Advanced Stochastic Control Systems with Engineering Applications

Guest Editors: Ming Liu, Peng Shi, Hamid Reza Karimi, Shen Yin, and Xiaojie Su



Advanced Stochastic Control Systems with Engineering Applications

Advanced Stochastic Control Systems with Engineering Applications

Guest Editors: Ming Liu, Peng Shi, Hamid Reza Karimi, Shen Yin, and Xiaojie Su



Editorial Board

Ravi P. Agarwal, USA Bashir Ahmad, Saudi Arabia M.O. Ahmedou, Germany Nicholas D. Alikakos, Greece Debora Amadori, Italy Pablo Amster, Argentina Douglas R. Anderson, USA Jan Andres, Czech Republic Giovanni Anello, Italy Stanislav Antontsev, Portugal Mohamed Kamal Aouf, Egypt Narcisa C. Apreutesei, Romania Natig M. Atakishiyev, Mexico Ferhan M. Atici, USA Ivan G. Avramidi, USA Soohyun Bae, Republic of Korea Zhanbing Bai, China Chuanzhi Bai, China Dumitru Baleanu, Turkey Józef Banas, Poland Gerassimos Barbatis, Greece Martino Bardi, Italy Roberto Barrio, Spain Feyzi Başar, Turkey Abdelghani Bellouquid, Morocco Daniele Bertaccini, Italy Michiel Bertsch, Italy Lucio Boccardo, Italy Igor Boglaev, New Zealand Martin J. Bohner, USA Julian F. Bonder, Argentina Geraldo Botelho, Brazil Elena Braverman, Canada Romeo Brunetti, Italy Janusz Brzdek, Poland Detlev Buchholz, Germany Sun-Sig Byun, Republic of Korea Fabio M. Camilli, Italy Jinde Cao, China Anna Capietto, Italy Jianqing Chen, China Wing-Sum Cheung, Hong Kong Michel Chipot, Switzerland C. Chun, Republic of Korea Soon Y. Chung, Republic of Korea

Jaeyoung Chung, Republic of Korea Lorenzo Giacomelli, Italy Silvia Cingolani, Italy Jean M. Combes, France Monica Conti, Italy Diego Córdoba, Spain Juan Carlos Cortés López, Spain Graziano Crasta, Italy Bernard Dacorogna, Switzerland Vladimir Danilov, Russia Mohammad T. Darvishi, Iran Luis F. Pinheiro de Castro, Portugal T. Diagana, USA Jesús I. Díaz, Spain Josef Diblík, Czech Republic Fasma Diele, Italy Tomas Dominguez, Spain Alexander I. Domoshnitsky, Israel Marco Donatelli, Italy Bo-Qing Dong, China Ondřej Došlý, Czech Republic Wei-Shih Du, Taiwan Luiz Duarte, Brazil Roman Dwilewicz, USA Paul W. Eloe, USA Ahmed El-Sayed, Egypt Luca Esposito, Italy Jose A. Ezquerro, Spain Khalil Ezzinbi, Morocco Dashan Fan, USA Angelo Favini, Italy Marcia Federson, Brazil Stathis Filippas, Equatorial Guinea Alberto Fiorenza, Italy Tore Flåtten, Norway Ilaria Fragala, Italy Bruno Franchi, Italy Xianlong Fu, China Massimo Furi, Italy Giovanni P. Galdi, USA Isaac Garcia, Spain Jesús García Falset, Spain José A. García-Rodríguez, Spain Leszek Gasinski, Poland György Gát, Hungary

Vladimir Georgiev, Italy

Jaume Giné, Spain Valery Y. Glizer, Israel Laurent Gosse, Italy Jean P. Gossez, Belgium Jose L. Gracia, Spain Maurizio Grasselli, Italy Qian Guo, China Yuxia Guo, China Chaitan P. Gupta, USA Uno Hämarik, Estonia Ferenc Hartung, Hungary Behnam Hashemi, Iran Norimichi Hirano, Japan Jafari Hossein, Iran Jiaxin Hu, China Chengming Huang, China Zhongyi Huang, China Gennaro Infante, Italy Ivan Ivanov, Bulgaria Jaan Janno, Estonia Aref Jeribi, Tunisia Un C. Ji, Republic of Korea Zhongxiao Jia, China L. Jódar, Spain Jong Soo Jung, Republic of Korea Henrik Kalisch, Norway Hamid Reza Karimi, Norway Satyanad Kichenassamy, France Tero Kilpeläinen, Finland Sung Guen Kim, Republic of Korea Ljubisa Kocinac, Serbia Andrei Korobeinikov, Spain Pekka Koskela, Finland Victor Kovtunenko, Austria Ren-Jieh Kuo, Taiwan Pavel Kurasov, Sweden Miroslaw Lachowicz, Poland Kunguan Lan, Canada Ruediger Landes, USA Irena Lasiecka, USA Matti Lassas, Finland Chun-Kong Law, Taiwan Ming-Yi Lee, Taiwan Gongbao Li, China

Elena Litsyn, Israel Yansheng Liu, China Shengqiang Liu, China Carlos Lizama, Chile Milton C. Lopes Filho, Brazil Julian López-Gómez, Spain Guozhen Lu, USA Iinhu Lü, China Grzegorz Lukaszewicz, Poland Shiwang Ma, China Wanbiao Ma, China Eberhard Malkowsky, Turkey Salvatore A. Marano, Italy Cristina Marcelli, Italy Paolo Marcellini, Italy Jesús Marín-Solano, Spain Jose M. Martell, Spain M. Mastyłfjo, Poland Ming Mei, Canada Taras Mel'nyk, Ukraine Anna Mercaldo, Italy Changxing Miao, China Stanislaw Migorski, Poland Mihai Mihäilescu, Romania Feliz Minhós, Portugal Dumitru Motreanu, France Roberta Musina, Italy G. M. N'Guérékata, USA Maria Grazia Naso, Italy Sylvia Novo, Spain Micah Osilike, Nigeria Mitsuharu Ôtani, Japan Turgut Öziş, Turkey Filomena Pacella, Italy Nikolaos S. Papageorgiou, Greece Sehie Park, Repubic of Korea Alberto Parmeggiani, Italy Kailash C. Patidar, South Africa Kevin R. Payne, Italy Ademir Fernando Pazoto, Brazil Josip E. Pečarić, Croatia Shuangjie Peng, China Sergei V. Pereverzyev, Austria Maria Eugenia Perez, Spain Josefina Perles, Spain Allan Peterson, USA Andrew Pickering, Spain Cristina Pignotti, Italy

Somyot Plubtieng, Thailand Milan Pokorny, Czech Republic Sergio Polidoro, Italy Ziemowit Popowicz, Poland Maria M. Porzio, Italy Enrico Priola, Italy Vladimir S. Rabinovich, Mexico Irena Rachůková, Czech Republic Maria Alessandra Ragusa, Italy Simeon Reich, Israel Abdelaziz Rhandi, Italy Hassan Riahi, Malaysia Juan P. Rincón-Zapatero, Spain Luigi Rodino, Italy Yuriy V. Rogovchenko, Norway Julio D. Rossi, Argentina Wolfgang Ruess, Germany Bernhard Ruf, Italy Marco Sabatini, Italy Satit Saejung, Thailand Stefan G. Samko, Portugal Martin Schechter, USA Javier Segura, Spain Sigmund Selberg, Norway Valery Serov, Finland Naseer Shahzad, Saudi Arabia Andrey Shishkov, Ukraine Stefan Siegmund, Germany Abdel-Maksoud A. Soliman, Egypt Pierpaolo Soravia, Italy Marco Squassina, Italy Svatoslav Staněk, Czech Republic Stevo Stevic, Serbia Antonio Suárez, Spain Wenchang Sun, China Robert Szalai, UK Sanyi Tang, China Chun-Lei Tang, China Youshan Tao, China Gabriella Tarantello, Italy Nasser-eddine Tatar, Saudi Arabia Susanna Terracini, Italy Gerd Teschke, Germany Alberto Tesei, Italy Bevan Thompson, Australia Sergey Tikhonov, Spain

Claudia Timofte, Romania

Thanh Tran, Australia

Juan J. Trujillo, Spain Ciprian A. Tudor, France Gabriel Turinici, France Milan Tvrdy, Czech Republic Mehmet Unal, Turkey Csaba Varga, Romania Carlos Vazquez, Spain Gianmaria Verzini, Italy Jesus Vigo-Aguiar, Spain Qing-Wen Wang, China Qing Wang, USA Yushun Wang, China Shawn X. Wang, Canada Youyu Wang, China Jing Ping Wang, UK Peixuan Weng, China Noemi Wolanski, Argentina Ngai-Ching Wong, Taiwan Patricia J. Y. Wong, Singapore Zili Wu, China Yong Hong Wu, Australia Shanhe Wu, China Tie-cheng Xia, China Xu Xian, China Yanni Xiao, China Fuding Xie, China Gongnan Xie, China Naihua Xiu, China Daoyi Xu, China Zhenya Yan, China Xiaodong Yan, USA Norio Yoshida, Japan Beong In Yun, Republic of Korea Vjacheslav Yurko, Russia Agacik Zafer, Turkey Sergey V. Zelik, UK Jianming Zhan, China Meirong Zhang, China Weinian Zhang, China Chengjian Zhang, China Zengqin Zhao, China Sining Zheng, China Tianshou Zhou, China Yong Zhou, China Qiji J. Zhu, USA Chun-Gang Zhu, China Malisa R. Zizovic, Serbia Wenming Zou, China

Contents

Advanced Stochastic Control Systems with Engineering Applications, Ming Liu, Peng Shi,

Hamid Reza Karimi, Shen Yin, and Xiaojie Su Volume 2014, Article ID 320412, 2 pages

The Flow Field Analysis and Flow Calculation of Ultrasonic Flowmeter Based on the Fluent Software,

Ling Guo, Yue Sun, Ling Liu, Zhixi Shen, Ruizhen Gao, and Kai Zhao Volume 2014, Article ID 528602, 8 pages

Robust Adaptive Reactive Power Control for Doubly Fed Induction Generator, Huabin Wen, Yu Zeng,

Lei Wang, Feng Yang, and Y. D. Song

Volume 2014, Article ID 369349, 8 pages

Stochastic Maximum Principle for Partial Information Optimal Control Problem of Forward-Backward Systems Involving Classical and Impulse Controls, Yan Wang, Aimin Song, and Enmin Feng

Volume 2014, Article ID 452124, 8 pages

Consensus of Multiagent Systems with Packet Losses and Communication Delays Using a Novel Control

Protocol, Zheping Yan, Di Wu, Wei Zhang, and Yibo Liu Volume 2014, Article ID 159609, 13 pages

Adaptive Predictive Control: A Data-Driven Closed-Loop Subspace Identification Approach,

Xiaosuo Luo and Yongduan Song

Volume 2014, Article ID 869879, 11 pages

AP Deployment Research Based on Physical Distance and Channel Isolation, Dangui Yan,

Chengchang Zhang, Honghua Liao, Lisheng Yang, Ping Li, and Guogang Yang Volume 2014, Article ID 941547, 7 pages

Decentralized H_{∞} Control for Uncertain Interconnected Systems of Neutral Type via Dynamic Output

Feedback, Heli Hu and Dan Zhao

Volume 2014, Article ID 989703, 11 pages

Robust Guaranteed Cost Observer Design for Singular Markovian Jump Time-Delay Systems with

Generally Incomplete Transition Probability, Yanbo Li, Yonggui Kao, and Jing Xie

Volume 2014, Article ID 832891, 11 pages

Relative Orbit Stabilization Control for the Agile Satellite under Stochastic Disturbance, Xiande Wu,

Fengzhi Guo, Wenbo Yang, Jiangtao Xu, and Ting Song

Volume 2014, Article ID 789583, 9 pages

Robust Stability Criteria of Roesser-Type Discrete-Time Two-Dimensional Systems with Parameter

Uncertainties, Yan Zhao, Tieyan Zhang, Dan Zhao, Fucai You, and Miao Li

Volume 2014, Article ID 159745, 6 pages

Stochastic Maximum Principle of Near-Optimal Control of Fully Coupled Forward-Backward Stochastic Differential Equation, Maoning Tang

Volume 2014, Article ID 361259, 12 pages

Robust Adaptive Fault-Tolerant Control of Stochastic Systems with Modeling Uncertainties and Actuator Failures, Wenchuan Cai, Lingling Fan, and Yongduan Song Volume 2014, Article ID 450521, 11 pages

Dynamic Neural Network Identification and Decoupling Control Approach for MIMO Time-Varying Nonlinear Systems, Zhixi Shen and Kai Zhao

Volume 2014, Article ID 316206, 10 pages

Prescribed Performance Fuzzy Adaptive Output-Feedback Control for Nonlinear Stochastic Systems, Lili Zhang, Shuai Sui, and Shaocheng Tong

Volume 2014, Article ID 836378, 9 pages

Finite-Time Terminal Sliding Mode Tracking Control for Piezoelectric Actuators, Jin Li and Liu Yang

Volume 2014, Article ID 760937, 9 pages

Numerical Implementation of Stochastic Operational Matrix Driven by a Fractional Brownian Motion for Solving a Stochastic Differential Equation, R. Ezzati, M. Khodabin, and Z. Sadati Volume 2014, Article ID 523163, 11 pages

Variable Torque Control of Offshore Wind Turbine on Spar Floating Platform Using Advanced RBF Neural Network, Lei Wang, Shan Zuo, Y. D. Song, and Zheng Zhou Volume 2014, Article ID 903493, 7 pages

T-S Fuzzy Model-Based Approximation and Filter Design for Stochastic Time-Delay Systems with Hankel Norm Criterion, Yanhui Li and Xiujie Zhou

Volume 2014, Article ID 937495, 12 pages

Volume 2014, Article ID 807102, 10 pages

 H_{∞} Filtering for Discrete-Time Genetic Regulatory Networks with Random Delay Described by a Markovian Chain, Yantao Wang, Xingming Zhou, and Xian Zhang Volume 2014, Article ID 257971, 12 pages

 ${\bf Adaptive\ Neural\ Networks\ Synchronization\ of\ a\ Four-Dimensional\ Energy\ Resource\ Stochastic\ System}, \\ {\bf Duo\ Meng}$

Volume 2014, Article ID 863902, 8 pages

Fuzzy Pruning Based LS-SVM Modeling Development for a Fermentation Process, Weili Xiong,

Wei Zhang, Dengfeng Liu, and Baoguo Xu Volume 2014, Article ID 794368, 7 pages

Study on the Characteristics of Electromagnetic Noise of Axial Flux Permanent Magnet Synchronous

Motor, Wei Wang, Hang Wang, and Hamid Reza Karimi

Volume 2014, Article ID 764105, 8 pages

Event-Based H_{∞} Filter Design for Sensor Networks with Missing Measurements, Jinliang Liu,

Shumin Fei, and Engang Tian

Volume 2014, Article ID 512037, 9 pages

Finite-Horizon Robust Kalman Filter for Uncertain Attitude Estimation System with Star Sensor

Measurement Delays, Hua-Ming Qian, Wei Huang, and Biao Liu

Volume 2014, Article ID 494060, 11 pages

Fuzzy Modeling and Control for a Class of Inverted Pendulum System, Liang Zhang, Xiaoheng Chang,

and Hamid Reza Karimi

Volume 2014, Article ID 936868, 6 pages

Ergodicity of Stochastic Burgers' System with Dissipative Term, Guoli Zhou, Boling Guo, Daiwen Huang, and Yongqian Han

Volume 2013, Article ID 267328, 23 pages

A New Real-Time Path Planning Method Based on the Belief Space, Yu-xin Zhao, Xin-an Wu, and Yan Ma Volume 2013, Article ID 260578, 14 pages

Robust Backstepping Control for Cold Rolling Main Drive System with Nonlinear Uncertainties,

Xu Yang, Kai-xiang Peng, and Chao-nan Tong

Volume 2013, Article ID 387890, 7 pages

Model Predictive Control of Piecewise Affine System with Constrained Input and Time Delay,

Zhilin Liu, Lutao Liu, Jun Zhang, and Xin Yuan

Volume 2013, Article ID 937274, 9 pages

Exponential Stabilization for Timoshenko Beam with Distributed Delay in the Boundary Control,

Xiu Fang Liu and Gen Qi Xu

Volume 2013, Article ID 726794, 15 pages

Hybrid Artificial Neural Networks Modeling for Faults Identification of a Stochastic Multivariate

Process, Yuehjen E. Shao and Chia-Ding Hou

Volume 2013, Article ID 386757, 10 pages

State-Feedback Stabilization for a Class of Stochastic Feedforward Nonlinear Time-Delay Systems, Liang Liu, Zhandong Yu, Qi Zhou, and Hamid Reza Karimi Volume 2013, Article ID 151374, 8 pages

Nonlinear Model Predictive Control with Terminal Invariant Manifolds for Stabilization of Underactuated Surface Vessel, Lutao Liu, Zhilin Liu, and Jun Zhang Volume 2013, Article ID 846389, 8 pages

Hindawi Publishing Corporation Abstract and Applied Analysis Volume 2014, Article ID 320412, 2 pages http://dx.doi.org/10.1155/2014/320412

Editorial

Advanced Stochastic Control Systems with Engineering Applications

Ming Liu,¹ Peng Shi,² Hamid Reza Karimi,³ Shen Yin,⁴ and Xiaojie Su⁵

- ¹ School of Astronautics, Harbin Institute of Technology, Harbin, Heilongjiang, China
- ² School of Electrical and Electronic Engineering, The University of Adelaide, SA 5005, Australia
- ³ Department of Engineering, Faculty of Engineering and Science, University of Agder, 4898 Grimstad, Norway
- ⁴ Institute of Automation and Complex Systems, University of Duisburg-Essen, Duisburg, Germany
- ⁵ College of Automation, Chongqing University, Chongqing 400044, China

Correspondence should be addressed to Ming Liu; mingliu23@hit.edu.cn

Received 26 May 2014; Accepted 26 May 2014; Published 12 June 2014

Copyright © 2014 Ming Liu et al. This is an open access article distributed under the Creative Commons Attribution License, which permits unrestricted use, distribution, and reproduction in any medium, provided the original work is properly cited.

Stochastic phenomenon has played an important role in various branches of science such as biology, economics, and aircraft. Stochastic modeling approach has achieved a great number of distinguished contributions for a wide spectrum of systems including Markovian jumping systems, Itô stochastic systems, networked control systems with random communication delays, and/or packet losses. Over the past few decades, considerable attention has been paid to modeling, stability analysis, stabilization, robust filtering, model reduction, and practical applications of stochastic dynamical systems. In spite of the extensive and systemic development of stochastic approaches and techniques, there still remain various types of open problems desired to be further strengthened, which includes modeling, filtering, nonparametric methods, system realization and identification, and so forth. Meanwhile, novel and updated developed theories and results are required to be investigated for application of stochastic systems in practical engineering.

This special issue contains thirty-four papers, which are summarized as follows.

"Event-based H_{∞} filter design for sensor networks with missing measurements" by J. Liu et al. proposes an event triggered mechanism based on sampled-data information, which has some advantages over existing ones. Considering the missing sensor measurements and the network-induced delay in the transmission, a new event-based H_{∞} filtering is constructed by taking the effect of sensor faults with different

failure rates. By using the Lyapunov stability theory and the stochastic analysis theory, sufficient criteria are derived for the existence of a solution to the algorithm of the event-based filter design.

"Finite-horizon robust Kalman filter for uncertain attitude estimation system with star sensor measurement delays" by H.-M. Qian et al. addresses the robust Kalman filtering problem for uncertain attitude estimation system with star sensor measurement delays. Combined with the misalignment errors and scale factor errors of gyros in the process model and the misalignment errors of star sensors in the measurement model, the uncertain attitude estimation model can be established to indicate that uncertainties not only appear in the state and output matrices but also affect the statistic of the process noise. Meanwhile, the phenomenon of star sensor measurement delays is described by introducing Bernoulli random variables with different delay characteristics. A finite-horizon robust Kalman filter is proposed to solve this estimation problem which takes into account the effects of star sensor measurement delays and model

"Robust adaptive fault-tolerant control of stochastic systems with modeling uncertainties and actuator failures" by W. Cai et al. deals with the problem of actuator fault-tolerant control of a class of uncertain stochastic systems with model uncertainties. A robust adaptive control scheme is developed to solve this problem. The proposed approach does not require

the fault detection and diagnosis roles and thus simplifies the design procedure and achieve a low cost.

"Prescribed performance fuzzy adaptive output-feedback control for nonlinear stochastic systems" by L. Zhang et al. proposes a prescribed performance for a class of single-input and single-output nonlinear stochastic systems with unmeasured states, and a fuzzy state observer is designed for estimating the unmeasured states. Based on the back-stepping recursive design technique and the predefined performance technique, a new fuzzy adaptive output feedback control method is developed. It is shown that all the signals of the resulting closed-loop system are bounded in probability and the tracking error remains an adjustable neighborhood of the origin with the prescribed performance bounds.

"Consensus of multiagent systems with packet losses and communication delays using a novel control protocol" by Z. Yan et al. addresses the consensus problem of multiagent system with packet losses and communication delays under directed communication channels from a practical point of view. A novel control protocol is proposed depending only on periodic sampling and transmitting data in order to be convenient for practical implementation and economical for limited system resources. It is proved that for single integrator agents and double integrator systems with only communication delays consensusability can be ensured through stochastic matrix theory provided that the designed communication topology contains a directed spanning tree. For double integrator agents and high-order integrator agents, the interval system theory is introduced to investigate the consensus of multiagent system.

"State-feedback stabilization for a class of stochastic feed-forward nonlinear time-delay systems" by L. Liu et al. investigates the state-feedback stabilization problem for a class of stochastic feedforward nonlinear time-delay systems. By using the homogeneous domination approach and choosing an appropriate Lyapunov-Krasovskii functional, the delay-independent state-feedback controller is explicitly constructed such that the closed-loop system is globally asymptotically stable in probability.

"Robust guaranteed cost observer design for singular Markovian jump time-delay systems with generally incomplete transition probability" by Y. Li et al. investigates the design of robust guaranteed cost observer for a class of linear singular Markovian jump time-delay systems with generally incomplete transition probability. In this design, each transition rate can be completely unknown or only its estimate value is known. Based on stability theory of stochastic differential equations and linear matrix inequality technique, an observer is designed to ensure that for all uncertainties the resulting augmented system is regular, impulse free, and robust stochastically stable with the proposed guaranteed cost performance.

Of course, the selected issues and papers are not a comprehensive representation of the area of this special issue. Nonetheless, they represent the rich and many-faceted knowledge that we have the pleasure of sharing with the readers.

Acknowledgments

We would like to express appreciation to the authors for their excellent contributions and patience in assisting us. The hard work of all reviewers on these papers is also very greatly acknowledged.

Ming Liu Peng Shi Hamid Reza Karimi Shen Yin Xiaojie Su Hindawi Publishing Corporation Abstract and Applied Analysis Volume 2014, Article ID 528602, 8 pages http://dx.doi.org/10.1155/2014/528602

Research Article

The Flow Field Analysis and Flow Calculation of Ultrasonic Flowmeter Based on the Fluent Software

Ling Guo, 1,2 Yue Sun, Ling Liu, Zhixi Shen, Ruizhen Gao, and Kai Zhao

- ¹ School of Automation, Chongqing University, Chongqing 400044, China
- ² Logistic Engineering University, Chongqing 400016, China

Correspondence should be addressed to Zhixi Shen; shenzhixi@cqu.edu.cn

Received 26 January 2014; Accepted 3 March 2014; Published 22 May 2014

Academic Editor: Xiaojie Su

Copyright © 2014 Ling Guo et al. This is an open access article distributed under the Creative Commons Attribution License, which permits unrestricted use, distribution, and reproduction in any medium, provided the original work is properly cited.

We can build the three-dimensional structure model based on the Gambit software and achieve the distribution of flow field in the pipe and reflux flow condition at the position of transducer in regard to the real position of transducer according to the Fluent software. Under the framework, define the reflux length based on the distance of reflux along the channel and evaluate the effect of reflux on flow field. Then we can correct the power factor with the transmission speed difference method in the ideal condition and obtain the matching expression of power correction factor according to the practice model. In the end, analyze the simulation experience and produce the sample table based on the proposed model. The comparative analysis of test results and simulation results demonstrates the validity and feasibility of the proposed simulation method. The research in this paper will lay a foundation for further study on the optimization of ultrasonic flowmeter, enhance the measurement precision, and extend the application of engineering.

1. Introduction

Compared with the conventional flowmeter, the ultrasonic flowmeter has a better performance since it has no moving parts, no pressure loss, wide measuring range, excellent repeatability, and high precision [1], and it is widely used in industrial production [2, 3], especially for large diameter pipes and larger flows [4, 5]. The ultrasonic flowmeter is mainly comprised of an ultrasonic transducer installed on the measuring pipe and the related sensors of temperature and pressure [6]. The ultrasonic transducer has two installations: intrusive and nonintrusive [7, 8]. With the nonintrusive installation, the signal emitted by the ultrasonic transducer needs to go through the pipe wall twice, which will weaken the strength of the signal largely, while the low SNR will affect the stability and accuracy of signal receiving. The intrusive installation is currently used in normal situations [9]. For the single-path ultrasonic flowmeter, the intrusive installation requires a through-hole in the pipe wall, where the ultrasonic transducer can be built. This structure and ultrasonic transducer generate disturbance in the flow field,

cause measuring errors, and may be the key problem in the measurement of ultrasonic flowmeter. Reference [10] pointed out that the unevenness near the pipe wall induced by the ultrasonic transducer distorts the flow field and leads to lower measuring values. The measuring value would be lower by 0.05% while the length of the channel is 5 m; the measuring value would be lower by 0.35% while the length of the channel is 1 m. However, for the pipe with small diameter and low flow, the length of channel will be shorter, far less than 1 m; the reference had not stated the magnitude of error. Raišutis [11] analysed the flow at the recess in the pipe with a diameter of 70 mm; the flow field was distorted and the symmetry of the velocity distribution was destroyed; this also influenced the measurement of flow. Yet the velocity of flow was large in this reference, and the Reynolds number was large; this belonged to the turbulent flow. Zhang et al. [6] and Zheng et al. [12] did research on the non-flow-calibrated method of ultrasonic flowmeter, using the computational fluid dynamics numerical simulation method, and analyzed the influences of DN500-the multichannel transducer ultrasonic flowmeter—on the accuracy of measurement. The analysis

³ Chongqing Vocational Institute of Engineering, Chongqing 400037, China

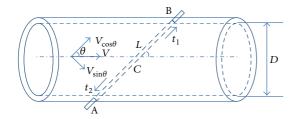


FIGURE 1: The diagram of the principle of ultrasonic flowmeter.

of flow field pointed out that since there might be a reflux near the transducer, the average measurement of velocity of each channel was lower, and the measuring values of flows were lower as well.

With analysis of the related references, we found that (1) the ultrasonic flowmeter uses double-path and multipath measurement generally [13, 14]; the shortcomings can be listed as follows: on one hand the complex pipe structure requires higher accuracy of installation; on the other hand the use of multiple ultrasonic transducers will increase the costs; (2) few researches have been done for the fluid with low Reynolds number in the single-path ultrasonic flowmeter. And for this kind of ultrasonic flowmeter, the intrusive installation and transducer have nonignorable disturbance on flow field.

In order to estimate the measuring errors caused by disturbance, this paper proposed a novelty model that builds the practice structure of a single-path ultrasonic transducer with a 50 mm pipe diameter and calculates the disturbance of transducer to the flow field approximately using the Fluent software for flow field analysis combined with test data; based on the above model we can analyze the measurement effects on the accuracy by quantitative methods.

This paper is structured in the following way. In Section 2, the measurement principle of the single-path ultrasonic flowmeter is presented. In Section 3, we can model and analyze the flow field based on Fluent software. The simulation results demonstrate the effectiveness and generality of the proposed algorithm in Section 4. Finally, Section 5 summarizes the conclusion.

2. Measurement Principle of the Single-Path Ultrasonic Flowmeter

2.1. Operational Principle. We can see the measurement principle of transmission speed difference method in the single-path ultrasonic flowmeter [15–20] from Figure 1. The diameter of the pipe is represented by D, ultrasonic transducers are installed on A and B sides, which could emit and receive the ultrasonic signals, L represents the distance of A and B, and θ is the angle of AB with the pipe axis. It will need time t_1 for the signal from A to B and the circuit delay is τ_1 . For the same reason, the signal will cost time t_2 from B to A and the circuit delay is τ_2 ; in addition, the actual pressure is P and the actual temperature is T.

It is assumed that the fluid will flow with velocity V and the direction is parallel to the axis to the right, so on

the channel L the propagation velocity of the ultrasonic signal is composited by the acoustic velocity C and component of flow velocity $V_{\cos\theta}$, then the propagation time of ultrasonic signal in both downstream and upstream directions can be shown, respectively:

Downstream:
$$t_1 = \frac{L}{C + V_{\cos \theta}}$$
, (1)
Upstream: $t_2 = \frac{L}{C - V_{\cos \theta}}$.

Using (1), the linear mean velocity V_L will be calculated by

$$V_{L} = \frac{L}{2\cos\theta} \left(\frac{1}{t_{1} - \tau_{1}} - \frac{1}{t_{2} - \tau_{2}} \right). \tag{2}$$

Because of the presence of the actual fluid velocity distribution in the pipe cross-section, linear mean velocity V_L is not equal to the cross-section mean velocity V_A . Assume that there is a power correction factor K between the linear mean velocity V_L and the cross-section mean velocity V_A , the expression is that

$$K = \frac{V_{\rm A}}{V_{\rm I}}.\tag{3}$$

Then we can get that the flow of the pipe is

$$Q = K \frac{\pi D^2}{4} V_L. \tag{4}$$

Considering the influences of pressure and temperature, the flow can be converted under the standard working conditions:

$$Q = K \frac{\pi D^2}{4} V_L \cdot \frac{P}{P_0} \cdot \frac{T_0}{T}.$$
 (5)

2.2. Model of Ideal Channel. Based on the hydrodynamic theory, the fluid has viscosity so that the fluid shows different velocities at the points of different diameter in the crosssection. And the Reynolds number can be the only parameter that distinguishes moving patterns of viscous fluid. Whether the fluid moving as laminar or turbulent flow can be decided by the value of Reynolds number, there is a lower bound around 2000 for the critical Reynolds number, which transits laminar flow to turbulence. In the moving of laminar flows, the tiny disturbance in the flow field such as the roughness of pipe wall and free changes of surface will attenuate gradually so that the fluid flows as laminar flow. However, the tiny disturbance can be increased and flow becomes unstable if Reynolds number is bigger, so it is difficult to make sure the final status after disturbance increased as the equations are of nonlinearity, we can only conclude that the final stage is connected with structure of flow field and Reynolds number.

With regard to the ideal laminar flow shown in Figure 1, the fluid may flow symmetrically if the gravity effects are ignored, and the velocity will be a function of radius r in

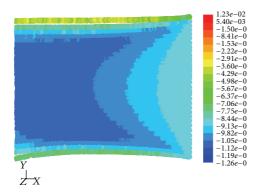


FIGURE 2: The velocity profile in the laminar flow.

the horizontal direction. Presume that the pressure drop on the pipe is ΔP and the radius of the pipe R = D/2, the velocity distribution at cross-section can be shown by the Hagen-Poiseuille formula:

$$u = \frac{\Delta P}{4\,\mu\text{L}} \left(R^2 - r^2 \right). \tag{6}$$

Based on the equation above, each point velocity distributed parabolically with radius r; the largest velocity is on the pipe axis as r = 0:

$$u_{\text{max}} = \frac{\Delta P}{4 \,\mu \text{L}} R^2 = \frac{\Delta P}{16 \,\mu \text{L}} D^2.$$
 (7)

Through the simulation, we can get the flow results with parabolic distribution in Figure 2; the distribution is shown clearly.

According to the distribution of flow velocity, the cross-sectional area of the flow can be calculated as

$$dQ = udA = \frac{\Delta P}{4\mu L} \left(R^2 - r^2\right) 2\pi r dr. \tag{8}$$

After integration:

$$Q = \int_0^R \frac{\Delta P}{4 \,\mu L} \left(R^2 - r^2 \right) 2\pi r dr = \frac{\pi \Delta P}{128 \,\mu L} D^4. \tag{9}$$

The mean flow velocity at cross-section can be presented as

$$V_{\rm A} = \frac{Q}{A} = \frac{\Delta P}{32 \,\mu \rm L} D^2 = \frac{1}{2} u_{\rm max}.$$
 (10)

Under the normal circumstances, the path of ultrasonic flowmeter is installed in the middle of the pipe, then the linear mean velocity is

$$V_{L} = \frac{1}{L} \int_{L} u(r) dL = \frac{1}{R} \int_{0}^{R} u_{\text{max}} \left(1 - \frac{r^{2}}{R^{2}} \right) dr = \frac{2}{3} u_{\text{max}}.$$
(11)

On the basis of (4), (10), and (11), we can compute the power correction factor K:

$$K = \frac{V_{\rm A}}{V_{\rm L}} = \frac{3}{4}. (12)$$

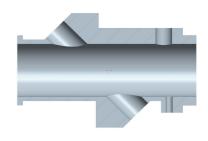


FIGURE 3: The cross-section of ultrasonic flowmeter.

We can achieve the relationship between the cross-section mean velocity, linear mean velocity, and the maximum flow rate based on the above theory; meanwhile the relationship between the cross-section mean velocity and linear mean velocity is obtained. However, the magnitude and position of maximum velocity cannot be measured directly in practice and engineering application.

3. Fluent-Based Modeling and Analysis of Flow Field

The laminar flow velocity distribution and the value of power correction factor have been derived under the ideal circumstances. However, the pipe is not smooth in practice, and the pipe will be installed with temperature and pressure sensors inside it, which may disturb the flow field making the velocity of flow field dissatisfy the standard parabolic distribution. Therefore, the power correction factor *K* is not a fixed value.

In this paper, we design the actual structure of ultrasonic flowmeter with small diameter and small flow as shown in Figure 3. Then, the model processing of the simulation and modeling is as follows.

In the first step, we can use the Gambit software to build the geometric model of the flowmeter. The pipe is cylindrical with a 50 mm-diameter with holes at the 45-degree angle along with pipe axis, where the transducer is installed; the pressure and temperature sensors are built separately inside the two holes on the left side.

Secondly, mesh the model. Since the pipe has a throughhole structure that the transducer and sensors are installed in, the shape of flow field is not cylindrical any more. Thence, the surface and volume of flow field can ensure the grid near the transducer and sensors is dense enough and can control the number of grids by choosing tetrahedral mesh.

Next, put the grid file into the Fluent software in order to do the fluid calculation. As the pipe is of small diameter, small flow, and small Reynolds number, we should employ the laminar flow model to make the fluid calculation.

At last, set the parameters for calculations. Using the Fluent software to deal with the laminar flow model when the minimum flow is $0.6 \,\mathrm{m}^3/\mathrm{h}$ and the corresponding Reynolds number R_e is 140. Based on the calculation above, we can set

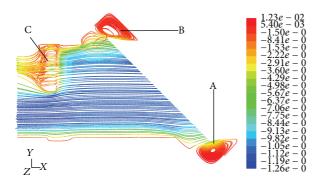


Figure 4: The diagram of sound channel ($R_e = 145$).

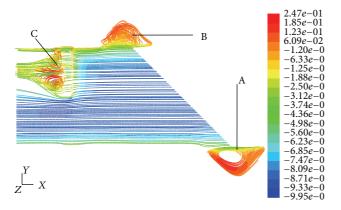


Figure 5: The diagram of sound channel ($R_e = 1168$).

the uniform speed entrance and free exit to do the simulated calculation and analyze the output after convergence.

3.1. The Disturbance of Pipe Structure in the Flow Field. In Figures 4 and 5, the fluid flows into the pipe from the right side and the flow field will be affected by the structures of the transducer and the sensor installed therefore generating reflux near the attachments of transducer and sensor at point A and B. The strength of reflux is changing every time according to Reynolds number and it will be increased when Reynolds number is bigger. The reflux will go through the test channel, produce opposite flow, and decrease the linear average velocity of the path, which may affect the measuring accuracy directly. For flowmeter with large diameter, the influences of reflux can be ignored generally. But these influences may be significant with the small-diameter and small-flow condition.

In addition, the fluid velocity has parabolic distribution in the ideal laminar flow model and is parallel to the axis, but in the actual structure we can get the curve of fluid velocity along AB in Figures 6 and 7. In Figure 6, velocity is not symmetrically distributed in the *X* direction along AB. At point A the velocity is exactly positive which means the fluid flows to the opposite direction. The reflux will have larger influence at point A than point B. Figure 7 shows that particles were distributed along the velocity to the *Y* axis

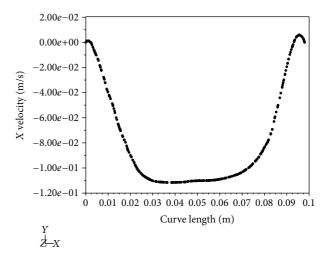


FIGURE 6: The velocity curve in the *X* direction along AB.

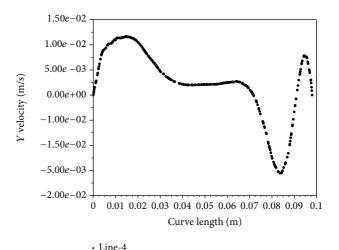


FIGURE 7: The velocity curve in the *Y* direction along AB.

along AB; on the axis of pipe there is tiny flow to the *Y* axis, but apparent flow to the *Y* axis exists near the ends of AB.

The curve of cross-sectional velocity distribution at the midpoint of output pipe (the midpoint of AB) can be seen in Figure 8. Being influenced by actual pipe structure and transducer, it is no more standard parabolic distribution.

3.2. Estimating the Influence of Reynolds Number on Reflux. To the fluid, the Reynolds number can be estimated by

$$R_e = \frac{\rho VR}{\eta},\tag{13}$$

where R_e is the Reynolds number, ρ is the density of gas, V is velocity of flow, and R means the radius of the pipe.

In the model shown in Figure 3, the distance AB for transducer installation is $0.098 \, \text{m}$, the air viscosity is $1.84e-05 \, \text{Pa·S}$, and the density can be seen as $1.225 \, \text{kg/m}^3$. According to whether the particles on the line in the trajectories of AB are circulated or not, we can ensure the length of reflux on

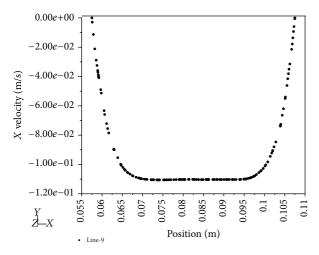


FIGURE 8: The curve of cross-sectional velocity distribution at the midpoint of output pipe AB.

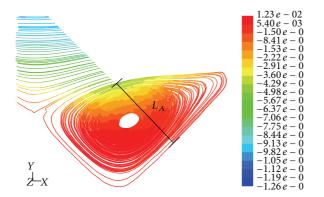


FIGURE 9: The length of reflux at point A.

Table 1: The length of refluxes L_A and L_B .

Number	R_e	$L_{ m A}$	L_{B}	Percentage (%)
1	145	0.01191	0.00798	20.3
2	226	0.01198	0.00815	20.5
3	459	0.01212	0.00956	22.1
4	1168	0.01339	0.01110	25.0
5	1853	0.01451	0.01361	28.7

the propagation path. At the same time, the length of reflux at point A is $L_{\rm A}$ and at point B is $L_{\rm B}$, as in Figures 9 and 10.

Simulating under different Reynolds numbers, we can get the reflux of fluid at the transducer and the length of refluxes $L_{\rm A}$ and $L_{\rm B}$; the statistics are expressed in Table 1.

On the basis of Table 1, the length of reflux will be raised if Reynolds number is larger. The curve that shows the relationship between Reynolds number and length of reflux is drawn in Figure 11.

3.3. Power Correction Factor Analysis. From (12) above, the power correction factor K plays an important role in measurement accuracy of ultrasonic flowmeter, which is the key parameter of ultrasonic flowmeter calibration [9]. The

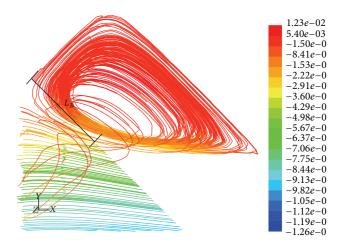


FIGURE 10: The length of reflux at point B.

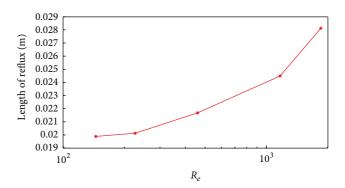


Figure 11: The relationship diagram of R_e and length of reflux.

value of K is highly related to the Reynolds number, pipe structure, and other factors. If the pipe structure is certain, K changes all the time when the Reynolds number changes. And among the references related to the power correction factor K, two assumptions can be concluded.

First, assume that the fluid is flowing parallel to the pipe axis in Figure 1. But in practice, the fluid direction is influenced by the pipe shape; it will not certainly and completely be parallel to axis; the velocity V of transducer and sensor is not in the horizontal direction. If the actual flowing direction is not parallel to the axis, according to (5), the measurement will generate large errors.

Second, suppose that the pipes are all smooth tubes; we can ignore the influences on the fluid of exact pipe structure. However, because of the actual structure of the transducer by intrusive installation, especially for the pipes with small diameters, the fluid flow will be affected.

In engineering, we can get the power correction factor generally from the test when correcting the flowmeter against the fluid with low Reynolds number, if, considering the actual shape, structure of pipe, and the influences on the measurement of the non-axis-parallel flowing fluid, the relationship between flow field that affects power correction factor and measurement error of pipe flow can be analyzed.

Reflux makes the linear average velocity less so that the measurement is lower and the error is negative. Now considering the influences of reflux, we can rewrite (2):

$$\begin{split} V &= \frac{L - L_{\rm A} - L_{\rm B}}{2\cos\theta} \left(\frac{1}{t_1 - t_{\rm A1} - t_{\rm B1} - \tau_1} - \frac{1}{t_2 - t_{\rm A2} - t_{\rm B2} - \tau_2} \right) \\ &= \frac{L - L_{\rm A} - L_{\rm B}}{2\cos\theta} \frac{t_2 - t_{\rm A2} - t_{\rm B2} - \tau_2 - t_1 + t_{\rm A1} + t_{\rm B1} + \tau_1}{(t_1 - t_{\rm A1} - t_{\rm B1} - \tau_1) \left(t_2 - t_{\rm A2} - t_{\rm B2} - \tau_2 \right)} \\ &= \frac{L - L_{\rm A} - L_{\rm B}}{2\cos\theta} \frac{\Delta T_{\rm sim} - \Delta T_{\rm A} - \Delta T_{\rm B} + \left(\tau_1 - \tau_2 \right)}{(t_1 - t_{\rm A1} - t_{\rm B1} - \tau_1) \left(t_2 - t_{\rm A2} - t_{\rm B2} - \tau_2 \right)}. \end{split}$$

Considering that the type and size of the transducer in part A are generally the same as part B, so the hardware delay can be regarded as the same: $\tau_1 = \tau_2$. Then

$$V = \frac{L - L_{A} - L_{B}}{2\cos\theta} \frac{\Delta T_{\text{sim}} - \Delta T_{A} - \Delta T_{B}}{(t_{1} - t_{A1} - t_{B1} - \tau_{1})(t_{2} - t_{A2} - t_{B2} - \tau_{2})}.$$
(15)

According to the simulation output data we can get $t_1, t_{A1}, t_{B1}, t_2, t_{A2}$, and t_{B2} . Since τ_1 and τ_2 are errors caused by circuit board delay, which can be ignored, getting the linear average velocity by calculation, then the power correction factor K is calculated basing on (3) and (4).

4. Simulation

To test the effectiveness of simulation analysis, make a trial version of ultrasonic flowmeter shown in Figure 3; then test with the nozzle flow calibration test device.

4.1. Time Difference Correction of Ultrasonic Propagation. The analysis from the last section leads to the conclusion that the actual structure of the pipe generates reflux at points A and B; the reflux raises the downstream ultrasonic propagation time and lowers the upstream time so that the time difference is less, the flow measurement is lower, the errors will be negative, with the same diameters, and the measuring errors will increase gradually along with the increasing entrance velocity.

To estimate the exact influences on measurement of reflux, this paper is based on the output of Fluent and counts the propagation time and time difference of ultrasonic wave between two transducers, as Table 2 states. From the table, the time difference of reflux at point A is $\Delta T_{\rm A}$, the time difference of reflux at point B is $\Delta T_{\rm B}$, the downstream and upstream time difference through the AB channel is $\Delta T_{\rm sim}$, and the unit is nanosecond (ns).

4.2. Power Correction Factor K. The power correction factor *K* is calculated based on (3) and (4), and the results are shown in Table 3.

Data from Table 3 suggests that the power factor will change in the same direction with Reynolds number. This also proves that power factor K may have negative errors using ideal model and the errors increase as Reynolds number

TABLE 2: Time difference of ultrasonic wave at points A and B.

Number	R_e	$\Delta T_{ m A}$	$\Delta T_{ m B}$	$\Delta T_{ m sim}$	Percentage (%)
1	145	1.874	1.608	97.5	3.6
2	226	3.283	1.883	147.2	3.5
3	459	5.60	3.810	277.1	3.4
4	1168	17.723	2.366	683.4	2.94
5	1853	23.10	1.59	1037.8	2.38

TABLE 3: The result of mean linear velocity.

Number	R_e	Mean linear velocity	Power correction factor
1	145	0.0816	1.067
2	226	0.123	1.105
3	459	0.231	1.196
4	1168	0.569	1.235
5	1853	0.863	1.290

TABLE 4: The relationship of time difference and R_{ρ} .

Number	R_e	$\Delta T_{ m exp}$
1	145	90.5
2	226	202.2
3	459	346.8
4	1168	746.4
5	1853	1119.2

increases. On the basis of Table 3 and using the logarithm of fitting method in the Matlab software, we can fit the power factor and Reynolds number as follows:

$$K = 0.08444 \log (R_e) + 0.6532.$$
 (16)

The curve that indicates the relationship between the power factor and Reynolds number is drawn in Figure 12.

4.3. The Relationship of Time Difference and $R_{\rm e}$. During the test, $\Delta T_{\rm exp}$ represents the time difference of downstream and upstream, the related experimental results are shown in Table 4.

Based on Table 4, draw the diagram of relationships among simulated time differences, testing time differences, and Reynolds number in Figure 13.

The simulation and test outputs have the same trend with Reynolds number, but there are some offsets in Figure 13; the related seasons can be listed as follows.

Firstly, when installing two transducers along AB, some installation errors always exist.

Secondly, when building the finite element model of flow field, the meshing type and the size of grids will affect the accuracy and then generate the errors.

Thirdly, while using Fluent to simulate and calculate, the setting of related parameters in the laminar flow model will influence the accuracy of outputs.

It is effective to converge the tested and simulated results by improving the accuracy of meshing, setting the reasonable parameters and installation accuracy.

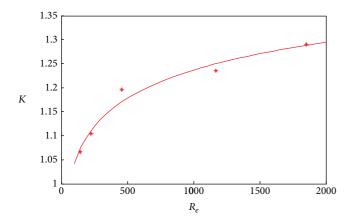


FIGURE 12: The relationship of power factor K and R_e .

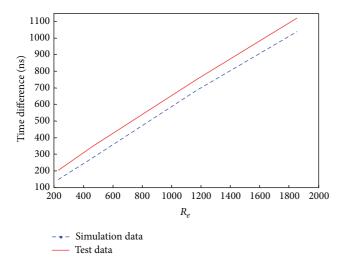


Figure 13: The relationship curve of time difference and R_e .

5. Conclusion

In this paper, we analyze the flow field of ultrasonic mono flowmeter with small diameter and low flow and discuss the influences on the flow field and power factor of exact pipe structure and the variation using different Reynolds number. The main conclusions are as follows.

- (1) The installation point of ultrasonic transducer and temperature/pressure sensor will disturb the laminar flow field, the velocity will not be standard parabolic distribution any longer, and the reflux is generated at the transducer; the length of reflux has the same trend with Reynolds number.
- (2) Near the transducer, the reflux decreases the linear average velocity and makes the measurement of flow lower; the errors will be negative.
- (3) The expression of power correction factor by simulated data is fit.
- (4) Through the test, the effectiveness of simulation is tested. Numerical simulation method can be a good reaction to flow state of flow field; it may be an important way to design and develop ultrasonic flowmeter.

In further work, we will take into account the main reason which causes the error between the test data and the simulation data and fit the power correction factor more accurately so that the proposed method is a more effective tool.

Conflict of Interests

The authors declare that there is no conflict of interests regarding the publication of this paper.

Acknowledgment

This work was supported by the Fundamental Research Funds for the Central Universities (no. CDJZR10170007).

References

- [1] P.-Y. Zhang, D.-D. Zheng, T.-S. Xu, L.-X. Zhang, and H.-M. Hu, "Study on the influence of ultrasonic probes on flow field and measurement performance of ultrasonic flowmeter," *Journal of Experiments in Fluid Mechanics*, vol. 25, no. 3, pp. 60–65, 2011.
- [2] L. C. Lynnworth, "Ultrasonic flow meters," *Physical Acoustics: Principles and Methods*, vol. 14, pp. 407–525, 1979.
- [3] D. W. Spitzer, Flow Measurement: Practical Guides for Measurement and Control, Instrument society of Amer, 1993.
- [4] D. Z. Huo, "Large flow-rate measurement and multichords ultrasonic flowmeter," in *Proceedings of the Flow-Rate Measurement Conference*, pp. 158–166, Zhengzhou, China, 2006.
- [5] J. G. Drenthen and G. De Boer, "The manufacturing of ultrasonic gas flow meters," *Flow Measurement and Instrumentation*, vol. 12, no. 2, pp. 89–99, 2001.
- [6] L. Zhang, T. Meng, C. Wang, H. M. Hu, and C. L. Qin, "Probe installation effects on the accuracy of feed thru ultrasonic flowmeters," *Chinese Journal of Scientific Instrument*, vol. 33, no. 10, pp. 2307–2314, 2012.
- [7] C. Ruppel and F. Peters, "Effects of upstream installations on the reading of an ultrasonic flowmeter," *Flow Measurement and Instrumentation*, vol. 15, no. 3, pp. 167–177, 2004.
- [8] M. L. Sanderson and H. Yeung, "Guidelines for the use of ultrasonic non-invasive metering techniques," *Flow Measurement and Instrumentation*, vol. 13, no. 4, pp. 125–142, 2002.
- [9] Y. Hu, T. Zhang, and D. D. Zheng, "Estimation on influence of probe protrusion length of ultrasonic flowmeter on measurement," *Journal of Tianjin University*, vol. 46, no. 9, pp. 776–783, 2013.
- [10] The American Society of Mechanical Engineer, ASME PTC18-2011 Hydraulic Turbines and Pump Turbines Performance Test Codes, The American Society of Mechanical Engineer, 2011.
- [11] R. Raišutis, "Investigation of the flow velocity profile in a metering section of an invasive ultrasonic flowmeter," Flow Measurement and Instrumentation, vol. 17, no. 4, pp. 201–206, 2006.
- [12] D. Zheng, P. Zhang, and T. Xu, "Effect of installation position of ultrasonic flowmeter probe on flow measurement," *Journal of Mechanical Engineering*, vol. 47, no. 12, pp. 13–18, 2011.
- [13] L. Y. Zhong and L. Chang, "Modeling and simulating of multi path ultrasonic gas flowmeters," *Journal of Huazhong University of Science and Technology*, vol. 34, no. 4, 2006.

- [14] S. He, L. Peng, and H. Nakazato, "Computational fluid dynamics based sound path optimization for ultrasonic flow meter," *Chinese Journal of Scientific Instrument*, vol. 30, no. 4, pp. 852– 856, 2009.
- [15] X. Wang and Z. Tang, "Model simulation and error quantitative analysis of pipeline of ultrasonic gas flowmeter," *Chinese Journal* of Scientific Instrument, vol. 30, no. 12, pp. 2612–2618, 2009.
- [16] L. S. Bao, J. D. Liang, and J. Lu, "Mathematic model of multipath ultrasonic gas flowmeter," *Technical Acoustics*, vol. 29, no. 4, pp. 392–395, 2010.
- [17] Y. Li and C. Li, "Modeling and simulating of multi-path ultrasonic gas flowmeters," *Journal of Huazhong University of Science and Technology*, vol. 34, no. 4, pp. 852–856, 2006.
- [18] J. T. Liang, J. Lu, and S. M. Zhu, "Principles and calibrations of the multipath ultrasonic gas flowmeter," *Chinese Journal of Scientific Instrument*, vol. 22, no. 3, 2001.
- [19] Y. L. Chen, C. M. Liu, C. Y. Chiang, S. M. Yuan, and J. H. Wang, "Building Communication Software: a project-based approach for teaching C⁺⁺ object-oriented Programming," *International Journal of Innovative Computing, Information and Control*, vol. 9, no. 8, pp. 3415–3436, 2013.
- [20] K. Shirai, Y. Amano, and S. Omatu, "Process throughput analysis for manufacturing process under incomplete information based on physical approach," *International Journal of Innovative Computing, Information and Control*, vol. 9, no. 11, pp. 4431– 4445, 2013.

Hindawi Publishing Corporation Abstract and Applied Analysis Volume 2014, Article ID 369349, 8 pages http://dx.doi.org/10.1155/2014/369349

Research Article

Robust Adaptive Reactive Power Control for Doubly Fed Induction Generator

Huabin Wen,¹ Yu Zeng,² Lei Wang,³ Feng Yang,⁴ and Y. D. Song³

- ¹ School of Electrical Engineering, Beijing Jiaotong University, Beijing 100044, China
- ² School of Energy Science and Engineering, UESTC, Chengdu 611731, China
- ³ School of Automation, Chongqing University, Chongqing 400044, China

Correspondence should be addressed to Y. D. Song; ydsong@cqu.edu.cn

Received 3 February 2014; Accepted 19 March 2014; Published 20 May 2014

Academic Editor: Peng Shi

Copyright © 2014 Huabin Wen et al. This is an open access article distributed under the Creative Commons Attribution License, which permits unrestricted use, distribution, and reproduction in any medium, provided the original work is properly cited.

The problem of reactive power control for mains-side inverter (MSI) in doubly fed induction generator (DFIG) is studied in this paper. To accommodate the modelling nonlinearities and inherent uncertainties, a novel robust adaptive control algorithm for MSI is proposed by utilizing Lyapunov theory that ensures asymptotic stability of the system under unpredictable external disturbances and significant parametric uncertainties. The distinguishing benefit of the aforementioned scheme consists in its capabilities to maintain satisfactory performance under varying operation conditions without the need for manually redesigning or reprogramming the control gains in contrast to the commonly used PI/PID control. Simulations are also built to confirm the correctness and benefits of the control scheme.

1. Introduction

Doubly fed induction generator (DFIG) enjoys more noticeable advantages compared with other kinds of wind generators [1]. For example, by keeping the rotor current frequency at a constant level, DFIG can produce nearly constant power from the stator, and by keeping an optimal tip-speed ratio, DFIG is able to capture the maximum wind power at different wind speeds [2]. A wind power generation system equipped with DFIG requires a converter with only one-third of the power rating, leading to a less expensive system with reduced power loss [3]. DFIG can also control reactive power separately from active power with a reasonable adoption of orientation frame [4]. Especially, DFIG can stabilize the power network voltage by providing some controllable reactive power, thus improving power factor or voltage characteristics [5].

Researches on the blackout in Canada and America in 2003 indicated that if reactive power was provided in time the cascaded outages of several power system devices might have been avoided. Reactive power is closely related

to voltage level and power factor (pf) and terminal voltage. To prevent power network instability problem, some power companies have proposed several standards which must be strictly met when the wind generators connect to the system [6]. Therefore, reactive power control in DFIG for wind turbines has become a research topic of theoretical and practical importance that has attracted considerable attention during the past decade, leading to a number of technical results on reactive power control of DFIG in wind turbines. Brekken and Mohan [7] deal with the harmonic component on the frame with a low bandwidth filter. A PI and a state space based controller for reactive power are studied by Machmoum et al. [8]. The limitation of generation capability on both converters of DFIG is analysed in Engelhardt et al. [9]. Slootweg et al. [10] study the voltage control scheme by reactive power compensation on the RSI, without considering reactive power generation ability of grid-side inverter (MSI). In Tapia et al. [11] a similar problem is investigated in which MSI contribution to voltage control is ignored. It should be noted that MSI can be the main reactive compensator as a STATCOM as shown in Kayikci and Milanovic [12].

⁴ School of Automation Engineering, UESTC, Chengdu 611731, China

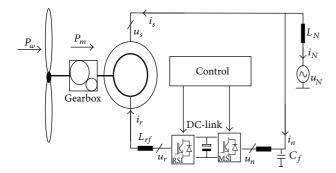


FIGURE 1: DFIG drive topology.

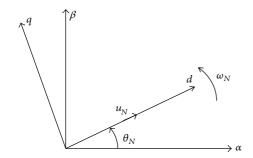


FIGURE 2: Voltage orientation.

An interesting effort has been made on using both the RSI and the MSI to design reactive power regulator in DFIG [13]. There are several other coordinated RSI and MSI based voltage-control methods suggested in the literature (see, e.g., Akhmatov [14] and Ackermann [15] and the references cited therein).

While reactive power control of DFIG has been extensively studied during the past few years, there are some open issues which have practical and theoretical importance in this area. For instance, from a reliable operation and realtime implementation point of view, currently there is no uniform framework for the design of a cost-effective and reliable method for reactive power adjustment. As a matter of fact, in most existing works, either the control development and closed-loop system stability conditions are based on largely oversimplified linear dynamics or the resultant control algorithms are prohibitively too complex for real-time implementation. One reason leading to such barrier is the fact that differential equations of DFIG are nonlinear and complex in nature. To facilitate control design, most existing methods have carried on the tradition of using linear model, without fully recognizing modelling uncertainty, external disturbance, or implementation cost. As such, these control methods which heavily depend on linear model and precise system parameters seldom satisfactorily work in practice. It is interesting to notice that different applications of adaptive control method have been studied in various fields, such as in power systems [16, 17] and in robot controlling [18]. Adaptive control method can help to solve the above problems.

This paper proposes a computationally inexpensive control algorithm for controlling reactive power in DFIG for wind turbines. The main interest in the mentioned method is primarily motivated by some practical implementation situations, where algorithm cost-effectiveness appears to be the prior concern. Meanwhile, there exist the possibilities that the system parameters and dynamics are not always fully available for the sake of some constraints. A dynamic model which reflects the electrical connection effects of the MSI of DIFG wind turbine system is established in this paper. Inspired by the recent work on using core information for control design [19], a simple yet effective robust adaptive control scheme is developed. The superior features of the resultant control scheme consist in the significance in dealing with unpredictable lumped disturbances and simple structure. In fact, only little information of the parameters/dynamics is necessary for the construction of the control algorithm. Meanwhile complicated and painful trail-anderror process for control gains determination is no longer needed. These friendly advantages are favourable in practical implementations.

2. System Topology and Dynamic Equations

Drive topologies of DFIG have been intensively studied in the literature [13]. Drive topology of DFIG containing the current and power flow is shown in Figure 1. Wind power captured from the wind turbine transfers into electric power through the gear box and the induction generator. The induction generator is quite special since it has a dual converter which is made of electric devices such as IGBTs. The size of the converter is determined according to the desired speed range. With a proper control for the RSI and MSI, the separate control of reactive power from active power is achieved. The DFIG employs some inductors between the rotor terminals and the RSI as filters. In order to suppress harmonics, output filters are also used in the DFIG.

- 2.1. Voltage Orientation. Considering the deep coupling nature between reactive and active power, a well-chosen orientation can help to control the two variables independently. In this paper, the coordinate system rotates synchronously along with mains voltage vector. By adopting the phase-locked loop (PLL) scheme [20], the mains voltage vector is well tracked by d-axis in the frame. Thus we obtain $u_N = u_{Nd}$ and $u_{Nq} = 0$. Based on such voltage orientation, current components on the q- and d-axis are considered, separately, as reactive component and active component. Thus the q-axis current component is responsible for controlling the reactive power production which will be used in later discussion. This implication is illustrated in Figure 2, and ω_N is the angular speed of u_N .
- 2.2. Generator Model. In this work, we follow the modelling methods as described in Rabelo et al. [13]. The stator voltage frequency is the same as the net frequency; that is, $\omega_N = \omega_S$, and the slip frequency is determined by $\omega_r = S\omega_N$. u_s and

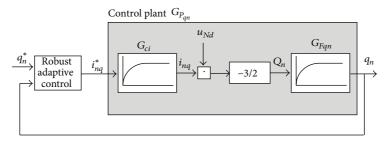


FIGURE 3: Block diagram of the system.

 u_r are obtained by using the synchronous rotating frame for induction generator in Leonhard [2]. Consider

$$u'_{r} = R'_{r}i'_{r} + \frac{d\psi_{r}}{dt} + jSw_{N}\psi_{r},$$

$$u_{s} = R_{s}i_{s} + \frac{d\psi_{s}}{dt} + jw_{N}\psi_{s}.$$
(1)

Flux linkage of the rotor ψ_r and flux linkage of the stator ψ_s are calculated as

$$\psi_r = L_r' i_r' + L_m i_s, \qquad \psi_s = L_s i_s + L_m i_r'.$$
 (2)

Electromagnetic torque of the drive system is established by

$$T_e = \frac{3}{2} n \frac{L_m}{L_s} \cdot \mathfrak{F} \left\{ \psi_s i_r^{\prime *} \right\},\tag{3}$$

where "*" denotes the conjugate complex value and $\mathfrak{F}\{\cdot\}$ denotes the imaginary part and n represents pole pairs.

The current components on the stator side with orthogonal coordinate are written as

$$i_{sd} = -\frac{L_m}{L_s} i_{rd},$$

$$i_{sq} = \frac{\psi_{sq}}{L_s} - \frac{L_m}{L_s} i_{rq},$$
(4)

where i_{sd} is the stator current component on the d-axis and i_{sq} is the stator current component on the q-axis.

Using the flux linkage equations above and replacing the stator current component, the following equations can be obtained:

$$u_{rq} = R_r i_{rq} + \sigma L_r \frac{di_{rq}}{dt} - Sw_N \sigma L_r i_{rq},$$

$$u_{rd} = R_r i_{rd} + \sigma L_r \frac{di_{rd}}{dt} + Sw_N \sigma L_r i_{rq} + Sw_N \frac{L_m}{L_s} \psi_{sq},$$
(5)

where $\sigma = 1 - (Lm^2/L_sL_r)$. The basic electrical formulas above will be used to construct the inner rotor current controller.

2.3. LC Filter Model. Considering the inverter synchronized with the mains voltage and ignoring the voltage drop on the L_N , the MSI output current dynamics can be described as follows:

$$u_{Nq} = R_f i_{nq} + L_f \frac{di_{nq}}{dt} - w_N L_f i_{nd} + u_{nq} = 0,$$
 (6)

$$u_{Nd} = R_f i_{nd} + L_f \frac{di_{nd}}{dt} - w_N L_f i_{nq} + u_{nd}.$$
 (7)

The block diagram in Figure 1, together with the above equations, indicated the mutual and internal relationship in the drive topology of DFIG and the wind power generation system.

3. Reactive Power Control Design

Considering the external disturbance acting on the system, reactive power at the MSI is governed by the dynamic equation as given in (8): that is,

$$\ddot{q}_n T_1 T_2 + \dot{q}_n (T_1 + T_2) + q_n + h(\cdot) = K_{an} i_{na}^*, \tag{8}$$

which can be shown in detail as follows.

3.1. Current Inner Loop Control. This is a cross-coupled 2D problem. The transfer function of the plant $G_i(s)$ is described as

$$G_i(s) = \frac{K_i}{sT_i + 1},\tag{9}$$

where $K_i = 1/R$ and $T_i = L/R$. The transfer functions are identical on both d and q axes. The time delay of signal preconditioning and processing can be regarded as a small time constant $T_{\rm sum} \ll T_i$. Note that $T_{\rm sum}$ is small and its accurate value is normally difficult to obtain. The first-order transfer function of such time constant part is described as

$$G_{\text{sum}}(s) = \frac{1}{sT_{\text{sum}} + 1}.$$
 (10)

By utilizing of a simple controller G_{Ri} , the following open-loop transfer function is established:

$$G_{oi}(s) = G_{Ri}G_{i}G_{sum} = K_{Pi}\frac{sT_{Ii}+1}{sT_{Ii}}\frac{K_{i}}{sT_{i}+1}\frac{1}{sT_{sum}+1},$$
 (11)

where K_{Pi} is the differential parameter and T_{Ii} is the integrated time.

3.2. Output Current Control. Output current control should track the input current without heavy overshoots. A general method to solve such problems is proposed in Föllinger [21]. To achieve a well damping factor $1/\sqrt{2}$, we can set K_{Pi} and T_{Ii} as follows:

$$K_{Pi} = \frac{L}{2T_{\text{sum}}}, \qquad T_{Ii} = T_i. \tag{12}$$

The closed-loop transfer function becomes

$$G_{ci}(s) = \frac{G_{oi}}{1 + G_{oi}} = \frac{1}{2T_{\text{sum}}^2 s^2 + 2T_{\text{sum}} s + 1}.$$
 (13)

Since $T_{\text{sum}} \ll T_i$, the square value in the s^2 term can be ignored. Thus, the closed-loop function of the current inner control is simplified and obtained as

$$G_{ci}(s) \cong \frac{1}{2T_{\text{sum}}s + 1}.$$
 (14)

At the mains-side inverter and under the voltage orientation discussed above, the reactive power is established by

$$Q_n = \frac{3}{2} \Im \left\{ u_n i_n^* \right\} = \frac{3}{2} \left(u_{Nq} i_{nd} - u_{Nd} i_{nq} \right) = -\frac{3}{2} u_{Nd} i_{nq}. \quad (15)$$

Before passing into the controller, the data of the input reactive power pass through a filter. The filter is given by a one-order transfer function as described in Rabelo et al. [13]. Consider

$$G_{F_{qn}} = \frac{q_n}{Q_n} = \frac{1}{\left(sT_{F_{qn}} + 1\right)},$$
 (16)

where q_n is the ultimate actual reactive power through the filter and $T_{F_{om}}$ is the filter time constant.

We take the current inner control in (13) into account. Thus the control plant becomes the following second-order transfer function:

$$G_{P_{qn}} = K_{qn}G_{ci}G_{F_{qn}} = \frac{K_{qn}}{\left(s2T_{sum} + 1\right)\left(sT_{F_{sm}} + 1\right)},$$
 (17)

where

$$K_{qn} = -\left(\frac{3}{2}\right)u_{Nd}.\tag{18}$$

The block diagram of the system adopting robust adaptive control methods is shown in Figure 3. The primary objective is to build the reference current i_{nq}^* which makes the actual reactive power q_n regulate the reference one q_n^* asymptotically.

We rewrite control plant equation (16) as

$$\frac{q_n}{i_{nq}^*} = \frac{K_{nq}}{\left(sT_1 + 1\right)\left(sT_2 + 1\right)},\tag{19}$$

where $T_1=2T_{\rm sum},\,T_2=T_{F_{nq}}.$ Using Laplace inverse transform, it follows that

$$\ddot{q}_n T_1 T_2 + \dot{q}_n (T_1 + T_2) + q_n = K_{an} i_{na}^*. \tag{20}$$

Taking the external disturbances acting on the system into account, (20) becomes (8) where $h(\cdot)$ is the external disturbances.

3.3. Robust Adaptive Control for Mains-Side Reactive Power. In this section, a robust adaptive control for mains-side reactive power will be proposed. To build a meaningful adaptive control scheme, two realistic assumptions are adopted.

Assumption 1. Voltage amplitude at net connecting point remains nonzero. Thus with the voltage orientation and (6), u_{Nd} can be regarded as a positive known number so that K_{qn} with respect to (18) is a negative known number.

Remark 2. Assumption 1 imposed here, rather standard in addressing system stabilization, is practical because the wind power generation system will be shut off if the voltage at the net is extremely low; thus the zero voltage does not occur for the situation under consideration.

To design the tracking controller, we define the reactive power tracking error as

$$e = q_n - q_n^*. \tag{21}$$

To simplify controller design, we introduce ε and define ε as

$$\varepsilon = \beta e + \dot{e},\tag{22}$$

where $\beta > 0$ is a designed constant.

Apparently if ε converges to zero as time increases, e and \dot{e} also converge to zero, which means if we can design a controller that forces ε to converge to zero as time increases, then problem will be solved.

Taking derivative of (22) with respect to time, we get

$$\dot{\varepsilon} = \beta \dot{e} + \ddot{e}. \tag{23}$$

Substituting \ddot{e} with (21) and using \ddot{q}_n as given in (8), we obtain

$$\dot{\varepsilon} = \frac{K_{qn}}{T_1 T_2} i_{nq}^* + \frac{1}{T_1 T_2} \left[-h(\cdot) - q_n - (T_1 + T_2) \dot{q}_n \right] + \beta \dot{e} - \ddot{q}_n^*.$$
(24)

Or equivalently,

$$\dot{\varepsilon} = Bu + L(\cdot), \tag{25}$$

where $u = -i_{nq}^*$,

$$B = -\frac{K_{qn}}{T_1 T_2},$$

$$L(\cdot) = \frac{1}{T_1 T_2} \left[-h(\cdot) - q_n - (T_1 + T_2) \dot{q}_n \right] + \beta \dot{e} - \ddot{q}_n^*.$$
(26)

Obviously B is positive because of the definition of K_{qn} as given in (18). Note that

$$L(\cdot) \le \left| \frac{1}{T_1 T_2} \right| \left[|h(\cdot)| + |q_n| + |(T_1 + T_2)| |\dot{q}_n| \right] + |\beta \dot{e}| + |\ddot{q}_n^*|.$$
(27)

Assumption 3. In this assumption, the characteristic of the disturbance is discussed. The external disturbance $h(\cdot)$ is bounded which leads to the existence of an unknown constant such that

$$|h(\cdot)| \le a_1 < \infty. \tag{28}$$

Also, the time constants T_1 and T_2 , although unknown in general, are bounded so that

$$\left|\frac{1}{T_1 T_2}\right| \le a_2 < \infty, \qquad \left|\left(T_1 + T_2\right)\right| \le a_3 < \infty, \qquad (29)$$

where a_2 and a_3 are some unknown positive constants.

This assumption, quite reasonable in practice, allows for the establishment of

$$|L(\cdot)| \le a\varphi\left(q_n\right),\tag{30}$$

where

$$a = \max(a_2 \cdot a_1, a_2, a_2 \cdot a_3, 1),$$
 (31)

$$\varphi(q_n) = 1 + |q_n| + |\dot{q}_n| + \beta |\dot{e}| + |\ddot{q}_n^*|. \tag{32}$$

We design the input as

$$u = -\left(K_0 + \widehat{K}\right)\varepsilon,\tag{33a}$$

where $K_0 > 0$ is a design constant and \widehat{K} is updated as

$$\widehat{K} = \frac{\widehat{a}\varphi}{|\varepsilon|},\tag{33b}$$

where \hat{a} is the estimation of a and is updated as

$$\dot{\hat{a}} = |\varepsilon|\,\varphi. \tag{33c}$$

Theorem 4. For such system established by (8) under the assumptions, if u is calculated by (33a), (33b), and (33c), then the reactive power is ensured to track the desired one asymptotically.

Proof. The result can be justified using the following Lyapunov function:

$$V = \frac{1}{2}\varepsilon^2 + \frac{1}{2B_{\min}} (a - \hat{a}B_{\min})^2,$$
 (34)

where B_{\min} is constant and $0 < B_{\min} \le B$ for $\forall B \in L_{\infty}$. Differentiating V leads to

$$\dot{V} = \varepsilon \dot{\varepsilon} - (a - \hat{a}B_{\min})\,\dot{\hat{a}}.\tag{35}$$

From (25) and (33a), we get

$$\dot{\varepsilon} = -BK_0\varepsilon - B\widehat{K}\varepsilon + L. \tag{36}$$

Equation (35) becomes

$$\dot{V} = \varepsilon \left(-BK_0 \varepsilon - B\widehat{K}\varepsilon + L \right) - \left(a - \widehat{a}B_{\min} \right) \dot{\widehat{a}}. \tag{37}$$

Substituting \widehat{K} with (33b) and $\dot{\widehat{a}}$ with (33c),

$$\dot{V} = \varepsilon L - BK_0 \varepsilon^2 - B\hat{a}\varphi |\varepsilon| - \varphi |\varepsilon| (a - \hat{a}B_{\min})$$

$$\leq |\varepsilon| |L| - BK_0 \varepsilon^2 - B\hat{a}\varphi |\varepsilon| - \varphi |\varepsilon| (a - \hat{a}B_{\min})$$

$$= -BK_0 \varepsilon^2 + (|\varepsilon| |L| - |\varepsilon| \varphi a) + (B_{\min} \hat{a}\varphi |\varepsilon| - B\hat{a}\varphi |\varepsilon|).$$
(38)

Because we have

$$|L(\cdot)| \le a\varphi, \qquad 0 < B_{\min} \le B,$$
 (39)

we can get

$$\dot{V} \le -B_{\min} K_0 \varepsilon^2 < 0. \tag{40}$$

As $B_{\min} > 0$, it is readily shown from (40) that both ε and \widehat{a} are bounded. Furthermore, we can show that $\dot{\varepsilon}$ is bounded and thus ε is uniformly continuous. Therefore, using Barbalat Lemma [22] the reality is obtained that ε converges to zero asymptotically. By utilizing (22), ultimately, e and \dot{e} converge to zero asymptotically; then the result is established.

Remark 5. It should be noted that when the states get closer to zero, the control scheme might experience chattering. This, however, can be avoided by using the simple but classic means of replacing z/|z| with $z/(|z| + \tau)$, where τ is small. Meanwhile, in order to prevent the estimate \hat{a} from drifting, (33c) can be modified to

$$\dot{\hat{a}} = -\sigma_1 \hat{a} + \sigma_2 \frac{\varepsilon^2 \varphi^2}{|\varepsilon| \, \varphi + \tau}, \quad \sigma_1 > 0, \ \sigma_2 > 0.$$
 (41a)

In this case, we have the following ultimately uniformly bounded (UUB) tracking control result.

Theorem 6. Also for system established by (8) under the assumptions, if the following robust adaptive control algorithm is adopted,

$$u = -\left(K_0 + \widehat{K}\right)\varepsilon,\tag{41b}$$

where $K_0 > 0$ is a design constant and \widehat{K} is updated as

$$\widehat{K} = \frac{\widehat{a}\varphi}{|\varepsilon| + \tau},\tag{41c}$$

where \hat{a} is the estimation of a and is updated by (33a), then the system is ensured to be UUB stable.

Proof. This theorem can be proved by utilizing of the methods in Cai et al. [23].

Remark 7. Instead of using PI controller as in Rabelo et al. [13], a simple robust adaptive control scheme is developed here in which one only needs to specify the parameters in a clear direction; that is, $K_0 > 0$ and $\beta > 0$.

Remark 8. The significance of the developed control scheme is twofold.

- (1) The control scheme developed here does not rely on the precise value for the time constants T_1 , T_2 . Also, there is no need for analytical estimation of the unknown parameters a_1, a_2, a_3 . Such fact can sufficiently simplify the design procedure and implementation of the proposed control algorithm.
- (2) As the parameter \hat{a} involved in the controller is updated automatically via the algorithm, and such process is independent of operation conditions, no redesign or reprogramming is needed during the system operation.

4. Simulation Verification

Aiming at validating the correctness of the robust adaptive reactive control scheme, simulations with Matlab/Simulink are presented here.

Per unit (p.u.) value is introduced to simplify calculation and simulation. The datum voltage V_{av} and datum capacity S_{av} , respectively, are set as 330 V and 1 MVar. The net voltage u_{Nd} under voltage orientation is chosen as 220 V and thus K_{qn} with respect to (17) is calculated as –1. Other parameters used for simulation are chosen as $T_{\rm sum}=0.5$, $T_{F_{qn}}=1$, $\beta=1$, and $K_0=1$. The PI control algorithm described in Ackermann [15] for reactive power is rebuilt for comparison. Three types of working conditions are simulated here.

4.1. Regulating under Steady Working Condition. In real application, DFIG can work as a compensator to provide constant reactive power. Based on this fact, we set the desired reactive power output as 1 p.u. The desired reactive power and actual one are together plotted in Figure 4.

Compared with the adopted PI scheme, adaptive method eliminates overshoot and has a shorter regulate time and a longer rise time. Both of the control schemes can obtain stabilization.

4.2. Regulating under Modelling Uncertainty. In this kind of simulation, the influence of modelling uncertainty is investigated. Assume that the time constant $T_{\rm sum}$ has a deviation of 5%; then $T_{\rm sum}=0.525$. The result of the proposed adaptive method is illustrated in Figure 5 and the PI method is shown in Figure 6.

The result shows that, by utilizing the proposed scheme, the tracking trajectory almost remains the same even under such modelling uncertainty and parameter deviation. From the point of detail, the proposed adaptive scheme enjoys a better tracking trajectory compared with the PI controller under such condition.

4.3. Tracking under Dynamic Reactive Power Compensation. If the voltage begins to drop during an unsymmetrical grid fault, the DFIG will work as a dynamic reactive compensator to keep the voltage to a certain degree. Once the fault is moved, the reactive power generating capacity of DFIG will be resumed [24]. Based on this fact, we set the desired reactive power output as illustrated in Figure 7. Specifically, the DFIG is ordered to provide 1 p.u. before 7 s and provide an extra

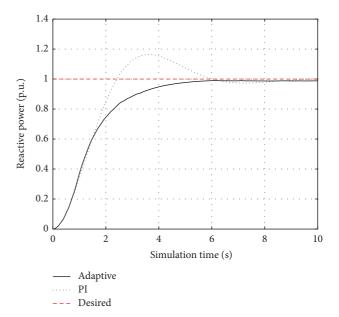


FIGURE 4: Reactive power regulation trajectories.

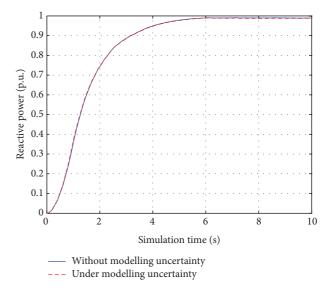


FIGURE 5: Adaptive controller tracking trajectories.

0.2 p.u. reactive power in the time from 7 s to 8 s, because the proposed scheme uses the derivative of the desired input. The reference has been smoothed before putting into the controller

The result of PI controller is also compared to the proposed adaptive method. Figure 7 illustrates that, compared with PI controller, the proposed method can track the desired reactive power better. This is because PI controller fails to track the reference value at the time of 7 s. The result shows that the adopted PI controller fails to deal with such problem which, however, the adaptive scheme proposed in this paper can deal with.

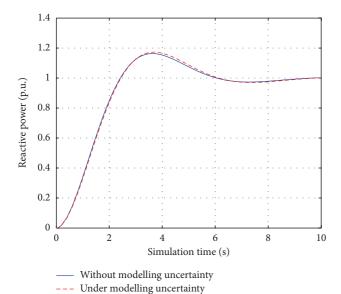


FIGURE 6: PI controller tracking trajectories.

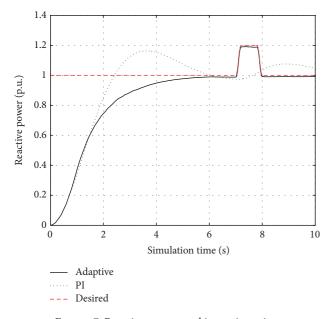


FIGURE 7: Reactive power tracking trajectories.

5. Conclusions

Reactive power control for mains-side inverter (MSI) in DFIG represents an important issue in wind power generation systems. A robust adaptive control scheme for MSI is developed. As confirmed by theoretical analysis the proposed method is able to maintain satisfactory performance under varying operation conditions without the need for manually redesigning or reprogramming the control gains. Numerical simulations also validate the correctness and benefits of the proposed algorithm.

Conflict of Interests

The authors declare that there is no conflict of interests regarding the publication of this paper.

Acknowledgments

This work was supported in part by the National Basic Research Program of China (973 Program no. 2012CB215200) and in part by the National Natural Science Foundation of China (no. 51205046).

References

- [1] Y. She, X. She, and M. E. Baran, "Universal tracking control of wind conversion system for purpose of maximum power acquisition under hierarchical control structure," *IEEE Transactions on Energy Conversion*, vol. 26, no. 3, pp. 766–775, 2011.
- [2] W. Leonhard, Control of Electrical Drives, Springer, 2000.
- [3] Rabelo and B. Hofmann W, "Power flow optimisation and grid integration of wind turbines with the Doubly-Fed induction generator," in *Proceedings of the 36th International Conference* on *Power Electronics Specialists Conference*, pp. 2930–2936, Recife, Brazil, June 2005.
- [4] R. Pena, J. C. Clare, and G. M. Asher, "Doubly fed induction generator using back-to-back PWM converters and its application to variable-speed wind-energy generation," *IEE Proceedings: Electric Power Applications*, vol. 143, no. 3, pp. 231–241, 1996.
- [5] M. El Moursi, G. Joos, and C. Abbey, "A secondary voltage control strategy for transmission level interconnection of wind generation," *IEEE Transactions on Power Electronics*, vol. 23, no. 3, pp. 1178–1190, 2008.
- [6] E. O. N. Netz, "Grid code high and extra high voltage," 2006.
- [7] T. K. A. Brekken and N. Mohan, "Control of a doubly fed induction wind generator under unbalanced grid voltage conditions," IEEE Transactions on Energy Conversion, vol. 22, no. 1, pp. 129–135, 2007.
- [8] M. Machmoum, F. Poitiers, C. Darengosse, and A. Queric, "Dynamic performances of a doubly-fed induction machine for a variable-speed wind energy generation," in *Proceedings of the International Conference on Power System Technology*, pp. 2431– 2436, October 2002.
- [9] S. Engelhardt, I. Erlich, C. Feltes, J. Kretschmann, and F. Shewarega, "Reactive power capability of wind turbines based on doubly fed induction generators," *IEEE Transactions on Energy Conversion*, vol. 26, no. 1, pp. 364–372, 2011.
- [10] J. G. Slootweg, S. W. H. de Haan, H. Polinder, and W. L. Kling, "Voltage control methods with grid connected wind turbines: a tutorial review," *Wind Engineering*, vol. 25, no. 6, pp. 353–366, 2001.
- [11] A. Tapia, G. Tapia, J. Xabier Ostolaza, and J. R. Sáenz, "Modeling and control of a wind turbine driven doubly fed induction generator," *IEEE Transactions on Energy Conversion*, vol. 18, no. 2, pp. 194–204, 2003.
- [12] M. Kayikci and J. V. Milanovic, "Reactive power control strategies for DFIG-based plants," *IEEE Transactions on Energy Conversion*, vol. 22, no. 2, pp. 389–396, 2007.
- [13] B. C. Rabelo Jr., W. Hofmann, J. L. da Silva, R. G. de Oliveira, and S. R. Silva, "Reactive power control design in doubly fed

- induction generators for wind turbines," *IEEE Transactions on Industrial Electronics*, vol. 56, no. 10, pp. 4154–4162, 2009.
- [14] V. Akhmatov, Analysis of Dynamic Behaviour of Electric Power Systems with Large Amount of Wind Power, Electric Power Engineering, Ørsted-DTU, Technical University of Denmark, 2003.
- [15] T. Ackermann, Ed., Wind Power in Power Systems, John Wiley and Sons, New York, NY, USA, 2005.
- [16] Y. Song, X. Li, and W. Cai, "Adaptive and fault-tolerant reactive power compensation in power systems," *International Journal* of *Innovative Computing, Information and Control*, vol. 9, no. 8, pp. 3403–3413, 2013.
- [17] D. Niu and Y. Wei, "A novel social-environmental-economic dispatch model for thermal/wind power generation and application," *International Journal of Innovative Computing, Information and Control*, vol. 9, no. 7, pp. 3005–3014, 2013.
- [18] Y. Chen, G. Mei, G. Ma, S. Lin, and J. Gao, "Robust adaptive inverse dynamics control for uncertain robot manipulator," *International Journal of Innovative Computing, Information and Control*, vol. 10, no. 2, pp. 575–587, 2014.
- [19] Y.-D. Song, H.-N. Chen, and D.-Y. Li, "Virtual-point-based fault-tolerant lateral and longitudinal control of 4W-steering vehicles," *IEEE Transactions on Intelligent Transportation Systems*, vol. 12, no. 4, pp. 1343–1351, 2011.
- [20] V. Kaura and V. Blasko, "Operation of a phase locked loop system under distorted utility conditions," *IEEE Transactions on Industry Applications*, vol. 33, no. 1, pp. 58–63, 1997.
- [21] O. Föllinger, Regelungstechnik, Springer, 8th edition, 1999.
- [22] J. J. Slotine and W. Lei, Applied Nonlinear Control, Prentice-Hall, 1991
- [23] W. Cai, X. H. Liao, and Y. D. Song, "Indirect robust adaptive fault-tolerant control for attitude tracking of spacecraft," *Journal* of Guidance, Control, and Dynamics, vol. 31, no. 5, pp. 1456–1463, 2008.
- [24] S. Seman, J. Niiranen, and A. Arkkio, "Ride-through analysis of doubly fed induction wind-power generator under unsymmetrical network disturbance," *IEEE Transactions on Power Systems*, vol. 21, no. 4, pp. 1782–1789, 2006.

Hindawi Publishing Corporation Abstract and Applied Analysis Volume 2014, Article ID 452124, 8 pages http://dx.doi.org/10.1155/2014/452124

Research Article

Stochastic Maximum Principle for Partial Information Optimal Control Problem of Forward-Backward Systems Involving Classical and Impulse Controls

Yan Wang, 1 Aimin Song, 1 and Enmin Feng2

¹ School of Science, Dalian Jiaotong University, Dalian 116028, China

Correspondence should be addressed to Yan Wang; wymath@163.com

Received 1 January 2014; Revised 28 March 2014; Accepted 29 March 2014; Published 15 April 2014

Academic Editor: Xiaojie Su

Copyright © 2014 Yan Wang et al. This is an open access article distributed under the Creative Commons Attribution License, which permits unrestricted use, distribution, and reproduction in any medium, provided the original work is properly cited.

We study the partial information classical and impulse controls problem of forward-backward systems driven by Lévy processes, where the control variable consists of two components: the classical stochastic control and the impulse control; the information available to the controller is possibly less than the full information, that is, partial information. We derive a maximum principle to give the sufficient and necessary optimality conditions for the local critical points of the classical and impulse controls problem. As an application, we apply the maximum principle to a portfolio optimization problem with piecewise consumption processes and give its explicit solutions.

1. Introduction

The classical and impulse controls problems have received considerable attention in recent years due to their wide applicability in different areas, such as optimal control of the exchange rate between different currencies (see, e.g., [1–3]), optimal financing and dividend control problem of an insurance company facing fixed and proportional transaction costs (see, e.g., [4, 5]), stochastic differential game (see, e.g., [6]), and dynamic output feedback controller design problem (see, e.g., [7] and the references therein).

In the existing literatures, the dynamic programming principle and the maximum principle are two main approaches in solving these problems.

In dynamic programming principle, the classical and impulse controls can be solved by a verification theorem and the value function is a solution to some quasi-variational inequalities. However, the dynamic programming approach relies on the assumption that the controlled system is Markovian; see, for example, [8–10].

There have been some pioneering works on deriving maximum principles for the classical and impulse controls

problems. For example, Wu and Zhang [11] established maximum principle for stochastic recursive optimal control problems involving impulse controls; Wu and Zhang [12] gave maximum principle for classical and impulse controls of forward-backward systems. In their control problems, the information available to the controller is full information.

In many practical systems, the controller only gets partial information, instead of full information, such as delayed information (see, e.g., [13–16]). The partial information stochastic control problem is not of a Markovian type and hence cannot be solved by dynamic programming. As a result, maximum principles are established to solve the partial information stochastic control problem. There is already a rich literature and versions of corresponding maximum principles for partial information control problems. For example, Baghery and Øksendal [17] derived the maximum principle for partial information stochastic control problem, where the stochastic system is described by stochastic differential equations (SDE hereafter). An and Øksendal [18] gave a maximum principle for the stochastic differential game under partial information. Øksendal and Sulèm [19] established maximum

² School of Mathematical Sciences, Dalian University of Technology, Dalian 116023, China

principles for stochastic control of forward-backward systems driven by Lévy processes. In their control problems, the control variable is just the classical stochastic control process $u(\cdot)$. To the best of our knowledge, there is no literature on studying the maximum principle for partial information classical and impulse controls problems, which motivates our work.

In this paper, we study classical and impulse controls problems of forward-backward systems, where the stochastic systems are represented by forward-backward SDEs driven by Lévy processes, the control variable consists of two components: the stochastic control $u(\cdot)$ and the impulse control $\xi(\cdot)$, and the information available to the controller is possibly partial information, rather than full information. Because of the non-Markovian nature of the partial information, we cannot use dynamic programming principle to solve the problems. Instead, we derive a maximum principle which allows us to handle the partial information case.

The similar maximum principle is also studied by Wu and Zhang [11] in the complete information case and with the Brownian motion setting. There are three main differences between our paper and [11]. Firstly, we study the more general cases: the forward-backward system is driven by Lévy processes and the information available to the controller is partial information. Secondly, their proof differs from ours. They used convex perturbation technique to establish the maximum principle. Thirdly, they assumed the concavity conditions of Hamiltonian and utility functional to make the necessary optimality conditions turn out to be sufficient. However, the concavity conditions may not hold in many applications. Consequently, in our maximum principle formulation, we give the sufficient and necessary optimality conditions for the local critical points, instead of global optimums, without the assumption of concavity condition.

The paper is organized as follows: in the next section we formulate the partial information classical and impulse controls of the forward-backward system driven by Lévy processes. In Section 3 we derive the stochastic maximum principle for the considered classical and impulse controls problem. In Section 4 we apply the general results obtained in Section 3 to give the solutions of the example. Finally we conclude this paper in Section 5.

2. Problem Formulation

Let $(\Omega, \mathcal{F}, \{\mathcal{F}_t\}_{t\geq 0}, P)$ be a filtered probability space and let $\eta(\cdot)$ be a Lévy process defined on it. Let B(t) be an \mathcal{F}_t -Brownian motion and let $\widetilde{N}(dt,dz) = N(dt,dz) - \nu(dz)dt$ be compensated Poisson random measures independent of B(t), where ν is the Lévy measure of Lévy process $\eta(t)$ with jump measure N such that $E[\eta_i^2(t)] < \infty$ for all $t, t \in [0,\infty)$. $\{\mathcal{F}_t\}_{t\geq 0}$ is the filtration generated by B(t) and $\widetilde{N}(dt,dz)$ (as usual augmented with all the P-null sets). We refer to [8] for more information about Lévy processes.

Suppose that we are given a subfiltration $\mathcal{G}_t \subseteq \mathcal{F}_t$ representing the information available to the controller at time $t, t \in [0, T]$. It is remarked that the partial information of classical and impulse controls is different from the classical

and impulse controls of delay systems, where the state function is described by the solution of stochastic differential delay equation (see, e.g., [20]).

Let $\{\tau_i, i \geq 1\}$ be a given sequence of increasing \mathcal{G}_t -stopping times such that $\tau_i \uparrow +\infty$. At τ_i we are free to intervene and give the system an impulse $\xi_i \in \mathbb{R}$, where ξ_i is \mathcal{G}_{τ_i} -measurable random variable. We define impulse process $\xi(t)$ by

$$\xi(t) = \sum_{i>1} \xi_i \mathbf{1}_{[\tau_i, T]}(t), \quad t \le T.$$
 (1)

It is worth noting that the assumption $\tau_i \uparrow +\infty$ implies that at most finitely many impulses may occur on [0, T].

Now we consider the forward-backward systems involving classical and impulse controls. Given $a \in \mathbb{R}$ and $\mu \in \mathbb{R}_0$, let $b:[0,T]\times\mathbb{R}\times U\to\mathbb{R}$, $\sigma:[0,T]\times\mathbb{R}\times U\to\mathbb{R}$, $\gamma:[0,T]\times\mathbb{R}\times U\times\mathbb{R}_0\to\mathbb{R}$, $g:[0,T]\times\mathbb{R}\times\mathbb{R}\times\mathbb{R}\times\mathbb{R}\times U\to\mathbb{R}$, $f:[0,T]\times\mathbb{R}\times U\to\mathbb{R}$, $f:[0,T]\times\mathbb{R}\times\mathbb{R}\times\mathbb{R}\times U\to\mathbb{R}$, and $f:[0,T]\to\mathbb{R}$ be measurable mappings. $f:[0,T]\to\mathbb{R}$ is a nonempty convex set of $f:[0,T]\to\mathbb{R}$. Then the forward-backward systems are described by forward-backward SDEs in the unknown processes $f:[0,T]\to\mathbb{R}$, and $f:[0,T]\to\mathbb{R}$, and f:

$$dA(t) = b(t, A(t), u(t)) dt + \sigma(t, A(t), u(t)) dB(t)$$

$$+ \int_{\mathbb{R}_{0}} \gamma(t, A(t), u(t), z) \widetilde{N}(dt, dz) + C(t) d\xi(t),$$

$$dX(t) = -g(t, A(t), X(t), Y(t), u(t)) dt$$

$$+ Y(t) dB(t) + \int_{\mathbb{R}_{0}} K(t, z) \widetilde{N}(dt, dz)$$

$$- D(t) d\xi(t),$$

$$X(T) = \mu A(T), \quad A(0) = a.$$
(2)

The result of giving the impulse ξ_i is that the state jumps from $(A(\tau_i-), X(\tau_i-))$ to $(A(\tau_i), X(\tau_i)) = (A(\tau_i-)+C(\tau_i)\xi_i, X(\tau_i-)-D(\tau_i)\xi_i)$. We call (u, ξ) classical and impulse controls.

There are two different jumps in the system (2). One jump is the jump of $(A(\tau), X(\tau))$ stemming from the random measure N, denoted by $(\Delta_N A(\tau), \Delta_N X(\tau))$. The other jump is the jump caused by the impulse ξ , given by $(\Delta_\xi A(\tau_i), \Delta_\xi X(\tau_i)) = (C(\tau_i)\xi_i, V(\tau_i)\xi_i)$. Let

$$\mathcal{M} = \left\{ \left(\Delta_{N} A \left(\tau \right), \Delta_{N} X \left(\tau \right) \right); 0 \leq \tau \leq T \right\},$$

$$\mathcal{N} = \left\{ \left(\Delta_{\xi} A \left(\tau_{i} \right), \Delta_{\xi} X \left(\tau_{i} \right) \right); 0 \leq \tau_{i} \leq T \right\}.$$
(3)

Assumption 1. A jump $(\Delta A(t), \Delta X(t))$ at time $t, 0 \le t \le T$, satisfies

$$(\Delta A(t), \Delta X(t)) \in \mathcal{M} \cup \mathcal{N},$$

$$(\Delta A(t), \Delta X(t)) \notin \mathcal{M} \cap \mathcal{N}.$$
(4)

Let $\mathcal{U}_{\mathcal{G}}$ denote a given family of controls, contained in the set of \mathcal{G}_t -predictable controls $u(\cdot)$ such that the system (2) has a unique strong solution. We denote by \mathcal{F} the class

of processes $\xi(\cdot) = \sum_{i \geq 1} \xi_i \chi_{[\tau_i, T]}(\cdot)$ such that each ξ_i is an \mathbb{R} -valued \mathcal{G}_{τ_i} -measurable random variable. Let $\mathcal{K}_{\mathcal{G}}$ be the class of impulse process $\xi \in \mathcal{F}$ such that $E(\sum_{i \geq 1} |\xi_i|)^2 < \infty$. We call $\mathcal{A}_{\mathcal{G}} = \mathcal{U}_{\mathcal{G}} \times \mathcal{K}_{\mathcal{G}}$ the admissible control set.

Suppose we are given a performance functional of the form

$$\begin{split} \mathcal{J}\left(u,\xi\right) &= E\left[\int_{0}^{T} f\left(t,A\left(t\right),X\left(t\right),Y\left(t\right),K\left(t,\cdot\right),u\left(t\right)\right)dt \right. \\ &+ h_{1}\left(X\left(0\right)\right) + h_{2}\left(A\left(T\right)\right) + \sum_{i\geq1} l\left(\tau_{i},\xi_{i}\right)\right], \end{split}$$

where E denotes expectation with respect to P and f, h_1 , and h_2 are given functions such that

$$E\left[\int_{0}^{T}\left|f\left(t,A\left(t\right),X\left(t\right),Y\left(t\right),K\left(t,\cdot\right),u\left(t\right)\right)\right|dt\right.\right.\right.$$

$$\left.+\left|h_{1}\left(X\left(0\right)\right)\right|+\left|h_{2}\left(A\left(T\right)\right)\right|+\sum_{i\geq1}\left|l\left(\tau_{i},\xi_{i}\right)\right|\right]<\infty.$$
(6)

Then the classical and impulse controls problem is to find the value function $\Phi_{\mathscr{G}}(a) \in \mathbb{R}$ and optimal classical and impulse controls $(u^*, \xi^*) \in \mathscr{A}_{\mathscr{G}}$ such that

$$\Phi_{\mathcal{G}}(a) = \sup_{(u,\xi) \in \mathcal{A}_{\varphi}} \mathcal{J}(u,\xi) = \mathcal{J}(u^*,\xi^*). \tag{7}$$

3. Maximum Principle for Partial Information Classical and Impulse Controls Problems

In this section, we derive a maximum principle for the optimal control problems (7). We will give the necessary and sufficient conditions for the local critical points (u^*, ξ^*) .

Firstly, we make the following assumptions.

Assumption 2. (1) For all $s \in [0,T)$ and bounded \mathcal{G}_s -measurable random variables $\theta(\omega)$, the control β_s defined by

$$\beta_s(t) = \theta(\omega) \chi_{(s,T]}; \quad s \in [0,T]$$
 (8)

belongs to $\mathcal{U}_{\mathcal{G}}$.

(2) For all (u, ξ) , $(\beta, \varsigma) \in \mathscr{A}_{\mathscr{C}}$ where (β, ς) is bounded, there exists $\delta > 0$ such that the control

$$(u(t) + y\beta(t), \xi(t) + y\varsigma(t)) \in \mathcal{A}_{\mathcal{G}},$$

$$\forall y \in (-\delta, \delta), \ t \in [0, T].$$
(9)

Next we give the definition of the Hamiltonian process.

Definition 3 (see [19]). We define a Hamiltonian process

$$H: [0,T] \times \mathbb{R} \times \mathbb{R} \times \mathbb{R} \times L^{2}(\nu) \times U \times \mathbb{R} \longrightarrow \mathbb{R}$$
 (10)

as follows:

$$H(t, a, x, y, k, u, \lambda)$$

$$= f(t, a, x, y, k, u) + \lambda(t) g(t, a, x, y, u)$$

$$+ b(t, a, u) p(t) + \sigma(t, a, u) q(t)$$

$$+ \int_{\mathbb{R}_0} \gamma(t, a, u, z) r(t, z) \nu(dz),$$
(11)

where H is Fréchet differentiable in the variables a, x, y, k; $\nabla_k H$ denotes the Fréchet derivative in k of H; the adjoint processes p(t), q(t), r(t, z), and $\lambda(t)$ are given by a pair of forward-backward SDEs as follows.

(i) Forward system in the unknown process $\lambda(t)$

$$= \frac{\partial H}{\partial x} \left(t, A(t), X(t), Y(t), K(t, \cdot), \right.$$

$$u(t), \lambda(t), p(t), q(t), r(t, z) \right) dt$$

$$+ \frac{\partial H}{\partial y} \left(t, A(t), X(t), Y(t), K(t, \cdot), u(t), \right.$$

$$\lambda(t), p(t), q(t), r(t, z) \right) dB(t)$$

$$+ \int_{\mathbb{R}_0} \nabla_k H \left(t, A(t), X(t), Y(t), K(t, \cdot), u(t), \right.$$

$$\lambda(t), p(t), q(t), r(t, z) \right) \widetilde{N}(dt, dz)$$

$$\lambda(0) = h'_1(X(0)). \tag{12}$$

(ii) Backward system in the unknown processes p(t), q(t), and $r(t, \cdot)$,

$$dp(t)$$

$$= -\frac{\partial H}{\partial a} \left(t, A(t), X(t), Y(t), K(t, \cdot), u(t), \lambda(t), p(t), q(t), r(t, z) \right) dt$$

$$+ q(t) dB(t) + \int_{\mathbb{R}_0} r(t, z) \widetilde{N}(dt, dz)$$

$$p(T) = \mu \lambda(T) + h'_2(A(T)). \tag{13}$$

For the sake of simplicity, we use the short hand notation in the following:

$$\frac{\partial b}{\partial a}(t, A(t), u(t), \omega) = \frac{\partial b}{\partial a}(t),$$

$$\frac{\partial b}{\partial u}(t, A(t), u(t), \omega) = \frac{\partial b}{\partial u}(t),$$
(14)

and similarly for $(\partial \sigma/\partial a)(t)$, $(\partial \sigma/\partial u)(t)$, $(\partial \gamma/\partial a)(t)$, $(\partial \gamma/\partial u)(t)$, $(\partial f/\partial a)(t)$, $(\partial f/\partial x)(t)$, $(\partial f/\partial y)(t)$, $(\partial f/\partial u)(t)$, $\nabla_k f(t,z)$, $(\partial g/\partial a)(t)$, $(\partial g/\partial x)(t)$, $(\partial g/\partial y)(t)$, and $(\partial g/\partial u)(t)$.

Theorem 4 (maximum principle). Let $(u, \xi) \in \mathcal{A}_{\mathscr{G}}$ with corresponding solutions A(t), X(t), Y(t), K(t, z), and $\lambda(t)$ of (2), (12), and (13). Assume that for all $(u, \xi) \in \mathcal{A}_{\mathscr{G}}$ the following growth conditions hold:

$$E\left[\int_{0}^{T}X^{2}(t)\left(\left(\frac{\partial H}{\partial y}(t)\right)^{2}+\int_{\mathbb{R}_{0}}\left\|\nabla_{k}H\left(t,z\right)\right\|^{2}\nu\left(dz\right)\right)dt\right]<\infty,$$

$$E\left[\int_{0}^{T}\lambda^{2}(t)\left(Y^{2}(t)+\int_{\mathbb{R}_{0}}K^{2}(t,z)\nu\left(dz\right)\right)dt\right]<\infty,$$

$$E\left[\int_{0}^{T}A^{2}(t)\left(q^{2}(t)+\int_{\mathbb{R}_{0}}r^{2}(t,z)\nu\left(dz\right)\right)dt\right]<\infty,$$

$$E\left[\int_{0}^{T}p^{2}(t)\left(\left(\sigma^{2}(t)\right)^{2}+\int_{\mathbb{R}_{0}}\gamma^{2}(t,z)\nu\left(dz\right)\right)dt\right]<\infty.$$

$$(15)$$

Then the following are equivalent.

(1) (u, ξ) is a critical point for $\mathcal{J}(u, \xi)$, in the sense that

$$\frac{d}{dy}\mathcal{J}(u+y\beta,\xi+y\varsigma)|_{y=0}=0$$

$$\forall bounded(\beta,\varsigma)\in\mathcal{A}_{\mathcal{C}}.$$
(16)

(2) Consider

$$E\left[\frac{\partial}{\partial u}H(t,A(t),X(t),Y(t),K(t,\cdot),u,\lambda(t))_{u=u(t)}|\mathcal{G}_{t}\right]=0$$
(17)

for a.a. $(t, \omega) \in [0, T] \times \Omega$ and

$$\sum_{\tau_{i} \leq T} E\left[\left\{p\left(\tau_{i}\right) C\left(\tau_{i}\right) + \frac{\partial l}{\partial \xi}\left(\tau_{i}\right) - \lambda\left(\tau_{i}\right) D\left(\tau_{i}\right)\right\} \mid \mathscr{G}_{\tau_{i}}\right] = 0.$$
(18)

Proof. Define

$$\check{A}(t,\beta,\varsigma) = \frac{d}{dy}A(t,u+y\beta,\xi+y\varsigma)|_{y=0},$$

$$\check{X}(t,\beta,\varsigma) = \frac{d}{dy}X(t,u+y\beta,\xi+y\varsigma)|_{y=0},$$

$$\check{Y}(t,\beta,\varsigma) = \frac{d}{dy}Y(t,u+y\beta,\xi+y\varsigma)|_{y=0},$$

$$\check{K}(t,z,\beta,\varsigma) = \frac{d}{dy}K(t,z,u+y\beta,\xi+y\varsigma)|_{y=0}.$$
(19)

Then we have

$$\check{A}(0,\beta,\varsigma) = \frac{d}{dy}A(0,u+y\beta,\xi+y\varsigma)|_{y=0} = 0;$$

$$\check{A}(T,\beta,\varsigma) = \frac{d}{dy}A(T,u+y\beta,\xi+y\varsigma)|_{y=0} = \frac{1}{\mu}\check{X}(T,\beta,\varsigma);$$

$$d\check{A}(t,\beta,\varsigma) = \left[\frac{\partial b}{\partial a}(t)\check{A}(t,\beta,\varsigma) + \frac{\partial b}{\partial u}(t)\beta(t)\right]dt$$

$$+ \int_{0}^{t} \left[\frac{\partial \sigma}{\partial a}(s)\check{A}(t,\beta,\varsigma) + \frac{\partial \sigma}{\partial u}(s)\beta(s)\right]dB(s)$$

$$+ \int_{\mathbb{R}_{0}} \left[\frac{\partial \gamma}{\partial a}(t)\check{A}(t,\beta,\varsigma) + \frac{\partial \gamma}{\partial u}(t)\beta(t)\right]\widetilde{N}(dt,dz)$$

$$+ C(t)d\varsigma(t),$$

$$d\check{X}(t,\beta,\varsigma) = -\left[\frac{\partial g}{\partial a}(t)\check{A}(t,\beta,\varsigma) + \frac{\partial g}{\partial x}(t)\check{X}(t,\beta,\varsigma)\right]$$

$$+ \frac{\partial g}{\partial y}(t)\check{Y}(t,\beta,\varsigma) + \frac{\partial g}{\partial u}(t)\beta(t)\right]dt$$

$$+ \check{Y}(t,\beta,\varsigma)dB(t)$$

$$+ \int_{\mathbb{R}_{0}} \check{K}(t,z,\beta,\varsigma)\widetilde{N}(dt,dz) + D(t)d\varsigma(t).$$
(20)

Firstly, we prove $(1) \Rightarrow (2)$. Assume that (1) holds. Then we have

$$0 = \frac{d}{dy} \mathcal{J} \left(u + y\beta, \xi + y\varsigma \right) |_{y=0}$$

$$= E \left[\int_{0}^{T} \left\{ \frac{\partial f}{\partial a} \left(t \right) \check{A} \left(t, \beta, \varsigma \right) + \frac{\partial f}{\partial x} \left(t \right) \check{X} \left(t, \beta, \varsigma \right) \right. \right.$$

$$\left. + \frac{\partial f}{\partial y} \left(t \right) \check{Y} \left(t, \beta, \varsigma \right) \right.$$

$$\left. + \int_{\mathbb{R}_{0}} \nabla_{k} f \left(t, z \right) \check{K} \left(t, z, \beta, \varsigma \right) \nu \left(dz \right) \right.$$

$$\left. + \frac{\partial f}{\partial u} \left(t \right) \beta \left(t \right) \right\} dt + h'_{1} \left(X \left(0 \right) \right) \check{X} \left(0, \beta, \varsigma \right)$$

$$\left. + h'_{2} \left(A \left(T \right) \right) \check{A} \left(T, \beta, \varsigma \right) + \sum_{\tau, s'} \frac{\partial l}{\partial \eta} \left(\tau_{i} \right) \varsigma_{i} \right].$$

$$\left. - \frac{\partial f}{\partial u} \left(t \right) \check{A} \left(T, \beta, \varsigma \right) + \sum_{\tau, s'} \frac{\partial l}{\partial \eta} \left(\tau_{i} \right) \varsigma_{i} \right].$$

By Itô formula, we get

$$E\left[h'_{1}\left(X\left(0\right)\right)\check{X}\left(0,\beta,\varsigma\right)\right]$$
$$=E\left[\lambda\left(0\right)\check{X}\left(0,\beta,\varsigma\right)\right]$$

$$= E \left[\lambda \left(T \right) \check{X} \left(T, \beta, \varsigma \right) - \int_{0}^{T} \check{X} \left(t, \beta, \varsigma \right) \frac{\partial H}{\partial x} \left(t \right) dt \right.$$

$$- \int_{0}^{T} \frac{\partial H}{\partial y} \left(t \right) \check{Y} \left(t, \beta, \varsigma \right) dt$$

$$+ \int_{0}^{T} \lambda \left(t \right) \left(\frac{\partial g}{\partial a} \left(t \right) \check{A} \left(t, \beta, \varsigma \right) \right.$$

$$+ \frac{\partial g}{\partial x} \left(t \right) \check{X} \left(t, \beta, \varsigma \right) + \frac{\partial g}{\partial y} \left(t \right) \check{Y} \left(t, \beta, \varsigma \right)$$

$$+ \frac{\partial g}{\partial y} \left(t \right) \beta \left(t \right) \right) dt$$

$$- \int_{0}^{T} \int_{\mathbb{R}_{0}} \nabla_{k} H \left(t, z \right) \check{K} \left(t, z, \beta, \varsigma \right) \nu \left(dz \right) dt$$

$$- \sum_{i \ge 1} \lambda \left(\tau_{i} \right) D \left(\tau_{i} \right) \varsigma_{i} \right], \tag{22}$$

where $0 \le \tau_i \le T$. Now we consider

$$E\left[h'_{2}(A(T))\check{A}(T,\beta,\varsigma)\right]$$

$$= E\left[\left(p(T) - \mu\lambda(T)\right)\check{A}(T,\beta,\varsigma)\right]$$

$$= E\left[p(T)\check{A}(T,\beta,\varsigma)\right] - E\left[\lambda(T)\check{X}(T,\beta,\varsigma)\right].$$
(23)

Applying Itô formula to $E[p(T)\check{A}(T, \beta, \varsigma)]$, we get

$$E\left[p\left(T\right)\check{A}\left(T,\beta,\varsigma\right)\right]$$

$$=E\left[p\left(0\right)\check{A}\left(0,\beta,\varsigma\right)\right]$$

$$+\int_{0}^{T}p\left(t\right)\left(\frac{\partial b}{\partial a}\left(t\right)\check{A}\left(t,\beta,\varsigma\right)+\frac{\partial b}{\partial u}\left(t\right)\beta\left(t\right)\right)dt$$

$$+\sum_{i\geq 1}p\left(\tau_{i}\right)C\left(\tau_{i}\right)\varsigma_{i}-\int_{0}^{T}\frac{\partial H}{\partial a}\left(t\right)\check{A}\left(t,\beta,\varsigma\right)dt$$

$$+\int_{0}^{T}\left(\frac{\partial\sigma}{\partial a}\left(t\right)\check{A}\left(t,\beta,\varsigma\right)+\frac{\partial\sigma}{\partial u}\left(t\right)\beta\left(t\right)\right)q\left(t\right)dt$$

$$+\int_{0}^{T}\int_{\mathbb{R}_{0}}r\left(t,z\right)\left(\frac{\partial\gamma}{\partial a}\left(t,z\right)\check{A}\left(t,\beta,\varsigma\right)\right)$$

$$+\frac{\partial\gamma}{\partial u}\left(t,z\right)\beta\left(t\right)\right)\nu\left(dz\right)dt\right],$$
(2

where $0 \le \tau_i \le T$. By substituting (22), (23), and (24) into (21), we obtain

$$0 = E\left[\sum_{i\geq 1} \left(p\left(\tau_{i}\right) C\left(\tau_{i}\right) + \frac{\partial l}{\partial \eta}\left(\tau_{i}\right) - \lambda\left(\tau_{i}\right) D\left(\tau_{i}\right)\right) \varsigma_{i}\right] \right]$$

$$+ E\left[\int_{0}^{T} \left\{\left(\frac{\partial f}{\partial a}\left(t\right) + \lambda\left(t\right) \frac{\partial g}{\partial a}\left(t\right) + p\left(t\right) \frac{\partial b}{\partial a}\left(t\right)\right.\right.\right.\right.$$

$$+ q\left(t\right) \frac{\partial \sigma}{\partial a}\left(t\right) + \int_{\mathbb{R}_{0}} \frac{\partial \gamma}{\partial a}\left(t, z\right) r\left(t, z\right) \nu\left(dz\right)$$

$$- \frac{\partial H}{\partial a}\left(t\right)\right) \breve{A}\left(t, \beta, \varsigma\right)$$

$$+ \left(\frac{\partial f}{\partial x}\left(t\right) + \lambda\left(t\right) \frac{\partial g}{\partial x}\left(t\right) - \frac{\partial H}{\partial x}\left(t\right)\right) \breve{X}\left(t, \beta, \varsigma\right)$$

$$+ \left(\frac{\partial f}{\partial y}\left(t\right) + \lambda\left(t\right) \frac{\partial g}{\partial y}\left(t\right) - \frac{\partial H}{\partial y}\left(t\right)\right) \breve{Y}\left(t, \beta, \varsigma\right)$$

$$+ \int_{\mathbb{R}_{0}} \left(\nabla_{k} f\left(t, z\right) - \nabla_{k} H\left(t, z\right)\right) \breve{K}\left(t, z, \beta, \varsigma\right) \nu\left(dz\right)$$

$$+ \left(\frac{\partial f}{\partial u}\left(t\right) + \lambda\left(t\right) \frac{\partial g}{\partial u}\left(t\right) + p\left(t\right) \frac{\partial b}{\partial u}\left(t\right)$$

$$+ q\left(t\right) \frac{\partial \sigma}{\partial u}\left(t\right)$$

$$+ \left(\frac{\partial \sigma}{\partial u}\left(t\right) + \left(\frac{\partial \sigma}{\partial u}\left(t\right)\right) \left(\frac{\partial \sigma}{\partial u}\left(t\right)\right) \left(\frac{\partial \sigma}{\partial u}\left(t\right)\right) \left(\frac{\partial \sigma}{\partial u}\left(t\right)\right)$$

$$+ \left(\frac{\partial \sigma}{\partial u}\left(t\right)\right) \left(\frac{\partial \sigma}{\partial u}\left(t\right$$

Depending on the definition of Hamiltonian H, we get

$$\frac{\partial H}{\partial x}(t) = \frac{\partial f}{\partial x}(t) + \frac{\partial g}{\partial x}(t)\lambda(t);$$

$$\frac{\partial H}{\partial y}(t) = \frac{\partial f}{\partial y}(t) + \frac{\partial g}{\partial y}(t)\lambda(t);$$

$$\nabla_k H(t,z) = \nabla_k f(t,z);$$

$$\frac{\partial H}{\partial a}(t) = \frac{\partial f}{\partial a}(t) + \lambda(t)\frac{\partial g}{\partial a}(t) + p(t)\frac{\partial b}{\partial a}(t)$$

$$+ q(t)\frac{\partial \sigma}{\partial a}(t) + \int_{\mathbb{R}_0} \frac{\partial \gamma}{\partial a}(t,z)r(t,z)\nu(dz);$$

$$\frac{\partial H}{\partial u}(t) = \frac{\partial f}{\partial u}(t) + \lambda(t)\frac{\partial g}{\partial u}(t) + p(t)\frac{\partial b}{\partial u}(t)$$

$$+ q(t)\frac{\partial \sigma}{\partial u}(t) + \int_{\mathbb{R}_0} r(t,z)\frac{\partial \gamma}{\partial u}(t,z)\nu(dz).$$
(26)

Hence (25) simplifies to

$$0 = E\left[\sum_{i \ge 1} \left(p\left(\tau_{i}\right) C\left(\tau_{i}\right) + \frac{\partial l}{\partial \eta}\left(\tau_{i}\right) - \lambda\left(\tau_{i}\right) D\left(\tau_{i}\right)\right) \varsigma_{i}\right] + E\left[\int_{0}^{T} \frac{\partial H}{\partial u}\left(t\right) \beta\left(t\right) dt\right],$$
(27)

for all bounded $(\beta, \varsigma) \in \mathscr{A}_{\mathscr{C}}$. It is obvious that $\beta(t)$ is independent of $\varsigma(t)$, $0 \le t \le T$. So we obtain from (27) that

$$E\left[\int_0^T \frac{\partial H}{\partial u}(t) \beta(t) dt\right] = 0, \tag{28}$$

$$E\left[\sum_{i\geq 1}\left(p\left(\tau_{i}\right)C\left(\tau_{i}\right)+\frac{\partial l}{\partial \eta}\left(\tau_{i}\right)-\lambda\left(\tau_{i}\right)D\left(\tau_{i}\right)\right)\varsigma_{i}\right]=0,$$
(29)

holds for all bounded $\beta \in \mathcal{U}_{\mathcal{G}}$ and $\varsigma \in \mathcal{F}_{\mathcal{G}}$.

Now we prove that (17) holds for all $\beta(t) \in \mathcal{U}_{\mathcal{G}}$. We know that (28) holds for all bounded $\beta \in \mathcal{U}_{\mathcal{G}}$. So (28) holds for all bounded $\beta \in \mathcal{U}_{\mathcal{G}}$ of the form

$$\beta(t) = \beta_s(t, \omega) = \theta(\omega) \chi_{[s,T]}(t), \quad t \in [0, T], \quad (30)$$

for a fixed $s \in [0, T)$, where $\theta(\omega)$ is a bounded \mathcal{G}_s -measurable random variable. Then we have

$$E\left[\frac{\partial H}{\partial u}(s)\theta\right] = 0\tag{31}$$

which holds for all bounded \mathcal{G}_s -measurable random variable θ . As a result, we conclude that

$$E\left[\left.\frac{\partial H}{\partial u}\left(s\right)\right|\mathcal{G}_{s}\right]=0. \tag{32}$$

Moreover, since (29) holds for all bounded \mathcal{G}_{τ_i} -measurable random variable ς_i , we conclude that (18) holds. Therefore, we conclude that (1) \Rightarrow (2).

 $(2) \Rightarrow (1)$ Each bounded $\beta \in \mathcal{U}_G$ can be approximated by linear combinations of controls β_s of the form. Then we prove that $(2) \Rightarrow (1)$ by reversing the above argument.

Remark 5. Let $x \to h_1(x)$, $a \to h_2(a)$, $\xi \to l(t, \xi)$, and $(t, a, x, k, u) \to H(t, a, x, y, k, u, \lambda)$ be concave, for all $t \in [0, T]$. Then the local critical point (u, ξ) , which is obtained by Theorem 4, is also a global optimum for the control problem (7).

Remark 6. Let $\mathcal{G}_t = \mathcal{F}_t$, K(t,z) = 0, and $\gamma(t,a,u,z) = 0$. Then our maximum principle (Theorem 4) coincides with the maximum principle (Theorem 3.1) in [11].

4. Application

Example 7 (portfolio optimization problem). In a financial market, we are given a subfiltration

$$\mathcal{G}_t \subseteq \mathcal{F}_t \quad \forall t \in [0, T],$$
 (33)

representing the information available to the trader at time t. Let $\xi(t) = \sum_{i \geq 1} \xi_i \mathbf{1}_{[\tau_i,T]}(t), \ t \leq T$, be a piecewise consumption process (see, e.g., [11]), where $\{\tau_i\}$ is a fixed sequence of increasing \mathcal{G}_t -stopping times and each ξ_i is an \mathcal{G}_{τ_i} -measurable random variable. Then the wealth process $A(t) = A^{u,\eta}(t)$ corresponding to the portfolio u(t) is given by

$$dA(t) = u(t) \left[\zeta(t) dt + \pi(t) dB(t) + \int_{\mathbb{R}_0} \varrho(t, z) \widetilde{N}(dt, dz) \right] - \omega d\xi(t),$$
 (34)

$$A(0) = a > 0$$

where $\omega \geq 0$, $\mathbb{R}_0 = \mathbb{R} \setminus \{0\}$, and $\pi(t)$ and $\varrho(t,z)$ are \mathscr{F}_t -predictable processes such that $\varrho(t,z) \geq -1 + \epsilon$ for some $\epsilon > 0$ and

$$\int_{0}^{T} \left\{ \left| \zeta(t) \right| + \pi^{2}(t) + \int_{\mathbb{R}_{0}} \varrho^{2}(t, z) \nu(dz) \right\} dt < \infty \quad \text{a.s.}$$
(35)

Endowed with initial wealth a > 0, an investor wants to find a portfolio strategy $u(\cdot)$ and a consumption strategy $\xi(\cdot)$ minimizing an expected functional which composes of three parts: the first part is the total utility of the consumption $-\int_0^T (u^2(t)/2)dt$; the second part represents the risk of the terminal wealth $\rho(A(T)) = X_g^{-A_u(T)}(0)$, where $X_g^{-A_u(T)}(0)$ is the value at t = 0 of the solution X(t) of the following backward stochastic differential equation ([19]):

$$dX(t) = -g(t, X(t)) dt + Y(t) dB(t)$$

$$+ \int_{\mathbb{R}_0} K(t, z) \widetilde{N}(dt, dz) - \vartheta d\xi(t)$$
(36)

and the third part is the utility derived from the consumption process $\xi(\cdot)$. More precisely, for any admissible control $(u(\cdot), \xi(\cdot))$, the utility functional is defined by

X(T) = -A(T);

$$J\left(u\left(\cdot\right),\xi\left(\cdot\right)\right) = E\left[-\int_{0}^{T} \frac{u^{2}\left(t\right)}{2} dt + \rho\left(A\left(T\right)\right) + \frac{S}{2} \sum_{\tau_{i} \leq T} \xi_{i}^{2}\right],\tag{37}$$

where *E* denotes the expectation with respect to the probability measure *P*, and S > 0. Therefore, the control problem is to find $\Phi(a)$ and $(u^*(\cdot), \xi^*(\cdot))$ such that

$$\Phi(a) = \inf_{(u,\xi) \in \mathscr{A}_{\mathscr{G}}} E\left[-\int_{0}^{T} \frac{u^{2}(t)}{2} dt + \rho(A(T)) + \frac{S}{2} \sum_{\tau_{i} \leq T} \xi_{i}^{2}\right]$$

$$= E\left[-\int_{0}^{T} \frac{u^{*2}(t)}{2} dt + X_{g}^{-A_{u^{*}}(T)}(0) + \frac{S}{2} \sum_{\tau_{i} \leq T} \xi_{i}^{*2}\right].$$
(38)

The control problem (38) is a classical and impulse controls problem of forward-backward systems driven by Lévy processes under partial information \mathcal{G}_t . Next we solve the control problem (38) by Theorem 4. With the notation of the previous section we see that in Example 7 we have

$$f(t, a, x, y, k, u, \omega) = -\frac{u^2}{2}; \qquad h_1(x) = x; \qquad h_2(s, \omega) = 0;$$

$$b(t, a, u, \omega) = u\zeta(t); \qquad \sigma(t, a, u, \omega) = u\pi(t);$$

$$\gamma(t, a, u, z, \omega) = u\varrho(t, z); \qquad l(\tau_i, \xi_i) = \frac{S}{2}\xi_i^2;$$

$$C(t) = \omega; \qquad D(t) = \vartheta; \qquad \mu = -1.$$
(39)

Then by (11) the Hamiltonian is

$$H\left(t,a,x,y,k,u,\lambda,\omega\right) = -\frac{u^{2}}{2} + \lambda\left(t\right)g\left(t,x\right)$$

$$+ u\left(t\right)\zeta\left(t\right)p\left(t\right) + u\left(t\right)\pi\left(t\right)q\left(t\right)$$

$$+ \int_{\mathbb{R}_{0}} u\left(t\right)\varrho\left(t,z\right)r\left(t,z\right)\nu\left(dz\right),$$
(40)

where

$$dp(t) = q(t) dB(t) + \int_{\mathbb{R}_0} r(t, z) \widetilde{N}(dt, dz)$$

$$p(T) = -\lambda(T),$$
(41)

and $\lambda(t)$ is given by (12); that is,

$$d\lambda(t) = \lambda(t) g_x(t, X(t)) dt,$$

$$\lambda(0) = 1,$$
(42)

where $g_x(t, x) = (\partial/\partial x)g(t, x)$. We can easily obtain the solution of (42) as follows:

$$\lambda(t) = \exp\left\{ \int_0^t g_x(s, X(s)) \, ds \right\}; \quad 0 \le t \le T.$$
 (43)

If $(u^*(t), \xi^*(t))$ is a local critical point with corresponding $X^*(t) = X^{(u^*)}(t)$, then, by the sufficient and necessary optimality condition (17) in Theorem 4, we get

$$E\left[u^{*}\left(t\right)\mid\mathcal{G}_{t}\right] = E\left[\zeta\left(t\right)p\left(t\right) + \pi\left(t\right)q\left(t\right)\right.$$

$$+ \int_{\mathbb{R}_{0}} \varrho\left(t,z\right)r\left(t,z\right)\nu\left(dz\right)\mid\mathcal{G}_{t}\right].$$

$$(44)$$

Since $u^*(t)$ is \mathcal{G}_t -adapted, we have

$$u^{*}(t) = E\left[\zeta(t) p(t) + \pi(t) q(t) + \int_{\mathbb{R}_{0}} \varrho(t, z) r(t, z) \nu(dz) \mid \mathcal{G}_{t}\right],$$

$$(45)$$

where p(t), q(t), and r(t, z) are given by (41).

On the other hand, by the sufficient and necessary optimality condition (17) in Theorem 4, we obtain

$$\sum_{\tau_{i} < T} E\left[S\xi_{i}^{*} + \omega p\left(\tau_{i}\right) - \vartheta\lambda\left(\tau_{i}\right) \mid \mathcal{G}_{\tau_{i}}\right] = 0. \tag{46}$$

That is, for each $\tau_i < T$, we have

$$E\left[\xi_{i}^{*}\mid\mathscr{G}_{\tau_{i}}\right]=\frac{1}{S}E\left[\vartheta\lambda\left(\tau_{i}\right)-\varpi p\left(\tau_{i}\right)\mid\mathscr{G}_{\tau_{i}}\right].$$
 (47)

Since ξ_i is an \mathcal{G}_{τ_i} -measurable random variable, we have

$$\xi_{i}^{*} = \frac{1}{S} E \left[\vartheta \lambda \left(\tau_{i} \right) - \omega p \left(\tau_{i} \right) \mid \mathcal{G}_{\tau_{i}} \right], \tag{48}$$

where $\lambda(t)$ is given by (43) and p(t) is given by (41). Consequently, we summarize the above results in the following theorem.

Theorem 8. Let p(t), q(t), and r(t,z) be the solutions of (41) and let $\lambda(t)$ be the solution of (43). Then the pair $(u^*(t), \xi^*(t))$ is given by

$$u^{*}(t) = E\left[\zeta(t) p(t) + \pi(t) q(t) + \int_{\mathbb{R}_{0}} \varrho(t, z) r(t, z) \nu(dz) \mid \mathcal{G}_{t}\right], \qquad (49)$$

$$\xi^{*}(t) = \sum_{i \ge 1} \xi_{i}^{*} \mathbf{1}_{[\tau_{i}, T]}(t), \quad t \le T,$$

where ξ_i^* given by (48) is the local critical point of the classical and impulse controls problem (38).

5. Conclusion

We consider the partial information classical and impulse controls problem of forward-backward systems driven by Lévy processes. The control variable consists of two components: the classical stochastic control and the impulse control. Because of the non-Markovian nature of the partial information, dynamic programming principle cannot be used to solve partial information control problems. As a result, we derive a maximum principle for this partial information problem. Because the concavity conditions of the utility functions and the Hamiltonian process may not hold in many applications, we give the sufficient and necessary optimality conditions for the local critical points of the control problem. To illustrate the theoretical results, we use the maximum principle to solve a portfolio optimization problem with piecewise consumption processes and give its explicit solutions.

In this paper, we assume that the two different jumps in our system do not occur at the same time (Assumption 1). This assumption makes the problem easier to analyze. However, it may fail in many applications. Without this assumption, it requires more attention to distinguish between the two different jumps. This will be explored in our subsequent work.

Conflict of Interests

The authors declare that there is no conflict of interests regarding the publication of this paper.

Acknowledgment

This work was supported by the National Natural Science Foundation of China under Grant 11171050.

References

- [1] G. Mundaca and B. Øksendal, "Optimal stochastic intervention control with application to the exchange rate," *Journal of Mathematical Economics*, vol. 29, no. 2, pp. 225–243, 1998.
- [2] A. Cadenillas and F. Zapatero, "Classical and impulse stochastic control of the exchange rate using interest rates and reserves," *Mathematical Finance*, vol. 10, no. 2, pp. 141–156, 2000.
- [3] R. R. Lumley and M. Zervos, "A model for investments in the natural resource industry with switching costs," *Mathematics of Operations Research*, vol. 26, no. 4, pp. 637–653, 2001.
- [4] H. Meng and T. K. Siu, "Optimal mixed impulse-equity insurance control problem with reinsurance," *SIAM Journal on Control and Optimization*, vol. 49, no. 1, pp. 254–279, 2011.
- [5] H. Meng and T. K. Siu, "On optimal reinsurance, dividend and reinvestment strategies," *Economic Modelling*, vol. 28, no. 1-2, pp. 211–218, 2011.
- [6] F. Zhang, "Stochastic differential games involving impulse controls," ESAIM: Control, Optimisation and Calculus of Variations, vol. 17, no. 3, pp. 749–760, 2011.
- [7] L. G. Wu, X. J. Su, and P. Shi, "Output feedback control of Markovian jump repeated scalar nonlinear systems," *IEEE Transactions on Automatic Control*, vol. 59, no. 1, pp. 199–204, 2014.
- [8] B. Øksendal and A. Sulem, Applied Stochastic Control of Jump Diffusions, Springer, Berlin, Germany, 2nd edition, 2007.
- [9] R. C. Seydel, "Existence and uniqueness of viscosity solutions for QVI associated with impulse control of jump-diffusions," *Stochastic Processes and Their Applications*, vol. 119, no. 10, pp. 3719–3748, 2009.
- [10] Y. Wang, A. Song, C. Zheng, and E. Feng, "Nonzero-sum stochastic differential game between controller and stopper for jump diffusions," *Abstract and Applied Analysis*, vol. 2013, Article ID 761306, 7 pages, 2013.
- [11] Z. Wu and F. Zhang, "Stochastic maximum principle for optimal control problems of forward-backward systems involving impulse controls," *IEEE Transactions on Automatic Control*, vol. 56, no. 6, pp. 1401–1406, 2011.
- [12] Z. Wu and F. Zhang, "Maximum principle for stochastic recursive optimal control problems involving impulse controls," *Abstract and Applied Analysis*, vol. 2012, Article ID 709682, 16 pages, 2012.
- [13] R. Yang, Z. Zhang, and P. Shi, "Exponential stability on stochastic neural networks with discrete interval and distributed delays," *IEEE Transactions on Neural Networks*, vol. 21, no. 1, pp. 169–175, 2010.
- [14] R. Yang, H. Gao, and P. Shi, "Delay-dependent robust H_{∞} control for uncertain stochastic time-delay systems," *International Journal of Robust and Nonlinear Control*, vol. 20, no. 16, pp. 1852–1865, 2010.

- [15] X. Gao, K. L. Teo, and G. Duan, "An optimal control approach to robust control of nonlinear spacecraft rendezvous system with θ-D technique," *International Journal of Innovative Computing, Information and Control*, vol. 9, no. 5, pp. 2099–2110, 2013.
- [16] X. Su, P. Shi, L. Wu, and Y. D. Song, "A novel control design on discrete-time Takagi–Sugeno fuzzy systems with time-varying delays," *IEEE Transactions on Fuzzy Systems*, vol. 21, no. 4, pp. 655–671, 2013.
- [17] F. Baghery and B. Øksendal, "A maximum principle for stochastic control with partial information," *Stochastic Analysis and Applications*, vol. 25, no. 3, pp. 705–717, 2007.
- [18] T. T. K. An and B. Øksendal, "Maximum principle for stochastic differential games with partial information," *Journal of Opti*mization Theory and Applications, vol. 139, no. 3, pp. 463–483, 2008
- [19] B. Øksendal and A. Sulèm, "Maximum principles for optimal control of forward-backward stochastic differential equations with jumps," *SIAM Journal on Control and Optimization*, vol. 48, no. 5, pp. 2945–2976, 2009.
- [20] Z. Yu, "The stochastic maximum principle for optimal control problems of delay systems involving continuous and impulse controls," *Automatica*, vol. 48, no. 10, pp. 2420–2432, 2012.

Hindawi Publishing Corporation Abstract and Applied Analysis Volume 2014, Article ID 159609, 13 pages http://dx.doi.org/10.1155/2014/159609

Research Article

Consensus of Multiagent Systems with Packet Losses and Communication Delays Using a Novel Control Protocol

Zheping Yan, Di Wu, Wei Zhang, and Yibo Liu

College of Automation, Harbin Engineering University, Heilongjiang 150001, China

Correspondence should be addressed to Di Wu; roaddywu@gmail.com

Received 16 January 2014; Revised 23 February 2014; Accepted 24 February 2014; Published 7 April 2014

Academic Editor: Peng Shi

Copyright © 2014 Zheping Yan et al. This is an open access article distributed under the Creative Commons Attribution License, which permits unrestricted use, distribution, and reproduction in any medium, provided the original work is properly cited.

This paper studies the consensus problem of multiagent system with packet losses and communication delays under directed communication channels. Different from previous research results, a novel control protocol is proposed depending only on periodic sampling and transmitting data in order to be convenient for practical implementation. Due to the randomicity of transmission delays and packet losses, each agent updates its input value asynchronously at discrete time instants with synchronized time stamped information and evolves in continuous time. Consensus conditions for multiagent system consists of three typical dynamics including single integrator, double integrator, and high-order integrator that are all discussed in this paper. It is proved that, for single integrator agents and double integrator systems with only communication delays, consensusability can be ensured through stochastic matrix theory if the designed communication topology contains a directed spanning tree. While, for double integrator agents and high-order integrator agents with packet losses and communication delays, the interval system theory is introduced to prove the consensus of multiagent system under the condition that the designed communication topology is a directed spanning tree. Finally, simulations are carried out to validate the effectiveness of the proposed solutions.

1. Introduction

Consensus of multiagent system has attracted increasing focuses of researchers from different areas including multiple robotics system, large-scale oceanographic survey, and wireless sensor networks [1–4]. Among all the problems studied aiming at achieving consensus through local interaction, packet losses and communication delays that usually result from unreliable communication links are significant factors which influence the consensusability of multiagent system [5–25]. Considering those problems, three typical agent dynamics, single integrator [5, 9, 16, 23], double integrator [6, 8, 10, 12, 14, 17, 18], and high-order integrator [11, 15], are most widely discussed because they can represent a majority of autonomous systems.

Even though plenty of research results have been carried out about consensus problem of multiagent systems with communication delays, most of the controllers designed cannot be easily practiced. Take two typical controllers; for example, in Gao and Wang [10], the structure of controller implies that each agent has to memorize system states all the

time between two sampling instants because of the randomicity of communication delay. In Lin and Jia [12], to deploy the control protocol, each agent has to broadcast the information all the time and only one transmitted data is useful to calculate the control input. In both cases, system resources are wasted to some extent, especially for embedded systems whose resources are ordinarily limited. So in this paper, in order to be convenient for practical implementation and economical for limited system resource, a novel controller structure is proposed depending only on periodic sampling and transmitting data which is the main contribution of this paper. Compared with previously proposed solutions, this protocol greatly relieves the computational burden of each agent. In addition, with this control protocol, it is worth being noticed that since the communication delays are random, each agent updates its input asynchronously at discrete time instants based on received data. But the information transmitted is with synchronized time stamp and the whole system evolves in continuous time.

With the proposed control protocol, interaction topology is time varying due to communication delays and packet

losses. Also, many research results about consensus of multiagent systems with dynamically changing topology have been obtained based on stochastic matrix theory and Lyapunov theory. However, Lyapunov theory usually needs the topology to be undirected or balanced [7, 13, 14]. When random transmission delays and packet losses are concerned, undirected or balanced assumption is unreasonable. With the novel control protocol proposed in this paper, it will be shown that, for single integrator agent and second order agent without packet losses, similar results can be obtained as in [8, 9] according to stochastic matrix theory. That is, the consensus can be reached as long as the designed communication topology contains a directed spanning tree. However, when it comes to second order and high-order agent with packet losses and communication delays, stochastic theory is no longer easily applicable since the nonnegativity of the system matrix is not always guaranteed. Actually, to the best of the authors' knowledge, few results have been obtained to handle this problem. Based on the theory of interval matrix, it will be proved that the consensus of the system can be reached as long as the designed communication topology is a directed spanning tree which is another contribution of this paper. Of course, in this situation, the states of all agents will converge to the root node and average consensus cannot be obtained. However, this assumption can also simplify the system architecture indicating that one agent can only receive message from its superior and send information to its inferiors; this kind of hierarchy structure is actually more efficient and convenient in real-world application. Since the protocol proposed in this paper can be easily implemented for system with limited resources and unreliable communication links, it would have a wide application prospect in multiple autonomous systems, especially for multiple marine systems such AUVs, UUVs, and USVs, that rely on acoustic communication which is characterized by intermittent failures and latency [16].

The rest of the paper is organized as follows. In Section 2, preliminaries are presented and problems concerned are formulated. In Section 3, consensus of the multiagent system with single integrator, double integrator, and high-order integrator are analyzed under different situations. And simulations to prove the results are given in Section 4. Conclusions are made in Section 5.

2. Preliminaries and Problem Formulation

2.1. Graph Theory. Graph theory has played an important role in analysis of multiagent systems for its advantages in modeling the interactions between agents. As graph theory has been introduced in many relative articles, only necessary notations are put forward here. Consider a system with n agents and the topology graph consists of a vertex set $v = \{1, 2, \ldots, n\}$, an edge set $\varepsilon = \{(j, i) : i, j \in v\} \subseteq v \times v$, and an adjacent matrix $A = [a_{ij}] \in R^{n \times n}$. If $\varepsilon_{ji} \in \varepsilon$, then $a_{ij} > 0$ which means that agent i can receive information from agent j; else $a_{ij} = 0$. The set of neighbors of agent i is denoted by $N_i = \{v_j : (v_j, v_i) \in \varepsilon\}$. A directed spanning tree is a graph that has one node called root node, which has a directed path

to all of the other nodes. The Laplacian matrix $L \in \mathbb{R}^{n \times n}$ is defined as follows:

$$L = \begin{cases} -a_{ij}, & i \neq j; i, j \in v \\ & \sum_{j=1, j \neq i}^{n} a_{ij}. \end{cases}$$
 (1)

The following definitions are introduced for further discussion.

Definition 1 (subgraph [8]). Considering a topology graph $G = (v, \varepsilon, A)$, then $G_1 = (v_1, \varepsilon_1, A_1)$ is a subgraph of G if $(1) \ v_1 \subseteq v$; $(2) \ \varepsilon_1 \subseteq \varepsilon$.

Definition 2 (union of graphs [7]). Set the union of topology graphs $G_k = (v_k, \varepsilon_k, A_k)$ as $G = (v, \varepsilon, A)$; then, (1) $v_k \in v$; (2) $\varepsilon_k \in \varepsilon$.

2.2. Control Protocol. In this paper, system states are sampled and transmitted at discrete instants and the controller is designed based on the periodic sampling and transmitting information. For agent i, control input between $[t_k, t_{k+1})$ can be presented as follows:

$$u_{i}(t) = K \sum_{j \in N_{i}} a_{ij}(t) \left(x_{j}(t_{k}) - x_{i}(t_{k}) \right) \quad t_{k} \le t < t_{k+1},$$
 (2)

where K is controller gain with proper dimension to be decided, the value of $a_{ij}(t)$ should be defined as

$$a_{ij}(t) = \begin{cases} 0 & t_k \le t < t_k + \tau_{ij}(k) \\ 1 & t_k + \tau_{ij}(k) \le t < t_{k+1}. \end{cases}$$
 (3)

In the above equation, $\tau_{ij}(k)$ denotes the transmission delay between agent i and agent j during the period $[t_k,t_{k+1})$. From the structure of the controller, it is obvious that the control input is not constant during $[t_k,t_{k+1})$ and each agent in the system updates its input asynchronously. It is also worth noticing that (3) implies that $\tau_{ij} < t_{k+1} - t_k$, which is not necessarily guaranteed for communication system with random delays. So the following assumption is introduced about communication delays.

Assumption 3 (bounded transmission delays). There exist positive constant values τ_{\min} and τ_{ij} denoting the delay between agent i and agent j; T presents the time period for sampling and transmitting data. The following condition is satisfied;

$$T - \tau_{ij}(k) > \tau_{\min}, \quad \text{for any } k.$$
 (4)

From a practical point of view, it can be assumed that, for any packet with transmission delay that cannot satisfy Assumption 3, the packets are regarded as being lost.

2.3. Model. With the proposed control algorithm as in (2), the multiagent systems consist of three typical dynamics that are concerned. And the corresponding discrete-time system presentations are also presented in Table 1.

For *m*th high-order system, the matrices *A* and *B* are as follows:

$$A = \begin{bmatrix} 0 & 1 & 0 & \cdots & 0 \\ 0 & 0 & 1 & \ddots & \vdots \\ 0 & 0 & 0 & \ddots & 0 \\ \vdots & \vdots & \vdots & \ddots & 1 \\ 0 & 0 & 0 & \cdots & 0 \end{bmatrix} \in \mathbf{R}^{m \times m},$$

$$B = \begin{bmatrix} 0 & \cdots & 0 & 1 \end{bmatrix}^T \in \mathbf{R}^{m \times 1}.$$
(5)

Definition 4 (consensus [11]). Consensus of the multiagent system is regarded as being achieved when the following equation is satisfied:

$$\lim_{t \to \infty} \left\| x_i(t) - x_j(t) \right\| = 0, \quad \forall i, j \in v.$$
 (6)

3. Consensus of Multiagent System

In this section, consensus problem of multiagent system consists of different agent dynamics that is discussed separately. With proper assumptions made, we have proposed the conditions needed for consensusability of the multiagent system.

3.1. Case 1: Single Integrator Agent

3.1.1. With Communication Delays and No Packet Losses. Define $X(t) = \begin{bmatrix} x_1(t) & x_2(t) & \cdots & x_n(t) \end{bmatrix}^T$ as the state of the multiagent system. Since it can be easily extended to multistate through Kronecker production, it is assumed here that each agent has only one state for briefness of description. Based on the controller as (2) and the discrete time model in Table 1, the dynamics of multiagent system can be denoted by

$$X\left(t_{k+1}\right) = \left(I - \alpha\left(t_0L_0 + t_1L_1 + \dots + t_mL_m\right)\right)X\left(t_k\right),\tag{7}$$

where controller gain K is presented as $\alpha \in R$ in this case. Because of transmission delays, Laplacian matrix is not invariant. So L_0, L_1, \ldots, L_m represent the Laplacian matrices that exist during $[t_k, t_{k+1})$ and t_0, t_1, \ldots, t_m are the durations for corresponding Laplacian matrices satisfying $t_0 + t_1 + \cdots + t_m = T$. In fact, L_0 is a Laplacian matrix with no connections between agents and since no packet losses are concerned, for any $0 \le i \le m-1$, the topology associated with L_i is a subgraph of the topology associated L_{i+1} . To prove the consensusability of discrete-time system as in (7), following lemmas about nonnegative matrix and stochastic matrix are introduced beforehand.

Lemma 5 (see [26]). Let $M \in \mathbb{R}^{n \times n}$ be a stochastic matrix. If M has an eigenvalue $\lambda = 1$ with algebraic multiplicity equal to one and all of the other eigenvalues satisfy $|\lambda| < 1$, then M is SIA. That is, $\lim_{n \to \infty} M^n \to \mathbf{1} y^T$.

Lemma 6 (see [9]). A stochastic matrix has algebraic multiplicity equal to one for its eigenvalue $\lambda = 1$ if and

only if the graph associated with the matrix has a spanning tree. Furthermore, a stochastic matrix with positive diagonal elements has the property that $|\lambda| < 1$ for every eigenvalue not equal to one.

Lemma 7 (see [27]). Let $S_1, S_2, ..., S_k$ be a finite set of SIA matrices with property that, for each sequence $S_{i_1}, S_{i_2}, ..., S_{i_j}$ of positive length, the matrix product $S_{i_j}S_{i_{j-1}} \cdots S_{i_1}$ is SIA. Then, for each infinite sequence $S_{i_1}, S_{i_2}, ...,$ there exists a column vector y such that $\lim_{j\to\infty} S_{i_j}, S_{i_{j-1}}, ..., S_{i_1} = \mathbf{1}y^T$.

Lemma 8 (Gershgorin circle criterion [28]). All eigenvalues of a matrix $E = [e_{ij}] \in \mathbb{R}^{N \times N}$ are located within the union of N discs as follows:

$$\bigcup_{i=1}^{N} \left\{ z \in C : \left| z - e_{ii} \right| \le \sum_{j \neq i} \left| e_{ij} \right| \right\}.$$
 (8)

Lemma 9 (see [29]). Let $m \ge 2$ be a positive integer and let P_1, P_2, \ldots, P_m be nonnegative matrices with positive diagonal elements; then, $P_1P_2\cdots P_m \ge \gamma(P_1+P_2+\cdots+P_m)$, with $\gamma>0$. And if the digraph associated with $\gamma(P_1+P_2+\cdots+P_m)$ has a spanning tree, the graph associated with $P_1P_2\cdots P_m$ also has a spanning tree.

Besides, some assumptions also need to be proposed.

Assumption 10 (quantized transmission delays). There exists a small positive value Δ such that, for all $i, j \in 1, 2, ..., n$,

$$\tau_{ij}(k) = q\Delta, \qquad q \in 1, 2, \dots, m_q. \tag{9}$$

Assumption 10 indicates that transmission delays can be quantized and must be a multiple of fundamental delay time Δ . Assumption 10 is realizable and practical because all agents are operated under digital computers and the smaller the Δ is, the higher the accuracy is.

Assumption 11. The designed communication topology for the multiagent system has a directed spanning tree.

This assumption means that if there are no packet losses and communication delays, the topology of the multiagent system has a spanning tree at every instant t_k . Combing with Assumption 3, it can be derived that the union of digraphs associated with L_0, L_1, \ldots, L_m has a directed spanning tree. Then based on introduced lemmas and assumptions, the consensus of the system described as in (7) can be proposed.

Theorem 12. For multiagent system consisting of single integrator dynamics, with control protocol designed as (2) and Assumptions 3–11, the consensus of the multiagent system can be reached if the controller gain is set to be $\alpha = 1/Td_{\text{max}}$, where d_{max} is the largest in-degree of the Laplacian matrices $L_0, L_1, \ldots L_m$.

Proof. First of all, since there are a limited number of possible Laplacian matrices for fixed number of agents, $d_{\rm max}$ can be precalculated without consideration about communication

delays; then, it can be viewed as a constant in subsequent presentation. By substituting $\alpha = 1/Td_{\rm max}$ into (7), the system can be transformed as

$$X\left(t_{k+1}\right) = \left(I - \frac{1}{d_{\max}} \left(\frac{t_0}{T} L_0 + \frac{t_1}{T} L_1 + \dots + \frac{t_m}{T} L_m\right)\right) X\left(t_k\right)$$
$$= M_k X\left(t_k\right). \tag{10}$$

Since Assumption 11 holds and there are no packet losses, L_m has a spanning tree and the interaction graphs associated with $L_0, L_1, \ldots, L_{m-1}$ are subgraphs of the topology associated with L_m . Then, for the union of graphs $L_0, L_1, \ldots, L_{m-1}$, there is a simple eigenvalue equal to zero. According to Lemma 8, it is not difficult to conclude that all of other eigenvalues of $(1/d_{\max})((t_0/T)L_0+(t_1/T)L_1+\cdots+(t_m/T)L_m)$ are located within the circle with origin point of (1,0) and radius of 1. Thus, it can be obtained that M_k is a matrix with simple eigenvalues equal to one and the others within the unit circle of the complex plane which means that the topology associated with M_k has a spanning tree according to Lemma 6.

In addition, since all the nondiagonal entries of Laplacian matrices are nonpositive, the nondiagonal entries of M_k are nonnegative. All diagonal elements of M_k are less than one due to the choice of α . And since Laplacian matrices L_0, L_1, \ldots, L_m all have zero row sums, M_k has row sum equal to one; that is, M_k is a stochastic matrix. As a conclusion, M_k is a stochastic nonnegative matrix with positive diagonal elements and it can be derived from Lemma 5 that M_k is SIA.

Because M_k has a spanning tree, $M_k M_{k+1} \cdots M_{k+l}$ also has a spanning tree according to Lemma 9. In addition, the stochastic matrices with positive diagonal entries are closed under matrix multiplication, so that $M_k M_{k+1} \cdots M_{k+l}$ is also a stochastic matrix with positive diagonal elements. According to Lemmas 6 and 5, the matrix $M_k M_{k+1} \cdots M_{k+l}$ is SIA.

With Assumption 10, it can be derived that there is a finite number of M_k . After that, Lemma 7 can be applied to acquire that the multiagent system as in (10) can reach a consensus. Theorem 12 is proved.

3.1.2. With Packet Losses and Communication Delays. In the above section, consensus problem with communication delays has been solved that lay firm foundation for the problem concerned in the situation where packet losses must be taken into consideration. In this case, Assumption 3 is no longer satisfied. As mentioned previously, Assumption 3 is a relative strict condition to be fulfilled in practice. So the following assumption is proposed in addition.

Assumption 13. Set the success ratio of transmission between two agents as $p \in (0,1)$, $\forall \mu \in (0,1)$; there exists an integer l that satisfies $1-(1-p)^l>\mu$. If μ is chosen to be close to 1 enough, it is reasonable to assume that the transmission can be successful for at least one time during l periods. Besides, under Assumption 13, the communication delay can still satisfy Assumption 3 for the successful transmitted information. With Assumption 11, this assumption essentially

means that the union of digraphs within l periods has a directed spanning tree.

Theorem 14. For multiagent system consisting of single integrator dynamics satisfying Assumptions 10–13, with control protocol designed as in (2), the consensus of the multiagent system can be reached with the same controller gain α adopted as in Theorem 12.

Proof. In this situation, since Assumption 3 is no longer satisfied all the time, L_m cannot always have a spanning tree. However, according to Assumptions II and I3, the digraph associated with $M_k+M_{k+1}+\cdots+M_{k+l-1}$ will have a spanning tree. Since M_k is still a stochastic nonnegative matrix with positive diagonal elements, Lemma 9 still holds; that is, the relation $M_kM_{k+1}\cdots M_{k+l-1} \geq \gamma(M_k+M_{k+1}+\cdots+M_{k+l-1})$ exists. Thus, define $Q_{k,l}=M_kM_{k+1}\cdots M_{k+l-1}$ such that

$$X(t_{k+l}) = M_k M_{k+1} \cdots M_{k+l-1} X(t_k) = Q_{k,l} X(t_k).$$
 (11)

Since $Q_{k,l}$ is a stochastic nonnegative matrix with positive diagonal elements and the associated graph has a spanning tree, the problem regarding packet losses and communication delays can be handled in a similar way as in proof of Theorem 12. So, the consensusability of multiagent system with packet losses and communication delays is guaranteed. \Box

Remark 15. Based on the analysis of this section, it can be found that Theorem 12 can be viewed as a special case of Theorem 14 with l=1. With the proposed control protocol and proper choice of controller gain, the multiagent system can reach consensus as long as the union of the digraphs within finite periods has a spanning tree.

3.2. Case 2: Double Integrator Agent

3.2.1. With Communication Delays and No Packet Losses. For second order multiagent system, the corresponding variables are defined as $X(t) = \begin{bmatrix} x_1(t) & x_2(t) & \cdots & x_n(t) \end{bmatrix}^T$, $V(t) = \begin{bmatrix} v_1(t) & v_2(t) & \cdots & v_n(t) \end{bmatrix}^T$, respectively. Then based on the discrete time model of second order system in Table 1, it can be obtained that for agent i

$$v_i(t_{k+1}) = v_i(t_k) + \sum_{j \in N_i, j=0} (T - \tau_{ij}(k)) u_{ij}(k),$$
 (12)

$$x_{i}(t_{k+1}) = x_{i}(t_{k}) + Tv_{i}(t_{k}) + \sum_{i \in V_{k+1}} \frac{\left(T - \tau_{ij}(k)\right)^{2}}{2} u_{ij}(k),$$
(13)

where $u_{ij}(k)$ is the control input results from the relative state information between agent i and agent j. u_{i0} denotes the default control value of agent i that is usually set as 0 and $\tau_{i0}=0$ since the input is default.

To make (13) more concise, some transformations need to be carried out. Set $u_{ij}(k) = (2/(T - \tau_{ij}(k))^2)u'_{ij}(k)$. The transformation process is applicable because, during the

period $[t_k, t_{k+1}), \tau_{ij}(k)$ are known to the agent *i*. Equations (12) and (13) are revised as

$$v_{i}(t_{k+1}) = v_{i}(t_{k}) + \sum_{j \in N_{i}, j=0} \frac{2}{\left(t_{k+1} - \tau_{ij}\right)} u'_{ij},$$

$$x_{i}(t_{k+1}) = x_{i}(t_{k}) + Tv_{i}(t_{k}) + \sum_{j \in N_{i}, j=0} u'_{ij}.$$
(14)

With the controller gain chosen as $K = [\alpha \ \beta]$, $u'_{ij}(k) = \alpha(x_j(t_k) - x_i(k)) + \beta(v_j(t_k) - v_i(k))$. The dynamics of the multiagent system can be presented as

$$\begin{bmatrix} X\left(t_{k+1}\right) \\ V\left(t_{k+1}\right) \end{bmatrix} = \begin{bmatrix} I_{n} - \alpha L_{k} & TI_{n} - \beta L_{k} \\ -\alpha L_{k}' & I_{n} - \beta L_{k}' \end{bmatrix} \begin{bmatrix} X\left(t_{k}\right) \\ V\left(t_{k}\right) \end{bmatrix}. \tag{15}$$

As we know, topology associated with L_k will have a spanning tree if Assumption 11 holds. L'_k has the same structure as L_k except for all its items that have been multiplied by $2/(T - \tau_{ij}(k))$. Thus, topology of L'_k also has a spanning tree. The consensus problem for system depicted as (15) can be discussed in a similar way as in Cao and Ren [8].

Lemma 16 (Cao and Ren [8]). With the decomposition of system transfer matrix as in (16), since L_k , L'_k all have spanning tree, if the conditions (1) and (2) are satisfied, consensus of the system can be reached

$$\begin{bmatrix} I_{n} - \alpha L_{k} & TI_{n} - \beta L_{k} \\ -\alpha L_{k}' & I_{n} - \beta L_{k}' \end{bmatrix}$$

$$= \begin{bmatrix} I_{n} - TI_{n} - \alpha L_{k} & TI_{n} - \beta L_{k} \\ TI_{n} - \alpha L_{k}' & I_{n} - TI_{n} - \beta L_{k}' \end{bmatrix} + \begin{bmatrix} TI_{n} & \mathbf{0} \\ -TI_{n} & TI_{n} \end{bmatrix}.$$
(16)

- (1) $I_n TI_n \alpha L_k$, $(1 T)I_n \beta L'_k$ are nonnegative matrices with positive diagonal entries and $TI_n \beta L_k$, $TI_n \alpha L'_k$ are nonnegative matrices.
- (2) The infinite norm of matrix $\begin{bmatrix} TI_n & \mathbf{0} \\ -TI_n & TI_n \end{bmatrix}$ is less than 1.

The first condition is aimed to guarantee that the first matrix is a nonnegative one with positive diagonal entries. In addition, it is not difficult to find that the matrix is also stochastic. Then the matrix is SIA and Lemma 7 is applicable. And the second condition is to make sure that multiplication of infinite number of the second matrix goes to zero. More detailed proofs can be found in Cao and Ren [8].

Theorem 17. For multiagent system consisting of double integrator agents, with Assumptions 3–11 holding, if the sampling and transmitting period T and controller gain K can satisfy the following conditions, the consensus of the multiagent system is guaranteed:

(1)
$$1/4 < T < 1/2$$
;

(2)
$$\alpha = \beta = \tau_{\min}/4d_{\max}$$
.

Proof. If condition (1) is satisfied, the infinite norm of matrix $\begin{bmatrix} TI_n & \mathbf{0} \\ -TI_n & TI_n \end{bmatrix}$ is less than 1. Define d_{\max} , d'_{\max} that represent the largest in-degree for L_k , L'_k , respectively. d'_{\max} is random due to the randomicity of transmission delays. From Assumption 3, it is obvious that

$$\tau_{\min} d'_{\max} < d_{\max}. \tag{17}$$

Then, with the second condition, it can be acquired that

$$\sup\left(\frac{\tau_{\min}}{4d_{\max}}d'_{\max}\right) < \frac{1}{4}.\tag{18}$$

As a result, $T - \alpha d'_{\max} > 0$. Besides, it is not difficult to find that $1 - T - \beta d'_{\max} > 0$ since $\tau_{\min} < T$. As a result, it can be concluded that if the conditions are satisfied, Lemma 16 is also fulfilled and the consensusability of the multiagent system with double integrator dynamics is proved.

3.2.2. With Communication Delays and Packet Losses. For second order system with packet losses, Assumption 11 cannot hold and the Laplacian matrices L_k , L_k' discussed in the above section no longer have a spanning tree all the time. In this situation, Lemma 16 cannot directly be applied. Inspired by Qin et al. [17], a covariable can be introduced here with definition as

$$y_{i}(t_{k}) = av_{i}(t_{k}) + bx_{i}(t_{k}),$$
 (19)

where a, b are constant parameters. It is easily derived that if $x(t_k)$ and $y(t_k)$ can reach consensus, the velocity of the system will also achieve consensus. So in the following discussion, the consensus problem of system states $x(t_k)$ and $y(t_k)$ is concerned. Besides, default control of agent i also needs to be set as $u'_{i0} = -cv_i(t_k)$, $i \in \{1, 2, ..., n\}$.

As a result, the multiagent system can be transformed into

$$\begin{bmatrix} x(t_{k+1}) \\ y(t_{k+1}) \end{bmatrix} = \begin{bmatrix} \left(1 - \frac{bT}{a}(1 - cT)\right)I_n - \left(\alpha - \frac{b\beta}{a}\right)L_k & \frac{T}{a}(1 - cT)I_n - \frac{\beta}{a}L_k \\ \left(cbT - \frac{b^2T}{a}(1 - cT)\right)I_n - \left(\alpha - \frac{b\beta}{a}\right)L'_k & \left(\frac{bT}{a}(1 - cT) + 1 - cT\right)I_n - \frac{\beta}{a}L'_k \end{bmatrix} \begin{bmatrix} x(t_k) \\ y(t_k) \end{bmatrix}.$$
(20)

With proper choices of parameters α , β , a, b, and T, the system matrix can be a nonnegative stochastic matrix with

positive diagonal elements. In fact, to ensure that the transfer matrix is stochastic, $b \equiv 1$. Then if Assumption 13 holds, the

system described as (20) can reach a consensus with similar proof as Theorem 14. However, because of the existence of default control input, the consensus value of system velocity is zero which is usually the case for rendezvous problem not for formation control or flocking. So in order to obtain the consensus for multiagent system without adding the control input u_{i0}' , in the subsequence of this paper, a different assumption about interaction topology needs to be made.

Assumption 18. The designed communication topology for the multiagent system is a directed spanning tree. Similarly, with Assumption 13, this assumption essentially means that the union of digraphs within \boldsymbol{l} periods is a directed spanning tree.

Consider two agents i, j and assume that there is a directed link from agent i to j. According to Assumption 13, there exist a positive integer g with $1 \le g \le l$ such that the data transmission is successful during the period $[t_{k+g-1},t_{k+g})$ and packets dropout during the previous g-1 periods. Define the delay during $[t_{k+g-1},t_{k+g})$ as $\tau_{ij}(t_k^g)$ which satisfies Assumption 3. Adopt the controller gain as $\alpha_j(t_k^g) = \beta_j(t_k^g) = (T - \tau_{ij}(t_k^g))/4$ and the following dynamics can be obtained for agents i and j:

$$\begin{bmatrix} x_{i}(t_{k+g}) \\ x_{j}(t_{k+g}) \\ v_{i}(t_{k+g}) \\ v_{j}(t_{k+g}) \end{bmatrix} = \begin{bmatrix} 1 & 0 & gT & 0 \\ \frac{(T - \tau_{ij}(t_{k}^{g}))}{4} & 1 - \frac{(T - \tau_{ij}(t_{k}^{g}))}{4} & \frac{T - \tau_{ij}(t_{k}^{g})}{4} & (1 + (g - 1)T) & gT - \frac{T - \tau_{ij}(t_{k}^{g})}{4} & (1 + (g - 1)T) \\ 0 & 0 & 1 & 0 \\ \frac{1}{2} & -\frac{1}{2} & \frac{1}{2}(1 + (g - 1)T) & \frac{1}{2}(1 - (g - 1)T) \end{bmatrix}$$

$$\times \begin{bmatrix} x_{i}(t_{k}) \\ x_{j}(t_{k}) \\ v_{i}(t_{k}) \\ v_{j}(t_{k}) \end{bmatrix}.$$

$$(21)$$

Define the states error between agents i and j at time instants as t_k and t_{k+q} as follows:

$$\begin{split} &\zeta_{ij}\left(d+1\right) = x_{j}\left(t_{k+g}\right) - x_{i}\left(t_{k+g}\right), \\ &\xi_{ij}\left(d+1\right) = v_{j}\left(t_{k+q}\right) - v_{i}\left(t_{k+q}\right), \end{split}$$

$$\zeta_{ij}(d) = x_j(t_k) - x_i(t_k),$$

$$\xi_{ij}(d) = v_j(t_k) - v_i(t_k),$$
(22)

where d represents the number of successful transmissions. Then the following equation is acquired denoting the error dynamics between agents i and j:

$$\begin{bmatrix} \zeta_{ij} (d+1) \\ \xi_{ij} (d+1) \end{bmatrix} = \begin{bmatrix} \left(1 - \frac{\left(T - \tau_{ij} (t_k^g) \right)}{4} \right) \left(gT - \frac{T - \tau_{ij} (t_k^g)}{4} (1 + (g-1)T) \right) \\ -\frac{1}{2} & \frac{1}{2} (1 - (g-1)T) \end{bmatrix} \begin{bmatrix} \zeta_{ij} (d) \\ \xi_{ij} (d) \end{bmatrix}.$$
(23)

According to the error dynamics depicted as above, the following lemma can be proposed.

Theorem 19. For multiagent system consisting of double integrator dynamics as in Table 1, with Assumptions 13 and 18, the consensusability of the system can be guaranteed with packet

losses and transmission delays as long as the discrete error dynamics as in (23) is stable.

Proof. Without loss of generality, set agent i as the root node of the directed spanning tree. Define N_i^0 as the set of agents that receive information from agent i. If the error dynamics as

Agent type	Continuous time system	Discrete time presentation
Single integrator	$\dot{x}_i(t) = u_i(t)$	$x_i\left(t_{k+1}\right) = x_i\left(t_k\right) + TK \sum_{j \in N_i} a_{ij}\left(x_j\left(t_k\right) - x_i\left(t_k\right)\right)$
Double integrator	$\dot{x}_i(t) = v_i(t)$ $\dot{v}_i(t) = u_i(t)$	$x_{i}(t_{k+1}) = x_{i}(t_{k}) + Tv_{i}(t_{k}) + \frac{T^{2}}{2}K\sum_{j \in N_{i}}a_{ij}(x_{j}(t_{k}) - x_{i}(t_{k}))$ $v_{i}(t_{k+1}) = v_{i}(t_{k}) + TK\sum_{j \in N_{i}}a_{ij}(x_{j}(t_{k}) - x_{i}(t_{k}))$
High-order integrator	$\dot{x}_i(t) = Ax_i(t) + Bu_i(t)$	$x_{i}(t_{k+1}) = e^{AT}x_{i}(t_{k}) + \int_{0}^{T} e^{At}BK \sum_{j \in N_{i}} a_{ij}(x_{j}(t_{k}) - x_{i}(t_{k})) dt$

TABLE 1: Continuous time and discrete time presentations of agent dynamics.

in (23) is stable, that is, $\lim_{d\to\infty}\zeta_{ij}(d)=0$, $\lim_{d\to\infty}\xi_{ij}(d)=0$. It is obvious that agents i and j can reach a consensus for any $j\in N_i^0$ with finite time periods since Assumption 18 holds.

Then there exist a positive number m_j and a time instant t_{m_j} such that $\left[\zeta_{ij}(m_j) \ \xi_{ij}(m_j)\right]^T = \begin{bmatrix} 0 \ 0 \end{bmatrix}^T$ for $t > t_{m_j}$. With definition of $t_m = \max\{t_{m_j}\}, j \in N_i^0$, it can be derived that when $t > t_m, x_j(t) = x_i(t), v_j(t) = v_i(t)$, for all $j \in N_i^0$ which means that the consensus has been reached between agents i and N_i^0 . Since the discrete error dynamics is as in

(23) set no restrictions on initial states of agents and the agents belonging to N_j^0 will reach consensus with agent j in a similar way. Finally, the whole multiagent system will reach a consensus.

To be more illustrative, the process can be shown in Figure 1. The error dynamics between different agents in the dash line circle can be presented as (23). The agents in the real line circle mean that the consensus has been reached among them

In the following, an algorithm to testify the Schur stability of discrete-time dynamics system as in (23) is proposed. Since all communication delay τ_{ij} is random, the transfer matrix

$$M = \begin{bmatrix} \left(1 - \frac{T - \tau_{ij} (t_k^g)}{4}\right) \left(gT - \frac{T - \tau_{ij} (t_k^g)}{4} (1 + (g - 1)T)\right) \\ -\frac{1}{2} & \frac{1}{2} (1 - (g - 1)T) \end{bmatrix}$$
(24)

can be viewed as an interval matrix $[M^m, M^M] = \{M = [m_{ij}] : m_{ij}^m < m_{ij} < m_{ij}^M, i, j = 1, 2\}$ for fixed g with the expressions of M^m and M^M as follows:

$$M^{m} = \begin{bmatrix} 1 - \frac{T}{4} & gT - \frac{T}{4} \left(1 + (g - 1)T \right) \\ -\frac{1}{2} & \frac{1}{2} \left(1 - (g - 1)T \right) \end{bmatrix};$$

$$M^{M} = \begin{bmatrix} 1 - \frac{\tau_{\min}}{4} & gT - \frac{\tau_{\min}}{4} \left(1 + (g - 1)T \right) \\ -\frac{1}{2} & \frac{1}{2} \left(1 - (g - 1)T \right) \end{bmatrix}.$$
(25)

The following lemma needs to be introduced concerning the stability of interval matrix.

Lemma 20. An interval matrix $[R^m, R^M]$ is Schur stable if and only if there are finitely subinterval matrices $[R_i^m, R_i^M] \subset [R^m, R^M]$, $1 \le i \le k$, such that

$$[R^m, R^M] = \bigcup_{i=1}^k [R_i^m, R_i^M].$$
 (26)

And for each $i, 1 \le i \le k$, $[R_i^m, R_i^M]$ satisfies the following conditions.

(1) R_{i0} is Schur stable and there exists a positive definite matrix $P = P^{T}$ satisfying

$$R_{i0}^{T} P_i R_{i0} - P_i + I = 0. (27)$$

(2) $\phi(\Delta R_i) < [\phi(R_{i0})^2 + 1/|P_i|_{\infty}]^{1/2} - \phi(R_{i0})$. $\phi(\cdot)$ is an operator $\phi(R) = \max\{|R|_1, |R|_{\infty}\}$ and the definitions of ΔR_i and R_{i0} are as follows:

$$\Delta R_{i} = \frac{1}{2} \left(R_{i}^{M} - R_{i}^{m} \right),$$

$$R_{i0} = \frac{1}{2} \left(R_{i}^{M} + R_{i}^{m} \right).$$
(28)

(3) Subinterval matrices $\bigcup_{i=1}^{k} [R_i^m, R_i^M]$ are complete decomposition of interval matrix $[R^m, R^M]$ which means that $\forall R \in [R^m, R^M]$, $\exists i \in [1, 2, ..., k]$ such that $R \in [R_i^m, R_i^M]$.

Proof. See Wang et al. [30] and Liao et al. [31] for details. \Box

Consider the parameters in (23), according to Assumption 3 and τ_{min} actually denotes the smallest processing

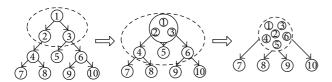


FIGURE 1: Consensus process of multiagent system under directed spanning tree.

time available for the embedded system. T is the sampling and transmitting period for the multiagent system and for acoustic communication system it also indicates the largest distance available between two linked agents since the relation Dis $< v_c(T - \tau_{\min})$ has to be satisfied, where v_c is the acoustic velocity. Due to the physical meanings of τ_{\min} , T, they usually are predetermined once the multiagent system structure is determined. As for g, according to Assumption 13 and the derivation of (23), g is a time varying positive integrator variable satisfying $1 \le g \le l$. So the following lemma is put forward.

Lemma 21. The system transfer matrix in (23) is Schur stable if, for every fixed $g \in [1, 2, ..., l]$, $[M^m, M^M]$ is Schur stable.

Proof. Define the interval matrix $[M^m, M^M]$ as $[M_j^m, M_j^M]$ when $g = j, 1 \le j \le l$. If $[M_j^m, M_j^M]$ is Schur stable, then there exist a finite number of subinterval matrices $[M_j^m, M_j^M] = \bigcup_{i=1}^k [M_{ij}^m, M_{ij}^M]$ satisfying conditions in Lemma 20. In addition, the system matrix in (23) can be completely decomposed as

$$\left[M^{m}, M^{M}\right] = \bigcup_{j=1}^{l} \left[M_{j}^{m}, M_{j}^{M}\right]. \tag{29}$$

Then it can be derived that

$$\left[M^{m}, M^{M}\right] = \left\{ \bigcup_{i=1}^{k} \left[M_{i1}^{m}, M_{i1}^{M}\right] \right\} \cup \left\{ \bigcup_{i=1}^{k} \left[M_{i2}^{m}, M_{i2}^{M}\right] \right\} \\
\cup \cdots \cup \left\{ \bigcup_{i=1}^{k} \left[M_{il}^{m}, M_{il}^{M}\right] \right\}.$$
(30)

The above equation means that the system matrix can be decomposed into finite number of subinterval matrices that all satisfy the conditions in Lemma 20. The matrix is Schur stable. \Box

Even though Lemmas 20 and 21 have provided conditions to guarantee the Schur stability of the discrete interval system matrix, method to completely decompose an interval matrix is needed. Based on the definition of R_{i0} and ΔR_i in (28), the interval matrix $[R^m, R^M]$ can be presented as $[R_0 \pm \Delta R]$. With this presentation, it is natural to adopt the decomposition as $[R^m, R^M] = [R_0 - \Delta R, R_0] \cup [R_0, R_0 + \Delta R]$. However, the decomposition is not always complete. Denote the element of the interval matrix at ith row and jth

column by $[R^m(i, j), R^M(i, j)]$. Then divide the interval into two subintervals as follows:

$$\left[R^{m}\left(i,j\right),R^{M}\left(i,j\right)\right]=R_{L}\left(i,j\right)\cup R_{H}\left(i,j\right)\tag{31}$$

with $R_L(i, j)$ and $R_H(i, j)$ defined as

$$R_{L}(i, j) = [R_{0}(i, j) - \Delta R(i, j), R_{0}(i, j)],$$

$$R_{H}(i, j) = [R_{0}(i, j), R_{0}(i, j) + \Delta R(i, j)]$$
(32)

If R^m , $R^M \in \mathbf{R}^{n \times n}$, the interval matrix can be decomposed as follows:

$$[R^m, R^M] = \bigcup_{k=1}^{2^{m \times n}} R_{\text{inv}}(k).$$
 (33)

Each element in $R_{\rm inv}(k)$ at ith row and jth column will be either $R_L(i,j)$ or $R_H(i,j)$. Then, it is obvious that the decomposition is complete. Now, Algorithm 1 is proposed in pseudocode to testify the Schur stability of the interval matrix. If a limited number of subintervals can be obtained for each $[M_j^m, M_j^M]$, $1 \le j \le l$ that satisfy the Schur stability conditions in Lemma 20, the system matrix in (23) is stable according to Lemma 21. That is, the multiagent system consists of second order agent with communication delays and packet losses can reach a consensus.

Through Algorithm 1, the consensusability of the multiagent system concerned can be testified. However, since the controller gain and the system parameters are predefined, no analytical solutions are provided by this method for multiagent system that could not reach consensus. Besides, the computational burden of the algorithm will increase exponentially with the order of agents. Therefore, in the next section, a theorem will be proposed to design the controller gain and solve the consensus problem of multiagent system with high-order integrator agents.

3.3. High-Order Integrator Agent. Assume that Assumption 18 still holds; similar result can be obtained as in Theorem 19; that is, if the root agent i and agent j, $j \in N_i^0$, can reach consensus, the multiagent system can reach consensus. So for the high-order integrator dynamics introduced in Table 1, with communication delays, the discrete system dynamics for agent i and agent j can be presented as

$$X_{i}\left(t_{k+1}\right) = e^{AT}X_{i}\left(t_{k}\right),$$

$$X_{j}\left(t_{k+1}\right) = e^{AT}X_{j}\left(t_{k}\right) + \int_{o}^{T-\tau_{ij}\left(t_{k}\right)} e^{At}dt \qquad (34)$$

$$\cdot BK\left(X_{i}\left(t_{k}\right) - X_{j}\left(t_{k}\right)\right)$$

with $K = [k_1 \ k_2 \cdots k_m]$ as the controller gain to be designed; $\tau_{ij}(t_k)$ is the communication delay satisfying Assumption 3. Let the states error between agent i and agent j at time t_k

$$\delta(t_k) = X_i(t_k) - X_j(t_k). \tag{35}$$

```
Initialization of parameters \tau_{\min}, T and l;

For j=1:l

Test the Schur stability \left(\left[M_{j}^{m},M_{j}^{M}\right]\right)

{

If \left[M_{j}^{m},M_{j}^{M}\right] is Schur stable

Break;

Else

If M_{j}^{o} is not Hurwitz stable

\left[M_{j}^{m},M_{j}^{M}\right] is not stable; break;

Else

Decompose \left[M_{j}^{m},M_{j}^{M}\right];

Test the Schur stability (each subinterval);

}

End
```

Algorithm 1

The error dynamics between two agents is

$$\delta\left(t_{k+1}\right) = \left(e^{AT} - \int_{o}^{T - \tau_{ij}(t_k)} e^{At} dt \cdot BK\right) \delta\left(t_k\right). \tag{36}$$

Considering packet losses and according to Assumption 13, there exists an integer $g \in [1, ..., l]$ such that the error dynamics during the period $[t_k, t_{k+g})$ can be presented as

$$\delta\left(t_{k+g}\right) = e^{(g-1)AT} \left(e^{AT} - \int_{o}^{T-\tau_{ij}(t_k^g)} e^{At} dt \cdot BK\right) \delta\left(t_k\right). \tag{37}$$

Algorithm 1 can still be applied to test the Schur stability of system matrix equation (36) and (37). Except for the computational complexity increases exponentially with the system order, the controller gain is also difficult to design comparing with second order multiagent system. So in order to circumvent those difficulties, the following lemmas are applied to achieve the controller gain.

Lemma 22 (see [32]). For discrete time interval system as in (38), $M \in \mathbf{R}^{n \times n}, N \in \mathbf{R}^{n \times p}$, the system is stabilizable if and only if there exist a matrix $G \in \mathbf{R}^{p \times n}$ and a symmetric positive definite matrix $H \in \mathbf{R}^{n \times n}$ and scalars $\lambda_{ij} > 0$, i, j = 1, 2, ..., n, $\delta_{ij} > 0$, i = 1, 2, ..., n, j = 1, 2, ..., p, satisfying (39). And the controller gain can be adopted as $K = GH^{-1}$. Consider

$$\delta (d+1) = \left[M_{\min}, M_{\max} \right] \delta (d) + \left[N_{\min}, N_{\max} \right] u (d),$$

$$u (d) = K\delta (d),$$
(38)

$$\begin{bmatrix} -H & HM_o^T + GN_o^T & H_d & G_d \\ M_0H + N_0G & -H + \Sigma & 0 & 0 \\ H_d^T & 0 & -\Lambda \\ G_d^T & 0 & -\Delta \end{bmatrix} < 0,$$
 (39)

where $\Sigma = \sum_{i,j=1}^{n} \lambda_{ij} |\Delta m_{ij}|^2 e_i e_i^T + \sum_{i=1}^{n} \sum_{j=1}^{p} \delta_{ij} |\Delta n_{ij}|^2 e_i e_i^T$, e_i is a column vector with ith element being 1. And

$$H_d = \underbrace{[H, \dots, H]}_{n}, \qquad G_d = \underbrace{[G^T, \dots, G^T]}_{n},$$

$$\Lambda = \operatorname{diag} \{\lambda_{11}, \lambda_{12}, \dots, \lambda_{1n}, \dots, \lambda_{n1}, \lambda_{n2}, \dots, \lambda_{nn}\},$$

$$\Delta = \operatorname{diag} \{\delta_{11}, \delta_{12}, \dots, \delta_{1n}, \dots, \delta_{n1}, \delta_{n2}, \dots, \delta_{nn}\}.$$

$$(40)$$

Lemma 23. The interval system matrices $[M_{\min}, M_{\max}]$ and $[N_{\min}, N_{\max}]$ are stabilizable if there are a finite number of subintervals $[M^i_{\min}, M^i_{\max}]$, $[N^i_{\min}, N^i_{\max}]$, $1 \le i \le k$ such that, for each $i \in \{1, 2, \dots, k\}$, the system matrices $[M^i_{\min}, M^i_{\max}]$, $[N^i_{\min}, N^i_{\max}]$ are stabilizable. And the interval system is completely decomposed which means that, at any time instant t, if $N(t) \in [N^i_{\min}, N^i_{\max}]$, then $M(t) \in [M^i_{\min}, M^i_{\max}]$, $1 \le i \le k$. And the complete decomposition can be denoted by

$$\begin{bmatrix} M_{\min}, M_{\max} \end{bmatrix} = \bigcup_{i=1}^{k} \begin{bmatrix} M_{\min}^{i}, M_{\max}^{i} \end{bmatrix},$$

$$[N_{\min}, N_{\max}] = \bigcup_{i=1}^{k} \begin{bmatrix} N_{\min}^{i}, N_{\max}^{i} \end{bmatrix}.$$
(41)

Proof. Since the system matrices $[M_{\min}^i, M_{\max}^i]$, $[N_{\min}^i, N_{\max}^i]$ are stabilizable, suppose that the controller gain is denoted by K; then, it can be derived that $[M_{\min}^i, M_{\max}^i] + [N_{\min}^i, N_{\max}^i]K$ is Schur stable. Because the interval system is completely decomposed, the following decomposition is also complete

$$\begin{split} \left[M_{\min}, M_{\max}\right] + \left[N_{\min}, N_{\max}\right] K \\ &= \bigcup_{i=1}^{k} \left(\left[M_{\min}^{i}, M_{\max}^{i}\right] + \left[N_{\min}^{i}, N_{\max}^{i}\right] K\right). \end{split} \tag{42}$$

Then according to Lemma 21, the Schur stability of $[M^i_{\min}, M^i_{\max}] + [N^i_{\min}, N^i_{\max}]K, i \in \{1, 2, \dots, k\}$ indicated Schur stability of the multiagent system.

Comparing (36) with (37), it can be concluded that (36) is the special case of (37) when g = 1. Actually, the interval matrices in (37) are piecewise interval, and the system can be completely decomposed into l subinterval systems easily. The subinterval systems can be presented as follows:

$$\delta\left(t_{k+g}\right) = e^{gAT}\delta\left(t_{k}\right) - e^{(g-1)AT} \int_{o}^{T-\tau_{ij}(t_{k}^{g})} e^{At}Bdt \cdot u\left(t_{k}\right)$$

$$= M_{g}\delta\left(t_{k}\right) + N_{g}u\left(t_{k}\right)$$
for $g \in \{1, 2, \dots, l\}$.
$$(43)$$

Theorem 24. For multiagent system consisting of high order agents, under Assumptions 13 and 18, the consensusability of the system can be guaranteed with transmission delays and packet losses if there exists a controller gain K such that the conditions in Lemma 22 can be satisfied for each $M_g + N_g K$, $g \in \{1, 2, \ldots, l\}$.

Proof. If the conditions in Lemma 22 are satisfied, $M_g + N_g K$ is Schur stable. From (43), the interval system in (37) can be completely decomposed by M_g and N_g , $g \in \{1, 2, ..., l\}$. Then according to Lemma 23, the theorem is established.

In fact, the existence of controller gain K is important in the above lemma. According to (39) in Lemma 22, matrix K can be obtained by solving the LMI with matlab. In order to guarantee the conditions in Lemma 23, l LMIs should be solved simultaneously to calculate the feedback gain K. Besides, it should be noticed that Theorem 24 is a general solution for controller gain of multiagent system and can be applied to all kinds of agent dynamics including single integrator, second order integrator, and general linear system.

4. Simulations

In this section, simulation results will be presented to demonstrate the theoretical results in Section 3. A multiagent system consists of five agents with the designed interaction topology as in Figure 2 that is concerned. The success ratio p in Assumption 13 is set as 0.8 according to the property of ordinary acoustic communication equipment; if μ is chosen to be 0.999, then l can be set as 5 which means that the transmission will be successful at least one time during five periods. τ_{\min} is set to be 0.1, which is long enough for system to calculate the system inputs. Sampling and transmitting period T=0.5. With all above initialization, single integrator, second order, and high-order agents are discussed separately and consensusability for every typical multiagent system is testified with packet losses and communication delays.

4.1. Single Integrator Agent. In this case, the initial state of each agent in the multiagent system is chosen randomly from 0 to 50, $\alpha = 2$. Simulation result is shown in Figure 3. It can be concluded that, for single integrator system, the position of each agent will converge to the state of agent 1 and the consensus of the system will be reached fast.

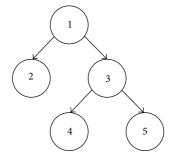


FIGURE 2: Interaction topology.

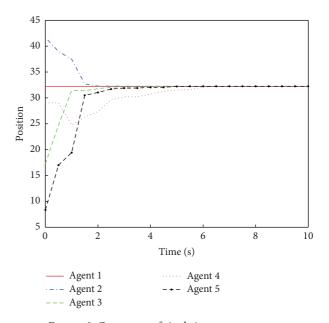


FIGURE 3: Consensus of single integrator system.

4.2. Second Order Agent. In this case, we need to test Schur stability of the error dynamics with Algorithm 1; it can be calculated that, with 582 subintervals, the conditions in Lemma 20 can be satisfied for every subinterval. Similar to Case 1, the initial values for position and velocity are randomly adopted within [0, 50] and [0, 10], respectively. The simulation results are shown in Figures 4 and 5. It can be seen that, during some time intervals at the beginning, the difference of states may increase, especially for velocity of the agent, but the consensus will be reached with enough time. It is also worth noticing that the sampling and transmitting period T adopted in this case cannot satisfy the condition in Theorem 17; however, the consensus can still be guaranteed which indicated that the condition from stochastic matrix theory is more conservative if Assumption 18 holds.

4.3. High-Order Agent. Considering the third order integrator agent, corresponding structure of matrices A and B can be obtained through Table 1. Then according to Lemmas 22 and 23, the controller gain K can be calculated through solving the 5 LMIs with matlab. It can be found that $K = \begin{bmatrix} 2.36 & 2.57 & 3.59 \end{bmatrix}$ is a proper solution and the simulations

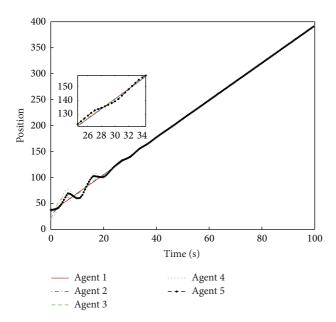


FIGURE 4: Consensus of position for second order system.

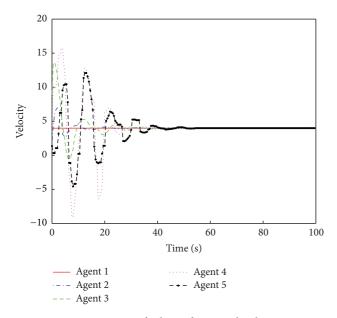
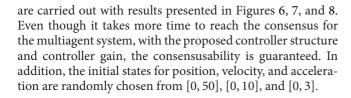


FIGURE 5: Consensus of velocity for second order system.



5. Conclusions

In this paper, the consensus problem of multiagent system with packet losses and communication delays is discussed. A novel control protocol that depends on periodic sampling

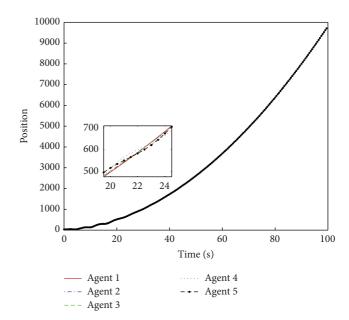


FIGURE 6: Consensus of position for high-order system.

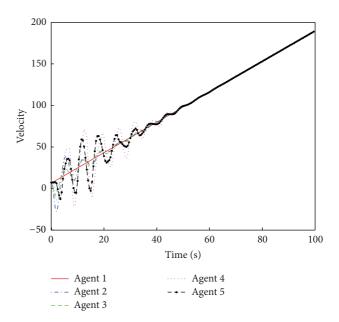


Figure 7: Consensus of velocity for high-order system.

and transmitting information is proposed to make it more convenient for implementation. Then, sufficient conditions for consensusability of multiagent systems consist of single integrator, second order, and high-order agents that are established, respectively, according to stochastic matrix theory and interval matrix theory. Finally, simulations are carried out to verify the theoretical results obtained. However, to reach the consensus for second and high-order systems with packet losses and communication delays, the directed communication topology is limited to a directed spanning tree. Even though this kind of structure has its own advantages in real-world applications, being convenient and economical, for

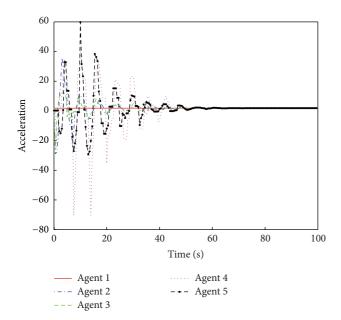


FIGURE 8: Consensus of acceleration for high-order system.

example, it also has some flaws in modeling the system with massive agents such as flock and fish school. Therefore, in the follow-up study of this research, the directed topology will not be limited to a directed spanning tree in order to make the whole system more distributive.

Conflict of Interests

The authors declare that they have no conflict of interests regarding the publication of this paper.

Acknowledgments

This work is supported by the National Natural Science Foundation of China (Grant nos. 5179038, 51109043, and 51309067) and New Century Excellent Talents in University of China (Grant no. NCET-10-0053).

References

- [1] K. Nagatani, Y. Okada, N. Tokunaga et al., "Multirobot exploration for search and rescue missions: a report on map building in RoboCupRescue 2009," *Journal of Field Robotics*, vol. 28, no. 3, pp. 373–387, 2011.
- [2] S. Zhang, J. Yu, A. Zhang, L. Yang, and Y. Shu, "Marine vehicle sensor network architecture and protocol designs for ocean observation," *Sensors*, vol. 12, no. 1, pp. 373–390, 2012.
- [3] S. Iyengar and R. Brooks, *Distributed Sensor Networks: Sensor Networking and Applications*, CRC Press, 2012.
- [4] R. Cui, S. S. Ge, B. Voon Ee How, and Y. Sang Choo, "Leader-follower formation control of underactuated autonomous underwater vehicles," *Ocean Engineering*, vol. 37, no. 17-18, pp. 1491–1502, 2010.
- [5] R. Olfati-Saber and R. M. Murray, "Consensus problems in networks of agents with switching topology and time-delays,"

- *IEEE Transactions on Automatic Control*, vol. 49, no. 9, pp. 1520–1533, 2004.
- [6] Y. Zhang and Y.-P. Tian, "Consensus of data-sampled multiagent systems with random communication delay and packet loss," *IEEE Transactions on Automatic Control*, vol. 55, no. 4, pp. 939–943, 2010.
- [7] W. Ni and D. Cheng, "Leader-following consensus of multiagent systems under fixed and switching topologies," *Systems and Control Letters*, vol. 59, no. 3-4, pp. 209–217, 2010.
- [8] Y. Cao and W. Ren, "Sampled-data discrete-time coordination algorithms for double-integrator dynamics under dynamic directed interaction," *International Journal of Control*, vol. 83, no. 3, pp. 506–515, 2010.
- [9] W. Ren and R. W. Beard, "Consensus seeking in multiagent systems under dynamically changing interaction topologies," *IEEE Transactions on Automatic Control*, vol. 50, no. 5, pp. 655– 661, 2005.
- [10] Y. Gao and L. Wang, "Consensus of multiple double-integrator agents with intermittent measurement," *International Journal of Robust and Nonlinear Control*, vol. 20, no. 10, pp. 1140–1155, 2010.
- [11] P. Lin, Z. Li, Y. Jia, and M. Sun, "High-order multi-agent consensus with dynamically changing topologies and timedelays," *IET Control Theory and Applications*, vol. 5, no. 8, pp. 976–981, 2011.
- [12] P. Lin and Y. Jia, "Consensus of second-order discrete-time multi-agent systems with nonuniform time-delays and dynamically changing topologies," *Automatica*, vol. 45, no. 9, pp. 2154– 2158, 2009.
- [13] Y. Liu, H. Min, S. Wang, Z. Liu, and S. Liao, "Distributed adaptive consensus for multiple mechanical systems with switching topologies and time-varying delay," *Systems & Control Letters*, vol. 64, pp. 119–126, 2014.
- [14] Y. Gao, J. Ma, M. Zuo, T. Jiang, and J. Duc, "Consensus of discrete-time second-order agents with time-varying topology and time-varying delays," *Journal of the Franklin Institute*, vol. 349, no. 8, pp. 2598–2608, 2012.
- [15] J. Zhu and L. Yuan, "Consensus of high-order multi-agent systems with switching topologies," *Linear Algebra and Its Applications*, vol. 443, pp. 105–119, 2014.
- [16] J. Almeida, C. Silverstre, and A. M. Pascoal, "Continuous time consensus with discrete time communications," *Systems & Control Letters*, vol. 61, no. 7, pp. 788–796, 2012.
- [17] J. Qin, H. Gao, and W. X. Zheng, "Consensus strategy for a class of multi-agents with discrete second-order dynamics," *International Journal of Robust and Nonlinear Control*, vol. 22, no. 4, pp. 437–452, 2012.
- [18] D. Goldin and J. Raisch, "Consensus for agents with double integrator dynamics in heterogeneous networks," *Asian Journal of Control*, vol. 15, no. 4, pp. 1–10, 2013.
- [19] G. Parlangeli, "Collaborative diagnosis and compensation of misbehaving nodes in acyclic consensus networks: analysis and algorithms," *International Journal of Innovative Computing Information and Control*, vol. 9, no. 3, pp. 915–938, 2009.
- [20] X. Su, L. Wu, Shi, and P.:, "Sensor networks with random link failures: distributed filtering for T-S fuzzy systems," *IEEE Transactions on Industrial Informatics*, vol. 9, no. 3, pp. 1739–1750, 2013.
- [21] X. Su, X. Yang, P. Shi, and L. Wu, "Fuzzy control of nonlinear electromagnetic suspension systems," *Mechatronics*, 2013.
- [22] X. Su, P. Shi, L. Wu, and Y.-D. Song, "A novel control design on discrete-time Takagi-Sugeno fuzzy systems with time-varying

- delays," *IEEE Transactions on Fuzzy Systems*, vol. 21, no. 4, pp. 655–671, 2013.
- [23] J. Yu and L. Wang, "Group consensus in multi-agent systems with switching topologies and communication delays," *Systems and Control Letters*, vol. 59, no. 6, pp. 340–348, 2010.
- [24] B. Iantovics and C. B. Zamfirescu, "ERMS: an evolutionary reorganizing multiagent system," *International Journal of Innovative Computing Information and Control*, vol. 9, no. 3, pp. 1171–1188, 2013.
- [25] L. Wu, X. Su, and P. Shi, "Sliding mode control with bounded L2 gain performance of Markovian jump singular time-delay systems," *Automatica*, vol. 48, no. 8, pp. 1929–1933, 2012.
- [26] R. A. Horn and C. R. Johnson, Matrix Analysis, Cambridge University Press, 2012.
- [27] J. Wolfowitz, "Products of indecomposable, aperiodic, stochastic matrices," *Proceedings of the American Mathematical Society*, vol. 14, no. 5, pp. 733–736, 1963.
- [28] F. Lewis, Cooperative Control of Multi-Agent Systems: Optimal and Adaptive Design Approaches, Springer, Berlin, Germany, 2013
- [29] A. Jadbabaie, J. Lin, and A. S. Morse, "Coordination of groups of mobile autonomous agents using nearest neighbor rules," *IEEE Transactions on Automatic Control*, vol. 48, no. 6, pp. 988–1001, 2003.
- [30] K. Wang, A. N. Michel, and D. Liu, "Necessary and sufficient conditions for the Hurwitz and Schur stability of interval matrices," *IEEE Transactions on Automatic Control*, vol. 39, no. 6, pp. 1251–1255, 1994.
- [31] X. Liao, Q. Luo, Z. Mei, and W. Hu, "Notes on necessary and sufficient conditions of stability, observability and controllability for interval matrices," *Acta Automatica Sinica*, vol. 24, no. 6, pp. 829–833, 1998.
- [32] D.-Q. Zhang, Q.-L. Zhang, and Y.-P. Chen, "Controllability and quadratic stability quadratic stabilization of discrete-time interval systems—an LMI approach," *IMA Journal of Mathematical Control and Information*, vol. 23, no. 4, pp. 413–431, 2006.

Hindawi Publishing Corporation Abstract and Applied Analysis Volume 2014, Article ID 869879, 11 pages http://dx.doi.org/10.1155/2014/869879

Research Article

Adaptive Predictive Control: A Data-Driven Closed-Loop Subspace Identification Approach

Xiaosuo Luo^{1,2} and Yongduan Song¹

¹ School of Automation, Chongqing University, Chongqing 400044, China

Correspondence should be addressed to Yongduan Song; ydsong@cqu.edu.cn

Received 13 January 2014; Accepted 13 February 2014; Published 1 April 2014

Academic Editor: Peng Shi

Copyright © 2014 X. Luo and Y. Song. This is an open access article distributed under the Creative Commons Attribution License, which permits unrestricted use, distribution, and reproduction in any medium, provided the original work is properly cited.

This paper presents a data-driven adaptive predictive control method using closed-loop subspace identification. As the predictor is the key element of the predictive controller, we propose to derive such predictor based on the subspace matrices which are obtained through the closed-loop subspace identification algorithm driven by input-output data. Taking advantage of transformational system model, the closed-loop data is effectively processed in this subspace algorithm. By combining the merits of receding window and recursive identification methods, an adaptive mechanism for online updating subspace matrices is given. Further, the data inspection strategy is introduced to eliminate the negative impact of the harmful (or useless) data on the system performance. The problems of online excitation data inaccuracy and closed-loop identification in adaptive control are well solved in the proposed method. Simulation results show the efficiency of this method.

1. Introduction

With the development of industrial technology, the industrial processes become more complex than before and it is more difficult to build the accurate mechanism models of these processes. Hence, the data-driven approach has obtained widespread attention since it emerged. Data-driven control also turns into focus of study. Simply, the data-driven control is a method from data to design controller directly [1, 2]. Model predictive control (MPC) has been attractive for decades in control theory field. It has become more established as the one of the choices for the control architecture in the industry, especially with the improvement of computational capabilities of processors [3-8]. But one drawback of the traditional industrial predictive control is based on inputoutput model, including parametric and nonparametric ones. In order to improve the control performance, a state-space model should be adopted, so the modern filter theory and the design method of controller developed in recent years can play a role [9]. Subspace identification is one of the system identification algorithms for state-space modeling. The control workers may relieve completely from the tedious mechanism modeling and the accurate state-space model can be obtained when there is enough process input-output data [10–12]. More attractively, the subspace matrices obtained through the subspace identification algorithm can be used to derive the predictor of predictive controllers, eliminating the intermediate step of process model identification and providing a method of data-driven predictive control [13]. This method has been applied in some industrial processes and achieved good results.

Most data-driven predictive controllers are designed based on open-loop subspace identification, but in practice it is often necessary to perform identification experiments on systems operating in closed-loop. This is especially true when open-loop experiments are not allowed due to safety (unstable processes) or production (undesirable open-loop behavior) reasons [14]. It is found that the regular open-loop subspace identification algorithm yields a biased estimate

² Chongqing College of Electronic Engineering, Chongqing 401331, China

when applied to closed-loop data [15]. The closed-loop data-driven predictive control methods in [16, 17] have been presented. But the predictor is derived with the estimated Markov parameters which lead to a complicated predictor. We get a simple predictor constructed by subspace matrices. Jansson [18] developed a subspace method that can perform well on data collected both in open- and closed-loop conditions.

It is a major problem to implement adaptive control in closed-loop system. In this paper, based on the subspace prediction model derived from [18], we design a closed-loop data-driven predictive controller to solve this problem that obtains subspace matrices simply from Hankel matrices for a better implementation of the following adaptive mechanism in closed-loop system.

The control performance of predictive control is dependent on the model quality [19]. The linear fixed model is used to design the controller in conventional data-driven predictive control method. It is applied to a linear system showed good results in a short period. But there are nonlinear and time-varying characteristics of long period in industrial processes, resulting in a poor performance when using the fixed model. It is highly desirable to implement adaptive mechanism to adjust the system model online. The feature of subspace identification is suitable for designing adaptive predictive controller perfectly. The adaptive mechanism is realized by online updating subspace matrices. At present, there are two ways of online adaptive subspace identification [20]. One is recursive identification method; by using different weighting to the new and old data, the variation of the process is tracked. The size of modeling data set will become larger with the process operation which needs enough memory storage. The other one is receding window method; the size of modeling data set remains unchanged and the oldest data is removed at the arriving of the new data. It is unfavorable that the harmless (or useless) data will increase information missing in the whole window and the computation time is longer than recursive one [21]. The recursive adaptive predictive control method is shown in [22, 23]; in [22] an adaptive predictive control strategy based on recursive subspace identification has been presented, adopting the prediction model with the smallest matching error. Mardi and Wang [23] presented an approach to constrained subspace-based MPC of time-varying systems. The central ideas are to find the predictive control law recursively using a subspace identification technology and to update the control law once a plant-model mismatch is detected. Although both of them consider the forgetting factor to weaken the negative impact of the old data on the identification model, the identification accuracy will be declined as the old data more or less. Accordingly, we can find the receding window method in [24, 25]. Yang and Li [24] designed a subspacebased predictive controller, using receding window method to update subspace matrices at each time step for adaptive mechanism. Wahab et al. [25] proposed a direct adaptive MPC method which requires a single QR decomposition for obtaining the controller parameters and uses a receding horizon approach to process input-output data for the identification. These two methods require QR decomposition at

every time instant which increase the computational load and have incapability of handling harmless (or useless) data that bring performance degradation. Only one way of online adaptive subspace identification is employed in the above adaptive predictive control methods. We have been trying to combine the two ways, in our previous work [26]; an adaptive mechanism through online updating of the R matrix is proposed. By comparing the prediction error before and after updating, we consider whether or not to update the prediction model. This method employs a recursive strategy to derive *R* matrix but it requires us to compute every element value of *R* matrix that increases the computation time. The model inspection can bring a promotion in harmless (or useless) data suppression but it cannot eliminate the harmless (or useless) data. Kameyama et al. [27] derived a recursive subspace-based identification algorithm with fixed inputoutput data size. It only solves the identification problem. We get the online updated subspace matrices from partial results in [27] but stress the derivation of the key elements of *R* matrix which can reduce the computation time compared to the method in [26] and extend it to design the predictive controller. Another major problem to implement adaptive control is the inaccuracy of online excitation data. When the model or system parameters change, it needs to be adequately excited. Otherwise, some of the obtained data become harmless (or useless) ones which have a negative impact on system performance. The data inspection strategy introduced is a good solution for this problem through comparing the prediction error.

The main contribution of the paper is the development of a new solution of data-driven adaptive predictive control ensuring adaptation of closed-loop systems. The method can offer an attractive alternative for industrial nonlinear, timevarying systems of long period in closed-loop condition and there is no need for obtaining the system explicit model which can reduce the complexity. Through transforming system model form, the closed-loop subspace identification algorithm is developed and the subspace matrices are obtained from the closed-loop data. The adaptive mechanism is implemented by combining the advantages of receding window and recursive identification methods. The subspace matrices are derived by recursive method using a fixed modest size of data set with receding window method. The proposed mechanism can sufficiently fade the influence of the old data better than only recursive method and bring less computation load than only receding window method. By comparing the prediction error before and after updating, we consider whether or not to add the new data in data inspection strategy. The purpose of the strategy is to eliminate the new arrival of harmful (or useless) data produced by the online insufficient excitation. The control performance is superior to adopt open-loop identification and other methods of data-driven adaptive predictive control.

The paper is organized as follows. In Section 2 the open-loop data-driven predictive control method is given. Section 3 provides the closed-loop data-driven predictive control method. The adaptive mechanism is highlighted in Section 4. Some simulation results are presented and discussed in Section 5. Section 6 gives the conclusions.

2. Open-Loop Data-Driven Predictive Control

Consider a discrete state-space system of order n described by innovations form

$$x_{k+1} = Ax_k + Bu_k + Ke_k,$$

$$y_k = Cx_k + Du_k + e_k,$$
(1)

where $u_k \in \mathbb{R}^m$, $y_k \in \mathbb{R}^l$, and $x_k \in \mathbb{R}^n$ are input, output, and state vectors, respectively. K is the Kalman filter gain and $e_k \in \mathbb{R}^l$ is an innovation sequence where variance $E(e_k e_k^T) = S$. (A, B, C, D) are system matrices of appropriate dimensions and S is the innovations covariance matrix.

Construct the inputs block Hankel matrices using the data of u_k with $k \in \{1, 2, ..., N\}$ at instant t:

$$U_{p} = \begin{bmatrix} u_{1} & u_{2} & \cdots & u_{N-f-p+1} \\ u_{2} & u_{3} & \cdots & u_{N-f-p+1} \\ \vdots & \vdots & \ddots & \vdots \\ u_{p} & u_{p+1} & \cdots & u_{N-f} \end{bmatrix},$$

$$U_{f} = \begin{bmatrix} u_{p+1} & u_{p+2} & \cdots & u_{N-f+1} \\ u_{p+2} & u_{p+3} & \cdots & u_{N-f+2} \\ \vdots & \vdots & \ddots & \vdots \\ u_{p+f} & u_{p+f+1} & \cdots & u_{N} \end{bmatrix},$$

$$(2)$$

where the subscripts p and f represent the "past" and "future" time. Similarly, the outputs and noise Hankel matrices Y_p, Y_f, E_p , and E_f can also be obtained in the same way. The system past and future state sequences are defined as

$$X_p = [x_1 \ x_2 \ \cdots \ x_{N-f-p+1}],$$

 $X_f = [x_{p+1} \ x_{p+2} \ \cdots \ x_{N-f+1}].$ (3)

The subspace prediction expression of the outputs can be derived by recursive substitution of (1):

$$Y_f = \Gamma X_f + H U_f + H^s E_f, \tag{4}$$

where $\Gamma \in \mathbb{R}^{fl \times n}$ is the extended observability matrix and $H \in \mathbb{R}^{fl \times fm}$ and $H^s \in \mathbb{R}^{fl \times fl}$ are the low triangular Toeplitz matrices, respectively, denoted by

$$\Gamma = \begin{bmatrix} C \\ CA \\ \vdots \\ CA^{f-1} \end{bmatrix}, \qquad H = \begin{bmatrix} D & 0 & \cdots & 0 \\ CB & D & \ddots & \vdots \\ \vdots & \ddots & \ddots & 0 \\ CA^{f-2}B & \cdots & CB & D \end{bmatrix},$$

$$H^{S} = \begin{bmatrix} I_{l} & 0 & \cdots & 0 \\ CK & I_{l} & \ddots & \vdots \\ \vdots & \ddots & \ddots & 0 \\ CA^{f-2}K & \cdots & CK & I \end{bmatrix}.$$

$$(5)$$

The optimal prediction of Y_f can be written as

$$\widehat{Y}_f = L_w W_p + L_u U_f, \tag{6}$$

where W_p denotes the past input-output data matrix as $W_p = [Y_p^T \quad U_p^T]^T$, L_w is the subspace matrix that corresponds to the past input-output data, and L_u is the subspace matrix that corresponds to the future input data.

In order to calculate the subspace matrices L_w and L_u from block Hankel matrices, by solving the following least squares problem:

$$\min_{L_w, L_u} \left\| Y_f - (L_w, L_u) \begin{pmatrix} W_p \\ U_f \end{pmatrix} \right\|_F^2, \tag{7}$$

where $\|\cdot\|_F$ represents the Frobenius norm, the solution can be found from the orthogonal projection of the row space of Y_f onto the row space of the matrix $\binom{W_p}{U_f}$:

$$\widehat{Y}_f = \frac{Y_f}{\binom{W_p}{U_f}},\tag{8}$$

where / denotes the orthogonal projection. The solution for (8) can be done in an efficient way by performing a *QR*-decomposition:

$$\begin{bmatrix} W_p \\ U_f \\ Y_f \end{bmatrix} = R^T Q^T = \begin{bmatrix} R_{11} & 0 & 0 \\ R_{21} & R_{22} & 0 \\ R_{31} & R_{32} & R_{33} \end{bmatrix} \begin{bmatrix} Q_1^T \\ Q_2^T \\ Q_3^T \end{bmatrix}, \tag{9}$$

where R is a low triangular matrix and Q is an orthogonal matrix. By letting

$$L = \begin{bmatrix} R_{31} & R_{32} \end{bmatrix} \begin{bmatrix} R_{11} & 0 \\ R_{21} & R_{22} \end{bmatrix}^{\dagger}, \tag{10}$$

with

$$L = \begin{bmatrix} L_w & L_u \end{bmatrix}, \tag{11}$$

where superscript † represents the Moore-Penrose pseudoinverse and $L_w \in \mathbb{R}^{fl \times p(m+l)}$, $L_u \in \mathbb{R}^{fl \times fm}$.

The model predictive control problem is realized by the minimization of a cost function. A typical form of cost function in MPC is given as follows:

$$J = \sum_{k=1}^{N_p} (\widehat{y}_{t+k} - r_{t+k})^T G_Q (\widehat{y}_{t+k|t} - r_{t+k}) + \sum_{k=1}^{N_c} \Delta u_{t+k-1}^T G_R \Delta u_{t+k-1},$$
(12)

where r_t is the reference setpoint signal at the current time t, G_Q and G_R are the weight matrices, and N_p and N_c are the prediction and control horizon, respectively. N_p and N_c are defined as being equal to f, and (12) can be rewritten as

$$J = (\hat{y}_f - r_f)^T G_O(\hat{y}_f - r_f) + \Delta u_f^T G_R \Delta u_f.$$
 (13)

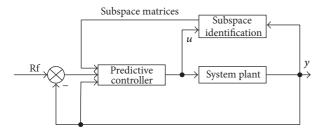


FIGURE 1: The structure of closed-loop data-driven predictive control.

In MPC framework, only the leftmost column is used to predict output. And to avoid steady-state error, the predictor of predictive controllers can be written in terms of incremental Δw_p and Δu_f as follows:

$$\widehat{y}_f = F_l y_t + \Gamma_l L_w \Delta w_p + \Gamma_l L_u \Delta u_f, \tag{14}$$

where

$$F_{l} = \begin{bmatrix} I_{l}^{T} & \cdots & I_{l}^{T} \end{bmatrix}^{T}, \qquad \Gamma_{l} = \begin{bmatrix} I_{l} & 0 & \cdots & 0 \\ I_{l} & I_{l} & \cdots & 0 \\ \vdots & \vdots & \ddots & \vdots \\ I_{l} & I_{l} & \cdots & I_{l} \end{bmatrix},$$

$$\Delta u_{f} = \begin{bmatrix} \Delta u_{t}^{T} & \Delta u_{t+1}^{T} & \cdots & \Delta u_{t+f-1}^{T} \end{bmatrix}^{T},$$

$$\Delta w_{p} = \begin{bmatrix} \Delta y_{t-p+1}^{T} & \cdots & \Delta y_{t}^{T} & \Delta u_{t-p}^{T} & \cdots & \Delta u_{t-1}^{T} \end{bmatrix}^{T}.$$
(15)

Using (14) in the minimization of cost function *J* of (13), the control sequence can be obtained as follows:

$$\Delta u_f = -\left(\left(\Gamma_l L_u\right)^T G_Q \left(\Gamma_l L_u\right) + G_R\right)^{-1} \times \left(\Gamma_l L_u\right)^T G_Q \left(\Gamma_l L_w \Delta w_p + F_l \left(y_t - r_t\right)\right).$$
(16)

At each time instance, only the first element of Δu_f is used for calculating the control input. Therefore the control input u_t is drawn as

$$u_t = u_{t-1} + \Delta u_t. \tag{17}$$

At the next instant, when the new input-output data arrive, the same optimization is repeated. The above results can also be seen in [28–32]. In the above objectives, subspace matrices are identified using the open-loop data and applied to the open-loop system suitably. But, in closed-loop system, as the data correlations due to feedback, above identification algorithm will result in a less accurate model and it will lead to degradation in control performance. To overcome the drawback, a closed-loop data-driven predictive control method is given in Section 3.

3. Closed-Loop Data-Driven Predictive Control

The structure of closed-loop data-driven predictive control method is shown in Figure 1.

In order to use the closed-loop structure of the subspace identification technique, the necessary steps are presented. Firstly, transform the system model in (1); define

$$\widetilde{A} = A - KC,$$

$$\widetilde{B} = B - KD.$$
(18)

It is well known that we can rewrite system model form as follows:

$$x_{k+1} = \widetilde{A}x_k + \widetilde{B}u_k + Ky_k,$$

$$y_k = Cx_k + Du_k + e_k.$$
(19)

The prediction model can be represented as the subspace expression:

$$Y_f = \widetilde{\Gamma} X_f + \widetilde{H} U_f + \widetilde{H}^s Y_f + E_f, \tag{20}$$

where

$$\widetilde{\Gamma} = \begin{bmatrix} C \\ C\widetilde{A} \\ \vdots \\ C\widetilde{A}^{f-1} \end{bmatrix}, \qquad \widetilde{H} = \begin{bmatrix} D & 0 & \cdots & 0 \\ C\widetilde{B} & D & \cdots & 0 \\ \vdots & \vdots & \ddots & \vdots \\ C\widetilde{A}^{f-2}\widetilde{B} & C\widetilde{A}^{f-3}\widetilde{B} & \cdots & D \end{bmatrix},$$

$$\widetilde{G} = \begin{bmatrix} 0 & 0 & \cdots & 0 \\ CK & 0 & \cdots & 0 \\ \vdots & \vdots & \ddots & \vdots \\ C\widetilde{A}^{f-2}K & C\widetilde{A}^{f-3}K & \cdots & 0 \end{bmatrix}.$$
(21)

Next, it's directly to obtain the system state-space model in previous paper [18]. But in this paper, we focus on the derivation of subspace matrices to implement data-driven predictive control. Equation (20) can be rewritten as

$$\widetilde{Y}_f = \widetilde{\Gamma} X_f + \widetilde{H} U_f + E_f, \tag{22}$$

where $\widetilde{Y}_f = (I - \widetilde{H}^s)Y_f$ and I is the appropriate identity matrix. \widetilde{Y}_f can be denoted by constituting the subspace matrices as follows:

$$\widetilde{Y}_f = \widetilde{L}_w X_f + \widetilde{L}_u U_f + E_f. \tag{23}$$

The intermediate subspace matrices \widetilde{L}_w and \widetilde{L}_u are provided by the least squares problem:

$$\begin{bmatrix} \widetilde{L}_w & \widetilde{L}_u \end{bmatrix} = \arg \min_{\widetilde{L}_w, \widetilde{L}_u} \left\| \widetilde{Y}_f - (\widetilde{L}_w, \widetilde{L}_u) \begin{pmatrix} W_p \\ U_f \end{pmatrix} \right\|_F^2. \tag{24}$$

The solution procedure is similar to the derivation of L_w and L_u in Section 2. Therefore, the closed-loop subspace matrices \overline{L}_w and \overline{L}_u can be calculated as

$$\overline{L}_{w} = \left(I - \widetilde{H}^{s}\right)^{-1} \widetilde{L}_{w},
\overline{L}_{u} = \left(I - \widetilde{H}^{s}\right)^{-1} \widetilde{L}_{u}.$$
(25)

We use incremental form to denote the predictor:

$$\widehat{y}_f = F_l y_t + \Gamma_l \overline{L}_w \Delta w_p + \Gamma_l \overline{L}_u \Delta u_f. \tag{26}$$

So the control sequence becomes

$$\Delta u_f = -\left(\left(\Gamma_l \overline{L}_u\right)^T G_Q \left(\Gamma_l \overline{L}_u\right) + G_R\right)^{-1} \times \left(\Gamma_l \overline{L}_u\right)^T G_Q \left(\Gamma_l \overline{L}_w \Delta w_p + F_l \left(y_t - r_t\right)\right), \qquad (27)$$

$$\Delta u_t = \begin{bmatrix} I_1 & 0 & \cdots & 0 \end{bmatrix} \Delta u_f,$$

where I_1 is an identity matrix of size 1. The control input is

$$u_t = u_{t-1} + \Delta u_t. \tag{28}$$

At the next time step, measuring the new input-output data and the new control input will be calculated using the above optimization.

The above method relies on transforming system model form for reducing the impact of the noise sequence E_f on input sequence U_f greatly. It can be applied in closed-loop system but also is suitable for open-loop system.

4. Adaptive Mechanism

The linear fixed model is used to design the controller in traditional data-driven predictive control. But, in industrial processes, in presence of nonlinear and time-varying characteristics, the control performance is difficult to achieve the desired control effect and it will cause great mismatch of the model. Therefore, the adaptive control methods, updating the model online according to the conditions, have been attractive for decades and gradually applied to industrial processes. The adaptive predictive control, one of the adaptive methods, also has achieved a number of applications [33]. In this paper, an adaptive predictive control method is presented. Drawing the advantages of the receding window approach, the size of window is maintained as modest a priori while the recursive approach is used for updating the model. Additionally, due to the system disturbance and noise, a larger match error will be produced between the test data with the real time data at some time when the model or system parameters change. Such data is referred to as the harmful (or useless) data. A data inspection strategy is suggested to use the 1-step output prediction error for filtering the harmful (or useless) data and eliminating the negative impact on the system of the harmful (or useless) data. Then, updating the subspace matrices online and implementing the adaptive mechanism are done.

The subspace matrices are obtained from *R* matrix, so we update the *R* matrix online using recursive method; then the prediction model can be obtained to calculate the control input.

Let $A^* \in \mathbb{R}^{2(p+f)(m+l)\times(N-f-p+1)}$ be the input-output Hankel matrix at instant t as

$$A^* = \begin{bmatrix} W_p^T(t) & U_f^T(t) & Y_f^T(t) \end{bmatrix}^T,$$
 (29)

where $W_p(t)$, $U_f(t)$, and $Y_f(t)$ are the past input-output data matrix, future input data matrix, and future output data matrix, respectively, in closed-loop system. The oldest column of A^* is defined as $b = \begin{bmatrix} w_p^T(1) & u_f^T(1) & y_f^T(1) \end{bmatrix}^T$, where

$$w_{p}(1) = \begin{bmatrix} y_{p}^{T}(1) & u_{p}^{T}(1) \end{bmatrix}^{T}$$

$$= \begin{bmatrix} y_{1}^{T} & \cdots & y_{p}^{T} & u_{1}^{T} & \cdots & u_{p}^{T} \end{bmatrix}^{T},$$

$$u_{f}(1) = \begin{bmatrix} u_{p+1}^{T} & u_{p+2}^{T} & \cdots & u_{p+f}^{T} \end{bmatrix}^{T},$$

$$y_{f}(1) = \begin{bmatrix} y_{p+1}^{T} & y_{p+2}^{T} & \cdots & y_{p+f}^{T} \end{bmatrix}^{T}.$$
(30)

Given a set of new input-output data $c = \begin{bmatrix} w_P^T(t+1) & u_f^T(t+1) & y_f^T(t+1) \end{bmatrix}^T$ at instant t+1, where

$$w_{p}(1) = \begin{bmatrix} y_{p}^{T}(t+1) & u_{p}^{T}(t+1) \end{bmatrix}^{T}$$

$$= \begin{bmatrix} y_{N-f-p+2}^{T} & \cdots & y_{N-f+1}^{T} & u_{N-f-p+2}^{T} & \cdots & u_{N-f+1}^{T} \end{bmatrix}^{T},$$

$$u_{f}(t+1) = \begin{bmatrix} u_{N-f+2}^{T} & u_{N-f+3}^{T} & \cdots & u_{t+1}^{T} \end{bmatrix}^{T},$$

$$y_{f}(t+1) = \begin{bmatrix} y_{N-f+2}^{T} & y_{N-f+3}^{T} & \cdots & y_{t+1}^{T} \end{bmatrix}^{T}.$$
(31)

The input-output Hankel matrix D^* at instant t + 1 is defined as

$$A^* = \begin{bmatrix} W_P^T(t) & U_f^T(t) & Y_f^T(t) \end{bmatrix}^T, \tag{32}$$

where $W_p(t+1)$, $U_f(t+1)$, and $Y_f(t+1)$ are similar to the definitions of $W_p(t)$, $U_f(t)$, and $Y_f(t)$.

In order to maintain the size of receding window constant, it is necessary to exclude b from A^* and add c to A^* .

So we can get the relation as $[A^* \ \vdots \ c] = [b \ \vdots \ D^*]$; then the relation $[A^* \ \vdots \ c][A^* \ \vdots \ c]^T = [b \ \vdots \ D^*][b \ \vdots \ D^*]^T$ gives

$$A^*A^{*T} + cc^T = bb^T + D^*D^{*T}. (33)$$

The QR decomposition of A^* is

$$A^* = R^T(t) Q^T(t) = \begin{bmatrix} R_{11}(t) & 0 & 0 \\ R_{21}(t) & R_{22}(t) & 0 \\ R_{31}(t) & R_{32}(t) & R_{33}(t) \end{bmatrix} \begin{bmatrix} Q_1^T(t) \\ Q_2^T(t) \\ Q_3^T(t) \end{bmatrix}$$

$$= \begin{bmatrix} R_{11}(t)Q_{1}^{T}(t) \\ R_{21}(t)Q_{1}^{T}(t) + R_{22}(t)Q_{2}^{T}(t) \\ R_{31}(t)Q_{1}^{T}(t) + R_{32}(t)Q_{2}^{T}(t) + R_{33}(t)Q_{3}^{T}(t) \end{bmatrix}.$$
(34)

The objective is to get the results from the QR decomposition of D^* :

$$D^* = R^T (t+1) Q^T (t+1)$$

$$= \begin{bmatrix} R_{11} (t+1) Q_1^T (t+1) & & \\ R_{21} (t+1) Q_1^T (t+1) + R_{22} (t+1) Q_2^T (t+1) & & \\ R_{31} (t+1) Q_1^T (t+1) + R_{32} (t+1) Q_2^T (t+1) + R_{33} (t+1) Q_3^T (t+1) \end{bmatrix}.$$
(35)

From (34)-(35), we have

$$\begin{split} A^*A^{*T} + cc^T \\ &= \begin{bmatrix} R_{11}\left(t\right)R_{11}^T\left(t\right) & R_{11}\left(t\right)R_{21}^T\left(t\right) & R_{11}\left(t\right)R_{31}^T\left(t\right) \\ R_{21}\left(t\right)R_{11}^T\left(t\right) & R_{21}\left(t\right)R_{21}^T\left(t\right) + R_{22}\left(t\right)R_{22}^T\left(t\right) & R_{21}\left(t\right)R_{31}^T\left(t\right) + R_{22}\left(t\right)R_{32}^T\left(t\right) \\ R_{31}\left(t\right)R_{11}^T\left(t\right) & R_{31}\left(t\right)R_{21}^T\left(t\right) + R_{32}\left(t\right)R_{22}^T\left(t\right) & R_{31}\left(t\right)R_{31}^T\left(t\right) + R_{32}\left(t\right)R_{32}^T\left(t\right) + R_{33}\left(t\right)R_{33}^T\left(t\right) \\ &+ \begin{bmatrix} w_p\left(t+1\right)w_p^T\left(t+1\right) & w_p\left(t+1\right)u_f^T\left(t+1\right) & w_p\left(t+1\right)y_f^T\left(t+1\right) \\ u_f\left(t+1\right)w_p^T\left(t+1\right) & u_f\left(t+1\right)u_f^T\left(t+1\right) & u_f\left(t+1\right)y_f^T\left(t+1\right) \\ y_f\left(t+1\right)w_p^T\left(t+1\right) & y_f\left(t+1\right)u_f^T\left(t+1\right) & y_f\left(t+1\right)y_f^T\left(t+1\right) \end{bmatrix}, \end{split}$$

$$bb^T + D^*D^{*T}$$

$$=\begin{bmatrix} w_{p}\left(1\right)w_{p}^{T}\left(1\right) & w_{p}\left(1\right)u_{f}^{T}\left(1\right) & w_{p}\left(1\right)y_{f}^{T}\left(1\right) \\ u_{f}\left(1\right)w_{p}^{T}\left(1\right) & u_{f}\left(1\right)u_{f}^{T}\left(1\right) & u_{f}\left(1\right)y_{f}^{T}\left(1\right) \\ y_{f}\left(1\right)w_{p}^{T}\left(1\right) & y_{f}\left(1\right)u_{f}^{T}\left(1\right) & y_{f}\left(1\right)y_{f}^{T}\left(1\right) \end{bmatrix} \\ + \begin{bmatrix} R_{11}\left(t+1\right)R_{11}^{T}\left(t+1\right) & R_{11}\left(t+1\right)R_{21}^{T}\left(t+1\right) & R_{11}\left(t+1\right)R_{31}^{T}\left(t+1\right) \\ R_{21}\left(t+1\right)R_{11}^{T}\left(t+1\right) & R_{21}\left(t+1\right)R_{22}^{T}\left(t+1\right) + R_{22}\left(t+1\right)R_{22}^{T}\left(t+1\right) \\ R_{31}\left(t+1\right)R_{11}^{T}\left(t+1\right) & R_{31}\left(t+1\right)R_{31}^{T}\left(t+1\right) + R_{32}\left(t+1\right)R_{33}^{T}\left(t+1\right) + R_{32}\left(t+1\right)R_{33}^{T}\left(t+1\right) + R_{33}\left(t+1\right)R_{33}^{T}\left(t+1\right) + R_{34}\left(t+1\right)R_{34}^{T}\left(t+1\right) + R_{34}\left(t+$$

From (33), firstly, we can get the first element $R_{11}(t+1)$ of R(t+1):

$$R_{11}(t+1)R_{11}^{T}(t+1) = R_{11}(t)R_{11}^{T}(t) + w_{p}(t+1)w_{p}^{T}(t+1) - w_{p}(1)w_{p}^{T}(1),$$

$$= R_{11}(t)R_{11}^{T}(t) + w_{p}(t+1)w_{p}^{T}(t+1) - w_{p}(1)w_{p}^{T}(1),$$

$$(37)$$

$$R_{22}(t+1) = \operatorname{chol}\left(R_{21}(t)R_{21}^{T}(t) + R_{22}(t)R_{22}^{T}(t) + R_{21}(t+1)u_{p}^{T}(t+1) - u_{p}(t+1)u_{p}^{T}(t+1) - u_{p}(t+1)u_{p}^{T}(t+1)\right),$$

$$-w_{p}(1)w_{p}^{T}(1),$$

$$(38)$$

$$R_{22}(t+1) = \operatorname{chol}\left(R_{21}(t)R_{21}^{T}(t) + R_{22}(t)R_{22}^{T}(t) + R_{21}(t+1)u_{p}^{T}(t+1)\right),$$

$$-R_{21}(t+1)R_{21}^{T}(t+1),$$

$$(38)$$

$$R_{22}(t+1) = \operatorname{chol}\left(R_{21}(t)R_{21}^{T}(t) + R_{21}(t)R_{21}^{T}(t) + R_{22}(t)R_{22}^{T}(t)\right),$$

where chol is Cholesky factorization [34]. The subspace matrices are obtained from R matrix as in (10), so we just calculate the elements required in R(t + 1):

$$R_{21}(t+1) = \left[R_{21}(t)R_{11}^{T}(t) + u_f(t+1)w_p^{T}(t+1)\right]$$

$$-u_{f}(1) w_{p}^{T}(1) \left[R_{11}^{T}(t+1) \right]^{-1},$$

$$R_{31}(t+1) = \left[R_{31}(t) R_{11}^{T}(t) + y_{f}(t+1) w_{p}^{T}(t+1) - y_{f}(1) w_{p}^{T}(1) \right] \left[R_{11}^{T}(t+1) \right]^{-1},$$

$$R_{22}(t+1) = \operatorname{chol} \left(R_{21}(t) R_{21}^{T}(t) + R_{22}(t) R_{22}^{T}(t) + u_{f}(t+1) u_{f}^{T}(t+1) - u_{f}(1) u_{f}^{T}(1) - R_{21}(t+1) R_{21}^{T}(t+1) \right),$$

$$R_{32}(t+1) = \left[R_{31}(t) R_{21}^{T}(t) + R_{32}(t) R_{22}^{T}(t) + y_{f}(t+1) u_{f}^{T}(t+1) - y_{f}(1) u_{f}^{T}(1) - R_{31}(t+1) R_{21}^{T}(t+1) \right] \left[R_{22}^{T}(t+1) \right]^{-1}.$$

$$(39)$$

Substituting (38) and (39) into (10), the subspace matrices at instant t + 1 can be derived by

$$\begin{split} \left[L_{w}\left(t+1\right) \;\; L_{u}\left(t+1\right)\right] \\ &= \left[R_{31}\left(t+1\right) \;\; R_{32}\left(t+1\right)\right] \begin{bmatrix} R_{11}(t+1) & 0 \\ R_{21}(t+1) & R_{22}(t+1) \end{bmatrix}^{\dagger}. \end{split} \tag{40}$$

By this way, the subspace matrices can be obtained through the above method; then the predictor will be calculated using (14) in open-loop system and (26) in closed-loop system. So we can get the control input at instant t+1. At the next time, repeat the above procedure to implement the online adaptive mechanism and it will result in a quicker response to process changes.

In presence of noise and online disturbance, it would result in an inaccurate identification precision and an unneglectable match error as the presence of the harmful (or useless) data in the online excitation. In our previous work [26], an inspection strategy of model precession was proposed, but it cannot eliminate the negative impact of harmful (or useless) data on system performance. In this paper, a data inspection strategy introduced is the use of prediction error to remove the harmful (or useless) data.

Calculate the following prediction error before adding new data:

$$e_{t+1|t} = |\widehat{y}_{t+1|t} - y_{t+1}|, \tag{41}$$

where y_{t+1} is the process output at t+1 time and $\hat{y}_{t+1|t}$ is the predictive output at t time predicting t+1 time before adding new data.

Similarly, the prediction error after adding new data can be also introduced:

$$e'_{t+1|t} = \left| \hat{y}'_{t+1|t} - y_{t+1} \right|,$$
 (42)

where $\hat{y}'_{t+1|t}$ is the output at t time predicting t+1 time after adding new data.

While $e_{k+1|k} \leq e'_{k+1|k}$, the new data is a harmful (or useless) one, so maintain R matrix and the system model invariably. Inversely, while $e_{k+1|k} > e'_{k+1|k}$, use the new data to update the R matrix and predictor. At the next sampling time, when the new data arrives, recycle the above progress.

For the sake of clarity, the proposed adaptive mechanism implemented in the closed-loop data-driven predictive controller is summarized in Algorithm 1.

5. Simulation Examples

In this section, a SISO (single input single output) example and a MIMO (multiple input multiple output) example identified and controlled by the proposed method are presented and discussed as follows.

Remark 1. The data used were preprocessed with the methods in Section 14 of [35].

TABLE 1: The prediction errors of open-loop and closed-loop identified hair dryer models.

Identified method	Open-loop	Closed-loop
Prediction error	15.6561	8.6039

5.1. A Hair Dryer Example. This hair dryer system is a simple mechanical device. The input u is the power of the heating device, which is a mesh of resistor wires. The output T is the outlet air temperature, which can be measured by thermocouple. Air is fanned through a tube and heated at the inlet. The details can be seen in [35]. In this example, we operated in case of closed-loop system. u was chosen to be a binary random signal shifting between 35 W and 65 W. The length of samples and sampling time were set to 1000 and 0.2 s, respectively. Firstly, totally 100 samples were used to verify the identification accuracy. The comparisons in Figure 2 show the response of the identified model and process output using open-loop data-driven predictive control (ODPC) in Section 1 and closed-loop data-driven predictive control (CDPC) in Section 2, where "Rf" is process output, "open-loop" is open-loop identified model, and "closed-loop" is closed-loop identified model.

To test the cross-validation in Figure 2, a form of prediction error in [10] is given as

$$\varepsilon = 100 \frac{1}{l} \sum_{c=1}^{l} \left[\sqrt{\frac{\sum_{k=1}^{N} \left((y_k)_c - (y_k^p)_c \right)^2}{\sum_{k=1}^{N} \left((y_k)_c \right)^2}} \right] \%, \quad (43)$$

where y_k and y_k^p are the values at instant k of process and model output, respectively. Table 1 illustrates the prediction errors of open-loop and closed-loop identified models.

The cross-validation results indicate that the closed-loop model is more accurate than open-loop model. Then, the system is given a performance of desired output changes to track using ODPC and CDPC. The sample N was set to 1000 and the sampling time t used was 0.2 s. The tuning parameters used in this simulation were p=f=3, $Q=I_3$, and $R=0.16*I_3$. Figure 3 depicts the output T tracking performance. It can be seen that CDPC shows the favorable control performance and has a better tracking ability compared to ODPC.

In order to verify the adaptive mechanism in Section 4, the model of closed-loop identification was identified as a state-space model:

$$A = \begin{bmatrix} 0.9398 & 0.1275 \\ -0.3046 & 0.8897 \end{bmatrix}, \qquad B = \begin{bmatrix} -0.0019 \\ -0.0721 \end{bmatrix},$$

$$C = \begin{bmatrix} -41.9003 \\ 5.5421 \end{bmatrix}, \qquad D = [0.1157].$$
(44)

We changed the system model at t = 600 as

$$A = \begin{bmatrix} 1.1762 & -0.1275 \\ -0.3046 & 0.8897 \end{bmatrix}, \qquad B = \begin{bmatrix} -0.0019 \\ -0.0721 \end{bmatrix},$$

$$C = \begin{bmatrix} -41.9003 \\ 5.5421 \end{bmatrix}, \qquad D = \begin{bmatrix} 0.1157 \end{bmatrix}.$$
(45)

- (1) Construct the block Hankel matrices from the closed-loop data.
- (2) Obtain the intermediate subspace matrices \tilde{L}_w and \tilde{L}_u by solving the least squares problem (24).
- (3) Compute the closed-loop subspace matrices \overline{L}_w and \overline{L}_u using (25).
- (4) Derive the predictor \hat{y}_f of predictive controller with (26).
- (5) Implement the control input u using (27) and (28).
- (6) At the next time, when new data arrives, implement the data inspection strategy. If the data is harmful (or useless), keep the *u* constant. Otherwise, implement the following steps.
- (7) Build the new input-output Hankel matrix D^* and the new R matrix is the QR decomposition results of D^* with (35).
- (8) Recursively computer the elements R_{11} , R_{21} , R_{22} , R_{31} , R_{32} of R matrix using (38) and (39).
- (9) Calculate the new subspace matrices using (40) and computer the control input by repeating steps 4-5. Then, back to step 6.

ALGORITHM 1: Summary of the proposed method.

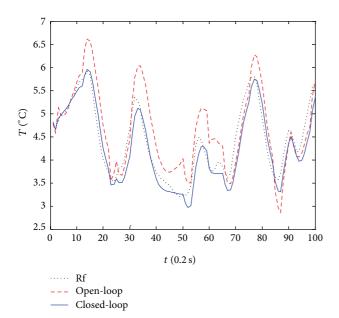


FIGURE 2: The response of the identified model and process output.

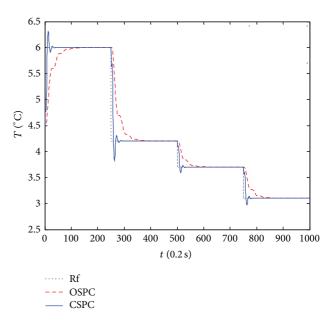


FIGURE 3: The output *T* tracking performance.

For comparison, the adaptive methods in [25, 26] are given. The method in [25] is an original receding window method which is performed by only *QR* decomposition. In [26], recursive approach is presented to obtain every element value of *R* matrix and the model inspection strategy is given. Figure 4 shows the response comparison in the presence of disturbance after the system model changes. We can get that, in performance of disturbance rejection, the method in this paper is better than the other two methods. The data inspection strategy makes the contribution for this result. The harmless (or useless) data are always produced when we implement online identification. The control performance depends on the better data preprocessing in this paper compared to the methods in [25, 26].

By comparing computation time of 1000 samples, the methods in [25, 26] and this paper take about 71 s, 62 s, and 52 s, respectively. The method in [25] requiring *QR* decomposition at every instant results in the most time of

the three methods. The computation time of our proposed method is less than that taken by the method in [26] since it only requires calculating the key elements R_{11} , R_{21} , R_{22} , R_{31} , and R_{32} of R matrix of our method but every element value of R matrix of the method in [26].

Additionally, to verify the usefulness of the data inspection strategy, the prediction error in (43) is used. When system model was changed, we introduced two identification ways, the data inspection strategy is used in one way and the other not. The prediction errors of these two ways are showed in Table 2 from 600 s to 1000 s. We can get that the data inspection strategy improves the accuracy of the method.

5.2. An Industrial 4-Stage Evaporator Example. The evaporator is a nonlinear and time-varying industrial process control system, and considering the stability of system the evaporator is often necessary to work in the closed-loop case. The conventional control methods, such as PID control,

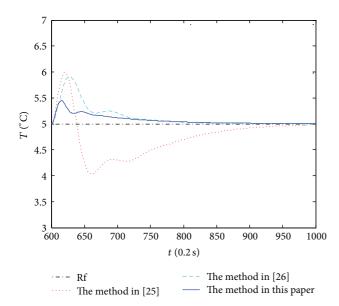


FIGURE 4: The response comparison in the presence of disturbance after the model changes.

TABLE 2: The prediction errors with and without the data inspection strategy in the hair dryer example.

Identification way in hair dryer	The method with the data inspection strategy	The method without the data inspection strategy
Prediction error	19.2230	26.0138

TABLE 3: The prediction errors of open-loop and closed-loop identified evaporator model.

Identification algorithm	Open-loop	Closed-loop
Prediction error	53.1732	28.0058

will result in poor control performance. The product quality will be also affected accordingly. The evaporator is used to reduce the water content of a product and is widely applied in chemical industry, food industry, pharmaceuticals, and others. Therefore, it is of an extremely important practical significance to use an effective control method to achieve fast and accurate control performance of the evaporator. A typical industrial 4-stage evaporator system and the detailed principle of operation can be seen in [36]. The system has three inputs and three outputs. The three inputs are input product flow q_i , vapour flow q_v to the first evaporator, and cooling water flow q_c to condenser, respectively. The three outputs are dry matter content TDS of output product, output product flow q_o , and output product temperature T, respectively [37].

The open-loop and closed-loop identification algorithms are applied in system. Using 1000 validation data for identification, the prediction errors in (43) are given in Table 3.

It is similar to the hair dryer example in Section 5.1; the closed-loop identification computes a more accurate model.

TABLE 4: The prediction errors with and without the data inspection strategy in the evaporator example.

Identification way in evaporator	The method with the data inspection strategy	The method without the data inspection strategy
Prediction error	32.1687	41.3125

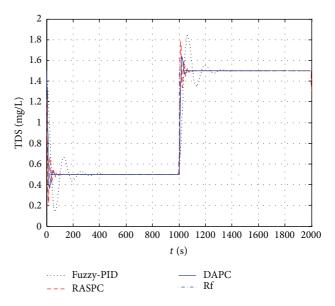


FIGURE 5: The tracking comparison of output TDS.

The target is set for the output TDS tracking the reference signal in the system. The parameters of proposed data-driven adaptive predictive control (DAPC) method were tuned as N=4000, t=1 s, p=f=10, $Q=I_{30}$, and $R=0.1*I_{30}$. The initial value of TDS was 1.5 mg/L. For comparison, the recursive adaptive subspace predictive control (RASPC) method in [23] and an adaptive fuzzy-PID controller in [38] were selected as competitors to compare the tracking capability. Figure 5 depicts the tracking comparison of these three controllers in the first 2000 samples and Figure 6 showed the partial enlarged drawing between 1000 s and 1200 s of Figure 5. At 1600 s, we changed q_i to increase by 10 percent; the response comparison after the parameters change is showed in Figure 7.

Through the simulation results, it may fairly be said that our proposed method is much better in output tracking and disturbance rejection than that performed by recursive method in [23] and fuzzy-PID controller in [38]. It can be interpreted that the reduction of the influence of the old data plays an important role.

As for the computation time, our method takes about 76 s for 1000 samples, while their recursive method in [23] is about 64 s; the latter method is somewhat superior to ours because it needs to add new data and eliminate old data at every instant in ours but theirs only add new data.

Similar to Section 5.1, the prediction errors with and without the data inspection strategy from 1600 s to 2000 s are listed in Table 4. Corresponding to the conclusion in the hair

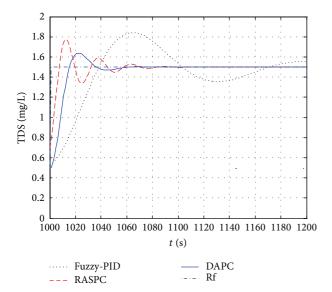


FIGURE 6: The partial enlarged comparison of Figure 5.

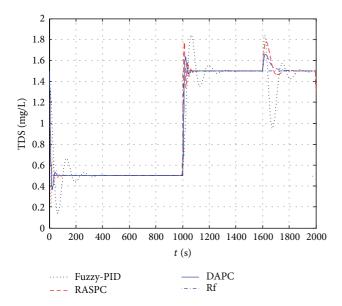


FIGURE 7: The response comparison in the presence of disturbance after the parameters change.

dryer example, the superior performance is obtained as using the data inspection strategy.

6. Conclusion

In this paper, the design of a data-driven adaptive predictive controller based on closed-loop subspace identification has been addressed. The predictor is identified through the closed-loop subspace identification and used to design a data-driven predictive controller. The adaptive mechanism is presented that combines the merits of both receding window and recursive identification methods, keeping the size of input-output data matrix constant and using recursive

identification to obtain the subspace matrices which can derive the predictor. Meanwhile, the data inspection strategy is used to eliminate the new harmless (or useless) data. By simulation studies for two examples its performance has been proved to be efficient by comparing with other methods.

Conflict of Interests

The authors declare that there is no conflict of interests regarding the publication of this paper.

Acknowledgments

This work was supported in part by the Major State Basic Research Development Program 973 (no. 2012CB215202), the National Natural Science Foundation of China (no. 61134001), and Key Laboratory of Dependable Service Computing in Cyber Physical Society (Chongqing University), Ministry of Education. The authors would like to thank Dr. Xiaojie Su and the reviewers for their helpful comments.

References

- [1] T. Katayama, T. McKelvey, A. Sano, C. G. Cassandras, and M. C. Campi, "Trends in systems and signals. Status report prepared by the IFAC Coordinating Committee on Systems and Signals," *Annual Reviews in Control*, vol. 30, no. 1, pp. 5–17, 2006.
- [2] Z. S. Hou and J. X. Xu, "On data-driven control theory: the state of the art and perspective," *Acta Automatica Sinica*, vol. 35, no. 6, pp. 650–667, 2009 (Chinese).
- [3] S. J. Qin and T. A. Badgwell, "A survey of industrial model predictive control technology," *Control Engineering Practice*, vol. 11, no. 7, pp. 733–764, 2003.
- [4] Huyck, H. J. Ferreau, M. Diehl et al., "Towards online model predictive control on a programmable logic controller: practical considerations," *Mathematical Problems in Engineering*, vol. 2012, Article ID 912603, 20 pages, 2012.
- [5] R. Hedjar, "Adaptive neural network model predictive control," International Journal of Innovative Computing, Information and Control, vol. 9, no. 3, pp. 1245–1257, 2013.
- [6] S. Bououden, M. Chadli, F. Allouani, and S. Filali, "A new approach for fuzzy predictive adaptive controller design using particle swarm optimization algorithm," *International Journal of Innovative Computing, Information and Control*, vol. 9, no. 9, pp. 3741–3758, 2013.
- [7] V. Vesely, D. Rosinova, and T. N. Quang, "Networked output feedback robust predictive controller design," *International Journal of Innovative Computing, Information and Control*, vol. 9, no. 10, pp. 3941–3953, 2013.
- [8] R. N. Yang, G. P. Liu, P. Shi, C. Thomas, and M. V. Basin, "Predictive output feedback control for networked control systems," *IEEE Transactions on Industrial Electronics*, vol. 61, no. 1, pp. 512–520, 2014.
- [9] B. C. Ding, Modern Predictive Control, CRC Press, Boca Raton, Fla, USA, 2010.
- [10] W. Favoreel, B. de Moor, and P. van Overschee, "Subspace state space system identification for industrial processes," *Journal of Process Control*, vol. 10, no. 2-3, pp. 149–155, 2000.

- [11] S. J. Qin, "An overview of subspace identification," Computers and Chemical Engineering, vol. 30, no. 10–12, pp. 1502–1513, 2006
- [12] S. Yin, S. Ding, A. Haghani, and H. Hao, "Data-driven monitoring for stochastic systems and its application on batch process," *International Journal of Systems Science*, vol. 44, no. 7, pp. 1366– 1376, 2013.
- [13] R. Kadali, B. Huang, and A. Rossiter, "A data driven subspace approach to predictive controller design," *Control Engineering Practice*, vol. 11, no. 3, pp. 261–278, 2003.
- [14] P. van Overschee and B. de Moor, "Closed loop subspace system identification," in *Proceedings of the 36th IEEE Conference on Decision and Control*, pp. 1848–1853, December 1997.
- [15] B. Huang, S. X. Ding, and S. J. Qin, "Closed-loop subspace identification: an orthogonal projection approach," *Journal of Process Control*, vol. 15, no. 1, pp. 53–66, 2005.
- [16] B. Kulcsár, J. W. van Wingerden, J. Dong, and M. Verhaegen, "Closed-loop subspace predictive control for Hammerstein systems," in *Proceedings of the 48th IEEE Conference on Decision* and Control held jointly with 28th Chinese Control Conference (CDC/CCC '09), pp. 2604–2609, December 2009.
- [17] J. Dong, M. Verhaegen, and E. Holweg, "Closed-loop subspace predictive control for fault tolerant MPC design," in *Proceedings* of the 17th World Congress, International Federation of Automatic Control (IFAC '08), pp. 3216–3221, July 2008.
- [18] M. Jansson, "A new subspace identification method for open and closed loop data," in *Proceedings of the 16th Triennial World Congress of International Federation of Automatic Control (IFAC* '05), pp. 500–505, July 2005.
- [19] Q. Zhou, P. Shi, S. Xu, and H. Li, "Adaptive output feedback control for nonlinear time-delay systems by fuzzy approximation approach," *IEEE Transactions on Fuzzy Systems*, vol. 21, no. 2, pp. 301–313, 2013.
- [20] L. Xie, W. Liang, Q. Zhang, J. Zhang, and S. Wang, "Adaptive subspace identification based on fast moving window QR decomposition," *Journal of Chemical Industry and Engineering*, vol. 59, no. 6, pp. 1448–1453, 2008 (Chinese).
- [21] B. Baykal and A. G. Constantinides, "Sliding window adaptive fast QR and QR-lattice algorithms," *IEEE Transactions on Signal Processing*, vol. 46, no. 11, pp. 2877–2887, 1998.
- [22] L. Sun and X. M. Jin, "Model-predictive-control based on subspace identification and its application," *Control Theory and Applications*, vol. 26, no. 3, pp. 313–315, 2009 (Chinese).
- [23] N. A. Mardi and L. Wang, "Subspace-based model predictive control of time-varying systems," in *Proceedings of the 48th IEEE Conference on Decision and Control held jointly with 28th Chinese Control Conference (CDC/CCC '09)*, pp. 4005–4010, December 2009.
- [24] H. Yang and S. Y. Li, "Subspace-based adaptive predictive control for a class of nonlinear systems," *International Journal* of *Innovative Computing, Information and Control*, vol. 1, no. 4, pp. 743–753, 2005.
- [25] N. A. Wahab, M. R. Katebi, and J. Balderud, "Data driven direct adaptive model based predictive control," in *Proceedings of the UKACC International Conference Control*, 2008.
- [26] X. S. Luo, B. C. Ding, and T. Zou, "Adaptive predictive control based on on-line subspace identification," *Control and Instruments in Chemical Industry*, vol. 37, no. 10, pp. 6–9, 2010 (Chinese).

- [27] K. Kameyama, A. Ohsumi, Y. Matsuura, and K. Sawada, "Recursive 4sid-based identification algorithm with fixed inputoutput data size," *International Journal of Innovative Computing, Information and Control*, vol. 1, no. 1, pp. 17–33, 2005.
- [28] W. Favorel, B. D. Moor, and M. Gevers, "SPC: subspace predictive control," in *Proceedings of the IFAC World Congress*, pp. 235–240, 1999.
- [29] I. H. Song, S. B. Lee, H. K. Rhee, and M. Mazzotti, "Identification and predictive control of a simulated moving bed process: purity control," *Chemical Engineering Science*, vol. 61, no. 6, pp. 1973–1986, 2006.
- [30] X. Wang, B. Huang, and T. Chen, "Data-driven predictive control for solid oxide fuel cells," *Journal of Process Control*, vol. 17, no. 2, pp. 103–114, 2007.
- [31] J. S. Zeng, C. H. Gao, and H. Y. Su, "Data-driven predictive control for blast furnace ironmaking process," *Computers and Chemical Engineering*, vol. 34, no. 11, pp. 1854–1862, 2010.
- [32] X. Lu, H. Chen, P. Wang, and B. Gao, "Design of a data-driven predictive controller for start-up process of AMT vehicles," *IEEE Transactions on Neural Networks*, vol. 22, no. 12, pp. 2201– 2212, 2011.
- [33] H. Fukushima, T. H. Kim, and T. Sugie, "Adaptive model predictive control for a class of constrained linear systems based on the comparison model," *Automatica*, vol. 43, no. 2, pp. 301– 308, 2007.
- [34] B. R. Woodley, J. P. How, and R. L. Kosut, "Subspace based direct adaptive H_{∞} control," *International Journal of Adaptive Control and Signal Processing*, vol. 15, no. 5, pp. 535–561, 2001.
- [35] L. Ljung, System Identification, Theory for the User, Prentice Hall, Upper Saddle River, NJ, USA, 1999.
- [36] Y. C. Zhu, P. V. Overschee, B. D. Moor, and L. Ljung, "Comparison of three classes of identification methods," in *Proceedings of the 10th IFAC Symposium on System Identification (SYSID '94)*, pp. 175–180, 1994.
- [37] P. V. Overschee and B. D. Moor, Subspace Identification for Linear Systems: Theory Implementation Applications, Kluwer Academic Publishers, Dordrecht, The Netherlands, 1996.
- [38] J. Carvajal, G. Chen, and H. Ogmen, "Fuzzy PID controller: design, performance evaluation, and stability analysis," *Infor*mation Sciences, vol. 123, no. 3-4, pp. 249–270, 2000.

Hindawi Publishing Corporation Abstract and Applied Analysis Volume 2014, Article ID 941547, 7 pages http://dx.doi.org/10.1155/2014/941547

Research Article

AP Deployment Research Based on Physical Distance and Channel Isolation

Dangui Yan, ¹ Chengchang Zhang, ² Honghua Liao, ³ Lisheng Yang, ² Ping Li, ² and Guogang Yang ²

¹ College of Mathematics and Physics, Chongaing University of Post and Telecommunications, Chongaing 400086, China

Correspondence should be addressed to Dangui Yan; yandg@cqupt.edu.cn

Received 5 January 2014; Revised 26 February 2014; Accepted 26 February 2014; Published 31 March 2014

Academic Editor: Hamid Reza Karimi

Copyright © 2014 Dangui Yan et al. This is an open access article distributed under the Creative Commons Attribution License, which permits unrestricted use, distribution, and reproduction in any medium, provided the original work is properly cited.

Aiming at the problem of inefficiency of wireless local area networks (WLAN) access point (AP) deployment in urban environment, a new algorithm for AP deployment based on physical distance and channel isolation (DPDCI) is proposed. First, it detects the position information of deployed APs and then calculates the interference penalty factor combined with physical distance and channel isolation, and finally gets the optimal location and channel of the new AP through the genetic algorithm. Comparing with NOOCA algorithm and NOFA-2 algorithm, the results of numerical simulation show that the new algorithm can minimize the mutual interference between basic service sets (BSS), can ensure the maximum of throughput based on quality of service (QoS) in BSS, and can effectively improve the system performance.

1. Introduction

With the development of information era, the growing importance of the wireless local area network (WLAN) becomes more and more obvious. Since the WLAN has the advantages of flexibility, simplicity, easy extension, and so on, it widely applies in hot places such as the markets, leisure clubs, and companies. However, there is no authoritative standards for commercial WLAN deployment and channel allocation and management standards, which leads to the current situation that each major telecom operator deploys its own WLAN equipment in the same hot spots in order to provide its own high-speed broadband multimedia business, respectively, which causes the repetitive construction of the coverage of the wireless access point (AP) and, at the same time, the large amount of channel interference in the limited frequency band due to the high-density deployment of AP. Therefore, how to effectively configure and optimize the AP channels becomes one of the leading problems to be solved for the large-scale commercial use of WLAN.

Aiming at AP channel interference problems, there have been some research results, most of which are mainly through the graph coloring [1], integer linear programming [2], and heuristic method [3] for allocating channels for APs in ISM (industrial, scientific, medical) band to make the whole interference minimum. Reference [4] uses the cognitive radio technology, combined with the service condition of the primary users' band, to allocate accessible primary users' channels for AP. However, the above algorithms improve the system throughput by minimizing interference, which neither considers the influence from different business on the throughput nor guarantees the quality of service (QoS) of the system. In order to ensure the QoS and fairness of different business in WLAN, based on Hsum algorithm [5], reference [6] introduces fairness index and puts forward the CAOTR (Channel Assignment based on the Order of Throughput Reduction) algorithm, but the complexity of the algorithm is higher. Reference [7] proposes the interference factor combining physical distance and channel isolation, but it is only suitable for the channel allocation of the fixedlocation AP and does not consider changing the deployment

² College of Communication Engineering, Chongqing University, Chongqing 400030, China

³ School of Information, Hubei University for Nationalities, Enshi 445000, China

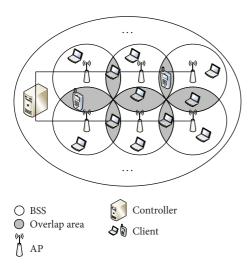


FIGURE 1: Work scene under the coexistence of high-density AP.

position of the AP. In [8], it gives a self-adapted algorithm based on neural network, which adapts retreat parameters in real time at Data Link Layer according to QoS request from Application Layer and channel state information from Physical Layer. In [9, 10], based on game theory algorithm, it seeks the optimal solution under the restricted condition of throughput, QoS, fairness, and so forth. However, [8–10] fail to involve the channel allocation of AP.

This paper considers synthetically the physical distance and channel isolation among APs and the position information of already deployed AP in detection area; a new algorithm for AP deployment based on physical distance and channel isolation (DPDCI) is proposed, which can effectively reduce interference and improve the system overall throughput.

2. System Model

2.1. Network Model. As shown in Figure 1, each AP and associated terminals in AP's communication range comprise a basic service set (BSS). In the BSS, terminals communicate with AP through the Media Access Control (MAC) protocol, while the communication between the APs is achieved by the IAPP [11], whose working principle is as follows: AP monitoring the adjacent AP beacon, including SNR information and the received signal strength and so on, and then AP will send its own information to the controller, including the number of terminals in the BSS. After the controller gets all the information from each AP, it will measure the overall throughput and allocate the channels. Because of the uncertainty of the AP position, it may cause the overlap on the range of BSS of different APs. In the overlap area, if channel allocation is not reasonable, it will cause interference problems when the terminals in the overlap area exchange data with the corresponding AP, especially when cochannel interference appears; it may even cause the communication interruption between client and its AP.

2.2. Interference Model. As shown in Figure 2, each AP owns two areas—one is communication area, and the other is interference area. Communication area is related to transmitter power and path loss and the receiver sensitivity corresponded to the real communication rate of the physical layer. While interference area is related to transmitter power, path loss and the receiver sensitivity corresponded to the minimum-supported communication rate of the physical layer. Apparently, the interference area is greater than or equal to communication area.

The communication radius (interference radius) is defined as [12]

$$r = 10^{(P_t - P_r - L_0)/10\alpha},\tag{1}$$

where P_t is transmitting power, P_r is receiving power; α is channel attenuation factor, and L_0 is the channel attenuation with one meter distance from receiver. The communication radius r_1 is obtained based on the minimum effective received power and the interference radius r_2 is obtained according to the minimum received power under interference. To simplify the analysis, we assume that the communication radius and interference radius of each AP are r_1 and r_2 , respectively.

2.2.1. Channel Interference Factor. Channel interference factor between APs is defined as follows;

$$\phi\left(c_{i},c_{j}\right) = \int_{-\infty}^{+\infty} S_{t}\left(f\right) S_{r}\left(f-\tau\right) df,\tag{2}$$

where c_i is the channel index number allocated to AP_i , c_i is the channel index number allocated to AP_j , $i, j \in \{1, ..., 11\}$, $S_t(f)$ is the transmitting power distribution of AP, $S_r(f)$ is the receiving power distribution of AP, and τ is off-set frequency.

In order to make it easy to analyze, the paper uses the IEEE 802.11b as the WiFi to analyze, and the channel isolation is set to 5 MHz and channel bandwidth is set to 22 MHz. The transmitting power distribution is defined as follows [7]:

$$S_{t}(f) = \begin{cases} -50 \text{ dB}, & \text{if } |f - f_{c}| > 22 \text{ MHz}, \\ -30 \text{ dB}, & \text{if } 11 \text{ MHz} < |f - f_{c}| < 22 \text{ MHz}, \\ 0 \text{ dB}, & \text{otherwise,} \end{cases}$$
 (3)

where f_c is the central frequency.

It is obvious that $\phi(c_i, c_j) \in [0, 1]$, and especially, $\phi(c_i, c_j) = 0$ when two APs' channels are completely orthogonal.

2.2.2. Physical Distance Interference. When the distance between AP_i and AP_j is bigger than the summation of r_1 and r_2 , its overlap area A_{ij} is illustrated in Figure 2, where the distance between adjacent AP_i and AP_j is d_{ij} , namely, AB, the communication radius of AP_i, namely, length of AC, is r_1 , and the interference radius of AP_j, namely, length of BC, is r_2 ; in $\triangle ABC$, we can obtain θ_1 and θ_2 according to the cosine theorem:

$$\theta_{1} = \arccos\left(\frac{r_{1}^{2} + d_{ij}^{2} - r_{2}^{2}}{2r_{1}d_{ij}}\right)$$

$$\theta_{2} = \arccos\left(\frac{r_{2}^{2} + d_{ij}^{2} - r_{1}^{2}}{2r_{2}d_{ij}}\right),$$
(4)

where S_1 is the difference value that corresponding sector area of θ_1 in the AP_i communication area minuses the area of ΔAOC , S_2 is the difference value that corresponding to sector area of θ_2 in AP_j communication area minuses the area of ΔBOC :

$$S_{1} = \frac{1}{2}\theta_{1}r_{1}^{2} - \frac{1}{2} \times r_{1} \sin \theta_{1} \times r_{1} \cos \theta_{1}$$

$$= \frac{1}{2}\theta_{1}r_{1}^{2} - \frac{1}{4}r_{1}^{2} \sin (2\theta_{1})$$

$$S_{2} = \frac{1}{2}\theta_{2}r_{2}^{2} - \frac{1}{2} \times r_{2} \sin \theta_{2} \times r_{2} \cos \theta_{2}$$

$$= \frac{1}{2}\theta_{2}r_{2}^{2} - \frac{1}{4}r_{2}^{2} \sin (2\theta_{2}).$$
(5)

According to symmetry, the expression of area A_{ij} is

$$A_{ij} = 2(S_1 + S_2)$$

$$= \frac{1}{2}r_1^2 \left[2\theta_1 - \sin(2\theta_1) \right] + \frac{1}{2}r_2^2 \left[2\theta_2 - \sin(2\theta_2) \right].$$
(6)

Therefore, A_{ii} can be expressed as

$$A_{ij} = \begin{cases} \frac{1}{2} r_1^2 \left[2\theta_1 - \sin\left(2\theta_1\right) \right] \\ + \frac{1}{2} r_2^2 \left[2\theta_2 - \sin\left(2\theta_2\right) \right], & d_{ij} < r_1 + r_2 \\ 0, & d_{ij} \ge r_1 + r_2. \end{cases}$$
 (7)

2.2.3. Signal to Interference Ratio in BSS. To facilitate analysis, we make such assumptions: AP receives the same power from the client and client obeys Poisson distribution in communication area, and each client transmits data equiprobably. Therefore, ignoring the noise, the APi's SIR [13] can be expressed as

$$SIR_{i} = \frac{\pi r_{1}^{2}}{\sum_{j=1, j \neq i}^{N} \phi(c_{i}, c_{j}) A_{ij}}.$$
 (8)

To guarantee the communication quality, SIR must satisfy the following condition:

$$SIR_i \le \gamma_i,$$
 (9)

where γ_i is the value of SIR threshold under AP_i.

3. Detection of Deployed APs

In an urban environment, a lot of the APs are located in some place which unable to be observed directly and the physical distance information of AP is hard to be measured directly, so wireless locating method is introduced [14]. It is assumed that the position of the already deployed AP is (x_0, y_0, z_0) , the position of the ith measuring point is (x_i, y_i, z_i) , the received signal intensity measured at the ith measuring point is r_i , and the numerical relationship between AP and the measuring point can be expressed as

$$\begin{bmatrix} -x_{1}^{2} - y_{1}^{2} - z_{1}^{2} + x_{k}^{2} + y_{k}^{2} + z_{k}^{2} \\ -x_{2}^{2} - y_{2}^{2} - z_{2}^{2} + x_{k}^{2} + y_{k}^{2} + z_{k}^{2} \\ \dots \\ -x_{k-1}^{2} - y_{k-1}^{2} - z_{k-1}^{2} + x_{k}^{2} + y_{k}^{2} + z_{k}^{2} \end{bmatrix}$$

$$= \begin{bmatrix} -2x_{1} + 2x_{k} & -2y_{1} + 2y_{k} & -2z_{1} + 2z_{k} & \frac{a_{1}(r_{1} - r_{k})}{5} \\ -2x_{2} + 2x_{k} & -2y_{2} + 2y_{k} & -2z_{2} + 2z_{k} & \frac{a_{1}(r_{2} - r_{k})}{5} \\ \dots & \dots & \dots \\ -2x_{k-1} + 2x_{k} & -2y_{k-1} + 2y_{k} & -2z_{k-1} + 2z_{k} & \frac{a_{1}(r_{k-1} - r_{k})}{5} \end{bmatrix} \begin{bmatrix} x_{0} \\ y_{0} \\ z_{0} \\ \frac{1}{n} \end{bmatrix}.$$

$$(10)$$

For simplicity, assume

$$\begin{bmatrix} -x_1^2 - y_1^2 - z_1^2 + x_k^2 + y_k^2 + z_k^2 \\ -x_2^2 - y_2^2 - z_2^2 + x_k^2 + y_k^2 + z_k^2 \\ \dots \\ -x_{k-1}^2 - y_{k-1}^2 - z_{k-1}^2 + x_k^2 + y_k^2 + z_k^2 \end{bmatrix} = a$$
(11)

$$\begin{bmatrix}
-2x_{1} + 2x_{k} & -2y_{1} + 2y_{k} & -2z_{1} + 2z_{k} & \frac{a_{1}(r_{1} - r_{k})}{5} \\
-2x_{2} + 2x_{k} & -2y_{2} + 2y_{k} & -2z_{2} + 2z_{k} & \frac{a_{1}(r_{2} - r_{k})}{5} \\
\dots & \dots & \dots & \dots \\
-2x_{k-1} + 2x_{k} & -2y_{k-1} + 2y_{k} & -2z_{k-1} + 2z_{k} & \frac{a_{1}(r_{k-1} - r_{k})}{5}
\end{bmatrix} = B.$$
(12)

According to the Least-Square Estimation, we can obtain

$$\begin{bmatrix} x_0 \\ y_0 \\ z_0 \\ \frac{1}{a} \end{bmatrix} = \left(B^T B \right)^{-1} B^T a. \tag{13}$$

So, the position information of the deployed AP can be calculated and the position information of all APs in the area can be measured.

4. Access Strategy in Authorized Frequency Band

We define s_t as the primary user channel state at time slot t, $s_t = 0$ indicates that the primary user's channel is busy, $s_t = 1$ stands for availability of primary user's channel, $\theta_0 = \Pr\{s_t = 0\}$ stands for busy probability of primary user's channel, and $\theta_1 = \Pr\{s_t = 1\}$ stands for available probability of primary user's channel. s'_t stands for the detection result of primary user's channel from secondary user, $s'_t = 0$ stands for that the detection of primary user's channel being busy, $s'_t = 1$ stands for that the detection of primary user's channel being available, $\pi_0 = \Pr\{s'_t = 0\}$ stands for probability that the detection of primary user's channel is busy, and $\pi_1 = \Pr\{s'_t = 1\}$ stands for probability that the detection of primary user's channel is available. The accuracy of the secondary user detection result is mainly expressed with detection probability $p_{\rm de}$ ($p_{\rm de} = \Pr\{s_t' = 0 \mid s_t = 0\}$) and false alarm probability $p_{\rm fa}$ ($p_{\rm fa} = \Pr\{s_t' = 0 \mid s_t = 1\}$). The access strategy of authorized frequency band can be expressed as [15]

$$\max_{\{r_{j},x_{j}\}} \sum_{j=0,1} \pi_{j} r_{j} \operatorname{Pr} \left\{ r_{j} \leq \log_{2} \left[1 + \frac{x_{j} g_{ss}}{\left(1 - z_{j} \right) Y g_{ps} + n} \right] \right\}$$
s.t.
$$\sum_{j=0,1} \pi_{j} x_{j} \leq \Gamma_{1}$$

$$\sum_{j=0,1} \pi_{j} \alpha_{0j} x_{j} g_{sp} \leq \Gamma_{2},$$

$$(14)$$

where r_j and x_j stand for the secondary user's state when channel state of authorized frequency band is j. g_{ss} is the channel power gain between the secondary user's transmitter and receiver. g_{ps} is the gain between the primary user's transmitter and secondary user's receiver. g_{sp} is the gain between the secondary user's transmitter and primary user's

receiver. $z_j = 0$ stands for the busy state of authorized frequency channel. $z_j = 1$ stands for the available state of authorized frequency channel. α_{ij} is the situation that, after authorization, the real state of frequency band is i and the detected result is the posterior probability of j. Γ_1 is the maximum power of secondary user. Γ_2 is the interference threshold of the primary user corresponding to secondary

5. The GA-Based AP Deployment Algorithm

In order to solve the optimal solution of the target channel allocation function reasonably, we introduce genetic algorithm [16] to solve the optimal channel allocation problem of ΔP

Genetic algorithm is viewed as a classic bionic algorithm, which imitates the selection process of the biological nature and selects the more adaptive individuals to reproduce with the rule of the survival of the fittest in order to form a new solution space through crossover and mutation and finally get the optimal solution of the problem. Each kind of AP deployment is viewed as an individual, and a limited kind of AP deployment constitutes a population.

5.1. Fitness Function. In order to obtain the optimal solution, we first build the fitness function. Fitness function reflects how adaptively an individual responds to the restricted conditions, and individuals with larger function values adapt better.

Assuming the positions of AP_i and AP_j are (x_i, y_i, z_i) and (x_j, y_j, z_j) , respectively, so the distance between AP_i and AP_j is

$$d_{ij} = \sqrt{(x_i - x_j)^2 + (y_i - y_j)^2 + (z_i - z_j)^2}.$$
 (15)

 I_c is defined as the whole interference factor in the area, and $I_c(i, j) = I_c(j, i)$, so I_c can be expressed as

$$I_{c} = 2\sum_{i=1}^{N} \sum_{j=i+1}^{N} I_{c}(i, j), \qquad (16)$$

where N is the number of APs in the area.

The system interference is minimized when the whole interference factor in the area is the minimum. To make the influence on the throughput of the whole area minimum, fitness function is defined as

$$fit = \frac{N}{I_c}.$$
 (17)

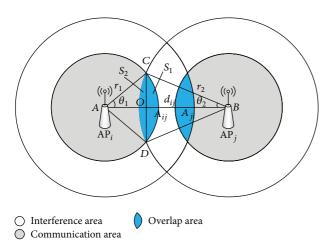


FIGURE 2: Diagram of interference model.

The probability that one individual is selected for crossover and mutation is defined as

$$p_i = \frac{\operatorname{fit}(i)}{\sum_{j=1}^{L} \operatorname{fit}(j)},$$
(18)

where *L* is the number of individuals in the population.

5.2. The Pseudocode of the Algorithm. The pseudocode of the algorithm is as in Algorithm 1.

The input of the algorithm is the position information of deployed AP, the number of new AP, and information of AP-usable position. First, it allocates channels randomly for the AP and then allocates deployment point for the new APs using the deployable positions and generate a not completely same allocation result to constitutes a population, and calculate the adaptability function value of each individual in the population, and the number of the iteration is initialized as 0. When the number of the iteration is smaller than the predefined maximum iteration number, calculating the selection probability according to (18), uses the Roulette method to select individual pair for hybrid processing, uses the Roulette method to select a single individual for mutation processing to get rid of individuals less adaptive individuals, and finally it refreshes the population and the number of iterations.

6. Simulations

To illustrate the performance of the algorithm, DPDCI algorithm is to be compared with the NOFA-2 algorithm [17] and the NOOCA algorithm [18].

The simulation parameters are shown in Table 1.

To estimate the interference of channel allocation algorithm over system performance, we define the average interference ratio η of system user from channel interference as follows:

$$\eta = \frac{1}{N} \sum_{i=1}^{N} \left(\frac{\sum_{j=1, j \neq i}^{N} A_{ij}}{\pi r_1^2} \right).$$
 (19)

TABLE 1: Main parameters of numerical analysis.

Network topology size	$1\mathrm{km} \times 1\mathrm{km}$
Transmit power of primary user's station $P_{\rm pt}$	43 dBm
Received power of primary user's receiver P_{pr}	-60 dBm
Antenna gain of primary user's station G_{pt}	15 dBi
Antenna gain of primary user's receiver G_{pr}	0 dBi
Path loss parameter α of cognitive network	4
Interference noise power δ	0.01 mw
The reserved average transmit rate of primary user C_0	4 Mbps
Signal bandwidth B	5 MHz
The total channel of primary user	11
Channel attenuation L_0 at 1 m	1
Available channel in authorized frequency band	15
Available probability of each channel in authorized frequency band	0.5
Communication radius r_1	100 m
Interference radius r_2	200 m

The simulation results are as in Figure 3.

In Figure 3, the horizontal coordinate indicates the accessed number *n* of AP and the vertical coordinate indicates the average interference of all the system users due to channel interference. At the first halves of the three algorithms, the tendencies of average interference are the same; this is due to the fact that the ISM band resource is relatively abundant under the situation that the number of AP is small. In particular, when the channel number is fewer than 3, the system average interference is 0 since ISM band owns three orthogonal channels (1/6/11). When AP takes orthogonal channel, there has no mutually interference.

With the increase of the number of AP, the average interference of NOFA-2 is always higher than NOOCA and DPDCI since NOFA-2 only assigns channel in ISM band, while, in the lower part of ISM band, AP's SIR is over its threshold value; if AP number increases on this base, it will increase the channel interference and lead to the increase of average interference. Moreover, the average interference of NOOCA is bigger than that of DPDCI, which is because the fact that when the NOOCA algorithm assigns channel in hybrid band, it fails to consider that the AP in unauthorized channel cannot interfere with AP in ISM band, which results in suboptimal allocation result of certain ISM band channel.

The comparison of normalization throughput of the three algorithms is shown in Figure 4. NOOCA and DPDCI algorithms introduce authorized band channel. When the number of communication channels increases, it decreases the interference between APs. Therefore, they are better than NOFA-2 algorithm in normalization throughput. The DPDCI algorithm considers that the AP in unauthorized channel cannot interfere with AP in ISM band which makes the channel allocation in ISM band more optimal. Therefore, it has a higher normalization throughput over NOOCA algorithm. As the accessing client increases, the advantage of

Input: a graph of APs with the No. of each AP

Output: an assigned channel for each AP

- (1) Initial a population with different individual
- (2) Calculated fitness for each individual
- (3) Let gen = 0
- (4) While gen < GMAX do
- (5) Assign a probability for each individual according to (18)
- (6) Select many pair of the individual using the roulette method
- (7) Crossover each pair of individual
- (8) Select many individual using the roulette method
- (9) Mutation each individual
- (10) Calculated fitness for each individual
- (11) Choose the right individual to form a new population
- (12) gen = gen + +
- (13) End while

ALGORITHM 1

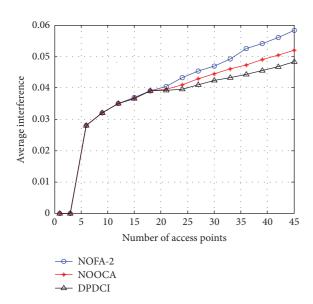


FIGURE 3: The comparison of average interference.

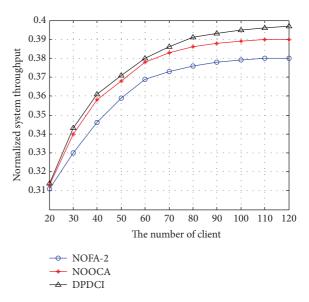


FIGURE 4: Comparison of normalization throughput.

DPDCI and NOOCA algorithms is highlighted and they are obviously higher than NOFA-2 algorithm.

Figure 5 shows the normalized throughput of DPDCI algorithm in the cases of detecting already deployed APs and not detecting already deployed APs. Because detecting already deployed AP can effectively avoid the strong interference between new AP and already deployed AP due to too close physical distance, the optimization result of this case is better than the case of not detecting already deployed AP. From the whole point of view, the normalized throughput is improved about 3.7%.

7. Conclusion

This paper gives a deep discussion on the new AP deployment in city area that has been deployed APs and uses the wireless locating method to detect the position of the already deployed APs that cannot be observed directly. Adopting genetic algorithm deploys new AP and allocates channels for AP; a new algorithm for AP deployment based on physical distance and channel isolation is proposed. The simulation results show that the new algorithm can minimize the mutual interference between BSS and ensure the maximum of throughput based on QoS in BSS and can also effectively improve the system performance. In order to achieve more practical oriented results, such as achieving dynamic configuration for the AP deployment, future work in the research will consider data-driven (measurements) framework [19–22].

Conflict of Interests

The authors declare that there is no conflict of interests regarding the publication of this paper.

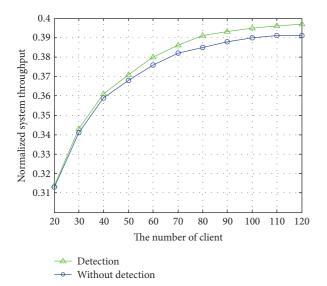


FIGURE 5: Comparison of DPDCI algorithm under detecting already deployed APs and not detecting already deployed APs.

Acknowledgments

The authors would like to thank the editors and the anonymous referees for their suggestions and comments. This work was supported in part by the National Natural Science Foundation of China (Grant no. 61263030), the Natural Science Foundation Project of CQCSTC (Grant no. 2010BB2240), and the Fundamental Research Funds for the Central Universities of China (Grants no. CDJZR12160018, no. CDJZR12160019).

References

- [1] E. Amaldi, S. Bosio, F. Malucelli, and D. Yuan, "Solving nonlinear covering problems arising in WLAN design," *Operations Research*, vol. 59, no. 1, pp. 173–187, 2011.
- [2] X.-N. Yue, C.-F. Wong, and S.-H. G. Chan, "CACAO: distributed client-assisted channel assignment optimization for uncoordinated WLANs," *IEEE Transactions on Parallel and Distributed Systems*, vol. 22, no. 9, pp. 1433–1440, 2011.
- [3] A. Farsi, N. Achir, and K. Boussetta, "Heuristic approaches for access points deployment and Frequency Assignment in WLANs," in *Proceedings of the Global Information Infrastructure Symposium (GIIS '11)*, pp. 1–7, IEEE Computer Society, Da Nang, Vietnam, August 2011.
- [4] F. Novillo, M. Churchman, R. Ferrús, and R. Agusti, "A channel allocation algorithm for OSA-enabled IEEE 802.11 WLANs," in *Proceedings of the 6th International Symposium on Wireless Communication Systems (ISWCS '09)*, pp. 468–472, Tuscany, Italy, September 2009.
- [5] A. Mishra, S. Banerjee, and W. Arbaugh, "Weighted coloring based channel assignment for WLANs," Sigmobile Mobile Computing and Communications Review, vol. 3, no. 11, pp. 19–31, 2005.
- [6] H. Zhang, H. Ji, and W.-D. Ge, "Channel assignment with fairness for multi-AP WLAN based on distributed coordination function," in *Proceedings of the IEEE Wireless Communications* and Networking Conference (WCNC '11), pp. 392–397, Cancun, Mexico, March 2011.

- [7] Y. Cui, W. Li, and X. Cheng, "Partially overlapping channel assignment based on "node orthogonality" for 802.11 wireless networks," in *Proceedings of the IEEE International Conference on Computer Communications (INFOCOM '11)*, pp. 361–365, Shanghai, China, April 2011.
- [8] C. Wang, T. Lin, and J.-L. Chen, "A cross-layer adaptive algorithm for multimedia QoS fairness in WLAN environments using neural networks," *IET Communications*, vol. 1, no. 5, pp. 858–865, 2007.
- [9] K.-L. Du, M. N. S. Swamy, and Q. Ni, "A dynamic spectrum access scheme for cognitive radio networks," in *Proceedings* of the Canadian Conference on Electrical and Computer Engineering (CCECE '09), pp. 450–454, IEEE Computer Society, St. John's, Canada, May 2009.
- [10] M. R. Javan and A. R. Sharafat, "Efficient and distributed SINR-based joint resource allocation and base station assignment in wireless CDMA networks," *IEEE Transactions on Communications*, vol. 59, no. 12, pp. 3388–3399, 2011.
- [11] M. Haidar, R. Akl, H. Al-Rizzo, and Y. Chan, "Channel assignment and load distribution in a power-managed WLAN," in Proceedings of the 18th Annual IEEE International Symposium on Personal, Indoor and Mobile Radio Communications (PIMRC '07), pp. 1–5, IEEE Computer Society, Athens, Greece, September 2007.
- [12] F. Novillo, M. Churchman, R. Ferrús, and R. Agustí, "A channel allocation algorithm for OSA-enabled IEEE 802.11 WLANs," in *Proceedings of the 6th International Symposium on Wireless Communication Systems (ISWCS '09)*, pp. 468–472, Tuscany, Italy, September 2009.
- [13] T. Kwon and J.-W. Choi, "Multi-group random access resource allocation for M2M devices in multicell systems," *IEEE Communications Letters*, vol. 16, no. 6, pp. 834–837, 2012.
- [14] J. Koo and H. Cha, "Localizing WiFi access points using signal strength," *IEEE Communications Letters*, vol. 15, no. 2, pp. 187–189, 2011.
- [15] W. Yuan, D. H. K. Tsang, L. Qian, and L. Meng, "Sensing based joint rate and power allocations for cognitive radio systems," *IEEE Communications Letters*, vol. 1, no. 2, pp. 113–116, 2012.
- [16] Y. Yang and X.-J. Yu, "Cooperative coevolutionary genetic algorithm for digital IIR filter design," *IEEE Transactions on Industrial Electronics*, vol. 54, no. 3, pp. 1311–1318, 2007.
- [17] W. El-Hajj and H. Alazemi, "Optimal frequency assignment for IEEE 802.11 wireless networks," Wireless Communications and Mobile Computing, vol. 9, no. 1, pp. 131–141, 2009.
- [18] F. Novillo, M. Churchman, R. Ferrús, and R. Agustí, "A channel allocation algorithm for OSA-enabled IEEE 802.11 WLANs," in *Proceedings of the 6th International Symposium on Wireless Communication Systems (ISWCS '09)*, pp. 468–472, Tuscany, Italy, September 2009.
- [19] M. de la Sen, "On the characterization of hankel and toeplitz operators describing switched linear dynamic systems with point delays," *Abstract and Applied Analysis*, vol. 2009, Article ID 670314, 34 pages, 2009.
- [20] H. Li, X. Jing, and H. R. Karimi, "Output-feedback-based H_{∞} control for vehicle suspension systems with control delay," *IEEE Transactions on Industrial Electronics*, vol. 1, no. 61, pp. 436–446, 2014.
- [21] S. Yin, H. Luo, and S. X. Ding, "Real-time implementation of fault-tolerant control systems with performance optimization," *IEEE Transactions on Industrial Electronics*, vol. 5, no. 61, pp. 2402–2411, 2014.
- [22] H. Li, X. Jing, H.-K. Lam, and P. Shi, "Fuzzy sampled-data control for uncertain vehicle suspension systems," *IEEE Transactions on Cybernetics*, no. 99, pp. 2168–2267, 2013.

Hindawi Publishing Corporation Abstract and Applied Analysis Volume 2014, Article ID 989703, 11 pages http://dx.doi.org/10.1155/2014/989703

Research Article

Decentralized H_{∞} Control for Uncertain Interconnected Systems of Neutral Type via Dynamic Output Feedback

Heli Hu¹ and Dan Zhao²

¹ Key Laboratory of Manufacturing Industrial Integrated Automation, Shenyang University, Shenyang 110044, China

Correspondence should be addressed to Heli Hu; huheli2004@126.com

Received 7 January 2014; Accepted 27 January 2014; Published 30 March 2014

Academic Editor: Ming Liu

Copyright © 2014 H. Hu and D. Zhao. This is an open access article distributed under the Creative Commons Attribution License, which permits unrestricted use, distribution, and reproduction in any medium, provided the original work is properly cited.

The design of the dynamic output feedback H_{∞} control for uncertain interconnected systems of neutral type is investigated. In the framework of Lyapunov stability theory, a mathematical technique dealing with the nonlinearity on certain matrix variables is developed to obtain the solvability conditions for the anticipated controller. Based on the corresponding LMIs, the anticipated gains for dynamic output feedback can be achieved by solving some algebraic equations. Also, the norm of the transfer function from the disturbance input to the controlled output is less than the given index. A numerical example and the simulation results are given to show the effectiveness of the proposed method.

1. Introduction

With the development of engineering systems, nowadays the systems become more and more complex and large. Therefore, there has been a growing interest in investigating the stability and stabilization problems for the large-scale interconnected systems [1-12]. In [5], Schuler et al. address a design of structured controllers for networks of interconnected multivariable discrete-time subsystems, in which a socalled degree of decentralization is introduced to characterize the sparsity level of the controller. In [6], Chen et al. consider the stabilization and H_{∞} disturbance attenuation problem for uncertain interconnected networked systems with both quantised output signal and quantised control inputs signal. A local-output dependent strategy is proposed to update the parameters of quantisers and achieve the H_{∞} disturbance attenuation level. In [7], Yan et al. consider the global decentralized stabilization of a class of interconnected systems with known and uncertain interconnections. Based on the Razumikhin-Lyapunov approach, they design a composite sliding surface and analyze the stability of the associated sliding motion, which is governed by a time delayed interconnected system. Not invoking the Lyapunov-Krasovskii functional approach and the Razumikhin Theorem approach, Ye provides a new method to globally stabilize a class of nonlinear large-scale systems with constant time-delay in [8], in which the Nussbaum gain is employed to tackle the unknown high-frequency-gain sign in the considered systems. Hua et al. investigate the model reference adaptive control problem and the exponential stabilization problem for a class of large-scale systems with time-varying delays in [9, 10], respectively. Different from the constraint on the derivatives of time-varying delays in [9, 10], Wu in [11] relaxes the constraint, that is, the derivatives of time-varying delays does not have to be less than one. It is worth pointing out that the nonlinear interconnections are subject to the matched condition in [9, 10] and the time-varying delays only appear in the interconnection in [11].

On the other hand, time delay frequently occurs in many engineering systems, such as the state, input, or related variable of dynamic systems [13, 14]. In particular, when it arises in the state derivative, the considered systems are called as neutral systems [15]. Neutral system is the general form of delay system and contains the same highest order derivatives for the state vector x(t), at both time t and past time(s) $t_s \leq t$. Due to the extensive applications of the neutral systems, in recent years, many efforts have been made for the stability analysis and control problem for neutral systems [16–22]. In [16], Xiong et al. construct a new class of stochastic Lyapunov-Krasovskii functionals to investigate

² Department of Fundamental Teaching, Shenyang Institute of Engineering, Shenyang 110136, China

the stability of neutral Markovian jump systems in the case of partly known transition probabilities. In [17], the Lyapunov-Krasovskii functional containing novel triple integral terms is developed to study the robust stabilization for a class of uncertain neutral system with discrete and distributed time delays. Based on the state feedback controller, an improved robust stability and stabilization criteria depending on the allowable maximum delay are derived. In [18], Kwon et al. propose a few delay-dependent stability criteria for uncertain neutral systems with time-varying delays, in which the augmented Lyapunov-Krasovskii functional is constructed and the reciprocal convex optimization approach is introduced. In [19], the delay-dependent exponential stability and stabilisation problems are investigated for a class of special neutral systems with actuator failures. A class of switching laws incorporating the average dwell time method is proposed to robustly stabilise the closed-loop system.

In practice, it is not always possible to have full access to the state variables and only the partial information through a measured output is available [23]. Therefore, it is more realistic in control engineering to design the output feedback control for the considered systems and there is a growing interest in it [24–29]. However, to the authors' best knowledge, there is little literature on designing dynamic output feedback control for interconnected systems of neutral type. This motivates the present study.

In this paper, the H_{∞} control problem for uncertain interconnected systems of neutral type is investigated via decentralized dynamic output feedback. Based on the Lyapunov stability theory, we develop a new technique to deal with the nonlinearity problem of certain matrix variables appearing in the solvable conditions of dynamic output feedback H_{∞} control. Furthermore, the parameterized characterization of the anticipated controller is achieved, which can be obtained by solving the corresponding LMIs and computing the corresponding algebraic equations. Also, it is guaranteed that the norm of the transfer function from the disturbance input to the controlled output is less than the given index. Finally, the effectiveness of the proposed method is elucidated by a numerical example and the simulation results.

2. Problem Formulation

Consider the following uncertain neutral interconnected systems composed of N subsystems:

$$\begin{split} \dot{x}_{i}\left(t\right) - A_{i\eta_{i}}\dot{x}_{i}\left(t - \eta_{i}\left(t\right)\right) \\ &= \left[A_{i} + \Delta A_{i}\left(t\right)\right]x_{i}\left(t\right) \\ &+ \left[A_{i\sigma_{i}} + \Delta A_{i\sigma_{i}}\left(t\right)\right]x_{i}\left(t - \sigma_{i}\left(t\right)\right) \\ &+ B_{i1}\omega_{i}\left(t\right) + \sum_{j=1, j \neq i}^{N} \left[A_{ij} + \Delta A_{ij}\right]x_{j}\left(t - \tau_{ij}\left(t\right)\right), \\ z_{i}\left(t\right) = C_{i1}x_{i}\left(t\right) + D_{i11}\omega_{i}\left(t\right), \\ x_{i}\left(t\right) = \phi_{i}\left(t\right), \quad t \in [-l, 0], \ i = 1, 2, \dots, N, \end{split}$$

where $x_i(t) \in \Re^{n_i}$, $z_i(t) \in \Re^{r_i}$, and $\omega_i(t) \in \Re^{p_i}$ are the state, the controlled output, and the disturbance input of the ith subsystem, respectively. A_i , $A_{i\sigma_i}$, $A_{i\eta_i}$, B_{i1} , A_{ij} , C_{i1} , and D_{i11} are known constant matrices of appropriate dimensions. $\phi_i(t)$ is the initial condition. $\sigma_i(t)$, $\eta_i(t)$, and $\tau_{ij}(t)$ are the time-varying delays. Assume that there exist constants f_{i0} , g_{i0} , l_{i0} , f_i , g_i , l_i , and l satisfying

$$0 \leq \sigma_{i}(t) \leq f_{i0}, \qquad 0 \leq \eta_{i}(t) \leq g_{i0}, \qquad 0 \leq \tau_{ij}(t) \leq l_{i0},$$

$$\dot{\sigma}_{i}(t) \leq f_{i} < 1, \qquad \dot{\eta}_{i}(t) \leq g_{i} < 1, \qquad \dot{\tau}_{ij}(t) \leq l_{i} < 1,$$

$$l = \max\{f_{i0}, g_{i0}, l_{i0}\}, \quad i, j = 1, 2..., N, j \neq i.$$

$$(2)$$

Time-varying parametric uncertainties $\Delta A_i(t)$, $\Delta A_{i\sigma_i}(t)$, and $\Delta A_{ii}(t)$ are assumed to satisfy

$$[\Delta A_i(t) \ \Delta A_{i\sigma_i}(t) \ \Delta A_{ij}(t)] = D_i F_i(t) [E_{i1} \ E_{i\sigma_i} \ L_{ij}],$$
 (3) where matrices D_i , E_{i1} , $E_{i\sigma_i}$, and L_{ij} are constant matrices of appropriate dimensions, and $F_i(t)$ is the unknown matrix function satisfying $F_i^T(t)F_i(t) \leq I$, for all $t \geq 0$.

Assumption 1 (see [30]). The matrix $A_{i\eta_i} \neq 0$ and $||A_{i\eta_i}|| < 1$.

As a general approach of dealing with the retarded argument in the state derivatives, it is assumed often that either there is no unstable neutral root chain or they can first use derivative feedback to assign the unstable neutral root chain to the left-hand side of the complex plane. Also, since $A_{i\eta_i} \neq 0$, it follows form that that the solution of (1) exists and is unique.

Lemma 2 (see [31]). Given any constant $\varepsilon > 0$ and matrices D, E, and F with compatible dimensions such that $F^TF < I$ then

$$2x^{T}DFEy \le \varepsilon x^{T}DD^{T}x + \varepsilon^{-1}y^{T}E^{T}Ey, \tag{4}$$

for all $x \in \mathbb{R}^n$, $y \in \mathbb{R}^n$.

3. Main Result

3.1. Robust H_{∞} Performance Analysis

Theorem 3. For given $\gamma_i > 0$, consider system (1) with (2) and (3). Under the condition of Assumption 1, system (1) is robustly asymptotically stable and satisfies $\|T_{z_i\omega_i}\|_{\infty} < \gamma_i$, if there exist matrices $P_i > 0$, $Q_{i1} > 0$, $Q_{i2} > 0$, $G_{ij} > 0$, and $G_{ji} > 0$ such that the following LMI holds:

$$\begin{bmatrix} \Gamma_{11}^{i} & \Gamma_{12}^{i} & \Gamma_{13}^{i} & \Gamma_{14}^{i} & \Gamma_{15}^{i} & \Gamma_{16}^{i} & \Gamma_{17}^{i} & 0 \\ * & \Gamma_{22}^{i} & \Gamma_{23}^{i} & \Gamma_{24}^{i} & 0 & 0 & 0 & 0 \\ * & * & \Gamma_{33}^{i} & \Gamma_{34}^{i} & 0 & 0 & 0 & 0 \\ * & * & * & \Gamma_{44}^{i} & \Gamma_{45}^{i} & 0 & 0 & \Gamma_{48}^{i} \\ * & * & * & * & \Gamma_{55}^{i} & \Gamma_{56}^{i} & 0 & 0 \\ * & * & * & * & * & -I & 0 & 0 \\ * & * & * & * & * & * & -I & 0 \\ * & * & * & * & * & * & * & * & -I \end{bmatrix}$$

where

$$\Gamma_{11}^{i} = P_{i}A_{i} + A_{i}^{T}P_{i} + \frac{1}{1 - f_{i}}Q_{i1} + \frac{1}{1 - g_{i}}Q_{i2} + \frac{1}{1 - l_{j}}\sum_{j=1,j\neq i}^{N}G_{ji} + 2E_{i1}^{T}E_{i1}, \qquad \Gamma_{12}^{i} = P_{i}A_{i\sigma_{i}} + 2E_{i1}^{T}E_{i\sigma_{i}},$$

$$\Gamma_{13}^{i} = \left[P_{i}A_{i1} + 2E_{i1}^{T}L_{i1} \cdots P_{i}A_{ii-1} + 2E_{i1}^{T}L_{ii-1} P_{i}A_{ii+1} + 2E_{i1}^{T}L_{ii+1} \cdots P_{i}A_{iN} + 2E_{i1}^{T}L_{iN}\right],$$

$$\Gamma_{14}^{i} = -A_{i}^{T}P_{i}A_{i\eta_{i}}, \qquad \Gamma_{15}^{i} = P_{i}B_{i1}, \qquad \Gamma_{16}^{i} = C_{i1}^{T}, \qquad \Gamma_{17}^{i} = P_{i}D_{i}, \qquad \Gamma_{22}^{i} = -Q_{i1} + 2E_{i\sigma_{i}}^{T}E_{i\sigma_{i}},$$

$$\Gamma_{24}^{i} = -A_{i\sigma_{i}}^{T}P_{i}A_{i\eta_{i}}, \qquad \Gamma_{23}^{i} = \left[2E_{i\sigma_{i}}^{T}L_{i1} \cdots 2E_{i\sigma_{i}}^{T}L_{ii-1} 2E_{i\sigma_{i}}^{T}L_{ii+1} \cdots 2E_{i\sigma_{i}}^{T}L_{iN}\right],$$

$$\Gamma_{33}^{i} = \operatorname{diag}\left\{-G_{i1} + 2L_{i1}^{T}L_{i1}, \dots, -G_{i-1} + 2L_{i-1}^{T}L_{ii-1}, -G_{i+1} + 2L_{i+1}^{T}L_{i+1}, \dots, -G_{iN} + 2L_{iN}^{T}L_{iN}\right\},$$

$$\Gamma_{34}^{i} = \left[-A_{i\eta_{i}}^{T}P_{i}A_{i1} \cdots -A_{i\eta_{i}}^{T}P_{i}A_{ii-1} -A_{i\eta_{i}}^{T}P_{i}A_{ii+1} \cdots -A_{i\eta_{i}}^{T}P_{i}A_{iN}\right]^{T}, \qquad \Gamma_{44}^{i} = -Q_{i2},$$

$$\Gamma_{45}^{i} = -A_{i\eta_{i}}^{T}P_{i}B_{i1}, \qquad \Gamma_{48}^{i} = -A_{i\eta_{i}}^{T}P_{i}D_{i}, \qquad \Gamma_{55}^{i} = -\gamma_{i}^{2}I, \qquad \Gamma_{56}^{i} = D_{i11}^{T}.$$

Proof. Construct the following Lyapunov-Krasovskii functional candidate of the form

$$V(x_{t}) = \sum_{i=1}^{N} V_{i}(x_{t})$$

$$= \sum_{i=1}^{N} \left\{ \left[x_{i}(t) - A_{i\eta_{i}} x_{i}(t - \eta_{i}(t)) \right]^{T} \right.$$

$$\times P_{i} \left[x_{i}(t) - A_{i\eta_{i}} x_{i}(t - \eta_{i}(t)) \right]$$

$$+ \frac{1}{1 - f_{i}} \int_{t - \sigma_{i}(t)}^{t} x_{i}^{T}(s) Q_{i1} x_{i}(s) ds$$

$$+ \frac{1}{1 - g_{i}} \int_{t - \eta_{i}(t)}^{t} x_{i}^{T}(s) Q_{i2} x_{i}(s) ds$$

$$+ \frac{1}{1 - l_{i}} \sum_{j=1, j \neq i}^{N} \int_{t - \tau_{ij}(t)}^{t} x_{j}^{T}(s) G_{ij} x_{j}(s) ds \right\}.$$

$$(7)$$

The time derivative of $V(x_t)$ along the trajectory of system (1) satisfies

$$\dot{V}(x_t) = \sum_{i=1}^{N} \dot{V}_i(x_t) \le \sum_{i=1}^{N} \dot{U}_i(x_t)$$

$$\le \sum_{i=1}^{N} \left\{ 2(x_i(t) - A_{i\eta_i} x_i(t - \eta_i(t)))^T \right.$$

$$\times P_i \left[(A_i + \Delta A_i(t)) x_i(t) + (A_{i\sigma_i} + \Delta A_{i\sigma_i}(t)) \times x_i(t - \sigma_i(t)) + B_{i1}\omega_i(t) \right]$$

$$+ \sum_{j=1,j\neq i}^{N} \left(A_{ij} + \Delta A_{ij} \right) x_{j} \left(t - \tau_{ij} \left(t \right) \right) \right]$$

$$+ \frac{1}{1 - f_{i}} x_{i}^{T} \left(t \right) Q_{i1} x_{i} \left(t \right)$$

$$+ \frac{1}{1 - g_{i}} x_{i}^{T} \left(t \right) Q_{i2} x_{i} \left(t \right)$$

$$- x_{i}^{T} \left(t - \sigma_{i} \left(t \right) \right) Q_{i1} x_{i} \left(t - \sigma_{i} \left(t \right) \right)$$

$$- x_{i}^{T} \left(t - \eta_{i} \left(t \right) \right) Q_{i2} x_{i} \left(t - \eta_{i} \left(t \right) \right)$$

$$+ \frac{1}{1 - l_{i}} \sum_{j=1,j\neq i}^{N} x_{j}^{T} \left(t \right) G_{ij} x_{j} \left(t \right)$$

$$- \sum_{j=1,j\neq i}^{N} x_{j}^{T} \left(t - \tau_{ij} \left(t \right) \right) G_{ij} x_{j} \left(t - \tau_{ij} \left(t \right) \right) \right\}.$$
(8)

In view of (3), applying Lemma 2, we obtain the following inequality:

$$2\left[x_{i}(t) - A_{i\eta_{i}}x_{i}\left(t - \eta_{i}(t)\right)\right]^{T}$$

$$\times P_{i}\left[\Delta A_{i}(t)x_{i}(t) + \Delta A_{i\sigma_{i}}(t)x_{i}\left(t - \sigma_{i}(t)\right)\right]$$

$$+ \sum_{j=1, j \neq i}^{N} \Delta A_{ij}x_{j}\left(t - \tau_{ij}(t)\right)\right]$$

$$\leq x_{i}^{T}(t)P_{i}D_{i}D_{i}^{T}P_{i}x_{i}(t) + 2\alpha_{i}^{T}(t)M_{i}^{T}M_{i}\alpha_{i}(t)$$

$$+ x_{i}^{T}\left(t - \eta_{i}(t)\right)A_{i\eta_{i}}^{T}P_{i}D_{i}D_{i}^{T}P_{i}A_{i\eta_{i}}x_{i}\left(t - \eta_{i}(t)\right),$$
(9)

where

$$\alpha_{i}(t) = \begin{bmatrix} x_{i}(t) & x_{i}(t - \sigma_{i}(t)) & x_{i1}(t - \tau_{i1}(t)) & \cdots & x_{ii-1}(t - \tau_{ii-1}(t)) & x_{ii+1}(t - \tau_{ii+1}(t)) & \cdots & x_{iN}(t - \tau_{iN}(t)) & x_{i}(t - \eta_{i}(t)) \end{bmatrix},$$

$$M_{i} = \begin{bmatrix} E_{i1} & E_{i\sigma_{i}} & L_{i1} & \cdots & L_{ii-1} & L_{ii+1} & \cdots & L_{iN} & 0 \end{bmatrix}.$$
(10)

It follows from (8) and (9) that

$$\dot{V}\left(x_{t}\right) = \sum_{i=1}^{N} \dot{V}_{i}\left(x_{t}\right) \leq \sum_{i=1}^{N} \alpha_{i}^{T}\left(t\right) \left[\Xi_{i} + 2M_{i}^{T}M_{i}\right] \alpha_{i}\left(t\right), \quad (11)$$

where

$$\begin{split} M_{i} &= \begin{bmatrix} E_{i1} & E_{i\sigma_{i}} & L_{i1} & \cdots & L_{ii-1} & L_{ii+1} & \cdots & L_{iN} & 0 \end{bmatrix}, \\ \Xi_{i} &= \begin{bmatrix} \Xi_{11}^{i} & P_{i}A_{i\sigma_{i}} & \Xi_{13}^{i} & -A_{i}^{T}P_{i}A_{i\eta_{i}} \\ * & -Q_{i1} & 0 & -A_{i\sigma_{i}}^{T}P_{i}A_{i\eta_{i}} \\ * & * & \Xi_{33}^{i} & \Xi_{34}^{i} \end{bmatrix}, \\ \Xi_{44}^{i} &= -Q_{i2} + A_{i\eta_{i}}^{T}P_{i}D_{i}D_{i}^{T}P_{i}A_{i\eta_{i}}, \\ \Xi_{11}^{i} &= P_{i}A_{i} + A_{i}^{T}P_{i} + \frac{1}{1 - f_{i}}Q_{i1} + \frac{1}{1 - g_{i}}Q_{i2} \\ &+ \frac{1}{1 - l_{j}}\sum_{j=1,j\neq i}^{N}G_{ji} + P_{i}D_{i}D_{i}^{T}P_{i}, \\ \Xi_{13}^{i} &= \begin{bmatrix} P_{i}A_{i1} & \cdots & P_{i}A_{ii-1} & P_{i}A_{ii+1} & \cdots & P_{i}A_{iN} \end{bmatrix}, \\ \Xi_{33}^{i} &= \operatorname{diag}\left\{ -G_{i1}, \dots, -G_{ii-1}, -G_{ii+1}, \dots, -G_{iN} \right\}, \\ \Xi_{34}^{i} &= \begin{bmatrix} -A_{i\eta_{i}}^{T}P_{i}A_{i1} & \cdots & -A_{i\eta_{i}}^{T}P_{i}A_{i-1} & -A_{i\eta_{i}}^{T}P_{i}A_{i+1} & \cdots & -A_{i\eta_{i}}^{T}P_{i}A_{iN} \end{bmatrix}^{T}. \end{split}$$

By the Schur Complement formula, it is easy to see that LMI (5) implies that $\Xi_i + 2M_i^T M_i < 0$. Then we can obtain that $\dot{V}(t) < 0$ for all $\alpha_i(t) \neq 0$ when $\omega_i(t) = 0$. Therefore, under the condition of Assumption 1, system (1) is asymptotically stable.

Next, consider the H_{∞} performance of system (1) under the zero initial condition. To this end, we introduce the following index:

$$J = \sum_{i=1}^{N} \int_{0}^{\infty} \left[z_{i}^{T}(t) z_{i}(t) - \gamma_{i}^{2} \omega_{i}^{T}(t) \omega_{i}(t) \right] dt.$$
 (13)

In view of the zero initial condition, it is easy to obtain that

$$J = \sum_{i=1}^{N} \int_{0}^{\infty} \left[z_{i}^{T}(t) z_{i}(t) - \gamma_{i}^{2} \omega_{i}^{T}(t) \omega_{i}(t) + \dot{V}_{i}(x_{t}) \right] dt$$

$$+ V(x_{t})|_{t=0} - V(x_{t})|_{t=\infty}, \qquad (14)$$

$$\leq \sum_{i=1}^{N} \xi_{i}^{T}(t) \left[\Pi_{i} + 2\overline{M}_{i}^{T} \overline{M}_{i} \right] \xi_{i}(t),$$

where

$$\Pi_{i} = \begin{bmatrix}
\Pi_{11}^{i} & P_{i}A_{i\sigma_{i}} & \Xi_{13}^{i} & -A_{i}^{T}P_{i}A_{i\eta_{i}} & \Pi_{15}^{i} \\
* & -Q_{i1} & 0 & -A_{i\sigma_{i}}^{T}P_{i}A_{i\eta_{i}} & 0 \\
* & * & \Xi_{33}^{i} & \Xi_{34}^{i} & 0 \\
* & * & * & \Xi_{44}^{i} & \Pi_{45}^{i} \\
* & * & * & * & \Pi_{55}^{i}
\end{bmatrix},$$

$$\xi_{i} = \begin{bmatrix} \alpha_{i}(t) \\ \omega_{i}(t) \end{bmatrix}, \qquad \overline{M}_{i} = \begin{bmatrix} M_{i} & 0 \end{bmatrix},$$

$$\Pi_{11}^{i} = P_{i}A_{i} + A_{i}^{T}P_{i} + \frac{1}{1 - f_{i}}Q_{i1} + \frac{1}{1 - g_{i}}Q_{i2}$$

$$+ \frac{1}{1 - l_{j}} \sum_{j=1, j \neq i}^{N} G_{ji} + P_{i}D_{i}D_{i}^{T}P_{i} + C_{i1}^{T}C_{i1},$$

$$\Pi_{15}^{i} = P_{i}B_{i1} + C_{i1}^{T}D_{i11}, \qquad \Pi_{45}^{i} = -A_{i\eta_{i}}^{T}P_{i}B_{i1},$$

$$\Pi_{55}^{i} = -\gamma_{i}^{2}I + D_{i11}^{T}D_{i11}.$$
(15)

It is obvious that $\Pi_i + 2\overline{M}_i^T\overline{M}_i < 0$ implies that J < 0, that is, $\|T_{z_i\omega_i}\|_{\infty} < \gamma_i$. By the Schur Complement formula, the inequality $\Pi_i + 2\overline{M}_i^T\overline{M}_i < 0$ is equivalent to LMI (5). This completes the proof.

3.2. H_{∞} Output Feedback Synthesis. Consider the following uncertain neutral interconnected systems composed of N subsystems:

$$\dot{x}_{i}(t) - A_{i\eta_{i}}\dot{x}_{i}(t - \eta_{i}(t))
= \left[A_{i} + \Delta A_{i}(t)\right]x_{i}(t)
+ \left[A_{i\sigma_{i}} + \Delta A_{i\sigma_{i}}(t)\right]x_{i}(t - \sigma_{i}(t))
+ B_{i1}\omega_{i}(t) + \sum_{j=1,j\neq i}^{N} \left[A_{ij} + \Delta A_{ij}\right]x_{j}(t - \tau_{ij}(t))
+ \left[B_{i2} + \Delta B_{i2}\right]u_{i}(t),
z_{i}(t) = C_{i1}x_{i}(t) + D_{i11}\omega_{i}(t) + D_{i12}u_{i}(t),
y_{i}(t) = C_{i2}x_{i}(t) + D_{i21}\omega_{i}(t),
x_{i}(t) = \phi_{i}(t), \quad t \in [-l, 0], i = 1, 2, ..., N,$$
(16)

where $u_i(t) \in \Re^{m_i}$ and $y_i(t) \in \Re^{q_i}$ are the control input and the measurement output. B_{i2} , C_{i2} , D_{i12} , and D_{i21}

are known constant matrices of appropriate dimensions. $\Delta B_{i2}(t)$ is the unknown matrix satisfying $B_{i2}(t) = D_i F_i(t) E_{i2}$, where E_{i2} is the known constant matrix with appropriate dimensions. The other signals are the same with system (1).

Consider the following output feedback controller for system (16):

$$\hat{\bar{x}}_i(t) = A_{iK}\hat{x}_i(t) + B_{iK}y_i(t),$$

$$u_{iK}(t) = C_{iK}\hat{x}_i(t),$$
(17)

where $\widehat{x}_i(t) \in \Re^{n_i \times n_i}$ is the controller state, and A_{iK} , B_{iK} , and C_{ik} are the gains to be designed.

Then the closed-loop system composed of system (16) with the controller (17) can be written as

$$\begin{split} \dot{\overline{x}}_{i}\left(t\right) - \overline{A}_{i\eta_{i}}\dot{x}_{i}\left(t - \eta_{i}\left(t\right)\right) \\ &= \left[\overline{A}_{i} + \Delta\overline{A}_{i}\left(t\right)\right]x_{i}\left(t\right) \\ &+ \left[\overline{A}_{i\sigma_{i}} + \Delta\overline{A}_{i\sigma_{i}}\left(t\right)\right]x_{i}\left(t - \sigma_{i}\left(t\right)\right) + \overline{B}_{i1}\omega_{i}\left(t\right) \\ &+ \sum_{j=1,j\neq i}^{N} \left[\overline{A}_{ij} + \Delta\overline{A}_{ij}\right]\overline{x}_{j}\left(t - \tau_{ij}\left(t\right)\right), \end{split}$$

where

$$\begin{split} \overline{A}_{i} &= \begin{bmatrix} A_{i} & B_{i2}C_{ik} \\ B_{iK}C_{i2} & A_{iK} \end{bmatrix}, \qquad \overline{A}_{i\sigma_{i}} = \begin{bmatrix} A_{i\sigma_{i}} & 0 \\ 0 & 0 \end{bmatrix}, \\ \overline{A}_{ij} &= \begin{bmatrix} A_{ij} & 0 \\ 0 & 0 \end{bmatrix}, \qquad \overline{A}_{i\eta_{i}} &= \begin{bmatrix} A_{i\eta_{i}} & 0 \\ 0 & 0 \end{bmatrix}, \\ \overline{A}_{i}(t) &= \begin{bmatrix} \Delta A_{i}(t) & \Delta B_{i2}C_{iK} \\ 0 & 0 \end{bmatrix} = \overline{D}_{i}F_{i}(t)\overline{E}_{i1} \\ &= \begin{bmatrix} D_{i} \\ 0 \end{bmatrix}F_{i}(t)\begin{bmatrix} E_{i1} & E_{i2}C_{iK} \end{bmatrix}, \\ \Delta \overline{A}_{i\sigma_{i}}(t) &= \begin{bmatrix} \Delta A_{i\sigma_{i}}(t) & 0 \\ 0 & 0 \end{bmatrix} = \overline{D}_{i}F_{i}(t)\overline{E}_{i\sigma_{i}} \\ &= \begin{bmatrix} D_{i} \\ 0 \end{bmatrix}F_{i}(t)\begin{bmatrix} E_{i\sigma_{i}} & 0 \end{bmatrix}, \end{split}$$

$$\Delta \overline{A}_{ij}(t) = \begin{bmatrix} \Delta A_{ij}(t) & 0 \\ 0 & 0 \end{bmatrix} = \overline{D}_{i} F_{i}(t) \overline{L}_{ij}$$

$$= \begin{bmatrix} D_{i} \\ 0 \end{bmatrix} F_{i}(t) [L_{ij} \quad 0],$$

$$\overline{B}_{i1} = \begin{bmatrix} B_{i1} \\ B_{iK} D_{i21} \end{bmatrix}, \qquad \overline{C}_{i1} = \begin{bmatrix} C_{i1} & D_{i12} C_{iK} \end{bmatrix},$$

$$\overline{x}_{i}(t) = \begin{bmatrix} x_{i}(t) \\ \widehat{x}_{i}(t) \end{bmatrix}, \qquad \overline{z}_{i}(t) = z_{i}(t).$$
(19)

The following theorem presents the solving method of the dynamic H_{∞} output feedback controller gains for uncertain neutral interconnected systems (16).

Theorem 4. For given $\gamma_i > 0$, consider system (16) with (2) and (3). Under the condition of Assumption 1, if there exist matrices $X_i > 0$, $Y_i > 0$, $Q_{i1} > 0$, $Q_{i2} > 0$, $G_{ij} > 0$, $G_{ji} > 0$ and invertible matrices N_i , matrices \widehat{A}_i , \widehat{B}_i , \widehat{C}_i , such that $\Psi_i = \begin{bmatrix} X_i & I \\ * & Y_i \end{bmatrix} > 0$ and the following LMI holds,

 Ω_i

then there exists a dynamic output feedback controller such that the closed-loop system (18) is asymptotically stable and satisfies $\|T_{z_i\omega_i}\| < \gamma_i \text{ with } A_{iK} = N_i^{-1}(\widehat{A}_i - Y_iA_iX_i - N_iB_{iK}C_{i2}X_i - Y_iB_{i2}C_{iK}M_i^T)M_i^{-T}, B_{iK} = N_i^{-1}\widehat{B}_i, C_{iK} = \widehat{C}_iM_i^{-T}, where$

$$\begin{split} M_{i} &= (I - X_{i}Y_{i})N_{i}^{-T}, \\ \Omega_{11}^{i} &= \begin{bmatrix} A_{i}X_{i} + X_{i}A_{i}^{T} + B_{12}\hat{C}_{i} + \hat{C}_{i}^{T}B_{12}^{T} & \widehat{A}_{i}^{T} + A_{i} \\ * & Y_{i}A_{i} + A_{i}^{T}Y_{i} + \hat{B}_{i}C_{12} + C_{12}^{T}\hat{B}_{i}^{T} \end{bmatrix}, \\ \Omega_{12}^{i} &= \begin{bmatrix} A_{ia_{i}} + 2X_{i}E_{i}^{T}E_{ia_{i}} + 2\hat{C}_{i}^{T}E_{12}^{T}E_{ia_{i}} & 0 \\ Y_{i}A_{ia_{i}} + 2E_{i}^{T}E_{ia_{i}} & 0 \end{bmatrix}, \\ \Omega_{13}^{i} &= \begin{bmatrix} A_{i1} + 2X_{i}E_{i}^{T}L_{i1} + 2\hat{C}_{i}^{T}E_{i}^{T}L_{i1} & 0 & \cdots & A_{i+1} + 2X_{i}E_{i}^{T}L_{i+1} + 2\hat{C}_{i}^{T}E_{i}^{T}L_{i+1} & 0 \\ Y_{i}A_{i+1} + 2\hat{E}_{i}^{T}L_{i+1} + 2\hat{C}_{i}^{T}E_{i}^{T}L_{i+1} & 0 & \cdots & A_{i+1} + 2X_{i}E_{i}^{T}L_{i+1} + 2\hat{C}_{i}^{T}E_{i}^{T}L_{in} & 0 \\ Y_{i}A_{i+1} + 2X_{i}E_{i}^{T}L_{i+1} + 2\hat{C}_{i}^{T}E_{i}^{T}L_{i+1} & 0 & \cdots & A_{i+1} + 2X_{i}E_{i}^{T}L_{i+1} + 2\hat{C}_{i}^{T}E_{i}^{T}L_{in} & 0 \\ Y_{i}A_{i+1} + 2X_{i}E_{i}^{T}L_{i+1} & 0 & \cdots & A_{i+1} + 2X_{i}E_{i}^{T}L_{i+1} + 2\hat{C}_{i}^{T}E_{i}^{T}L_{in} & 0 \\ X_{i+1} + 2X_{i}E_{i}^{T}L_{i+1} + 2\hat{C}_{i}^{T}E_{i}^{T}L_{i+1} & 0 & \cdots & A_{i+1} + 2X_{i}E_{i}^{T}L_{i+1} + 2\hat{C}_{i}^{T}E_{i}^{T}L_{in} & 0 \\ X_{i}A_{i+1} + 2X_{i}E_{i}^{T}L_{i+1} & 0 & \cdots & X_{i+1} + 2X_{i}E_{i}^{T}L_{i+1} & 0 \\ Y_{i}A_{i+1} + 2X_{i}E_{i}^{T}L_{i+1} & 0 & \cdots & X_{i+1} + 2X_{i}E_{i}^{T}L_{i+1} & 0 \\ X_{i+1} + X_{i}A_{i+1} + 2X_{i}E_{i}^{T}L_{i+1} & 0 & \cdots & X_{i+1} + 2X_{i}E_{i}^{T}L_{i+1} & 0 \\ X_{i+1} + X_{i}A_{i+1} + X_{i}A_{i}^{T}A_{i} & 0 & X_{i}A_{i} & X_{i}C_{i}^{T}+\hat{C}_{i}^{T}D_{i}A_{i} \\ X_{i}C_{i}^{T}+\hat{C}_{i}^{T}D_{i}^{T}D_{i}^{T}D_{i} & X_{i}C_{i}^{T}+\hat{C}_{i}^{T}D_{i}^{$$

Applying Theorem 3 to the closed-loop system (18), then system (18) is robustly asymptotically stable and satisfies $\|T_{z_i\omega_i}\|_{\infty} < \gamma_i$ under the condition of Assumption 1, if there exist matrices $P_i > 0$, $Q_{i1} > 0$, $Q_{i2} > 0$, $G_{ij} > 0$, and $G_{ji} > 0$

such that the LMI (5) holds, where A_i , $A_{i\sigma_i}$, $A_{i\eta_i}$, B_{i1} , A_{ij} , C_{i1} , D_{i11} , D_i , $E_{i\sigma_i}$, and L_{ij} are substituted with \overline{A}_i , $\overline{A}_{i\sigma_i}$, $\overline{A}_{i\eta_i}$, \overline{B}_{i1} , \overline{A}_{ij} , \overline{C}_{i1} , \overline{D}_{i11} , \overline{D}_i , $\overline{E}_{i\sigma_i}$, and \overline{L}_{ij} , respectively.

Firstly, decompose matrix P_i and its inverse as

$$P_{i} = \begin{bmatrix} Y_{i} & N_{i} \\ * & W_{i} \end{bmatrix}, \qquad P_{i}^{-1} = \begin{bmatrix} X_{i} & M_{i} \\ * & Z_{i} \end{bmatrix}, \tag{22}$$

where $Y_i, X_i \in \Re^{n_i}$ are positive definite matrices, and M_i and N_i are invertible matrices. According to $P_i^{-1}P_i = I$, we have

$$M_i N_i^T = I - X_i Y_i. (23)$$

Define $F_{i1} = \begin{bmatrix} X_i & I \\ M_i^T & 0 \end{bmatrix}$, $F_{i2} = \begin{bmatrix} I & Y_i \\ 0 & N^T \end{bmatrix}$, then it follows that

$$P_i F_{i1} = F_{i2}, F_{i1}^T P_i F_{i1} = F_{i2}^T F_{i1} = \begin{bmatrix} X_i & I \\ * & Y_i \end{bmatrix} > 0. (24)$$

Next, pre- and postmultiply the substitute of LMI (5) by the matrix

diag
$$\{F_{i1}^T, I, I, I, I, I, I, I\}$$
 (25)

and its transpose, respectively. By the Schur Complement formula, the following LMI can be obtained:

where

$$\begin{split} \Phi_{12}^{i} &= F_{i1}^{T} P_{i} \overline{A}_{i\sigma_{i}} + 2 F_{i1}^{T} \overline{E}_{i1}^{T} \overline{E}_{i\sigma_{i}}, \\ \Phi_{13}^{i} \\ &= \left[\begin{array}{cccc} F_{i1}^{T} P_{i} \overline{A}_{i1} + 2 F_{i1}^{T} \overline{E}_{i1}^{T} \overline{L}_{i1} & \cdots & F_{i1}^{T} P_{i} \overline{A}_{i-1} + 2 F_{i1}^{T} \overline{E}_{i1}^{T} \overline{L}_{i-1} \\ F_{i1}^{T} P_{i} \overline{A}_{ii+1} + 2 F_{i1}^{T} \overline{E}_{i1}^{T} \overline{L}_{ii+1} & \cdots & F_{i1}^{T} P_{i} \overline{A}_{iN} + 2 F_{i1}^{T} \overline{E}_{i1}^{T} \overline{L}_{iN} \end{array} \right], \\ \Phi_{14}^{i} &= -F_{i1}^{T} \overline{A}_{i}^{T} P_{i} \overline{A}_{i\eta_{i}}, & \Phi_{15}^{i} &= F_{i1}^{T} P_{i} \overline{B}_{i1}, \\ \Phi_{16}^{i} &= F_{i1}^{T} \overline{C}_{i1}^{T}, & \Phi_{17}^{i} &= F_{i1}^{T} P_{i} \overline{D}_{i}, \\ \Phi_{19}^{i} &= F_{i1}^{T}, & \Phi_{110}^{i} &= F_{i1}^{T}, \\ \Phi_{111}^{i} &= F_{i1}^{T}, & \Phi_{112}^{i} &= F_{i1}^{T} \overline{E}_{i1}^{T}, \\ \Phi_{22}^{i} &= -Q_{i1} + 2 \overline{E}_{i\sigma_{i}}^{T} \overline{E}_{i\sigma_{i}}, & \Phi_{24}^{i} &= - \overline{A}_{i\sigma_{i}}^{T} P_{i} \overline{A}_{i\eta_{i}}, \\ \Phi_{23}^{i} &= \left[2 \overline{E}_{i\sigma_{i}}^{T} \overline{L}_{i1} & \cdots & 2 \overline{E}_{i\sigma_{i}}^{T} \overline{L}_{ii-1} & 2 \overline{E}_{i\sigma_{i}}^{T} \overline{L}_{ii+1} & \cdots & 2 \overline{E}_{i\sigma_{i}}^{T} \overline{L}_{iN} \right], \end{split}$$

 $\Phi_{11}^i = F_{:1}^T P_i \overline{A}_i F_{:1} + F_{:1}^T \overline{A}_i^T P_i F_{:1},$

$$\Phi_{33}^{i} = \operatorname{diag} \left\{ -G_{i1} + 2\overline{L}_{i1}^{T}\overline{L}_{i1}, \dots, -G_{i\,i-1} + 2\overline{L}_{i\,i-1}^{T}\overline{L}_{i\,i-1}, \dots, -G_{i\,i+1} + 2\overline{L}_{i\,i+1}^{T}\overline{L}_{i\,i+1}, \dots, -G_{iN} + 2\overline{L}_{iN}^{T}\overline{L}_{iN} \right\},$$

$$\Phi_{34}^{i} = \left[-\overline{A}_{i\eta_{i}}^{T}P_{i}\overline{A}_{i1} \dots -\overline{A}_{i\eta_{i}}^{T}P_{i}\overline{A}_{i-1} - \overline{A}_{i\eta_{i}}^{T}P_{i}\overline{A}_{i+1} \dots -\overline{A}_{i\eta_{i}}^{T}P_{i}\overline{A}_{iN} \right]^{T},$$

$$\Phi_{44}^{i} = -Q_{i2}, \qquad \Phi_{45}^{i} = -\overline{A}_{i\eta_{i}}^{T}P_{i}\overline{B}_{i1},$$

$$\Phi_{48}^{i} = -\overline{A}_{i\eta_{i}}^{T}P_{i}\overline{D}_{i}, \qquad \Phi_{55}^{i} = -\gamma_{i}^{2}I,$$

$$\Gamma_{56}^{i} = \overline{D}_{i11}^{T}, \qquad \Phi_{99}^{i} = -(1 - f_{i})Q_{i1}^{-1},$$

$$\Phi_{1111}^{i} = -(1 - g_{i})Q_{i2},$$

$$\Phi_{1010}^{i} = \operatorname{diag} \left\{ -(1 - l_{1})G_{1i}, \dots, -(1 - l_{i-1})G_{i-1i}, -(1 - l_{i+1})G_{i+1i}, \dots, -(1 - l_{N})G_{Ni} \right\}.$$
(27)

By Lemma 2, we have

$$-F_{i2}^{T}Q_{i1}^{-1}F_{i2} - Q_{i1} \le -F_{i2}^{T} - F_{i2},$$

$$-F_{i2}^{T}Q_{i2}^{-1}F_{i2} - Q_{i2} \le -F_{i2}^{T} - F_{i2},$$

$$-F_{i2}^{T}G_{ji}^{-1}F_{i2} - G_{ji} \le -F_{i2}^{T} - F_{i2},$$

$$i, j = 1, 2, ..., N, j \ne i.$$
(28)

Pre- and postmultiplying the inequality (26) by the matrix

diag
$$\{I, I, I, I, I, I, I, F_{i2}^T, F_{i2}^T, F_{i2}^T, F_{i2}^T, I\}$$
, (29)

and its transpose, respectively, and utilizing (28), and denoting

$$\widehat{A}_i = Y_i A_i X_i + N_i B_{iK} C_{i2} X_i + Y_i B_{i2} C_{iK} M_i^T + N_i A_{iK} M_i^T,$$

$$\widehat{B}_i = N_i B_{iK}, \qquad \widehat{C}_i = C_{iK} M_i^T,$$
(30)

one can obtain Theorem 4 immediately. This completes the proof.

Algorithm 5. Given any solution of the LMI (20) in Theorem 4, a corresponding controller of the form (17) will be constructed as follows.

- (i) Utilizing the two positive definite solutions X_i , Y_i and the invertible matrix N_i ; compute the invertible M_i satisfying (23).
- (ii) Utilizing the matrices M_i and N_i obtained above; compute the gains A_{iK} , B_{iK} , and C_{iK} according to (30).

4. Illustrative Example

Consider system (16) composed of a three-order subsystem and a two-order subsystem with the following parameters:

$$\begin{split} A_1 &= \begin{bmatrix} 0.3 & -1.50.8 \\ -0.9 & -23.5 & 5.6 \\ 0.5 & 0.9 & -25.3 \end{bmatrix}, \qquad B_{11} = \begin{bmatrix} -0.1 & -0.2 \\ -0.3 & 0.2 \\ 0.1 & -0.1 \end{bmatrix}, \\ B_{12} &= \begin{bmatrix} 0.2 & 0.5 \\ -0.1 & -0.7 \\ -0.1 & 0.2 \end{bmatrix}, \qquad A_{1\sigma_1} &= \begin{bmatrix} -0.1 & 0.3 & -0.1 \\ 0.1 & -0.2 & -0.3 \\ 0.2 & 0.4 & 0.2 \end{bmatrix}, \\ A_{1\eta_1} &= \begin{bmatrix} 0.1 & -0.3 & -0.1 \\ 0.1 & 0.5 & -0.1 \\ 0.2 & 0.1 & -0.5 \end{bmatrix}, \qquad A_{12} &= \begin{bmatrix} -0.1 & 0.1 \\ -0.1 & 0.2 \\ -0.6 & -0.4 \end{bmatrix}, \end{split}$$

$$\begin{split} D_1 &= \begin{bmatrix} 0.01 & 0.5 & -0.01 \\ -0.1 & 0 & 0 \\ 0 & 0.1 & 0 \end{bmatrix}, \qquad E_{11} &= \begin{bmatrix} -0.1 & -0.1 & 0.1 \\ -0.1 & 0.2 & 0.1 \\ 0.1 & -0.1 & -0.2 \end{bmatrix}, \\ E_{12} &= \begin{bmatrix} -0.01 & 0.1 \\ 0.01 & -0.2 \\ 0.01 & -0.2 \end{bmatrix}, \qquad E_{1\sigma_1} &= \begin{bmatrix} 0.1 & 0.1 & -0.1 \\ -0.1 & -0.2 & -0.1 \\ -0.1 & -0.1 & 0.1 \end{bmatrix}, \\ E_{12} &= \begin{bmatrix} -0.1 & -0.3 \\ -0.1 & 0.1 \\ -0.4 & 0.2 \end{bmatrix}, \qquad C_{11} &= \begin{bmatrix} -0.4 & -0.1 & 0.1 \\ -0.1 & -0.2 & 0.3 \end{bmatrix}, \\ D_{111} &= \begin{bmatrix} -0.1 & 0.1 \\ 0.5 & 0.3 & -1.4 \end{bmatrix}, \qquad D_{112} &= \begin{bmatrix} 0.1 & -0.1 \\ 0.1 & 0.1 \end{bmatrix}, \\ C_{12} &= \begin{bmatrix} -0.1 & -0.1 & -0.1 \\ 0.5 & 0.3 & -1.4 \end{bmatrix}, \qquad D_{121} &= \begin{bmatrix} -0.2 & -0.1 \\ 0.1 & 0.1 \end{bmatrix}, \\ C_{12} &= \begin{bmatrix} -15.1 & 0.1 \\ -0.7 & -5.4 \end{bmatrix}, \qquad A_{2\sigma_2} &= \begin{bmatrix} -0.6 & -0.3 \\ -0.4 & 0.1 \end{bmatrix}, \\ A_{2\eta_2} &= \begin{bmatrix} -0.2 & 0.2 \\ 0.1 & -0.1 \end{bmatrix}, \qquad B_{21} &= \begin{bmatrix} -0.1 \\ -0.1 \end{bmatrix}, \\ A_{2\eta_2} &= \begin{bmatrix} 0.1 & -0.1 & -0.1 \\ -0.1 & 0.1 & 0.1 \end{bmatrix}, \qquad B_{22} &= \begin{bmatrix} 0.5 \\ 0.1 \end{bmatrix}, \\ D_2 &= \begin{bmatrix} 0.1 & 0.4 \\ -0.1 & 0.1 \end{bmatrix}, \qquad E_{21} &= \begin{bmatrix} -0.1 & 0.1 \\ 0.2 & -0.1 \end{bmatrix}, \\ E_{2\sigma_2} &= \begin{bmatrix} -0.1 & -0.1 \\ -0.1 & 0.1 \end{bmatrix}, \qquad E_{21} &= \begin{bmatrix} -0.1 & 0.1 \\ 0.2 & -0.1 \end{bmatrix}, \\ D_{211} &= 0.13, \qquad D_{221} &= -0.53, \\ C_{22} &= \begin{bmatrix} 0.1 & 0.5 \end{bmatrix}, \qquad D_{212} &= 0.16, \\ \sigma_2(t) &= 0.2 & (1 + \cos(t)), \\ \eta_2(t) &= 0.1 & (2 + \cos(t)), \\ \tau_{21}(t) &= 0.2 & (2 + \sin(t)), \\ \tau_{12}(t) &= 0.1 & (1 + \cos(t)), \\ \eta_1 &= 0.5, \qquad \gamma_2 &= 0.3. \\ \end{split}$$

Using the above parameters and applying Matlab Software to solving LMI (20), we can obtain the following results:

(31)

$$\begin{split} X_1 &= \left[\begin{array}{cccc} 0.0947 & 0.5569 & -0.1173 \\ 0.5569 & 6.1762 & 0.5942 \\ -0.1173 & 0.5942 & 7.2277 \end{array} \right], \\ Y_1 &= \left[\begin{array}{cccc} 0.2448 & -0.0612 & 0.2138 \\ -0.0612 & 0.1830 & -0.0255 \\ 0.2138 & -0.0255 & 0.2034 \end{array} \right], \end{split}$$

$$N_{1} = \begin{bmatrix} 1.2558 & -0.0000 & 0.0000 \\ -0.0000 & 1.2558 & -0.0000 \\ 0.0000 & -0.0000 & 1.2558 \end{bmatrix} \times 10^{5},$$

$$X_{2} = \begin{bmatrix} 4.4043 & 0.4772 \\ 0.4772 & 1.4044 \end{bmatrix}, \qquad Y_{2} = \begin{bmatrix} 1.4996 & 1.4523 \\ 1.4523 & 8.4219 \end{bmatrix},$$

$$N_{2} = \begin{bmatrix} 1.2075 & 0.0001 \\ 0.0001 & 1.2078 \end{bmatrix} \times 10^{5},$$

$$\widehat{A}_{1} = \begin{bmatrix} -1.4345 & -2.7721 & 5.7617 \\ -1.2489 & -9.1781 & 1.1119 \\ 0.3361 & 3.1163 & -5.0939 \end{bmatrix},$$

$$\widehat{C}_{1} = \begin{bmatrix} -1.6597 & -1.9990 & -0.3384 \\ -1.7543 & 0.5932 & 1.5744 \end{bmatrix},$$

$$\widehat{B}_{1} = \begin{bmatrix} -1.8297 & -4.1087 \\ 0.3341 & -0.3560 \\ -0.9167 & -0.6854 \end{bmatrix}, \qquad \widehat{A}_{2} = \begin{bmatrix} 0.5829 & -1.2895 \\ 1.5056 & -5.9999 \end{bmatrix},$$

$$\widehat{B}_{2} = \begin{bmatrix} -1.1894 \\ -2.1534 \end{bmatrix}, \qquad \widehat{C}_{2} = [-10.0067 & -3.6127].$$
(32)

Using the obtained solutions X_1 , Y_1 , N_1 , X_2 , Y_2 , and N_2 to solve (23), we have

$$M_{1} = \begin{bmatrix} 0.0825 & -0.0079 & 0.0014 \\ 0.0091 & -0.0064 & -0.0066 \\ -0.1178 & 0.0054 & -0.0342 \end{bmatrix} \times 10^{-4},$$

$$M_{2} = \begin{bmatrix} -0.5215 & -0.8623 \\ -0.2281 & -0.9538 \end{bmatrix} \times 10^{-4}.$$
(33)

Using the above solutions M_1 , N_1 , M_2 , and N_2 to compute A_{1K} , B_{1K} , C_{1K} , A_{2K} , B_{2K} , and C_{2K} according to (30), the following results are obtained:

$$A_{1K} = \begin{bmatrix} 5.6151 & 65.5141 & -14.4781 \\ -33.1939 & -343.0572 & 85.8446 \\ 3.9271 & 29.4768 & -64.3063 \end{bmatrix},$$

$$B_{1K} = \begin{bmatrix} -0.1457 & -0.3272 \\ 0.0266 & -0.0283 \\ -0.0730 & -0.0546 \end{bmatrix} \times 10^{-4},$$

$$C_{1K} = \begin{bmatrix} 0.0683 & 2.8751 & 0.3203 \\ -0.4408 & -2.2598 & 0.6995 \end{bmatrix} \times 10^{6},$$

$$A_{2K} = \begin{bmatrix} -25.1345 & 3.8472 \\ -24.1933 & -1.0036 \end{bmatrix}, \qquad B_{2K} = \begin{bmatrix} -0.0985 \\ -0.1783 \end{bmatrix} \times 10^{-4},$$

$$C_{2K} = \begin{bmatrix} 2.1380 & -0.1326 \end{bmatrix} \times 10^{5}.$$

$$(34)$$

When $F_1(t) = \text{diag}\{\sin(t), \sin(t), \sin(t)\}$ and $F_2(t) = \text{diag}\{\cos(t), \cos(t)\}$, the simulation results are shown in Figures 1–4 based on the above parameters. From Figures 1 and 2, one can see that the uncertain interconnected systems of neutral type (16) without controllers are not convergent. From Figures 3 and 4, one can see that the uncertain interconnected systems of neutral type (16) are indeed well stabilized.

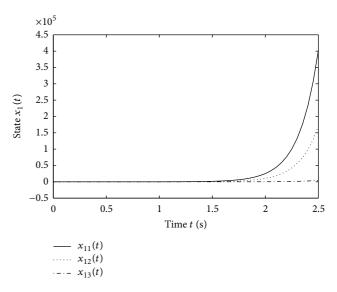


FIGURE 1: State response of the first open-loop subsystem.

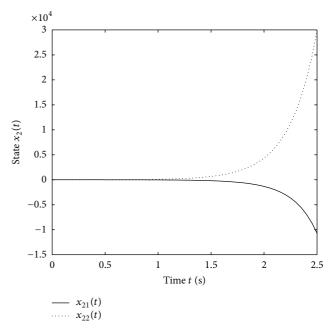


FIGURE 2: State response of the second open-loop subsystem.

5. Conclusion

The H_{∞} decentralized control problem via output feedback for uncertain neutral interconnected systems with time-varying delays is complex and challenging. Developing a novel mathematical technique for treating the nonlinear interconnection variable matrices, a sufficient condition of existing anticipated controller is obtained in terms of LMIs based on Lyapunov stability theory, which not only depends on the sizes of delays but also on the information of derivatives. The illustrative example shows that the results obtained in this paper are effective.

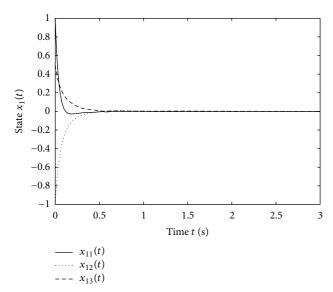


FIGURE 3: State response of the first closed-loop subsystem.

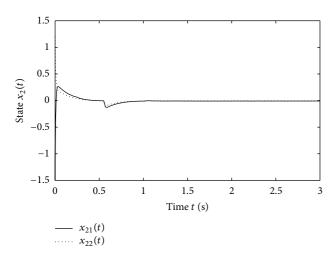


FIGURE 4: State response of the second closed-loop subsystem.

Conflict of Interests

The authors declare that there is no conflict of interests regarding the publication of this paper.

Acknowledgments

This research is supported by Natural Science Foundation of China (no. 61104106, 61372195, 61304069), Science Foundation of Department of Education of Liaoning Province (no. L2012422), and the Doctorial Science Foundation of Shenyang University (no. 1120212340).

References

[1] H. Mukaidani and H. Xu, "Pareto optimal strategy for stochastic weakly coupled large scale systems with state dependent system noise," *IEEE Transactions on Automatic Control*, vol. 54, no. 9, pp. 2244–2250, 2009.

- [2] A. Swarnakar, H. J. Marquez, and T. Chen, "A new scheme on robust observer-based control design for interconnected systems with application to an industrial utility boiler," *IEEE Transactions on Control Systems Technology*, vol. 16, no. 3, pp. 539–547, 2008.
- [3] M. Franceschelli, A. Gasparri, A. Giua, and G. Ulivi, "Decentralized stabilization of heterogeneous linear multi-agent systems," in *Proceedings of the 2010 IEEE International Conference on Robotics and Automation*, pp. 3556–3561, May 2010.
- [4] S. J. Yoo, N. Hovakimyan, and C. Cao, "Decentralised L_1 adaptive control for large-scale non-linear systems with interconnected unmodelled dynamics," *IET Control Theory & Applications*, vol. 4, no. 10, pp. 1972–1988, 2010.
- [5] S. Schuler, P. Li, J. Lam, and F. Allgöwer, "Design of structured dynamic output-feedback controllers for interconnected systems," *International Journal of Control*, vol. 84, no. 12, pp. 2081– 2091, 2011.
- [6] N. Chen, G. Zhai, W. Gui, C. Yang, and W. Liu, "Decentralised H_∞ quantisers design for uncertain interconnected networked systems," *IET Control Theory & Applications*, vol. 4, no. 2, pp. 177–185, 2010.
- [7] X.-G. Yan, S. K. Spurgeon, and C. Edwards, "Global decentralised static output feedback sliding-mode control for interconnected time-delay systems," *IET Control Theory & Applications*, vol. 6, no. 2, pp. 192–202, 2012.
- [8] X. Ye, "Decentralized adaptive stabilization of large-scale nonlinear time-delay systems with unknown high-frequency-gain signs," *IEEE Transactions on Automatic Control*, vol. 56, no. 6, pp. 1473–1478, 2011.
- [9] C. C. Hua, J. Leng, and X. P. Guan, "Decentralized MRAC for large-scale interconnected systems with time-varying delays and applications to chemical reactor systems," *Journal of Process Control*, vol. 22, no. 10, pp. 1985–1996, 2012.
- [10] C.-C. Hua, Q.-G. Wang, and X.-P. Guan, "Exponential stabilization controller design for interconnected time delay systems," *Automatica*, vol. 44, no. 10, pp. 2600–2606, 2008.
- [11] H. Wu, "Decentralised adaptive robust control of uncertain large-scale non-linear dynamical systems with time-varying delays," *IET Control Theory & Applications*, vol. 6, no. 5, pp. 629–640, 2012.
- [12] Y. Zhu and P. R. Pagilla, "Decentralized output feedback control of a class of large-scale interconnected systems," *IMA Journal of Mathematical Control and Information*, vol. 24, no. 1, pp. 57–69, 2007.
- [13] S. Yin, H. Luo, and S. Ding, "Real-time implementation of fault-tolerant control systems with performance optimization," *IEEE Transactions on Industrial Electronics*, vol. 64, no. 5, pp. 2402–2411, 2014.
- [14] S. Yin, G. Wang, and H. Karimi, "Data-driven design of robust fault detection system for wind turbines," *Mechatronics*, 2013.
- [15] V. Kolmanovskii and A. Myshkis, Introduction to the Theory and Applications of Functional Differential Equations, Kluwer Academic Publishers, Dordrecht, The Netherlands, 1999.
- [16] L. Xiong, J. Tian, and X. Liu, "Stability analysis for neutral Markovian jump systems with partially unknown transition probabilities," *Journal of the Franklin Institute*, vol. 349, no. 6, pp. 2193–2214, 2012.
- [17] R. Sakthivel, K. Mathiyalagan, and S. M. Anthoni, "Robust stability and control for uncertain neutral time delay systems," *International Journal of Control*, vol. 85, no. 4, pp. 373–383, 2012.

- [18] O. M. Kwon, M. J. Park, J. H. Park, S. M. Lee, and E. J. Cha, "New delay-partitioning approaches to stability criteria for uncertain neutral systems with time-varying delays," *Journal of the Franklin Institute*, vol. 349, no. 9, pp. 2799–2823, 2012.
- [19] L. Wang and C. Shao, "Stability analysis and control synthesis of uncertain neutral delay systems with actuator failures," *International Journal of Automation and Control*, vol. 4, no. 4, pp. 398–416, 2010.
- [20] F. Qiu and B. Cui, "Improved exponential stability criteria for uncertain neutral system with nonlinear parameter perturbations," *International Journal of Automation and Computing*, vol. 7, no. 4, pp. 413–418, 2010.
- [21] J. Yang, W. Luo, G. Li, and S. Zhong, "Reliable guaranteed cost control for uncertain fuzzy neutral systems," *Nonlinear Analysis: Hybrid Systems*, vol. 4, no. 4, pp. 644–658, 2010.
- [22] F. El Haoussi and H. El Tissir, "Delay and its time-derivative dependent robust stability of uncertain neutral systems with saturating actuators," *International Journal of Automation and Computing*, vol. 7, no. 4, pp. 455–462, 2010.
- [23] Y. Xiong and M. Saif, "Sliding mode observer for nonlinear uncertain systems," *IEEE Transactions on Automatic Control*, vol. 46, no. 12, pp. 2012–2017, 2001.
- [24] C. Jiang, "Observer design for neutral systems with delays and nonlinear perturbations: delay-dependent method," *International Journal of Control, Automation, and Systems*, vol. 11, no. 2, pp. 427–432, 2013.
- [25] S. Tong, Y. Li, G. Feng, and T. Li, "Observer-based adaptive fuzzy backstepping dynamic surface control for a class of non-linear systems with unknown time delays," *IET Control Theory & Applications*, vol. 5, no. 12, pp. 1426–1438, 2011.
- [26] W. P. M. H. Heemels, J. Daafouz, and G. Millerioux, "Observer-based control of discrete-time LPV systems with uncertain parameters," *IEEE Transactions on Automatic Control*, vol. 55, no. 9, pp. 2130–2135, 2010.
- [27] M. Chen and W. Chen, "Disturbance-observer-based robust control for time delay uncertain systems," *International Journal* of Control, Automation and Systems, vol. 8, no. 2, pp. 445–453, 2010.
- [28] N. Takahashi, M. Yokomichi, O. Sato, and M. Kono, "Observer-based control of a manipulator system with structured uncertainty," *Artificial Life and Robotics*, vol. 16, no. 2, pp. 234–238, 2011.
- [29] Y. Li, S. Tong, and Y. Li, "Observer-based adaptive fuzzy backstepping control of MIMO stochastic nonlinear strictfeedback systems," *Nonlinear Dynamics*, vol. 67, no. 2, pp. 1579– 1593, 2012.
- [30] Z. Wang, J. Lam, and K. J. Burnham, "Stability analysis and observer design for neutral delay systems," *IEEE Transactions* on Automatic Control, vol. 47, no. 3, pp. 478–483, 2002.
- [31] L. Huang and X. Mao, "Delay-dependent exponential stability of neutral stochastic delay systems," *IEEE Transactions on Automatic Control*, vol. 54, no. 1, pp. 147–152, 2009.

Hindawi Publishing Corporation Abstract and Applied Analysis Volume 2014, Article ID 832891, 11 pages http://dx.doi.org/10.1155/2014/832891

Research Article

Robust Guaranteed Cost Observer Design for Singular Markovian Jump Time-Delay Systems with Generally Incomplete Transition Probability

Yanbo Li,^{1,2} Yonggui Kao,² and Jing Xie³

Correspondence should be addressed to Yonggui Kao; kaoyonggui@sina.com

Received 29 November 2013; Revised 6 February 2014; Accepted 10 February 2014; Published 24 March 2014

Academic Editor: Shen Yin

Copyright © 2014 Yanbo Li et al. This is an open access article distributed under the Creative Commons Attribution License, which permits unrestricted use, distribution, and reproduction in any medium, provided the original work is properly cited.

This paper is devoted to the investigation of the design of robust guaranteed cost observer for a class of linear singular Markovian jump time-delay systems with generally incomplete transition probability. In this singular model, each transition rate can be completely unknown or only its estimate value is known. Based on stability theory of stochastic differential equations and linear matrix inequality (LMI) technique, we design an observer to ensure that, for all uncertainties, the resulting augmented system is regular, impulse free, and robust stochastically stable with the proposed guaranteed cost performance. Finally, a convex optimization problem with LMI constraints is formulated to design the suboptimal guaranteed cost filters for linear singular Markovian jump time-delay systems with generally incomplete transition probability.

1. Introduction

Descriptor systems are also referred to as singular systems, implicit systems, generalized state-space systems, or semistate systems and provide convenient and natural representations in the description of economic systems, power systems, robotics, network theory, and circuits systems [1]. The stability for singular system is more complicated than that for nonsingular systems because not only the asymptotic stability but also the system regularity and impulse elimination are needed to be addressed [2–5].

In practice, in many physical systems, such as aircraft control, solar receiver control, power systems, manufacturing systems, networked control systems, air intake systems, and other practical systems, abrupt variations may happen in their structure, due to random failures, repair of components, sudden environmental disturbances, changing subsystem interconnections, or abrupt variations in the operating points of a nonlinear plant [6–19]. Therefore, more and more attention has been paid to the problem of stochastic stability and stochastic admissibility for singular Markovian jump

systems (SMJSs) [20–30]. Long et al. [23] derived stochastic admissibility for a class of singular Markovian jump systems with mode-dependent time delays. Wang and Zhang [27] focused on the asynchronous l_2 – l_∞ filtering for discrete-time stochastic Markov jump systems with randomly occurring sensor nonlinearities. However, the TRs in the above mentioned literatures are assumed to be completely known.

In practice, the TRs in some jumping processes are difficult to be precisely estimated due to the cost and some other factors. Therefore, analysis and synthesis problems for normal MJSs with incomplete information on transition probability have attracted more and more attentions [31–49]. Xiong and Lam [32] probed robust H_2 control of Markovian jump systems with uncertain switching probabilities. Karan et al. [33] considered the stochastic stability robustness for continuous-time and discrete-time Markovian jump linear systems (MJLSs) with upper bounded TRs. Zhang and Boukas [34] discussed stability and stabilization for the continuous-time MJSs with partly unknown TRs. Lin et al. [38] considered delay-dependent H_{∞} filtering for discrete-time singular Markovian jump systems with time-varying

¹ School of Mathematical Sciences, Guangxi Teachers Education University, Guangxi 530001, China

² Department of Mathematics, Harbin Institute of Technology, Weihai 264209, China

³ College of Information Science and Engineering, Ocean University of China, Qingdao 266071, China

delay and partially unknown transition probabilities. Guo and Wang [49] proposed another description for the uncertain TRs, which is called generally uncertain TRs (GUTRs).

On the other hand, state estimation plays an important role in systems and control theory, signal processing, and information fusion [50, 51]. Certainly, the most widely used estimation method is the well-known Kalman filtering [52, 53]. A common feature in the Kalman filtering is that an accurate model is available. In some applications, however, when the system is subject to parameter uncertainties, the accurate system model is hard to obtain. To overcome this difficulty, the guaranteed cost filtering approach has been proposed to ensure the upper bound of guaranteed cost function [54]. Robust H_{∞} filtering for uncertain Markovian jump systems with mode-dependent time delays was proposed in [55]. In [56], guaranteed cost and H_{∞} filtering for timedelay systems were presented in terms of LMIs. However, to the best of our knowledge, there are few considering the robust guaranteed cost observer for a class of linear singular Markovian jump time-delay systems with generally incomplete transition probability, which is still an open problem.

In this paper, based on LMI method, we address the design problem of the robust guaranteed cost observer for a class of uncertain descriptor time-delay systems with Markovian jumping parameters and generally uncertain transition rates. The design problem proposed here is to design a memoryless observer such that for all uncertainties, including generally uncertain transition rates, the resulting augmented system is regular, impulse-free, and robust stochastically stable, and satisfies the proposed guaranteed cost performance.

2. Problem Formulation

Consider the following descriptor time-delay systems with Markovian jumping parameters:

$$E\dot{x}\left(t\right) = A\left(r_{t}, t\right)x\left(t\right) + A_{d}\left(r_{t}, t\right)x\left(t - d\right),$$

$$y\left(t\right) = C\left(r_{t}, t\right)x\left(t\right) + C_{d}\left(r_{t}, t\right)x\left(t - d\right), \qquad (1)$$

$$x\left(t\right) = \varphi\left(t\right), \quad \forall t \in [-d, 0],$$

where $x(t) \in \mathbb{R}^n$ and $y(t) \in \mathbb{R}^r$ are the state vector and the controlled output, respectively. d represents the state time delay. For convenience, the input terms in system (1) have been omitted. $\varphi(t) \in L_2[-d,0]$ is a continuous vector-valued initial function. The random parameter $\gamma(t)$ represents a continuous-time discrete-state Markov process taking values in a finite set $\mathbb{S} = \{1,2,\ldots,s\}$ and having the transition probability matrix $\Pi = [\pi_{ij}], i, j \in \mathbb{N}$. The transition probability from mode i to mode j is defined by

$$\Pr\left\{r_{t+\Delta} = j \mid r_t = i\right\} = \begin{cases} \pi_{ij}\Delta + o\left(\Delta\right), & i \neq j, \\ 1 + \pi_{ij}\Delta + o\left(\Delta\right), & i = j, \end{cases} \tag{2}$$

where $\Delta > 0$ satisfies $\lim_{\Delta \to 0} (o(\Delta)/\Delta) = 0$, $\pi_{ij} \ge 0$ is the transition probability from mode i to mode j and satisfies

$$\pi_{ii} = -\sum_{j=1, j \neq i}^{s} \pi_{ij} \le 0.$$
 (3)

In this paper, the transition rates of the jumping process are assumed to be partly available; that is, some elements in matrix Λ have been exactly known, some have been merely known with lower and upper bounds, and others may have no information to use. For instance, for system (1) with four operation modes, the transition rate matrix might be described by

$$\Lambda = \begin{bmatrix}
\widehat{\pi}_{11} + \Delta_{11} & ? & ? & \cdots & ? \\
? & ? & \widehat{\pi}_{23} + \Delta_{23} & \cdots & \widehat{\pi}_{2s} + \Delta_{2s} \\
\vdots & \vdots & \vdots & \ddots & \vdots \\
? & \widehat{\pi}_{s2} + \Delta_{s2} & ? & \cdots & ?
\end{bmatrix},$$
(4)

where $\widehat{\pi}_{ij}$ and $\Delta_{ij} \in [-\sigma_{ij},\sigma_{ij}]$ ($\sigma_{ij} \geq 0$) represent the estimate value and estimate error of the uncertain TR π_{ij} , respectively, where $\widehat{\pi}_{ij}$ and σ_{ij} are known. ? represents the complete unknown TR, which means that its estimate value $\widehat{\pi}_{ij}$ and estimate error bound are unknown.

For notational clarity, for all $i \in \mathbb{S}$, the set U^i denotes $U^i = U^i_k \cup U^i_{uk}$ with $U^i_k = \{j : \text{The estimate} \text{ value of } \pi_{ij} \text{ is known for } j \in \mathbb{S} \}, U^i_{uk} = \{j : \text{The estimate} \text{ value of } \pi_{ij} \text{ is unknown for } j \in \mathbb{S} \}.$ Moreover, if $U^i_k \neq \emptyset$, it is further described as $U^i_k = \{k^i_1, k^i_2, \ldots, k^i_m\}$, where $k^i_m \in \mathbb{N}^+$ represents the mth bound-known element with the index k^i_m in the ith row of matrix Π . We assume that the known estimate values of the TRs are well defined. That is

Assumption 1. If
$$U_k^i = \mathbb{S}$$
, then $\widehat{\pi}_{ij} - \sigma_{ij} \geq 0$ (for all $j \in \mathbb{S}$, $j \neq i$), $\widehat{\pi}_{ii} = -\sum_{j=1, j \neq i}^{N} \widehat{\pi}_{ij}$ and $\sigma_{ii} = -\sum_{j=1, j \neq i}^{s} \sigma_{ij}$.

Assumption 2. If $U_k^i \neq \mathbb{S}$ and $i \in U_k^i$, then $\widehat{\pi}_{ij} - \sigma_{ij} \geq 0$ (for all $j \in \mathbb{S}$, $j \neq i$), $\widehat{\pi}_{ii} + \sigma_{ii} \leq 0$ and $\sum_{j \in U_k^i} \widehat{\pi}_{ij}$.

Assumption 3. If $U_k^i \neq \mathbb{S}$ and $i \notin U_k^i$, then $\widehat{\pi}_{ij} - \sigma_{ij} \geq 0$ (for all $j \in \mathbb{S}$).

Remark 4. The above assumption is reasonable, since it is the direct result from the properties of the TRs (e.g., $\pi_{ij} \geq 0$ (for all $i, j \in \mathbb{S}$, $j \neq i$) and $\pi_{ii} = -\sum_{j=1,j\neq i}^s \pi_{ij}$). The above description about uncertain TRs is more general than either the MJSs model with bounded uncertain TRs or the MJSs model with partly uncertain TRs. If $U^i_{uk} = \emptyset$, for all $i \in \mathbb{S}$, then generally uncertain TR matrix (4) reduces to bounded uncertain TR matrix (5) as follows:

$$\begin{bmatrix} \hat{\pi}_{11} + \Delta_{11} & \hat{\pi}_{12} + \Delta_{12} & \cdots & \hat{\pi}_{1s} + \Delta_{1s} \\ \hat{\pi}_{21} + \Delta_{21} & \hat{\pi}_{22} + \Delta_{22} & \cdots & \hat{\pi}_{2s} + \Delta_{2s} \\ \vdots & \vdots & \ddots & \vdots \\ \hat{\pi}_{s1} + \Delta_{s1} & \hat{\pi}_{s2} + \Delta_{s2} & \cdots & \hat{\pi}_{ss} + \Delta_{ss} \end{bmatrix},$$
 (5)

where $\widehat{\pi}_{ij} - \Delta_{ij} \ge 0$ (for all $j \in \mathbb{S}$, $j \ne i$), $\widehat{\pi}_{ii} = -\sum_{j=1, j \ne i}^{s} \widehat{\pi}_{ij} \le 0$, and $\Delta_{ii} = \sum_{j=1, j \ne i}^{s} \Delta_{ij}$; if $\sigma_{ij} = 0$, for all $i \in \mathbb{S}$, for all $j \in \mathbb{S}$

 U_k^i , then generally uncertain TR matrix (4) reduces to partly uncertain TR matrix (6) as follows:

$$\begin{bmatrix} \pi_{11} & ? & ? & \cdots & ? \\ ? & ? & \pi_{23} & \cdots & \pi_{2s} \\ \vdots & \vdots & \vdots & \ddots & \vdots \\ ? & \pi_{s2} & ? & \cdots & ? \end{bmatrix}. \tag{6}$$

Our results in this paper can be applicable to the general Markovian jump systems with bounded uncertain or partly uncertain TR matrix.

 $A(\gamma(t),t), A_d(\gamma(t),t), C(\gamma(t),t)$, and $C_d(\gamma(t),t)$ are matrix functions of the random jumping process $\gamma(t)$. To simplify the notion, the notation $A_i(t)$ represents $A(\gamma(t),t)$ when $\gamma(t)=i$. For example, $A_d(\gamma(t),t)$ is denoted by $A_{di}(t)$ and so on. Further, for each $\gamma(t)=i\in N$, it is assumed that the matrices $A_i(t), A_{di}(t), C_i(t)$, and $C_{di}(t)$ can be described by the following form:

$$A_{i}(t) = A_{i} + \Delta A_{i}(t), \qquad A_{di}(t) = A_{di} + \Delta A_{di}(t),$$

$$C_{i}(t) = C_{i} + \Delta C_{i}(t), \qquad C_{di}(t) = C_{di} + \Delta C_{di}(t),$$
(7)

where A_i, A_{di}, C_i are C_{di} known real coefficient matrices with appropriate dimensions. Time-varying matrices $\Delta A_i(t), \ \Delta A_{di}(t), \ \Delta C_i(t), \ \text{and} \ \Delta C_{di}(t)$ represent normbounded uncertainties and satisfy

$$\begin{bmatrix} \Delta A_i(t) & \Delta A_{di}(t) \\ \Delta C_i(t) & \Delta C_{di}(t) \end{bmatrix} = \begin{bmatrix} M_{1i} \\ M_{2i} \end{bmatrix} F_i(t) \begin{bmatrix} N_{1i} & N_{2i} \end{bmatrix}, \quad (8)$$

where M_{1i} , M_{2i} , M_{1i} , and N_{2i} are known constant real matrices of appropriate dimensions, which represent the structure of uncertainties, and $F_i(t)$ is an unknown matrix function with Lebesgue measurable elements and satisfies $F_i(t)F_i^T(t) \leq I$.

Further, for convenience, we assume that the system has the same dimension at each mode and the Markov process is irreducible. Consider the following nominal unforced descriptor time-delay system:

$$E\dot{x}(t) = A_i x(t) + A_{di} x(t-d),$$

$$x(t) = \varphi(t), \quad \forall t \in [-d, 0].$$
(9)

Let x_0 , r_0 , and $x(t, \varphi, r_0)$ be the initial state, initial mode, and the corresponding solution of the system (9) at time t, respectively.

Definition 5. System (9) is said to be stochastically stable if, for all $\varphi(t) \in L_2[-d,0]$ and initial mode $r_0 \in N$, there exists a matrix M > 0 such that

$$E\left\{ \int_{0}^{\infty} \|x(t, \varphi, r_{0})\|^{2} dt \mid r_{0}, x(t) = \varphi(t), t \in [-d, 0] \right\}$$

$$\leq x_{0}^{T} M x_{0}.$$
(10)

The following definition can be regarded as an extension of the definition in [2].

Definition 6. (1) System (9) is said to be regular if $det(sE - A_i)$, i = 1, 2, ..., s are not identically zero.

- (2) System (9) is said to be impulse free if $deg(det(sE A_i)) = rank E_i$, i = 1, 2, ..., s.
- (3) System (9) is said to be admissible if it is regular, impulse free, and stochastically stable.

The linear memoryless observer under consideration is as follows:

$$E\hat{x}(t) = K_{1i}\hat{x}(t) + K_{2i}y(t),$$

$$\hat{x}_0 = 0, \qquad r(0) = r_0,$$
(11)

where $\widehat{x}(t) \in \mathbb{R}^n$ is the observer state, and the constant matrices K_{1i} and K_{2i} are observer parameters to be designed.

Denote the error state $e(t) = x(t) - \widehat{x}(t)$, and the augmented state vector $x_f = \begin{bmatrix} x^T(t) & e^T(t) \end{bmatrix}^T$. Let $\widetilde{x}(t) = Le(t)$ represent the output of the error states, where L is a known constant matrix. Define

$$A_{fi} = \begin{bmatrix} A_{i} & 0 \\ A_{i} - K_{1i} - K_{2i}C_{i} & K_{1i} \end{bmatrix},$$

$$A_{fdi} = \begin{bmatrix} A_{di} & 0 \\ A_{di} - K_{2i}C_{di} & 0 \end{bmatrix}, \qquad E_{f} = \begin{bmatrix} E & 0 \\ 0 & E \end{bmatrix},$$

$$M_{fi} = M_{f1i} = \begin{bmatrix} M_{1i} \\ M_{1i} - K_{2i}M_{2i} \end{bmatrix}, \qquad N_{fi} = \begin{bmatrix} N_{1i} & 0 \end{bmatrix},$$

$$\Delta A_{fi} = M_{fi}F_{i}(t)N_{fi}, \qquad N_{f1i} = \begin{bmatrix} N_{2i} & 0 \end{bmatrix},$$

$$\Delta A_{fdi} = M_{f1i}F_{i}(t)N_{f1i}, \qquad C_{f} = \begin{bmatrix} 0 & L \end{bmatrix}$$

and combine (1) and (11); then we derive the augmented systems as follows:

$$E_{f}\dot{x}_{f}(t) = \left(A_{fi} + \Delta A_{fi}\right)x_{f}(t) + \left(A_{fdi} + \Delta A_{fdi}\right)x_{f}(t-d),$$

$$z(t) = C_{f}x_{f}(t),$$
(13)

$$x_{f0}\left(t\right) = \left[\boldsymbol{\varphi}^{T}\left(t\right), \boldsymbol{\varphi}^{T}\left(t\right)\right]^{T}, \quad \forall t \in \left[-d, 0\right].$$

Similar to [5], it is also assumed in this paper that, for all $\varsigma \in [-d, 0]$, there exists a scalar h > 0 such that $||x_f(t + \varsigma)|| \le h||x_f(t)||$.

Associated with system (13) is the cost function

$$\mathcal{J} = \mathbb{E}\left\{\int_0^\infty z^T(t) z(t) dt\right\}. \tag{14}$$

Definition 7. Consider the augmented system (13), if there exist the observer parameters K_{1i} , K_{2i} and a positive scalar \mathcal{J}^* , for all uncertainties, such that the augmented system (13) is robust, stochastically stable and the value of the cost function (14) satisfies $\mathcal{J} \leq \mathcal{J}^*$, then \mathcal{J}^* is said to be a robust guaranteed cost and observer (11) is said to be a robust guaranteed cost observer for system (1) with (4).

Problem 8 (robust guaranteed cost observer problem for a class of linear singular Markovian jump time-delay systems

with generally incomplete transition probability). Given system (1) with GUTR Matrix (4), can we determine an observer (11) with parameters K_{1i} and K_{2i} such that the observer is a robust guaranteed cost observer for system (1) with GUTR Matrix (4)?

Lemma 9. Given any real number ε and any matrix Q, the matrix inequality $\varepsilon(Q + Q^T) \le \varepsilon^2 T + Q T^{-1} Q^T$ holds for any matrix T > 0.

3. Main Results

Theorem 10. Consider the augmented system (13) with GUTR Matrix (4) and the cost function (14). Then the robust guaranteed cost observer (11) with parameters K_{1i} and K_{2i} can be designed if there exist matrices P_i , K_{1i} , and K_{2i} , $i=1,2,\ldots,s$, and symmetric positive definite matrix Q, satisfying the following LMIs, respectively:

Case 1. If $i \notin U_k^i$ and $U_k^i = \{k_1^i, \dots, k_m^i\}$, there exist a set of symmetric positive definite matrices $T_{ij} \in \mathbb{R}^{n \times n}$ $(i \notin U_k^i, j \in U_k^i)$ such that

$$E_f^T P_i = P_i^T E_f \ge 0, \tag{15}$$

$$\begin{bmatrix} \Pi_i + C_f^T C_f & P_i \left(A_{fdi} + \Delta A_{fdi} \right) & \widehat{N}_1 \\ \left(A_{fdi} + \Delta A_{fdi} \right)^T P_i & -Q & 0 \\ * & * & \widehat{N}_2 \end{bmatrix} < 0, \quad (16)$$

$$P_i - P_j \ge 0, \quad \forall j \in U_{uk}^i, \ j \ne i.$$
 (17)

Case 2. If $i \in U_k^i$, $U_k^i = \{k_1^i, \dots, k_m^i\}$ and $U_{uk}^i \neq \emptyset$, there exist a set of symmetric positive definite matrices $V_{ijl} \in \mathbb{R}^{n \times n}$ $(i, j \in U_k^i, l \in U_{uk}^i)$ such that

$$E_f^T P_i = P_i^T E_f \ge 0, (18)$$

$$\begin{bmatrix} \Omega_{i} + C_{f}^{T}C_{f} & P_{i}\left(A_{fdi} + \Delta A_{fdi}\right) & \widehat{M}_{1} \\ \left(A_{fdi} + \Delta A_{fdi}\right)^{T}P_{i} & -Q & 0 \\ * & * & \widehat{M}_{2} \end{bmatrix} < 0. \quad (19)$$

Case 3. If $i \in U_k^i$ and $U_{uk}^i = \emptyset$, there exist a set of symmetric positive definite matrices $W_{ij} \in \mathbb{R}^{n \times n}$ $(i, j \in U_k^i)$ such that

$$E_f^T P_i = P_i^T E_f \ge 0, (20)$$

$$\begin{bmatrix} \Delta_{i} + C_{f}^{T} C_{f} & P_{i} \left(A_{fdi} + \Delta A_{fdi} \right) & \widehat{L}_{1} \\ \left(A_{fdi} + \Delta A_{fdi} \right)^{T} P_{i} & -Q & 0 \\ * & * & \widehat{L}_{2} \end{bmatrix} < 0, \quad (21)$$

where

$$\begin{split} \Pi_i &= \left(A_{fi} + \Delta A_{fi}\right)^T P_i + P_i \left(A_{fi} + \Delta A_{fi}\right) \\ &+ Q + \sum_{j \in U_k^i} \widehat{\pi}_{ij} E_f^T \left(P_j - P_i\right) + \sum_{j \in U_k^i} \frac{1}{4} \sigma_{ij}^2 T_{ij}, \end{split}$$

$$\Omega_{i} = \left(A_{fi} + \Delta A_{fi}\right)^{T} P_{i} + P_{i} \left(A_{fi} + \Delta A_{fi}\right) \\
+ Q + \sum_{j \in U_{k}^{i}} \widehat{\pi}_{ij} E_{f}^{T} \left(P_{j} - P_{l}\right) + \sum_{j \in U_{k}^{i}} \frac{1}{4} \sigma_{ij}^{2} V_{ijl}, \\
\Delta_{i} = \left(A_{fi} + \Delta A_{fi}\right)^{T} P_{i} + P_{i} \left(A_{fi} + \Delta A_{fi}\right) \\
+ Q + \sum_{j \in \mathbb{S}, j \neq i} \widehat{\pi}_{ij} E_{f}^{T} \left(P_{j} - P_{i}\right) + \sum_{j \in \mathbb{S}, j \neq i} \frac{1}{4} \sigma_{ij}^{2} W_{ij}, \\
\widehat{N}_{1} = \left[E_{f}^{T} \left(P_{ik_{1}^{i}} - P_{i}\right), E_{f}^{T} \left(P_{ik_{2}^{i}} - P_{i}\right), \dots, E_{f}^{T} \left(P_{ik_{m}^{i}} - P_{i}\right)\right], \\
\widehat{N}_{2} = \operatorname{diag} \left\{-T_{ik_{1}^{i}}, \dots, -T_{ik_{m}^{i}}\right\}, \\
\widehat{M}_{1} = \left[E_{f}^{T} \left(P_{k_{1}^{i}} - P_{l}\right), E_{f}^{T} \left(P_{k_{2}^{i}} - P_{l}\right), \dots, E_{f}^{T} \left(P_{k_{m}^{i}} - P_{l}\right)\right], \\
\widehat{M}_{2} = \operatorname{diag} \left\{-V_{ik_{1}^{i}l}, \dots, -V_{ik_{m}^{i}l}\right\}, \\
\widehat{L}_{1} = \left[E_{f}^{T} \left(P_{1} - P_{i}\right), \dots, E_{f}^{T} \left(P_{i-1} - P_{i}\right), \\
E_{f}^{T} \left(P_{i+1} - P_{i}\right), \dots, E_{f}^{T} \left(P_{s} - P_{i}\right)\right], \\
\widehat{L}_{2} = \operatorname{diag} \left\{-W_{i1}, \dots, -W_{is}\right\}. \tag{22}$$

Proof. According to Definition 2 and Theorem 1 in [2], we can derive from (15)–(21) that system (13) is regular and impulse free. Let the mode at time t be i, and consider the following Lyapunov function with respect to the augmented system (13)

$$V\left(x_{f}\left(t\right),\gamma\left(t\right)=i\right)=x_{f}^{T}\left(t\right)E_{f}^{T}P_{i}x_{f}\left(t\right)+\int_{t-d}^{t}x_{f}^{T}\left(s\right)Qx_{f}\left(s\right)dt,$$
(23)

where Q is the symmetric positive definite matrix to be chosen, and P_i is a matrix satisfying (15)–(21). The weak infinitesimal operator $\mathcal L$ of the stochastic process $\{\gamma(t), x_f(t)\}, \ t \ge 0$, is presented by

$$\mathcal{L}V\left(x_{f}(t), \gamma(t) = i\right)$$

$$= \lim_{\Delta \to 0} \frac{1}{\Delta} \left[E_{f} \left\{ V\left(x\left(t + \Delta\right), \gamma\left(t + \Delta\right)\right) x\left(t\right), \gamma\left(t\right) = i\right\} \right]$$

$$-V\left(x\left(t\right), \gamma\left(t\right) = i\right) \right]$$

$$= x_{f}^{T}(t) \left[\left(A_{fi} + \Delta A_{fi}\right)^{T} P_{i} + P_{i} \left(A_{fi} + \Delta A_{fi}\right) + \sum_{j=1}^{s} \pi_{ij} E_{f}^{T} P_{j} + Q \right] x_{f}(t)$$

$$+ 2x_{f}^{T}(t) P_{i} \left(A_{f1i} + \Delta A_{f1i}\right) x_{f}(t - d)$$

$$- x_{f}^{T}(t - d) Qx_{f}(t - d). \tag{24}$$

Case 1 ($i \notin U_k^i$). Note that in this case $\sum_{j \in U_{uk}^i, j \neq i} \pi_{ij} = -\sum_{j \in U_{k}^i, j \neq i} \pi_{ij} - \pi_{ii}$ and $\pi_{ij} \geq 0$, $j \in U_{uk}^i$, $j \neq i$; then from (24), we have

$$x_{f}^{T}(t) \left[\sum_{j=1}^{s} \pi_{ij} E_{f}^{T} P_{j} \right] x_{f}(t)$$

$$= x_{f}^{T}(t) \left[\sum_{j \in U_{k}^{i}} \pi_{ij} E_{f}^{T} P_{j} + \sum_{j \in U_{ik}^{i}, j \neq i} \pi_{ij} E_{f}^{T} P_{j} + \pi_{ii} E_{f}^{T} P_{j} \right] x_{f}(t)$$

$$= x_{f}^{T}(t) \left[\sum_{j \in U_{k}^{i}} \pi_{ij} E_{f}^{T} P_{j} + \left(-\pi_{ii} - \sum_{j \in U_{k}^{i}} \pi_{ij} \right) E_{f}^{T} P_{i} \right]$$

$$+ \pi_{ii} E_{f}^{T} P_{i} \right] x_{f}(t)$$

$$= x_{f}^{T}(t) E_{f}^{T} \left[\sum_{j \in U_{k}^{i}} \pi_{ij} \left(P_{j} - P_{i} \right) \right] x_{f}(t)$$

$$= x_{f}^{T}(t) E_{f}^{T} \left[\sum_{j \in U_{k}^{i}} \widehat{\pi}_{ij} \left(P_{j} - P_{i} \right) + \sum_{j \in U_{k}^{i}} \Delta_{ij} \left(P_{j} - P_{i} \right) \right] x_{f}(t).$$

$$(25)$$

On the other hand, in view of Lemma 9, we have

$$\sum_{j \in U_{k}^{i}} \Delta_{ij} E_{f}^{T} \left(P_{j} - P_{i} \right)$$

$$= \sum_{j \in U_{k}^{i}} \left[\frac{1}{2} \Delta_{ij} E_{f}^{T} \left(P_{j} - P_{i} \right) + \frac{1}{2} \Delta_{ij} E_{f}^{T} \left(P_{j} - P_{i} \right) \right]$$

$$\leq \sum_{j \in U_{k}^{i}} \left[\left(\frac{1}{2} \Delta_{ij} \right)^{2} T_{ij} + E_{f}^{T} \left(P_{j} - P_{i} \right) T_{ij}^{-1} \left(P_{j} - P_{i} \right) E_{f} \right]$$

$$\leq \sum_{j \in U_{k}^{i}} \left[\frac{1}{4} \sigma_{ij}^{2} T_{ij} + E_{f}^{T} \left(P_{j} - P_{i} \right) T_{ij}^{-1} \left(P_{j} - P_{i} \right) E_{f} \right]. \tag{26}$$

Case 2 ($i \in U_k^i$ and $U_{uk}^i \neq \emptyset$). Because of $U_k^i = \{k_1^i, \dots, k_m^i\}$ and $U_{uk}^i = \{u_1^i, \dots, u_{s-m}^i\}$, there must be $l \in U_{uk}^i$ so that $E_f^T P_l \geq E_f^T P_l$ (for all $j \in U_{uk}^i$):

$$\begin{aligned} x_{f}^{T}(t) \left[\sum_{j=1}^{s} \pi_{ij} E_{f}^{T} P_{j} \right] x_{f}(t) \\ &\leq x_{f}^{T}(t) \left[\sum_{j \in U_{k}^{i}} \pi_{ij} E_{f}^{T} P_{j} - \left(\sum_{j \in U_{k}^{i}, j \neq i} \pi_{ij} \right) E_{f}^{T} P_{l} \right] x_{f}(t) \\ &= x_{f}^{T}(t) E_{f}^{T} \left[\sum_{j \in U_{k}^{i}} \pi_{ij} \left(P_{j} - P_{l} \right) \right] x_{f}(t) \end{aligned}$$

$$= x_f^T(t) E_f^T \left[\sum_{j \in U_k^i} \widehat{\pi}_{ij} \left(P_j - P_l \right) + \sum_{j \in U_k^i} \Delta_{ij} \left(P_j - P_l \right) \right] x_f(t).$$
(27)

By using Lemma 9, we have

$$\sum_{j \in U_{k}^{I}} \Delta_{ij} E_{f}^{T} \left(P_{j} - P_{l} \right)$$

$$= \sum_{j \in U_{k}^{I}} \left[\frac{1}{2} \Delta_{ij} E_{f}^{T} \left(P_{j} - P_{l} \right) + \frac{1}{2} \Delta_{ij} E_{f}^{T} \left(P_{j} - P_{l} \right) \right]$$

$$\leq \sum_{j \in U_{k}^{I}} \left[\left(\frac{1}{2} \Delta_{ij} \right)^{2} V_{ijl} + E_{f}^{T} \left(P_{j} - P_{l} \right) V_{ijl}^{-1} \left(P_{j} - P_{l} \right) E_{f}^{T} \right]$$

$$\leq \sum_{j \in U_{k}^{I}} \left[\frac{1}{4} \sigma_{ij}^{2} V_{ijl} + E_{f}^{T} \left(P_{j} - P_{l} \right) V_{ijl}^{-1} \left(P_{j} - P_{l} \right) E_{f}^{T} \right]. \tag{28}$$

Case 3 ($i \in U_k^i$ and $U_{uk}^i = \emptyset$). Consider

$$x_{f}^{T}(t) \left[\sum_{j=1}^{s} \pi_{ij} E_{f}^{T} P_{j} \right] x_{f}(t)$$

$$= x_{f}^{T}(t) E_{f}^{T} \left[\sum_{j=1, j \neq i}^{s} \pi_{ij} \left(P_{j} - P_{i} \right) \right] x_{f}(t)$$

$$= x_{f}^{T}(t) E_{f}^{T} \left[\sum_{j=1, j \neq i}^{s} \widehat{\pi}_{ij} \left(P_{j} - P_{i} \right) + \sum_{j=1, j \neq i}^{s} \Delta_{ij} \left(P_{j} - P_{i} \right) \right] x_{f}(t).$$

$$(29)$$

Case 1. Substituting (25) and (26) into (24), it results in

$$\mathscr{L}V \leq \Lambda^{T}(t) \Phi(i) \Lambda(t), \qquad (30)$$

where $\Lambda^{T}(t) = [x_f^{T}(t), x_f^{T}(t-d)]$ and

$$\Phi_{i} = \begin{bmatrix}
\Pi_{i} + C_{f}^{T}C_{f} & P_{i}\left(A_{fdi} + \Delta A_{fdi}\right) & \widehat{N}_{1} \\
\left(A_{fdi} + \Delta A_{fdi}\right)^{T}P_{i} & -Q & 0 \\
* & * & \widehat{N}_{2}
\end{bmatrix}. (31)$$

Case 2. Substituting (27) and (28) into (24), it results in

$$\mathscr{L}V \leq \Lambda^{T}(t) \Psi(i) \Lambda(t),$$
 (32)

where $\Lambda^{T}(t) = [x_f^{T}(t), x_f^{T}(t-d)]$ and

$$\Psi_{i} = \begin{bmatrix} \Omega_{i} + C_{f}^{T}C_{f} & P_{i}\left(A_{fdi} + \Delta A_{fdi}\right) \widehat{M}_{1} \\ \left(A_{fdi} + \Delta A_{fdi}\right)^{T}P_{i} & -Q & 0 \\ * & * & \widehat{M}_{2} \end{bmatrix}. (33)$$

Case 3. Substituting (29) into (24), we get

$$\mathscr{L}V \leq \Lambda^{T}(t) \Gamma(i) \Lambda(t),$$
 (34)

where $\Lambda^{T}(t) = [x_f^{T}(t), x_f^{T}(t-d)]$ and

$$\Gamma_{i} = \begin{bmatrix} \Delta_{i} + C_{f}^{T}C_{f} & P_{i}\left(A_{fdi} + \Delta A_{fdi}\right) & \widehat{L}_{1} \\ \left(A_{fdi} + \Delta A_{fdi}\right)^{T}P_{i} & -Q & 0 \\ * & * & \widehat{L}_{2} \end{bmatrix}. \quad (35)$$

Similar to [5], using *Dynkin's* formula, we drive for each $i \in N$:

$$\lim_{T \to \infty} \mathbb{E} \left\{ \int_0^T x_f^T(t) x_f(t) dt \mid \varphi_f, \gamma_0 = i \right\} \le x_{f0}^T M x_{f0}. \quad (36)$$

By Definition 5, it is easy to see that the augmented system (13) is stochastically stable. Furthermore, from (16), (19), and (21), we have

$$\mathcal{L}V \le -x_f^T(t) C_f^T C_f x_f(t) < 0.$$
 (37)

On the other hand, we have

$$\mathcal{J} = \mathbb{E}\left\{\int_{0}^{\infty} x_{f}^{T}(t) C_{f}^{T} C_{f} x_{f}(t) dt\right\} < -\int_{0}^{\infty} \mathcal{L}V dt$$

$$= -\mathbb{E}\left\{\lim_{t \to \infty} V\left(x(t), \gamma(t)\right)\right\} + V\left(x_{0}, \gamma_{0}\right). \tag{38}$$

As the augmented system (13) is stochastically stable, it follows from (38) that $J < V(x_{f0}, r_0)$. From Definition 7, it is concluded that a robust guaranteed cost for the augmented system (13) can be given by $J^* = x_{f0}^T(t)E_{fr_0}^TP(r_0)x_{f0} + \int_{-d}^0 x_f^T(t)Qx_f(t)dt$.

In the following, based on the above sufficient condition, the design of robust guaranteed cost observers can be turned into the solvability of a system of LMIs.

Theorem 11. Consider system (13) with GUTR Matrix (4) and the cost function (14). If there exist matrices Y_{1i} and Y_{2i} , i = 1, 2, ..., s positive scalars ε_i , i = 1, 2, ..., s, symmetric positive definite matrix Q, and the full rank matrices P_{2i} , and matrices $P_i = \text{diag}(P_{1i}, P_{2i})$, i = 1, 2, ..., s, satisfying the following LMIs, respectively.

Case 1. If $i \notin U_k^i$ and $U_k^i = \{k_1^i, \dots, k_m^i\}$, a set of positive definite matrices $T_{ij} \in \mathbb{R}^{n \times n}$ $(i \notin U_k^i, j \in U_k^i)$ exist such that

$$E_f^T P_i = P_i^T E_f \ge 0, (39)$$

$$\begin{bmatrix} \phi_{1i} & \phi_{2i} & \overline{N}_{1} & \phi_{3i} \\ \phi_{2i}^{T} & -Q & 0 & 0 \\ \overline{N}_{1}^{T} & 0 & \overline{N}_{2} & 0 \\ \phi_{3i}^{T} & 0 & 0 & -\varepsilon_{i}I \end{bmatrix} < 0, \tag{40}$$

$$P_i - P_j \ge 0, \quad \forall j \in U_{uk}^i, \ j \ne i.$$
 (41)

Case 2. If $i \in U_k^i$ $(U_k^i = \{k_1^i, \dots, k_m^i\})$ and $U_{uk}^i \neq \emptyset$, a set of positive definite matrices $V_{ijl} \in \mathbb{R}^{n \times n}$ $(i, j \in U_k^i, l \in U_{uk}^i)$ exist such that

$$E_f^T P_i = P_i^T E_f \ge 0, \tag{42}$$

$$\begin{bmatrix} \varphi_{1i} & \varphi_{2i} & \overline{M}_{1} & \varphi_{3i} \\ \varphi_{2i}^{T} & -Q & 0 & 0 \\ \overline{M}_{1}^{T} & 0 & \overline{M}_{2} & 0 \\ \varphi_{3i}^{T} & 0 & 0 & -\varepsilon_{i}I \end{bmatrix} < 0.$$

$$(43)$$

Case 3. If $i \in U_k^i$ and $U_{uk}^i = \emptyset$, a set of positive definite matrices $W_{ij} \in \mathbb{R}^{n \times n}$ $(i, j \in U_k^i)$ exist such that

$$E_{fi}^{T} P_{i} = P_{i}^{T} E_{fi} \ge 0, (44)$$

$$\begin{bmatrix} \psi_{1i} & \psi_{2i} & \overline{L}_{1} & \psi_{3i} \\ \psi_{2i}^{T} & -Q & 0 & 0 \\ \overline{L}_{1}^{T} & 0 & \overline{L}_{2} & 0 \\ \psi_{2i}^{T} & 0 & 0 & -\varepsilon_{i}I \end{bmatrix} < 0, \tag{45}$$

where

$$\phi_{1i} = \varphi_{1i} = \psi_{1i}$$

$$= \begin{bmatrix} P_{1i}A_i + A_i^T P_{1i} & A_i^T P_{2i} - Y_{1i}^T - C_i^T Y_{2i}^T \\ P_{2i}A_i - Y_{1i} - Y_{2i}C_i & Y_{1i}^T + Y_{1i} \end{bmatrix}$$

$$+ Q + C_f^T C_f + \sum_{j \in U_k^i} \widehat{\pi}_{ij} E_f^T (P_j - P_i) + \sum_{j \in U_k^i} \frac{1}{4} \sigma_{ij}^2 T_{ij},$$

$$\phi_{2i} = \varphi_{2i} = \psi_{2i} = \begin{bmatrix} P_{1i}A_i & 0 \\ P_{2i}A_i - Y_{1i} - Y_{2i}C_i & 0 \end{bmatrix},$$

$$\phi_{3i} = \varphi_{3i} = \psi_{3i} = \begin{bmatrix} P_{1i}M_{1i} \\ P_{2i}M_{1i} - Y_{1i}M_{1i} - Y_{2i}M_{2i} \end{bmatrix},$$

$$\overline{N}_1 = \begin{bmatrix} E_f^T (P_{k_1^i} - P_i), E_f^T (P_{k_2^i} - P_i), \dots, E_f^T (P_{k_m^i} - P_i) \end{bmatrix},$$

$$\overline{N}_2 = \text{diag} \left\{ -T_{ik_1^i}, \dots, -T_{ik_m^i} \right\},$$

$$\overline{M}_1 = \begin{bmatrix} E_f^T (P_{k_1^i} - P_i), E_f^T (P_{k_2^i} - P_i), \dots, E_f^T (P_{k_m^i} - P_i) \end{bmatrix},$$

$$\overline{M}_2 = \text{diag} \left\{ -V_{ik_1^i}, \dots, -V_{ik_m^i} \right\},$$

$$\overline{L}_1 = \begin{bmatrix} E_f^T (P_1 - P_i), \dots, E_f^T (P_{i-1} - P_i), \\ E_f^T (P_{i+1} - P_i), \dots, E_f^T (P_s - P_i) \end{bmatrix},$$

$$\overline{L}_2 = \text{diag} \left\{ -W_{i1}, \dots, -W_{is} \right\}.$$

$$(46)$$

Then a suitable robust guaranteed cost observer in the form of (11) has parameters as follows:

(47) *Proof.* Define

$$K_{1i} = P_{1i}^{-1} Y_{1i}, K_{2i} = P_{2i}^{-1} Y_{2i} (47)$$

$$A_{i}^{1} = \begin{bmatrix} A_{fi}^{T} P_{i} + P_{i} A_{fi} + Q + \sum_{j \in U_{k}^{i}} \widehat{\pi}_{ij} \left(P_{j} - P_{i} \right) + \sum_{j \in U_{k}^{i}} \frac{1}{4} \sigma_{ij}^{2} T_{ij} + C_{f}^{T} C_{f} & P_{i} A_{fdi} & \overline{N}_{1} \\ A_{fdi}^{T} P_{i} & -Q & 0 \\ * & \overline{N}_{2} \end{bmatrix}, \tag{48}$$

Matrix (4).

$$A_{i}^{2} = \begin{bmatrix} A_{fi}^{T} P_{i} + P_{i} A_{fi} + Q + \sum_{j \in U_{k}^{i}} \widehat{\pi}_{ij} \left(P_{j} - P_{i} \right) + \sum_{j \in U_{k}^{i}} \frac{1}{4} \sigma_{ij}^{2} V_{ijl} + C_{f}^{T} C_{f} & P_{i} A_{fdi} & \overline{M}_{1} \\ A_{fdi}^{T} P_{i} & -Q & 0 \\ * & \overline{M}_{2} \end{bmatrix}, \tag{49}$$

$$A_{i}^{3} = \begin{bmatrix} A_{fi}^{T} P_{i} + P_{i} A_{fi} + Q + \sum_{j \in U_{k}^{i}} \widehat{\pi}_{ij} \left(P_{j} - P_{i} \right) + \sum_{j \in U_{k}^{i}} \frac{1}{4} \sigma_{ij}^{2} W_{ij} + C_{f}^{T} C_{f} & P_{i} A_{fdi} & \overline{L}_{1} \\ A_{fdi}^{T} P_{i} & -Q & 0 \\ * & \overline{L}_{2} \end{bmatrix} < 0.$$
 (50)

Then (16) is equivalent to

$$A_{i}^{1} + \begin{bmatrix} P_{i}M_{fi} \\ 0 \\ 0 \end{bmatrix} F_{i} \begin{bmatrix} N_{fi} & N_{f1i} & 0 \end{bmatrix} + \begin{bmatrix} N_{fi} & F_{f1i} & 0 \end{bmatrix}^{T} F_{i}^{T} \begin{bmatrix} P_{i}M_{fi} \\ 0 \\ 0 \end{bmatrix}^{T} < 0.$$
 (51)

Then (19) is equivalent to

$$A_{i}^{2} + \begin{bmatrix} P_{i}M_{fi} \\ 0 \\ 0 \end{bmatrix} F_{i} \begin{bmatrix} N_{fi} & N_{f1i} & 0 \end{bmatrix} + \begin{bmatrix} N_{fi} & F_{f1i} & 0 \end{bmatrix}^{T} F_{i}^{T} \begin{bmatrix} P_{i}M_{fi} \\ 0 \\ 0 \end{bmatrix}^{T} < 0.$$
(52)

Then (21) is equivalent to

$$A_{i}^{3} + \begin{bmatrix} P_{i}M_{fi} \\ 0 \\ 0 \end{bmatrix} F_{i} \begin{bmatrix} N_{fi} & N_{f1i} & 0 \end{bmatrix} + \begin{bmatrix} N_{fi} & F_{f1i} & 0 \end{bmatrix}^{T} F_{i}^{T} \begin{bmatrix} P_{i}M_{fi} \\ 0 \\ 0 \end{bmatrix}^{T} < 0.$$
(53)

By applying Lemma 2.4 in [57], (50), (51), and (52) hold for all uncertainties F_i satisfying $F_i^T F_i < I$ if and only if there exist positive scalars ε_i , i = 1, 2, ..., s, such that

and J^* is a robust guaranteed cost for system (13) with GUTR

$$A_{i}^{1} + \varepsilon_{i}^{-1} \begin{bmatrix} P_{i}M_{fi} \\ 0 \\ 0 \end{bmatrix} \begin{bmatrix} P_{i}M_{fi} \\ 0 \\ 0 \end{bmatrix}^{T} + \varepsilon_{i} [N_{fi} F_{f1i} 0]^{T} [N_{fi} F_{f1i} 0] < 0,$$

$$A_{i}^{2} + \varepsilon_{i}^{-1} \begin{bmatrix} P_{i}M_{fi} \\ 0 \\ 0 \end{bmatrix} \begin{bmatrix} P_{i}M_{fi} \\ 0 \\ 0 \end{bmatrix}^{T} + \varepsilon_{i} [N_{fi} F_{f1i} 0]^{T} [N_{fi} F_{f1i} 0] < 0,$$

$$A_{i}^{3} + \varepsilon_{i}^{-1} \begin{bmatrix} P_{i}M_{fi} \\ 0 \\ 0 \end{bmatrix} \begin{bmatrix} P_{i}M_{fi} \\ 0 \\ 0 \end{bmatrix}^{T} + \varepsilon_{i} [N_{fi} F_{f1i} 0]^{T} [N_{fi} F_{f1i} 0] < 0.$$

$$(54)$$

$$A_{i}^{3} + \varepsilon_{i}^{-1} \begin{bmatrix} P_{i}M_{fi} \\ 0 \\ 0 \end{bmatrix} \begin{bmatrix} P_{i}M_{fi} \\ 0 \\ 0 \end{bmatrix}^{T}$$

$$+ \varepsilon_{i} [N_{fi} F_{f1i} 0]^{T} [N_{fi} F_{f1i} 0] < 0.$$

Let $P_i = \operatorname{diag}(P_{1i}, P_{2i})$, and using (47), we can conclude from Schur complement results that the above matrix inequalities are equivalent to the coupled LMIs (40), (43), and (45). It further follows from Theorem 10 that J^* is a robust guaranteed cost for system (13) with (4).

Remark 12. The solution of LMIs (39)–(45) parameterizes the set of the proposed robust guaranteed cost observers. This parameterized representation can be used to design the guaranteed cost observer with some additional performance constraints. By applying the methods in [14], the suboptimal

guaranteed cost observer can be determined by solving a certain optimization problem. This is the following theorem.

Theorem 13. Consider system (13) with GUTR Matrix (4) and the cost function (14), and suppose that the initial conditions r_0 and x_{f0} are known; if the following optimization problem

$$\min_{Q_{i}P_{1i}, P_{2i}, \varepsilon_{i}, Y_{1i} \text{ and } Y_{2i}} J^{*}$$

$$s.t. LMIs (39) - (45)$$

has a solution Q, P_{1i} , P_{2i} , ε_i , Y_{1i} , and Y_{2i} , $i=1,2,\ldots,s$, then the observer (11) is a suboptimal guaranteed cost observer for system (1), where $J^* = x_{f0}^T E_{fr_0}^T P(r_0) x_{f0} + \operatorname{tr}(\int_{-d}^0 x_{f0}(t) x_{f0}(t) x_{f0}^T dt Q)$.

Proof. It follows from Theorem 11 that the observer (11) constructed in terms of the solution Q, P_{1i} , P_{2i} , ε_i , Y_{1i} , and Y_{2i} , $i=1,2,\ldots,s$, is a robust guaranteed cost observer. By noting that

$$\int_{-d}^{0} x_{f0}^{T}(t) Q x_{f0}(t) dt = \int_{-d}^{0} \operatorname{tr} \left(x_{f0}^{T}(t) Q x_{f0}(t) \right) dt$$

$$= \operatorname{tr} \left(\int_{-d}^{0} x_{f0}^{T}(t) x_{f0}(t) dt Q \right),$$
(56)

it follows that the suboptimal guaranteed cost observer problem is turned into the minimization problem (55). \Box

Remark 14. Theorem 13 gives the suboptimal guaranteed cost observer conditions of a class of linear Markovian jumping time-delay systems with generally incomplete transition probability and LMI constraints, which can be easily solved by the LMI toolbox in MATLAB.

4. Numerical Example

In this section, a numerical example is presented to demonstrate the effectiveness of the method mentioned in Theorem 11. Consider a 2-dimensional system (1) with 3 Markovian switching modes. In this numerical example, the singular system matrix is set as $E = \begin{bmatrix} 1 & 0 \\ 0 & 0 \end{bmatrix}$, and the 3-mode transition rate matrix is $\Lambda = \begin{bmatrix} -3.2 & ? & ? \\ ? & ? & 2 \\ 1.5 & 2.1 & -3.6 \end{bmatrix}$, where Δ_{11} , $\Delta_{31} \in [-0.15, 0.15]$; Δ_{23} , $\Delta_{33} \in [-0.12, 0.12]$ and $\Delta_{32} \in [-0.1, 0.1]$. The other system matrices are as follows.

For mode i = 1, there are

$$A_{1} = \begin{bmatrix} -3.2 & 0.65 \\ 1 & 0.2 \end{bmatrix}, \qquad A_{d1} = \begin{bmatrix} 0.2 & 0.5 \\ 1 & -0.68 \end{bmatrix},$$

$$C_{1} = \begin{bmatrix} 1.2 & 0.65 \\ -6.5 & 1.9 \\ -0.21 & -1.8 \end{bmatrix}, \qquad C_{d1} = \begin{bmatrix} -3.6 & -1.05 \\ 2.1 & 0.96 \\ 0.21 & -0.86 \end{bmatrix},$$

$$M_{11} = \begin{bmatrix} -0.2 \\ 0.8 \end{bmatrix}, \qquad M_{21} = \begin{bmatrix} 0.25 \\ 0.875 \\ -2 \end{bmatrix},$$

$$N_{11} = \begin{bmatrix} -1.2 & 3.1 \end{bmatrix}, \qquad N_{21} = \begin{bmatrix} -0.69 & -4.2 \end{bmatrix}.$$

$$(57)$$

For mode i = 2, there are

$$A_{2} = \begin{bmatrix} -1 & 6 \\ 2 & -3.6 \end{bmatrix}, \qquad A_{d2} = \begin{bmatrix} -3.1 & -1.6 \\ 3 & 0.75 \end{bmatrix},$$

$$C_{2} = \begin{bmatrix} 9 & -2.5 \\ 0.35 & -2 \\ 3.6 & -1.8 \end{bmatrix}, \qquad C_{d2} = \begin{bmatrix} 0.89 & -6 \\ -1.2 & 0.9 \\ -2.4 & 6 \end{bmatrix},$$

$$M_{12} = \begin{bmatrix} 2.3 \\ -4 \end{bmatrix}, \qquad M_{22} = \begin{bmatrix} 0.75 \\ -3.6 \\ 2.5 \end{bmatrix},$$

$$N_{12} = \begin{bmatrix} -7.2 & -6 \end{bmatrix}, \qquad N_{22} = \begin{bmatrix} 1 & 2 \end{bmatrix}.$$
(58)

For mode i = 3, there are

$$A_{3} = \begin{bmatrix} -10.6 & 2.9 \\ -0.3 & 3.6 \end{bmatrix}, \qquad A_{d3} = \begin{bmatrix} -5.6 & -1.2 \\ -3 & 4.5 \end{bmatrix},$$

$$C_{3} = \begin{bmatrix} -3 & -0.36 \\ 0.15 & -1.8 \\ 0.9 & -5 \end{bmatrix}, \qquad C_{d3} = \begin{bmatrix} -1.65 & 5 \\ -1.2 & 2.65 \\ -0.98 & -5.6 \end{bmatrix},$$

$$M_{13} = \begin{bmatrix} -8.2 \\ -0.3 \end{bmatrix}, \qquad M_{23} = \begin{bmatrix} -0.52 \\ 2.5 \\ -3.6 \end{bmatrix},$$

$$N_{13} = \begin{bmatrix} 1.05 & -5 \end{bmatrix}, \qquad N_{23} = \begin{bmatrix} -7.2 & -1.26 \end{bmatrix}.$$

$$(59)$$

Then, we set the error state matrix $L = \begin{bmatrix} -45 & 0.6 \\ 2 & -6 \end{bmatrix}$, and the positive scalars in Theorem 11 are $\varepsilon_1 = 0.2$, $\varepsilon_2 = 0.15$, $\varepsilon_3 = 0.32$. According to the definitions of augmented state matrices in (12), we can easily obtain the following parameter matrices in Theorem 11 by MATLAB

$$\begin{split} Y_{11} &= \begin{bmatrix} -8452.1006 & 0.0127 \\ 0.0127 & 8450.9001 \end{bmatrix}, \\ Y_{21} &= \begin{bmatrix} 0.02 & 0.1291 & 0.1435 \\ -2.3520 & -0.4080 & -0.8106 \end{bmatrix}, \\ Y_{12} &= \begin{bmatrix} -17.0991 & 26.9626 \\ 26.9626 & -24.6750 \end{bmatrix}, \\ Y_{22} &= \begin{bmatrix} -20.0744 & -13.2941 & 52.9388 \\ 21.6893 & 18.0120 & -50.6693 \end{bmatrix}, \\ Y_{13} &= \begin{bmatrix} -675.1329 & 22.4456 \\ 22.4456 & -897.6976 \end{bmatrix}, \\ Y_{23} &= \begin{bmatrix} -13.6021 & -146.1726 & 54.0500 \\ -3.4324 & -19.5125 & -10.3068 \end{bmatrix}, \\ P_{1} &= \begin{bmatrix} 6.3029 & 0 & 0 & 0 \\ 0 & 4.8620 & 0 & 0 \\ 0 & 0 & 2.2914 & 0 \\ 0 & 0 & 0.3169 \end{bmatrix}, \end{split}$$

$$P_2 = \begin{bmatrix} 0.8914 & 0 & 0 & 0 \\ 0 & 1.2505 & 0 & 0 \\ 0 & 0 & 7.3629 & 0 \\ 0 & 0 & 0 & 3.0056 \end{bmatrix},$$

$$P_3 = \begin{bmatrix} 3.0265 & 0 & 0 & 0 \\ 0 & 0.2156 & 0 & 0 \\ 0 & 0 & 0.8965 & 0 \\ 0 & 0 & 0 & 1.0002 \end{bmatrix},$$

$$Q = \begin{bmatrix} 0.5000 & 0 & 0 & 0 \\ 0 & 0.5001 & 0 & 0 \\ 0 & 0 & 0.5001 & 0 \\ 0 & 0 & 0 & 0.5001 \end{bmatrix},$$

$$T_{11} = \begin{bmatrix} 3417.3214 & -870.7765 & 0 & 0 \\ -870.7765 & 416.7216 & 0 & 0 \\ 0 & 0 & 2226.3598 & -320.7456 \\ 0 & 0 & -320.7456 & 1226.3101 \end{bmatrix},$$

 T_{23}

$$= \begin{bmatrix} 3775.3231 & -2799.9330 & 0 & 0 \\ -2799.9330 & 2810.7685 & 0 & 0 \\ 0 & 0 & 10690.7366 & -10743.2750 \\ 0 & 0 & -10743.2750 & 10855.5053 \end{bmatrix},$$

$$T_{31} = \begin{bmatrix} 951.8504 & -539.9245 & 0 & 0 \\ -539.9245 & 896.2029 & 0 & 0 \\ 0 & 0 & 1477.3012 & -207.7540 \\ 0 & 0 & -207.7540 & 1479.1256 \end{bmatrix},$$

$$T_{32} = \begin{bmatrix} 2161.7695 & -1209.4164 & 0 & 0 \\ -1209.4164 & 2037.1205 & 0 & 0 \\ 0 & 0 & 1.4786 & -0.9283 \\ 0 & 0 & -0.9283 & 1.4794 \end{bmatrix},$$

$$T_{33} = \begin{bmatrix} 1493.9313 & -839.8780 & 0 & 0 \\ -839.8780 & 1407.3689 & 0 & 0 \\ 0 & 0 & 147.8123 & -133.6452 \\ 0 & 0 & -133.6452 & 245.9347 \end{bmatrix},$$

$$V_{11} = \begin{bmatrix} 1.6650 & 0 & 0 & 0 \\ 0 & 1.6650 & 0 & 0 \\ 0 & 0 & 1.6650 & 0 \\ 0 & 0 & 0 & 1.6650 \end{bmatrix},$$

$$W_{31} = \begin{bmatrix} 1.5426 & 0 & 0 & 0 \\ 0 & 1.6650 & 0 & 0 \\ 0 & 0 & 1.6662 & 0 \\ 0 & 0 & 0 & 1.6650 \end{bmatrix},$$

$$W_{32} = \begin{bmatrix} 1.5428 & 0 & 0 & 0 \\ 0 & 1.6650 & 0 & 0 \\ 0 & 0 & 1.6622 & 0 \\ 0 & 0 & 0 & 1.6650 \end{bmatrix}.$$

Therefore, we can design a linear memoryless observer as (11) with the constant matrices

$$K_{11} = P_{11}^{-1} Y_{11} = \begin{bmatrix} -1340.9860 & 0.0020 \\ 0.0026 & 1738.1530 \end{bmatrix},$$

$$K_{21} = P_{21}^{-1} Y_{21} = \begin{bmatrix} 0.0087 & 0.0563 & 0.0626 \\ -7.4219 & -1.2875 & -2.5579 \end{bmatrix},$$

$$K_{12} = P_{12}^{-1} Y_{12} = \begin{bmatrix} -19.1823 & 30.2475 \\ 21.5615 & -19.7321 \end{bmatrix},$$

$$K_{22} = P_{22}^{-1} Y_{22} = \begin{bmatrix} -2.7264 & -1.8056 & 7.1899 \\ 7.2163 & 5.9928 & -16.8583 \end{bmatrix},$$

$$K_{13} = P_{13}^{-1} Y_{13} = \begin{bmatrix} -223.1402 & 7.4186 \\ 104.1076 & -4163.7180 \end{bmatrix},$$

$$K_{23} = P_{23}^{-1} Y_{23} = \begin{bmatrix} -15.1724 & -163.0481 & 60.2900 \\ -3.4317 & -19.5086 & -10.3047 \end{bmatrix}.$$

Finally, the observer (11) with the above parameter matrices for this numerical example is a suboptimal guaranteed cost observer by Theorems 11 and 13.

5. Conclusions

In this paper, the robust guaranteed cost observer problem for a class of uncertain descriptor time-delay systems with Markovian jumping parameters and generally uncertain transition rates is studied by using LMI method. In this GUTR singular model, each transition rate can be completely unknown or only its estimate value is known. The parameter's uncertainty is time varying and is assumed to be norm-bounded. Memoryless guaranteed cost observers are designed in terms of a set of linear coupled matrix inequalities. The suboptimal guaranteed cost observer is designed by solving a certain optimization problem. Our results can be applicable to the general Markovian jump systems with bounded uncertain or partly uncertain TR matrix.

Conflict of Interests

The authors declare that there is no conflict of interests regarding the publication of this paper.

Acknowledgments

(60)

This research is supported by the National Natural Science Foundations of China (10701020, 10971022, 60973048, 61272077, 60974025, 60673101, and 60939003), NCET-08-0755, National 863 Plan Project (2008 AA04Z401, 2009AA043404), SDPW IMZQWH010016, the Natural Science Foundation of Shandong Province (no. ZR2012FM006), the Scientific and Technological Project of Shandong Province (no. 2007GG3WZ04016), and the Natural Science Foundation of Guangxi Autonomous Region (no. 2012GXNSFBA053003).

References

- [1] L. Dai, Singular Control Systems, Springer, Berlin, Germany, 1989.
- [2] S. Xu, P. V. Dooren, R. Ştefan, and J. Lam, "Robust stability and stabilization for singular systems with state delay and parameter uncertainty," *IEEE Transactions on Automatic Control*, vol. 47, no. 7, pp. 1122–1128, 2002.
- [3] M. Fu and G. Duan, "Robust guaranteed cost observer for uncertain descriptor time-delay systems with Markovian jumping parameters," *Acta Automatica Sinica*, vol. 31, pp. 479–483, 2005.
- [4] Y. Q. Xia, E.-K. Boukas, P. Shi, and J. H. Zhang, "Stability and stabilization of continuous-time singular hybrid systems," *Automatica*, vol. 45, no. 6, pp. 1504–1509, 2009.
- [5] S. Xu and J. Lam, Robust Control and Filtering of Singular Systems, Springer, Berlin, Germany, 2006.
- [6] Y.-Y. Cao and J. Lam, "Robust H_{∞} control of uncertain Markovian jump systems with time-delay," *IEEE Transactions on Automatic Control*, vol. 45, no. 1, pp. 77–83, 2000.
- [7] Y. Li and Y. Kao, "Stability of stochastic reaction-diffusion systems with Markovian switching and impulsive perturbations," *Mathematical Problems in Engineering*, vol. 2012, Article ID 429568, 13 pages, 2012.
- [8] X. Mao and C. Yuan, Stochastic Differential Equations with Markovian Switching, Imperial College Press, London, UK, 2006.
- [9] E.-K. Boukas, Stochastic Switching Systems: Analysis and Design, Birkhäuser, Basel, Switzerland, 2005.
- [10] Y. Kao, C. Wang, and L. Zhang, "Delay-dependent exponential stability of impulsive markovian jumping Cohen-Grossberg neural networks with reaction-diffusion and mixed delays," *Neural Processing Letters*, vol. 38, no. 3, pp. 321–346, 2013.
- [11] Y.-G. Kao, J.-F. Guo, C.-H. Wang, and X.-Q. Sun, "Delay-dependent robust exponential stability of Markovian jumping reaction-diffusion Cohen-Grossberg neural networks with mixed delays," *Journal of the Franklin Institute*, vol. 349, no. 6, pp. 1972–1988, 2012.
- [12] Y. Kao, C. Wang, F. Zha, and H. Cao, "Stability in mean of partial variables for stochastic reaction—diffusion systems with Markovian switching," *Journal of the Franklin Institute*, vol. 351, no. 1, pp. 500–512, 2014.
- [13] N. Kumaresan and P. Balasubramaniam, "Optimal control for stochastic nonlinear singular system using neural networks," *Computers & Mathematics with Applications*, vol. 56, no. 9, pp. 2145–2154, 2008.
- [14] L. Yu and J. Chu, "An LMI approach to guaranteed cost control of linear uncertain time-delay systems," *Automatica*, vol. 35, no. 6, pp. 1155–1159, 1999.
- [15] S. Yin, H. Luo, and S. Ding, "Real-time implementation of fault-tolerant control systems with performance optimization," *IEEE Transactions on Industrial Electronics*, vol. 64, no. 5, pp. 2402–2411, 2014
- [16] S. Yin, G. Wang, and H. Karimi, "Data-driven design of robust fault detection system for wind turbines," *Mechatronics*, 2013.
- [17] S. Yin, S. X. Ding, A. H. A. Sari, and H. Hao, "Data-driven monitoring for stochastic systems and its application on batch process," *International Journal of Systems Science*, vol. 44, no. 7, pp. 1366–1376, 2013.
- [18] S. Yin, S. Ding, A. Haghani, H. Hao, and P. Zhang, "A comparison study of basic datadriven fault diagnosis and process

- monitoring methods on the benchmark Tennessee Eastman process," *Journal of Process Control*, vol. 22, no. 9, pp. 1567–1581, 2012.
- [19] Y. G. Kao and C. H. Wang, "Global stability analysis for stochastic coupled reaction-diffusion systems on networks," *Nonlinear Analysis. Real World Applications*, vol. 14, no. 3, pp. 1457–1465, 2013.
- [20] E. K. Boukas, "Stabilization of stochastic singular nonlinear hybrid systems," *Nonlinear Analysis. Theory, Methods & Applications*, vol. 64, no. 2, pp. 217–228, 2006.
- [21] E.-K. Boukas, Control of Singular Systems with Random Abrupt Changes, Springer, Berlin, Germany, 2008.
- [22] Y. Ding, H. Zhu, S. Zhong, and Y. Zeng, "Exponential mean-square stability of time-delay singular systems with Markovian switching and nonlinear perturbations," *Applied Mathematics and Computation*, vol. 219, no. 4, pp. 2350–2359, 2012.
- [23] S. Long, S. Zhong, and Z. Liu, "Stochastic admissibility for a class of singular Markovian jump systems with modedependent time delays," *Applied Mathematics and Computation*, vol. 219, no. 8, pp. 4106–4117, 2012.
- [24] Z. Wu, P. Shi, H. Su, and J. Chu, "Asynchronous I_2-I_{∞} filtering for discrete-time stochastic Markov jump systems with randomly occurred sensor nonlinearities," *Automatica*, vol. 50, no. 1, pp. 180–186, 2014.
- [25] Z. Wu, P. Shi, H. Su, and J. Chu, "Stochastic synchronization of Markovian jump neural networks with time-varying delay using sampled-data," *IEEE Transactions on Cybernetics*, vol. 43, no. 6, pp. 1796–1806, 2013.
- [26] S. Ma and E.-K. Boukas, "Guaranteed cost control of uncertain discrete-time singular Markov jump systems with indefinite quadratic cost," *International Journal of Robust and Nonlinear Control*, vol. 21, no. 9, pp. 1031–1045, 2011.
- [27] G. Wang and Q. Zhang, "Robust control of uncertain singular stochastic systems with Markovian switching via proportional-derivative state feedback," *IET Control Theory & Applications*, vol. 6, no. 8, pp. 1089–1096, 2012.
- [28] J. Wang, H. Wang, A. Xue, and R. Lu, "Delay-dependent H_∞ control for singular Markovian jump systems with time delay," Nonlinear Analysis. Hybrid Systems, vol. 8, pp. 1–12, 2013.
- [29] L. Wu, X. Su, and P. Shi, "Sliding mode control with bounded L_2 gain performance of Markovian jump singular time-delay systems," *Automatica*, vol. 48, no. 8, pp. 1929–1933, 2012.
- [30] Z.-G. Wu, J. H. Park, H. Su, and J. Chu, "Stochastic stability analysis for discrete-time singular Markov jump systems with timevarying delay and piecewise-constant transition probabilities," *Journal of the Franklin Institute*, vol. 349, no. 9, pp. 2889–2902, 2012.
- [31] J. Xiong, J. Lam, H. Gao, and D. W. C. Ho, "On robust stabilization of Markovian jump systems with uncertain switching probabilities," *Automatica*, vol. 41, no. 5, pp. 897–903, 2005.
- [32] J. Xiong and J. Lam, "Robust H₂ control of Markovian jump systems with uncertain switching probabilities," *International Journal of Systems Science*, vol. 40, no. 3, pp. 255–265, 2009.
- [33] M. Karan, P. Shi, and C. Y. Kaya, "Transition probability bounds for the stochastic stability robustness of continuous-and discrete-time Markovian jump linear systems," *Automatica*, vol. 42, no. 12, pp. 2159–2168, 2006.
- [34] L. Zhang and E.-K. Boukas, "Stability and stabilization of Markovian jump linear systems with partly unknown transition probabilities," *Automatica*, vol. 45, no. 2, pp. 463–468, 2009.

- [35] B. Du, J. Lam, Y. Zou, and Z. Shu, "Stability and stabilization for Markovian jump time-delay systems with partially unknown transition rates," *IEEE Transactions on Circuits and Systems. I. Regular Papers*, vol. 60, no. 2, pp. 341–351, 2013.
- [36] L. Zhang and J. Lam, "Necessary and sufficient conditions for analysis and synthesis of Markov jump linear systems with incomplete transition descriptions," *IEEE Transactions on Automatic Control*, vol. 55, no. 7, pp. 1695–1701, 2010.
- [37] Y. Guo and F. Zhu, "New results on stability and stabilization of Markovian jump systems with partly known transition probabilities," *Mathematical Problems in Engineering*, vol. 2012, Article ID 869842, 11 pages, 2012.
- [38] J. Lin, S. Fei, and J. Shen, "Delay-dependent H_{∞} filtering for discrete-time singular Markovian jump systems with time-varying delay and partially unknown transition probabilities," *Signal Processing*, vol. 91, no. 2, pp. 277–289, 2011.
- [39] J. Tian, Y. Li, J. Zhao, and S. Zhong, "Delay-dependent stochastic stability criteria for Markovian jumping neural networks with mode-dependent time-varying delays and partially known transition rates," *Applied Mathematics and Computation*, vol. 218, no. 9, pp. 5769–5781, 2012.
- [40] Y. Wei, J. Qiu, H. R. Karimi, and M. Wang, "A new design H_{∞} filtering for contrinuous-time Markovian jump systems with time-varying delay and partially accessible mode information," Signal Processing, vol. 93, pp. 2392–2407, 2013.
- [41] L. Zhang, E.-K. Boukas, and J. Lam, "Analysis and synthesis of Markov jump linear systems with time-varying delays and partially known transition probabilities," *IEEE Transactions on Automatic Control*, vol. 53, no. 10, pp. 2458–2464, 2008.
- [42] L. Zhang and E.-K. Boukas, "Mode-dependent H_{∞} filtering for discrete-time Markovian jump linear systems with partly unknown transition probabilities," *Automatica*, vol. 45, no. 6, pp. 1462–1467, 2009.
- [43] L. Zhang and E.-K. Boukas, "Mode-dependent H_{∞} control for discrete-time Markovian jump linear systems with partly unknown transition probabilities," *International Journal of Robust and Nonlinear Control*, vol. 19, no. 8, pp. 868–883, 2009.
- [44] Y. Zhang, Y. He, M. Wu, and J. Zhang, "Stabilization for Markovian jump systems with partial information on transition probability based on free-connection weighting matrices," *Automatica*, vol. 47, no. 1, pp. 79–84, 2011.
- [45] G. Zong, D. Yang, L. Hou, and Q. Wang, "Robust finite-time H_{∞} control for Markovian jump systems with partially known transition probabilities," *Journal of the Franklin Institute*, vol. 350, no. 6, pp. 1562–1578, 2013.
- [46] Y. Ding, H. Zhu, S. Zhong, and Y. Zhang, " $L_2 L_{\infty}$ filtering for Markovian jump systems with time-varying delays and partly unknown transition probabilities," *Communications in Nonlinear Science and Numerical Simulation*, vol. 17, no. 7, pp. 3070–3081, 2012.
- [47] Q. Ma, S. Xu, and Y. Zou, "Stability and synchronization for Markovian jump neural networks with partly unknown transition probabilities," *Neurocomputing*, vol. 74, pp. 3403– 3411, 2011.
- [48] E. Tian, D. Yue, and G. Wei, "Robust control for Markovian jump systems with partially known transition probabilities and nonlinearities," *Journal of the Franklin Institute*, vol. 350, no. 8, pp. 2069–2083, 2013.
- [49] Y. Guo and Z. Wang, "Stability of Markovian jump systems with generally uncertain transition rates," *Journal of the Franklin Institute*, vol. 350, no. 9, pp. 2826–2836, 2013.

- [50] L. Zhang, " H_{∞} estimation for discrete-time piecewise homogeneous Markov jump linear systems," *Automatica*, vol. 45, no. 11, pp. 2570–2576, 2009.
- [51] Z. Wu, H. Su, and J. Chu, "state estimation for discrete Markovian jumping neural networks with time delay," *Neuro-computing*, vol. 73, pp. 2247–2254, 2010.
- [52] I. R. Petersen and A. V. Savkin, Robust Kalman Filtering for Signals and Systems with Large Uncertainties, Birkhäuser, Boston, Mass, USA, 1999.
- [53] B. D. O. Anderson and J. B. Moore, Optimal Filtering, Prentice-Hall, Upper Saddle River, NJ, USA, 1979.
- [54] I. R. Petersen and D. C. McFarlane, "Optimal guaranteed cost control and filtering for uncertain linear systems," *IEEE Transactions on Automatic Control*, vol. 39, no. 9, pp. 1971–1977, 1994.
- [55] S. Xu, T. Chen, and J. Lam, "Robust H[∞] filtering for uncertain Markovian jump systems with mode-dependent time delays," *IEEE Transactions on Automatic Control*, vol. 48, no. 5, pp. 900– 907, 2003.
- [56] J. H. Kim, D. Oh, and H. Park, "Guaranteed cost and H_{∞} filtering for time-delay systems," in *Proceeding of the American Control Conference*, pp. 4014–4018, IEEE, Arlington, Va, USA, 2001.
- [57] L. Xie, "Output feedback H_{∞} control of systems with parameter uncertainty," *International Journal of Control*, vol. 63, no. 4, pp. 741–750, 1996.

Hindawi Publishing Corporation Abstract and Applied Analysis Volume 2014, Article ID 789583, 9 pages http://dx.doi.org/10.1155/2014/789583

Research Article

Relative Orbit Stabilization Control for the Agile Satellite under Stochastic Disturbance

Xiande Wu, Fengzhi Guo, Wenbo Yang, 2,3 Jiangtao Xu, and Ting Song 2

- ¹ College of Aerospace and Civil Engineering, Harbin Engineering University, Harbin 150001, China
- ² Shanghai Institute of Space Flight Control Technology, Shanghai 200030, China

Correspondence should be addressed to Xiande Wu; xiande_wu@163.com

Received 2 January 2014; Accepted 8 February 2014; Published 23 March 2014

Academic Editor: Ming Liu

Copyright © 2014 Xiande Wu et al. This is an open access article distributed under the Creative Commons Attribution License, which permits unrestricted use, distribution, and reproduction in any medium, provided the original work is properly cited.

This paper investigates the relative orbit control problem for a space communication satellite network. An observer-based state feedback control scheme is developed under the circumstance of faults and disturbance occurring in the sensors and actuators. The validity of sliding mode observer for the satellites' network is deduced and the analysis and proof of the relative orbit stabilization control are completed.

1. Introduction

The agile satellites have brought a great number of conveniences for modern spatial application; they have evolved from single satellite to constellation and formation [1]; furthermore, a spatial dynamic network is constructed. In order to expand the range of imaging services, orbit maneuver ability becomes an intrinsic ability of the satellite, and the satellites do not run on their preselected orbit. Therefore, the relative position and velocity need to be measured; all the members in the spatial agile imaging network need to be controlled real-timely [2].

The research of relative motion control is focusing on the two aspects, namely, relative orbit control and relative attitude control. Some methods are proposed for relative orbit control, such as optimal control for the orbit rendezvous [3] and predictive control for the rendezvous maneuver [4]. The relative control methods include the centralized and decentralized approach [5]. These methods pay more attention to the control law design in an ideal world where the status measurement sensors and control actuators work well. The modern control method is mentioned and analyzed [6–11] while, in the practical orbit control, the sensors and actuators will work in the fault or disturbance status.

This paper will complete the studies and analysis of sliding mode observer and state feedback control based on

designed observer. The relative motion dynamic model will be depicted in Section 2; the sliding mode observer will be discussed in Section 3; the state feedback controller will be designed and its stabilization analysis is completed in Section 4.

2. Dynamic Model of Network Members

The relative motion dynamics of satellite communication network is usually established in the local-vertical-local horizontal [LVLH] coordinate system [12]. The relative motion equation can be rewritten as in the following form:

$$\ddot{x}(t) - A_1 \dot{x} - A_2 x - C(x) = Bu. \tag{1}$$

Formula (1) can be expanded into the following form:

$$\begin{bmatrix} \ddot{x} \\ \ddot{y} \\ \ddot{z} \end{bmatrix} - \begin{bmatrix} 0 & 0 & 2\omega_t \\ 0 & 0 & 0 \\ -2\omega_t & 0 & 0 \end{bmatrix} \begin{bmatrix} \dot{x} \\ \dot{y} \\ \dot{z} \end{bmatrix} - \begin{bmatrix} \omega_t^2 & 0 & \dot{\omega}_t \\ 0 & 0 & 0 \\ -\dot{\omega}_t & 0 & \omega_t^2 \end{bmatrix} \begin{bmatrix} x \\ y \\ z \end{bmatrix}$$

³ Shanghai Key Laboratory of Aerospace Intelligent Control Technology, Shanghai 200030, China

(7)

$$-\begin{bmatrix} -\frac{\mu}{r_t^3} \delta x \\ -\frac{\mu}{r_t^3} \delta y \\ -\frac{\mu}{r_t^3} \delta z + \frac{\mu}{r_t^2} \delta - \frac{\mu}{r_t^2} \end{bmatrix} = \begin{bmatrix} a_x \\ a_y \\ a_z \end{bmatrix}.$$
 (2)

The x, y, and z are the relative coordinates to the target spacecraft, ω is the orbit angular of the target spacecraft, r_t is the orbit radius of the spacecrafts, a_x , a_y , a_z is the control acceleration, μ is the gravitational constant, and $\delta = \left[(x^2/r_t^2) + (y^2/r_t^2) + (z/r_t - 1)^2 \right]^{-3/2}$. Actually (2) is equivalent to

$$\ddot{x}(t) - 2\omega_t \dot{z} - \omega_t^2 x - \dot{\omega}_t z + \frac{\mu}{r_t^3} \delta x = a_x,$$

$$\ddot{y}(t) + \frac{\mu}{r_t^3} \delta y = a_y,$$
(3)

$$\ddot{z}\left(t\right)+2\omega_{t}\dot{x}+\dot{\omega}_{t}x-\omega_{t}^{2}z+\frac{\mu}{r_{t}^{3}}\delta z-\frac{\mu}{r_{t}^{2}}\delta+\frac{\mu}{r_{t}^{2}}=a_{z}.$$

Hence $\ddot{x}(t)$, $\ddot{y}(t)$, and $\ddot{z}(t)$ can be derived, and the expressions, respectively, are

$$\ddot{x}(t) = 2\omega_t \dot{z} + \omega_t^2 x + \dot{\omega}_t z - \frac{\mu}{r_t^3} \delta x + a_x,$$

$$\ddot{y}(t) = -\frac{\mu}{r_t^3} \delta y + a_y,$$
(4)

$$\ddot{z}\left(t\right)=-2\omega_{t}\dot{x}-\dot{\omega}_{t}x+\omega_{t}^{2}z-\frac{\mu}{r_{t}^{3}}\delta z+\frac{\mu}{r_{t}^{2}}\delta-\frac{\mu}{r_{t}^{2}}+a_{z}.$$

Consider each expression of variables in the system (4):

$$x = \begin{bmatrix} x \\ y \\ z \end{bmatrix}, \qquad u = \begin{bmatrix} a_x \\ a_y \\ a_z \end{bmatrix}, \qquad A_1 = \begin{bmatrix} 0 & 0 & 2\omega_t \\ 0 & 0 & 0 \\ -2\omega_t & 0 & 0 \end{bmatrix},$$
$$A_2 = \begin{bmatrix} \omega_t^2 & 0 & \dot{\omega}_t \\ 0 & 0 & 0 \\ -\dot{\omega}_t & 0 & \omega_t^2 \end{bmatrix},$$

$$C(x) = \begin{bmatrix} -\frac{\mu}{r_t^3} \delta x \\ -\frac{\mu}{r_t^3} \delta y \\ -\frac{\mu}{r_t^3} \delta z + \frac{\mu}{r_t^2} \delta + \frac{\mu}{r_t^2} \end{bmatrix}, \qquad B = \begin{bmatrix} 1 & 0 & 0 \\ 0 & 1 & 0 \\ 0 & 0 & 1 \end{bmatrix}.$$
 (5)

We define augmented variable as follows:

$$x_{a}(t) = \begin{bmatrix} x \\ y \\ z \\ \dot{x} \\ \dot{y} \\ \dot{z} \end{bmatrix}. \tag{6}$$

The system (4) can be rewritten as in the following form:

$$\dot{x}_{a}(t) = \begin{bmatrix} \dot{x} \\ \dot{y} \\ \dot{z} \\ \ddot{y} \\ \ddot{z} \end{bmatrix} = \begin{bmatrix} 0 & 0 & 0 & 1 & 0 & 0 \\ 0 & 0 & 0 & 0 & 1 & 0 \\ 0 & 0 & 0 & 0 & 0 & 1 \\ \omega_{t}^{2} - \frac{\mu}{r_{t}^{3}} \delta & 0 & \dot{\omega}_{t} & 0 & 0 & 2\omega_{t} \\ 0 & 0 & -\frac{\mu}{r_{t}^{3}} \delta & 0 & 0 & 0 \\ -\dot{\omega}_{t} & 0 & \omega_{t}^{2} - \frac{\mu}{r_{t}^{3}} \delta & -2\omega_{t} & 0 & 0 \end{bmatrix} \begin{bmatrix} x \\ y \\ z \\ \dot{x} \\ \dot{y} \\ \dot{z} \end{bmatrix}$$

$$+ \begin{bmatrix} 0 & 0 & 0 \\ 0 & 0 & 0 \\ 0 & 0 & 0 \\ 1 & 0 & 0 \\ 0 & 1 & 0 \\ 0 & 0 & 1 \end{bmatrix} \begin{bmatrix} a_{x} \\ a_{y} \\ a_{z} \end{bmatrix} + \begin{bmatrix} 0 \\ 0 \\ 0 \\ 0 \\ 0 \\ 0 \end{bmatrix}.$$

$$\frac{\mu}{a_{x}^{2}} \delta - \frac{\mu}{a_{x}^{2}} \end{bmatrix}.$$

Aiming at system (7), we consider more complex and practical situation: there exist sensors and actuators fault, constant input disturbance (namely, the last item in formula (7)), and the output disturbance in the system. Then we define system matrix as follows:

$$A = \begin{bmatrix} 0 & 0 & 0 & 1 & 0 & 0 \\ 0 & 0 & 0 & 0 & 1 & 0 \\ 0 & 0 & 0 & 0 & 0 & 1 \\ \omega_t^2 - \frac{\mu}{r_t^3} \delta & 0 & \dot{\omega}_t & 0 & 0 & 2\omega_t \\ 0 & 0 & -\frac{\mu}{r_t^3} \delta & 0 & 0 & 0 \\ -\dot{\omega}_t & 0 & \omega_t^2 - \frac{\mu}{r_t^3} \delta & -2\omega_t & 0 & 0 \end{bmatrix},$$

$$B = \begin{bmatrix} 0 & 0 & 0 \\ 0 & 0 & 0 \\ 0 & 0 & 0 \\ 1 & 0 & 0 \\ 0 & 1 & 0 \\ 0 & 0 & 1 \end{bmatrix}, \qquad u(t) = \begin{bmatrix} a_x \\ a_y \\ a_z \end{bmatrix}, \tag{8}$$

$$B_{\omega 1} = \begin{bmatrix} 0 \\ 0 \\ 0 \\ 0 \\ \frac{\mu}{r_t^2} \delta - \frac{\mu}{r_t^2} \end{bmatrix}.$$

The system (7) can be rewritten as

$$\dot{x}(t) = Ax(t) + Bu(t) + B_{\omega 1}\omega(t) + B_{a}f_{a}(t),$$

$$y(t) = Cx(t) + Du(t) + D_{a}f_{a}(t) + C_{s}f_{s}(t), \qquad (9)$$

$$+ D_{d}d(t) + B_{\omega 2}\omega(t).$$

Here, $B_a \in R^{n \times a}$, $D_a \in R^{p \times a}$, $C_s \in R^{p \times s}$, $D_d \in R^{p \times d}$, and $B_{\omega 2} \in R^{p \times 1}$ represent system matrix and $f_a(t) \in R^a$

and $f_s(t) \in R^s$, respectively, are actuators fault and sensors fault. $d(t) \in R^d$ is the sensors' disturbance. $\omega(t)$ is the constant disturbance. Here we pay attention to a more general situation: the disturbance $\omega(t)$ meanwhile exists in the state equation and output y(t) of system (9).

Defining $\overline{n} = n + a + \omega + 2p$, we do the following assumptions to the system (9).

(A1) fault and the perturbation vector: $f_a(t)$, $f_s(t)$, d(t), and $\omega(t)$ satisfy the following assumption:

$$||f_{s}(t)|| \leq r_{s1}, \qquad ||\dot{f}_{s}(t)|| \leq r_{s2},$$

$$||f_{a}(t)|| \leq r_{a1}, \qquad ||\dot{f}_{a}(t)|| \leq r_{a2},$$

$$||\omega(t)|| \leq r_{\omega 1}, \qquad ||\dot{\omega}(t)|| \leq r_{\omega 2},$$

$$||d(t)|| \leq r_{d1},$$
(10)

where $r_{s1}>0$, $r_{s2}>0$, $r_{a1}>0$, $r_{a2}>0$, $r_{\omega 1}>0$, $r_{\omega 1}>0$, $r_{\omega 2}>0$, and $r_d>0$ are known constant.

(A2) (A, C) is able to be observed, and there exists constant a > 0, which makes

$$\operatorname{rank} \begin{bmatrix} aI_n + A & B_a \\ C & D_a \end{bmatrix} = \overline{n}. \tag{11}$$

(A3) matrix: D_a , C_s , D_d , $B_{\omega 2}$ are column full rank matrix.

For the convenience of discussion, we define augmented vector and matrix as follows:

$$\overline{A} = \begin{bmatrix} A & 0 & 0 & 0 & 0 \\ 0 & -\alpha I_a & 0 & 0 & 0 \\ 0 & 0 & -\alpha I_\omega & 0 & 0 \\ 0 & 0 & 0 & -\alpha I_p & 0 \\ 0 & 0 & 0 & 0 & -I_p \end{bmatrix},$$

$$\overline{B} = \begin{bmatrix} B_{n \times m} \\ 0_{a \times m} \\ 0_{w \times m} \\ 0_{p \times m} \\ 0_{d \times m} \end{bmatrix} \overline{x}(t) = \begin{bmatrix} x(t) \\ f_a(t) \\ \omega(t) \\ C_s f_s(t) \\ D_d d(t) \end{bmatrix},$$

$$\overline{B}_a = \begin{bmatrix} \alpha^{-1}B_a & \alpha^{-1}B_\omega & 0_{n\times s} \\ I_a & 0_{a\times \omega} & 0 \\ 0 & I_\omega & 0 \\ 0 & 0 & C_s \\ 0 & 0 & 0 \end{bmatrix},$$

$$f(t) = \begin{bmatrix} \left(\alpha f_a(t) + \dot{f}_a(t)\right)_{a \times 1} \\ \left(\alpha \omega(t) + \dot{\omega}(t)\right)_{\omega \times 1} \\ \left(\alpha f_s(t) + \dot{f}_s(t)\right)_{s \times 1} \end{bmatrix}, \qquad \overline{N} = \begin{bmatrix} 0_n \\ 0_a \\ 0_\omega \\ 0_p \\ I_p \end{bmatrix},$$

$$\overline{E} = \begin{bmatrix} I_n & \alpha^{-1}B_a & 0 & 0 & 0 \\ 0 & I_a & 0 & 0 & 0 \\ 0 & 0 & I_\omega & 0 & 0 \\ 0 & 0 & 0 & I_p & 0 \\ 0 & 0 & 0 & 0 & 0 \end{bmatrix}, \qquad \overline{C} = \begin{bmatrix} C & D_a & B_{\omega 2} & I_p & I_p \end{bmatrix}.$$
(12)

Establish an augmented generalized system based on system (9) as follows:

$$\overline{Ex}(t) = \overline{Ax}(t) + \overline{Bu}(t) + \overline{B}_a f(t) + \overline{N} D_d d(t),$$

$$y(t) = \overline{Cx}(t) + Du(t).$$
(13)

Matrix \overline{E} and matrix \overline{C} have the following properties:

$$\operatorname{rank}\left[\frac{\overline{E}}{C}\right] = \begin{bmatrix} I_n & \alpha^{-1}B_a & 0 & 0 & 0\\ 0 & I_a & 0 & 0 & 0\\ 0 & 0 & I_\omega & 0 & 0\\ 0 & 0 & 0 & I_p & 0\\ 0 & 0 & 0 & 0 & 0\\ C & D_a & B_{\omega 2} & I_p & I_p \end{bmatrix}$$
(14)

 $= n + a + \omega + p + p = \overline{n}.$

Therefore, it can be inferred that, according to matrix knowledge, there must be an appropriate number of dimensions matrix \overline{L} which makes \overline{E} + \overline{LC} an invertible matrix. We may define a new matrix

$$\overline{L}_{D} = \begin{bmatrix}
0_{n \times p} \\
0_{a \times p} \\
0_{\omega \times p} \\
0_{p \times p} \\
\overline{L}_{D}^{(4)}
\end{bmatrix},$$
(15)

where $\overline{L}_D^{(4)} \in R^{p \times p}$ and $\overline{L}_D^{(4)} = \text{diag}\{\beta_1 \ \beta_2 \ \cdots \ \beta_p\}, \ \beta_i > 0,$ $i > 1, 2, \ldots, p$. Meanwhile, we define a new matrix $\overline{S} = \overline{E} + \overline{L}_D \overline{C}$. We can calculate directly

$$\overline{S} = \begin{bmatrix} I_n & \alpha^{-1}B_a & 0 & 0 & 0 \\ 0 & I_a & 0 & 0 & 0 \\ 0 & 0 & I_\omega & 0 & 0 \\ 0 & 0 & 0 & I_p & 0 \\ 0 & 0 & 0 & 0 & 0 \end{bmatrix} + \begin{bmatrix} 0_{n \times p} \\ 0_{a \times p} \\ 0_{\omega \times p} \\ 0_{p \times p} \\ \overline{L}_D^{(4)} \end{bmatrix} \begin{bmatrix} C & D_a & B_{\omega 2} & I_p & I_p \end{bmatrix}$$

$$\begin{bmatrix} I_n & \alpha^{-1}B_a & 0 & 0 & 0 \end{bmatrix}$$

$$= \begin{bmatrix} I_n & \alpha^{-1}B_a & 0 & 0 & 0 \\ 0 & I_a & 0 & 0 & 0 \\ 0 & 0 & I_\omega & 0 & 0 \\ 0 & 0 & 0 & I_p & 0 \\ 0 & 0 & 0 & 0 & 0 \end{bmatrix}$$

We can conclude that there must be \overline{S}^{-1} according to (16). Suppose that \overline{S}^{-1} has the following form:

$$\overline{S}^{-1} = \begin{bmatrix} I_n & -\alpha^{-1}B_a & 0 & 0 & 0\\ 0 & I_a & 0 & 0 & 0\\ 0 & 0 & I_\omega & 0 & 0\\ 0 & 0 & 0 & I_p & 0\\ X_1 & X_2 & X_3 & X_4 & X_5 \end{bmatrix}. \tag{17}$$

In formula (17), X_1 , X_2 , X_3 , X_4 , and X_5 are matrixes needed to be solved. Expand $\overline{SS}^{-1} = I_{\overline{n}}$ as follows:

$$\begin{bmatrix} I_{n} & \alpha^{-1}B_{a} & 0 & 0 & 0\\ 0 & I_{a} & 0 & 0 & 0\\ 0 & 0 & I_{\omega} & 0 & 0\\ 0 & 0 & 0 & I_{p} & 0\\ \overline{L}_{D}^{(4)}C & \overline{L}_{D}^{(4)}D_{a} & \overline{L}_{D}^{(4)}B_{\omega 2} & \overline{L}_{D}^{(4)} & \overline{L}_{D}^{(4)} \end{bmatrix} \times \begin{bmatrix} I_{n} & -\alpha^{-1}B_{a} & 0 & 0 & 0\\ 0 & I_{a} & 0 & 0 & 0\\ 0 & 0 & I_{\omega} & 0 & 0\\ 0 & 0 & 0 & I_{p} & 0\\ X_{1} & X_{2} & X_{3} & X_{4} & X_{5} \end{bmatrix} = I_{\overline{n}}.$$
(18)

Consider the elements in the last line of the expression $\overline{SS}^{-1} = I_{\overline{n}}$. Consider

$$\overline{L}_{D}^{(4)}C + \overline{L}_{D}^{(4)}X_{1} = 0,$$

$$-\alpha^{-1}\overline{L}_{D}^{(4)}CB_{a} + \overline{L}_{D}^{(4)}D_{a} + \overline{L}_{D}^{(4)}X_{2} = 0,$$

$$\overline{L}_{D}^{(4)}B_{\omega 2} + \overline{L}_{D}^{(4)}X_{3} = 0,$$

$$\overline{L}_{D}^{(4)} + \overline{L}_{D}^{(4)}X_{4} = 0,$$

$$\overline{L}_{D}^{(4)}X_{5} = I_{p}.$$
(19)

Formula (2) can be obtained by directly calculating

$$X_1 = -C,$$

$$X_2 = \alpha^{-1}CB_a - D_a,$$

$$X_3 = -B_{\omega 2},$$

$$X_4 = -I_p,$$

$$X_5 = \left(\overline{L}_D^{(4)}\right)^{-1}.$$
 (20)

3. Observer Design

To get the asymptotic estimates of the state of system (9) and, at the same time, solve the corresponding control problem, we introduce sliding-mode observer as follows:

$$\overline{S}\dot{z}(t) = \left(\overline{A} - \overline{L}_{p}\overline{C}\right)\overline{z}(t) - \overline{N}\left(y(t) - Du(t)\right)
+ \overline{B}u(t) + L_{s}u_{s}(t),$$

$$\widehat{x} = \overline{z}(t) + \overline{S}^{-1}\overline{L}_{D}\left(y(t) - Du(t)\right).$$
(21)

Here,

$$z(t) = \begin{bmatrix} z_{x}(t) \\ z_{a}(t) \\ z_{w}(t) \\ z_{s}(t) \\ z_{d}(t) \end{bmatrix}, \qquad \widehat{\overline{x}}(t) = \begin{bmatrix} \widehat{x}(t) \\ \widehat{f}_{a}(t) \\ \widehat{\omega}(t) \\ \widehat{f}_{s}(t) \\ \widehat{d}(t) \end{bmatrix}, \qquad (22)$$

where $z_x(t) \in R^n$, $z_a(t) \in R^a$, $z_\omega(t) \in R^\omega$, $z_s(t) \in R^p$, $z_d(t) \in R^p$, $\widehat{x}(t) \in R^n$, $\widehat{f}_a(t) \in R^a$, $\widehat{\omega}(t) \in R^\omega$, $\widehat{f}_s(t) \in R^p$, $\widehat{d}(t) \in R^p$, $\overline{L}_D \in R^{\overline{n} \times p}$, $\overline{L}_S \in R^{\overline{n} \times p}$, and $\overline{L}_S \in R^{\overline{n} \times p}$, respectively, are derivative gain, proportional gain, and sliding gain of the observer and $\overline{S} = \overline{E} + \overline{L}_D \overline{C}$ is defined previously. The $z_s(t)$ and $z_d(t)$ are not real estimation of $f_s(t)$ and d(t) in the observer (21). Assume that the real estimations of $z_s(t)$ and $z_d(t)$, respectively, are $f_s(t)$ and d(t); thus,

$$\widehat{f}_{s}(t) = C_{s} \widecheck{f}_{s}(t), \qquad \widehat{d}(t) = D_{d} \widecheck{d}(t). \tag{23}$$

According to the assumption (A3), C_s and D_d are column full rank, so $(C_s \ C_s)^{-1}$ and $(D_d \ D_d)^{-1}$ exist. It can be concluded from (23) that

$$\check{f}_s(t) = \left(C_s^T C_s\right)^{-1} C_s^T \widehat{f}_s(t),
\check{d}(t) = \left(D_d^T D_d\right)^{-1} D_d^T \widehat{d}(t).$$
(24)

Lemma 1. In the case of (A2), for the observer (21), there is a gain matrix \overline{L}_p , which makes $\overline{S}^{-1}(\overline{A} - \overline{L}_p\overline{C})$ Hurwitz.

Proof. First, considering matrix $\overline{S}^{-1}\overline{A}$, for the finite dimensions matrix, there must exist a constant $\mu > 0$, making $\text{Re}[\lambda_i(\overline{S}^{-1}\overline{A})] > -\mu$, $(i = 1, 2, ..., \overline{n})$, which means $\text{Re}[\lambda_i(-(\mu I + \overline{S}^{-1}\overline{A}))] < 0$, $(i = 1, 2, ..., \overline{n})$.

(29)

rank relationship existed:

$$\operatorname{rank}\left[\frac{\sigma I_{\overline{n}} - \overline{S}^{-1} \overline{A}}{\overline{C}}\right] = \operatorname{rank}\left[\overline{S}^{-1} \quad 0 \atop 0 \quad I_{p}\right] \left[\frac{\sigma\left(\overline{E} + \overline{L}_{D} \overline{C}\right) - \overline{A}}{\overline{C}}\right], \tag{25}$$

rank
$$\left(\sigma\left(\overline{E} + \overline{L}_D\overline{C}\right) - \overline{A}\right)$$

$$= \operatorname{rank} \begin{bmatrix} \sigma I_n - A & -\sigma \alpha^{-1} B_a & 0 & 0 & 0 \\ 0 & \sigma I_a + \alpha I_a & 0 & 0 & 0 \\ 0 & 0 & I_\omega + \alpha I_\omega & 0 & 0 \\ 0 & 0 & 0 & I_p + \alpha I_p & 0 \\ \sigma \overline{L}_D^{(4)} C & \sigma \overline{L}_D^{(4)} D_a & \sigma \overline{L}_D^{(4)} B_{\omega 2} & \sigma \overline{L}_D^{(4)} & \sigma \overline{L}_D^{(4)} + I_p \end{bmatrix}$$
(26)

In formula (26), notice that, for any $\sigma \in R^+$, rank $(\sigma \overline{L}_D^{(4)} + I_p) =$ p always existed. Therefore,

$$\begin{split} \operatorname{rank}\left(\sigma\left(\overline{E}+\overline{L}_D\overline{C}\right)-\overline{A}\right) \\ &=\operatorname{rank}\begin{bmatrix}\sigma I_n-A&-\sigma\alpha^{-1}B_a&0&0\\0&\sigma I_a+\alpha I_a&0&0\\0&0&I_\omega+\alpha I_\omega&0\\0&0&0&I_p+\alpha I_p\end{bmatrix}+p. \end{split}$$

(27)

On the other hand, we notice that

rank
$$(\sigma \overline{E} - \overline{A})$$

$$= \operatorname{rank} \begin{bmatrix} \sigma I - A & -\sigma \alpha^{-1} B_{a} & 0 & 0 & 0 \\ 0 & -\sigma I_{a} + \alpha I_{a} & 0 & 0 & 0 \\ 0 & 0 & \sigma I_{\omega} + \alpha I_{\omega} & 0 & 0 \\ 0 & 0 & 0 & \sigma I_{p} + \alpha I_{p} & 0 \\ 0 & 0 & 0 & 0 & I_{d} \end{bmatrix}$$

$$= \operatorname{rank} \begin{bmatrix} \sigma I - A & -\sigma \alpha^{-1} B_{a} & 0 & 0 \\ 0 & -\sigma I_{a} + \alpha I_{a} & 0 & 0 \\ 0 & 0 & \sigma I_{\omega} + \alpha I_{\omega} & 0 \\ 0 & 0 & \sigma I_{p} + \alpha I_{p} \end{bmatrix} + d.$$

So we can derive $\operatorname{rank}(\sigma(\overline{E} + \overline{L}_D \overline{C}) - \overline{A}) = \operatorname{rank}(\sigma \overline{E} - \overline{A}).$ According to (26), we can derive the following formula:

$$\operatorname{rank} \begin{bmatrix} \sigma I_{\overline{n}} - \overline{S}^{-1} \overline{A} \\ \overline{C} \end{bmatrix}$$

$$= \operatorname{rank} \begin{bmatrix} \sigma \left(\overline{E} + \overline{L}_{D} \overline{C} \right) - \overline{A} \\ \overline{C} \end{bmatrix}$$

$$= \operatorname{rank} \begin{bmatrix} \sigma \overline{E} - \overline{A} \\ \overline{C} \end{bmatrix}$$

So, for arbitrary real number
$$\sigma \in R^+$$
, the following matrix rank relationship existed:
$$\operatorname{rank} \begin{bmatrix} \sigma I_{\overline{n}} - \overline{S}^{-1} \overline{A} \\ \overline{C} \end{bmatrix} = \operatorname{rank} \begin{bmatrix} \overline{S}^{-1} & 0 \\ 0 & I_p \end{bmatrix} \begin{bmatrix} \sigma \left(\overline{E} + \overline{L}_D \overline{C} \right) - \overline{A} \\ \overline{C} \end{bmatrix},$$
 (25)
$$\operatorname{rank} \left(\sigma \left(\overline{E} + \overline{L}_D \overline{C} \right) - \overline{A} \right)$$

$$\operatorname{rank} \left(\sigma \left(\overline{E} + \overline{L}_D \overline{C} \right) - \overline{A} \right)$$

$$\operatorname{rank} \left(\sigma \left(\overline{E} + \overline{L}_D \overline{C} \right) - \overline{A} \right)$$

$$\operatorname{rank} \left(\sigma \left(\overline{E} + \overline{L}_D \overline{C} \right) - \overline{A} \right)$$

$$\operatorname{rank} \left(\sigma \left(\overline{E} + \overline{L}_D \overline{C} \right) - \overline{A} \right)$$

$$\operatorname{rank} \left(\sigma \left(\overline{E} + \overline{L}_D \overline{C} \right) - \overline{A} \right)$$

$$\operatorname{rank} \left(\sigma \left(\overline{E} + \overline{L}_D \overline{C} \right) - \overline{A} \right)$$

$$\operatorname{rank} \left(\sigma \left(\overline{E} + \overline{L}_D \overline{C} \right) - \overline{A} \right)$$

$$\operatorname{rank} \left(\sigma \left(\overline{E} + \overline{L}_D \overline{C} \right) - \overline{A} \right)$$

$$\operatorname{rank} \left(\sigma \left(\overline{E} + \overline{L}_D \overline{C} \right) - \overline{A} \right)$$

$$\operatorname{rank} \left(\sigma \left(\overline{E} + \overline{L}_D \overline{C} \right) - \overline{A} \right)$$

$$\operatorname{rank} \left(\sigma \left(\overline{E} + \overline{L}_D \overline{C} \right) - \overline{A} \right)$$

$$\operatorname{rank} \left(\sigma \left(\overline{E} + \overline{L}_D \overline{C} \right) - \overline{A} \right)$$

$$\operatorname{rank} \left(\sigma \left(\overline{E} + \overline{L}_D \overline{C} \right) - \overline{A} \right)$$

$$\operatorname{rank} \left(\sigma \left(\overline{E} + \overline{L}_D \overline{C} \right) - \overline{A} \right)$$

$$\operatorname{rank} \left(\sigma \left(\overline{E} + \overline{L}_D \overline{C} \right) - \overline{A} \right)$$

$$\operatorname{rank} \left(\sigma \left(\overline{E} + \overline{L}_D \overline{C} \right) - \overline{A} \right)$$

$$\operatorname{rank} \left(\sigma \left(\overline{E} + \overline{L}_D \overline{C} \right) - \overline{A} \right)$$

$$\operatorname{rank} \left(\sigma \left(\overline{E} + \overline{L}_D \overline{C} \right) - \overline{A} \right)$$

$$\operatorname{rank} \left(\sigma \left(\overline{E} + \overline{L}_D \overline{C} \right) - \overline{A} \right)$$

$$\operatorname{rank} \left(\sigma \left(\overline{E} + \overline{L}_D \overline{C} \right) - \overline{A} \right)$$

$$\operatorname{rank} \left(\sigma \left(\overline{E} + \overline{L}_D \overline{C} \right) - \overline{A} \right)$$

$$\operatorname{rank} \left(\sigma \left(\overline{E} + \overline{L}_D \overline{C} \right) - \overline{A} \right)$$

$$\operatorname{rank} \left(\sigma \left(\overline{E} + \overline{L}_D \overline{C} \right) - \overline{A} \right)$$

$$\operatorname{rank} \left(\sigma \left(\overline{E} + \overline{L}_D \overline{C} \right) - \overline{A} \right)$$

$$\operatorname{rank} \left(\sigma \left(\overline{E} + \overline{L}_D \overline{C} \right) - \overline{A} \right)$$

$$\operatorname{rank} \left(\sigma \left(\overline{E} + \overline{L}_D \overline{C} \right) - \overline{A} \right)$$

$$\operatorname{rank} \left(\sigma \left(\overline{E} + \overline{L}_D \overline{C} \right) - \overline{A} \right)$$

$$\operatorname{rank} \left(\sigma \left(\overline{E} + \overline{L}_D \overline{C} \right) - \overline{A} \right)$$

$$\operatorname{rank} \left(\sigma \left(\overline{E} + \overline{L}_D \overline{C} \right) - \overline{A} \right)$$

$$\operatorname{rank} \left(\sigma \left(\overline{E} + \overline{L}_D \overline{C} \right) - \overline{A} \right)$$

$$\operatorname{rank} \left(\sigma \left(\overline{E} + \overline{L}_D \overline{C} \right) - \overline{A} \right)$$

$$\operatorname{rank} \left(\sigma \left(\overline{E} + \overline{L}_D \overline{C} \right) - \overline{A} \right)$$

$$\operatorname{rank} \left(\sigma \left(\overline{E} + \overline{L}_D \overline{C} \right) - \overline{A} \right)$$

$$\operatorname{rank} \left(\overline{E} + \overline{L}_D \overline{C} \right) - \overline{A} \right)$$

Then we discuss the values of $\sigma \neq -\alpha$ and $\sigma = -\alpha$, based on formula (29).

First, we consider the situation of $\sigma \neq -\alpha$ and, at this time, formula (29) can be equivalent to

$$\operatorname{rank} \begin{bmatrix} \sigma I_n - A & -\sigma \alpha^{-1} B_a \\ C & D_a \end{bmatrix} + \omega + 2p. \tag{30}$$

We can draw the conclusion based on the assumption

$$\operatorname{rank}\left[\frac{\sigma I_{\overline{n}} - \overline{S}^{-1}\overline{A}}{\overline{C}}\right] = n + a + \omega + 2p = \overline{n}.$$
 (31)

On the other hand, consider the condition of $\sigma = -\alpha$ and, at this moment, formula (28) turns into

$$\operatorname{rank} \begin{bmatrix} -\alpha I_n - A & B_a & 0 & 0 \\ C & D_a & B_{\omega 2} & I_p \end{bmatrix} + p. \tag{32}$$

Notice that $B_{\omega 2}$ is column full rank and the above formula

$$\operatorname{rank} \begin{bmatrix} -\alpha I_n - A & B_a \\ C & D_a \end{bmatrix} + \omega + 2p = n + a + \omega + 2p = \overline{n}.$$
 (33)

Integrating the above two cases derived, we have proved that, for any $\sigma \in R^+$, rank $(\sigma(\overline{E} + \overline{L}_D \overline{C}) - \overline{A}) = \overline{n}$. Hence, $[\overline{S}^{-1} \ \overline{A} \ \overline{C}]$ is a couple observed, and can elicit that $\begin{bmatrix} -\overline{S}^{-1} & \overline{A} & \overline{C} \end{bmatrix}$ can be observed. Therefore, there exists matrix \overline{H} , making $-\overline{S}^{-1}\overline{A}-\overline{H}\overline{C}$ Hurwitz (i.e., the eigenvalues of $-\overline{S}^{-1}\overline{A} - \overline{H}\overline{C}$ are all negative). Thus there must exist matrix $\overline{X} > 0$ which makes

$$-\left(\mu I_{\overline{n}} + \overline{S}^{-1} \overline{A}\right) \overline{X} - \overline{X} \left(\mu I_{\overline{n}} + \overline{S}^{-1} \overline{A}\right) = -\overline{C}^{T} \overline{C}. \tag{34}$$

Let the proportion gain of observer (21) be equal to $\overline{L}_p =$ $\overline{S} \overline{X}^{-1} \overline{C}$; then, we can calculate

$$\left[\mu I_{\overline{n}} + \overline{S}^{-1} (\overline{A} - \overline{L}_{p} \overline{C})\right]^{T} \overline{X} + \overline{X} \left[\mu I_{\overline{n}} + \overline{S}^{-1} (\overline{A} - \overline{L}_{p} \overline{C})\right]$$

$$= -\overline{C}^{T} \overline{C}.$$
(35)

Therefore, $\text{Re}[\lambda_i(\overline{S}^{-1}(\overline{A} - \overline{L}_p\overline{C}))] < -\mu, (i = 1, 2, ..., \overline{n}).$ The proof completes.

4. Observer Error System

Then we derive the error system of the observer (21). Firstly, in the first formula of the system (13), we add $\overline{L}_D \overline{C} \dot{\overline{x}}(t)$ at the left and right side and we can get

$$(\overline{E} + \overline{L}_D \overline{C}) \dot{\overline{x}}(t)$$

$$= \overline{A}x(t) + \overline{B}u(t) + \overline{B}_a f(t) + \overline{L}_D \overline{C} \dot{\overline{x}}(t) + \overline{N} D_d d(t)$$

$$\iff \overline{S} \dot{\overline{x}}(t) = \overline{A}x(t) + \overline{B}u(t) + \overline{B}_a f(t)$$

$$+ \overline{L}_D \overline{C} \dot{\overline{x}}(t) + \overline{N} D_d d(t).$$
(36)

On the other hand, for the observer (21), we can get

$$\frac{\dot{S}\dot{\bar{x}}}{(t)} (t) = \bar{S}z(t) + \bar{L}_{D}(y(t) - Du(t))
= (\bar{A} - \bar{L}_{p}\bar{C})\bar{z}(t) - \bar{N}(y(t) - Du(t)) + \bar{B}u(t) + \bar{L}_{s}u_{s}(t)
+ \bar{L}_{D}(\dot{y}(t) - D\dot{u}(t))
= (\bar{A} - \bar{L}_{p}\bar{C})\hat{\bar{x}}(t) - (\bar{A} - \bar{L}_{p}\bar{C})\bar{S}^{-1}\bar{L}_{D}(y(t) - Du(t))
- \bar{N}(y(t) - Du(t)) + \bar{B}u(t) + \bar{L}_{s}u_{s}(t)
+ \bar{L}_{D}(\dot{y}(t) - D\dot{u}(t))
= (\bar{A} - \bar{L}_{p}\bar{C})\hat{\bar{x}}(t) - \bar{A}\bar{S}^{-1}\bar{L}_{D}(y(t) - Du(t))
+ \bar{L}_{p}\bar{C}\bar{S}^{-1}\bar{L}_{D}(y(t) - Du(t)) - \bar{N}(y(t) - Du(t)) + \bar{B}u(t)
+ \bar{L}_{s}u_{s}(t) + \bar{L}_{D}(\dot{y}(t) - D\dot{u}(t))
= [(\bar{A} - \bar{L}_{p}\bar{C})\hat{\bar{x}}(t) + \bar{L}_{pi}(y(t) - Du(t)) + \bar{B}u(t) + \bar{L}_{s}u_{s}(t)]
+ \bar{L}_{D}(\dot{y}(t) - D\dot{u}(t)).$$
(37)

Notice that $y(t) - Du(t) = \overline{C}\overline{x}(t)$, so $\dot{y}(t) - D\dot{u}(t) = \overline{C}\dot{x}(t)$. Therefore, from formula (36), we can obtain

$$\overline{S}\dot{\overline{x}} = \left(\overline{A} - \overline{L}_p \overline{C}\right) \hat{\overline{x}}(t) + \overline{L}_p \overline{C} \overline{x}(t) + \overline{B}u(t)
+ \overline{L}_s u_s(t) + \overline{L}_D \overline{C} \dot{\overline{x}}(t).$$
(38)

We define error variable as follows:

$$\overline{e}(t) = \widehat{\overline{x}}(t) - \overline{x}(t) = \begin{bmatrix} e_x(t) \\ e_a(t) \\ e_{\omega}(t) \\ e_s(t) \\ e_d(t) \end{bmatrix}.$$
(39)

Meanwhile considering (36) and (38), we obtain

$$\overline{S}\dot{\overline{e}}\left(t\right) = \left(\overline{A} - \overline{L}_{p}\overline{C}\right)\overline{e}\left(t\right) + \overline{L}_{s}u_{s}\left(t\right) - \overline{B}_{a}f\left(t\right) - \overline{N}D_{d}d\left(t\right). \tag{40}$$

This is equal to

$$\dot{\overline{e}}(t) = \overline{S}^{-1} \left(\overline{A} - \overline{L}_p \overline{C} \right) \overline{e}(t) + \overline{S}^{-1} \overline{L}_s u_s(t) - \overline{S}^{-1} \overline{B}_a f(t)
- \overline{S}^{-1} \overline{N} D_d d(t).$$
(41)

In formula (41),

$$\overline{S}^{-1}\overline{N} = \begin{bmatrix} I_n & -\alpha^{-1}B_a & 0 & 0 & 0 \\ 0 & I_a & 0 & 0 & 0 \\ 0 & 0 & I_\omega & 0 & 0 \\ 0 & 0 & 0 & I_p & 0 \\ X_1 & X_2 & X_3 & X_4 & X_5 \end{bmatrix} \begin{bmatrix} 0_n \\ 0_a \\ 0_\omega \\ 0_p \\ I_p \end{bmatrix} = \begin{bmatrix} 0 \\ 0 \\ 0 \\ (\overline{L}_D^{(4)})^{-1} \end{bmatrix}. \tag{42}$$

Here,

$$\overline{L}_{D}^{(4)} = \begin{pmatrix} \beta_{1} & \cdots & 0 \\ \vdots & \ddots & \vdots \\ 0 & \cdots & \beta_{p} \end{pmatrix}.$$
(43)

Hence, if the value of β_i ($i=1,2,\ldots,p$) is large enough, in the system (41), $\overline{S}^{-1}\overline{N}$ will become infinitesimal. Until now, we remove the influence of disturbance $D_dd(t)$ for the system stability.

On the other hand, for the $\overline{S}^{-1}\overline{L}_s u_s(t) - \overline{S}^{-1}\overline{B}_a f(t)$ of the system (41), we design $u_s(t)$ as the following form ($\rho > 0$ is design parameter):

$$u_{s}(t) = -\left(\alpha r_{a1} + r_{a2} + \alpha r_{\omega 1} + r_{\omega 2} + \alpha r_{s1} + r_{s2} + p\right) \operatorname{sgn}\left(s\left(t\right)\right),$$

$$s\left(t\right) = \overline{B}_{a}^{T} \overline{S}^{-1} \overline{P} \overline{e}\left(t\right) \in R^{a+\omega+s},$$

$$(44)$$

of which, \overline{P} is Lyapunov matrix required and $\overline{P} > 0$ satisfies

$$\overline{B}_a^T \overline{S}^{-1} \overline{P} = \overline{M} \overline{C}. \tag{45}$$

Here, $\overline{M} \in R^{(a+\omega+s)\times p}$ is matrix parameters waiting for being solved. Based on the above analysis, error system (41) changes

$$\dot{\overline{e}}(t) = \overline{S}^{-1} \left(\overline{A} - \overline{L}_p \overline{C} \right) \overline{e}(t) + \overline{S}^{-1} \overline{L}_s u_s(t) - \overline{S}^{-1} \overline{B}_a f(t).$$
(46)

The following section discusses the stability of error system (46) and then discusses stabilization problem of closed-loop system.

5. The Stability Analysis of the Error System

Theorem 2. For error system (46), let the sliding mode observer gain $\overline{L}_s = \overline{B}_a$, if there exists matrix $\overline{P} > 0$ making the following matrix inequality established:

$$\overline{P}\,\overline{S}^{-1}\left(\overline{A}-\overline{L}_{p}\overline{C}\right)+\left(\overline{A}-\overline{L}_{p}\overline{C}\right)^{T}\left(\overline{S}^{-1}\right)^{T}\overline{P}<0. \tag{47}$$

Then the system (46) states trajectory asymptotically stable convergence to the origin.

Proof. For the system (46), defining Lyapunov function v(t) = $\overline{e}^{T}(t)\overline{P}\overline{e}(t)$, $\overline{P} > 0$, along the system (46) state trajectory, we can calculate

$$\dot{v}(t)$$

$$= 2\overline{e}^{T}(t)\overline{P}\dot{\overline{e}}(t)$$

$$= 2\overline{e}^{T}(t)\overline{P}\left[\overline{S}^{-1}(\overline{A} - \overline{L}_{p}\overline{C})\overline{e}(t) + \overline{S}^{-1}\overline{L}_{s}u_{s}(t) - \overline{S}^{-1}\overline{B}_{a}f(t)\right]$$

$$\leq 2\overline{e}^{T}(t)\overline{P}\overline{S}^{-1}(\overline{A} - \overline{L}_{p}\overline{C})\overline{e}(t) + 2\overline{P}\overline{S}^{-1}(\overline{L}_{s}u_{s}(t) - \overline{B}_{a}f(t)).$$
(42)

Consider parts of above formula,

$$2\overline{e}(t) \overline{P} \overline{S}^{-1} \left(\overline{L}_{s} u_{s}(t) - \overline{B}_{a} f(t) \right)
\leq 2\overline{e}^{T}(t) \overline{P} \overline{S}^{-1} \overline{L}_{s} u_{s}(t) - 2\overline{e}^{T}(t) \overline{P} \overline{S}^{-1} \overline{B}_{a} f(t)
= 2\overline{e}^{T}(t) \overline{P} \overline{S}^{-1} \overline{B}_{a} \left(u_{s}(t) - f(t) \right)
\leq -2\overline{e}^{T}(t) \overline{P} \overline{S}^{-1} \overline{B}_{a} \left(\alpha r_{a1} + r_{a2} + \alpha r_{\omega_{1}} + r_{\omega_{2}} + \alpha r_{s_{1}} + r_{s_{2}} + p \right)
\times \operatorname{sgn}(s(t)) + 2 \left\| \overline{e}^{T}(t) \overline{P} \overline{S}^{-1} \overline{B}_{a} f(t) \right\|
\leq -2s^{T}(t) \left(\alpha r_{a1} + r_{a2} + \alpha r_{\omega_{1}} + r_{\omega_{2}} + \alpha r_{s_{1}} + r_{s_{2}} + p \right)
\times \operatorname{sgn}(s(t)) + 2 \left\| s^{T}(t) \right\| \left\| f(t) \right\|
= -2 \left| s(t) \right| \left(\alpha r_{a1} + r_{a2} + \alpha r_{\omega_{1}} + r_{\omega_{2}} + \alpha r_{s_{1}} + r_{s_{2}} + p \right)
\times \operatorname{sgn}(s(t)) + 2 \left\| s^{T}(t) \right\| \left\| f(t) \right\| .$$
(49)

The following formation can be derived based on assumption (A1):

$$||f(t)|| \le \alpha r_{a1} + r_{a2} + \alpha r_{\omega 1} + r_{\omega 2} + \alpha r_{s1} + r_{s2} + p.$$
 (50)

Therefore

$$2\overline{e}^{T}(t)\overline{P}\overline{S}^{-1}(\overline{L}_{s}u_{s}(t)-\overline{B}_{a}f(t))\leq0. \tag{51}$$

So we can derive

$$\dot{v}(t) \leq 2\overline{e}^{T}(t)\overline{P}\overline{S}^{-1}(\overline{A} - \overline{L}_{p}\overline{C})\overline{e}(t)$$

$$\leq \overline{e}^{T}(t)\left[\overline{P}\overline{S}^{-1}(\overline{A} - \overline{L}_{p}\overline{C}) + (\overline{A} - \overline{L}_{p}\overline{C})^{T}(\overline{S}^{-1})^{T}\overline{P}\right]\overline{e}(t)$$

$$\leq 0.$$
(52)

If $\overline{e}(t) \neq 0$, the inequality always holds. So the error system (46) is asymptotically stable. The proof completes.

6. The Stabilization of Closed-Loop System

Now we consider the stabilization problem of the closed-loop system based on the observer. Considering the system (9), we design a state feedback controller based on observer as follows:

$$u(t) = kx(t) - B^{-1}B_{\alpha}\hat{f}_{\alpha}(t) - B^{-1}B_{\omega 1}\hat{\omega}(t)$$
. (53)

Substitute formula (53) into the system (9) and we can

$$\dot{x}(t) = Ax(t) + B(kx(t) - B^{-1}B_{a}\hat{f}_{a}(t) - B^{-1}B_{\omega 1}\hat{\omega}(t))$$

$$+ B_{\omega 1}\omega(t) + B_{a}f_{a}(t)$$

$$= Ax(t) + Bkx(t) - B_{a}\hat{f}_{a}(t) - B_{\omega 1}\hat{\omega}(t) + B_{\omega 1}\omega(t)$$

$$+ B_{a}f_{a}(t)$$

$$= Ax(t) + Bkx(t) - B_{a}e_{a}(t) - B_{\omega 1}e_{\omega}(t).$$
(54)

Here, $e_a(t) = \hat{f}_a(t) - f_a(t)$, $e_{\omega}(t) = \hat{\omega}(t) - \omega(t)$. Formula (54) can be rewritten as

$$\dot{x}(t) = (A + Bk) x(t) - \overline{Fe}(t). \tag{55}$$

Here, $\overline{F} = \begin{bmatrix} 0_{n \times n} & B_a & B_{\omega 1} & 0_{n \times p} & 0_{n \times p} \end{bmatrix}$. For the close-loop system (55) and the error system (46), they can construct the following system:

$$\dot{x}\left(t\right) = \left(A + Bk\right)x\left(t\right) - \overline{Fe}\left(t\right),$$

$$\dot{\overline{e}}\left(t\right) = \overline{S}^{-1}\left(\overline{A} - \overline{L}_{p}\overline{C}\right)\overline{e}\left(t\right) + \overline{S}^{-1}\overline{L}_{s}u_{s}\left(t\right) - \overline{S}^{-1}\overline{B}_{a}f\left(t\right).$$
(56)

We present the following theorem.

Theorem 3. *If there is symmetric positive definite matrix* $Z \in$ $R^{\overline{n}}$ and the matrix $K \in R^{m \times \overline{n}}$, which makes the following constraint matrix established:

$$(A + BK)^{T}Z + Z(A + BK) < 0,$$
 (57)

then the system (56) is asymptotically stable.

Proof. For the system (56), we define Lyapunov function

$$v_{x}(t) = x^{T}(t) Zx(t)$$
. (58)

Here, Z > 0 is a positive definite symmetric matrix waiting for being solved. Along the system (56) trajectory, we can directly calculate

$$\dot{v}_{x}(t) = 2x^{T}(t) Z\dot{x}(t)$$

$$= 2x^{T}(t) Z \left[(A + Bk) x(t) - \overline{Fe}(t) \right]$$

$$= x^{T}(t) Z \left[(A + Bk)^{T} Z + Z(A + Bk) \right]$$

$$- 2x^{T}(t) Z \overline{Fe}(t).$$
(59)

Let
$$\Phi = (A + BK)^T Z + Z(A + BK)$$
 and then
$$\dot{v}_x(t) \le x^T(t) \Phi x(t) - 2x^T(t) Z\overline{Fe}(t)$$

$$\le \lambda_{\min}(\Phi) \|x(t)\|^2 + 2 \|x(t)\| \|Z\overline{Fe}(t)\|.$$
(60)

Here, $\lambda_{min}(\Phi)$ represents the minimum eigenvalue of the matrix Φ . We define a new Lyapunov function

$$v_0(t) = v_x(t) + \theta v(t). \tag{61}$$

Here, $\theta > 0$ is a parameter waiting for design, v(t) is defined in Theorem 2.

According to the proof in Theorem 2, we can obtain

$$\dot{v}(t) \le \varepsilon_1 \|\bar{e}(t)\|^2. \tag{62}$$

Here.

$$\varepsilon_1 = \lambda_{\min} \left(\overline{P} \, \overline{S}^{-1} \left(\overline{A} - \overline{L}_p \overline{C} \right) + \left(\overline{A} - \overline{L}_p \overline{C} \right)^T \left(\overline{S}^{-1} \right)^T \overline{P} \right) < 0.$$
(63)

In addition, the new parameters are defined as follows:

$$\varepsilon_2 = \lambda_{\min} (\Phi) < 0, \qquad \varepsilon_3 = 2 \| Z\overline{F} \|.$$
 (64)

Selecting parameters $\theta > 0$ and let it satisfy

$$\theta > \frac{\varepsilon_3^2}{\varepsilon_1 \varepsilon_2}.\tag{65}$$

Calculate formula (61) further and we can obtain

$$\dot{v}_{0}(t) \leq \varepsilon_{2} \|x(t)\|^{2} + \varepsilon_{3} \|x(t)\| \|\overline{e}(t)\| + \theta \varepsilon_{1} \|\overline{e}(t)\|^{2} \\
\leq \varepsilon_{2} \|x(t)\|^{2} + \varepsilon_{3} \|x(t)\| \|\overline{e}(t)\| + \frac{\varepsilon_{3}^{2}}{\varepsilon_{1}\varepsilon_{2}} \varepsilon_{1} \|\overline{e}(t)\|^{2} \\
\leq \varepsilon_{2} \|x(t)\|^{2} + \varepsilon_{3} \|x(t)\| \|\overline{e}(t)\| + \frac{\varepsilon_{3}^{2}}{\varepsilon_{2}} \|\overline{e}(t)\|^{2} \\
\leq 0.5\varepsilon_{2} \|x(t)\|^{2} + \varepsilon_{3} \|x(t)\| \|\overline{e}(t)\| + 0.5\frac{\varepsilon_{3}^{2}}{\varepsilon_{2}} \|\overline{e}(t)\|^{2} \\
+ 0.5\frac{\varepsilon_{3}^{2}}{\varepsilon_{2}} \|\overline{e}(t)\|^{2} + 0.5\varepsilon_{2} \|x(t)\|^{2} \\
\leq \left(\sqrt{\frac{\varepsilon_{2}}{2}} \|x(t)\| + \sqrt{\frac{\varepsilon_{3}^{2}}{2\varepsilon_{2}}} \|\overline{e}(t)\|\right)^{2} + 0.5\frac{\varepsilon_{3}^{2}}{\varepsilon_{2}} \|\overline{e}(t)\|^{2} \\
+ 0.5\varepsilon_{2} \|x(t)\|^{2} \\
\leq 0.5\frac{\varepsilon_{3}^{2}}{\varepsilon_{1}} \|\overline{e}(t)\|^{2} + 0.5\varepsilon_{2} \|x(t)\|^{2}.$$

Notice that $\varepsilon_3 > 0$, $\varepsilon_2 < 0$, so we have

$$\dot{v}_{0}(t) \le 0.5 \frac{\varepsilon_{3}^{2}}{\varepsilon_{2}} \|\bar{e}(t)\|^{2} + 0.5\varepsilon_{2} \|x(t)\|^{2} < 0.$$
 (67)

So we have proved that the system (56) is asymptotically stable. \Box

7. Conclusions and Future Works

The sliding mode observer and the state feedback controller is proposed and the controller's stabilization under stochastic disturbance is proved. The research provides a theoretical analysis of the controller design method based on sliding mode observer. In the future, we will give the simulation verification combined with the specific space mission.

Conflict of Interests

The authors declare that there is no conflict of interests regarding the publication of this paper.

Acknowledgments

This work is partially funded by the Fundamental Research Funds for the Central Universities (no. HEUCF021318), the Natural Science Foundation of Heilongjiang Province (no. A201312), the National Natural Science Funds (no. 11372080), the Harbin Science and Technology Innovation Talent Youth Fund (no. RC2013QN001007), and the Key Laboratory of Database and Parallel Computing, Heilongjiang Province.

References

- [1] M. Der-Ming, H. Zuu-Chang, L. Tzung-Hang, and C. Bo-Jyun, "Design of a micro-satellite constellation for communication," *Acta Astronautica*, vol. 82, no. 1, pp. 54–59, 2013.
- [2] Z. Guoqiang, H. Min, and Y. Hong, "Relative orbit estimation and formation keeping control of satellite formations in low Earth orbits," *Acta Astronautica*, vol. 76, no. 7-8, pp. 164–175, 2012
- [3] H. Peng, C. Yang, Y. Li, S. Zhang, and B. Chen, "Surrogate-based parameter optimization and optimal control for optimal trajectory of Halo orbit rendezvous," *Aerospace Science and Technology*, vol. 26, no. 1, pp. 176–184, 2012.
- [4] E. N. Hartley, P. A. Trodden, A. G. Richards, and J. M. Maciejowski, "Model predictive control system design and implementation for spacecraft rendezvous," *Control Engineering Practice*, vol. 20, no. 7, pp. 695–713, 2012.
- [5] I. Chang, S.-Y. Park, and K.-H. Choi, "Decentralized coordinated attitude control for satellite formation flying via the state-dependent Riccati equation technique," *International Journal of Non-Linear Mechanics*, vol. 44, no. 8, pp. 891–904, 2009.
- [6] S. Yin, H. Luo, and S. Ding, "Real-time implementation of fault-tolerant control systems with performance optimization," *IEEE Transactions on Industrial Electronics*, vol. 64, no. 5, pp. 2402–2411, 2014.
- [7] S. Yin, G. Wang, and H. Karimi, "Data-driven design of robust fault detection system for wind turbines," *Mechatronics*. In press.
- [8] S. Yin, S. Ding, A. Haghani, and H. Hao, "Data-driven monitoring for stochastic systems and its application on batch process," *International Journal of Systems Science*, vol. 44, no. 7, pp. 1366– 1376, 2013.
- [9] S. Yin, S. Ding, A. Haghani, H. Hao, and P. Zhang, "A comparison study of basic datadriven fault diagnosis and process monitoring methods on the benchmark Tennessee Eastman process," *Journal of Process Control*, vol. 22, no. 9, pp. 1567–1581, 2012.

- [10] W. Huanqing, C. Bing, and L. Chong, "Adaptive neural tracking control for a class of stochastic nonlinear systems with unknown dead-zone," *International Journal of Innovative Computing, Information and Control*, vol. 9, no. 8, pp. 3257–3269, 2013.
- [11] A. Leslie, M. Patricia, and C. Oscar, "Chemical optimization paradigm applied to a Fuzzy tracking controller for an autonomous mobile robot," *International Journal of Innovative Computing, Information and Control*, vol. 9, no. 5, pp. 2007–2018, 2013.
- [12] W. Shunan, W. Zhigang, R. Gianmarco, and W. Rui, "Adaptive control for spacecraft relative translation with parameteric uncertainty," *Aerospace Science and Technology*, vol. 31, no. 1, pp. 53–58, 2013.

Hindawi Publishing Corporation Abstract and Applied Analysis Volume 2014, Article ID 159745, 6 pages http://dx.doi.org/10.1155/2014/159745

Research Article

Robust Stability Criteria of Roesser-Type Discrete-Time Two-Dimensional Systems with Parameter Uncertainties

Yan Zhao, ¹ Tieyan Zhang, ¹ Dan Zhao, ¹ Fucai You, ¹ and Miao Li²

¹ School of Renewable Energy, Shenyang Institute of Engineering, Shenyang, Liaoning 110136, China

Correspondence should be addressed to Yan Zhao; zhaoyan_80@163.com

Received 9 January 2014; Accepted 2 February 2014; Published 16 March 2014

Academic Editor: Ming Liu

Copyright © 2014 Yan Zhao et al. This is an open access article distributed under the Creative Commons Attribution License, which permits unrestricted use, distribution, and reproduction in any medium, provided the original work is properly cited.

This paper is concerned with robust stability analysis of uncertain Roesser-type discrete-time two-dimensional (2D) systems. In particular, the underlying parameter uncertainties of system parameter matrices are assumed to belong to a convex bounded uncertain domain, which usually is named as the so-called polytopic uncertainty and appears typically in most practical systems. Robust stability criteria are proposed for verifying the robust asymptotical stability of the related uncertain Roesser-type discrete-time 2D systems in terms of linear matrix inequalities. Indeed, a parameter-dependent Lyapunov function is applied in the proof of our main result and thus the obtained robust stability criteria are less conservative than the existing ones. Finally, the effectiveness and applicability of the proposed approach are demonstrated by means of some numerical experiments.

1. Introduction

During the past several decades, the well-known Lyapunov stability theory has become an efficient tool for dealing with the problem of stability analysis of many kinds of uncertain systems [1-6]. However, those earlier results on stability analysis of uncertain systems are developed by using the socalled common quadratic Lyapunov function (CQLF) [7]. Actually, the CQLF applies a single Lyapunov matrix for all the submodels and therefore the obtained stability criteria are rather conservative. With the purpose of further releasing the conservatism of the stability criteria, the affine parameterdependent Lyapunov function (APDLF) has been proposed in [8], where the fixed quadratic Lyapunov function is replaced by a Lyapunov function with affine dependence on the underlying uncertain parameters. Because of the construction of such parameter-dependent Lyapunov functions, the conservatism could be released a lot as a tradeoff.

On the other hand, the famous 2D systems model could represent a wide range of practical plants, for example, water stream heating, thermal processes, biomedical imaging, gas absorption, river pollution modeling, data processing and transmission, process of gas filtration, grid based wireless sensor networks, and so forth, [9, 10]. As a result, a considerable interest in stability analysis of 2D systems has emerged

during the past two decades [11–15]. Recently, the 2D system theory has also been applied to address the problem of stability analysis 2D state-space digital filters with saturation arithmetic in [16–30]. However, it is worth noting that most of the aforementioned results are feasible for linear 2D systems without uncertainties. As is well known, most of the practical 2D dynamical systems in the realistic world are subject to parameter uncertainties and the above results would fail to work when some uncertain parameters occur in the practical settings.

In particular, it is worth noting that the Roesser-type discrete-time 2D system's information is propagated along two independent directions and this fact makes the problem of stability analysis more complicated. Due to the complexity of mathematical analysis of Roesser-type discrete-time 2D systems with parameter uncertainties, there has been little literature which focuses on robust stability analysis of uncertain Roesser-type discrete-time 2D systems so far. Thus, this problem needs to be further investigated and this fact motivates us to carry out this task in this paper.

Based on the above analysis, the problem of robust stability analysis of Roesser-type discrete-time 2D systems with parameter uncertainties will be addressed via the Lyapunov stability theory. The parameter uncertainties of 2D system's

² School of Engineering and Information Technology, Murdoch University, Perth, WA 6150, Australia

parameter matrices are assumed to belong to a convex bounded uncertain domain, which usually is named as the so-called polytopic uncertainty and appears typically in most modeling processes of uncertainties. An efficient parameter-dependent Lyapunov function is applied in the derivation of our main result and thus the obtained robust stability criteria are less conservative than the existing ones. Moreover, robust stability criteria are given to verify the robust asymptotical stability of the uncertain Roesser-type discrete-time 2D systems in terms of linear matrix inequalities. Finally, the effectiveness and applicability of the proposed approach are demonstrated by means of numerical examples.

The rest of this paper is organized as follows: following the introduction, some preliminaries are provided in Section 2. In Section 3, LMI-based robust stability criteria are proposed for verifying the robust asymptotical stability of the uncertain Roesser-type discrete-time 2D systems. A numerical example is given to demonstrate the effectiveness of the given approach in Section 4. Finally, some conclusions are also given in Section 5.

The following notations are applied for simplicity. A star * in a symmetric matrix denotes the transposed element in the symmetric position; the symbol I represents the identity matrix with appropriate dimension; X > 0 (or $X \ge 0$) means the matrix X is symmetric and positive definite (or symmetric and positive semidefinite); X^T denotes the transpose of X.

2. Preliminaries

Consider a class of uncertain discrete-time 2D systems which is described by the Roesser-type model

$$\mathbf{x}^{+}(k,l) = A(\alpha)\mathbf{x}(k,l), \qquad (1)$$

with

$$\mathbf{x}(k,l) = \begin{bmatrix} \mathbf{x}^{h}(k,l) \\ \mathbf{x}^{v}(k,l) \end{bmatrix}, \qquad \mathbf{x}^{+}(k,l) = \begin{bmatrix} \mathbf{x}^{h}(k+1,l) \\ \mathbf{x}^{v}(k,l+1) \end{bmatrix}, \quad (2)$$

where k and l are two integers in \mathbb{Z}^+ . $\mathbf{x}^h(\cdot,\cdot)$ is the horizontal state in \mathbf{R}^{n_1} and $\mathbf{x}^{\mathbf{v}}(\cdot,\cdot)$ is the vertical state in \mathbf{R}^{n_2} , where n_1 and n_2 are dimensions of the horizontal state vector and the vertical state vector, respectively. The system coefficient matrix $A(\alpha)$ is not precisely known but belongs to a convex bounded uncertain domain:

$$A(\alpha) = \begin{bmatrix} A^{11}(\alpha) & A^{12}(\alpha) \\ A^{21}(\alpha) & A^{22}(\alpha) \end{bmatrix}, \tag{3}$$

with $A^{11}(\alpha) \in \mathbf{R}^{n_1 \times n_1}$, $A^{12}(\alpha) \in \mathbf{R}^{n_1 \times n_2}$, $A^{21}(\alpha) \in \mathbf{R}^{n_2 \times n_1}$, and $A^{22}(\alpha) \in \mathbf{R}^{n_2 \times n_2}$, respectively. Specially, these matrices $A^{11}(\alpha)$, $A^{12}(\alpha)$, $A^{21}(\alpha)$, and $A^{22}(\alpha)$ belong to a convex bounded (polytope type) uncertain domain \mathscr{P} given as follows:

$$\mathcal{P} := \left\{ \left(A^{11}, A^{12}, A^{21}, A^{22} \right) (\alpha) : \left(A^{11}, A^{12}, A^{21}, A^{22} \right) (\alpha) \right.$$

$$= \sum_{i=1}^{r} \alpha_{i} \left(A_{i}^{11}, A_{i}^{12}, A_{i}^{21}, A_{i}^{22} \right) ; \alpha \in \Delta_{r} \right\}, \tag{4}$$

where Δ_r is the so-called unit simplex given by

$$\Delta_r = \left\{ \alpha \in \mathbf{R}^r : \sum_{i=1}^r \alpha_i = 1, \alpha_i \ge 0; i = 1, \dots, r \right\}. \tag{5}$$

Moreover, the boundary conditions along two independent directions are defined as $\mathbf{x}^h(0,l) = f(l)$ and $\mathbf{x}^v(k,0) = g(k)$, where f(l) and g(k) are boundary conditions along the horizontal direction and vertical direction, respectively.

Finally, let us end this section by giving a definition and a lemma which will play an important role in the following proof.

Denote $X_N = \sup\{\|\mathbf{x}(k,l)\| : N = k+l\}$, and then we give the definition of robust asymptotical stability for uncertain Roesser-type discrete-time 2D system (1).

Definition 1. The uncertain Roesser-type discrete-time 2D system (1) is robust asymptotically stable if $\lim_{k\to\infty,l\to\infty}X_N=0$ with the initial and boundary conditions $\mathbf{x}^h(0,l)=f(l)$ and $\mathbf{x}^v(k,0)=g(k)$.

Lemma 2 (see [7]). Given matrices $Q = Q^T$ and $R = R^T$ with appropriate dimensions, the inequality $\begin{pmatrix} Q & S \\ S^T & R \end{pmatrix} > 0$ is equivalent to R > 0, $Q - SR^{-1}S^T > 0$.

3. Main Results

In this section, by using the Lyapunov stability theory, sufficient robust stability criteria for ensuring the robust asymptotical stability of the underlying uncertain Roesser-type discrete-time 2D system (1) will be proposed in terms of linear matrix inequalities. Indeed, less conservative robust stability conditions are given by means of a parameter-dependent Lyapunov function and a slack method for exploiting the algebraic properties of the uncertain Roesser-type discrete-time 2D system (1).

Theorem 3. The uncertain Roesser-type discrete-time 2D system (1) is robust asymptotically stable if there exist appropriately dimensional matrices P_{ij} , i = 1, 2, ..., r; $i \le j \le r$, with

$$P_{ij} = \begin{bmatrix} P_{ij}^{1} & * \\ P_{ij}^{3} & P_{ij}^{2} \end{bmatrix}, \qquad P_{ij}^{1} \in \mathbf{R}^{n_{1} \times n_{1}},$$

$$P_{ij}^{2} \in \mathbf{R}^{n_{2} \times n_{2}}, \qquad P_{ij}^{3} \in \mathbf{R}^{n_{2} \times n_{1}},$$
(6)

such that the following LMIs hold:

$$\begin{bmatrix} -P_{ii} & * \\ P_{ii}A_i & -P_{ii} \end{bmatrix} < 0, \quad i = 1, 2, \dots, r;$$

$$\begin{bmatrix} -P_{ii} & * \\ P_{ii}A_j & -P_{ii} \end{bmatrix} + \begin{bmatrix} -P_{ij} & * \\ P_{ij}A_i & -P_{ij} \end{bmatrix} < 0,$$

$$i = 1, 2, \dots, r - 1, \quad i < j;$$

$$\begin{bmatrix} -P_{jj} & * \\ P_{jj}A_i & -P_{jj} \end{bmatrix} + \begin{bmatrix} -P_{ij} & * \\ P_{ij}A_j & -P_{ij} \end{bmatrix} < 0,$$

$$i = 1, 2, \dots, r - 1, \quad i < j;$$

$$\begin{bmatrix} -P_{ij} & * \\ P_{ij}A_l & -P_{ij} \end{bmatrix} + \begin{bmatrix} -P_{il} & * \\ P_{il}A_j & -P_{il} \end{bmatrix} + \begin{bmatrix} -P_{jl} & * \\ P_{jl}A_i & -P_{jl} \end{bmatrix} < 0,$$

$$i = 1, 2, \dots, r - 2, \quad i < j < l \le r.$$
(7)

Proof. Consider the following parameter-dependent Lyapunov function which is suitable for the uncertain Roessertype discrete-time 2D system (1):

$$V\left(\mathbf{x}\left(k,l\right)\right) = \mathbf{x}^{T}\left(k,l\right) P_{\alpha\alpha}\mathbf{x}\left(k,l\right),\tag{8}$$

where the matrix $P_{\alpha\alpha}$ is a positive definite matrix and with the following structure: $P_{\alpha\alpha} = \sum_{i=1}^r \sum_{i \leq j \leq r} \alpha_i \alpha_j \begin{bmatrix} P_{ij}^1 & * \\ P_{ij}^3 & P_{ij}^2 \end{bmatrix}, P^1 \in \mathbf{R}^{n_1 \times n_1}, P^2 \in \mathbf{R}^{n_2 \times n_2}, P^3 \in \mathbf{R}^{n_2 \times n_1}.$

Then, the variation of the parameter-dependent Lyapunov function $V(\mathbf{x}(k, l))$ could be described as

$$\Delta V\left(\mathbf{x}\left(k,l\right)\right) = \mathbf{x}^{T}\left(k,l\right) \left(A(\alpha)^{T} P_{\alpha\alpha} A\left(\alpha\right) - P_{\alpha\alpha}\right) \mathbf{x}\left(k,l\right). \tag{9}$$

By applying the Lyapunov stability theory, the uncertain Roesser-type discrete-time 2D system (1) is robust asymptotically stable if the following inequality holds:

$$A(\alpha)^{T} P_{\alpha\alpha} A(\alpha) - P_{\alpha\alpha} < 0. \tag{10}$$

Applying Lemma 2 to (10), it can be concluded that inequality (10) is equivalent to the following inequality:

$$\Phi = \begin{bmatrix} -P_{\alpha\alpha} & * \\ P_{\alpha\alpha}A(\alpha) & -P_{\alpha\alpha} \end{bmatrix} < 0.$$
 (11)

On the other hand, reordering the expression of Ψ , one can obtain

$$\Phi = \begin{bmatrix}
-P_{\alpha\alpha} & * \\
P_{\alpha\alpha}A(\alpha) & -P_{\alpha\alpha}
\end{bmatrix}$$

$$= \sum_{i=1}^{r} \alpha_{i}^{3} \Phi_{iii} + \sum_{i=1}^{r-1} \sum_{j>i} \alpha_{i}^{2} \alpha_{j} \Phi_{iij}$$

$$+ \sum_{i=1}^{r-1} \sum_{j>i} \alpha_{i}^{2} \Upsilon_{j} \Gamma_{ijj} + \sum_{i=1}^{r-2} \sum_{j>i} \sum_{l>i} \alpha_{i} \alpha_{j} \alpha_{l} \Phi_{ijl},$$
(12)

where we have

$$\begin{split} \Phi_{iii} &= \begin{bmatrix} -P_{ii} & * \\ P_{ii}A_i & -P_{ii} \end{bmatrix}, \\ \Phi_{iij} &= \begin{bmatrix} -P_{ii} & * \\ P_{ii}A_i & -P_{ii} \end{bmatrix} + \begin{bmatrix} -P_{ij} & * \\ P_{ii}A_i & -P_{ii} \end{bmatrix}, \end{split}$$

$$\Phi_{ijj} = \begin{bmatrix}
-P_{jj} & * \\
P_{jj}A_i & -P_{jj}
\end{bmatrix} + \begin{bmatrix}
-P_{ij} & * \\
P_{ij}A_j & -P_{ij}
\end{bmatrix},$$

$$\Phi_{ijl} = \begin{bmatrix}
-P_{ij} & * \\
P_{ij}A_l & -P_{ij}
\end{bmatrix} + \begin{bmatrix}
-P_{il} & * \\
P_{il}A_j & -P_{il}
\end{bmatrix}$$

$$+ \begin{bmatrix}
-P_{jl} & * \\
P_{jl}A_i & -P_{jl}
\end{bmatrix}.$$
(13)

From (10)–(12), if the LMI-based stability conditions (7) hold, inequality (10) evidently holds, which guarantee the robust asymptotical stability for the uncertain Roesser-type discrete-time 2D system (1).

This completes the proof.
$$\Box$$

Remark 4. From (1) and (4), the parameter uncertainties of 2D system parameter matrices are assumed to belong to a convex bounded uncertain domain. Then, LMI-based robust stability criteria are given for ensuring the robust asymptotical stability of the underlying uncertain Roesser-type discrete-time 2D systems in Theorem 3. Indeed, the parameter-dependent Lyapunov function $V(\mathbf{x}(k,l)) = \mathbf{x}^T(k,l)P_{\alpha\alpha}\mathbf{x}(k,l)$ is applied in the derivation of our main result and thus the obtained robust stability criteria are less conservative than before. Furthermore, the effectiveness and applicability of the proposed results will be demonstrated by means of numerical experiments in the following section.

4. Numerical Examples

Consider the uncertain Roesser-type discrete-time twodimensional systems described as follows:

$$\begin{bmatrix} x^h (k+1,l) \\ x^v (k,l+1) \end{bmatrix} = \sum_{i=1}^{2} \alpha_i \left(A_i \begin{bmatrix} x^h (k,l) \\ x^v (k,l) \end{bmatrix} \right), \tag{14}$$

where $A_1 = \left[\begin{smallmatrix} 1+a_1T_1 & (a_1a_2+a_0)T_1 \\ T_2 & 1+a_2T_2 \end{smallmatrix} \right]$ and $A_2 = \left[\begin{smallmatrix} 1+a_1T_1 & a_1a_2T_1 \\ T_2 & 1+a_2T_2 \end{smallmatrix} \right]$. And the following parameter values about $a_0, a_1, a_2, T_1,$ and T_2 are given: $a_0 = -2, a_1 = -3, T_1 = 0.1,$ and $T_2 = 0.2.$ Furthermore, the initial and boundary conditions of the above uncertain Roesser-type discrete-time two-dimensional systems are set as $x^h(0,l) = 6\cos(l)$ for l < 30 and $x^v(k,0) = 4\sin(k)$ for k < 30 and $x^h(0,l) = 0$ for $l \geq 30$ and $x^v(k,0) = 0$ for $k \geq 30$.

Let $a_2 = -0.6$; the stability criteria given in Theorem 3 are feasible by solving LMIs (7), which guarantee the robust asymptotical stability for the underlying uncertain Roessertype discrete-time 2D systems. On the other hand, Figures 1 and 2 show the state trajectory of the system state variables $x^h(k,l)$ and $x^v(k,l)$ with $\alpha_1 = 0.4$ and $\alpha_2 = 0.6$, respectively. From Figures 1 and 2, it is easy to see that the state trajectories of $x^h(k,l)$ and $x^v(k,l)$ are robust asymptotically stable in this case.

Let $a_2 = -2.9$; the stability criteria given in Theorem 3 are feasible by solving LMIs (7), which guarantee the robust asymptotical stability for the underlying uncertain Roessertype discrete-time 2D systems. On the other hand, Figures 3 and 4 show the state trajectory of the system state variables

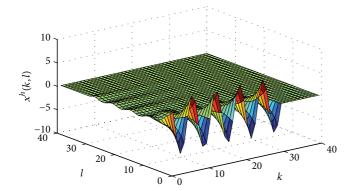


FIGURE 1: The state trajectory of $x^h(k, l)$ with $a_2 = -0.6$.

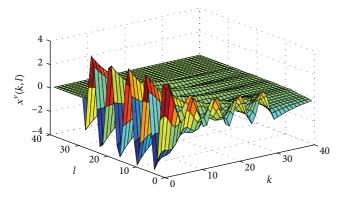
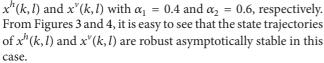


Figure 2: The state trajectory of $x^{\nu}(k, l)$ with $a_2 = -0.6$.



Let $a_2=-8.9$; the stability criteria given in Theorem 3 are not feasible by solving LMIs (7), which do not guarantee the robust asymptotical stability for the underlying uncertain Roesser-type discrete-time 2D systems. On the other hand, Figures 5 and 6 show the state trajectory of the system state variables $x^h(k,l)$ and $x^v(k,l)$ with $\alpha_1=0.4$ and $\alpha_2=0.6$, respectively. From Figures 5 and 6, it is easy to see that the state trajectories of $x^h(k,l)$ and $x^v(k,l)$ are not robust asymptotically stable in this case. Now, it could be concluded that the effectiveness and applicability of the proposed approach given in Theorem 3 are illustrated by means of numerical experiments.

5. Conclusions

The problem of robust stability analysis of a class of uncertain Roesser-type discrete-time 2D systems has been addressed by using an efficient parameter-dependent Lyapunov function. In particular, the parameter uncertainties of the underlying 2D system's parameter matrices belong to a convex bounded uncertain domain, which often is named as polytopic uncertainty and appears typically in most practical systems. In order to ensure the robust asymptotic stability of the

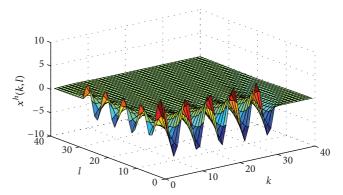


Figure 3: The state trajectory of $x^h(k, l)$ with $a_2 = -2.9$.

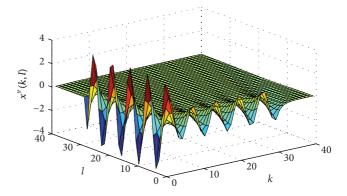


FIGURE 4: The state trajectory of $x^{\nu}(k, l)$ with $a_2 = -2.9$.

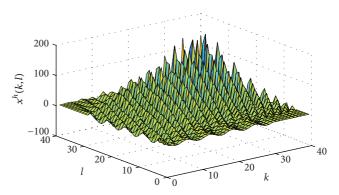


FIGURE 5: The state trajectory of $x^h(k, l)$ with $a_2 = -8.9$.

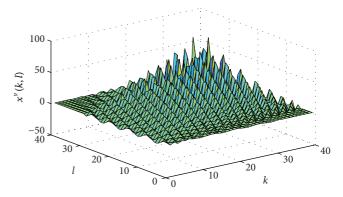


FIGURE 6: The state trajectory of $x^{\nu}(k, l)$ with $a_2 = -8.9$.

uncertain Roesser-type discrete-time 2D systems, LMI-based robust stability criteria are proposed by exploiting the algebraic properties of the convex bounded uncertain domain. Finally, a numerical example is provided to demonstrate the effectiveness and applicability of the approach given in this paper.

Conflict of Interests

The authors declare that there is no conflict of interests regarding the publication of this paper.

Acknowledgments

This work is supported by the National Nature Science Foundation of China under Grant 61304069 and 61372195, the National Nature Science Foundation of Liaoning Province under Grant 2013020124, 2012201010, and 201102160, the Key Project of Chinese Ministry of Education under Grant 212033, the Key Technologies R&D Program of Liaoning Province under Grant 2011224006, the Program for Liaoning Excellent Talents in University under Grant LJQ2011136, the Scientific Research Fund of Liaoning Provincial Education Department under Grant L2013494, and the Science and Technology Program of Shenyang under Grant F11-264-1-70.

References

- [1] D. Henrion, D. Arzelier, D. Peaucelle, and M. Śebek, "An LMI condition for robust stability of polynomial matrix polytopes," *Automatica*, vol. 37, no. 3, pp. 461–468, 2001.
- [2] S. Yin, H. Luo, and S. Ding, "Real-time implementation of fault-tolerant control systems with performance optimization," *IEEE Transactions on Industrial Electronics*, vol. 64, no. 5, pp. 2402–2411, 2014.
- [3] S. Yin, S. X. Ding, A. H. A. Sari, and H. Hao, "Data-driven monitoring for stochastic systems and its application on batch process," *International Journal of Systems Science*, vol. 44, no. 7, pp. 1366–1376, 2013.
- [4] S. Yin, S. Ding, A. Haghani, H. Hao, and P. Zhang, "A comparison study of basic datadriven fault diagnosis and process monitoring methods on the benchmark Tennessee Eastman process," *Journal of Process Control*, vol. 22, no. 9, pp. 1567–1581, 2012.
- [5] D. Henrion, D. Arzelier, and D. Peaucelle, "Positive polynomial matrices and improved LMI robustness conditions," *Automatica*, vol. 39, no. 8, pp. 1479–1485, 2003.
- [6] P. L. D. Peres and J. C. Geromel, "#2 control for discrete-time systems optimality and robustness," *Automatica*, vol. 29, no. 1, pp. 225–228, 1993.
- [7] P. L. D. Peres, J. C. Geromel, and J. Bernussou, "Quadratic stabilizability of linear uncertain systems in convex-bounded domains," *Automatica*, vol. 29, no. 2, pp. 491–493, 1993.
- [8] P. Gahinet, P. Apkarian, and M. Chilali, "Affine parameter-dependent Lyapunov functions and real parametric uncertainty," *IEEE Transactions on Automatic Control*, vol. 41, no. 3, pp. 436–442, 1996.
- [9] E. Fornasini and G. Marchesini, "State-space realization theory of two-dimensional filters," *IEEE Transactions on Automatic Control*, vol. 21, no. 4, pp. 484–492, 1976.

- [10] R. P. Roesser, "A discrete state-space model for linear image processing," *IEEE Transactions on Automatic Control*, vol. 20, pp. 1–10, 1975.
- [11] D. H. Owens, N. Amann, E. Rogers, and M. French, "Analysis of linear iterative learning control schemes: a 2D systems/ repetitive processes approach," *Multidimensional Systems and Signal Processing*, vol. 11, no. 1-2, pp. 125–177, 2000.
- [12] B. Sulikowski, K. Gałkowski, E. Rogers, and D. H. Owens, "Output feedback control of discrete linear repetitive processes," *Automatica*, vol. 40, no. 12, pp. 2167–2173, 2004.
- [13] B. Sulikowski, K. Galkowski, E. Rogers, and D. H. Owens, "PI control of discrete linear repetitive processes," *Automatica*, vol. 42, no. 5, pp. 877–880, 2006.
- [14] S. Yin, G. Wang, and H. Karimi, "Data-driven design of robust fault detection system for wind turbines, Mechatronics," 2013.
- [15] V. Singh, "Elimination of overflow oscillations in 2-D digital filters employing saturation arithmetic: an LMI approach," *IEEE Signal Processing Letters*, vol. 12, no. 3, pp. 246–249, 2005.
- [16] V. Singh, "Stability analysis of 2-D discrete systems described by the Fornasini-Marchesini second model with state saturation," *IEEE Transactions on Circuits and Systems II*, vol. 55, no. 8, pp. 793–796, 2008.
- [17] A. Dhawan and H. Kar, "Optimal guaranteed cost control of 2-D discrete uncertain systems: an LMI approach," *Signal Processing*, vol. 87, no. 12, pp. 3075–3085, 2007.
- [18] V. Singh, "New LMI condition for the nonexistence of overflow oscillations in 2-D state-space digital filters using saturation arithmetic," *Digital Signal Processing*, vol. 17, no. 1, pp. 345–352, 2007.
- [19] V. Singh, "Improved LMI-based criterion for global asymptotic stability of 2-D state-space digital filters described by Roesser model using two's complement arithmetic," *Digital Signal Pro*cessing, vol. 22, no. 3, pp. 471–475, 2012.
- [20] V. Singh, "On global asymptotic stability of 2-D discrete systems with state saturation," *Physics Letters A*, vol. 372, no. 32, pp. 5287–5289, 2008.
- [21] A. Dhawan and H. Kar, "An LMI approach to robust optimal guaranteed cost control of 2-D discrete systems described by the Roesser model," *Signal Processing*, vol. 90, no. 9, pp. 2648–2654, 2010
- [22] A. Dey and H. Kar, "Robust stability of 2-D discrete systems employing generalized overflow nonlinearities: an LMI approach," *Digital Signal Processing*, vol. 21, no. 2, pp. 262–269, 2011.
- [23] A. Dhawan and H. Kar, "An improved LMI-based criterion for the design of optimal guaranteed cost controller for 2-D discrete uncertain systems," *Signal Processing*, vol. 91, no. 4, pp. 1032– 1035, 2011.
- [24] V. Singh, "New approach to stability of 2-D discrete systems with state saturation," *Signal Processing*, vol. 92, no. 1, pp. 240–247, 2012.
- [25] H. Kar, "A new criterion for the global asymptotic stability of 2-D state-space digital filters with twos complement overflow arithmetic," *Signal Processing*, vol. 92, no. 9, pp. 2322–2326, 2012.
- [26] A. Dey and H. Kar, "An LMI based criterion for the global asymptotic stability of 2-D discrete state-delayed systems with saturation nonlinearities," *Digital Signal Processing*, vol. 22, no. 4, pp. 633–639, 2012.
- [27] W. Sun, H. Gao Sr., and O. Kaynak, "Finite frequency \mathcal{H}_{∞} control for vehicle active suspension systems," *IEEE Transactions on Control Systems Technology*, vol. 19, no. 2, pp. 416–422, 2011.

- [28] W. Sun, Y. Zhao, J. Li, L. Zhang, and H. Gao, "Active suspension control with frequency band constraints and actuator input delay," *IEEE Transactions on Industrial Electronics*, vol. 59, no. 1, pp. 530–537, 2012.
- [29] Y. Suzuki, S. Morioka, and H. Ueda, "Cooking support with information projection over ingredient," *International Journal of Innovative Computing, Information and Control*, vol. 9, no. 12, pp. 4753–4763, 2013.
- [30] M. Nakatani and T. Ohno, "An integrated model depicting psychology of active/Non-active internet users: how to motivate people to use internet at home," *International Journal of Innovative Computing, Information and Control*, vol. 9, no. 12, pp. 4765–4779, 2013.

Hindawi Publishing Corporation Abstract and Applied Analysis Volume 2014, Article ID 361259, 12 pages http://dx.doi.org/10.1155/2014/361259

Research Article

Stochastic Maximum Principle of Near-Optimal Control of Fully Coupled Forward-Backward Stochastic Differential Equation

Maoning Tang

Department of Mathematical Sciences, Huzhou University, Huzhou, Zhejiang 313000, China

Correspondence should be addressed to Maoning Tang; tangmaoning@hutc.zj.cn

Received 30 December 2013; Revised 29 January 2014; Accepted 6 February 2014; Published 16 March 2014

Academic Editor: Shen Yin

Copyright © 2014 Maoning Tang. This is an open access article distributed under the Creative Commons Attribution License, which permits unrestricted use, distribution, and reproduction in any medium, provided the original work is properly cited.

This paper first makes an attempt to investigate the near-optimal control of systems governed by fully nonlinear coupled forward-backward stochastic differential equations (FBSDEs) under the assumption of a convex control domain. By Ekeland's variational principle and some basic estimates for state processes and adjoint processes, we establish the necessary conditions for any ε -near optimal control in a local form with an error order of exact $\varepsilon^{1/2}$. Moreover, under additional convexity conditions on Hamiltonian function, we prove that an ε -maximum condition in terms of the Hamiltonian in the integral form is sufficient for near-optimality of order $\varepsilon^{1/2}$.

1. Introduction

Bismut [1] first investigated linear backward stochastic differential equations (BSDEs in short) as the adjoint equation of the forward stochastic system. The existence and uniqueness of BSDEs with nonlinear generators under Lipschitz condition were first proved by Pardoux and Peng [2] in 1990. Since then, the theory of BSDEs has extensive applications in both mathematical finance and stochastic control. Forwardbackward stochastic differential equations (FBSDEs in short) consist of forward stochastic differential equations (SDEs in short) of Itô type and BSDEs of Pardoux-Peng. Forwardbackward stochastic equations (FBSDEs) not only are widely used in stochastic control and differential games but also have profound applications in mathematical economics and mathematical finance. Therefore, it is natural to investigate control problems for systems governed by this kind of stochastic equations. In mathematical finance, FBSDEs can be formulated as the price equations of financial assets under model uncertainty. In the stochastic optimal control problem, FBSDEs arise as the Hamilton system which is composed of the optimality conditions, the adjoint equation, and the state equation and which completely characterizes the optimal control.

A classical approach for optimal control problems is to derive necessary conditions satisfied by an optimum, such as Pontryagin's maximum principle. Now the maximum principles for optimal controls of FBSDEs have rich literatures which can be referred to [3–12] and references therein.

The references stated in the above are all concerned with (exact) optimal control. But, in fact, the (exact) optimal control may not exist in many situations. So it becomes very important to study near-optimal controls which are more available and much easier to be obtained than optimal ones, both analytically and numerically. The near-optimal deterministic control problems have been investigated in [13–15]. Near-optimal control problems for SDEs with controlled diffusion coefficients were first investigated in 1998 by Zhou [16], where necessary and sufficient conditions are established by introducing second adjoint equation, for all near-optimal controls. Inspired by Zhou [16], we refer to [16–20] on the near-optimal control of other forward stochastic systems.

For forward-backward stochastic systems, Huang et al. [21] in 2010 and Bahlali et al. [22] in 2009, respectively, established the corresponding stochastic maximum principle for the near-optimal control of linear systems and nonlinear systems, where diffusion coefficients and control variables are each independently based on Ekeland's principle and spike

variation. In 2011, Hui et al. [23] studied the near-optimal control of nonlinear FBSDEs, where diffusion coefficients can be dependent on the control variable, with the assumption that the control domain is convex. In 2012, for linear FBSDEs, Zhang et al. [24] extended the results of [21–23] to the general case of control domains based on the Ekeland's principle, spike variation, reduction technique developed recently by Yong [25], and the methodology recently introduced by Wu [26].

The control systems of FBSDEs studied in references [21-24] are nonfully coupled which are only coupled in BSDE and not in SDE. For the control systems of fully coupled FBSDEs, the existing literatures mainly focused on exact optimal control problems and few on near-optimal control problems. The purpose of the present paper is to make the first attempt to discuss the near-optimal control for fully coupled FBSDEs. Its main contribution is the developments of maximum principle and verification theorem of the nearoptimal control in a uniform manner by Ekeland's variational principle. Compared with references [21-24], this paper mainly has three advantages as follows. Firstly, our systems studied are fully coupled FBSDEs, which are coupled not only in BSDEs but also in SDEs. Secondly, we get necessary optimality conditions for near-optimal control with an error order of exact $\varepsilon^{1/2}$, which is better than all in the existing literature on the cases of FBSDEs, where the error orders are almost $\varepsilon^{1/3}$. In fact, by Ekeland's variational principle, we know that the error order of exact $\varepsilon^{1/2}$ for the nearoptimal control is the best error order. Thirdly, different from [21–24], by continuous dependence theorem of FBSDEs (see Lemma 4), we obtain directly the basic estimates for state processes and adjoint processes (see Lemmas 10, 11, 12, and 14) which play a very important role in proving our main results. Therefore, our approach is simpler and more quickly.

The paper is organized as follows. In Section 2, we present the notations and give main theory on FBSDEs. In Section 3, the problem studied is formulated and basic assumptions are given. In Section 4, we prove some prior estimates for state trajectories and adjoint equation. In Section 5, we obtain a variational formula for the performance functional. Sections 6 and 7 are devoted to deriving verification theorem and stochastic maximum principle by Ekeland's variational principle. In Section 8, we conclude our paper.

2. Preliminary Notations and Basic Theory for FBSDEs

Now we first introduce some preliminary notations which will be used throughout this paper. Let (Ω, \mathcal{F}, P) be a probability space. Let $\{W(t), 0 \leq t \leq T\}$ be a d-dimensional Brownian motion. Let $\{\mathcal{F}_t\}_{0 \leq t \leq T}$ be P-completed natural filtration generated by $\{W(t), 0 \leq t \leq T\}$. Let E be a Euclidean space, where the inner product and norm are denoted by (\cdot, \cdot) and $|\cdot|$, respectively. For a given function, $\phi: \mathbb{R}^n \to \mathbb{R}$, we denote its gradient and Hessian by ϕ_x and ϕ_{xx} , respectively. If $\phi: \mathbb{R}^n \to \mathbb{R}^k$ (with $k \geq 2$), then $\phi_x = (\partial \phi_i/\partial x_j)$ is the corresponding $(k \times n)$ Jacobian matrix. By \mathcal{P} we denote the predictable σ field on $\Omega \times [0,T]$

and by $\mathscr{B}(\Lambda)$ the Borel σ -algebra of any topological space Λ . Denote by $M_{\mathscr{F}}^2(0,T;E)$ the space of all \mathscr{P} -measurable E-valued stochastic processes $f=\{f(t,\omega),(t,\omega)\in[0,T]\times\Omega\}$ satisfying $\|f\|_{M_{\mathscr{F}}^2(0,T;E)}\triangleq\sqrt{E\int_0^T|f(t)|^2dt}<\infty$, by $S_{\mathscr{F}}^2(0,T;E)$, the space of all \mathscr{F}_t -adapted E-valued stochastic càdlàg processes $f=\{f(t,\omega),(t,\omega)\in[0,T]\times\Omega\}$ such that $\|f\|_{S_{\mathscr{F}}^2(0,T;E)}\triangleq\sqrt{E\sup_{0\leq t\leq T}|f(t)|^2dt}<+\infty$, by $L^2(\Omega,\mathscr{F},P;E)$, and the set of all E-valued random variables ξ on (Ω,\mathscr{F},P) such that $\|\xi\|_{L^2(\Omega,\mathscr{F},P;E)}\triangleq\sqrt{E|\xi|^2}<\infty$. Finally, we define the space

$$\mathbb{M}^{2}\left[0,T\right] := S_{\mathcal{F}}^{2}\left(0,T;\mathbb{R}^{n}\right) \times S_{\mathcal{F}}^{2}\left(0,T;\mathbb{R}^{m}\right) \times M_{\mathcal{F}}^{2}\left(0,T;\mathbb{R}^{m\times d}\right). \tag{1}$$

Then $\mathbb{M}^2[0,T]$ is a Banach space with respect to the norm $\|\cdot\|_{\mathbb{M}^2}$ given by

$$\|\Theta(\cdot)\|_{\mathbb{M}^{2}}^{2} = E \sup_{0 \le t \le T} |x(t)|^{2} + E \sup_{0 \le t \le T} |y(t)|^{2} + E \int_{0}^{T} |z(t)|^{2} dt,$$
(2)

for $\Theta(\cdot) = (x(\cdot), y(\cdot), z(\cdot)) \in \mathbb{M}^2[0, T].$

Now we are in position to present the preliminary results of fully coupled FBSDEs. Consider a general FBSDE as follows:

$$dx(t) = b(t, x(t), y(t), z(t)) dt + \sigma(t, x(t), y(t), z(t)) dB(t),$$

$$y(t) = -f(t, x(t), y(t), z(t)) dt + z(t) dB(t),$$

$$x(0) = a,$$

$$y(T) = h(x(T)).$$
(3)

Here $f:[0,T]\times\Omega\times\mathbb{R}^n\times\mathbb{R}^m\times\mathbb{R}^{m\times d}\to\mathbb{R}^m, b:[0,T]\times\Omega\times\mathbb{R}^n\times\mathbb{R}^m\times\mathbb{R}^{m\times d}\to\mathbb{R}^n, h:\Omega\times\mathbb{R}^n\to\mathbb{R}^m,$ and $\sigma:[0,T]\times\Omega\times\mathbb{R}^n\times\mathbb{R}^m\times\mathbb{R}^{m\times d}\to\mathbb{R}^{n\times d}$ are given mappings and $a\in\mathbb{R}^n$. For a given full-rank $m\times n$ matrix G, we use the notations $v=\begin{pmatrix}x\\y\\z\end{pmatrix}$ and $A(t,u)=\begin{pmatrix}-G^*f\\Gb\\G\sigma\end{pmatrix}$, where G^* is the transpose matrix of G.

Definition 1. A stochastic process $(x(\cdot), y(\cdot), z(\cdot)) \in \mathbb{M}^2[0, T]$ for the coefficients (a, b, σ, f, h) is said to be an adapted solution of (3) if, for any $t \in [0, T]$, it follows almost surely

$$x(t) = a + \int_{0}^{t} b(r, x(r), y(r), z(r)) dr$$

$$+ \int_{0}^{t} \sigma(r, x(r), y(r), z(r)) dB(r),$$

$$y(t) = h(x(T)) + \int_{t}^{T} f(r, x(r), y(r), z(r)) dr$$

$$- \int_{t}^{T} z(r) dB(r).$$
(4)

Furthermore, FBSDE (3) is said to be solvable if it has an adapted solution. An FBSDE is said to be nonsolvable if it is not solvable.

In order to get the solvability of FBSDE (3), we make the basic assumptions as follows.

Assumption 2. (i) The random mappings b, σ , and f are $\mathscr{P} \otimes \mathscr{B}(\mathbb{R}^n) \otimes \mathscr{B}(\mathbb{R}^m) \times \mathscr{B}(\mathbb{R}^{m \times d})$ measurable with $b(\cdot,0,0,0) \in M_{\mathscr{F}}^2(0,T;\mathbb{R}^n)$, $\sigma(\cdot,0,0,0) \in M_{\mathscr{F}}^2(0,T;\mathbb{R}^{m \times d})$, and $f(\cdot,0,0,0) \in M_{\mathscr{F}}^2(0,T;\mathbb{R}^m)$. And h is $\mathscr{F}_T \times \mathscr{B}(\mathbb{R}^m)$ measurable with $h(0) \in L^2(\Omega,\mathscr{F}_T,P;\mathbb{R}^m)$. Moreover, b, σ , and f are uniformly Lipschitz continuous in (x,y,z) and h is uniformly Lipschitz continuous in x.

(ii) Monotonicity conditions

$$\langle A(t,u) - A(t,\overline{u}), u - \overline{u} \rangle$$

$$\leq -\gamma_1 |G\widehat{x}|^2 - \gamma_2 \left(|G^*\widehat{y}|^2 + |G^*\widehat{z}|^2 \right), \qquad (5)$$

$$\langle x - \overline{x}, h(x) - h(\overline{x}) \rangle \geq \theta_1 |G\widehat{x}|^2,$$

Οľ

$$\langle A(t,u) - A(t,\overline{u}), u - \overline{u} \rangle$$

$$\geq \gamma_1 |G\widehat{x}|^2 + \gamma_2 \left(|G^*\widehat{y}|^2 + |G^*\widehat{z}|^2 \right), \tag{6}$$

$$\langle h(x) - h(\overline{x}), x - \overline{x} \rangle \leq -\theta_1 |G\widehat{x}|^2,$$

for all u = (x, y, z) and $\overline{u} = (\overline{x}, \overline{y}, \overline{z})$, $\widehat{x} = x - \overline{x}$, $\widehat{y} = y - \overline{y}$, $\widehat{z} = z - \overline{z}$, where γ_1, γ_2 and θ_1 are nonnegative constants with $\gamma_1 + \gamma_2 \ge 0$, $\gamma_2 + \theta_1 \ge 0$. Moreover, we have $\gamma_1 > 0$, $\theta_1 > 0$ (resp., $\gamma_2 > 0$), if m > n (resp., m < n).

The following two lemmas present the solvability results and continuous dependence theorem of FBSDE (3), respectively, which will be used to demonstrate the basic estimates for the state equation and adjoint equation (see Lemmas 10, 11, 12, and 14).

Lemma 3. Let Assumption 2 be satisfied. Then (3) admits a unique solution $(x(\cdot), y(\cdot), z(\cdot)) \in \mathbb{M}^2[0, T]$.

The proof can be found in Peng and Wu [27].

Lemma 4. Let $(x(\cdot), y(\cdot), z(\cdot))$ and $(\overline{x}(\cdot), \overline{y}(\cdot), \overline{z}(\cdot))$ be the solutions of the FBSDE (3) corresponding to two given coefficients (b, σ, f, h, a) and $(\overline{b}, \overline{\sigma}, \overline{f}, \overline{h}, \overline{a})$ which both satisfy Assumption 2, respectively. Then there exists a constant such that

$$\begin{aligned} \left\| \left(\widehat{x} \left(\cdot \right), \widehat{y} \left(\cdot \right), \widehat{z} \left(\cdot \right) \right) \right\|_{\mathbb{M}^{2}[0,T]} \\ &\leq K \left[\left| a - \overline{a} \right|^{2} \right. \\ &+ E \int_{0}^{T} \left| b \left(r, \overline{x} \left(r \right), \overline{y} \left(r \right), \overline{z} \left(r \right) \right) \right. \\ &- \overline{b} \left(r, \overline{x} \left(r \right), \overline{y} \left(r \right), \overline{z} \left(r \right) \right) \right|^{2} dr \end{aligned}$$

$$+ E \int_{0}^{T} \left| \sigma \left(r, \overline{x} \left(r \right), \overline{y} \left(r \right), \overline{z} \left(r \right) \right) \right.$$

$$\left. - \overline{\sigma} \left(r, \overline{x} \left(r \right), \overline{y} \left(r \right), \overline{z} \left(r \right) \right) \right|^{2} dr$$

$$+ E \int_{0}^{T} \left| f \left(r, \overline{x} \left(r \right), \overline{y} \left(r \right), \overline{z} \left(r \right) \right) \right.$$

$$\left. - \overline{f} \left(r, \overline{x} \left(r \right), \overline{y} \left(r \right), \overline{z} \left(r \right) \right) \right|^{2} dr$$

$$+ E \left| h \left(\overline{x} \left(T \right) \right) - \overline{h} \left(\overline{x} \left(T \right) \right) \right|^{2} \right]. \tag{7}$$

Particularly, if $(\overline{b}, \overline{\sigma}, \overline{f}, \overline{h}, \overline{a}) = (0, 0, 0, 0)$, we have

$$\|(x(\cdot), y(\cdot), z(\cdot))\|_{\mathbb{M}^2[0,T]}$$

$$\leq K \left[|a|^{2} + E \int_{0}^{T} |b(t, 0, 0, 0)|^{2} dt + E \int_{0}^{T} |\sigma(t, 0, 0, 0)|^{2} dt + E \int_{0}^{T} |f(t, 0, 0, 0)|^{2} dt + E |h(0)|^{2} \right].$$
(8)

The proof can be found in Lin [28].

3. Statement of the Problem and Basic Assumptions

Suppose that U is a given compact convex subset of \mathbb{R}^k . The stochastic process $u(\cdot):[0,T]\times\Omega\to\mathbb{R}^k$ is said to be admissible, if it is an \mathcal{F}_t -adopted process taking values in U. We denote all admissible controls by the set \mathscr{A} .

For any admissible control $u(\cdot) \in \mathcal{A}$, we consider the following controlled FBSDE:

$$dx(s) = b(r, x(r), y(r), z(r), u(r)) dr + \sigma(r, x(r), y(r), z(r), u(r)) dB(r),$$

$$dy(r) = -f(r, x(r), y(r), z(r), u(r)) dr + z(r) dB(r),$$

$$x(0) = a \in \mathbb{R}^{n},$$

$$y(T) = h(x(T)),$$
(9)

with the performance functional

$$J(u(\cdot)) = E\left[\int_{0}^{T} l(t, x(t), y(t), z(t), u(t)) dt + \phi(x(T)) + \gamma(y(0))\right].$$
(10)

In the above, b, σ, f, h, l, ϕ , and γ are given random mappings. $b: [0,T] \times \Omega \times \mathbb{R}^n \times \mathbb{R}^m \times \mathbb{R}^{m \times d} \times U \to \mathbb{R}^n, \sigma: [0,T] \times \Omega \times \mathbb{R}^n \times \mathbb{R}^m \times \mathbb{R}^{m \times d} \times U \to \mathbb{R}^{n \times d}, f: [0,T] \times \Omega \times \mathbb{R}^n \times \mathbb{R}^m \times \mathbb{R}^m$

The basic assumptions on coefficients $(b, \sigma, f, h, l, \phi, \gamma)$ are given as follows.

Assumption 5. (i) For any $u \in U$, (a,b,σ,f,h) satisfy Assumption 2. Moreover, b, f, and σ are differentiable in (x, y, z, u), h is differentiable in x, and the corresponding derivatives are continuous and uniformly bounded for all $(t,\omega) \in [0,T] \times \Omega$.

(ii) $l:[0,T]\times\Omega\times\mathbb{R}^n\times\mathbb{R}^m\times\mathbb{R}^{m\times d}\times U\to\mathbb{R}^1$ is continuous differentiable in (x,y,z,u), $\phi:\Omega\times\mathbb{R}^n\to\mathbb{R}^1$ is continuous differentiable in x, and $y:\Omega\times\mathbb{R}^m\to\mathbb{R}^1$ is continuous differentiable in y. For all $(t,\omega)\in[0,T]\times\Omega$, there is a constant C such that, for all $(x,y,z,u)\in\mathbb{R}^n\times\mathbb{R}^m\times\mathbb{R}^{m\times d}\times U$,

$$|l| \le C \left(1 + |y|^2 + |x|^2 + |z|^2 + |u|^2 \right),$$

$$|\gamma| \le C \left(|y|^2 + 1 \right), \qquad |\phi| \le C \left(|x|^2 + 1 \right),$$

$$|l_x| + |l_y| + |l_z| + |l_u| \le C \left(1 + |z| + |x| + |y| + |u| \right),$$

$$|\phi_x| \le C \left(|x| + 1 \right),$$

$$|\gamma_y| \le C \left(|y| + 1 \right).$$
(11)

Under Assumption 5, from Lemma 3, we know that, for every $u(\cdot) \in \mathcal{A}$, (9) has a unique solution. The corresponding strong solution is denoted by $(x^u(\cdot), y^u(\cdot), z^u(\cdot))$ or $(x(\cdot), y(\cdot), z(\cdot))$. Then $(x(\cdot), y(\cdot), z(\cdot))$ is said to be the state processes associated with the admissible control $u(\cdot)$ and $(u(\cdot); x(\cdot), y(\cdot), z(\cdot))$ is called the admissible control pair. Moreover, under Assumption 5, using a priori estimates (8), we can deduce the fact that

$$|J(u(\cdot))| < \infty. \tag{12}$$

The so-called stochastic optimal control problem is to minimize the cost function $J(u(\cdot))$, over all $u(\cdot) \in \mathcal{A}$. The corresponding value function is defined as

$$V(a) = \inf_{u(\cdot) \in \mathscr{A}} J(u(\cdot)). \tag{13}$$

We denote the above problem (9)–(13) by *PRO*. Any $\overline{u}(\cdot) \in \mathcal{A}$ is said to be an optimal control of Problem *PRO*, if $\overline{u}(\cdot)$ achieves the infimum of $J(u(\cdot))$ over \mathcal{A} . The state process $(\overline{x}(\cdot), \overline{y}(\cdot), \overline{z}(\cdot))$ is said to be the optimal state. And $(\overline{u}(\cdot); \overline{x}(\cdot), \overline{y}(\cdot), \overline{z}(\cdot))$ is called an optimal pair of Problem *PRO*.

Since this paper is devoted to discussing the near-optimal problem of FBSDEs, we recall the definition of the near-optimal control, following [16].

Definition 6. An admissible control pair $(u^{\varepsilon}(\cdot); x^{\varepsilon}(\cdot), y^{\varepsilon}(\cdot), z^{\varepsilon}(\cdot))$ is said to be an ε -optimal control for some $\varepsilon \ge 0$, if

$$\left| J\left(u^{\varepsilon}\left(\cdot \right) \right) - V\left(a \right) \right| \le \varepsilon. \tag{14}$$

Definition 7. The set of parameterized admissible control pairs $\{(u^{\varepsilon}(\cdot); x^{\varepsilon}(\cdot), y^{\varepsilon}(\cdot), z^{\varepsilon}(\cdot))\}$ is said to be near-optimal for sufficient small ε , if

$$\left|J\left(u^{\varepsilon}\left(\cdot\right)\right) - V\left(a\right)\right| \le r\left(\varepsilon\right). \tag{15}$$

Here r is a function with respect to ε satisfying $r(\varepsilon) \to 0$ as $\varepsilon \to 0$. We call the estimate $r(\varepsilon)$ an error bound. If $r(\varepsilon) = c\varepsilon^{\delta}$ for some $\delta > 0$ independent of the constant c, then we call $u^{\varepsilon}(\cdot)$ the near-optimal control with order ε^{δ} .

Before we conclude this section, let us recall the definition of the Clarke generalized gradient as well as Ekeland's variational principle which will be used to prove our main results.

Definition 8 (see Zhou [16]). Let X be a convex set in \mathbb{R}^d and let $\eta(\cdot): \to R$ be a locally Lipschitz function. At any given $x \in X$, we define the generalized gradient of η as a set given by

$$\partial_{x} \eta = \left\{ \xi : \left\langle \xi, \beta \right\rangle \leq \lim_{y \to x, y \in X, h \downarrow 0} \sup \frac{\eta \left(y + h\beta \right) - \eta \left(x \right)}{h},$$
for any $\beta \in \mathbb{R}^{d} \right\}.$
(16)

Lemma 9 (Ekeland's variational principle [29]). Suppose that (S,d) is a complete metric space and $\rho(\cdot): S \to \mathbb{R}$ is bounded from below and lower-semi-continuous. For $\varepsilon > 0$, let $u^{\varepsilon} \in S$ satisfy the following inequality:

$$\rho\left(u^{\varepsilon}\right) \le \inf_{u \in S} \rho\left(u\right) + \varepsilon. \tag{17}$$

Then, for any $\lambda > 0$, there exists u^{λ} such that

- (1) $\rho(u^{\lambda}) \leq \rho(u^{\varepsilon}),$
- (2) $d(u^{\lambda}, u^{\varepsilon}) \leq \lambda$,
- (3) $\rho(u^{\lambda}) \leq \rho(u) + (\varepsilon/\lambda)d(u^{\lambda}, u)$, for all $u \in S$.

4. Some Prior Estimates for State Trajectories and Adjoint Equations

In order to apply Ekeland's variational principle to obtain our main result, we must define a distance d on the space of admissible controls such that (\mathcal{A}, d) is a complete metric space. For any given $v(\cdot), u(\cdot) \in \mathcal{A}$, we define

$$d(v(\cdot), u(\cdot)) = \left[E \int_0^T |v(r) - u(r)|^2 dr \right]^{1/2}.$$
 (18)

To simplify our notation, for any admissible control pair $(u(\cdot); x^u(\cdot), y^u(\cdot), z^u(\cdot))$, we set

$$\Theta^{u}(t) := (x^{u}(t), y^{u}(t), z^{u}(t)). \tag{19}$$

The following is devoted to proving the boundedness and continuity of the state and adjoint processes with the control processes under the metric (18). Note that, in the following, *C* is a generic constants, which may change from line to line.

Lemma 10. Let Assumption 5 be satisfied. Then there exists a constant C s.t. that, for every admissible pair $(u(\cdot); \Theta^u(\cdot)) = (u(\cdot); x^u(\cdot), y^u(\cdot), z^u(\cdot)),$

$$\|\Theta^u(\cdot)\|_{\mathbb{M}^2} \le C. \tag{20}$$

Proof. Under Assumption 5, by the estimate (8), we have

$$\|\Theta^{u}(\cdot)\|_{\mathbb{M}^{2}} \leq C \left[E \int_{0}^{T} |b(t,0,0,0,u(t))|^{2} dt + E \int_{0}^{T} |\sigma(t,0,0,0,u(t))|^{2} dt + E \int_{0}^{T} |f(t,0,0,0,u(t))|^{2} dt + E |h(0)|^{2} + |a|^{2} \right]$$

$$\leq C \left[E \int_{0}^{T} |b(t,0,0,0,0)|^{2} dt + E \int_{0}^{T} |\sigma(t,0,0,0,0)|^{2} dt + E \int_{0}^{T} |f(t,0,0,0,0)|^{2} dt + E \int_{0}^{T} |f(t,0,0,0,0,0)|^{2} dt + E |h(0)|^{2} + 1 + |a|^{2} \right],$$

$$(21)$$

where the last inequality is obtained by the boundedness of the control domain U. The proof is complete. \Box

Lemma 11. Let Assumption 5 be satisfied. Then there is a positive constant C s.t. for any given two admissible pairs $(u(\cdot); \Theta^u(\cdot)) = (u(\cdot); x^u(\cdot), y^u(\cdot), z^u(\cdot))$ and $(v(\cdot); \Theta^v(\cdot)) = (v(\cdot); x^v(\cdot), y^v(\cdot), z^v(\cdot))$,

$$\left\|\Theta^{u}\left(\cdot\right) - \Theta^{v}\left(\cdot\right)\right\|_{\mathbb{M}^{2}}^{2} \le Cd(u\left(\cdot\right), v\left(\cdot\right))^{2}.\tag{22}$$

Proof. Under Assumption 5, from the estimate (7), we have

$$\|\Theta^{u}(\cdot) - \Theta^{v}(\cdot)\|_{\mathbb{M}^{2}}^{2}$$

$$\leq C \left[E \int_{0}^{T} \left| b(r, \Theta^{u}(r), u(r)) - b(r, \Theta^{u}(r), v(r)) \right|^{2} dr + E \int_{0}^{T} \left| \sigma(r, \Theta^{u}(r), u(r)) - \sigma(r, \Theta^{u}(r), v(r)) \right|^{2} dr + E \int_{0}^{T} \left| f(r, \Theta^{u}(r), u(r)) - f(r, \Theta^{u}(r), v(r)) \right|^{2} dr \right]$$

$$\leq CE \int_{0}^{T} \left| u(r) - v(r) \right|^{2} dr$$

$$= Cd(u(\cdot), v(\cdot))^{2}, \tag{23}$$

where the second inequality is obtained by the mean value theorem and the boundedness of b_u , σ_u , and f_u . The proof is complete.

We know that the adjoint process plays a key role in establishing stochastic maximum principle. In the following, we will study certain boundedness and continuity of adjoint processes with the control variable under the metric d.

For a given admissible pair $(u(\cdot); \Theta^u(\cdot))$, corresponding adjoint process $\Lambda^u(\cdot) = (k^u(\cdot), p^u(\cdot), q^u(\cdot))$ is defined as the solution to the following FBSDE:

$$dk_{t} = -\left[b_{y}^{*}\left(t,\Theta^{u}\left(t\right),u\left(t\right)\right)p_{t} + \sigma_{y}^{*}\left(t,\Theta^{u}\left(t\right),u\left(t\right)\right)q_{t}\right]$$

$$-f_{y}^{*}\left(t,\Theta^{u}\left(t\right),u\left(t\right)\right)k_{t}$$

$$+l_{y}\left(t,\Theta^{u}\left(t\right),u\left(t\right)\right)dt$$

$$-\left[b_{z}^{*}\left(t,\Theta^{u}\left(t\right),u\left(t\right)\right)p_{t}\right]$$

$$+\sigma_{z}^{*}\left(t,\Theta^{u}\left(t\right),u\left(t\right)\right)q_{t}$$

$$-f_{z}^{*}\left(t,\Theta^{u}\left(t\right),u\left(t\right)\right)k_{t} + l_{z}\left(t,\Theta^{u}\left(t\right),u\left(t\right)\right)dt_{t}$$

$$dp_{t} = -\left[b_{x}^{*}\left(t,\Theta^{u}\left(t\right),u\left(t\right)\right)p_{t}\right]$$

$$+\sigma_{x}^{*}\left(t,\Theta^{u}\left(t\right),u\left(t\right)\right)q_{t} - f_{x}^{*}\left(t,\Theta^{u}\left(t\right),u\left(t\right)\right)k_{t}$$

$$+l_{x}\left(t,\Theta^{u}\left(t\right),u\left(t\right)\right)dt + q_{t}dB_{t},$$

$$k_{0} = -\gamma_{y}\left(y^{u}\left(0\right)\right),$$

$$p_{T} = -h_{x}^{*}\left(x^{u}\left(T\right)\right)k\left(T\right) + \phi_{x}\left(x^{u}\left(T\right)\right),$$

$$0 \le t \le T.$$

$$(24)$$

The adjoint equation (24) is a linear FBSDE whose solution consists of $(p^u(\cdot), q^u(\cdot), k^u(\cdot))$. Under Assumption 5, by Lemma 3, the adjoint equation has a unique solution $\Lambda^u(\cdot) = (k^u(\cdot), p^u(\cdot), q^u(\cdot)) \in \mathbb{M}^2$.

Next, the Hamiltonian $H: [0,T] \times \mathbb{R}^n \times \mathbb{R}^m \times \mathbb{R}^{m \times d} \times U \times \mathbb{R}^m \times \mathbb{R}^n \times \mathbb{R}^{n \times d} \to \mathbb{R}$ is defined as follows:

$$H(t, x, y, z, u, k, p, q)$$

$$= (k, -f(t, x, y, z, u)) + (p, b(t, x, y, z, u)) + (q, \sigma(t, x, y, z, u)) + l(t, x, y, z, u).$$
(25)

Then (24) can be rewritten in Hamiltonian system as follows:

$$dk(t) = -H_{y}(t, \Theta^{u}(t), u(t), \Lambda^{u}(t)) dt$$

$$-H_{z}(t, \Theta^{u}(t), u(t), \Lambda^{u}(t)) dB(t),$$

$$dp(t) = -H_{x}(t, \Theta^{u}(t), u(t) \Lambda^{u}(t)) dt + q(t) dB(t), \quad (26)$$

$$k_{0} = -\gamma_{y}(y^{u}(0)),$$

$$p(t) = -h_{x}^{*}(x^{u}(T)) k(T) + \phi_{x}(x(T)).$$

Lemma 12. Let Assumption 5 be satisfied. Then there is a constant C s.t. for all control pairs $(u(\cdot); \Theta(\cdot)) = (u(\cdot); x^u(\cdot), y^u(\cdot), z^u(\cdot))$; it holds

$$\left\| \Lambda^{u} \left(\cdot \right) \right\|_{\mathbb{M}^{2}} \le C. \tag{27}$$

Proof. Under Assumption 5, by the estimate (8), we have

$$\|\Lambda^{u}(\cdot)\|_{\mathbb{M}^{2}} \leq C \left\{ E \int_{0}^{T} \left| l_{x} \left(r, \Theta^{u}(r), u(r) \right) \right|^{2} dr + E \int_{0}^{T} \left| l_{y} \left(r, \Theta^{u}(r), u(r) \right) \right|^{2} dr + E \int_{0}^{T} \left| l_{z} \left(r, \Theta^{u}(r), u(r) \right) \right|^{2} dr + E \left| \phi_{x} \left(x^{u}(T) \right) \right|^{2} + E \left| \gamma_{y} \left(y^{u}(0) \right) \right|^{2} \right\}$$

$$\leq C \left\{ \|\Theta^{u}(\cdot)\|_{\mathbb{M}^{2}} + 1 \right\} \leq C,$$
(28)

where the last inequality is obtained by Lemma 10. The proof is complete. $\hfill\Box$

Assumption 13. There is a constant C > 0 s.t. for every $(t, \theta, u) = (t, x, y, z, u), (t, \overline{\theta}, \overline{u}) = (t, \overline{x}, \overline{y}, \overline{z}, \overline{u}) \in [0, T] \times \mathbb{R}^n \times \mathbb{R}^m \times \mathbb{R}^{m \times d} \times U$ and a.s. $\omega \in \Omega$,

$$\left| l_{\alpha}\left(t,\theta,u\right) - l_{\alpha}\left(t,\overline{\theta},\overline{u}\right) \right| \leq C\left(\left|\widehat{x}\right| + \left|\widehat{z}\right| + \left|\widehat{y}\right| + \left|\widehat{u}\right|\right),$$

$$\left| \phi_{x}\left(x\right) - \phi_{x}\left(\overline{x}\right) \right| \leq C\left|\widehat{x}\right|,$$

$$\left| \gamma_{y}\left(y\right) - \gamma_{y}\left(\overline{y}\right) \right| \leq C\left|\widehat{y}\right|,$$
(29)

where $\alpha = x, y, z, u$.

Lemma 14. Let Assumptions 5 and 13 be satisfied. Let $\Lambda^u(\cdot) = (k^u(\cdot), p^u(\cdot), q^u(\cdot))$ and $\Lambda^v(\cdot) = (k^v(\cdot), p^v(\cdot), q^v(\cdot))$ be adjoint processes corresponding to two admissible pairs $(u(\cdot); \Theta^u(\cdot)) = (u(\cdot); x^u(\cdot), y^u(\cdot), z^u(\cdot))$ and $(v(\cdot); \Theta^v(\cdot)) = (v(\cdot); x^v(\cdot), y^v(\cdot), z^v(\cdot))$, respectively. Then we have

$$\left\|\Lambda^{u}\left(\cdot\right) - \Lambda^{v}\left(\cdot\right)\right\|_{\mathbb{M}^{2}}^{2} \le Cd(u\left(\cdot\right), v\left(\cdot\right))^{2}.\tag{30}$$

Proof. Under Assumptions 5 and 13, from the estimate (7), we have

$$\|\Lambda^{u}(\cdot) - \Lambda^{v}(\cdot)\|_{\mathbb{M}^{2}}^{2}$$

$$\leq C \left\{ E \int_{0}^{T} |l_{x}(r, \Theta^{u}(r), u(r)) + l_{z}(r, \Theta^{u}(r), u(r)) + l_{y}(r, \Theta^{u}(r), u(r)) + l_{z}(r, \Theta^{u}(r), u(r)) - l_{x}(r, \Theta^{v}(r), v(r)) - l_{y}(r, \Theta^{v}(r), v(r)) + l_{z}(r, \Theta^{u}(r), v(r)) - l_{z}(r, \Theta^{u}(r), v(r))|^{2} dr + E|\phi_{x}(x^{u}(T)) - \phi_{x}(x^{v}(T))|^{2} + E|\gamma_{x}(y^{u}(0)) - \gamma_{x}(y^{v}(0))|^{2} \right\}$$

$$\leq C \left\{ \|\Theta(\cdot) - \Theta(\cdot)\|_{\mathbb{M}_{2}}^{2} + E \int_{0}^{T} |u(r) - v(r)|^{2} dr \right\}$$

$$\leq Cd(u(\cdot), v(\cdot))^{2}, \tag{31}$$

where the last inequality is obtained by Lemma 11 directly.

5. A Variational Formula

The purpose of this section is to obtain a variational formula for the cost functional (10). For any two given control pairs $(\overline{u}(\cdot); \Theta^{\overline{u}}(\cdot)) = (\overline{u}(\cdot); x^{\overline{u}}(\cdot), y^{\overline{u}}(\cdot), z^{\overline{u}}(\cdot))$ and $(u(\cdot); \Theta^{u}(\cdot)) = (u(\cdot); x^{u}(\cdot), y^{u}(\cdot), z^{u}(\cdot))$, from the convex property of the control domain U, we can define an admissible control process as follows:

$$u^{\delta}(\cdot) = \overline{u}(\cdot) + \delta(u(\cdot) - \overline{u}(\cdot)), \quad 0 \le \delta \le 1.$$
 (32)

We denote the corresponding state process by $\Theta^{u^{\delta}}(\cdot) = (x^{u^{\delta}}(\cdot), y^{u^{\delta}}(\cdot), z^{u^{\delta}}(\cdot)).$

In the following, using the Hamiltonian H (see (25)) and adjoint process $\Lambda^{\overline{u}}(\cdot) = (k^{\overline{u}}(\cdot), p^{\overline{u}}(\cdot), q^{\overline{u}}(\cdot))$ associated with the admissible control pair $(\overline{u}(\cdot); \Theta^{\overline{u}}(\cdot))$, we will state and prove a presentation for the difference $J(u^{\delta}(\cdot)) - J(\overline{u}(\cdot))$.

Lemma 15. Let Assumption 5 be satisfied. Then we get

$$\begin{split} J\left(u^{\delta}\left(\cdot\right)\right) - J\left(\overline{u}\left(\cdot\right)\right) \\ &= E\int_{0}^{T} \left[H\left(r,\Theta^{u^{\delta}}\left(r\right),u^{\delta}\left(r\right),\Lambda^{\overline{u}}\right)\right. \\ &- H\left(r,\Theta^{\overline{u}}\left(r\right),\overline{u}\left(r\right),\Lambda^{\overline{u}}\left(r\right)\right) \\ &- H_{x}\left(r,\Theta^{\overline{u}}\left(r\right),\overline{u}\left(r\right),\Lambda^{\overline{u}}\left(r\right)\right) \\ &\times \left(x^{u^{\delta}}\left(r\right) - x^{\overline{u}}\left(r\right)\right) \\ &- H_{y}\left(r,\Theta^{\overline{u}}\left(r\right),\overline{u}\left(r\right),\Lambda^{\overline{u}}\left(r\right)\right) \\ &\times \left(y^{u^{\delta}}\left(r\right) - y^{\overline{u}}\left(r\right)\right) \\ &- H_{z}\left(r,\Theta^{\overline{u}}\left(r\right),\overline{u}\left(r\right),\Lambda^{\overline{u}}\left(r\right)\right) \\ &\times \left(z^{u^{\delta}}\left(r\right) - z^{\overline{u}}\left(r\right)\right)\right] dr \\ &+ E\left[\phi\left(x^{u^{\delta}}\left(T\right)\right) - \phi\left(x^{\overline{u}}\left(T\right)\right) \\ &- \phi_{x}\left(x^{\overline{u}}\left(T\right)\right) \cdot \left(x^{u^{\delta}}\left(T\right) - x^{\overline{u}}\left(T\right)\right)\right] \\ &+ E\left[\gamma\left(y^{u^{\delta}}\left(0\right)\right) - \gamma\left(y^{\overline{u}}\left(0\right)\right) \\ &- \gamma_{y}\left(y^{\overline{u}}\left(0\right)\right) \cdot \left(y^{u^{\delta}}\left(0\right) - y^{\overline{u}}\left(0\right)\right)\right] \\ &- E\left[\left(h\left(x^{u^{\delta}}\left(T\right)\right) - h\left(x^{\overline{u}}\left(T\right)\right),k^{\overline{u}}\left(T\right)\right) \\ &- \left(h_{x}\left(x^{\overline{u}}\left(T\right)\right) \cdot \left(x^{u^{\delta}}\left(T\right) - x^{\overline{u}}\left(T\right)\right),k^{\overline{u}}\left(T\right)\right)\right] \\ \triangleq \beta^{(u^{\delta},\overline{u})}. \end{split}$$

(33)

Proof. Applying the definitions of $J(u(\cdot))$ and Hamilton H, we obtain

$$J(u^{\delta}(\cdot)) - J(\overline{u}(\cdot))$$

$$= E \int_{0}^{T} \left[H(r, \Theta^{u^{\delta}}(r), u^{\delta}(r), \Lambda^{\overline{u}}(r)) - H(r, \Theta^{\overline{u}}(r), \overline{u}(r), \Lambda^{\overline{u}}(r)) - (b(r, \Theta^{u^{\delta}}(r), u^{\delta}(r)) - (b(r, \Theta^{u^{\delta}}(r), u^{\delta}(r)), p^{\overline{u}}(r)) - (\sigma(r, \Theta^{u^{\delta}}(r), u^{\delta}(r)), p^{\overline{u}}(r)) - (\sigma(r, \Theta^{u^{\delta}}(r), u^{\delta}(r)) - (\sigma(r, \Theta^{\overline{u}}(r), \overline{u}(r)), q^{\overline{u}}(r)) + (f(r, \Theta^{u^{\delta}}(r), u^{\delta}(r)) - f(r, \Theta^{\overline{u}}(r), \overline{u}(r)), k^{\overline{u}}(r)) \right] dr$$

$$+ E \left[\phi(x^{u^{\delta}}(T)) - \phi(x^{\overline{u}}(T)) \right]$$

$$+ E \left[\gamma(y^{u^{\delta}}(0)) - \gamma(y^{\overline{u}}(0)) \right].$$

Applying Itô formula to $(p^{\overline{u}}(r), x^{u^{\delta}}(r) - x^{\overline{u}}(r)) + (k^{\overline{u}}(r), y^{u^{\delta}}(r) - y^{\overline{u}}(r))$, we have

$$\begin{split} E \int_{0}^{T} \left[\left(b \left(r, \Theta^{u^{\delta}} \left(r \right), u^{\delta} \left(r \right) \right) - b \left(r, \Theta^{\overline{u}} \left(r \right), \overline{u} \left(r \right) \right), p^{\overline{u}} \left(r \right) \right) \right. \\ &+ \left(\sigma \left(r, \Theta^{u^{\delta}} \left(r \right), u^{\delta} \left(r \right) \right) \right. \\ &- \sigma \left(r, \Theta^{\overline{u}} \left(r \right), \overline{u} \left(r \right) \right), q^{\overline{u}} \left(r \right) \right) \\ &- \left(f \left(r, \Theta^{u^{\delta}} \left(r \right), u^{\delta} \left(r \right) \right) \right. \\ &- f \left(r, \Theta^{\overline{u}} \left(r \right), \overline{u} \left(r \right) \right), k^{\overline{u}} \left(r \right) \right) \right] dr \\ &= E \int_{0}^{T} \left[H_{x} \left(r, \Theta^{\overline{u}} \left(r \right), \overline{u} \left(r \right), \Lambda^{\overline{u}} \left(r \right) \right) \left(x^{u^{\delta}} \left(r \right) - x^{\overline{u}} \left(r \right) \right) \right. \\ &+ H_{y} \left(r, \Theta^{\overline{u}} \left(r \right), \overline{u} \left(r \right), \Lambda^{\overline{u}} \left(r \right) \right) \\ &\times \left(y^{u^{\delta}} \left(r \right) - y^{\overline{u}} \left(r \right) \right) \\ &+ H_{z} \left(r, \Theta^{\overline{u}} \left(r \right), \overline{u} \left(r \right), \Lambda^{\overline{u}} \left(r \right) \right) \\ &\times \left(z^{u^{\delta}} \left(r \right) - z^{\overline{u}} \left(r \right) \right) \right] dr \\ &+ E \left[\phi_{x} \left(x^{\overline{u}} \left(T \right) \right) \cdot \left(x^{u^{\delta}} \left(T \right) - x^{\overline{u}} \left(T \right) \right) \right] \\ &+ E \left[\gamma_{y} \left(y^{\overline{u}} \left(0 \right) \right) \cdot \left(y^{u^{\delta}} \left(0 \right) - y^{\overline{u}} \left(0 \right) \right) \right] \end{split}$$

$$+ E\left[\left(h\left(x^{u^{\delta}}\left(T\right)\right) - h\left(x^{\overline{u}}\left(T\right)\right), k^{\overline{u}}\left(T\right)\right) - \left(h_{x}\left(x^{\overline{u}}\left(T\right)\right) \cdot \left(x^{u^{\delta}}\left(T\right) - x^{\overline{u}}\left(T\right)\right), k^{\overline{u}}\left(T\right)\right)\right]. \tag{35}$$

Now putting (35) into (34), we deduce the fact that (33) holds. The proof is complete. $\hfill\Box$

Remark 16. According to the above proof, it is easy to check that $u^{\delta}(\cdot)$ can be changed as any admissible control and need not have the form of the convex variation $u^{\delta}(\cdot) = \overline{u}(\cdot) + \delta(u(\cdot) - \overline{u}(\cdot))$.

Now we state and prove the variational formula for the cost functional (10) as follows.

Theorem 17. Suppose that Assumption 5 holds. Let $\overline{u}(\cdot)$ be any given admissible control. Then we have

$$\frac{d}{d\delta} J(\overline{u}(\cdot) + \delta(u(\cdot) - \overline{u}(\cdot)))|_{\delta=0}$$

$$:= \lim_{\delta \to 0} \frac{J(\overline{u}(\cdot) + \delta(v(\cdot) - \overline{u}(\cdot))) - J(\overline{u}(\cdot))}{\delta}$$

$$= E \int_{0}^{T} \left(H_{u}\left(r, \Theta^{\overline{u}}(r), \overline{u}(r), \Lambda^{\overline{u}}(r)\right), u(r) - \overline{u}(r) \right) dr, \tag{36}$$

where $u(\cdot)$ is any given admissible control and $\delta > 0$.

Proof. Define $u^{\delta}(\cdot) = \overline{u}(\cdot) + \delta(v(\cdot) - \overline{u}(\cdot))$; by Lemma 15, we have

$$J(u^{\delta}(\cdot)) - J(\overline{u}(\cdot))$$

$$= J(\overline{u}(\cdot) + \delta(u(\cdot) - \overline{u}(\cdot))) - J(\overline{u}(\cdot))$$

$$= E \int_{0}^{T} H_{u}(r, \Theta^{\overline{u}}(r), \overline{u}(r), \Lambda^{\overline{u}}(r)) (u^{\delta}(r) - \overline{u}(r)) dr$$

$$+ \beta^{(u^{\delta}, \overline{u})} - E \int_{0}^{T} H_{u}(r, \Theta^{\overline{u}}(r), \overline{u}(r), \Lambda^{\overline{u}}(r))$$

$$\times (u^{\delta}(r) - \overline{u}(r)) dr$$

$$= \delta E \int_{0}^{T} H_{u}(r, \Theta^{\overline{u}}(r), \overline{u}(r), \Lambda^{\overline{u}}(r)) (v(r) - \overline{u}(r)) dr$$

$$+ \beta^{(u^{\delta}, \overline{u})} - E \int_{0}^{T} H_{u}(r, \Theta^{\overline{u}}(r), \overline{u}(r), \Lambda^{\overline{u}}(r))$$

$$\times (u^{\delta}(r) - \overline{u}(r)) dr.$$

$$(37)$$

Applying Lemma 11 and Assumption 5, we get

$$\beta^{(u^{\delta},\overline{u})} - E \int_{0}^{T} H_{u}\left(r,\Theta^{\overline{u}}\left(r\right),\overline{u}\left(r\right),\Lambda^{\overline{u}}\left(r\right)\right) \times \left(u^{\delta}\left(r\right) - \overline{u}\left(r\right)\right) dr = o\left(\delta\right).$$
(38)

Hence, by (38) and (37), we get

$$\lim_{\delta \to 0} \frac{J\left(u^{\delta}\left(\cdot\right)\right) - J\left(\overline{u}\left(\cdot\right)\right)}{\delta}$$

$$= E \int_{0}^{T} \left(H_{u}\left(r, \Theta^{\overline{u}}\left(r\right), \overline{u}\left(r\right), \Lambda^{\overline{u}}\left(r\right)\right), v\left(r\right) - \overline{u}\left(r\right)\right) dr. \tag{39}$$

The proof is complete.

6. Necessary Conditions for Near-Optimality

In this section, we will state and prove our main results, that is, the stochastic maximum principle of the near-optimal control of Problem *PRO*. Moreover, we give the additional assumption as follows.

Assumption 18. There is a constant C > 0 s.t. for all $(t, x, y, z, \overline{x}, \overline{y}, \overline{z}, u, \overline{u})$ and a.s. $\omega \in \Omega$,

$$|l(t, x, z, y, u) - l(t, \overline{x}, \overline{z}, \overline{y}, u)|$$

$$\leq C(|\widehat{x}| + |\widehat{z}| + |\widehat{y}| + |\widehat{u}|).$$
(40)

Theorem 19. Suppose that Assumptions 5 and 13 hold. Let $(u^{\varepsilon}(\cdot); \Theta^{\varepsilon}(\cdot)) = (u^{\varepsilon}(\cdot); x^{\varepsilon}(\cdot), y^{\varepsilon}(\cdot), z^{\varepsilon}(\cdot))$ be ε -optimal pair of problem PRO. Then, for any given $\varepsilon > 0$, there is a positive constant C s.t.:

$$H_{u}\left(r,\Theta^{\varepsilon}\left(r\right),u^{\varepsilon}\left(r\right),\Lambda^{\varepsilon}\left(r\right)\right)\cdot\left(u-u^{\varepsilon}\left(r\right)\right)\geq-C\varepsilon^{1/2},$$

$$\forall u\in U,\ a.e.\ (r,\omega)\in\left[0,T\right]\times\Omega,$$

$$(41)$$

where $\Lambda^{\epsilon}(\cdot) = (k^{\epsilon}(\cdot), p^{\epsilon}(\cdot), q^{\epsilon}(\cdot))$ is the adjoint process corresponding to $(u^{\epsilon}(\cdot); \Theta^{\epsilon}(\cdot))$.

Proof. By Lemma 11 and Assumption 13, we can deduce the fact that $J(u(\cdot))$ is continuous on $\mathscr A$ with respect to the metric (18). Using Ekeland's variational principle (see [16]) with $\delta = \varepsilon^{1/2}$, there exists an admissible pair $(\overline{u}^{\varepsilon}(\cdot); \overline{\Theta}^{\varepsilon}(\cdot)) = (\overline{u}^{\varepsilon}(\cdot); \overline{x}^{\varepsilon}(\cdot), \overline{y}^{\varepsilon}(\cdot), \overline{z}^{\varepsilon}(\cdot))$ such that

$$d\left(u^{\varepsilon}\left(\cdot\right), \overline{u}^{\varepsilon}\left(\cdot\right)\right) \le \varepsilon^{1/2},\tag{42}$$

$$J(u(\cdot)) - J(\overline{u}^{\varepsilon}(\cdot)) \ge -\varepsilon^{1/2} d(u(\cdot), \overline{u}^{\varepsilon}(\cdot)),$$

$$\forall u(\cdot) \in \mathcal{A}.$$
(43)

Now we define a convex perturbed control $u^{\varepsilon,h}(\cdot)$ of $\overline{u}^{\varepsilon}(\cdot)$ as

$$u^{\varepsilon,h}(\cdot) = \overline{u}^{\varepsilon}(\cdot) + h(\overline{u}^{\varepsilon}(\cdot) - u(\cdot)), \tag{44}$$

where $u(\cdot) \in \mathcal{A}$ is an arbitrary given admissible control and 0 < h < 1.

Then by the variational formula (36), (43), and the fact that

$$d\left(u^{\varepsilon,h}\left(\cdot\right),\overline{u}^{\varepsilon}\left(\cdot\right)\right)\leq Ch,$$
 (45)

we have

$$E \int_{0}^{T} H_{u}\left(t, \overline{\Theta}^{\varepsilon}(r), \overline{u}^{\varepsilon}(r), \overline{\Lambda}^{\varepsilon}(r)\right) \cdot \left(u(r) - \overline{u}^{\varepsilon}(t)\right) dt$$

$$= \lim_{\varepsilon \to 0^{+}} \frac{J\left(u^{\varepsilon, h}(\cdot)\right) - J\left(\overline{u}^{\varepsilon}(\cdot)\right)}{h}$$

$$\geq \lim_{\varepsilon \to 0^{+}} \frac{-\varepsilon^{1/2} d\left(u^{\varepsilon, h}(\cdot), \overline{u}^{\varepsilon}(\cdot)\right)}{h}$$

$$\geq -C\varepsilon^{1/2},$$
(46)

where $\overline{\Lambda}^{\varepsilon} = (\overline{p}^{\varepsilon}(\cdot), \overline{q}^{\varepsilon}(\cdot), \overline{k}^{\varepsilon}(\cdot))$ is the adjoint process corresponding to $(\overline{u}^{\varepsilon}(\cdot); \overline{\Theta}^{\varepsilon}(\cdot))$.

Now in order to obtain the optimal condition (41), we now have to estimate the following formula:

$$I^{\varepsilon} := E \int_{0}^{T} H_{u}\left(t, \Theta^{\varepsilon}\left(r\right), u^{\varepsilon}\left(r\right), \Lambda^{\varepsilon}\left(r\right)\right) \cdot \left(u\left(r\right) - u^{\varepsilon}\left(r\right)\right) dr$$
$$- E \int_{0}^{T} H_{u}\left(t, \overline{\Theta}^{\varepsilon}\left(r\right), \overline{u}^{\varepsilon}\left(r\right), \overline{\Lambda}^{\varepsilon}\left(r\right)\right) \cdot \left(u\left(r\right) - \overline{u}^{\varepsilon}\left(r\right)\right) dr. \tag{47}$$

First, by adding and subtracting $E \int_0^T H_u(t, \Theta^{\varepsilon}(r), u^{\varepsilon}(r), \Lambda^{\varepsilon}(r)) \cdot (u(r) - \overline{u}^{\varepsilon}(r)) dr$, we have

$$I^{\varepsilon} = E \int_{0}^{T} H_{u} \left(t, \Theta^{\varepsilon} \left(r \right), u^{\varepsilon} \left(r \right), \Lambda^{\varepsilon} \left(r \right) \right) \cdot \left(\overline{u}^{\varepsilon} \left(r \right) - u^{\varepsilon} \left(r \right) \right) dr$$

$$+ E \int_{0}^{T} \left(H_{u} \left(r, \Theta^{\varepsilon} \left(r \right), u^{\varepsilon} \left(r \right), \Lambda^{\varepsilon} \left(r \right) \right) \right)$$

$$- H_{u} \left(t, \overline{\Theta}^{\varepsilon} \left(r \right), \overline{u}^{\varepsilon} \left(r \right), \overline{\Lambda}^{\varepsilon} \left(r \right) \right) \right)$$

$$\cdot \left(u \left(r \right) - \overline{u}^{\varepsilon} \left(r \right) \right) dr$$

$$= I_{1}^{\varepsilon} + I_{2}^{\varepsilon}. \tag{48}$$

Next, using Lemmas 11 and 14 and (42), we have

$$\begin{split} \left|I_{2}^{\varepsilon}\right| &\leq CE \int_{0}^{T} \left|H_{u}\left(t,\Theta^{\varepsilon}\left(r\right),u^{\varepsilon}\left(r\right),\Lambda^{\varepsilon}\left(r\right)\right)\right| \\ &-H_{u}\left(t,\overline{\Theta}^{\varepsilon}\left(r\right),\overline{u}^{\varepsilon}\left(r\right),\overline{\Lambda}^{\varepsilon}\left(r\right)\right)\right| dr \\ &\leq CE \int_{0}^{T} \left|H_{u}\left(t,\Theta^{\varepsilon}\left(r\right),u^{\varepsilon}\left(r\right),\Lambda^{\varepsilon}\left(r\right)\right)\right| \\ &-H_{u}\left(t,\overline{\Theta}^{\varepsilon}\left(r\right),\overline{u}^{\varepsilon}\left(r\right),\Lambda^{\varepsilon}\left(r\right)\right)\right| dr \\ &+CE \int_{0}^{T} \left|H_{u}\left(t,\overline{\Theta}^{\varepsilon}\left(r\right),\overline{u}^{\varepsilon}\left(r\right),\Lambda^{\varepsilon}\left(r\right)\right)\right| dr \\ &-H_{u}\left(t,\overline{\Theta}^{\varepsilon}\left(r\right),\overline{u}^{\varepsilon}\left(r\right),\overline{\Lambda}^{\varepsilon}\left(r\right)\right)\right| dr \end{split}$$

$$\leq C \left(E \sup_{0 \leq r \leq T} |\overline{x}^{\varepsilon}(r) - x^{\varepsilon}(r)|^{2} \right)^{1/2} \\
+ C \left(E \sup_{0 \leq r \leq T} |\overline{p}^{\varepsilon}(r) - p^{\varepsilon}(r)|^{2} \right)^{1/2} \\
+ C \left(E \int_{0}^{T} |\overline{q}^{\varepsilon}(r) - q^{\varepsilon}(r)|^{2} dr \right)^{1/2} \\
+ C \left(E \int_{0}^{T} |\overline{u}^{\varepsilon}(r) - u^{\varepsilon}(r)|^{2} dr \right)^{1/2} \\
+ \left(E \sup_{0 \leq r \leq T} |\overline{k}^{\varepsilon}(r) - k^{\varepsilon}(r)|^{2} \right)^{1/2} \\
\leq C \left(E \int_{0}^{T} |\overline{u}^{\varepsilon}(r) - u^{\varepsilon}(r)|^{2} dr \right)^{1/2} \\
\leq C \varepsilon^{1/2}. \tag{49}$$

Then, combining Schwarz's inequality and Lemmas 10 and 12 and (42), we have

$$\begin{aligned}
|I_{1}^{\varepsilon}| &\leq E \left(\int_{0}^{T} \left| H_{u} \left(t, \Theta^{\varepsilon} \left(r \right), u^{\varepsilon} \left(r \right), \Lambda^{\varepsilon} \left(r \right) \right) \right|^{2} dr \right)^{1/2} \\
&\times \left(E \int_{0}^{T} \left| \overline{u}^{\varepsilon} \left(r \right) - u^{\varepsilon} \left(r \right) \right|^{2} dr \right)^{1/2} \\
&\leq C \left(E \int_{0}^{T} \left| \overline{u}^{\varepsilon} \left(t \right) - u^{\varepsilon} \left(r \right) \right|^{2} dr \right)^{1/2} \\
&\leq C \varepsilon^{1/2}.
\end{aligned} \tag{50}$$

Therefore, combining (46), (47), (49), and (50), we have

$$E \int_{0}^{T} H_{u}\left(r, \Theta^{\varepsilon}\left(r\right), u^{\varepsilon}\left(t\right), \Lambda^{\epsilon}\left(r\right)\right) \cdot \left(u\left(r\right) - u^{\varepsilon}\left(r\right)\right) dr$$

$$= E \int_{0}^{T} H_{u}\left(t, \overline{\Theta}^{\varepsilon}\left(r\right), \overline{u}^{\varepsilon}\left(r\right), \overline{\Lambda}^{\epsilon}\left(r\right)\right)$$

$$\cdot \left(u\left(r\right) - \overline{u}^{\varepsilon}\left(r\right)\right) dr + I^{\varepsilon}$$

$$= E \int_{0}^{T} H_{u}\left(r, \overline{\Theta}^{\varepsilon}\left(r\right), \overline{u}^{\varepsilon}\left(r\right), \overline{\Lambda}^{\epsilon}\left(r\right)\right)$$

$$\cdot \left(u\left(r\right) - \overline{u}^{\varepsilon}\left(r\right)\right) dr + I_{1}^{\varepsilon} + I_{2}^{\varepsilon}$$

$$\geq -C\varepsilon^{1/2}$$

$$(51)$$

which implies that (41) holds. The proof is complete.

7. Sufficient Optimality Conditions

In this section, we will show that, under certain convex conditions, the near-maximum condition of the Hamiltonian function in the integral form is sufficient for near-optimality. **Theorem 20.** Under Assumption 5, let $(u^{\varepsilon}(\cdot); \Theta^{\varepsilon}(\cdot)) = (u^{\varepsilon}(\cdot); x^{\varepsilon}(\cdot), y^{\varepsilon}(\cdot), z^{\varepsilon}(\cdot))$ be an admissible pair with $\overline{y}(T) = Mx^{\varepsilon}(T)$, $M \in L^{2}(\Omega, \mathcal{F}_{T}, P; \mathbb{R}^{m \times n})$. Let $\Lambda^{\varepsilon}(\cdot) = (p^{\varepsilon}(\cdot), q^{\varepsilon}(\cdot), k^{\varepsilon}(\cdot))$ be the adjoint process associated with $(u^{\varepsilon}(\cdot); \Theta^{\varepsilon}(\cdot))$. Assume that for almost all $(t, \omega) \in [0, T] \times \Omega$, $H(t, x, y, z, u, \Lambda^{\varepsilon}(t))$ is convex in (x, y, z, u), $\gamma(y)$ is convex in y, and $\phi(x)$ is convex in x, respectively, and for some ε , the optimality conditions,

$$E \int_{0}^{T} H\left(r, \Theta^{\varepsilon}\left(r\right), u^{\varepsilon}\left(r\right), \Lambda^{\varepsilon}\left(r\right)\right) dr$$

$$\leq E \inf_{u(\cdot) \in \mathcal{A}} \int_{0}^{T} H\left(r, \Theta^{\varepsilon}\left(r\right), u\left(r\right), \Lambda^{\varepsilon}\left(r\right)\right) dr + \varepsilon,$$
(52)

hold. Then

$$J\left(u^{\varepsilon}\left(\cdot\right)\right) \leq \inf_{u(\cdot) \in \mathscr{A}} J\left(u\left(\cdot\right)\right) + C_{1} \varepsilon^{1/2},\tag{53}$$

where C_1 is a constant independent of ε .

Proof. In the following, C_1 is a constant which may change from line to line and is independent of ε .

According to Lemma 15, we deduce the fact that

$$J(u(\cdot)) - J(u^{\varepsilon}(\cdot))$$

$$= E \int_{0}^{T} \left[H(t, \Theta^{u}(r), u(r), \Lambda^{\varepsilon}(r)) - H(r, \Theta^{\varepsilon}(r), u^{\varepsilon}(r), \Lambda^{\varepsilon}(r)) - H_{x}(r, \Theta^{\varepsilon}(r), u^{\varepsilon}(r), \Lambda^{\varepsilon}(r)) \right]$$

$$\times (x^{u}(r) - x^{\varepsilon}(r))$$

$$- H_{y}(r, \Theta^{\varepsilon}(r), u^{\varepsilon}(r), \Lambda^{\varepsilon}(r))$$

$$\times (y^{u}(r) - y^{\varepsilon}(r)) - H_{z}(r, \Theta^{\varepsilon}(r), u^{\varepsilon}(r), \Lambda^{\varepsilon}(r))$$

$$\times (z^{u}(r) - z^{\varepsilon}(r)) \right] dr$$

$$+ E \left[\phi(x^{u}(T)) - \phi(x^{\varepsilon}(T)) - \Phi_{x}(x^{\varepsilon}(T)) \cdot (x^{u}(R) - x^{\varepsilon}(T)) \right]$$

$$+ E \left[\gamma(y^{u}(0)) - \gamma(y^{\varepsilon}(0)) - \gamma_{y}(y^{\varepsilon}(0)) \right],$$

where $(u(\cdot); x^u(\cdot), y^u(\cdot), z^u(\cdot))$ are any given admissible control pairs. By the convexity of H, ϕ , and γ , we have

$$H\left(t,\Theta^{u}\left(r\right),u\left(r\right),\Lambda^{\varepsilon}\left(r\right)\right)$$

$$-H\left(r,\Theta^{\varepsilon}\left(r\right),u^{\varepsilon}\left(r\right),\Lambda^{\varepsilon}\left(r\right)\right)$$

$$\geq H_{x}\left(r,\Theta^{\varepsilon}\left(r\right),u^{\varepsilon}\left(r\right),\Lambda^{\varepsilon}\left(r\right)\right)\left(x^{u}\left(r\right)-x^{\varepsilon}\left(r\right)\right)$$

$$+H_{y}\left(r,\Theta^{\varepsilon}\left(r\right),u^{\varepsilon}\left(r\right),\Lambda^{\varepsilon}\left(r\right)\right)\left(y^{u}\left(r\right)-y^{\varepsilon}\left(r\right)\right)$$

$$+H_{z}\left(r,\Theta^{\varepsilon}\left(r\right),u^{\varepsilon}\left(r\right),\Lambda^{\varepsilon}\left(r\right)\right)\left(z^{u}\left(r\right)-z^{\varepsilon}\left(r\right)\right)$$

$$+H_{u}\left(r,\Theta^{\varepsilon}\left(r\right),u^{\varepsilon}\left(r\right),\Lambda^{\varepsilon}\left(r\right)\right)\left(u\left(r\right)-u^{\varepsilon}\left(r\right)\right),$$

$$E\left[\phi\left(x^{u}\left(T\right)\right)-\phi\left(x^{\varepsilon}\left(T\right)\right)$$

$$-\phi_{x}\left(x^{\varepsilon}\left(T\right)\right)\cdot\left(x^{u}\left(T\right)-x^{\varepsilon}\left(T\right)\right)\right]$$

$$+E\left[\gamma\left(y^{u}\left(0\right)\right)-\gamma\left(y^{\varepsilon}\left(0\right)\right)$$

$$-\gamma_{y}\left(y^{u}\left(0\right)\right)\cdot\left(y^{u}\left(0\right)-y^{\varepsilon}\left(0\right)\right)\right]\geq0.$$
(55)

Putting (55) into (54), we have

$$J\left(u^{\varepsilon}\left(\cdot\right)\right) - J\left(u\left(\cdot\right)\right)$$

$$\leq -E \int_{0}^{T} H_{u}\left(r, \Theta^{\varepsilon}\left(r\right), u^{\varepsilon}\left(r\right), \Lambda^{\varepsilon}\left(r\right)\right) \left(u\left(r\right) - u^{\varepsilon}\left(r\right)\right) dr.$$
(56)

Therefore, the rest of the proof is only to estimate the term $H_u(r, \Theta^{\varepsilon}(r), u^{\varepsilon}(r), \Lambda^{\varepsilon}(r))(u(r) - u^{\varepsilon}(r))$. To this end, for a given $\varepsilon > 0$, let us introduce a new metric \tilde{d} on $\mathscr A$ as follows:

$$\widetilde{d}\left(u\left(\cdot\right),u'\left(\cdot\right)\right)=E\int_{0}^{T}v^{\varepsilon}\left(r\right)\left|u\left(r\right)-u'\left(r\right)\right|dr,\tag{57}$$

where

$$v^{\varepsilon}(r) = 1 + \left| p^{\varepsilon}(r) \right| + \left| q^{\varepsilon}(r) \right| + \left| k^{\varepsilon}(r) \right| \ge 1. \tag{58}$$

Now on \mathcal{A} we define a new functional F by

$$F(u(\cdot)) = E \int_0^T H(r, \Theta^{\varepsilon}(r), u(r), \Lambda^{\varepsilon}(r)) dr.$$
 (59)

It is easy to check that

$$\left| F\left(u\left(\cdot \right) \right) - F\left(u'\left(\cdot \right) \right) \right| \le CE \int_{0}^{T} v^{\varepsilon}\left(r\right) \left| u\left(r\right) - u'\left(r\right) \right| dr. \tag{60}$$

Therefore F is continuous on $\mathscr A$ with respect to metric $\widetilde d$. Using (52) and Ekeland's variational principle, we can find an admissible control $\overline u^\varepsilon(\cdot) \in \mathscr A$ such that

$$\tilde{d}\left(u^{\varepsilon}\left(\cdot\right), \overline{u}^{\varepsilon}\left(\cdot\right)\right) \le \varepsilon^{1/2},$$
(61)

$$E \int_{0}^{T} \widetilde{H}\left(r, \Theta^{\varepsilon}\left(r\right), \overline{u}^{\varepsilon}\left(r\right), \Lambda^{\varepsilon}\left(r\right)\right)$$

$$= \max_{u(\cdot) \in \mathscr{A}} E \int_{0}^{T} \widetilde{H}\left(t, \Theta^{\varepsilon}\left(r\right), u\left(r\right), \Lambda^{\varepsilon}\left(r\right)\right),$$
(62)

where

$$\widetilde{H}\left(t,\Theta^{\varepsilon}\left(r\right),u\left(r\right),\Lambda^{\varepsilon}\left(r\right)\right)$$

$$=H\left(t,\Theta^{\varepsilon}\left(r\right),u\left(r\right),\Lambda^{\varepsilon}\left(r\right)\right)-\varepsilon^{1/2}v^{\varepsilon}\left(r\right)\left|u\left(r\right)-\overline{u}^{\varepsilon}\left(r\right)\right|.$$

(63)

By standard methods, the maximum condition (52) implies that

$$\widetilde{H}\left(t, \Theta^{\varepsilon}\left(r\right), \overline{u}^{\varepsilon}\left(r\right), \Lambda^{\varepsilon}\left(r\right)\right) = \max_{u(\cdot) \in \mathcal{A}} \widetilde{H}\left(t, \Theta^{\varepsilon}\left(r\right), u\left(r\right), \Lambda^{\varepsilon}\left(r\right)\right),$$

$$\text{a.e. } (r, \omega) \in [0, T] \times \Omega.$$
(64)

Applying Proposition 2.3.2 in [30], we have

$$0 \in \partial_{u} H\left(t, \Theta^{\varepsilon}\left(r\right), \overline{u}^{\varepsilon}\left(r\right), \Lambda^{\varepsilon}\left(r\right)\right)$$

$$\subset \partial_{u} H\left(t, \Theta^{\varepsilon}\left(r\right), \overline{u}^{\varepsilon}\left(r\right), \Lambda^{\varepsilon}\left(r\right)\right)$$

$$+ \left[-\varepsilon^{1/2} v^{\varepsilon}\left(r\right), \varepsilon^{1/2} v^{\varepsilon}\left(r\right)\right],$$
(65)

which implies that there exists $\beta^{\varepsilon}(r) \in [-\varepsilon^{1/2}v^{\varepsilon}(r), \varepsilon^{1/2}v^{\varepsilon}(r)]$ such that

$$H_{u}\left(r,\Theta^{\varepsilon}\left(r\right),\overline{u}^{\varepsilon}\left(r\right),\Lambda^{\varepsilon}\left(r\right)\right)+\beta^{\varepsilon}\left(r\right)=0.\tag{66}$$

Therefore, under Assumptions 13 and 5,

$$\begin{aligned} & \left| H_{u} \left(r, \Theta^{\varepsilon} \left(r \right), u^{\varepsilon} \left(r \right), \Lambda^{\varepsilon} \left(r \right) \right) \right| \\ & - H_{u} \left(r, \Theta^{\varepsilon} \left(r \right), \overline{u}^{\varepsilon} \left(r \right), \Lambda^{\varepsilon} \left(r \right) \right) \Big| \\ & + \left| H_{u} \left(r, \Theta^{\varepsilon} \left(r \right), \overline{u}^{\varepsilon} \left(r \right), \Lambda^{\varepsilon} \left(r \right) \right) \right| \\ & \leq C \left(1 + \left| p^{\varepsilon} \left(r \right) \right| + \left| q^{\varepsilon} \left(r \right) \right| + \left| k^{\varepsilon} \left(r \right) \right| \right) \\ & \times \left| u^{\varepsilon} \left(t \right) - \overline{u}^{\varepsilon} \left(t \right) \right| + \varepsilon^{1/2} v^{\varepsilon} \\ & \leq C \left(1 + \left| p^{\varepsilon} \left(r \right) \right| + \left| q^{\varepsilon} \left(r \right) \right| + \left| k^{\varepsilon} \left(r \right) \right| \right) \\ & \times \left(\left| u^{\varepsilon} \left(r \right) - \overline{u}^{\varepsilon} \left(r \right) \right| + \varepsilon^{1/2} \right). \end{aligned}$$

Then, applying Holder's inequality and Lemma 12 and (61), we deduce

$$E \int_{0}^{T} \left| H_{u} \left(t, \Theta^{\varepsilon} \left(r \right), u^{\varepsilon} \left(r \right), \Lambda^{\varepsilon} \left(r \right) \right) \right| dr$$

$$\leq d \left(u^{\varepsilon} \left(\cdot \right), \overline{u}^{\varepsilon} \left(\cdot \right) \right) + C \varepsilon^{1/2}$$

$$\leq C \varepsilon^{1/2}. \tag{68}$$

By (56) and (68), we get

$$J(u^{\varepsilon}(\cdot)) \le J(u(\cdot)) + C\varepsilon^{1/2}.$$
 (69)

Since $u(\cdot)$ is arbitrary, $u(\cdot)$ is a near-optimal control with order $\varepsilon^{1/2}$.

8. Conclusion

This paper is the near-optimal control problem for a stochastic system driven by fully coupled FBSDEs. Stochastic maximum principle and verification theory of the near-optimal control are obtained. The control variable appears in both drift and diffusion coefficients of the FBSDEs. The control domain is assumed to be convex. The reviewers suggest that the data-driven control has extensive applications in industry and finance (see, e.g., [31–33] and the references therein) and the model discussed in this present paper may has the potential to achieve more practical oriented results under data-driven framework. Some investigations on this topic will be studied and carried out in our future publications.

Conflict of Interests

The author declares that there is no conflict of interests regarding the publication of this paper.

Acknowledgments

Financial supports by the National Natural Science Foundation of China (Grant nos. 11101140 and 11301177), China Postdoctoral Science Foundation (2011M500721 and 2012T50391), and the Natural Science Foundation of Zhejiang (Grant nos. Y6110775 and Y6110789) are gratefully acknowledged.

References

- [1] J.-M. Bismut, "Conjugate convex functions in optimal stochastic control," *Journal of Mathematical Analysis and Applications*, vol. 44, no. 3, pp. 384–404, 1973.
- [2] É. Pardoux and S. G. Peng, "Adapted solution of a backward stochastic differential equation," *Systems & Control Letters*, vol. 14, no. 1, pp. 55–61, 1990.
- [3] S. Peng, "Backward stochastic differential equations and applications to optimal control," *Applied Mathematics and Optimization*, vol. 27, no. 2, pp. 125–144, 1993.
- [4] W. S. Xu, "Stochastic maximum principle for optimal control problem of forward and backward system," *Journal of the Australian Mathematical Society B*, vol. 37, no. 2, pp. 172–185, 1995.
- [5] Z. Wu, "Maximum principle for optimal control problem of fully coupled forward-backward stochastic systems," *Systems Science and Mathematical Sciences*, vol. 11, no. 3, pp. 249–259, 1998.
- [6] J. T. Shi and Z. Wu, "Maximum principle for partially-observed optimal control of fully-coupled forward-backward stochastic systems," *Journal of Optimization Theory and Applications*, vol. 145, no. 3, pp. 543–578, 2010.
- [7] J.-T. Shi and Z. Wu, "The maximum principle for fully coupled forward-backward stochastic control system," *Acta Automatica Sinica*, vol. 32, no. 2, pp. 161–169, 2006.
- [8] G. Wang and Z. Wu, "The maximum principles for stochastic recursive optimal control problems under partial information," *IEEE Transactions on Automatic Control*, vol. 54, no. 6, pp. 1230– 1242, 2009.
- [9] G. Wang, Z. Wu, and J. Xiong, "Maximum principles for forward-backward stochastic control systems with correlated state and observation noises," *SIAM Journal on Control and Optimization*, vol. 51, no. 1, pp. 491–524, 2013.
- [10] S. Ji and Q. Wei, "A maximum principle for fully coupled forward-backward stochastic control systems with terminal state constraints," *Journal of Mathematical Analysis and Appli*cations, vol. 407, no. 2, pp. 200–210, 2013.
- [11] Q. Meng, "A maximum principle for optimal control problem of fully coupled forward-backward stochastic systems with partial information," *Science in China A*, vol. 52, no. 7, pp. 1579–1588, 2009.
- [12] M. Tang and Q. Meng, "Stochastic differential games of fully coupled forward-backward stochastic systems under partial information," in *Proceedings of the 29th Chinese Control Conference (CCC '10)*, pp. 1150–1155, IEEE, July 2010.

- [13] X. Y. Zhou, "Deterministic near-optimal control. I. Necessary and sufficient conditions for near-optimality," *Journal of Opti*mization Theory and Applications, vol. 85, no. 2, pp. 473–488, 1995
- [14] X. Y. Zhou, "Deterministic near-optimal controls. II. Dynamic programming and viscosity solution approach," *Mathematics of Operations Research*, vol. 21, no. 3, pp. 655–674, 1996.
- [15] I. Ekeland, "On the variational principle," *Journal of Mathematical Analysis and Applications*, vol. 47, pp. 324–353, 1974.
- [16] X. Y. Zhou, "Stochastic near-optimal controls: necessary and sufficient conditions for near-optimality," SIAM Journal on Control and Optimization, vol. 36, no. 3, pp. 929–947, 1998.
- [17] F. Chighoub and B. Mezerdi, "Near optimality conditions in stochastic control of jump diffusion processes," *Systems & Control Letters*, vol. 60, no. 11, pp. 907–916, 2011.
- [18] M. Hafayed, P. Veverka, and S. Abbas, "On maximum principle of near-optimality for diffusions with jumps, with application to consumption-investment problem," *Differential Equations and Dynamical Systems*, vol. 20, no. 2, pp. 111–125, 2012.
- [19] M. Hafayed and S. Abbas, "On near-optimal mean-field stochastic singular controls: necessary and sufficient conditions for near-optimality," *Journal of Optimization Theory and Appli*cations, 2013.
- [20] M. Hafayed, S. Abbas, and P. Veverka, "On necessary and sufficient conditions for near-optimal singular stochastic controls," *Optimization Letters*, vol. 7, no. 5, pp. 949–966, 2013.
- [21] J. Huang, X. Li, and G. Wang, "Near-optimal control problems for linear forward-backward stochastic systems," *Automatica*, vol. 46, no. 2, pp. 397–404, 2010.
- [22] K. Bahlali, N. Khelfallah, and B. Mezerdi, "Necessary and sufficient conditions for near-optimality in stochastic control of FBSDEs," *Systems & Control Letters*, vol. 58, no. 12, pp. 857–864, 2009.
- [23] E. Hui, J. Huang, X. Li, and G. Wang, "Near-optimal control for stochastic recursive problems," *Systems & Control Letters*, vol. 60, no. 3, pp. 161–168, 2011.
- [24] L. Zhang, J. Huang, and X. Li, "Stochastic maximum principle for nearoptimal control of fbsdes," 2012, http://arxiv.org/pdf/1203.1774.pdf.
- [25] J. Yong, "Optimality variational principle for controlled forward-backward stochastic differential equations with mixed initial-terminal conditions," SIAM Journal on Control and Optimization, vol. 48, no. 6, pp. 4119–4156, 2010.
- [26] Z. Wu, "A general maximum principle for optimal control of forward-backward stochastic systems," *Automatica*, vol. 49, no. 5, pp. 1473–1480, 2013.
- [27] S. Peng and Z. Wu, "Fully coupled forward-backward stochastic differential equations and applications to optimal control," SIAM Journal on Control and Optimization, vol. 37, no. 3, pp. 825–843, 1999.
- [28] Q. Lin, "Optimal control of coupled forward-backward stochastic system with jumps and related hamilton-jacobi-bellman equations," 2011, http://arxiv.org/pdf/1111.4642.pdf.
- [29] J. Yong and X. Y. Zhou, Stochastic Controls, vol. 43 of Applications of Mathematics, Springer, New York, NY, USA, 1999.
- [30] F. H. Clarke, Optimization and Nonsmooth Analysis, vol. 5 of Classics in Applied Mathematics, SIAM, Philadelphia, Pa, USA, Second edition, 1990.
- [31] S. Yin, S. X. Ding, A. H. A. Sari, and H. Hao, "Data-driven monitoring for stochastic systems and its application on batch process," *International Journal of Systems Science*, vol. 44, no. 7, pp. 1366–1376, 2013.

- [32] S. Yin, S. X. Ding, A. Haghani, H. Hao, and P. Zhang, "A comparison study of basic data-driven fault diagnosis and process monitoring methods on the benchmark tennessee eastman process," *Journal of Process Control*, vol. 22, no. 9, pp. 1567–1581, 2012.
- [33] S. Yin, H. Luo, and S. Ding, "Real-time implementation of fault-tolerant control systems with performance optimization," *IEEE Transactions on Industrial Electronics*, vol. 61, no. 5, pp. 2402–2411, 2013.

Hindawi Publishing Corporation Abstract and Applied Analysis Volume 2014, Article ID 450521, 11 pages http://dx.doi.org/10.1155/2014/450521

Research Article

Robust Adaptive Fault-Tolerant Control of Stochastic Systems with Modeling Uncertainties and Actuator Failures

Wenchuan Cai, Lingling Fan, and Yongduan Song^{1,2}

¹ School of Electronic and Information Engineering, Beijing Jiaotong University, Beijing 100044, China

Correspondence should be addressed to Yongduan Song; ydsong@cqu.edu.cn

Received 2 January 2014; Revised 27 January 2014; Accepted 30 January 2014; Published 13 March 2014

Academic Editor: Xiaojie Su

Copyright © 2014 Wenchuan Cai et al. This is an open access article distributed under the Creative Commons Attribution License, which permits unrestricted use, distribution, and reproduction in any medium, provided the original work is properly cited.

This paper deals with the problem of fault-tolerant control (FTC) of uncertain stochastic systems subject to modeling uncertainties and actuator failures. A robust adaptive fault-tolerant controller design method based on stochastic Lyapunov theory is developed to accommodate the negative impact on system performance arising from uncertain system parameters and external disturbances as well as actuation faults. There is no need for on-line fault detection and diagnosis (FDD) unit in the proposed FTC scheme, which not only simplifies the design process but also makes the implementation inexpensive. Numerical examples are provided to validate and illustrate the benefits of the proposed control method.

1. Introduction

Stability analysis and control design of stochastic systems have received increasing attention during the past decades. Under the framework of Itô equations together with the notion of mean-square stability, some interesting results have been obtained in terms of generalized algebraic Riccati equations, linear matrix inequality (LMI), or spectra of some operators (see, for instance, [1–4] and the references cited therein).

However, to our knowledge, very few works have dealt with the stabilization of general stochastic systems where actuator failures, parameter uncertainties, and state-dependent disturbances are involved simultaneously. This motivates us to investigate the reliable control problem of stochastic systems, aiming at maintaining an acceptable performance for the closed-loop systems in the presence of actuator failures and modeling uncertainties.

Actuator failures can cause severe performance deterioration of control systems, or even system instability, leading to catastrophic accidents. Fault-tolerant control (FTC) has been viewed as one of the most promising methods to increase system safety and reliability and has thus received considerable attention from control and system engineering

research community [5-17]. Most existing FTC methods can be broadly classified as active FTC and passive FTC. The active FTC requires a fault detection and diagnosis (FDD) mechanism to detect and identify the faults in real time, and a mechanism to reconfigure the controller according to the on-line fault information from the FDD [9-17]. The main idea of the passive FTC approach is to design a single controller that is robust against faults and uncertainties. In contrast to the passive approach, active methods utilize control reconfiguration to adjust controllers in real time so that the impacts of the failures can be compensated and the stability as well as the acceptable performance of the system can be maintained. Remarkable progress have been made in the area of actuator accommodation control with various effective design methods developed such as linear quadratic [18], multiple model designs [19-21], model following [2], FDD-dependent designs [22-24], and sliding mode controlbased designs [10, 25].

It is noted that, by blending adaptive control into FTC, the resultant control scheme turns out to be effective in reconfigurable control of systems with actuator failures [9, 26–30]. However, it is noted that few of the aforementioned works address the fault-tolerant control problem of stochastic systems.

² School of Automation, Chongqing University, Chongqing 400044, China

In this research, we will consider robust adaptive FTC for uncertain stochastic systems subject to actuator faults. The system under consideration involves parameter uncertainties and state-dependent disturbances. Moreover, there involves actuation faults that are assumed to be unpredictable during the system operation. We are interested in developing an FTC control scheme without the need for FDD. The developed FTC scheme is user friendly in the fact that no complicated computation is involved in its design and implementation.

The remaining part of the paper is organized as follows. In Section 2, the control problem is formulated. The design and analysis of the proposed control schemes are given in Section 3. Numerical simulations are conducted to demonstrate various features of the proposed control method and the results are presented in Section 4. Finally, the paper is closed with some concluding comments in Section 5.

Notation. The notations in this paper are quite standard. Rⁿ and $R^{n \times m}$ denote, respectively, the *n* dimensional Euclidean space and the set of all $n \times m$ real matrices. The superscript "T" denotes the transpose and the notation $X \ge Y$ (resp., X > Y) where X and Y are symmetric matrices, which means that X - Y is positive semidefinite (resp., positive definite). *I* is the identity matrix with compatible dimension. $|\cdot|$ is the Euclidean norm in \mathbb{R}^n . If A is a matrix, denote by ||A|| its operator norm; that is, $||A|| = \sup\{|Ax| : |x| = \max\{|Ax| : |x| = \max[|Ax| : |x| = \max[$ 1} = $\lambda_{\max}^{1/2}(A^T A)$, where $\lambda_{\max}(\cdot)$ [resp., $\lambda_{\min}(\cdot)$] means the largest (resp., smallest) eigenvalues of A. Moreover, (Ω, F, P) is probability space with Ω the sample space, **F** the σ -algebra of subsets of the sample space, and **P** the probability measure. $\Xi\{\cdot\}$ stands for the mathematical expectation operator with respect to the given probability measure **P**. L_2 and L_{∞} denote the spaces of square-integrable vector and bounded vector functions over $[0, \infty)$, respectively.

2. Problem Statement

Consider the stabilization problem of the following uncertain stochastic systems subject to actuator faults and external disturbances:

$$dx(t) = \left[(A + \Delta A(t)) x(t) + B(u_a(t) + f(x(t))) \right] dt + (C + \Delta C(t)) x(t) d\omega(t),$$
(1)

where $x(t) \in \mathbb{R}^n$ is state, $u_a(t) \in \mathbb{R}^m$ is actual control input, $f(x,t) \in \mathbb{R}^m$ is unknown external disturbances.

Here, $\omega(t)$ is a one-dimensional Brownian motion defined on the probability space $(\Omega, \mathbf{F}, \mathbf{P})$ with $\Xi\{\omega(t)\} = 0$ and $\Xi\{\omega^2(t)\} = 1$. A; B and C are known real constant matrices with appropriate dimensions. Without loss of generality, it is assumed that the pair (A, B) is controllable. $\Delta A(t)$, $\Delta C(t)$, and C denote parameter uncertainties and satisfy

$$\Delta A(t) = BF_1(t)$$
 $\Delta C(t) = BF_2(t)$ $C = BF_3$, (2)

where F_3 is known constant matrix, $F_1(t)$ and $F_2(t)$ are unknown time-varying matrix satisfying $||F_1(t)|| \le a_{F1} < \infty$ and $(||F_2(t)|| + ||F_3||)^2 \le a_{F2} < \infty$.

Table 1: Representations of typical actuator failures.

Type of actuator failures	$\delta_i(t)$	$\kappa(t)$
Healthy actuator	1	0
Loss of effectiveness only	$0<\delta_i(t)\leq 1$	0
Loss of effectiveness and partially out of control	$0<\delta_i(t)\leq 1$	Time-varying
Loss of effectiveness and partially jammed	$0<\delta_i(t)\leq 1$	Constant

Remark 1. It is observed that the parameter uncertainty structure as in (2) is more relaxed than the most existing methods. The parameter uncertainty structure which has been widely used in the problems of robust control and robust filtering of uncertain systems is assumed to be $\left(\Delta A(t)^T \ \Delta C(t)^T\right)^T = \left(E_1^T \ E_2^T\right)^T F(t)H$, where E_1, E_2 , and H are known constant matrices and F(t) is an known time-varying matrix satisfying $F^T(t)F(t) < I$ (see, for instance, [31–34]). Obviously, the structure herein which only needs the existence of the upper bound of F(t) is easier to be satisfied.

To formulate the fault-tolerant control problem, the fault model must be established first. In system (1), the types of faults under consideration include loss of effectiveness, stuck, or combination of all. The actual control input $u_a(t)$ able to impact the system and the designed control input u(t) designed are not the same in general. In this paper, the relationship between them will be adopted. Consider

$$u_{a}(t) = \Delta(\cdot) u(t) + \kappa(t), \qquad (3)$$

where $\Delta(\cdot)=\operatorname{diag}\{\delta_i(t)\}$ is a diagonal matrix with $\delta_i(t)$ ($i=1,2,\ldots,m$) being the unknown and time-varying scalar function called actuator efficiency factor, or "health indicator." For every fault mode, $\underline{\delta}_i$ and $\overline{\delta}_i$ represent the lower and upper bounds of δ_i , respectively. Note that, when $\underline{\delta}_i=\overline{\delta}=1$, there is no fault for the ith actuator u_i . When $\underline{\delta}_i=\overline{\delta}=0$, the ith actuator u_i is outage. When $0<\underline{\delta}_i\leq\overline{\delta}<1$, the type of actuator is loss of effectiveness. $\kappa(t)$ denotes a vector function reflecting the portion of the control action produced by the actuator that is completely out of control.

The type of actuator failures considered in this work is listed in Table 1.

In order for the system to admit a feasible FTC, the following assumptions are imposed.

Assumption 2. The unparametrizable stuck-actuator fault and external disturbance are piecewise continuous bounded functions; that is, there exist unknown positive constants a_{κ} and a_f such that

$$\|\kappa(t)\| \le a_{\kappa} < \infty, \qquad \|f(\cdot)\| \le a_f \psi_f(\cdot) < \infty.$$
 (4)

Assumption 3. For the system under consideration, there exist some constants $\alpha > 0$ and $\beta > 0$ such that for all possible actuator faults, the following relation holds:

$$\alpha \|B^T Px\|^2 \le \beta \|B^T Px \sqrt{\Delta(\cdot)}\|^2,$$
 (5)

where

$$\sqrt{\Delta(\cdot)} = \operatorname{diag}\left\{\sqrt{\delta_i(t)}\right\},
\delta_i(t) \in (0, 1] \quad (i = 1, 2, ..., m).$$
(6)

Remark 4. Assumption 2 confines the vector $\kappa(t)$ and external disturbances are bounded. Assumption 3, slightly less restrictive, sets constraint on the actuation faults, which a feasible FTC is able to deal with. Clearly, such condition is well justified if all the actuators with faults are still functional (i.e., $\delta_i(t) \neq 0$), whereas the too extreme faults in that all the actuators completely fail to work (i.e., $\delta_i(t) = 0$) make the assumption invalid, which, if not impossible, is significantly challenging to develop a globally stable control for the stochastic system (1); thus it is not considered in this work.

Remark 5. Since (A, B) is controllable, one can choose N_0 properly such that $\overline{A} = A - BN_0$ is Hurwitz. Namely, for given $Q = Q^T > 0$, there exists a symmetric and positive definite P such that the following matrix inequality is established:

$$\overline{A}^T P + P \overline{A} + \rho I < -Q, \tag{7}$$

where $\rho = \|B^T P B\| a_{F2}$. Note that we can find the proper *P* very easily because (7) is much simpler than those complex LMIs. The method in frame of linear matrix inequality is well used in many existing works [8, 13, 31, 33].

In the end of this section, the following important lemma is given, which will be used for the development of our result.

Lemma 6 (see [35]). The trivial solution of the stochastic differential equation

$$dx(t) = a(x,t) dt + b(x,t) d\omega,$$
 (8)

with a(x,t) and b(x,t) sufficiently differentiable maps, is globally asymptotically stable in probability, if there exists a positive definite, radially unbounded, twice continuously differentiable function V(x(t),t) such that the infinitesimal generator is

$$L[V(x(t),t)] = \frac{\partial V}{\partial t} + \left(\frac{\partial V}{\partial x}\right)^{T} a(x,t)$$

$$+ \frac{1}{2}b(x(t),t)^{T} \frac{\partial^{2} V}{\partial x^{2}} b(x(t),t) < 0.$$
(9)

3. Fault-Tolerant Control Design

To show the idea of this work explicitly, several fault-tolerant control schemes are developed under different conditions in this section. At the beginning, a robust fault-tolerant control method is presented.

3.1. Robust Fault-Tolerant Control. In this section, a robust fault-tolerant control of the form

$$u(t) = -N_0 x + N(t) \tag{10a}$$

is proposed, where N_0 is chosen such that $A - BN_0$ is Hurwitz, and N(t) is generated by

$$N(t) = -\frac{a}{\lambda_m} \varphi(\cdot) \frac{B^T P x}{\|B^T P x\|},$$
 (10b)

with $0 < \lambda_m \le \alpha/\beta$ being a constant, where λ_m represents the lower bound of the health indicator matrix $\Delta(\cdot)$; that is, $0 < \lambda_m \le \lambda_{\min}(\Delta)$ and $\alpha > 0$, $\beta > 0$ are suitable constants such that

$$\alpha \|B^T P x\|^2 \le \beta \|B^T P x \sqrt{\Delta(\cdot)}\|^2,$$
 (10c)

$$\begin{split} \varphi\left(\cdot\right) &= 1 + \left\|N_{0}x\right\| + \left\|\varphi_{f}\left(x\right)\right\| + \left\|x\right\|,\\ a &= \max\left\{1, a_{N}, a_{f}, a_{F1}\right\}. \end{split} \tag{10d}$$

Theorem 7. Under Assumptions 2 and 3, the FTC as given in ((10a), (10b), (10c), and (10d)) exponentially stabilizes (in mean square) the stochastic system described by (1), for all admissible uncertainties as well as all actuator failures corresponding to (3).

Proof. When the system is subject to the actuator failure as described in (3), its dynamic behavior becomes

$$dx(t) = \left[(A + \Delta A(t)) x(t) + B(\Delta(\cdot) u(t) + \kappa(t) + f(x(t))) \right] dt$$
 (11)

$$+ (C + \Delta C(t)) x(t) d\omega(t).$$

With the proposed control ((10a), (10b), (10c), (10d)), one has

$$dx(t) = \left[(A + \Delta A(t)) x(t) + B(\Delta(\cdot) u(t) + \kappa(t) + f(x(t))) \right] dt$$

$$+ (C + \Delta C(t)) x(t) d\omega(t)$$

$$= \left[(A + \Delta A(t)) x(t) + B(\Delta(\cdot) (-N_0 x + N(t)) + \kappa(t) + f(x(t))) \right] dt$$

$$+ (C + \Delta C(t)) x(t) d\omega(t)$$

$$= (A - BN_0) x(t) dt$$

$$+ B[\Delta(\cdot) N(t) + Z(t)] dt$$

$$+ (C + \Delta C(t)) x(t) d\omega(t),$$
(12)

where

$$Z(\cdot) = (I - \Delta(\cdot)) N_0 x(t) + \kappa(t) + f(\cdot) + F_1(t) x(t), \quad (13)$$

which is bounded as

$$||Z(\cdot)|| \le ||N_0 x|| + ||\kappa(\cdot)|| + ||f(\cdot)|| + ||F_1(t) x(t)||$$

$$\le a (1 + ||N_0 x|| + ||\psi(x)|| + ||x||),$$
(14)

based on Assumption 2, where $a=\max\{1,a_N,a_f,a_{F1}\}$ and $\varphi(\cdot)=1+\|N_0x\|+\|\varphi_f(x)\|+\|x\|.$ Thus, it is not difficult to get

$$(B^{T}Px)^{T}Z \le a\varphi(\cdot) \|B^{T}Px\|. \tag{15}$$

Consider the following Lyapunov function candidate:

$$V(x(t),t) = x^{T}(t) Px(t)$$
. (16)

Then, by Itô's formula, the infinitesimal generator of (12) is

$$L\left[V\left(x\left(t\right),t\right)\right] = x^{T}\left(t\right)P\left(A - BN_{0}\right)x\left(t\right)$$

$$+\left(\left(A - BN_{0}\right)x(t)\right)^{T}Px\left(t\right)$$

$$+2\left(B^{T}Px\right)^{T}\left[-\Delta\left(\cdot\right)\frac{a}{\lambda_{m}}\varphi\left(\cdot\right)\frac{B^{T}Px}{\left\|B^{T}Px\right\|}\right]$$

$$+2\left(B^{T}Px\right)^{T}Z$$

$$+x^{T}\left(t\right)\left(C + \Delta C\left(t\right)\right)^{T}P\left(C + \Delta C\left(t\right)\right)x\left(t\right).$$
(17)

Note that the last term of (17) cannot be combined with $Z(\cdot)$; thus the adaptive updating law cannot be used to compensate its effect as usual. To establish the robust stability of the closed-loop system (12), we need to have the following development. From the fact that $(\|F_2(t)\| + \|F_3\|)^2 \le a_{F2} < \infty$ and using (2), it is seen that the last term of (17) can be expressed as

$$x^{T}(t) (C + \Delta C(t))^{T} P (C + \Delta C(t)) x (t)$$

$$= x^{T}(t) \left[B(F_{2}(t) + F_{3})^{T} P B(F_{2}(t) + F_{3}) \right] x (t)$$

$$\leq x^{T}(t) \left[\|B^{T} P B\| a_{F_{2}} \right] x (t);$$
(18)

from (10c), it holds that

$$-\left(B^{T}Px\right)^{T}\Delta\left(\cdot\right)\left(B^{T}Px\right) \leq -\frac{\alpha}{\beta}\left\|B^{T}Px\right\|^{2} \leq -\lambda_{m}\left\|B^{T}Px\right\|^{2}.$$
(19)

and by defining $\rho = \|B^T P B\| a_{F2}$, the inequality (17) can be shown to satisfy

$$L[V(x(t),t)] \leq x^{T}(t) \left(\overline{A}^{T} P + P\overline{A}\right) x(t)$$

$$-2 \frac{a}{\lambda_{m}} \frac{\varphi(\cdot)}{\|B^{T} P x\|} \left(B^{T} P x\right)^{T} \Delta(\cdot) \left(B^{T} P x\right)$$

$$+ a\varphi(\cdot) \|B^{T} P x\| + x^{T}(t) \|B^{T} P B\| \|F_{2}\|^{2} x(t)$$

$$\leq x^{T}(t) \left(\overline{A}^{T} P + P\overline{A} + \rho I\right) x(t)$$

$$\leq -\frac{1}{2} x^{T} Q x < 0 \quad \text{for } x(t) \neq 0,$$
(20)

where matrixes P and Q are chosen properly to satisfy $\overline{A}^T P + P \overline{A} + \rho I \leq -Q$. Therefore, it is confirmed from Lemma 6 that the closed-loop system (11) is asymptotically mean square stable in probability despite faulty actuators with the proposed FTC.

Remark 8. Note that if proper constants α and β can be obtained in advance, the proposed control ((10a), (10b), (10c), and (10d)) achieved exponential stability in mean square for the stochastic system under Assumptions 2 and 3. However, it is a little difficult to select such α and β to ensure $\lambda_m \leq \alpha/\beta$, since λ_m the lower bound of the eigenvalue of the health indicator matrix is not available in general. In view of this, a more feasible method is developed in the next subsection.

3.2. Robust Adaptive Fault-Tolerant Control. In order to develop a control scheme that is not only robust but also adaptive yet fault-tolerant, we modify the previous one to get

$$u(t) = -N_0 x + \widehat{N}(t), \qquad (21a)$$

where $N_0 > 0$ is chosen such that $A - BN_0$ is Hurwitz and $\widehat{N}(t)$ is on-line updated by

$$\widehat{N}(t) = \frac{\widehat{a}(t)\,\varphi(x)\,B^T P x}{\|B^T P x\|},\tag{21b}$$

with

$$\varphi(x) = 1 + ||N_0 x|| + ||\varphi_f(x)|| + ||x||,$$
 (21c)

$$\dot{\hat{a}}(t) = -\gamma \varphi(x) \|B^T P x\|, \quad \gamma > 0.$$
 (21d)

Theorem 9. Consider the uncertain stochastic system (11) under Assumptions 2 and 3. If the robust adaptive fault-tolerant controller ((21a), (21b), (21c), and (21d)) is implemented, the closed-loop system is ensured to be asymptotically stable.

Proof. Substituting the proposed control ((21a), (21b), (21c), and (21d)) into the stochastic system (11), we obtain the closed-loop system dynamics as follows:

$$dx(t) = [(A + \Delta A(t)) x(t) + B(\Delta(\cdot) u(t) + \kappa(t) + f(x(t)))] dt$$

$$+ (C + \Delta C(t)) x(t) d\omega(t)$$

$$= [(A + \Delta A(t)) x(t) + B(\Delta(\cdot) (-N_0 x + \widehat{N}(t)) + \kappa(t) + f(x(t)))] dt$$

$$+ (C + \Delta C(t)) x(t) d\omega(t)$$

$$= (A - BN_0) x(t) dt$$

$$+ B[\Delta(\cdot) \widehat{N}(t) + Z(t)] dt$$

$$+ (C + \Delta C(t)) x(t) d\omega(t).$$
(22)

Consider the following Lyapunov function candidate:

$$V(x(t),t) = x^{T}Px + \frac{1}{\lambda_{m}\gamma}(a - \hat{a}\lambda_{m})^{2}, \qquad (23)$$

where $\gamma > 0$ is a constant related to adaptation rate chosen by the designer and $\lambda_m > 0$ is constant defined as before. Upon using the control scheme with the adaptive algorithm, it is not difficult to show that

$$L[V(x(t),t)] = x^{T}(t) P(A - BN_{0}) x(t)$$

$$+ ((A - BN_{0}) x(t))^{T} Px(t)$$

$$+ 2(a - \hat{a}\lambda_{m}) (-\dot{a}\gamma^{-1})$$

$$+ x^{T}(t) (C + \Delta C(t))^{T} P(C + \Delta C(t)) x(t)$$

$$= [\overline{A}x + B(\Delta(\cdot)\widehat{N}(t)x + Z(\cdot))]^{T} Px$$

$$+ x^{T} P[\overline{A}x + B(\Delta(\cdot)\widehat{N}(t)x + Z(\cdot))]$$

$$+ 2(a - \hat{a}\lambda_{m}) (-\dot{a}\gamma^{-1})$$

$$+ x^{T}(t) (C + \Delta C(t))^{T} P(C + \Delta C(t)) x(t)$$

$$= x^{T} (\overline{A}^{T} P + P\overline{A}) x$$

$$+ 2x^{T} PB(\Delta(\cdot)\widehat{N}(t)x + Z(\cdot))$$

$$+ 2(a - \hat{a}\lambda_{m}) (-\dot{a}\gamma^{-1})$$

$$+ x^{T}(t) (C + \Delta C(t))^{T} P(C + \Delta C(t)) x(t). \tag{24}$$

Then

$$L[V(x(t),t)]$$

$$= x^{T} \left(\overline{A}^{T} P + P \overline{A}\right) x$$

$$+ 2x^{T} P B \left\{ \Delta(\cdot) \left[-\frac{\widehat{a} \varphi(x) \left(B^{T} P x\right)}{\|B^{T} P x\|} \right] + Z(\cdot) \right\}$$

$$+ 2 \left(a - \lambda_{m} \widehat{a}\right) \left(-\gamma^{-1} \dot{\overline{a}} \right)$$

$$+ x^{T} (t) \left(C + \Delta C(t)\right)^{T} P \left(C + \Delta C(t)\right) x(t).$$
(25)

In light of the definition of λ_m , it is true that $(B^T P x)^T \Delta(\cdot)(B^T P x) \ge \lambda_m \|B^T P x\|^2$; thus the second term in (25) can be rewritten as

$$2x^{T}PB\left\{\Delta\left(\cdot\right)\left[-\frac{\widehat{a}\varphi\left(x\right)\left(B^{T}P\right)}{\left\|B^{T}Px\right\|}\right]x+Z\left(\cdot\right)\right\}$$

$$=-2\frac{\widehat{a}\varphi\left(x\right)}{\left\|B^{T}Px\right\|}\left(B^{T}Px\right)^{T}\Delta\left(\cdot\right)\left(B^{T}Px\right)$$

$$+2\left(B^{T}Px\right)^{T}Z\left(\cdot\right)$$

$$\leq 2\left(a-\lambda_{m}\widehat{a}\right)\varphi\left(x\right)\left\|B^{T}Px\right\|.$$
(26)

The fact $x^{T}(t)(C + \Delta C(t))^{T}P(C + \Delta C(t))x(t) \le x^{T}(t)[\|B^{T}PB\|a_{F2}]x(t) \le x^{T}(t)(\rho I)x(t)$ leads (25) to

$$L\left[V\left(x\left(t\right),t\right)\right] \leq x^{T}\left(t\right)\left(\overline{A}^{T}P + P\overline{A}\right)x\left(t\right)$$

$$+ 2\left(a - \lambda_{m}\widehat{a}\right)\varphi\left(x\right)\left\|B^{T}Px\right\|$$

$$+ 2\left(a - \lambda_{m}\widehat{a}\right)\left(-\gamma^{-1}\dot{a}\right)$$

$$+ x^{T}\left(t\right)\left(\left\|B^{T}PB\right\|\left\|F_{2}\right\|^{2}\right)x\left(t\right)$$

$$\leq x^{T}\left(t\right)\left(\overline{A}^{T}P + P\overline{A} + \rho I\right)x\left(t\right).$$
(27)

Using the updating law (21d) and choosing the proper matrixes P and Q to ensure that the matric inequality is established, one obtains from (27) that

$$L[V(x(t),t)] \le -\frac{1}{2}x^{T}Qx < 0 \text{ for } x(t) \ne 0.$$
 (28)

Consequently, according to Lemma 6, it can be obtained that the closed-loop system (11) is globally asymptotically stable in probability in presence of actuator failures. \Box

Remark 10. Note that in designing and implementing the first robust fault-tolerant control method we need to predetermine the parameters a and λ_m . This might present analytical and technical difficulty in practice. The second robust adaptive FTC scheme, which does not need the analytic computation of the parameters a and λ_m , circumvents this shortcoming. Although the existence of $\lambda_m>0$ is used in stability analysis, none of them are used in the control algorithm.

Remark 11. It is seen that the proposed control is independent of explicit information on faults and disturbances. As with most variable structure control methods, when the states get closer to zero, the control scheme might experience chattering, which can be easily avoided by replacing $z/\|z\|$ with $z/(\|z\| + \varsigma)$, where ς is a small number, as commonly

adopted in the literature. Also to prevent the estimate \hat{a} from drifting, (21d) can be modified as

$$\hat{a}(t) = -\sigma \hat{a} + \gamma \frac{\varphi(x)^2 \left\| B^T P x \right\|^2}{\varphi(x) \left\| B^T P x \right\| + \varsigma}, \quad \gamma > 0, \ \sigma > 0. \quad (29a)$$

In this case, we have the following ultimately uniformly bounded (UUB) stabilization result.

Theorem 12. Consider the uncertain stochastic system (11). Let the Assumptions 2 and 3 hold. If the following robust adaptive control is applied:

$$u(t) = -N_0 x + \widehat{N}(t), \qquad (29b)$$

where $N_0 > 0$ is chosen such that $A - BN_0$ is Hurwitz, and $\widehat{N}(t)$ is generated by

$$\widehat{N}(t) = \frac{\widehat{a}(t)\varphi(x)^2 B^T P x}{\|B^T P x\|\varphi(x) + \varsigma}$$
(29c)

and \hat{a} is updated by (29a), then the closed-loop system (11) is ensured to UUB stable.

Proof. The result can be established by using the method similar to that as in [15].

Remark 13. Since the robust FTC with the fixed gain may bring more conservatives, a new robust adaptive FTC is further addressed in the next subsection. By means of the online estimation of effectiveness values of faulty actuators, the robust adaptive FTC gain is adaptively updated to compensate the effects of actuator faults.

3.3. Improved Robust Adaptive Fault-Tolerant Control. Consider that the elements of the actuator efficiency factor $\Delta(\cdot)$ are constants. A robust and adaptive control scheme integrated with on-line fault estimation is designed as

$$u(t) = -\widehat{\Delta}(t)^{-1} N_0 x + \widehat{N}(t),$$
 (30a)

where $\widehat{\Delta}(t) = \text{diag}\{\widehat{\delta}_1(t), \widehat{\delta}_2(t), \dots, \widehat{\delta}_m(t)\}$, $\widehat{\delta}_i(t)$ is the estimated values of effectiveness for ith actuator, and the updating law for $\widehat{\delta}_i(t)$ ($i = 1, 2, \dots, m$) is given as

$$\dot{\overline{\delta}}_{i}\left(t\right) = \Pr_{\left[\underline{\delta}_{i}, \overline{\delta}_{i}\right]} \begin{cases} 0, & \text{if } \widehat{\delta}_{i} = \underline{\delta}_{i}, \ U_{i} \leq 0, \text{ or } \widehat{\delta}_{i} = \overline{\delta}_{i}, \ U_{i} \geq 0 \\ U_{i}, & \text{otherwise}, \end{cases}$$
(30b)

where $U_i = \eta_i x(t)^T (PB)_i \widehat{\Delta}(\cdot)^{-1} N_0^i x(t)$, $\eta_i > 0$ is the adaptive law gain to be chosen according to practical applications. Here, M^i and M_i denote the *i*th row and *i*th column of a matrix M, respectively.

 $N_0 > 0$ is chosen such that $A - BN_0$ is Hurwitz, and $\widehat{N}(t)$ is on-line updated by

$$\widehat{N}(t) = \frac{\widehat{a}(t) \psi(x) B^{T} P x}{\|B^{T} P x\|},$$
(30c)

with

$$\psi(x) = 1 + \|\varphi_f(x)\| + \|x\|,$$
 (30d)

$$\dot{\hat{a}}(t) = -\gamma \psi(x) \|B^T P x\|, \quad \gamma > 0.$$
 (30e)

Remark 14. It is noted from (30b) that $\Pr\{\cdot\}$ is a projection operator [28], which projects the estimate $\widehat{\delta}_i$ into the interval $[\underline{\delta}_i, \overline{\delta}_i]$ so as to satisfy the assumption on the bound of effectiveness values in (3). Because this updating law can ensure the estimated values $\widehat{\delta}_i(t)$ are not zero, the control signal u(t) will take effect on the plant.

Theorem 15. For the uncertain stochastic system (11), the robust adaptive fault-tolerant controller given as ((30a), (30b), (30c), (30d), and (30e)) can ensure that the state will asymptotically tend to zero.

Proof. Substituting ((30a), (30b), (30c), (30d), and (30e)) into the stochastic system (11), we obtain the closed-loop system equation as follows:

$$dx(t) = \left[(A + \Delta A(t)) x(t) + B(\Delta(t)) u(t) + \kappa(t) + f(x(t)) \right] dt$$

$$+ (C + \Delta C(t)) x(t) d\omega(t)$$

$$= \left[(A + \Delta A(t)) x(t) + B(\Delta(t)) \left(-\widehat{\Delta}(t)^{-1} N_0 x + \widehat{N}(t) \right) + \kappa(t) + f(x(t)) \right] dt$$

$$+ (C + \Delta C(t)) x(t) d\omega(t)$$

$$= (A - BN_0) x(t) dt$$

$$+ B\left[\left(I - \Delta(t) \widehat{\Delta}(t)^{-1} \right) N_0 x + \Delta(t) \widehat{N}(t) + Z(t) \right] dt$$

$$+ (C + \Delta C(t)) x(t) d\omega(t),$$
(31)

where $Z(\cdot) = \kappa(t) + f(\cdot) + F_1(t)x(t)$, which is bounded by

$$||Z(\cdot)|| \le ||\kappa(\cdot)|| + ||f(\cdot)|| + ||F_1(t)x(t)||$$

$$\le a(1 + ||\varphi(x)|| + ||x||)$$
(32)

under Assumption 2.

Consider the following Lyapunov function candidate

$$V(x(t),t) = x^{T} P x + \frac{1}{\lambda_{m} \gamma} (a - \hat{a} \lambda_{m})^{2} + \sum_{i=1}^{m} \eta_{i}^{-1} \tilde{\delta}_{i}^{2}(t), \quad (33)$$

where $\gamma>0$ and $\eta>0$ are constants related to adaptation rate chosen by the designer and $\lambda_m>0$ is constant defined as before. Upon using the control scheme with the adaptive

algorithm, it is not difficult to show that the infinitesimal operator

$$L[V(x(t),t)] = x^{T}(t) P(A - BN_{0}) x(t)$$

$$+ ((A - BN_{0}) x(t))^{T} P x(t)$$

$$+ 2 (a - \hat{a}\lambda_{m}) (-\dot{a}\gamma^{-1})$$

$$+ 2 \sum_{i=1}^{m} \eta_{i}^{-1} \tilde{\delta}_{i}(t) \dot{\hat{\delta}}_{i}(t)$$

$$= \left[\overline{A}x + B (-\tilde{\delta}\hat{\delta}^{-1} N_{0}x + \Delta (\cdot) \hat{N}(t) x + Z (\cdot) \right]^{T} P x$$

$$+ x^{T} P \left[\overline{A}x + B (-\tilde{\delta}\hat{\delta}^{-1} N_{0}x + \Delta (\cdot) \hat{N}(t) x + Z (\cdot) \right]$$

$$+ 2 (a - \hat{a}\lambda_{m}) (-\dot{a}\gamma^{-1})$$

$$+ 2 \sum_{i=1}^{m} \eta_{i}^{-1} \tilde{\delta}_{i}(t) \dot{\hat{\delta}}_{i}(t)$$

$$= x^{T} (\overline{A}^{T} P + P \overline{A}) x + 2x^{T} P B \tilde{\delta} \hat{\delta}^{-1} N_{0}x$$

$$+ 2x^{T} P B (\Delta (\cdot) \hat{N}(t) x + Z (\cdot))$$

$$+ 2 (a - \hat{a}\lambda_{m}) (-\dot{a}\gamma^{-1})$$

$$+ 2 \sum_{i=1}^{m} \eta_{i}^{-1} \tilde{\delta}_{i}(t) \dot{\hat{\delta}}_{i}(t).$$
(34)

Considering that $PB\delta\delta\delta^{-1} = \sum_{i=1}^{m} \delta(PB)^{i}\delta^{-1}$ and the adaptive law (30b), we have

$$-2x^{T}PB\widetilde{\delta}\widehat{\delta}^{-1}N_{0}x + 2\sum_{i=1}^{m}\eta_{i}^{-1}\widetilde{\delta}_{i}\left(t\right)\widehat{\delta}_{i}\left(t\right) \leq 0. \tag{35}$$

Then, L[V(x(t), t)] becomes

$$L[V(x(t),t)]$$

$$= x^{T} \left(\overline{A}^{T} P + P \overline{A}\right) x$$

$$+ 2x^{T} P B \left\{ \Delta \left(\cdot \right) \left[-\frac{\widehat{a} \psi(x) \left(B^{T} P x \right)}{\|B^{T} P x\|} \right] + Z(\cdot) \right\}$$

$$+ 2 \left(a - \lambda_{m} \widehat{a} \right) \left(-\gamma^{-1} \dot{\overline{a}} \right)$$

$$+ x^{T} (t) \left(C + \Delta C(t) \right)^{T} P \left(C + \Delta C(t) \right) x(t),$$
(36)

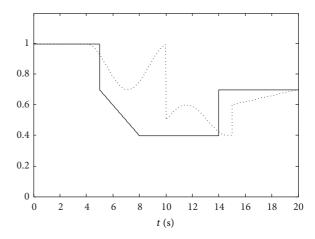


FIGURE 1: Profile of the time-varying actuator efficiency variable (δ_1 (solid), δ_2 (dot)).

in which the second term in (36) can be rewritten as

$$2x^{T}PB\left\{\Delta\left(\cdot\right)\left[-\frac{\widehat{a}\psi\left(x\right)\left(B^{T}P\right)}{\left\|B^{T}Px\right\|}\right]x+Z\left(\cdot\right)\right\}$$

$$=-2\frac{\widehat{a}\psi\left(x\right)}{\left\|B^{T}Px\right\|}\left(B^{T}Px\right)^{T}\Delta\left(\cdot\right)\left(B^{T}Px\right)$$

$$+2\left(B^{T}Px\right)^{T}Z\left(\cdot\right)$$

$$\leq 2\left(a-\lambda_{m}\widehat{a}\right)\psi\left(x\right)\left\|B^{T}Px\right\|;$$
(37)

by using (19) it is true that $(B^T P x)^T \Delta(\cdot) (B^T P x) \ge \lambda_m \|B^T P x\|^2$. Thus by using the fact that $x^T (t) (C + \Delta C(t))^T P (C + \Delta C(t)) x(t) \le x^T (t) (\rho I) x(t)$ and the updating law (30e), the function L[V(x(t),t)] eventually is bounded as

$$L[V(x(t),t)] \leq x^{T} \left(\overline{A}^{T} P + P\overline{A} + \rho I\right) x$$

$$+ 2(a - \lambda_{m} \widehat{a}) \psi(x) \|B^{T} P x\|$$

$$+ 2(a - \lambda_{m} \widehat{a}) \left(-\gamma^{-1} \dot{\overline{a}}\right)$$

$$\leq -\frac{1}{2} x^{T} Q x < 0 \quad \text{for } x(t) \neq 0,$$

$$(38)$$

as long as proper matrixes P and Q are select to ensure (7). Therefore, it can be obtained from Lemma 6 that the state of the stochastic system is asymptotically stable in probability and the estimation parameters $(a - \lambda_m \widehat{a})$ and $\widetilde{\delta}_i$ are bounded.

4. Numerical Simulation

Two examples are used to demonstrate the features of the proposed control scheme.

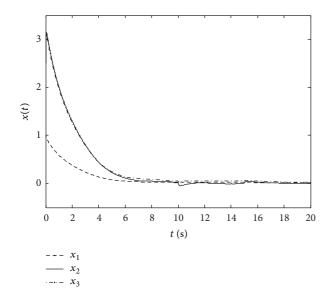


FIGURE 2: The curve of x(t) with the proposed control scheme ((29a), (29b), and (29c)).

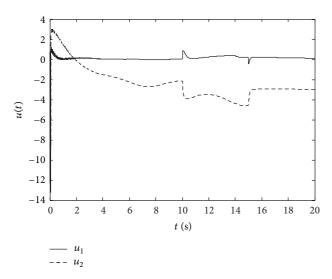


FIGURE 3: The curve of u(t) with the proposed control scheme ((29a), (29b), and (29c)).

Example 1. Consider the uncertain stochastic system (11) with

$$A = \begin{bmatrix} 0.2 & -0.2 & 0 \\ -0.2 & -0.6 & 0.3 \\ 0.2 & -0.4 & -0.2 \end{bmatrix}, \qquad B = \begin{bmatrix} -0.2 & 0.2 \\ 1 & -1.7 \\ 0.6 & -0.7 \end{bmatrix},$$

$$C = \begin{bmatrix} -0.04 & 0.2 & 0.07 \\ -0.03 & 0.1 & 0.04 \\ 0.04 & -0.2 & -0.07 \end{bmatrix},$$

$$\Delta A = \begin{bmatrix} 0.02\sin(t) & 0.04\cos^2(t) & 0.04\cos(2t) \\ 0.02 & 0.04\sin(2t)\cos(t) & 0.04 \\ 0.03\cos(t) & 0.06 & 0.06\sin(t) \end{bmatrix}$$

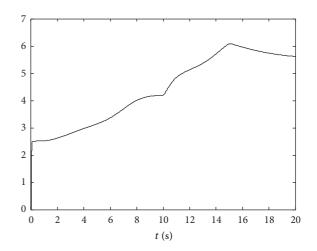


FIGURE 4: Updating of $\hat{a}(t)$ with the proposed control scheme ((29a), (29b), and (29c)).

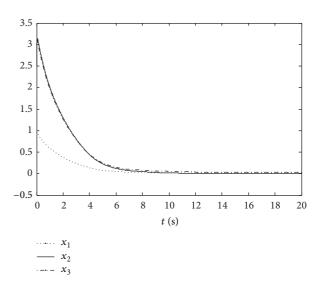


FIGURE 5: System responses under the control of the proposed FTC ((30a), (30b), (30c), (30d), and (30e)).

$$\Delta C = \begin{bmatrix} -0.007\cos\left(t\right) & 0.014 & 0.014\sin\left(2t\right) \\ 0.004\cos^{2}\left(t\right) & 0.008\sin^{2}\left(t\right) & 0.008 \\ -0.007 & -0.014\sin\left(t\right)\cos\left(2t\right) & -0.014\sin\left(t\right)\cos\left(3t\right) \end{bmatrix},$$

$$f\left(x\left(t\right)\right) = \begin{pmatrix} \sin\left(x_{1}\left(t\right)\right)\sin\left(x_{2}\left(t\right)\right) \\ 2x_{1}\left(t\right)\cos\left(x_{2}\left(t\right)\right) \end{pmatrix}.$$
(39)

It is seen that the uncertainties ΔA and ΔC are complex to be described by the form of $\left(\Delta A(t)^T \ \Delta C(t)^T\right)^T = \left(E_1^T \ E_2^T\right)^T F(t)H$. But the form of (2) is easy to satisfy. The external disturbance $f(\cdot)$ is state-dependent and unknown. For the simulation, the initial conditions are x(0) = [1, 2.5, 3] and $\widehat{a}(0) = 0$.

The actuator efficiency variables for each of the two control channels simulated are as illustrated in Figure 1, where two of the actuators suffer from the failure as shown in the figure.

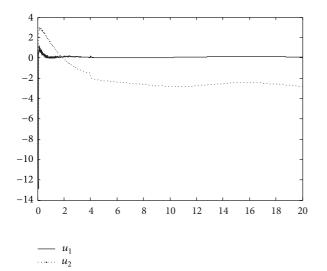


FIGURE 6: The curve of u(t) with the proposed control scheme ((30a), (30b), (30c), (30d), and (30e)).

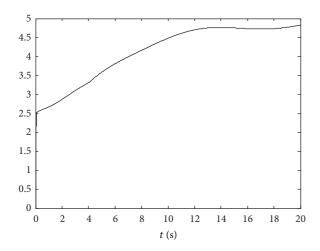


FIGURE 7: Updating of $\hat{a}(t)$ with the proposed control scheme ((30a), (30b), (30c), (30d), and (30e)).

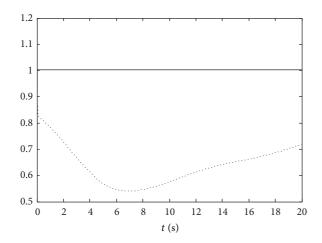


FIGURE 8: The curve of the estimate $\widehat{\Delta}(t)$ with $\eta=2$ ($\widehat{\delta}_1$ (solid), $\widehat{\delta}_2$ (dot)).

The scenario simulated is that the system operates normally at the beginning, and the disturbances always exist during the system operation. After 4 seconds of the operation some faults in actuators occur: the first and the second actuators encounter severe failures in the fact that both channels lose their effectiveness by over 50% at some time and the faults are fast time-varying for some period.

The objective in this work is to design a reliable robust adaptive fault-tolerant controller such that the closed-loop system is asymptotically stable in probability despite the presence of actuator faults. In applying the control scheme ((29a), (29b), and (29c)), one can easily determine all the control parameters:

$$N_{0} = \begin{bmatrix} -1.0912 & 0.3210 & 0.0695 \\ 8.0245 & -3.8070 & 0.0239 \end{bmatrix},$$

$$\gamma = 5, \quad \sigma = 0.08, \quad \varepsilon = 0.001,$$

$$\varphi(x) = 1 + \|N_{0}x\| + \|\varphi_{f}(x)\| + \|x\|.$$

$$(40)$$

The simulation results in terms of stabilization of the three states are presented in Figure 2. It can be seen that the states x_1 , x_2 , and x_3 can converge to a small neighborhood around zero. Figure 3 shows the control signals of the two inputs. The estimated parameter $\hat{a}(t)$ is shown in Figure 4. The results confirm the theoretical prediction.

Example 2. The second simulation is made for robust adaptive fault-tolerant controller ((30a), (30b), (30c), (30d), and (30e)). It is assumed that at t=4 s, the first actuator u_1 is still normal and the second actuator u_2 is faulty with $\delta_2=0.5$. The simulations are shown in Figures 5, 6, 7, and 8. Also it should be pointed out from [36] that the estimated value $\hat{\delta}_i(t)$ (i=1,2) can converge but may not converge to its true value $\delta_i(t)$. And in our controller design procedure, only the estimated value $\hat{\delta}_i(t)$ is needed to construct adaptive controller and whether $\hat{\delta}_i(t)$ can converge to its true values or not is not necessary.

From Figure 5, the FTC scheme ((30a), (30b), (30c), (30d), and (30e)) makes the curves relatively smooth via the adaptive estimate $\hat{\delta}_i(t)$ of efficiency value. The simulation results confirm that the robust adaptive FTC can achieve a good performance on dealing with the reliable control problem of stochastic systems in presence of actuator failures, parameter uncertainty, and state-dependent disturbance.

5. Conclusion

In this paper, the problem of robust adaptive FTC for stochastic systems with faulty actuators has been considered. By blending adaptive control into robust FTC, the proposed control method is able to accommodate actuation faults and modeling uncertainties concurrently. Both theoretical analysis and numerical simulations validate the benefits and effectiveness of the proposed approach.

Conflict of Interests

The authors declare that there is no conflict of interests regarding the publication of this paper.

Acknowledgments

The paper is supported by the Major State Basic Research Development Program 973 (no. 2012CB215202), the National Natural Science Foundation of China (no. 61134001 and 61203124), and Fundamental Research Funds for the Central Universities (2013YJS021).

References

- D. Hinrichsen and A. J. Pritchard, "Stochastic H_∞," SIAM Journal on Control and Optimization, vol. 36, no. 5, pp. 1504– 1538, 1998.
- [2] J. Zhang, M. Ren, Y. Tian, G. Hou, and F. Fang, "Constrained stochastic distribution control for nonlinear stochastic systems with non-Gaussian noises," *International Journal of Innovative Computing, Information and Control*, vol. 9, no. 4, pp. 1759–1767, 2013.
- [3] I. R. Petersen, V. A. Ugrinovskii, and A. V. Savkin, Robust control design using H_∞-methods, Springer, London, UK, 2000.
- [4] X. Su, L. Wu, P. Shi, and Y. D. Song, "H_{co} model reduction of Takagi-Sugeno fuzzy stochastic systems," *IEEE Transactions on Systems, Man, and Cybernetics B*, vol. 42, no. 6, pp. 1574–1585, 2012.
- [5] A. S. Willsky, "A survey of design methods for failure detection in dynamic systems," *Automatica*, vol. 12, no. 6, pp. 601–611, 1976.
- [6] L.-L. Fan and Y.-D. Song, "Neuro-adaptive model-reference fault-tolerant control with application to wind turbines," *IET Control Theory and Applications*, vol. 6, no. 4, pp. 475–486, 2012.
- [7] R. J. Veillette, J. B. Medanic, and W. R. Perkins, "Design of reliable control systems," *IEEE Transactions on Automatic Control*, vol. 37, no. 3, pp. 290–304, 1992.
- [8] Z. Wang, B. Huang, and K. J. Burnham, "Stochastic reliable control of a class of uncertain time-delay systems with unknown nonlinearities," *IEEE Transactions on Circuits and Systems*, vol. 48, no. 5, pp. 646–650, 2001.
- [9] G. Tao, S. M. Joshi, and X. L. Ma, "Adaptive state feedback and tracking control of systems with actuator failures," *IEEE Transactions on Automatic Control*, vol. 46, no. 1, pp. 78–95, 2001.
- [10] Z. Hu, Z. Han, and Z. Tian, "Fault detection and diagnosis for singular stochastic systems via B-spline expansions," ISA Transactions, vol. 48, no. 4, pp. 519–524, 2009.
- [11] M. L. Corradini and G. Orlando, "Actuator failure identification and compensation through sliding modes," *IEEE Transactions* on Control Systems Technology, vol. 15, no. 1, pp. 184–190, 2007.
- [12] P. Mhaskara, C. McFallb, A. Ganib, P. D. Christofidesb, and J. F. Davis, "Isolation and handling of actuator faults in nonlinear systems," *Automatica*, vol. 44, no. 1, pp. 53–62, 2008.
- [13] F. Tao and Q. Zhao, "Design of stochastic fault tolerant control for H_2 performance," *International Journal of Robust and Nonlinear Control*, vol. 17, no. 1, pp. 1–24, 2007.
- [14] Z.-H. Mao and B. Jiang, "Fault estimation and accommodation for networked control systems with transfer delay," *Acta Automatica Sinica*, vol. 33, no. 7, pp. 738–743, 2007.

- [15] W. Cai, X. H. Liao, and Y. D. Song, "Indirect robust adaptive fault-tolerant control for attitude tracking of spacecraft," *Journal* of Guidance, Control, and Dynamics, vol. 31, no. 5, pp. 1456–1463, 2008.
- [16] X. Su, L. Wu, and P. Shi, "Senor networks with random link failures: distributed filtering for T-S fuzzy systems," *IEEE Transactions on Industrial Informatics*, vol. 9, no. 3, pp. 1739–1750, 2013.
- [17] M. Zhong, S. Li, and Y. Zhao, "Robust H_{∞} fault detection for uncertain LDTV systems using Krein space approach," *International Journal of Innovative Computing, Information and Control*, vol. 9, no. 4, pp. 1637–1649, 2013.
- [18] D. P. Looze, J. L. Weiss, J. S. Eterno, and N. M. Barrett, "An automatic redesign approach for restructurable control systems," *IEEE Control Systems Magazine*, vol. 5, no. 2, pp. 16–22, 1985.
- [19] J. D. Boskovic, S.-H. Yu, and R. K. Mehra, "Stable adaptive fault-tolerant control of over actuated aircraft using multiple models, switching and tuning," in *Proceedings of the AIAA Guidance, Navigation and Control Conference*, pp. 739–749, Boston, Mass, USA, 1998.
- [20] J. D. Boskovic and R. K. Mehra, "Stable multiple model adaptive flight control for accommodation of a large class of control effector failures," in *Proceedings of the American Control Conference (ACC*,99), pp. 1920–1924, San Diego, Calif, USA, June 1999.
- [21] J. D. Boskovic, J. A. Jackson, R. K. Mehra, and N. T. Nguyen, "Multiple-model adaptive fault-tolerant control of a planetary lander," *Journal of Guidance, Control, and Dynamics*, vol. 32, no. 6, pp. 1812–1826, 2009.
- [22] M. A. Demetriou and M. M. Polycarpou, "Incipient fault diagnosis of dynamical systems using online approximators," *IEEE Transactions on Automatic Control*, vol. 43, no. 11, pp. 1612–1617, 1998.
- [23] A. T. Vemuri and M. M. Polycarpou, "Robust nonlinear fault diagnosis in input-output systems," *International Journal of Control*, vol. 68, no. 2, pp. 343–360, 1997.
- [24] X. Zhang, T. Parisini, and M. M. Polycarpou, "Adaptive fault-tolerant control of nonlinear uncertain systems: an information-based diagnostic approach," *IEEE Transactions on Automatic Control*, vol. 49, no. 8, pp. 1259–1274, 2004.
- [25] M. L. Corradini and G. Orlando, "A sliding mode controller for actuator failure compensation," in *Proceedings of the 42nd IEEE Conference on Decision and Control (CDC '03)*, pp. 4291–4296, Maui, Hawaii, USA, December 2003.
- [26] Q. Zhao and J. Jiang, "Reliable state feedback control system design against actuator failures," *Automatica*, vol. 34, no. 10, pp. 1267–1272, 1998.
- [27] G. Tao, S. Chen, and S. M. Joshi, "An adaptive actuator failure compensation controller using output feedback," *IEEE Transactions on Automatic Control*, vol. 47, no. 3, pp. 506–511, 2002.
- [28] G.-H. Yang and D. Ye, "Reliable H_{∞} control of linear systems with adaptive mechanism," *IEEE Transactions on Automatic Control*, vol. 55, no. 1, pp. 242–247, 2010.
- [29] X. Tang, G. Tao, and S. M. Joshi, "Adaptive actuator failure compensation for parametric strict feedback systems and an aircraft application," *Automatica*, vol. 39, no. 11, pp. 1975–1982, 2003.
- [30] X. D. Tang, G. Tao, and S. M. Joshi, "Adaptive actuator failure compensation for nonlinear MIMO systems with an aircraft

- control application," Automatica, vol. 43, no. 11, pp. 1869–1883, 2007.
- [31] G. Wang and Q. Zhang, "Robust control of uncertain singular stochastic systems with Markovian switching via proportional-derivative state feedback," *IET Control Theory & Applications*, vol. 6, no. 8, pp. 1089–1096, 2012.
- [32] C. Wang and Y. Shen, "Delay partitioning approach to robust stability analysis for uncertain stochastic systems with interval time-varying delay," *IET Control Theory & Applications*, vol. 6, no. 7, pp. 875–883, 2012.
- [33] R. Sakthivel, K. Mathiyalagan, and S. M. Anthoni, "Robust H_{∞} control for uncertain discrete-time stochastic neural networks with time-varying delays," *IET Control Theory & Applications*, vol. 6, no. 9, pp. 1220–1228, 2012.
- [34] J. Hu, Z. Wang, H. Gao, and L. K. Stergioulas, "Robust sliding mode control for discrete stochastic systems with mixed time delays, randomly occurring uncertainties, and randomly occurring nonlinearities," *IEEE Transactions on Industrial Electronics*, vol. 59, no. 7, pp. 3008–3015, 2012.
- [35] R. Z. Khasminskii, *Stochastic Stability of Differential Equations*, Sijthoff and Noordhoff, Amsterdam, The Netherlands, 1980.
- [36] P. A. Ioannou and J. Sun, *Robust Adaptive Control*, Prentice-Hall, Englewood Cliffs, NJ, USA, 1996.

Hindawi Publishing Corporation Abstract and Applied Analysis Volume 2014, Article ID 316206, 10 pages http://dx.doi.org/10.1155/2014/316206

Research Article

Dynamic Neural Network Identification and Decoupling Control Approach for MIMO Time-Varying Nonlinear Systems

Zhixi Shen and Kai Zhao

School of Automation, Chongqing University, Chongqing 400044, China

Correspondence should be addressed to Zhixi Shen; shenzhixi@cqu.edu.cn

Received 12 December 2013; Accepted 7 January 2014; Published 13 March 2014

Academic Editor: Xiaojie Su

Copyright © 2014 Z. Shen and K. Zhao. This is an open access article distributed under the Creative Commons Attribution License, which permits unrestricted use, distribution, and reproduction in any medium, provided the original work is properly cited.

Overcoming the coupling among variables is greatly necessary to obtain accurate, rapid and independent control of the real nonlinear systems. In this paper, the main methodology, on which the method is based, is dynamic neural networks (DNN) and adaptive control with the Lyapunov methodology for the time-varying, coupling, uncertain, and nonlinear system. Under the framework, the DNN is developed to accommodate the identification, and the weights of DNN are iteratively and adaptively updated through the identification errors. Based on the neural network identifier, the adaptive controller of complex system is designed in the latter. To guarantee the precision and generality of decoupling tracking performance, Lyapunov stability theory is applied to prove the error between the reference inputs and the outputs of unknown nonlinear system which is uniformly ultimately bounded (UUB). The simulation results verify that the proposed identification and control strategy can achieve favorable control performance.

1. Introduction

Coupling is a widespread phenomenon existing in nonlinear systems. Due to the existence of the coupling, the variables among systems often suffer impact from each other's fluctuations. Besides, time-varying and time delay is frequently encountered in many real control systems, and these may be the root of instability in the performance of closed-loop system. If the problems which have attracted many researchers cannot be solved effectively, they would not only delay achieving the steady states, but also realize the goal of independent control at all. Thereby, in order to achieve accurate, rapid, and independent control, it is essential to decouple among these variables and take the related methods. However, how to select the proper methodology according to the characteristics of control object is a thorny question.

In the open pieces of literature, the traditional decoupling ways to a multi-input multioutput (MIMO) system are primarily represented by frequency domain methods such as state variable method, diagonal dominance matrix, characteristic curve method, inverse Nyquist array, and relative gain analysis method [1]. These methods, which are based

on rigorous transfer functions or state spaces, play a significant role in decoupling the linear time-invariant systems. Nevertheless, these methods are hard to accomplish dynamic decoupling for uncertain, nonlinear, and time-variant MIMO systems because precise system models are difficult to develop for these systems. Hence, the above traditional decoupling methods are limited to a certain extent.

With the development of decoupling control, many other decoupling approaches, such as adaptive decoupling [2, 3], energy decoupling [4, 5], disturbance decoupling [6, 7], robust decoupling [8, 9], prediction decoupling, intelligent decoupling methods mainly represented by fuzzy decoupling [10], and neural network (NN) decoupling [11], have been proposed and applied in many real control practices. Adaptive decoupling has merits in decoupling a system with uncertain factors and can solve the system's uncertainty to some extent. However, the algorithm of adaptive controller has a large amount of calculation and is much time consumed [12] so that it is hard to be implemented in the processing of real-time control. Energy decoupling can be applied in linear uncertain systems, but, up to now, the method is also confined to the research stage [13]. Disturbance decoupling

[14, 15] tries to perfectly eliminate the external influences on system outputs, but the feasibility of this method has closer relationship with the development of nonlinear system differential geometry theory which is too strict and complex, so some researchers think this approach is very trouble to be widely used in the real control processes. Robust decoupling attempts to design a compensator with both good dynamic performance and strong robustness, but it is tough to deal well with the inner contradiction between the dynamic performance and the optimal decoupling controller parameters of robustness. Intelligent decoupling methods have obvious advantages in decoupling nonlinear systems and have received a lot of interest in decoupling control fields. The representative of intelligent decoupling methods, NN decoupling, has self-learning, adaptive, and fault tolerance abilities and is an universal approximator which has the capability of approximating any nonlinear function to any desired degree of accuracy, making it a useful tool for decoupling control in MIMO nonlinear systems. But NN decoupling commonly requires to be combined with other related algorithms to realize decoupling control [11, 16]. Fuzzy decoupling accomplishes the system decoupling by defuzzification based on the fuzzy rules which are often summarized by practical experiences. For the simple systems, it can be achieved easily, but for more complex MIMO nonlinear systems the accurate multidimensional fuzzy rules are very difficult, even impossible, to be established [17].

In practice, allowing for a complicated MIMO nonlinear system with uncertainty and strong coupling, the common PID controller with fixed parameters can hardly achieve the desired steady sate at all. At the same time, the physical system is often difficult to obtain accurate and faithful mathematical model so that the conventional control schemes based on precise mathematical model can hardly achieve good performance in the real control process. Motivated by the seminal paper [18], there is a continuously increasing interest in applying neural network to identification and control of nonlinear system. In structure, neural networks can be classified as dynamic and feedforward ones. However, most of practical applications use the feedforward structures [19, 20], which are suitable for the approximation of complex static functions. Nevertheless, the major shortcomings of such structure of neural networks in describing dynamic functions are that the weight updating does not utilize the information on the local date structure and the function approximation is sensitive to the purity of training data. On the other hand, the dynamic neural networks [21-24] incorporate feedback not merely having concise structure but more importantly having adaptive mechanism incorporated to fine tune the approximation accuracy and convergent speed. So dynamic neural network (DNN) is being developed, which is superior to the static neural network such as radial basis function (RBF) and backpropagation (BP) neural network on the dynamic characteristic [25, 26] recent years, and it is now widely applied in the fields of system identification and MIMO nonlinear control.

In this paper, we focus on developing an indirect adaptive NN controller for complex nonlinear systems including strong coupling, unknown or uncertain models, and

disturbances simultaneously. The proposed method is the combination of NN-based identifier and adaptive controller, and the controller is designed based on the identified NN model. The main merits of this paper can be summarized as follows.

- (1) A novel and generalized decoupling control strategy based on indirect adaptive control is presented for nonlinear systems. Firstly, we construct a dynamic neural network (DNN) identifier without coupling to replace the real coupled systems. Then, we design the adaptive controller to deal with the nonlinear systems based on DNN identifier models.
- (2) According to the Lyapunov methodology, the online weights updating laws of DNN are developed to accommodate the identification and to guarantee that the error between the DNN identifier and the real unknown systems is UUB.
- (3) According to the Lyapunov methodology, the adaptive control laws are designed to deal with modeling uncertainties, system nonlinearities, and external disturbances and to guarantee stable tracking performance of the real outputs related to the reference inputs.

This paper is structured in the following way. In Section 2, the problem formulation and preliminaries are presented, in which a general nonlinear dynamic system model and its neural network approximator are presented to establish a basis for designing and analyzing the system identification and control. In Section 3, a DNN-based identification algorithm is developed to approximate the nonlinear system. Section 4 proposed the adaptive decoupling control algorithm based on the DNN identifier. In Section 5, the whole procedure for the identification and control is described to provide a step by step guide for potential users. The simulation results demonstrate the effectiveness and generality of the proposed algorithm in Section 6. Finally, in Section 7 the conclusion is summarized.

2. Problem Formulation and Preliminaries

The equation of MIMO continuous-time-varying nonlinear coupling system can be generally described as

$$y = g(x, u, t), \tag{1}$$

where $x = [x_1, x_2, ..., x_n]^T$ is the state vector of nonlinear system, $u = [u_1, u_2, ..., u_n]^T$ is the bounded control input vector, $y = [y_1, y_2, ..., y_n]^T$ is the output vector, and $g(\cdot)$ is an unknown continuous nonlinear smooth function.

In this study, the following assumptions are imposed.

Assumption 1. The whole system can be decomposed as N coupling subsystems. The architecture of the multi-input multioutput nonlinear system is shown in Figure 1.

Assumption 2. All the states of system are bounded and measurable at every instant. The desired output trajectory and its first derivative are bounded.

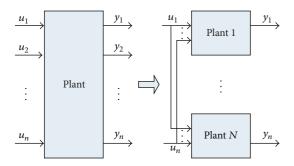


FIGURE 1: The architecture of the MIMO nonlinear system.

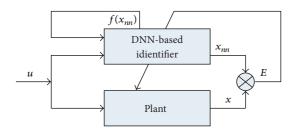


FIGURE 2: The architecture of system identification based on DNN.

In order to analyze the dynamic characteristic of nonlinear system more conveniently, we use the state-space equation to describe system (1) as follows:

$$\dot{x}_{1} = g_{1}(x, u_{1}, u_{2}, \dots, u_{n})$$

$$\dot{x}_{2} = g_{2}(x, u_{1}, u_{2}, \dots, u_{n})$$

$$\vdots$$

$$\dot{x}_{n} = g_{n}(x, u_{1}, u_{2}, \dots, u_{n})$$

$$y_{1} = x_{1}$$

$$y_{2} = x_{2}$$

$$\vdots$$

$$y_{n} = x_{n}.$$
(2)

By qualitatively analyzing the above model (2), it can be seen that the system is a coupling, time-varying, and uncertain nonlinear system. It is difficult, even impossible, to establish the accurate mathematical model and achieve prefect performance by using traditional decoupling control methods. In this paper, the dynamic neural network $g_{nn}(x_{nn})$ will be employed to approximate the continuous nonlinear function g(x), so that

$$g(x) = g_{nn}(x_{nn}). (3)$$

To identify the coupling, uncertain, and nonlinear dynamic system (2), we use dynamic neural network as the identifier and construct the identification structure as shown in Figure 2.

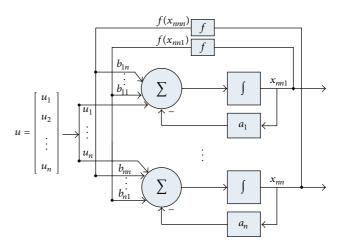


FIGURE 3: The architecture of DNN-based identifier.

We consider a single-layer, fully interconnected DNN as follows [25, 27]:

$$g_{nn}(x_{nn}) = \dot{x}_{nn} = Ax_{nn} + Bf(x_{nn}) + u,$$
 (4)

where $x_{nn} \in \Re^n$ is the state variables of DNN, $A = \operatorname{diag}[-a_1, \dots, -a_n] \in \Re^{n \times n}$, $a_i > 0$, $i = 1, \dots, n$ is the unknown matrix for the linear part of NN model, $B \in \Re^{n \times n}$ is the matrix of synaptic weights for nonlinear system feedback, $f(x_{nn}) = [f(x_{nn1}), \dots, f(x_{nnn})]^T$ is the vector of network feedback, $f(\cdot)$ represents the neuron activation function, and $u = [u_1, \dots, u_n]^T$ is the control force vector of adaptive controller, which will be designed subsequently. In this work, the architecture of DNN-based identifier is shown in Figure 3.

Remark 1. The real system is a coupling, time-varying, and uncertain nonlinear system. Since neural network is a universal approximator which is capable of approximating any nonlinear function to any desired degree of accuracy, we can use DNN model without coupling to replace the real coupled system. This idea motivates a novel and generalized decoupling control strategy based on indirect adaptive control as described in what follows. Using this basic idea, the specific design for DNN-based identifier can be developed in the next section.

3. System Identification Based on Neural Networks

The nonlinear system (2) can be approximated by the following continuous dynamic neural networks:

$$\dot{x} = A^* x + B^* f(x) + u,$$
 (5)

where A^* and B^* are ideal nominal constant matrices and the state and output variables are physically bounded.

In the process of approximating the time-varying, coupling, nonlinear system, DNN model (4) can be rewritten as follows:

$$\dot{x}_{nn} = \widehat{A}x_{nn} + \widehat{B}f(x_{nn}) + u, \tag{6}$$

where the activation function is specified as a monotonically increased function and bounded with

$$0 \le f(x) - f(y) \le k \cdot (x - y) \tag{7}$$

for any x, y, $k \in \Re$ and $x \le y$, k > 0, such as $f(x) = \tanh(x)$. The identification errors are defined as

$$E = x_m - x. (8)$$

From (5) and (6), we can obtain the error dynamics equation as follows:

$$\dot{E} = \dot{x}_{nn} - \dot{x}$$

$$= \left\{ \widehat{A}x_{nn} + \widehat{B}f\left(x_{nn}\right) + u \right\} - \left\{ A^*x + B^*f\left(x\right) + u \right\}$$

$$= \left(\widehat{A}x_{nn} - A^*x \right) + \left(\widehat{B}f\left(x_{nn}\right) - B^*f\left(x\right) \right)$$

$$= \widetilde{A}x_{nn} + A^*E + \widetilde{B}f\left(x_{nn}\right) + B^*\widetilde{f}\left(E\right),$$
(9)

where
$$\widetilde{A} = \widehat{A} - A^*$$
, $\widetilde{B} = \widehat{B} - B^*$, and $\widetilde{f}(E) = f(x_{nn}) - f(x)$.

Remark 2. In model (6), we use a DNN model without coupling to approximate the real coupled system (2). If we could develop effective weights updating laws of DNN model (6) to make the error (8) become zero or uniformly ultimately bounded, it is indicated that the DNN-based identifier without coupling has the ability of approximating the coupled, nonlinear systems, namely, instead of the real systems. Using this idea, the objective of decoupling among the subsystems would be realized.

Lemma 3. If $M \in \Re^{n \times n}$ is a positive define symmetric matrix and $q \in \Re^n$ is a vector arbitrarily, then there exist positive constants λ_{\min} and λ_{\max} such that

$$\lambda_{\min} \|q\|^2 \le q^T M q \le \lambda_{\max} \|q\|^2, \tag{10}$$

where $0 < \lambda_{min} \le \lambda_{max}$ denotes the minimum and maximum eigenvalues of M, respectively.

Lemma 4. If $L \in \mathbb{R}^{1 \times m}$, $M \in \mathbb{R}^{m \times n}$, and $Q \in \mathbb{R}^{n \times 1}$ are any real matrix, there is the following property:

$$\operatorname{tr}(LMQ) = \operatorname{tr}(MQL) = \operatorname{tr}(QLM) = LMQ.$$
 (11)

Theorem 5. Considering the identification model (6), the identification error (8) will be uniformly ultimately bounded (UUB) if the weights updating laws are as follows:

$$\dot{\widehat{A}} = -\Lambda_1 \left[E x_{nn}^T + \sigma_1 \widehat{A} \right],
\dot{\widehat{B}} = -\Lambda_2 \left[E f^T (x_{nn}) + \sigma_2 \widehat{B} \right],$$
(12)

where Λ_i is a free positive define symmetric constant matrix picked arbitrarily which is related to the approximation precision and $\sigma_i > 0$ is a design parameter introduced to ensure the boundedness of \hat{A} , \hat{B} (the term $\sigma_1 \hat{A}$ or $\sigma_2 \hat{B}$ in (12) is to make suitable corrections to prevent parameter drift).

Proof. Consider a Lyapunov function candidate as

$$V_{I1} = \frac{1}{2}E^{T}E. {(13)}$$

The time derivative of V_{I1} is given by

$$\dot{V}_{I1} = E^T \dot{E}. \tag{14}$$

Now applying the error dynamics equation (9) leads to

$$\dot{V}_{I1} = E^{T} \left\{ \widetilde{A} x_{nn} + A^{*} E + \widetilde{B} f \left(x_{nn} \right) + B^{*} \widetilde{f} \left(E \right) \right\}$$

$$= E^{T} \widetilde{A} x_{nn} + E^{T} A^{*} E + E^{T} \widetilde{B} f \left(x_{nn} \right) + E^{T} B^{*} \widetilde{f} \left(E \right).$$
(15)

According to the properties (7) of the active function,

$$E^{T}B^{*}\tilde{f}(E) = E^{T}B^{*}[f(x_{nn}) - f(x)]$$

$$\leq E^{T}B^{*}k(x_{nn} - x) = E^{T}B^{*}kE.$$
(16)

In the view of Lemma 4, (16) can be rewritten as

$$E^{T}B^{*}\tilde{f}(E) \leq \frac{1}{2}k^{2}E^{T}E + \frac{1}{2}E^{T}B^{*}(B^{*})^{T}E.$$
 (17)

Then, substituting (17) into (15) yields the following:

$$\dot{V}_{I1} \le E^{T} \widetilde{A} x_{nn} + E^{T} A^{*} E + E^{T} \widetilde{B} f (x_{nn})$$

$$+ \frac{1}{2} k^{2} E^{T} E + \frac{1}{2} E^{T} B^{*} (B^{*})^{T} E.$$
(18)

Namely,

$$\dot{V}_{I1} \leq E^{T} \widetilde{A} x_{nn} + E^{T} A^{*} E + E^{T} \widetilde{B} f (x_{nn})
+ \frac{1}{2} k^{2} E^{T} E + \frac{1}{2} E^{T} B^{*} (B^{*})^{T} E - \eta_{1} V_{I1} + \frac{\eta_{1}}{2} E^{T} E
= -\eta_{1} V_{I1} + E^{T} \left\{ \frac{\eta_{1}}{2} + A^{*} + \frac{1}{2} k^{2} + \frac{1}{2} B^{*} (B^{*})^{T} \right\} E
+ E^{T} \widetilde{A} x_{nn} + E^{T} \widetilde{B} f (x_{nn}),$$
(19)

where η_1 is a positive real number which is picked arbitrarily. As \widetilde{A} , \widetilde{B} contain the ideal weight matrices, we will cancel them in the following step:

$$V_{I2} = \frac{1}{2} \operatorname{tr} \left(\widetilde{A}^T \Lambda_1^{-1} \widetilde{A} + \widetilde{B}^T \Lambda_2^{-1} \widetilde{B} \right). \tag{20}$$

The time derivative of V_{I2} is given by

$$\dot{V}_{I2} = \operatorname{tr}\left(\widetilde{A}^T \Lambda_1^{-1} \dot{\widetilde{A}} + \widetilde{B}^T \Lambda_2^{-1} \dot{\widetilde{B}}\right) = \operatorname{tr}\left(\widetilde{A}^T \Lambda_1^{-1} \dot{\widehat{A}} + \widetilde{B}^T \Lambda_2^{-1} \dot{\widetilde{B}}\right). \tag{21}$$

Using the updating laws (12) and Lemma 4 yields

$$\dot{V}_{I2} = -\operatorname{tr}\left[\widetilde{A}^{T}Ex_{nn}^{T}\right] - \sigma_{1}\operatorname{tr}\left(\widetilde{A}^{T}\widehat{A}\right)
-\operatorname{tr}\left[\widetilde{B}^{T}Ef^{T}\left(x_{nn}\right)\right] - \sigma_{2}\operatorname{tr}\left(\widetilde{B}^{T}\widehat{B}\right)
= -E^{T}\widetilde{A}x_{nn} - E^{T}\widetilde{B}f\left(x_{nn}\right) - \sigma_{1}\operatorname{tr}\left(\widetilde{A}^{T}\widehat{A}\right) - \sigma_{2}\operatorname{tr}\left(\widetilde{B}^{T}\widehat{B}\right).$$
(22)

At the same time, it is clear that

$$\widetilde{A}^T \widehat{A} = \widetilde{A}^T \left(\widetilde{A} + A^* \right) = \widetilde{A}^T \widetilde{A} + \widetilde{A}^T A^*$$

$$\geq \frac{1}{2} \widetilde{A}^T \widetilde{A} - \frac{1}{2} (A^*)^T A^*, \tag{23}$$

$$\widetilde{B}^T\widehat{B} = \widetilde{B}^T \left(\widetilde{B} + B^*\right) \geq \frac{1}{2}\widetilde{B}^T\widetilde{B} - \frac{1}{2} \big(B^*\big)^T B^*.$$

Substituting (23) into (22), we can obtain that

$$\dot{V}_{I2} \leq -E^{T} \widetilde{A} x_{nn} - E^{T} \widetilde{B} f \left(x_{nn} \right)
- \frac{\sigma_{1}}{2} \operatorname{tr} \left(\widetilde{A}^{T} \widetilde{A} \right) + \frac{\sigma_{1}}{2} \operatorname{tr} \left(\left(A^{*} \right)^{T} A^{*} \right)
- \frac{\sigma_{2}}{2} \operatorname{tr} \left(\widetilde{B}^{T} \widetilde{B} \right) + \frac{\sigma_{2}}{2} \operatorname{tr} \left(\left(B^{*} \right)^{T} B^{*} \right).$$
(24)

In the view of Lemma 3, we can obtain the following property:

$$\widetilde{A}^{T} \Lambda_{1}^{-1} \widetilde{A} \leq \lambda_{\max(\Lambda_{1}^{-1})} \widetilde{A}^{T} \widetilde{A},$$

$$\widetilde{B}^{T} \Lambda_{2}^{-1} \widetilde{B} \leq \lambda_{\max(\Lambda_{2}^{-1})} \widetilde{B}^{T} \widetilde{B}.$$
(25)

Using the characteristics of the positive define matrices (25), (24) can be rewritten as

$$\dot{V}_{I2} \leq -E^{T}\widetilde{A}x_{nn} - E^{T}\widetilde{B}f\left(x_{nn}\right) + \frac{\sigma_{1}}{2}\operatorname{tr}\left(\left(A^{*}\right)^{T}A^{*}\right)
+ \frac{\sigma_{2}}{2}\operatorname{tr}\left(\left(B^{*}\right)^{T}B^{*}\right) - \frac{\sigma_{1}}{2\lambda_{\max(\Lambda_{1}^{-1})}}\operatorname{tr}\left(\widetilde{A}^{T}\Lambda_{1}^{-1}\widetilde{A}\right)
- \frac{\sigma_{2}}{2\lambda_{\max(\Lambda_{2}^{-1})}}\operatorname{tr}\left(\widetilde{B}^{T}\Lambda_{2}^{-1}\widetilde{B}\right)
\leq -\eta_{2}V_{I2} - E^{T}\widetilde{A}x_{nn} - E^{T}\widetilde{B}f\left(x_{nn}\right)
+ \frac{\sigma_{1}}{2}\operatorname{tr}\left(\left(A^{*}\right)^{T}A^{*}\right) + \frac{\sigma_{2}}{2}\operatorname{tr}\left(\left(B^{*}\right)^{T}B^{*}\right),$$
(26)

where $\eta_2 = \min(\sigma_i/\lambda_{\max(\Lambda_i^{-1})})$, i = 1, 2.

We choose the following Lyapunov function $V_I = V_{I1} + V_{I2}$, and its time derivative is

$$\dot{V}_{I} = \dot{V}_{I1} + \dot{V}_{I2}
\leq -\eta_{1} V_{I1} + E^{T} \left\{ \frac{\eta_{1}}{2} + A^{*} + \frac{1}{2} k^{2} + \frac{1}{2} B^{*} (B^{*})^{T} \right\} E
- \eta_{2} V_{I2} + \frac{\sigma_{1}}{2} \operatorname{tr} \left((A^{*})^{T} A^{*} \right) + \frac{\sigma_{2}}{2} \operatorname{tr} \left((B^{*})^{T} B^{*} \right)
\leq -\eta V_{I} + E^{T} \Psi E + \Omega,$$
(27)

where

$$\Omega = \frac{\sigma_1}{2} \operatorname{tr} \left((A^*)^T A^* \right) + \frac{\sigma_2}{2} \operatorname{tr} \left((B^*)^T B^* \right) > 0,$$

$$\Psi = \frac{\eta_1}{2} + A^* + \frac{1}{2} k^2 + \frac{1}{2} B^* (B^*)^T,$$

$$\eta = \min(\eta_1, \eta_2) > 0.$$
(28)

Make Ψ < 0 to specify A^* as follows:

$$A^* < -\left(\frac{\eta_1}{2} + \frac{1}{2}k^2 + \frac{1}{2}B^*(B^*)^T\right). \tag{29}$$

Therefore we arrive at

$$\dot{V}_I < -\eta V_I + \Omega \tag{30}$$

and it can be concluded that

$$V_{I} < \left(V_{I}\left(0\right) - \frac{\Omega}{\eta}\right) \exp\left(-\eta t\right) + \frac{\Omega}{\eta}.$$
 (31)

We assume that $V_I(0) = 0$; then

$$V_I < \left(-\frac{\Omega}{\eta}\right) \exp\left(-\eta t\right) + \frac{\Omega}{\eta}.$$
 (32)

As $V_I > (1/2)E^T E$, then

$$\lim_{t \to \infty} ||E|| = \sqrt{\frac{2\Omega}{\eta}}.$$
 (33)

According to the Boundedness Theorem [5], we can get the error using dynamic neural network to approximate the nonlinear system which is uniformly ultimately bounded (UUB) and converges to a set containing origin with a rate at least as fast as $e^{-\eta t/2}$.

4. Adaptive Decoupling Control Based on System Identification

In this section, the aim of controller design is to drive outputs of system properly following a prespecified trajectory. In addition, model errors of DNN-based identifier and external disturbances should be considered. The architecture of indirect adaptive control for the time-varying, coupling, and nonlinear system is shown in Figure 4, which combines the dynamic neural network and the adaptive controller.

In Figure 4, x represents the real outputs, and x_{nn} is the identification outputs of dynamic neural network. According to the errors E, the identification model of dynamic neural network is used to approximate the unknown nonlinear system. x_d is the reference inputs, E_d is the errors between the given value x_d and real output x in every instant, and u is the manipulated variables.

In Section 3, we know that the nonlinear system can be modeled by DNN-based identifier with the weights updating laws (12). In this section, we should consider model errors and external disturbances. If

$$q_{nn}(x_{nn}) = q(x) - \tilde{q}, \tag{34}$$

the nonlinear system can be represented as follows:

$$\dot{x} = \widehat{A}x_{nn} + \widehat{B}f(x_{nn}) + u + \widetilde{q}, \tag{35}$$

where \tilde{g} is the lump model errors and external disturbances, which is assumed to be bounded and $|\tilde{g}| < d^*$, d^* is an unknown constant.

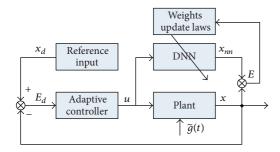


FIGURE 4: The architecture of indirect adaptive decoupling control.

The desired reference inputs x_d are defined as follows:

$$\dot{x}_d = h_d(t). \tag{36}$$

The states errors E_d are defined as follows:

$$E_d = x - x_d. (37)$$

So we can obtain the errors dynamics equation as follows:

$$\dot{E}_d = \dot{x} - \dot{x}_d = \widehat{A}x_{nn} + \widehat{B}f(x_{nn}) + u + \widetilde{g} - h_d. \tag{38}$$

Then, we design the control action u as follows:

$$u = u_c + u_r, \tag{39}$$

where u_c is a compensation action for the nonlinearity and u_r is dedicated to deal with the model errors and external disturbances.

Remark 6. If model errors and external disturbances are zero or negligible, u_r can be chosen to be zero and will drive the error dynamics to converge to the origin. From the control point of view, the system stability will not be affected. However, even if the DNN-based identifier has superb learning ability to represent the dynamic process of nonlinear system, model errors and environment disturbances are sometimes inevitable or even may affect the system stability. So the following controller design will consider this factor and will be suitable for general situations.

Theorem 7. The states errors (37) between reference model and real output will asymptotically converge to zero, if the adaptive control laws are as follows:

$$u_{c} = -\widehat{A}x_{nn} - \widehat{B}f(x_{nn}) + h_{d},$$

$$u_{r} = -k_{0} \cdot E_{d} - \operatorname{diag}(\operatorname{sgn}(E_{d})) \cdot \widehat{d}$$

$$\dot{\widehat{d}} = ||E_{d}||.$$
(40)

Proof. Substituting (40) into (38), we can obtain the equation as follows:

$$\dot{E}_{d} = \dot{x} - \dot{x}_{d}$$

$$= \widehat{A}x_{nn} + \widehat{B}f(x_{nn}) - \widehat{A}x_{nn} - \widehat{B}f(x_{nn}) + h_{d}$$

$$- k_{0} \cdot E_{d} - \operatorname{diag}(\operatorname{sgn}(E_{d})) \cdot \widehat{d} + \widetilde{g} - h_{d}$$

$$= -k_{0} \cdot E_{d} - \operatorname{diag}(\operatorname{sgn}(E_{d})) \cdot \widehat{d} + \widetilde{g}.$$
(41)

Consider the Lyapunov function candidate of controller design as follows:

$$V_C = \frac{1}{2} E_d^T E_d + \frac{1}{2} \tilde{d}^T \tilde{d}.$$
 (42)

We can obtain the time derivative of the Lyapunov function candidate (42) as follows:

$$\dot{V}_C = E_d^T \dot{E}_d + \tilde{d}^T \dot{\tilde{d}}. \tag{43}$$

Then, substituting (41) into (43),

$$V_{C}$$

$$= E_{d}^{T} \left[-k_{0}E_{d} - \operatorname{diag}\left(\operatorname{sgn}\left(E_{d}\right)\right) \cdot \hat{d} + \tilde{g} \right] + \tilde{d}^{T}\dot{\tilde{d}}$$

$$= E_{d}^{T} \left[-k_{0}E_{d} - \operatorname{diag}\left(\operatorname{sgn}\left(E_{d}\right)\right) \cdot \hat{d} + \tilde{g} \right] + \tilde{d}^{T}\dot{\tilde{d}}$$

$$= -k_{0}E_{d}^{T}E_{d} - \left\| E_{d}^{T} \right\| \hat{d} + E_{d}^{T}\tilde{g} + \tilde{d}^{T}\dot{\tilde{d}}$$

$$\leq -k_{0}E_{d}^{T}E_{d} - \left\| E_{d}^{T} \right\| \hat{d} + \left\| E_{d}^{T} \right\| \left\| \tilde{g} \right\| + \tilde{d}^{T}\dot{\tilde{d}}$$

$$\leq -k_{0}E_{d}^{T}E_{d} - \left\| E_{d}^{T} \right\| \hat{d} + \left\| E_{d}^{T} \right\| d^{*} + \tilde{d}^{T}\dot{\tilde{d}}$$

$$= -k_{0}E_{d}^{T}E_{d} - \left\| E_{d}^{T} \right\| \tilde{d} + \tilde{d}^{T}\dot{\tilde{d}}$$

$$= -k_{0}E_{d}^{T}E_{d} - \left\| E_{d}^{T} \right\| \tilde{d} + \tilde{d}^{T}\dot{\tilde{d}}$$

$$= -k_{0}E_{d}^{T}E_{d}$$

$$< 0.$$

where $\tilde{d} = \hat{d} - d^*$.

Thus, we have $V_C \in \ell_\infty$, implying that $E_d \in \ell_2 \cap \ell_\infty$, $\widehat{d} \in \ell_\infty$. From (38), it is readily shown that $\dot{E}_d \in \ell_\infty$; namely, E_d is uniformly continuous. According to $\dot{V}_C \leq -k_0 E_d^{\ T} E_d \leq 0$, we can obtain $\int_0^t k_0 E_d^{\ T} E_d d\tau \leq V_C(0) < \infty$. By Barbalat's lemma, it can be concluded that $E_d \to 0$ and $x \to x_d$ as $t \to \infty$.

The online computational algorithm for the system identification and controller design will be described in next section.

Remark 8. If considering the identification and control as a whole process, we can prove the system stability by defining the final Lyapunov function candidate as $V = V_I + V_C$. Since the stability of system identification and adaptive control has already been proven in Theorems 5 and 7, respectively, we can make a conclusion that the errors between the real system states and the desired reference inputs are uniformly ultimately bounded (UUB).

5. Algorithm for Implement

In this section, a step by step procedure is listed to implement the identification and control strategy.

Step 1. Assign the initial values of gain matrices Λ_i and σ_i in weight updating laws, and the initial values of the estimated parameters \widehat{A} , \widehat{B} .

Step 2. Based on the initial states x(0) and system inputs u, calculate the states of neural network x_{nn} according to (6).

Step 3. Calculate the new parameter values of \widehat{A} , \widehat{B} by weight updating laws (12) and then calculate the state variables x_{nn} once again.

Step 4. Choose the suitable control gain k and calculate the values of u_c and u_r according to Theorem 7.

Step 5. Go to Step 2.

This is the algorithm of online identification and control scheme for the MIMO system with time varying, coupling, and nonlinearity.

6. Simulation Example

In this section, in order to verify the effectiveness of indirect adaptive controller based on DNN, we choose a coupled two-input two-output, time-varying, nonlinear system as the simulation model

$$\dot{x}_1 = -2x_1 + 5\operatorname{sign}(x_2) + u_1 + u_2,$$

$$\dot{x}_2 = -0.8x_1 - 3x_2 + 5\operatorname{sign}(x_2) - 1.2u_1 + 0.8u_2,$$
(45)

where x_1 and x_2 are state variables and u_1 and u_2 are control inputs. As a coupled system, u_1 and u_2 can impact every subsystem, respectively.

6.1. Nonlinear System Identification. It is assumed that the structure of two-input two-output system is a black box system. In this experiment, this test was to validate the feasibility of the proposed DNN-based identifier to approximate the unknown, coupled, and nonlinear system.

In this study, $u_1 = 4\sin(0.2t)$, $u_2 = 4\cos(0.6t)$. The DNN model was selected as follows:

$$\dot{x}_{nn} = \widehat{A}x_{nn} + \widehat{B}f(x_{nn}) + u \tag{46}$$

which was structured with single layer, 2 neurons and the activation functions were selected as hyperbolic tangent; namely, $\tanh(x) = (e^x - e^{-x})/(e^x + e^{-x})$. Assigned the initials $\widehat{A}(0)$ and $\widehat{B}(0)$ as null matrices, $\Lambda_i = \begin{bmatrix} 6000 & 550 \\ 50 & 6000 \end{bmatrix}$, $\sigma_1 = 0.1$, and $\sigma_2 = 0.02$. Then run the online identification procedure and the whole process was run for 50s. The identification results are shown in Figures 5 and 6.

The real system (45) is a coupled nonlinear system, and the DNN model (46) is constructed without coupling. We use the DNN (46) to approximate the real system (45) on the basis of the weights updating laws (12) which is derived by the Lyapunov method. In Figures 5 and 6, x_1 and x_2 are the state variables of the real system, x_{nn1} and x_{nn2} are the state variables of the DNN model, and E_1 and E_2 stand for the errors of state variables between the real system and the DNN model. We can explicitly see that the errors are small enough and the effectiveness of the DNN model according to the relevant algorithm although the DNN model has no coupling features.

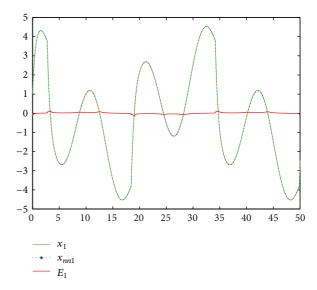


FIGURE 5: Identification result for system state x_1 .

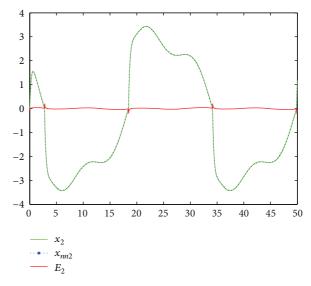


FIGURE 6: Identification result for system state x_2 .

6.2. Nonlinear System Control. Although the DNN has the ability to approximate any nonlinear systems, however, the DNN model errors and environment disturbances are inevitable in the real systems. In the control point of view, we should consider these factors which include neural network model errors and uncertain disturbance forces acting on the real nonlinear systems.

The control objective is to make the real outputs of the unknown, coupled, and MIMO nonlinear systems tracking the perspecified inputs; namely, the system states $x = [x_1, x_2]^T$ to follow the prespecified inputs $x_d = [x_{d1}, x_{d2}]^T$. So a comprehensive control scheme was shown in Section 4, and the controller designed could deal with the compensation of the nonlinearity, the uncertain model errors, and environment disturbances.

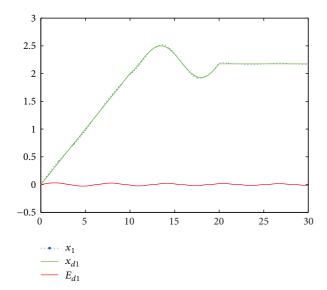


FIGURE 7: Trajectory tracking result for system state x_1 .

In the view of this paper, the real systems can be formulated as

$$\dot{x} = \widehat{A}x_{nn} + \widehat{B}f\left(x_{nn}\right) + u + \widetilde{g}\left(t\right),\tag{47}$$

where $\tilde{g} = (\tilde{g}_1, \tilde{g}_2)^T$ represents the lump model errors and disturbances.

In this study, first we simply define $\tilde{g}_1 = 0.8 \sin(t)$, $\tilde{g}_2 = 1.5 \cos(t)$ and the reference model inputs are defined as

$$\dot{x}_{d1} = \dot{x}_{d2} = \begin{cases} 0.2 & 0 \le t \le 10\\ \sin(0.7t) & 10 \le t \le 20\\ 0 & 20 \le t. \end{cases}$$
 (48)

In fact, the desired inputs x_{d1} and x_{d2} are the piecewise functions of ramp signal, cosine signal, and step signal.

By using the DNN-based identifier to approximate the real systems, the adaptive controller is designed as follows:

$$u_{c} = -\widehat{A}x_{nn} - \widehat{B}f(x_{nn}) + h_{d},$$

$$u_{r} = -k_{0} \cdot E_{d} - \operatorname{diag}(\operatorname{sgn}(E_{d})) \cdot \widehat{d}$$

$$\dot{\widehat{d}} = ||E_{d}||.$$
(49)

Assigned the initials $\widehat{A}(0)$ and $\widehat{B}(0)$ as null matrices, $\Lambda_i = \begin{bmatrix} 6000 & 50 \\ 50 & 6000 \end{bmatrix}$, $\sigma_1 = 0.1$, $\sigma_2 = 0.02$, and $k_0 = 25$. Then run the proposed controller design procedure and the whole process was run for 30 s. The response curves of trajectory tracking are shown in Figures 7 and 8.

In Figures 7 and 8, x_1 and x_2 are the state variables identified by DNN model, x_{d1} and x_{d2} are the reference input signals, and E_{d1} and E_{d2} stand for the errors of trajectory tracking. We can see no matter how the reference input signals change; E_{d1} and E_{d2} are bounded as time goes by when considering the model errors and environment disturbances. At the same time, there is no large magnitude of overshoot

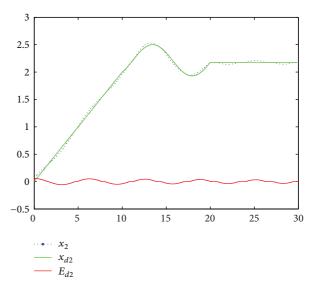


FIGURE 8: Trajectory tracking result for system state x_2 .

in the response curves. It is concluded that the proposed adaptive controller is able to achieve excellent dynamic performance and high antidisturbance capability in trajectory tracking, which agrees with our theoretic prediction.

For the purpose of verifying the generality and effectiveness of the proposed method for more complex nonlinear signal, we choose another reference input signal as follows:

$$\dot{x}_{d1} = \sin t,
\dot{x}_{d2} = \cos t.$$
(50)

The lump model errors and disturbances \tilde{g}_i are defined as the square signals

$$\widetilde{g}_1 = 4 \text{ square } (0.5, t),$$

$$\widetilde{g}_2 = 3 \text{ square } (1, t).$$
(51)

And the other conditions are the same with the above. The response curves of trajectory tracking are shown in Figures 9 and 10.

From Figures 9 and 10, there is explicitly fluctuation in the first 20 s, but the errors are always bounded and become smaller and smaller as time goes on. And the simulation results once again demonstrate the effectiveness of the proposed control scheme, and it can be observed with the excellent performance of the system states following the prespecified inputs.

7. Conclusion

In this paper, we present the DNN identification and adaptive control strategy for the real systems which is of nonlinearity, coupling, and uncertain environment disturbances. According to the Lyapunov methodology, the weights updating laws of DNN-based identifier and the control laws of indirect adaptive controller have been derived to ensure the stability

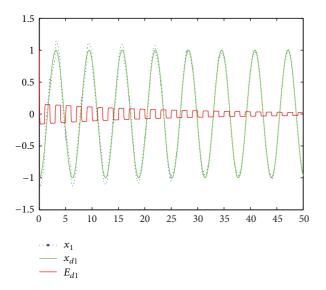


FIGURE 9: Trajectory tracking result for system state x_1 .

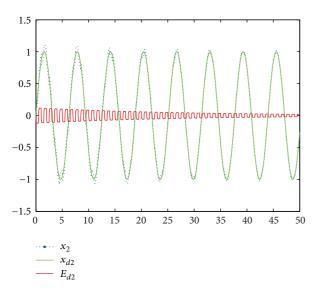


FIGURE 10: Trajectory tracking result for system state x_2 .

of decoupling control and to achieve favorable tracking performance for the real system. The simulation results have indicated that the success of decoupling and the proper dynamic response of the plant states to follow the desired input trajectories.

Conflict of Interests

The authors declare that there is no conflict of interests regarding the publication of this paper.

Acknowledgments

This work was supported by the Fundamental Research Funds for the Central Universities (no. CDJZR10170007) and

the National Key Basic Research and Development Program of China (973 Program) (no. 2012CB215202).

References

- [1] X. Z. Wang, "A Summary of multivariable decoupling methods," *Journal of Shenyang Architectural and Civil Engineering*, vol. 16, no. 2, pp. 143–145, 2000.
- [2] T. Y. Chai, S. J. Lang, and X. Y. Gu, "A generalized self-tuning feed forward controller and multivariable application," in *Processings of 24th IEEE Conference on Decision and Control*, pp. 862–867, 1985.
- [3] B. Wittenmark, R. H. Middleton, and G. C. Goodwin, "Adaptive decoupling of multivariable systems," *International Journal of Control*, vol. 46, no. 6, pp. 1993–2009, 1987.
- [4] W. J. Mao and J. Chu, "Input-output energy decoupling of linear time-invariant systems," *Control Theory & Applications*, vol. 19, no. 1, pp. 146–148, 2002.
- [5] X. Z. Dong and Q. L. Zhang, "Input-output energy decoupling of linear singular systems," *Journal of Northeastern University*, vol. 25, no. 6, pp. 523–526, 2004.
- [6] Z. Gao, "Active disturbance rejection control: a paradigm shift in feedback control system design," in *Proceedings of the American Control Conference*, pp. 2399–2405, June 2006.
- [7] Q. Zheng, Z. Chen, and Z. Gao, "A practical approach to disturbance decoupling control," *Control Engineering Practice*, vol. 17, no. 9, pp. 1016–1025, 2009.
- [8] T. E. Djaferis, Robust Decoupling for Systems With Parameters Modeling, Identification and Robust Control, B V North-Holland, Elsevier Science, 1986.
- [9] G. Z. Pang and Z. Y. Chen, "The relation between robust stability and robust diagonal dominance," *Acta Atuomatic Sinica*, vol. 18, no. 3, pp. 273–281, 1992.
- [10] T. H. Lee, J. H. Nie, and M. W. Lee, "A fuzzy controller with decoupling for multivariable nonlinear servo-mechanisms, with application to real-time control of a passive line-of-sight stabilization system," *Mechatronics*, vol. 7, no. 1, pp. 83–104, 1997.
- [11] H. Li, "Design of multivariable fuzzy-neural network decoupling controller," *Kongzhi yu Juece/Control and Decision*, vol. 21, no. 5, pp. 593–596, 2006.
- [12] J. Maldacena, "The large-*N* limit of superconformal field theories and supergravity," *International Journal of Theoretical Physics*, vol. 38, no. 4, pp. 1113–1133, 1999, Quantum gravity in the southern cone (Bariloche, 1998).
- [13] Y. B. Dai, W. D. Yang, and S. F. Wang, "A summary of multivariable predictive decoupling control methods," *Electrical Automation*, vol. 30, no. 6, pp. 1–3, 2008.
- [14] R. Pothin, "Disturbance decoupling for a class of nonlinear MIMO systems by static measurement feedback," *Systems & Control Letters*, vol. 43, no. 2, pp. 111–116, 2001.
- [15] Q. X. Gong, Research on disturbance decoupling and attenuation control for nonlinear systems, [Doctor dissertation of Northeastern University], 2008.
- [16] L. M. Wu and T. Y. Chai, "A neural network decoupling strategy for a class of nonlinear discrete time systems," *Acta Atuomatic Sinica*, vol. 23, no. 2, pp. 207–212, 1997.
- [17] X. Su, P. Shi, L. Wu, and Y. D. Song, "Novel control design on discrete-time Takagi-Sugeno fuzzy systems with time-varying delays," *IEEE Transactions on Fuzzy Systems*, vol. 20, no. 6, pp. 655–671, 2013.

- [18] K. S. Narendra and K. Parthasarathy, "identification and control of dynamical systems using neural networks," *IEEE Transac*tions on Neural Networks, vol. 1, no. 1, pp. 4–27, 1990.
- [19] M. M. Gupta and D. H. Rao, Neuro-Control Systems: Theory and Applications, IEEE Press, Piscataway, NJ, USA, 1994.
- [20] K. Hunt, G. Irwin, and K. Warwick, Neural Networks Engineering in Dynamic Control Systems: Advances in Industrial Control, Springer, New York, NY, USA, 1995.
- [21] Y. Kourd, D. Lefebvre, and N. Guersi, "Fault diagnosis based on neural networks and decision trees: application to DAMADICS," *International Journal of Innovative Computing, Information and Control*, vol. 9, no. 8, pp. 3185–3196, 2013.
- [22] P. L. Liu, "Delay-dependent robust stability analysis for recurrent neural networks with time-varying delay," *International Journal of Innovative Computing, Information and Control*, vol. 9, no. 8, pp. 3341–3355, 2013.
- [23] S. Sefriti, J. Boumhidi, M. Benyakhlef, and I. Boumhidi, "Adaptive decentralized sliding mode neural network control of a class of nonlinear interconnected systems," *International Journal of Innovative Computing, Information and Control*, vol. 9, no. 7, pp. 2941–2947, 2013.
- [24] X. Su, Z. Li, Y. Feng, and L. Wu, "New global exponential stability criteria for interval-delayed neural networks," *Proceedings of the Institution of Mechanical Engineers I: Journal of Systems and Control Engineering*, vol. 225, no. 1, pp. 125–136, 2011.
- [25] C.-H. Wang, P.-C. Chen, P.-Z. Lin, and T.-T. Lee, "A dynamic neural network model for nonlinear system identification," in Proceedings of the IEEE International Conference on Information Reuse and Integration, IRI 2009, pp. 440–441, August 2009.
- [26] X.-J. Wu, Q. Huang, and X.-J. Zhu, "Power decoupling control of a solid oxide fuel cell and micro gas turbine hybrid power system," *Journal of Power Sources*, vol. 196, no. 3, pp. 1295–1302, 2011.
- [27] Z. J. Fu, W. F. Xie, X. Han, and W. D. Luo, "Nonlinear system identification and control via dynamic multitime scales neural networks," *IEEE Transactions on Neural Networks and Learning Systems*, vol. 24, no. 11, pp. 1814–1823, 2013.

Hindawi Publishing Corporation Abstract and Applied Analysis Volume 2014, Article ID 836378, 9 pages http://dx.doi.org/10.1155/2014/836378

Research Article

Prescribed Performance Fuzzy Adaptive Output-Feedback Control for Nonlinear Stochastic Systems

Lili Zhang, Shuai Sui, and Shaocheng Tong

Department of Basic Mathematics, Liaoning University of Technology, Jinzhou, Liaoning 121000, China

Correspondence should be addressed to Lili Zhang; lutzhanglili@163.com

Received 4 January 2014; Accepted 4 February 2014; Published 12 March 2014

Academic Editor: Ming Liu

Copyright © 2014 Lili Zhang et al. This is an open access article distributed under the Creative Commons Attribution License, which permits unrestricted use, distribution, and reproduction in any medium, provided the original work is properly cited.

A prescribed performance fuzzy adaptive output-feedback control approach is proposed for a class of single-input and single-output nonlinear stochastic systems with unmeasured states. Fuzzy logic systems are used to identify the unknown nonlinear system, and a fuzzy state observer is designed for estimating the unmeasured states. Based on the backstepping recursive design technique and the predefined performance technique, a new fuzzy adaptive output-feedback control method is developed. It is shown that all the signals of the resulting closed-loop system are bounded in probability and the tracking error remains an adjustable neighborhood of the origin with the prescribed performance bounds. A simulation example is provided to show the effectiveness of the proposed approach.

1. Introduction

In the past decade, control design and stability analysis on stochastic systems have received considerable attention, since stochastic modeling has come to play an important role in many real systems, including nuclear processes, thermal processes, chemical processes, biology, socioeconomics, and immunology [1-4]. Especially, the investigations on the control design methods of nonlinear stochastic systems have received more attention in recent years based on backstepping technique. For example, the adaptive backstepping control problem has been investigated in [5] for a class of SISO strict-feedback stochastic systems by a risk-sensitive cost criterion. An output-feedback stabilization method has been proposed for a class of strict-feedback stochastic nonlinear systems by using the quartic Lyapunov function in [6]. Two backstepping control design approaches have been developed for nonlinear stochastic systems with the Markovian switching in [7, 8]. By using a linear reduced-order state observer, several different output-feedback controllers have been developed for strict-feedback nonlinear stochastic systems with unmeasured states, such as tracking control [9], decentralized control [10], and time-delay systems [11]. However, these proposed control methods are only suitable for

those nonlinear stochastic systems with nonlinear dynamic models known exactly or with the unknown parameters appearing linearly with respect to known nonlinear functions. To cope with the problems that the nonlinear dynamic models are unknown or the system uncertainties are not linearly parameterized, the adaptive output-feedback control approaches have been proposed for a class of uncertain nonlinear stochastic systems by using neural networks in [12, 13]. The decentralized adaptive neural networks control methods have been developed in [14, 15] for a class of uncertain large-scale nonlinear stochastic systems on the basis of [12, 13].

Although the adaptive neural networks backstepping control approaches in [12–15] can solve the problem of the unmeasured states by designing a linear state observer, there is a limit; that is, uncertain terms are only the functions of the output of the controlled systems, not related to the other states variables. To solve this limit, some adaptive fuzzy output feedback control methods have been proposed for a class of nonlinear stochastic systems by designing nonlinear fuzzy state observers in [16–18].

It should be mentioned that the control methods [12–18] can only solve output-feedback stabilization problem and cannot solve the output feedback tracking control problem.

In addition, the tracking performance in the above control methods confined to converge to a small residual set, whose size depends on the design parameters and some unknown bounded terms; they cannot offer the guaranteed transient performance at time instants. As we know, the practical engineering often requires the proposed control scheme to satisfy certain quality of the performance indices, such as overshoot, convergence rate, and steady-state error. Prescribed performance issues are extremely challenging and difficult to be achieved, even in the case of the nonlinear behavior of the system in the presence of unknown uncertainties and external disturbances. More recently, a design solution called prescribed performance control for the problem has been proposed in [19] for a class of feedback linearization nonlinear systems and was extended to the class of nonlinear systems in [20]. Its main idea is to introduce predefined performance bounds of the tracking errors and is able to adjust control performance indices. However, to the author's best knowledge, by far, the prescribed performance design methodology has not been applied to nonlinear strictfeedback systems with unknown functions and immeasurable states, which is important and more practical; thus, it has motivated us for this study.

In this paper, an adaptive fuzzy output-feedback control design with prescribed performance is developed for a class of uncertain SISO nonlinear stochastic systems with unmeasured states. With the help of fuzzy logic systems identifying the unknown nonlinear systems, a fuzzy adaptive observer is developed to estimate the immeasurable states. The backstepping control design technique based on predefined performance bounds is presented to design adaptive fuzzy output-feedback controller. It is shown that all the signals of the resulting closed-loop system are bounded in probability. Moreover, the tracking error converges to an adjustable neighborhood of the origin and remains within the prescribed performance bounds. Compared with the existing results, the main advantages of the proposed control scheme are as follows: (i) the restrictive assumption that all the states of the system be measured directly can be removed by designing a state observer; and (ii) by introducing predefined performance, the proposed adaptive control method can ensure that the tracking error converges to a predefined arbitrarily small residual set.

2. System Descriptions and Preliminaries

2.1. Nonlinear System Descriptions. Consider the following SISO strict-feedback nonlinear stochastic system:

$$\begin{aligned} dx_1 &= \left(x_2 + f_1\left(x_1\right) + d_1\left(t\right)\right) dt + g_1\left(x\right) dw, \\ dx_2 &= \left(x_3 + f_2\left(\overline{x}_2\right) + d_2\left(t\right)\right) dt + g_2\left(x\right) dw, \\ &\vdots \\ dx_{n-1} &= \left(x_n + f_{n-1}\left(\overline{x}_{n-1}\right) + d_{n-1}\left(t\right)\right) dt \\ &+ g_{n-1}\left(x\right) dw, \end{aligned}$$

$$dx_n = (u + f_n(\overline{x}_n) + d_n(t)) dt + g_n(x) dw,$$

$$y = x_1,$$
(1)

where $\overline{x}_i = [x_1, x_2, \dots, x_i]^T \in R^i$, $i = 1, 2, \dots, n$ ($x = \underline{x}_n$) is the state vector; $u \in R$ and $y \in R$ are the control input and system output, respectively. $f_i(\overline{x}_i)$ and $g_i(x)$ $i = 1, 2, \dots, n$ are unknown continuous nonlinear functions, and $d_i(t)$, $i = 1, 2, \dots, n$ is the external disturbance. $w \in R$ is an independent standard Wiener process defined on a complete probability space with the incremental covariance $E\{dw \cdot dw_i^T\} = \sigma(t)\sigma(t)^T dt$.

In this paper, the states x_i ($i \ge 2$) are assumed not to be available for measurement.

Our control objective is to design a stable output feedback control scheme for system (1) to ensure that all the signals are bounded in probability and that the system output y(t) can track the given reference signal $y_d(t)$ with the given prescribed performance bounds.

Assumption 1. The external disturbances $d_i(t)$ are bounded; that is, $|d_i(t)| \le d_i^*$ with d_i^* being an unknown constant.

Assumption 2 (see [17]). Assume that functions $f_i(\cdot)$ satisfy the global Lipschitz condition; that is, there exist known constants m_i , $i=1,2,\ldots,n$ such that for all $X_1,X_2\in R^i$, the following inequalities hold:

$$|f_i(X_1) - f_i(X_2)| \le m_i ||X_1 - X_2||,$$
 (2)

where ||X|| denotes the 2-norm of a vector X.

Assumption 3 (see [9]). The disturbance covariance $g^T \sigma \sigma^T g = \overline{\sigma} \overline{\sigma}^T$ is bounded, where $g = [g_1, \dots, g_n]^T$.

2.2. Prescribed Performance. This section introduces preliminary knowledge on the prescribed performance concept reported in [20]. According to [20], the prescribed performance is achieved by ensuring that each error $z_i(t)$ evolves strictly within predefined decaying bounds as follows:

$$-\delta_{i\min}\mu_i(t) < z_i(t) < \delta_{i\max}\mu_i(t), \quad \forall t \ge 0,$$
 (3)

where $1 \leq i \leq n$, $\delta_{i\,\mathrm{min}}$ and $\delta_{i\,\mathrm{max}}$ are design constants, and the performance functions $\mu_i(t)$ are bounded and strictly positive decreasing smooth functions with the property $\lim_{t\to\infty}\mu_i(t)=\mu_{i,\infty};\ \mu_{i,\infty}>0$ are a constant. In this paper, the performance functions are chosen as the exponential form $\mu_i(t)=(\mu_{i,0}-\mu_{i,\infty})e^{-n_it}+\mu_{i,\infty}$, where $n_i,\ \mu_{i,0}$, and $\mu_{i,\infty}$ are strictly positive constants, $\mu_{i,0}>\mu_{i,\infty}$, and $\mu_{i,0}=\mu_i(0)$ is selected such that $-\delta_{i\,\mathrm{min}}\mu_i(0)< z_i(0)<\delta_{i\,\mathrm{max}}\mu_i(0)$ is satisfied. The constant $\mu_{i,\infty}$ denotes the maximum allowable size of $z_i(t)$ at steady state that is adjustable to an arbitrary small value reflecting the resolution of the measurement device. The decreasing rate n_i represents a lower bound on the required speed of convergence of $z_i(t)$. Furthermore, the maximum overshoot of $z_i(t)$ is prescribed less than $\max\{\delta_{i\,\mathrm{min}}\mu_i(0),\delta_{i\,\mathrm{max}}\mu_i(0)\}$. Therefore, choosing the performance function $\mu_i(t)$ and the constants $\delta_{i\,\mathrm{min}}$, $\delta_{i\,\mathrm{max}}$

appropriately determines the performance bounds of the error $z_i(t)$.

To represent (3) by an equality form, we employ an error transformation as

$$z_i = \mu_i(t) \Phi_i(\zeta_i(t)), \quad \forall t \ge 0,$$
 (4)

where $\Phi_i(\zeta_i) = (\delta_{i \max} e^{\zeta_i} - \delta_{i \min} e^{-\zeta_i})/(e^{\zeta_i} + e^{-\zeta_i})$. Since the function $\Phi_i(\zeta_i)$ is strictly monotonic increasing. its inverse function can be expressed as

$$\zeta_{i}(t) = \Phi^{-1}\left(\frac{z_{i}(t)}{\mu_{i}(t)}\right) = \frac{1}{2}\ln\frac{\Phi_{i} - \delta_{i\min}}{\delta_{i\max} - \Phi_{i}},$$

$$\dot{\zeta}_{i}(t) = p_{i}\left(\dot{z}_{i} - \frac{\dot{\mu}_{i}z_{i}}{\mu_{i}}\right)$$
(5)

with $p_i = (1/2\mu_i)[(1/(\Phi_i + \delta_{i\min})) - (1/(\Phi_i - \delta_{i\max}))].$

For the output-feedback control design of the nonlinear system, we design the following state transformation:

$$z_{i}(t) = \zeta_{i}(t) - \frac{1}{2} \ln \frac{\delta_{i \min}}{\delta_{i \max}}.$$
 (6)

And the transformation state dynamics is

$$\dot{z}_i(t) = p_i \left(\dot{z}_i - \frac{\dot{\mu}_i z_i}{\mu_i} \right). \tag{7}$$

2.3. Fuzzy Logic Systems. A fuzzy logic system (FLS) consists of four parts: the knowledge base, the fuzzifier, the fuzzy inference engine working on fuzzy rules, and the defuzzifier. The knowledge base for FLS comprises a collection of fuzzy IF-THEN rules of the following form:

$$R^{l}: \text{If } x_{1} \text{ is } F_{1}^{l}, x_{2} \text{ is } F_{2}^{l}, \dots, x_{n} \text{ is } F_{n}^{l},$$

$$\text{Then } y \text{ is } G^{l}, \quad l = 1, 2, \dots, N,$$
(8)

where $x = (x_1, ..., x_n)^T$ and y are the FLS input and output, respectively. Fuzzy sets F_i^l and G^l are associated with the fuzzy functions $\mu_{F_i^l}(x_i)$ and $\mu_{G^l}(y)$, respectively. N is the rule number of IF-THEN.

Through singleton function, center average defuzzification, and product inference [21], the FLS can be expressed as

$$y(x) = \frac{\sum_{l=1}^{N} \overline{y}_{l} \prod_{i=1}^{n} \mu_{F_{i}^{l}}(x_{i})}{\sum_{l=1}^{N} \left[\prod_{i=1}^{n} \mu_{F_{i}^{l}}(x_{i}) \right]},$$
 (9)

where $\overline{y}_l = \max_{v \in R} \mu_{G^l}(y)$.

Define the fuzzy basis functions as

$$\varphi_{l} = \frac{\prod_{i=1}^{n} \mu_{F_{i}^{l}}(x_{i})}{\sum_{l=1}^{N} \left(\prod_{i=1}^{n} \mu_{F_{i}^{l}}(x_{i})\right)}.$$
(10)

Denoting $\theta^T = [\overline{y}_1, \overline{y}_2, \dots, \overline{y}_N] = [\theta_1, \theta_2, \dots, \theta_N]$ and $\varphi(x) = [\theta_1, \theta_2, \dots, \theta_N]$ $[\varphi_1(x), \dots, \varphi_N(x)]^T$, then FLS (9) can be rewritten as

$$y(x) = \theta^T \varphi(x). \tag{11}$$

Lemma 4 (see [21]). Let f(x) be a continuous function defined on a compact set Ω . Then for any constant $\varepsilon > 0$, there exists a FLS (11) such as

$$\sup_{x \in \Omega} \left| f(x) - \theta^{T} \varphi(x) \right| \le \varepsilon. \tag{12}$$

3. Fuzzy State Observer Design

Since the states x_2, \ldots, x_n in system (1) are not available for measurement, a state observer is to be established to estimate them in this section.

Rewrite (1) in the following form:

$$\overline{dx}_{n} = \left(A\overline{x}_{n} + Ky + \sum_{i=1}^{n} B_{i} \left[f_{i}\left(\overline{x}_{i}\right) + d_{i}\left(t\right)\right] + Bu\right) dt
+ g\left(x\right) dw
= \left(A\overline{x}_{n} + Ky + \sum_{i=1}^{n} B_{i} \left[f_{i}\left(\widehat{\overline{x}}_{i}\right) + \Delta f_{i} + d_{i}\left(t\right)\right] + Bu\right) dt
+ g\left(x\right) dw,$$
(13)

where $\widehat{\overline{x}}_i = (\widehat{x}_1, \widehat{x}_2, \dots, \widehat{x}_i)^T$ is the estimate of $\overline{x}_i = (x_1, x_2, \dots, x_i)^T$, $A = \begin{bmatrix} -k_1 \\ \vdots & 1 \\ -k_n & 0 & 0 \end{bmatrix}$, $K = [k_1, k_2, \dots, k_n]^T$, $B_i = [0 \cdots 1 \cdots 0]^T$, $B = [0 \cdots 0 \cdots 1]^T$, $\Delta f_i = f_i(\overline{x}_i) - f_i(\widehat{\overline{x}}_i)$, $g(x) = [g_1(x), \dots, g_n(x)]^T$.

The vector *K* is chosen such that *A* is a Hurwitz matrix. Thus, given a positive definite matrix $Q = Q^T > 0$, there exists a positive definite matrix $P = P^T > 0$ satisfying

$$A^T P + PA = -2Q. (14)$$

By Lemma 4, we can assume that nonlinear terms $f_i(\widehat{x}_i)$, i = $1, 2, \dots, n$ in (13) can be approximated by the following FLSs:

$$\widehat{f}_{i}\left(\widehat{\overline{x}}_{i}\theta_{i}\right) = \theta_{i}^{T}\varphi_{i}\left(\widehat{\overline{x}}_{i}\right). \tag{15}$$

Define the optimal parameter vectors θ_i^* as

$$\theta_{i}^{*} = \underset{\theta_{i} \in \Omega_{i}}{\operatorname{arg \, min}} \left[\underset{\widehat{x}_{i} \in U_{i}}{\sup} \left| \widehat{f}_{i} \left(\widehat{\overline{x}}_{i} \mid \theta_{i} \right) - f_{i} \left(\widehat{\overline{x}}_{i} \right) \right| \right], \quad (16)$$

where Ω_i and U_i are bounded compact sets for θ_i and \overline{x}_i , respectively. Also, the fuzzy minimum approximation error ε_i is defined as

$$\varepsilon_{i} = f_{i}\left(\widehat{\overline{x}}_{i}\right) - \widehat{f}_{i}\left(\widehat{\overline{x}}_{i} \mid \theta_{i}^{*}\right), \tag{17}$$

where ε_i satisfies $|\varepsilon_i| \le \varepsilon_i^*$, with ε_i^* being a positive constant. The state observer for (13) is designed as

$$\dot{\overline{x}}_{n} = A\widehat{x}_{n} + Ky + \sum_{i=1}^{n} B_{i} \left[\widehat{f}_{i} \left(\widehat{\overline{x}}_{i} \mid \theta_{i} \right) \right] + Bu,$$

$$\hat{y} = C\widehat{x}_{n},$$
(18)

where
$$C = [1 \cdots 0 \cdots 0]$$
.

4. Adaptive Controller Design

In this section, an adaptive fuzzy output-feedback control scheme will be developed by using the above fuzzy state observer and the backstepping technique, and the stability of the closed-loop system will be given.

The controller design consists of step *n*; each step is based on the following change of coordinates:

$$z_1 = y - y_d,$$
 $z_i = \hat{x}_i - \alpha_{i-1},$ $(i = 2, ..., n),$ (19)

where α_{i-1} is referred to as the intermediate control function, which will be designed later.

Step 1. From (1), (7), and (19), according to Itô's differentiation rule, we can obtain

$$dz_{1} = p_{1} \left(x_{2} + f_{1} \left(x_{1} \right) + d_{1} - \dot{y}_{d} - \frac{\dot{\mu}_{1} z_{1}}{\mu_{1}} \right) dt$$

$$+ p_{1} g_{1} \left(x \right) dw$$

$$= p_{1} \left(z_{2} + \alpha_{1} + e_{2} + \theta_{1}^{T} \varphi_{1} \left(\hat{x}_{1} \right) \right)$$

$$+ \tilde{\theta}_{1}^{T} \varphi_{1} \left(\hat{x}_{1} \right) + \varepsilon_{1} + d_{1} - \dot{y}_{d}$$

$$+ \Delta f_{1} - \frac{\dot{\mu}_{1} z_{1}}{\mu_{1}} \right) dt + p_{1} g_{1} \left(x \right) dw.$$

$$(20)$$

Choose the intermediate control function α_1 and the adaptation law for θ_1 as follows:

$$\alpha_{1} = -c_{1}z_{1}p_{1} - \frac{9}{4}z_{1}p_{1}^{1/3} - \frac{3}{4}z_{1}p_{1}^{3} - z_{1}^{3}p_{1}$$

$$-\theta_{1}^{T}\varphi_{1}(\widehat{x}_{1}) + \dot{y}_{d} + \frac{\dot{\mu}_{1}z_{1}}{\mu_{1}},$$

$$\dot{\theta}_{1} = \eta_{1}z_{1}^{3}p_{1}\varphi_{1}(\widehat{x}_{1}) - \sigma_{1}\theta_{1},$$
(21)

where $c_1 > 0$, $\sigma_1 > 0$ and $\eta_1 > 0$ are design parameters and θ_1 is the estimate of θ_1^* .

Step i ($2 \le i \le n - 1$). Similar to Step 1, we have

$$\begin{split} dz_i &= \left[p_i \left(z_{i+1} + \alpha_i + k_i e_1 + \theta_i^T \varphi \left(\widehat{\overline{x}}_i \right) \right. \\ &- \sum_{l=1}^{i-1} \frac{\partial \alpha_{l-1}}{\partial \widehat{x}_l} \widehat{x}_l - \sum_{l=1}^{i-1} \frac{\partial \alpha_{l-1}}{\partial \theta_l} \dot{\theta}_l \right. \\ &- \sum_{l=1}^{i-1} \frac{\partial \alpha_{l-1}}{\partial y_d^{(l-1)}} y_d^l - \frac{\partial \alpha_1}{\partial y} \dot{y} - \frac{\dot{\mu}_i z_i}{\mu_i} \right) \right] dt \\ &- p_i \frac{\partial \alpha_{i-1}}{\partial y} g_1 \left(x \right) dw \end{split}$$

$$= \left[p_{i} \left(z_{i+1} + \alpha_{i} + k_{i} e_{1} + \theta_{i}^{T} \varphi \left(\widehat{\overline{x}}_{i} \right) + \widetilde{\theta}_{i}^{T} \varphi \left(\widehat{\overline{x}}_{i} \right) - \widetilde{\theta}_{i}^{T} \varphi \left(\widehat{\overline{x}}_{i} \right) - \frac{\partial \alpha_{1}}{\partial y} \right] \times \left[\widetilde{\theta}_{1}^{T} \varphi_{1} \left(\widehat{x}_{1} \right) + e_{2} + \varepsilon_{1} + \Delta f_{1} + d_{1} \right] - H_{i} - \frac{\dot{\mu}_{i} z_{i}}{\mu_{i}} \right] dt - p_{i} \frac{\partial \alpha_{i-1}}{\partial y} g_{1} (x) dw,$$

$$(23)$$

where

$$H_{i} = -\sum_{l=1}^{i-1} \frac{\partial \alpha_{l-1}}{\partial \hat{x}_{l}} \left[\hat{x}_{l+1} + \theta_{l}^{T} \varphi_{l} \left(\hat{\overline{x}}_{l} \right) + k_{l} e_{1} \right]$$

$$- \frac{\partial \alpha_{1}}{\partial \theta_{1}} \dot{\theta}_{1} - \frac{\partial \alpha_{1}}{\partial y_{d}^{(l-1)}} \dot{y}_{d} - \frac{\partial \alpha_{1}}{\partial y} \left[\hat{x}_{2} + \theta_{1}^{T} \varphi_{1} \left(\hat{x}_{1} \right) \right].$$

$$(24)$$

Choose intermediate control function α_i and adaptation law θ_i as

$$\alpha_{i} = -c_{i}z_{i}p_{i} - k_{i}e_{1} - \overline{H}_{i} - \theta_{i}^{T}\varphi_{i}\left(\widehat{\overline{x}}_{i}\right)$$

$$-\frac{3}{4}z_{i}p_{i}^{1/3} - \frac{1}{4}z_{i} + \frac{\dot{\mu}_{i}z_{i}}{\mu_{i}},$$
(25)

$$\dot{\theta}_i = \eta_i z_i^3 p_i \varphi_i \left(\widehat{\overline{x}}_i \right) - \sigma_i \theta_i, \tag{26}$$

where $c_i > 0$, $\sigma_i > 0$ and $\eta_i > 0$ are design parameters and θ_i is the estimate of θ_i^* , and

$$\overline{H}_{i} = H_{i} + \left(\frac{\partial \alpha_{i-1}}{\partial x_{1}}\right)^{2} z_{i}^{3} p_{i} + \frac{3}{4} z_{i} p_{i}^{3} \left(\frac{\partial \alpha_{i-1}}{\partial y}\right)^{4} + \frac{1}{2} z_{i}^{3} p_{i} + \frac{1}{4} z_{i}^{3} p_{i} \left(\frac{\partial^{2} \alpha_{i-1}}{\partial y^{2}}\right)^{2}.$$
(27)

Step n. In the final design step, the actual control input u will be designed. Similar to Step i we have

$$dz_{n} = p_{n} \left(u + k_{n} e_{1} + \theta_{n}^{T} \varphi_{n} \left(\widehat{\overline{x}}_{n} \right) - \dot{\alpha}_{n-1} - \frac{\dot{\mu}_{n} z_{n}(t)}{\mu_{n}} \right) dt$$
$$- p_{n} \frac{\partial \alpha_{n-1}}{\partial y} g_{1}(x) dw. \tag{28}$$

The controller u and adaptation law θ_n are chosen as

$$u = -c_n z_n p_n - k_n e_1 - \theta_n^T \varphi_n \left(\widehat{\overline{x}}_n\right) - \overline{H}_n - \frac{1}{4} z_n + \frac{\dot{\mu}_n z_n}{\mu_n}, \quad (29)$$

$$\dot{\theta}_n = \eta_n z_n^3 p_n \varphi_n \left(\widehat{\overline{x}}_n \right) - \sigma_n \theta_n, \tag{30}$$

where $c_n > 0$, $\sigma_n > 0$ and $\eta_i > 0$ are design parameters and θ_n is the estimate of θ_n^* .

(35)

5. Stability Analysis

Consider the total Lyapunov candidate functions V as the sum of local Lyapunov candidate functions V_0 and V_i , namely, $V = V_0 + V_i$, with $V_0 = (1/2)e^T P e$, and $V_i = \sum_{i=1}^n ((1/4)z_i^4 + (1/2\eta_i)\widetilde{\theta}_i^T \widetilde{\theta}_i)$, where $e = \overline{x} - \widehat{x}$ is the observer error vector, η_i is positive design constant, and $\widetilde{\theta}_i = \theta_i^* - \theta_i$.

Theorem 5. For the stochastic nonlinear system (1), if Assumptions 1–3 are satisfied, the controller (29) with the state observer (18), together with the intermediate control functions (21) and (25), and adaptation laws (22), (26), and (30) can guarantee that all signals in the closed-loop system are semiglobally uniformly ultimately bounded in probability, and the tracking error remains in a neighborhood of the origin within the prescribed performance bounds for all $t \ge 0$.

Proof. The infinitesimal generator of *V* is

$$\ell V = \ell V_0 + \ell V_i. \tag{31}$$

From (13) and (18), we have the observer error equation

$$de = \left(Ae + \sum_{i=1}^{n} B_{i} \left[f_{i}\left(\widehat{x}_{i}\right) - \widehat{f}_{i}\left(\widehat{x}_{i} \mid \theta_{i}\right) + \Delta f_{i} + d_{i}\right]\right) dt + g(x) dw$$

$$= \left(Ae + \sum_{i=1}^{n} B_{i} \left[\varepsilon_{i} + \widetilde{\theta}_{i}^{T} \varphi_{i}\left(\widehat{x}_{i}\right) + \Delta f_{i} + d_{i}\right]\right) dt + g(x) dw$$

$$= \left(Ae + \varepsilon + d + \Delta f\right)$$

$$+ \sum_{i=1}^{n} B_{i} \widetilde{\theta}_{i}^{T} \varphi_{i}\left(\widehat{x}_{i}\right)\right) dt + g(x) dw,$$
(32)

where $\Delta f = [\Delta f_1, \dots, \Delta f_n]^T$, $\varepsilon = [\varepsilon_1, \dots, \varepsilon_n]^T$, $d = [d_1, \dots, d_n]^T$, $\tilde{\theta}_i = \theta_i^* - \theta_i$.

The infinitesimal generator of V_0 along with (32) is

$$\ell V_{0} \leq -\lambda_{\min}(Q) \|e\|^{2} + e^{T} P\left(\varepsilon + d + \Delta f\right) + \sum_{i=1}^{n} e^{T} P B_{i} \widetilde{\theta}_{i}^{T} \varphi_{i}\left(\widehat{\overline{x}}_{i}\right) + Tr\left[\sigma g^{T} P g \sigma^{T}\right].$$

$$(33)$$

By Young's inequality, Assumptions 1–3, we have

$$\begin{split} e^T P \left(d + \varepsilon + \Delta f \right) & \leq \frac{3}{2} \| \varepsilon \|^2 + \frac{1}{2} \| P \|^2 \| \varepsilon^* \|^2 \\ & + \frac{1}{2} \| P \|^2 \| d^* \|^2 + \frac{1}{2} \| P \|^2 \| \Delta f \|^2 \end{split}$$

$$\leq \left(\frac{3}{2} + \frac{1}{2} \|P\|^{2} \sum_{i=1}^{n} m_{i}^{2}\right) \|e\|^{2} + \frac{1}{2} \|P\|^{2} \|\epsilon^{*}\|^{2} + \frac{1}{2} \|P\|^{2} \|d^{*}\|^{2},$$

$$Tr\left[\sigma g^{T} P g \sigma^{T}\right] \leq \frac{1}{2} \|P\|^{2} + \frac{1}{2} |\overline{\sigma} \overline{\sigma}^{T}|^{2},$$
(34)

where $\varepsilon^* = [\varepsilon_1^*, \dots, \varepsilon_n^*]^T$, $d^* = [d_1^*, \dots, d_n^*]^T$. Note that $\varphi_i^T(\widehat{x}_i)\varphi_i(\widehat{x}_i) \leq 1$; by Young's inequality, we have

$$\begin{split} e^T P \sum_{i=1}^n B_i \widetilde{\theta}_i^T \varphi_i \left(\widehat{\overline{x}}_i \right) &\leq \frac{1}{4} e^T P P^T e + \sum_{i=1}^n \widetilde{\theta}_i^T \varphi_i \left(\widehat{\overline{x}}_i \right) \varphi_i^T \left(\widehat{\overline{x}}_i \right) \widetilde{\theta}_i \\ &\leq \frac{1}{4} \lambda_{\max}^2 \left(P \right) \| e \|^2 + \sum_{i=1}^n \widetilde{\theta}_i^T \widetilde{\theta}_i, \end{split}$$

where $\lambda_{\max}(P)$ is the largest eigenvalue of P. Substituting (34)-(35) into (33) gives

$$\dot{V}_{0} \le -q_{0} \|e\|^{2} + \sum_{i=1}^{n} \tilde{\theta}_{i}^{T} \tilde{\theta}_{i} + \lambda_{0},$$
 (36)

where $q_0 = \lambda_{\min}(Q) - ((3/2) + (1/2)\|P\|^2 \sum_{i=1}^n m_i^2 + (1/4)\lambda_{\max}^2(P)), \ \lambda_0 = (1/2)\|P\|^2 \|\epsilon^*\|^2 + (1/2)\|P\|^2 \|d^*\|^2 + (1/2)\|P\|^2 + (1/2)|\overline{\sigma}\,\overline{\sigma}^T|^2$, and $\lambda_{\min}(Q)$ is the minimal eigenvalue of Q.

From (19), (20), (23), and (28) we have

$$\begin{split} z_{1}^{3}\dot{z}_{1} &= z_{1}^{3}p_{1}\left(x_{2} + f_{1}\left(x_{1}\right) + d_{1} - \dot{y}_{d} - \frac{\dot{\mu}_{1}z_{1}}{\mu_{1}}\right) \\ &+ \frac{3}{2}z_{1}^{2}p_{1}^{2}g_{1}^{T}\sigma\sigma^{T}g_{1} \\ &= z_{1}^{3}p_{1}\left(z_{2} + \alpha_{1} + e_{2} + \theta_{1}^{T}\varphi_{1}\left(\hat{x}_{1}\right) + \widetilde{\theta}_{1}^{T}\varphi_{1}\left(\hat{x}_{1}\right) \right. \\ &+ \varepsilon_{1} + d_{1} - \dot{y}_{d} + \Delta f_{1} - \frac{\dot{\mu}_{1}z_{1}}{\mu_{1}}\right) \\ &+ \frac{3}{2}z_{1}^{2}p_{1}^{2}g_{1}^{T}\sigma\sigma^{T}g_{1}, \\ z_{i}^{3}\dot{z}_{i} &= z_{i}^{3}p_{i}\left(z_{i+1} + \alpha_{i} + k_{i}e_{1} - \frac{\partial\alpha_{1}}{\partial y}\right. \\ & \times \left[\widetilde{\theta}_{1}^{T}\varphi_{1}\left(\hat{x}_{1}\right) + e_{2} + \Delta f_{1} + d_{1} + \varepsilon_{1}\right] \\ &+ \theta_{i}^{T}\varphi_{i}\left(\widehat{x}_{i}\right) + \widetilde{\theta}_{i}^{T}\varphi_{i}\left(\widehat{x}_{i}\right) - \widetilde{\theta}_{i}^{T}\varphi_{i}\left(\widehat{x}_{i}\right) - H_{i} \\ &- \frac{1}{2}\frac{\partial^{2}\alpha_{i-1}}{\partial y^{2}}g_{1}^{T}\sigma\sigma^{T}g_{1} - \frac{\dot{\mu}_{i}z_{i}}{\mu_{i}}\right) \\ &+ \frac{3}{2}p_{i}^{2}z_{i}^{2}\left(\frac{\partial\alpha_{i-1}}{\partial y}\right)^{2}g_{1}^{T}\sigma\sigma^{T}g_{1}, \end{split}$$

$$z_{n}^{3}\dot{z}_{n} = z_{n}^{3}p_{n}\left(\theta_{n}^{T}\varphi_{n}\left(\widehat{\overline{x}}_{n}\right) + u + \frac{1}{4}z_{n} + k_{n}e_{1} - \overline{H}_{n} - \frac{\dot{\mu}_{n}z_{n}\left(t\right)}{\mu_{n}}\right) + \widetilde{\theta}_{n}^{T}\varphi_{n}\left(\widehat{\overline{x}}_{n}\right) - \widetilde{\theta}_{n}^{T}\varphi_{n}\left(\widehat{\overline{x}}_{n}\right) + \frac{3}{2}p_{n}^{2}z_{n}^{2}\left(\frac{\partial\alpha_{n-1}}{\partial y}\right)^{2}g_{1}^{T}\sigma\sigma^{T}g_{1}.$$

$$(37)$$

By Young's inequality and Assumptions 1-3, we have

$$\begin{split} z_{1}^{3}p_{1}z_{2} + z_{1}^{3}p_{1}e_{2} + z_{1}^{3}p_{1}\varepsilon_{1} + z_{1}^{3}p_{1}d_{1} + z_{1}^{3}p_{1}\Delta f_{1} \\ &\leq \frac{3}{4}z_{1}^{4}p_{1}^{4/3} + \frac{1}{4}z_{2}^{4} + \frac{1}{2}z_{1}^{6}p_{1}^{2} + \frac{1}{2}\|e\|^{2} + \frac{3}{4}z_{1}^{4}p_{1}^{4/3} \\ &\quad + \frac{1}{4}\varepsilon_{1}^{*4} + \frac{3}{4}z_{1}^{4}p_{1}^{4/3} + \frac{1}{4}d_{1}^{*4} + \frac{1}{2}z_{1}^{6}p_{1}^{2} + \frac{1}{2}\Delta f_{1}^{2} \\ &\leq \frac{9}{4}z_{1}^{4}p_{1}^{4/3} + z_{1}^{6}p_{1}^{2} + \frac{1}{4}z_{2}^{4} + \frac{1}{4}\varepsilon_{1}^{*4} + \frac{1}{4}d_{1}^{*4} \\ &\quad + \frac{1}{2}\|e\|^{2} + \frac{1}{2}\|e\|^{2}m_{1}^{2}, \end{split} \tag{39}$$

$$z_{i}^{3} p_{i} z_{i+1} - z_{i}^{3} p_{i} \widetilde{\theta}_{i}^{T} \varphi_{i} \left(\widehat{\overline{x}}_{i} \right)$$

$$\leq \frac{3}{4} z_{i}^{4} p_{i}^{4/3} + \frac{1}{4} z_{i+1}^{4} + \frac{1}{2} z_{i}^{6} p_{i}^{2} + \frac{1}{2} \widetilde{\theta}_{i}^{T} \widetilde{\theta}_{i}, \tag{40}$$

$$-z_{i}^{3} p_{i} \frac{\partial \alpha_{i-1}}{\partial x_{1}} e_{2} \leq \frac{1}{2} \|e\|^{2} + \frac{1}{2} \left(\frac{\partial \alpha_{i-1}}{\partial x_{1}}\right)^{2} z_{i}^{6} p_{i}^{2}, \tag{41}$$

$$-z_i^3 p_i \frac{\partial \alpha_{i-1}}{\partial x_1} \widetilde{\theta}_1^T \varphi_1\left(\widehat{x}_1\right) \le \frac{1}{2} \widetilde{\theta}_1^T \widetilde{\theta}_1 + \frac{1}{2} \left(\frac{\partial \alpha_{i-1}}{\partial x_1}\right)^2 z_i^6 p_i^2, \quad (42)$$

$$-z_{i}^{3} p_{i} \frac{\partial \alpha_{i-1}}{\partial x_{1}} \left[\varepsilon_{1} + \Delta f_{1} + d_{1} \right]$$

$$\leq \frac{3}{2} \left(\frac{\partial \alpha_{i-1}}{\partial x_{1}} \right)^{2} z_{i}^{6} p_{i}^{2} + \frac{1}{2} \varepsilon_{1}^{*2} + \frac{1}{2} d_{1}^{*2} + \frac{m_{1}^{2}}{2} \| e \|^{2},$$

$$- \frac{1}{2} z_{i}^{3} p_{i} \frac{\partial^{2} \alpha_{i-1}}{\partial y^{2}} g_{1}^{T} \sigma \sigma^{T} g_{1} + \frac{3}{2} p_{i}^{2} z_{i}^{2} \left(\frac{\partial \alpha_{i-1}}{\partial y} \right)^{2} g_{1}^{T} \sigma \sigma^{T} g_{1}$$

$$\leq \frac{1}{4} z_{i}^{6} p_{i}^{2} \left(\frac{\partial^{2} \alpha_{i-1}}{\partial y^{2}} \right)^{2} + \frac{1}{4} |\overline{\sigma} \overline{\sigma}|^{2} + \frac{3}{4} p_{i}^{4} z_{i}^{4} \left(\frac{\partial \alpha_{i-1}}{\partial y} \right)^{4}$$

$$(44)$$

$$+\frac{3}{4}\left|\overline{\sigma}\,\overline{\sigma}^T\right|^2$$
.

From (21)-(22), (25)-(26), (29)-(30), and (41)-(44), we have

$$\begin{aligned} \ell V &\leq -q_n \|e\|^2 - \sum_{i=1}^n c_i z_i^4 p_i^2 + \sum_{i=1}^n \frac{\sigma_i}{\eta_i} \widetilde{\theta}_i^T \theta_i \\ &+ 2 \sum_{i=1}^n \widetilde{\theta}_i^T \widetilde{\theta}_i + \frac{n-1}{2} \widetilde{\theta}_1^T \widetilde{\theta}_1 + \lambda_n, \end{aligned} \tag{45}$$

where $q_n = q_0 - (n/2) - (nm_1^2/2)$, $\lambda_n = \lambda_0 + (n/2)\varepsilon_1^2 + (n/2)d_1^{*2} + n|\overline{\sigma}\overline{\sigma}|^2$.

Note that

$$\sum_{i=1}^{n} \frac{\sigma_i}{\eta_i} \widetilde{\theta}_i^T \theta_i \le -\frac{1}{2} \sum_{i=1}^{n} \frac{\sigma_i}{\eta_i} \widetilde{\theta}_i^T \widetilde{\theta}_i + \frac{1}{2} \sum_{i=1}^{n} \frac{\sigma_i}{\eta_i} \theta_i^{*T} \theta_i^*. \tag{46}$$

Substituting the above inequality into (52) gives

$$\begin{split} \ell V & \leq -q_n \|e\|^2 - \sum_{i=1}^n c_i z_i^4 p_i^2 - \sum_{i=2}^n \left(\frac{\sigma_i}{2\eta_i} - 2\right) \widetilde{\theta}_i^T \widetilde{\theta}_i \\ & - \left(\frac{\sigma_1}{2\eta_1} - \frac{n+3}{2}\right) \widetilde{\theta}_1^T \widetilde{\theta}_1 + \lambda, \end{split} \tag{47}$$

where $D = \sum_{i=1}^{n} (\sigma_i/2\eta_i)\theta_i^{*T}\theta_i^* + \lambda_n$. Let $q_n > 0$, $c_i > 0$, $(\sigma_i/2\eta_i) > 1$, and define

$$C = \min \left\{ \frac{2q_n}{\lambda_{\min}(P)}, 4c_i p_i^2, (i = 1, ..., n), \right.$$

$$\sigma_1 - (n+3) \eta_1, 2(\sigma_i - 4\eta_i), (i = 2, ..., n) \right\}.$$
(48)

Then (47) can be written as

$$\ell V \le -CV + D. \tag{49}$$

Multiplying V by e^{Ct} and by Itô formula leads to

$$d\left(e^{Ct}V\right) = e^{Ct}\left(CV + \ell V\right)dt + e^{Ct}\Omega_1 dw, \qquad (50)$$

where $\Omega_1 = (\partial V/\partial z_1)g_1(x) - \sum_{i=2}^n (\partial V/\partial z_i)(\partial \alpha_{i-1}/\partial y)g_1(x) + (\partial V/\partial e)g(x)$.

From (49) and (50), we have

$$d\left(e^{Ct}V\right) \le e^{Ct}Ddt + e^{Ct}\Omega_1 dw. \tag{51}$$

Integrating (51) over [0, T], we get

$$V(T) \le e^{CT}V(0) + \frac{D}{C} + e^{CT} \int_{0}^{T} e^{Cs}\Omega_{1}dw(s)$$
. (52)

Taking expectation on (52), it follows that

$$E[V(T)] \le EV(0)e^{-CT} + \frac{D}{C},$$
 (53)

where $E(\cdot)$ is probability expectation.

The above inequality means that E[V(T)] is bounded by D/C in mean square. Thus, according to [12–18], it is concluded that all the signals of the closed-loop system are SGUUB in the sense of the four-moment. Moreover, it follows that the tracking errors and virtual tracking errors remain within the prescribed performance bounds for all time $t \geq 0$.

6. Simulation Study

In this section, a simulation example is provided to evaluate the control performance of the proposed adaptive outputfeedback control method.

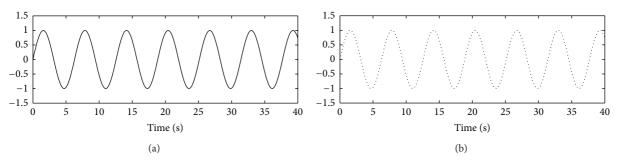


Figure 1: The curves of y (solid line) and y_d (dot line).

Consider a stochastic system governed by the following form:

$$dx_{1} = [x_{2} + f_{1}(x_{1})] dt + g_{1}(x) dw,$$

$$dx_{2} = [f_{2}(x_{1}, x_{2})] dt + u + g_{2}(x) dw,$$

$$y = x_{1},$$
(54)

where $f_1(x_1) = \sin(x_1^2)$, $f_2(x_1, x_2) = x_1 \sin(x_2^2) - x_1 e^{0.5x_1}$, $g_1(x) = \sin(x_1)/(1+0.5\cos(x_2))$, $g_2(x) = x_1x_2/(1+(x_1x_2)^2)$. $\dot{w}(t)$ is assumed to be a Gaussian white noise with zero mean and variance 1.0. The tracking reference signal is chosen as $y_d(t) = \sin(t)$.

Choose fuzzy membership functions as

$$\mu_{F_i^l}(\widehat{x}_i) = \exp\left[-\frac{(\widehat{x}_i - 3 + l)^2}{16}\right], \quad l = 1, 2, 3, 4, 5. \quad (55)$$

Construct the FLSs $\hat{f}_i(\hat{x}_i \mid \theta_i) = \theta_i^T \varphi_i(\hat{x}_i)$ to appreciate the unknown nonlinear functions $f_i(\cdot)$, i = 1, 2.

Choose the design parameters and performance functions as $k_1 = 0.8$, $k_2 = 10$, $c_1 = 0.01$, $c_2 = 1$, $\eta_1 = \eta_2 = 0.01$, $\mu_{1,0} = 2$, $\mu_{1,\infty} = 0.5$, $n_1 = 0.5$, $\sigma_1 = \sigma_2 = 0.01$, $\delta_{1\,\text{min}} = 0.01$, $\delta_{1\,\text{max}} = 0.02$, and $\mu_1(t) = 1.5e^{-0.5t} + 0.5$.

The initial conditions are chosen as follows: $x_1(0) = 0$, $x_2(0) = 0.1$, $\widehat{x}_1(0) = 0$, $\widehat{x}_2(0) = -0.1$, $\theta_1^T(0) = [0, 0, -0.1, 0, 0]$, and $\theta_2^T(0) = [0, 0, 0, -0.1, 0]$.

Applying the control method in this paper to control (54), the simulation results are shown by Figures 1–4, where Figure 1 expresses the curves of the output yand tracking signal y_d ; Figure 2 expresses the curves of the observer error e_1 and e_2 ; Figure 3 expresses the curve of the control input u. Figure 4 express the curve the tracking error of the proposed control method. Figure 4 reveals that the evolution of the proposed adaptive controller remains within the prescribed performance bounds for all $t \geq 0$; that is, the prescribed performance is satisfied.



In this paper, fuzzy adaptive output feedback tracking control problem has been investigated for a class of nonlinear stochastic systems in strict-feedback form. The addressed stochastic nonlinear systems contain unknown nonlinear

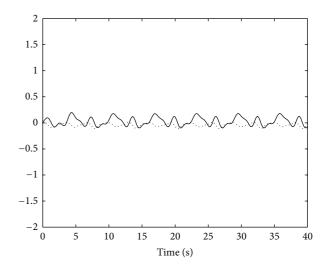


Figure 2: The curves of e_1 (solid line) and e_2 (dot line).

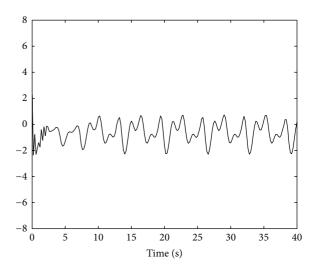


FIGURE 3: The curve of *u*.

functions and without the measurements of the states. Fuzzy logic systems are used to identify the unknown nonlinear functions, and a fuzzy state filter observer has been designed for estimating the unmeasured states. By applying

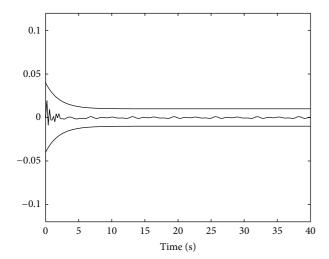


FIGURE 4: The curves of z_1 and performance bounds.

the backstepping recursive design technique and the predefined performance technique, a new robust fuzzy adaptive output-feedback control approach has been developed, and the stability of the closed-loop system has been proved. The main advantages of the proposed control approach are that it cannot only solve the state unmeasured problem of nonlinear stochastic systems, but can also guarantee that the tracking error converges to an adjustable neighborhood of the origin and remains within the prescribed performance bounds. Future research will be concentrated on an adaptive fuzzy output-feedback tracking control for multiinput and multioutput stochastic nonlinear systems with unmeasured states based on the results of [22, 23] and this paper.

Conflict of Interests

None of the authors of the paper have declared any conflict of interests.

Acknowledgments

This work was supported by the National Natural Science Foundation of China (nos. 61374113, 61074014, and 61203008) and Liaoning Innovative Research Team in University (LT2012013).

References

- [1] Y. G. Niu, W. C. H. Daniel, and J. Lam, "Robust integral sliding mode control for uncertain stochastic systems with time-varying delay," *Automatica*, vol. 41, no. 5, pp. 873–880, 2005
- [2] P. Shi, Y. Q. Xia, G. P. Liu, and D. Rees, "On designing of sliding-mode control for stochastic jump systems," *IEEE Transactions on Automatic Control*, vol. 51, no. 1, pp. 97–103, 2006.
- [3] M. Liu, D. W. C. Ho, and Y. G. Niu, "Stabilization of Markovian jump linear system over networks with random communication delay," *Automatica*, vol. 45, no. 2, pp. 416–421, 2009.

- [4] H. Y. Li, C. Wang, P. Shi, and H. Gao, "New passivity results for uncertain discrete-time stochastic neural networks with mixed time delays," *Neurocomputing*, vol. 73, no. 16–18, pp. 3291–3299, 2010.
- [5] Z. G. Pan and T. Başar, "Adaptive controller design for tracking and disturbance attenuation in parametric strict-feedback nonlinear systems," *IEEE Transactions on Automatic Control*, vol. 43, no. 8, pp. 1066–1083, 1998.
- [6] H. Deng and M. Krstic, "Output-feedback stochastic nonlinear stabilization," *IEEE Transactions on Automatic Control*, vol. 44, no. 2, pp. 328–333, 1999.
- [7] Z. Wu, X. Xie, P. Shi, and Y.-q. Xia, "Backstepping controller design for a class of stochastic nonlinear systems with Markovian switching," *Automatica*, vol. 45, no. 4, pp. 997–1004, 2009.
- [8] Y. Xia, M. Fu, P. Shi, Z. Wu, and J. Zhang, "Adaptive back-stepping controller design for stochastic jump systems," *IEEE Transactions on Automatic Control*, vol. 54, no. 12, pp. 2853–2859, 2009.
- [9] H. B. Ji and H. S. Xi, "Adaptive output-feedback tracking of stochastic nonlinear systems," *IEEE Transactions on Automatic Control*, vol. 51, no. 2, pp. 355–360, 2006.
- [10] S. J. Liu, J. F. Zhang, and Z. P. Jiang, "Decentralized adaptive output-feedback stabilization for large-scale stochastic nonlinear systems," *Automatica*, vol. 43, no. 2, pp. 238–251, 2007.
- [11] S. J. Liu, S. S. Ge, and J. F. Zhang, "Adaptive output-feedback control for a class of uncertain stochastic non-linear systems with time delays," *International Journal of Control*, vol. 81, no. 8, pp. 1210–1220, 2008.
- [12] W. S. Chen, L. C. Jiao, J. Li, and R. Li, "Adaptive NN backstepping output-feedback control for stochastic nonlinear strictfeedback systems with time-varying delays," *IEEE Transactions* on Systems, Man, and Cybernetics B, vol. 40, no. 3, pp. 939–950, 2010.
- [13] J. Li, W. S. Chen, J. M. Li, and Y. Q. Fang, "Adaptive NN output-feedback stabilization for a class of stochastic nonlinear strict-feedback systems," *ISA Transactions*, vol. 48, no. 4, pp. 468–475, 2009.
- [14] J. Li, W. S. Chen, and J. M. Li, "Adaptive NN output-feedback decentralized stabilization for a class of large-scale stochastic nonlinear strict-feedback systems," *International Journal of Robust and Nonlinear Control*, vol. 21, no. 4, pp. 452–472, 2011.
- [15] Q. Zhou, P. Shi, H. H. Liu, and S. Y. Xu, "Neural-network-based decentralized adaptive output-feedback control for large-scale stochastic nonlinear systems," *IEEE Transactions on Systems*, *Man, and Cybernetics B*, vol. 42, no. 6, pp. 1608–1619, 2012.
- [16] S. C. Tong, Y. Li, Y. M. Li, and Y. Liu, "Observer-based adaptive fuzzy backstepping control for a class of stochastic nonlinear strict-feedback systems," *IEEE Transactions on Systems, Man, and Cybernetics B*, vol. 41, no. 6, pp. 1693–1704, 2011.
- [17] S. C. Tong, T. Wang, Y. M. Li, and B. Chen, "A combined backstepping and stochastic small-gain approach to robust adaptive fuzzy output feedback control," *IEEE Transactions on Fuzzy Systems*, vol. 21, no. 2, pp. 314–327, 2013.
- [18] S. C. Tong, Y. M. Li, and T. Wang, "Adaptive fuzzy decentralized output feedback control for stochastic nonlinear large-scale systems using DSC technique," *International Journal of Robust* and Nonlinear Control, vol. 23, no. 4, pp. 381–399, 2013.
- [19] C. P. Bechlioulis and G. A. Rovithakis, "Robust adaptive control of feedback linearizable MIMO nonlinear systems with prescribed performance," *IEEE Transactions on Automatic Control*, vol. 53, no. 9, pp. 2090–2099, 2008.

- [20] C. P. Bechlioulis and G. A. Rovithakis, "Prescribed performance adaptive control for multi-input multi-output affine in the control nonlinear systems," *IEEE Transactions on Automatic Control*, vol. 55, no. 5, pp. 1220–1226, 2010.
- [21] L. X. Wang, Adaptive Fuzzy Systems and Control: Design and Stability Analysis, Prentice Hall, Englewood Cliffs, NJ, USA, 1994.
- [22] H. Y. Li, X. J. Jing, H. K. Lam, and P. Shi, "Fuzzy sampled-data control for uncertain vehicle suspension systems," *IEEE Transactions on Cybernetics*, no. 99, 1 page, 2013.
- [23] H. Y. Li, X. J. Jing, and H. R. Karimi, "Output-feedback based H_{∞} control for active suspension systems with control delay," *IEEE Transactions on Industrial Electronics*, vol. 61, no. 1, pp. 436–446, 2014.

Hindawi Publishing Corporation Abstract and Applied Analysis Volume 2014, Article ID 760937, 9 pages http://dx.doi.org/10.1155/2014/760937

Research Article

Finite-Time Terminal Sliding Mode Tracking Control for Piezoelectric Actuators

Jin Li¹ and Liu Yang^{1,2}

¹ College of Automation, Harbin Engineering University, Harbin, Heilongjiang 150001, China

Correspondence should be addressed to Liu Yang; yangliuheu@gmail.com

Received 22 January 2014; Accepted 3 February 2014; Published 12 March 2014

Academic Editor: Shen Yin

Copyright © 2014 J. Li and L. Yang. This is an open access article distributed under the Creative Commons Attribution License, which permits unrestricted use, distribution, and reproduction in any medium, provided the original work is properly cited.

This paper proposes a continuous finite-time control scheme using a new form of terminal sliding mode (TSM) combined with a sliding mode disturbance observer (SMDO). The proposed controller is applied for nanopositioning of piezoelectric actuators (PEAs). Nonlinearities, mainly hysteresis, can drastically degrade the system performance. Same as the model imperfection, hysteresis can also be treated as uncertainties of the system. These uncertainties can be addressed by terminal sliding mode control (TSMC) for it is promising for positioning and tracking control. To further improve the robustness of the TSM controller, the SMDO is employed to estimate the bounded disturbances and uncertainties. The robust stability of the TSMC is proved through a Lyapunov stability analysis. Simulation results demonstrate the effectiveness of the proposed TSM/SMDO controller for both positioning and tracking applications. The fast response, few chattering, and high precision positioning and tracking performances can be achieved in finite time by the proposed controller.

1. Introduction

Different from other traditional actuators, piezoelectric actuators (PEAs) possess the advantages of high positioning resolution, fast response, large actuating force, and free of backlash and friction [1]. Therefore, PEAs have been widely used in a variety of applications, such as adaptive optics [2], scanning tunneling microscopy [3, 4], data storage [1, 5, 6], and nanofabrication. However, there are also some challenges in the use of PEAs. The main problems come from the nonlinear behaviors like creep and hysteresis that often occur when the PEAs are driven by an amplifier. These nonlinearities can greatly degrade the performance of PEAs and even compromise the stability of the closed-loop system [2, 7]. For these two types of nonlinearity, creep is a slow drifting behavior in the displacement of PEAs, when responding to a step command voltage. Creep can cause a drifting steady state error in static or slow moving applications, but this effect can be easily eliminated by feedback techniques.

Hysteresis, on the other hand, is another typical nonlinear behavior that needs to be tackled in applications of PEAs. The hysteresis relation between the input voltage and the output displacement can cause normally 10%–15% of open-loop positioning error in the displacement range of PEAs. Figure 1 shows the simulated hysteresis response of the PEA model employed in this research [8]. This phenomenon can largely degrade the performance of controllers that have not considered its influence. Some earlier works dealt with this problem by using charge amplifier [1, 9–11] or restricting the amplitude of the input voltage small enough [12]. However, these two methods were either too complex or not practical in implementation. Therefore, researchers start to employ advanced control methods to suppress hysteresis in various applications of PEAs.

Past research proposed various control methods to deal with the influence of hysteresis. To generally summarize, mainly two ways of control strategies were employed in related literature. One way is using some inverse-based feedforward compensation methods, and another is using feedback control methods. In feedforward based methods, different hysteresis models are used to compensate this effect inversely. Typical models are Prandt-Ishlinskii model [13, 14], Preisach model [15, 16], Bouc-Wen model [17], and

² Department of Earth and Space Science and Engineering, York University, Toronto, ON, Canada M3J 1P3

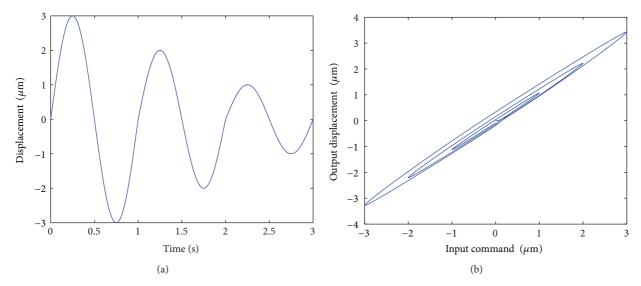


FIGURE 1: (a) A 1 Hz input displacement signal applied to the PEA model and (b) hysteresis loop obtained by simulation.

Maxwell resistive capacitor (MRC) model [18, 19]. However, these methods are based on precise hysteresis model; degraded compensation performance is unavoidable if modeling error exists. On the other hand, in feedback control methods, the hysteresis model is usually not needed since nonlinearities can be treated as disturbances that can be suppressed by feedback controller, related methods include PID (proportional-integral-derivative) control [20], repetitive control [21], robust control [22–26], and SMC (sliding mode control) [8, 27–29]. In addition, [30, 31] combined those two types of methods by employing both feedforward and feedback control design.

It is well known that finite-time stabilization of dynamical systems will improve the systems performance of highprecision and finite-time convergence to the equilibrium. Therefore, discontinuous terminal sliding mode control with robustness for matched disturbances and parametric uncertainties with known bounds has been widely adopted in nonlinear systems for finite-time stability [32-35]. However, because of the chattering of discontinuous control, it may induce poor tracking performance and create undesirable oscillations in the control signal and even may excite highfrequency dynamics neglected in the course of modeling [8]. In order to alleviate chattering, the boundary layer technique is usually adopted. However, both the attractive SMC feature of insensitivity to uncertainties and disturbances and the finite time stability are lost. Recently, a continuous TSMC scheme has been developed for robotic manipulators to avoid this problem [36]. In this paper, a new continuous finite-time terminal sliding mode control combined with a sliding mode disturbance observer is proposed, which is then applied in a piezoelectric actuator system with finite-time stability. To improve the robustness of the TSMC, the SMDO is adopted to estimate the bounded disturbances and uncertainties in finite time. Here, the PEA is considered as a second-order nonlinear system to design the proposed controller, and the hysteresis considered as the main nonlinearity is modeled for accurate simulation. The stability of the proposed controller

is proved by using the Lyapunov stability theory, and the positioning and tracking performances of the resulting control system illustrate that the proposed controller can provide the fast convergence in finite time and high tracking precision.

This paper is organized as follows. In Section 2, the problem formulation is presented. In Section 3, the continuous finite-time terminal sliding mode control with sliding mode disturbance observer scheme is designed. Simulations demonstration of the proposed controller is shown in Section 4. Section 5 concludes this paper.

2. Problem Formulation

A class of second-order single input nonlinear systems with dynamic processes can be defined as follows:

$$\ddot{x} = f(x, \dot{x}) + b(x)u + f_d, \tag{1}$$

where x and \dot{x} are the system state variables, $f(x,\dot{x})$ is in general nonlinear and possibly time-varying, b(x) expresses the control gain, u is the control input, and f_d represents the bounded external disturbance with $|f_d| \leq d$. $f(x,\dot{x}) = f_n(x,\dot{x}) + \Delta f(x,\dot{x})$, and $b(x) = b_n(x) + \Delta b(x)$. Here $f_n(x,\dot{x})$ and $d_n(x)$ are the nominal parts, whereas $d_n(x)$ and $d_n(x)$ represent the perturbations in the system. Then, the second-order system can be rewritten as

$$\ddot{x} = f_n(x, \dot{x}) + b_n(x) u + F_d,$$
 (2)

where $f_n(x, \dot{x})$, $b_n(x)$ are the nominal parts and $F_d = \Delta f(x, \dot{x}) + \Delta b(x)u + f_d$ is the lumped system uncertainty, which is assumed to be bounded by $|F_d| \leq D$. D is a given positive constant.

Consider the piezoelectric actuator as a second-order system [37], which can be written as

$$\ddot{x} + 2\xi\omega_n\dot{x} + \omega_n^2x = k\omega_n^2u + F_d,\tag{3}$$

where ξ , ω_n , and k are the damping ratio, the natural frequency, and the gain of the second-order system, respectively.

3. Controller Design

To have a concise manner of representation, in the rest of this paper, the system state variables x and \dot{x} will be omitted.

3.1. Terminal Sliding Mode Controller Design. For simplicity of expression and used in the analysis and design of the TSM controller, the following notion, which was used in [38], is introduced in this paper:

$$\operatorname{sig}(x)^{\lambda} = |x|^{\lambda} \operatorname{sign}(x), \tag{4}$$

where $0.5 < \lambda < 1$.

Remark 1. A TSM and a fast TSM can be described by the following first-order nonlinear differential equations [36]:

$$s = \dot{x} + \mu \operatorname{sig}(x)^{\lambda} = 0, \tag{5}$$

$$s = \dot{x} + ax + \mu \operatorname{sig}(x)^{\lambda} = 0, \tag{6}$$

respectively, where $x \in R$, $a, \mu > 0$, $0.5 < \lambda < 1$.

Remark 2. According to the definition of finite-time stability [39], the equilibrium point x = 0 of the differential equations (5) and (6) is globally finite-time stable; for example, for any given initial condition $x(0) = x_0$, the system state x will converge to 0 in finite time as follows:

$$T = \frac{1}{\mu (1 - \lambda)} |x_0|^{(1 - \lambda)},$$

$$T = \frac{1}{a (1 - \lambda)} \ln \frac{a|x_0|^{(1 - \lambda)} + \mu}{\mu},$$
(7)

respectively, and it stays there forever, such as x = 0 for t > T. Define the tracking error as

$$e_0 = x - x_d, \tag{8}$$

where x_d represents the desired position trajectory, and for the tracking task to be achievable using a feedback control u, the actuator output x tracks the desired trajectory x_d in finite time.

Introduce three auxiliary variables e_{01} , e_{02} , and e, where $\dot{e}_{01}=e_0$, $\dot{e}_{02}=e_{01}$, and

$$e = \dot{e}_{01} + k_0 e_{02},\tag{9}$$

where k_0 is a positive constant.

Hence, a TSM sliding surface is defined as

$$s = \dot{e} + \mu \operatorname{sig}(e)^{\lambda}, \tag{10}$$

where $\mu > 0$ and 0.5 < λ < 1. A continuous fast TSM-type reaching law is selected to achieve continuous control as follows:

$$\dot{s} = -k_1 s - k_2 \operatorname{sig}(s)^{\rho},\tag{11}$$

where k_1 , $k_2 > 0$ and $0 < \rho < 1$.

By differentiating the sliding variable s with respect to time, we have

$$\dot{s} = -2\xi\omega_n \dot{x} - \omega_n^2 x + k\omega_n^2 u + F_d - \ddot{x}_d + \mu \lambda |e|^{\lambda - 1} \dot{e}. \tag{12}$$

Substituting (11) into (12), the control law of the finitetime TSM controller can be obtained as follows:

$$u = B^{-1} \left[-A - k_1 s - k_2 \operatorname{sig}(s)^{\rho} - F_d \right], \tag{13}$$

where $A = -2\xi\omega_n\dot{x} - \omega_n^2x + \mu\lambda|e|^{\lambda-1}\dot{e} - \ddot{x}_d$ and $B = k\omega_n^2$.

It can be seen from the expression equation (12) that the term $|e|^{\lambda-1}\dot{e}$ is included in the control law u which has the negative fractional power $\lambda-1$ because of $0.5<\lambda<1$. Therefore, singularity will occur as e=0 and $\dot{e}\neq 0$. To avoid the singularly problem, the approach proposed in [40] is used in this paper. Define a new auxiliary variable \overline{e} to replace the original e, which is written as

$$\bar{e} = \begin{cases}
|e|^{\lambda^{-1}} \dot{e} & \text{if } e \neq 0 \text{ and } \dot{e} \neq 0 \\
|\Delta|^{\lambda^{-1}} \dot{e} & \text{if } e = 0 \text{ and } \dot{e} \neq 0 \\
0 & \text{if } e = 0 \text{ and } \dot{e} = 0,
\end{cases}$$
(14)

where $\Delta > 0$ is a small positive constant.

It should be noted that the bounded system uncertainty F_d is always unknown and not available in general. Therefore, in order to increase the robustness of the controller and improve the control performance, a sliding mode disturbance observer is incorporated to estimate the uncertain terms.

3.2. Sliding Mode Disturbance Observer. The SMDO is designed as an effective way to improve the robustness to external disturbances and modeling uncertainties which can finish the estimation in finite time [41, 42]. To design a SMDO for estimating the bounded system uncertainty F_d , an auxiliary system is introduced as

$$\sigma = s + z,$$

$$\dot{z} = -A - Bu - v.$$
(15)

where σ and z are the auxiliary sliding variable and intermediate variable, respectively. ν is the auxiliary traditional SMC.

The σ dynamic is derived, differentiating it with respect to time, we have

$$\dot{\sigma} = \dot{s} + \dot{z} = F_d - \nu. \tag{16}$$

Then the auxiliary traditional sliding mode control ν is designed to stabilize the sliding variable σ at zero in finite time as follows:

$$v = (D + \epsilon) \operatorname{sign}(\sigma),$$
 (17)

where $\epsilon > 0$. Introduce a Lyapunov function $V = (1/2)\sigma^2$ to drive σ to zero in finite time, and then compute its differentiating, we have

$$V = \sigma \dot{\sigma} = \sigma \left(F_d - \nu \right) \le |\sigma| D - |\sigma| \left(D + \epsilon \right) = -\epsilon |\sigma|. \tag{18}$$

It can be conclude by using (17) that σ converges to zero in finite time t_f [41], which is

$$t_f \le \frac{|\sigma(0)|}{\epsilon}.\tag{19}$$

Therefore, the auxiliary system dynamics can be governed by equivalent control $\nu_{\rm eq}$. $\nu_{\rm eq}$ is obtained by filtering the high-frequency switching control ν using a low pass filter, which is

$$v_{\rm eq} = \frac{1}{\tau s + 1} v,\tag{20}$$

where $\tau > 0$. For any t satisfied $t > t_f$, the system uncertain term F_d is estimated by $v_{\rm eq}$ in finite time t_f , which is written as

$$\widehat{F}_d = \nu_{\rm eq},\tag{21}$$

where \hat{F}_d is the estimation of F_d . Then the final continuous TSM control law with SMDO is designed as

$$u = B^{-1} \left[-A - k_1 s - k_2 \operatorname{sig}(s)^{\rho} - \widehat{F}_d \right]. \tag{22}$$

Remark 3. The convergence of the auxiliary sliding variable σ must be faster than that of s to make sure that the terminal sliding variable is stabilized to zero only after the system uncertainty is estimated.

3.3. Stability Analysis

Lemma 4. Suppose that $c_1, c_2, ..., c_n$ and 0 are all positive numbers; then the following inequality holds:

$$\left(c_1^2 + c_2^2 + \dots + c_n^2\right)^p \le \left(c_1^p + c_2^p + \dots + c_n^p\right)^2. \tag{23}$$

Lemma 5. An extended Lyapunov description of finite-time stability can be given with the form of fast TSM equation (6) as [36]

$$\dot{V}(x) + aV(x) + \mu V^{\lambda}(x) \le 0, \tag{24}$$

and the settling time can be given by

$$T \le \frac{1}{a(1-\lambda)} \ln \frac{aV^{1-\lambda}(x_0) + \mu}{\mu}.$$
 (25)

It is evident that the inequalities (24) and (25) mean exponential stability as well as faster finite-time stability.

Theorem 6. For a single-input second-order nonlinear system given by (3), with the terminal sliding surface defined by (10) and the reaching law given by (11), both the system robust stability and tracking convergence are guaranteed in finite time if the control law is designed as (22) based on the combination of SMDO.

Proof. Consider the following positive definite Lyapunov function:

$$V = \frac{1}{2}s^2.$$
 (26)

By taking the time derivative of V with respect to time, we have

$$\dot{V} = s\dot{s}$$

$$= s\left(A + F_d + Bu\right)$$

$$= s \left\{ A + F_d + B \left[B^{-1} \left(-A - k_1 s - k_2 \operatorname{sig}(s)^{\rho} - \widehat{F}_d \right) \right] \right\}$$

$$= -k_1 s^2 - s k_2 \operatorname{sig}(s)^{\rho} + s \widetilde{F}_d,$$
(27)

where $A=-2\xi\omega_n\dot{x}-\omega_n^2x+\mu\lambda|\overline{e}|^{\lambda-1}\dot{\overline{e}}-\ddot{x}_d$. $\widetilde{F_d}=F_d-\widehat{F}_d$ since the sliding variable s converges to zero only after the system uncertainty F_d is estimated in finite time t_f . Thus, $\widetilde{F_d}=F_d-\widehat{F}_d\to 0$, if $t>t_f$.

Therefore, for any $t > t_f$, from Lemma 4, we have

$$\dot{V} \le -2k_1V - 2^{(\rho+1)/2}k_2V^{(\rho+1)/2},\tag{28}$$

where $1/2 < \rho < 1$. According to Lemma 5, the proposed terminal sliding surface equation (10) will be reached in the finite time as follows:

$$T \le \frac{1}{k_1 (1 - \rho)} \ln \frac{k_1 V^{(1 - \rho)/2} + 2^{(\rho - 1)/2} k_2}{2^{(\rho - 1)/2} k_2}.$$
 (29)

Thus, according to the definition of (8), (9), and (10), if $s \to 0$ in finite time T, then $e \to 0$ and $\dot{e} \to 0$ in finite time T, and then $e_0 \to 0$ and $\dot{e}_0 \to 0$ in finite time T; hence, $x \to x_d$ and $\dot{x} \to \dot{x}_d$ in finite time T. This shows that the proposed TSM controller combined with the SMDO ensures both the robust stability of the system and the convergence of the motion tracking.

4. Simulation Results

In this section, the proposed TSM controller combined with SMDO is validated through simulations. The results are shown and discussed in this section.

4.1. PEA Model. For the purpose of simulation, a Bouc-Wen model which can describe the hysteresis is applied in this work. Consider the fact that the hysteresis is the major nonlinearity which can be handled as the uncertainty of the PEAs system. Thus, the hysteresis is modeled and integrated into the second-order PEA model for exact simulation. The Bouc-Wen model has already been verified that it is adaptive to describe the hysteresis loop of PEAs [43]. The piezoelectric actuator model with nonlinear hysteresis for simulation can be written as

$$\ddot{x} + 2\xi\omega_n\dot{x} + \omega_n^2 x = \omega_n^2 (Ku - h), \qquad (30)$$

$$\dot{h} = \alpha d\dot{u} - \beta |\dot{u}| h |h|^{n-1} - \gamma \dot{u} |h|^n,$$
 (31)

where h is the nonlinear hysteresis which indicates the hysteretic loop in terms of displacement whose magnitude and shape are determined by parameters α , β , γ , the parameter d is the piezoelectric coefficient, u denotes the input voltage, and the order n governs the smoothness of the transition from elastic to plastic response. For the elastic structure and material, n=1 is assigned in (31) as usual. These parameters used in this paper are from [8] and the values of these parameters are shown in Table 1.

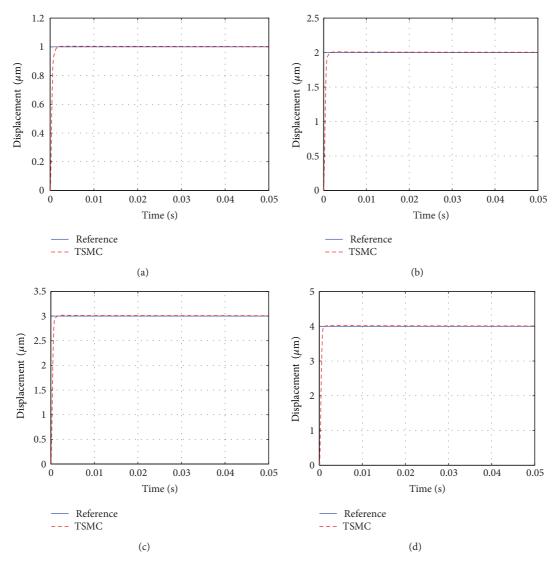


Figure 2: Simulation responses to step signals with amplitudes of (a) 1 μ m, (b) 2 μ m, (c) 3 μ m, and (d) 4 μ m.

TABLE 1: Parameters of the PEA with Bouc-Wen model.

Value Parameter 1 n ξ 1.2315×10^4 1.2225×10^6 ω_n 1.7339×10^{-6} k 0.3575 α β 0.0364 0.0272 γ

4.2. Step Responses. The transient response capability of the proposed controller is examined firstly. The controller parameters for all simulations of this paper are shown in Table 2, and the results for steps of different amplitudes are described in Figure 2 and tabulated in Table 3 for a clear expression.

The simulation results observed from Figure 2 and Table 3 show that the proposed controller provides a smooth

TABLE 2: Parameters of the implemented controller.

Parameter	Value
μ	1
λ	0.85
ρ	0.5
τ	0.01
k_0	2.5×10^4
$k_0 \ k_1$	1.5×10^{7}
$k_2 \\ D + \epsilon$	1.5×10^{7}
$D + \epsilon$	5

control with chattering free and fast convergence in finite time. Specifically, it can produce a fast response with a small overshoot.

4.3. Sinusoidal Tracking. The performances for tracking a sinusoidal waveform of $4\,\mu m$ peak-to-peak (p-p) amplitude

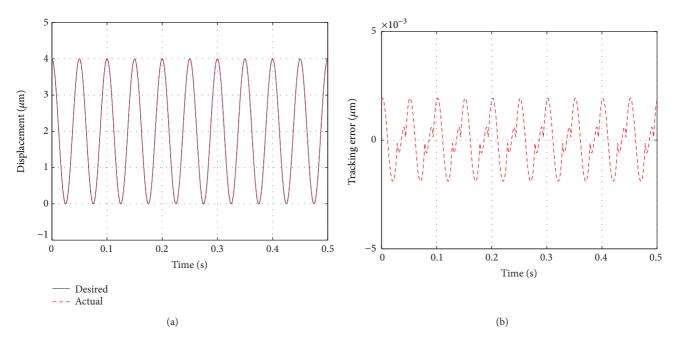


FIGURE 3: Simulation results of response to a 20 Hz sinusoidal signal.

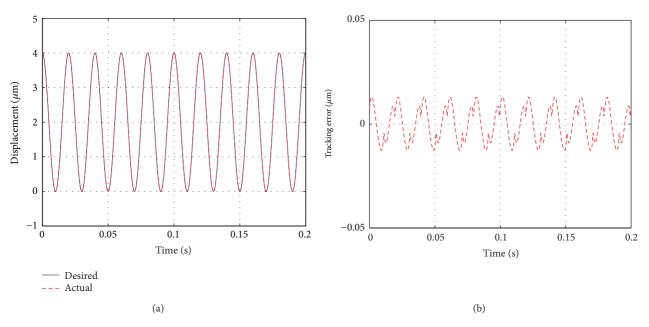


FIGURE 4: Simulation results of response to a 50 Hz sinusoidal signal.

TABLE 3: Control performance in step tracking.

Performance	TSMC			
(with different amplitudes)	$1 \mu m$	$2 \mu \mathrm{m}$	$3 \mu m$	$4\mu\mathrm{m}$
1% settling time (ms)	1.40	1.27	1.16	0.87
Overshoot	0.50%	0.55%	0.67%	0.72%

in different frequencies using the proposed controller are depicted in Figures 3-4 and described in Table 4. It can be observed from the trajectories and tracking errors that the TSM controller can track the sinusoidal trajectory precisely and chattering free. It produces a maximum error of $\pm 0.0019 \, \mu m$ at 20 Hz and $0.0130 \, \mu m$ at 50 Hz.

4.4. Responses to Staircase Signal. The staircase signal is applied to the proposed controller for the PEA. Figures 5(a) and 5(b) show that a step of the staircase signal covering the range of $1\,\mu\mathrm{m}$ by 100 steps with each step lasting for 0.01s. The proposed controller can guarantee the steady-state error of 0 nm for approximating 80% duration of the step. Shorter distance positioning response is described in

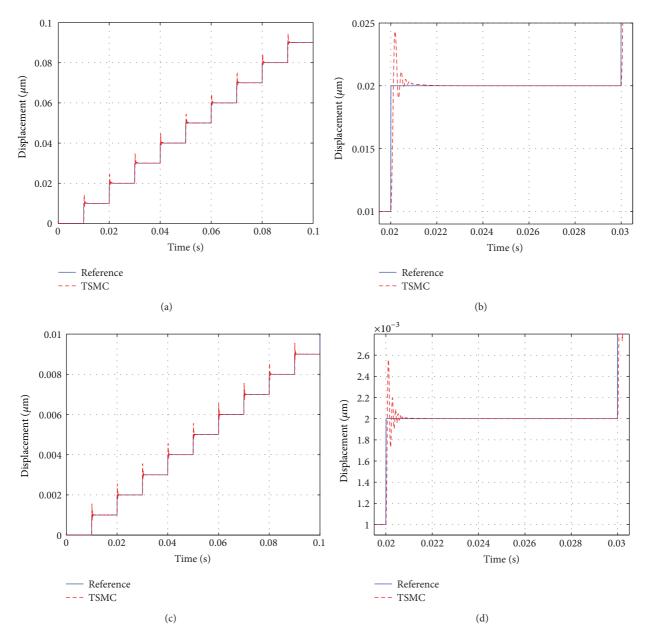


FIGURE 5: Simulation responses to staircase signals covering the range 1 µm with (a)-(b) 100 steps and (c)-(d) 1000 steps.

TABLE 4: Performance of the controller with sinusoidal signal.

Performance	SMC		
(with different frequencies)	RMSE (μ m)	Max. $E(\mu m)$	
5 HZ	1.3791×10^{-8}	-2.1021×10^{-4}	
10 HZ	1.0575×10^{-7}	-5.0846×10^{-4}	
20 HZ	1.4110×10^{-6}	±0.0019	
50 HZ	6.8825×10^{-5}	0.0130	
100 HZ	0.0012	0.0515	

Figures 5(c) and 5(d) in which the amplitude of each step is 1 nm. The proposed controller can realize the steady-state error of ± 0.5 nm for approximating 85% duration of the step.

Therefore, the steps can be identified which indicates that the positioning resolution of the proposed controller is less than 1 nm.

4.5. Discussions on Control Performance. In view of the simulation results, it can be concluded that the proposed TSM controller can obtain good performances in both positioning control and tracking control of the PEA. In the step signal simulations, the proposed controller enables a fast transient response without much overshoot, and especially, it removes the chattering without steady-state error. The TSM controller is also suitable for tracking control because of its small tracking error, fast response, and high resolution in both sinusoidal tracking and stair signals tracking.

5. Conclusions

In this paper, a robust control strategy based on a new TSMC combined with a SMDO is developed for piezoelectric actuators. In order to get accurate motion tracking performance, the hysteresis model is considered in the PEA model for simulation. The step response simulation results show that the proposed controller can accelerate the transient response with low overshoot. In addition, it provides a smooth control and excellent performance in the control implementation yielding few chattering and fast convergence. The sinusoidal motion and stair signal tracking simulation results illustrate that the proposed controller can give a rise to the tracking performance with a small tracking error and high resolution. Based on this control strategy, the design of the controller is simple and convenient to drive the piezoelectric actuator. Robust stability of the proposed controller is guaranteed with the nonlinear uncertainties and external disturbance.

In the future research, fault detection and fault tolerant control of piezoelectric actuators will be an interesting work based on related results [44, 45].

Conflict of Interests

The authors declare that there is no conflict of interests regarding the publication of this paper.

Acknowledgment

The authors would like to acknowledge the financial support of the National Key Scientific Instrument and Equipment Development Projects of China through grant nos. 2012YQ04014001 and 2012YQ04014010.

References

- [1] S. Devasia, E. Eleftheriou, and S. O. R. Moheimani, "A survey of control issues in nanopositioning," *IEEE Transactions on Control Systems Technology*, vol. 15, no. 5, pp. 802–823, 2007.
- [2] H. Song, G. Vdovin, R. Fraanje, G. Schitter, and M. Verhaegen, "Extracting hysteresis from nonlinear measurement of wavefront-sensorless adaptive optics system," *Optics Letters*, vol. 34, no. 1, pp. 61–63, 2009.
- [3] D. Croft, G. Shedd, and S. Devasia, "Creep, hysteresis, and vibration compensation for piezoactuators: atomic force microscopy application," in *Proceedings of the American Control Conference*, vol. 3, pp. 2123–2128, Chicago, Ill, USA, June 2000.
- [4] S. O. R. Moheimani, "Invited review article: accurate and fast nanopositioning with piezoelectric tube scanners: emerging trends and future challenges," *Review of Scientific Instruments*, vol. 79, no. 7, Article ID 071101, 2008.
- [5] K. W. Chan and W.-H. Liao, "Precision positioning of hard disk drives using piezoelectric actuators with passive damping," in Proceedings of the IEEE International Conference on Mechatronics and Automation (ICMA '06), pp. 1269–1274, Luoyang, China, June 2006.
- [6] E. Eleftheriou, "Nanopositioning for storage applications," *Annual Reviews in Control*, vol. 36, no. 2, pp. 244–254, 2012.

- [7] H. J. M. T. A. Adriaens, W. L. de Koning, and R. Banning, "Modeling piezoelectric actuators," *IEEE/ASME Transactions on Mechatronics*, vol. 5, no. 4, pp. 331–341, 2000.
- [8] J. Li and L. Yang, "Adaptive pi-based sliding mode control for nanopositioning of piezoelectric actuators," *Mathematical Problems in Engineering*, vol. 2014, Article ID 357864, 10 pages, 2014.
- [9] G. M. Clayton, S. Tien, A. J. Fleming, S. O. R. Moheimani, and S. Devasia, "Inverse-feedforward of charge-controlled piezopositioners," *Mechatronics*, vol. 18, no. 5-6, pp. 273–281, 2008.
- [10] J. Minase, T.-F. Lu, B. Cazzolato, and S. Grainger, "A review, supported by experimental results, of voltage, charge and capacitor insertion method for driving piezoelectric actuators," *Precision Engineering*, vol. 34, no. 4, pp. 692–700, 2010.
- [11] Y. T. Ma, L. Huang, Y. B. Liu, and Z. H. Feng, "Note: creep character of piezoelectric actuator under switched capacitor charge pump control," *Review of Scientific Instruments*, vol. 82, no. 4, Article ID 046106, 2011.
- [12] K. K. Leang, Q. Zou, and S. Devasia, "Feedforward control of piezoactuators in atomic force microscope systems," *IEEE Con*trol Systems Magazine, vol. 29, no. 1, pp. 70–82, 2009.
- [13] D. Pesotski, H. Janocha, and K. Kuhnen, "Adaptive compensation of hysteretic and creep non-linearities in solid-state actuators," *Journal of Intelligent Material Systems and Structures*, vol. 21, no. 14, pp. 1437–1446, 2010.
- [14] B. Mokaberi and A. A. G. Requicha, "Compensation of scanner creep and hysteresis for AFM nanomanipulation," *IEEE Transactions on Automation Science and Engineering*, vol. 5, no. 2, pp. 197–206, 2008.
- [15] M.-J. Jang, C.-L. Chen, and J.-R. Lee, "Modeling and control of a piezoelectric actuator driven system with asymmetric hysteresis," *Journal of the Franklin Institute*, vol. 346, no. 1, pp. 17–32, 2009.
- [16] L. Liu, K. Tan, S. Chen, C. Teo, and T. Lee, "Discrete composite control of piezoelectric actuators for high-speed and precision scanning," *IEEE Transactions on Industrial Informatics*, vol. 9, no. 2, pp. 859–868, 2013.
- [17] Y. C. Huang and D. Y. Lin, "Ultra-fine tracking control on piezoelectric actuated motion stage using piezoelectric hysteretic model," *Asian Journal of Control*, vol. 6, no. 2, pp. 208–216, 2004.
- [18] T.-J. Yeh, H. Ruo-Feng, and L. Shin-Wen, "An integrated physical model that characterizes creep and hysteresis in piezoelectric actuators," *Simulation Modelling Practice and Theory*, vol. 16, no. 1, pp. 93–110, 2008.
- [19] L. Juhász, J. Maas, and B. Borovac, "Parameter identification and hysteresis compensation of embedded piezoelectric stack actuators," *Mechatronics*, vol. 21, no. 1, pp. 329–338, 2011.
- [20] H. G. Xu, T. Ono, and M. Esashi, "Precise motion control of a nanopositioning PZT microstage using integrated capacitive displacement sensors," *Journal of Micromechanics and Micro-engineering*, vol. 16, no. 12, article 2747, 2006.
- [21] C.-Y. Lin and P.-Y. Chen, "Precision tracking control of a biaxial piezo stage using repetitive control and double-feedforward compensation," *Mechatronics*, vol. 21, no. 1, pp. 239–249, 2011.
- [22] A. Sebastian and S. M. Salapaka, "Design methodologies for robust nano-positioning," *IEEE Transactions on Control Systems Technology*, vol. 13, no. 6, pp. 868–876, 2005.
- [23] M. Boukhnifer and A. Ferreira, " H_{∞} loop shaping bilateral controller for a two-fingered tele-micromanipulation system," *IEEE Transactions on Control Systems Technology*, vol. 15, no. 5, pp. 891–905, 2007.

- [24] S. Yin, S. X. Ding, A. H. A. Sari, and H. Hao, "Data-driven monitoring for stochastic systems and its application on batch process," *International Journal of Systems Science*, vol. 44, no. 7, pp. 1366–1376, 2013.
- [25] J. Dong, S. M. Salapaka, and P. M. Ferreira, "Robust control of a parallel-kinematic nanopositioner," *Journal of Dynamic Systems, Measurement and Control*, vol. 130, no. 4, Article ID 0410071, 15 pages, 2008.
- [26] T. W. Seo, H. S. Kim, D. S. Kang, and J. Kim, "Gain-scheduled robust control of a novel 3-DOF micro parallel positioning platform via a dual stage servo system," *Mechatronics*, vol. 18, no. 9, pp. 495–505, 2008.
- [27] H. C. Liaw, B. Shirinzadeh, and J. Smith, "Enhanced sliding mode motion tracking control of piezoelectric actuators," Sensors and Actuators A, vol. 138, no. 1, pp. 194–202, 2007.
- [28] H. C. Liaw, B. Shirinzadeh, and J. Smith, "Sliding-mode enhanced adaptive motion tracking control of piezoelectric actuation systems for micro/nano manipulation," *IEEE Transactions on Control Systems Technology*, vol. 16, no. 4, pp. 826–833, 2008.
- [29] J.-C. Shen, W.-Y. Jywe, C.-H. Liu, Y.-T. Jian, and J. Yang, "Sliding-mode control of a three-degrees-of-freedom nanopositioner," *Asian Journal of Control*, vol. 10, no. 3, pp. 267–276, 2008.
- [30] G. Song, J. Zhao, X. Zhou, and J. A. de Abreu-García, "Tracking control of a piezoceramic actuator with hysteresis compensation using inverse Preisach model," *IEEE/ASME Transactions on Mechatronics*, vol. 10, no. 2, pp. 198–209, 2005.
- [31] C.-J. Lin and S.-R. Yang, "Precise positioning of piezo-actuated stages using hysteresis-observer based control," *Mechatronics*, vol. 16, no. 7, pp. 417–426, 2006.
- [32] O. Barambones and V. Etxebarria, "Robust sliding composite adaptive control for mechanical manipulators with finite error convergence time," *International Journal of Systems Science*, vol. 32, no. 9, pp. 1101–1108, 2001.
- [33] O. Barambones and V. Etxebarria, "Energy-based approach to sliding composite adaptive control for rigid robots with finite error convergence time," *International Journal of Control*, vol. 75, no. 5, pp. 352–359, 2002.
- [34] S. Yin, G. Wang, and H. R. Karimi, "Data-driven design of robust fault detection system for wind turbines," *Mechatronics*, 2013.
- [35] Y. Feng, X. Yu, and Z. Man, "Non-singular terminal sliding mode control of rigid manipulators," *Automatica*, vol. 38, no. 12, pp. 2159–2167, 2002.
- [36] S. Yu, X. Yu, B. Shirinzadeh, and Z. Man, "Continuous finitetime control for robotic manipulators with terminal sliding mode," *Automatica*, vol. 41, no. 11, pp. 1957–1964, 2005.
- [37] J. Y. Peng and X. B. Chen, "Integrated pid-based sliding mode state estimation and control for piezoelectric actuators," *IEEE/ASME Transactions on Mechatronics*, vol. 19, no. 1, pp. 88– 99, 2012
- [38] V. T. Haimo, "Finite time controllers," SIAM Journal on Control and Optimization, vol. 24, no. 4, pp. 760–770, 1986.
- [39] Y. Hong, J. Huang, and Y. Xu, "On an output feedback finitetime stabilization problem," *IEEE Transactions on Automatic Control*, vol. 46, no. 2, pp. 305–309, 2001.
- [40] D. Zhao, S. Li, and F. Gao, "A new terminal sliding mode control for robotic manipulators," *International Journal of Control*, vol. 82, no. 10, pp. 1804–1813, 2009.

- [41] C. E. Hall and Y. B. Shtessel, "Sliding mode disturbance observer-based control for a reusable launch vehicle," *Journal of Guidance, Control, and Dynamics*, vol. 29, no. 6, pp. 1315–1328, 2006.
- [42] S. Yin, X. Yang, and H. R. Karimi, "Data-driven adaptive observer for fault diagnosis," *Mathematical Problems in Engi*neering, vol. 2012, Article ID 832836, 21 pages, 2012.
- [43] T. S. Low and W. Guo, "Modeling of a three-layer piezoelectric bimorph beam with hysteresis," *Journal of Microelectromechanical Systems*, vol. 4, no. 4, pp. 230–237, 1995.
- [44] S. Yin, H. Luo, and S. Ding, "Real-time implementation of fault-tolerant control systems with performance optimization," *IEEE Transactions on Industrial Electronics*, vol. 61, no. 5, pp. 2402–2411, 2014.
- [45] S. Yin, S. Ding, A. Haghani, H. Hao, and P. Zhang, "A comparison study of basic data-driven fault diagnosis and process monitoring methods on the benchmark tennessee eastman process," *Journal of Process Control*, vol. 22, no. 9, pp. 1567–1581, 2012.

Hindawi Publishing Corporation Abstract and Applied Analysis Volume 2014, Article ID 523163, 11 pages http://dx.doi.org/10.1155/2014/523163

Research Article

Numerical Implementation of Stochastic Operational Matrix Driven by a Fractional Brownian Motion for Solving a Stochastic Differential Equation

R. Ezzati, M. Khodabin, and Z. Sadati

Department of Mathematics, Karaj Branch, Islamic Azad University, Karaj, Iran

Correspondence should be addressed to R. Ezzati; ezati@kiau.ac.ir

Received 16 November 2013; Revised 20 January 2014; Accepted 20 January 2014; Published 11 March 2014

Academic Editor: Hamid Reza Karimi

Copyright © 2014 R. Ezzati et al. This is an open access article distributed under the Creative Commons Attribution License, which permits unrestricted use, distribution, and reproduction in any medium, provided the original work is properly cited.

An efficient method to determine a numerical solution of a stochastic differential equation (SDE) driven by fractional Brownian motion (FBM) with Hurst parameter $H \in (1/2,1)$ and n independent one-dimensional standard Brownian motion (SBM) is proposed. The method is stated via a stochastic operational matrix based on the block pulse functions (BPFs). With using this approach, the SDE is reduced to a stochastic linear system of m equations and m unknowns. Then, the error analysis is demonstrated by some theorems and definitions. Finally, the numerical examples demonstrate applicability and accuracy of this method.

1. Introduction

In many fields of science and engineering, there are a large number of problems which are intrinsically involving stochastic excitations of a Gaussian white noise type. Having in mind a Gaussian white noise mathematically described as a formal derivative of a Brownian motion process, all such problems are mathematically modeled by stochastic differential equations. Most of them cannot be solved analytically, so it is important to provide their numerical solutions. There has been a growing interest in numerical solutions of stochastic differential equations for the last years [1–10].

In the presented work, we consider SDE as follows:

$$dx(s) = k(s,t) x(s) ds + \sum_{i=1}^{n} ti(s,t) x(s) dB_{i}(s)$$

$$+ r(s,t) x(s) dB_{s}^{H}, \quad s \in (0,T), T < 1,$$

$$x(0) = x_{0},$$
(1)

or

$$x(t) = x_0 + \int_0^t k(s, t) x(s) ds$$

$$+ \sum_{i=1}^n \int_0^t ti(s, t) x(s) dB_i(s)$$

$$+ \int_0^t r(s, t) x(s) dB_s^H, \quad t \in (0, T), \ T < 1,$$
(2)

where B_s^H denotes the FBM with Hurst parameter $H \in ((1/2), 1)$ on probability space (Ω, \mathcal{F}, P) and $B_i(s)$ (i = 1, 2, ..., n) is n independent one-dimensional SBM defined on the same probability space. Also, k(s, t), $t_i(s, t) : (0, T) \times (0, T) \to \mathbb{R}$ (i = 1, 2, ..., n) and x(t) is the stochastic process of unknown on the probability space.

Investigations concerning the SDE driven by the FBM have been done by Zähle [11], Coutin [12], Decreusefond and Üstünel [13], Nualart [4, 14], Lisei and Soós [15], and other authors. Also, there exist several ways for solving it, pathwise and related techniques, Dirichlet forms, Euler approximations, Malliavin calculus, and Skorohod integral

[1, 4, 15–17]; almost all methods have very poor numerical convergence.

It is important to find approximate solutions of the stochastic equations driven by the FBM, since these equations cannot be solved analytically in most cases and have many applications in models arising in physics, telecommunication networks, and finance [18]. Also, we cannot use from the classical Ito theory for their stochastic calculus, since these processes are not Markovian and semimartingale. Hence, in this work, we implement the stochastic operational matrix based on the BPFs for solving (2). The benefits of this method are lower cost of setting up the system of equations; moreover, the computational cost of operations is low. Also, convergence of this method is faster than other methods. These advantages make the method easier to apply.

The rest of the paper is organized as follows. In Section 2, some essential definitions and the following assumptions on the coefficients of (2) are stated. Also, the necessary properties of the block pulse functions (BPFs) are introduced. In Section 3, first a theorem is proved; then (2) is reduced to a stochastic linear system by using the properties of the BPFs. In Section 4, the error analysis is demonstrated. Efficiency of this method and good reasonable degree of accuracy are confirmed by some numerical examples, in Section 5. Finally, in Section 6, a brief conclusion is given.

2. Preliminaries

Definition 1. Let be the step $r(t) = \sum_{j=1}^{m-1} d_j \chi_{[t_j, t_{j+1}(t)]}$ function and χ denotes the characteristic function on [0, p], $d_j \in \mathbb{R}$, and $0 = t_1 < t_2 < \cdots < t_m = p$. Then, the wiener integral with respect to the FBM is defined as

$$\int_{0}^{p} r(t) dB_{t}^{H} = \sum_{i=1}^{m-1} d_{j} \left(B_{t_{j+1}}^{H} - B_{t_{j}}^{H} \right), \tag{3}$$

where $H \in ((1/2), 1)$ and p > 0 (see [19]).

Definition 2. Let $\nu = \nu[\alpha, \lambda]$ denote the class of function h on $[\alpha, \lambda] \times \Omega$ such that

- (1) the function *h* is $\beta \times F$ measurable;
- (2) the function *h* is adapted to $\{F_t\}_{t\geq 0}$;

(3)
$$\int_{a}^{\lambda} \int_{a}^{s} E[h^{2}(s)]|s - t| dt ds < \infty \text{ and } s, t \in [\alpha, \lambda].$$

Let us consider the following assumptions on the coefficients.

(A₁) (r(s,t)x(s)) is differentiable in x(s) and there exist constants $\alpha, \beta \le 1$ and $K_1, K_2, K_3 > 0$ such that

$$|r(s,t) x(s) - r(s,t) y(s)|$$

 $\leq K_1 |x(s) - y(s)|$ (Lipschitz continuity),

$$\begin{aligned} \left| \partial_{x} r\left(s,t\right) x\left(s\right) - \partial_{x} r\left(s,t\right) y\left(s\right) \right| \\ &\leq K_{2} \left| x\left(s\right) - y\left(s\right) \right|^{\alpha} \quad \left(\text{Holder continuity} \right), \\ \left| r\left(s,t\right) x\left(s\right) - r\left(u,t\right) x\left(s\right) \right| + \left| \partial_{x} r\left(s,t\right) x\left(s\right) - \partial_{x} r\left(u,t\right) x\left(s\right) \right| \\ &\leq K_{3} \left| s - u \right|^{\beta}. \end{aligned} \tag{4}$$

(A₂) There exist constants K_{4i} , $K_{5i} > 0$ (i = 1, ..., n) such that

$$|ti(s,t) x(s) - ti(s,t) y(s)|$$

$$\leq K_{4i} |x(s) - y(s)| \quad \text{(Lipschitz continuity)}, \qquad (5)$$

$$|ti(s,t) x(s)| \leq K_{5i} (1 + |x(s)|) \quad \text{(Linear growth)}.$$

(A₃) There exist constants $K_6, K_7 > 0$ (i = 1, ..., n) such that

$$|k(s,t) x(s) - k(s,t) y(s)|$$

$$\leq K_6 |x(s) - y(s)| \quad \text{(Lipschitz continuity)}, \qquad (6)$$

$$|k(s,t) x(s)| \leq K_7 (1 + |x(s)|) \quad \text{(Linear growth)},$$

for all t, s, $u \in (0, T)$.

Theorem 3. Let k(s,t)x(s), ti(s,t)x(s) and r(s,t)x(s) hold in condition (A_1) , (A_2) , (A_3) , and $H < \{(1/2), (\alpha/(\alpha+1)), \beta\}$. Then, there exists a unique solution for (2).

Now, we review the main properties of the BPFs which are necessary for this paper. Note that the BPFs are discussed in [7, 8].

(1) A function $p(x) \in L^2([0,T))$ is approximated by using properties of the BPFs as

$$p(x) \approx \hat{p}(x) = P^{T} \Psi(x) = \Psi^{T}(x) P,$$
 (7)

where

$$\Psi(x) = (\Psi_1(x), \Psi_2(x), \dots, \Psi_i(x), \dots, \Psi_m(x))^T,$$
 (8)

with

$$\Psi_i(x) = \begin{cases} 1 & (i-1)\frac{T}{m} \le x < i\frac{T}{m}, \ i = 1, \dots, m, \\ 0 & \text{otherwise,} \end{cases}$$
 (9)

where $\Psi_i(x)$ denotes the BPFs and

$$P = (p_1, p_2, \dots, p_i, \dots, p_m)^T,$$
 (10)

with

$$p_i = \frac{m}{T} \int_0^T p(x) \Psi_i(x) dx.$$
 (11)

(2) A function $p(x, y) \in L^2([0, T) \times [0, T))$ is approximated as follows:

$$p(x, y) \approx \hat{p}(x, y) = \Psi^{T}(x) P\Psi(y) = \Psi^{T}(y) P^{T}\Psi(x),$$
(12)

where

$$P = \left(p_{ij}\right)_{m \times m},$$

$$p_{ij} = \frac{m^2}{T^2} \left\{ \int_0^T p(x, y) \Psi_i(x) \Psi_j(y) dx dy, \right\}$$
(13)

$$i = 1, 2, \ldots, m, j = 1, 2, \ldots, m.$$

(3) Consider

$$\Psi(x) \Psi^{T}(x)$$

$$= \begin{pmatrix} \Psi_{1}(x) & 0 & 0 & \cdots & 0 \\ 0 & \Psi_{2}(x) & 0 & \cdots & 0 \\ 0 & 0 & \Psi_{3}(x) & \cdots & 0 \\ \vdots & \vdots & \vdots & \ddots & \vdots \\ 0 & 0 & 0 & \cdots & \Psi_{m}(x) \end{pmatrix}_{m \times m}$$

$$(14)$$

$$\begin{array}{c} 2m \\ \vdots & \vdots & \vdots \\ 0 & 0 & 0 \\ \vdots & \vdots & \vdots \\ 0 & 0 & 0 \end{array}$$

$$(6) \text{ In [8], it is proved that}$$

$$\left(\int_{0}^{t} \Psi(x) \Psi^{T}(x) dB(t) dt \right) dt = 0$$

(4) $\Psi(x)\Psi^{T}(x)L = \widehat{L}\Psi(x)$, where

$$\hat{L} = \begin{pmatrix} l_{11}, l_{21}, \dots, l_{m1} \end{pmatrix}^{T},$$

$$\hat{L} = \begin{pmatrix} l_{11} & 0 & 0 & \cdots & 0 \\ 0 & l_{21} & 0 & \cdots & 0 \\ 0 & 0 & l_{31} & \cdots & 0 \\ \vdots & \vdots & \vdots & \ddots & \vdots \\ 0 & 0 & 0 & 1 \end{pmatrix} .$$
(15)

(5) In [8], it is proved that

$$\left(\int_{0}^{t} \Psi(x) \Psi^{T}(x) dx\right) A \Psi(t) = R \Psi(t), \qquad (16)$$

$$A = (a_{ij})_{m \times m},$$

$$R = \frac{T}{2m} \begin{pmatrix} a_{11} & 2a_{12} & 2a_{13} & \cdots & 2a_{1m} \\ 0 & a_{22} & 2a_{23} & \cdots & 2a_{2m} \\ 0 & 0 & a_{33} & \cdots & 2a_{3m} \\ \vdots & \vdots & \vdots & \ddots & \vdots \\ 0 & 0 & 0 & \cdots & a_{mm} \end{pmatrix}_{m \times m}$$

$$(17)$$

$$\left(\int_{0}^{t} \Psi(x) \Psi^{T}(x) dB(x)\right) A\Psi(t) = E\Phi(t), \quad (18)$$

where

$$E = \begin{pmatrix} a_{11}B\left(\frac{h}{2}\right) & a_{12}B(h) & a_{13}B(h) & \cdots & a_{1m}B(h) \\ 0 & a_{22}\left(B\left(\frac{3h}{2}\right) - B(h)\right) & a_{23}\left(B(2h) - B(h)\right) & \cdots & a_{2m}\left(B(2h) - B(h)\right) \\ 0 & 0 & a_{33}\left(B\left(\frac{5h}{2}\right) - B(2h)\right) & \cdots & a_{3m}\left(B(3h) - B(2h)\right) \\ \vdots & \vdots & \vdots & \ddots & \vdots \\ 0 & 0 & 0 & \cdots & a_{mm}\left(B\left(\frac{(2m-1)h}{2}\right) - B((m-1)h)\right) \end{pmatrix}_{m \times m}$$

$$h = \frac{T}{m}.$$
(19)

3. Solving the SDE Driven by FBM and *n* Independent One-Dimensional SBM

Theorem 4. Let $\Psi(t)$ denote the BPFs, h = (T/m), and $R = (r_{ij})_{m \times m}$, i, j = 1, ..., m; then

$$\left(\int_{0}^{t} \Psi(s) \Psi^{T}(s) dB_{s}^{H}\right) R\Psi(t) \approx B\Psi(t), \quad t \in (0, T), \quad (20)$$

where

$$B = \begin{pmatrix} r_{11}B_{h/2}^{H} & r_{12}B_{h}^{H} & \cdots & r_{1m}B_{h}^{H} \\ 0 & r_{22}\left(B_{3h/2}^{H} - B_{h}^{H}\right) & \cdots & r_{2m}\left(B_{2h}^{H} - B_{h}^{H}\right) \\ \vdots & \vdots & \ddots & \vdots \\ 0 & 0 & \cdots & r_{mm}\left(B_{((2m-1)h/2)}^{H} - B_{(m-1)h}^{H}\right) \end{pmatrix}_{m \times m}$$

$$(21)$$

Proof. First, we compute stochastic operational matrix driven by the FBM based on the BPFs as follows.

(A1) If $0 \le t < (i - 1)h$, then

$$\int_{0}^{t} \Psi_{i}(s) dB_{s}^{H} = 0.$$
 (22)

(A2) If $(i-1)h \le t < ih$, the function $\Psi_i(s)$ is defined as

$$\Psi_i(s) = \sum_{k=1}^{m+1} f_{ik} \chi_{[s_{k-1}, s_k)}(s), \quad i = 1, \dots, m,$$
 (23)

where χ denotes the characteristic function and $0 = s_0 < s_1 < \cdots < s_{i-1} \le s_i = t < s_{i+1} < \cdots < s_{m+1}$, where $s_k = kh$ if $k = 0, 1, \ldots, i-1$ and $s_k = (k-1)h$ if $k = i+1, \ldots, m+1$. Also,

$$f_{ik} = \begin{cases} 1 & k = i \lor k = i + 1, \\ 0 & \text{otherwise.} \end{cases}$$
 (24)

Now, for computation $\int_0^t \Psi_i(s) dB_s^{H_i}$ ($s \in [0,t]$), we can write

$$\Psi_{i}(s) = \sum_{k=1}^{i} f_{ik} \chi_{[s_{k-1}, s_{k})}(s), \quad i = 1, \dots, m.$$
 (25)

Then by using Definition 1, we obtain

$$\int_{0}^{t} \Psi_{i}(s) dB_{s}^{H} = \sum_{k=1}^{i} f_{ik} \left(B_{s_{k}}^{H} - B_{s_{k-1}}^{H} \right)$$

$$= B_{t}^{H} - B_{(i-1)h}^{H}, \quad i = 1, 2, \dots, m.$$
(26)

(A3) If $ih \le t < T$, then

$$\Psi_{i}(s) = \sum_{k=1}^{m+1} c_{ik} \chi_{[s_{k-1}, s_{k})}(s), \quad i = 1, \dots, m,$$
 (27)

where $0 = s_0 < s_1 < \dots < s_i \le s_{i+1} = t < s_{i+2} < \dots < s_{m+1}$, $s_k = kh$ if $k = 0, 1, \dots, i$, $s_k = (k-1)h$ if $k = i+2, \dots, m+1$, and

$$c_{ik} = \begin{cases} 1 & k = i, \\ 0 & k \neq i. \end{cases}$$
 (28)

For computation $\int_0^t \Psi_i(s) dB_s^{H_i}$ ($s \in [0, t]$), we can write

$$\Psi_i(s) = \sum_{k=1}^{i+1} c_{ik} \chi_{[s_{k-1}, s_k)}(s), \quad i = 1, \dots, m,$$
 (29)

so, we get

$$\int_{0}^{t} \Psi_{i}(s) dB_{s}^{H} = \sum_{k=1}^{i+1} c_{ik} \left(B_{s_{k}}^{H} - B_{s_{k-1}}^{H} \right)$$

$$= B_{ih}^{H} - B_{(i-1)h}^{H}, \quad i = 1, 2, \dots, m.$$
(30)

From (A1), (A2), and (A3), we get

$$\int_{0}^{t} \Psi_{i}(s) dB_{s}^{H} = \begin{cases} 0 & 0 \le t < (i-1)h, \\ B_{t}^{H} - B_{(i-1)h}^{H} & (i-1)h \le t < ih, \\ B_{ih}^{H} - B_{(i-1)h}^{H} & ih \le t < T. \end{cases}$$
(31)

Furthermore, we suppose that

$$B_t^H - B_{(i-1)h}^H \approx B_{(i-0.5)h}^H - B_{(i-1)h}^H, \quad (i-1)h \le t < ih, \quad (32)$$

so, we can write

$$\int_{0}^{t} \Psi_{i}(s) dB_{s}^{H} \approx \left(0, \dots, 0, B_{(i-0.5)h}^{H} - B_{(i-1)h}^{H}, B_{(i-1)h}^{H}, \dots, B_{ih}^{H} - B_{(i-1)h}^{H}\right) \Psi(t).$$
(33)

Hence, by using the relation (33), we can write

$$\int_{0}^{t} \Psi(s) dB_{s}^{H} \approx P_{H} \Psi(t), \qquad (34)$$

where

$$P_{H} = \begin{pmatrix} B_{h/2}^{H} & B_{h}^{H} & B_{h}^{H} & \cdots & B_{h}^{H} \\ 0 & B_{3h/2}^{H} - B_{h}^{H} & B_{2h}^{H} - B_{h}^{H} & \cdots & B_{2h}^{H} - B_{h}^{H} \\ 0 & 0 & B_{5h/2}^{H} - B_{2h}^{H} & \cdots & B_{3h}^{H} - B_{2h}^{H} \\ \vdots & \vdots & \vdots & \ddots & \vdots \\ 0 & 0 & 0 & \cdots & B_{((2m-1)h/2)}^{H} - B_{(m-1)h}^{H} \end{pmatrix}_{m \times m}$$

$$(35)$$

Now, let C_{R^i} be the *i*th row of matrix $C_R = \text{Diag}(R)$, let P_H^i be the ith row of the matrix P_H , and let R^i be the ith row of matrix *R*. We have

$$\left(\int_{0}^{t} \Psi\left(s\right) \Psi^{T}\left(s\right) dB_{s}^{H} \right) R\Psi\left(t\right) \\ + \sum_{i=1}^{n} x^{T} \int_{0}^{t} \Psi\left(s\right) \Psi^{T}\left(s\right) Ti\Psi\left(t\right) dB_{i}\left(s\right) \\ + x^{T} \int_{0}^{t} \Psi\left(s\right) \Psi^{T}\left(s\right) Ti\Psi\left(t\right) dB_{i}\left(s\right) \\ + x^{T} \int_{0}^{t} \Psi\left(s\right) \Psi^{T}\left(s\right) R\Psi\left(t\right) dB_{s}^{H}, \\ + x^{T} \left(\int_{0}^{t} \Psi\left(s\right) \Psi^{T}\left(s\right) dS\right) R\Psi\left(t\right) dB_{s}^{H}, \\ + x^{T} \left(\int_{0}^{t} \Psi\left(s\right) \Psi^{T}\left(s\right) dB_{s}^{H}, \\ + x^{T} \left(\int_{0}^{t} \Psi\left(s\right) \Psi\left(s\right) dB_{s}^{H}, \\ + x^{T} \left(\int_{0}^{t} \Psi\left(s\right) \Psi\left(s\right) dB_{s}^{H}, \\ + x^{T} \left$$

where B is given by (21).

Let

$$x(t) \approx x^{T} \Psi(t) = \Psi^{T}(t) x,$$

$$x_{0} \approx x_{0}^{T} \Psi(t) = \Psi^{T}(t) x_{0},$$

$$k(s,t) \approx \Psi^{T}(s) K \Psi(t) = \Psi^{T}(t) K^{T} \Psi(s),$$

$$r(s,t) \approx \Psi^{T}(s) R \Psi(t) = \Psi^{T}(t) R^{T} \Psi(s),$$

$$ti(s,t) \approx \Psi^{T}(s) Ti \Psi(t)$$

$$= \Psi^{T}(t) Ti^{T} \Psi(s), \quad i = 1, 2, ..., n,$$
(37)

where x and x_0 are the block pulse coefficients vector and K, R, and Ti, i = 1, ..., n, are the block pulse coefficients matrix.

By substituting the relation (37) in (2), we get

$$x^{T}\Psi(t) \approx x_{0}^{T}\Psi(t) + x^{T} \int_{0}^{t} \Psi(s) \Psi^{T}(s) K\Psi(t) ds$$

$$+ \sum_{i=1}^{n} x^{T} \int_{0}^{t} \Psi(s) \Psi^{T}(s) Ti\Psi(t) dB_{i}(s) \qquad (38)$$

$$+ x^{T} \int_{0}^{t} \Psi(s) \Psi^{T}(s) R\Psi(t) dB_{s}^{H},$$

$$x^{T}\Psi(t) \approx x^{T}\Psi(t) + x^{T} \left(\int_{0}^{t} \Psi(s) \Psi^{T}(s) ds \right) K\Psi(t)$$

$$x^{T}\Psi(t) \approx x_{0}^{T}\Psi(t) + x^{T}\left(\int_{0}^{t}\Psi(s)\Psi^{T}(s)\,ds\right)K\Psi(t)$$

$$+ x^{T}\sum_{i=1}^{n}\left(\int_{0}^{t}\Psi(s)\Psi^{T}(s)\,dB_{i}(s)\right)Ti\Psi(t) \qquad (39)$$

$$+ x^{T}\left(\int_{0}^{t}\Psi(s)\Psi^{T}(s)\,dB_{s}^{H}\right)R\Psi(t).$$

Therefore, by using properties of the BPFs and Theorem 4, we can write

$$x^{T}\Psi(t) \approx x_{0}^{T}\Psi(t) + x^{T}A\Psi(t) + x^{T}\sum_{i=1}^{n}C_{i}\Psi(t) + x^{T}B\Psi(t),$$

$$(40)$$

where

$$A = \frac{T}{2m} \begin{pmatrix} k_{11} & 2k_{12} & 2k_{13} & \cdots & 2k_{1m} \\ 0 & k_{22} & 2k_{23} & \cdots & 2k_{2m} \\ 0 & 0 & k_{33} & \cdots & 2k_{3m} \\ \vdots & \vdots & \vdots & \ddots & \vdots \\ 0 & 0 & 0 & \cdots & k_{mm} \end{pmatrix}, \tag{41}$$

with

$$k_{ij} = \frac{m^2}{T^2} \iint_0^T k(s, t) \, \Psi_i(s) \, \Psi_j(t) \, ds \, dt,$$
$$i = 1, 2, \dots, m, \quad j = 1, 2, \dots, m,$$

$$C_{i} = \begin{pmatrix} ti_{11}B\left(\frac{h}{2}\right) & ti_{12}B\left(h\right) & ti_{13}B\left(h\right) & \cdots & ti_{1m}B\left(h\right) \\ 0 & ti_{22}\left(B\left(\frac{3h}{2}\right) - B\left(h\right)\right) & ti_{23}\left(B\left(2h\right) - B\left(h\right)\right) & \cdots & ti_{2m}\left(B\left(2h\right) - B\left(h\right)\right) \\ 0 & 0 & ti_{33}\left(B\left(\frac{5h}{2}\right) - B\left(2h\right)\right) & \cdots & ti_{3m}\left(B\left(3h\right) - B\left(2h\right)\right) \\ \vdots & \vdots & \ddots & \vdots \\ 0 & 0 & \cdots & ti_{mm}\left(B\left(\frac{(2m-1)h}{2}\right) - B\left((m-1)h\right)\right) \end{pmatrix}_{\substack{m \times m \\ (42)}}$$

with

$$ti_{pq} = \frac{m^2}{T^2} \iint_0^T ti(s,t) \Psi_p(s) \Psi_q(t) ds dt,$$

$$p = 1, 2, \dots, m, \quad q = 1, 2, \dots, m,$$

$$B = \begin{pmatrix} r_{11} B_{h/2}^H & r_{12} B_h^H & \cdots & r_{1m} B_h^H \\ 0 & r_{22} \left(B_{3h/2}^H - B_h^H \right) & \cdots & r_{2m} \left(B_{2h}^H - B_h^H \right) \\ \vdots & \vdots & \ddots & \vdots \\ 0 & 0 & \cdots & r_{mm} \left(B_{((2m-1)h/2)}^H - B_{(m-1)h}^H \right) \end{pmatrix}_{m \times m}$$

$$(43)$$

with

$$r_{ij} = \frac{m^2}{T^2} \iint_0^T r(s, t) \, \Psi_i(s) \, \Psi_j(t) \, ds \, dt,$$

$$i = 1, 2, \dots, m, \quad j = 1, 2, \dots, m.$$
(44)

Now, with replacing \approx by =, we have

$$x^{T}\left(I - A - \sum_{i=1}^{n} C_{i} - B\right)\Psi(t) = x_{0}^{T}\Psi(t),$$
 (45)

or

$$Mx = x_0, (46)$$

where $M = (I - A - \sum_{i=1}^{n} C_i - B)^T$. Clearly, (46) is the stochastic linear system of m equations and m unknowns.

4. Error Analysis

In [20], it is stated that if $f(t) \in \nu[\alpha, \beta]$ and (1/2) < H < 1, then

$$E\left[\left(\int_{\alpha}^{\beta} f(x) dB_{x}^{H}\right)^{2}\right]$$
$$= \int_{\alpha}^{\beta} E\left[\left(f(x)\right)^{2}\right] (dx)^{2H}$$

$$= 2H (2H - 1)$$

$$\times \int_{\alpha}^{\beta} \int_{\alpha}^{y} (y - x)^{2H-2} E[f^{2}(x)] dx dy.$$
(47)

Theorem 5. Let r(s) be an arbitrary bounded function on [0,1) and $e(s) = r(s) - \hat{r}(s)$ such that $\hat{r}(s)$ is the BPFs of r(s). Then,

$$|e(s)|^2 \le O(h^2), \quad 0 \le s < 1.$$
 (48)

Proof. See [7].
$$\Box$$

Theorem 6. Let r(x, y) be an arbitrary bounded function on $I = [0, 1) \times [0, 1)$ and $e(x, y) = r(x, y) - \hat{r}(x, y)$ such that $\hat{r}(x, y)$ is the BPFs of r(x, y). Then,

$$|e(x,y)|^2 \le O(h^2), \quad (x,y) \in I.$$
 (49)

Proof. See [7].
$$\Box$$

Let
$$e(t) = x(t) - \hat{x}(t) = x_0 - \hat{x}_0$$

$$+ \int_0^t (k(s,t) x(s) - \hat{k}(s,t) \hat{x}(s)) ds$$

$$+ \sum_{i=1}^n \int_0^t (ti(s,t) x(s) - ti(s,t) \hat{x}(s)) dB_i(s)$$

$$+ \int_0^t (r(s,t) x(s) - \hat{r}(s,t) \hat{x}(s)) dB_s^H,$$
(50)

where $\hat{x}(t)$ is the approximate solution of x(t) defined in (46) and \hat{x}_0 , $\hat{k}(s,t)$, $\hat{t}i(s,t)$, and $\hat{r}(s,t)$ are approximated by using properties of the BPFs.

Theorem 7. Let $\hat{x}(t)$ be the approximate solution of (2) which is the solution of (46), $||x(t)||^2 \le N$, $||k(s,t)||^2 \le l_1$, $||ti(s,t)||^2 \le l_2$, i = 1, 2, ..., n, and $||r(s,t)||^2 \le l_3$, for all $(s,t) \in I = [0,1) \times [0,1)$. Then,

$$\|x(t) - \widehat{x}(t)\|^2 \le O(h^2), \quad t \in [0, 1),$$
 (51)

where $||x|| = (E[x^2])^{1/2}$.

Proof. Consider

$$e(t) = x(t) - \hat{x}(t) = x_0 - \hat{x}_0$$

$$+ \int_0^t \left(k(s, t) x(s) - \hat{k}(s, t) \hat{x}(s) \right) ds$$

$$+ \sum_{i=1}^n \int_0^t \left(ti(s, t) x(s) - \hat{t}i(s, t) \hat{x}(s) \right) dB_i(s)$$

$$+ \int_0^t \left(r(s, t) x(s) - \hat{r}(s, t) \hat{x}(s) \right) dB_s^H;$$
(52)

by using $(\sum_{i=1}^{n+3} x_i)^2 \le (n+3)(\sum_{i=1}^{n+3} x_i^2)$, we can write $||x(t) - \widehat{x}(t)||^2$

$$\leq (n+3) \left(\|x_{0} - \widehat{x}_{0}\|^{2} + \left\| \int_{0}^{t} (k(s,t)x(s) - \widehat{k}(s,t)\widehat{x}(s))ds \right\|^{2} + \sum_{i=1}^{n} \left\| \int_{0}^{t} \left(ti(s,t)x(s) - \widehat{t}i(s,t)\widehat{x}(s) \right) dB_{i}(s) \right\|^{2} + \left\| \int_{0}^{t} (r(s,t)x(s) - \widehat{r}(s,t)\widehat{x}(s)) dB_{s}^{H} \right\|^{2} \right).$$
(53)

First, by using the relation (47), we can write

$$E\left[\left(\int_{0}^{t} (r(s,t) x(s) - \hat{r}(s,t) \hat{x}(s)) dB_{s}^{H}\right)^{2}\right]$$

$$= \int_{0}^{t} E\left[(r(s,t) x(s) - \hat{r}(s,t) \hat{x}(s))^{2}\right] (ds)^{2H}$$

$$= 2H (2H - 1)$$

$$\times \int_{0}^{t} \int_{0}^{p} (p - s)^{2H-2}$$

$$\times E \left[(r(s,t) x(s) - \hat{r}(s,t) \hat{x}(s))^{2} \right] ds dp$$

$$= 2H (2H - 1)$$

$$\times \int_{0}^{t} \int_{s}^{t} (p - s)^{2H-2}$$

$$\times E \left[(r(s,t) x(s) - \hat{r}(s,t) \hat{x}(s))^{2} \right] dp ds$$

$$= 2H (2H - 1) \int_{0}^{t} E \left[(r(s,t) x(s) - \hat{r}(s,t) \hat{x}(s))^{2} \right]$$

$$\times \int_{s}^{t} (p - s)^{2H-2} dp ds$$

$$= 2H \int_{0}^{t} E \left[(r(s,t) x(s) - \hat{r}(s,t) \hat{x}(s))^{2} \right] (t - s)^{2H-1} ds.$$
(54)

Cleary, we have

$$0 < s < t < 1,$$

$$0 < 2H - 1 < 1,$$
(55)

and consequently,

$$0 < (t - s)^{2H - 1} < 1. (56)$$

Hence,

$$E\left[\left(\int_{0}^{t} r(s,t) x(s) - \widehat{r}(s,t) \widehat{x}(s) dB_{s}^{H}\right)^{2}\right]$$

$$\leq 2 \int_{0}^{t} E\left[\left(r(s,t) x(s) - \widehat{r}(s,t) \widehat{x}(s)\right)^{2}\right] ds,$$
(57)

or

$$\left\| \int_{0}^{t} (r(s,t) x(s) - \hat{r}(s,t) \hat{x}(s)) dB_{s}^{H} \right\|^{2}$$

$$\leq 2 \int_{0}^{t} \|r(s,t) x(s) - \hat{r}(s,t) \hat{x}(s)\|^{2} ds.$$
(58)

Now, by using the property of the Ito isometry for the SBM defined in [21] and $(x + y)^2 \le 2(x^2 + y^2)$, we get

$$\|x(t) - \widehat{x}(t)\|^{2}$$

$$\leq (n+3) \left(\|x_{0} - \widehat{x}_{0}\|^{2} + \int_{0}^{t} \|k(s,t) x(s) - \widehat{k}(s,t) \widehat{x}(s)\|^{2} ds + \sum_{i=1}^{n} \int_{0}^{t} \|ti(s,t) x(s) - \widehat{ti}(s,t) \widehat{x}(s)\|^{2} ds + 2 \int_{0}^{t} \|r(s,t) x(s) - \widehat{r}(s,t) \widehat{x}(s)\|^{2} ds \right)$$

4	\overline{x}	=	%95 confidence interval for mean	
ι	X	3	Lower	Upper
0.05	1.6470×10^{-4}	1.0272×10^{-4}	1.1968×10^{-4}	2.0972×10^{-4}
0.1	2.1125×10^{-4}	1.3531×10^{-4}	1.5195×10^{-4}	2.7055×10^{-4}
0.15	3.8495×10^{-4}	3.2763×10^{-4}	2.4135×10^{-4}	5.2855×10^{-4}
0.2	4.3880×10^{-4}	2.7714×10^{-4}	3.1734×10^{-4}	5.6026×10^{-4}

TABLE 1: Mean, standard deviation, and confidence interval for error mean (T = 0.25, H = 2/3).

Table 2: Mean, standard deviation, and confidence interval for numerical solution mean (T = 0.25, H = 3/4).

4	\overline{x}		%95 confidence interval for mean	
ı	X	3	Lower	Upper
0.05	1.9830×10^{-4}	1.3868×10^{-4}	1.1235×10^{-4}	2.8425×10^{-4}
0.1	1.8920×10^{-4}	1.7302×10^{-4}	8.196×10^{-5}	2.9644×10^{-4}
0.15	3.7490×10^{-4}	1.9789×10^{-4}	2.5225×10^{-4}	4.9755×10^{-4}
0.2	3.0940×10^{-4}	2.8441×10^{-4}	1.3312×10^{-4}	4.8568×10^{-4}

$$\leq 2 (n+3) \left(\|x_0 - \bar{x}_0\|^2 + 2 \sum_{i=1}^n \int_0^t \left(\|ti(s,t) - \hat{ti}(s,t)\|^2 \right) \right) \\ + \int_0^t \|k(s,t)(x(s) - \bar{x}(s)) + (k(s,t) - \hat{k}(s,t)) + (k(s,t) - \hat{ti}(s,t)) + (k(s,t) -$$

%95 confidence interval for mean t \overline{x} Lower Upper 0.05 1.9270×10^{-4} 1.3065×10^{-4} 1.1172×10^{-4} 2.7368×10^{-4} 1.7260×10^{-4} 1.6552×10^{-4} 7.001×10^{-5} 2.7519×10^{-4} 0.1 0.15 3.5330×10^{-4} 2.1775×10^{-4} 2.1834×10^{-5} 4.8826×10^{-4} 0.2 2.8700×10^{-4} 2.6380×10^{-4} 1.2349×10^{-4} 4.5051×10^{-4}

TABLE 3: Mean, standard deviation, and confidence interval for numerical solution mean (T = 0.25, H = 9/10).

Table 4: Mean, standard deviation, and confidence interval for numerical solution mean (T = 0.25, H = 2/3).

+			%95 confidence interval for mean	
ι	X	3	Lower	Upper
0.05	4.1685×10^{-4}	2.8249×10^{-4}	2.9305×10^{-4}	5.4065×10^{-4}
0.1	4.8485×10^{-4}	3.1651×10^{-4}	3.4613×10^{-4}	6.2357×10^{-4}
0.15	5.7120×10^{-4}	5.3911×10^{-4}	3.3491×10^{-4}	8.0749×10^{-4}
0.2	7.3150×10^{-4}	5.4920×10^{-4}	4.9081×10^{-4}	9.7219×10^{-4}

$$+ \int_{0}^{t} (\|r(s,t) - \hat{r}(s,t)\|^{2}) + l_{3} \int_{0}^{t} \|x(s) - \hat{x}(s)\|^{2} ds$$

$$\times (\|x(s) - \hat{x}(s)\|^{2} + \|x(s)\|^{2}) ds + k_{4}h^{2} \left(\int_{0}^{t} \|x(s) - \hat{x}(s)\|^{2} ds + N \right) ,$$
(59)

or

By using Theorems 5 and 6, we can write

$$\|x_{0} - \widehat{x}_{0}\|^{2} \leq k_{1}h^{2},$$

$$\|k(s,t) - \widehat{k}(s,t)\|^{2} \leq k_{2}h^{2},$$

$$\|ti(s,t) - \widehat{ti}(s,t)\|^{2} \leq k_{3i}h^{2}, \quad i = 1, \dots, n,$$

$$\|r(s,t) - \widehat{r}(s,t)\|^{2} \leq k_{4}h^{2}.$$
(60)

By substituting the relation (60) in (59), we get

$$||x(t) - \widehat{x}(t)||^{2}$$

$$\leq 8 (n+3)$$

$$\times \left(k_{1}h^{2} + l_{1} \int_{0}^{t} ||x(s) - \widehat{x}(s)||^{2} ds + k_{2}h^{2} \left(\int_{0}^{t} ||x(s) - \widehat{x}(s)||^{2} ds + N\right) + \sum_{i=1}^{n} l_{2i} \int_{0}^{t} ||x(s) - \widehat{x}(s)||^{2} ds + \sum_{i=1}^{n} k_{3i}h^{2} \left(\int_{0}^{t} ||x(s) - \widehat{x}(s)||^{2} ds + N\right)$$

$$\|x(t) - \widehat{x}(t)\|^2 \le \mu + \lambda \int_0^t \|x(s) - \widehat{x}(s)\|^2 ds,$$
 (62)

where $\mu = 8(n+3)(k_1h^2 + k_2h^2N + \sum_{i=1}^n k_{3i}h^2N + k_4h^2N)$ and $\lambda = 8(n+3)(l_1 + k_2h^2 + \sum_{i=1}^n l_{2i} + \sum_{i=1}^n k_{3i}h^2 + l_3 + k_4h^2)$. If $f(s) = \|x(s) - \widehat{x}(s)\|^2$, we get

$$f(t) \le \mu + \lambda \int_0^t f(s) \, ds. \tag{63}$$

Now, by using Gronwall inequality, we have

$$f(t) \le \mu \left(1 + \lambda \int_0^t \exp\left(\lambda (t - s)\right) ds\right), \quad t \in [0, 1), \quad (64)$$

or

$$\|x(t) - \widehat{x}(t)\|^{2} \le O\left(h^{2}\right). \tag{65}$$

5. Numerical Examples

The SDE driven by the FBM

$$S(t) = S_0 + \int_0^t \mu(s) S(s) ds + \sum_{i=1}^n \int_0^t \sigma i(s) S(s) dB_i(s)$$

$$+ \int_0^t \alpha(s) S(s) dB_s^H, \quad t \in (0, T),$$
(66)

+	~		%95 confidence interval for mean	
ι	x	3	Lower	Upper
0.05	5.0950×10^{-4}	1.8639×10^{-4}	3.9397×10^{-4}	6.2503×10^{-4}
0.1	5.0980×10^{-4}	2.9898×10^{-4}	3.2449×10^{-4}	6.9511×10^{-4}
0.15	4.0610×10^{-4}	3.3768×10^{-4}	1.9680×10^{-4}	6.1540×10^{-4}
0.2	4.9960×10^{-4}	3.0343×10^{-4}	3.1153×10^{-4}	6.8767×10^{-4}

TABLE 5: Mean, standard deviation, and confidence interval for numerical solution mean (T = 0.25, H = 3/4).

Table 6: Mean, standard deviation, and confidence interval for numerical solution mean (T = 0.25, H = 9/10).

+	\overline{x} \overline{s}		%95 confidence interval for mean	
ι		Lower	Upper	
0.05	4.9780×10^{-4}	2.0137×10^{-4}	3.7299×10^{-4}	6.2261×10^{-4}
0.1	6.9850×10^{-4}	3.4267×10^{-4}	4.8611×10^{-4}	9.1089×10^{-4}
0.15	7.7470×10^{-4}	5.1518×10^{-4}	4.5537×10^{-4}	1.0940×10^{-3}
0.2	1.2516×10^{-3}	6.3210×10^{-4}	8.5982×10^{-4}	1.6434×10^{-3}

is applied in modeling the price *S* of a stock with various Hurst parameters (see [18]). Hence, we show applicability and accuracy of this method in two numerical examples.

Example 1. Let us consider a SDE

$$dx(s) = -\frac{1}{5}s^{2}x(s) ds - \frac{1}{10}x(s) dB_{s}^{H}$$

$$-\frac{1}{6}x(s) dB_{1}(s) - \frac{1}{30}x(s) dB_{2}(s),$$

$$s \in (0, T), T < 1,$$

$$x(0) = \frac{1}{30},$$
(67)

with the exact solution $x(t) = (1/30) \exp(-(1/10)B_t^H - (1/15)t^3 - (1/200) \times t^{2H} - (1/6)B_1(t) - (1/72)t - (1/30)B_2(t) - (1/1800)t)$. The numerical results have been shown in Tables 1, 2, and 3 (with various Hurst parameters), where \overline{x} and \overline{s} are error mean and standard deviation of error, respectively.

Example 2. Let us consider a SDE

$$dx(s) = -\frac{1}{6}s^{2}x(s) ds - \frac{1}{30}x(s) dB_{s}^{H}$$

$$-\frac{1}{10(1-s)}x(s) dB_{1}(s) - \frac{1}{30}x(s) dB_{2}(s),$$

$$s \in (0,T), T < 1,$$

$$x(0) = \frac{1}{12},$$
(68)

with the exact solution $x(t) = (1/12) \exp(-(1/30)B_t^H - (1/18)t^3 - (1/1800)t^{2H} - \int_0^t (1/10(1-s))dB_1(s) - (1/30)B_2(t) - (1/1800)t + (1/(200(1-s))))$. The numerical results have been shown in Tables 4, 5, and 6 (with various Hurst parameters), where \overline{x} and \overline{s} are error mean and standard deviation of error, respectively.

6. Conclusion

This paper presents a numerical comparison between the approximation solution of the SDE driven by the FBM with Hurst parameter $H \in ((1/2), 1)$ and n independent one-dimensional SBM and the exact solution of it. Also, the method is applied with two examples to illustrate the accuracy and implementation of the method.

Conflict of Interests

The authors declare that there is no conflict of interests regarding the publication of this paper.

Acknowledgments

The authors thank Islamic Azad University for supporting this work. The authors are also grateful to the anonymous referee for his/her constructive comments and suggestions.

References

- [1] J. Bertoin, "Sur une intégrale pour les processus à α -variation bornée," *The Annals of Probability*, vol. 17, no. 4, pp. 1277–1699, 1989.
- [2] P. Cheng and M. Webster, "Stability analysis of impulsive stochastic functional differential equations with delayed impulses via comparison principle and impulsive delay differential inequality," *Abstract and Applied Analysis*, vol. 2014, Article ID 710150, 2014.
- [3] W. Gao, F. Deng, R. Zhang, and W. Liu, "Finite-time H_{∞} control for time-delayed stochastic systems with Markovian switching," Abstract and Applied Analysis, vol. 2014, Article ID 809290, 2014.
- [4] J. Guerra and D. Nualart, "Stochastic differential equations driven by fractional Brownian motion and standard Brownian motion," *Stochastic Analysis and Applications*, vol. 26, no. 5, pp. 1053–1075, 2008.
- [5] D. Huang and S. K. Nguang, "Robust H_{∞} static output feedback control of fuzzy systems: an ILMI approach," *IEEE Transactions*

- on Systems, Man, and Cybernetics B, vol. 36, no. 1, pp. 216–222, 2006.
- [6] A. Mark, F. Yao, and M. Hua, "Abstract functional stochastic evolution equations driven by fractional Brownian motion," *Abstract and Applied Analysis*, vol. 2014, Article ID 516853, 2014.
- [7] K. Maleknejad, M. Khodabin, and M. Rostami, "A numerical method for solving *m*-dimensional stochastic Itô-Volterra integral equations by stochastic operational matrix," *Computers & Mathematics with Applications*, vol. 63, no. 1, pp. 133–143, 2012.
- [8] K. Maleknejad, M. Khodabin, and M. Rostami, "Numerical solution of stochastic Volterra integral equations by a stochastic operational matrix based on block pulse functions," *Mathematical and Computer Modelling*, vol. 55, no. 3-4, pp. 791–800, 2012.
- [9] J. Wang and K. Zhang, "Non-fragile H_{∞} control for stochastic systems with Markovian jumping parameters and random packet losses," *Abstract and Applied Analysis*, vol. 2014, Article ID 934134, 2014.
- [10] H. Zhang, Y. Shi, and A. Saadat Mehr, "Robust static output feedback control and remote PID design for networked motor systems," *IEEE Transactions on Industrial Electronics*, vol. 58, no. 12, pp. 5396–5405, 2011.
- [11] M. Zähle, "Integration with respect to fractal functions and stochastic calculus. I," *Probability Theory and Related Fields*, vol. 111, no. 3, pp. 333–374, 1998.
- [12] L. Coutin, "An introduction to (stochastic) calculus with respect to fractional Brownian motion," in *Séminaire de Probabilités XL*, vol. 1899, pp. 3–65, Springer, Berlin, Germany, 2007.
- [13] L. Decreusefond and A. S. Üstünel, "Fractional Brownian motion: theory and applications," in *Systèmes Différentiels Fractionnaires*, vol. 5 of *ESAIM Proceedings*, pp. 75–86, 1998.
- [14] D. Nualart and A. Răşcanu, "Differential equations driven by fractional Brownian motion," *Collectanea Mathematica*, vol. 53, no. 1, pp. 55–81, 2002.
- [15] H. Lisei and A. Soós, "Approximation of stochastic differential equations driven by fractional Brownian motion," in Seminar on Stochastic Analysis, Random Fields and Applications Progress in Probability, vol. 59, pp. 227–241, 2008.
- [16] Y. Mishura and G. Shevchenko, "The rate of convergence for Euler approximations of solutions of stochastic differential equations driven by fractional Brownian motion," *Stochastics*, vol. 80, no. 5, pp. 489–511, 2008.
- [17] F. Russo and P. Vallois, "Forward, backward and symmetric stochastic integration," *Probability Theory and Related Fields*, vol. 97, no. 3, pp. 403–421, 1993.
- [18] F. Biagini, Y. Hu, B. Øksendal, and T. Zhang, Stochastic Calculus for Fractional Brownian Motion and Applications, Springer, London, UK, 2008.
- [19] T. Caraballo, M. J. Garrido-Atienza, and T. Taniguchi, "The existence and exponential behavior of solutions to stochastic delay evolution equations with a fractional Brownian motion," *Nonlinear Analysis. Theory, Methods & Applications*, vol. 74, no. 11, pp. 3671–3684, 2011.
- [20] L. Longjin, F.-Y. Ren, and W.-Y. Qiu, "The application of fractional derivatives in stochastic models driven by fractional Brownian motion," *Physica A*, vol. 389, no. 21, pp. 4809–4818, 2010.
- [21] B. Øksendal, Stochastic Differential Equations. An Introduction with Application, Springer, New York, NY, USA, 5th edition, 1998.

Hindawi Publishing Corporation Abstract and Applied Analysis Volume 2014, Article ID 903493, 7 pages http://dx.doi.org/10.1155/2014/903493

Research Article

Variable Torque Control of Offshore Wind Turbine on Spar Floating Platform Using Advanced RBF Neural Network

Lei Wang,^{1,2} Shan Zuo,² Y. D. Song,^{1,2} and Zheng Zhou³

- ¹ Intelligent Systems and New Energy Technology Research Institute, Chongqing University, Chongqing 400044, China
- ² Institute of Intelligent System and Renewable Energy Technology, University of Electronic Science and Technology of China, Chengdu 611731, China

Correspondence should be addressed to Lei Wang; leiwang08@cqu.edu.cn

Received 2 January 2014; Revised 14 January 2014; Accepted 15 January 2014; Published 6 March 2014

Academic Editor: Xiaojie Su

Copyright © 2014 Lei Wang et al. This is an open access article distributed under the Creative Commons Attribution License, which permits unrestricted use, distribution, and reproduction in any medium, provided the original work is properly cited.

Offshore floating wind turbine (OFWT) has been a challenging research spot because of the high-quality wind power and complex load environment. This paper focuses on the research of variable torque control of offshore wind turbine on Spar floating platform. The control objective in below-rated wind speed region is to optimize the output power by tracking the optimal tip-speed ratio and ideal power curve. Aiming at the external disturbances and nonlinear uncertain dynamic systems of OFWT because of the proximity to load centers and strong wave coupling, this paper proposes an advanced radial basis function (RBF) neural network approach for torque control of OFWT system at speeds lower than rated wind speed. The robust RBF neural network weight adaptive rules are acquired based on the Lyapunov stability analysis. The proposed control approach is tested and compared with the NREL baseline controller using the "NREL offshore 5 MW wind turbine" model mounted on a Spar floating platform run on FAST and Matlab/Simulink, operating in the below-rated wind speed condition. The simulation results show a better performance in tracking the optimal output power curve, therefore, completing the maximum wind energy utilization.

1. Introduction

Wind energy has been an important part of the renewable energy. It is significantly meaningful for optimizing the energy system structure, easing the energy crisis, and protecting the environment by actively developing wind energy. With the rapidly development of wind energy all over the world, promising and reliable wind turbine concepts have been developed. Offshore wind turbine makes it possible to go further into water deeper than 60 m [1]; therefore, it has become the key research in the field of renewable energy.

The floating offshore wind turbine (OFWT) concept provides a groundbreaking strategy to fully utilize the high-quality wind power in deep waters. The design concept of "large floating offshore wind turbine" was firstly proposed by Heronemus from Massachusetts Institute of Technology (MIT) in 1972 [2, 3]. American Renewable Energy

Laboratory (NREL) and MIT have completed the dynamic system modeling of OFWT and the three types of floating platform: tension leg platform with suction pile anchors, Spar-buoy with catenary mooring, drag-embedded anchors and barge with catenary mooring lines through OC3 projects [4]. Figure 1 shows the three primary types of floating offshore wind turbine concepts.

Previous research results show that, compared to onshore wind turbines, OFWTs with six degrees of freedom are prone to pitching motion and to produce complex dynamic load because of proximity to load centers and strong wave coupling [5]. Meanwhile, with the larger scale (the capacity of OFWTs reaches up to 10 MW, the diameter of blades approximates 200 meters), the blades of OFWT produce higher uneven loads due to the effect of turbulence, wind shear, tower shadow, and spindle tilt. Accumulating of the above two types of loads will result in devastating impact on the fatigue life and output power quality of the OFWT system.

³ Web Science Center, University of Electronic Science and Technology of China, Chengdu 611731, China

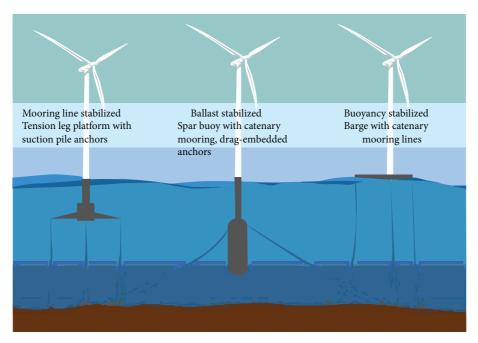


FIGURE 1: Floating offshore wind turbine concepts (image from Google).

Therefore, it is urgently needed to reduce fatigue loads and improve output power quality for OFWT system by utilizing advanced control strategies.

Control of OFWT is a relatively new yet challenging research area. There have been a large number of recent achievements in the research of blade pitch control for OFWT in the above-rated wind speed region [6–13]. In our previous work [6], we propose a computationally inexpensive robust adaptive control approach with memory-based compensation for blade pitch control. However, works on the variable speed control for OFWT system in below-rated wind speed region are relatively few.

In this study, to address the challenge that the system parameters of OFWT are varying and uncertain due to the complex external wind and wave disturbances, an adaptive radial basis function (RBF) neural network approach is proposed for torque control of OFWT system at speeds lower than rated wind speed. The robust RBF neural network weight adaptive rules are acquired based on the Lyapunov stability analysis. The proposed torque controller based on RBF neural network is presented and mounted on a Spar floating platform for performance comparison with the baseline torque controller in the below-rated wind speed region.

Section 2 briefly presents the wind turbine model and the Spar floating platform utilized in this paper. Section 3 describes the two implemented controllers: the baseline torque controller and the proposed variable torque controller based on RBF neural network. Section 4 shows the simulation and results, in which performances of the above two controllers are compared with each other on Spar floating platform. Eventually, conclusions are reported in Section 5.

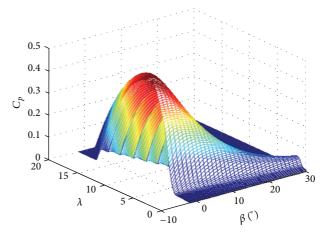


FIGURE 2: Power coefficients for VSVP wind turbine.

2. Wind Turbine and Platform Models

2.1. 5 MW Offshore Wind Turbine Model. The basic properties of future offshore turbines can be estimated by considering the amount of kinetic energy density in the wind, which can be converted into kinetic energy of the turbine shaft. The expression for power produced by the wind is simply given by

$$P_{S} = \frac{1}{2} C_{p} \left(\lambda, \beta \right) \rho A v^{3}, \tag{1}$$

where ρ is air density and A is the swept area of the turbine rotor with a radius R, giving $A = \pi R^2$. ν is wind speed passing the rotor. C_p denotes power coefficient of wind turbine, which is a nonlinear function of the tip-speed ratio λ and the pitch angle β [14]. Figure 2 depicts the curve of

power coefficients for variable speed and variable pitch wind turbine. It indicates that, for a different β , there will be a different curve for the $C_p - \lambda$, while, for a fixed β , there will be an optimal λ at which the power output is maximum. In addition, for any tip-speed ratio λ , power coefficient C_p is relatively maximum when blade pitch angle $\beta = 0^\circ$. When β increases, C_p decreases simultaneously.

Note that the tip-speed ratio is defined as

$$\lambda = \frac{\nu_{\text{Tip}}}{\nu} = \frac{R\omega_r}{\nu},\tag{2}$$

where v_{Tip} is the tip speed and ω_r is the rotor speed.

For a constant value of $\beta = 0^{\circ}$, the mathematical model of C_{D} is expressed as

$$C_{p}(\lambda) = c_{1} \left(\frac{c_{2}}{\lambda_{1}} - c_{4}\right) e^{-c_{5}/\lambda_{1}} + c_{6}\lambda,$$

$$\frac{1}{\lambda_{1}} = \left(\frac{1}{\lambda} - 0.035\right),$$
(3)

where the coefficients $(c_1, c_2, c_4, c_5, c_6)$ depend on the aero-dynamic design of the blade and operating conditions of the wind turbine. In this paper, the coefficients are $c_1 = 0.5176$, $c_2 = 116$, $c_4 = 5$, $c_5 = 21$, and $c_6 = 0.0068$ [15]. For the "NREL 5 MW reference offshore wind turbine" model simulated in this paper, the peak power coefficient of 0.482 occurred at a tip-speed ratio of 7.55 and a rotor-collective blade-pitch angle of 0.0° [16].

In the case of the variable speed wind power generation system, the maximum power point control from the wind turbine can be adopted. The maximum power of the wind turbine is given by

$$P_{\text{max}} = \frac{1}{2} \frac{\rho \pi R^5 C_{p-\text{max}}}{\lambda^{*3}} \omega_r^{*3}.$$
 (4)

The physical properties of the specified wind turbine model used for analysis, the "NREL 5 MW reference offshore wind turbine," are listed in Table 1 [16]. This wind turbine is mounted on a Spar floating platform.

2.2. Floating Platform. The Spar-buoy platform is modeled for the support structure. The NREL 5 MW offshore floating platform input properties for the OC3-Hywind Spar-buoy used in this paper are briefly summarized in Table 2 [4].

3. Implemented Controllers

This section gives the detailed information about the two controllers simulated in the analysis.

3.1. The Baseline Generator Torque Controller. The baseline generator torque controller is built on the best performance presented by Jonkman in his previous research on the Sparbuoy platform [17].

In the below rated wind speed region, the purpose is to optimize power capture. The generator torque is proportional

TABLE 1: NREL 5 MW turbine model properties.

Power rating	5 MW
Rotor orientation, Configuration	Upwind, 3 blades
Control	Variable speed, variable pitch, active yaw
Rotor, hub diameter	126 m, 3 m
Hub height	90 m
Cut-in, rated, cut-out wind speed	3 m/s, 11.4 m/s, 25 m/s
Rated rotor, generator speed	12.1 rpm, 1173.7 rpm
Rotor mass	110000 kg
Optimal tip-speed-ratio	7.55
Blade operation	Pitch to feather
Maximum blade pitch rate	8°/s
Rated generator torque	43,093 Nm
Maximum generator torque	47,402 Nm

Using the turbine model data from [16].

TABLE 2: Physical properties for the OC3-hywind spar-buoy.

Diameter	6.5 m
Draft	120.0 m
Platform mass	7,466,330 kg
Water depth	320.0 m
Number of mooring lines	3

Using the barge platform data from [4].

to the square of the filtered generator speed to maintain a constant optimal tip-speed ratio.

The generator torque for this region is expressed as

$$T_g^{\omega_r} = T_g^1 + \frac{T_g^* - T_g^1}{\omega_{r,2} - \omega_{r,1}} \left(\omega_r - \omega_{r,1} \right), \tag{5}$$

where ω_r is rotor speed, T_g^1 is the generator torque at the rotor speed in which this region starts $(\omega_{r,1})$, T_g^* is rated torque, and $\omega_{r,2}$ is the rotor speed in which the rated torque is reached.

3.2. Advanced Generator Torque Controller Based on RBF Neural Network. We propose a RBF neural network for variable torque control of the OFWT system. The total number of input signals in the OFWT torque control system is no more than 4. Consequently, it is a computationally inexpensive approach to utilize the RBF neural network for linearization and approximation.

In this paper, the RBF neural network is a three-layer forward network, including an input layer, a hidden layer with a Gaussian activation function, and a linear output layer. The mapping from input to output is nonlinear, while the mapping from hidden layer to output layer is linear, therefore speeding up the process of study obviously and avoiding local minimum problem. The topological structure of RBF network is presented in Figure 3.

The control block diagram of RBF neural network is illustrated in Figure 4.

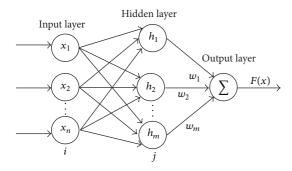


FIGURE 3: Topological graph of RBF neural network.

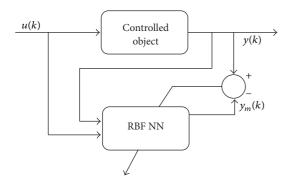


FIGURE 4: Control block diagram of RBF neural network.

In RBF network, $X = [x_1, x_1, ..., x_n]^T$ is the input vector, h_q is a nonlinear RBF activation function, which is given by

$$h_g = \Phi(\|X - C_g\|) = \exp\left(-\frac{\|X - C_g\|^2}{2b_g^2}\right),$$
 (6)

where m is the number of neurons in the hidden layer and $C_g = [c_{1g}, c_{2g}, \ldots, c_{ig}, \ldots, c_{ng}]^T$ is the central vector of gth hidden neuron. $B = [b_1, b_2, \ldots, b_g, \ldots, b_m]^T$ is the basis-width vector, $b_g > 0$ is the base width constant of gth mode, and the weight vector of the linear output neurons is $w = [w_1, w_2, \ldots, w_g, \ldots, w_m]^T$.

The output $R^n \to R$ of the neural network is defined as

$$F(x) = wH = \sum_{g=1}^{m} w_g \Phi\left(\left\|x - C_g\right\|\right). \tag{7}$$

From previous research results [13, 18–25], we could learn that, a RBF neural network with enough hidden neurons can approximate any nonlinear continuous functions with arbitrary precision. In this paper, in order to train the RBF neural network, we utilize the Lyapunov stability to get the weights updating rules of the RBF neural network.

In the first mode of operating at variable torque control, where the wind speed is less than the rated speed region, the electrical torque of the wind turbine must be adjusted to make the rotor speed track the desired speed that is specified

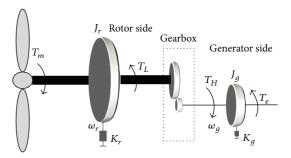


FIGURE 5: Layout of drive train model.

according to the optimal tip-speed ratio. The drive train dynamics are depicted in Figure 5. The mechanical motion equations are given by

$$\begin{split} J_r \dot{\omega}_r + K_r \omega_r + B_r \theta_r &= T_m \left(\omega, \beta, \nu, \dot{x} \right) - T_L, \\ J_g \dot{\omega}_g + K_g \omega_g + B_g \theta_g &= T_H - T_e, \\ n &= \frac{\omega_g}{\omega_r} &= \frac{T_L}{T_H}, \end{split} \tag{8}$$

where J_r and J_g are the moment of inertia of the rotor and the generator. K_r and K_g are the coefficient of viscous reaction of rotor and generator, respectively. B_r and B_g are the coefficient and stiffness of rotor and generator, respectively. T_m , T_e , T_L , and T_H are the shaft torque at wind turbine end, generator end, and before and after gear box, respectively. x is the tower displacement and n is the gearbox ratio. θ_r and θ_g are the mechanical angular position of the rotor and generator.

We rewrite the above mechanical motion equations in a compact form as follows:

$$J\dot{\omega}_r + K\omega_r + B\theta_r = T_m(\omega, \beta, \nu, \dot{x}) - nT_e, \tag{9}$$

where, B are lumped parameters given by

$$J = J_r + n^2 J_g,$$

$$K = K_r + n^2 K_g,$$

$$B = B_r + n^2 B_a.$$
(10)

 T_m is given by

$$T_m = \frac{\rho \pi R^3 C_p (\lambda, \beta)}{2\lambda} (\nu - \dot{x})^2. \tag{11}$$

The affine form of the rotor speed equation can be characterized by the following equation:

$$\dot{\omega}_r = \Gamma\left(\omega_r, \nu\right) + \gamma T_e,\tag{12}$$

where γ is a constant negative value and T_e is the input signal, with

$$\Gamma(\omega_r, \nu) = \frac{\left(\rho \pi R^3 C_p(\lambda, \beta) / 2\lambda\right) \nu^2 - K \omega_r - B\theta_r}{J},$$

$$\gamma = \frac{-n}{J}.$$
(13)

Construct a nonlinear approximation function through RBF neural network given by

$$\frac{\Gamma(\omega_r, \nu)}{\gamma} = \Phi(\omega_r, \nu) w + L(\omega_r, \nu), \qquad (14)$$

where $|L(\omega_r, v)| \le L_{\text{max}}$ represents the lumped RBF neural network approximation error.

To design the rotor speed tracking controller, define the rotor tracking error *e* as follows:

$$e = \omega_r - \omega_r^*, \tag{15}$$

where ω_r^* is the optimal rotor speed, which is defined as

$$\omega_r^* = \frac{\lambda^* \nu}{R},\tag{16}$$

where the optimum tip speed ratio λ^* is given in Table 1.

The control system can be justified by considering the Lyapunov function candidate as follows:

$$V = \frac{1}{-2\gamma}e^2 + \frac{1}{2\theta_1}\widetilde{w}^T\widetilde{w},\tag{17}$$

where $\theta_1>0$ is the positive adaptation gain. $\widetilde{w}=w-\widehat{w}$ is the weight error. w and \widehat{w} are the ideal weight and estimated weight of the network, respectively. The Lyapunov function candidate V is a positive definite function and $\dot{V}\leq 0$ is the sufficient condition for the robust stability of the nonlinear system. We can get the following:

$$\dot{V} = \left(\omega_r - \omega_r^*\right) \left(-\frac{\Gamma\left(\omega_r, \nu\right)}{\gamma} - T_e + \frac{\lambda^* \dot{\nu}}{R \gamma}\right) - \frac{1}{\theta_1} \widetilde{w}^T \dot{\overline{w}}. \quad (18)$$

Deriving the approximation through the neural networks $\Gamma(\omega_r, \nu)/\gamma = \Phi(\omega_r, \nu)w + L(\omega_r, \nu)$ and $\widehat{\Gamma}(\omega_r, \nu)/\widehat{\gamma} = \Phi(\omega_r, \nu)\widehat{w}$. For the stability of the nonlinear system, consider the following controller:

$$\widehat{u} = T_e = -\Phi\left(\omega_r, \nu\right)\widehat{w} + \kappa\left(\omega_r - \omega_r^*\right) + \omega_r,\tag{19}$$

where $\kappa > 0$ is the rotor speed tracking error feedback gain.

Proof. Based on (18) and (19), we can get

$$\dot{V} = (\omega - \omega^*) \left(-L(\omega_r, \nu) - \kappa (\omega_r - \omega_r^*) - \omega_r + \frac{\lambda^* \dot{\nu}}{R \gamma} \right) + \widetilde{\omega}^T \left(-\Phi^T(\omega_r, \nu) (\omega_r - \omega_r^*) - \frac{1}{\theta_1} \dot{\widehat{\omega}} \right).$$
(20)

The weight updating rule of the network can be obtained through the e-modification method given by

$$\dot{\widehat{w}} = -\theta_1 \left(\Phi^T \left(\omega_r, v \right) \left(\omega_r - \omega_r^* \right) + v \left| \omega_r - \omega_r^* \right| \widehat{w} \right), \quad (21)$$

where v is a constant positive value. Combine (20) and (21) to get the following:

$$\dot{V} = (\omega_r - \omega_r^*) \left(-L(\omega_r, v) - \omega_r + \frac{\lambda^* \dot{v}}{R \gamma} \right) - \kappa (\omega_r - \omega_r^*)^2 + v |\omega_r - \omega_r^*| \widetilde{w}^T \widetilde{w}.$$
(22)

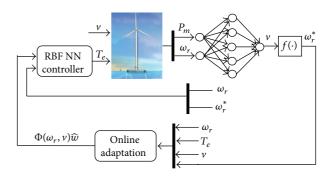


FIGURE 6: Block diagram of the RBF NN variable speed control scheme.

It is assumed that ω_r and $\dot{\omega}_r^*$ are bounded, so

$$\left|\omega_r\right| \leq L_1, \qquad \left|\dot{\omega}_r^*\right| = \left|\frac{\lambda^*\dot{\nu}}{R\gamma}\right| \leq L_2,$$

$$\dot{V} \le \left| \omega_r - \omega_r^* \right|$$

$$\cdot \left(\left(L_{\max} + L_1 + L_2 \right) - \kappa \left| \omega_r - \omega_r^* \right| - v \widetilde{w}^T \widetilde{w} + v \widetilde{w}^T w \right). \tag{23}$$

$$\begin{split} & \text{If } |\omega_r - \omega_r^*| \geq (L_{\max} + L_w)/\kappa + (vw^2)/4\kappa \text{ or } \|\widetilde{w}\| \geq (w/2) + \\ & \sqrt{(L_{\max} + L_w)/v + w^2/4}, \text{ we could get} \end{split}$$

$$\dot{V} \le 0. \tag{24}$$

Therefore, the overall dynamic system is uniformly ultimately bounded.

From the above equations, we can see that the estimated wind speed input enables the generator to track the optimal output power curve by generating a reference rotor speed. There are many previous researches working on estimating wind speed without directly measuring the wind speed. In this paper, we utilize the sensorless scheme presented in [26] to estimate wind speed based on neural network. Then we could get the reference rotor speed by the following equation:

$$\omega_r^* = f(v) = \frac{\lambda^* v}{R}.$$
 (25)

The block diagram of the RBF neural network variable speed control scheme of the OFWT system is depicted in Figure 6. \Box

4. Simulation and Results

In this section, the "NREL 5 MW reference offshore wind turbine" installed on a OC3-Hywind Spar-buoy floating platform is tested and simulated with the FAST and MAT-LAB/Simulink under mean value of 8 m/s turbulence wind speed, which is below the rated wind speed.

To verify the robustness and self-adaptation of the proposed variable torque controller based on RBF neural network, compared simulations of two types of controllers,

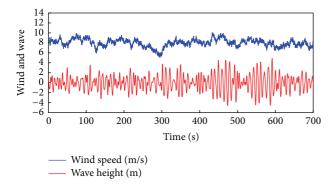


FIGURE 7: Wind and wave conditions.

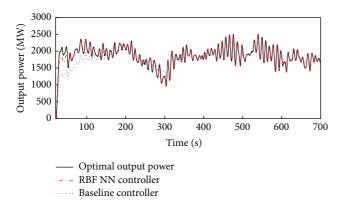


FIGURE 8: Comparison in generator output power.

the baseline torque controller and the proposed torque controller, have been performed on the same offshore wind turbine system. Two comparison performances are simulated based on power tracking: generator output power and torque regulations.

Figure 7 shows the turbulence wind and wave conditions.

Figure 8 compares the average generator output power tracking for the proposed torque controller based on RBF neural network and the baseline torque controller with the optimal output power trajectory. It can be observed that, the proposed adaptive torque controller is able to follow the optimal output power curve with better tracking accuracy than the baseline torque controller, therefore completing the maximum offshore wind energy utilization.

Figure 9 presents the compared curve in generator torque.

5. Conclusions

This paper mainly focuses on the variable torque control of OFWT system for power tracking in below-rated wind speed region on a Spar-buoy floating platform. In allusion to the external disturbances and uncertain system parameters of OFWT due to the much more complicated external load environment and strong wave coupling compared to the onshore wind turbine, a robust adaptive torque controller based on RBF neural network is proposed and tested. Two

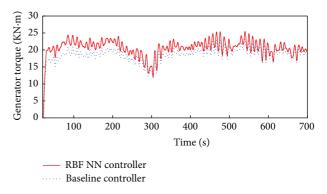


FIGURE 9: Comparison in generator torque.

types of controllers are implemented on the OC3-Hywind Spar-buoy floating platform for performance comparison: the baseline torque controller and the proposed torque controller

According to the average simulation results, the proposed torque controller based on RBF neural network is not only robust to complex wind and wave disturbances but also adaptive to varying and uncertain system parameters as well. As a result, the advanced controller shows a better performance in tracking the optimal generator output power curve, therefore completing the maximum wind energy utilization.

Conflict of Interests

The authors declare that there is no conflict if interests regarding the publication of this paper.

Acknowledgments

This work was supported in part by the National High Technology Research and Development Program of China (SS2012AA052302), the National Natural Science Foundation of China (no. 51205046), and the Fundamental Research Funds for the Central Universities (no. CDJZR170008).

References

- [1] F. G. Nielsen, T. D. Hanson, and B. Skaare, "Integrated dynamic analysis of floating offshore wind turbines," in *Proceedings of the 25TH International Conference on Offshore Mechanics and Arctic Engineering (OMAE '06)*, pp. 671–679, Hamburg, Germany, June 2006.
- [2] W. E. Heronemus, "Pollution-free energy from offshore wind," in Proceedings of the 8th Annual Conference and Exposition Marine Technology Society, Washington, DC, USA, 1972.
- [3] W. Musial and S. Butterfield, "Future for offshore wind energy in the United States," Tech. Rep. 36313, National Renewable Energy Laboratory, Golden, Colo, USA, 2004.
- [4] J. M. Jonkman, "Dynamics modeling and loads analysis of an offshore floating wind turbine," Tech. Rep. 41958, National Renewable Energy Laboratory, Golden, Colo, USA, 2007.
- [5] J. M. Jonkman and D. Matha, "Dynamics of offshore floating wind turbines-analysis of three concepts," *Wind Energy*, vol. 14, no. 4, pp. 557–569, 2011.

- [6] S. Zuo, Y. D. Song, L. Wang, and Q.-W. Song, "Computationally inexpensive approach for pitch control of offshore wind turbine on barge floating platform," *The Scientific World Journal*, vol. 2013, Article ID 357849, 9 pages, 2013.
- [7] W. Lei, Y.-L. He, X. Jin, J. Du, and S. Ma, "Dynamic simulation analysis of floating wind turbine," *Journal of Central South University: Science and Technology*, vol. 43, no. 4, pp. 1309–1314, 2012.
- [8] L. Wang, B. Wang, Y. Song et al., "Fatigue loads alleviation of floating offshore wind turbine using individual pitch control," *Advances in Vibration Engineering*, vol. 12, no. 4, pp. 377–390, 2013.
- [9] H. Namik and K. Stol, "Individual blade pitch control of floating offshore wind turbines," Wind Energy, vol. 13, no. 1, pp. 74–85, 2010.
- [10] M. A. Lackner, "An investigation of variable power collective pitch control for load mitigation of floating offshore wind turbines," Wind Energy, vol. 16, no. 3, pp. 435–444, 2012.
- [11] Y. D. Song, "Control of wind turbines using memory-based method," *Journal of Wind Engineering and Industrial Aerodynamics*, vol. 85, no. 3, pp. 263–275, 2000.
- [12] Y. D. Song, B. Dhinakaran, and X. Bao, "Control of wind turbines using nonlinear adaptive field excitation algorithms," in *Proceedings of the IEEE American Control Conference*, vol. 3, pp. 1551–1555, Chicago, Ill, USA, 2000.
- [13] L. Wu, W. X. Zheng, and H. Gao, "Dissipativity-based sliding mode control of switched stochastic systems," *IEEE Transactions on Automatic Control*, vol. 58, no. 3, pp. 785–793, 2013.
- [14] J. F. Conroy and R. Watson, "Frequency response capability of full converter wind turbine generators in comparison to conventional generation," *IEEE Transactions on Power Systems*, vol. 23, no. 2, pp. 649–656, 2008.
- [15] J. Zaragoza, J. Pou, A. Arias, C. Spiteri, E. Robles, and S. Ceballos, "Study and experimental verification of control tuning strategies in a variable speed wind energy conversion system," *Renewable Energy*, vol. 36, no. 5, pp. 1421–1430, 2011.
- [16] J. Jonkman, S. Butterfield, W. Musial, and G. Scott, "Definition of a 5-MW reference wind turbine for offshore system development," Tech. Rep. TP 500-38060, National Renewable Energy Laboratory, Golden, Colo, USA, 2009.
- [17] J. M. Jonkman, "Influence of control on the pitch damping of a floating wind turbine," in *Proceedings of the 46th AIAA Aerospace Sciences Meeting and Exhibit*, Reno, Nev, USA, January 2008.
- [18] R. M. Sanner and J.-J. E. Slotine, "Gaussian networks for direct adaptive control," *IEEE Transactions on Neural Networks*, vol. 3, no. 6, pp. 837–863, 1992.
- [19] Y. Kourd, D. Lefebvre, and N. Guersi, "Fault diagnosis based on neural networks and decision trees: application to DAMADICS," *International Journal of Innovative Computing, Information and Control*, vol. 9, no. 8, pp. 3185–3196, 2013.
- [20] C. K. Ahn and M. K. Song, "New sets of criteria for exponential L_2-L_∞ stability of Takagi-Sugeno fuzzy systems combined with Hopfield neural networks," *International Journal of Innovative Computing, Information and Control*, vol. 9, no. 7, pp. 2979–2986, 2013.
- [21] S. Sefriti, J. Boumhidi, M. Benyakhlef, and I. Boumhidi, "Adaptive decentralized sliding mode neural network control of a class of nonlinear interconnected systems," *International Journal of Innovative Computing, Information and Control*, vol. 9, no. 7, pp. 2941–2947, 2013.

- [22] K. S. Narendra and K. Parthasarathy, "Identification and control of dynamical systems using neural networks," *IEEE Transactions on Neural Networks*, vol. 1, no. 1, pp. 4–27, 1990.
- [23] L. Wu, X. Su, P. Shi, and J. Qiu, "Model approximation for discrete-time state-delay systems in the T-S fuzzy framework," *IEEE Transactions on Fuzzy Systems*, vol. 19, no. 2, pp. 366–378, 2011.
- [24] X. Su, Z. Li, Y. Feng, and L. Wu, "New global exponential stability criteria for interval-delayed neural networks," *Journal* of *Systems and Control Engineering*, vol. 225, Proceedings of the Institution of Mechanical Engineers, no. 1, pp. 125–136, 2011.
- [25] X. Su, P. Shi, L. Wu, and Y.-D. Song, "A novel control design on discrete-time Takagi-Sugeno fuzzy systems with time-varying delays," *IEEE Transactions on Fuzzy Systems*, vol. 20, no. 6, pp. 655–671, 2013.
- [26] H. Li, K. L. Shi, and P. G. McLaren, "Neural-network-based sensorless maximum wind energy capture with compensated power coefficient," *IEEE Transactions on Industry Applications*, vol. 41, no. 6, pp. 1548–1556, 2005.

Hindawi Publishing Corporation Abstract and Applied Analysis Volume 2014, Article ID 937495, 12 pages http://dx.doi.org/10.1155/2014/937495

Research Article

T-S Fuzzy Model-Based Approximation and Filter Design for Stochastic Time-Delay Systems with Hankel Norm Criterion

Yanhui Li and Xiujie Zhou

College of Electrical and Information Engineering, Northeast Petroleum University, Daqing, Heilongjiang Province 163318, China

Correspondence should be addressed to Yanhui Li; ly_hui@hotmail.com

Received 3 January 2014; Accepted 21 January 2014; Published 4 March 2014

Academic Editor: Shen Yin

Copyright © 2014 Y. Li and X. Zhou. This is an open access article distributed under the Creative Commons Attribution License, which permits unrestricted use, distribution, and reproduction in any medium, provided the original work is properly cited.

This paper investigates the Hankel norm filter design problem for stochastic time-delay systems, which are represented by Takagi-Sugeno (T-S) fuzzy model. Motivated by the parallel distributed compensation (PDC) technique, a novel filtering error system is established. The objective is to design a suitable filter that guarantees the corresponding filtering error system to be mean-square asymptotically stable and to have a specified Hankel norm performance level γ . Based on the Lyapunov stability theory and the Itô differential rule, the Hankel norm criterion is first established by adopting the integral inequality method, which can make some useful efforts in reducing conservativeness. The Hankel norm filtering problem is casted into a convex optimization problem with a convex linearization approach, which expresses all the conditions for the existence of admissible Hankel norm filter as standard linear matrix inequalities (LMIs). The effectiveness of the proposed method is demonstrated via a numerical example.

1. Introduction

The filtering problem can be briefly described as the design of an estimator from the measured output to estimate the state of the given systems and plays an important role in control fields and signal processing. During the last decades, various methodologies have been developed for the filter designs, such as Kalman filter [1, 2], H_{∞} filter [3, 4], and H_2 or H_2/H_{∞} filter [5, 6]. To mention a few, the earlier appeared Kalman filter is based on the precise noise statistics, while H_{∞} filter can be designed without the statistical assumption on the noise signals. With the continuous development of filtering technology, research on the above filtering methods has made a lot of achievements. In recent years, more and more scholars pay their attentions to other performance index, such as L_1 , L_2 - L_{∞} , and Hankel norm, where the analysis of Hankel norm takes the effects of past inputs on the future outputs into account. Since the inputs and outputs of the plants for actual control systems change over time, environment and any other factors, the past inputs will affect the future outputs, which is one issue need to consider in the filtering analysis. Therefore, the study on Hankel norm filter has significance of theoretical guidance and engineering application.

On another research frontline, a great number of results on stochastic systems have been reported since stochastic modeling has come to be a key part in many branches of science and engineering. As far as we know, the study of stochastic systems mainly focusses on the stability analysis [7, 8], controller design [9, 10], filtering [11], model reduction [12] and fault detection [13], and so forth. Among them, the literature [8] proposed some sufficient conditions to ensure that the stochastic interval delay system is exponentially stable by using the Razumikhin-type theorem, and the robust H_{∞} control and filtering problem for a class of uncertain stochastic time-delay systems were discussed in [9, 11], respectively. In the literature [12], the Hankel norm gain criterion of model reduction was established for neutral stochastic time-delay systems by using the projection lemma. For the existence of nonlinearity and unknown measured noise as well as stochastic perturbation, researchers have proposed different methods as data-driven approach [14, 15] and fault tolerant control with an iterative optimization scheme [16]. It is noted that the research on the filtering problem for stochastic time-delay systems has great significance and the major works are obtained with H_{∞} performance, while being relatively less with other performance constraints, especially Hankel norm.

As well known, a significant body of research on the aforementioned filter design problem has been investigated up to now and the closely related results of nonlinear systems are also fruitful with the T-S fuzzy model approach. Over the past few years, the T-S fuzzy model has been recognised as a powerful tool in approximating complex nonlinear systems to a number of linear subsystems by employing piecewise smooth membership functions. It has been proved that some stability analysis and synthesis methods in the linear systems can be effectively extended to the T-S fuzzy systems [17, 18]. Through the T-S fuzzy model approach, the filtering problem for nonlinear systems has undergone a fast development in recent year. Some results are cited in the study [19, 20], where the literature [19] considered both continuous and differential uniformly bounded time-varying delays and proposed some novel delay-dependent H_{∞} filtering criteria for nonlinear systems via a T-S fuzzy model approach, and [20] is concerned with the design problem of H_{∞} filter for continuous T-S fuzzy systems based on the delay partitioning idea. However, it should be pointed out that the mentioned results are mostly established with the induced norms, such as H_2 and H_{∞} , while more and more researchers have switched their interests to Hankel norm very recently. Different from other norms, the analysis of the Hankel norm included both the past inputs and the future outputs. By estimating the effect of the system past inputs on the system future outputs, the Hankel norm can be used to achieve the system performance analysis more efficiently. So far, the applications of the Hankel norm is mainly in system model reduction [12, 21, 22]. To the best of the authors' knowledge, the Hankel norm filtering problem for T-S model-based stochastic timedelay systems has not been investigated, which motivates the current research.

The goal of this paper is to design a robust Hankel norm filter for stochastic time-delay systems. Firstly, based on the T-S fuzzy model approximation and the parallel distributed compensation (PDC) technique, a novel filtering error system is established. Then, two appropriate Lyapunov-Krasovskii functions are chosen for the stability and Hankel norm performance analysis. By using the Itô differential rule and the integral inequality method, the Hankel norm criterion is first proposed for the existence of admissible filter that guarantees the mean-square asymptotic stability and Hankel norm performance of the corresponding filtering error system. Finally, the existence conditions of the admissible Hankel norm filter can be expressed as LMIs and the filter parameters are obtained by using standard numerical software. An example is illustrated to show the efficiency of the proposed filter design methods.

The notation used in this paper is standard. \mathbb{R}^n denotes the n-dimensional real Euclidean space, $\mathbb{R}^{n\times m}$ is the set of $n\times m$ real matrices. \mathbb{N} denotes the natural numbers set. The notation X^T and X^{-1} denote its transpose and inverse when it exists, respectively. Given a symmetric matrix $X = X^T$, the notation X > 0 ($X \ge 0$) means that the matrix X is real positive definiteness (semidefiniteness). By diag we denote a block diagonal matrix with its input arguments on the

diagonal. I denotes the identity matrix. The symbol * within a matrix represents the symmetric entries. $L_2[0,\infty)$ denotes the space of square integrable functions over $[0,\infty)$. The notation $\mathcal{E}\{\cdot\}$ stands for the expectation operator.

2. Problem Statement

Consider a stochastic time-delay system which could be approximated by a T-S fuzzy model with r plant rules.

Plant Rule i. If $\theta_1(t)$ is $W_{i1},\theta_2(t)$ is W_{i2} and . . and $\theta_g(t)$ is W_{ig} , then

$$dx(t) = [A_{i}x(t) + A_{di}x(t - \tau) + B_{i}v(t)] dt + [M_{i}x(t) + M_{di}x(t - \tau) + N_{i}v(t)] d\omega(t),$$

$$dy(t) = [C_{i}x(t) + C_{di}x(t - \tau) + D_{i}v(t)] dt + [E_{i}x(t) + E_{di}x(t - \tau) + F_{i}v(t)] d\omega(t),$$

$$z(t) = L_{i}x(t),$$

$$x(t) = 0, \quad t \in [-\tau, 0], \quad i = 1, 2, ..., r,$$

$$(1)$$

where $x(t) \in \mathbb{R}^n$ is the state vector, $y(t) \in \mathbb{R}^m$ is the measured output signal, and $v(t) \in \mathbb{R}^p$ is the exogenous disturbance that is assumed to be an arbitrary signal belonging to $L_2[0,\infty)$. $z(t) \in \mathbb{R}^q$ is the signal to be estimated. $\omega(t)$ is a zero-mean real scalar Wiener process on $(\Omega, \mathcal{F}, \mathcal{P})$. And $\mathcal{E}\{d\omega(t)\} = 0$, $\mathcal{E}\{d\omega^2(t)\} = 0$. τ is the time delay and is assumed to be constant in the whole dynamic process. $\theta(t) = [\theta_1(t), \theta_2(t), \ldots, \theta_g(t)]$ is the premise variables vector, W_{ij} $(i=1,2,\ldots,r,\ j=1,2,\ldots,g)$ is the fuzzy set, and r is the number of IF-THEN rules. $A_i, A_{di}, B_i, M_i, M_{di}, N_i, C_i, C_{di}, D_i, E_i, E_{di}, F_i$, and L_i are known constant matrices with appropriate dimensions.

The fuzzy system (1) is supposed to have singleton fuzzifier, product inference, and centroid difuzzifier. The final output of the fuzzy system is inferred as follows:

$$dx(t) = \sum_{i=1}^{r} h_{i}(\theta(t))$$

$$\times \{ [A_{i}x(t) + A_{di}x(t-\tau) + B_{i}v(t)] dt + [M_{i}x(t) + M_{di}x(t-\tau) + N_{i}v(t)] d\omega(t) \},$$

$$dy(t) = \sum_{i=1}^{r} h_{i}(\theta(t))$$

$$\times \{ [C_{i}x(t) + C_{di}x(t-\tau) + D_{i}v(t)] dt + [E_{i}x(t) + E_{di}x(t-\tau) + F_{i}v(t)] d\omega(t) \},$$

$$z(t) = \sum_{i=1}^{r} h_{i}(\theta(t)) L_{i}x(t),$$

$$x(t) = 0, \quad t \in [-\tau, 0], \quad i = 1, 2, ..., r,$$
(2)

where

$$h_{i}(\theta(t)) = \frac{\mu_{i}(\theta(t))}{\sum_{i=1}^{r} \mu_{i}(\theta(t))},$$

$$\mu_{i}(\theta(t)) = \prod_{j=1}^{g} W_{ij}(\theta_{j}(t)),$$
(3)

and $W_{ij}(\theta_j(t))$ representing the grade of membership of $\theta_j(t)$ in W_{ij} . Here, for all $t, h_i(\theta(t)) \geq 0$ and $\sum_{i=1}^r h_i(\theta(t)) = 1$.

In this paper, we will design the following Hankel norm filter by employing the parallel distributed compensation technique.

Filter Rule i. If $\theta_1(t)$ is $W_{i1}, \theta_2(t)$ is W_{i2} and . . . and $\theta_g(t)$ is W_{ig} , then

$$d\hat{x}(t) = A_{fi}\hat{x}(t) + B_{fi}dy(t),$$

$$\hat{z}(t) = C_{fi}\hat{x}(t),$$
(4)

where $\widehat{x}(t) \in \mathbb{R}^n$ and $\widehat{z}(t) \in \mathbb{R}^q$ are the state and output of the filter, respectively. The matrices $A_{\rm fi}$, $B_{\rm fi}$, and $C_{\rm fi}$ are filter parameters to be determined.

The defuzzified output of (4) is referred by

$$d\widehat{x}(t) = \sum_{i=1}^{r} h_i(\theta(t)) \left\{ A_{fi}\widehat{x}(t) + B_{fi}dy(t) \right\}$$

$$\widehat{z}(t) = \sum_{i=1}^{r} h_i(\theta(t)) C_{fi}\widehat{x}(t).$$
(5)

Defining the augmented state vector $\xi^T(t) = [x^T(t) \ \hat{x}^T(t)]$ and $e(t) = z(t) - \hat{z}(t)$, then the filtering error system can be written in the following form:

$$d\xi(t)$$

$$= \left[\overline{A}(t) \xi(t) + \overline{A}_{d}(t) G \xi(t-\tau) + \overline{B}(t) v(t) \right] dt$$

$$+ \left[\overline{M}(t) \xi(t) + \overline{M}_{d}(t) G \xi(t-\tau) + \overline{N}(t) v(t) \right] d\omega(t),$$

$$e(t) = \overline{L}(t) \xi(t),$$
(6)

where $G = \begin{bmatrix} I & 0 \end{bmatrix}$,

$$\begin{split} \overline{A}\left(t\right) &= \sum_{i=1}^{r} h_{i}\left(\theta\left(t\right)\right) \sum_{j=1}^{r} h_{j}\left(\theta\left(t\right)\right) \begin{bmatrix} A_{j} & 0 \\ B_{\mathrm{fi}}C_{j} & A_{\mathrm{fi}} \end{bmatrix} \\ &= \begin{bmatrix} A\left(t\right) & 0 \\ B_{f}\left(t\right)C\left(t\right) & A_{f}\left(t\right) \end{bmatrix}, \\ \overline{A}_{d}\left(t\right) &= \sum_{i=1}^{r} h_{i}\left(\theta\left(t\right)\right) \sum_{j=1}^{r} h_{j}\left(\theta\left(t\right)\right) \begin{bmatrix} A_{dj} \\ B_{\mathrm{fi}}C_{dj} \end{bmatrix} \\ &= \begin{bmatrix} A_{d}\left(t\right) \\ B_{f}\left(t\right)C_{d}\left(t\right) \end{bmatrix}, \end{split}$$

$$\overline{B}(t) = \sum_{i=1}^{r} h_{i}(\theta(t)) \sum_{j=1}^{r} h_{j}(\theta(t)) \begin{bmatrix} B_{j} \\ B_{f}D_{j} \end{bmatrix}
= \begin{bmatrix} B(t) \\ B_{f}(t)D(t) \end{bmatrix},
\overline{M}(t) = \sum_{i=1}^{r} h_{i}(\theta(t)) \sum_{j=1}^{r} h_{j}(\theta(t)) \begin{bmatrix} M_{j} & 0 \\ B_{f}E_{j} & 0 \end{bmatrix}
= \begin{bmatrix} M(t) & 0 \\ B_{f}(t)E(t) & 0 \end{bmatrix},
\overline{M}_{d}(t) = \sum_{i=1}^{r} h_{i}(\theta(t)) \sum_{j=1}^{r} h_{j}(\theta(t)) \begin{bmatrix} M_{dj} \\ B_{fi}E_{dj} \end{bmatrix}
= \begin{bmatrix} M_{d}(t) \\ B_{f}(t)E_{d}(t) \end{bmatrix},
\overline{N}(t) = \sum_{i=1}^{r} h_{i}(\theta(t)) \sum_{j=1}^{r} h_{j}(\theta(t)) \begin{bmatrix} N_{j} \\ B_{fi}F_{j} \end{bmatrix}
= \begin{bmatrix} N(t) \\ B_{f}(t)F(t) \end{bmatrix},
\overline{L}(t) = \sum_{i=1}^{r} h_{i}(\theta(t)) \sum_{j=1}^{r} h_{j}(\theta(t)) [L_{j} - C_{fi}]
= [L(t) - C_{f}(t)].$$
(7)

The Hankel norm filtering problem addressed in this paper can be expressed as follows.

Given a scalar $\gamma > 0$, determine the matrices $A_{\rm fi}$, $B_{\rm fi}$, and $C_{\rm fi}$ to find a suitable filter in the form of (5) such that

- (i) the filtering error system (6) with v(t) = 0 is mean-square asymptotically stable;
- (ii) subjected to the zero initial condition ($\xi(t) = 0$, for all t < 0)

$$\mathscr{E}\left\{\int_{\mathcal{T}}^{\infty} e^{T}\left(t\right) e\left(t\right) dt\right\} < \gamma^{2} \int_{0}^{\mathcal{T}} v^{T}\left(t\right) v\left(t\right) dt; \qquad (8)$$

for all $v(t) \in L_2[0, \infty)$ with v(t) = 0, for all $t \ge \mathcal{T}$.

Then, the filtering error system (6) is said to be mean-square asymptotically stable with a Hankel norm performance level γ .

Lemma 1. Given matrix $R = R^T \ge 0$ and scalar $\tau > 0$, $\overline{y}(t)$ is a vector function which satisfies $\overline{y}(t)dt = d\xi(t)$, then

$$-\tau \int_{t-\tau}^{t} \overline{y}^{T}(s) R \overline{y}(s) ds$$

$$\leq \left[\xi^{T}(t) \quad \xi^{T}(t-\tau) \right] \begin{bmatrix} -R & R \\ R & -R \end{bmatrix} \begin{bmatrix} \xi(t) \\ \xi(t-\tau) \end{bmatrix}.$$
(9)

Remark 2. $\overline{y}(t)$ in Lemma 1 is not equivalent to $\dot{\xi}(t)$ in deterministic time-delay systems and cannot be expressed by the known system parameters for the existence of the stochastic perturbation $d\omega(t)$. If $d\omega(t) = 0$, $\overline{v}(t) = \dot{\xi}(t)$.

3. Hankel Norm Performance Analysis

In this subsection, we will derive a sufficient condition for the existence of the Hankel norm filter that guarantees the filtering error system (6) to be mean-square asymptotically stable with a specified Hankel norm performance level. By making use of the Itô differential rule, the stochastic differentials of Lyapunov functions along the solution of system (6) are obtained and the integral inequality method is also used during the derivation. Based on these, the Hankel norm criterion of filtering problem is first established. Now, we will first give the following theorem which will play a key role in the derivation of our main results.

Theorem 3. The filtering error system (6) is mean-square asymptotically stable and has a guaranteed Hankel norm performance γ if there exist $P_1 > 0$, $P_2 > 0$, $Q_1 > 0$, $Q_2 > 0$, $R_1 > 0$, $R_2 > 0$, and S_1 , S_2 satisfying

$$\begin{bmatrix} -P_{1} & P_{1}\overline{M}(t) & P_{1}\overline{M}_{d}(t) & 0 & P_{1}\overline{N}(t) \\ * & P_{1}\overline{A}(t) + \overline{A}^{T}(t) P_{1} + G^{T}\left(Q_{1} - \frac{R_{1}}{\tau}\right)G & P_{1}\overline{A}_{d}(t) + G^{T}\frac{R_{1}}{\tau} & \overline{A}^{T}(t) G^{T}S_{1} & P_{1}\overline{B}(t) \\ * & * & -Q_{1} - \frac{R_{1}}{\tau} & \overline{A}_{d}^{T}(t) G^{T}S_{1} & 0 \\ * & * & * & \tau R_{1} - S_{1} - S_{1}^{T} S_{1}^{T}G\overline{B}(t) \\ * & * & * & -\gamma^{2}I \end{bmatrix} < 0, \quad (10)$$

$$\begin{bmatrix} -P_{2} & P_{2}\overline{M}(t) & P_{2}\overline{M}_{d}(t) & 0 & 0 \\ * & P_{2}\overline{A}(t) + \overline{A}^{T}(t) P_{2} + G^{T}\left(Q_{2} - \frac{R_{2}}{\tau}\right)G & P_{2}\overline{A}_{d}(t) + G^{T}\frac{R_{2}}{\tau} & \overline{A}^{T}(t) G^{T}S_{2} & \overline{L}^{T}(t) \\ * & * & -Q_{2} - \frac{R_{2}}{\tau} & \overline{A}_{d}^{T}(t) G^{T}S_{2} & 0 \\ * & * & \tau R_{2} - S_{2} - S_{2}^{T} & 0 \\ * & * & * & -I \end{bmatrix}$$

$$\begin{bmatrix}
-P_{2} & P_{2}\overline{M}(t) & P_{2}\overline{M}_{d}(t) & 0 & 0 \\
* & P_{2}\overline{A}(t) + \overline{A}^{T}(t) P_{2} + G^{T}\left(Q_{2} - \frac{R_{2}}{\tau}\right)G & P_{2}\overline{A}_{d}(t) + G^{T}\frac{R_{2}}{\tau} & \overline{A}^{T}(t) G^{T}S_{2} & \overline{L}^{T}(t) \\
* & * & -Q_{2} - \frac{R_{2}}{\tau} & \overline{A}_{d}^{T}(t) G^{T}S_{2} & 0 \\
* & * & * & \tau R_{2} - S_{2} - S_{2}^{T} & 0 \\
* & * & * & * & -I
\end{bmatrix} < 0, (11)$$

$$P_1 - P_2 \ge 0,$$
 (12)

$$G^{T}(Q_{1}-Q_{2})G \geq 0, \tag{13}$$

$$G^{T}\left(R_{1}-R_{2}\right)G\geq0.\tag{14}$$

Proof. Choose the Lyapunov-Krasovskii functionals as

$$V_{1}\left(\xi_{t},t\right) = \xi^{T}\left(t\right)P_{1}\xi\left(t\right) + \int_{t-\tau}^{t} \xi^{T}\left(\alpha\right)G^{T}Q_{1}G\xi\left(\alpha\right)d\alpha$$

$$+ \int_{-\tau}^{0} \int_{t+\beta}^{t} \overline{y}^{T}\left(\alpha\right)G^{T}R_{1}G\overline{y}\left(\alpha\right)d\alpha\,d\beta,$$
(15)

$$V_{2}(\xi_{t},t) = \xi^{T}(t) P_{2}\xi(t) + \int_{t-\tau}^{t} \xi^{T}(\alpha) G^{T} Q_{2}G\xi(\alpha) d\alpha$$

$$+ \int_{-\tau}^{0} \int_{t+\beta}^{t} \overline{y}^{T}(\alpha) G^{T} R_{2}G\overline{y}(\alpha) d\alpha d\beta,$$
(16)

where P_1 , P_2 , Q_1 , Q_2 , R_1 , and R_2 are real symmetric positive definite matrices to be determined, $\xi_t = \xi(t + \iota), -\tau \le \iota \le 0$.

 $\overline{y}(t)$ is defined as $\overline{y}(t)dt = d\xi(t)$, and according to the Newton-Leibniz formula, we have

$$\int_{t-\tau}^{t} \overline{y}(\alpha) d\alpha = \xi(t) - \xi(t-\tau). \tag{17}$$

Then by making use of the Itô differential rule, the stochastic differential $dV_1(\xi_t, t)$ along the solution of system (6) can be obtained as

$$dV_{1}(\xi_{t},t)$$

$$= \mathcal{L}V_{1}(\xi_{t},t) dt + 2\xi^{T}(t) P_{1}$$

$$\times \left[\overline{M}(t) \xi(t) + \overline{M}_{d}(t) G\xi(t-\tau) + \overline{N}(t) v(t) \right] d\omega(t),$$
(18)

where

$$\mathcal{L}V_{1}\left(\xi_{t},t\right) = 2\xi^{T}\left(t\right)P_{1}\left[\overline{A}\left(t\right)\xi\left(t\right) + \overline{A}_{d}\left(t\right)G\xi\left(t-\tau\right) + \overline{B}\left(t\right)v\left(t\right)\right] \\
+ \left[\overline{M}\left(t\right)\xi\left(t\right) + \overline{M}_{d}\left(t\right)G\xi\left(t-\tau\right) + \overline{N}\left(t\right)v\left(t\right)\right]^{T} \\
\times P_{1}\left[\overline{M}\left(t\right)\xi\left(t\right) + \overline{M}_{d}\left(t\right)G\xi\left(t-\tau\right) + \overline{N}\left(t\right)v\left(t\right)\right] \\
+ \xi^{T}\left(t\right)G^{T}Q_{1}G\xi\left(t\right) \\
- \xi^{T}\left(t-\tau\right)G^{T}Q_{1}G\xi\left(t-\tau\right) + \tau\overline{y}^{T}\left(t\right)G^{T}R_{1}G\overline{y}\left(t\right) \\
- \int_{t-\tau}^{t} \overline{y}^{T}\left(s\right)G^{T}R_{1}G\overline{y}\left(s\right)ds. \tag{19}$$

Applying Lemma 1 to $\mathscr{L}V_1(\xi_t,t)$, we have

$$\mathscr{L}V_{1}\left(\xi_{t},t\right)$$

$$\leq \xi^{T}(t) \left[2P_{1}\overline{A}(t) + \overline{M}^{T}(t) P_{1}\overline{M}(t) + G^{T}\left(Q_{1} - \frac{R_{1}}{\tau}\right)G \right]
\times \xi(t) + \xi^{T}(t) \left[2P_{1}\overline{A}_{d}(t) + \overline{M}^{T}(t) P_{1}\overline{M}_{d}(t) + G^{T}\frac{R_{1}}{\tau} \right]
\times G\xi(t-\tau)
+ \xi^{T}(t) \left[2P_{1}\overline{B}(t) + \overline{M}^{T}(t) P_{1}\overline{N}(t) \right] v(t)
+ \xi^{T}(t-\tau)G^{T}\left[\overline{M}_{d}^{T}(t) P_{1}\overline{M}(t) + \frac{R_{1}}{\tau}G \right] \xi(t)
+ \xi^{T}(t-\tau)G^{T}
\times \left[\overline{M}_{d}^{T}(t) P_{1}\overline{M}_{d}(t) - \left(Q_{1} + \frac{R_{1}}{\tau}\right) \right] G\xi(t-\tau)
+ \xi^{T}(t-\tau)G^{T}
\times \left[\overline{M}_{d}^{T}(t) P_{1}\overline{N}(t) \right] v(t) + v^{T}(t) \left[\overline{N}^{T}(t) P_{1}\overline{M}(t) \right] \xi(t)
+ v^{T}(t) \left[\overline{N}^{T}(t) P_{1}\overline{M}_{d}(t) \right] G\xi(t-\tau)
+ v^{T}(t) \left[\overline{N}^{T}(t) P_{1}\overline{M}_{d}(t) \right] v(t)
+ \tau \overline{y}^{T}(t) G^{T}R_{1}G\overline{y}(t) .$$
(20)

Noting that $\overline{y}(t)dt = d\xi(t)$ and system (6), for arbitrary matrix $S_1 \in \mathbb{R}^{n \times n}$ it can be seen that

$$0 = 2\overline{y}^{T}(t) G^{T} S_{1}^{T} G$$

$$\times \left\{ \left[\overline{M}(t) \xi(t) + \overline{M}_{d}(t) G \xi(t-\tau) + \overline{N}(t) v(t) \right] d\omega(t) + \left[\overline{A}(t) \xi(t) + \overline{A}_{d}(t) G \xi(t-\tau) + \overline{B}(t) v(t) - \overline{y}(t) \right] dt \right\}.$$

$$(21)$$

Thus, it follows from (18) and (21) that

$$dV_{1}(\xi_{t},t) = \mathcal{L}\widetilde{V}_{1}(\xi_{t},t) dt$$

$$+ 2\left[\xi^{T}(t) P_{1} + \overline{y}^{T}(t) G^{T} S_{1}^{T} G\right]$$

$$\times \left[\overline{M}(t) \xi(t) + \overline{M}_{d}(t) G \xi(t-\tau) + \overline{N}(t) v(t)\right]$$

$$\times d\omega(t),$$
(22)

where

$$\mathcal{L}\widetilde{V}_{1}\left(\xi_{t},t\right) = \mathcal{L}V_{1}\left(\xi_{t},t\right) + 2\overline{y}^{T}\left(t\right)G^{T}S_{1}^{T}G
\times \left[\overline{A}\left(t\right)\xi\left(t\right) + \overline{A}_{d}\left(t\right)G\xi\left(t-\tau\right)
+ \overline{B}\left(t\right)v\left(t\right) - \overline{y}\left(t\right)\right]
\leq \xi^{T}\left(t\right)\left[2P_{1}\overline{A}\left(t\right) + \overline{M}^{T}\left(t\right)P_{1}\overline{M}\left(t\right)
+ G^{T}\left(Q_{1} - \frac{R_{1}}{\tau}\right)G\right]
\times \xi\left(t\right) + 2\xi^{T}\left(t\right)\left[P_{1}\overline{A}_{d}\left(t\right) + \overline{M}^{T}\left(t\right)P_{1}\overline{M}_{d}\left(t\right)
+ G^{T}\frac{R_{1}}{\tau}G^{T}S_{1}G\overline{y}\left(t\right)
+ 2\xi^{T}\left(t\right)\left[\overline{A}\left(t\right)^{T}G^{T}S_{1}G\overline{y}\left(t\right)
+ 2\xi^{T}\left(t\right)\left[P_{1}\overline{B}\left(t\right) + \overline{M}^{T}\left(t\right)P_{1}\overline{N}\left(t\right)\right]v\left(t\right)
+ \xi^{T}\left(t-\tau\right)G^{T}
\times \left[\overline{M}_{d}^{T}\left(t\right)P_{1}\overline{M}_{d}\left(t\right) - Q_{1} - \frac{R_{1}}{\tau}\right]
\times G\xi\left(t-\tau\right) + 2\xi^{T}\left(t-\tau\right)G^{T}
\times \left[\overline{A}_{d}^{T}\left(t\right)G^{T}S_{1}G\overline{y}\left(t\right)
+ 2\xi^{T}\left(t-\tau\right)G^{T}\left[\overline{M}_{d}^{T}\left(t\right)P_{1}\overline{N}\left(t\right)\right]v\left(t\right)
+ 7\overline{y}^{T}\left(t\right)G^{T}\left[\tau R_{1} - S_{1} - S_{1}^{T}G\overline{y}\left(t\right)
+ 2\overline{y}^{T}\left(t\right)G^{T}\left[S_{1}^{T}G\overline{B}\left(t\right)\right]v\left(t\right)
+ v^{T}\left(t\right)\left[\overline{N}^{T}\left(t\right)P_{1}\overline{N}\left(t\right)\right]v\left(t\right) . \tag{23}$$

Therefore, when assuming zero input v(t) = 0, it follows that

$$\mathscr{L}\widetilde{V}_{1}\left(\xi_{t},t\right)\leq\eta^{T}\left(t\right)\Theta_{1}\eta\left(t\right),\tag{24}$$

where

$$\eta^{T}(t) = \begin{bmatrix} \xi^{T}(t) & \xi^{T}(t - \tau) G^{T} & \overline{y}^{T}(t) G^{T} \end{bmatrix},
\Theta_{1} = \begin{bmatrix} \Pi_{11} & \Pi_{12} & \overline{A}^{T}(t) G^{T} S_{1} \\ * & \Pi_{22} & \overline{A}^{T}_{d}(t) G^{T} S_{1} \\ * & * & \tau R_{1} - S_{1} - S_{1}^{T} \end{bmatrix},
\Pi_{11} = P_{1}\overline{A}(t) + \overline{A}^{T}(t) P_{1} + \overline{M}^{T}(t) P_{1}\overline{M}(t)
+ G^{T} \left(Q_{1} - \frac{R_{1}}{\tau} \right) G,
\Pi_{12} = P_{1}\overline{A}_{d}(t) + \overline{M}^{T}(t) P_{1}\overline{M}_{d}(t) + G^{T} \frac{R_{1}}{\tau},
\Pi_{22} = \overline{M}^{T}_{d}(t) P_{1}\overline{M}_{d}(t) - Q_{1} - \frac{R_{1}}{\tau}.$$
(25)

By using the Schur complement lemma, the inequality (10) implies the negative definiteness of Θ_1 . Then, we have $\mathscr{L}\widetilde{V}_1(\xi_t,t)<0$, and the filtering error system (6) with v(t)=0 is guaranteed to be mean-square asymptotically stable. And the next step is to establish the Hankel norm performance:

$$\mathscr{E}\left\{\int_{\mathscr{T}}^{\infty} e^{T}\left(t\right)e\left(t\right)dt\right\} < \gamma^{2}\int_{0}^{\mathscr{T}} \nu^{T}\left(t\right)\nu\left(t\right)dt,\tag{26}$$

under zero initial condition and $v(t) \in L_2[0,\infty)$ with v(t) = 0, for all $t \ge \mathcal{T}$.

For any nonzero $v(t) \in L_2[0,\infty)$ with v(t) = 0, for all $t \ge \mathcal{T}$, the inequality of (23) can be rewritten in the following quadratic form:

$$\mathscr{L}\widetilde{V}_{1}\left(\xi_{t},t\right)\leq\zeta^{T}\left(t\right)\widetilde{\Theta}_{1}\zeta\left(t\right),\tag{27}$$

where

$$\zeta^{T}(t) = \begin{bmatrix} \xi^{T}(t) & \xi^{T}(t-\tau)G^{T} & \overline{y}^{T}(t)G^{T} & v^{T}(t) \end{bmatrix},$$

$$\widetilde{\Theta}_{1} = \begin{bmatrix} \Pi_{11} & \Pi_{12} & \overline{A}^{T}(t)G^{T}S_{1} & P_{1}\overline{B}(t) + \overline{M}^{T}(t)P_{1}\overline{N}(t) \\ * & \Pi_{22} & \overline{A}^{T}_{d}(t)G^{T}S_{1} & M_{d}^{T}(t)P_{1}\overline{N}(t) \\ * & * & \tau R_{1} - S_{1} - S_{1}^{T} & S_{1}^{T}G\overline{B}(t) \\ * & * & * & \overline{N}^{T}(t)P_{1}\overline{N}(t) \end{bmatrix}.$$
(28)

The inequalities (10) and (27) imply

$$\mathcal{L}\widetilde{V}_{1}\left(\xi_{t},t\right)-\gamma^{2}v^{T}\left(t\right)v\left(t\right)$$

$$\leq\zeta^{T}\left(t\right)\widetilde{\Theta}_{1}\zeta\left(t\right)-\gamma^{2}v^{T}\left(t\right)v\left(t\right)<0.$$
(29)

Integrating both sides of (22) and (29), respectively, from 0 to \mathcal{T} and then taking expectation, we have

$$\mathcal{E}\left\{V_{1}\left(\xi_{\mathcal{T}},\mathcal{T}\right)\right\}$$

$$=\mathcal{E}\left\{\int_{0}^{\mathcal{T}}\mathcal{L}\widetilde{V}_{1}\left(\xi_{t},t\right)dt\right\} < \gamma^{2}\int_{0}^{\mathcal{T}}v^{T}\left(t\right)v\left(t\right)dt,$$
(30)

where zero initial condition is used.

Second, introduce $V_2(\xi_t,t)$ in (16). By following similar lines as above, it is not difficult to obtain the stochastic differential $dV_2(\xi_t,t)$ as

$$dV_{2}(\xi_{t},t) = \mathcal{L}\widetilde{V}_{2}(\xi_{t},t) dt$$

$$+ 2\left[\xi^{T}(t) P_{2} + \overline{y}^{T}(t) G^{T} S_{2}^{T} G\right]$$

$$\times \left[\overline{M}(t) \xi(t) + \overline{M}_{d}(t) G \xi(t-\tau) + \overline{N}(t) v(t)\right]$$

$$\times d\omega(t),$$
(31)

where

$$\mathcal{L}\widetilde{V}_{2}\left(\xi_{t},t\right) \leq \zeta^{T}\left(t\right)\widetilde{\Theta}_{2}\zeta\left(t\right),$$

$$\left[\Gamma_{11} \quad \Gamma_{12} \quad \overline{A}^{T}\left(t\right)G^{T}S_{2} \quad P_{2}\overline{B}\left(t\right) + \overline{M}^{T}\left(t\right)P_{2}\overline{N}\left(t\right)\right] \\ * \quad \Gamma_{22} \quad \overline{A}_{d}^{T}\left(t\right)G^{T}S_{2} \qquad M_{d}^{T}\left(t\right)P_{2}\overline{N}\left(t\right) \\ * \quad * \quad \tau R_{2} - S_{2} - S_{2}^{T} \qquad S_{2}^{T}G\overline{B}\left(t\right) \\ * \quad * \quad * \qquad \overline{N}^{T}\left(t\right)P_{2}\overline{N}\left(t\right)\right],$$

$$\Gamma_{11} = P_{2}\overline{A}\left(t\right) + \overline{A}^{T}\left(t\right)P_{2} + \overline{M}^{T}\left(t\right)P_{2}\overline{M}\left(t\right) \\ + G^{T}\left(Q_{2} - \frac{R_{2}}{\tau}\right)G,$$

$$\Gamma_{12} = P_{2}\overline{A}_{d}\left(t\right) + \overline{M}^{T}\left(t\right)P_{2}\overline{M}_{d}\left(t\right) + G^{T}\frac{R_{2}}{\tau},$$

$$\Gamma_{22} = \overline{M}_{d}^{T}\left(t\right)P_{2}\overline{M}_{d}\left(t\right) - Q_{2} - \frac{R_{2}}{\tau},$$

$$(32)$$

By Schur complement lemma, the inequality (11) is equivalent to

$$\begin{bmatrix} \Gamma_{11} & \Gamma_{12} & \overline{A}^{T}(t) G^{T} S_{2} \\ * & \Gamma_{22} & \overline{A}_{d}^{T}(t) G^{T} S_{2} \\ * & * & \tau R_{2} - S_{2} - S_{2}^{T} \end{bmatrix} + \begin{bmatrix} \overline{L}^{T}(t) \\ 0 \\ 0 \end{bmatrix} [\overline{L}(t) \ 0 \ 0] < 0.$$
(33)

Thus, we have

$$Y = \xi^{T}(t) \left[P_{2}\overline{A}(t) + \overline{A}^{T}(t) P_{2} + \overline{M}^{T}(t) P_{2}\overline{M}(t) + G^{T}\left(Q_{2} - \frac{R_{2}}{\tau}\right) G \right] \xi(t)$$

$$+ 2\xi^{T}(t) \left[P_{2}\overline{A}_{d}(t) + \overline{M}^{T}(t) P_{2}\overline{M}_{d}(t) + G^{T}\frac{R_{2}}{\tau} \right]$$

$$\times G\xi(t - \tau)$$

$$+ 2\xi^{T}(t) \left[\overline{A}(t)^{T}G^{T}S_{2} \right] G\overline{y}(t)$$

$$+ \xi^{T}(t - \tau) G^{T} \left[\overline{M}_{d}^{T}(t) P_{2}\overline{M}_{d}(t) - Q_{2} - \frac{R_{2}}{\tau} \right]$$

$$\times G\xi(t - \tau)$$

$$+ 2\xi^{T}(t - \tau) G^{T} \left[\overline{A}_{d}^{T}(t) G^{T}S_{2} \right] G\overline{y}(t)$$

$$+ \overline{y}^{T}(t) G^{T} \left[\tau R_{2} - S_{2} - S_{2}^{T} \right] G \overline{y}(t)$$

$$+ \left[\overline{L}(t) \xi(t) \right]^{T} \left[\overline{L}(t) \xi(t) \right]$$

$$< 0. \tag{34}$$

By considering v(t) = 0, for all $t \ge \mathcal{T}$ and (32), for any $t \ge \mathcal{T}$, inequalities (32) and (34) guarantee

$$\mathscr{L}\widetilde{V}_{2}(\xi_{t},t)+e^{T}(t)e(t)<0, \quad \forall t\geq \mathscr{T}.$$
 (35)

Integrating both sides of (31) and (35), respectively, from \mathcal{T} to ∞ and then taking expectation, we have

$$\mathcal{E}\left\{\int_{\mathcal{T}}^{\infty} \mathcal{L}\widetilde{V}_{2}\left(\xi_{t},t\right)dt\right\} + \mathcal{E}\left\{\int_{\mathcal{T}}^{\infty} e^{T}\left(t\right)e\left(t\right)dt\right\} < 0. \quad (36)$$

Due to $\mathscr{E}\{\int_{\mathscr{T}}^{\infty}\mathscr{L}\widetilde{V}_2(\xi_t,t)dt\} = \mathscr{E}\{V_2(\xi_\infty,\infty)\} - \mathscr{E}\{V_2(\xi_{\mathscr{T}},\mathscr{T})\}$ and $\mathscr{E}\{V_2(\xi_\infty,\infty)\} \geq 0$, then

$$\mathscr{E}\left\{\int_{\mathscr{T}}^{\infty} e^{T}\left(t\right)e\left(t\right)dt\right\} < \mathscr{E}\left\{V_{2}\left(\xi_{\mathscr{T}},\mathscr{T}\right)\right\}. \tag{37}$$

By considering (12), (13), (14), (30), and (37), we obtain (26), the proof is concluded. \Box

Remark 4. For general continuous time stochastic time-delay systems, the delay-independent results can be obtained by choosing the following form of Lyapunov functional:

$$V(t) = \xi^{T}(t) P\xi(t) + \int_{t-\tau}^{t} \xi^{T}(s) Q\xi(s) ds.$$
 (38)

However, the presence of stochastic perturbation (Wiener process) in the stochastic time-delay systems makes $\dot{\xi}(t)$ undefined and the above function is not suitable for its large conservative. Thus, we adopt the Lyapunov functionals in the form of (15) and (16) in the original version and obtain delay-dependent criterion of filtering problem for stochastic time-delay systems. It should be pointed out that the Lyapunov functions are chosen with constant delay τ in this paper, and the proposed method can be also extended to the case of time-varying delay $\tau(t)$, which can have more conservative results.

Remark 5. Theorem 3 provides a delay-dependent sufficient condition of the robustly mean-square asymptotic stability with a Hankel norm performance level γ for the filtering error system (6). By introducing the assistant vector $\overline{\gamma}(t)$ and free-weighting matrices S_i , the derivation of the above theorem is completed without using any model transformations and cross terms bounding techniques. The introduction of S_i helps establishing the contact of $\xi(t)$, $\overline{\gamma}(t)$, and $\xi(t-\tau)$ and then the delay-dependent results are obtained. This approach has been proved to be less conservative.

4. Hankel Norm Filter Design

In this section, we will provide the solution to Hankel norm filtering problem for stochastic time-delay systems. As mentioned above, Theorem 3 gives a sufficient condition for the existence of a filter that guarantees the filtering error system mean-square asymptotically stable with Hankel norm performance. However, the inequalities (10) and (11) in Theorem 3 cannot be solved directly for the coupled matrix variables. To solve this problem, we will make decoupling process and adopt the convex linearization approach to transform (10) and (11) into LMI forms, which can be solved easily with the standard numerical software.

Theorem 6. For the given positive constants $\tau > 0$ and $0 < \alpha \le 1$, an admissible Hankel norm filter in the form of (5) exists such that the filtering error system (6) is meansquare asymptotically stable and has a guaranteed Hankel norm performance level γ if there exist X > 0, Y > 0, Q > 0, R > 0, S, $\overline{A}_f(t)$, $\overline{B}_f(t)$, and $\overline{C}_f(t)$ satisfying

$$\begin{bmatrix}
-X & -Y & \Phi_{13} & 0 & \Phi_{15} & 0 & \Phi_{17} \\
* & -Y & \Phi_{23} & 0 & \Phi_{25} & 0 & \Phi_{27} \\
* & * & \Phi_{33} & \Phi_{34} & \Phi_{35} & A^{T}(t) S & \Phi_{37} \\
* & * & * & \Phi_{44} & \Phi_{45} & 0 & \Phi_{47} \\
* & * & * & * & \Phi_{55} & A_{d}^{T}(t) S & 0 \\
* & * & * & * & * & \Phi_{66} & S^{T}B(t) \\
* & * & * & * & * & * & * & -y^{2}I
\end{bmatrix} < 0, (39)$$

$$\begin{bmatrix} -\alpha X & -\alpha Y & \Psi_{13} & 0 & \Psi_{15} & 0 & 0 \\ * & -\alpha Y & \Psi_{23} & 0 & \Psi_{25} & 0 & 0 \\ * & * & \Psi_{33} & \Psi_{34} & \Psi_{35} & \alpha A^T(t) S & L^T(t) \\ * & * & * & \Psi_{44} & \Psi_{45} & 0 & -\overline{C}_f^T(t) \\ * & * & * & * & \Psi_{55} & \alpha A_d^T(t) S & 0 \\ * & * & * & * & * & \Psi_{66} & 0 \\ * & * & * & * & * & * & -I \end{bmatrix} < 0,$$

$$(40)$$

where

$$\begin{split} & \Phi_{13} = XM\left(t\right) + \overline{B}_{f}\left(t\right)E\left(t\right), \\ & \Phi_{15} = XM_{d}\left(t\right) + \overline{B}_{f}\left(t\right)E_{d}\left(t\right), \\ & \Phi_{17} = XN\left(t\right) + \overline{B}_{f}\left(t\right)F\left(t\right), \\ & \Phi_{23} = YM\left(t\right) + \overline{B}_{f}\left(t\right)E\left(t\right), \\ & \Phi_{25} = YM_{d}\left(t\right) + \overline{B}_{f}\left(t\right)E_{d}\left(t\right), \\ & \Phi_{27} = YN\left(t\right) + \overline{B}_{f}\left(t\right)F\left(t\right), \\ & \Phi_{33} = XA\left(t\right) + A^{T}\left(t\right)X + \overline{B}_{f}\left(t\right)C\left(t\right) \\ & + C^{T}\left(t\right)\overline{B}_{f}^{T}\left(t\right) + Q - \frac{R}{\tau}, \end{split}$$

$$\begin{split} &\Phi_{34} = \overline{A}_f\left(t\right) + A^T\left(t\right)Y + C^T\left(t\right)\overline{B}_f^T\left(t\right), \\ &\Phi_{35} = XA_d\left(t\right) + \overline{B}_f\left(t\right)C_d\left(t\right) + \frac{R}{\tau}, \\ &\Phi_{37} = XB\left(t\right) + \overline{B}_f\left(t\right)D\left(t\right), \\ &\Phi_{44} = \overline{A}_f\left(t\right) + \overline{A}_f^T\left(t\right), \\ &\Phi_{45} = YA_d\left(t\right) + \overline{B}_f\left(t\right)C_d\left(t\right), \\ &\Phi_{47} = YB\left(t\right) + \overline{B}_f\left(t\right)D\left(t\right), \\ &\Phi_{55} = -Q - \frac{R}{\tau}, \\ &\Phi_{66} = \tau R - S - S^T, \\ &\Psi_{13} = \alpha\left(XM\left(t\right) + \overline{B}_f\left(t\right)E\left(t\right)\right), \\ &\Psi_{15} = \alpha\left(XM_d\left(t\right) + \overline{B}_f\left(t\right)E_d\left(t\right)\right), \\ &\Psi_{23} = \alpha\left(YM\left(t\right) + \overline{B}_f\left(t\right)E\left(t\right)\right), \\ &\Psi_{25} = \alpha\left(YM_d\left(t\right) + \overline{B}_f\left(t\right)E_d\left(t\right)\right), \\ &\Psi_{33} = \alpha\left(XA\left(t\right) + A^T\left(t\right)X + \overline{B}_f\left(t\right)C\left(t\right) \\ &\quad + C^T\left(t\right)\overline{B}_f^T\left(t\right) + Q - \frac{R}{\tau}\right), \\ &\Psi_{34} = \alpha\left(\overline{A}_f\left(t\right) + A^T\left(t\right)Y + C^T\left(t\right)\overline{B}_f^T\left(t\right)\right), \end{split}$$

$$\begin{split} \Psi_{35} &= \alpha \left(X A_d \left(t \right) + \overline{B}_f \left(t \right) C_d \left(t \right) + \frac{R}{\tau} \right), \\ \Psi_{44} &= \alpha \left(\overline{A}_f \left(t \right) + \overline{A}_f^T \left(t \right) \right), \\ \Psi_{45} &= \alpha \left(Y A_d \left(t \right) + \overline{B}_f \left(t \right) C_d \left(t \right) \right), \\ \Psi_{55} &= -\alpha \left(Q + \frac{R}{\tau} \right), \\ \Psi_{66} &= \alpha \left(\tau R - S - S^T \right). \end{split} \tag{41}$$

Proof. Inequality (39) implies X > 0 and Y > 0. For arbitrary symmetric positive definite matrix Y, one can always find a nonsingular matrix V and symmetric positive definite matrix W satisfying $Y = VW^{-1}V^{T}$. Now we introduce, respectively, the following matrix variables

$$P = \begin{bmatrix} X & V \\ V^T & W \end{bmatrix}, \qquad J_1 = \begin{bmatrix} I & 0 \\ 0 & W^{-1}V^T \end{bmatrix}. \tag{42}$$

By Schur complement lemma, we can infer from (39) that $X - VW^{-1}V^T = X - Y > 0$, and then P > 0.

Defining $P_1 = P$, $P_2 = \alpha P$, $Q_1 = Q$, $Q_2 = \alpha Q$, $R_1 = R$, $R_2 = \alpha R$, and applying the congruence transformation by matrix $\hat{\Delta} = \text{diag}\{J_1, J_1, I, I, I\}$ to (10) and (11), respectively, we can easily infer the following inequalities:

$$\begin{bmatrix} -X & -Y & \widetilde{\Phi}_{13} & 0 & \widetilde{\Phi}_{15} & 0 & \widetilde{\Phi}_{17} \\ * & -Y & \widetilde{\Phi}_{23} & 0 & \widetilde{\Phi}_{25} & 0 & \widetilde{\Phi}_{27} \\ * & * & \widetilde{\Phi}_{33} & \widetilde{\Phi}_{34} & \widetilde{\Phi}_{35} & A^T(t) S & \widetilde{\Phi}_{37} \\ * & * & * & \widetilde{\Phi}_{44} & \widetilde{\Phi}_{45} & 0 & \widetilde{\Phi}_{47} \\ * & * & * & * & -Q - \frac{R}{\tau} & A_d^T(t) S & 0 \\ * & * & * & * & * & \tau R - S - S^T & S^T B(t) \\ * & * & * & * & * & * & -\gamma^2 I \end{bmatrix} \\ \begin{bmatrix} -\alpha X & -\alpha Y & \widetilde{\Psi}_{13} & 0 & \widetilde{\Psi}_{15} & 0 & 0 \\ * & -\alpha Y & \widetilde{\Psi}_{23} & 0 & \widetilde{\Psi}_{25} & 0 & 0 \\ * & * & \widetilde{\Psi}_{33} & \widetilde{\Psi}_{34} & \widetilde{\Psi}_{35} & \alpha A^T(t) S & L^T(t) \\ * & * & * & \widetilde{\Psi}_{44} & \widetilde{\Psi}_{45} & 0 & -\overline{C}_f^T(t) \\ * & * & * & * & * & * & \alpha (\tau R - S - S^T) & 0 \\ * & * & * & * & * & * & * & -I \end{bmatrix} < 0,$$

where

$$\begin{split} \widetilde{\Phi}_{13} &= XM\left(t\right) + VB_{f}\left(t\right)E\left(t\right), \\ \widetilde{\Phi}_{15} &= XM_{d}\left(t\right) + VB_{f}\left(t\right)E_{d}\left(t\right), \\ \widetilde{\Phi}_{17} &= XN\left(t\right) + VB_{f}\left(t\right)F\left(t\right), \\ \widetilde{\Phi}_{23} &= YM\left(t\right) + VB_{f}\left(t\right)E\left(t\right), \\ \widetilde{\Phi}_{25} &= YM_{d}\left(t\right) + VB_{f}\left(t\right)E_{d}\left(t\right), \\ \widetilde{\Phi}_{27} &= YN\left(t\right) + VB_{f}\left(t\right)F\left(t\right), \\ \widetilde{\Phi}_{33} &= XA\left(t\right) + A^{T}\left(t\right)X + VB_{f}\left(t\right)C\left(t\right) \\ &+ C^{T}\left(t\right)B_{f}^{T}\left(t\right)V^{T} + Q - \frac{R}{\tau}, \\ \widetilde{\Phi}_{34} &= VA_{f}\left(t\right)W^{-1}V^{T} + A^{T}\left(t\right)Y + C^{T}\left(t\right)B_{f}^{T}\left(t\right)V^{T}, \\ \widetilde{\Phi}_{35} &= XA_{d}\left(t\right) + VB_{f}\left(t\right)C_{d}\left(t\right) + \frac{R}{\tau}, \\ \widetilde{\Phi}_{37} &= XB\left(t\right) + VB_{f}\left(t\right)D\left(t\right), \\ \widetilde{\Phi}_{44} &= VA_{f}\left(t\right)W^{-1}V^{T} + VW^{-1}A_{f}^{T}\left(t\right)V^{T}, \\ \widetilde{\Phi}_{45} &= YA_{d}\left(t\right) + VB_{f}\left(t\right)C_{d}\left(t\right), \\ \widetilde{\Phi}_{47} &= YB\left(t\right) + VB_{f}\left(t\right)D\left(t\right), \\ \widetilde{\Psi}_{13} &= \alpha\left(XM_{d}\left(t\right) + VB_{f}\left(t\right)E_{d}\left(t\right)\right), \\ \widetilde{\Psi}_{23} &= \alpha\left(YM_{d}\left(t\right) + VB_{f}\left(t\right)E_{d}\left(t\right)\right), \\ \widetilde{\Psi}_{25} &= \alpha\left(YM_{d}\left(t\right) + VB_{f}\left(t\right)E_{d}\left(t\right)\right), \\ \widetilde{\Psi}_{33} &= \alpha\left(XA\left(t\right) + A^{T}\left(t\right)X + VB_{f}\left(t\right)C\left(t\right) \\ &+ C^{T}\left(t\right)B_{f}^{T}\left(t\right)V^{T} + Q - \frac{R}{\tau}\right), \\ \widetilde{\Psi}_{34} &= \alpha\left(VA_{f}\left(t\right)W^{-1}V^{T} + A^{T}\left(t\right)Y + C^{T}\left(t\right)B_{f}^{T}\left(t\right)V^{T}\right), \\ \widetilde{\Psi}_{35} &= \alpha\left(XA_{d}\left(t\right) + VB_{f}\left(t\right)C_{d}\left(t\right) + \frac{R}{\tau}\right), \\ \end{array}$$

$$\begin{split} \widetilde{\Psi}_{44} &= \alpha \left(VA_{f}\left(t\right)W^{-1}V^{T} + VW^{-1}A_{f}^{T}\left(t\right)V^{T}\right), \\ \widetilde{\Psi}_{45} &= \alpha \left(YA_{d}\left(t\right) + VB_{f}\left(t\right)C_{d}\left(t\right)\right). \end{split} \tag{44}$$

Letting $\overline{A}_f(t) = VA_f(t)W^{-1}V^T$, $\overline{B}_f(t) = VB_f(t)$, $\overline{C}_f(t) = C_f(t)W^{-1}V^T$, we readily obtain (39) and (40). The proof is completed.

Remark 7. It is noted that there exist different approaches to solve the Hankel norm filtering problem as mentioned above, such as the well-known projection lemma and the convex linearization approach. In this paper, the later approach is employed to solve the Hankel norm filtering problem. Compared with the projection lemma, the convex linearization approach has been proved to be less conservative. The contrast analysis of the two methods can be referred in the literature [19].

Remark 8. Although Theorem 6 overcome the coupled problem in Theorem 3, the inequalities (39) and (40) still cannot be used to solve the filter parameters in (5) directly. Therefore, the next step of using $\Delta(t) = \sum_{i=1}^r h_i(\theta(t))\Delta_i$ to substitute the matrix functions in Theorem 6 is necessary, where Δ denotes system matrices A, A_d , B, M, M_d , N, C, C_d , D, E, E_d , F, E, E, and corresponding parameters \overline{A}_f , \overline{B}_f , \overline{C}_f . By this way, the following theorem is obtained to present the final results.

Theorem 9. For the given positive constants $\tau > 0$ and $0 < \alpha \le 1$, the filtering error system (6) is mean-square asymptotically stable and has a guaranteed Hankel norm performance level γ if there exist X > 0, Y > 0, Q > 0, R > 0, S_i , \overline{A}_{fi} , \overline{B}_{fi} , and \overline{C}_{fi} $(i = 1, 2, \ldots, r)$ satisfying

$$\Omega_1^{ij} + \Omega_1^{ji} < 0,$$

$$\Omega_2^{ij} + \Omega_2^{ji} < 0, \quad i \le j,$$
 (45)

where Ω_1^{ij} and Ω_2^{ij} are given as

$$\Omega_{1}^{ij} = \begin{bmatrix} -X & -Y & XM_{j} + \overline{B}_{fi}E_{j} & 0 & XM_{dj} + \overline{B}_{fi}E_{dj} & 0 & XN_{j} + \overline{B}_{fi}F_{j} \\ * & -Y & YM_{j} + \overline{B}_{fi}E_{j} & 0 & YM_{dj} + \overline{B}_{fi}E_{dj} & 0 & YN_{j} + \overline{B}_{fi}F_{j} \\ * & * & \Lambda_{33} & \Lambda_{34} & XA_{dj} + \overline{B}_{fi}C_{dj} + \frac{R}{\tau} & A_{j}^{T}S_{i} & XB_{j} + \overline{B}_{fi}D_{j} \\ * & * & * & \Lambda_{44} & YA_{dj} + \overline{B}_{fi}C_{dj} & 0 & YB_{j} + \overline{B}_{fi}D_{j} \\ * & * & * & * & -Q - \frac{R}{\tau} & A_{dj}^{T}S_{i} & 0 \\ * & * & * & * & \tau R - S_{i} - S_{i}^{T} & S_{i}^{T}B_{j} \\ * & * & * & * & * & -\gamma^{2}I \end{bmatrix},$$

(46)

$$\Omega_{2}^{ij} = \begin{bmatrix} -\alpha X & -\alpha Y & \alpha \left(XM_{j} + \overline{B}_{fi}E_{j} \right) & 0 & \alpha \left(XM_{dj} + \overline{B}_{fi}E_{dj} \right) & 0 & 0 \\ * & -\alpha Y & \alpha \left(YM_{j} + \overline{B}_{fi}E_{j} \right) & 0 & \alpha \left(YM_{dj} + \overline{B}_{fi}E_{dj} \right) & 0 & 0 \\ * & * & \widetilde{\Lambda}_{33} & \widetilde{\Lambda}_{34} & \alpha \left(XA_{dj} + \overline{B}_{fi}C_{dj} + \frac{R}{\tau} \right) & \alpha A_{j}^{T}S_{i} & L^{T}\left(t \right) \\ * & * & * & \widetilde{\Lambda}_{44} & \alpha \left(YA_{dj} + \overline{B}_{fi}C_{dj} \right) & 0 & -\overline{C}_{fi}^{T} \\ * & * & * & * & -\alpha \left(Q + \frac{R}{\tau} \right) & \alpha A_{dj}^{T}S_{i} & 0 \\ * & * & * & * & * & \alpha \left(\tau R - S_{i} - S_{i}^{T} \right) & 0 \\ * & * & * & * & * & * & * & -I \end{bmatrix}$$

$$\begin{split} &\Lambda_{33} = XA_j + A_j^T X + \overline{B}_{fi} C_j + C_j^T \overline{B}_{fi}^T + Q - \frac{R}{\tau}, \\ &\Lambda_{34} = \overline{A}_{fi} + A_j^T Y + C_j^T \overline{B}_{fi}^T, \qquad \Lambda_{44} = \overline{A}_{fi} + \overline{A}_{fi}^T, \\ &\widetilde{\Lambda}_{33} = \alpha \left(XA_j + A_j^T X + \overline{B}_{fi} C_j + C_j^T \overline{B}_{fi}^T + Q - \frac{R}{\tau} \right), \\ &\widetilde{\Lambda}_{34} = \alpha \left(\overline{A}_{fi} + A_j^T Y + C_j^T \overline{B}_{fi}^T \right), \qquad \widetilde{\Lambda}_{44} = \alpha \left(\overline{A}_{fi} + \overline{A}_{fi}^T \right). \end{split}$$

In this case, the filter parameters in (5) are given by

$$A_{fi} = Y^{-1}\overline{A}_{fi}, \qquad B_{fi} = Y^{-1}\overline{B}_{fi},$$

$$C_{fi} = \overline{C}_{fi}, \quad i = 1, 2, \dots, r.$$

$$(47)$$

Proof. Based on Theorems 3 and 6, we set

$$\overline{A}_{f}(t) = \sum_{i=1}^{r} h_{i}(\theta(t)) \overline{A}_{fi},$$

$$\overline{B}_{f}(t) = \sum_{i=1}^{r} h_{i}(\theta(t)) \overline{B}_{fi},$$

$$\overline{C}_{f}(t) = \sum_{i=1}^{r} h_{i}(\theta(t)) \overline{C}_{fi},$$

$$S(t) = \sum_{i=1}^{r} h_{i}(\theta(t)) S_{i}.$$
(48)

From (39) and (40), we have

$$\begin{split} \Omega_{1}\left(t\right) &= \sum_{i=1}^{r} h_{i}^{2}\left(\theta\left(t\right)\right) \Omega_{1}^{ii} \\ &+ \sum_{i=1}^{r} h_{i}\left(\theta\left(t\right)\right) \sum_{j=1}^{r} h_{j}\left(\theta\left(t\right)\right) \left(\Omega_{1}^{ij} + \Omega_{1}^{ji}\right) < 0, \\ \Omega_{2}\left(t\right) &= \sum_{i=1}^{r} h_{i}^{2}\left(\theta\left(t\right)\right) \Omega_{2}^{ii} \\ &+ \sum_{i=1}^{r} h_{i}\left(\theta\left(t\right)\right) \sum_{i=1}^{r} h_{j}\left(\theta\left(t\right)\right) \left(\Omega_{2}^{ij} + \Omega_{2}^{ji}\right) < 0. \end{split} \tag{49}$$

By virtue of Theorems 3 and 6, the Hankel norm filter design problem is solvable and the filter parameters are given by

$$A_{f}(t) = V^{-1}\overline{A}_{f}(t)V^{-T}W, \qquad B_{f}(t) = V^{-1}\overline{B}_{f}(t),$$

$$C_{f}(t) = \overline{C}_{f}(t)V^{-T}W,$$
(50)

where matrices W > 0 and V are such that $Y = VW^{-1}V^T$. Or equivalently under transformation $V^{-T}W\widehat{x}(t)$, the filter parameters can be obtained as (47). The proof is completed.

Remark 10. Notice that the obtained conditions in Theorem 9 are all in LMI forms and the Hankel norm filtering problem can be solved by the following convex optimization problem with LMI Toolbox in MATLAB:

$$\min_{X>0,Y>0,Q>0,R>0,S_{i},\overline{A}_{fi},\overline{B}_{fi},\overline{C}_{fi}} \lambda \quad \text{Subject to } (45)\,, \qquad (51)$$

where $\lambda = \gamma^2$, and the admissible filter parameters can be determined by (47).

5. Numerical Example

In this section, we will present a numerical example to demonstrate the validity of the developed results. Consider a stochastic system of the form (2) with the following parameters (r = 2):

$$A_1 = \begin{bmatrix} -1.5 & 0.5 \\ -1 & -3 \end{bmatrix}, \qquad A_{d1} = \begin{bmatrix} -0.8 & 0.2 \\ 0.2 & -0.2 \end{bmatrix},$$
 (52)

$$B_1 = \begin{bmatrix} 0.2 \\ -0.2 \end{bmatrix}, \qquad M_1 = \begin{bmatrix} -0.8 & 0.2 \\ 0.5 & -0.5 \end{bmatrix},$$
 (53)

$$M_{d1} = \begin{bmatrix} 0.5 & 0.5 \\ 0.2 & 0.3 \end{bmatrix}, \qquad N_1 = \begin{bmatrix} -0.2 \\ 0.5 \end{bmatrix}, \tag{54}$$

$$C_1 = \begin{bmatrix} 0.2 & 0.1 \end{bmatrix}, \qquad C_{d1} = \begin{bmatrix} -0.1 & 0.2 \end{bmatrix}, \qquad D_1 = 0.2,$$
 (55)

$$E_1 = \begin{bmatrix} -0.2 & 0.2 \end{bmatrix}, \qquad E_{d1} = \begin{bmatrix} 0.2 & -0.5 \end{bmatrix}, \tag{56}$$

$$F_1 = 0.5, L_1 = \begin{bmatrix} -1 & 0.5 \end{bmatrix}, (57)$$

$$A_2 = \begin{bmatrix} -1 & 0.5 \\ 0.5 & -1.3 \end{bmatrix}, \qquad A_{d2} = \begin{bmatrix} 0.02 & 0.14 \\ 0 & 0.15 \end{bmatrix}, \tag{58}$$

$$B_2 = \begin{bmatrix} 0.3 \\ 0.1 \end{bmatrix}, \qquad M_2 = \begin{bmatrix} -1 & 0 \\ -0.5 & -1.3 \end{bmatrix},$$
 (59)

$$M_{d2} = \begin{bmatrix} 0.1 & 0\\ 0.02 & 0.03 \end{bmatrix}, \qquad N_2 = \begin{bmatrix} 0.2\\ -0.5 \end{bmatrix},$$
 (60)

$$C_2 = \begin{bmatrix} 0.5 & 0.1 \end{bmatrix}, \qquad C_{d2} = \begin{bmatrix} -0.1 & 0.5 \end{bmatrix}, \qquad D_2 = 0.1,$$
 (61)

$$E_2 = \begin{bmatrix} -0.1 & 0.2 \end{bmatrix}, \qquad E_{d2} = \begin{bmatrix} 0.1 & -0.5 \end{bmatrix}, \tag{62}$$

$$F_2 = 0.2, L_2 = [0.5 -0.1]. (63)$$

According to Theorem 9, we can get the minimum performance level $\gamma = 0.5253$ for $\tau = 0.5$ and $\alpha = 1$, and the solutions of corresponding parameters are as follows:

$$Y = \begin{bmatrix} 0.1901 & -0.1134 \\ -0.1134 & 0.1207 \end{bmatrix}, \qquad \overline{A}_{f1} = \begin{bmatrix} -0.5394 & -0.0057 \\ -0.0057 & -0.3529 \end{bmatrix},$$

$$\overline{B}_{f1} = \begin{bmatrix} 0.2148 \\ -0.1394 \end{bmatrix}, \qquad \overline{C}_{f1} = \begin{bmatrix} -0.6610 & 0.0083 \end{bmatrix}$$

$$\overline{A}_{f2} = \begin{bmatrix} -0.4336 & 0.5944 \\ 0.5944 & -0.9336 \end{bmatrix}, \qquad \overline{B}_{f2} = \begin{bmatrix} -0.0247 \\ -0.1454 \end{bmatrix},$$

$$\overline{C}_{f2} = \begin{bmatrix} 0.6553 & -1.1762 \end{bmatrix}.$$
(64)

Then the Hankel norm filter parameter matrices are computed from (47) as

$$A_{f1} = \begin{bmatrix} -6.5154 & -4.0327 \\ -6.1661 & -6.7104 \end{bmatrix}, \qquad B_{f1} = \begin{bmatrix} 1.0035 \\ -0.2123 \end{bmatrix},$$

$$C_{f1} = \begin{bmatrix} -0.6610 & 0.0083 \end{bmatrix}, \qquad A_{f2} = \begin{bmatrix} 0.7727 & -3.3775 \\ 5.6483 & -10.9038 \end{bmatrix},$$

$$B_{f2} = \begin{bmatrix} -1.9283 \\ -3.0147 \end{bmatrix}, \qquad C_{f2} = \begin{bmatrix} 0.6553 & -1.1762 \end{bmatrix}.$$
(65)

Table 1: Minimum index γ for different τ .

	$\tau = 0.5$	$\tau = 0.6$	$\tau = 0.8$	$\tau = 1.0$
γ	0.5253	0.5553	0.6387	0.8138

The solvability of the filter parameters indicates that the proposed approach is effective. Furthermore, different value of τ may yield different γ_{\min} . By selecting several different values of τ , the computation results of minimum γ are obtained in Table 1. Table 1 shows that the results presented in this paper are delay-dependent and less conservative.

6. Conclusions

In this paper, the problem of Hankel norm filter design for stochastic time-delay systems via T-S fuzzy-model-based approach has been investigated. A new filtering error system is established by designing local linear filters for each linear subsystem according to the parallel distributed compensation (PDC) method. Based on the Lyapunov stability theory and LMI techniques, a delay-dependent sufficient condition is developed in terms of LMIs for the mean-square asymptotic stability with Hankel norm performance of the filtering error system. The integral inequality method is adopted and an assistant vector and free matrices are introduced, which helps achieving much less conservative results. The results of numerical example are presented to demonstrate the effectiveness of the proposed approach.

Conflict of Interests

The authors declare that there is no conflict of interests regarding the publication of this paper.

Acknowledgment

This work is supported by the China Petroleum Science and Technology Innovation Foundation (no. 2012D-5006-0209).

References

- [1] P. Shi, E.-K. Boukas, and R. K. Agarwal, "Kalman filtering for continuous-time uncertain systems with Markovian jumping parameters," *IEEE Transactions on Automatic Control*, vol. 44, no. 8, pp. 1592–1597, 1999.
- [2] F. Yang, Z. Wang, and Y. S. Hung, "Robust Kalman filtering for discrete time-varying uncertain systems with multiplicative noises," *IEEE Transactions on Automatic Control*, vol. 47, no. 7, pp. 1179–1183, 2002.
- [3] H. Gao, X. Meng, and T. Chen, "A parameter-dependent approach to robust H_{∞} filtering for time-delay systems," *IEEE Transactions on Automatic Control*, vol. 53, no. 10, pp. 2420–2425, 2008.
- [4] H. Gao, X. Meng, and T. Chen, " H_{∞} filter design for discrete delay systems: a new parameter-dependent approach," *International Journal of Control*, vol. 82, no. 6, pp. 993–1005, 2009.
- [5] L. Wu and W. X. Zheng, "On design of reduced-order H_{∞} filters for discrete repetitive processes," in *Proceedings of the IEEE*

- International Symposium of Circuits and Systems (ISCAS '11), pp. 2137–2140, May 2011.
- [6] Y. C. Lin and J. C. Lo, "Robust mixed H_2 / H_{∞} filtering for time-delay fuzzy systems," *IEEE Transactions on Signal Processing*, vol. 54, pp. 2897–2909, 2006.
- [7] E. K. Boukas, "Stabilization of stochastic nonlinear hybrid systems," *International Journal of Innovative Computing, Information and Control*, vol. 1, pp. 131–141, 2005.
- [8] X. X. Liao and X. Mao, "Exponential stability of stochastic delay interval systems," Systems & Control Letters, vol. 40, no. 3, pp. 171–181, 2000.
- [9] S. Xu and T. Chen, "Robust H_{∞} control for uncertain stochastic systems with state delay," *IEEE Transactions on Automatic Control*, vol. 47, no. 12, pp. 2089–2094, 2002.
- [10] M. Liu, L. X. Zhang, P. Shi, and H. R. Karimi, "Robust control of stochastic systems against bounded disturbances with application to flight control," *IEEE Transactions on Industrial Electronics*, vol. 61, pp. 1504–1515, 2014.
- [11] S. Xu and T. Chen, "Robust H_{∞} filtering for uncertain stochastic time-delay systems," *Asian Journal of Control*, vol. 5, no. 3, pp. 364–373, 2003.
- [12] Y. Li, J. Lam, and X. Luo, "Hankel norm model reduction of uncertain neutral stochastic time-delay systems," *International Journal of Innovative Computing, Information and Control*, vol. 5, no. 9, pp. 2819–2828, 2009.
- [13] S. Yin, G. Wang, and H. Karimi, "Data-driven design of robust fault detection system for wind turbines," *Mechatronics*, 2013.
- [14] S. Yin, S. X. Ding, A. H. A. Sari, and H. Hao, "Data-driven monitoring for stochastic systems and its application on batch process," *International Journal of Systems Science*, vol. 44, no. 7, pp. 1366–1376, 2013.
- [15] S. Yin, S. Ding, A. Haghani, H. Hao, and P. Zhang, "A comparison study of basic datadriven fault diagnosis and process monitoring methods on the benchmark Tennessee Eastman process," *Journal of Process Control*, vol. 22, pp. 1567–1581, 2012.
- [16] S. Yin, H. Luo, and S. Ding, "Real-time implementation of fault-tolerant control systems with performance optimization," *IEEE Transactions on Industrial Electronics*, vol. 64, pp. 2402–2411, 2014.
- [17] L. Wu, X. Su, P. Shi, and J. Qiu, "A new approach to stability analysis and stabilization of discrete-time T-S fuzzy time-varying delay systems," *IEEE Transactions on Systems, Man, and Cybernetics B*, vol. 41, no. 1, pp. 273–286, 2011.
- [18] H. K. Lam, H. Li, and H. Liu, "Stability analysis and control synthesis for fuzzy-observer-based controller of nonlinear systems: a fuzzy-model-based control approach," *IET Control Theory & Applications*, vol. 7, no. 5, pp. 663–672, 2013.
- [19] J. Liu, Z. Gu, E. Tian, and R. Yan, "New results on H_{∞} filter design for nonlinear systems with time-delay through a T-S fuzzy model approach," *International Journal of Systems Science*, vol. 43, no. 3, pp. 426–442, 2012.
- [20] Y. Zhao, H. Gao, and J. Lam, "New results on H_{∞} filtering for fuzzy systems with interval time-varying delays," *Information Sciences*, vol. 181, no. 11, pp. 2356–2369, 2011.
- [21] H. Gao, J. Lam, C. Wang, and Q. Wang, "Hankel norm approximation of linear systems with time-varying delay: continuous and discrete cases," *International Journal of Control*, vol. 77, no. 17, pp. 1503–1520, 2004.
- [22] L. Wu, P. Shi, and X. Su, "Hankel-norm model approximation for LPV systems with parameter-varying time delays," *International Journal of Systems Science*, vol. 41, no. 10, pp. 1173–1185, 2010.

Hindawi Publishing Corporation Abstract and Applied Analysis Volume 2014, Article ID 807102, 10 pages http://dx.doi.org/10.1155/2014/807102

Research Article

Finite-Time Cooperative Tracking Control Algorithm for Multiple Surface Vessels

Jianfang Jiao and Mingyu Fu

College of Automation, Harbin Engineering University, Harbin, Heilongjiang 150001, China

Correspondence should be addressed to Mingyu Fu; fumingyu@hrbeu.edu.cn

Received 9 December 2013; Accepted 5 January 2014; Published 4 March 2014

Academic Editor: Shen Yin

Copyright © 2014 J. Jiao and M. Fu. This is an open access article distributed under the Creative Commons Attribution License, which permits unrestricted use, distribution, and reproduction in any medium, provided the original work is properly cited.

We investigate the problem of finite-time cooperative tracking for multiple surface vessels in the presence of external disturbances. A robust finite-time cooperative tracking algorithm based on terminal sliding-mode control is proposed for multiple surface vessels. In light of the leader-follower strategy, a virtual leader vessel is defined to provide reference point for other surface vessels to form the desired formation. Specifically, the proposed algorithm only requires the communication topology among the surface vessels to be a directed graph with a directed spanning tree. The robustness is achieved by compensating the upper bound of external disturbance in the control input, and the global finite-time stability is proved by Lyapunov stability theory. Finally, the effectiveness of the proposed finite-time cooperative tracking control algorithm is demonstrated by simulation results.

1. Introduction

With the rapid development of marine technology, the cooperative motion control for multiple vessels has received increasing attention during the last decades. The cooperative formation of multiple vessels has become popular for military and commercial applications. For example, coast patrol requires multiple vessels to perform cooperative tracking operation while maintaining a desired formation pattern. During winter, the tanker must be escorted by icebreakers, which requires the tanker to keep a fixed distance to the icebreakers. Besides, underway replenishment is performed by coordinating one or more supply vessels and the receiving vessel such that all vessels maintain the desired relative distances and hold the equal course and forward speed. These complicated operations of multiple vessels are carried out by moving collectively as a whole formation. Compared with individual vessel, cooperative operations of multiple vessels have higher operational efficiency, larger serve areas, better fault-tolerant property, and stronger robustness [1]. Based on these broad applications and several superiorities mentioned above, study on cooperative control algorithm for multiple surface vessels is important and significative.

With respect to the cooperative control issues, formation control as a special case, a large number of studies have been widely reported in existing publications. The formation strategies mainly include leader-follower strategy, virtual structures strategy, and behavioral strategy [2]. In order to achieve robustness and improve cooperative performance, some robust control approaches had been proposed, such as model predictive control [3], Lagrangian method [4], and null-space-based behavioral control [5]. Some advanced cooperative control approaches had also been investigated, such as graph theory [6], passivity-based control [7, 8], and hybrid control [9], to name just a few. In particular, the leader-follower strategy is utilized widely in practice due to its easy manipulation and implementation. For maritime applications, Kyrkjebø et al. proposed a leaderfollower synchronization algorithm to solve the ship underway replenishment, which realizes feedback control law by estimating velocity and acceleration of all ships based on nonlinear observers [10]. Breivik et al. proposed a guided leader-follower approach for ship formation control using integrator backstepping and cascade theory [11]. Thorvaldsen and Skjetne researched the formation control of fully actuated marine vessels and proposed group agreement protocols based on leader-follower strategy [7]. Overall, the cooperative task based on leader-follower strategy is achieved through that the appointed leaders track the predefined desired paths or trajectories, while the followers track the leaders. However, the main shortcoming of this formation strategy in the aforementioned studies is that it depends heavily on the leader. The formation task cannot be achieved if the leader has failure in the process of operations. To avoid this problem, the concept of virtual leader is introduced and used to solve the formation control of multiagent systems [12, 13]. It is a good choice to design cooperative control algorithm based on the virtual leader strategy.

When multiple agents are to be coordinated to perform complicated task, information exchange between them is a necessary condition. In order to accomplish cooperative tracking operations, both position and velocity information need to be shared. In practice, the communication topology among these agents might be directed as a result of the external disturbances. That means one agent might receive the information from neighbors but cannot send his own information to the neighbors. Under directed communication topologies, Ren had studied the consensus tracking algorithm for multiagent with single-integrator kinematics [14]. Yu et al. provided a consensus algorithm for multiagent systems with nonlinear dynamics [15, 16]. Zhang et al. studied the cooperative control problem of multiple uncertain Lagrangian systems [17]. Besides, Fu et al. proposed a coordinated formation control algorithm under directed communication topology for multiple surface vessels [18]. However, it is still a big problem to design a cooperative control algorithm under directed communication for the leaderfollower multiagent systems, especially in the case that the information of the leader is not available to all the followers; that is, only a portion of followers can communicate with the leader and the communication links are directed.

For marine control, finite-time control is quite desirable when considering the huge inertia of the surface vessels. Compared to asymptotic stability control, the convergence rate of finite-time control is faster, and the system with finitetime convergence has better disturbance rejection properties and robustness against uncertainties [19]. However, a common trait of the existing cooperative tracking control algorithms for multiple surface vessels is that they only provide asymptotic stability [9, 20]. In other words, the cooperative operations can be achieved in infinite time, which may not be applicable to practical operation. So the finite-time cooperative control has received considerable attention. Wang and Xiao and Khoo et al. developed finite-time consensus algorithm for multiagent systems in [21, 22]. The finitetime formation control algorithms had been investigated for multiagent systems in [23, 24]. Furthermore, both finitetime position consensus and collision avoidance problems had been investigated for multiple autonomous underwater vehicle [25]. The cooperative performance of multiple surface vessels is often influenced by the environmental disturbances; therefore, robust cooperative tracking algorithm is significative, and the real-time implementation of fault-tolerant control is also important [26-29]. The sliding-mode control is a better method for solving this problem, which possesses the

robustness to external disturbances [30]. A robust tracking control algorithm is proposed based on sliding-mode control for a single surface vessel to achieve robustness to the wind, wave, and current environment disturbances in [31, 32]. The sliding-mode control approach is also used to design the robust cooperative control algorithm in [20, 33, 34]. The terminal sliding-mode control can be achieved by the finite-time cooperative operations [35], which motivates the research of the finite-time cooperative tracking for multiple surface vessels.

In this paper, the problem of robust cooperative tracking control for multiple surface vessels is considered, and the communication topology among these surface vessels is directed graph which has a directed spanning tree. The finite-time cooperative tracking control algorithm is designed using the terminal sliding-mode control method, and the desired formation configuration is achieved using the virtual leader-follower strategy. The rest of this paper is organized as follows. In Section 2, the basic notations for the graph theory are introduced and the vessel mathematic model is established. Section 3 describes a detailed algorithm of the finite-time cooperative tracking control for multiple surface vessels. The simulation is carried out to demonstrate the validity of the proposed cooperative control algorithm in Section 4. At last, we draw conclusion in Section 5.

2. Preliminaries

2.1. Vessel Model. With respect to the surface vessels, only the motions on the surge, sway, and yaw are considered. If we define the generalized position and orientation which are expressed in the inertial reference frame as $\eta = [n, e, \psi]^T$, the linear-angular velocity vector expressed in the body-fixed reference frame is denoted as $v = [u, v, r]^T$. Then we can obtain the 3 degrees of freedom (DOF) mathematical model for the surface vessels as follows [36]:

$$\dot{\eta} = R(\psi) v,$$

$$M_{\nu}\dot{v} + C_{\nu}(\nu) v + D_{\nu}(\nu) v = \tau_{\nu} + R^{-T}(\psi) \omega,$$
(1)

where $R(\psi)$ is a transformation matrix from the body-fixed reference to the inertial reference frame and the form is

$$R(\psi) = \begin{bmatrix} \cos(\psi) & -\sin(\psi) & 0\\ \sin(\psi) & \cos(\psi) & 0\\ 0 & 0 & 1 \end{bmatrix}. \tag{2}$$

It is obvious that $R_i^{-1}(\psi_i) = R_i^T(\psi_i)$, for all ψ_i .

 M_{ν} denotes a positive definite matrix of inertia mass which includes added mass. $C_{\nu}(\nu)$ is a matrix which arises from the coriolis and centripetal forces and $D_{\nu}(\nu)$ represents a damping matrix. The detailed expression of the above three matrices can be seen in [36]. τ_{ν} represents the forces and torques input vector from the thruster system. ω denoted the forces and torques input vector from the external disturbances. And we assume that the disturbances are bounded; $|\omega| < \omega_{\rm max} \in \mathbb{R}^3$.

In order to design the tracking controller for surface vessels in the sequel, the expression of vessel model can be transformed as

$$M(\eta)\ddot{\eta} + C(\eta,\dot{\eta})\dot{\eta} + D(\eta,\dot{\eta})\dot{\eta} = \tau + \omega. \tag{3}$$

The above expression is vessel mathematic model in the inertial reference frame, which is obtained by using the following transformations:

$$M(\eta) = R^{-T}(\psi) M_{\nu} R^{-1}(\psi),$$

$$C(\eta, \dot{\eta}) = R^{-T}(\psi) \left[C_{\nu}(\nu) - M_{\nu} R^{-1}(\psi) \dot{R}(\psi) \right] R^{-1}(\psi),$$

$$D(\eta, \dot{\eta}) = R^{-T}(\psi) D_{\nu}(\nu) R^{-1}(\psi),$$

$$\tau = R^{-T}(\psi) \tau_{\nu}.$$
(4)

The vessel model as (3) holds the following properties.

(1) Inertia mass matrix $M(\eta)$ is symmetric positive definite and satisfies

$$\lambda_{\min}(M) I \le M(\eta) \le \lambda_{\max}(M) I,$$
 (5)

where $\lambda_{\min}(M)$ represents the minimum eigenvalue of the matrix M and $\lambda_{\max}(M)$ represents the maximal eigenvalue of the matrix M;

(2) $\dot{M}(\eta) - 2C(\eta, \dot{\eta})$ satisfies

$$\eta^{T} \left(\dot{M} \left(\eta \right) - 2C \left(\eta, \dot{\eta} \right) \right) \eta = 0, \quad \forall \eta \in \mathbb{R}^{3}$$
(6)

which means it is skew symmetric;

(3) $D(\eta, \dot{\eta})$ is positive definite matrix which satisfies

$$\eta^T D(\eta, \dot{\eta}) \eta > 0, \quad \forall \eta \neq 0.$$
(7)

2.2. Notations. In order to model the information transmit relationship between the group of surface vessels, several basic concepts of directed graph are given here [20]. If we define ν as a set of vertices and define $\varepsilon \in \nu^2$ as a set of edges, then we can represent a directed graph as $G = (\nu, \varepsilon)$. Furthermore, the edges of directed graph are directed. The directed edge $\langle i, j \rangle \in \varepsilon$ can represent the information that flows from vertex j to vertex i, and $\langle j, i \rangle \in \varepsilon$ represents the information that flows from vertex *i* to vertex *j*. Let $A \in \mathbb{R}^{n \times n}$ be the adjacent matrix of a directed graph G. The matrix A is defined as follows: the off-diagonal entries are a_{ii} = 1 if $\langle i, j \rangle \in \varepsilon$ and 0; otherwise, the diagonal entries are 0. $D \in \mathbb{R}^{n \times n}$ is called the degree matrix, which is defined as follows: off-diagonal entries are 0 and diagonal entries are $d_{ii} = \sum_{j \neq i} a_{ij}$. The Laplacian matrix can be calculated as $L = D - A \in \mathbb{R}^{n \times n}$. The matrix $L = [l_{ij}] \in \mathbb{R}^{n \times n}$ is defined as follows: $l_{ii} = \sum_{j \neq i} a_{ij}$, $l_{ij} = -a_{ij}$.

Let one vertex represent one vessel in the group and the edges represent information exchange links by available directed communication; then the communication relationship between the group of vessels is described by a directed graph. Specially, in this paper we consider the communication topology as a directed graph with a directed spanning tree; that is, the digraph has at least one vertex with a directed path to all other vertexes.

Define the Kronecker product of two matrices $A \in \mathbb{R}^{n \times n}$ and $B \in \mathbb{R}^{p \times q}$ as

$$A \otimes B = \begin{bmatrix} a_{11}B & \cdots & a_{1n}B \\ \vdots & \ddots & \vdots \\ a_{m1}B & \cdots & a_{mn}B \end{bmatrix} \in \mathbb{R}^{mp \times nq}.$$
 (8)

The Kronecker product holds the following properties:

- $(1) (A \otimes B)^T = A^T \otimes B^T;$
- (2) $C(A \otimes B) = (CA) \otimes B = A \otimes (CB)$;
- $(3) (A \otimes I_p)(C \otimes I_p) = AC \otimes I_p, I_p \in \mathbb{R}^{p \times p}.$

Given a variable vector $x = [x_1, ..., x_n]^T \in \mathbb{R}^n$ and an integer α , define $x^{\alpha} = [x_1^{\alpha}, ..., x_n^{\alpha}]^T$, diag $(x) = \begin{bmatrix} x_1 & ... & ... \\ & ... & ... \end{bmatrix}$.

2.3. Some Lemmas

Lemma 1 (see [14]). Let the Laplacian matrix of a directed graph G be defined as $L = [l_{ij}] \in \mathbb{R}^{p \times p}$, where L is not necessarily symmetric. The Laplacian matrix satisfies the following conditions:

$$l_{ij} \le 0, \ i \ne j; \quad \sum_{j=1}^{p} l_{ij} = 0, \quad i = 1, \dots p.$$
 (9)

The Laplacian matrix L of a directed graph G has a simple zero eigenvalue with an associated eigenvector $\mathbf{1}_p$, and all the other eigenvalues have positive real parts if and only if the directed graph has a directed spanning tree. Furthermore, if Laplacian matrix L has a simple zero eigenvalue, then Rank (L) = p - 1.

Lemma 2 (see [37]). For the non-Lipschitz system

$$\dot{x} = f(x), \quad f(0) = 0, \quad x \in \mathbb{R}^n, \tag{10}$$

where $f(\cdot)$ is a continuous nonlinear function on an open neighborhood U of the origin x=0 in \mathbb{R}^n . Suppose there exist a continuous function $V(x):U\to\mathbb{R}$, real numbers C>0 and $0<\alpha<1$, and an open neighborhood $U_0\subset U$ of x=0, such that

- (1) V(x) is positive definite;
- (2) $\dot{V}(x) + C(V(x))^{\alpha} \le 0, x \in U_0 \setminus \{0\}.$

Then the origin x=0 is a finite-time stable equilibrium of system (10). Furthermore, if $U=U_0=\mathbb{R}^n$, the origin x=0 is a globally finite-time stable equilibrium of system (10). And the finite settling time satisfies $T \leq V^{1-\alpha}(x_0)/C(1-\alpha)$, where x_0 is the initial state of the system.

3. Finite-Time Cooperative Tracking Controller Design

In this section, we will design the finite-time cooperative tracking controller based on terminal sliding-mode control.

Here we consider n vessels to perform the cooperative tracking task with desired formation. And these vessels are identified by the index set I = [1, 2, ...n]. We define the communication topology relationship among these vessels as a directed graph G; then the adjacent matrix of G is

$$A = \begin{bmatrix} a_{11} & a_{12} & \cdots & a_{1n} \\ \vdots & \vdots & \vdots & \vdots \\ a_{n1} & a_{n2} & \cdots & a_{nn} \end{bmatrix} \in \mathbb{R}^{n \times n}.$$
 (11)

The degree matrix is defined as $D = \text{diag}\{d_1 \ d_2 \ \cdots \ d_n\} \in \mathbb{R}^{n \times n}$; then we can know that the Laplacian matrix is L = D - A

The desired formation pattern among the surface vessels is established based on the leader-follower strategy. The leader vessel is virtual and it is labeled by 0. Then the communication topology among all the vessels (include the virtual leader) is described by a directed graph \overline{G} ; the adjacent matrix of \overline{G} is denoted as

$$\overline{A} = \begin{bmatrix} 0 & 0 & 0 & 0 \\ a_{10} & a_{11} & \cdots & a_{1n} \\ \vdots & \vdots & \vdots & \vdots \\ a_{n0} & a_{n1} & \cdots & a_{nn} \end{bmatrix} \in \mathbb{R}^{(n+1)\times(n+1)}.$$
 (12)

The connected relationship between the leader vessel and the practical vessels is denoted by $B = \text{diag}\{b_1 \ b_2 \ \cdots \ b_n\}$.

Remark 3. Consider the following.

$$a_{ij} = \begin{cases} 1, & \text{if } (j,i) \in \varepsilon \\ 0, & \text{otherwise,} \end{cases}$$

 $b_i = \begin{cases} 1, & \text{if vessel } i \text{ can receive the leader's information} \\ 0, & \text{otherwise.} \end{cases}$

(13)

We assume that the position of the virtual leader vessel is denoted as η_0 and the desired trajectory of the whole formation is given by the leader vessel. Here we define the desired trajectory of the leader as η_d , where $\eta_d = [n_d(t), e_d(t), \psi_d(t)]^T$, $n_d(t)$, $e_d(t)$ are sufficiently smooth functions, and the motion direction of the virtual leader vessel can be chosen as the tangential vector of its desired trajectory; that is, $\psi_d(t) =$ $\arctan(\dot{e}_d(t)/\dot{n}_d(t))$. In order to form the desired formation, we define the relative distance between the *i*th follower vessel and the virtual leader vessel as $l_i = [x_{0i}, y_{0i}, \psi_{0i}]^T$ and $\psi_{0i} = 0$; then we can define the formation reference point of the ith vessel as $x_i = \eta_i + l_i$. It is obvious that $l_0 = 0$; then $x_0 = \eta_0$. In order to maintain the desired formation among these surface vessels, it is necessary for all the formation reference points to synchronize. That is, $x_1 = \cdots = x_i = \cdots = x_n = \eta_0$. And the cooperative tracking while keeping the desired formation is achieved by $x_1 = \cdots = x_i = \cdots = x_n = \eta_d$.

The virtual vessel is free to external disturbances, so the leader vessel model in the inertial reference frame can be written as

$$M_0(\eta_0)\ddot{\eta}_0 + C_0(\eta_0,\dot{\eta}_0)\dot{\eta}_0 + D_0(\eta_0,\dot{\eta}_0)\dot{\eta}_0 = \tau_0.$$
 (14)

Design the tracking control law τ_0 using the backstepping control approach to make $\eta_0 \to \eta_d$ as in the literature [20].

We assume that the position of the virtual vessel and its velocity are available to its neighbors only and the control force input τ_0 is unknown to any practical vessels, but its upper bound $\overline{\tau}_0$ is available to its neighbors. The detailed design process of the finite-time cooperative tracking algorithm is as follows.

Define the relative position error of the formation reference point for the *i*th vessel as

$$e_{1}^{i} = \sum_{j=1}^{n} a_{ij} (x_{i} - x_{j}) + b_{i} (x_{i} - x_{0})$$

$$= \sum_{i=1}^{n} a_{ij} (\eta_{i} + l_{i} - \eta_{j} - l_{j}) + b_{i} (\eta_{i} + l_{i} - \eta_{0}).$$
(15)

Define the the relative velocity error of the formation reference point for for the *i*th vessel in the inertial reference frame as

$$e_{2}^{i} = \sum_{j=1}^{n} a_{ij} (\dot{x}_{i} - \dot{x}_{j}) + b_{i} (\dot{x}_{i} - \dot{x}_{0})$$

$$= \sum_{j=1}^{n} a_{ij} (\dot{\eta}_{i} - \dot{\eta}_{j}) + b_{i} (\dot{\eta}_{i} - \dot{\eta}_{0})$$

$$= \left(\sum_{j=1}^{n} a_{ij}\right) \dot{\eta}_{i} - \left(\sum_{j=1}^{n} a_{ij}\right) \dot{\eta}_{j} + b_{i} \dot{\eta}_{i} - b_{i} \dot{\eta}_{0}.$$
(16)

Define the terminal sliding-mode surface of the *i*th vessel as

$$s_i = e_1^i + (e_2^i)^{\alpha},$$
 (17)

where $(e_2^i)^{\alpha} = \left[(e_2^i(1))^{\alpha} \ (e_2^i(2))^{\alpha} \ (e_2^i(3))^{\alpha} \right]^T$. The real-time control input τ_0 of the virtual leader is unknown to any following vessels due to time delay or information transmission failure in the communication channel; while the upper bound of the control input $\overline{\tau}_0$ is available to the adjacent vessels. The control input of each vessel can be chosen as

$$\tau_{i} = C_{i} (\eta_{i}, \dot{\eta}_{i}) \dot{\eta}_{i} + D_{i} (\eta_{i}, \dot{\eta}_{i}) \dot{\eta}_{i}$$

$$+ \sum_{j=1, j \neq i}^{n} (a_{ij} + b_{i})^{-1} M_{i}$$

$$\times \left\{ \frac{\left(e_{2}^{i}\right)^{2-\alpha}}{\alpha} + \sum_{j=1, j \neq i}^{n} a_{ij} M_{j}^{-1} \right.$$

$$\times \left[-C_{j} (\eta_{j}, \dot{\eta}_{j}) \dot{\eta}_{j} - D_{j} (\eta_{j}, \dot{\eta}_{j}) \dot{\eta}_{j} + \tau_{j} \right]$$

$$+ b_{i} M_{0}^{-1} \left[-C_{0} (\eta_{0}, \dot{\eta}_{0}) \dot{\eta}_{0} - D_{0} (\eta_{0}, \dot{\eta}_{0}) \dot{\eta}_{0} \right]$$

$$- \operatorname{diag} \left(2n M_{\min}^{-1} \omega_{\max} + b_{i} M_{\min}^{-1} \overline{\tau}_{0} + \kappa_{1} \right)$$

$$\times \operatorname{sign} (s_{i}) \right\},$$
(18)

where $\kappa_1 \in \mathbb{R}^{3\times 1}$ is positive vector and $0 < M_{\min} \le \min\{M_1, \dots, M_n\}$.

Theorem 4. Consider the vessel with the nonlinear model as in (1) and (3), if the communication topology among all the vessels (include the virtual leader) is a directed graph which has a directed spanning tree and the terminal sliding-mode surface is defined as (17), the control input force is chosen as (18). Then, the cooperative tracking of multiple surface vessels can be reached in finite time.

Proof. The Laplacian matrix of the communication graph among these surface vessels is

$$L = D - A = \begin{bmatrix} \left(\sum_{j=1}^{n} a_{1j}\right) - a_{11} & \cdots & -a_{1n} \\ \vdots & \ddots & \vdots \\ -a_{n1} & \cdots & \left(\sum_{j=1}^{n} a_{nj}\right) - a_{nn} \end{bmatrix}.$$

$$(19)$$

The connected relationship between the leader vessel and the practical vessels is denoted as

$$B = \begin{bmatrix} b_1 & & \\ & \ddots & \\ & & b_n \end{bmatrix}. \tag{20}$$

If we define

$$E_{1} = [e_{1}^{1} \cdots e_{1}^{n}]^{T} \in \mathbb{R}^{3n \times 1},$$

$$E_{2} = [e_{2}^{1} \cdots e_{2}^{n}]^{T} \in \mathbb{R}^{3n \times 1},$$

$$\eta = [\eta_{1} \cdots \eta_{n}]^{T} \in \mathbb{R}^{3n \times 1},$$

$$1_{n} = [1, \dots, 1]^{T} \in \mathbb{R}^{n \times 1},$$

$$I_{3} = \operatorname{diag}(1 \ 1 \ 1) \in \mathbb{R}^{3 \times 3},$$
(21)

then the error dynamics of multiple surface vessels can be written in terms of matrix and vector:

$$\begin{split} \dot{E}_1 &= E_2, \\ \dot{E}_2 &= \left[(L+B) \otimes I_3 \right] \ddot{\eta} - \left(B \otimes I_3 \right) \left(1_n \otimes \ddot{\eta}_0 \right). \end{split} \tag{22}$$

For representing conveniently, we define

$$\eta = \begin{bmatrix} \eta_1^T & \eta_2^T & \cdots & \eta_n^T \end{bmatrix}^T;
l = \begin{bmatrix} l_1^T & l_2^T & \cdots & l_n^T \end{bmatrix}^T;
\tau = \begin{bmatrix} \tau_1^T & \tau_2^T & \cdots & \tau_n^T \end{bmatrix}^T;
M(\eta) = \operatorname{diag}(M_1(\eta_1) & \cdots & M_n(\eta_n)),
C(\eta, \dot{\eta}) = \operatorname{diag}(C_1(\eta_1, \dot{\eta}_1) & \cdots & C_n(\eta_n, \dot{\eta}_n)),
D(\eta, \dot{\eta}) = \operatorname{diag}(D_1(\eta_1, \dot{\eta}_1) & \cdots & D_n(\eta_n, \dot{\eta}_n)).$$
(23)

We can redefine the error dynamics with the matrix or vector form with the vessel model; then we can obtain that

$$\begin{split} \dot{E}_1 &= E_2, \\ \dot{E}_2 &= \left[(L+B) \otimes I_3 \right] \\ &\times \left[M^{-1} \left(\eta \right) \times \left(\tau + \omega - C \left(\eta, \dot{\eta} \right) \dot{\eta} - D \left(\eta, \dot{\eta} \right) \dot{\eta} \right) \right] \\ &- \left(B \otimes I_3 \right) \\ &\times \left\{ 1_n \otimes \left[M_0^{-1} \left(\eta_0 \right) \right. \\ &\left. \times \left. \left(\tau_0 - C_0 \left(\eta_0, \dot{\eta}_0 \right) \dot{\eta}_0 - D_0 \left(\eta_0, \dot{\eta}_0 \right) \dot{\eta}_0 \right) \right] \right\}. \end{split}$$

The terminal sliding-mode variable vector can be written as $S = \begin{bmatrix} s_1 & \cdots & s_n \end{bmatrix}^T$; then we can obtain that

$$S = E_1 + E_2^{\alpha}. (25)$$

Consider the Lyapunov function

$$V = \frac{1}{2}S^T S. (26)$$

Differentiating V with respect to time, we can obtain that

$$\dot{V} = S^{T} \dot{S}$$

$$= S^{T} \left[E_{2} + \alpha \operatorname{diag} \left(E_{2}^{\alpha - 1} \right) \dot{E}_{2} \right]$$

$$= S^{T} \left\{ E_{2} + \alpha \operatorname{diag} \left(E_{2}^{\alpha - 1} \right) \right.$$

$$\times \left[\left((L + B) \otimes I_{3} \right) \right.$$

$$\times \left(M^{-1} \left(\eta \right) \left(\tau + \omega - C \left(\eta, \dot{\eta} \right) \dot{\eta} - D \left(\eta, \dot{\eta} \right) \dot{\eta} \right) \right)$$

$$- \left(B \otimes I_{3} \right)$$

$$\times \left(1_{n} \otimes \left(M_{0}^{-1} \left(\eta_{0} \right) \right.$$

$$\times \left(\tau_{0} - C_{0} \left(\eta_{0}, \dot{\eta}_{0} \right) \dot{\eta}_{0} \right.$$

$$- D_{0} \left(\eta_{0}, \dot{\eta}_{0} \right) \dot{\eta}_{0} \right) \right] \right\}.$$
(27)

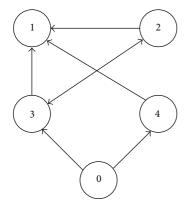


FIGURE 1: The information exchange topology among all the vessels.

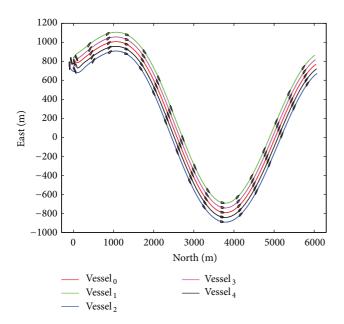


FIGURE 2: The dynamic trajectory of each vessel.

The control input vector of all these vessels can be written as

$$\tau = C(\eta, \dot{\eta}) \dot{\eta} + D(\eta, \dot{\eta}) \dot{\eta} + \left[(D + B)^{-1} \otimes I_3 \right] M$$

$$\times \left\{ \frac{(E_2)^{2-\alpha}}{\alpha} + (A \otimes I_3) M^{-1} \right.$$

$$\times \left(\tau - C(\eta, \dot{\eta}) \dot{\eta} - D(\eta, \dot{\eta}) \dot{\eta} \right)$$

$$+ (B \otimes I_{3})$$

$$\times \left(1_{n} \otimes M_{0}^{-1} \left(-C_{0} \left(\eta_{0}, \dot{\eta}_{0}\right) \dot{\eta}_{0} - D_{0} \left(\eta_{0}, \dot{\eta}_{0}\right) \dot{\eta}_{0}\right)\right)$$

$$- \operatorname{diag} \left\{\operatorname{diag} \left(M_{\min}^{-1} \left(2n\omega_{\max} + b_{i}\overline{\tau}_{0}\right) + \kappa_{1}\right), \dots, \operatorname{diag} \left(M_{\min}^{-1} \left(2n\omega_{\max} + b_{i}\overline{\tau}_{0}\right) + \kappa_{1}\right)\right\}$$

$$\times \operatorname{sign}(S) \right\}.$$

$$(28)$$

We can note that

$$I_{3n} - \left\{ \left[(D+B)^{-1} \otimes I_3 \right] M \left(A \otimes I_3 \right) M^{-1} \right\}$$

$$= MM^{-1} - \left\{ \left[(D+B)^{-1} \otimes I_3 \right] M \left(A \otimes I_3 \right) M^{-1} \right\}$$

$$= M \left[(D+B)^{-1} \otimes I_3 \right] \left[(D+B) \otimes I_3 \right] M^{-1}$$

$$- \left\{ \left[(D+B)^{-1} \otimes I_3 \right] M \left(A \otimes I_3 \right) M^{-1} \right\}$$

$$= M \left[(D+B)^{-1} \otimes I_3 \right] \left[(D+B) \otimes I_3 - (A \otimes I_3) \right] M^{-1}$$

$$= M \left[(D+B)^{-1} \otimes I_3 \right] \left[(D+B-A) \otimes I_3 \right] M^{-1}$$

$$= M \left[(D+B)^{-1} \otimes I_3 \right] \left[(D+B-A) \otimes I_3 \right] M^{-1}.$$
(29)

Then the control input can be rewritten as

$$\tau = M\left((L+B)^{-1} \otimes I_{3}\right)$$

$$\times \left((D+B) \otimes I_{3}\right) M^{-1}$$

$$\times \left\{C\left(\eta, \dot{\eta}\right) \dot{\eta} + D\left(\eta, \dot{\eta}\right) \dot{\eta}$$

$$+ \left((D+B)^{-1} \otimes I_{3}\right) M$$

$$\times \left\{\frac{\left(E_{2}\right)^{2-\alpha}}{\alpha} + \left(A \otimes I_{3}\right) M^{-1}$$

$$\times \left(\tau - C\left(\eta, \dot{\eta}\right) \dot{\eta} - D\left(\eta, \dot{\eta}\right) \dot{\eta}\right) + \left(B \otimes I_{3}\right)$$

$$\times \left(1_{n} \otimes M_{0}^{-1} \left(-C_{0}\left(\eta_{0}, \dot{\eta}_{0}\right) \dot{\eta}_{0} - D_{0}\left(\eta_{0}, \dot{\eta}_{0}\right) \dot{\eta}_{0}\right)\right)$$

$$- \operatorname{diag}\left\{\operatorname{diag}\left(M_{\min}^{-1} \left(2n\omega_{\max} + b_{i}\overline{\tau}_{0}\right) + \kappa_{1}\right),$$

$$\ldots, \operatorname{diag}\left(M_{\min}^{-1} \left(2n\omega_{\max} + b_{i}\overline{\tau}_{0}\right) + \kappa_{1}\right)\right\}$$

$$\times \operatorname{sign}(S)\right\}\right\}.$$
(30)

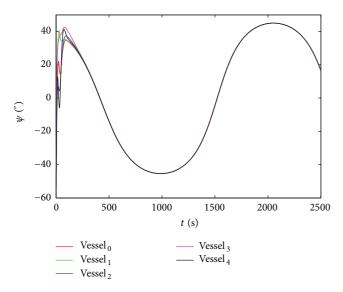


FIGURE 3: The heading consensus for these vessels.

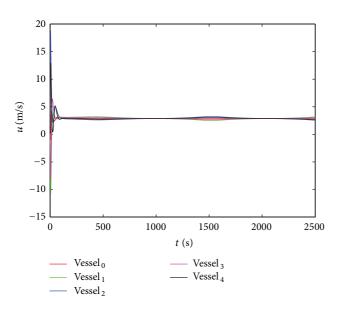


FIGURE 4: The surge velocities consensus of the vessels.

Substituting the control input (30) into (27), then

$$\begin{split} \dot{V} &= \boldsymbol{S}^T \\ &\times \left\{\alpha \operatorname{diag}\left(E_2^{\alpha-1}\right) \right. \\ &\times \left[\left(\left(L+B\right) \otimes I_3\right) \boldsymbol{M}^{-1}\left(\boldsymbol{\eta}\right) \boldsymbol{\omega} \right. \\ &\left. - \left(B \otimes I_3\right) \left(\boldsymbol{1}_n \otimes \left(\boldsymbol{M}_0^{-1}\left(\boldsymbol{\eta}_0\right) \boldsymbol{\tau}_0\right)\right) \right. \\ &\left. - \operatorname{diag}\left\{\operatorname{diag}\left(\boldsymbol{M}_{\min}^{-1}\left(2n\boldsymbol{\omega}_{\max} + b_i \overline{\boldsymbol{\tau}}_0\right) + \kappa_1\right), \right. \\ &\left. \ldots, \operatorname{diag}\left(\boldsymbol{M}_{\min}^{-1}\left(2n\boldsymbol{\omega}_{\max} + b_i \overline{\boldsymbol{\tau}}_0\right) + \kappa_1\right)\right\} \end{split}$$

$$\times \operatorname{sign}(S) \}$$

$$= -\alpha \sum_{i=1}^{n} \left[s_{i}^{T} \left(e_{2}^{i} \right)^{\alpha - 1} \right.$$

$$\times \operatorname{diag} \left(M_{\min}^{-1} \left(2n\omega_{\max} + b_{i} \overline{\tau}_{0} \right) + \kappa_{1} \right)$$

$$\times \operatorname{sign}(s_{i})$$

$$+ \alpha \sum_{i=1}^{n} \left[s_{i}^{T} \left(e_{2}^{-i} \right)^{\alpha - 1} \right.$$

$$\times \left(\left(\sum_{j=1, j \neq i}^{n} a_{ij} + b_{i} \right) \left(M_{i}^{-1} \left(\eta_{i} \right) |\omega_{i}| \right) \right.$$

$$+ \sum_{j=1, j \neq i}^{n} a_{ij} \left(M_{j}^{-1} \left(\eta_{j} \right) |\omega_{j}| \right) \right)$$

$$+ b_{i} M_{i}^{-1} \left(\eta_{i} \right) |\tau_{0}|$$

$$\times \operatorname{diag} \left(M_{\min}^{-1} \left(2n\omega_{\max} + b_{i} \overline{\tau}_{0} \right) + \kappa_{1} \right) 1_{3} \right]$$

$$+ \alpha \sum_{i=1}^{n} \left[\left| s_{i}^{T} \left(e_{2}^{i} \right)^{\alpha - 1} \right.$$

$$\times \left(\left(\sum_{j=1, j \neq i}^{n} a_{ij} + b_{i} \right) \left(M_{i}^{-1} \left(\eta_{i} \right) |\omega_{i}| \right) \right.$$

$$+ \sum_{j=1, j \neq i}^{n} a_{ij} \left(M_{j}^{-1} \left(\eta_{j} \right) |\omega_{j}| \right) \right)$$

$$+ b_{i} M_{i}^{-1} \left(\eta_{i} \right) |\tau_{0}|$$

$$\le -\alpha \sum_{i=1}^{n} \left| s_{i}^{T} \left| \left(e_{2}^{i} \right)^{\alpha - 1} \kappa_{1} \right.$$

$$(31)$$

Let

$$\rho(E_{2}) = \min \left[\frac{\alpha(e_{2}^{1}(k))^{\alpha-1} \kappa_{1}(k), \dots \alpha(e_{2}^{n}(k))^{\alpha-1} \kappa_{1}(k)}{k = 1, 2, 3} \right].$$
(32)

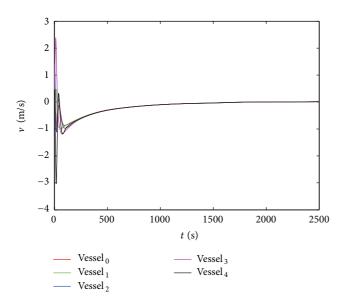


FIGURE 5: The sway velocities consensus of the vessels.

For $e_2^k \neq 0, k = 1, 2, ..., n, \rho(E_2) > 0$, then we have

$$\dot{V} \leq -\alpha \sum_{i=1}^{n} \left| s_{i}^{T} \right| \left(e_{2}^{i} \right)^{\alpha - 1} \kappa_{1}$$

$$\leq -\rho \left(E_{2} \right) \sum_{l=1}^{3n} |S(l)|$$

$$\leq -\rho \left(E_{2} \right) \left(\sum_{l=1}^{3n} |S(l)|^{2} \right)^{1/2}$$

$$= -2^{1/2} \rho \left(E_{2} \right) V^{1/2}.$$
(33)

Therefore, we can know that the terminal sliding surface S = 0 can be reached in a finite time for the case of $e_2^k \neq 0$, k = 1, 2, ..., n, because the condition of finite-time stability is satisfied.

Substituting the control input (30) into the error dynamics (24), then

$$\dot{E}_{2} = -\frac{(E_{2})^{2-\alpha}}{\alpha}$$

$$-\left(\operatorname{diag}\left(2n\omega_{\max} + \kappa_{1}\right) + \left(B \otimes I_{3}\right)\left(1_{n} \otimes \tau_{0}\right)\right) \times \operatorname{sign}\left(S\right)$$

$$+\left(L + B\right)\omega + \left(B \otimes I_{3}\right)\left(1_{n} \otimes \tau_{0}\right).$$
(34)

If $S \neq 0$, $\dot{e}_2^i \leq -\kappa_1$ or $\dot{e}_2^i \geq \kappa_1$, we can know that $E_2 = 0$ is not an attractor.

However, on this new terminal sliding-mode surface, that is, S=0, $E_1+E_2^\alpha=0$, so $E_2=-E_1^{1/\alpha}$.

Define the Lyapunov function as

$$V_{E_1} = \frac{1}{2} E_1^T E_1. (35)$$

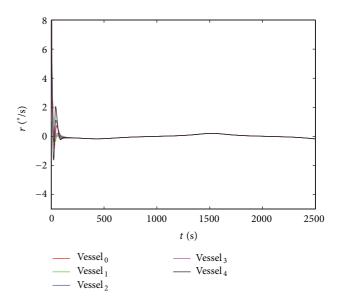


FIGURE 6: The angular velocities consensus of the vessels.

And it follows that

$$\dot{V}_{E_1} = -E_1^T E_1^{1/\alpha} \le -2^{(1+\alpha)/2\alpha} (V_{E_1})^{(1+\alpha)/2\alpha}. \tag{36}$$

In light of Lemma 2, the error functions E_1 and E_2 will converge to zero in finite time.

4. Simulation Results

In this section, simulation results are presented to evaluate the performance of the proposed finite-time cooperative formation control algorithm. We consider four surface vessels to perform the cooperative tracking task. For detailed system parameters matrices of vessel mathematic model, we can refer to the literature [7]. Here, we suppose that the information of virtual leader is available only to vessel 3 and vessel 4. The information exchange topology among all the vessels (including the virtual vessel) can be denoted as a directed graph in Figure 1.

From the above information exchange topology graph, we can know that the adjacent matrix of the graph is as follows:

$$\overline{A} = \begin{bmatrix} 0 & 0 & 0 & 0 & 0 \\ 0 & 0 & 1 & 1 & 1 \\ 0 & 0 & 0 & 1 & 0 \\ 1 & 0 & 1 & 0 & 0 \\ 1 & 0 & 0 & 0 & 0 \end{bmatrix}. \tag{37}$$

Then the Laplacian matrix of the information exchange topology graph of the practical vessels can be written as

$$L = \begin{bmatrix} 3 & -1 & -1 & -1 \\ 0 & 1 & -1 & 0 \\ 0 & -1 & 1 & 0 \\ 0 & 0 & 0 & 0 \end{bmatrix}.$$
 (38)

And the matrix for the communication relationship between the virtual vessel and the practical vessels is

$$B = \text{diag} (0 \ 0 \ 1 \ 1). \tag{39}$$

The initial conditions are $\eta_0(0) = \begin{bmatrix} 27 & 782 & -\pi/3 \end{bmatrix}^T$, $\eta_1(0) = \begin{bmatrix} 80 & 831 & -7\pi/30 \end{bmatrix}^T$, $\eta_2(0) = \begin{bmatrix} -94 & 753 & -\pi/2 \end{bmatrix}^T$, $\eta_3(0) = \begin{bmatrix} 40 & 700 & -\pi/4 \end{bmatrix}^T$ and $\eta_4(0) = \begin{bmatrix} -50 & 800 & -\pi/3 \end{bmatrix}^T$, respectively. The desired trajectory for the virtual vessel is chosen as $\eta_d(t) = \begin{bmatrix} n_d & e_d & \psi_d \end{bmatrix}^T$, and the detailed expressions are $n_d = t$, $e_d = 800 \sin(t/800)$, and $\psi_d = \arctan(\dot{e}_d/\dot{n}_d)$. In order to maintain the desired formation pattern, the relative distance between the practical vessels and the virtual leader vessel is defined as $l_1 = \begin{bmatrix} 0 & 100 & 0 \end{bmatrix}^T$, $l_2 = \begin{bmatrix} 0 & -100 & 0 \end{bmatrix}^T$, $l_3 = \begin{bmatrix} 0 & 50 & 0 \end{bmatrix}^T$, and $l_4 = \begin{bmatrix} 0 & -50 & 0 \end{bmatrix}^T$, respectively.

With the proposed finite-time cooperative tracking control law, the dynamic trajectory of each vessel is shown in Figure 2. It can be seen that these vessels move collectively along the sinusoid with maintaining a beeline formation pattern in the plane. The heading consensus for these vessels is achieved in finite time as shown in Figure 3. Furthermore, in the process of cooperative tracking, the surge velocities, the sway velocities, and the angular velocities of all these surface vessels converge to the desired values as a whole in finite time, which are presented in Figures 4, 5, and 6, respectively. From Figure 4, it is clearly seen that the surge velocities consensus of these vessels cannot be achieved absolutely at the inflexion of the curves. This is a natural phenomenon because all the desired trajectories are curve and all the curvatures are distinct.

Based on the above simulation results, we can know that the cooperative tracking task of multiple surface vessels is achieved by the proposed finite-time cooperative control algorithm. That means that these surface vessels can form the desired formation and perform the cooperative tracking as a whole formation in finite time. Overall, the proposed finite-time cooperative tracking control algorithm for multiple surface vessels is effective and satisfactory.

5. Conclusion

In this paper, the finite-time cooperative tracking control scheme for multiple surface vessels has been proposed. The cooperative formation is achieved by defining the formation reference point of each vessel based on the virtual leader-follower strategy. Furthermore, the communication topology among these vessels (include the virtual leader) is only the directed graph with a directed spanning tree. The cooperative tracking control scheme is designed using the terminal sliding-mode control approach which requires defining a nonlinear sliding variable function. In addition, the robustness against the external disturbances is achieved by compensating for the upper bound in the control input. It is proved that the cooperative tracking with desired formation can be achieved in finite time. Finally, the effectiveness of the proposed finite-time cooperative tracking control algorithm is validated by the simulation results.

Conflict of Interests

The authors declare that there is no conflict of interests regarding the publication of this paper.

Acknowledgments

The authors would like to acknowledge the support of the National Technology Momentous Special Program of China (2011ZX05027-002), High Technology of ships Research Program of China (Z12SJENA0011), the National Natural Science Fund of China (NSFC51209056), and the Basic Research Business Particular Item Fund of the Central High School of China (HEUCF041405).

References

- [1] I. Ihle, *Coordinated control of marine craft [Ph.D. thesis*], Norwegian University of Science and Technology, 2006.
- [2] W. Ren, R. W. Beard, and E. M. Atkins, "A survey of consensus problems in multi-agent coordination," in *Proceedings of the American Control Conference (ACC '05)*, pp. 1859–1864, June 2005.
- [3] F. Fahimi, "Non-linear model predictive formation control for groups of autonomous surface vessels," *International Journal of Control*, vol. 80, no. 8, pp. 1248–1259, 2007.
- [4] I.-A. F. Ihle, J. Jouffroy, and T. I. Fossen, "Formation control of marine surface craft: a lagrangian approach," *IEEE Journal of Oceanic Engineering*, vol. 31, no. 4, pp. 922–934, 2006.
- [5] F. Arrichiello, S. Chiaverini, and T. Fossen, "Formation control of underactuated surface vessels using the null-space-based behavioral control," in *Proceedings of IEEE International Con*ference on Interlligent Robots and Systems, pp. 5942–5947, 2006.
- [6] J. Almeida, C. Silvestre, and A. M. Pascoal, "Cooperative control of multiple surface vessels with discrete-time periodic communications," *International Journal of Robust and Nonlinear Control*, vol. 22, no. 4, pp. 398–419, 2012.
- [7] C. Thorvaldsen and R. Skjetne, "Formation control of fully-actuated marine vessels using group agreement protocols," in *Proceedings the 50th IEEE Conference on Decision and Control and European Control Conference*, pp. 4132–4139, 2011.
- [8] Y. Wang, W. Yan, and J. Li, "Passivity-based formation control of autonomous underwater vehicles," *IET Control Theory & Applications*, vol. 6, no. 4, pp. 518–525, 2012.
- [9] M. Fu and J. Jiao, "A hybrid approach for coordinated formation control of multiple surface vessels," *Mathematical Problems in Engineering*, vol. 2013, Article ID 794284, 8 pages, 2013.
- [10] E. Kyrkjebø, K. Y. Pettersen, M. Wondergem, and H. Nijmeijer, "Output synchronization control of ship replenishment operations: theory and experiments," *Control Engineering Practice*, vol. 15, no. 6, pp. 741–755, 2007.
- [11] M. Breivik, V. E. Hovstein, and T. I. Fossen, "Ship formation control: a guided leader-follower approach," in *Proceedings of the 17th World Congress, International Federation of Automatic Control (IFAC '08)*, pp. 16008–16014, July 2008.
- [12] N. E. Leonard and E. Fiorelli, "Virtual leaders, artificial potentials and coordinated control of groups," in *Proceedings of the 40th IEEE Conference on Decision and Control (CDC '01)*, pp. 2968–2973, December 2001.

- [13] H. Shi, L. Wang, and T. Chu, "Virtual leader approach to coordinated control of multiple mobile agents with asymmetric interactions," *Physica D*, vol. 213, no. 1, pp. 51–65, 2006.
- [14] W. Ren, "Consensus tracking under directed interaction topologies: algorithms and experiments," *IEEE Transactions on Control Systems Technology*, vol. 18, no. 1, pp. 230–237, 2010.
- [15] W. Yu, G. Chen, and M. Cao, "Consensus in directed networks of agents with nonlinear dynamics," *IEEE Transactions on Automatic Control*, vol. 56, no. 6, pp. 1436–1441, 2011.
- [16] W. Yu, G. Chen, M. Cao, and J. Kurths, "Second-Order consensus for multiagent systems with directed topologies and nonlinear dynamics," *IEEE Transactions on Systems, Man, and Cybernetics B*, vol. 40, no. 3, pp. 881–891, 2010.
- [17] W. Zhang, Z. Wang, and Y. Guo, "Adaptive backstepping-based synchronization of uncertain networked Lagrangian systems," in *Proceedings of the American Control Conference (ACC '11)*, pp. 1057–1062, July 2011.
- [18] M. Fu, J. Jiao, J. Liu, and Y. Wang, "Coordinated formation control of nonlinear marine vessels under directed communication topology," in *Proceedings of MTS/IEEE Conference on Oceans*, pp. 1–7, 2013.
- [19] S. P. Bhat and D. S. Bernstein, "Finite-time stability of continuous autonomous systems," *SIAM Journal on Control and Optimization*, vol. 38, no. 3, pp. 751–766, 2000.
- [20] M. Fu, J. Jiao, and S. Yin, "Robust coordinated formation for multiple surface vessels based on backstepping sliding mode control," *Abstract and Applied Analysis*, vol. 2013, Article ID 681319, 10 pages, 2013.
- [21] L. Wang and F. Xiao, "Finite-time consensus problems for networks of dynamic agents," *IEEE Transactions on Automatic Control*, vol. 55, no. 4, pp. 950–955, 2010.
- [22] S. Khoo, L. Xie, and Z. Man, "Robust finite-time consensus tracking algorithm for multirobot systems," *IEEE/ASME Trans*actions on Mechatronics, vol. 14, no. 2, pp. 219–228, 2009.
- [23] F. Xiao, L. Wang, J. Chen, and Y. Gao, "Finite-time formation control for multi-agent systems," *Automatica*, vol. 45, no. 11, pp. 2605–2611, 2009.
- [24] H. Du, S. Li, and X. Lin, "Finite-time formation control of multiagent systems via dynamic output feedback," *International Journal of Robust and Nonlinear Control*, vol. 23, no. 14, pp. 1609–1628, 2013.
- [25] S. Li and X. Wang, "Finite-time consensus and collision avoidance control algorithms for multiple AUVs," *Automatica*, vol. 49, no. 11, pp. 3359–3367, 2013.
- [26] S. Yin, S. Ding, and H. Luo, "Real-time implementation of fault tolerant control system with performance optimization," *IEEE Transactions on Industrial Electronics*, vol. 64, no. 5, pp. 2402–2411, 2014.
- [27] S. Yin, G. Wang, and H. Karimi, "Data-driven design of robust fault detection system for wind turbines," *Mechatronics*, 2013.
- [28] S. Yin, S. Ding, A. Haghani, H. Hao, and P. Zhang, "A comparison study of basic data-driven fault diagnosis and process monitoring methods on the benchmark Tennessee Eastman process," *Journal of Process Control*, vol. 22, no. 9, pp. 1567–1581, 2012.
- [29] S. Yin, S. X. Ding, A. H. A. Sari, and H. Hao, "Data-driven monitoring for stochastic systems and its application on batch process," *International Journal of Systems Science*, vol. 44, no. 7, pp. 1366–1376, 2013.
- [30] J. Huang, H. Li, Y. Chen, and Q. Xu, "Robust position control of PMSM using fractional-order sliding mode controller," *Abstract* and *Applied Analysis*, vol. 2012, Article ID 512703, 33 pages, 2012.

- [31] E. A. Tannuri, A. C. Agostinho, H. M. Morishita, and L. Moratelli, "Dynamic positioning systems: an experimental analysis of sliding mode control," *Control Engineering Practice*, vol. 18, no. 10, pp. 1121–1132, 2010.
- [32] H. Ashrafiuon, K. R. Muske, L. C. McNinch, and R. A. Soltan, "Sliding-mode tracking control of surface vessels," *IEEE Transactions on Industrial Electronics*, vol. 55, no. 11, pp. 4004–4012, 2008.
- [33] F. Fahimi, "Sliding-mode formation control for underactuated surface vessels," *IEEE Transactions on Robotics*, vol. 23, no. 3, pp. 617–622, 2007.
- [34] M. Defoort, T. Floquet, A. Kökösy, and W. Perruquetti, "Sliding-mode formation control for cooperative autonomous mobile robots," *IEEE Transactions on Industrial Electronics*, vol. 55, no. 11, pp. 3944–3953, 2008.
- [35] D. Zhao and T. Zou, "A finite-time approach to formation control of multiple mobile robots with terminal sliding mode," *International Journal of Systems Science*, vol. 43, no. 11, pp. 1998– 2014, 2012.
- [36] T. Fossen, Marine Control Systems: Guidance, Navigation and Control of Ships, Rigs and Underwater Vehicles, Marine Cybernetics, Trondheim, Norway, 2002.
- [37] S. P. Bhat and D. S. Bernstein, "Finite-time stability of continuous autonomous systems," *SIAM Journal on Control and Optimization*, vol. 38, no. 3, pp. 751–766, 2000.

Hindawi Publishing Corporation Abstract and Applied Analysis Volume 2014, Article ID 257971, 12 pages http://dx.doi.org/10.1155/2014/257971

Research Article

H_{∞} Filtering for Discrete-Time Genetic Regulatory Networks with Random Delay Described by a Markovian Chain

Yantao Wang, Xingming Zhou, and Xian Zhang

School of Mathematical Science, Heilongjiang University, Harbin 150080, China

Correspondence should be addressed to Xian Zhang; zhangx663@126.com

Received 14 December 2013; Accepted 22 January 2014; Published 2 March 2014

Academic Editor: Xiaojie Su

Copyright © 2014 Yantao Wang et al. This is an open access article distributed under the Creative Commons Attribution License, which permits unrestricted use, distribution, and reproduction in any medium, provided the original work is properly cited.

This paper is concerned with the H_{∞} filtering problem for a class of discrete time genetic regulatory networks with random delay and external disturbance. The aim is to design H_{∞} filter to estimate the true concentrations of mRNAs and proteins based on available measurement data. By introducing an appropriate Lyapunov function, a sufficient condition is derived in terms of linear matrix inequalities (LMIs) which makes the filtering error system stochastically stable with a prescribed H_{∞} disturbance attenuation level. The filter gains are given by solving the LMIs. Finally, an illustrative example is given to demonstrate the effectiveness of the proposed approach; that is, our approach is available for a smaller H_{∞} disturbance attenuation level than one in (Liu et al., 2012).

1. Introduction

Genetic regulatory networks (GRNs) are collections of DNA segments in a cell which interact with each other indirectly through their mRNAs, protein expression products, and other substances. Understanding the nature and functions of various GRNs is very interesting and crucially important for the treatment of many diseases such as cancers [1, 2]. Therefore, in the past decade, the study on GRNs has been put more emphasis by the researchers at interdisciplinary field. Mathematical modeling of GRNs provides a powerful tool for studying gene regulation processes. In general, genetic network models can be classified into two types, that is, the discrete model [3, 4] and the continuous model [5–8]. Usually, a continuous model is described by a (functional) differential equation. Due to slow biochemical reactions such as gene transcription and translation, time delays can play an important role in GRNs, which results that the (functional) differential equation model has been one of the most fashionable GRN models, and a lot of research on analysis and synthesis of GRNs have been recently done based on (functional) differential equation models (see, e.g., [9-15]).

The concentrations of gene products, such as mRNAs and proteins, are described as system states in a (functional)

differential equation model. In practice, biologists hope to gain actual concentrations of gene products in GRNs. However, due to model errors, external perturbation, time delays, and parameters jump, the steady-state values of GRNs can hardly be obtained. In order to obtain the steady-state values through available measurement data, the design of filter and estimator for (functional) differential equation models of GRNs has been investigated by some scholars (see, e.g., [16-23]). However, due to the requirement for implementing and application of GRNs for computer-based simulation, it is of vital importance to design filter or estimator for delayed discrete-time GRNs (i.e., discretized (functional) differential equation models of GRNs) in today's digital world, although there are, to the best author's knowledge, only three results reported at present [24-26]. Zhang et al. [25] is concerned with the set-values filtering for a class of discrete-time GRNs with time-varying parameters, constant time-delay, and bounded external noise. For a class of discrete-time GRNs with random delays described by a Markov chain, Liu et al. [26] designed a filter ensuring that the filtering error system is stochastically stable and has a prescribed H_{∞} performance. By utilizing the Lyapunov stability theory and stochastic analysis technique, Wang et al. [24] investigated the existing conditions and explicit expressions of H_{∞} state estimators for a class of stochastic discrete-time GRNs with probabilistic measurement delays described by Bernoulli distributed white sequences. These conditions are given in terms of LMIs and are dependent on the lower and upper bounds of the time-varying delays.

It should also be emphasized that for delayed discrete-time GRNs, the stability problem (as the most important properties for any dynamics systems) [27–29], H_{∞} stabilization problem [30], and passivity problem [31] have been exploited. On the other hand, researchers have been paying attention to the problems of analysis and synthesis for Markovian jump system [32–36] and the filtering problems for some nonlinear systems [37–41].

Motivated by the above discussion, in this paper, we will deal with the H_{∞} filtering problem for a class of discrete-time GRNs with random delay which is described by a Markovian chain. By constructing a novel Lyapunov function different from one in [26], a sufficient LMI condition is first established to ensure the existence of the desired filter. The condition is dependent on the transition probability matrix of the random delay. Then, the explicit expression of the desired filter is shown to ensure the resulting filtering error system to be stochastically stable and have a prescribed H_{∞} disturbance attenuation level. Moreover, an optimization problem with LMIs constraints is established to design an H_{∞} filter which ensures an optimal H_{∞} disturbance attenuation level. Finally, a numerical example is given to show the effectiveness of the proposed approach.

2. Problem Formulation

Consider the following discrete-time GRN with random delays, *n* mRNAs, and *n* proteins [27, 28]:

$$\begin{split} M_{i}\left(k+1\right) &= e^{-a_{i}h} M_{i}\left(k\right) + \phi_{i}\left(h\right) \\ &\times \left[\sum_{j=1}^{n} b_{ij} f_{j}\left(P_{j}\left(k-d\left(k\right)\right)\right) + V_{i}\right], \\ \\ P_{i}\left(k+1\right) &= e^{-c_{i}h} P_{i}\left(k\right) + \varphi_{i}\left(h\right) d_{i} M_{i}\left(k-d\left(k\right)\right), \\ \\ i &= 1, 2, \dots, n, \end{split}$$

where $M_i(k)$ and $P_i(k)$, respectively, are the concentrations of mRNA and protein of the ith gene; $\phi_i(h) = (1 - e^{-a_i h})/a_i > 0$ and $\phi_i(h) = (1 - e^{-c_i h})/c_i > 0$, where h is a given positive real number standing for the uniform discretionary step size; d(k) denotes the random time delay of mRNAs and proteins, and is assumed to be a Markovian chain with state space $\mathcal{N} := \{1, 2, \ldots, d\}$, and d is a fixed positive integer; $a_i > 0$ and $c_i > 0$ are the degradation rates of mRNA and protein, respectively; d_i is the translation rate; $V_i = \sum_{j \in I_i} v_{ij}$, where v_{ij} is a bounded constant denoting the dimensionless transcriptional rate of

gene j to i, and I_i is the set of all the repressors of ith gene; b_{ij} (i, j = 1, 2, ..., n) are the coupling coefficients satisfying

$$b_{ij} = \begin{cases} v_{ij}, & \text{if transcription factor } j \text{ is} \\ & \text{an activator of gene } i, \\ 0, & \text{if there is no link from} \\ & \text{link node } j \text{ to } i, \\ -v_{ij}, & \text{if transcription factor } j \text{ is} \\ & \text{a repressor of gene } i; \end{cases}$$
 (2)

the nonlinear function f_j ($j=1,2,\ldots,n$) denotes the feedback regulation of protein in process of transcription. In general, f_j is a monotonic function in Hill form; namely, $f_j(s) = s^{h_j}/(1+s^{h_j})$ ($j=1,2,\ldots,n$), where h_j is the Hill coefficient. Denote by $\pi:=[\pi_{ij}]_{n\times n}$ the transition probability matrix of d(k), where $\pi_{ij}=\operatorname{Prob}\{d(k+1)=j\mid d(k)=i\}$.

Let us rewrite GRN (1) as the following compact matrix form:

$$M(k+1) = AM(k) + Bf(P(k-d(k))) + V,$$

$$P(k+1) = CP(k) + DM(k-d(k)),$$
(3)

where

$$M(k) = [M_1(k) \ M_2(k) \ \cdots \ M_n(k)]^T,$$

 $P(k) = [P_1(k) \ P_2(k) \ \cdots \ P_n(k)]^T,$

$$f(P(k-d(k)))$$

$$= [f_{1}(P_{1}(k-d(k))) \quad f_{2}(P_{2}(k-d(k))) \quad \cdots \quad f_{n}(P_{n}(k-d(k)))]^{T},$$

$$V = [\phi_{1}(h)V_{1} \quad \phi_{2}(h)V_{2} \quad \cdots \quad \phi_{n}(h)V_{n}]^{T},$$

$$A = \operatorname{diag}(e^{-a_{1}h}, e^{-a_{2}h}, \dots, e^{-a_{n}h}),$$

$$C = \operatorname{diag}(e^{-c_{1}h}, e^{-c_{2}h}, \dots, e^{-c_{n}h}),$$

$$D = \operatorname{diag}(\phi_{1}(h) d_{1}, \phi_{2}(h) d_{2}, \dots, \phi_{n}(h) d_{n}),$$

$$B = [\phi_{i}(h)b_{ij}]_{n \times n} \quad (i = 1, 2, \dots, n).$$

$$(4)$$

Let (M^*, P^*) be an equilibrium point of GRN (3), where $M^* = \begin{bmatrix} M_1^* & \cdots & M_n^* \end{bmatrix}^T$ and $P^* = \begin{bmatrix} P_1^* & \cdots & P_n^* \end{bmatrix}^T$; that is,

$$M^* = AM^* + Bf(P^*) + V, \qquad P^* = CP^* + DM^*.$$
 (5)

To simplify the analysis, one can transform the equilibrium point to the origin by the relation $x_m(k) = M(k) - M^*$ and $x_p(k) = P(k) - P^*$. Then the transformed system is changed as follows:

$$x_{m}(k+1) = Ax_{m}(k) + Bg(x_{p}(k-d(k))),$$

 $x_{p}(k+1) = Cx_{p}(k) + Dx_{m}(k-d(k)),$
(6)

where $g(x_p(k)) = f(x_p(k) + P^*) - f(P^*)$. For every i = 1, 2, ..., n, since f_i is a monotonic function in Hill form, one

can easily obtain that g_i is a monotonically increasing function with saturation and satisfies the following inequality:

$$g_i(0) = 0, \quad 0 \le \frac{g_i(s_1) - g_i(s_2)}{s_1 - s_2} \le l_i, \quad \forall s_1, s_2 \in R, \ s_1 \ne s_2,$$

$$(7)$$

where l_i is a given constant.

When we take extracellular perturbations into account, a class of stochastic discrete-time GRN model with random delays is represented as follows:

$$x_{m}(k+1) = Ax_{m}(k) + Bg(x_{p}(k-d(k))) + E_{1}w(k),$$

$$x_{p}(k+1) = Cx_{p}(k) + Dx_{m}(k-d(k)) + F_{1}v(k),$$

$$y_{m}(k) = C_{1}x_{m}(k) + E_{2}w(k),$$

$$y_{p}(k) = C_{2}x_{p}(k) + F_{2}v(k),$$

$$z_{m}(k) = G_{1}x_{m}(k),$$

$$z_{p}(k) = G_{2}x_{p}(k),$$

$$x_{m}(k) = \theta_{m}(k), \quad x_{p}(k) = \theta_{p}(k),$$

$$k = -d, -d + 1, \dots, 0,$$
(8)

where $A, B, C, D, C_1, C_2, E_1, E_2, F_1, F_2, G_1,$ and G_2 are constant matrices of appropriate dimension; $y_m(k) := [y_{m1}(k) \cdots y_{mn}(k)]^T$ and $y_p(k) := [y_{p1}(k) \cdots y_{pn}(k)]^T$ denote the expression levels of mRNA and protein, respectively; $z_m(k) := [z_{m1}(k) \cdots z_{ml}(k)]^T$ and $z_p(k) := [z_{p1}(k) \cdots z_{pl}(k)]^T$ are the estimated signals; both w(k) and v(k) are exogenous disturbance signals; and $\theta_m(k)$ and $\theta_p(k)$ are the initial conditions of $x_m(k)$ and $x_p(k)$, respectively.

In complex GRNs, only the partial information of the network components can be usually obtained. Therefore, in order to obtain the states of GRNs, we need to estimate them via available measurements [42]. The full order linear filter which need to be designed as the following form:

$$\widehat{x}_{m}(k+1) = A_{f}\widehat{x}_{m}(k) + B_{f}y_{m}(k),$$

$$\widehat{x}_{p}(k+1) = C_{f}\widehat{x}_{p}(k) + D_{f}y_{p}(k),$$

$$\widehat{z}_{m}(k) = G_{1f}\widehat{x}_{m}(k) + H_{1f}y_{m}(k),$$

$$\widehat{z}_{p}(k) = G_{2f}\widehat{x}_{p}(k) + H_{2f}y_{p}(k),$$

$$(9)$$

where $\widehat{x}_m(k)$, $\widehat{x}_p(k)$, $\widehat{z}_m(k)$, and $\widehat{z}_p(k)$ are the estimates of $x_m(k)$, $x_p(k)$, $z_m(k)$, and $z_p(k)$, respectively; A_f , B_f , C_f , $D_f \in R^{n \times n}$ and G_{1f} , G_{2f} , H_{1f} , $H_{2f} \in R^{l \times n}$ are filter parametric matrices to be determined.

Set

$$\begin{split} \widetilde{x}_{m}\left(k\right) &= \begin{bmatrix} x_{m}\left(k\right) \\ \widehat{x}_{m}\left(k\right) \end{bmatrix}, \qquad \widetilde{x}_{p}\left(k\right) &= \begin{bmatrix} x_{p}\left(k\right) \\ \widehat{x}_{p}\left(k\right) \end{bmatrix}, \\ e_{m}\left(k\right) &= z_{m}\left(k\right) - \widehat{z}_{m}\left(k\right), \qquad e_{p}\left(k\right) &= z_{p}\left(k\right) - \widehat{z}_{p}\left(k\right). \end{split}$$

$$(10)$$

Then the filtering error system can be expressed as

$$\widetilde{x}_{m}(k+1) = \overline{A}\widetilde{x}_{m}(k) + \overline{B}g\left(Z_{1}\widetilde{x}_{p}(k-d(k))\right) + \overline{E}w(k),$$

$$\widetilde{x}_{p}(k+1) = \overline{C}\widetilde{x}_{p}(k) + \overline{D}Z_{1}\widetilde{x}_{m}(k-d(k)) + \overline{F}v(k),$$

$$e_{m}(k) = \overline{G}_{1f}\widetilde{x}_{m}(k) + \overline{H}_{1f}w(k),$$

$$e_{p}(k) = \overline{G}_{2f}\widetilde{x}_{p}(k) + \overline{H}_{2f}v(k),$$

$$\widetilde{x}_{m}(k) = \widetilde{\theta}_{m}(k), \qquad \widetilde{x}_{p}(k) = \widetilde{\theta}_{p}(k),$$

$$k = -d, -d + 1, \dots, 0,$$
(11)

where

$$\widetilde{\theta}_{m}(k) = \begin{bmatrix} \theta_{m}(k) \\ 0 \end{bmatrix}, \qquad \widetilde{\theta}_{p}(k) = \begin{bmatrix} \theta_{p}(k) \\ 0 \end{bmatrix},
\overline{A} = \begin{bmatrix} A & 0 \\ B_{f}C_{1} & A_{f} \end{bmatrix}, \qquad \overline{B} = \begin{bmatrix} B \\ 0 \end{bmatrix}, \qquad \overline{C} = \begin{bmatrix} C & 0 \\ D_{f}C_{2} & C_{f} \end{bmatrix},
\overline{D} = \begin{bmatrix} D \\ 0 \end{bmatrix}, \qquad \overline{E} = \begin{bmatrix} E_{1} \\ B_{f}E_{2} \end{bmatrix}, \qquad \overline{F} = \begin{bmatrix} F_{1} \\ D_{f}F_{2} \end{bmatrix},
\overline{G}_{1f} = \begin{bmatrix} G_{1} - H_{1f}C_{1} & -G_{1f} \end{bmatrix},
\overline{G}_{2f} = \begin{bmatrix} G_{2} - H_{2f}C_{2} & -G_{2f} \end{bmatrix}, \qquad \overline{H}_{1f} = -H_{1f}E_{2},
\overline{H}_{2f} = -H_{2f}F_{2}, \qquad Z_{1} = \begin{bmatrix} I & 0 \end{bmatrix}.$$
(12)

For convenience, for a nonnegative integer k we define

$$\Theta_{k} = \left\{ \widetilde{x}_{m}(k), \widetilde{x}_{m}(k-1), \dots, \widetilde{x}_{m}(k-d), \right.$$

$$\widetilde{x}_{p}(k), \widetilde{x}_{p}(k-1), \dots, \widetilde{x}_{p}(k-d) \right\}.$$
(13)

Definition 1 (see [26]). The delay d(k) is said to be the random delay described by a Markovian chain if it is bound by $1 \le d(k) \le d$, and $\{d(k) \in \mathcal{N}, k = 0, 1, 2, ...\}$ is a Markovian chain with state space \mathcal{N} and transition probability matrix π .

Definition 2 (see [26]). When w(k) = 0 and v(k) = 0, the filtering error system (11) is said to be stochastically stable, if

$$\sum_{k=0}^{\infty} E\left\{ \left\| \widetilde{x}_{m}(k) \right\|^{2} + \left\| \widetilde{x}_{p}(k) \right\|^{2} \mid \Theta_{0}, d\left(0\right) \right\} < \infty$$
 (14)

for every initial condition Θ_0 and initial mode d(0), where $E\{\cdot\}$ represents the mathematical expectation operator.

Definition 3. For a given constant $\gamma > 0$, the filtering error system (11) is said to be stochastically stable with H_{∞} disturbance attenuation level γ if it is stochastically stable with

w(k) = 0 and v(k) = 0, and under the zero initial conditions it satisfies the following inequality:

$$\sum_{k=0}^{\infty} E\left\{ \begin{bmatrix} e_{m}(k) \\ e_{p}(k) \end{bmatrix}^{T} \begin{bmatrix} e_{m}(k) \\ e_{p}(k) \end{bmatrix} \mid \Theta_{0}, d(0) \right\}$$

$$< \gamma^{2} \sum_{k=0}^{\infty} \begin{bmatrix} w(k) \\ v(k) \end{bmatrix}^{T} \begin{bmatrix} w(k) \\ v(k) \end{bmatrix}$$
(15)

for all nonzero w(k), $v(k) \in l_2[0, +\infty)$, and initial mode d(0).

The objective of this paper is to design a filter of form (9) such that the filtering error system (11) is stochastically stable with H_{∞} disturbance attenuation level γ . In order to realize the aim, we first introduce the following lemma.

Lemma 4 (see [43]). For symmetric matrices P > 0 and Q > 0, the matrix inequality

$$\begin{bmatrix} -P^{-1} & A \\ * & -Q \end{bmatrix} < 0 \tag{16}$$

holds, if and only if there is a matrix R such that

$$\begin{bmatrix} P - R - R^T & R^T A \\ * & -Q \end{bmatrix} < 0. \tag{17}$$

3. Stability Analysis and H_{∞} Filter Design

The stability analysis for the filtering error system (11) with w(k) = 0 and v(k) = 0 is presented by the following theorem.

Theorem 5. The filtering error system (11) with w(k) = 0 and v(k) = 0 is stochastically stable, if there exist matrices $\varsigma := \operatorname{diag}(\varsigma_1, \varsigma_2, \ldots, \varsigma_n) > 0$, $\mu := \operatorname{diag}(\mu_1, \mu_2, \ldots, \mu_n) > 0$, $P_i^T(r) = P_i(r) > 0 (i = 1, 2, \ldots, 6; r = 1, 2, \ldots, d)$, and $P_j^T = P_j > 0$ (j = 2, 3, 5, 6) such that the following matrix inequalities (18) and (19) hold for all $r \in \mathcal{N}$:

$$\Omega := \widetilde{\Omega} + \widehat{\Omega} < 0, \tag{18}$$

$$\overline{P}_{i}(r) < P_{i}, \quad j = 2, 3, 5, 6,$$
 (19)

where

$$\begin{split} \widehat{\Omega} &= \Lambda_1^T \overline{P}_1 \left(r \right) \Lambda_1 + \Lambda_2^T \left(d \overline{P}_3 \left(r \right) + \frac{d^2 + d}{2} P_3 \right) \Lambda_2 \\ &+ \Lambda_3^T \overline{P}_4 \left(r \right) \Lambda_3, \\ \Lambda_1 &= \left[\overline{A} \ 0 \ 0 \ \overline{B} \ 0 \ 0 \right], \\ \Lambda_2 &= \left[\overline{A} - I \ 0 \ 0 \ \overline{B} \ 0 \ 0 \right], \\ \Lambda_3 &= \left[0 \ \overline{C} \ \overline{D} Z_1 \ 0 \ 0 \ 0 \right], \end{split}$$

$$\widetilde{\Omega} = \begin{bmatrix} \Omega_{11} & 0 & \Omega_{13} & 0 & 0 & 0 \\ * & -P_4(r) & 0 & 0 & -Z_1^T \varsigma L & -Z_1^T C^T \mu L \\ * & * & \Omega_{33} & 0 & 0 & -Z_1^T D^T \mu L \\ * & * & * & \Omega_{44} & \Omega_{45} & 0 \\ * & * & * & * & \Omega_{55} & \Omega_{56} \\ * & * & * & * & * & \Omega_{66} \end{bmatrix},$$

$$\Omega_{11} = (d-1) P_2 + \overline{P}_2(r) - P_1(r) - \Omega_{13},$$

$$\Omega_{13} = \frac{1}{r} P_3(r) + \frac{1}{r} P_3, \qquad \Omega_{33} = -P_2(r) - \Omega_{13},$$

$$\Omega_{44} = -P_5(r) - \Omega_{45}, \qquad \Omega_{45} = \frac{1}{r} P_6(r) + \frac{1}{r} P_6,$$

$$\Omega_{55} = (d-1) P_5 + \overline{P}_5(r) - \Omega_{56} - \Omega_{45} - \varsigma,$$

$$\Omega_{56} = -d\overline{P}_6(r) - \frac{(d^2 + d) P_6}{2}, \qquad \Omega_{66} = -\Omega_{56} - \mu,$$

$$L = \operatorname{diag}\left(-\frac{l_1}{2}, -\frac{l_2}{2}, \dots, -\frac{l_n}{2}\right),$$

$$\overline{P}_i(r) = \sum_{s=1}^d \pi_{rs} P_i(s), \quad i = 1, 2, \dots, 6.$$
(20)

Proof. Choose an appropriate Lyapunov function $V(\Theta_k, k, d(k))$ for the filtering error system (11) with w(k) = 0 and v(k) = 0 as follows:

$$V\left(\Theta_{k},k,d\left(k\right)\right) = \sum_{i=1}^{3} \left(V_{m,i}\left(\Theta_{k},k,d\left(k\right)\right) + V_{p,i}\left(\Theta_{k},k,d\left(k\right)\right)\right)$$
(21)

 $V_{m,1}\left(\Theta_{k},k,d\left(k\right)\right)=\widetilde{x}_{m}^{T}\left(k\right)P_{1}\left(d\left(k\right)\right)\widetilde{x}_{m}\left(k\right),$

 $V_{p,1}\left(\Theta_{k},k,d\left(k\right)\right)=\tilde{x}_{p}^{T}\left(k\right)P_{4}\left(d\left(k\right)\right)\tilde{x}_{p}\left(k\right),$

with

$$\begin{split} V_{m,2}\left(\Theta_{k},k,d\left(k\right)\right) &= \sum_{i=k-d(k)}^{k-1} \widetilde{x}_{m}^{T}\left(i\right) P_{2}\left(d\left(k\right)\right) \widetilde{x}_{m}\left(i\right) \\ &+ \sum_{j=-d+1}^{l} \sum_{i=k+j}^{k-1} \widetilde{x}_{m}^{T}\left(i\right) P_{2}\widetilde{x}_{m}\left(i\right), \\ V_{p,2}\left(\Theta_{k},k,d\left(k\right)\right) &= \sum_{i=k-d(k)}^{k-1} g^{T}\left(Z_{1}\widetilde{x}_{p}\left(i\right)\right) P_{5}\left(d\left(k\right)\right) g\left(Z_{1}\widetilde{x}_{p}\left(i\right)\right) \\ &+ \sum_{j=-d+1}^{l} \sum_{i=k+j}^{k-1} g^{T}\left(Z_{1}\widetilde{x}_{p}\left(i\right)\right) P_{5}g\left(Z_{1}\widetilde{x}_{p}\left(i\right)\right), \\ V_{m,3}\left(\Theta_{k},k,d\left(k\right)\right) &= \sum_{j=-d(k)}^{l} \sum_{i=k+j}^{k-1} \eta^{T}\left(i\right) P_{3}\left(d\left(k\right)\right) \eta\left(i\right) \\ &+ \sum_{j=-d}^{l} \sum_{l=j}^{l} \sum_{i=k+l}^{k-1} \eta^{T}\left(i\right) P_{3}\eta\left(i\right), \end{split}$$

$$\begin{split} V_{p,3}\left(\Theta_{k},k,d\left(k\right)\right) &= \sum_{j=-d(k)}^{-1} \sum_{i=k+j}^{k-1} \zeta^{T}\left(i\right) P_{6}\left(d\left(k\right)\right) \zeta\left(i\right) \\ &+ \sum_{j=-d}^{-1} \sum_{l=j}^{-1} \sum_{i=k+l}^{k-1} \zeta^{T}\left(i\right) P_{6}\zeta\left(i\right), \end{split} \tag{22}$$

where $\eta(k) = \tilde{x}_m(k+1) - \tilde{x}_m(k)$ and $\zeta(k) = g(Z_1\tilde{x}_p(k+1)) - g(Z_1\tilde{x}_p(k))$. By taking the forward difference of the function $V_{m,1}(\Theta_k,k,d(k))$ along with the solution of system (11), one can obtain that

$$\begin{split} &E\left\{V_{m,1}\left(\Theta_{k+1},k+1,d\left(k+1\right)\right)\mid\Theta_{k},d\left(k\right)=r\right\}\\ &-V_{m,1}\left(\Theta_{k},k,r\right)\\ &=\sum_{s=1}^{d}\pi_{rs}\widetilde{x}_{m}^{T}\left(k+1\right)P_{1}\left(s\right)\widetilde{x}_{m}\left(k+1\right)-\widetilde{x}_{m}^{T}\left(k\right)P_{1}\left(r\right)\widetilde{x}_{m}\left(k\right)\\ &=\widetilde{x}_{m}^{T}\left(k+1\right)\overline{P}_{1}\left(r\right)\widetilde{x}_{m}\left(k+1\right)-\widetilde{x}_{m}^{T}\left(k\right)P_{1}\left(r\right)\widetilde{x}_{m}\left(k\right). \end{split} \tag{23}$$

Additionally, it can be verified that

$$\begin{split} &E\left\{V_{m,2}\left(\Theta_{k+1},k+1,d\left(k+1\right)\right)\mid\Theta_{k},d\left(k\right)=r\right\}\\ &-V_{m,2}\left(\Theta_{k},k,r\right)\\ &=\sum_{s=1}^{d}\pi_{rs}\sum_{i=k+1-s}^{k}\widetilde{x}_{m}^{T}\left(i\right)P_{2}\left(s\right)\widetilde{x}_{m}\left(i\right)\\ &-\sum_{i=k-r}^{k-1}\widetilde{x}_{m}^{T}\left(i\right)P_{2}\left(r\right)\widetilde{x}_{m}\left(i\right)\\ &+\sum_{j=-d+1}^{-1}\sum_{i=k+1+j}^{k}\widetilde{x}_{m}^{T}\left(i\right)P_{2}\widetilde{x}_{m}\left(i\right)\\ &-\sum_{j=-d+1}^{-1}\sum_{i=k+j}^{k-1}\widetilde{x}_{m}^{T}\left(i\right)P_{2}\widetilde{x}_{m}\left(i\right)\\ &=\widetilde{x}_{m}^{T}\left(k\right)\overline{P}_{2}\left(r\right)\widetilde{x}_{m}\left(k\right)-\widetilde{x}_{m}^{T}\left(k-r\right)P_{2}\left(r\right)\widetilde{x}_{m}\left(k-r\right)\\ &+\sum_{i=k+1-s}^{k-1}\widetilde{x}_{m}^{T}\left(i\right)\overline{P}_{2}\left(r\right)\widetilde{x}_{m}\left(i\right)-\sum_{i=k+1-r}^{k-1}\widetilde{x}_{m}^{T}\left(i\right)P_{2}\left(r\right)\widetilde{x}_{m}\left(i\right)\\ &+\sum_{j=-d+1}^{-1}\widetilde{x}_{m}^{T}\left(k\right)P_{2}\widetilde{x}_{m}\left(k\right)-\sum_{j=k+1-d}^{k-1}\widetilde{x}_{m}^{T}\left(j\right)P_{2}\widetilde{x}_{m}\left(j\right)\\ &\leq\widetilde{x}_{m}^{T}\left(k\right)\overline{P}_{2}\left(r\right)\widetilde{x}_{m}\left(k\right)-\widetilde{x}_{m}^{T}\left(k-r\right)P_{2}\left(r\right)\widetilde{x}_{m}\left(k-r\right)\\ &+\left(d-1\right)\widetilde{x}_{m}^{T}\left(k\right)P_{2}\widetilde{x}_{m}\left(k\right)\\ &+\sum_{i=k+1-d}^{k-1}\widetilde{x}_{m}^{T}\left(i\right)\overline{P}_{2}\left(r\right)\widetilde{x}_{m}\left(i\right)-\sum_{i=k+1-d}^{k-1}\widetilde{x}_{m}^{T}\left(i\right)P_{2}\widetilde{x}_{m}\left(i\right) \end{split}$$

$$\leq \widetilde{X}_{m}^{T}(k) \left[(d-1) P_{2} + \overline{P}_{2}(r) \right] \widetilde{X}_{m}^{T}(k) \\ - \widetilde{X}_{m}^{T}(k-r) P_{2}(r) \widetilde{X}_{m}^{T}(k-r),$$

$$E\left\{ V_{m,3} \left(\Theta_{k+1}, k+1, d\left(k+1\right) \right) \mid \Theta_{k}, d\left(k\right) = r \right\} \\ - V_{m,3} \left(\Theta_{k}, k, r \right) \\ = \sum_{s=1}^{d} \pi_{rs} \sum_{j=-s}^{-1} \sum_{i=k+1+j}^{k} \eta^{T}(i) P_{3}(s) \eta(i) \\ - \sum_{j=-r}^{-1} \sum_{i=k+j}^{k-1} \eta^{T}(i) P_{3}(r) \eta(i) \\ + \sum_{j=-d}^{-1} \sum_{l=j}^{-1} \left[\sum_{i=k+1+l}^{k} \eta^{T}(i) P_{3}\eta(i) - \sum_{i=k+l}^{k-1} \eta^{T}(i) P_{3}\eta(i) \right] \\ \leq \sum_{j=-d}^{-1} \eta^{T}(k) \overline{P}_{3}(r) \eta(k) - \sum_{j=-r}^{-1} \eta^{T}(k+j) P_{3}(r) \eta(k+j) \\ + \sum_{j=-d}^{-1} \sum_{i=k+1+j}^{k-1} \eta^{T}(i) \overline{P}_{3}(r) \eta(i) + \frac{d^{2}+d}{2} \eta^{T}(k) P_{3}\eta(k) \\ - \sum_{j=-d}^{-1} \sum_{i=k+1+j}^{k-1} \eta^{T}(i) P_{3}\eta(i) - \sum_{j=-d}^{-1} \eta^{T}(k+j) P_{3}\eta(k+j) \\ \leq \eta^{T}(k) \left[d\overline{P}_{3}(r) + \frac{d^{2}+d}{2} P_{3} \right] \eta(k) \\ - \sum_{j=-r}^{-1} \eta^{T}(k+j) \frac{1}{r} P_{3}(r) \sum_{j=-r}^{-1} \eta(k+j) \\ + \sum_{j=-d}^{-1} \sum_{i=k+1+j}^{k-1} \eta^{T}(i) \overline{P}_{3}(r) \eta(i) - \sum_{j=-d}^{-1} \sum_{i=k+1+j}^{k-1} \eta^{T}(i) P_{3}\eta(i) \\ - \sum_{j=-r}^{-1} \eta^{T}(k+j) \frac{1}{r} P_{3} \sum_{j=-r}^{-1} \eta(k+j) \\ \leq \eta^{T}(k) \left[d\overline{P}_{3}(r) + \frac{d^{2}+d}{2} P_{3} \right] \eta(k) \\ - \sum_{j=-r}^{-1} \eta^{T}(k+j) \frac{1}{r} (P_{3}(r) + P_{3}) \sum_{j=-r}^{-1} \eta(k+j) .$$

$$(24)$$

Similarly, the following inequalities (25) can be derived:

$$\begin{split} &E\left\{V_{p,1}\left(\Theta_{k+1},k+1,d\left(k+1\right)\right)\mid\Theta_{k},d\left(k\right)=r\right\}\\ &-V_{p,1}\left(\Theta_{k},k,r\right)\\ &=\sum_{s=1}^{d}\pi_{rs}\widetilde{x}_{p}^{T}\left(k+1\right)P_{4}\left(s\right)\widetilde{x}_{p}\left(k+1\right)-\widetilde{x}_{p}^{T}\left(k\right)P_{4}\left(r\right)\widetilde{x}_{p}\left(k\right)\\ &=\widetilde{x}_{p}^{T}\left(k+1\right)\overline{P}_{4}\left(r\right)\widetilde{x}_{p}\left(k+1\right)-\widetilde{x}_{p}^{T}\left(k\right)P_{4}\left(r\right)\widetilde{x}_{p}\left(k\right), \end{split}$$

$$\begin{split} &E\left\{V_{p,2}\left(\Theta_{k+1},k+1,d\left(k+1\right)\right)\mid\Theta_{k},d\left(k\right)=r\right\}\\ &-V_{p,2}\left(\Theta_{k},k,r\right)\\ &=\sum_{s=1}^{d}\pi_{rs}\sum_{i=k+1-s}^{k}g^{T}\left(Z_{1}\tilde{x}_{p}\left(i\right)\right)P_{5}\left(s\right)g\left(Z_{1}\tilde{x}_{p}\left(i\right)\right)\\ &-\sum_{i=k-r}^{k-1}g^{T}\left(Z_{1}\tilde{x}_{p}\left(i\right)\right)P_{5}\left(r\right)g\left(Z_{1}\tilde{x}_{p}\left(i\right)\right)\\ &+\sum_{j=-d+1}^{l}\sum_{i=k+1+j}^{k}g^{T}\left(Z_{1}\tilde{x}_{p}\left(i\right)\right)P_{5}g\left(Z_{1}\tilde{x}_{p}\left(i\right)\right)\\ &-\sum_{j=-d+1}^{l}\sum_{i=k+j}^{k-1}g^{T}\left(Z_{1}\tilde{x}_{p}\left(i\right)\right)P_{5}g\left(Z_{1}\tilde{x}_{p}\left(i\right)\right)\\ &-g^{T}\left(Z_{1}\tilde{x}_{p}\left(k\right)\right)\overline{P}_{5}\left(r\right)g\left(Z_{1}\tilde{x}_{p}\left(k\right)\right)\\ &-g^{T}\left(Z_{1}\tilde{x}_{p}\left(k-r\right)\right)P_{5}\left(r\right)g\left(Z_{1}\tilde{x}_{p}\left(k-r\right)\right)\\ &+\sum_{s=1}^{d}\pi_{rs}\sum_{i=k+1-s}^{k-1}g^{T}\left(Z_{1}\tilde{x}_{p}\left(i\right)\right)P_{5}\left(s\right)g\left(Z_{1}\tilde{x}_{p}\left(i\right)\right)\\ &-\sum_{i=k+1-r}^{k-1}\left[g^{T}\left(Z_{1}\tilde{x}_{p}\left(i\right)\right)P_{5}\left(r\right)g\left(Z_{1}\tilde{x}_{p}\left(k\right)\right)\right.\\ &-g^{T}\left(Z_{1}\tilde{x}_{p}\left(k\right)\right)\left[\left(d-1\right)P_{5}+\overline{P}_{5}\left(r\right)\right]g\left(Z_{1}\tilde{x}_{p}\left(k\right)\right)\\ &-g^{T}\left(Z_{1}\tilde{x}_{p}\left(k\right)\right)\left[\left(d-1\right)P_{5}+\overline{P}_{5}\left(r\right)\right]g\left(Z_{1}\tilde{x}_{p}\left(k\right)\right)\\ &-\sum_{i=k+1-d}^{k-1}g^{T}\left(Z_{1}\tilde{x}_{p}\left(i\right)\right)\overline{P}_{5}\left(r\right)g\left(Z_{1}\tilde{x}_{p}\left(i\right)\right)\\ &-\sum_{i=k+1-d}^{k-1}g^{T}\left(Z_{1}\tilde{x}_{p}\left(i\right)\right)P_{5}g\left(Z_{1}\tilde{x}_{p}\left(i\right)\right)\\ &-g^{T}\left(Z_{1}\tilde{x}_{p}\left(k\right)-r\right)P_{5}\left(r\right)g\left(Z_{1}\tilde{x}_{p}\left(i\right)\right)\\ &-g^{T}\left(Z_{1}\tilde{x}_{p}\left(k\right)-r\right)P_{5}\left(r\right)g\left(Z_{1}\tilde{x}_{p}\left(i\right)\right)\\ &-g^{T}\left(Z_{1}\tilde{x}_{p}\left(k\right)-r\right)P_{5}\left(r\right)g\left(Z_{1}\tilde{x}_{p}\left(k\right)\right)\\ &-g^{T}\left(Z_{1}\tilde{x}_{p}\left(k\right)-r\right)P_{5}\left(r\right)g\left(Z_{1}\tilde{x}_{p}\left(k\right)\right)\\ &-g^{T}\left(Z_{1}\tilde{x}_{p}\left(k\right)-r\right)P_{5}\left(r\right)g\left(Z_{1}\tilde{x}_{p}\left(k\right)\right)\\ &-g^{T}\left(Z_{1}\tilde{x}_{p}\left(k\right)-r\right)P_{5}\left(r\right)g\left(Z_{1}\tilde{x}_{p}\left(k\right)\right)\\ &-g^{T}\left(Z_{1}\tilde{x}_{p}\left(k\right)-r\right)P_{5}\left(r\right)g\left(Z_{1}\tilde{x}_{p}\left(k\right)\right)\\ &-p^{T}\left(Z_{1}\tilde{x}_{p}\left(k\right)-r\right)P_{5}\left(r\right)g\left(Z_{1}\tilde{x}_{p}\left(k\right)\right)\\ &-p^{T}\left(Z_{1}\tilde{x}_{p}\left(k\right)-r\right)P_{5}\left(r\right)g\left(Z_{1}\tilde{x}_{p}\left(k\right)\right)\\ &-p^{T}\left(Z_{1}\tilde{x}_{p}\left(k\right)-r\right)P_{5}\left(r\right)g\left(Z_{1}\tilde{x}_{p}\left(k\right)\right)\\ &-p^{T}\left(Z_{1}\tilde{x}_{p}\left(k\right)-r\right)P_{5}\left(r\right)g\left(Z_{1}\tilde{x}_{p}\left(k\right)\right)\\ &-p^{T}\left(Z_{1}\tilde{x}_{p}\left(k\right)-r\right)P_{5}\left(r\right)g\left(Z_{1}\tilde{x}_{p}\left(k\right)\right)\\ &-p^{T}\left(Z_{1}\tilde{x}_{p}\left(k\right)-r\right)P_{5}\left(r\right)g\left(Z_{1}\tilde{x}_{p}\left(k\right)\right)\\ &-p^{T}\left(Z_{1}\tilde{x}_{p}\left(k\right)-r\right)P_{5}\left(r\right)P_{5}\left(r\right)\left(r\right)P_{5}\left(r\right)P_{5}\left(r\right)P_{5}\left(r\right)P_{5}\left(r\right)P_{5}\left(r\right)P_{$$

$$\leq \sum_{s=1}^{d} \pi_{rs} \sum_{j=-d}^{-1} \zeta^{T}(k) P_{6}(s) \zeta(k) \\
- \sum_{j=-r}^{-1} \zeta^{T}(k+j) P_{6}(r) \zeta(k+j) \\
+ \sum_{s=1}^{d} \pi_{rs} \sum_{j=-d}^{-1} \sum_{i=k+1+j}^{k-1} \zeta^{T}(i) P_{6}(s) \zeta(i) \\
- \sum_{j=-r}^{-1} \sum_{i=k+1+j}^{k-1} \zeta^{T}(i) P_{6}(r) \zeta(i) + \frac{d^{2}+d}{2} \zeta^{T}(k) P_{6}\zeta(k) \\
- \sum_{j=-d}^{-1} \sum_{i=k+1+j}^{k-1} \zeta^{T}(i) P_{6}\zeta(i) - \sum_{j=-d}^{-1} \zeta^{T}(k+j) P_{6}\zeta(k+j) \\
\leq \zeta^{T}(k) \Omega_{56}\zeta(k) - \sum_{j=-r}^{-1} \zeta^{T}(k+j) \Omega_{45} \sum_{j=-r}^{-1} \zeta(k+j). \tag{25}$$

In view of (7), we can conclude that

$$g_i(s)[g_i(s) - l_i s] \le 0, \quad \forall s \in R, i = 1, 2, ..., n.$$
 (26)

Then, it follows from (26) that

$$-g^{T}\left(Z_{1}\widetilde{x}_{p}\left(k\right)\right)\varsigma g\left(Z_{1}\widetilde{x}_{p}\left(k\right)\right)-2\widetilde{x}_{p}^{T}\left(k\right)Z_{1}^{T}\varsigma Lg\left(Z_{1}\widetilde{x}_{p}\left(k\right)\right)$$

$$\geq0,$$

$$-g^{T}\left(Z_{1}\widetilde{x}_{p}\left(k+1\right)\right)\mu g\left(Z_{1}\widetilde{x}_{p}\left(k+1\right)\right)$$

$$-2\widetilde{x}_{p}^{T}\left(k+1\right)Z_{1}^{T}\mu Lg\left(Z_{1}\widetilde{x}_{p}\left(k+1\right)\right)\geq0.$$
(27)

Now, combining (23)-(25) and (27) results in

$$E\left\{V\left(\Theta_{k+1}, k+1, d\left(k+1\right)\right) \mid \Theta_{k}, d\left(k\right) = r\right\} - V\left(\Theta_{k}, k, r\right) \leq \xi^{T}\left(k\right) \Omega \xi\left(k\right),$$
(28)

where $\xi^T(k) = [\widetilde{x}_m^T(k)\ \widetilde{x}_p^T(k)\ \widetilde{x}_m^T(k-r)\ g^T(Z_1\widetilde{x}_p(k-r))$ $g^T(Z_1\widetilde{x}_p(k))\ g^T(Z_1\widetilde{x}_p(k+1))]$, and Ω is defined as in (18). Due to (18), formula (28) results in

$$E\left\{V\left(\Theta_{k+1}, k+1, d\left(k+1\right)\right) \mid \Theta_{k}, d\left(k\right) = r\right\}$$

$$\leq V\left(\Theta_{k}, k, r\right) - \lambda_{\min}\left\{\widetilde{x}_{m}^{T}\left(k\right)\widetilde{x}_{m}\left(k\right) + \widetilde{x}_{p}^{T}\left(k\right)\widetilde{x}_{p}\left(k\right)\right\},\tag{29}$$

where λ_{min} denotes the minimal eigenvalue of $-\Omega$. Since

$$E\left\{E\left\{V\left(\Theta_{k+1}, k+1, d\left(k+1\right)\right) \mid \Theta_{k}, d\left(k\right)\right\} \mid \Theta_{0}, d\left(0\right)\right\} = E\left\{V\left(\Theta_{k+1}, k+1, d\left(k+1\right)\right) \mid \Theta_{0}, d\left(0\right)\right\},$$
(30)

we obtain

$$E\left\{\left\|\widetilde{x}_{m}\left(k\right)\right\|^{2}+\left\|\widetilde{x}_{p}\left(k\right)\right\|^{2}\mid\Theta_{0},d\left(0\right)\right\}\leq\lambda_{\min}^{-1}V\left(\Theta_{0},0,d\left(0\right)\right)$$
< \infty.
(31)

by taking the conditional expectation $E\{\cdot \mid \Theta_0, d(0)\}$ and summing from k=0 to $+\infty$ on both sides of (29). Consequently, by Definition 2, one can conclude from the above inequality that the filtering error system (11) is stochastically stable, and the proof is thus completed.

Remark 6. It is worth noting that the H_{∞} filtering problem for (8) has been studied in [26], but the obtained results in [26] are not dependent on the transition probability matrix of the random delay described by a Markovian chain. In order to reduce the conservatism and give the explicit expression of the desired filter, in the above theorem we have constituted intensive studying of the H_{∞} filtering problem for (8) and have investigated a result dependent on the transition probability matrix of the random delay described by a Markovian chain.

Remark 7. The novel Lyapunov functional in this paper is selected to be of (21). Since in (21) we have not only chosen the triple summation term but also considered sufficiently the information of the random delay described by a Markovian chain, the conservatism might be reduced than one in [26], which will be illustrated through a numerical example in Section 4.

Theorem 5 does not give a design procedure for the desired filter. Based on Theorem 5, the following theorem offers an approach to design a H_{∞} filter for GRN (8) such that the filtering error system (11) is stochastically stable with H_{∞} disturbance attenuation level γ .

Theorem 8. For given a scalar $\gamma > 0$ and a positive integer d, if for each $r \in \mathcal{N}$, there exist matrices $P_i^T(r) = P_i(r) > 0$ (i = 1, 2, ..., 6), $P_j^T = P_j > 0$ (j = 2, 3, 5, 6),

$$R_k := \begin{bmatrix} R_{k1} & R_{k2} \\ R_{k3} & R_{k2} \end{bmatrix}^T$$
, $\det R_{k2} \neq 0$, $k = 1, 2$, (32)

 $\varsigma := \operatorname{diag}(\varsigma_1, \varsigma_2, \dots, \varsigma_n) > 0, \ \mu := \operatorname{diag}(\mu_1, \mu_2, \dots, \mu_n) > 0, \ \overline{A}_f, \ \overline{B}_f, \ \overline{C}_f, \ \overline{D}_f, \ G_{1f}, \ H_{1f}, \ G_{2f}, \ and \ H_{2f}, \ such \ that \ the \ following \ LMIs (34) \ and (35) \ hold, \ then \ the \ filtering \ error \ system (11) \ is stochastically \ stable \ with \ H_{\infty} \ disturbance \ attenuation \ level \ \gamma.$ Moreover, the required filter is given by (9) with

$$A_{f} = R_{12}^{-1} \overline{A}_{f}, \qquad B_{f} = R_{12}^{-1} \overline{B}_{f},$$

$$C_{f} = R_{22}^{-1} \overline{C}_{f}, \qquad D_{f} = R_{22}^{-1} \overline{D}_{f},$$
(33)

$$\Upsilon := \begin{bmatrix}
\Upsilon_{11} & 0 & 0 & 0 & 0 & \Upsilon_{16} \\
* & \Upsilon_{22} & 0 & 0 & 0 & \Upsilon_{26} \\
* & * & \Upsilon_{33} & 0 & 0 & \Upsilon_{36} \\
* & * & * & -I & 0 & \Upsilon_{46} \\
* & * & * & * & -I & \Upsilon_{56} \\
* & * & * & * & * & \Upsilon_{66}
\end{bmatrix} < 0,$$
(34)

$$\overline{P}_{j}(r) < P_{j}, \quad j = 2, 3, 5, 6,$$
 (35)

where

$$Y_{11} = \overline{P}_{1}(r) - R_{1} - R_{1}^{T},$$

$$Y_{22} = d\overline{P}_{3}(r) + \frac{d^{2} + d}{2}P_{3} - R_{1} - R_{1}^{T},$$

$$Y_{33} = \overline{P}_{4}(r) - R_{2} - R_{2}^{T},$$

$$\overline{P}_{i}(r) = \sum_{s=1}^{d} \pi_{rs}P_{i}(s), \quad i = 1, 2, ..., 6,$$

$$Y_{16} = R_{1}^{T}\Psi_{1} + (Z_{1} + Z_{2})^{T}(\overline{B}_{f}\Psi_{2} + \overline{A}_{f}\Psi_{3}),$$

$$Y_{26} = R_{1}^{T}\Psi_{4} + (Z_{1} + Z_{2})^{T}(\overline{B}_{f}\Psi_{2} + \overline{A}_{f}\Psi_{3}),$$

$$Y_{36} = R_{2}^{T}\Psi_{5} + (Z_{1} + Z_{2})^{T}(\overline{D}_{f}\Psi_{6} + \overline{C}_{f}\Psi_{7}),$$

$$Z_{1} = \begin{bmatrix} I & 0 \end{bmatrix}, \quad Z_{2} = \begin{bmatrix} 0 & I \end{bmatrix},$$

$$\Psi_{1} = \begin{bmatrix} AZ_{1} & 0 & 0 & B & 0 & 0 & E_{1} & 0 \\ 0 & 0 & 0 & 0 & 0 & 0 & 0 & 0 \end{bmatrix},$$

$$\Psi_{2} = \begin{bmatrix} C_{1}Z_{1} & 0 & 0 & 0 & 0 & 0 & E_{2} & 0 \end{bmatrix},$$

$$\Psi_{3} = \begin{bmatrix} Z_{2} & 0 & 0 & 0 & 0 & 0 & 0 & E_{1} & 0 \\ -Z_{2} & 0 & 0 & 0 & 0 & 0 & 0 & 0 \end{bmatrix},$$

$$\Psi_{4} = \begin{bmatrix} AZ_{1} & 0 & 0 & B & 0 & 0 & E_{1} & 0 \\ -Z_{2} & 0 & 0 & 0 & 0 & 0 & 0 & 0 \end{bmatrix},$$

$$\Psi_{5} = \begin{bmatrix} 0 & CZ_{1} & DZ_{1} & 0 & 0 & 0 & 0 & F_{1} \\ 0 & 0 & 0 & 0 & 0 & 0 & 0 & 0 \end{bmatrix},$$

$$\Psi_{6} = \begin{bmatrix} 0 & CZ_{1} & DZ_{1} & 0 & 0 & 0 & 0 & F_{2} \end{bmatrix},$$

$$\Psi_{7} = \begin{bmatrix} 0 & Z_{2} & 0 & 0 & 0 & 0 & 0 & \overline{H}_{1f} & 0 \end{bmatrix},$$

$$Y_{66} = \begin{bmatrix} \overline{G}_{1f} & 0 & 0 & 0 & 0 & 0 & \overline{H}_{2f} \end{bmatrix},$$

$$\Phi_{2} = \begin{bmatrix} 0 & 0 & 0 & 0 & 0 & -F_{1}^{T}\mu L \end{bmatrix}^{T},$$

and L, \overline{G}_{1f} , \overline{G}_{2f} , \overline{H}_{1f} , and \overline{H}_{2f} are defined as previously.

Proof. A_f , B_f , C_f , and D_f are defined as in (33). Then it is easy to verify that $\Upsilon_{16} = R_1^T \overline{\Lambda}_1$, $\Upsilon_{26} = R_1^T \overline{\Lambda}_2$, and $\Upsilon_{36} = R_2^T \overline{\Lambda}_3$, where

$$\overline{\Lambda}_{1} = \begin{bmatrix} \Lambda_{1} & \overline{E} & 0 \end{bmatrix}, \qquad \overline{\Lambda}_{2} = \begin{bmatrix} \Lambda_{2} & \overline{E} & 0 \end{bmatrix},
\overline{\Lambda}_{3} = \begin{bmatrix} \Lambda_{3} & 0 & \overline{F} \end{bmatrix},$$
(37)

(36)

and Λ_1 , Λ_2 , Λ_3 , \overline{E} , and \overline{F} are defined as previously. This, together with (34) and Lemma 4, implies that

$$\begin{bmatrix} -\overline{P}_{1}^{-1}(r) & 0 & 0 & 0 & 0 & \overline{\Lambda}_{1} \\ * & -\left(d\overline{P}_{3}(r) + \frac{d^{2} + d}{2}P_{3}\right)^{-1} & 0 & 0 & 0 & \overline{\Lambda}_{2} \\ * & * & -\overline{P}_{4}^{-1}(r) & 0 & 0 & \overline{\Lambda}_{3} \\ * & * & * & -I & 0 & \Upsilon_{46} \\ * & * & * & * & -I & \Upsilon_{56} \\ * & * & * & * & * & \Upsilon_{66} \end{bmatrix} < 0.$$

$$(38)$$

Due to the Schur complement lemma, inequality (38) is equal to

$$\Phi + \overline{\Phi} < 0, \tag{39}$$

where

$$\overline{\Phi} = \begin{bmatrix} 0 & 0 & 0 \\ 0 & -\gamma^{2}I & 0 \\ 0 & 0 & -\gamma^{2}I \end{bmatrix} + \Upsilon_{46}^{T} \Upsilon_{46} + \Upsilon_{56}^{T} \Upsilon_{56},$$

$$\Phi = \begin{bmatrix} \widetilde{\Omega} & 0 & \Phi_{2} \\ 0 & 0 & 0 \\ \Phi_{2}^{T} & 0 & 0 \end{bmatrix} + \overline{\Lambda}_{1}^{T} \overline{P}_{1}(r) \overline{\Lambda}_{1}$$

$$+ \overline{\Lambda}_{2}^{T} \left(d\overline{P}_{3}(r) + \frac{d^{2} + d}{2} P_{3} \right) \overline{\Lambda}_{2} + \overline{\Lambda}_{3}^{T} \overline{P}_{4}(r) \overline{\Lambda}_{3}.$$
(40)

Thus

$$\Lambda := \Upsilon_{66} + \overline{\Lambda}_{1}^{T} \overline{P}_{1}(r) \overline{\Lambda}_{1} + \overline{\Lambda}_{2}^{T} \left(d\overline{P}_{3}(r) + \frac{d^{2} + d}{2} P_{3} \right) \overline{\Lambda}_{2}$$

$$+ \overline{\Lambda}_{3}^{T} \overline{P}_{4}(r) \overline{\Lambda}_{3} < 0. \tag{41}$$

Noting that Ω is a submatrix of Λ , we can conclude that $\Omega < 0$. By Theorem 5, the filtering error system (11) with w(k) = 0 and v(k) = 0 is stochastically stable.

Choose the same Lyapunov function as in (21) for the filtering error system (11) and employ the similar approach in the proof of Theorem 5, one has

$$\Delta V_{k} := E\left\{V\left(\Theta_{k+1}, k+1, d\left(k+1\right)\right) \mid \Theta_{k}, d\left(k\right) = r\right\}$$

$$-V\left(\Theta_{k}, k, r\right)$$

$$\leq E\left\{\delta^{T}\left(k\right) \Phi \delta\left(k\right)\right\},$$

$$(42)$$

where $\delta(k) = \left[\xi^T(k) \ w^T(k) \ v^T(k)\right]^T$, and $\xi(k)$ is defined as previously. To deal with the H_{∞} performance, the following performance function is considered

$$J_{K} := \sum_{k=0}^{K} E\left\{\begin{bmatrix} e_{m}(k) \\ e_{p}(k) \end{bmatrix}^{T} \begin{bmatrix} e_{m}(k) \\ e_{p}(k) \end{bmatrix} - \gamma^{2} \begin{bmatrix} w(k) \\ v(k) \end{bmatrix}^{T} \begin{bmatrix} w(k) \\ v(k) \end{bmatrix} \mid \Theta_{0}, d(0) \right\}.$$

$$(43)$$

Due to the zero initial condition and

$$E\left\{E\left\{V\left(\Theta_{k+1}, k+1, d\left(k+1\right)\right) \mid \Theta_{k}, d\left(k\right)\right\} \mid \Theta_{0}, d\left(0\right)\right\}$$

$$= E\left\{V\left(\Theta_{k+1}, k+1, d\left(k+1\right)\right) \mid \Theta_{0}, d\left(0\right)\right\},$$
(44)

it is easy to see from (39) and (42) that

$$J_{K} = \sum_{k=0}^{K} E\left\{ \begin{bmatrix} e_{m}(k) \\ e_{p}(k) \end{bmatrix}^{T} \begin{bmatrix} e_{m}(k) \\ e_{p}(k) \end{bmatrix} - \gamma^{2} \begin{bmatrix} w(k) \\ v(k) \end{bmatrix}^{T} \begin{bmatrix} w(k) \\ v(k) \end{bmatrix} + \Delta V_{k} \mid \Theta_{0}, d(0) \right\}$$

$$- \sum_{k=0}^{K} E\left\{ \Delta V_{k} \mid \Theta_{0}, d(0) \right\}$$

$$= \sum_{k=0}^{K} E\left\{ \begin{bmatrix} e_{m}(k) \\ e_{p}(k) \end{bmatrix}^{T} \begin{bmatrix} e_{m}(k) \\ e_{p}(k) \end{bmatrix} - \gamma^{2} \begin{bmatrix} w(k) \\ v(k) \end{bmatrix}^{T} \begin{bmatrix} w(k) \\ v(k) \end{bmatrix} + \Delta V_{k} \mid \Theta_{0}, d(0) \right\}$$

$$- E\left\{ V\left(\Theta_{K+1}, K+1, d(K+1)\right) \mid \Theta_{0}, d(0) \right\}$$

$$+ V\left(\Theta_{0}, 0, d(0)\right)$$

$$\leq \sum_{k=0}^{K} E\left\{ e_{m}^{T}(k) e_{m}(k) + e_{p}^{T}(k) e_{p}(k) - \gamma^{2} w^{T}(k) w(k) - \gamma^{2} v^{T}(k) v(k) + \Delta V_{k} \mid \Theta_{0}, d(0) \right\}$$

$$\leq \sum_{k=0}^{K} E\left\{ \delta^{T}(k) \left(\Phi + \overline{\Phi}\right) \delta(k) \mid \Theta_{0}, d(0) \right\} < 0. \tag{45}$$

Let $k \to \infty$; it is concluded from Definition 3 that the filtering error system (11) is stochastically stable with H_{∞} disturbance attenuation level γ .

The proof is thus completed.

Remark 9. What can be seen from Theorem 8 is that the scalar γ can be calculated as an optimization variable to obtain the minimum H_{∞} disturbance attenuation level. To be more specific, the minimal H_{∞} disturbance attenuation level

can be obtained by solving the following convex optimization problem:

$$\min_{\text{s.t. } (34)-(35)} \beta, \quad \beta = \gamma^2.$$
 (46)

Note that if there exists a solution β^* to the problem (46), then the minimal H_{∞} disturbance attenuation level is $\sqrt{\beta^*}$.

4. Illustrative Example

In this section we illustrate the effectiveness of the proposed approach by testing the following numerical example which has been used in [26].

Consider GRN (8) with the following parameters:

$$A = \begin{bmatrix} 0.3679 & 0 & 0 \\ 0 & 0.3679 & 0 \\ 0 & 0 & 0.3679 \end{bmatrix},$$

$$B = \begin{bmatrix} 0 & 0 & -0.126 \\ -0.126 & 0 & 0 \\ 0 & -0.126 & 0 \end{bmatrix},$$

$$E_1 = \begin{bmatrix} 0.3 \\ 0.5 \\ 0 \end{bmatrix}, \qquad F_1 = \begin{bmatrix} 0.6 \\ 0.4 \\ 0.2 \end{bmatrix},$$

$$C = \begin{bmatrix} 0.3679 & 0 & 0 \\ 0 & 0.6065 & 0 \\ 0 & 0 & 0.3679 \end{bmatrix},$$

$$D = \begin{bmatrix} 0.6321 & 0 & 0 \\ 0 & 0.3935 & 0 \\ 0 & 0 & 0.6321 \end{bmatrix},$$

$$E_2 = \begin{bmatrix} 0.5 \\ 0.4 \\ 0.2 \end{bmatrix}, \qquad F_2 = \begin{bmatrix} 0.2 \\ 0.6 \\ 0.3 \end{bmatrix},$$

$$G_2 = G_1 = C_2 = C_1 = \begin{bmatrix} 0.3 & 0 & 0 \\ 0 & 0.2 & 0 \\ 0 & 0 & 0.3 \end{bmatrix}.$$

The regulation function is taken as $g_i(x) = x^2/(1+x^2)$ (i = 1, 2, 3). It is easy to know that the derivative of $g_i(x)$ is less than l = 0.65, which shows L = diag(-0.325, -0.325, -0.325). Suppose the bound of the time delay is d = 3: then $d(k) \in \mathcal{N} = \{1, 2, 3\}$. The transition probability matrix Π is given by

$$\Pi = \begin{bmatrix} 0.3 & 0.5 & 0.2 \\ 0.4 & 0.3 & 0.3 \\ 0.2 & 0.5 & 0.3 \end{bmatrix}. \tag{48}$$

By solving the optimization problem (46), it can be obtained that the optimal disturbance attenuation level γ^* is 0.2289,

which is better than one (i.e., 1.5046) in [26]. And the corresponding filter gain matrices are as follows:

$$A_{f} = \begin{bmatrix} 0.3033 & 0.0362 & -0.0085 \\ -0.1172 & 0.0675 & 0.0442 \\ -0.0196 & -0.0232 & 0.3032 \end{bmatrix},$$

$$B_{f} = \begin{bmatrix} -1.3657 & 1.0166 & -0.1168 \\ 0.2405 & -1.8421 & -0.0969 \\ 0.0521 & 0.4326 & -1.7666 \end{bmatrix},$$

$$C_{f} = \begin{bmatrix} 0.0604 & -0.0945 & -0.0015 \\ -0.2121 & 0.4325 & 0.0640 \\ -0.1054 & 0.1555 & 0.1184 \end{bmatrix},$$

$$D_{f} = \begin{bmatrix} 0.4505 & -2.1899 & -0.2779 \\ 0.0936 & -1.8583 & 0.3270 \\ -0.4267 & 1.2589 & -2.8255 \end{bmatrix},$$

$$G_{1f} = \begin{bmatrix} -0.0965 & -0.1809 & 0.0340 \\ -0.0772 & -0.1447 & 0.0272 \\ -0.0386 & -0.0724 & 0.0136 \end{bmatrix},$$

$$G_{2f} = \begin{bmatrix} 0.0413 & -0.0725 & -0.0097 \\ 0.1240 & -0.2175 & -0.0292 \\ 0.0620 & -0.1087 & -0.0146 \end{bmatrix},$$

$$H_{1f} = \begin{bmatrix} 0.6784 & -0.9047 & 0.1134 \\ -0.2573 & 0.2762 & 0.0907 \\ -0.1286 & -0.3619 & 1.0454 \end{bmatrix},$$

$$H_{2f} = \begin{bmatrix} 1.1304 & -0.3575 & -0.0320 \\ 0.3912 & -0.0724 & -0.0960 \\ 0.1956 & -0.5362 & 0.9520 \end{bmatrix}.$$

In the following simulation setup, the noise signal is chosen as

$$w(k) = v(k) = \begin{cases} \sin(0.3k), & k \le 20, \\ 0, & k > 20. \end{cases}$$
 (50)

Let the filtering error system run by random sequence d(k), the trajectories and their estimations of the mRNAs and proteins are shown in Figures 1 and 2, where the solid line and dotted line describe the state trajectories and estimations of mRNAs and proteins, respectively. The filtering errors are shown in Figures 3 and 4. It can be seen from Figures 3 and 4 that the filtering error converges to zero in the absence of disturbances.

Next, we illustrate the H_{∞} performance of the filtering error system (11). By direct computation, we have

$$\sum_{k=0}^{60} \begin{bmatrix} w(k) \\ v(k) \end{bmatrix}^T \begin{bmatrix} w(k) \\ v(k) \end{bmatrix} = 20.9454.$$
 (51)

For values of 1000 random sequences of d(k), we obtain by MATLAB that the maximum of $\sum_{k=0}^{60} \left[\frac{e_m(k)}{e_p(k)}\right]^T \left[\frac{e_m(k)}{e_p(k)}\right]$ is

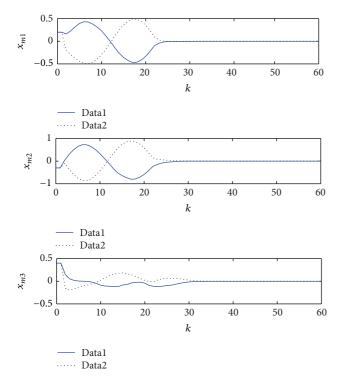


FIGURE 1: Trajectories and estimations of mRNAs.

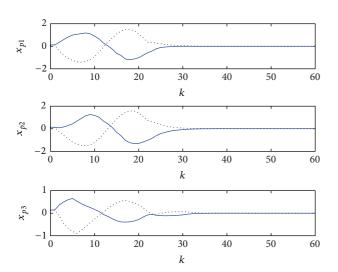


FIGURE 2: Trajectories and estimations of proteins.

0.1647, and hence the maximum disturbance attenuation level is

$$\sqrt{\frac{\sum_{k=0}^{60} \begin{bmatrix} e_{m}(k) \\ e_{p}(k) \end{bmatrix}^{T} \begin{bmatrix} e_{m}(k) \\ e_{p}(k) \end{bmatrix}}{\sum_{k=0}^{60} \begin{bmatrix} w(k) \\ v(k) \end{bmatrix}^{T} \begin{bmatrix} w(k) \\ v(k) \end{bmatrix}}} = \sqrt{\frac{0.1647}{20.9454}} = 0.0887 < \gamma^{*}.$$
(52)

This verifies that the H_{∞} disturbance attenuation level is below the given upper bound.

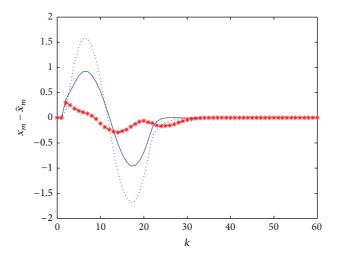


FIGURE 3: Estimation error of mRNAs.

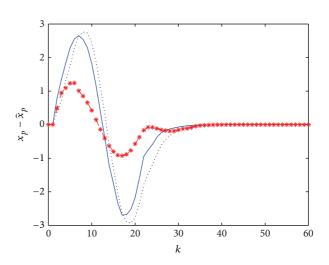


FIGURE 4: Estimation error of proteins.

5. Conclusion

In this paper, we investigate the filtering problem on a class of discrete-time GRNs with random delays. The filtering error system is established as a Markovian switched system and the random delay is described as a Markovian chain. By introducing an appropriate Lyapunov function, sufficient conditions for concerned problems are derived in terms of LMIs. The designed filter guarantees that the filtering error system is stochastically stable with H_{∞} disturbance attenuation level. Finally, the effectiveness and performance of the obtained results are demonstrated by a numerical example.

Conflict of Interests

The authors declare that there is no conflict of interests regarding the publication of this paper.

Acknowledgments

This work is supported by the National Natural Science Foundation of China under Grant no. 11371006, the fund of Heilongjiang Province Innovation Team Support Plan under Grant no. 2012TD007, the fund of Heilongjiang University Innovation Team Support Plan under Grant no. Hdtd2010-03, the Fund of Key Laboratory of Electronics Engineering, College of Heilongjiang Province, (Heilongjiang University), China, the fund of Heilongjiang Education Committee, and the Heilongjiang University Innovation Fund for Graduates. The authors thank the anonymous referees for their helpful comments and suggestions which improve greatly this note.

References

- [1] F. K. Ahmad, S. Deris, and N. H. Othman, "The inference of breast cancer metastasis through gene regulatory networks," *Journal of Biomedical Informatics*, vol. 45, no. 2, pp. 350–362, 2012.
- [2] H.-Y. Yeh, S.-W. Cheng, Y.-C. Lin, C.-Y. Yeh, S.-F. Lin, and V.-W. Soo, "Identifying significant genetic regulatory networks in the prostate cancer from microarray data based on transcription factor analysis and conditional independency," *BMC Medical Genomics*, vol. 2, article 70, 2009.
- [3] R. Somogyi and C. A. Sniegoski, "Modeling the complexity of genetic networks: understanding multigenic and pleiotropic regulation," *Complexity*, vol. 1, no. 6, pp. 45–63, 1995/96.
- [4] D. C. Weaver, C. T. Workman, and G. D. Stormo, "Modeling regulatory networks with weight matrices," in *Proceedings of the Pacific Symposium on Biocomputing*, vol. 4, pp. 112–123, World Scientific, Maui, Hawaii, 1999.
- [5] M. B. Elowitz and S. Leibier, "A synthetic oscillatory network of transcriptional regulators," *Nature*, vol. 403, no. 6767, pp. 335– 338, 2000.
- [6] T. Chen, H. L. He, and G. M. Church, "Modeling gene expression with differential equations," *Pacific Symposium on Biocomputing*, vol. 4, pp. 29–40, 1999.
- [7] D. Thieffry and R. Thomas, "Qualitative analysis of gene networks," *Pacific Symposium on Biocomputing*, vol. 3, pp. 77– 88, 1998.
- [8] L. Chen and K. Aihara, "Stability of genetic regulatory networks with time delay," *IEEE Transactions on Circuits and Systems I*, vol. 49, no. 5, pp. 602–608, 2002.
- [9] X. Zhang, A. H. Yu, and G. D. Zhang, "M-matrix-based delay-range-dependent global asymptotical stability criterion for genetic regulatory networks with time-varying delays," *Neurocomputing*, vol. 113, pp. 8–15, 2013.
- [10] Y. He, J. Zeng, M. Wu, and C.-K. Zhang, "Robust stabilization and H_{∞} controllers design for stochastic genetic regulatory networks with time-varying delays and structured uncertainties," *Mathematical Biosciences*, vol. 236, no. 1, pp. 53–63, 2012.
- [11] F.-X. Wu, "Stability and bifurcation of ring-structured genetic regulatory networks with time delays," *IEEE Transactions on Circuits and Systems I*, vol. 59, no. 6, pp. 1312–1320, 2012.
- [12] Y. T. Wang, A. H. Yu, and X. Zhang, "Robust stability of stochastic genetic regulatory networks with time-varying delays: a delay fractioning approach," *Neural Computing and Applications*, vol. 23, no. 5, pp. 1217–1227, 2013.
- [13] J. H. Koo, D. H. Ji, S. C. Won, and J. H. Park, "An improved robust delay-dependent stability criterion for genetic regulatory

- networks with interval time delays," *Communications in Nonlinear Science and Numerical Simulation*, vol. 17, no. 8, pp. 3399–3405, 2012.
- [14] J. Liu and D. Yue, "Asymptotic and robust stability of T-S fuzzy genetic regulatory networks with time-varying delays," *International Journal of Robust and Nonlinear Control*, vol. 22, no. 8, pp. 827–840, 2012.
- [15] W. Wang and S. Zhong, "Delay-dependent stability criteria for genetic regulatory networks with time-varying delays and nonlinear disturbance," *Communications in Nonlinear Science* and Numerical Simulation, vol. 17, no. 9, pp. 3597–3611, 2012.
- [16] P. Li, J. Lam, and Z. Shu, "On the transient and steadystate estimates of interval genetic regulatory networks," *IEEE Transactions on Systems, Man, and Cybernetics B*, vol. 40, no. 2, pp. 336–349, 2010.
- [17] B. Lv, J. Liang, and J. Cao, "Robust distributed state estimation for genetic regulatory networks with Markovian jumping parameters," *Communications in Nonlinear Science and Numerical Simulation*, vol. 16, no. 10, pp. 4060–4078, 2011.
- [18] J. Liang, J. Lam, and Z. Wang, "State estimation for Markov-type genetic regulatory networks with delays and uncertain mode transition rates," *Physics Letters A*, vol. 373, no. 47, pp. 4328–4337, 2009.
- [19] W. Yu, J. Lü, G. Chen, Z. Duan, and Q. Zhou, "Estimating uncertain delayed genetic regulatory networks: an adaptive filtering approach," *IEEE Transactions on Automatic Control*, vol. 54, no. 4, pp. 892–897, 2009.
- [20] M. Mohammadian, A. Hossein Abolmasoumi, and H. Reza Momeni, " H_{∞} mode-independent filter design for Markovian jump genetic regulatory networks with time-varying delays," Neurocomputing, vol. 87, pp. 10–18, 2012.
- [21] B. Chen, L. Yu, and W.-A. Zhang, "H_∞ filtering for Markovian switching genetic regulatory networks with time-delays and stochastic disturbances," *Circuits, Systems, and Signal Process*ing, vol. 30, no. 6, pp. 1231–1252, 2011.
- [22] W. Wang, S. Zhong, and F. Liu, "Robust filtering of uncertain stochastic genetic regulatory networks with time-varying delays," *Chaos, Solitons & Fractals*, vol. 45, no. 7, pp. 915–929, 2012.
- [23] D. Zhang, L. Yu, and Q.-G. Wang, "Exponential H_{∞} filtering for switched stochastic genetic regulatory networks with random sensor delays," *Asian Journal of Control*, vol. 13, no. 5, pp. 749–755, 2011.
- [24] T. Wang, Y. S. Ding, L. Zhang, and K. R. Hao, "Robust state estimation for discrete-time stochastic genetic regulatory networks with probabilistic measurement delays," *Neurocomputing*, vol. 111, pp. 1–12, 2013.
- [25] D. Zhang, H. Song, L. Yu, Q.-G. Wang, and C. Ong, "Set-values filtering for discrete time-delay genetic regulatory networks with time-varying parameters," *Nonlinear Dynamics*, vol. 69, no. 1-2, pp. 693–703, 2012.
- [26] A. Liu, L. Yu, W.-A. Zhang, and B. Chen, " H_{∞} filtering for discrete-time genetic regulatory networks with random delays," *Mathematical Biosciences*, vol. 239, no. 1, pp. 97–105, 2012.
- [27] J. Cao and F. Ren, "Exponential stability of discrete-time genetic regulatory networks with delays," *IEEE Transactions on Neural Networks*, vol. 19, no. 3, pp. 520–523, 2008.
- [28] Q. Ye and B. Cui, "Mean square exponential and robust stability of stochastic discrete-time genetic regulatory networks with uncertainties," *Cognitive Neurodynamics*, vol. 4, no. 2, pp. 165–176, 2010.

- [29] Q. Ma, S. Xu, Y. Zou, and J. Lu, "Robust stability for discretetime stochastic genetic regulatory networks," *Nonlinear Analy*sis. Real World Applications, vol. 12, no. 5, pp. 2586–2595, 2011.
- [30] K. Mathiyalagan and R. Sakthivel, "Robust stabilization and H_{∞} control for discrete-time stochastic genetic regulatory networks with time delays," *Canadian Journal of Physics*, vol. 90, no. 10, pp. 939–953, 2012.
- [31] K. Mathiyalagan, R. Sakthivel, and S. M. Anthoni, "New robust passivity criteria for discrete-time genetic regulatory networks with Markovian jumping parameters," *Canadian Journal of Physics*, vol. 90, no. 2, pp. 107–118, 2012.
- [32] L. G. Wu, X. J. Su, and P. Shi, "Output feedback control of Markovian jump repeated scalar nonlinear systems," *IEEE Transactions on Automatic Control*, vol. 59, no. 1, pp. 199–204, 2014
- [33] L. Wu, P. Shi, and H. Gao, "State estimation and sliding-mode control of Markovian jump singular systems," *IEEE Transactions on Automatic Control*, vol. 55, no. 5, pp. 1213–1219, 2010.
- [34] L. Wu, X. Su, and P. Shi, "Sliding mode control with bounded L_2 gain performance of Markovian jump singular time-delay systems," *Automatica*, vol. 48, no. 8, pp. 1929–1933, 2012.
- [35] L. Wu, P. Shi, H. Gao, and C. Wang, " H_{∞} filtering for 2D Markovian jump systems," *Automatica*, vol. 44, no. 7, pp. 1849–1858, 2008.
- [36] L. Wu, X. Yao, and W. X. Zheng, "Generalized H₂ fault detection for two-dimensional Markovian jump systems," *Automatica*, vol. 48, no. 8, pp. 1741–1750, 2012.
- [37] X. J. Su, L. G. Wu, and P. Shi, "Sensor networks with random link failures: distributed filtering for T-S fuzzy systems," *IEEE Transactions on Industrial Informatics*, vol. 9, no. 3, pp. 1739–1750, 2013.
- [38] L. Wu and D. W. C. Ho, "Fuzzy filter design for Itô stochastic systems with application to sensor fault detection," *IEEE Transactions on Fuzzy Systems*, vol. 17, no. 1, pp. 233–242, 2009.
- [39] X. Su, P. Shi, L. Wu, and S. K. Nguang, "Induced filtering of fuzzy stochastic systems with time-varying delays," *IEEE Transactions* on Computers, vol. 43, no. 4, pp. 1251–1264, 2012.
- [40] A. Hmamed, C. E. Kasri, E. H. Tissir, T. Alvarez, and F. Tadeo, "Robust H_{∞} filtering for uncertain 2-D continuous systems with delays," *International Journal of Innovative Computing Information and Control*, vol. 9, no. 5, pp. 2167–2183, 2013.
- [41] F. B. Li and X. Zhang, "Delay-range-dependent robust H1 filtering for singular LPV systems with time variant delay," *International Journal of Innovative Computing Information and Control*, vol. 9, no. 1, pp. 339–353, 2013.
- [42] J. Liang and J. Lam, "Robust state estimation for stochastic genetic regulatory networks," *International Journal of Systems Science*, vol. 41, no. 1, pp. 47–63, 2010.
- [43] M. C. de Oliveira, J. Bernussou, and J. C. Geromel, "A new discrete-time robust stability condition," *Systems & Control Letters*, vol. 37, no. 4, pp. 261–265, 1999.

Hindawi Publishing Corporation Abstract and Applied Analysis Volume 2014, Article ID 863902, 8 pages http://dx.doi.org/10.1155/2014/863902

Research Article

Adaptive Neural Networks Synchronization of a Four-Dimensional Energy Resource Stochastic System

Duo Meng

School of Civil and Architectural Engineering, Liaoning University of Technology, Jinzhou 121001, China

Correspondence should be addressed to Duo Meng; mengduo2004@163.com

Received 31 December 2013; Accepted 19 January 2014; Published 2 March 2014

Academic Editor: Ming Liu

Copyright © 2014 Duo Meng. This is an open access article distributed under the Creative Commons Attribution License, which permits unrestricted use, distribution, and reproduction in any medium, provided the original work is properly cited.

An adaptive neural networks chaos synchronization control method is proposed for a four-dimensional energy resource demandsupply system with input constraints. Assuming the response system contains unknown uncertain nonlinearities and unknown stochastic disturbances, the neural networks and robust terms are used to identify the nonlinearities and overcome the stochastic disturbances, respectively. Based on stochastic Lyapunov stability and robust adaptive theories, an adaptive neural networks synchronization control method is developed. In the design process, an auxiliary design system is employed to address input constraints. Simulation results, which fully coincide with theoretical results, are presented to demonstrate the obtained results.

1. Introduction

Energy resource system is a kind of complex nonlinear system. Over the last two decades, much attention has been paid to the chaos synchronization in this class system. Reference [1] established a three-dimensional energy resource demand-supply system based on the real energy resources demand-supply system in the East and the West of China. By adding a new variable to consider the renewable resources, a four-dimensional energy resource system was proposed in [2]. The dynamics behaviors of the four-dimensional energy resource system have been analyzed by means of the Lyapunov exponents and bifurcation diagrams. Also the same as the above-mentioned power systems, this fourdimensional energy resource system is with rich chaos behaviors. The problem of chaotic control for the energy resource system was considered in [3]. Feedback control and adaptive control methods were used to suppress chaos to unstable equilibrium or unstable periodic orbits, where only three of the system's parameters were supposed to be unknown. Reference [4] investigated the robust chaos synchronization problem for the four-dimensional energy resource systems based on the sliding mode control technique. The control of energy resource chaotic system was investigated by timedelayed feedback control method in [5]. Four linear control

schemes are proposed to a four-dimensional energy resource system in [6]. Based on stability criterion of linear system and Lyapunov stability theory, respectively, the chaos synchronization problems for energy resource demand-supply system were discussed using two novel different control methods in [7].

In many practical dynamic systems (including the energy resource demand-supply system), physical input saturation on hardware dictates that the magnitude of the control signal is always constrained. Saturation is a potential problem for actuators of control systems. It often severely limits system performance, giving rise to undesirable inaccuracy or leading instability [8, 9]. The development of control schemes for systems with input saturation has been a task of major practical interest as well as theoretical significance. The proposed approaches in [1-7] assume that all the components of the considered energy resource demand-supply systems are in good operating conditions and do not consider the problem of saturation. Reference [10] proposed two different chaos synchronization methods for a class of energy resource demand-supply systems with input saturation, but the response system in [10] did not contain unknown uncertain nonlinearities and unknown stochastic disturbances. It is well known that stochastic disturbances also often exist in many practical systems. Their existence is a source of instability of the control systems; thus, the investigations on stochastic control systems have received considerable attention in recent years [11–22]. Since the emergence of the stochastic stabilization theory in the 1960s, the progress has been constructed by a fundamental technical Itô lemma, and the control design for stochastic systems is more difficult compared with deterministic systems.

Motivated by the above observations, an adaptive neural networks chaos synchronization method is proposed for a four-dimensional energy resource demand-supply system with input constraints. Assume that the response system contains unknown uncertain nonlinearities and unknown stochastic disturbances. In the design, the neural networks and robust terms are used to identify the nonlinearities and overcome the stochastic disturbances, respectively. Based on Lyapunov stability, an adaptive synchronization method is developed in order to make the states of two chaotic systems asymptotically synchronized. The new auxiliary design system is employed to address input constraints. Numerical simulations are provided to illustrate the effectiveness of the proposed approach.

Compared with the existing results, the main contributions of the proposed method are as follows: (i) the controlled response system of this paper contains unknown nonlinearities, and the proposed method can solve the unknown nonlinearity problem by neural networks, but the methods of [1–8, 10] cannot solve this problem; (ii) the controlled response system of this paper contains stochastic disturbances, and the proposed method can solve the stochastic disturbances problem based on Itô's lemma and stochastic LaSalle's theorem, but the methods of [1–8, 10] cannot solve this problem; (iii) an auxiliary design system is employed to address input constraints problem, and the methods of [1–8] can solve this problem.

2. Energy Resource Chaotic System

The four-dimensional energy resource system can be expressed as follows (see [2, 4, 6]):

$$\dot{x} = a_1 x \left(1 - \frac{x}{M} \right) - a_2 (y + z) - d_3 w,
\dot{y} = -b_1 y - b_2 z + b_3 x [N - (x - z)],
\dot{z} = c_1 z (c_2 x - c_3),
\dot{w} = d_1 x - d_2 w,$$
(1)

where x(t) is the energy resource shortage in A region, y(t) is the energy resource supply increment in B region, and z(t) and w(t) are energy resource import in A region and renewable energy resource in A region, respectively; M, N, a_i , b_j , c_j , and d_j (i = 1, 2, j = 1, 2, 3) are parameters that are all positive real. The dynamics of this system has been extensively studied in [2, 4, 6].

When the system parameters are taken as the following values, this system exhibits chaotic behavior: M = 1.8, N = 1, $a_1 = 0.1$, $a_2 = 0.15$, $b_1 = 0.06$, $b_2 = 0.082$, $b_3 = 0.07$, $c_1 = 0.2$, $c_2 = 0.5$, $c_3 = 0.4$, $d_1 = 0.1$, $d_2 = 0.06$, and $d_3 = 0.07$.

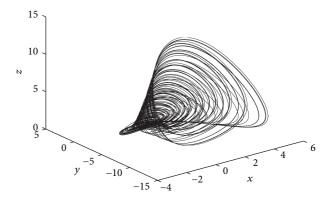


FIGURE 1: Three-dimensional view x - y - z.

Without the particular statement, these values are adopted in this whole paper. Figures 1, 2, and 3 show the phase portraits with initial conditions of x(0) = 0.82, y(0) = 0.29, z(0) = 0.48, and w(0) = 0.1.

3. Synchronization of the Energy Resource System

In this section, a controller will be designed in order to make the response system track the drive system. The drive system with subscript 1 is written as

$$\dot{x}_{1} = a_{1}x_{1} \left(1 - \frac{x_{1}}{M} \right) - a_{2} \left(y_{1} + z_{1} \right) - d_{3}w_{1},
\dot{y}_{1} = -b_{1}y_{1} - b_{2}z_{1} + b_{3}x_{1} \left[N - (x_{1} - z_{1}) \right],
\dot{z}_{1} = c_{1}z_{1} \left(c_{2}x_{1} - c_{3} \right),
\dot{w}_{1} = d_{1}x_{1} - d_{2}w_{1}.$$
(2)

Assume that the controlled response system with subscript 2 contained uncertain nonlinearities (unknown smooth nonlinear functions) and unknown external stochastic disturbance, and it can be expressed as the following dynamics:

$$dx_{2} = \left[a_{1}x_{2}\left(1 - \frac{x_{2}}{M}\right) - a_{2}\left(y_{2} + z_{2}\right) - d_{3}w_{2}\right]$$

$$+ f_{1}\left(x_{2}\right) + u_{1}\left(v_{1}\left(t\right)\right) dt + p_{1}\left(e_{1}\right) dW,$$

$$dy_{2} = \left[-b_{1}y_{2} - b_{2}z_{2} + b_{3}x_{2}\left[N - \left(x_{2} - z_{2}\right)\right]\right]$$

$$+ f_{2}\left(y_{2}\right) + u_{2}\left(v_{2}\left(t\right)\right) dt + p_{2}\left(e_{2}\right) dW, \quad (3)$$

$$dz_{2} = \left[c_{1}z_{2}\left(c_{2}x_{2} - c_{3}\right) + f_{3}\left(z_{2}\right) + u_{3}\left(v_{3}\left(t\right)\right)\right] dt$$

$$+ p_{3}\left(e_{3}\right) dW,$$

$$dw_{2} = \left[d_{1}x_{2} - d_{2}w_{2} + f_{4}\left(w_{2}\right) + u_{4}\left(v_{4}\left(t\right)\right)\right] dt$$

$$+ p_{4}\left(e_{4}\right) dW,$$

where v_i is the actual controller to be designed and $u_i(v_i(t))$ (i = 1, 2, 3, 4) is the plant input subject to saturation

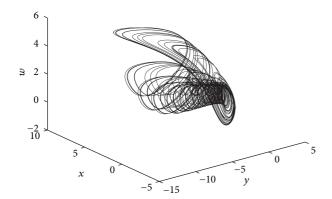


FIGURE 2: Three-dimensional view y - x - w.

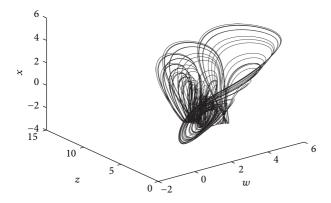


FIGURE 3: Three-dimensional view w - z - x.

type nonlinearly. $p_i(e_i)$, i = 1, 2, 3, 4, are uncertain functions, and $W \in \mathbb{R}^n$ is an independent standard Brownian motion defined on a complete probability space, with the incremental covariance $E\{dW \cdot dW^T\} = \sigma(t)\sigma(t)^T dt$.

Remark 1. If no input saturation, uncertain nonlinearities, and unknown external stochastic disturbance (i.e., $u_i(v_i(t)) = v_i(t)$), $p_i(t) = 0$, and $f_i(\cdot) = 0$ (i = 1, 2, 3, 4)) are included in (3), then (3) becomes the chaotic systems studied widely, see [8, 10], where $u_i(v_i(t))$ can be described as

$$u_{i}(v_{i}(t)) = \operatorname{sat}(v_{i}(t))$$

$$= \begin{cases} \operatorname{sign}(v_{i}(t)) u_{iM}, & |v_{i}(t)| \ge u_{iM}, \\ v_{i}(t), & |v_{i}(t)| < u_{iM}, \end{cases}$$
(4)

where u_{iM} is a known bound of $u_i(v_i(t))$.

To design an adaptive controller, the following basic assumption is made for the system (3).

Assumption 2. The disturbance covariance $P^T \sigma \sigma^T P \leq \sum_{i=1}^4 e_i \overline{\sigma}_i(e_i)$, where $P = \begin{bmatrix} p_1(e_1) & p_2(e_2) & p_3(e_3) & p_4(e_4) \end{bmatrix}^T$ and $\overline{\sigma}_i(e_i)$ is a known function.

To establish stochastic stability as a preliminary, consider a stochastic nonlinear system:

$$dx = f(x,t) dt + g(x,t) dW,$$
 (5)

where $x \in R^n$, W is an independent r-dimensional Wiener process, defined on the probability space (Ω, F, P) , with the incremental covariance $E\{dW, dW^T = \sigma(t)\sigma(t)^T de\}$, and $f: R^n \times R \to R^n$ and $f: R^n \times R \to R^{n \times r}$ are locally Lipschitz continuous in x, uniformly in $t \in R$, with f(0,t) = 0 and g(0,t) = 0, for all $t \geq 0$.

Lemma 3 (see [16, 17] (stochastic LaSalle's theorem)). Consider (5) and suppose that there exists a twice continuously differentiable function V(x,t), which is positive definite, decrescent, and radially unbounded, and another nonnegative continuous function $Q(x) \ge 0$ such that the infinitesimal generator V(x,t) along (5) satisfies

$$\ell V := \frac{\partial V}{\partial t} + \frac{\partial V}{\partial x} f(x) + \frac{1}{2} \operatorname{Tr} \left\{ \sigma^T g^T \frac{\partial^2 V}{\partial x^2} g \sigma \right\} \le -Q(x),$$

$$\forall x \in \mathbb{R}^n, \ t \ge 0,$$

where Tr denotes the matrix trace. Then, the equilibrium x = 0 is globally stable in probability and

$$P\left\{\lim_{t\to\infty}Q\left(x\left(t\right)\right)=0\right\}=1,\quad\forall x\left(0\right)\in R^{n}.\tag{7}$$

In order to solve the unknown nonlinear $f_i(\cdot)$ (i=1,2,3,4), the following radial basis function neural networks (RBFNNs) [23] are used to identify them similar to fuzzy logic systems [24–27].

An RBFNN can approximate a continuous function h(X): $\mathbb{R}^q \to \mathbb{R}$,

$$h_{nn}(X) = W^{T} \varphi(X), \qquad (8)$$

where the input vector $X \in \Omega \subset \mathbb{R}^q$, weight vector $W = [W_1, \ldots, W_m]^T \in \mathbb{R}^m$, the NN node number m > 1, and $\varphi(X) = [\varphi_1(X) \cdots \varphi_m(X)]^T$, with $\varphi_i(X)$ being Gaussian functions, which have the form

$$\varphi_i(X) = \exp\left[\frac{-\left(X - \mu_i\right)^T \left(X - \mu_i\right)}{\eta^2}\right], \quad i = 1, 2, \dots, m,$$
(9)

where $\mu_i = [\mu_{i1}, \dots, \mu_{iq}]^T$ is the center of the receptive field and η is the width of the Gaussian function.

According to the literatures [23], the neural network (8) can approximate any continuous function h(X) over a compact set $D \in \mathbb{R}^q$ to arbitrary any accuracy as

$$h(X) = W^{*T} \varphi(X) + \varepsilon(X), \quad \forall X \in D, \tag{10}$$

where W^* is an ideal constant weight, $\varepsilon(X)$ is the bounded approximation error, and W^* is defined as

$$W^* = \arg\min_{W \in \Omega} \left\{ \sup_{X \in D} \left| h(X) - W^T \varphi(X) \right| \right\}. \tag{11}$$

4. Adaptive Synchronization of the Energy Resource System

For different initial conditions of systems (2) and (3), the two coupled systems can achieve synchronization by designing an appropriate control input $u_i(t)$. First, we define the synchronization error vector between systems (2) and (3) as

$$e_1 = x_2 - x_1 - h_1,$$
 $e_2 = y_2 - y_1 - h_2,$
 $e_3 = z_2 - z_1 - h_3,$ $e_4 = w_2 - w_1 - h_4,$ (12)

where h_i (i = 1, 2, 3, 4) is filter signal and will be given later. From (2), (3), and (12), the error dynamical system can be written as

$$de_{1} = \left[-\dot{h}_{1} + a_{1}e_{1} - a_{2} \left(e_{2} + e_{3} \right) - \frac{a_{1}x_{2}^{2}}{M} + \frac{a_{1}x_{1}^{2}}{M} - d_{3}e_{4} \right.$$

$$\left. + a_{1}h_{1} - a_{2} \left(h_{2} + h_{3} \right) - d_{3}h_{4} + f_{1} \left(x_{2} \right) \right.$$

$$\left. + u_{1} \left(v_{1} \left(t \right) \right) \right] dt + p_{1} \left(e_{1} \right) dW,$$

$$de_{2} = \left[-\dot{h}_{2} - b_{1}e_{2} - b_{2}e_{3} + b_{3}Ne_{1} - b_{3}x_{2}^{2} + b_{3}x_{1}^{2} + b_{3}x_{2}z_{2} \right.$$

$$\left. - b_{3}x_{1}z_{1} - b_{1}h_{2} - b_{2}h_{3} + b_{3}Nh_{1} \right.$$

$$\left. + f_{2} \left(y_{2} \right) + u_{2} \left(v_{2} \left(t \right) \right) \right] dt + p_{2} \left(e_{2} \right) dW,$$

$$de_{3} = \left[-\dot{h}_{3} - c_{1}c_{3}e_{3} + c_{1}c_{2}x_{2}z_{2} - c_{1}c_{2}x_{1}z_{1} - c_{1}c_{3}h_{3} \right.$$

$$\left. + f_{3} \left(z_{2} \right) + u_{3} \left(v_{3} \left(t \right) \right) \right] dt + p_{3} \left(e_{3} \right) dW,$$

$$de_{4} = \left[-\dot{h}_{4} + d_{1}e_{1} - d_{2}e_{4} + d_{1}h_{1} - d_{2}h_{4} + f_{4} \left(w_{2} \right) \right.$$

$$\left. + u_{4} \left(v_{4} \left(t \right) \right) \right] dt + p_{4} \left(e_{4} \right) dW.$$

$$(13)$$

RBFNNs are used to identify $f_i(\cdot)$ (i=1,2,3,4), and (13) can be rewritten as

$$de_{1} = \left[-\dot{h}_{1} + a_{1}e_{1} - a_{2} \left(e_{2} + e_{3} \right) - \frac{a_{1}x_{2}^{2}}{M} + \frac{a_{1}x_{1}^{2}}{M} - d_{3}e_{4} \right.$$

$$+ a_{1}h_{1} - a_{2} \left(h_{2} + h_{3} \right) - d_{3}h_{4} + W_{1}^{*T} \varphi_{1} \left(x_{2} \right) + \varepsilon_{1} \left(x_{2} \right)$$

$$+ u_{1} \left(v_{1} \left(t \right) \right) \right] dt + p_{1} \left(e_{1} \right) dW,$$

$$de_{2} = \left[-\dot{h}_{2} - b_{1}e_{2} - b_{2}e_{3} + b_{3}Ne_{1} - b_{3}x_{2}^{2} + b_{3}x_{1}^{2} \right.$$

$$+ b_{3}x_{2}z_{2} - b_{3}x_{1}z_{1} - b_{1}h_{2} - b_{2}h_{3} + b_{3}Nh_{1}$$

$$+ W_{2}^{*T} \varphi_{2} \left(y_{2} \right) + \varepsilon_{2} \left(y_{2} \right) + u_{2} \left(v_{2} \left(t \right) \right) \right] dt + p_{2} \left(e_{2} \right) dW,$$

$$de_{3} = \left[-\dot{h}_{3} - c_{1}c_{3}e_{3} + c_{1}c_{2}x_{2}z_{2} - c_{1}c_{2}x_{1}z_{1} - c_{1}c_{3}h_{3} + W_{3}^{*T}\varphi_{3}(z_{2}) + \varepsilon_{3}(z_{2}) + u_{3}(v_{3}(t)) \right] dt + p_{3}(e_{3}) dW,$$

$$de_{4} = \left[-\dot{h}_{4} + d_{1}e_{1} - d_{2}e_{4} + d_{1}h_{1} - d_{2}h_{4} + W_{4}^{*T}\varphi_{4}(w_{2}) + \varepsilon_{4}(w_{2}) + u_{4}(v_{4}(t)) \right] dt + p_{4}(e_{4}) dW,$$

$$(14)$$

where $|\varepsilon_i| \le \varepsilon_i^*$ (i = 1, 2, 3, 4) and ε_i^* is a positive constant.

In this section, we assume that all the parameters of the energy resource system are unknown. For convenience, similar to [7], we define $a_3 = a_1/M$, $b_4 = b_3N$, $q_1 = c_1c_2$, and $q_2 = c_1c_3$; the system (14) can be rewritten as

$$de_{1} = \left[-\dot{h}_{1} + a_{1}e_{1} - a_{2} \left(e_{2} + e_{3} \right) - a_{3}x_{2}^{2} + a_{3}x_{1}^{2} - d_{3}e_{4} \right.$$

$$\left. + a_{1}h_{1} - a_{2} \left(h_{2} + h_{3} \right) - d_{3}h_{4} + W_{1}^{*T}\varphi_{1} \left(x_{2} \right) + \varepsilon_{1} \left(x_{2} \right) \right.$$

$$\left. + u_{1} \left(v_{1} \left(t \right) \right) \right] dt + p_{1} \left(e_{1} \right) dW,$$

$$de_{2} = \left[-\dot{h}_{2} - b_{1}e_{2} - b_{2}e_{3} + b_{4}e_{1} - b_{3}x_{2}^{2} \right.$$

$$\left. + b_{3}x_{1}^{2} + b_{3}x_{2}z_{2} - b_{3}x_{1}z_{1} - b_{1}h_{2} \right.$$

$$\left. - b_{2}h_{3} + b_{4}h_{1} + W_{2}^{*T}\varphi_{2} \left(y_{2} \right) + \varepsilon_{2} \left(y_{2} \right) \right.$$

$$\left. + u_{2} \left(v_{2} \left(t \right) \right) \right] dt + p_{2} \left(e_{2} \right) dW,$$

$$de_{3} = \left[-\dot{h}_{3} - q_{2}e_{3} + q_{1}x_{2}z_{2} - q_{1}x_{1}z_{1} - q_{2}h_{3} + W_{3}^{*T}\varphi_{3} \left(z_{2} \right) \right.$$

$$\left. + \varepsilon_{3} \left(z_{2} \right) + u_{3} \left(v_{3} \left(t \right) \right) \right] dt + p_{3} \left(e_{3} \right) dW,$$

$$de_{4} = \left[-\dot{h}_{4} + d_{1}e_{1} - d_{2}e_{4} + d_{1}h_{1} - d_{2}h_{4} + W_{4}^{*T}\varphi_{4} \left(w_{2} \right) \right.$$

$$\left. + \varepsilon_{4} \left(w_{2} \right) + u_{4} \left(v_{4} \left(t \right) \right) \right] dt + p_{4} \left(e_{3} \right) dW.$$

$$(15)$$

Define the dynamic system as

$$\dot{h}_i = -h_i + (u_i - v_i), \quad i = 1, 2, 3, 4.$$
 (16)

Choose the following Lyapunov function candidate V as

$$\begin{split} V &= \frac{1}{2} \left(e_1^2 + e_2^2 + e_3^2 + e_4^2 \right) + \widetilde{W}_1^T \widetilde{W}_1 + \widetilde{W}_2^T \widetilde{W}_2 + \widetilde{W}_3^T \widetilde{W}_3 \\ &+ \widetilde{W}_4^T \widetilde{W}_4 + \widetilde{a}_1^2 + \widetilde{a}_2^2 + \widetilde{a}_3^2 + \widetilde{b}_1^2 + \widetilde{b}_2^2 + \widetilde{b}_3^2 + \widetilde{b}_4^2 \\ &+ \widetilde{d}_1^2 + \widetilde{d}_2^2 + \widetilde{d}_3^2 + \widetilde{q}_1^2 + \widetilde{q}_2^2, \end{split} \tag{17}$$

where
$$\tilde{a}_i = a_i - \hat{a}_i$$
, $\tilde{d}_i = d_i - \hat{d}_i$ $(i = 1, 2, 3)$, $\widetilde{W}_j = W_j^* - \widehat{W}_j$, $\widetilde{b}_j = b_j - \hat{b}_j$ $(j = 1, 2, 3, 4)$, and $\widetilde{q}_k = q_k - \widehat{q}_k$ $(k = 1, 2)$.

Similar to [16, 17], the ℓ infinitesimal generator of V along with the solutions of (15) is

$$\begin{split} \ell V &= e_1 \left[h_1 + v_1 + a_1 \hat{e}_1 - \hat{a}_2 \left(e_2 + e_3 \right) - \hat{a}_3 x_2^2 + \hat{a}_3 x_1^2 \right. \\ &\quad - \hat{d}_3 e_4 + \hat{a}_1 h_1 - \hat{a}_2 \left(h_2 + h_3 \right) - \hat{d}_3 h_4 + p_1 \left(t \right) \\ &\quad + \widehat{W}_1^T \varphi_1 \left(x_2 \right) + \varepsilon_1 \left(x_2 \right) \right] \\ &\quad + e_2 \left[h_2 + v_2 - \hat{b}_1 e_2 - \hat{b}_2 e_3 + \hat{b}_4 e_1 - \hat{b}_3 x_2^2 \right. \\ &\quad + \hat{b}_3 x_1^2 + \hat{b}_3 x_2 z_2 - \hat{b}_3 x_1 z_1 - \hat{b}_1 h_2 - \hat{b}_2 h_3 \\ &\quad + \hat{b}_4 h_1 + p_2 \left(t \right) + \widehat{W}_2^T \varphi_2 \left(y_2 \right) + \varepsilon_2 \left(y_2 \right) \right] \\ &\quad + e_3 \left[h_3 + v_3 - \hat{q}_2 e_3 + \hat{q}_1 x_2 z_2 - \hat{q}_1 x_1 z_1 - \hat{q}_2 h_3 \right. \\ &\quad + p_3 \left(t \right) + \widehat{W}_3^T \varphi_3 \left(z_2 \right) + \varepsilon_3 \left(z_2 \right) \right] \\ &\quad + e_4 \left[h_4 + v_4 + \hat{d}_1 e_1 - \hat{d}_2 e_4 + \hat{d}_1 h_1 - \hat{d}_2 h_4 \right. \\ &\quad + p_4 \left(t \right) + \widehat{W}_4^T \varphi_4 \left(w_2 \right) + \varepsilon_4 \left(w_2 \right) \right] \\ &\quad + \widehat{W}_1^T \left[e_1 \varphi_1 \left(x_2 \right) - \widehat{W}_1 \right] + \widehat{W}_2^T \left[e_2 \varphi_2 \left(y_2 \right) - \widehat{W}_2 \right] \\ &\quad + \widehat{W}_3^T \left[e_3 \varphi_3 \left(z_2 \right) - \widehat{W}_3 \right] + \widehat{W}_4^T \left[e_4 \varphi_4 \left(w_2 \right) - \widehat{W}_4 \right] \right. \\ &\quad + \widehat{a}_1 \left[e_1^2 + e_1 h_1 - \widehat{a}_1 \right] \\ &\quad + \widehat{a}_2 \left[e_1 \left(e_2 + e_3 \right) - e_1 \left(h_2 + h_3 \right) - \widehat{a}_2 \right] \\ &\quad + \widehat{a}_3 \left[- e_1 x_2^2 + e_1 x_1^2 - \widehat{a}_3 \right] + \widehat{b}_1 \left[- e_2^2 - e_2 h_2 - \widehat{b}_1 \right] \\ &\quad + \widehat{b}_2 \left[- e_2 e_3 - e_2 h_3 - \widehat{b}_2 \right] \\ &\quad + \widehat{b}_3 \left[- e_2 x_2^2 + e_2 x_1^2 + e_2 x_2 z_2 - e_2 x_1 z_1 - \widehat{b}_3 \right] \\ &\quad + \widehat{b}_4 \left[e_2 e_1 + e_2 h_1 - \widehat{b}_4 \right] + \widehat{d}_1 \left[e_4 e_1 + e_4 h_4 + e_4 h_1 - \widehat{d}_1 \right] \\ &\quad + \widehat{d}_2 \left[- e_4^2 - \widehat{d}_2 \right] + \widehat{d}_3 \left[- e_1 \left(e_4 + h_4 \right) - \widehat{d}_3 \right] \\ &\quad + \widehat{q}_1 \left[e_3 x_2 z_2 - e_3 x_1 z_1 - \widehat{q}_1 \right] + \widehat{q}_2 \left[- e_3^2 - e_3 h_3 - \widehat{q}_2 \right] \\ &\quad + \sum_{i=1}^4 e_i \overline{\phi}_i \left(e_i \right). \end{aligned}$$

Design the actual controllers v_j and parameters update laws of \widehat{W}_j , \widehat{a}_i , \widehat{d}_i (i=1,2,3), \widehat{b}_j (j=1,2,3,4), and \widehat{q}_k (k=1,2) as follows:

$$v_{1} = -l_{1}e_{1} - \overline{\sigma}_{1}(e_{1}) - h_{1} - \hat{a}_{1}e_{1} + \hat{a}_{2}(e_{2} + e_{3})$$

$$+ \hat{a}_{3}x_{2}^{2} - \hat{a}_{3}x_{1}^{2} + \hat{d}_{3}e_{4} - \hat{a}_{1}h_{1} + \hat{a}_{2}(h_{2} + h_{3})$$

$$+ \hat{d}_{3}h_{4} - \widehat{W}_{1}^{T}\varphi_{1}(x_{2}) - \operatorname{sgn}(e_{1})(\varepsilon_{1}^{*} + \alpha_{1}),$$
(19)

$$v_{2} = -l_{2}e_{2} - \overline{\sigma}_{2}(e_{2}) - h_{2} + \hat{b}_{1}e_{2} + \hat{b}_{2}e_{3} - \hat{b}_{4}e_{1}$$

$$+ \hat{b}_{3}x_{2}^{2} - \hat{b}_{3}x_{1}^{2} - \hat{b}_{3}x_{2}z_{2} + \hat{b}_{3}x_{1}z_{1} + \hat{b}_{1}h_{2} + \hat{b}_{2}h_{3}$$

$$- \hat{b}_{4}h_{1} - \widehat{W}_{2}^{T}\varphi_{2}(y_{2}) - \operatorname{sgn}(e_{2})(\varepsilon_{2}^{*} + \alpha_{2}),$$
(20)

$$v_{3} = -\bar{l}_{3}e_{3} - \overline{\sigma}_{3}(e_{3}) - h_{3} + \widehat{q}_{2}e_{3} - \widehat{q}_{1}x_{2}z_{2} + \widehat{q}_{1}x_{1}z_{1} + \widehat{q}_{2}h_{3} - \widehat{W}_{3}^{T}\varphi_{3}(z_{2}) - \operatorname{sgn}(e_{3})(\varepsilon_{3}^{*} + \alpha_{3}),$$
(21)

$$v_{4} = -l_{4}e_{4} - \overline{\sigma}_{4}(e_{4}) - h_{4} - \widehat{d}_{1}e_{1} + \widehat{d}_{2}e_{4} - \widehat{d}_{1}h_{1} + \widehat{d}_{2}h_{4} - \widehat{W}_{4}^{T}\varphi_{4}(w_{2}) - \operatorname{sgn}(e_{4})(\varepsilon_{4}^{*} + \alpha_{4}),$$
(22)

where l_i (i = 1, 2, 3, 4) are positive design parameters. Consider the following:

$$\dot{\widehat{W}}_1 = e_1 \varphi_1 \left(x_2 \right), \tag{23}$$

$$\dot{\widehat{W}}_{2} = e_{2}\varphi_{2}\left(y_{2}\right),\tag{24}$$

$$\dot{\widehat{W}}_3 = e_3 \varphi_3 \left(z_2 \right), \tag{25}$$

$$\dot{\widehat{W}}_{A} = e_{A} \varphi_{A} \left(w_{2} \right), \tag{26}$$

$$\dot{\hat{a}}_1 = e_1^2 + e_1 h_1, \tag{27}$$

$$\dot{\hat{a}}_2 = e_1 \left(e_2 + e_3 \right) - e_1 \left(h_2 + h_3 \right), \tag{28}$$

$$\dot{\hat{a}}_3 = -e_1 x_2^2 + e_1 x_1^2,\tag{29}$$

$$\dot{\hat{b}}_1 = -e_2^2 - e_2 h_2,\tag{30}$$

$$\dot{\hat{b}}_2 = -e_2 e_3 - e_2 h_3,\tag{31}$$

$$\dot{\hat{b}}_3 = -e_2 x_2^2 + e_2 x_1^2 + e_2 x_2 z_2 - e_2 x_1 z_1, \tag{32}$$

$$\dot{\hat{b}}_4 = e_2 e_1 + e_2 h_1,\tag{33}$$

$$\dot{\hat{d}}_1 = e_4 e_1 + e_4 h_4 + e_4 h_1, \tag{34}$$

$$\dot{\hat{d}}_2 = -e_4^2,\tag{35}$$

$$\dot{\hat{d}}_3 = -e_1 (e_4 + h_4), \tag{36}$$

$$\dot{\hat{q}}_1 = e_3 x_2 z_2 - e_3 x_1 z_1,\tag{37}$$

$$\dot{\hat{q}}_2 = -e_3^2 - e_3 h_3. \tag{38}$$

Substituting (19)–(38) into (18) results in

(18)

$$\ell V \le -l_1 e_1^2 - l_2 e_2^2 - l_3 e_3^2 - l_4 e_4^2. \tag{39}$$

From (39) and Lemma 3, we can conclude that the states x_2 , y_2 , z_2 , and w_2 of response system (2) and the states x_1 , y_1 , z_1 , and w_1 of drive system (3) are ultimately synchronized asymptotically in probability.

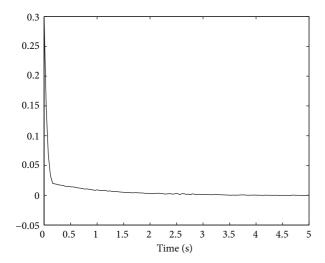


FIGURE 4: The trajectory of e_1 .

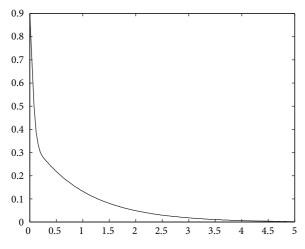


FIGURE 5: The trajectory of e_2 .

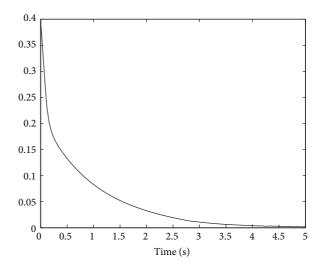


FIGURE 6: The trajectory of e_3 .

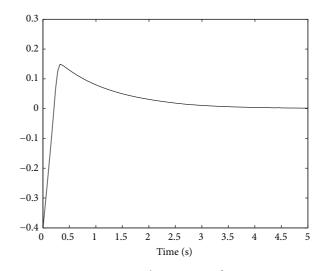


Figure 7: The trajectory of e_4 .

5. Simulation Results

In this section, external perturbations $p_i(e_i) = e_i$; uncertain nonlinear $f_1(x_2) = 0.1x_2^2$, $f_2(y_2) = 0.1y_2^2$, $f_3(z_2) = z_2$, and $f_4(w_2) = w_2$. Consider $\alpha_1 = \alpha_2 = \alpha_2 = \alpha_2 = 0.1$ and $\varepsilon_1^* = \varepsilon_2^* = \varepsilon_3^* = \varepsilon_4^* = 0.1$. RBFNNs, $\widehat{W}_i^T \varphi_i(\cdot)$, contain 25 nodes, with centers evenly spaced in [-4, 4] and width is 2. $\widehat{W}(t)$ is assumed to be Gaussian white noise with zero mean and variance 1.0.

The initial values are chosen as $x_1(0) = 0.1$, $y_1(0) = -0.8$, $z_1(0) = 0.2$, $w_1(0) = 0.1$, $x_2(0) = 0.4$, $y_2(0) = 0.1$, $z_2(0) = 0.6$, and $w_2(0) = -0.3$, and the other initial values are chosen as zeros. The saturation values are $u_{2M} = 5$, $u_{3M} = 2$, and $u_{4M} = 2$. Design parameters in controllers are $l_1 = 20$, $l_2 = 20$, $l_3 = 20$, and $l_4 = 20$. The simulation results are shown in Figures 4, 5, 6, 7, 8, 9, 10, and 11.

Remark 4. It is worth pointing out that the method of [10] cannot be used to control the systems of this paper. There exist three reasons: (i) the system of this paper is four dimensional

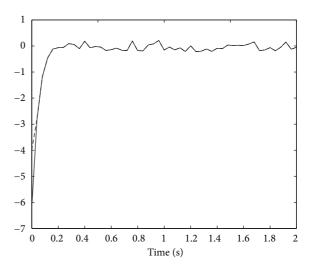


Figure 8: The trajectories of v_1 (solid line) and u_1 (dash-dotted line).

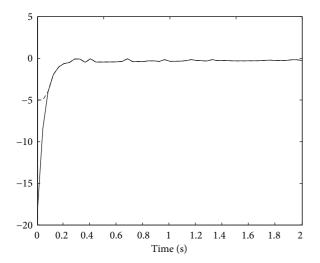


FIGURE 9: The trajectories of v_2 (solid line) and u_2 (dash-dotted line).

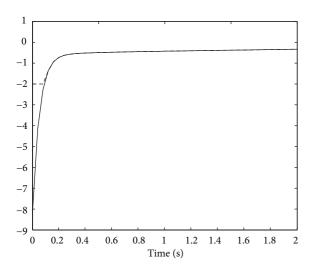


FIGURE 10: The trajectories of v_3 (solid line) and u_3 (dash-dotted line).

and the system in [10] is three dimensional; (ii) the system of this paper contains stochastic disturbances, and the system in [10] does not contain them; (iii) the controlled response system of this paper contains unknown nonlinearities, and [10] does not contain them.

6. Conclusions

This paper has solved the synchronization problems of a class of unknown parameters four-dimensional energy resource system. The main features of the proposed algorithm are that (i) the problems of the input constraint have been solved by employing a new auxiliary system; (ii) the unknown nonlinearities and stochastic disturbances that existed in the response system have been overcome by the neural networks and some special robust terms, respectively; (iii) the stability

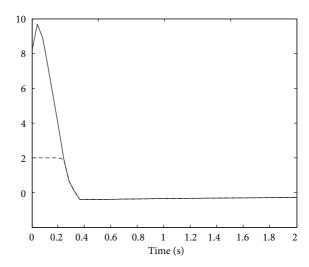


FIGURE 11: The trajectories of v_4 (solid line) and u_4 (dash-dotted line).

of the energy resource demand-supply system has been guaranteed based on stochastic Lyapunov theory.

Conflict of Interests

The author declares that there is no conflict of interests regarding the publication of this paper.

Acknowledgments

This work was supported by the National Natural Science Foundation of China (no. 51308275) and the Foundation of Liaoning Educational Committee (no. L2012225).

References

- M. Sun, L. X. Tian, and Y. Fu, "An energy resources demandsupply system and its dynamical analysis," *Chaos, Solitons & Fractals*, vol. 32, no. 1, pp. 168–180, 2007.
- [2] M. Sun, Q. Jia, and L. X. Tian, "A new four-dimensional energy resources system and its linear feedback control," *Chaos, Solitons & Fractals*, vol. 39, no. 1, pp. 101–108, 2009.
- [3] M. Sun, L. X. Tian, Y. Fu, and W. Qian, "Dynamics and adaptive synchronization of the energy resource system," *Chaos, Solitons & Fractals*, vol. 31, no. 4, pp. 879–888, 2007.
- [4] C.-F. Huang, K.-H. Cheng, and J.-J. Yan, "Robust chaos synchronization of four-dimensional energy resource systems subject to unmatched uncertainties," *Communications in Nonlinear Science and Numerical Simulation*, vol. 14, no. 6, pp. 2784–2792, 2009
- [5] M. Sun, L. X. Tian, and J. Xu, "Time-delayed feedback control of the energy resource chaotic system," *International Journal of Nonlinear Science*, vol. 1, no. 3, pp. 172–177, 2006.
- [6] Z. L. Wang and X. R. Shi, "Synchronization of a four-dimensional energy resource system via linear control," *Communications in Nonlinear Science and Numerical Simulation*, vol. 16, no. 1, pp. 463–474, 2011.

- [7] X. C. Li, W. Xu, and R. H. Li, "Chaos synchronization of the energy resource system," *Chaos, Solitons & Fractals*, vol. 40, no. 2, pp. 642–652, 2009.
- [8] C. Y. Wen, J. Zhou, Z. T. Liu, and H. Y. Su, "Robust adaptive control of uncertain nonlinear systems in the presence of input saturation and external disturbance," *IEEE Transactions on Automatic Control*, vol. 56, no. 7, pp. 1672–1678, 2011.
- [9] Y. M. Li, T. S. Li, and X. J. Jing, "Indirect adaptive fuzzy control for input and output constrained nonlinear systems using a barrier Lyapunov function," *International Journal of Adaptive Control and Signal Processing*, vol. 28, no. 2, pp. 184–199, 2014.
- [10] D. Meng, "Robust adaptive synchronization of the energy resource system with constraint," *Mathematical Problems in Engineering*, vol. 2013, Article ID 494218, 7 pages, 2013.
- [11] Z. G. Yan and W. H. Zhang, "Finite-time stability and stabilization of Itô-type stochastic singular systems," Abstract and Applied Analysis, vol. 2014, Article ID 263045, 9 pages, 2014.
- [12] J. Cui, L. T. Yan, and X. C. Sun, "Existence and stability for stochastic partial differential equations with infinite delay," *Abstract and Applied Analysis*, vol. 2014, Article ID 235937, 8 pages, 2014.
- [13] L. Liu, Z. D. Yu, Q. Zhou, and H. R. Karimi, "State-feedback stabilization for a class of stochastic feedforward nonlinear timedelay systems," *Abstract and Applied Analysis*, vol. 2013, Article ID 151374, 8 pages, 2013.
- [14] L. G. Wu and D. W. C. Ho, "Sliding mode control of singular stochastic hybrid systems," *Automatica*, vol. 46, no. 4, pp. 779– 783, 2010.
- [15] X. J. Su, L. G. Wu, P. Shi, and Y. D. Song, " H_{∞} model reduction of Takagi-Sugeno fuzzy stochastic systems," *IEEE Transactions on Systems, Man, and Cybernetics B*, vol. 42, no. 6, pp. 1574–1585, 2012.
- [16] S.-C. Tong, Y. Li, and Y. M. Li, "Observer-based adaptive fuzzy backstepping control for a class of stochastic nonlinear strict-feedback systems," *IEEE Transactions on Systems, Man, and Cybernetics B*, vol. 41, no. 6, pp. 1693–1704, 2011.
- [17] S.-C. Tong, T. Wang, Y. M. Li, and B. Chen, "A combined back-stepping and stochastic small-gain approach to robust adaptive fuzzy output feedback control," *IEEE Transactions on Fuzzy Systems*, vol. 21, pp. 314–327, 2013.
- [18] H. Li, C. Wang, P. Shi, and H. J. Gao, "New passivity results for uncertain discrete-time stochastic neural networks with mixed time delays," *Neurocomputing*, vol. 73, no. 16–18, pp. 3291–3299, 2010.
- [19] M. Liu, D. W. C. Ho, and Y. G. Niu, "Stabilization of Markovian jump linear system over networks with random communication delay," *Automatica*, vol. 45, no. 2, pp. 416–421, 2009.
- [20] Q. Zhou, P. Shi, H. H. Liu, and S. Y. Xu, "Neural-network-based decentralized adaptive output-feedback control for large-scale stochastic nonlinear systems," *IEEE Transactions on Systems*, *Man, and Cybernetics B*, vol. 42, no. 6, pp. 1608–1619, 2012.
- [21] L. G. Wu and W. X. Zheng, " L_2 - L_∞ control of nonlinear fuzzy Itô stochastic delay systems via dynamic output feedback," *IEEE Transactions on Systems, Man, and Cybernetics B*, vol. 39, no. 5, pp. 1308–1315, 2009.
- [22] Q. Zhou, P. Shi, S. Y. Xu, and H. Y. Li, "Observer-based adaptive neural network control for nonlinear stochastic systems with time-delay," *IEEE Transactions on Neural Networks and Learn*ing Systems, vol. 24, no. 1, pp. 71–80, 2013.
- [23] F. Lewis, S. Jaganathan, and A. Yesildirek, Neural Network Control of Robust Manipulator and Nonlinear Systems, Taylor & Francis, New York, NY, USA, 1998.

- [24] H. Y. Li, X. J. Jing, and H. R. Karimi, "Output-feedback based H_{∞} control for active suspension systems with control delay," *IEEE Transactions on Industrial Electronics*, vol. 61, no. 1, pp. 436–446, 2014.
- [25] S. C. Tong and Y. M. Li, "Adaptive fuzzy output feedback tracking backstepping control of strict-feedback nonlinear systems with unknown dead zones," *IEEE Transactions on Fuzzy Systems*, vol. 20, no. 1, pp. 168–180, 2012.
- [26] H. Y. Li, X. J. Jing, H. K. Lam, and P. Shi, "Fuzzy sampled-data control for uncertain vehicle suspension systems," *IEEE Transactions on Cybernetics*, 2013.
- [27] Y. M. Li, S. C. Tong, Y. J. Liu, and T. S. Li, "Adaptive fuzzy robust output feedback control of nonlinear systems with unknown dead zones based on small-gain approach," *IEEE Transactions on Fuzzy Systems*, vol. 22, no. 1, pp. 164–176, 2014.

Hindawi Publishing Corporation Abstract and Applied Analysis Volume 2014, Article ID 794368, 7 pages http://dx.doi.org/10.1155/2014/794368

Research Article

Fuzzy Pruning Based LS-SVM Modeling Development for a Fermentation Process

Weili Xiong, 1,2 Wei Zhang, 2 Dengfeng Liu, 2 and Baoguo Xu2

¹ Key Laboratory of Advanced Process Control for Light Industry (Ministry of Education), Jiangnan University, Wuxi 214122, China

Correspondence should be addressed to Weili Xiong; greenpre@163.com

Received 16 December 2013; Revised 14 January 2014; Accepted 14 January 2014; Published 27 February 2014

Academic Editor: Shen Yin

Copyright © 2014 Weili Xiong et al. This is an open access article distributed under the Creative Commons Attribution License, which permits unrestricted use, distribution, and reproduction in any medium, provided the original work is properly cited.

Due to the complexity and uncertainty of microbial fermentation processes, data coming from the plants often contain some outliers. However, these data may be treated as the normal support vectors, which always deteriorate the performance of soft sensor modeling. Since the outliers also contaminate the correlation structure of the least square support vector machine (LS-SVM), the fuzzy pruning method is provided to deal with the problem. Furthermore, by assigning different fuzzy membership scores to data samples, the sensitivity of the model to the outliers can be reduced greatly. The effectiveness and efficiency of the proposed approach are demonstrated through two numerical examples as well as a simulator case of penicillin fermentation process.

1. Introduction

For the limitation of advanced measurement techniques, some important process variables in biochemical industrial processes, such as product composition, product concentration, and biomass concentration, are difficult or impossible to measure online. However, these variables are very important for the products quality and the result of the whole reaction process. A soft sensor model is always needed to construct between variables which are easy to measure online and one which is difficult to measure. Then a value of an objective variable can be inferred by this model. The approaches and corresponding applications of soft sensors have been discussed in some literature [1-4]. For example, partial least squares (PLS) and principal component analysis (PCA) [5, 6] are the most popular projection based soft sensor modeling methods for modeling and prediction. However, a drawback of these models is their linear nature. If it is known that the relation between the easy-to-measure and the difficult-tomeasure variables is nonlinear, then a nonlinear modeling method should be used. In last decades, data-based soft sensor modeling approaches have been intensively studied, such as nonlinear partial least squares (NPLS), nonlinear principal component analysis (NPCA), artificial neural networks (ANNs), and support vector machine (SVM) [7-10]. Although the NPCA is a well-established and powerful algorithm, it has several drawbacks. One of them is that the principal components describe very well the input space but do not reflect the relation between the input and the output data space. A solution to this drawback is given by the NPLS method. NPLS models are appropriate to study the behavior of the process. Unfortunately, sometimes the algorithm of NPLS is available only for specific nonlinear relationships. To break through the limitation of NPLS, ANN is adopted to solve the complexity and highly nonlinear problem in the case of the sample data tending to infinity. The disadvantage of ANNs is that during their learning they are prone to get stuck in local minima, which can result in suboptimal performance. Meanwhile, SVM has been demonstrated to work very well for a wide spectrum of applications under the limited training data samples, so it is not surprising that it has also been successfully applied as soft sensor.

Support vector machine (SVM) proposed by Vapnik [11, 12], which is based on statistical learning theory, obtains the optimal classification of the sample data through a quadratic programming. So it can balance the risk of learning algorithm and promotion of the extension ability. As a sophisticated soft sensor modeling method, SVM has a lot of advantages in solving small sample data and nonlinear and high dimensional pattern recognition and has been applied to the fermentation process successfully [13, 14]. Least squares

² School of Internet of Things Engineering, Jiangnan University, Wuxi 214122, China

support vector machine (LS-SVM) proposed by Suykens and Vandewalle [15] is an extension of the standard SVM. It can solve linear equations with faster solution speed and figure out the robustness, sparseness, and large-scale computing problems. However, all training data are treated as the normal support vector which loses the sparseness of SVM [16–19]. In this paper, the effective work addressed in Section 3 could improve the performance of the standard LS-SVM effectively.

Penicillin fermentation process is a typical biochemical reaction process with the features of nonlinearity and dynamic, which is caused by the factors such as genetic variation of somatic cell, microbial sensitivity to environment changing, and instability of raw material and seed quality that bring about serious nonlinearity and uncertainty [20]. For this process, key variables are concentration of the biomass, product, and substrate which are difficult to measure directly. However, some other auxiliary variables are easy to measure. So we choose aeration rate, dissolved oxygen concentration, agitator power, and others as auxiliary variables and the concentration of penicillin as the quality variable in this process. The next step is to construct the inferred model between the auxiliary variables and the quality variable. Outliers are commonly encountered in penicillin fermentation process which may be treated as the normal support vector and always has a bad influence on the precision of the soft sensor model. So applying the idea of fuzzy pruning for LS-SVM algorithm to cut off these outliers and reduce the number of support vectors will improve the sparseness and precision of the original LS-SVM model. Also assigning different fuzzy membership scores to sample data, the sensitivity to the outliers is reduced and the accuracy of the model is further improved as well. Finally, the LS-SVM and fuzzy pruning based LS-SVM soft sensor models for the penicillin fermentation process are constructed based on the optimal parameters obtained by using particle swarm optimization algorithm [21, 22]. Thus a soft sensor model with higher prediction precision and better generalization capability for penicillin fermentation process is completed.

The remainder of this paper is organized as follows. Section 2 begins with the revisit of LS-SVM algorithm and lays out the mathematical formulations. Detailed descriptions of improved LS-SVM based on fuzzy pruning algorithm are provided in Section 3. Two numerical simulation examples are illustrated in Section 4 which aims to demonstrate the effectiveness of the proposed method in developing soft sensors. Thereafter, a soft sensor application for the penicillin fermentation process using the proposed approach is presented in Section 5. Section 6 draws conclusions based on the results obtained in this paper.

2. The LS-SVM Revisit

Given the training data $\{T = (x_i, y_i), i = 1, 2, 3, ..., l\}, x_i \in$ R^n and $y_i \in R$ denote the input patterns and one-dimension output data, respectively. Similar to the standard SVM, LS-SVM nonlinear regression is mapping the data to a higher dimension space F by using a nonlinear function $\phi(x)$ and

constructing an optimal linear regression function in the higher dimension space:

$$y(x) = \omega^T \cdot \phi(x) + b. \tag{1}$$

Here ω is the weight value and b is the threshold.

The main difference between LS-SVM and SVM is that LS-SVM adopts the equality constraints instead of inequality constraints, and empirical risk is the deviation of the quadratic rather than one square deviation. By introducing the Kernel function σ and the penalty factor C, one considers the following optimization problem:

$$\min_{\omega,b,e} J(\omega,e) = \frac{1}{2}\omega^{T}\omega + \frac{1}{2}C\sum_{i=1}^{l}e_{i}^{2}$$
(2)

s.t.
$$y_i = \omega^T \phi(x_i) + b + e_i$$
, $i = 1, 2, ... l$.

To solve the optimization problem, the constrained optimization problem should be converted to unconstrained optimization problem first. By introducing Lagrange multiplier α_i , we obtain the following Lagrange function as follows:

$$L(\omega, b, e, \alpha) = J(\omega, e) - \sum_{i=1}^{l} \alpha_i \left\{ \omega^T \phi(x_i) + b + e_i - y_i \right\}. \quad (3)$$

Then according to the Mercer condition, the specific form of the nonlinear mapping does not need to be known a priori. Suppose the kernel function takes the form $k(x_i, x_i) =$ $\phi(x_i) \cdot \phi(x_i)$; this optimization problem could be changed into several linear equations. Based on the conditions of Karush-Kuhn-Tucker, calculating the partial derivative of $L(\omega, b, e_i, \alpha_i)$ with respect to ω, b, e_i , and α_i , respectively, and setting to zero yield

$$\frac{\partial L}{\partial \omega} = 0, \qquad \omega = \sum_{i=1}^{l} \alpha_i \phi(x_i),$$

$$\frac{\partial L}{\partial b} = 0, \qquad \sum_{i=1}^{l} \alpha_i = 0,$$

$$\frac{\partial L}{\partial e_i} = 0, \qquad \alpha_i = Ce_i,$$
(4)

$$\frac{\partial L}{\partial \alpha_i} = 0, \qquad \omega^T \phi(x_i) + b + e_i - y_i = 0.$$

To simplify the equations, we can get a compressed matrix equation:

$$\begin{pmatrix} 0 & e^T \\ e & Q + \frac{1}{C}I \end{pmatrix} \begin{pmatrix} b \\ \alpha \end{pmatrix} = \begin{pmatrix} 0 \\ y \end{pmatrix}, \tag{5}$$

where $Q_{ij} = \phi(x_i) \cdot \phi(x_j) = k(x_i, x_j), e = (1, 1, 1 ... 1)^T, y =$ $(y_1, y_2 ... y_l)^T$, $\alpha = (\alpha_1, \alpha_2 ... \alpha_l)^T$ i = 1, 2, 3 ... l, C > 0denotes the penalty factor, and *I* denotes the identity matrix. Solving the matrix equation (5), eventually the function of least squares vector machines is estimated as

$$y(x) = \sum_{i=1}^{l} \alpha_i k(x, x_i) + b.$$
 (6)

3. Improved LS-SVM with Fuzzy **Pruning Algorithm**

3.1. The Idea of Fuzzy Pruning Algorithm. Compared with SVM, the computational load of LS-SVM is reduced greatly. However, LS-SVM loses its sparseness because all training data are treated as support vectors even the outliers which always have a bad influence on the precision of the soft sensor model. In this paper, aiming to minimize effects of the outliers as well as the antidisturbance ability of sampling data [23, 24], fuzzy pruning approach is employed to handle the problem. The number of the support vectors is reduced which improves the sparseness of LS-SVM and model accuracy as well. Furthermore, the sensitivity to outliers of the proposed algorithm can be reduced through the fuzzy membership score assigned to the data samples.

The absolute value of Lagrange multiplier determines the importance of data in the training process which means the higher the absolute value, the greater the influence degree. The absolute value of Lagrange multiplier of outliers is often higher than that of the normal data. Based on this situation, the data which have the higher absolute value of Lagrange multiplier will be cut off according to certain proportion (e.g., 5%). When these data are cut off, the impact of outlier data is minimized, and the model sparseness and accuracy are improved simultaneously.

Since Lagrange multiplier plays an important role in constructing model, a fuzzy membership score is introduced to adjust the weight of data for modeling. Fuzzy membership value is defined as

$$s_i = (1 - \delta) \frac{|\alpha_i| - |\alpha|_{\min}}{|\alpha|_{\max} - |\alpha|_{\min}}, \quad 0 \le \delta < 1, \tag{7}$$

where s_i is the fuzzy membership score and α_i is the Lagrange multiplier of the *i*th sample data. Meanwhile, δ need to be given an appropriate value between 0 and 1.

It is noticed that the fuzzy membership score is near to zero when Lagrange multiplier is very small. So the corresponding sampling data may play no role in modeling, which means a part of sample data can be cut off according to the absolute value of Lagrange multiplier that is very small. As a result, the sparseness of the proposed LS-SVM algorithm is further improved.

3.2. Description of Fuzzy Pruning Based LS-SVM Algorithm. Adding fuzzy membership score s_i to error e_i , the new quadratic programming problem is expressed as follows:

$$\min_{\omega,b,e} J(\omega,e) = \frac{1}{2}\omega^{T}\omega + \frac{1}{2}C\sum_{i=1}^{l} s_{i}e_{i}^{2}$$
s.t. $v_{i} = \omega^{T}\Phi(x_{i}) + b + e_{i}, i = 1, 2, ... l.$ (8)

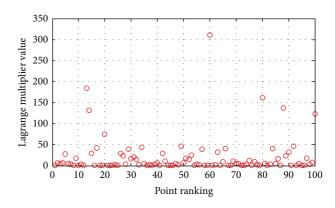
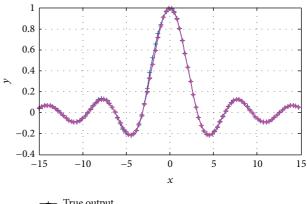


FIGURE 1: Lagrange multiplier value.



True output

LS-SVM output

Pruning fuzzy LS-SVM output

FIGURE 2: Prediction output of one-dimension function.

Since the direct optimization is not tractable, Lagrange method is introduced to convert it to become an unconstrained optimization problem. Therefore, the Lagrange function can be obtained as

$$L(\omega, b, e, \alpha) = J(\omega, e) - \sum_{i=1}^{l} \alpha_i \left\{ \omega^T \phi(x_i) + b + e_i - y_i \right\}. \quad (9)$$

The optimization requires the computation of the derivative of $L(\cdot)$ with respect to ω , b, e_i , and α_i , respectively. Thereafter, a set of linear equations are obtained and can be simplified as

$$\begin{pmatrix} 0 & e^T \\ e & Q + M_n \end{pmatrix} \begin{pmatrix} b^* \\ \alpha^* \end{pmatrix} = \begin{pmatrix} 0 \\ y \end{pmatrix}, \tag{10}$$

where $Q_{ij} = (\phi(x_i) \cdot \phi(x_j)) = k(x_i, x_j), e = (1, 1, 1 ... 1)^T$, $y = (y_1, y_2 \dots y_l)^T$, $\alpha^* = (\alpha_1, \alpha_2 \dots \alpha_l)^T$, $M_n = \text{diag}\{1/Cs_1, \dots, 1/Cs_l\}$, and C > 0 denotes the penalty factor.

Eventually, the fuzzy pruning based LS-SVM function takes the form as follows:

$$y(x) = \sum_{i=1}^{l} \alpha_i^* k(x, x_i) + b^*.$$
 (11)

3.3. The Modeling Steps Based on Fuzzy Pruning LS-SVM. The proposed LS-SVM algorithm based on fuzzy pruning technique can be summarized as follows.

- (1) Based on the training data set $\{x_i, y_i\}_{i=1}^l$, we can calculate the Lagrange multiplier α_i .
- (2) Choose a suitable δ ; the fuzzy membership scores s_i of training data are obtained from (7).
- (3) Build a new data set $\{x_i, y_i, s_i\}_{i=1}^l$, and train the new data set under the scheme of fuzzy pruning LS-SVM algorithm again; then we can get the new α_i^* .
- (4) Sort the Lagrange multiplier α_i , and cut off the data taking larger Lagrange multiplier according to certain proportion (e.g., 5%).
- (5) Then the fuzzy pruning based LS-SVM algorithm is applied to train the current data set. If the fitting performance degrades, the training procedure is done. Otherwise, switch to (4).

4. Two Numerical Simulations

4.1. One-Dimension Function. The effectiveness and efficiency of handing the outliers through the proposed approach are evaluated through two numerical functions. All the simulation experiments are run on a 2.8 GH CPU with 1024 MB RAM PC using Matlab 7.11.

Consider one-dimension function defined as follows:

$$y = \frac{\sin x}{x}, \quad -15 < x < 15. \tag{12}$$

100 data are generated in [-15, 15] randomly as the training data set. To test the performance of detecting outliers, 30% disturbance is added to the 20th, 40th, 60th, 80th, and 100th data sample, respectively. And another 100 data are collected for evaluation.

It can be seen from Figure 1 that the outliers have the higher value of Lagrange multiplier as mentioned above. Using PSO algorithm (w keeps linear decline from 1.2 to 0.4, population size is 20, and maximum number of iterations of the population is 200) to optimize kernel parameter σ and the penalty factor C, then the LS-SVM and fuzzy pruning LS-SVM models are constructed to predict and compare (Figures 2 and 3). Figure 3 is the 45-degree line comparison between different measurements. If two measurements agree with the true outputs, then all data points will fall into the black 45-degree line. The blue circles denote the LS-SVM measurements and the pink asterisks denote the model predictions of fuzzy pruning LS-SVM. We can see that the estimation with the fuzzy pruning LS-SVM fits the black line better and thus provides a superior performance compared to the LS-SVM observation.

The detailed results such as the maximum absolute error (Max EE), the mean absolute error (Mean EE), and root mean square error (RMSE) are calculated and listed in Table 1. The RMSE decreased from 1.21% to 0.052%, which indicates the fuzzy pruning LS-SVM has higher prediction performance and better antidisturbance.

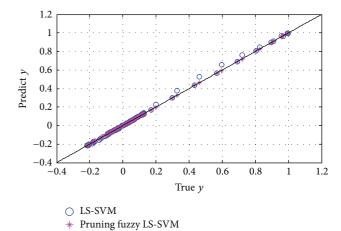


FIGURE 3: 45-degree comparison of the two soft sensors.

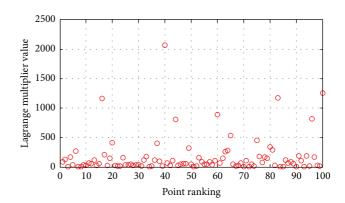


FIGURE 4: Lagrange multiplier value.

4.2. Two-Dimension Function. A two-dimension function is described as

$$z = \sin x \cos y, \quad x \ge -\pi, \ y \le \pi. \tag{13}$$

100 data are generated randomly in the range of $[-\pi,\pi]$, which makes up a training data set. Then the 20th, 40th, 60th, 80th, and 100th data points are added with 30% disturbance separately and the performance is tested by using another different 100 data. As is shown in Figure 4, Lagrange multiplier value of data points that corrupted by some disturbance always has the higher value. Compared results are shown in Figure 5. From Table 2, prediction accuracy of fuzzy pruning LS-SVM is much higher than LS-SVM, which indicates the five outliers have been detected and cut off effectively using the proposed method.

5. An Experiment Simulation

The Pensim simulator provides a simulation of a fed-batch fermentation process for penicillin production. The main component of the process is a fermenter, where the biological reaction takes place. It fully considers the most factors influencing the penicillin fermentation process, such as PH, aeration rate, substrate feed rate, carbon dioxide, and

Table 1: One-dimension function predicted results.

Model	С	σ	Max EE	Mean EE	RMSE
LS-SVM	4616.2	1.5118	0.0640	0.0079	0.0121
Fuzzy pruning LS-SVM	4616.2	1.5118	0.0028	0.0002	5.2456e (-4)

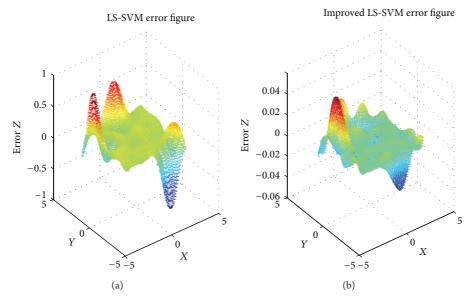


FIGURE 5: Prediction error of two-dimension function.

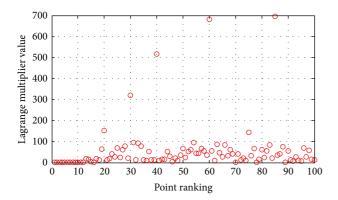


FIGURE 6: Lagrange multiplier value.

penicillin production. The practicability and validity of the platform have been fully verified [25–27] and it has been a benchmark problem for modeling and diagnosis detection.

In this paper Pensim simulation platform is used to generate the original 100 training data. Then 30% disturbance is added to the 20th, 30th, 40th, 60th, and 85th, respectively, and another 100 data are used as test data to verify the constructed model. The simulation results are shown in Figures 7 and 8.

To further exhibit the difference of the two methods, the indexes of Max EE, Mean EE, and RMSE of each method are also calculated and listed in Table 3.

Compared to LS-SVM, the proposed approach makes RMSE decrease from 2.44% to 0.97%, which indicates the fuzzy pruning LS-SVM has better prediction performance.

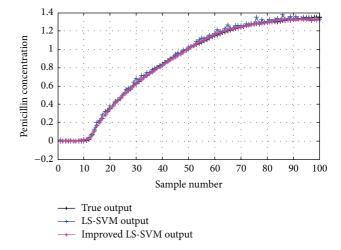


FIGURE 7: Penicillin concentration prediction.

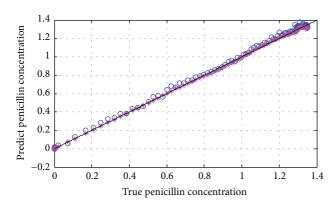
Lagrange multiplier values according to each data point are shown in Figure 6, and we can easily find out the outliers obviously have much bigger Lagrange multiplier. Figure 8 is the 45-degree line comparison between two different soft sensors. Clearly, the fuzzy pruning based LS-SVM exhibits the better capability of approximating the true process. It has effectively handled the disturbance of the outliers so that their impact on modeling is minimized to lowest.

TABLE 2: Two-dimension function predicted results.

Model	С	σ	Max EE	Mean EE	RMSE
LS-SVM	9528.2	1.4557	0.0475	0.0146	0.0207
Pruning fuzzy LS-SVM	9528.2	1.4557	0.0415	0.0029	0.0066

TABLE 3: The predicted concentration of penicillin.

Model	С	σ	Max EE	Mean EE	RMSE
LS-SVM	2131.3	2.5448	0.0678	0.0191	0.0244
Pruning fuzzy LS-SVM	2131.3	2.5448	0.0261	0.0075	0.0097



- o LS-SVM
- * Pruning fuzzy LS-SVM

FIGURE 8: 45-degree comparison of the two soft sensors.

6. Conclusions

A novel LS-SVM method based on fuzzy pruning technique is investigated in this paper. Pruning algorithm is applied to cut off the outliers. Therefore the number of support vectors is reduced which improves the sparseness and accuracy of LS-SVM algorithm. On the other hand, assigning different fuzzy membership score to each of the sample data makes those sample data that play a small role in soft sensor modeling not participate in the construction of the model. Furthermore, the sensitivity to the outliers of the proposed algorithm can be reduced through the fuzzy membership score. The simulation examples demonstrated that the proposed method can effectively handle the outliers and achieved satisfied performance of modeling and prediction.

Conflict of Interests

The authors declare that there is no conflict of interests regarding the publication of this paper.

Acknowledgments

The authors thank the financial support by the National Natural Science Foundation of China (nos. 21206053, 21276111, and 61273131) and partial support by the 111 Project (B12018)

and the Priority Academic Program Development of Jiangsu Higher Education Institutions (PAPD).

References

- [1] S. Yin, H. Luo, and S. Ding, ". Real-time implementation of fault-tolerant control systems with performance optimization," *IEEE Transactions on Industrial Electronics*, vol. 64, no. 5, pp. 2402–2411, 2014.
- [2] Q.-D. Yang, F.-L. Wang, and Y.-Q. Chang, "Soft sensor of biomass based on improved BP neural network," *Control and Decision*, vol. 23, no. 8, pp. 869–878, 2008.
- [3] G. Liu, D. Zhou, H. Xu, and C. Mei, "Soft sensor modeling using SVM in fermentation process," *Chinese Journal of Scientific Instrument*, vol. 30, no. 6, pp. 1228–1232, 2009.
- [4] L. Huang, Y. Sun, X. Ji, Y. Huang, and B. Wang, "Soft sensor of lysine fermentation based on tPSO-BPNN," *Chinese Journal of Scientific Instrument*, vol. 31, no. 10, pp. 2317–2321, 2010.
- [5] S. J. Qin, "Recursive PLS algorithms for adaptive data modeling," *Computers and Chemical Engineering*, vol. 22, no. 4-5, pp. 503–514, 1998.
- [6] W. Li, H. H. Yue, S. Valle-Cervantes, and S. J. Qin, "Recursive PCA for adaptive process monitoring," *Journal of Process Control*, vol. 10, no. 5, pp. 471–486, 2000.
- [7] S. J. Qin and T. J. McAvoy, "Nonlinear PLS modeling using neural networks," *Computers and Chemical Engineering*, vol. 16, no. 4, pp. 379–391, 1992.
- [8] D. Dong and T. J. Mcavoy, "Nonlinear principal component analysis: based on principal curves and neural networks," Computers and Chemical Engineering, vol. 20, no. 1, pp. 65–78, 1996.
- [9] J. C. B. Gonzaga, L. A. C. Meleiro, C. Kiang, and R. Maciel Filho, "ANN-based soft-sensor for real-time process monitoring and control of an industrial polymerization process," *Computers and Chemical Engineering*, vol. 33, no. 1, pp. 43–49, 2009.
- [10] S. Yin, G. Wang, and H. Karimi, "Data-driven design of robust fault detection system for wind turbines," *Mechatronics*, 2013.
- [11] V. N. Vapnik, *The Nature Statistical Learning Theory*, Springer, New York, NY, USA, 1999.
- [12] V. N. Vapnik, "An overview of statistical learning theory," *IEEE Transactions on Neural Networks*, vol. 10, no. 5, pp. 988–999, 1999.
- [13] G. Liu, D. Zhou, H. Xu, and C. Mei, "Microbial fermentation process soft sensors modeling research based on the SVM," *Chinese Journal of Scientific Instrument*, vol. 30, no. 6, pp. 1228– 1232, 2009.
- [14] X.-J. Gao, P. Wang, C.-Z. Sun, J.-Q. Yi, Y.-T. Zhang, and H.-Q. Zhang, "Modeling for Penicillin fermentation process based on

- support vector machine," *Journal of System Simulation*, vol. 18, no. 7, pp. 2052–2055, 2006.
- [15] J. A. K. Suykens and J. Vandewalle, "Least squares support vector machine classifiers," *Neural Processing Letters*, vol. 9, no. 3, pp. 293–300, 1999.
- [16] X. Wang, J. Chen, C. Liu, and F. Pan, "Hybrid modeling of penicillin fermentation process based on least square support vector machine," *Chemical Engineering Research and Design*, vol. 88, no. 4, pp. 415–420, 2010.
- [17] L. LI, H. SU, and J. CHU, "Modeling of isomerization of C8 aromatics by online least squares support vector machine," *Chinese Journal of Chemical Engineering*, vol. 17, no. 3, pp. 437–444, 2009
- [18] L. Li, K. Song, and Y. Zhao, "Modeling of ARA fermentation based on affinity propagation clustering," *CIESC Journal*, vol. 62, no. 8, pp. 2116–2121, 2011.
- [19] J. W. Cao and H. W. Ma, *Microbial Engineering*, Science press, Beijing, China, 2002.
- [20] G. Guo, S. Z. Li, and K. L. Chan, "Support vector machines for face recognition," *Image and Vision Computing*, vol. 19, no. 9-10, pp. 631–638, 2001.
- [21] R.-Q. Chen and J.-S. Yu, "Soft sensor modeling based on particle swarm optimization and least squares support vector machines," *Journal of System Simulation*, vol. 19, no. 22, pp. 5307–5310, 2007.
- [22] L. Huang, Y. Sun, X. Ji, Y. Huang, and T. Du, "Soft sensor modeling of fermentation process based on the combination of CPSO and LSSVM," *Chinese Journal of Scientific Instrument*, vol. 32, no. 9, pp. 2066–2070, 2011.
- [23] X. Zhang, "Using class-center vectors to build support vector machines," in *Proceedings of the 9th IEEE Workshop on Neural Networks for Signal Processing (NNSP '99)*, pp. 3–11, August 1999.
- [24] C.-F. Lin and S.-D. Wang, "Fuzzy support vector machines," IEEE Transactions on Neural Networks, vol. 13, no. 2, pp. 464– 471, 2002.
- [25] S. Yin, S. Ding, A. Haghani, and H. Hao, "Data-driven monitoring for stochastic systems and its application on batch process," *International Journal of Systems Science*, vol. 44, no. 7, pp. 1366– 1376, 2013.
- [26] Y. Liu and H.-Q. Wang, "Pensim simulator and its application in penicillin fermentation process," *Journal of System Simulation*, vol. 18, no. 12, pp. 3524–3527, 2006.
- [27] S. Yin, S. Ding, A. Haghani, H. Hao, and P. Zhang, "A comparison study of basic data driven fault diagnosis and process monitoring methods on the benchmark Tennessee Eastman process," *Journal of Process Control*, vol. 22, no. 9, pp. 1567–1581, 2012.

Hindawi Publishing Corporation Abstract and Applied Analysis Volume 2014, Article ID 764105, 8 pages http://dx.doi.org/10.1155/2014/764105

Research Article

Study on the Characteristics of Electromagnetic Noise of Axial Flux Permanent Magnet Synchronous Motor

Wei Wang, 1 Hang Wang, 1 and Hamid Reza Karimi 2

Correspondence should be addressed to Wei Wang; wangwei_yang@126.com

Received 19 December 2013; Accepted 18 January 2014; Published 27 February 2014

Academic Editor: Ming Liu

Copyright © 2014 Wei Wang et al. This is an open access article distributed under the Creative Commons Attribution License, which permits unrestricted use, distribution, and reproduction in any medium, provided the original work is properly cited.

The normal electromagnetic force distribution in stator system of axial flux permanent magnet synchronous motor (PMSM) has been thoroughly analyzed in this paper. The main composition of force wave causing vibration and noise has been proposed, and at the same time a calculation method of stator natural frequency of axial flux PMSM has been raised. Through this method electromagnetic force wave, natural frequency, vibration response, and electromagnetic noise of a 15 kW axial flux PMSM with 22 poles and 24 slots have been calculated; calculations and measured values are consistent by comparison. The noise sources of axial flux PMSM have been found in this paper, which provides the theoretical support for the suppression of electromagnetic noise of axial flux PMSM.

1. Introduction

Currently, noise, water pollution, and exhaust gas have been the three public hazards of environmental pollution. With the implementation of ISO14001 standard, the motor noise level has been listed as an important indicator of measuring its quality. Therefore, low noise motor will surely become one of the key products to in the 21st century. Internationally, for the motor, the merits and defects of noise control have become a domain factor of market competition for electronic motor, which has been widely recognized by this industry. The level of controlling motor noise has attracted more and more attention of manufacturers and users. And the laws and regulations connected with the working environment noise are becoming more rigid.

Various reasons cause the motor vibration, which are mainly divided into electromagnetic noise, mechanical noise, and aerodynamic noise. A research on how to apply effective fault diagnosis method to make noise fault diagnosis is very significant [1–8]. And the first problem to be solved is how to effectively calculate the vibration and noise of the motor. Compared with the electrical excitation motors, permanent magnet motors, especially rare earth permanent

magnet motors, have simple structure, reliable operation, small volume, light weight, low loss, high efficiency, and diverse shapes and sizes as well as other remarkable advantages [5]. PMSM with multiphase, multipole, and few slots (especially the ratio of poles to slots was 1 to 1) has been applied more and more widely at present. However, compared with the traditional motor, the number and amplitude of air gap harmonics magnetic field, the intensity and frequency of electromagnetic noise, and the adapted suppression methods of this kind of PMSM have distinctive difference.

Although the research about the electromagnetic vibration and noise of motors has made great achievements [6-25], there are still no mature methods to analyze and calculate the modal and natural frequency of axial flux PMSM. Thus this paper will explore the electromagnetic noise of PMSM with multipole and few slots.

2. The Generation Mechanism of Electromagnetic Noise

The normal electromagnetic force, which consists of different frequencies and different distribution rotation force waves

¹ College of Engineering, Bohai University, Jinzhou 121013, China

² Department of Engineering, Faculty of Engineering and Science, The University of Agder, 4898 Grimstad, Norway

caused by the mutual action of stator and rotor and acting on the inner surface of stator core, is the main source of motors vibration and electromagnetic noise.

According to Maxwell law, the instantaneous value of normal electromagnetic force per unit area can be expressed as

$$p_r(\theta, t) = \frac{b^2(\theta, t)}{2\mu_0},\tag{1}$$

where μ_0 is the permeability of vacuum and $b(\theta, t)$ is the air gap flux density, which was superposed by stator flux and rotor flux, and can be expressed as

$$b(\theta, t) = b_{\nu}(\theta, t) + b_{\mu}(\theta, t)$$

$$= \sum_{\nu} B_{\nu} \cos(\nu\theta - \omega_{1}t - \phi_{\nu r})$$

$$+ \sum_{\mu} B_{\mu} \cos(\mu\theta - \omega_{\mu}t - \phi_{\mu r}),$$
(2)

where $b_{\nu}(\theta,t)$, $b_{\mu}(\theta,t)$, respectively, represent the instantaneous value of flux density produced at stator side and rotor side which changed with position angle and time. Then substitute (2) into (1), the following equation can be obtained:

$$\begin{split} p_{r} \left(\theta, t \right) \\ &= \frac{1}{2\mu_{0}} \left\{ \sum_{\nu} B_{\nu}^{2} \cos^{2} \left(\nu \theta - \omega_{1} t - \phi_{\nu r} \right) \right. \\ &+ \sum_{\mu} B_{\mu}^{2} \cos^{2} \left(\mu \theta - \omega_{\mu} t - \phi_{\mu r} \right) \\ &+ 2 \sum_{\nu_{1}, \nu_{2}} B_{\nu_{1}} B_{\nu_{2}} \cos \left(\nu_{1} \theta - \omega_{1} t - \phi_{\nu_{1} r} \right) \\ &\times \cos \left(\nu_{2} \theta - \omega_{1} t - \phi_{\nu_{2} r} \right) \\ &+ 2 \sum_{\nu, \mu} B_{\nu} B_{\mu} \cos \left(\nu \theta - \omega_{1} t - \phi_{\nu r} \right) \\ &\times \cos \left(\mu \theta - \omega_{\mu} t - \phi_{\mu r} \right) \\ &+ 2 \sum_{\mu_{1}, \mu_{2}} B_{\mu_{1}} B_{\mu_{2}} \cos \left(\mu_{1} \theta - \omega_{\mu_{1}} t - \phi_{\mu_{1} r} \right) \\ &\times \cos \left(\mu_{2} \theta - \omega_{\mu_{2}} t - \phi_{\mu_{2} r} \right) \right\} . \end{split}$$

According to (3), the normal electromagnetic force acting on the stator tooth consists of five parts. And the force waves with large amplitude and low order are the primary sources. To PMSM, the electromagnetic force waves, caused by the interaction between rotor and stator harmonic magnetic flux density (the fourth item) and the interaction of various harmonic magnetic flux density produced by permanent magnet (the fifth item), are the major sources of electromagnetic noise.

Under plane radiation, the power of electromagnetic noise caused by electromagnetism acting on stator teeth can be expressed as

$$W = 2\rho c \pi^2 f_r^2 Y^2 S_0, (4)$$

where ρ is the medium density of sound, c is the velocity of sound in medium density, f_r is the frequency of electromagnetic force wave, and S_0 is the vibrating area in vertical direction of the sound wave propagation. Y is the displacement of vibration under stator electromagnetic force and $Y = P'/K - \omega_r^2 M$ when damping neglected. P' is the amplitude of electromagnetic force wave acting on stator teeth. K is the stiffness of stator system. M is the mass of fixed system. ω_r is the angular frequency of electromagnetic force wave

3. The Analysis of Electromagnetic Force Wave of Axial Flux PMSM

The rotating force wave per unit area, causing the electromagnetic noise, can be expressed as

$$p_r(\theta, t) = \sum_r P_r \cos(\omega_r t - r\theta + \varphi_n), \qquad (5)$$

where P_r , r (r = 1, 2, 3, ...) represent the amplitude and the order of electromagnetic force wave.

In a moment of time, the distribution of normal electromagnetic force from zero to third harmonic of axial flux PMSM is shown in Figure 1, where solid dots stand for outward and crossing lines stand for inward. Different sizes of solid dots and crossing lines signify the size and direction of electromagnetic force.

After further clarification of fourth and fifth formulas in formula (3), the main values of electromagnetic force in the realm of amplitude, order, and frequency can be obtained.

$$\begin{split} p_r \left(\theta, t \right) \\ &\approx \frac{1}{2\mu_0} \left\{ 2 \sum_{\nu,\mu} B_{\nu} B_{\mu} \cos \left(\nu \theta - \omega_1 t - \phi_{\nu r} \right) \right. \\ &\quad \times \cos \left(\mu \theta - \omega_{\mu} t - \phi_{\mu r} \right) \\ &\quad + 2 \sum_{\mu_1, \mu_2} B_{\mu_1} B_{\mu_2} \cos \left(\mu_1 \theta - \omega_{\mu_1} t - \phi_{\mu_1 r} \right) \\ &\quad \times \cos \left(\mu_2 \theta - \omega_{\mu_2} t - \phi_{\mu_2 r} \right) \right\} \\ &\quad = \frac{1}{2\mu_0} \sum_{\nu,\mu} B_{\nu} B_{\mu} \\ &\quad \times \cos \left[\left(\nu + \mu \right) \theta - \left(\omega_1 + \omega_{\mu} \right) t - \left(\phi_{\nu r} + \phi_{\mu r} \right) \right] \end{split}$$

Item Harmonic source Amplitude Frequency Order $[(2k_1+1) p_1 \pm k_2 Z_1] t - v_p$ $2k_1 f_1$ $(1/2\mu_0) B_{\nu}B_{\mu}$ The interaction between rotor and stator harmonic $2(k_1+1)f_1$ $[(2k_1+1) p_1 \pm k_2 Z_1] t + \nu_p$ $[2(k_1-k_3)p_1\pm(k_2\pm k_4)Z_1]t$ $2(k_1 - k_3) f_1$ $(1/2\mu_0) B_{\mu 1}B_{\mu 2}$ The interaction of different rotor harmonic $2(k_1 + k_3 + 1)f_1$ $[2(k_1 + k_3 + 1) p_1 \pm (k_2 \pm k_4) Z_1] t$

TABLE 1: Main normal electromagnetic force.

Remark: k_1 , k_2 , k_3 , k_4 are defined as 0, 1, 2, 3, ..., respectively f_1 is fundamental frequency; v_p is harmonic order produced by stator winding.

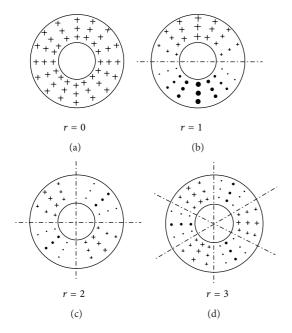


FIGURE 1: Normal electromagnetic forces distribution of axial flux permanent magnet synchronous motor.

$$+ \frac{1}{2\mu_0} \sum_{\mu_1, \mu_2} B_{\mu_1} B_{\mu_2} \times \cos \left[\left(\mu_1 + \mu_2 \right) \theta - \left(\omega_{\mu_1} + \omega_{\mu_2} \right) t - \left(\phi_{\mu_1 r} + \phi_{\mu_2 r} \right) \right]. \tag{6}$$

The electromagnetic noise of axial flux PMSM with the characteristics of 22 poles and 24 slots, six phases, dual-Y, and 30° shifts was studied in this paper. The main normal electromagnetic force was illustrated in formula (6) and its amplitude, order, and frequency were shown in Table 1.

As for PMSM, the main electromagnetic force was from the interactions of different harmonic waves of rotor in which the electromagnetic force generated from the interactions between fundamental harmonic magnetic flux density and first-order tooth harmonic magnetic density of permanent magnet was the most important. The frequency of the electromagnetic force was 2 multiple of fundamental frequency. The order of the electromagnetic force r is

$$r = (p_1 + (p_1 - Z_1))t = (2p_1 - Z_1)t.$$
 (7)

A $15\,\mathrm{kW}$ axial flux PMSM with 22 poles and 24 slots was taken as an example in this paper. The frequency and

TABLE 2: Main electromagnetic force with 22 Poles and 24 Slots.

$\overline{\nu_1}$				μ_1			
-1	$(9)_{3}$	11	$(-13)_1$	33	$(35)_1$	$[-37]_1$	55
5	$4/2 f_1$						
-7		$4/2f_1$					
11	$2/2f_1$		$2/2f_1$				
$(-13)_1$	$4/4 f_1$	$2/2f_1$					
17			$4/2f_1$				
29				$4/2 f_1$			
-31				$2/4f_1$	$4/2 f_1$		
$(35)_{1}$				$2/2f_1$			
$[-37]_{1}$				$4/4f_{1}$	$2/2f_1$		
41						$4/2f_1$	

order of the electromagnetic force were shown in Table 2, where () stands for first slot harmonic, [] stands for second slot harmonic, the subscripts out of parentheses represent that the slot harmonic in parentheses was generated by its interactions, and ν_1 , μ_1 were the harmonic order of stator side and rotor. Also, low-order harmonic force wave would be generated from the interactions between μ_1 and μ_2 . The harmonic order with bold font also represented ν_1 and μ_2 .

As seen from Table 2, firstly, the electromagnetic force wave, which order is 2 and frequency is $2f_1$, has been generated from the interactions between 11th fundamental harmonic of permanent magnet and first slot harmonic magnetic flux density (-13) of stator and rotor. Secondly, loworder force wave generated from the interactions between 11th fundamental harmonic of stator and first slot harmonic magnetic flux density (-13) of rotor was equally important. Thirdly, another electromagnetic force wave was the second gear force wave (the frequency was $2f_1$) which was generated from the interactions between 33th harmonic (the flux density was 3 times of fundamental wave) and 35th step first slot harmonic wave of rotor. The above will be the largest sources of force wave.

The power spectral density of electromagnetic force wave (the step was less than 4) could be derived by using analytic method. The fundamental frequency (f_1) of motor was 82.5 Hz. As seen in Figure 2, each frequency of electromagnetic force was an even multiple of fundamental frequency, where the energy of electromagnetic force whose frequency was 2 multiple of fundamental frequency was the biggest, which was consistent with analysis of Table 2.

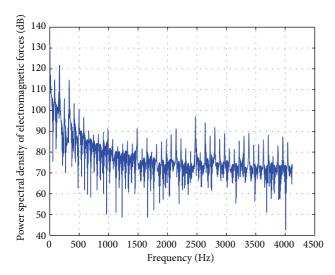


FIGURE 2: Power spectral density of electromagnetic forces used analytical methods.

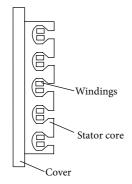


FIGURE 3: Stator system of axial flux PMSM.

4. The Analysis of Natural Frequency of Stator System of Axial Flux PMSM

4.1. The Analysis of Natural Frequency. The vibrating direction of axial flux PMSM stator system was axial. Based on the analysis, the vibration characteristics of stator yoke were similar to doughnut-shaped steel plate, so choosing the circular plate as a replacement. The stator structure and the stress direction of stator tooth were shown in Figures 3 and 4.

With reference to calculative method of stator natural frequency for radial flux PMSM, the calculation formula of stator natural frequency of axial flux PMSM was presented as follows:

$$f_m = \frac{1}{2\pi} \sqrt{\frac{K_m^{(c)} + K_m^{(f)}}{\Delta_w M_m^{(c)} + \Delta_f M_m^{(f)}}},$$
 (8)

where $K_m^{(c)}$ is the equivalent stiffness of stator core, $K_m^{(f)}$ is the equivalent stiffness of the cover, $M_m^{(c)}$ is the equivalent mass of stator core, $M_m^{(f)}$ is the equivalent mass of the cover, $\Delta_\omega = 1 + (M_t + M_w)/M_m^{(c)}$ is the additional coefficient of core mass, M_t , M_w is the mass of stator tooth and stator winding,

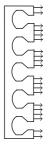


FIGURE 4: Stress direction of stator tooth of axial flux PMSM stator system of axial flux PMSM.

 $\Delta_f=1+M_f/K_m^{(f)}$ is the additional coefficient of the cover, and M_f is the mass of shell.

From (8), we can see that the key to getting stator natural frequency was how to determine the equivalent stiffness of iron core and cover in different vibrational modes.

When computed through the distribution of the quality system and the centralized quality system, the calculation formula of natural frequency of annular plate was presented as follows:

$$f_m = \frac{a_{ns}}{2\pi a^2} \sqrt{\frac{D}{\rho_A}} \tag{9}$$

$$f_m = \frac{1}{2\pi} \sqrt{\frac{K_m}{M_m}},\tag{10}$$

where D is the bending rigidity of plate and E is the modulus of elasticity of plate. h is the thickness of laminated plate and μ is Poisson's ratio. a is the outer radius of annular plates, ρ_A is the surface density of circular plate with a radius of a, and a_{ns} is the frequency constants, determined by boundary conditions, vibrational mode, and the ratio of inside to outside diameter.

According to (9),

$$f_{m} = \frac{a_{ns}}{2\pi a^{2}} \sqrt{\frac{D}{\rho_{A}}} = \frac{1}{2\pi} \sqrt{\frac{a_{ns}^{2} D\pi \left(a^{2} - b^{2}\right)}{a^{4} \rho_{A} \pi \left(a^{2} - b^{2}\right)}} = \frac{1}{2\pi} \sqrt{\frac{K_{m}}{M_{m}}},$$
(11)

where

$$K_{m} = \frac{a_{ns}^{2} D\pi \left(a^{2} - b^{2}\right)}{a^{4}}$$

$$M_{m} = \rho_{A} \pi \left(a^{2} - b^{2}\right),$$
(12)

where b the inside radius of the annular plate.

4.2. The Calculations of Stator System Natural Frequency of a 15 kW Axial Flux PMSM. The natural frequency of a 15 kW axial flux PMSM was calculated in this paper. The structure parameters of stator system were listed in Table 3 and the computational results of equivalent stiffness and natural frequency were listed in Table 4. To verify the effectiveness

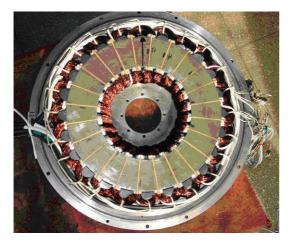


FIGURE 5: Stator system for 15 kW motor example of a figure caption.

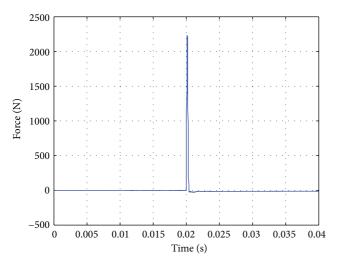


FIGURE 6: Excitation signal imposed on stator system.

Table 3: Parameters of stator system of 15 kW motor.

Parameters	Value
Outerdiameter of stator	250 mm
Innerdiameter of stator	144 mm
Height of iron core yoke	12.7 mm
Weight of statorteeth	$2.4 \mathrm{kg}$
Weight of iron core yoke	2.9 kg
Weight of stator winding	3.4 kg

of the calculation method presented in this paper, the 15 kW axial flux PMSM was tested by using PULSE system produced by Denmark B&K company. Figure 5 was stator system for 15 kW motor. Figures 6, 7, and 8 were, respectively, curves of excitation, response, and transfer functions. According to Figure 8, the natural frequency of stator system can be obtained, and test results were listed in Table 4.

The natural frequency of stator system must be away from the electromagnetic force wave; otherwise the motor will cause resonance, resulting in serious consequences.

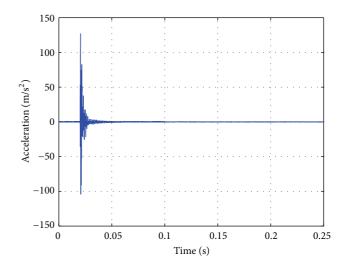


FIGURE 7: Response by stator system natural frequency experiment.

Table 4: Calculation and test results for natural frequencies of stator core of 15 kW motor.

(n, s)	$K_m^{(c)}/\mathrm{M \ N\cdot m}^{-1}$	$f_{\rm ma}/{\rm Hz}$	$f_{\rm me}/{\rm Hz}$	err/%
(2, 0)	91.75	258.3	280	-7.75
(3, 0)	777.42	691.2	675	2.40
(1, 1)	238.67	1174.5	1135	3.48
(4, 0)	2746.05	1265.0	1313	-3.65
(5,0)	6943.36	1985.2	2040	-2.68

Remark: n is pitch diameter number; s is pitch circle number; $f_{\rm ma}$ is calculation natural frequency; $f_{\rm me}$ is measured value of natural frequency; err is relative error.

5. The Analysis of Electromagnetic Noise of Axial Flux PMSM

5.1. The Dynamic Response of Motor. The vibration of motor caused by normal electromagnetic force acting on stator system is the main source of electromagnetic noise and an analytic relationship exists between the vibration and noise. Therefore it is very important to calculate the vibration of motor. When the motor was at work, vibration at every point was caused all by different electromagnetic forces, which synthesized by vibration waveform of different amplitudes and different frequencies. When a lumped parameter mechanical system suffered a harmonic force with ω_r frequency and P_{rs} amplitude, the vibration velocity of the system can be expressed as follows:

$$\dot{Y} = \frac{\omega_r P_{rs}}{\left(K_r^{(c)} + K_r^{(f)}\right) - \omega_r^2 \left(\Delta_w M_m^{(c)} + \Delta_f M_m^{(f)}\right)},\tag{13}$$

where $K_r^{(c)}$, $K_r^{(f)}$ is equivalent stiffness of stator core and shields with the same number between number of pitch diameter and force wave.

The spectrum curve of vibrator acceleration of motor cover was obtained through experiment, which is shown in Figure 9. We can obtain the amplitude of vibration acceleration in maximal frequency from curve. Calculation and

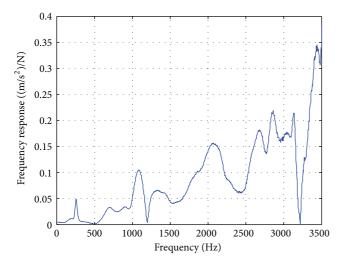


FIGURE 8: Transfer function by stator system natural frequency experiment.

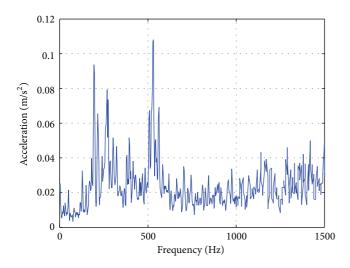


FIGURE 9: Spectrogram of vibration accelerations of motor cover.

measured value of vibration acceleration of motor shield were listed in Table 5.

The most important frequency component of the vibration acceleration level is $165 \, \text{Hz}$ and $330 \, \text{Hz}$. From Table 5, the calculate errors -5.2% and -0.47% indicate that the calculation results are consistent with the actual value.

5.2. The Electromagnetic Noise. Four steps must be completed before obtaining electromagnetic noise: calculating magnetic field and its harmonic, calculating normal electromagnetic force, calculating natural frequency and vibratory response of stator system, and calculating noise power level. On the basis of the previous three steps, you can successfully get the electromagnetic noise of the motor. Under nonloaded operation, the electromagnetic noise of axial flux PMSM was calculated by author edited programming, and at the same time the electromagnetic noise of the motor was measured



FIGURE 10: Experiment of 15 kW motor.

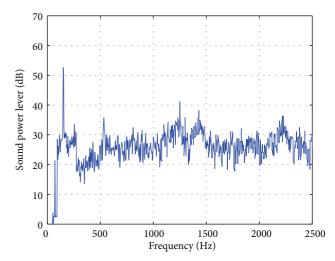


FIGURE 11: Spectrum of electromagnetic noise sound power lever L_I of 15 kW motor.

in an anechoic chamber which is shown in Figures 10 and 11. And the test value and calculated value were listed in Table 6.

The calculation results of acoustic noise in Table 6 have been modified, and the correction factor is 1.082. The noise of 165 Hz is the most significant from the measured spectrum of acoustic noise, and theoretical calculations have the same conclusion. So rationality about analysis and calculation methods of axial flux PMSM electromagnetic noise mentioned by this paper has been proved.

6. Conclusion

The methods of analyses and calculation for electromagnetic vibration and noise have been researched in this paper. Using a 15 kW axial flux PMSM with 22 poles and 24 slots as an example, a verification calculation has been completed. The conclusions are illustrated.

(1) The direction of electromagnetic vibration: the direction of electromagnetic vibration was axial; thus typical estimation method for calculating electromagnetic vibration is not suitable.

TABLE 5: Calculated and experimental values of accelerations level of 15 kW motor.

Item		Value		
Frequency/Hz	165	330	495	825
Calculation/dB	94.5	84.1	82.3	62.36
Measured value/dB	99.7	84.5	78.1	74.66
Error/%	-5.2	-0.47	5.3	16.4

Table 6: Comparation between calculated and measured values of Sound power lever.

Frequency/Hz	Calculation after correction/dB (A)	Measured value/dB (A)	Error/%
165	72.60	72.6	0
330	59.73	59.1	1.06
660	48.15	48.5	-0.7
Combining	72.6	72.6	0

- (2) The stator system structure of axial flux PMSM: the stator system of axial flux PMSM can be equivalent to annular steel plate and vibration mode was indicated by the number of pitch diameter and pitch, where the stator core thickness replaced with annular plate of stator yoke to calculate the height, teeth of the stator, and winding as additional quality were included in the stator core; shell as additional quality was included in the shield.
- (3) The frequency of electromagnetic noise and vibration: the frequencies of electromagnetic noise and vibration were even multiple of fundamental wave. The frequency of vibration with highest energy was 2 times of fundamental frequency, which was caused by the normal electromagnetic force with frequency of double fundamental frequency. The main components of the electromagnetic force are listed below.
 - (a) One of the main components of the electromagnetic force: the low order force was caused by the interaction between fundamental flux density of permanent magnet and first-order slot harmonic magnetic density of rotor and stator.
 - (b) Another one of the main components of the electromagnetic force: the low order force was caused by the interaction between fundamental flux density of stator and first-order tooth harmonic magnetic density of rotor.
 - (c) The third main components of the electromagnetic force: the low order force was caused by the interaction between 3 times of the fundamental flux density of rotor and first-order slot harmonic magnetic density of rotor and stator.
 - (d) The forth main components of the electromagnetic force: the electromagnetic vibration and noise sources of axial flux PMSM have been presented in this paper, which provides

the theoretical support for the suppression of electromagnetic noise of axial flux PMSM.

Conflict of Interests

The authors declare that there is no conflict of interests regarding the publication of this paper.

Acknowledgments

The research leading to these results has received funding from the Research Foundation Program for Doctor of Liaoning Province (20131001) and the Polish-Norwegian Research Programme operated by the National Centre for Research and 24 Development under the Norwegian Financial Mechanism 2009–2014 in the frame of Project Contract no. Pol-Nor/200957/47/2013.

References

- [1] S. Yin, S. X. Ding, A. H. A. Sari, and H. Hao, "Data-driven monitoring for stochastic systems and its application on batch process," *International Journal of Systems Science: Principles and Applications of Systems and Integration*, vol. 44, no. 7, pp. 1366–1376, 2013.
- [2] S. Yin, S. X. Ding, A. Haghani, H. Hao, and P. Zhang, "A comparison study of basic data-driven fault diagnosis and process monitoring methods on the benchmark Tennessee Eastman process," *Journal of Process Control*, vol. 22, no. 9, pp. 1567–1581, 2012.
- [3] S. Yin, H. Luo, and S. Ding, "Real-time implementation of fault-tolerant control systems with performance optimization," *IEEE Transactions on Industrial Electronics*, vol. 61, no. 5, pp. 2402–22411, 2013.
- [4] S. Yin, X. Yang, and H. R. Karimi, "Data-driven adaptive observer for fault diagnosis," *Mathematical Problems in Engineering*, vol. 2012, Article ID 832836, 21 pages, 2012.
- [5] X. Zhao, X. Liu, S. Yin, and H. Li, "Improved results on sta-bility of continuous-time switched positive linear systems," *Automat*ica, 2013
- [6] X. Zhao, P. Shi, and L. Zhang, "Asynchronously switched control of a class of slowly switched linear systems," *Systems & Control Letters*, vol. 61, no. 12, pp. 1151–1156, 2012.
- [7] X. Zhao, L. Zhang, and P. Shi, "Stability of a class of switched positive linear time-delay systems," *International Journal of Ro*bust and Nonlinear Control, vol. 23, no. 5, pp. 578–589, 2013.
- [8] X. Zhao, L. Zhang, P. Shi, and H. Karimi, "Robust control of continuous-time systems with state-dependent uncertainties and its application to electronic circuits," *IEEE Transactions on Industrial Electronics*, no. 99, 1 page, 2013.
- [9] Z. Q. Zhu and D. Howe, "Instantaneous magnetic field distribution in permanent magnet brushless DC motors. Part IV: magnetic field on load," *IEEE Transactions on Magnetics*, vol. 29, no. 1, pp. 152–158, 1993.
- [10] Y.-X. Chen, Z.-Q. Zhu, and S.-C. Ying, Analysis and Control of Moto, Zhejiang University Press, Hangzhou, China, 1987.
- [11] Z. Q. Zhu, D. Howe, and C. C. Chan, "Improved analytical model for predicting the magnetic field distribution in brushless permanent-magnet machines," *IEEE Transactions on Magnetics*, vol. 38, no. 1, pp. 229–238, 2002.

- [12] Z. Q. Zhu, Z. P. Xia, L. J. Wu, and G. W. Jewell, "Analytical modelling and finite element computation of radial vibration force in fractional-slot permanent magnet brushless machines," in *Proceedings of the IEEE International Electric Machines and Drives Conference (IEMDC '09)*, pp. 144–151, Miami, Fla, USA, May 2009.
- [13] S. A. Long, Z. Q. Zhu, and D. Howe, "Vibration behaviour of stators of switched reluctance motors," *IEE Proceedings: Electric Power Applications*, vol. 148, no. 3, pp. 257–264, 2001.
- [14] D. Žarko, D. Ban, and T. A. Lipo, "Analytical solution for cogging torque in surface permanent-magnet motors using conformal mapping," *IEEE Transactions on Magnetics*, vol. 44, no. 1, pp. 52–65, 2008.
- [15] H. R. Izadfar, S. Shokri, and M. Ardebili, "Magnetic field analysis in permanent magnet synchronous machine by analytical method," in *Proceedings of the International Conference on Electrical Machines and Systems (ICEMS '07)*, pp. 670–674, Seoul, South Korea, October 2007.
- [16] X. Wang, Q. Li, S. Wang, and Q. Li, "Analytical calculation of air-gap magnetic field distribution and instantaneous characteristics of brushless DC motors," *IEEE Transactions on Energy Conversion*, vol. 18, no. 3, pp. 424–432, 2003.
- [17] D. Žarko, D. Ban, and T. A. Lipo, "Analytical calculation of magnetic field distribution in the slotted air gap of a surface permanent-magnet motor using complex relative air-gap permeance," *IEEE Transactions on Magnetics*, vol. 42, no. 7, pp. 1828– 1837, 2006.
- [18] J. Azzouzi, G. Barakat, and B. Dakyo, "Quasi-3-D analytical modeling of the magnetic field of an axial flux permanentmagnet synchronous machine," *IEEE Transactions on Energy Conversion*, vol. 20, no. 4, pp. 746–752, 2005.
- [19] F. Ishibashi, K. Kamimoto, S. Noda, and K. Itomi, "Small induction motor noise calculation," *IEEE Transactions on Energy Conversion*, vol. 18, no. 3, pp. 357–361, 2003.
- [20] L. Yang, C. Lixiang, T. Renyuan, and C. Jian, "Test and analysis of vibration and noise for permanent magnet synchronous motor," *Electrical Engineering*, no. 4, pp. 18–20, 2009.
- [21] S. Yu, J. Xu, Q. Zhao, and R. Tang, "Experimental research of permanent magnet synchronous motor vibration and noise characteristics," *Journal of Northeastern University*, vol. 23, no. 1, pp. S72–S76, 2002.
- [22] S. Yu, Q. Zhao, and R. Tang, "Researches on noise and vibration characteristics of large-capacity permanent magnet synchronous machine," in *Proceedings of the 5th International Conference on Electrical Machines and Systems (ICEMS '01)*, vol. 2, pp. 846–849, Shenyang, China, 2001.
- [23] K.-T. Kim, K.-S. Kim, S.-M. Hwang, T.-J. Kim, and Y.-H. Jung, "Comparison of magnetic forces for IPM and SPM motor with rotor eccentricity," *IEEE Transactions on Magnetics*, vol. 37, no. 5 I, pp. 3448–3451, 2001.
- [24] H.-S. Ko and K.-J. Kim, "Characterization of noise and vibration sources in interior permanent-magnet brushless DC motors," *IEEE Transactions on Magnetics*, vol. 40, no. 6, pp. 3482–3489, 2004.
- [25] S. Yu and R. Tang, "Electromagnetic and mechanical characterizations of noise and vibration in permanent magnet synchronous machines," *IEEE Transactions on Magnetics*, vol. 42, no. 4, pp. 1335–1338, 2006.

Hindawi Publishing Corporation Abstract and Applied Analysis Volume 2014, Article ID 512037, 9 pages http://dx.doi.org/10.1155/2014/512037

Research Article

Event-Based H_{∞} Filter Design for Sensor Networks with Missing Measurements

Jinliang Liu,^{1,2} Shumin Fei,² and Engang Tian³

Correspondence should be addressed to Shumin Fei; smfei@seu.edu.cn

Received 26 December 2013; Accepted 16 January 2014; Published 24 February 2014

Academic Editor: Ming Liu

Copyright © 2014 Jinliang Liu et al. This is an open access article distributed under the Creative Commons Attribution License, which permits unrestricted use, distribution, and reproduction in any medium, provided the original work is properly cited.

In order to save network resources and network bandwidth, this paper proposed an event triggered mechanism based on sampled-data information, which has some advantages over existing ones. Considering the missing sensor measurements and the network-induced delay in the transmission, we construct a new event-based H_{∞} filtering by taking the effect of sensor faults with different failure rates. By using the Lyapunov stability theory and the stochastic analysis theory, sufficient criteria are derived for the existence of a solution to the algorithm of the event-based filter design. Finally, an example is exploited to illustrate the effectiveness of the proposed method.

1. Introduction

The application of network technologies is becoming increasingly important in many areas for its predominant advantages (such as low cost, simple installation and maintenance, and high reliability). However, it is known that implementing a communication network can induce multiple channel transmission, packet dropout, and so on. This has motivated much attention to the research. Various techniques have been proposed to deal with the above issues, such as time triggered communication scheme [1, 2] and event triggered communication scheme [3–7]. In general, under a time triggered communication scheme, a fixed sampling interval should be selected under worse conditions such as external disturbances and time delay. However, such situation rarely occurs. Hence, time triggered communication scheme can lead to transmit much unnecessary information and inefficient utilization of limited network resources. Comparing with time triggered scheme, the event triggered scheme can save the network resources such as network bandwidth while maintaining the control performance. The adoption of the event triggered scheme has drawn a great deal of interest to the researchers. The authors in [3] firstly proposed a kind

of event triggered scheme which decided whether the newly sampled signal should be transmitted to the controller and invested the controller design problem. In [8], the authors took the sensor and actuator faults into consideration and studied the reliable control design for networked control system under event triggered scheme. The authors in [9] were concerned with the control design problem of event triggered networked systems with both state and control input quantization. In [10], the authors discussed the event-based fault detection for the networked systems with communication delay and nonlinear perturbation.

On the other hand, the filtering problem has been a hot topic over the past decades. A large number of outstanding results have been published [9, 11–18]. For example, the researchers in [9] studied the problem of event-based H_{∞} filtering for networked systems with communication delay. Most of them are based on an assumption that sensors are working without any flaws. However, the distortion of the sensor usually occurs due to the internal noise or external disturbance. Therefore, it is necessary to discuss the situation when the filter cannot receive the value of the process accurately. Fortunately, much effort has been put into this issue. The authors in [19] were concerned with reliable

¹ Department of Applied Mathematics, Nanjing University of Finance and Economics, Nanjing, Jiangsu 210023, China

² School of Automation, Southeast University, Nanjing 210096, China

³ Institute of Information and Control Engineering Technology, Nanjing Normal University, Nanjing, Jiangsu 210042, China

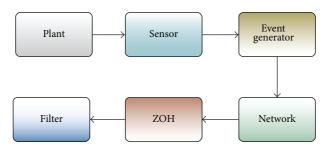


FIGURE 1: The structure of an event triggered filter design system.

 H_{∞} filter design for sampled-data systems with probabilistic sensor signal distortion. In [20], the authors investigated reliable H_{∞} filter design for T-S fuzzy model based networked control systems with random sensor failure.

To the best of our knowledge, the filter design of event triggering network-based systems with random sensor failures is still an open problem, which motivates our present paper. The main contributions of the obtained results are as follows: (I) the insertion of the event triggering generator saves the network resources and network bandwidth. (II) A new kind of event triggering network-based systems with probabilistic sensor failures and network induced delay, which has not been investigated in the existing literatures, is proposed.

This paper is outlined as follows. Section 2 presents the modeling. Section 3 presents our main stability theorem and develops a filter design method. In Section 4, an example is given to illustrate the effectiveness of the proposed method.

 \mathbb{R}^n and $\mathbb{R}^{n\times m}$ denote the n-dimensional Euclidean space and the set of $n\times m$ real matrices; the superscript "T" stands for matrix transposition; I is the identity matrix of appropriate dimension; $\|\cdot\|$ stands for the Euclidean vector norm or the induced matrix 2-norm as appropriate; the notation X>0 (resp., $X\geq 0$), for $X\in\mathbb{R}^{n\times n}$ means that the matrix X is real symmetric positive definite (resp., positive semidefinite), when X is a stochastic variable. For a matrix X and two symmetric matrices X and X and X denotes a symmetric matrix, where X denotes the entries implied by symmetry.

2. System Description

As shown in Figure 1, our aim in this paper is to investigate an event-based reliable filtering design problem by taking the effect of sensor faults. Suppose the plant model is governed by

$$x(k+1) = Ax(k) + Bw(k),$$

$$y(k) = Cx(k),$$

$$z(k) = Lx(k),$$
(1)

where $x(k) \in \mathbb{R}^n$ is the state vector, $y(k) \in \mathbb{R}^m$ is the measured output, z(k) is the signal to be estimated, w(k) is the process noise belonging to $\mathbb{L}_2(0,\infty)$, A, B, C, and L are known constant matrices with appropriate dimensions.

Remark 1. Considering the network induced delay, the transmission time of measured output y(k) from sensor to filt cannot be neglected. The input of the filter is not y(k), but $\hat{y}(k)$, in fact, $\hat{y}(k) = y(k + \tau(k))$. $\tau(k)$ is the network induced delay, and $\tau(k) \in [0, \tau^M)$, where τ^M is a positive real number.

For the network-based system in described in Figure 1, we propose the following filter:

$$x_{f}\left(k+1\right) = A_{f}x_{f}\left(k\right) + B_{f}\widehat{y}\left(k\right),$$

$$z_{f}\left(k\right) = C_{f}x_{f}\left(k\right),$$
 (2)

where $x_f(k)$ is the filter state, $\hat{y}(k)$ is the input of the filter, A_f, B_f, C_f are the filter matrices of appropriate dimensions. If we take the missing sensor measurements into consideration, (2) can be described as

$$x_{f}(k+1) = A_{f}x_{f}(k) + B_{f}\Xi\widehat{y}(k),$$

$$z_{f}(k) = C_{f}x_{f}(k),$$
(3)

where $\Xi = \operatorname{diag}\{\Xi_1, \Xi_2, \dots, \Xi_m\}$, $\Xi_i \in [0, \theta_1]$ $(i = 1, 2, \dots)$ $(\theta_1 > 1)$ being m unrelated random variables, and the mathematical expectation and variance of Ξ_i are α_i and σ_i^2 , respectively.

Remark 2. When $\alpha_i = 1$, it means the sensor i works normally. When $\alpha_i = 0$, it means the sensor i completely failed and the signal transmitted by sensor i is lost. When $\Xi_i \in [0, 1]$, it means the signal at the filter is smaller or greater than it actually is [20].

In order to reduce the load of network transmission and save the network resources such as network bandwidth, it is necessary to introduce an event triggered mechanism. As is shown in Figure 1, an event generator is constructed between the sensor and filter, which is used to decide whether the measured output should be sent to the filter. We adopt the following judgement algorithm:

$$\left[\mathbb{E}\left\{\Xi y\left(k\right)\right\} - \mathbb{E}\left\{\Xi y\left(s_{i}\right)\right\}\right]^{T} \Omega\left[\mathbb{E}\left\{\Xi y\left(k\right)\right\} - \mathbb{E}\left\{\Xi y\left(s_{i}\right)\right\}\right]$$

$$\leq \sigma\left[\mathbb{E}\left\{\Xi y\left(k\right)\right\}\right]^{T} \Omega\left[\mathbb{E}\left\{\Xi y\left(k\right)\right\}\right],$$
(4)

where $\Omega \in \mathbb{R}^m \times m$ is a symmetric positive definite matrix, $\sigma \in [0, 1), \Xi = \text{diag}\{\Xi_1, \Xi_2, \ldots\}$, and $\Xi_i \in [0, \theta_1]$ $(i = 1, 2, \ldots)$

are m unrelated random variables. Only when the expectation of a certain function of current sampled value y(k) and the previously transmitted one $y(s_i)$ violate (4), it can be sent out to the filter.

Remark 3. Under the event triggering (4), the release times are assumed to be s_0, s_1, s_2, \ldots . Due to the delay in the network transmission, the measured output will arrive at the filter at the instants $s_0 + \tau(s_0), s_1 + \tau(s_1), s_2 + \tau(s_2), \ldots$, respectively.

Based on the above analysis, considering the behavior of ZOH, the input of the filter is

$$\Xi \widehat{y}\left(k\right) = \Xi \widehat{y}\left(s_{i}\right), \quad k \in \left[s_{i} + \tau\left(s_{i}\right), s_{i+1} + \tau\left(s_{i+1}\right) - 1\right]. \tag{5}$$

Similar to [4, 6, 11], for technical convenience, consider the following two cases.

Case 1. When $s_i + 1 + \tau^M \ge s_{i+1} + \tau(s_{i+1}) - 1$, define a function d(k) as

$$d(k) = k - s_i, \quad k \in [s_i + \tau(s_i), s_{i+1} + \tau(s_{i+1}) - 1].$$
 (6)

Obviously,

$$\tau(s_i) \le d(k) \le (s_{i+1} - s_i) + \tau(s_{i+1}) - 1 \le 1 + \tau^M.$$
 (7)

Case 2. When $s_i + 1 + \tau^M \le s_{i+1} + \tau(s_{i+1}) - 1$, consider the following two intervals:

$$\left[s_{i}+\tau\left(s_{i}\right),s_{i}+\tau^{M}\right], \qquad \left[s_{i}+\tau^{M}+l,s_{i}+\tau^{M}+l+1\right]. \tag{8}$$

From $\tau(k) \le \tau^M$, we can deduce that there must exist d satisfying

$$s_i + d + \tau^M < s_{i+1} + \tau \left(s_{i+1} \right) - 1 \le s_i + d + 1 + \tau^M. \tag{9}$$

Moreover, $y(s_i)$ and $y(s_i + l)$ l = 1, 2, ..., d satisfy (4). Set

$$I_{0} = \left[s_{i} + \tau \left(s_{i} \right), s_{i} + \tau^{M} + 1 \right),$$

$$I_{l} = \left[s_{i} + \tau^{M} + l, s_{i} + \tau^{M} + l + 1 \right),$$

$$I_{d} = \left[s_{i} + d + \tau^{M}, s_{i+1} + \tau \left(s_{i+1} \right) - 1 \right],$$
(10)

where l = 1, 2, ..., d - 1. Clearly, we have

$$[s_i + \tau(s_i), s_{i+1} + \tau(s_{i+1}) - 1] = \bigcup_{i=0}^{i=d} I_i.$$
 (11)

Define d(k) as

$$d(k) = \begin{cases} k - s_i, & k \in I_0, \\ k - s_i - l, & k \in I_l, l = 1, 2, \dots, d - 1, \\ k - s_i - d, & k \in I_d. \end{cases}$$
 (12)

Then, one can easily get

$$\tau\left(s_{i}\right) \leq d\left(k\right) \leq 1 + \tau^{M} \triangleq d^{M}, \quad k \in I_{0},$$

$$\tau\left(s_{i}\right) \leq \tau^{M} \leq d\left(k\right) \leq d^{M}, \quad k \in I_{l}, \ l = 1, 2, \dots, d - 1,$$

$$\tau\left(s_{i}\right) \leq \tau^{M} \leq d\left(k\right) \leq d^{M}, \quad k \in I_{d}.$$

$$(13)$$

Due to $s_{i+1} + \tau(s_{i+1}) - 1 \le s_i + d + 1 + \tau^M$, the third row in (13) holds. Obviously,

$$\tau(s_i) \le \tau^M \le d(k) \le d^M, \quad k \in I_d. \tag{14}$$

In Case 1, for $k \in [s_i + \tau(s_i), s_{i+1} + \tau(s_{i+1}) - 1]$, define $e_i(k) = 0$. When it comes to Case 2, define

 $\overline{\Xi}e_{i}(k)$

$$=\begin{cases} 0, & k \in I_0, \\ \overline{\Xi}y(s_i) - \overline{\Xi}y(s_i+l), & k \in I_l, l = 1, 2, \dots, d-1, \\ \overline{\Xi}y(s_i) - \overline{\Xi}y(s_i+d), & k \in I_d. \end{cases}$$

$$(15)$$

It can be deduced from the definition of $\overline{\Xi}e_i(k)$ and the event triggering scheme (4); for $k \in [s_i + \tau(s_i), s_{i+1} + \tau(s_{i+1}) - 1]$, the following inequality holds

$$e_{i}^{T}(k)\overline{\Xi}^{T}\Omega\overline{\Xi}e_{i}(k) \leq \sigma y^{T}(k-d(k))\overline{\Xi}^{T}\Omega\overline{\Xi}y(k-d(k)).$$
(16)

Remark 4. From (15), it can be easily obtained that

 $e_i(k)$

$$=\begin{cases} 0, & k \in I_0, \\ y(s_i) - y(s_i + l), & k \in I_l, l = 1, 2, \dots, d - 1, \\ y(s_i) - y(s_i + d), & k \in I_d. \end{cases}$$
(17)

Employing d(k) $e_i(k)$, the input of the filter $\Xi \hat{y}(k)$ can be rewritten as

$$\Xi \widehat{y}(k) = \Xi y(s_i) = \Xi (y(k - d(k)) + \Xi e_i(k)),$$

$$k \in [s_i + \tau(s_i), s_{i+1} + \tau(s_{i+1}) - 1].$$
(18)

Obviously,

$$\widehat{y}(k) = y(s_{i}) = (y(k - d(k)) + e_{i}(k)), k \in [s_{i} + \tau(s_{i}), s_{i+1} + \tau(s_{i+1}) - 1].$$
(19)

Combining (19) and (3), we can get

$$x_{f}\left(k+1\right) = A_{f}x_{f}\left(k\right) + B_{f}\Xi\left(Cx\left(k-d\left(k\right)\right) + e_{i}\left(k\right)\right),$$

$$z_{f}\left(k\right) = C_{f}x_{f}\left(k\right). \tag{20}$$

Define $\eta(k) = \begin{bmatrix} x(k) \\ x_f(k) \end{bmatrix}$, $e(k) = z(k) - z_f(k)$; the following filtering-error system based on (1) and (20) can be obtained as

$$\eta(k+1) = \overline{A}\eta(k) + Dx(k-d(k)) + D_k x(k-d(k))$$

$$+ \overline{B}e_i(k) + \overline{B}_k e_i(k) + \overline{B}_1 w(k),$$

$$e(k) = \overline{L}\eta(k),$$
(21)

$$\begin{split} &\text{where } \overline{A} = \left[\begin{smallmatrix} A & 0 \\ 0 & A_f \end{smallmatrix} \right], D = \left[\begin{smallmatrix} 0 \\ B_f \overline{\Xi}C \end{smallmatrix} \right], D_k = \left[\begin{smallmatrix} 0 \\ B_f (\Xi - \overline{\Xi})C \end{smallmatrix} \right], \overline{B} = \left[\begin{smallmatrix} 0 \\ B_f \Xi \end{smallmatrix} \right], \\ \overline{B}_k = \left[\begin{smallmatrix} 0 \\ B_f (\Xi - \overline{\Xi}) \end{smallmatrix} \right], \overline{B}_1 = \left[\begin{smallmatrix} B \\ 0 \end{smallmatrix} \right], \overline{L} = \left[\begin{smallmatrix} L & -C_f \end{smallmatrix} \right]. \end{split}$$

Remark 5. The event triggering scheme (4) can be applied to the situation when the sensor have failures. Besides, the effect of the network environment is also taken into consideration. From the modeling process, we can see that the system (21) is more general.

Before giving the main results in the next section, the following lemmas will be introduced, which will be helpful in deriving the main results.

Lemma 6 (see [21]). For any vectors $x, y \in \mathbb{R}^n$, and positive definite matrix $Q \in \mathbb{R}^{n \times n}$, the following inequality holds:

$$2x^{T}y \le x^{T}Qx + y^{T}Q^{-1}y. (22)$$

Lemma 7 (see [22]). Ω_1 , Ω_2 , and Ω are matrices with appropriate dimensions, $d(k) \in [0, d^M]$; then

$$d(k)\Omega_1 + \left(d^M - d(k)\right)\Omega_2 + \Omega < 0, \tag{23}$$

if and only if the following two inequalities hold

$$d^{M}\Omega_{1} + \Omega < 0,$$

$$d^{M}\Omega_{2} + \Omega < 0.$$
(24)

3. Main Results

In this section, we will invest a new approach to guarantee the filter error system (21) to be globally asymptotically stable. A sufficient condition is established for (21). Then, the explicit filter design method in (20) is given.

Theorem 8. For given scalars α_i , μ_i (i = 1, ..., m), $\rho \in [0, 1)$, $0 \le d(k) \le d^M$, and γ , under the event triggered communication scheme (4), the augmented system (21) is asymptotically stable with an H_{∞} performance index γ for the disturbance attention, if there exist positive definite matrices P, Q, R and matrices P, P, P with appropriate dimensions, such that

$$\Omega(s) = \begin{bmatrix} \Omega_{11} + \Gamma + \Gamma^{T} & * & * & * \\ \Omega_{21} & \Omega_{22} & * & * \\ \Omega_{31} & 0 & \Omega_{33} & * \\ \Omega_{41}(s) & 0 & 0 & -R \end{bmatrix} < 0, \quad s = 1, 2,$$
(25)

where

$$\Omega_{11} = \begin{bmatrix} P\overline{A} + \overline{A}^P - 2P + H^TQH & * & * & * & * \\ D^TP & 0 & * & * & * \\ 0 & 0 & -Q & * & * \\ \overline{B}^TP & 0 & 0 & -\overline{\Xi}^T\Omega\overline{\Xi} & * \\ \overline{B}_1^TP & 0 & 0 & 0 & -\gamma^2I \end{bmatrix},$$

$$\Gamma = \begin{bmatrix} NH & M - N & -M & 0 & 0 \end{bmatrix},$$

$$\Omega_{21} = \begin{bmatrix} P\left(\overline{A} - I\right) & PD & 0 & P\overline{B} & P\overline{B}_1 \\ \sqrt{d^M}RH\left(\overline{A} - I\right) & \sqrt{d^M}RHD & 0 & \sqrt{d^M}RH\overline{B} & \sqrt{d^M}RH\overline{B}_1 \\ \overline{L} & 0 & 0 & 0 & 0 \\ 0 & \sqrt{\sigma}\Omega\overline{\Xi}C & 0 & 0 & 0 \end{bmatrix},$$

$$\Omega_{22}=\mathrm{diag}\left\{ -P,-R,-I,-\Omega\right\} ,$$

$$\Omega_{31} = \begin{bmatrix} 0 & \delta_1 P \widehat{D}_1 & 0 & 0 & 0 \\ 0 & \vdots & 0 & 0 & 0 \\ 0 & \delta_m P \widehat{D}_m & 0 & 0 & 0 \\ 0 & 0 & 0 & \delta_1 P \widehat{B}_1 & 0 \\ 0 & 0 & 0 & \vdots & 0 \\ 0 & 0 & 0 & \delta_m P \widehat{B}_m & 0 \end{bmatrix},$$

$$\Omega_{41}(1) = \sqrt{d^{M}} N^{T}, \qquad \Omega_{41}(2) = \sqrt{d^{M}} M^{T},
N^{T} = \begin{bmatrix} N_{1}^{T} & N_{2}^{T} & N_{3}^{T} & N_{4}^{T} & N_{5}^{T} \end{bmatrix},
M^{T} = \begin{bmatrix} M_{1}^{T} & M_{2}^{T} & M_{3}^{T} & M_{4}^{T} & M_{5}^{T} \end{bmatrix},
\widehat{D}_{i} = \begin{bmatrix} 0 \\ B_{f}E_{i}C \end{bmatrix}, \quad \widehat{B}_{i} = \begin{bmatrix} 0 \\ B_{f}E_{i} \end{bmatrix}, \quad (i = 1, 2, ..., m),
E_{i} = \operatorname{diag} \left\{ \underbrace{0, ..., 0}_{i-1}, 1, \underbrace{0, ..., 0}_{m-i} \right\}, \qquad H = \begin{bmatrix} I & 0 \end{bmatrix}.$$
(26)

Proof. Set $\delta(k) = x(k+1) - x(k)$, $\overline{\eta}(k) = \eta(k+1) - \eta(k)$; choose the Lyapunov functional candidate

$$V(k) = \eta^{T}(k) P \eta(k) + \sum_{k=d^{M}}^{k-1} x^{T}(i) Qx(i)$$

$$+ \sum_{i=-d^{M}}^{-1} \sum_{j=k+i}^{k-1} \delta^{T}(j) R\delta(j).$$
(27)

Calculating the difference of V(k) along the solution of (27) and taking the mathematical expectation, we obtain

$$\mathbb{E}\left\{\Delta V\left(k\right)\right\} = 2\eta^{T}\left(k\right)P\left[\left(\overline{A}-I\right)\eta\left(k\right) + Dx\left(k-d\left(k\right)\right)\right] + \overline{B}e_{i}\left(k\right) + \overline{B}_{1}w\left(k\right)\right] + \mathcal{A}^{T}P\mathcal{A}$$

$$+ \sum_{i=1}^{m}\sigma_{i}^{2}x^{T}\left(k-d\left(k\right)\right)\left[\begin{matrix} 0\\ B_{f}E_{i}C\end{matrix}\right]^{T}$$

$$\times P\left[\begin{matrix} 0\\ B_{f}E_{i}C\end{matrix}\right]x\left(k-d\left(k\right)\right)$$

$$+ \sum_{i=1}^{m}\sigma_{i}^{2}e_{i}^{T}\left(k\right)\left[\begin{matrix} 0\\ B_{f}E_{i}\end{matrix}\right]^{T}P\left[\begin{matrix} 0\\ B_{f}E_{i}\end{matrix}\right]e_{i}\left(k\right)$$

$$+ \eta^{T}\left(k\right)H^{T}QH\eta\left(k\right)$$

$$- x^{T}\left(k-d^{M}\right)Qx\left(k-d^{M}\right)$$

$$+ \mathbb{E}\left\{d^{M}\delta^{T}\left(k\right)R\delta\left(k\right)\right\} - \sum_{i=k-d^{M}}^{k-1}\delta^{T}\left(k\right)R\delta\left(k\right),$$
(28)

where
$$\mathcal{A} = (\overline{A} - I)\eta(k) + Dx(k - d(k)) + \overline{B}e_i(k) + \overline{B}_1w(k)$$
 and

$$\mathbb{E}\left\{d^{M}\delta^{T}(k)R\delta(k)\right\} = \mathbb{E}\left\{d^{M}\overline{\eta}^{T}(k)H^{T}RH\overline{\eta(k)}\right\}$$
$$= d^{M}\mathcal{A}^{T}H^{T}RH\mathcal{A}.$$
 (29)

Then by employing free weight matrix method [23, 24], we have

$$2\xi^{T}(k) M\left[x(k-d(k)) - x(k-d^{M})\right] - \sum_{i=k-d^{M}}^{k-d(k)-1} \delta(i) = 0,$$

$$2\xi^{T}(k) N\left[x(k) - x(k-d(k))\right] - \sum_{i=k-d^{M}}^{k-1} \delta(i) = 0,$$
(30)

where $\xi^{T}(k) = [\eta^{T}(k) \ x^{T}(k - d(k)) \ x^{T}(k - d^{M}) \ e_{i}^{T}(k) \ w^{T}(k)]^{T}$.

By Lemma 6, we can easily get

$$-2\xi^{T}(k) M \sum_{i=k-d^{M}}^{k-d(k)-1} \delta(i) \le (d^{M} - d(k)) \xi^{T}(k) M R^{-1} M^{T} \xi(k)$$

$$+\sum_{i=k-d^{M}}^{k-d(k)-1} \delta^{T}(i) R\delta(i),$$
(31)

$$-2\xi^{T}(k) N \sum_{i=k-d^{M}}^{k-1} \delta(i) \leq d(k) \xi^{T}(k) N R^{-1} N^{T} \xi(k) + \sum_{i=k-d(k)}^{k-1} \delta^{T}(i) R \delta(i).$$
(32)

Combine (28)-(31) and (16), we have

$$\mathbb{E} \left\{ \Delta V(k) \right\} - \gamma^{2} w^{T}(k) w(k) + e^{T}(k) e(k)$$

$$\leq \xi^{T}(k) \left[\Omega_{11} + \Gamma + \Gamma^{T} \right] \xi(k)$$

$$+ \left(d^{M} - d(k) \right) \xi^{T}(k) M R^{-1} M^{T} \xi(k)$$

$$+ d(k) \xi^{T}(k) N R^{-1} N^{T} \xi(k)$$

$$+ \mathcal{A}^{T} P \mathcal{A} + \sum_{i=1}^{m} \sigma_{i}^{2} x^{T}(k - d(k)) \left[\begin{matrix} 0 \\ B_{f} E_{i} C \end{matrix} \right]^{T}$$

$$\times P \left[\begin{matrix} 0 \\ B_{f} E_{i} C \end{matrix} \right] x(k - d(k))$$

$$+ \sum_{i=1}^{m} \sigma_{i}^{2} e_{i}^{T}(k) \left[\begin{matrix} 0 \\ B_{f} E_{i} \end{matrix} \right]^{T} P \left[\begin{matrix} 0 \\ B_{f} E_{i} \end{matrix} \right] e_{i}(k)$$

$$+ \sigma x^{T}(k - d(k)) C^{T} \overline{\Xi}^{T} \Omega \overline{\Xi} C x(k - d(k))$$

$$+ d^{M} \mathcal{A}^{T} H^{T} R H \mathcal{A} + \eta^{T}(k) \overline{L}^{T} \overline{L} \eta(k).$$

Subsequently, by the well known Schur complement and Lemma 7, from (25), we can deduce

$$\mathbb{E} \{ \Delta V(k) \} - \gamma^2 w^T(k) w(k) + e^T(k) e(k) \le 0.$$
 (34)

Similar to the method in [25], the filter error system (21) is asymptotically stable. \Box

Based on Theorem 8, a design method of the reliable filter in the form of (20) is given in Theorem 9.

Theorem 9. For given parameters α , σ_i $(i=1,2,\ldots,m)$, $\rho \in [0,1)$, and $0 \leq d(k) \leq d^M$, the filter error system (21) is asymptotically stable with H_{∞} performance level γ , if there exist positive definite matrices X, Q, \widehat{R} , and A_f , B_f , C_f , N_{10} , N_{11} , M_{10} , M_{11} , M_i , and N_i (i=2,3,4,5) with appropriate dimensions, such that

$$\widehat{\Omega}(s) = \begin{bmatrix} \widehat{\Omega}_{11} + \widehat{\Gamma} + \widehat{\Gamma}^T & * & * & * & * \\ \widehat{\Omega}_{21} & \widehat{\Omega}_{22} & * & * & * \\ \widehat{\Omega}_{31} & 0 & \widehat{\Omega}_{33} & * & * \\ \widehat{\Omega}_{41} & 0 & 0 & \widehat{\Omega}_{44} & * \\ \widehat{\Omega}_{51}(s) & B_w & 0 & 0 & -R \end{bmatrix} < 0, \quad s = 1, 2,$$
(35)

$$P_1 - \overline{P}_3 > 0, \tag{36}$$

where

$$\widehat{\Omega}_{11} = \begin{bmatrix} P_1A + A^T P_1 - 2P_1 + Q & * & * & * & * & * \\ \overline{P}_3A + \overline{A}_3^T - 2\overline{P}_3 & A_f + A_f^T - 2P_3 & * & * & * & * \\ \overline{P}_3A + \overline{A}_3^T - 2\overline{P}_3 & A_f + A_f^T - 2P_3 & * & * & * & * \\ C^T \overline{\Xi}^T \overline{B}_f^T & C^T \overline{\Xi}^T \overline{B}_f^T & 0 & * & * & * \\ 0 & 0 & 0 & -Q & * & * & * \\ \overline{\Xi}^T \overline{B}_f^T & \overline{\Xi}^T \overline{B}_f^T & 0 & 0 & -\overline{\Xi}^T \Omega \overline{\Xi} & * \\ \overline{B}^T P_1 & \overline{B}^T \overline{P}_3 & 0 & 0 & 0 & -\gamma^2 I \end{bmatrix},$$

$$\widehat{\Omega}_{21} = \begin{bmatrix} P_1(A-I) & \overline{A}_f - \overline{P}_3 & \overline{B}_f \overline{\Xi}C & 0 & \overline{B}_f \overline{\Xi} & P_1 B \\ \overline{P}_3(A-I) & \overline{A}_f - \overline{P}_3 & \overline{B}_f \overline{\Xi}C & 0 & \overline{B}_f \overline{\Xi} & \overline{P}_3 B \end{bmatrix}, \qquad \widehat{\Omega}_{22} = \begin{bmatrix} -P_1 & * \\ -\overline{P}_3 & -\overline{P}_3 \end{bmatrix},$$

$$\widehat{\Omega}_{31} = \begin{bmatrix} \sqrt{dM}R(A-I) & 0 & 0 & 0 & 0 & \sqrt{dM}RB \\ L & -C_f & 0 & 0 & 0 & 0 \\ 0 & \sqrt{\sigma}\Omega \overline{\Xi}C & 0 & 0 & 0 & 0 \\ 0 & 0 & \delta_1\overline{B}_f E_1C & 0 & 0 & 0 \\ 0 & 0 & \delta_1\overline{B}_f E_1C & 0 & 0 & 0 \\ 0 & 0 & \delta_1\overline{B}_f E_1C & 0 & 0 & 0 \\ 0 & 0 & \delta_1\overline{B}_f E_1C & 0 & 0 & 0 \\ 0 & 0 & 0 & 0 & \delta_1\overline{B}_f E_1 & 0 \\ 0 & 0 & 0 & \delta_1\overline{B}_f E_1 & 0 \\ 0 & 0 & 0 & \delta_1\overline{B}_f E_1 & 0 \\ 0 & 0 & 0 & \delta_1\overline{B}_f$$

The filter parameters are given by

Proof. Since $\overline{P}_3 > 0$, there exist nonsingular matrix P_2 and symmetrical matrix $P_3 > 0$ satisfying $\overline{P}_3 = P_2^T P_3^{-1} P_2$.

$$A_f = \overline{A}_f \overline{P}_3^{-1}$$
, Define

$$B_f = \overline{B}_f,$$

$$C_f = \overline{C}_f \overline{P}_3^{-1}.$$
(38)

$$P = \begin{bmatrix} P_1 & P_2^T \\ P_2 & P_3 \end{bmatrix}, \qquad J = \begin{bmatrix} I & 0 \\ 0 & P_2^T P_3^{-1} \end{bmatrix}.$$
 (39)

Now premultiply and postmultiply Equation (25) with = diag $\{J, \underbrace{I, I, \dots, I}_{4}, J, I, I, I, \underbrace{J, J, \dots, J}_{2m}, I\}$ and Y^{T} , and

define new variables as

$$\overline{A}_{f} = \widehat{A}_{f} \overline{P}_{3}, \qquad \widehat{A}_{f} = P_{2}^{T} A_{f} P_{2}^{-T},$$

$$\overline{B}_{f} = P_{2}^{T} B_{f},$$

$$\overline{C}_{f} = \widehat{C}_{f} \overline{P}_{3}, \qquad \widehat{C}_{f} = C_{f} P_{2}^{-T},$$

$$N_{1}^{T} J^{T} = \left[\overline{N}_{10}^{T} \ \overline{N}_{11}^{T} \right], \qquad M_{1}^{T} J^{T} = \left[\overline{M}_{10}^{T} \ \overline{M}_{11}^{T} \right].$$

$$(40)$$

We can obtain (35). Therefore, (35) holds, only if (25) holds. From Theorem 8, the filter error system (21) is asymptotic stable with H_{∞} performance level γ .

Similar to the analysis of [25], the filter parameters in (20) can be obtained as (38).

4. Simulation Examples

Consider a specific network controlled system of Equation (21) under a structure:

$$A = \begin{bmatrix} 0.1 & 0.4 \\ -0.4 & 0.1 \end{bmatrix}, \qquad B = \begin{bmatrix} -0.7 \\ 0.2 \end{bmatrix},$$

$$C = \begin{bmatrix} 0 & 1 \end{bmatrix}, \qquad L = \begin{bmatrix} 1 & 1 \end{bmatrix}.$$
(41)

Assume $0 \le d(k) \le 4$ and the failure rates of the sensors are $\alpha_1 = 0.8$ and $\sigma_1 = 0.05$.

According to Theorem 9, when H_{∞} performance level $\gamma = 0.8$, the following parameters can be obtained from the solution of (35) and (36) by using the LMI technique:

$$\overline{P}_3 = \begin{bmatrix} 0.7521 & 0.5801 \\ 0.5801 & 1.4216 \end{bmatrix}, \qquad \overline{A}_f = \begin{bmatrix} -0.0837 & 0.3567 \\ -0.3238 & 0.2977 \end{bmatrix},$$

$$\overline{B}_f = \begin{bmatrix} -0.0036 \\ -0.0019 \end{bmatrix}, \qquad \overline{C}_f = \begin{bmatrix} -0.6268 & -0.6181 \end{bmatrix}.$$
 (42)

From (38), the corresponding filter parameters can be obtained as

$$A_f = \begin{bmatrix} -0.4448 & 0.4325 \\ -0.8641 & 0.5620 \end{bmatrix}, \qquad B_f = \begin{bmatrix} -0.0036 \\ -0.0019 \end{bmatrix},$$

$$C_f = \begin{bmatrix} -0.7268 & -0.1382 \end{bmatrix}$$
(43)

and the parameter in the event triggering scheme (4) is Ω =

Suppose the initial condition $x(0) = \begin{bmatrix} 0.2 & 0.1 \end{bmatrix}^T$ and external disturbance

$$w(k) = \begin{cases} 0.05 & 5s \le k \le 15s \\ 0 & \text{else.} \end{cases}$$
 (44)

Based on the designed filter above, the response of the error e(k) and the probabilistic failure Ξ are given in Figures 2 and 3, respectively. Figure 4 describes the release instants and release interval. It is easy to see from Figures 2-4 that the filter design method in this paper is effectiveness.

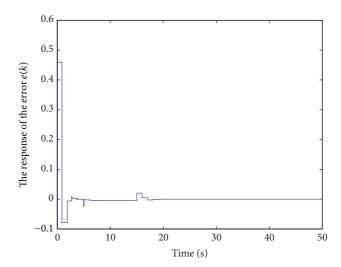


FIGURE 2: The response of the error e(k).

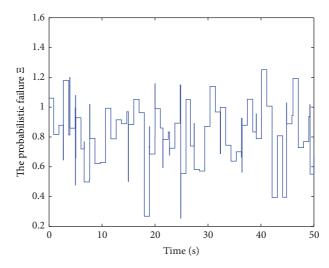


FIGURE 3: The probabilistic failure Ξ .

5. Conclusion

This paper investigates a H_{∞} filter design for a class of network-based systems under an event triggered mechanism. In particular, the system under study is a more general sensor failure model. Considering the uncertain time delay, the uncertain network environment and probabilistic missing sensor measurements, we introduce an event triggered mechanism into the system. By using the free-weighting matrix method and the LMI techniques, the fundamental stability conditions are obtained and the filter design methods are developed. Finally, a numerical example is given to demonstrate the effectiveness of the proposed designed method.

We would like to point out that it is possible to extend our main results to the nonlinear systems such as T-S fuzzy systems, and complex network systems. This will also be one of our future research issues.

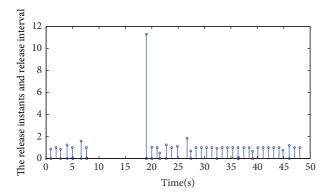


FIGURE 4: The release instants and release interval.

Conflict of Interests

The authors declare that there is no conflict of interests regarding the publication of this paper.

Acknowledgments

This work is partly supported by the National Natural Science Foundation of China (no. 11226240 and no. 61273115), National Center for International Joint Research on E-Business Information Processing under Grant no. 2013B01035, the Natural Science Foundation of Jiangsu Province of China (nos. BK2012469, BK2012211, and BK2012847), the Natural Science Foundation of the Jiangsu Higher Education Institutions of China (no. 12KJD120001 and no. 13KJB110010), and a Project Funded by the Priority Academic Program Development of Jiangsu Higher Education Institutions (PAPD).

References

- [1] H. Yang, Y. Xia, and P. Shi, "Stabilization of networked control systems with nonuniform random sampling periods," *International Journal of Robust and Nonlinear Control*, vol. 21, no. 5, pp. 501–526, 2011.
- [2] Q.-L. Han, "A discrete delay decomposition approach to stability of linear retarded and neutral systems," *Automatica*, vol. 45, no. 2, pp. 517–524, 2009.
- [3] D. Yue, E. Tian, and Q. Han, "A delay system method for designing event-triggered controllers of networked control systems," *IEEE Transactions on Automatic Control*, vol. 58, no. 2, pp. 475–481, 2013.
- [4] C. Peng and T. Yang, "Event-triggered communication and H_{∞} control co-design for networked control systems," *Automatica*, vol. 49, no. 5, pp. 1326–1332, 2013.
- [5] A. Molin and S. Hirche, "On the optimality of certainty equivalence for event-triggered control systems," *IEEE Transactions on Automatic Control*, vol. 58, no. 2, pp. 470–474, 2013.
- [6] C. Peng, Q. Han, and D. Yue, "To transmit or not to transmit: a discrete event-triggered communication scheme for networked takagisugeno fuzzy systems," *IEEE Transactions on Fuzzy Sys*tems, vol. 21, no. 1, pp. 164–170, 2013.
- [7] X. Yin and D. Yue, "Event-triggered tracking control for heterogeneous multi-agent systems with markov communication

- delays," Journal of the Franklin Institute, vol. 350, no. 3, pp. 651–669, 2013.
- [8] J. Liu and D. Yue, "Event-triggering in networked systems with probabilistic sensor and actuator faults," *Information Sciences*, vol. 240, no. 10, pp. 145–160, 2013.
- [9] S. Hu and D. Yue, "Event-based H_{∞} filtering for networked system with communication delay," *Signal Processing*, vol. 92, no. 9, pp. 2029–2039, 2012.
- [10] J. Liu and D. Yue, "Event-based fault detection for networked systems with communication delay and nonlinear perturbation," *Journal of the Franklin Institute*, vol. 350, no. 9, pp. 2791– 2807, 2013.
- [11] M. Liu, P. Shi, L. Zhang, and X. Zhao, "Fault-tolerant control for nonlinear markovian jump systems via proportional and derivative sliding mode observer technique," *IEEE Transactions* on Circuits and Systems I, vol. 58, no. 11, pp. 2755–2764, 2011.
- [12] M. Liu and P. Shi, "Sensor fault estimation and tolerant control for itô stochastic systems with a descriptor sliding mode approach," Automatica, vol. 49, no. 5, pp. 1242–1250, 2013.
- [13] P. Shi, X. Luan, and F. Liu, " H_{∞} filtering for discrete-time systems with stochastic incomplete measurement and mixed delays," *IEEE Transactions on Industrial Electronics*, vol. 59, no. 6, pp. 2732–2739, 2012.
- [14] F. Li and X. Zhang, "Delay-range-dependent robust H_{∞} filtering for singular lpv systems with time variant delay," *International Journal of Innovative Computing, Information and Control*, vol. 9, no. 1, pp. 339–353, 2013.
- [15] Y. Xu, H. Su, Y. Pan, and Z. Wu, "Robust H_{∞} filtering for networked stochastic systems with randomly occurring sensor nonlinearities and packet dropouts," *Signal Processing*, vol. 93, no. 7, pp. 1794–1803, 2013.
- [16] J. Liu, Z. Gu, and S. Hu, " H_{∞} filtering for Markovian jump systems with time-varying delays," *International Journal of Innovative Computing, Information and Control*, vol. 7, no. 3, pp. 1299–1310, 2011.
- [17] C. Peng, D. Yue, E. Tian, and Z. Gu, "Observer-based fault detection for networked control systems with network quality of services," *Applied Mathematical Modelling*, vol. 34, no. 6, pp. 1653–1661, 2010.
- [18] C. Peng, Y.-C. Tian, and D. Yue, "Output feedback control of discrete-time systems in networked environments," *IEEE Transactions on Systems, Man, and Cybernetics A*, vol. 41, no. 1, pp. 185–190, 2011.
- [19] Z. Gu, E. Tian, and J. Liu, "Reliable H_{∞} filter design for sampled-data systems with consideration of probabilistic sensor signal distortion," *IET Signal Processing*, vol. 7, no. 5, pp. 420–426, 2013.
- [20] E. Tian and D. Yue, "Reliable H_{∞} filter design for T-S fuzzy model-based networked control systems with random sensor failure," *International Journal of Robust and Nonlinear Control*, vol. 23, no. 1, pp. 15–32, 2013.
- [21] Y. Wang, L. Xie, and C. E. de Souza, "Robust control of a class of uncertain nonlinear systems," *Systems and Control Letters*, vol. 19, no. 2, pp. 139–149, 1992.
- [22] D. Yue, E. Tian, Y. Zhang, and C. Peng, "Delay-distribution-dependent stability and stabilization of T-S fuzzy systems with probabilistic interval delay," *IEEE Transactions on Systems, Man, and Cybernetics B*, vol. 39, no. 2, pp. 503–516, 2009.
- [23] Y. He, M. Wu, J.-H. She, and G.-P. Liu, "Parameter-dependent Lyapunov functional for stability of time-delay systems with polytopic-type uncertainties," *IEEE Transactions on Automatic Control*, vol. 49, no. 5, pp. 828–832, 2004.

- [24] D. Yue, Q.-L. Han, and J. Lam, "Network-based robust H_{∞} control of systems with uncertainty," Automatica, vol. 41, no. 6, pp. 999–1007, 2005.
- [25] X.-M. Zhang and Q.-L. Han, "Delay-dependent robust H_{∞} filtering for uncertain discrete-time systems with time-varying delay based on a finite sum inequality," *IEEE Transactions on Circuits and Systems II*, vol. 53, no. 12, pp. 1466–1470, 2006.

Hindawi Publishing Corporation Abstract and Applied Analysis Volume 2014, Article ID 494060, 11 pages http://dx.doi.org/10.1155/2014/494060

Research Article

Finite-Horizon Robust Kalman Filter for Uncertain Attitude Estimation System with Star Sensor Measurement Delays

Hua-Ming Qian, Wei Huang, and Biao Liu²

Correspondence should be addressed to Wei Huang; huangwei2393@163.com

Received 10 October 2013; Accepted 6 January 2014; Published 23 February 2014

Academic Editor: Xiaojie Su

Copyright © 2014 Hua-Ming Qian et al. This is an open access article distributed under the Creative Commons Attribution License, which permits unrestricted use, distribution, and reproduction in any medium, provided the original work is properly cited.

This paper addresses the robust Kalman filtering problem for uncertain attitude estimation system with star sensor measurement delays. Combined with the misalignment errors and scale factor errors of gyros in the process model and the misalignment errors of star sensors in the measurement model, the uncertain attitude estimation model can be established, which indicates that uncertainties not only appear in the state and output matrices but also affect the statistic of the process noise. Meanwhile, the phenomenon of star sensor measurement delays is described by introducing Bernoulli random variables with different delay characteristics. The aim of the addressed attitude estimation problem is to design a filter such that, in the presence of model uncertainties and star sensors delays for the attitude estimation system, the optimized filter parameters can be obtained to minimize the upper bound on the estimation error covariance. Therefore, a finite-horizon robust Kalman filter is proposed to cope with this question. Compared with traditional attitude estimation algorithms, the designed robust filter takes into account the effects of star sensor measurement delays and model uncertainties. Simulation results illustrate the effectiveness of the developed robust filter.

1. Introduction

Attitude estimation has played an important role in many actual applications, such as aerospace, satellites, marine, and robots. For attitude estimation system, due to the high measurement precision of star sensor, the rate gyro and star sensor are often integrated to determinate the spacecraft attitude. Furthermore, the filter design is one of the key technologies in attitude estimation. As is well known, Kalman filter has been employed to solve the attitude estimation filtering problem [1–3]. Although these attitude estimation filtering algorithms are available for handling attitude estimation problem, they need to know the accurate model with Gaussian noises and assume exact alignment of gyro and star sensor. However, in practical problems, the measurement misalignment errors of these sensors are inevitable, which will severely degrade the filtering performance. To overcome the sensor misalignment problem in attitude estimation, many researches have been reported in some recent notes [4-8]. For example, Shuster et al. [4] utilize the batch estimation technique to calibrate

the misalignment of the sensors. Pittelkau [5, 6] develops the Kalman filtering technique to estimate the calibration parameters of gyro and star sensor. Lai and Crassidis [7] derived a new spacecraft sensor alignment estimation approach based on the unscented filter. Vandersteen [8] presents the real-time moving horizon estimation of a spacecraft's attitude and sensor calibration parameters. Unfortunately, even though misalignment calibration is accomplished, the measurement misalignment error of gyro and star sensor cannot be removed completely, which lead to model uncertainty. Therefore, in the case that an exact uncertain model is established, the robust filtering technique can be used to deal with the filtering problem with model uncertainty. For the purpose, in the past few decades, many researchers' attentions have been drawn to the robust filtering problem with model uncertainties, including the H_{∞} filter [9], new energy-to-peak FIR filter [10], fuzzy filter design [11], and robust Kalman filter [12, 13]. Among them, the robust Kalman filter design based on the minimum variance theory has been approved to be an effective methodology. Based on

¹ College of Automation, Harbin Engineering University, Harbin 150001, China

² Dongguan Techtotop Microelectronics Co., Ltd., Chengdu R & D Branch, Chengdu 610041, China

this, Wang et al. [14] proposed a regularized robust filter for attitude determination system to deal with the installation error of star trackers. In this work, the installation error of star trackers is expressed as model uncertainty in the measurement model, but the measurement misalignment error of gyros is not taken into account.

In this paper, all the misalignment errors and scale factor errors of gyros introduced into the process model and the misalignment errors of star sensors in the measurement model are described as model uncertainties, so that uncertain attitude estimation model is established. From the uncertain model, we can find that the attitude estimation filtering problem suffers from uncertainties in the state and output matrices and uncertainty in the process noise matrix. A typical way is to represent the model uncertainties as normbounded uncertainties. Recently, the finite-horizon robust Kalman filter design has been investigated to be available for handling the filtering problem with model uncertainties in the state, output, and noise matrices by getting an optimized upper bound on the estimation error covariance [15]. Souto and Ishihara [16] extend this work by considering correlated noises with unknown mean and variance.

However, the above works have been based on this assumption that all the observations should be available at the time of estimation. In many situations, the sensor measurements are disturbed by complicated signal processing circuit, leading to the sensor measurement delays or measurement failures [17–20]. Therefore, the filtering problems with sensor measurement delays have stirred considerable research attention, such as [21-26]. In attitude estimation system, due to optics imaging, star recognition, and attitude determination, the attitude information output of star sensors has the random delay characteristic. Up to now, the attitude estimation filtering problem with model uncertainties in the state, output, and process noise matrices and star sensor delays has not been reported. So, there is great desire to present a robust Kalman filter for uncertain attitude estimation system with star sensor delays.

Based on the above discussion, a finite-horizon robust Kalman filter is proposed for uncertain attitude estimation system with star sensor delays. The star sensor measurement is assumed as one-step randomly delayed measurement with different delay characteristics. The main contributions of the paper are as follows. (1) The uncertain attitude estimation model is established to take into consideration measurement errors of gyros and star sensors, which indicates that the norm-bounded uncertainties appear in the state, output, and process noise matrices. (2) Combined with star sensor delays, a new finite-horizon robust Kalman filter design is derived for the uncertain attitude estimation system. (3) The Hadamard product is employed to help the robust Kalman filter development. (4) The presented robust filter is recursive, which is suitable for online applications.

This paper is organized as follows. In Section 2, the uncertainty attitude estimation model with star sensor delays is set up. In Section 3, a finite-horizon robust Kalman filter for uncertainty attitude estimation system with star sensor delays is developed. In Section 4, the simulation results and analysis are given. In Section 5, some conclusions are drawn.

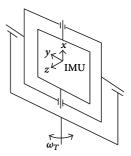


FIGURE 1: A brief principal diagram of the gyro.

2. Uncertainty Attitude Estimation Model with Star Sensor Delays

2.1. Gyro Error Model. As Figure 1 shows, x, y, and z are three axes of the gyro, respectively. The gyro model with misalignment errors and scale factor errors is given as follows:

$$\widetilde{\boldsymbol{\omega}} = (\mathbf{I}_{3\times3} + \mathbf{M})\,\boldsymbol{\omega} + \boldsymbol{\beta} + \boldsymbol{\eta}_{v}$$

$$\dot{\boldsymbol{\beta}} = \boldsymbol{\eta}_{v},$$
(1)

where $\widetilde{\boldsymbol{\omega}}$ is the gyro measured output, $\boldsymbol{\omega}$ is the actual gyro angular rate, $\boldsymbol{\beta}$ is the gyro bias, $\boldsymbol{\eta}_v$ and $\boldsymbol{\eta}_u$ are independent Gaussian white-noise processes with zero means and covariance σ_v^2 and covariance σ_u^2 , and \boldsymbol{M} is an unknown matrix with misalignment errors and scale factor errors, which is defined by

$$\mathbf{M} = \begin{bmatrix} \lambda_x & \delta_{xy} & \delta_{xz} \\ \delta_{yx} & \lambda_y & \delta_{yz} \\ \delta_{zx} & \delta_{zy} & \lambda_z \end{bmatrix}, \tag{2}$$

where $\lambda = \begin{bmatrix} \lambda_x & \lambda_y & \lambda_z \end{bmatrix}^T$ is the unknown scale factor error vector and δ_{ij} is the projection of the *i*-gyro axis on the *j* body-axis, which is assumed to be a small and unknown misalignment angle.

2.2. Uncertainty Process Model. The quaternion is employed to express the attitude for the attitude estimation system consisting of the gyro and star tracker. So, the quaternion orientation equation is described as

$$\dot{\mathbf{q}} = \frac{1}{2} \begin{bmatrix} \boldsymbol{\omega} \\ 0 \end{bmatrix} \otimes \mathbf{q} = \frac{1}{2} \boldsymbol{\Omega} (\boldsymbol{\omega}) \cdot \mathbf{q},$$
 (3)

where $\mathbf{q} = \begin{bmatrix} q_1 & q_2 & q_3 & q_4 \end{bmatrix}^T = \begin{bmatrix} \boldsymbol{\rho}^T & q_4 \end{bmatrix}^T$ is the attitude quaternion, $\boldsymbol{\rho}$ is the quaternion vector, q_4 is the quaternion scalar part, \otimes is the quaternion product, and $\Omega(\boldsymbol{\omega})$ can be defined as follows:

$$\Omega\left(\boldsymbol{\omega}\right) = \begin{bmatrix} -\begin{bmatrix} \boldsymbol{\omega} \times \end{bmatrix} & \boldsymbol{\omega} \\ -\boldsymbol{\omega}^T & 0 \end{bmatrix},\tag{4}$$

where $[\boldsymbol{\omega} \times]$ is a cross-product matrix defined by

$$[\boldsymbol{\omega} \times] = \begin{bmatrix} 0 & -\omega_3 & \omega_2 \\ \omega_3 & 0 & -\omega_1 \\ -\omega_2 & \omega_1 & 0 \end{bmatrix}.$$
 (5)

Using quaternion multiplication, the quaternion error is expressed as

$$\delta \mathbf{q} = \mathbf{q} \otimes \hat{\mathbf{q}}^{-1} = \begin{bmatrix} \Delta \boldsymbol{\rho}^T & \Delta q_4 \end{bmatrix}^T, \tag{6}$$

where \mathbf{q} is the true quaternion, $\hat{\mathbf{q}}$ is the estimated quaternion, \mathbf{q}^{-1} is the inverse quaternion, which is given by $\mathbf{q}^{-1} = \begin{bmatrix} -\boldsymbol{\rho}^T & q_4 \end{bmatrix}^T$, and $\Delta \boldsymbol{\rho}$ is the quaternion error vector part.

The gyro error angular rate $\delta \omega$ is assumed as the difference between the estimated and actual angular rate: $\delta \omega = \omega - \widehat{\omega}$. According to (1), using a small angle approximation, we have

$$\delta \boldsymbol{\omega} = \boldsymbol{\omega} - \widehat{\boldsymbol{\omega}} = \boldsymbol{\omega} - \left(\mathbf{I}_{3\times3} + \mathbf{M}\right)^{-1} \left(\widetilde{\boldsymbol{\omega}} - \widehat{\boldsymbol{\beta}}\right)$$

$$= \boldsymbol{\omega} - \left(\mathbf{I}_{3\times3} + \mathbf{M}\right)^{-1} \left[\left(\mathbf{I}_{3\times3} + \mathbf{M}\right) \boldsymbol{\omega} + \boldsymbol{\beta} + \boldsymbol{\eta}_{\nu} - \widehat{\boldsymbol{\beta}}\right]$$

$$= -\left(\mathbf{I}_{3\times3} + \mathbf{M}\right)^{-1} \left(\Delta \boldsymbol{\beta} + \boldsymbol{\eta}_{\nu}\right) \approx -\left(\mathbf{I}_{3\times3} - \mathbf{M}\right) \left(\Delta \boldsymbol{\beta} + \boldsymbol{\eta}_{\nu}\right),$$
(7)

where $\Delta \beta$ is the gyro bias error vector.

Differentiating (6) with respect to time and combining the quaternion multiplication, we obtain

$$\delta \dot{\mathbf{q}} = \dot{\mathbf{q}} \otimes \widehat{\mathbf{q}}^{-1} + \mathbf{q} \otimes \dot{\widehat{\mathbf{q}}}^{-1} = \dot{\mathbf{q}} \otimes \widehat{\mathbf{q}}^{-1} + \mathbf{q} \otimes \frac{1}{2} \widehat{\mathbf{q}}^{-1} \otimes \begin{bmatrix} \widehat{\boldsymbol{\omega}} \\ 0 \end{bmatrix}^{-1}$$

$$= \frac{1}{2} \begin{bmatrix} \boldsymbol{\omega} \\ 0 \end{bmatrix} \otimes \delta \mathbf{q} - \frac{1}{2} \delta \mathbf{q} \otimes \begin{bmatrix} \widehat{\boldsymbol{\omega}} \\ 0 \end{bmatrix}$$

$$= \frac{1}{2} \begin{bmatrix} \widehat{\boldsymbol{\omega}} \\ 0 \end{bmatrix} \otimes \delta \mathbf{q} - \frac{1}{2} \delta \mathbf{q} \otimes \begin{bmatrix} \widehat{\boldsymbol{\omega}} \\ 0 \end{bmatrix} + \frac{1}{2} \begin{bmatrix} \delta \boldsymbol{\omega} \\ 0 \end{bmatrix} \otimes \delta \mathbf{q}$$

$$= \begin{bmatrix} -\begin{bmatrix} \widehat{\boldsymbol{\omega}} \times \end{bmatrix} \Delta \boldsymbol{\rho} \\ 0 \end{bmatrix} + \frac{1}{2} \begin{bmatrix} \Delta q_4 \cdot \delta \boldsymbol{\omega} - \begin{bmatrix} \delta \boldsymbol{\omega} \times \end{bmatrix} \Delta \boldsymbol{\rho} \\ -\delta \boldsymbol{\omega}^T \Delta \boldsymbol{\rho} \end{bmatrix}.$$
(8)

In order to avoid the quaternion normalization constraint, only the vector component of the quaternion error $\delta \mathbf{q}$ is considered in the states. Inserting (7) into (8), by neglecting the second-order terms, we have

$$\Delta \dot{\boldsymbol{\rho}} = -\left[\widehat{\boldsymbol{\omega}}\times\right] \Delta \boldsymbol{\rho} + \frac{1}{2} \delta \boldsymbol{\omega}$$

$$= -\left[\widehat{\boldsymbol{\omega}}\times\right] \Delta \boldsymbol{\rho} - \frac{1}{2} \left(\mathbf{I}_{3\times 3} - \mathbf{M}\right) \left(\Delta \boldsymbol{\beta} + \boldsymbol{\eta}_{\nu}\right). \tag{9}$$

The quaternion error vector part $\Delta \rho$ and the gyro bias error vector $\Delta \beta$ are constructed as the error state vector: $\mathbf{x} = \left[\Delta \rho^T \ \Delta \beta^T\right]^T$. An error state process model with unknown misalignment errors and scale factor errors can be expressed

$$\dot{\mathbf{x}} = \begin{bmatrix} \Delta \dot{\boldsymbol{\rho}} \\ \Delta \dot{\boldsymbol{\beta}} \end{bmatrix} = \begin{bmatrix} -\left[\widehat{\boldsymbol{\omega}}\times\right] \Delta \boldsymbol{\rho} - \frac{1}{2} \left(\mathbf{I}_{3\times3} - \mathbf{M}\right) \left(\Delta \boldsymbol{\beta} + \boldsymbol{\eta}_{\nu}\right) \\ \boldsymbol{\eta}_{\nu} \end{bmatrix}. (10)$$

According to (10), the discrete-time process equation can be developed as

$$\mathbf{x}_{k+1} = (\mathbf{A}_k + \Delta \mathbf{A}_k) \mathbf{x}_k + (\mathbf{B}_k + \Delta \mathbf{B}_k) \mathbf{w}_k, \tag{11}$$

where \mathbf{w}_k is the zero mean Gaussian noise with covariance $\mathbf{Q}_k = \begin{bmatrix} \Delta t \sigma_v^2 \mathbf{I}_{3 \times 3} & \mathbf{0}_{3 \times 3} \\ \mathbf{0}_{3 \times 3} & \Delta t \sigma_u^2 \mathbf{I}_{3 \times 3} \end{bmatrix}$,

$$\mathbf{A}_{k} = \begin{bmatrix} \mathbf{I}_{3\times3} - [\widehat{\boldsymbol{\omega}}\times] & -\frac{1}{2}\mathbf{I}_{3\times3} \\ \mathbf{0}_{3\times3} & \mathbf{I}_{3\times3} \end{bmatrix}, \qquad \Delta\mathbf{A}_{k} = \begin{bmatrix} \mathbf{0}_{3\times3} & \frac{1}{2}\mathbf{M} \\ \mathbf{0}_{3\times3} & \mathbf{0}_{3\times3} \end{bmatrix},$$

$$\mathbf{B}_{k} = \begin{bmatrix} -\frac{1}{2}\mathbf{I}_{3\times3} & \mathbf{0}_{3\times3} \\ \mathbf{0}_{3\times3} & \mathbf{I}_{3\times3} \end{bmatrix}, \qquad \Delta\mathbf{B}_{k} = \begin{bmatrix} \frac{1}{2}\mathbf{M} & \mathbf{0}_{3\times3} \\ \mathbf{0}_{3\times3} & \mathbf{0}_{3\times3} \end{bmatrix}.$$

$$(12)$$

From (11), it can be seen that the unknown error matrix M not only appears in the state matrix but also affects the statistic of the process noise. In order to realize the robust filtering design, the unknown error matrix M can be rewritten as

$$\mathbf{M} = \mathbf{HFE},\tag{13}$$

where $\delta_{ij} = \Delta_{ij}\sigma_{ij}$ $(i, j = x, y, z, \text{ and } i \neq j)$; $\lambda_i = \gamma_i \Delta \lambda_i$ (i = x, y, z),

$$\mathbf{H} = \begin{bmatrix} \gamma_{x} & \sigma_{xy} & \sigma_{xz} \\ & \sigma_{yx} & \gamma_{y} & \sigma_{yz} \\ & & \sigma_{zx} & \sigma_{zy} & \gamma_{z} \end{bmatrix}$$

$$\mathbf{F} = \operatorname{diag}([\Delta \lambda_{1} \ \Delta_{xy} \ \Delta_{xz} \ \Delta_{yx} \ \Delta \lambda_{2} \ \Delta_{yz} \ \Delta_{zx} \ \Delta_{zy} \ \Delta \lambda_{3}])$$

$$\mathbf{E} = \begin{bmatrix} 1 & 0 & 0 & 1 & 0 & 0 & 1 & 0 & 0 \\ 0 & 1 & 0 & 0 & 1 & 0 & 0 & 1 & 0 \\ 0 & 0 & 1 & 0 & 0 & 1 & 0 & 0 & 1 \end{bmatrix}^{T}.$$
(14)

The parameters σ_{ij} and γ_i are positive constants, which can be chosen by the priori information of the gyro installation errors. If the σ_{ij} and γ_i are set to be large enough, the inequalities $\Delta_{ij}\Delta_{ij}^T \leq 1$ and $\Delta\lambda_i\Delta\lambda_i^T \leq 1$ can be fulfilled, so that the inequality $\mathbf{FF}^T \leq \mathbf{I}$ is satisfied. According to (13), the model error matrices $\Delta \mathbf{A}_k$ and $\Delta \mathbf{B}_k$ can be described as

$$\Delta \mathbf{A}_{k} = \mathbf{H}_{1,k} \mathbf{F}_{1,k} \mathbf{E}_{1,k}, \qquad \Delta \mathbf{B}_{k} = \mathbf{H}_{1,k} \mathbf{F}_{1,k} \mathbf{E}_{2,k},$$
 (15)

where $\mathbf{F}_{1,k}\mathbf{F}_{1,k}^T \leq \mathbf{I}$,

$$\mathbf{H}_{1,k} = \begin{bmatrix} \frac{1}{2} \mathbf{H} \\ \mathbf{0}_{3\times 9} \end{bmatrix}, \qquad \mathbf{F}_{1,k} = \begin{bmatrix} \mathbf{F} \\ \mathbf{0}_{9\times 9} \end{bmatrix},$$

$$\mathbf{E}_{1,k} = \begin{bmatrix} \mathbf{0}_{9\times 3} & \mathbf{E} \\ \mathbf{0}_{9\times 3} & \mathbf{0}_{9\times 3} \end{bmatrix}, \qquad \mathbf{E}_{2,k} = \begin{bmatrix} \mathbf{E} & \mathbf{0}_{9\times 3} \\ \mathbf{0}_{9\times 3} & \mathbf{0}_{9\times 3} \end{bmatrix}.$$

$$(16)$$

2.3. Uncertainty Measurement Model with Star Sensor Delays. To obtain the attitude information, three star sensors are chosen. Considering the misalignment error of star sensors, the measurement model with model errors is expressed as

$$\begin{bmatrix} \Delta \boldsymbol{\rho}_{A} \\ \Delta \boldsymbol{\rho}_{B} \\ \Delta \boldsymbol{\rho}_{C} \end{bmatrix} = \begin{bmatrix} \mathbf{I}_{3 \times 3} - [\boldsymbol{\varphi}_{A} \times] & \mathbf{0}_{3 \times 3} \\ \mathbf{I}_{3 \times 3} - [\boldsymbol{\varphi}_{B} \times] & \mathbf{0}_{3 \times 3} \\ \mathbf{I}_{3 \times 3} - [\boldsymbol{\varphi}_{C} \times] & \mathbf{0}_{3 \times 3} \end{bmatrix} \begin{bmatrix} \Delta \boldsymbol{\rho} \\ \Delta \boldsymbol{\beta} \end{bmatrix} + \begin{bmatrix} \mathbf{v}_{A} \\ \mathbf{v}_{B} \\ \mathbf{v}_{C} \end{bmatrix}, \quad (17)$$

where A, B, and C denote different star sensors, $\Delta \rho_i$ (i = A, B, C) are the measured quaternion error vector parts of star sensors, $\boldsymbol{\varphi}_i = \begin{bmatrix} \varphi_{ix} & \varphi_{iy} & \varphi_{iz} \end{bmatrix}^T$ (i = A, B, C) is the unknown misalignment error vector, and \mathbf{v}_i (i = A, B, C) are the zero mean Gaussian white noises with covariance matrix $\sigma_s^2 \mathbf{I}_{3 \times 3}$. The unknown cross-product matrix $[\boldsymbol{\varphi}_i \times]$ (i = A, B, C) can be written as

$$-\left[\boldsymbol{\varphi}_{i}\times\right] = -\begin{bmatrix} 0 & -\varphi_{iz} & \varphi_{iy} \\ \varphi_{iz} & 0 & -\varphi_{ix} \\ -\varphi_{iy} & \varphi_{ix} & 0 \end{bmatrix} = \mathbf{N}_{i}\Delta_{i}\mathbf{U}_{i} \quad (i = A, B, C),$$
(18)

where

$$\mathbf{N}_{i} = \begin{bmatrix} 0 & 0 & \pi_{iy} & 0 & \pi_{iz} & 0 \\ \pi_{ix} & 0 & 0 & 0 & 0 & \pi_{iz} \\ 0 & \pi_{ix} & 0 & \pi_{iy} & 0 & 0 \end{bmatrix},$$

$$\Delta_{i} = \operatorname{diag} \left(\begin{bmatrix} \Delta_{ix} & \Delta_{ix} & \Delta_{iy} & \Delta_{iy} & \Delta_{iz} & \Delta_{iz} \end{bmatrix} \right);$$

$$\mathbf{U}_{i} = \begin{bmatrix} 0 & 0 & 0 & 1 & 0 & -1 \\ 0 & -1 & 0 & 0 & 1 & 0 \\ 1 & 0 & -1 & 0 & 0 & 0 \end{bmatrix}^{T};$$

$$\Delta_{ij} = \frac{\varphi_{ij}}{\pi_{ij}}, \quad j = x, y, z.$$

$$(19)$$

The parameters π_{ij} are positive constants. If π_{ij} are large enough, the inequalities $\Delta_i^T \Delta_i \leq \mathbf{I}$ and $\Delta_i \Delta_i^T \leq \mathbf{I}$ can be satisfied. For convenience, the uncertain measurement with misalignment errors can be rewritten as

$$\mathbf{z}_k = \left(\mathbf{C}_k + \Delta \mathbf{C}_k\right) \mathbf{x}_k + \mathbf{v}_k,\tag{20}$$

where \mathbf{v}_k is the zero mean Gaussian white-noise process with covariance $\mathbf{R}_k = \sigma_s^2 \mathbf{I}_{9 \times 9}$,

$$\mathbf{z}_{k} = \begin{bmatrix} \Delta \rho_{A} \\ \Delta \rho_{B} \\ \Delta \rho_{C} \end{bmatrix}, \qquad \mathbf{C}_{k} = \begin{bmatrix} \mathbf{I}_{3 \times 3} & \mathbf{0}_{3 \times 3} \\ \mathbf{I}_{3 \times 3} & \mathbf{0}_{3 \times 3} \\ \mathbf{I}_{3 \times 3} & \mathbf{0}_{3 \times 3} \end{bmatrix},$$

$$\Delta \mathbf{C}_{k} = \mathbf{H}_{2,k} \mathbf{F}_{2,k} \mathbf{E}_{1,k}^{*}, \qquad \mathbf{H}_{2,k} = \begin{bmatrix} \mathbf{N}_{A} \\ \mathbf{N}_{B} \\ \mathbf{N}_{C} \end{bmatrix}, \qquad (21)$$

$$\mathbf{F}_{2,k} = \begin{bmatrix} \Delta_{A} \\ \Delta_{B} \\ \Delta_{C} \end{bmatrix}, \qquad \mathbf{E}_{1,k}^{*} = \begin{bmatrix} \mathbf{U}_{A} & \mathbf{0}_{6 \times 3} \\ \mathbf{U}_{B} & \mathbf{0}_{6 \times 3} \\ \mathbf{U}_{C} & \mathbf{0}_{6 \times 3} \end{bmatrix}.$$

Since the attitude information of star sensors is given by the complicated data processing and transmission, the output measurement is delayed. The delayed star sensor measurement is assumed as

$$\mathbf{y}_k = (\mathbf{I} - \mathbf{\Gamma}_k) \, \mathbf{z}_k + \mathbf{\Gamma}_k \mathbf{z}_{k-1}, \tag{22}$$

where $\mathbf{y}_k \in \mathbf{R}^m$ is the true measurement output vector, $\Gamma_k = \text{diag}\{\mu_{k,1}, \mu_{k,2}, \dots, \mu_{k,m}\}$ accounts for the different delay

rates, and $\mu_{k,i} \in \mathbf{R}$ (i = 1, 2, ..., m) are independent random variables taking the values of 1 or 0 with

$$p(\mu_{k,i} = 1) = E[\mu_{k,i}] = p_{k,i}$$

$$p(\mu_{k,i} = 0) = 1 - E[\mu_{k,i}] = 1 - p_{k,i},$$
(23)

where $p_{k,i} \in [0, 1)$ is a known scalar.

Remark 1. The measurement errors of sensors are inevitable in real applications, and the gyro and star sensor are no exception. Though the literature [14] takes into consideration the misalignment error of star sensors, no attention is paid to the misalignment errors and scale factor errors of the gyro. However, they can lead to the uncertainty process model. As shown in (11), the uncertainty error matrix exists in the state matrix and noise matrix, which influences the design of robust filter. Besides, the sensor measurement signal transmission is susceptible to interference from the external environment and limited bandwidth of network, which makes the sensor measurement delay occur. In (22), the delayed star sensor measurement model is established. As discussed in the work [25], different delay rates are taken into account by introducing the diagonal matrix Γ_k .

3. Finite-Horizon Robust Kalman Filter for Attitude Estimation

3.1. Problem Description. Considering the uncertain discrete-time linear stochastic system with sensor delays

$$\mathbf{x}_{k+1} = (\mathbf{A}_k + \Delta \mathbf{A}_k) \mathbf{x}_k + (\mathbf{B}_k + \Delta \mathbf{B}_k) \mathbf{w}_k$$

$$\mathbf{z}_k = (\mathbf{C}_k + \Delta \mathbf{C}_k) \mathbf{x}_k + \mathbf{v}_k$$

$$\mathbf{y}_k = (\mathbf{I} - \mathbf{\Gamma}_k) \mathbf{z}_k + \mathbf{\Gamma}_k \mathbf{z}_{k-1},$$
(24)

where $\mathbf{x}_k \in \mathbf{R}^n$ is the state vector, $\mathbf{z}_k \in \mathbf{R}^m$ is the measurement vector, $\mathbf{y}_k \in \mathbf{R}^m$ is the true measurement output vector, \mathbf{w}_k and \mathbf{v}_k are uncorrelated process and measurement Gaussian noises with zero means and covariance \mathbf{Q}_k and covariance \mathbf{R}_k , and \mathbf{A}_k , \mathbf{B}_k , and \mathbf{C}_k are known matrices with appropriate dimensions. The matrices $\Delta \mathbf{A}_k$, $\Delta \mathbf{B}_k$, and $\Delta \mathbf{C}_k$ represent uncertainties in the state, process noise, and output matrices, which have the following form:

$$\Delta \mathbf{A}_{k} = \mathbf{H}_{1,k} \mathbf{F}_{1,k} \mathbf{E}_{1,k}, \qquad \Delta \mathbf{B}_{k} = \mathbf{H}_{1,k} \mathbf{F}_{1,k} \mathbf{E}_{2,k},$$

$$\Delta \mathbf{C}_{k} = \mathbf{H}_{2,k} \mathbf{F}_{2,k} \mathbf{E}_{1,k}^{*},$$
(25)

where $\mathbf{H}_{1,k}$, $\mathbf{E}_{1,k}$, $\mathbf{E}_{2,k}$, $\mathbf{H}_{2,k}$, and $\mathbf{E}_{1,k}^*$ are known matrices with appropriate dimensions and $\mathbf{F}_{1,k}$ and $\mathbf{F}_{2,k}$ are the normbounded uncertainties satisfying $\mathbf{F}_{1,k}\mathbf{F}_{1,k}^T \leq \mathbf{I}$ and $\mathbf{F}_{2,k}\mathbf{F}_{2,k}^T \leq \mathbf{I}$.

Due to the delayed measurement model, we need to obtain a concise model for convenience. By defining

$$\begin{split} \mathbf{X}_{k} &= \begin{bmatrix} \mathbf{x}_{k} \\ \mathbf{x}_{k-1} \end{bmatrix}, \qquad \overline{\mathbf{A}}_{k} = \begin{bmatrix} \mathbf{A}_{k} & \mathbf{0} \\ \mathbf{0} & \mathbf{A}_{k-1} \end{bmatrix}, \\ \overline{\mathbf{B}}_{k} &= \begin{bmatrix} \mathbf{B}_{k} & \mathbf{0} \\ \mathbf{0} & \mathbf{B}_{k-1} \end{bmatrix}, \\ \Delta \overline{\mathbf{A}}_{k} &= \overline{\mathbf{H}}_{1,k} \overline{\mathbf{F}}_{1,k} \overline{\mathbf{E}}_{1,k}, \qquad \Delta \overline{\mathbf{B}}_{k} = \overline{\mathbf{H}}_{1,k} \overline{\mathbf{F}}_{1,k} \overline{\mathbf{E}}_{2,k}, \\ \overline{\mathbf{H}}_{1,k} &= \begin{bmatrix} \mathbf{H}_{1,k} & \mathbf{0} \\ \mathbf{0} & \mathbf{H}_{1,k-1} \end{bmatrix}, \qquad \overline{\mathbf{F}}_{1,k} &= \begin{bmatrix} \mathbf{F}_{1,k} & \mathbf{0} \\ \mathbf{0} & \mathbf{F}_{1,k-1} \end{bmatrix}, \\ \overline{\mathbf{E}}_{1,k} &= \begin{bmatrix} \mathbf{E}_{1,k} & \mathbf{0} \\ \mathbf{0} & \mathbf{E}_{1,k-1} \end{bmatrix}, \qquad \overline{\mathbf{E}}_{2,k} &= \begin{bmatrix} \mathbf{E}_{2,k} & \mathbf{0} \\ \mathbf{0} & \mathbf{E}_{2,k-1} \end{bmatrix}, \\ \overline{\mathbf{C}}_{k} &= \begin{bmatrix} \mathbf{C}_{k} & \mathbf{0} \\ \mathbf{0} & \mathbf{C}_{k-1} \end{bmatrix}, \qquad \overline{\mathbf{F}}_{2,k} &= \begin{bmatrix} \mathbf{F}_{2,k} & \mathbf{0} \\ \mathbf{0} & \mathbf{F}_{2,k-1} \end{bmatrix}, \\ \overline{\mathbf{E}}_{1,k}^{*} &= \begin{bmatrix} \mathbf{E}_{1,k}^{*} & \mathbf{0} \\ \mathbf{0} & \mathbf{E}_{1,k-1}^{*} \end{bmatrix}, \qquad \overline{\mathbf{w}}_{k} &= \begin{bmatrix} \mathbf{w}_{k} \\ \mathbf{w}_{k-1} \end{bmatrix}, \\ \overline{\mathbf{v}}_{k} &= \begin{bmatrix} \mathbf{v}_{k} \\ \mathbf{v}_{k-1} \end{bmatrix}, \qquad \mathbf{Y}_{k} &= [\mathbf{I} - \mathbf{\Gamma}_{k} & \mathbf{\Gamma}_{k}], \end{split}$$

we have the following form:

$$\mathbf{X}_{k+1} = \left(\overline{\mathbf{A}}_k + \Delta \overline{\mathbf{A}}_k\right) \mathbf{X}_k + \left(\overline{\mathbf{B}}_k + \Delta \overline{\mathbf{B}}_k\right) \overline{\mathbf{w}}_k$$

$$\mathbf{y}_k = \mathbf{Y}_k \left[\left(\overline{\mathbf{C}}_k + \Delta \overline{\mathbf{C}}_k\right) \mathbf{X}_k + \overline{\mathbf{v}}_k \right],$$
(27)

where it is known that

$$E\left[\overline{\mathbf{w}}_{k}\overline{\mathbf{w}}_{k}^{T}\right] = \overline{\mathbf{Q}}_{k} = \begin{bmatrix} \mathbf{Q}_{k} & \mathbf{0} \\ \mathbf{0} & \mathbf{Q}_{k-1} \end{bmatrix},$$

$$E\left[\overline{\mathbf{v}}_{k}\overline{\mathbf{v}}_{k}^{T}\right] = \overline{\mathbf{R}}_{k} = \begin{bmatrix} \mathbf{R}_{k} & \mathbf{0} \\ \mathbf{0} & \mathbf{R}_{k-1} \end{bmatrix}.$$
(28)

According to the definition, \mathbf{Y}_k can be expressed as

$$\overline{\mathbf{Y}}_{k} = E\left[\mathbf{Y}_{k}\right] = \begin{bmatrix} \mathbf{I} - \overline{\mathbf{\Gamma}}_{k} & \overline{\mathbf{\Gamma}}_{k} \end{bmatrix}
\widetilde{\mathbf{Y}}_{k} = \mathbf{Y}_{k} - \overline{\mathbf{Y}}_{k} = \begin{bmatrix} \overline{\mathbf{\Gamma}}_{k} - \mathbf{\Gamma}_{k} & \overline{\mathbf{\Gamma}}_{k} - \overline{\mathbf{\Gamma}}_{k} \end{bmatrix},$$
(29)

where $\overline{\Gamma}_k = \text{diag}\{p_{k,1}, p_{k,2}, \dots, p_{k,m}\}$. For the uncertain system (27), a required filter form is assumed as

$$\widehat{\mathbf{X}}_{k+1} = \mathbf{A}_o \widehat{\mathbf{X}}_k + \mathbf{K}_o \left(\mathbf{y}_k - \overline{\mathbf{Y}}_k \overline{\mathbf{C}}_k \widehat{\mathbf{X}}_k \right), \tag{30}$$

where $\widehat{\mathbf{X}}_k$ is the state estimation value with $\widehat{\mathbf{X}}_0 = \begin{bmatrix} \mathbf{x}_0^T & 0 \end{bmatrix}^T$ and A_o and K_o are the filter parameters to be determined. According to the above analysis, the robust filtering problem for delayed uncertain system (24) can be converted to the robust filter design problem for uncertain system (27). Therefore, our aim is to find an upper bound on the estimation error covariance and design a finite-horizon robust filter for (30) to minimize the upper bound.

Remark 2. Compared with the literature [15, 16], it is obvious that the designed robust Kalman filter does not apply to the case that the measurement delay appears in the system. Meanwhile, the definition of the uncertainty matrices $\Delta \mathbf{A}_k$ and $\Delta \mathbf{C}_k$ is different from the definition of the corresponding matrices in [15, 16]. So, in order to facilitate the robust filter design, we need to utilize the state augmentation method to obtain a new uncertain system in (27).

3.2. Upper Bound of the Estimation Error Covariance. Because there are uncertain and delay rate terms for the system (27), it is difficult to obtain the true estimation error covariance. Our objective is to find the upper bound $\overline{\Xi}_k$, where

$$E\left[\left(\mathbf{X}_{k}-\widehat{\mathbf{X}}_{k}\right)\left(\mathbf{X}_{k}-\widehat{\mathbf{X}}_{k}\right)^{T}\right] \leq \overline{\mathbf{\Xi}}_{k}.\tag{31}$$

Considering the system (27) and the filter structure (30), we define an augmented state $\eta_k = \left[\mathbf{X}_k^T \ \widehat{\mathbf{X}}_k^T \right]^T$. Then, the augmented state-space model is expressed as

$$\eta_{k+1} = \left(\widehat{\mathbf{A}}_k + \widehat{\mathbf{H}}_{1,k}\widehat{\mathbf{F}}_{1,k}\widehat{\mathbf{E}}_{1,k}\right)\eta_k + \widehat{\mathbf{A}}_{1,k}\eta_k
+ \left(\widehat{\mathbf{B}}_k + \widehat{\mathbf{H}}_{2,k}\widehat{\mathbf{F}}_{2,k}\widehat{\mathbf{E}}_{2,k}\right)\widehat{\mathbf{w}}_k + \widehat{\mathbf{B}}_{1,k}\widehat{\mathbf{w}}_k,$$
(32)

where

$$\begin{split} \widehat{\mathbf{A}}_{k} &= \begin{bmatrix} \overline{\mathbf{A}}_{k} & \mathbf{0} \\ \mathbf{K}_{o} \overline{\mathbf{Y}}_{k} \overline{\mathbf{C}}_{k} & \mathbf{A}_{o} - \mathbf{K}_{o} \overline{\mathbf{Y}}_{k} \overline{\mathbf{C}}_{k} \end{bmatrix}, \\ \widehat{\mathbf{H}}_{1,k} &= \begin{bmatrix} \overline{\mathbf{H}}_{1,k} & \mathbf{0} \\ \mathbf{0} & \mathbf{K}_{o} \overline{\mathbf{Y}}_{k} \overline{\mathbf{H}}_{2,k} \end{bmatrix}, \\ \widehat{\mathbf{E}}_{1,k} &= \begin{bmatrix} \overline{\mathbf{E}}_{1,k} & \mathbf{0} \\ \overline{\mathbf{E}}_{1,k} & \mathbf{0} \end{bmatrix}, \qquad \widehat{\mathbf{F}}_{1,k} &= \begin{bmatrix} \overline{\mathbf{F}}_{1,k} & \mathbf{0} \\ \mathbf{0} & \overline{\mathbf{F}}_{2,k} \end{bmatrix}, \\ \widehat{\mathbf{A}}_{1,k} &= \begin{bmatrix} \mathbf{0} & \mathbf{0} & \mathbf{0} \\ \mathbf{K}_{o} \overline{\mathbf{Y}}_{k} (\overline{\mathbf{C}}_{k} + \overline{\mathbf{H}}_{2,k} \overline{\mathbf{F}}_{2,k} \overline{\mathbf{E}}_{1,k}^{*}) & \mathbf{0} \end{bmatrix}, \\ \widehat{\mathbf{B}}_{k} &= \begin{bmatrix} \overline{\mathbf{B}}_{k} & \mathbf{0} \\ \mathbf{0} & \mathbf{K}_{o} \overline{\mathbf{Y}}_{k} \end{bmatrix}, \\ \widehat{\mathbf{H}}_{2,k} &= \begin{bmatrix} \overline{\mathbf{H}}_{1,k} & \mathbf{0} \\ \mathbf{0} & \mathbf{0} \end{bmatrix}, \qquad \widehat{\mathbf{F}}_{2,k} &= \begin{bmatrix} \overline{\mathbf{F}}_{1,k} & \mathbf{0} \\ \mathbf{0} & \mathbf{0} \end{bmatrix}, \\ \widehat{\mathbf{E}}_{2,k} &= \begin{bmatrix} \overline{\mathbf{E}}_{2,k} & \mathbf{0} \\ \mathbf{0} & \mathbf{0} \end{bmatrix}, \\ \widehat{\mathbf{W}}_{k} &= \begin{bmatrix} \overline{\mathbf{W}}_{k} \\ \overline{\mathbf{v}}_{k} \end{bmatrix}. \end{split}$$

The state covariance matrix of η_k in augmented system (32) is denoted as

$$\mathbf{\Xi}_{k} = E\left[\boldsymbol{\eta}_{k}\boldsymbol{\eta}_{k}^{T}\right] = \begin{bmatrix} \mathbf{\Xi}_{11,k} & \mathbf{\Xi}_{12,k} \\ \mathbf{\Xi}_{12,k}^{T} & \mathbf{\Xi}_{22,k} \end{bmatrix}. \tag{34}$$

So, the evolution equation can be expressed as

$$\begin{split} \Xi_{k+1} &= \left(\widehat{\mathbf{A}}_{k} + \widehat{\mathbf{H}}_{1,k} \widehat{\mathbf{F}}_{1,k} \widehat{\mathbf{E}}_{1,k}\right) \Xi_{k} \left(\widehat{\mathbf{A}}_{k} + \widehat{\mathbf{H}}_{1,k} \widehat{\mathbf{F}}_{1,k} \widehat{\mathbf{E}}_{1,k}\right)^{T} + \Psi_{1} \\ &+ \left(\widehat{\mathbf{B}}_{k} + \widehat{\mathbf{H}}_{2,k} \widehat{\mathbf{F}}_{2,k} \widehat{\mathbf{E}}_{2,k}\right) W_{k} \left(\widehat{\mathbf{B}}_{k} + \widehat{\mathbf{H}}_{2,k} \widehat{\mathbf{F}}_{2,k} \widehat{\mathbf{E}}_{2,k}\right)^{T} + \Psi_{2}, \end{split} \tag{35}$$

where

$$W_{k} = \begin{bmatrix} \overline{\mathbf{Q}}_{k} & \mathbf{0} \\ \mathbf{0} & \overline{\mathbf{R}}_{k} \end{bmatrix}, \qquad \widehat{\mathbf{F}}_{1,k} \widehat{\mathbf{F}}_{1,k}^{T} \leq \mathbf{I}, \qquad \widehat{\mathbf{F}}_{2,k} \widehat{\mathbf{F}}_{2,k}^{T} \leq \mathbf{I}$$

$$\Psi_{1} = E \begin{bmatrix} \widehat{\mathbf{A}}_{1,k} \boldsymbol{\eta}_{k} \boldsymbol{\eta}_{k}^{T} \widehat{\mathbf{A}}_{1,k}^{T} \end{bmatrix}$$

$$= E \begin{pmatrix} \begin{bmatrix} \mathbf{0} & \mathbf{0} & \mathbf{0} \\ \mathbf{K}_{o} \widetilde{\mathbf{Y}}_{k} \begin{pmatrix} \overline{\mathbf{C}}_{k} + \overline{\mathbf{H}}_{2,k} \overline{\mathbf{F}}_{2,k} \overline{\mathbf{E}}_{1,k}^{*} \end{pmatrix} & \mathbf{0} \end{bmatrix} \begin{bmatrix} \mathbf{X}_{k} \\ \widehat{\mathbf{X}}_{k} \end{bmatrix}$$

$$\times \begin{bmatrix} \mathbf{X}_{k} \\ \widehat{\mathbf{X}}_{k} \end{bmatrix}^{T} \begin{bmatrix} \mathbf{0} & \mathbf{0} & \mathbf{0} \\ \mathbf{K}_{o} \widetilde{\mathbf{Y}}_{k} \begin{pmatrix} \overline{\mathbf{C}}_{k} + \overline{\mathbf{H}}_{2,k} \overline{\mathbf{F}}_{2,k} \overline{\mathbf{E}}_{1,k}^{*} \end{pmatrix} & \mathbf{0} \end{bmatrix}^{T}$$

$$= \begin{bmatrix} \mathbf{0} & \mathbf{0} \\ \mathbf{0} & \mathbf{K}_{o} E \begin{bmatrix} \widetilde{\mathbf{Y}}_{k} (\overline{\mathbf{C}}_{k} + \overline{\mathbf{H}}_{2,k} \overline{\mathbf{F}}_{2,k} \overline{\mathbf{E}}_{1,k}^{*}) \mathbf{X}_{k} \mathbf{X}_{k}^{T} (\overline{\mathbf{C}}_{k} + \overline{\mathbf{H}}_{2,k} \overline{\mathbf{F}}_{2,k} \overline{\mathbf{E}}_{1,k}^{*})^{T} \widetilde{\mathbf{Y}}_{k}^{T} \end{bmatrix} \mathbf{K}_{o}^{T} \end{bmatrix}$$

$$= E \begin{pmatrix} \begin{bmatrix} \mathbf{0} & \mathbf{0} \\ \mathbf{0} & \mathbf{K}_{o} \widetilde{\mathbf{Y}}_{k} \end{bmatrix} \begin{bmatrix} \overline{\mathbf{w}}_{k} \\ \overline{\mathbf{v}}_{k} \end{bmatrix} \begin{bmatrix} \overline{\mathbf{w}}_{k} \\ \overline{\mathbf{v}}_{k} \end{bmatrix}^{T} \begin{bmatrix} \mathbf{0} & \mathbf{0} \\ \mathbf{0} & \mathbf{K}_{o} \widetilde{\mathbf{Y}}_{k} \end{bmatrix}^{T} \end{pmatrix}$$

$$= \begin{bmatrix} \mathbf{0} & \mathbf{0} \\ \mathbf{0} & \mathbf{K}_{o} E \begin{bmatrix} \widetilde{\mathbf{Y}}_{k} \overline{\mathbf{v}}_{k} \overline{\mathbf{v}}_{k}^{T} \widetilde{\mathbf{Y}}_{k}^{T} \end{bmatrix} \mathbf{K}_{o}^{T} \end{bmatrix}.$$
(36)

In order to obtain the upper bound of the error covariance in (35), the following two lemmas are employed.

Lemma 3 (see [27]). Given matrices A, H, E, and F with compatible dimensions such that $FF^T \leq I$, let X be a symmetric positive definite matrix and let γ be an arbitrary positive constant such that

$$\gamma^{-1}\mathbf{I} - \mathbf{E}\mathbf{X}\mathbf{E}^T > 0. \tag{37}$$

Then, the following matrix inequality holds:

$$(\mathbf{A} + \mathbf{H}\mathbf{F}\mathbf{E}) \mathbf{X}(\mathbf{A} + \mathbf{H}\mathbf{F}\mathbf{E})^{T}$$

$$\leq \mathbf{A} (\mathbf{X}^{-1} - \gamma \mathbf{E}^{T} \mathbf{E})^{-1} \mathbf{A}^{T} + \gamma^{-1} \mathbf{H} \mathbf{H}^{T}.$$
(38)

Lemma 4 (see [28]). Let $\mathbf{A} = [a_{ij}]_{n \times n}$ be a real matrix and let $\mathbf{B} = \operatorname{diag}(b_1, b_2, \dots, b_n)$ be a diagonal random matrix. Then,

$$E\left\{\mathbf{B}\mathbf{A}\mathbf{B}^{T}\right\} = \begin{bmatrix} E\left\{b_{1}^{2}\right\} & E\left\{b_{1}b_{2}\right\} & \cdots & E\left\{b_{1}b_{n}\right\} \\ E\left\{b_{2}b_{1}\right\} & E\left\{b_{2}^{2}\right\} & \cdots & E\left\{b_{2}b_{n}\right\} \\ \vdots & \vdots & \ddots & \vdots \\ E\left\{b_{n}b_{1}\right\} & E\left\{b_{n}b_{2}\right\} & \cdots & E\left\{b_{n}^{2}\right\} \end{bmatrix} \circ \mathbf{A}, \quad (39)$$

where • is the Hadamard product.

Then, the following conclusion can be given by making use of the two lemmas.

Theorem 5. If there exist three positive scalars λ_1 , λ_2 , and λ_3 , such that

$$\lambda_{1}^{-1}\mathbf{I} - \widehat{\mathbf{E}}_{1,k} \mathbf{\Xi}_{k} \widehat{\mathbf{E}}_{1,k}^{T} > 0$$

$$\lambda_{2}^{-1}\mathbf{I} - \widehat{\mathbf{E}}_{2,k} \mathbf{W}_{k} \widehat{\mathbf{E}}_{2,k}^{T} > 0$$

$$\lambda_{3}^{-1}\mathbf{I} - \overline{\mathbf{E}}_{1,k}^{*} \mathbf{\Xi}_{11,k} (\overline{\mathbf{E}}_{1,k}^{*})^{T} > 0$$

$$(40)$$

and there exists a symmetric positive-definite matrix $\tilde{\Xi}_k$, such that

$$\widetilde{\Xi}_{k+1} = \widehat{\mathbf{A}}_{k} \left(\widetilde{\Xi}_{k}^{-1} - \lambda_{1} \widehat{\mathbf{E}}_{1,k}^{T} \widehat{\mathbf{E}}_{1,k} \right)^{-1} \widehat{\mathbf{A}}_{k}^{T}
+ \lambda_{1}^{-1} \widehat{\mathbf{H}}_{1,k} \widehat{\mathbf{H}}_{1,k}^{T} + \lambda_{2}^{-1} \widehat{\mathbf{H}}_{2,k} \widehat{\mathbf{H}}_{2,k}^{T}
+ \widehat{\mathbf{B}}_{k} \left(\mathbf{W}_{k}^{-1} - \lambda_{2} \widehat{\mathbf{E}}_{2,k}^{T} \widehat{\mathbf{E}}_{2,k} \right)^{-1} \widehat{\mathbf{B}}_{k}^{T}
+ \begin{bmatrix} \mathbf{0} & \mathbf{0} \\ \mathbf{0} & \mathbf{K}_{2} \left(\mathbf{\Phi}_{1,k} + \mathbf{\Phi}_{2,k} \right) \mathbf{K}_{2}^{T} \end{bmatrix},$$
(41)

where

$$\Phi_{1,k} = \check{\mathbf{\Gamma}}_{k} \circ \left\{ \overline{\mathbf{H}} \left[\overline{\mathbf{C}}_{k} \left(\widetilde{\mathbf{\Xi}}_{11,k} + \widetilde{\mathbf{\Xi}}_{11,k} (\overline{\mathbf{E}}_{1,k}^{*})^{T} \right. \right. \right. \\
\left. \times \left(\lambda_{3}^{-1} \mathbf{I} - \overline{\mathbf{E}}_{1,k}^{*} \widetilde{\mathbf{\Xi}}_{11,k} (\overline{\mathbf{E}}_{1,k}^{*})^{T} \right)^{-1} \right. \\
\left. \times \overline{\mathbf{E}}_{1,k}^{*} \widetilde{\mathbf{\Xi}}_{11,k} \right) \overline{\mathbf{C}}_{k}^{T} + \lambda_{3}^{-1} \overline{\mathbf{H}}_{2,k} \overline{\mathbf{H}}_{2,k}^{T} \right] \overline{\mathbf{H}}^{T} \right\} \\
\Phi_{2,k} = \check{\mathbf{\Gamma}}_{k} \circ \left(\overline{\mathbf{H}} \overline{\mathbf{R}}_{k} \overline{\mathbf{H}}^{T} \right), \qquad \overline{\mathbf{H}} = \left[\mathbf{I}_{m} - \mathbf{I}_{m} \right] \\
\check{\mathbf{\Gamma}}_{k} = \operatorname{diag} \left\{ p_{k,1} \left(1 - p_{k,1} \right), p_{k,2} \left(1 - p_{k,2} \right), \dots, p_{k,m} \left(1 - p_{k,m} \right) \right\} \tag{42}$$

with initial value $\widetilde{\Xi}_0 = \text{diag}\{\mathbf{U}_0, \mathbf{0}\}$, then $\Xi_k \leq \widetilde{\Xi}_k$ for $0 \leq k \leq N$.

Proof. According to Lemma 4, we have

$$E\left[\widetilde{\mathbf{Y}}_{k}\overline{\mathbf{v}}_{k}\overline{\mathbf{v}}_{k}^{T}\widetilde{\mathbf{Y}}_{k}^{T}\right] = \check{\mathbf{\Gamma}}_{k} \circ \left(\overline{\mathbf{H}}\overline{\mathbf{R}}_{k}\overline{\mathbf{H}}^{T}\right)$$

$$E\left[\widetilde{\mathbf{Y}}_{k}\left(\overline{\mathbf{C}}_{k} + \overline{\mathbf{H}}_{2,k}\overline{\mathbf{F}}_{2,k}\overline{\mathbf{E}}_{1,k}^{*}\right)\mathbf{X}_{k}\mathbf{X}_{k}^{T}\left(\overline{\mathbf{C}}_{k} + \overline{\mathbf{H}}_{2,k}\overline{\mathbf{F}}_{2,k}\overline{\mathbf{E}}_{1,k}^{*}\right)^{T}\widetilde{\mathbf{Y}}_{k}^{T}\right]$$

$$= \check{\mathbf{\Gamma}}_{k} \circ \left\{\overline{\mathbf{H}}\left[\left(\overline{\mathbf{C}}_{k} + \overline{\mathbf{H}}_{2,k}\overline{\mathbf{F}}_{2,k}\overline{\mathbf{E}}_{1,k}^{*}\right)\mathbf{\Xi}_{11,k}\right] \times \left(\overline{\mathbf{C}}_{k} + \overline{\mathbf{H}}_{2,k}\overline{\mathbf{F}}_{2,k}\overline{\mathbf{E}}_{1,k}^{*}\right)^{T}\overline{\mathbf{H}}^{T}\right\}.$$

$$(43)$$

Since the assumptions in (40) hold, using Lemma 3, we can get

$$\Xi_{k+1} \leq \widehat{\mathbf{A}}_{k} \left(\Xi_{k}^{-1} - \lambda_{1} \widehat{\mathbf{E}}_{1,k}^{T} \widehat{\mathbf{E}}_{1,k}\right)^{-1} \widehat{\mathbf{A}}_{k}^{T} \\
+ \lambda_{1}^{-1} \widehat{\mathbf{H}}_{1,k} \widehat{\mathbf{H}}_{1,k}^{T} + \lambda_{2}^{-1} \widehat{\mathbf{H}}_{2,k} \widehat{\mathbf{H}}_{2,k}^{T} \\
+ \widehat{\mathbf{B}}_{k} \left(\mathbf{W}_{k}^{-1} - \lambda_{2} \widehat{\mathbf{E}}_{2,k}^{T} \widehat{\mathbf{E}}_{2,k}\right)^{-1} \widehat{\mathbf{B}}_{k}^{T} \\
+ \begin{bmatrix} \mathbf{0} & \mathbf{0} \\ \mathbf{0} & \mathbf{K}_{o} \left(\overline{\mathbf{\Phi}}_{1,k} + \mathbf{\Phi}_{2,k}\right) \mathbf{K}_{o}^{T} \end{bmatrix}, \tag{44}$$

where

$$\overline{\boldsymbol{\Phi}}_{1,k} = \widecheck{\boldsymbol{\Gamma}}_{k} \circ \left\{ \overline{\mathbf{H}} \left[\overline{\mathbf{C}}_{k} \left(\Xi_{11,k}^{-1} - \lambda_{3} \left(\overline{\mathbf{E}}_{1,k}^{*} \right)^{T} \overline{\mathbf{E}}_{1,k}^{*} \right)^{-1} \overline{\mathbf{C}}_{k}^{T} \right. \right.$$

$$\left. + \lambda_{3}^{-1} \overline{\mathbf{H}}_{2,k} \overline{\mathbf{H}}_{2,k}^{T} \right] \overline{\mathbf{H}}^{T} \right\}$$

$$\left. \boldsymbol{\Phi}_{2,k} = \widecheck{\boldsymbol{\Gamma}}_{k} \circ \left(\overline{\mathbf{H}} \overline{\mathbf{R}}_{k} \overline{\mathbf{H}}^{T} \right), \quad \overline{\mathbf{H}} = \left[\mathbf{I}_{m} - \mathbf{I}_{m} \right]$$

$$\widecheck{\boldsymbol{\Gamma}}_{k} = \operatorname{diag} \left\{ p_{k,1} \left(1 - p_{k,1} \right), p_{k,2} \left(1 - p_{k,2} \right), \dots, \right.$$

$$\left. p_{k,m} \left(1 - p_{k,m} \right) \right\}.$$

$$(45)$$

Then, when k = 0, we have $\Xi_0 = \widetilde{\Xi}_0 = \text{diag}\{\mathbf{U}_0, \mathbf{0}\}$. When k = n, suppose that $\Xi_n \leq \widetilde{\Xi}_n$.

When k = n + 1, comparing (41) with (44), it is easy to obtain that $\Xi_{n+1} \leq \widetilde{\Xi}_{n+1}$. According to the mathematical induction, the proof is complete.

Assume that
$$\overline{\Xi}_k = \begin{bmatrix} \mathbf{I} & -\mathbf{I} \end{bmatrix} \widetilde{\Xi}_k \begin{bmatrix} \mathbf{I} & -\mathbf{I} \end{bmatrix}^T$$
; then

$$E\left[\left(\mathbf{X}_{k}-\widehat{\mathbf{X}}_{k}\right)\left(\mathbf{X}_{k}-\widehat{\mathbf{X}}_{k}\right)^{T}\right] \leq \overline{\mathbf{\Xi}}_{k}.\tag{46}$$

Therefore, for the upper bound $\overline{\Xi}_k$, we need to choose the filter parameters \mathbf{A}_o and \mathbf{K}_o to obtain an optimized upper bound. In the next part, we will find the value of $\overline{\Xi}_k$ and design the finite-horizon robust Kalman filter to minimize the upper bound.

3.3. Finite-Horizon Robust Kalman Filter Design. In order to obtain a solution to the above question and design the robust filter, the main result is presented in the following theorem.

Theorem 6. Assume that the positive scalars λ_1 , λ_2 , and λ_3 fulfill the assumptions in (40); then the upper bound $\tilde{\Xi}_k$ can be expressed as

$$\widetilde{\Xi}_{n} = \begin{bmatrix} \widetilde{\Xi}_{11,n} & \widetilde{\Xi}_{12,n} \\ \widetilde{\Xi}_{12,n}^{T} & \widetilde{\Xi}_{22,n} \end{bmatrix} = \begin{bmatrix} \widetilde{\Xi}_{11,n} & \widetilde{\Xi}_{22,n} \\ \widetilde{\Xi}_{22,n} & \widetilde{\Xi}_{22,n} \end{bmatrix}, \quad n \in [0, N]. \quad (47)$$

If the filter parameters A_o and K_o can be written as

$$\mathbf{A}_{o} = \overline{\mathbf{A}}_{k} + \left(\overline{\mathbf{A}}_{k} - \mathbf{K}_{o} \overline{\mathbf{Y}}_{k} \overline{\mathbf{C}}_{k}\right) \overline{\mathbf{\Xi}}_{k} \mathbf{G}_{k}^{T} \left(\lambda_{1}^{-1} \mathbf{I} - \mathbf{G}_{k} \overline{\mathbf{\Xi}}_{k} \mathbf{G}_{k}^{T}\right)^{-1} \mathbf{G}_{k}$$

$$(48)$$

$$\mathbf{K}_{o} = \overline{\mathbf{A}}_{k} \mathbf{S}_{k} \overline{\mathbf{C}}_{k}^{T} \overline{\mathbf{Y}}_{k}^{T} \left[\overline{\mathbf{Y}}_{k} \overline{\mathbf{C}}_{k} \mathbf{S}_{k} \overline{\mathbf{C}}_{k}^{T} \overline{\mathbf{Y}}_{k}^{T} + \overline{\mathbf{Y}}_{k} \left(\lambda_{1}^{-1} \overline{\mathbf{H}}_{2,k} \overline{\mathbf{H}}_{2,k}^{T} + \overline{\mathbf{R}}_{k}\right) \right]^{-1}$$

$$\times \overline{\mathbf{Y}}_{k}^{T} + \mathbf{\Phi}_{1,k} + \mathbf{\Phi}_{2,k}^{T} \left[\mathbf{Y}_{k} \overline{\mathbf{C}}_{k} \mathbf{Y}_{k}^{T} + \mathbf{\Phi}_{2,k}^{T} \right]^{-1},$$

$$(49)$$

where

$$\overline{\mathbf{E}}_{1,k}^T \overline{\mathbf{E}}_{1,k} + \left(\overline{\mathbf{E}}_{1,k}^*\right)^T \overline{\mathbf{E}}_{1,k}^* = \mathbf{G}_k^T \mathbf{G}_k, \tag{50}$$

$$\mathbf{S}_{k} = \overline{\Xi}_{k} + \overline{\Xi}_{k} \mathbf{G}_{k}^{T} \left(\lambda_{1}^{-1} \mathbf{I} - \mathbf{G}_{k} \overline{\Xi}_{k} \mathbf{G}_{k}^{T} \right)^{-1} \mathbf{G}_{k} \overline{\Xi}_{k}, \tag{51}$$

then $\operatorname{tr}(\overline{\Xi}_k)$ is minimized. So, the state covariance can be obtained as

$$\widetilde{\Xi}_{11,k+1} = \overline{\mathbf{A}}_{k} \left(\widetilde{\Xi}_{11,k} + \widetilde{\Xi}_{11,k} \mathbf{G}_{k}^{T} \left(\lambda_{1}^{-1} \mathbf{I} - \mathbf{G}_{k} \widetilde{\Xi}_{11,k} \mathbf{G}_{k}^{T} \right)^{-1} \right.$$

$$\times \mathbf{G}_{k} \widetilde{\Xi}_{11,k} \right) \overline{\mathbf{A}}_{k}^{T} + \overline{\mathbf{B}}_{k} \left(\overline{\mathbf{Q}}_{k}^{-1} - \lambda_{2} \overline{\mathbf{E}}_{2,k}^{T} \overline{\mathbf{E}}_{2,k} \right)^{-1} \overline{\mathbf{B}}_{k}^{T}$$

$$+ \left(\lambda_{1}^{-1} + \lambda_{2}^{-1} \right) \overline{\mathbf{H}}_{1,k} \overline{\mathbf{H}}_{1,k}^{T}$$

$$(52)$$

and the estimation error covariance can be given as

$$\overline{\Xi}_{k+1} = \overline{\mathbf{A}}_{k} \mathbf{S}_{k} \overline{\mathbf{A}}_{k}^{T} + \overline{\mathbf{B}}_{k} \left(\overline{\mathbf{Q}}_{k}^{-1} - \lambda_{2} \overline{\mathbf{E}}_{2,k}^{T} \overline{\mathbf{E}}_{2,k} \right)^{-1} \overline{\mathbf{B}}_{k}^{T} - \overline{\mathbf{A}}_{k} \mathbf{S}_{k} \overline{\mathbf{C}}_{k}^{T} \overline{\mathbf{Y}}_{k}^{T}
\times \left[\overline{\mathbf{Y}}_{k} \overline{\mathbf{C}}_{k} \mathbf{S}_{k} \overline{\mathbf{C}}_{k}^{T} \overline{\mathbf{Y}}_{k}^{T} + \overline{\mathbf{Y}}_{k} \left(\lambda_{1}^{-1} \overline{\mathbf{H}}_{2,k} \overline{\mathbf{H}}_{2,k}^{T} + \overline{\mathbf{R}}_{k} \right) \overline{\mathbf{Y}}_{k}^{T}
+ \Phi_{1,k} + \Phi_{2,k} \right]^{-1} \overline{\mathbf{Y}}_{k} \overline{\mathbf{C}}_{k} \mathbf{S}_{k}^{T} \overline{\mathbf{A}}_{k}^{T}
+ \left(\lambda_{1}^{-1} + \lambda_{2}^{-1} \right) \overline{\mathbf{H}}_{1,k} \overline{\mathbf{H}}_{1,k}^{T}.$$
(53)

Proof. when n=0, we have $\tilde{\Xi}_0 = \begin{bmatrix} \tilde{\Xi}_{11,0} & \tilde{\Xi}_{22,0} \\ \tilde{\Xi}_{22,0} & \tilde{\Xi}_{22,0} \end{bmatrix} = \begin{bmatrix} \mathbf{U_0} & \mathbf{0} \\ \mathbf{0} & \mathbf{0} \end{bmatrix}$. When n=k, assume that (47) is valid. When n=k+1, we will prove that (47) is still valid. From (47), suppose that the upper

bound $\tilde{\Xi}_{k+1}$ can be partitioned as $\begin{bmatrix} \tilde{\Xi}_{11,k+1} & \tilde{\Xi}_{12,k+1} \\ \tilde{\Xi}_{12,k+1}^T & \tilde{\Xi}_{22,k+1} \end{bmatrix}$. According to the definitions of (50), inserting $\tilde{\Xi}_k$ into (41), we have

$$\widetilde{\Xi}_{11,k+1} = \overline{\mathbf{A}}_{k} \widetilde{\Xi}_{11c,k} \overline{\mathbf{A}}_{k}^{T} + \overline{\mathbf{B}}_{k} \left(\overline{\mathbf{Q}}_{k}^{-1} - \lambda_{2} \overline{\mathbf{E}}_{2,k}^{T} \overline{\mathbf{E}}_{2,k} \right)^{-1} \overline{\mathbf{B}}_{k}^{T}
+ \left(\lambda_{1}^{-1} + \lambda_{2}^{-1} \right) \overline{\mathbf{H}}_{1,k} \overline{\mathbf{H}}_{1,k}^{T},$$

$$\widetilde{\Xi}_{12,k+1} = \overline{\mathbf{A}}_{k} \widetilde{\Xi}_{11c,k} \left(\mathbf{K}_{o} \overline{\mathbf{Y}}_{k} \overline{\mathbf{C}}_{k} \right)^{T} + \overline{\mathbf{A}}_{k} \widetilde{\Xi}_{12c,k} \left(\mathbf{A}_{o} - \mathbf{K}_{o} \overline{\mathbf{Y}}_{k} \overline{\mathbf{C}}_{k} \right)^{T},$$

$$\widetilde{\Xi}_{22,k+1} = \mathbf{K}_{o} \overline{\mathbf{Y}}_{k} \overline{\mathbf{C}}_{k} \widetilde{\Xi}_{11c,k} \left(\mathbf{K}_{o} \overline{\mathbf{Y}}_{k} \overline{\mathbf{C}}_{k} \right)^{T}
+ \left(\mathbf{A}_{o} - \mathbf{K}_{o} \overline{\mathbf{Y}}_{k} \overline{\mathbf{C}}_{k} \right) \widetilde{\Xi}_{12c,k}^{T} \left(\mathbf{K}_{o} \overline{\mathbf{Y}}_{k} \overline{\mathbf{C}}_{k} \right)^{T}
+ \left(\mathbf{K}_{o} \overline{\mathbf{Y}}_{k} \overline{\mathbf{C}}_{k} \right) \widetilde{\Xi}_{12c,k} \left(\mathbf{A}_{o} - \mathbf{K}_{o} \overline{\mathbf{Y}}_{k} \overline{\mathbf{C}}_{k} \right)^{T}
+ \left(\mathbf{A}_{o} - \mathbf{K}_{o} \overline{\mathbf{Y}}_{k} \overline{\mathbf{C}}_{k} \right) \widetilde{\Xi}_{22c,k} \left(\mathbf{A}_{o} - \mathbf{K}_{o} \overline{\mathbf{Y}}_{k} \overline{\mathbf{C}}_{k} \right)^{T}
+ \mathbf{K}_{o} \left[\overline{\mathbf{Y}}_{k} \left(\lambda_{1}^{-1} \overline{\mathbf{H}}_{2,k} \overline{\mathbf{H}}_{2,k}^{T} + \overline{\mathbf{R}}_{k} \right) \overline{\mathbf{Y}}_{k}^{T}
+ \Phi_{1,k} + \Phi_{2,k} \right] \mathbf{K}_{o}^{T},$$
(56)

where

$$\mathbf{M}_{k} = \mathbf{G}_{k}^{T} \left(\lambda_{1}^{-1} \mathbf{I} - \mathbf{G}_{k} \widetilde{\Xi}_{11,k} \mathbf{G}_{k}^{T} \right)^{-1} \mathbf{G}_{k},$$

$$\widetilde{\Xi}_{11c,k} = \widetilde{\Xi}_{11,k} + \widetilde{\Xi}_{11,k} \mathbf{M}_{k} \widetilde{\Xi}_{11,k},$$

$$\widetilde{\Xi}_{12c,k} = \widetilde{\Xi}_{12,k} + \widetilde{\Xi}_{11,k} \mathbf{M}_{k} \widetilde{\Xi}_{12,k},$$

$$\widetilde{\Xi}_{22c,k} = \widetilde{\Xi}_{22,k} + \widetilde{\Xi}_{12,k}^{T} \mathbf{M}_{k} \widetilde{\Xi}_{12,k},$$

$$\mathbf{S}_{k} = \widetilde{\Xi}_{11c,k} - \widetilde{\Xi}_{12c,k} \widetilde{\Xi}_{22c,k}^{-1} \widetilde{\Xi}_{12c,k}^{T}.$$

$$(57)$$

Due to the fact that $\overline{\Xi}_k = \begin{bmatrix} \mathbf{I} & -\mathbf{I} \end{bmatrix} \widetilde{\Xi}_k \begin{bmatrix} \mathbf{I} & -\mathbf{I} \end{bmatrix}^T$, using (54)–(56), the required upper bound $\overline{\Xi}_{k+1}$ can be calculated as

$$\begin{split} \overline{\Xi}_{k+1} &= \widetilde{\Xi}_{11,k+1} - \widetilde{\Xi}_{12,k+1} - \widetilde{\Xi}_{12,k+1}^T + \widetilde{\Xi}_{22,k+1} \\ &= \left(\overline{\mathbf{A}}_k - \mathbf{K}_o \overline{\mathbf{Y}}_k \overline{\mathbf{C}}_k\right) \widetilde{\Xi}_{11c,k} \left(\overline{\mathbf{A}}_k - \mathbf{K}_o \overline{\mathbf{Y}}_k \overline{\mathbf{C}}_k\right)^T \\ &- \left(\overline{\mathbf{A}}_k - \mathbf{K}_o \overline{\mathbf{Y}}_k \overline{\mathbf{C}}_k\right) \widetilde{\Xi}_{12c,k} \left(\mathbf{A}_o - \mathbf{K}_o \overline{\mathbf{Y}}_k \overline{\mathbf{C}}_k\right)^T \\ &- \left(\mathbf{A}_o - \mathbf{K}_o \overline{\mathbf{Y}}_k \overline{\mathbf{C}}_k\right) \widetilde{\Xi}_{12c,k}^T \left(\overline{\mathbf{A}}_k - \mathbf{K}_o \overline{\mathbf{Y}}_k \overline{\mathbf{C}}_k\right)^T \\ &+ \left(\mathbf{A}_o - \mathbf{K}_o \overline{\mathbf{Y}}_k \overline{\mathbf{C}}_k\right) \widetilde{\Xi}_{22c,k} \left(\mathbf{A}_o - \mathbf{K}_o \overline{\mathbf{Y}}_k \overline{\mathbf{C}}_k\right)^T \\ &+ \overline{\mathbf{B}}_k \left(\overline{\mathbf{Q}}_k^{-1} - \lambda_2 \overline{\mathbf{E}}_{2,k}^T \overline{\mathbf{E}}_{2,k}\right)^{-1} \overline{\mathbf{B}}_k^T \\ &+ \left(\lambda_1^{-1} + \lambda_2^{-1}\right) \overline{\mathbf{H}}_{1,k} \overline{\mathbf{H}}_{1,k}^T \\ &+ \mathbf{K}_o \left[\overline{\mathbf{Y}}_k \left(\lambda_1^{-1} \overline{\mathbf{H}}_{2,k} \overline{\mathbf{H}}_{2,k}^T + \overline{\mathbf{R}}_k\right) \overline{\mathbf{Y}}_k^T \\ &+ \Phi_{1,k} + \Phi_{2,k}\right] \mathbf{K}_o^T. \end{split}$$

Computing the first-order variation of (58) with respect to \mathbf{A}_o and \mathbf{K}_o and making them equal to zero, we have

$$\frac{\partial \operatorname{tr}\left(\overline{\Xi}_{k+1}\right)}{\partial \mathbf{A}_{o}} = -2\left(\overline{\mathbf{A}}_{k} - \mathbf{K}_{o}\overline{\mathbf{Y}}_{k}\overline{\mathbf{C}}_{k}\right)\widetilde{\Xi}_{12c,k}
+ 2\left(\mathbf{A}_{o} - \mathbf{K}_{o}\overline{\mathbf{Y}}_{k}\overline{\mathbf{C}}_{k}\right)\widetilde{\Xi}_{22c,k} = 0,
\frac{\partial \operatorname{tr}\left(\overline{\Xi}_{k+1}\right)}{\partial \mathbf{K}_{o}} = -2\left(\overline{\mathbf{A}}_{k} - \mathbf{K}_{o}\overline{\mathbf{Y}}_{k}\overline{\mathbf{C}}_{k}\right)\widetilde{\Xi}_{11c,k}\overline{\mathbf{C}}_{k}^{T}\overline{\mathbf{Y}}_{k}^{T}
+ 2\overline{\mathbf{A}}_{k}\widetilde{\Xi}_{12c,k}\overline{\mathbf{C}}_{k}^{T}\overline{\mathbf{Y}}_{k}^{T} + 2\mathbf{A}_{o}\widetilde{\Xi}_{12c,k}^{T}\overline{\mathbf{C}}_{k}^{T}\overline{\mathbf{Y}}_{k}^{T}
- 2\mathbf{K}_{o}\left[\overline{\mathbf{Y}}_{k}\overline{\mathbf{C}}_{k}\left(\widetilde{\Xi}_{12c,k} + \widetilde{\Xi}_{12c,k}^{T}\right)\overline{\mathbf{C}}_{k}^{T}\overline{\mathbf{Y}}_{k}^{T}\right]
- 2\left(\mathbf{A}_{o} - \mathbf{K}_{o}\overline{\mathbf{Y}}_{k}\overline{\mathbf{C}}_{k}\right)\widetilde{\Xi}_{22c,k}\overline{\mathbf{C}}_{k}^{T}\overline{\mathbf{Y}}_{k}^{T}
+ 2\mathbf{K}_{o}\left[\overline{\mathbf{Y}}_{k}\left(\lambda_{1}^{-1}\overline{\mathbf{H}}_{2,k}\overline{\mathbf{H}}_{2,k}^{T} + \overline{\mathbf{R}}_{k}\right)\overline{\mathbf{Y}}_{k}^{T}
+ \Phi_{1,k} + \Phi_{2,k}\right] = 0.$$
(59)

According to (59) and (60), the optimal parameters \mathbf{A}_o and \mathbf{K}_o to minimize the required upper bound can be calculated by

$$\mathbf{A}_{o} = \overline{\mathbf{A}}_{k} + \left(\overline{\mathbf{A}}_{k} - \mathbf{K}_{o} \overline{\mathbf{Y}}_{k} \overline{\mathbf{C}}_{k}\right) \left(\widetilde{\Xi}_{12c,k} \widetilde{\Xi}_{22c,k}^{-1} - \mathbf{I}\right), \tag{61}$$

$$\mathbf{K}_{o} = \overline{\mathbf{A}}_{k} \mathbf{S}_{k} \overline{\mathbf{C}}_{k}^{T} \overline{\mathbf{Y}}_{k}^{T} \left[\overline{\mathbf{Y}}_{k} \overline{\mathbf{C}}_{k} \mathbf{S}_{k} \overline{\mathbf{C}}_{k}^{T} \overline{\mathbf{Y}}_{k}^{T} + \overline{\mathbf{Y}}_{k} \left(\lambda_{1}^{-1} \overline{\mathbf{H}}_{2,k} \overline{\mathbf{H}}_{2,k}^{T} + \overline{\mathbf{R}}_{k}\right)\right]$$

$$\times \overline{\mathbf{Y}}_{k}^{T} + \mathbf{\Phi}_{1,k} + \mathbf{\Phi}_{2,k}$$

$$\tag{62}$$

Then, substituting (61) and (62) into (55) and (56), we can obtain

$$\begin{split} \widetilde{\Xi}_{12,k+1} &= \widetilde{\Xi}_{12,k+1}^T = \widetilde{\Xi}_{22,k+1} \\ &= \overline{\mathbf{A}}_k \widetilde{\Xi}_{12c,k} \widetilde{\Xi}_{22c,k}^{-1} \widetilde{\Xi}_{12c,k}^T \overline{\mathbf{A}}_k^T + \overline{\mathbf{A}}_k \mathbf{S}_k \overline{\mathbf{C}}_k^T \overline{\mathbf{Y}}_k^T \\ &\times \left[\overline{\mathbf{Y}}_k \overline{\mathbf{C}}_k \mathbf{S}_k \overline{\mathbf{C}}_k^T \overline{\mathbf{Y}}_k^T + \overline{\mathbf{Y}}_k \left(\lambda_1^{-1} \overline{\mathbf{H}}_{2,k} \overline{\mathbf{H}}_{2,k}^T + \overline{\mathbf{R}}_k \right) \overline{\mathbf{Y}}_k^T \right. \\ &+ \left. \Phi_{1,k} + \Phi_{2,k} \right]^{-1} \overline{\mathbf{Y}}_k \overline{\mathbf{C}}_k \mathbf{S}_k^T \overline{\mathbf{A}}_k^T. \end{split}$$

$$(63)$$

Thus, when n = k + 1, (47) is still valid. We can deduce that (50) is valid, for $n \in [0, N]$. From (47), we can know that $\overline{\Xi}_k = \widetilde{\Xi}_{11,k} - \widetilde{\Xi}_{22,k}$. Utilizing (57), we have

$$\widetilde{\Xi}_{12c,k}\widetilde{\Xi}_{22c,k}^{-1} - \mathbf{I} = \overline{\Xi}_k \mathbf{G}_k^T (\lambda_1^{-1} \mathbf{I} - \mathbf{G}_k \overline{\Xi}_k \mathbf{G}_k^T)^{-1} \mathbf{G}_k, \qquad (64)$$

$$\mathbf{S}_{k} = \widetilde{\Xi}_{11c,k} - \widetilde{\Xi}_{12c,k} \widetilde{\Xi}_{22c,k}^{-1} \widetilde{\Xi}_{12c,k}^{T}$$

$$= \overline{\Xi}_{k} + \overline{\Xi}_{k} \mathbf{G}_{k}^{T} (\lambda_{1}^{-1} \mathbf{I} - \mathbf{G}_{k} \overline{\Xi}_{k} \mathbf{G}_{k}^{T})^{-1} \mathbf{G}_{k} \overline{\Xi}_{k}.$$
(65)

Substituting (64) into (61), (48) can be given. Furthermore, using (59), the required upper bound $\overline{\Xi}_{k+1}$ can

be rewritten as (56). Therefore, the theorem has been proved. \Box

Based on the above theorems, the finite-horizon robust Kalman filter can be summarized as follows.

Step 1. The initial values can be given as $\widehat{\mathbf{X}}_0 = \begin{bmatrix} \mathbf{x}_0^T & 0 \end{bmatrix}^T$ and $\overline{\mathbf{\Xi}}_0 = \mathbf{U}_0$.

Step 2. In the presence of uncertainties and sensor delays, the parameters of the filter can be calculated by (48) and (49).

Step 3. According to (30) and (53), the state estimation $\widehat{\mathbf{X}}_k$ and the filtering error covariance $\overline{\mathbf{\Xi}}_k$ can be obtained.

Remark 7. The finite-horizon robust Kalman filter design is accomplished by using Theorems 5 and 6 for uncertain attitude estimation system with star sensor delays. Different from the most existing attitude estimation filtering algorithms, the finite-horizon robust Kalman filter presented in this paper has the advantage to consider the misalignment errors and scale factor errors of gyros and measurement delays of star sensors for attitude estimation system. Note that these phenomena of the misalignment errors of gyro and star sensor and star sensor measurement delays are often encountered in real attitude estimation systems. To compensate the misalignment errors of sensor and star sensor measurement delays, we have designed a finite-horizon robust Kalman filter by finding the upper bound of the estimation error covariance and minimizing the upper bound. It is worth mentioning that, due to the presence of the star sensor measurement delays, the upper bound of the estimation error covariance in (35) and the filter parameters A_o and K_o in (48) and (49) distinguished our work from the counterpart in [15, 16]. In addition, this paper talks about the filter problem with only one type of noise disturbance. The filter problem with multiple disturbances can be considered to achieve more practical oriented results, as discussed in [28, 29], which will be one of our future research topics.

4. Simulations and Analysis

4.1. Simulation Conditions. The simulation utilizes the data from a satellite. The initial orbit elements of the satellite are set as follows: the semimajor axis $a=7.087457\times 10^3$ km, the eccentricity $e=1.99\times 10^{-3}$, the inclination $i=98.153^\circ$, the ascending node longitude $\Omega=-30.534^\circ$, and the argument of perigee $\omega^*=-0.133^\circ$. Numerical simulation gives the measurement data of gyro. The standard deviation of gyros' measurement noise is $\sigma_v=1.45444\times 10^{-6}\,\mathrm{rad/s^{1/2}}$; the standard deviation of gyros' drift noise is $\sigma_u=1.3036\times 10^{-9}\,\mathrm{rad/s^{3/2}}$; the gyro sampling interval is $\Delta t=0.25\,\mathrm{s}$; the components of the gyro scale factor error vector are chosen randomly at the interval $[-6\times 10^{-6}, 6\times 10^{-6}]$; the misalignment error of gyro is chosen randomly at the interval $[-3\times 10^{-6}, 3\times 10^{-6}]$; three star sensors are used and the standard deviation of star sensors' measurement noise is all $\sigma_s=18''$. The misalignment error of star sensor is set to

[-5'', 5'']. Three star sensors have different delay rates, so the random variables $\mu_{k,i}$ ($i=1,2,\ldots,9$) satisfy the Bernoulli distribution with

$$\overline{\Gamma}_k = \text{diag}\{0.2, 0.2, 0.2, 0.1, 0.1, 0.1, 0.05, 0.05, 0.05\}.$$
 (66)

The initial attitude quaternion of the system is taken as $\mathbf{q}_0 = \begin{bmatrix} 0 & 0 & 1 \end{bmatrix}^T$; the gyros' initial bias is set as $\boldsymbol{\beta} = \begin{bmatrix} 0.1 & 0.1 & 0.1 \end{bmatrix}^{T^\circ} /h$; all the filters are initialized with no attitude errors and zero bias estimate; the initial attitude error covariance is set at 0.1° for the quaternion components and 0.2° for the bias components. In order to complete the robust filter design and ensure the estimation precision, the parameters λ_1 , λ_2 , and λ_3 are set to satisfy the condition (40).

4.2. Simulation Results. To validate the effectiveness of the proposed robust filter for controlling the measurement errors of gyros and star sensors and star sensor delays, the proposed approach (FRKF) is compared with the traditional Kalman filter (KF) and the robust Kalman filter (RKF) in the literature [15]. For a fair comparison, the root-mean square error (RMSE) and accumulative RMSE (ARMSE) [30, 31] of the attitude are employed to describe the quality of the attitude estimation. Monte-Carlo simulation runs are set as $N_{\rm MC}=50$, and the RMSE of attitude angles can be defined by

RMSE_{att}
$$(k) = \sqrt{\frac{1}{N_{\text{MC}}} \sum_{i=1}^{N_{\text{MC}}} \|\mathbf{ae}_i(k)\|^2},$$
 (67)

where $\mathbf{ae}_i(k)$ expresses the attitude estimation error vector at the ith Monte-Carlo run. Then, the ARMSE of the attitude is defined by

$$AMSE_{att} = \sqrt{\frac{1}{N} \sum_{i=1}^{N} RMSE_{att}^{2}(k)},$$
 (68)

where N denotes the simulation time. The simulation results are shown in Figures 2–4.

From Figures 2 and 3, it is obvious to be seen that the FRKF performs much better than the RKF and KF, and the KF performs the worst. This is because the traditional KF is not suitable for handling the model uncertainties in the system model and star sensor delays. However, the RKF compensates the measurement errors of gyros and star sensors, whose precisions are better than the KF. But the RKF cannot control the effect of the star sensor delays. Compared with the RKF, the FRKF has higher estimation precision that the RKF, which indicates that the FRKF not only deals with the measurement errors of gyros and star sensors but also cope with the star sensor delays.

For the sake of accounting for the effect of star sensor delays, three star sensors are assumed to have the same delay rate, such as $p_{k,i}$ (i=1,2,...,m) = p. Figure 4 shows the ARMSE of the attitude angles from three filters when p=0,0.1,0.2,...,1.0. From Figure 4, it can be seen that if there are no star sensor delays, that is, p=0, the FRKF is equal to the RKF. Meanwhile, it is apparent that the KF and RKF

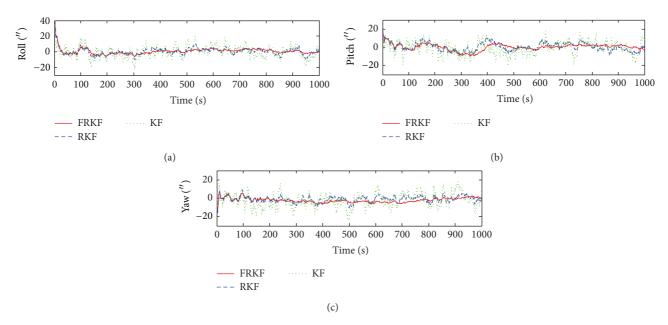


FIGURE 2: Attitude estimation errors.

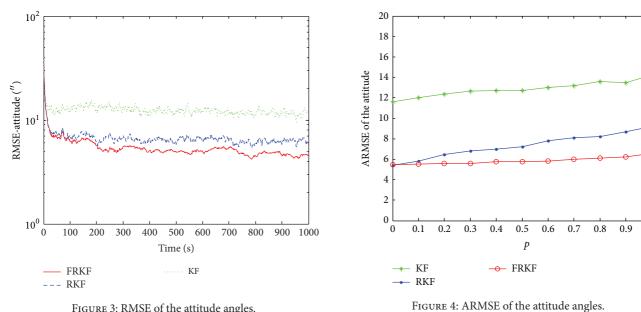


FIGURE 3: RMSE of the attitude angles.

increase faster than the FRKF as the delay probability p is

greater, which illustrates the efficiency of the FRKF to control the star sensor delays.

5. Conclusion

By the fact that the misalignment errors and scale factor errors of gyros and the misalignment errors of star sensors are difficult to be removed entirely by the attitude estimation filter calibration, these measurement errors of sensors are assumed as the norm-bounded uncertainties in the attitude estimation model. At the same time, due to the complicated signal processing of star sensors, the star sensor delay is one of the most important problems for attitude estimation system. Therefore, a finite-horizon robust Kalman filter for the uncertain attitude estimation system with star sensor delays is proposed in this paper. The uncertain attitude estimation model with star sensor delays is constructed, and the finite-horizon robust Kalman filter design is developed. Finally, the applicability and effectiveness of the proposed filter have been demonstrated by the simulation.

Conflict of Interests

The authors declare that there is no conflict of interests regarding the publication of this paper.

References

- [1] E. J. Lefferts, F. L. Markley, and M. D. Shuster, "Kalman filtering for spacecraft attitude estimation," *Journal of Guidance, Control, and Dynamics*, vol. 5, no. 5, pp. 417–429, 1982.
- [2] F. L. Markley, "Attitude error representations for Kalman filtering," *Journal of Guidance, Control, and Dynamics*, vol. 26, no. 2, pp. 311–317, 2003.
- [3] J. L. Crassidis, F. L. Markley, and Y. Cheng, "Survey of nonlinear attitude estimation methods," *Journal of Guidance, Control, and Dynamics*, vol. 30, no. 1, pp. 12–28, 2007.
- [4] M. D. Shuster, D. S. Pitone, and G. J. Bierman, "Batch estimation of spacecraft sensor alignments—relative alignment estimation," *Journal of the Astronautical Sciences*, vol. 39, no. 4, pp. 519– 546, 1991.
- [5] M. Pittelkau, "Kalman filtering for spacecraft system alignment calibration," *Journal of Guidance, Control, and Dynamics*, vol. 24, no. 6, pp. 1187–1195, 2001.
- [6] M. Pittelkau, "Survey of calibration algorithms for spacecraft attitude sensors and gyros," Advances in the Astronautical Sciences, vol. 129, paper no. AAS 07-295, pp. 651-706, 2008.
- [7] K. L. Lai and J. L. Crassidis, "In-space spacecraft alignment calibration using the unscented filter," in *Proceedings of the AIAA Guidance, Navigation, and Control Conference and Exhibit*, pp. 1–11, 2003.
- [8] J. Vandersteen, M. Diehl, C. Aerts, and J. Swevers, "Spacecraft attitude estimation and sensor calibration using moving horizon estimation," *Journal of Guidance, Control, and Dynamics*, vol. 36, no. 3, pp. 734–742, 2013.
- [9] A. Hmamed, C. E. Kasri, E. H. Tissir, T. Alvarez, and F. Tadeo, "Robust H_{∞} filtering for uncertain 2-D continuous systems with delays," *International Journal of Innovative Computing, Information and Control*, vol. 9, no. 5, pp. 2167–2183, 2013.
- [10] C. K. Ahn and P. S. Kim, "New energy-to-peak FIR filter design for systems with disturbance: a convex optimization approach," *International Journal of Innovative Computing, Information and Control*, vol. 9, no. 5, pp. 1987–1993, 2013.
- [11] L. G. Wu and D. W. C. Ho, "Fuzzy filter design for Itô stochastic systems with application to sensor fault detection," *IEEE Transactions on Fuzzy Systems*, vol. 17, no. 1, pp. 233–242, 2009.
- [12] J. Hu, Z. D. Wang, H. J. Gao, and L. K. Stergioulas, "Extended Kalman filtering with stochastic nonlinearities and multiple missing measurements," *Automatica*, vol. 48, no. 9, pp. 2007– 2015, 2012.
- [13] J. Hu, Z. D. Wang, B. Shen, and H. J. Gao, "Quantised recursive filtering for a class of nonlinear systems with multiplicative noises and missing measurements," *International Journal of Control*, vol. 86, no. 4, pp. 650–663, 2013.
- [14] J. Q. Wang, Z. M. He, H. Y. Zhou, and Y. Y. Jiao, "Regularized robust filter for attitude determination system with relative installation error of star trackers," *Acta Astronautica*, vol. 87, pp. 88–95, 2013.
- [15] Z. Dong and Z. You, "Finite-horizon robust Kalman filtering for uncertain discrete time-varying systems with uncertaincovariance white noises," *IEEE Signal Processing Letters*, vol. 13, no. 8, pp. 493–496, 2006.
- [16] R. F. Souto and J. Y. Ishihara, "Comments on 'finite: horizon robust Kalman filtering for uncertain discrete time: varying systems with uncertain: covariance white noises," *IEEE Signal Processing Letters*, vol. 17, no. 2, pp. 213–216, 2010.

- [17] X. Su, L. Wu, and P. Shi, "Sensor networks with random link failures: distributed filtering for T-S fuzzy systems," *IEEE Transactions on Industrial Informatics*, vol. 9, no. 3, pp. 1739–1750, 2013.
- [18] X. Su, P. Shi, L. Wu, and S. K. Nguang, "Induced l₂ filtering of fuzzy stochastic systems with time-varying delays," *IEEE Transactions on Cybernetics*, vol. 43, no. 4, pp. 1251–1264, 2013.
- [19] R. Yang, P. Shi, and G. Liu, "Filtering for discrete-time networked nonlinear systems with mixed random delays and packet dropouts," *IEEE Transactions on Automatic Control*, vol. 56, no. 11, pp. 2655–2660, 2011.
- [20] R. Caballero-Aguila, A. Hermoso-Carazo, J. D. Jimenez-Lopez, J. Linares-Perez, and S. Nakamori, "Recursive estimation of discrete-time signals from nonlinear randomly delayed observations," *Computers & Mathematics with Applications*, vol. 58, no. 6, pp. 1160–1168, 2009.
- [21] R. Caballero-Aguilaa, A. Hermoso-Carazo, J. D. Jimenez-Lopez, J. Linares-Perez, and S. Nakamori, "Signal estimation with multiple delayed sensors using covariance information," *Digital Signal Processing*, vol. 20, no. 2, pp. 528–540, 2010.
- [22] H. H. Dam, "Variable fractional delay filter with sub-expression coefficients," *International Journal of Innovative Computing, Information and Control*, vol. 9, no. 7, pp. 2995–3003, 2013.
- [23] F. O. Hounkpevi and E. Yaz, "Minimum variance generalized state estimators for multiple sensors with different delay rates," *Signal Processing*, vol. 87, no. 4, pp. 602–613, 2007.
- [24] X. X. Wang, Y. Liang, Q. Pan, and C. H. Zhao, "Gaussian filter for nonlinear systems with one-step randomly delayed measurements," *Automatica*, vol. 49, no. 4, pp. 976–986, 2013.
- [25] J. Hu, Z. D. Wang, B. Shen, and H. J. Gao, "Gain-constrained recursive filtering with stochastic nonlinearities and probabilistic sensor delays," *IEEE Transactions on Signal Processing*, vol. 61, no. 5, pp. 1230–1238, 2013.
- [26] L. Xie, Y. C. Soh, and C. E. de Souza, "Robust Kalman filtering for uncertain discrete-time systems," *IEEE Transactions on Automatic Control*, vol. 39, no. 6, pp. 1310–1314, 1994.
- [27] R. A. Horn and C. R. Johnson, Topics in Matrix Analysis, Cambridge University Press, New York, NY, USA, 1991.
- [28] X. M. Yao and L. Guo, "Composite anti-disturbance control for Markovian jump nonlinear systems via disturbance observer," *Automatica*, vol. 49, no. 8, pp. 2538–2545, 2013.
- [29] X. M. Yao, Z. Dong, and D. F. Wang, "Full-order disturbanceobserver-based control for singular hybrid system," *Mathematical Problems in Engineering*, Article ID 352198, 7 pages, 2013.
- [30] X. J. Tang, Z. B. Liu, and J. S. Zhang, "Square-root quaternion cubature Kalman filtering for spacecraft attitude estimation," *Acta Astronautica*, vol. 76, pp. 84–94, 2012.
- [31] I. Arasaratnam, S. Haykin, and T. R. Hurd, "Cubature Kalman filtering for continuous-discrete systems: theory and simulations," *IEEE Transactions on Signal Processing*, vol. 58, no. 10, pp. 4977–4993, 2010.

Hindawi Publishing Corporation Abstract and Applied Analysis Volume 2014, Article ID 936868, 6 pages http://dx.doi.org/10.1155/2014/936868

Research Article

Fuzzy Modeling and Control for a Class of Inverted Pendulum System

Liang Zhang, 1 Xiaoheng Chang, 1 and Hamid Reza Karimi 2

Correspondence should be addressed to Liang Zhang; md18638@126.com

Received 14 December 2013; Accepted 24 December 2013; Published 29 January 2014

Academic Editor: Ming Liu

Copyright © 2014 Liang Zhang et al. This is an open access article distributed under the Creative Commons Attribution License, which permits unrestricted use, distribution, and reproduction in any medium, provided the original work is properly cited.

Focusing on the issue of nonlinear stability control system about the single-stage inverted pendulum, the T-S fuzzy model is employed. Firstly, linear approximation method would be applied into fuzzy model for the single-stage inverted pendulum. At the same time, for some nonlinear terms which could not be dealt with via linear approximation method, this paper will adopt fan range method into fuzzy model. After the T-S fuzzy model, the PDC technology is utilized to design the fuzzy controller secondly. Numerical simulation results, obtained by Matlab, demonstrate the well-controlled effectiveness based on the proposed method for the model of T-S fuzzy system and fuzzy controller.

1. Introduction

Traditional control theory has perfect control ability for explicitly controlled system, however, which is a little weak to describe too complex or difficult system accurately. Therefore, many researchers seek ways to resolve this problem; those researchers have also focused on fuzzy mathematics and applied it to control problems. Zadeh [1] created fuzzy mathematics on an uncertainty system of control which is great contribution. Since the 70s, some practical controllers appear in succession, so that we have a big step forward in the control field. A number of control design approaches using adaptive control [2–4], sliding mode control [5, 6], H_{∞} [7–9], optimal control [10-12], control based data driven [10, 13-15], and fuzzy control [16, 17]. The inverted pendulum system is controlled by the method of fuzzy control and realizes steady control. The inverted pendulum is a typical automatic control in the field of controlled object [18], which is multivariable and nonlinear and strong coupling characteristics, and so on. The inverted pendulum system reveals a natural unstable object, which can accomplish the stability and good performance by the control methods.

For the stability control of inverted pendulum system, the establishment of the model takes an important role. T-S fuzzy control [19] is the most popular one of the most promising methods based on modeling of fuzzy control research platform. At present, the T-S fuzzy control is one of the methods for nonlinear system control research [20], which is very popular. Based on T-S fuzzy model of inverted pendulum system modeling and control have a certain research. For inverted pendulum system based on T-S fuzzy mode, there are two methods [21]: the first one is the fan of nonlinear method. Although this method has high precision in describing the nonlinear system, it obtains many fuzzy rules. Thus it brings to the controller design difficulty, especially for the nonlinear term system. The second one is linear approximation modeling method, the method at the expense of the modeling accuracy and less number of rules of T-S fuzzy model. Since the second method can obtain a simple T-S fuzzy model, so in the inverted pendulum system modeling it is widely applied, but there is a very important problem, which is that if for one type of inverted pendulum system it contains the approximate method to deal with the nonlinear term, then the fuzzy modeling becomes the key to study.

Based on the above analysis and discussion, this thesis will carry the fuzzy modeling and control on inverted pendulum system of complex nonlinear term. For this point, sector nonlinear and linear approximation method will be adopted in the T-S fuzzy modeling of some inverted pendulums and the design of fuzzy controller. The fuzzy modeling and control

¹ College of Engineering, Bohai University, Jinzhou 121013, China

² Department of Engineering, Faculty of Engineering and Science, The University of Agder, 4898 Grimstad, Norway

method can achieve the stability control of the single inverted pendulum system through the simulation.

2. Fuzzy Modeling for the Inverted Pendulum System

Assume that the car's quality is M, the pendulum's quality is m, the pendulum's length is l, the pendulum's angle is θ at an

instant (the angle between the pendulum rod and the vertical direction), the initial displacement is x, $g = 9.8 \text{ m/s}^2$ is the gravity constant, the level for control is forced acting on the car is F, a = 1/(m + M), and the inverted pendulum's state space is as follows:

$$\begin{pmatrix} \dot{x}_{1}(t) \\ \dot{x}_{2}(t) \end{pmatrix} = \begin{pmatrix} \frac{x_{2}(t)}{(4l/3) - amlcos^{2}(x_{1}(t))} \left[g \sin(x_{1}(t)) - \frac{amlx_{2}^{2}(t)\sin^{2}(x_{1}(t))}{2} - x_{2}(t) - au(t) \right] \end{pmatrix},$$
 (1)

where θ is $x_1(t)$, $\dot{\theta}$ is $x_2(t)$, F = u(t), and $x_1(t) \in (0, \pm \pi/2)$, $x_2(t) \in [-\alpha, \alpha]$.

When $x_1(t) = \pm \pi/2$, the system is uncontrollable, so we take $x_1(t) \in [-88^\circ, 88^\circ]$ as the range. For this inverted pendulum system, T-S fuzzy model can be considered as follows:

$$R^{i}$$
: if $x_{1}(t)$ is $M_{1}^{i}, \dots x_{n}(t)$ is M_{n}^{i}
then $\dot{x}(t) = A_{i}x(t) + B_{i}u(t)$, (2)

where $x(t) = \begin{bmatrix} x_1(t) & x_2(t) & \cdots & x_n(t) \end{bmatrix}^T \in R^n$ is the state variables for the fuzzy system, M_k^i is the fuzzy sets and where $k = 1, 2, \ldots, n, i = 1, 2, \ldots, r$, the input vector is $u(t) \in R^m$, $A_i \in R^{n \times n}$, $B_i \in R^{n \times m}$ are coefficient matrix for the system. The number of fuzzy rules for the system is r.

The total fuzzy control system is as follows:

$$\dot{x}(t) = \frac{\sum_{i=1}^{r} \omega_i(x(t)) \left(A_i x(t) + B_i u(t) \right)}{\sum_{i=1}^{r} \omega_i(x(t))},$$
 (3)

where $\omega_i(x(t)) = \prod_{k=1}^n M_k^i(x_k(t))$, and $M_k^i(x_k(t))$ is denotes the membership degree, and where $x_k(t)$ for M_k^i . The $h_i(x(t)) = \omega_i(x(t)) / \sum_{j=1}^r \omega_j(x(t))$ and (2) will be as follows:

$$\dot{x}(t) = \sum_{i=1}^{r} h_i(x(t)) \left(A_i x(t) + B_i u(t) \right), \tag{4}$$

where $h_i(x(t)) \ge 0$ and $\sum_{i=1}^r h_i(x(t)) = 1$.

There is an important nonlinear term in this inverted pendulum system, in other words $x_2^2(t)\sin^2(x_1(t))$, which should be paid more attention. The nonlinear term cannot be conducted through the linear approximation method on this inverted pendulum system. Thus, the thesis will combine the linear approximation method with the fan of nonlinear method to establish the fuzzy model. The process is as follows.

(1) If $x_1(t)$ is about 0, through approximate treatment the system with the linear approximation method, the fuzzy model of system can be obtained as follows:

then

$$\begin{pmatrix}
\dot{x}_{1}(t) \\
\dot{x}_{2}(t)
\end{pmatrix} = \begin{pmatrix}
0 & 1 \\
\frac{g}{(4l/3) - aml} & \frac{-1}{(4l/3) - aml}
\end{pmatrix} \begin{pmatrix}
x_{1}(t) \\
x_{2}(t)
\end{pmatrix}
+ \begin{pmatrix}
0 \\
\frac{-a}{(4l/3) - aml}
\end{pmatrix} u(t)
\begin{pmatrix}
\dot{x}_{1}(t) \\
\dot{x}_{2}(t)
\end{pmatrix} = \begin{pmatrix}
0 & 1 \\
\frac{3g}{4l - 3aml} & \frac{-3}{4l - 3aml}
\end{pmatrix} \begin{pmatrix}
x_{1}(t) \\
x_{2}(t)
\end{pmatrix}
+ \begin{pmatrix}
0 \\
\frac{-3a}{4l - 3aml}
\end{pmatrix} u(t).$$
(5)

(2) If $x_1(t)$ is about $\pm \pi/2$, and consider the fan of nonlinear method, and $z(t) = x_2(t)\sin^2(x_1(t))$,

then

$$\max_{x_1(t), x_2(t)} z(t) = x_2(t) \sin^2(x_1(t)) \equiv c_1 = 0.2595.$$
 (6)

Then

$$\min_{x_1(t), x_2(t)} z(t) = x_2(t) \sin^2(x_1(t)) \equiv c_2 = -0.2595.$$
 (7)

(1) If z(t) is c_1 , through the linear approximation method and the fan of nonlinear method to approximate treatment, the fuzzy model of system can be obtained as follows:

$$\begin{pmatrix} \dot{x}_{1}(t) \\ \dot{x}_{2}(t) \end{pmatrix} = \begin{pmatrix} 0 \\ \frac{g(2/\pi)}{4l/3} - \left(\frac{1}{4l/3} \frac{amlc_{1}}{2} + \frac{1}{4l/3}\right) \end{pmatrix} \begin{pmatrix} x_{1}(t) \\ x_{2}(t) \end{pmatrix}$$

$$+ \begin{pmatrix} 0 \\ \frac{-a}{4l/3} \end{pmatrix} u(t),$$

$$\begin{pmatrix} \dot{x}_{1}(t) \\ \dot{x}_{2}(t) \end{pmatrix} = \begin{pmatrix} 0 \\ \frac{3g}{2\pi l} - \left(\frac{3amc_{1}}{8} + \frac{3}{4l}\right) \end{pmatrix} \begin{pmatrix} x_{1}(t) \\ x_{2}(t) \end{pmatrix} + \begin{pmatrix} 0 \\ \frac{-3a}{4l} \end{pmatrix} u(t).$$

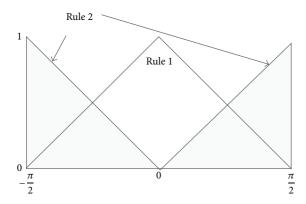


FIGURE 1: Membership functions of two-rule model.

(2) If z(t) is c_2 , through the linear approximation method and the fan of nonlinear method to approximate treatment, the fuzzy model of system can be obtained as follows:

$$\begin{pmatrix} \dot{x}_1(t) \\ \dot{x}_2(t) \end{pmatrix} = \begin{pmatrix} 0 \\ \frac{g(2/\pi)}{4l/3} - \left(\frac{1}{4l/3} \frac{amlc_2}{2} + \frac{1}{4l/3}\right) \end{pmatrix} \begin{pmatrix} x_1(t) \\ x_2(t) \end{pmatrix}$$

$$+ \begin{pmatrix} 0 \\ \frac{-a}{4l/3} \end{pmatrix} u(t),$$

$$\langle \dot{x}_1(t) \rangle = \begin{pmatrix} 0 \\ \frac{-a}{4l/3} \end{pmatrix} u(t),$$

$$\langle \dot{x}_1(t) \rangle = \begin{pmatrix} 0 \\ \frac{-a}{4l/3} \end{pmatrix} u(t),$$

$$\begin{pmatrix} \dot{x}_{1}\left(t\right) \\ \dot{x}_{2}\left(t\right) \end{pmatrix} = \begin{pmatrix} 0 \\ \frac{3g}{2\pi l} - \left(\frac{3amc_{2}}{8} + \frac{3}{4l}\right) \end{pmatrix} \begin{pmatrix} x_{1}\left(t\right) \\ x_{2}\left(t\right) \end{pmatrix} + \begin{pmatrix} 0 \\ -3a \\ 4l \end{pmatrix} u\left(t\right).$$
 (9)

Here define membership functions. For the part of linear approximation, the membership function is shown as Figure 1.

Rule 1: Consider

$$H_{1}(t) = \begin{cases} \frac{2}{\pi} x_{1}(t) + 1, & \left(-\frac{\pi}{2} \le x_{1}(t) \le 0\right) \\ \frac{2}{\pi} x_{1}(t) + 1, & \left(0 < x_{1}(t) \le \frac{\pi}{2}\right) \end{cases}.$$
(10)

Rule 2: Consider

$$H_2(t) = 1 - H_1(t)$$
. (11)

Figure 2 is the membership function for the fan of nonlinear method. z(t) can be rewritten as $z(t) = \sum_{i=1}^{2} E_i(z(t))c_i$, where $E_1(z(t)) = (z(t)-c_2)/(c_1-c_2)$ and $E_2(z(t)) = (c_1-z(t))/(c_1-c_2)$. The membership functions $E_1(z(t))$ and $E_2(z(t))$ will meet the equation $E_1(z(t)) + E_2(z(t)) = 1$.

In conclusion, the finally fuzzy model for the system will be shown as follows.

> Rule 1: if $x_1(t)$ tends to 0, then $\dot{x}(t) = A_1 x(t) + B_1 u(t)$. Rule 2: if $x_1(t)$ tends to $\pm (\pi/2)(|x_1(t)| < \pi/2)$ and z(t) takes the maximum value, then $\dot{x}(t) = A_2 x(t) + B_2 u(t)$.

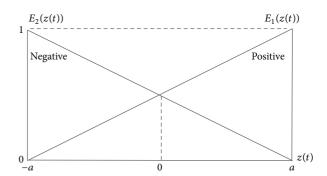


FIGURE 2: Membership function for the fan of nonlinear method.

TABLE 1: Function parameters.

Parameter	Function	Value
M	The mass of the cart	1.096 kg
m	The mass of the pendulum	0.109 kg
1	The length of the pendulum	0.25 m
θ	The angle of the pendulum from the vertical	
F	The force applied to the cart	

Rule 3: if $x_1(t)$ tends to $\pm (\pi/2)(|x_1(t)| < \pi/2)$ and z(t) takes the minimum value, then $\dot{x}(t) = A_3 x(t) + B_3 u(t)$.

The function and value of every parameter are shown in Table 1.

All the parameters defined in Table 1 are taken to account, then the system coefficient matrix can be obtained as follow

$$A_{1} = \begin{pmatrix} 0 & 1 \\ \frac{3g}{4l - 3aml} & \frac{-3}{4l - 3aml} \end{pmatrix} = \begin{pmatrix} 0 & 1 \\ 31.5397 & -3.2183 \end{pmatrix},$$

$$B_{1} = \begin{pmatrix} 0 \\ -3a \\ \frac{1}{4l - 3aml} \end{pmatrix} = \begin{pmatrix} 0 \\ -2.6708 \end{pmatrix},$$

$$A_{2} = \begin{pmatrix} 0 & 1 \\ \frac{3g}{2\pi l} & -\left(\frac{3amc_{1}}{8} + \frac{3}{4l}\right) \end{pmatrix} = \begin{pmatrix} 0 & 1 \\ 18.7166 & -3.0088 \end{pmatrix},$$

$$B_{2} = \begin{pmatrix} 0 & 1 \\ \frac{-3a}{4l} \end{pmatrix} = \begin{pmatrix} 0 \\ -2.4896 \end{pmatrix},$$

$$A_{3} = \begin{pmatrix} 0 & 1 \\ \frac{g(2/\pi)}{4l/3} & -\left(\frac{1}{4l/3}\frac{amlc_{2}}{2} + \frac{1}{4l/3}\right) \end{pmatrix}$$

$$= \begin{pmatrix} 0 & 1 \\ 18.7166 & -2.9912 \end{pmatrix},$$

$$B_{3} = \begin{pmatrix} 0 & 0 \\ \frac{-a}{4l/3} & -\frac{1}{4l/3} & -\frac{1}{4l/3$$

(12)

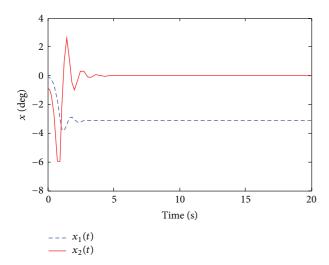


FIGURE 3: Simulation result without the controller.

The model rules can be represented as follows:

$$h_{1}(t) = H_{1}(t),$$

$$h_{2}(t) = H_{2}(t) \times E_{1}(z(t)) = H_{2}(t) \times \left[\frac{z(t) - c_{2}}{c_{1} - c_{2}}\right], \quad (13)$$

$$h_{3}(t) = H_{2}(t) \times E_{2}(z(t)) = H_{2}(t) \times \left[\frac{c_{1} - z(t)}{c_{1} - c_{2}}\right].$$

For the T-S model of the control object, a parallel distributed compensation control scheme (PDC) is employed. And the regulations are described as follow:

$$R^{i}$$
: if $x_{1}(t)$ is $M_{1}^{i}, \dots x_{n}(t)$ is M_{n}^{i}
then $u(t) = K_{i}x(t)$. (14)

Here the fuzzy controller and the fuzzy system adopt the same fuzzy rule. The overall model for the fuzzy controller is as follows:

$$u(t) = \sum_{i=1}^{r} h_i(x(t)) K_i x(t).$$
 (15)

The closed control system can be obtained by combining (2) and (4):

$$\dot{x} = \sum_{i=1}^{r} \sum_{j=1}^{r} h_i h_j \left(A_i + B_i K_j \right) x.$$
 (16)

3. Based on Linear Matrix Inequalities (LMI) and the Matlab Simulation

Without the controller, the simulation output curves of the angular velocity and angular acceleration are shown in Figure 3.

Figure 3 shows that the inverted pendulum system is unstable without the controller.

In the following, by using the linear matrix inequalities technique [23], the fuzzy controller is designed.

Let us define the Lyapunov function as $(x(t)) = x^{T}(t)Px(t)$, P > 0, then the stable criterion of the system for (16) is as follows:

$$\sum_{i=1}^{r} \sum_{j=1}^{r} h_{i} h_{j} \left(A_{i} + B_{i} K_{j} \right)^{T} P + P \sum_{i=1}^{r} \sum_{j=1}^{r} h_{i} h_{j} \left(A_{i} + B_{i} K_{j} \right) < 0.$$

$$(17)$$

Define $Q = P^{-1}$; we can obtain (18) by multiplying Q on both sides contemporary:

$$Q\sum_{i=1}^{r}\sum_{j=1}^{r}h_{i}h_{j}\left(A_{i}+B_{i}K_{j}\right)^{T}+\sum_{i=1}^{r}\sum_{j=1}^{r}h_{i}h_{j}\left(A_{i}+B_{i}K_{j}\right)Q<0. \tag{18}$$

After defining $K_jQ=N_j$, the system stability discriminant conditions can be obtained. And this will guarantee a positive definite matrix Q and matrix N_j can be searched, then the following matrix inequality can be established:

$$QA_{i}^{T} + N_{i}^{T}B_{i}^{T} + A_{i}Q + B_{i}N_{i} < 0,$$

$$QA_{i}^{T} + N_{j}^{T}B_{i}^{T} + A_{i}Q + B_{i}N_{j} + QA_{j}^{T} + N_{i}^{T}B_{j}^{T} + A_{j}Q + B_{j}N_{i} < 0,$$

$$i = 1, 2, ..., r, i < j,$$
(19)

where the stable controller will be obtained from (20):

$$K_j = N_j Q^{-1}. (20)$$

Through solving (19) by linear matrix inequality with LMI of Matlab [24], we can obtain

$$Q = \begin{bmatrix} 1.1127 & -0.4874 \\ -0.4874 & 1.9975 \end{bmatrix},$$

$$N_1 = \begin{bmatrix} 14.6725 & -7.9846 \end{bmatrix},$$

$$N_2 = \begin{bmatrix} 9.7868 & -5.9077 \end{bmatrix},$$

$$N_3 = \begin{bmatrix} 9.7836 & -5.8945 \end{bmatrix}.$$
(21)

Moreover, taking advantage of (20), the fuzzy controller gain will be obtained and shown as follows:

$$K_1 = [12.8038 - 0.8733],$$

 $K_2 = [8.3975 - 0.9086],$ (22)
 $K_3 = [8.3975 - 0.9020].$

Put the controller gain into (16); design the simulation program in the simulink environment. Here the initial value $x(0) = \begin{bmatrix} -0.01 & -0.1 \end{bmatrix}$ is selected. The results of the fuzzy control simulation of the level single inverted pendulum system are shown in Figures 4, 5, and 6.

Simulation results show that the system responses converge to the equilibrium point, which indicates that the design of the controller is stable.

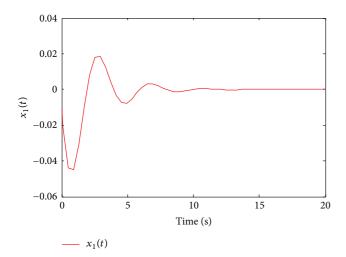


FIGURE 4: Simulation result of the angle.

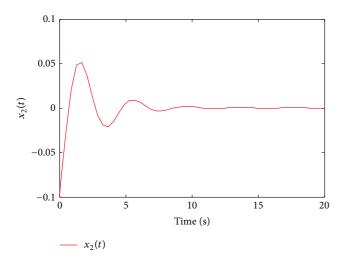


FIGURE 5: Simulation result of the angular velocity.

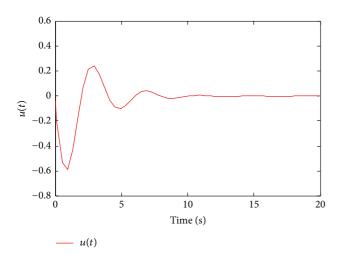


FIGURE 6: Simulation result of the controller.

4. Conclusion

This thesis takes a class of an inverted pendulum system as the research object. The system fuzzy model was established by the methods that combining with the linearization approximation processing and fan-shaped interval, and then the fuzzy controller was designed. Matlab-Simulink software toolbox was employed to be on computer simulation. The results show that it achieved a stable control of the single-stage inverted pendulum system through fuzzy control method on the basis of this fuzzy model. This model has the advantages of less fuzzy rules, high precision, and simple structure. The research results can provide an effective way for the subsequent instability in other nonlinear system modeling and fuzzy control.

Conflict of Interests

The authors declare that there is no conflict of interests regarding the publication of this paper.

Acknowledgments

This work is supported by the National Nature Science Foundation of China under Grant (Project no. 61104071), by the Program for Liaoning Excellent Talents in University, China, under Grant (Project no. LJQ2012095), by the Open Program of the Key Laboratory of Manufacturing Industrial Integrated Automation, Shenyang University, China, under Grant (Project no. 1120211415), and Natural Science Foundation of Liaoning, China (Project no. 2013020044). The authors highly appreciate the above financial supports.

References

- [1] L. A. Zadeh, "Fuzzy sets," *Information and Computation*, vol. 8, pp. 338–353, 1965.
- [2] B. Xiao, Q. Hu, and Y. Zhang, "Adaptive sliding mode fault tolerant attitude tracking control for flexible spacecraft under actuator saturation," *IEEE Transactions on Control Systems Technology*, vol. 20, no. 6, pp. 1605–1612, 2012.
- [3] B. Xiao, Q. Hu, and Y. Zhang, "Fault-tolerant attitude control for flexible spacecraft without angular velocity magnitude measurement," *Journal of Guidance, Control, and Dynamics*, vol. 34, no. 5, pp. 1556–1561, 2011.
- [4] Y. Zhao, W. Sun, and H. Gao, "Robust control synthesis for seat suspension systems with actuator saturation and time-varying input delay," *Journal of Sound and Vibration*, vol. 329, no. 21, pp. 4335–4353, 2010.
- [5] L. Wu, X. Su, and P. Shi, "Sliding mode control with bounded L_2 gain performance of Markovian jump singular time-delay systems," *Automatica*, vol. 48, no. 8, pp. 1929–1933, 2012.
- [6] Q. Hu, "Sliding mode maneuvering control and active vibration damping of three-axis stabilized flexible spacecraft with actuator dynamics," *Nonlinear Dynamics*, vol. 52, no. 3, pp. 227–248, 2008.
- [7] G. Pujol, "Reliable H_∞ control of a class of uncertain interconnected systems: an LMI approach," *International Journal of Systems Science*, vol. 40, no. 6, pp. 649–657, 2009.

- [8] Q. Zheng and F. Wu, "Nonlinear H_{∞} control designs with axisymmetric spacecraft control," *Journal of Guidance, Control, and Dynamics*, vol. 32, no. 3, pp. 850–859, 2009.
- [9] W. Sun, H. Gao Sr., and O. Kaynak, "Finite frequency H_{∞} control for vehicle active suspension systems," *IEEE Transactions on Control Systems Technology*, vol. 19, no. 2, pp. 416–422, 2011.
- [10] S. Yin, H. Luo, and S. Ding, "Real-time implementation of fault-tolerant control systems with performance optimization," *IEEE Transactions on Industrial Electronics*, vol. 61, no. 5, pp. 2402–2411, 2013.
- [11] M. V. Levskii, "Optimal control of reorientation of a spacecraft using free trajectory method," *Cosmic Research*, vol. 49, no. 2, pp. 131–149, 2011.
- [12] E. M. Queen and L. Silverberg, "Optimal control of a rigid body with dissimilar actuators," *Journal of Guidance, Control, and Dynamics*, vol. 19, no. 3, pp. 738–740, 1996.
- [13] S. Yin, S. X. Ding, A. H. A. Sari, and H. Hao, "Data-driven monitoring for stochastic systems and its application on batch process," *International Journal of Systems Science*, vol. 44, no. 7, pp. 1366–1376, 2013.
- [14] S. Yin, S. X. Ding, A. Haghani, H. Hao, and P. Zhang, "A comparison study of basic data-driven fault diagnosis and process monitoring methods on the benchmark Tennessee Eastman process," *Journal of Process Control*, vol. 22, no. 9, pp. 1567–1581, 2012.
- [15] S. Yin, X. Yang, and H. R. Karimi, "Data-driven adaptive observer for fault diagnosis," *Mathematical Problems in Engineering*, vol. 2012, Article ID 832836, 21 pages, 2012.
- [16] S.-J. Dong, Y.-Z. Li, J. Wang, and J. Wang, "Fuzzy incremental control algorithm of loop heat pipe cooling system for space-craft applications," *Computers & Mathematics with Applications*, vol. 64, no. 5, pp. 877–886, 2012.
- [17] Z. Gao, X. Shi, and S. X. Ding, "Fuzzy state/disturbance observer design for T-S fuzzy systems with application to sensor fault estimation," *IEEE Transactions on Systems, Man, and Cybernetics B*, vol. 38, no. 3, pp. 875–880, 2008.
- [18] S. Udomsin, "Inverted pendulum control," *KKU Engineering Journal*, vol. 25, pp. 41–65, 2013.
- [19] C.-H. Fang, Y.-S. Liu, S.-W. Kau, L. Hong, and C.-H. Lee, "A new LMI-based approach to relaxed quadratic stabilization of T-S fuzzy control systems," *IEEE Transactions on Fuzzy Systems*, vol. 14, no. 3, pp. 386–397, 2006.
- [20] H. O. Wang, K. Tanaka, and M. F. Griffin, "An approach to fuzzy control of nonlinear systems: stability and design issues," *IEEE Transactions on Fuzzy Systems*, vol. 4, no. 1, pp. 14–23, 1996.
- [21] H. O. Wang, K. Tanaka, and M. Griffin, "Parallel distributed compensation of nonlinear systems by Takagi-Sugeno fuzzy model," in Proceedings of the International Joint Conference of the 4th IEEE International Conference on Fuzzy Systems and the 2nd International Fuzzy Engineering Symposium, vol. 2, pp. 531– 538, March 1995.
- [22] K. Tanaka, T. Ikeda, and H. O. Wang, "Fuzzy regulators and fuzzy observers: relaxed stability conditions and LMI-based designs," *IEEE Transactions on Fuzzy Systems*, vol. 6, no. 2, pp. 250–265, 1998.
- [23] S. Boyd, L. EI Ghaoul, E. Feron, and V. Balakrishnan, Linear Matrix Inequalities in System and Control Theory, vol. 15 of Studies in Applied Mathematics, Society for Industrial Mathematics, 1994.
- [24] P. Gahinet, A. Nemirovski, A. J. Laub, and M. Chilali, LMI Control Toolbox, vol. 1 of User's Guide Versión, Manuales de MATLAB, 1992.

Hindawi Publishing Corporation Abstract and Applied Analysis Volume 2013, Article ID 267328, 23 pages http://dx.doi.org/10.1155/2013/267328

Research Article

Ergodicity of Stochastic Burgers' System with Dissipative Term

Guoli Zhou, 1,2 Boling Guo, 2 Daiwen Huang, 2 and Yongqian Han 2

¹ College of Mathematics and Statistics, Chong Qing University, Chong Qing 401331, China

Correspondence should be addressed to Guoli Zhou; zhouguoli736@126.com

Received 9 October 2013; Revised 6 November 2013; Accepted 6 November 2013

Academic Editor: Hamid Reza Karimi

Copyright © 2013 Guoli Zhou et al. This is an open access article distributed under the Creative Commons Attribution License, which permits unrestricted use, distribution, and reproduction in any medium, provided the original work is properly cited.

A 2-dimensional stochastic Burgers equation with dissipative term perturbed by Wiener noise is considered. The aim is to prove the well-posedness, existence, and uniqueness of invariant measure as well as strong law of large numbers and convergence to equilibrium.

1. Introduction

The paper is concerned with the 2-dimensional Burgers equation in a bounded domain with Wiener noise as the body forces like this

$$du = (\nu \Delta u + (u \cdot \nabla) u) dt + dW, \quad \text{on } [0, T] \times D,$$

$$u(t, x) = 0, \quad t \in [0, T], \ x \in \partial D, \tag{1}$$

$$u(0, x) = u_0(x), \quad x \in D,$$

where $u(t,x) = (u^1(t,x), u^2(t,x))$ is the velocity field, v >0 is viscid coefficient, Δ denotes the Laplace operator, ∇ represents the gradient operator, W stands for the Q-Wiener process, and D is a regular bounded open domain of \mathbb{R}^2 . Burgers equation has received an extensive amount of attention since the studies by Burgers in the 1940s (and it has been considered even earlier by Beteman [1] and Forsyth [2]). But it is well known that the Burgers' equation is not a good model for turbulence since it does not perform any chaos. Even if a force is added to equation, all solutions will converge to a unique stationary solution as time goes to infinity. However, if the force is a random one, the result is completely different. So, several authors have indeed suggested to use the stochastic Burgers' equation to model turbulence, see [3–6]. The stochastic equation has also been proposed in [7] to study the dynamics of interfaces.

So far, most of the monographs concerning the equation focus on one-dimensional case, for example, Bertini et al. [8]

solved the equation with additive space-time white noise by an adaptation of the Hopf-cole transformation. Da Prato et al. [9] studied the equation via a different approach based on semigroup property for the heat equation on a bounded interval. The more general equation with multiplicative noise was considered by Da Prato and Debussche [10]. With a similar method, Gyöngy and Nualart [11] extended the Burgers equation from bounded interval to real line. A large deviation principle for the solution was obtained by Gourcy [12]. Concerning the ergodicity, an important paper by Weinan et al. [13] proved that there exists a unique stationary distribution for the solutions of the random inviscid Burgers equation, and typical solutions are piecewise smooth with a finite number of jump discontinuities corresponding to shocks. For model with jumps, Dong and Xu [14] proved that the global existence and uniqueness of the strong, weak, and mild solutions for a one-dimensional Burgers equation perturbed by Lévy noise. When the noise is fractal, Wang et al. [15] get the well-posedness.

The main aim in our paper is to study the large time behavior of stochastic system. There are lots of the literature about the topic (see [16-20]).

Burgers system is a well-known model for mechanics problems. But as far as we know, there are no results about the long-term behavior of stochastic Burgers' system. We think that the difficulty lies in the fact that the dissipative term Δu cannot dominate the nonlinear term $(u \cdot \nabla)u$. However, in many practical cases, we cannot ignore the energy dissipation and external forces, especially considering the long-term

² Institute of Applied Physics and Computational Mathematics, P.O. Box 8009, Beijing 100088, China

behavior. Therefore, we introduce dissipative term f(u) and study the ergodicity of the following equation:

$$du = \left[\Delta u + (u \cdot \nabla) u - f(u)\right] dt + dW, \quad \text{on } [0, T] \times D,$$

$$u(t, x) = 0, \quad t \in [0, T], \ x \in \partial D,$$

$$u(0, x) = u_0(x), \quad x \in D,$$
(2)

where $f(u) = \vartheta |u(t, x)|^2 u(t, x)$, $\vartheta > 0$, $|\cdot|$ denote the absolute value or norm for the real number or two-dimensional vector, respectively.

We believe that our work is new and is worth researching. The methods and results in this paper can be applied to stochastic reaction diffusion equations and stochastic real valued Ginzburg Landau equation in high dimensions. But we cannot extend our result to dynamical systems with statedelays. Since in order to show the existence of an invariant measure, we should consider the segments of a solution. In contrast to the scalar solution process, the process of segments is a Markov process. We show that the process of segments is also Feller and that there exists a solution of which the segments are tight. Then, we apply the Krylov-Bogoliubov method. Since the segment process has values in the infinitedimensional space C([-r, 0], H), boundedness in probability does not automatically imply tightness. For solution processes of infinite-dimensional equations, one often uses compactness of the orbits of the underlying deterministic equation to obtain tightness. For an infinite-dimensional formulation of the functional differential equation, however, such a compactness property does not hold. For ergodicity of stochastic delay equations, we can see [21]. We believe that stochastic Burgers' system with state-delays is a very interesting problem.

In order to study ergodicity of problem (2), we use a remarkable dissipativity property of the stochastic dynamic to obtain the existence of the invariant measure. For uniqueness, we try to use the method from [22] to prove that the distributions $P(t, x, \cdot)$ induced by the solution are equivalent. It is well known that the equivalence of the distributions implies uniqueness, a strong law of large numbers, and the convergence to equilibrium.

The remaining of this paper is organized as follows. Some preliminaries are presented in Section 2, the local existence and global existence are presented, respectively, in Sections 3 and 4. In Section 5, we obtain the existence and uniqueness of the invariant measure as well as strong law of large numbers, and convergence to equilibrium. As usual, constants C may change from one line to the next; we denote by C_a a constant which depends on some parameter a.

2. Preliminaries on the Burgers Equation

Let $u(t, x) = (u^1(t, x), u^2(t, x))$ be a row vector valued function on $[0, \infty) \times \mathbb{R}^2$. And it denotes the following:

$$|u|^2 := \sum_{i=1}^2 |u^i|^2, \quad \partial_i u^j := \frac{\partial u^j}{\partial x_i}, \quad i, j = 1, 2.$$
 (3)

Let $[C^{\infty}(D)]^2$ be infinitely differentiable 2-dimensional vector field on D, and let $[C_0^{\infty}(D)]^2$ be infinitely differentiable 2-dimensional vector field with compact support strictly contained in D. We denote by H^{α} the closure of $[C^{\infty}(D)]^2$ in $[H^{\alpha}(D)]^2$, whose norms are denoted by $\|\cdot\|_{H^{\alpha}}$, when $\alpha \neq 0$. Let H_0^1 , H be the closure of $[C_0^{\infty}(D)]^2$ in $[H^1(D)]^2$ and $[L^2(D)]^2$ whose norms are denoted by $\|\cdot\|_{H^1}$ and $\|\cdot\|_{H^2}$ respectively. Without confusion, set $\langle \cdot, \cdot \rangle$ as the inner product in *H* or $L^2(D)$. For p > 0, let $\|\cdot\|_{L^p}$ be the norm of vector filed in Lebesgue spaces $[L^p(D)]^2$. $|\cdot|_{H^{\alpha}}$ represents the norm in the usual sobolev spaces $H^{\alpha}(D)$ for real valued functions on D and $\alpha \in \mathbb{R}$; $|\cdot|_{L^p}$ stands for the norm in the usual Lebesgue spaces $L^p(D)$ for real valued functions on D. Denote $A := -\Delta$; then $A: D(A) \subset H \to H$ and $D(A) = [H^2(D)]^2 \cap H_0^1$. Since H_0^1 coincides with $D(A^{1/2})$, we can endow H_0^1 with the norm $\|u\|_{H^1} = \|A^{1/2}u\|_H$. The operator A is positive self-adjoint with compact resolvent; we denote by $0 < \alpha_1 \le \alpha_2 \le \cdots$ the eigenvalues of A, and by e_1, e_2, \ldots the eigenvectors which is a corresponding complete orthonormal system in H satisfying

(i)
$$e_i \in \left[C_0^{\infty}(D)\right]^2$$
,
(ii) $|e_i(x)| \le C$, $|\nabla e_i(x)| \le C\sqrt{\alpha_i}$, (4)
 $x \in D, i = 1, 2, \dots$,

for some positive constant C. We remark that $\|u\|_{H^1}^2 \ge \alpha_1 \|u\|_H^2$. We define the bilinear operator $B(u,v): H^1 \times H^1 \to H^{-1}$ as

$$\langle B(u,v), z \rangle = \int_{D} z(x) \cdot (u(x) \cdot \nabla) v(x) dx,$$
 (5)

for all $z \in H^1$. Then, (2) is equivalent to the following abstract equation:

$$du(t) + [Au(t) + B(u(t), u(t)) + f(u(t))] dt = dW(t).$$
 (6)

 ${\cal W}$ is the ${\cal Q}$ Wiener process having the following representative:

$$W(t) = \sum_{n=1}^{\infty} \sqrt{\lambda_n} e_n \beta_n(t), \quad t \in [0, T],$$
 (7)

in which $\sum_{n=1}^{\infty} \lambda_n < \infty$ and β_k are a sequence of mutually independent 1-dimensional Brownian motions in a fixed probability space (Ω, \mathcal{F}, P) adapted to a filtration $\{\mathcal{F}_t\}_{t>0}$.

It can be derived from [23] that the solution to the linear problem corresponding to (2) with the following initial condition:

$$du = \Delta u dt + dW,$$

$$u(t, x) = 0, \quad t \in [0, T], \quad x \in \partial D,$$

$$u(0, x) = u_0(x), \quad x \in D,$$
(8)

is unique, and when $u_0 = 0$, it has the form of

$$W_A(t) = \int_0^t e^{(t-s)A} dW(s).$$
 (9)

Let

$$v(t) = u(t) - W_A(t), \quad t \ge 0,$$
 (10)

then u is a solution to (2) if and only if it solves the following evolution equation:

$$\begin{split} \frac{\partial v}{\partial t} + Av + B\left(v + W_A, v + W_A\right) + f\left(v + W_A\right) &= 0, \\ v\left(t, x\right) &= 0, \quad t \in [0, T], \ x \in \partial D, \\ v\left(0\right) &= u_0. \end{split} \tag{11}$$

So, we see that when $w \in \Omega$ is fixed, this equation is in fact a deterministic equation. From now on, we will study the equation of the form (11) to get the existence and uniqueness of the solution a.s. $w \in \Omega$.

3. Local Existence in Time

Definition 1 (see Definition 5.1.1 in [24]). We say a $(\mathcal{F}(t))_{t\geq 0}$ adapted process v(t) is a mild solution to (11), if $v(t) \in C([0,T];H_0^1)$ and it satisfies

$$v(t) = e^{tA}v_0 + \int_0^t e^{(t-s)A}B(v + W_A, v + W_A) ds - \int_0^t e^{(t-s)A}f(v + W_A) ds, \quad t \in [0, T].$$
(12)

Lemma 2. For any $\theta \in (0,1)$, if $\sum_{i=1}^{\infty} \lambda_i(\alpha_i)^{\theta} < \infty$, then $A^{1/2}W_A$ has a version which is α -Hölder continuous with respect to $t \in [0,T], x \in D$ with any $\alpha \in]0,\theta/2[$.

Proof. Let T > 0 and $s, t \in [0, T]$; then

$$E \left| A^{1/2} W_A(t, x) - A^{1/2} W_A(s, x) \right|^2$$

$$= \sum_{i=1}^{\infty} \lambda_i \int_s^t \left| A^{1/2} S(t - \tau) e_i(x) \right|^2 ds$$

$$+ \sum_{i=1}^{\infty} \lambda_i \int_0^s \left| A^{1/2} [S(t - \tau) - S(s - \tau)] e_i(x) \right|^2 d\tau$$

$$=: I_1(t, s, x) + I_2(t, s, x).$$
(13)

Then, we have

$$I_{1}(t, s, x)$$

$$\leq C \sum_{i=1}^{\infty} \lambda_{i} \alpha_{i} \int_{s}^{t} e^{-2(t-\tau)\alpha_{i}} d\tau$$

$$= C \sum_{i=1}^{\infty} \lambda_{i} \alpha_{i} \left(\frac{1 - e^{-2(t-s)\alpha_{i}}}{2\alpha_{i}} \right)$$

$$\leq C \sum_{i=1}^{\infty} \lambda_{i} (\alpha_{i})^{\theta} |t - s|^{\theta},$$

$$I_{2}(t, s, x)$$

$$\leq \frac{1}{2} C \sum_{i=1}^{\infty} \lambda_{i} \alpha_{i} \int_{0}^{s} \left| \left[e^{-(t - \tau)\alpha_{i}} - e^{-(s - \tau)\alpha_{i}} \right] \right|^{2} d\tau$$

$$= C \sum_{i=1}^{\infty} \lambda_{i} \alpha_{i} \frac{1}{2\alpha_{i}} \left[\left(e^{-(t - s)\alpha_{i}} - 1 \right)^{2} - \left(e^{-t\alpha_{i}} - e^{-s\alpha_{i}} \right)^{2} \right]$$

$$\leq C \sum_{i=1}^{\infty} \lambda_{i} (\alpha_{i})^{\theta} |t - s|^{\theta}.$$
(14)

So, by the estimate of I_1 and I_2 , we arrive at

$$E\left|A^{1/2}W_{A}(t,x) - A^{1/2}W_{A}(s,x)\right|^{2} \le C\sum_{i=1}^{\infty} \lambda_{i}(\alpha_{i})^{\theta}|t-s|^{\theta}.$$
(15)

For $t \in [0, T]$, $x, y \in D$, we get

$$E\left|A^{1/2}W_{A}(t,x) - A^{1/2}W_{A}(t,y)\right|^{2}$$

$$= \sum_{i=1}^{\infty} \lambda_{i} \alpha_{i} \int_{0}^{t} e^{-2\alpha_{i}(t-s)} \left|e_{i}(x) - e_{i}(y)\right|^{2} ds$$

$$\leq \sum_{i=1}^{\infty} \lambda_{i} \left|e_{i}(x) - e_{i}(y)\right|^{2}$$

$$\leq \sum_{i=1}^{\infty} \lambda_{i} (\alpha_{i})^{\theta} \left|x - y\right|^{\theta}.$$
(16)

Therefore,

$$E\left|A^{1/2}W_{A}\left(t,x\right) - A^{1/2}W_{A}\left(s,y\right)\right|^{2}$$

$$\leq C\left(\left|t-s\right|^{\theta} + \left|x-y\right|^{\theta}\right).$$
(17)

As $A^{1/2}W_A(t,x)-A^{1/2}W_A(s,y)$ is a Gaussian random variable, we obtain

$$E\left|A^{1/2}W_{A}\left(t,x\right)-A^{1/2}W_{A}\left(s,y\right)\right|^{2m}$$

$$\leq C\left(\left|t-s\right|^{m\theta}+\left|x-y\right|^{m\theta}\right),$$
(18)

for $m=1,2,\ldots$ By Kolmogorov' test theorem, we get the conclusion.

Remark 3. An example of the noise satisfying condition of Lemma 2 is

$$dW(t) = \sum_{n=1}^{\infty} \sqrt{\lambda_n} e_n d\beta_n(t), \qquad (19)$$

where $\{\beta_n\}$ is a sequence of independent 1-dimensional Brownian motion, and $\{\lambda_n\}$ satisfies

$$\lambda_n = n^{-(1+2\theta)}, \quad \alpha_n = n \quad \forall n \in \mathbb{N}.$$
 (20)

It is so because the eigenvalues α_n of the operator A, in 2-dimensional space, behave like n.

Remark 4. Another example of stochastic noise satisfying Lemma 2 is

$$A^{-\gamma}LdW(t), \qquad (21)$$

where $W(t) = \sum_{n=1}^{\infty} e_n \beta_n(t)$, L is an isomorphism in H, and

$$\gamma \ge \frac{1}{2} + \theta. \tag{22}$$

To prove the local existence of the solution of (1) in sense of Definition 1, we introduce the space \mathcal{B}_m defined by

$$\mathcal{B}_{m} = \left\{ v : v \in C\left(\left[0, T^{*}\right]; H_{0}^{1}\right), \|v\|_{H^{1}} \le m, \forall t \in \left[0, T^{*}\right] \right\},$$
(23)

where $T^* \ge 0$ which in fact is a stopping time and m > 0, p > 0.

Lemma 5. For $u_0 = (u^1(0), u^2(0)), \|u_0\|_{H^1} < m$, and $u^i(0)$ is adapted to \mathcal{F}_0 , i = 1, 2; then there exists a unique mild solution v in sense of Definition 1 to (11) in \mathcal{B}_m .

Proof. Choose a v in \mathcal{B}_m , and set

$$\mathcal{L}(v) := e^{-tA} u_0$$

$$+ \int_0^t e^{-(t-s)A} \left[(v + W_A) \cdot \nabla \right] (v + W_A) ds \qquad (24)$$

$$- \int_0^t e^{-(t-s)A} f(v + W_A) ds.$$

Then,

$$\|\mathcal{L}(v)\|_{H^{1}} \leq \|e^{-tA}u_{0}\|_{H^{1}} + \|\int_{0}^{t} e^{-(t-s)A} \left[(v+W_{A}) \cdot \nabla \right] (v+W_{A}) ds \|_{H^{1}} + \|\int_{0}^{t} e^{-(t-s)A} f(v+W_{A}) ds \|_{H^{1}}.$$
(25)

For the second term on the right hand side of (25),

$$\begin{aligned} \left\| e^{-(t-s)A} \left[(v + W_A) \cdot \nabla \right] (v + W_A) \right\|_{H^1} \\ &= \left\| e^{-(t-s)A} \left[u \cdot \nabla \right] u \right\|_{H^1} \\ &\leq \frac{1}{2} \left| e^{-(t-s)A} \partial_1 (u^1)^2 \right|_{H^1} \\ &+ \frac{1}{2} \left| e^{-(t-s)A} \partial_2 (u^2)^2 \right|_{H^1} \\ &+ \left| e^{-(t-s)A} u^2 \partial_2 u^1 \right|_{H^1} \\ &+ \left| e^{-(t-s)A} u^1 \partial_1 u^2 \right|_{H^1} \\ &:= I_1 + I_2 + I_3 + I_4. \end{aligned}$$
(26)

In the following, we will estimate I_i , respectively, i = 1, 2, 3, 4. Since $\{e^{-tA}\}_{t\geq 0}$ is contraction on $L^p(D)$, $p \geq 1$, it is known that

$$\left| e^{-tA} z \right|_{W^{s_2,r}} \le C_1 t^{(s_1 - s_2)/2} |z|_{W^{s_1,r}},$$
 (27)

for all $z \in W^{s_1,r}(D)$, $s_1, s_2 \in \mathbb{R}$, $s_1 \leq s_2, r \geq 1$, and C_1 only depends on s_1, s_2 , and r. Before calculating each I_i , we outline the Sobolev embedding principle in fractional Sobolev spaces as follows:

$$W^{\eta_1,p_1}(D) \in W^{\eta_2,q_1}(D),$$
 (28)

when

$$\frac{1}{p_1} - \frac{1}{n} (\eta_1 - \eta_2) \le \frac{1}{q_1} \le \frac{1}{p_1},\tag{29}$$

where *n* is the dimension of the spatial. Let $\eta_1 = 3/4$, $p_1 = 2$, $\eta_2 = 1/4$, $q_1 = 4$ satisfying (29) such that

$$W^{3/4,2}(D) \subset W^{1/4,4}(D)$$
. (30)

For I_1 , by (27) and Theorem A.8 in [25], we get

$$\begin{split} I_{1} &\leq C_{1} |t-s|^{-7/8} \left| \partial_{1} \left(u^{1} \right)^{2} \right|_{H^{-3/4}} \\ &= C_{1} |t-s|^{-7/8} \left| A^{1/8} \left(u^{1} \right)^{2} \right|_{H} \\ &= C_{1} |t-s|^{-7/8} \left| 2u^{1} A^{1/8} u^{1} + R \right|_{H}, \end{split}$$
(31)

where

$$R = A^{1/8} (u^1)^2 - 2A^{1/8} u^1, (32)$$

satisfying

$$|R|_{H} \le \left|A^{1/16}u^{1}\right|_{L^{4}}^{2} \le \left|u^{1}\right|_{H^{1}}^{2}.$$
 (33)

The last inequality follows by (30). For the other term added to R, we have

$$\left|2u^{1}A^{1/8}u^{1}\right|_{H} \le \left|u_{1}\right|_{L^{4}}^{2} + \left|A^{1/8}u^{1}\right|_{L^{4}}^{2} \le 2\left|u^{1}\right|_{H^{1}}^{2}.$$
 (34)

So, by (31)–(34), we have

$$I_1 \le 3C_1|t-s|^{-7/8}|u^1|_{H^1}^2.$$
 (35)

Similarly, we get for I_2 that

$$I_2 \le 3C_1|t-s|^{-7/8}|u^2|_{H^1}^2.$$
 (36)

For I_3 , by Theorem A.8 in [25], we get

$$I_{3} \leq \left| e^{-(t-s)A} u^{2} A^{1/2} u^{1} \right|_{H^{1}}$$

$$= \left| e^{-(t-s)A} \left[A^{1/4} \left(u^{2} A^{1/4} u^{1} \right) - \left(A^{1/4} u^{1} \right) \left(A^{1/4} u^{2} \right) - R_{1} \right] \right|_{H^{1}}, \tag{37}$$

where

$$R_1 = A^{1/4} \left(u^2 A^{1/4} u^1 \right) - \left[A^{1/4} u^2 \right] \left[A^{1/4} u^1 \right] - u^2 A^{1/2} u^1.$$
(38)

For R_1 , we have

$$\begin{aligned} \left| e^{-(t-s)A} R_1 \right|_{H^1} \\ &\leq C_1 |t-s|^{-1/2} |R_1|_H \\ &\leq C_1 |t-s|^{-1/2} |A^{1/4} u^1|_{L^4} \cdot |A^{1/4} u^2|_{L^4} \\ &\leq C_1 |t-s|^{-1/2} \left(\left| u^1 \right|_{H^1}^2 + \left| u^2 \right|_{H^1}^2 \right). \end{aligned}$$
(39)

For the first term on the right hand side of (37), by (27), we have

$$\begin{aligned} \left| e^{-(t-s)A} A^{1/4} \left(u^2 A^{1/4} u^1 \right) \right|_{H^1} \\ &= \left| e^{-(t-s)A} A^{3/4} \left(u^2 A^{1/4} u^1 \right) \right|_{H} \\ &\leq C_1 |t-s|^{-3/4} \left| u^2 A^{1/4} u^1 \right|_{H} \\ &\leq C_1 |t-s|^{-3/4} \left(\left| u^2 \right|_{L^4}^2 + \left| A^{1/4} u^1 \right|_{L^4}^2 \right) \\ &\leq C_1 |t-s|^{-3/4} \left(\left| u^2 \right|_{H^1}^2 + \left| u^1 \right|_{H^1}^2 \right). \end{aligned}$$

$$(40)$$

For the second term on the right hand side of (37), by (27), we obtain

$$\begin{split} \left| e^{-(t-s)A} [A^{1/4} u^2 \cdot A^{1/4} u^1] \right|_{H^1} \\ & \leq C_1 |t-s|^{-1/2} \left| A^{1/4} u^2 \cdot A^{1/4} u^1 \right|_H \\ & \leq C_1 |t-s|^{-1/2} \left(\left| u^1 \right|_{H^1}^2 + \left| u^2 \right|_{H^1}^2 \right). \end{split} \tag{41}$$

From (37) to (41), we get for I_3 that

$$I_3 \le C \left(|t - s|^{-1/2} + |t - s|^{-3/4} \right) \left(\left| u^1 \right|_{H^1}^2 + \left| u^2 \right|_{H^1}^2 \right). \tag{42}$$

Analogously, for I_4 , we get

$$I_4 \le C \left(|t - s|^{-1/2} + |t - s|^{-3/4} \right) \left(\left| u^1 \right|_{H^1}^2 + \left| u^2 \right|_{H^1}^2 \right). \tag{43}$$

By (26), (35), (36), (42), and (43), we have

$$\begin{aligned} \left\| e^{-(t-s)A} \left[(v + W_A) \cdot \nabla \right] (v + W_A) \right\|_{H^1} \\ &\leq C \left(|t - s|^{-1/2} + |t - s|^{-3/4} + |t - s|^{-7/8} \right) \\ &\times \left(\left| u^1 \right|_{H^1}^2 + \left| u^2 \right|_{H^1}^2 \right). \end{aligned}$$
(44)

As $u = v + W_{\Delta}$, by (44), for $t \le T^*$, we have

$$\int_{0}^{t} ds \|e^{-(t-s)A} \left[\left(v + W_{A} \right) \cdot \nabla \right] \left(v + W_{A} \right) \|_{H^{1}} \\
\leq C \left(t^{1/8} + t^{1/4} + t^{1/2} \right) \left(\sup_{t \in [0, T^{*}]} \|v\|_{H^{1}}^{2} + \sup_{t \in [0, T]} \|W_{A}\|_{H^{1}}^{2} \right). \tag{45}$$

Since by Lemma 2,

$$\sup_{t \in [0,T]} \|W_A\|_{H^1}^2 < \infty. \tag{46}$$

For the last term on the right hand side of (25), we have

$$\begin{aligned} \left\| e^{-(t-s)A} f \left(v + W_A \right) \right\|_{H^1} \\ &\leq C |t-s|^{-1/2} \left(\left\| v + W_A \right\|_{L^6}^3 \right) \\ &\leq C |t-s|^{-1/2} \left(\left\| W_A \right\|_{H^1}^3 + \left\| v \right\|_{H^1}^3 \right). \end{aligned}$$
(47)

Therefore,

$$\left\| \int_{0}^{t} e^{-(t-s)A} f(v + W_{A}) ds \right\|_{H^{1}}$$

$$\leq C \left(1 + m^{3} \right) \int_{0}^{t} |t - s|^{-1/2} ds \tag{48}$$

$$\leq C \left(1 + m^{3} \right) T^{*1/2}.$$

So by (25), (45), and (48), when T^* is small enough,

$$\|\mathscr{L}(v)\|_{H^1} \le m. \tag{49}$$

For each $v_1, v_2 \in \mathcal{B}_m$, set $u_i = v_i + W_A$, i = 1, 2. To simplify the notation in the following calculation, we denote $u_i = (u_i^1, u_i^2)$, i = 1, 2. Then,

$$\mathcal{L}(v_1) - \mathcal{L}(v_2)$$

$$= \int_0^t e^{-(t-s)A} \left[(u_1 \cdot \nabla) u_1 - (u_2 \cdot \nabla) u_2 \right] ds$$

$$+ \int_0^t e^{-(t-s)A} \left[f(u_1) - f(u_2) \right] ds.$$
(50)

Sc

$$\|\mathscr{L}(v_{1}) - \mathscr{L}(v_{2})\|_{H^{1}}$$

$$\leq \int_{0}^{t} \|e^{-(t-s)A} [(u_{1} \cdot \nabla) u_{1} - (u_{2} \cdot \nabla) u_{2}]\|_{H^{1}} ds \qquad (51)$$

$$+ \int_{0}^{t} \|e^{-(t-s)A} [f(u_{1}) - f(u_{2})]\|_{H^{1}} ds.$$

In order to simplify the notation, we set

$$(u_1 \cdot \nabla) u_1 - (u_2 \cdot \nabla) u_2 = (f_1 + f_2, f_3 + f_4),$$
 (52)

where

$$f_{1} = \frac{1}{2}\partial_{1}\left[\left(u_{1}^{1}\right)^{2} - \left(u_{2}^{1}\right)^{2}\right],$$

$$f_{2} = u_{1}^{2}\partial_{2}u_{1}^{1} - u_{2}^{2}\partial_{2}u_{2}^{1},$$

$$f_{3} = \frac{1}{2}\partial_{2}\left[\left(u_{1}^{2}\right)^{2} - \left(u_{2}^{2}\right)^{2}\right],$$

$$f_{4} = u_{1}^{1}\partial_{1}u_{1}^{2} - u_{2}^{1}\partial_{1}u_{2}^{2}.$$
(53)

Then, we estimate f_i , i=1,2,3,4, respectively. For f_1 , we have

$$\begin{split} \left| e^{-(t-s)A} f_1 \right|_{H^1} \\ &= \left| e^{-(t-s)A} A^{1/2} \left[\left(u_1^1 - u_2^1 \right) \left(u_1^1 + u_2^1 \right) \right] \right|_{H^1} \\ &\leq C |t - s|^{-7/8} \left| A^{1/8} \left[\left(u_1^1 \right)^2 - \left(u_2^1 \right)^2 \right] \right|_{H} \\ &= C |t - s|^{-7/8} \left| A^{1/8} \left[\left(u_1^1 - u_1^2 \right) \left(u_1^1 + u_1^2 \right) \right] \right|_{H} \\ &= C |t - s|^{-7/8} \left| \left[A^{1/8} \left(u_1^1 - u_1^2 \right) \right] \left(u_1^1 + u_1^2 \right) \right|_{H} \\ &+ C |t - s|^{-7/8} \left| \left[A^{1/8} \left(u_1^1 + u_1^2 \right) \right] \left(u_1^1 - u_1^2 \right) + R_2 \right|_{H}. \end{split}$$
(54)

We first consider

$$\begin{aligned} \left| R_{2} \right|_{H} &\leq C \left| A^{1/16} \left(u_{1}^{1} - u_{2}^{1} \right) \right|_{L^{4}} \cdot \left| A^{1/16} \left(u_{1}^{1} + u_{2}^{1} \right) \right|_{L^{4}} \\ &\leq C \left| u_{1}^{1} - u_{2}^{1} \right|_{H^{1}} \cdot \left| u_{1}^{1} + u_{2}^{1} \right|_{H^{1}}. \end{aligned} \tag{55}$$

For the other term added to R_2 ,

$$\begin{aligned}
&\left| \left[A^{1/8} \left(u_1^1 + u_2^1 \right) \right] \left(u_1^1 - u_2^1 \right) \right|_{H} \\
&\leq \left| u_1^1 + u_2^1 \right|_{H^1} \cdot \left| u_1^1 - u_2^1 \right|_{H^1}.
\end{aligned} (56)$$

By (54)–(56),

$$\left| e^{-(t-s)A} f_1 \right|_{H^1} \le C |t-s|^{-7/8} \left| u_1^1 - u_2^1 \right|_{H^1} \cdot \left| u_1^1 + u_2^1 \right|_{H^1}.$$
 (57)

Analogously, for f_3 ,

$$\left| e^{-(t-s)A} f_3 \right|_{H^1} \le C |t-s|^{-7/8} \left| u_1^1 - u_2^1 \right|_{H^1} \cdot \left| u_1^1 + u_2^1 \right|_{H^1}.$$
 (58)

For f_2 , by (53), we have

$$\begin{aligned} \left| e^{-(t-s)A} f_2 \right|_{H^1} &= \left| e^{-(t-s)A} \left(u_1^2 \partial_2 u_1^1 - u_2^2 \partial_2 u_2^1 \right) \right|_{H^1} \\ &\leq \left| e^{-(t-s)A} \left(u_1^2 \left(\partial_2 u_1^1 - \partial_2 u_2^1 \right) \right) \right|_{H^1} \\ &+ \left| e^{-(t-s)A} \left(\left(u_1^2 - u_2^2 \right) \partial_2 u_2^1 \right) \right|_{H^1}. \end{aligned} (59)$$

For the first term on the right hand side of (59), we have

$$\begin{aligned} \left| e^{-(t-s)A} \left(u_1^2 \left(\partial_2 u_1^1 - \partial_2 u_2^1 \right) \right) \right|_{H^1} \\ & \leq \left| e^{-(t-s)A} \left(u_1^2 A^{1/2} \left(u_1^1 - u_2^1 \right) \right) \right|_{H^1} \\ & = \left| e^{-(t-s)A} \left\{ A^{1/4} \left[u_1^2 A^{1/4} \left(u_1^1 - u_2^1 \right) \right] \right. \\ & \left. - \left[A^{1/4} u_1^2, A^{1/4} \left(u_1^1 - u_2^1 \right) \right] - R_3 \right\} \right|_{H^1}. \end{aligned}$$

$$(60)$$

For R_3 ,

$$\begin{aligned} \left| e^{-(t-s)A} R_3 \right|_{H^1} \\ & \leq |t-s|^{-1/2} |R_3|_H \\ & \leq |t-s|^{-1/2} |A^{1/4} u_1^2|_{L^4} \cdot |A^{1/4} \left(u_1^1 - u_2^1 \right)|_{L^4} \\ & = |t-s|^{-1/2} |u_1^2|_{L^1} \cdot |u_1^1 - u_2^1|_{L^1}. \end{aligned}$$

$$(61)$$

For the first term on the right hand side of (60), we arrive at

$$\begin{aligned} \left| e^{-(t-s)A} A^{1/4} \left[u_1^2 A^{1/4} \left(u_1^1 - u_2^1 \right) \right] \right|_{H^1} \\ &= \left| e^{-(t-s)A} A^{3/4} \left[u_1^2 A^{1/4} \left(u_1^1 - u_2^1 \right) \right] \right|_{H} \\ &\leq \left| t - s \right|^{-3/4} \left| u_1^2 A^{1/4} \left(u_1^1 - u_2^1 \right) \right|_{H} \\ &\leq \left| t - s \right|^{-3/4} \left| u_1^2 \right|_{L^4} \cdot \left| A^{1/4} \left(u_1^1 - u_2^1 \right) \right|_{L^4} \\ &\leq \left| t - s \right|^{-3/4} \left| u_1^2 \right|_{H^1} \cdot \left| u_1^1 - u_2^1 \right|_{H^1}. \end{aligned}$$

$$(62)$$

For the second term on the right hand side of (60), we obtain

$$\begin{aligned} \left| e^{-(t-s)A} \left[\left(A^{1/4} u_1^2 \right) \left(A^{1/4} \left(u_1^1 - u_2^1 \right) \right) \right] \right|_{H^1} \\ & \leq |t-s|^{-1/2} \left| \left[A^{1/4} u_1^2 \right] \cdot \left[A^{1/4} \left(u_1^1 - u_2^1 \right) \right] \right|_{H} \\ & \leq |t-s|^{-1/2} \left| A^{1/4} u_1^2 \right|_{L^4} \cdot \left| A^{1/4} \left(u_1^1 - u_2^1 \right) \right|_{L^4} \\ & \leq |t-s|^{-1/2} \left| u_1^2 \right|_{H^1} \cdot \left| u_1^1 - u_2^1 \right|_{H^1}. \end{aligned} \tag{63}$$

By (59)–(63), we get for f_2 that

$$\begin{aligned} \left| e^{(t-s)A} f_2 \right|_{H^1} \\ &\leq C \left(\left| t - s \right|^{-1/2} + \left| t - s \right|^{-3/4} \right) \\ &\times \left(\left\| u_1 \right\|_{H^1} + \left\| u_2 \right\|_{H^1} \right) \left\| u_1 - u_2 \right\|_{H^1}. \end{aligned}$$
(64)

Similarly, we get for f_4 that

$$\begin{aligned} \left| e^{(t-s)A} f_4 \right|_{H^1} \\ &\leq C \left(|t-s|^{-1/2} + |t-s|^{-3/4} \right) \\ &\times \left(\left\| u_1 \right\|_{H^1} + \left\| u_2 \right\|_{H^1} \right) \left\| u_1 - u_2 \right\|_{H^1}. \end{aligned}$$
(65)

By (52), (53), (57), (58), (64), and (65), we have

$$\begin{aligned} \left\| e^{-(t-s)A} \left[\left(u_{1} \cdot \nabla \right) u_{1} - \left(u_{2} \cdot \nabla \right) u_{2} \right] \right\|_{H^{1}} \\ &\leq \sum_{i=1}^{4} \left| e^{-(t-s)A} f_{i} \right|_{H^{1}} \\ &\leq C \left(\left| t - s \right|^{-1/2} + \left| t - s \right|^{-3/4} + \left| t - s \right|^{-7/8} \right) \\ &\qquad \times \left(\left\| u_{1} \right\|_{H^{1}} + \left\| u_{2} \right\|_{H^{1}} \right) \left\| u_{1} - u_{2} \right\|_{H^{1}} \\ &\leq C \left(2m + 1 \right) \left(\left| t - s \right|^{-1/2} + \left| t - s \right|^{-3/4} + \left| t - s \right|^{-7/8} \right) \\ &\qquad \times \left\| v_{1} - v_{2} \right\|_{H^{1}}. \end{aligned}$$

$$(66)$$

For the second term on the right hand side of (51), we have

$$f(u_1) - f(u_2) = (h_1, h_2),$$
 (67)

where

$$h_{1} = |u_{1}|^{2} u_{1}^{1} - |u_{2}|^{2} u_{2}^{1},$$

$$h_{2} = |u_{1}|^{2} u_{1}^{2} - |u_{2}|^{2} u_{2}^{2}.$$
(68)

Then,

$$\begin{split} \left| e^{(t-s)A} h_1 \right|_{H^1} \\ &\leq C |t-s|^{-1/2} \left| \left| u_1 \right|^2 u_1^1 - \left| u_2 \right|^2 u_2^1 \right|_{H} \\ &\leq C |t-s|^{-1/2} \left| \left| u_1 \right|^2 u_1^1 - \left| u_2 \right|^2 u_1^1 \right|_{H} \\ &+ C |t-s|^{-1/2} \left| \left| u_2 \right|^2 u_1^1 - \left| u_2 \right|^2 u_2^1 \right|_{H} \\ &\leq C |t-s|^{-1/2} \left| \left| v_1 - v_2 \right| \cdot \left(\left| v_1 \right| + \left| v_2 \right| + 2 \left| W_A \right| \right) \cdot \left| u_1^1 \right| \right|_{H} \\ &+ C |t-s|^{-1/2} \left| \left| u_2 \right|^2 \cdot \left| v_1^1 - v_2^1 \right| \right|_{H} \\ &\leq C |t-s|^{-1/2} \left\| v_1 - v_2 \right\|_{L^4} \cdot \left| \left(\left| v_1 \right| + \left| v_2 \right| + 2 \left| W_A \right| \right) \cdot \left| u_1^1 \right| \right|_{L^4} \\ &+ C |t-s|^{-1/2} \left\| v_1 - v_2 \right\|_{L^4} \cdot \left| \left| u_2 \right|_{L^4}^2 \\ &\leq C |t-s|^{-1/2} \left\| v_1 - v_2 \right\|_{L^4} \left(\left\| v_1 \right\|_{L^8}^2 + \left\| v_2 \right\|_{L^8}^2 + 1 \right) \\ &\leq C |t-s|^{-1/2} \left\| v_1 - v_2 \right\|_{H^1} \left(\left\| v_1 \right\|_{H^1}^2 + \left\| v_2 \right\|_{H^1}^2 + 1 \right). \end{split}$$

Similarly, we can get the same estimate for h_2 . So, we have

$$\int_{0}^{t} \left\| e^{(t-s)A} \left[f\left(u_{1}\right) - f\left(u_{2}\right) \right] \right\|_{H^{1}} ds$$

$$\leq C \left(1 + m^{2} \right) T^{*1/2} \sup_{t \in [0, T^{*}]} \left\| v_{1}\left(t\right) - v_{2}\left(t\right) \right\|_{H^{1}}.$$
(70)

By (51), (66), and (70), we have

$$\|\mathscr{L}(\nu_{1}) - \mathscr{L}(\nu_{2})\|_{H^{1}} \le C \left[T^{*1/2} + T^{*1/4} + T^{*1/8} \right] \cdot \left(\sup_{t \in [0, T^{*}]} \|\nu_{1} - \nu_{2}\|_{H^{1}} \right).$$
(71)

By (49), (71), and fixed point principle, we get the conclusion.

Remark 6. By making some minor modifications in the proof of Lemma 5, we can see that the conclusion in Lemma 5 is also true for (1). Our original aim is to get the global well-posedness of (1), but we find that the dissipative term Δu cannot dominate the nonlinear term $(u \cdot \nabla)u$. So, we introduce the dissipative term $|u|^2u$ which will also play an important role in obtaining the ergodicity.

4. Global Existence

Theorem 7. With conditions in Lemma 2, for $v \in C([0,T]; H_0^1)$ satisfying (12), when $\theta > 1/16$, one has

$$\|v\|_{H^1} \le \left(C_T + \|v_0\|_{H^1}^2\right) e^{C_T}.$$
 (72)

Subsequently, one gets the existence of the global solution belonging to $C([0,T];H_0^1)$.

Proof. Let $\{u_n^0\}_{n\geq 1}$ be a sequence of vectors which satisfies $u_n^0=(u_n^{0,1},u_n^{0,2})$ and $u_n^{0,i}\in C_0^\infty(D), i=1,2,n\geq 1$, such that

$$u_n^0 \longrightarrow u_0$$
, as $n \longrightarrow \infty$, (73)

in sense of $\|\cdot\|_{H^1}$. Let $\{W_n\}_{n\geq 1}$ be a sequence of regular process, such that

$$A^{a/2}W_A^n := A^{a/2} \int_0^t e^{(t-s)A} dW_n(s) \longrightarrow A^{a/2}W_A(t),$$
as $n \to \infty$,
$$(74)$$

in $C(T \times D)$ when a = 0 or a = 1. For $h = (h_1, h_2)$, $h_i \in C([0, T] \times D; \mathbb{R}), \|h\|_{C(T \times D)} := \sum_{i=1}^2 |h_i|_{C(T \times D)}$, where $|h_i|_{C(T \times D)} = \sup_{(t,x) \in [0,T] \times D} |h_i|$. Then, by (74), we have

$$\sup_{\{n>1\}} \|W_A^n\|_{C(T \times D)} < \infty, \tag{75}$$

$$\sup_{\{n\geq 1\}} \sup_{t\in[0,T]} \left| A^{1/2} W_A^n \right| < \infty. \tag{76}$$

If v_n satisfies

$$v_{n} = e^{tA}u_{n}^{0} + \int_{0}^{t} e^{(t-s)A} \left[(v_{n} + W_{A}) \cdot \nabla \right] (v_{n} + W_{A}) ds$$

$$- \int_{0}^{t} e^{(t-s)A} f(v_{n} + W_{A}),$$
(77)

then, v_n is regular, such that

$$\frac{\partial v_n}{\partial t} + Av_n + B\left(v_n + W_A^n, v_n + W_A^n\right) + f\left(v_n + W_A^n\right) = 0.$$
(78)

Taking inner product with respect to v_n in (78), we have

$$\left\langle \frac{\partial v_n}{\partial t}, v_n \right\rangle + \left\langle A v_n, v_n \right\rangle + \left\langle B \left(v_n + W_A^n, v_n + W_A^n \right), v_n \right\rangle$$

$$+ \left\langle f \left(v_n + W_A^n \right), v_n \right\rangle = 0.$$

$$(79)$$

For simplicity, we calculate the third term on the left hand side of (79) first as follows:

$$\langle B(v_{n} + W_{A}^{n}, v_{n} + W_{A}^{n}), v_{n} \rangle$$

$$= \langle (v_{n}^{1} + W_{A,1}^{n}) \partial_{1} (v_{n}^{1} + W_{A,1}^{n}), v_{n}^{1} \rangle$$

$$+ \langle (v_{n}^{2} + W_{A,2}^{n}) \partial_{2} (v_{n}^{1} + W_{A,1}^{n}), v_{n}^{1} \rangle$$

$$+ \langle (v_{n}^{1} + W_{A,1}^{n}) \partial_{1} (v_{n}^{2} + W_{A,2}^{n}), v_{2}^{n} \rangle$$

$$+ \langle (v_{n}^{2} + W_{A,2}^{n}) \partial_{2} (v_{n}^{2} + W_{A,2}^{n}), v_{n}^{2} \rangle$$

$$= I_{1} + I_{2} + I_{3} + I_{4},$$
(80)

where $W_A^n = (W_{A,1}^n, W_{A,2}^n)$. For I_1 , we have

$$I_{1} = \left\langle \left(v_{n}^{1} + W_{A,1}^{n}\right) \partial_{1} \left(v_{n}^{1} + W_{A,1}^{n}\right), v_{n}^{1} \right\rangle$$

$$= \left\langle v_{n}^{1} \partial_{1} v_{n}^{1}, v_{n}^{1} \right\rangle + \left\langle W_{A,1}^{n} \partial_{1} v_{n}^{1}, v_{n}^{1} \right\rangle$$

$$+ \left\langle v_{n}^{1} \partial_{1} W_{A,1}^{n}, v_{n}^{1} \right\rangle + \left\langle W_{A,1}^{n} \partial_{1} W_{A,1}^{n}, v_{n}^{1} \right\rangle. \tag{81}$$

In the following, we estimate the four terms for I_1 , respectively. For the first term,

$$\left\langle v_n^1 \partial_1 v_n^1, v_n^1 \right\rangle = \int_D \left(v_n^1 \right)^2 \partial_1 v_n^1 dx$$

$$= \int_D \partial_1 \left[\frac{\left(v_n^1 \right)^3}{3} \right] dx = 0. \tag{82}$$

For the second term, by (75), we have

$$\langle W_{A,1}^{n} \partial_{1} v_{n}^{1}, v_{n}^{1} \rangle$$

$$\leq C \left| v_{n}^{1} \right|_{H}^{2} + \varepsilon \int_{D} \left(\partial_{1} v_{n}^{1} \right)^{2} dx \qquad (83)$$

$$\leq C \left| v_{n}^{1} \right|_{H}^{2} + \varepsilon \left| v_{n}^{1} \right|_{H}^{2}.$$

similarly, for the third term,

$$\left| \left\langle v_n^1 \partial_1 W_{A,1}^n, v_n^1 \right\rangle \right|$$

$$= \left| \int_D \left(v_n^1 \right)^2 \partial_1 W_{A,1}^n dx \right|$$

$$= \left| \int_D W_{A,1}^n \partial_1 \left(v_n^1 \right)^2 dx \right|$$

$$\leq C \left| \int_D v_n^1 \partial_1 v_n^1 dx \right|$$

$$\leq C \left| v_n^1 \right|_H^2 + \varepsilon \left| v_n^1 \right|_{H^1}^2.$$
(84)

For the last term, by (75) and (76),

$$\left| \left\langle W_{A,1}^{n} \partial_{1} W_{A,1}^{n}, v_{n}^{1} \right\rangle \right|$$

$$\leq C \left| \int_{D} \partial_{1} v_{n}^{1} dx \right|$$

$$\leq C + \varepsilon \left| v_{n}^{1} \right|_{L^{1}}^{2}.$$
(85)

By (81)–(85), it follows that

$$I_1 \le C \left(1 + \| v_n \|_H^2 \right) + 4\varepsilon \| v_n \|_{H^1}^2.$$
 (86)

Similarly,

$$I_4 \le C \left(1 + \| v_n \|_H^2 \right) + 4\varepsilon \| v_n \|_{H^1}^2.$$
 (87)

For I_3 ,

$$I_{3} = \langle v_{n}^{1} \partial_{1} v_{n}^{2}, v_{n}^{2} \rangle + \langle v_{n}^{1} \partial_{1} W_{A,2}^{n}, v_{n}^{2} \rangle$$

$$+ \langle W_{A,1}^{n} \partial_{1} v_{n}^{2}, v_{n}^{2} \rangle + \langle W_{A,1}^{n} \partial_{1} W_{A,2}^{n}, v_{n}^{2} \rangle.$$
(88)

For the first term on the right hand side of (88), we deduce that

$$\left| \left\langle v_{n}^{1} \partial_{1} v_{n}^{2}, v_{n}^{2} \right\rangle \right| = \frac{1}{2} \left| \int_{D} v_{n}^{1} \partial_{1} \left(v_{n}^{2} \right)^{2} dx \right|$$

$$= \frac{1}{2} \left| \int_{D} \partial_{1} v_{n}^{1} \cdot \left(v_{n}^{2} \right)^{2} dx \right|$$

$$\leq \frac{1}{2} \left| v_{n}^{2} \right|_{L^{4}}^{2} \cdot \left| v_{n}^{1} \right|_{H^{1}}$$

$$\leq \frac{1}{4} \epsilon \left| v_{n}^{2} \right|_{L^{4}}^{4} + \frac{1}{4\epsilon} \left| v_{n}^{1} \right|_{H^{1}}^{2},$$
(89)

where $\epsilon > 0$. For the second term on the right hand side of (88), we have

$$\left| \left\langle v_{n}^{1} \partial_{1} W_{A,2}^{n}, v_{n}^{2} \right\rangle \right| \leq \varepsilon \left\| v^{n} \right\|_{H^{1}}^{2} + C \left\| v^{n} \right\|_{H}^{2}. \tag{90}$$

Analogously, for the third term on the right hand side of (88), we see that

$$\left| \left\langle W_{A,1}^{n} \partial_{1} v_{n}^{2}, v_{n}^{2} \right\rangle \right| \le C \|v^{n}\|_{H}^{2} + \varepsilon \|v^{n}\|_{H^{1}}^{2}.$$
 (91)

For the last term, by (75) and (76), we have

$$\left| \left\langle W_{A,1}^n \partial_x W_{A,2}^n, v_n^2 \right\rangle \right| \le C + \varepsilon \|v^n\|_{H^1}^2. \tag{92}$$

By (88)–(92), we get

$$I_{3} \leq \frac{1}{4\epsilon} \|v_{n}^{2}\|_{L^{4}}^{4} + \frac{\epsilon}{4} \|v_{n}^{1}\|_{H^{1}}^{2} + 3\epsilon \|v_{n}\|_{H^{1}}^{2} + C \|v_{n}\|_{H}^{2} + C.$$

$$(93)$$

Analogously, for I_2 , it follows that

$$I_{2} \leq \frac{1}{4\epsilon} \|v_{n}^{1}\|_{L^{4}}^{4} + \frac{\epsilon}{4} \|v_{n}^{2}\|_{H^{1}}^{2} + 3\epsilon \|v_{n}\|_{H^{1}}^{2} + C \|v_{n}\|_{H}^{2} + C.$$

$$(94)$$

By (80) and the estimates of I_1 , I_2 , I_3 , and I_4 , see (86), (87), (93), and (94), we have

$$\langle B\left(\nu_{n} + W_{A}^{n}, \nu_{n} + W_{A}^{n}\right), \nu_{n} \rangle$$

$$\leq C\left(1 + \left\|\nu_{n}\right\|_{H}^{2}\right) + \left(\frac{\epsilon}{4} + 14\epsilon\right) \left\|\nu_{n}\right\|_{H^{1}}^{2} \qquad (95)$$

$$+ \frac{1}{4\epsilon} \left\|\nu_{n}\right\|_{L^{4}}^{4}.$$

For the last term on the left hand side of (79), we have

$$\langle f(v_{v} + W_{A}^{n}), v_{n} \rangle$$

$$= \vartheta \|v_{n}\|_{L^{4}}^{4} + 3\vartheta \int_{D} |v_{n}|^{2} \left(v_{n}^{1} W_{A,1}^{n} + v_{n}^{2} W_{A,2}^{n}\right) dx$$

$$+ \vartheta \int_{D} |v_{n}|^{2} |W_{A}^{n}|^{2} dx$$

$$+ \vartheta \int_{D} \left(v_{n}^{1} W_{A,1}^{n} + v_{n}^{2} W_{A,2}^{n}\right) |W_{A}^{n}|^{2} dx \qquad (96)$$

$$+ 2\vartheta \int_{D} \left(\left|W_{A,1}^{n}\right|^{2} |v_{n}^{1}|^{2} + \left|W_{A,2}^{n}\right|^{2} |v_{n}^{2}|^{2}\right) dx$$

$$+ 4\vartheta \int_{D} W_{A,1}^{n} W_{A,2}^{n} v_{n}^{1} v_{n}^{2} dx$$

$$\leq (\vartheta + \varepsilon) \|v_{n}\|_{L^{4}}^{4} + C\left(1 + \|v_{n}\|_{H}^{2}\right).$$

By (79), (95), and (96), we get

$$\frac{1}{2} \frac{\partial}{\partial t} \|v_{n}\|_{H}^{2} + \|v_{n}\|_{H^{1}}^{2} + \vartheta \|v_{n}\|_{L^{4}}^{4}$$

$$\leq C \left(1 + \|v_{n}\|_{H}^{2}\right) + \left(\frac{\epsilon}{4} + 14\epsilon\right) \|v_{n}\|_{H^{1}}^{2}$$

$$+ \left(\frac{1}{4\epsilon} + \epsilon\right) \|v_{n}\|_{L^{4}}^{4}.$$
(97)

Rearranging the above inequality, we deduce that

$$\begin{split} &\frac{1}{2}\frac{\partial}{\partial t}\left\|\boldsymbol{v}_{n}\right\|_{H}^{2}+\left(1-\frac{\epsilon}{4}-14\varepsilon\right)\left\|\boldsymbol{v}_{n}\right\|_{H^{1}}^{2}\\ &+\left(\vartheta-\frac{1}{4\epsilon}-\varepsilon\right)\left\|\boldsymbol{v}_{n}\right\|_{L^{4}}^{4}\leq C\left(1+\left\|\boldsymbol{v}_{n}\right\|_{H}^{2}\right). \end{split} \tag{98}$$

Let $\epsilon \in (1/49, 4)$, and ϵ be small enough, such that

$$1 - \frac{\epsilon}{4} - 14\epsilon > 0, \qquad \vartheta - \frac{1}{4\epsilon} - \epsilon > 0. \tag{99}$$

So, we integrate with respect to t on both sides of (98) to obtain

$$\|v_{n}(t)\|_{H}^{2} + C_{\varepsilon} \int_{0}^{t} \|v_{n}(s)\|_{H^{1}}^{2} ds$$

$$\leq \|v_{n}(0)\|_{H}^{2} + Ct + C \int_{0}^{t} \|v_{n}(s)\|_{H}^{2} ds,$$
(100)

where $C_{\epsilon}=2(1-\epsilon/4-14\epsilon)$, by Gronwall's inequality, we arrive at

$$\|v_n(t)\|_H^2 \le (\|v_n(0)\|_H^2 + Ct)e^{Ct} \le C_T.$$
 (101)

By (100) and (101), we have

$$\int_{0}^{t} \|v_{n}(s)\|_{H^{1}}^{2} ds \le C_{T}.$$
 (102)

Multiplying Av_n on both sides of (78), and integrating with respect to $x \in D$, we have

$$\left\langle \frac{\partial v_n}{\partial t}, A v_n \right\rangle + \left\langle A v_n, A v_n \right\rangle + \left\langle f \left(v_n + W_A^n \right), A v_n \right\rangle$$

$$= \left\langle B \left(v_n + W_A^n, v_n + W_A^n \right), A v_n \right\rangle, \tag{103}$$

which is equivalent to

$$\frac{1}{2} \frac{\partial}{\partial t} \| v_n \|_{H^1}^2 + \| v_n \|_{H^2}^2$$

$$= - \left\langle f \left(v_n + W_A^n \right), A v_n \right\rangle$$

$$+ \left\langle B \left(v_n + W_A^n, v_n + W_A^n \right), A v_n \right\rangle.$$
(104)

We first estimate the second term on the right hand side of (104) as follows:

$$\langle B(v_{n} + W_{A}^{n}, v_{n} + W_{A}^{n}), Av_{n} \rangle$$

$$= \langle v_{n}^{1} + W_{A,1}^{n} \partial_{1} (v_{n}^{1} + W_{A,1}^{n}), Av_{n}^{1} \rangle$$

$$+ \langle v_{n}^{2} + W_{A,2}^{n} \partial_{2} (v_{n}^{1} + W_{A,1}^{n}), Av_{n}^{1} \rangle$$

$$+ \langle v_{n}^{1} + W_{A,1}^{n} \partial_{1} (v_{n}^{2} + W_{A,2}^{n}), Av_{n}^{2} \rangle$$

$$+ \langle v_{n}^{2} + W_{A,2}^{n} \partial_{2} (v_{n}^{2} + W_{A,2}^{n}), Av_{n}^{2} \rangle$$

$$= J_{1} + J_{2} + J_{3} + J_{4}.$$
(105)

For J_1 , we have

$$J_{1} = \left\langle v_{n}^{1} \partial_{1} v_{n}^{1}, A v_{n}^{1} \right\rangle + \left\langle v_{n}^{1} \partial_{1} W_{A,1}^{n}, A v_{n}^{1} \right\rangle$$
$$+ \left\langle W_{A,1}^{n} \partial_{1} v_{n}^{1}, A v_{n}^{1} \right\rangle + \left\langle W_{A,1}^{n} \partial_{1} W_{A,1}^{n}, A v_{n}^{1} \right\rangle \qquad (106)$$
$$= k_{1} + k_{2} + k_{3} + k_{4}.$$

For k_1 , we have

$$k_1 \le \varepsilon |v_n^1|_{H^2}^2 + C |v_n^1|_{I^4}^2 \cdot |v_n^1|_{W^{1,4}}^2.$$
 (107)

By interpolation inequality, there exists some C > 0, such that

$$\begin{aligned} \left| v_n^1 \right|_{L^4} &\le C \left| v_n^1 \right|_H^{1/2} \left| v_n^1 \right|_{H^1}^{1/2}, \\ \left| v_n^1 \right|_{W^{1,4}} &\le C \left| v_n^1 \right|_H^{1/4} \left| v_n^1 \right|_{H^2}^{3/4}. \end{aligned} \tag{108}$$

Then,

$$k_{1} \leq \varepsilon \left| v_{n}^{1} \right|_{H^{2}}^{2} + C \left| v_{n}^{1} \right|_{H}^{3/2} \cdot \left| v_{n}^{1} \right|_{H^{1}} \cdot \left| v_{n}^{1} \right|_{H^{2}}^{3/2}$$

$$\leq \varepsilon \left| v_{n}^{1} \right|_{H^{2}}^{2} + \varepsilon \left| v_{n}^{1} \right|_{H^{2}}^{2} + C \left| v_{n}^{1} \right|_{H}^{6} \left| v_{n}^{1} \right|_{H^{1}}^{4}$$

$$\leq 2\varepsilon \left| v_{n}^{1} \right|_{H^{2}}^{2} + C_{T} \left| v_{n}^{1} \right|_{H^{1}}^{4},$$

$$(109)$$

where the last inequality follows from (101). For k_2 , we deduce that

$$k_{2} \leq \varepsilon |v_{n}^{1}|_{H^{2}}^{2} + C \int_{D} (v_{n}^{1})^{2} (\partial_{1} W_{A,1}^{n})^{2} dx$$

$$\leq \varepsilon |v_{n}^{1}|_{H^{2}}^{2} + C |v_{n}^{1}|_{H}^{2}$$

$$\leq \varepsilon |v_{n}^{1}|_{L^{2}}^{2} + C_{T}.$$
(110)

For k_3 , we arrive at

$$k_3 \le C \int_D \left| \partial_1 v_n^1 \cdot A v_n^1 \right| dx \le \varepsilon \left| v_n^1 \right|_{H^2}^2 + C \left| v_n^1 \right|_{H^1}^2.$$
 (111)

For k_4 , we obtain

$$k_4 \le C + \varepsilon |v_n^1|_{H^2}^2.$$
 (112)

By (106) and (109)-(112),

$$J_1 \le 5\varepsilon \left| v_n^1 \right|_{L^2}^2 + C_T \left| v_n^1 \right|_{L^1}^4 + C \left| v_n^1 \right|_{L^1}^2 + C_T. \tag{113}$$

Similarly, for J_4 , we infer that

$$J_4 \le 5\varepsilon \left| v_n^2 \right|_{H^2}^2 + C_T \left| v_n^2 \right|_{H^1}^4 + C \left| v_n^2 \right|_{H^1}^2 + C_T. \tag{114}$$

For J_2 , we have

$$J_{2} = \left\langle v_{n}^{2} \partial_{2} v_{n}^{1}, A v_{n}^{1} \right\rangle + \left\langle W_{A,2}^{n} \partial_{2} v_{n}^{1}, A v_{n}^{1} \right\rangle$$

$$+ \left\langle v_{n}^{2} \partial_{2} W_{A,1}^{n}, A v_{n}^{1} \right\rangle + \left\langle W_{A,2}^{n} \partial_{2} W_{A,1}^{n}, A v_{n}^{1} \right\rangle$$

$$= l_{1} + l_{2} + l_{3} + l_{4}.$$

$$(115)$$

By interpolation inequality and (101), we deduce that

$$\begin{split} &l_{1} \leq \varepsilon \left| v_{n}^{1} \right|_{H^{2}}^{2} + C \left| v_{n}^{2} \right|_{L^{4}}^{2} \cdot \left| v_{n}^{1} \right|_{W^{1,4}}^{2} \\ &\leq \varepsilon \left| v_{n}^{1} \right|_{H^{2}}^{2} + C \left| v_{n}^{2} \right|_{H} \cdot \left| v_{n}^{2} \right|_{H^{1}} \cdot \left| v_{n}^{1} \right|_{H}^{1/2} \cdot \left| v_{n}^{1} \right|_{H^{2}}^{3/2} \\ &\leq 2\varepsilon \left| v_{n}^{1} \right|_{L^{2}}^{2} + C_{T} \left| v_{n}^{2} \right|_{H^{1}}^{4}. \end{split} \tag{116}$$

For l_2 , we have

$$l_{2} \leq C \int_{D} \left| \partial_{2} v_{n}^{1} \right| \cdot \left| A v_{n}^{1} \right| dx \leq \varepsilon \left| v_{n}^{1} \right|_{H^{2}}^{2} + C \left| v_{n}^{1} \right|_{H^{1}}^{2}. \tag{117}$$

Similarly, for l_3 ,

$$l_3 \le C \int_D |v_n^2| \cdot |Av_n^1| dx \le \varepsilon |v_n^1|_{H^2}^2 + C_T.$$
 (118)

As for l_4 , we get

$$l_4 \le \varepsilon |v_n^1|_{H^2}^2 + C_T.$$
 (119)

By (115)-(119), we arrive at

$$J_{2} \leq 5\varepsilon \left\| v_{n}^{1} \right\|_{H^{2}}^{2} + C_{T} \left\| v_{n}^{2} \right\|_{H^{1}}^{4} + C \left\| v_{n}^{1} \right\|_{H^{1}}^{2} + C_{T}.$$
 (120)

Analogously to J_2 , we have

$$J_{3} \leq 5\varepsilon \left\| v_{n}^{2} \right\|_{H^{2}}^{2} + C_{T} \left\| v_{n}^{1} \right\|_{H^{1}}^{4} + C \left\| v_{n}^{2} \right\|_{H^{1}}^{2} + C_{T}.$$
 (121)

By (105) and the estimates of $J_1 - J_4$, see (113), (114), (120), and (121), we get that

$$\langle B(\nu_{n} + W_{A}^{n}, \nu_{n} + W_{A}^{n}), A\nu_{n} \rangle$$

$$\leq 10\varepsilon \|\nu_{n}\|_{H^{2}}^{2} + C_{T} \|\nu_{n}\|_{H^{1}}^{4}$$

$$+ C \|\nu_{n}\|_{H^{1}}^{2} + C_{T}.$$
(122)

For the first term on the right hand side of (104), we have

$$\begin{aligned} \left| \left\langle f \left(v_{n} + W_{A}^{n} \right), A v_{n} \right\rangle \right| \\ &\leq \varepsilon \left\| v_{n} \right\|_{H^{2}}^{2} + C \left\| v_{n} + W_{A}^{n} \right\|_{L^{6}}^{6} \\ &\leq \varepsilon \left\| v_{n} \right\|_{H^{2}}^{2} + C \left\| v_{n} \right\|_{L^{6}}^{6} + C_{T} \\ &\leq \varepsilon \left\| v_{n} \right\|_{H^{2}}^{2} + C_{T} \left\| v_{n} \right\|_{H^{1}}^{2} \left\| v_{n} \right\|_{H}^{4} + C_{T} \\ &\leq \varepsilon \left\| v_{n} \right\|_{H^{2}}^{2} + C_{T} \left(1 + \left\| v_{n} \right\|_{H^{1}}^{2} \right). \end{aligned} \tag{123}$$

By (104), (122), and (123),

$$\frac{1}{2} \frac{\partial}{\partial t} \| v_n \|_{H^1}^2 + \| v_n \|_{H^2}^2
\leq 11 \varepsilon \| v_n \|_{H^2}^2 + C_T \left(1 + \| v_n \|_{H^1}^2 \right) \| v_n \|_{H^1}^2 + C_T.$$
(124)

By the Gronwall inequality, we get

$$\|v_{n}(t)\|_{H^{1}}^{2}$$

$$\leq (\|v_{n}(0)\|_{H^{1}}^{2} + C_{T})e^{C_{T}\int_{0}^{t}(1+\|v_{n}(s)\|_{H^{1}}^{2}ds)}$$

$$\leq (\|v_{n}(0)\|_{H^{1}}^{2} + C_{T})e^{C_{T}}.$$
(125)

Let $n \to \infty$, by Fatou Lemma,

$$\|v(t)\|_{H^{1}}^{2} \le (\|v(0)\|_{H^{1}}^{2} + C_{T})e^{C_{T}}.$$
 (126)

5. Invariant Measures

5.1. Existence. In this section, we will establish the existence of invariant measure for (2). Analogously to [24], we extend the Wiener process W(t) to \mathbb{R} by setting

$$W(t) := W^{1}(t), \quad t \le 0,$$
 (127)

where $W^1(t)$ is another H-valued Wiener process satisfying conditions in Lemma 2 and being independent of W(t). For any $\tau \ge 0$, we consider the following equation:

$$du_{\tau} + [Au_{\tau} + B(u_{\tau}, u_{\tau}) + f(u_{\tau})] dt = dW,$$
on $[0, T] \times D$, $u_{\tau}(-\tau) = 0$. (128)

By Theorem 7, we know that there exists unique solution. In order to obtain the invariant measure, we should show that the family of laws $\{\mathscr{L}(u_{\tau}(0))\}_{\tau\geq 0}$ is tight. Since $H^{1+\delta}\subset H^1$

is compact, for any $\delta > 0$, we only need to show that $\{\mathscr{L}(u_{\tau}(0))\}_{\tau>0}$ is bounded in probability in $H^{1+\delta}$. As we know,

$$W_{A}(t) = \int_{-\infty}^{t} e^{-(t-s)A} dW(s), \quad t \in \mathbb{R}$$
 (129)

is the mild solution of (8) with the following initial condition:

$$W_A(0) = \int_{-\infty}^0 e^{sA} dW(s).$$
 (130)

Making the classical change of variable $v_{\tau}(t) = u_{\tau}(t) - W_A(t)$, (128) is equivalent to

$$\frac{dv_{\tau}(t)}{dt} = Av_{\tau}(t) + B\left(v_{\tau}(t) + W_{A}(t), v_{\tau}(t) + W_{A}(t)\right) + f\left(v_{\tau}(t) + W_{A}(t)\right),$$
(131)

with initial condition

$$v_{\tau}(-\tau) = -W_A(-\tau). \tag{132}$$

In order to get the invariant measure of (131), it is enough to show that $\nu_{\tau}(0)$ is bounded in probability in $H^{1+\delta}$, for some $\delta>0$. That is what we have to do in Theorem 8 below.

Theorem 8. With conditions in Lemma 2, when $\theta > 1/4$, there exists an invariant measure for (2).

Proof. Multiplying (131) by v_{τ} and integrating on D, we get

$$\frac{1}{2} \frac{d}{dt} \| v_{\tau}(t) \|_{H}^{2} + \| v_{\tau}(t) \|_{H^{1}}^{2}
+ \langle f(v_{\tau}(t) + W_{A}(t)), v_{\tau}(t) \rangle
= \langle B(v_{\tau}(t) + W_{A}(t), v_{\tau}(t) + W_{A}(t)), v_{\tau}(t) \rangle.$$
(133)

For the third term on the left hand side of (133), we deduce that

$$\begin{split} & \left\langle f\left(\nu_{\tau}\left(t\right) + W_{A}\left(t\right)\right), \nu_{\tau}\left(t\right)\right\rangle \\ & = \vartheta\left\langle \left|\nu_{\tau}\left(t\right) + W_{A}\left(t\right)\right|^{2}\left(\nu_{\tau}\left(t\right) + W_{A}\left(t\right)\right), \nu_{\tau}\left(t\right) + W_{A}\left(t\right)\right\rangle \\ & - \vartheta\left\langle \left|\nu_{\tau}\left(t\right) + W_{A}\left(t\right)\right|^{2}\left(\nu_{\tau}\left(t\right) + W_{A}\left(t\right)\right), W_{A}\left(t\right)\right\rangle \\ & = \vartheta\left\|\nu_{\tau}\left(t\right) + W_{A}\left(t\right)\right\|_{L^{4}}^{4} \\ & - \vartheta\left\langle \left\|\nu_{\tau}\left(t\right) + W_{A}\left(t\right)\right\|_{L^{4}}^{2}\left(\nu_{\tau}\left(t\right) + W_{A}\left(t\right)\right), W_{A}\left(t\right)\right\rangle \\ & \ge \vartheta\left[\left\|\nu_{\tau}\left(t\right)\right\|_{L^{4}} - \left\|W_{A}\left(t\right)\right\|_{L^{4}}^{4} \\ & - \vartheta\left\langle \left\|\nu_{\tau}\left(t\right) + W_{A}\left(t\right)\right\|_{L^{4}}^{2}\left(\nu_{\tau}\left(t\right) + W_{A}\left(t\right)\right), W_{A}\left(t\right)\right\rangle \\ & \ge \vartheta\left\|\nu_{\tau}\left(t\right)\right\|_{L^{4}}^{4} - 4\vartheta\left\|\nu_{\tau}\left(t\right)\right\|_{L^{4}}^{3}\left\|W_{A}\left(t\right)\right\|_{L^{4}} \\ & - 4\vartheta\left\|\nu_{\tau}\left(t\right)\right\|_{L^{4}}^{1}\left\|W_{A}\left(t\right)\right\|_{L^{4}}^{3} \\ & - \vartheta\left\langle \left\|\nu_{\tau}\left(t\right) + W_{A}\left(t\right)\right\|_{L^{4}}^{2} \\ & - \vartheta\left\langle \left\|\nu_{\tau}\left(t\right) + W_{A}\left(t\right)\right\|_{L^{4}}^{2} \right\} \right\rangle . \end{split}$$

$$(134)$$

Substituting (134) into (133), we have

$$\begin{split} &\frac{1}{2} \frac{d}{dt} \left\| v_{\tau}\left(t\right) \right\|_{H}^{2} + \left\| v_{\tau}\left(t\right) \right\|_{H^{1}}^{2} + \vartheta \left\| v_{\tau}\left(t\right) \right\|_{L^{4}}^{4} \\ &\leq 4\vartheta \left\| v_{\tau}\left(t\right) \right\|_{L^{4}}^{3} \left\| W_{A}\left(t\right) \right\|_{L^{4}} \\ &+ 4\vartheta \left\| v_{\tau}\left(t\right) \right\|_{L^{4}} \left\| W_{A}\left(t\right) \right\|_{L^{4}}^{3} \\ &+ \vartheta \left\langle \left\| v_{\tau}\left(t\right) + W_{A}\left(t\right) \right\|_{L^{2}}^{2} \left(v_{\tau}\left(t\right) + W_{A}\left(t\right) \right), W_{A}\left(t\right) \right\rangle \\ &+ \left\langle B\left(v_{\tau}\left(t\right) + W_{A}\left(t\right), v_{\tau}\left(t\right) + W_{A}\left(t\right) \right), v_{\tau}\left(t\right) \right\rangle. \end{split} \tag{135}$$

For the third term on the right hand side of (135), we get by the Young inequality that

$$\vartheta \left\langle \left\| v_{\tau}(t) + W_{A}(t) \right\|^{2} \left(v_{\tau}(t) + W_{A}(t) \right), W_{A}(t) \right\rangle \\
\leq \varepsilon \left\| v_{\tau}(t) \right\|_{I^{4}}^{4} + C \left\| W_{A}(t) \right\|_{I^{4}}^{4}.$$
(136)

For the last term on the right hand side of (135),

$$\langle B\left(v_{\tau}\left(t\right) + W_{A}\left(t\right), v_{\tau}\left(t\right) + W_{A}\left(t\right)\right), v_{\tau}\left(t\right)\rangle$$

$$= \langle \left(v_{\tau}\left(t\right) \cdot \nabla\right) v_{\tau}\left(t\right), v_{\tau}\left(t\right)\rangle$$

$$+ \langle \left(W_{A}\left(t\right) \cdot \nabla\right) v_{\tau}\left(t\right), v_{\tau}\left(t\right)\rangle$$

$$+ \langle \left(v_{\tau}\left(t\right) \cdot \nabla\right) W_{A}\left(t\right), v_{\tau}\left(t\right)\rangle$$

$$+ \langle \left(W_{A}\left(t\right) \cdot \nabla\right) W_{A}\left(t\right), v_{\tau}\left(t\right)\rangle$$

$$= r_{1} + r_{2} + r_{3} + r_{4}.$$
(137)

Since $v_{\tau}(t)$ is vector field, we denote it by $v_{\tau}(t) = (v_{\tau}^{1}(t), v_{\tau}^{2}(t))$, where $v_{\tau}^{i}(t)$ is real valued function, i = 1, 2. For r_{1} , we have

$$r_{1} = \left\langle v_{\tau}^{1}(t) \partial_{1} v_{\tau}^{1}(t) + v_{\tau}^{2}(t) \partial_{2} v_{\tau}^{1}(t), v_{\tau}^{1}(t) \right\rangle$$

$$+ \left\langle v_{\tau}^{1}(t) \partial_{1} v_{\tau}^{2}(t) + v_{\tau}^{2}(t) \partial_{2} v_{\tau}^{2}(t), v_{\tau}^{2}(t) \right\rangle$$

$$= \left\langle v_{\tau}^{2}(t) \partial_{2} v_{\tau}^{1}(t), v_{\tau}^{1}(t) \right\rangle$$

$$+ \left\langle v_{\tau}^{1}(t) \partial_{1} v_{\tau}^{2}(t), v_{\tau}^{2}(t) \right\rangle$$

$$\leq -\frac{1}{2} \left\langle \partial_{2} v_{\tau}^{2}(t), \left(v_{\tau}^{1}(t) \right)^{2} \right\rangle$$

$$-\frac{1}{2} \left\langle \partial_{1} v_{\tau}^{1}(t), \left(v_{\tau}^{2}(t) \right)^{2} \right\rangle$$

$$\leq \frac{1}{4} \left| \partial_{1} v_{\tau}^{1}(t) \right|_{H}^{2} + \frac{1}{4} \left| v_{\tau}^{2}(t) \right|_{L^{4}}^{4}$$

$$+ \frac{1}{4} \left| \partial_{2} v_{\tau}^{2}(t) \right|_{H}^{2} + \frac{1}{4} \left| v_{\tau}^{1}(t) \right|_{L^{4}}^{4}$$

$$\leq \frac{1}{4} \left\| v_{\tau}(t) \right\|_{H^{1}}^{2} + \frac{1}{4} \left\| v_{\tau}(t) \right\|_{L^{4}}^{4}.$$
(138)

Similarly for r_2 ,

$$r_{2} = \left\langle W_{A,1}(t) \, \partial_{1} v_{\tau}^{1}(t) + W_{A,2}(t) \, \partial_{2} v_{\tau}^{1}(t), v_{\tau}^{1}(t) \right\rangle$$

$$+ \left\langle W_{A,1}(t) \, \partial_{1} v_{\tau}^{2}(t) + W_{A,2}(t) \, \partial_{2} v_{\tau}^{2}(t), v_{\tau}^{2}(t) \right\rangle$$

$$= -\left\langle \partial_{1} W_{A,1}(t), \left(v_{\tau}^{1}(t) \right)^{2} \right\rangle$$

$$- \left\langle \partial_{2} W_{A,2}(t), \left(v_{\tau}^{1}(t) \right)^{2} \right\rangle$$

$$- \left\langle \partial_{1} W_{A,1}(t), \left(v_{\tau}^{2}(t) \right)^{2} \right\rangle$$

$$- \left\langle \partial_{2} W_{A,2}(t), \left(v_{\tau}^{2}(t) \right)^{2} \right\rangle$$

$$\leq \varepsilon \| v_{\tau}(t) \|_{L^{4}}^{4} + C \| W_{A}(t) \|_{H^{1}}^{2}.$$

$$(139)$$

Analogously to r_1 , we deduce that

$$r_{3} = \left\langle v_{\tau}^{1}(t) \, \partial_{1} W_{A,1}(t) + v_{\tau}^{2}(t) \, \partial_{2} W_{A,1}(t), v_{\tau}^{1}(t) \right\rangle$$

$$+ \left\langle v_{\tau}^{1}(t) \, \partial_{1} W_{A,2}(t) + v_{\tau}^{2}(t) \, \partial_{2} W_{A,2}(t), v_{\tau}^{2}(t) \right\rangle \qquad (140)$$

$$\leq \varepsilon \|v_{\tau}(t)\|_{L^{4}}^{4} + C \|W_{A}(t)\|_{H^{1}}^{2}.$$

For r_4 , we have

$$\begin{split} r_{4} &= \left\langle W_{A,1}\left(t\right) \partial_{1} W_{A,1}\left(t\right) + W_{A,2}\left(t\right) \partial_{2} W_{A,1}\left(t\right), v_{\tau}^{1}\left(t\right) \right\rangle \\ &+ \left\langle W_{A,1}\left(t\right) \partial_{1} W_{A,2}\left(t\right) + W_{A,2}\left(t\right) \partial_{2} W_{A,2}\left(t\right), v_{\tau}^{2}\left(t\right) \right\rangle \\ &\leq \varepsilon \Big| v_{\tau}^{1}\left(t\right) \Big|_{H}^{2} + C \Big| W_{A,1}\left(t\right) \partial_{1} W_{A,1}\left(t\right) \Big|_{H}^{2} \\ &+ \varepsilon \Big| v_{\tau}^{1}\left(t\right) \Big|_{H}^{2} + C \Big| W_{A,2}\left(t\right) \partial_{2} W_{A,1}\left(t\right) \Big|_{H}^{2} \\ &+ \varepsilon \Big| v_{\tau}^{2}\left(t\right) \Big|_{H}^{2} + C \Big| W_{A,2}\left(t\right) \partial_{1} W_{A,2}\left(t\right) \Big|_{H}^{2} \\ &+ \varepsilon \Big| v_{\tau}^{2}\left(t\right) \Big|_{H}^{2} + C \Big| W_{A,2}\left(t\right) \partial_{2} W_{A,2}\left(t\right) \Big|_{H}^{2} \\ &\leq \varepsilon \Big| v_{\tau}^{1}\left(t\right) \Big|_{H}^{2} + \Big| W_{A,1}\left(t\right) \Big|_{L^{4}}^{2} \cdot \Big| W_{A,1}\left(t\right) \Big|_{W^{1,4}}^{2} \\ &+ C \Big| W_{A,2}\left(t\right) \Big|_{H}^{2} + C \Big| W_{A,1}\left(t\right) \Big|_{W^{1,4}}^{2} \\ &+ \varepsilon \Big| v_{\tau}^{2}\left(t\right) \Big|_{H}^{2} + C \Big| W_{A,1}\left(t\right) \Big|_{L^{4}}^{2} \cdot \Big| W_{A,2}\left(t\right) \Big|_{W^{1,4}}^{2} \\ &\leq \varepsilon \Big\| v_{\tau}\left(t\right) \Big\|_{H}^{2} + C \Big\| W_{A}\left(t\right) \Big\|_{L^{4}}^{2} \cdot \Big\| W_{A}\left(t\right) \Big\|_{W^{1,4}}^{2} . \end{split}$$

Since $\{A^{1/2}W_A(t)\}_{t\in\mathbb{R}}$ is a Gaussian process, we infer that

$$E(|A^{1/2}W_A(t)|^4) \le C[E(|A^{1/2}W_A(t)|^2)]^2.$$
 (142)

Then, with the proof of Lemma 2, we know that $||W_A(t)||^2_{W^{1,4}}$ is continuous with respect to t. By (137)–(141), we have

$$\langle B\left(\nu_{\tau}(t) + W_{A}(t), \nu_{\tau}(t) + W_{A}(t)\right), \nu_{\tau}(t) \rangle
\leq \left(\frac{1}{4} + \varepsilon\right) \|\nu_{\tau}(t)\|_{H^{1}}^{2} + \left(\frac{1}{4} + 2\varepsilon\right) \|\nu_{\tau}(t)\|_{L^{4}}^{4}
+ C\left(\|W_{A}(t)\|_{H^{1}}^{2} + \|W_{A}(t)\|_{L^{4}}^{2} \|W_{A}(t)\|_{W^{1,4}}^{2}\right).$$
(143)

By (135), (136), and (143), we arrive at

$$\begin{split} &\frac{1}{2}\frac{d}{dt}\left\|\nu_{\tau}\left(t\right)\right\|_{H}^{2}+\left\|\nu_{\tau}\left(t\right)\right\|_{H^{1}}^{2}+\vartheta\left\|\nu_{\tau}\left(t\right)\right\|_{L^{4}}^{4}\\ &\leq\left(\frac{1}{4}+3\varepsilon\right)\left\|\nu_{\tau}\left(t\right)\right\|_{L^{4}}^{4}+\left(\frac{1}{4}+\varepsilon\right)\left\|\nu_{\tau}\left(t\right)\right\|_{H^{1}}^{2}\\ &+C\left\|W_{A}\left(t\right)\right\|_{W^{1,4}}^{4}+C. \end{split} \tag{144}$$

It is equivalent to

$$\frac{1}{2} \frac{d}{dt} \| v_{\tau}(t) \|_{H}^{2} + \left(\frac{3}{4} - \varepsilon \right) \| v_{\tau}(t) \|_{H^{1}}^{2}
+ \left(9 - \frac{1}{4} - 3\varepsilon \right) \| v_{\tau}(t) \|_{L^{4}}^{4}
\leq C \left(1 + \| W_{A}(t) \|_{W^{1,4}}^{4} \right).$$
(145)

Since $\vartheta > 1/4$, let ε be small enough, such that

$$\frac{3}{4} - \varepsilon > 0; \qquad \vartheta - \frac{1}{4} - 3\varepsilon > 0. \tag{146}$$

Then, the above estimates can be changed into

$$\frac{d}{dt} \| v_{\tau}(t) \|_{H}^{2} + \alpha_{1} \| v_{\tau}(t) \|_{H^{1}}^{2} + C_{\nu} \| v_{\tau}(t) \|_{L^{4}}^{4}
\leq C \left(1 + \| W_{A}(t) \|_{W^{1,4}}^{4} \right).$$
(147)

By the Gronwall inequality, we get

$$\begin{aligned} \left\| v_{\tau} \left(t \right) \right\|_{H}^{2} & \leq \left\| W_{A} \left(-\tau \right) \right\|_{H}^{2} e^{-\alpha_{1} \left(\tau + t \right)} \\ & + C \int_{-\tau}^{t} \left(1 + \left\| W_{A} \left(s \right) \right\|_{W^{1,4}}^{4} \right) e^{\alpha_{1} \left(s - t \right)} ds \\ & \leq \left\| W_{A} \left(-\tau \right) \right\|_{H}^{2} e^{-\alpha_{1} \left(\tau + t \right)} \\ & + C \int_{-\infty}^{0} \left(1 + \left\| W_{A} \left(s \right) \right\|_{W^{1,4}}^{4} \right) e^{\alpha_{1} \left(s - t \right)} ds. \end{aligned} \tag{148}$$

Similarly to the argument of [26], we will prove that $\|W_A(t)\|_{W^{1,4}}$ has at most polynomial growth, when $t \to -\infty$ a.s. So, we conclude that

$$\sup_{0 \le \tau; t \le T} \left\| \nu_{\tau}(t) \right\|_{H}^{2} < \infty. \quad \text{a.s.}$$
 (149)

Multiplying $e^{\delta t}$ on both sides of (147) and integrating with respect to t, we have

$$\int_{-\tau}^{t} e^{\delta s} \|v_{\tau}(s)\|_{H^{1}}^{2} ds$$

$$\leq e^{-\delta \tau} \|W_{A}(-\tau)\|_{H}^{2} + \alpha_{1} \int_{-\tau}^{t} e^{\delta s} \|v_{\tau}(s)\|_{H}^{2} ds$$

$$+ C \int_{-\tau}^{t} \left(1 + \|W_{A}(t)\|_{W^{1,4}}^{4}\right) e^{\delta s} ds$$

$$\leq e^{-\delta \tau} \|W_{A}(-\tau)\|_{H}^{2}$$

$$+ \alpha_{1} \int_{-\infty}^{0} e^{\delta s} \|v_{\tau}(s)\|_{H}^{2} ds$$

$$+ C \int_{-\infty}^{0} \left(1 + \|W_{A}(t)\|_{W^{1,4}}^{4}\right) e^{\delta s} ds.$$
(150)

As

$$\int_{-\infty}^{0} \left(1 + \left\| W_A(t) \right\|_{W^{1,4}}^4 \right) e^{\delta s} ds < \infty, \tag{151}$$

by (149), we have

$$\sup_{0 \le \tau; t \le T} \int_{-\tau}^{t} e^{\delta s} \| \nu_{\tau}(s) \|_{H^{1}}^{2} ds < \infty. \quad \text{a.s.}$$
 (152)

By Theorem 7, we know that for problem (131) there exists unique mild solution, which has the following:

$$\begin{aligned} v_{\tau}\left(0\right) &= e^{\tau A} W_{A}\left(-\tau\right) \\ &+ \int_{-\tau}^{0} e^{t A} B\left(\left(v_{\tau}\left(t\right) + W_{A}\left(t\right), v_{\tau}\left(t\right) + W_{A}\left(t\right)\right)\right) dt \\ &+ \int_{-\tau}^{0} e^{t A} f\left(v_{\tau}\left(t\right) + W_{A}\left(t\right)\right) dt. \end{aligned} \tag{153}$$

Then, for any $\zeta \in (0, \theta) \cap (0, 1/4)$, where the θ is the parameter in Lemma 2,

$$\begin{split} & \left\| A^{(1+\zeta)/2} v_{\tau} \left(0 \right) \right\|_{H} \\ & \leq \left\| e^{\tau A} A^{(1+\zeta)/2} W_{A} \left(-\lambda \right) \right\|_{H} \\ & + \int_{-\tau}^{0} \left\| A^{(1+\zeta)/2} e^{tA} B(\left(v_{\tau} \left(t \right) + W_{A} \left(t \right), v_{\tau} \left(t \right) + W_{A} \left(t \right) \right) \right\|_{H} dt \\ & + \int_{-\tau}^{0} \left\| A^{(1+\zeta)/2} e^{tA} f\left(v_{\tau} \left(t \right) + W_{A} \left(t \right) \right) \right\|_{H} dt. \end{split} \tag{154}$$

Since

$$B\left(\left(v_{\tau}\left(t\right) + W_{A}\left(t\right), v_{\tau}\left(t\right) + W_{A}\left(t\right)\right)\right)$$

$$= \left(v_{\tau}\left(t\right) \cdot \nabla\right) v_{\tau}\left(t\right) + \left(v_{\tau}\left(t\right) \cdot \nabla\right) W_{A}\left(t\right)$$

$$+ \left(W_{A}\left(t\right) \cdot \nabla\right) v_{\tau}\left(t\right) + \left(W_{A}\left(t\right) \cdot \nabla\right) W_{A}\left(t\right),$$
(155)

then,

$$\begin{split} \left\| A^{(1+\zeta)/2} e^{tA} B\left(\left(v_{\tau}\left(t \right) + W_{A}\left(t \right), v_{\tau}\left(t \right) + W_{A}\left(t \right) \right) \right) \right\|_{H} \\ & \leq \left\| A^{(1+\zeta)/2} e^{tA} \left[v_{\tau}\left(t \right) \cdot \nabla \right] v_{\tau}\left(t \right) \right\|_{H} \\ & + \left\| A^{(1+\zeta)/2} e^{tA} \left[v_{\tau}\left(t \right) \cdot \nabla \right] W_{A}\left(t \right) \right\|_{H} \\ & + \left\| A^{(1+\zeta)/2} e^{tA} \left[W_{A}\left(t \right) \cdot \nabla \right] v_{\tau}\left(t \right) \right\|_{H} \\ & + \left\| A^{(1+\zeta)/2} e^{tA} \left[W_{A}\left(t \right) \cdot \nabla \right] W_{A}\left(t \right) \right\|_{H} \\ & = z_{1} + z_{2} + z_{3} + z_{4}. \end{split} \tag{156}$$

For z_1 , we have

$$\begin{split} z_{1} &\leq \left| A^{(1+\zeta)/2} e^{tA} \left[v_{\tau}^{1}(t) \, \partial_{1} v_{\tau}^{1}(t) \right] \right|_{H} \\ &+ \left| A^{(1+\zeta)/2} e^{tA} \left[v_{\tau}^{2}(t) \, \partial_{2} v_{\tau}^{1}(t) \right] \right|_{H} \\ &+ \left| A^{(1+\zeta)/2} e^{tA} \left[v_{\tau}^{1}(t) \, \partial_{1} v_{\tau}^{2}(t) \right] \right|_{H} \\ &+ \left| A^{(1+\zeta)/2} e^{tA} \left[v_{\tau}^{2}(t) \, \partial_{2} v_{\tau}^{2}(t) \right] \right|_{H} \\ &= z_{1,1} + z_{1,2} + z_{1,3} + z_{1,4}. \end{split} \tag{157}$$

In the following, we use Theorem 6.13 in chapter two of [27] to estimate them respectively as follows:

$$\begin{split} z_{1,1} &= \frac{1}{2} \left| e^{tA} A^{(1+\zeta)/2} \partial_1 \left(v_{\tau}^1 \right)^2 \right|_H \\ &\leq \frac{1}{2} \left| e^{tA} A^{(3+2\zeta)/4} \left(v_{\tau}^1 \right)^2 \right|_{H^{1/2}} \\ &\leq C |t|^{-(3+2\zeta)/4} e^{\delta t} \left| \left(v_{\tau}^1 \right)^2 \right|_{H^{1/2}} \\ &\leq C |t|^{-(3+2\zeta)/4} e^{\delta t} \left| 2 v_{\tau}^1 \left(t \right) A^{1/4} v_{\tau}^1 \left(t \right) + R_4 \right|_H, \end{split} \tag{158}$$

the last inequality follows by Theorem A.8 in [25], where $\delta > 0$, $R_4 = A^{1/4}(v_\tau^1)^2 - 2v_\tau^1A^{1/4}v_\tau^1$, and $|R_4|_H \leq C|A^{1/8}v_\tau^1(t)|_{L^4}^2 \leq C|v_\tau^1(t)|_{H^1}^2$. So, by Hölder inequality and interpolation inequality, we have

$$z_{1,1} \le C|t|^{-(3+2\zeta)/4} e^{\delta t} \|\nu_{\tau}(t)\|_{H^{1}}^{2}.$$
 (159)

For $z_{1,2}$, we have

$$\begin{split} z_{1,2} &= \left| A^{(1+\zeta)/2} e^{tA} \left[v_{\tau}^{2}(t) \, \partial_{2} v_{\tau}^{1}(t) \right] \right|_{H} \\ &\leq \left| A^{(1+\zeta)/2} e^{tA} \left[A^{1/4} \left(v_{\tau}^{2}(t) \, A^{1/4} v_{\tau}^{1}(t) \right) \right] \right|_{H} \\ &+ \left| A^{(1+\zeta)/2} e^{tA} \left[A^{1/4} v_{\tau}^{1}(t) \, A^{1/4} v_{\tau}^{2}(t) \right] \right|_{H} \\ &+ \left| A^{(1+\zeta)/2} e^{tA} R_{5} \right|_{H}, \end{split} \tag{160}$$

where

$$R_{5} = A^{1/4} \left[v_{\tau}^{2}(t) A^{1/4} v_{\tau}^{1}(t) \right]$$

$$- \left[A^{1/4} v_{\tau}^{1}(t), A^{1/4} v_{\tau}^{2}(t) \right]$$

$$- v_{\tau}^{2}(t) A^{1/2} v_{\tau}^{1}(t).$$

$$(161)$$

Analogously to estimating $z_{1,1}$, we have

$$\begin{split} z_{1,2} &\leq C|t|^{-(3+2\zeta)/4} e^{\delta t} \Big| v_{\tau}^{2}\left(t\right) \Big|_{L^{4}} \Big| v_{\tau}^{1}\left(t\right) \Big|_{W^{1/2,4}} \\ &+ C|t|^{-(1+\zeta)/2} e^{\delta t} \Big| v_{\tau}^{1}\left(t\right) \Big|_{W^{1/2,4}} \Big| v_{\tau}^{2}\left(t\right) \Big|_{W^{1/2,4}} \\ &\leq C\left(\big|t\big|^{-(3+2\zeta)/4} + \big|t\big|^{-(1+\zeta)/2} \right) e^{\delta t} \big\| v_{\tau}\left(t\right) \big\|_{W^{1/2,4}}^{2} \\ &\leq C\left(\big|t\big|^{-(3+2\zeta)/4} + \big|t\big|^{-(1+\zeta)/2} \right) e^{\delta t} \big\| v_{\tau}\left(t\right) \big\|_{H^{1}}^{2}. \end{split} \tag{162}$$

Similarly, we can get the same estimates for $z_{1,3}$ and $z_{1,4}$. Therefore,

$$z_1 \le C \left(|t|^{-(3+2\zeta)/4} + |t|^{-(1+\zeta)/2} \right) e^{\delta t} \|v_{\tau}(t)\|_{H^1}^2.$$
 (163)

Analogously to estimating z_1 , we can get for z_2 , z_3 , and z_4 that

$$z_{2} \leq C \left(|t|^{-(3+2\zeta)/4} + |t|^{-(1+\zeta)/2} \right)$$

$$\times e^{\delta t} \left(\|W_{A}(t)\|_{H^{1}}^{2} + \|\nu_{\tau}(t)\|_{H^{1}}^{2} \right),$$

$$z_{3} \leq C \left(|t|^{-(3+2\zeta)/4} + |t|^{-(1+\zeta)/2} \right)$$

$$\times e^{\delta t} \left(\|W_{A}(t)\|_{H^{1}}^{2} + \|\nu_{\tau}(t)\|_{H^{1}}^{2} \right),$$

$$z_{4} \leq C \left(|t|^{-(3+2\zeta)/4} + |t|^{-(1+\zeta)/2} \right)$$

$$\times e^{\delta t} \|W_{A}(t)\|_{H^{1}}^{2}.$$

$$(164)$$

So, by (163)–(164) and (156), we get

$$\|A^{(1+\zeta)/2}e^{tA}B\left(\left(\nu_{\tau}(t) + W_{A}(t), \nu_{\tau}(t) + W_{A}(t)\right)\right)\|_{H}$$

$$\leq C\left(|t|^{-(3+2\zeta)/4} + |t|^{-(1+\zeta)/2}\right)$$

$$\times e^{\delta t}\left(\|W_{A}(t)\|_{H^{1}}^{2} + \|\nu_{\tau}(t)\|_{H^{1}}^{2}\right).$$
(165)

For the third term on the right hand side of (154), we obtain

$$\begin{split} \left\| A^{(1+\zeta)/2} e^{tA} f \left(v_{\tau}(t) + W_{A}(t) \right) \right\|_{H} \\ &\leq C |t|^{-(1+\zeta)/2} e^{\delta t} \left(\left\| v_{\tau}(t) \right\|_{L^{6}}^{3} + \left\| W_{A}(t) \right\|_{L^{6}}^{3} \right) \\ &\leq C |t|^{-(1+\zeta)/2} \\ &\qquad \times e^{\delta t} \left(\left\| v_{\tau}(t) \right\|_{H} \cdot \left\| v_{\tau}(t) \right\|_{H^{1}}^{2} + \left\| W_{A}(t) \right\|_{H^{1}}^{3} \right) \\ &\leq C |t|^{-(1+\zeta)/2} e^{\delta t} \\ &\qquad \times e^{\delta t} \left(\left\| v_{\tau}(t) \right\|_{H^{1}}^{2} + \left\| W_{A}(t) \right\|_{H^{1}}^{2} \right), \end{split}$$

$$(166)$$

since $\|v_{\tau}(t)\|_{H}$ and $e^{\delta t}\|W_{A}(t)\|_{H^{1}}^{2}$ are bounded for $t, \tau \in (-\infty, T]$, the last inequality follows. For the first term on the right hand side of (154), we have

$$\|e^{\tau A}A^{(1+\zeta)/2}W_A(-\tau)\|_H \le e^{-\delta\tau}\|A^{(1+\zeta)/2}W_A(-\tau)\|_H.$$
 (167)

Similar to [26], we can prove that $||A^{(1+\zeta)/2}W_A(-\tau)||_H$ has at most polynomial growth when $\tau \to \infty$. For the reader

convenience, we sketch a proof. By Lemma 2, we know that W(t) - W(s) is a $D(A^{\theta/2})$ valued Brownian motion, for $s \le t \le 0$. So, by the law of iterated logarithm, we have

$$w_n := \sup_{1 \le s \le t \le n+1} \frac{\|W(t) - W(s)\|_{H^{\theta}}}{|t - s|^{1/2 + (\zeta - \theta)/4}} < \infty, \quad \text{a.s. } n \in \mathbb{Z}.$$
 (168)

Obviously, w_n is a i.i.d sequence. By the law of large numbers, there exists an integer-valued random variable $n_0(w) > 0$, when $n \ge n_0(w)$, we have

$$\frac{w_{-n}}{n} \le \frac{w_{-n} + \dots + w_{-1}}{n} \le Ew_0 + 1 < \infty. \tag{169}$$

This implies that

$$w_{-n} \le C_0(w) n, \tag{170}$$

for all n > 0. In other words,

$$\|W(t) - W(s)\|_{H^{\theta}} \le C_0(w) \|[s]\| \cdot |t - s|^{1/2 + (\zeta - \theta)/4},$$
 (171)

when $s \le t \le [s] + 1$. By the law of iterated logarithm, we have

$$||W(t)||_{H^{\theta}} \le C_1(w)|t|, \quad t \in (-\infty, 0],$$
 (172)

for some positive random variable. By Theorem 5.14 in [23], we know that

$$W_{A}(t) = \int_{-\infty}^{t} Ae^{-(t-s)A} (W(t) - W(s)) ds.$$
 (173)

So, we have that

$$\begin{split} & \left\| A^{(1+\zeta)/2} W_{A}(t) \right\|_{H} \\ & \leq \int_{-\infty}^{t} \left\| A^{1+1/2+\zeta/2} e^{-(t-s)A} \left(W(t) - W(s) \right) \right\|_{H} ds \\ & = \int_{-\infty}^{t} \left\| A^{1+1/2+(\zeta-\theta)/2} e^{-(t-s)A} \left[A^{\theta/2} \left(W(t) - W(s) \right) \right] \right\|_{H} ds \\ & \leq \int_{-\infty}^{t} \frac{e^{-\delta(t-s)}}{|t-s|^{1+1/2+(\zeta-\theta)/2}} \left\| W(t) - W(s) \right\|_{H^{\theta}} ds \\ & \leq \int_{[t]-1}^{t} \frac{e^{-\delta(t-s)}}{|t-s|^{1+(\zeta-\theta)/4}} \cdot \frac{\left\| W(t) - W(s) \right\|_{H^{\theta}}}{|t-s|^{1/2+(\zeta-\theta)/4}} \\ & + \int_{-\infty}^{[t]-1} \frac{e^{-\delta(t-s)}}{|t-s|^{1+(\zeta-\theta)/4}} \cdot \frac{C_{1}(w) \left(|t| + |s| \right)}{|t-s|^{1/2+(\zeta-\theta)/4}} \\ & \leq \int_{[t]-1}^{t} \frac{e^{-\delta(t-s)}}{|t-s|^{1+(\zeta-\theta)/4}} \cdot C_{0}(w) \left| [s] \right| ds \\ & + \int_{-\infty}^{[t]-1} e^{-\delta(t-s)} C_{1}(w) \left(|t| + |s| \right) \\ & \leq \left(C_{0}(w) + C_{1}(w) \right) \left(|t| + 1 \right), \end{split}$$

since $s \le [t] - 1$, the fourth inequality follows. By (167) and (174), we know that

$$\sup_{\tau>0} \left\| e^{\tau A} A^{(1+\zeta)/2} W_A(-\tau) \right\|_H < \infty, \quad \text{a.s.}$$
 (175)

If we let $\zeta=1/2<\theta$, repeating the argument of (174), we can see that $\|W_A(t)\|_{W^{1,4}}$ also has at most polynomial growth, when $t\to-\infty$ a.s., since we have the Sobolev embedding $H^{3/2}\subset W^{1,4}$. Consider the second term on the right hand side of (154), by (165),

$$\int_{-\tau}^{0} \|A^{(1+\zeta)/2} e^{tA} B\left(\left(\nu_{\tau}(t) + W_{A}(t), \nu_{\tau}(t) + W_{A}(t)\right)\right)\|_{H} dt
\leq \int_{-\tau}^{0} C\left(|t|^{-(3+2\zeta)/4} + |t|^{-(1+\zeta)/2}\right)
\times e^{\delta t} \left(\|W_{A}(t)\|_{H^{1}}^{2} + \|\nu_{\tau}(t)\|_{H^{1}}^{2}\right) dt
\leq \int_{-1}^{0} C\left(|t|^{-(3+2\zeta)/4} + |t|^{-(1+\zeta)/2}\right)
\times e^{\delta t} \left(\|W_{A}(t)\|_{H^{1}}^{2} + \|\nu_{\tau}(t)\|_{H^{1}}^{2}\right) dt
+ \int_{-\infty}^{-1} Ce^{\delta t} \left(\|W_{A}(t)\|_{H^{1}}^{2} + \|\nu_{\tau}(t)\|_{H^{1}}^{2}\right) dt < \infty, \tag{176}$$

where the last inequality follows by (152). Analogously, we can prove that

$$\int_{-\tau}^{0} \left\| A^{(1+\zeta)/2} e^{tA} f\left(\nu_{\tau}(t) + W_{A}(t)\right) \right\|_{H} dt$$

$$\leq \int_{-\tau}^{0} C\left(\left|t\right|^{-(1+\zeta)/2}\right)$$

$$\times e^{\delta t} \left(\left\|\nu_{\tau}(t)\right\|_{H} \left\|\nu_{\tau}(t)\right\|_{H^{1}}^{2} + \left\|W_{A}(t)\right\|_{H^{1}}^{3}\right)$$

$$< \infty,$$
(177)

where we used (149) and (152) for the last inequality. By (154) and (175)–(177), we get

$$||A^{(1+\zeta)/2}\nu_{\tau}(0)||_{tt} \le \xi(w), \quad \text{a.s.,}$$
 (178)

for some positive random variable $\xi(w)$. As $H^{1+\delta} \subset H^1$ is compact, by Prohorov Theorem, we know that the family of laws for $(v_{\tau}(0))_{\tau \geq 0}$ taking values in H^1 is tight. Since $v_{\tau}(0) = u_{\tau}(0) - W_A(0)$, then so does the law of $(u_{\tau}(0))_{\tau \geq 0}$ taking values in the same space. For $t \geq 0$, set

$$(P, f)(x) = Ef(u(t, .; 0, x)),$$
 (179)

where $f \in C_b(H_0^1)$. Following the arguments in [24], for all $t_0 < s < t$ and all $u_t \in H_0^1$, by proving

$$E\left(f\left(u\left(t;t_{0},u_{t_{0}}\right)\right)\mid\mathcal{F}_{s}\right)=P_{t-s}\left(u\left(s;t_{0},u_{t_{0}}\right)\right),\quad(180)$$

we can show that u is a Markov process. Here, \mathscr{F}_s is the σ -algebra generated by W(r) for $r \leq s$. So, $(P_t)_{t\geq 0}$ is the Markov semigroup. Define a dual semigroup P_t^* in the space $P(H_0^1)$ of probability measures on H_0^1 as follows:

$$\int_{H_{\epsilon}^{1}} fd\left(P_{t}^{*}\mu\right) = \int_{H_{\epsilon}^{1}} P_{t} fd\mu. \tag{181}$$

Let μ_{τ} be the law of $u_{\tau}(0)$, which is the solution of (2) with initial condition $u(-\tau) = 0$. Then, we have

$$\mu_{\tau}(f) = Ef(u_{-\tau}(0)) = Ef(u(\tau, \cdot; 0, 0))$$

$$= (P_{\tau}f)(0) = \int_{H_0^1} P_{\tau}fd\delta_0$$

$$= \int_{H_0^1} fd(P_{\tau}^*\delta_0),$$
(182)

where we use the fact that $u(\tau, \cdot; 0, 0)$ and $u_{\tau}(0)$ have the same law, the second equality follows. Therefore,

$$P_{\tau_1}^* \mu_{\tau} = \mu_{\tau + \tau_1}. \tag{183}$$

Since $(\mu_{\tau})_{\tau\geq 0}$ is tight, then by Prokhorov theorem, we know that $(\mu_{\tau})_{\tau\geq 0}$ is relatively compact. We can choose a subsequence of $(\mu_{\tau})_{\tau\geq 0}$ denoted by $(\mu_{\tau_n})_{n\in\mathbb{N}}$ such that for $\mu\in P(H^{\sigma})$,

$$\int_{H_0^1} (P_t f)(x) \mu(dx)
= \lim_{n \to \infty} \int_{H_0^1} (P_t f)(x) \mu_{\tau_n}(dx)
= \lim_{n \to \infty} \int_{H_0^1} f(x) P_t^* \mu_{\tau_n}(dx)
= \lim_{n \to \infty} \int_{H_0^1} f(x) \mu_{\tau_{n+t}}(dx)
= \int_{H_0^1} f(x) \mu(dx).$$
(184)

5.2. *Uniqueness*. The main result of this part is as follows.

Theorem 9. Assume $\theta > 1/2$ in Lemma 2 and $\theta > 1/4$; then,

- (i) the stochastic Burgers equation (2) has a unique invariant measure u;
- (ii) for all $u_0 \in H_0^1 \varphi$, $H_0^1 \to \mathbb{R}$, such that $\int_{H_0^1} |\varphi| d\mu < \infty$,

$$\lim_{T \to \infty} \frac{1}{T} \int_0^T \varphi(u(t; u_0)) dt = \int_{H_0^1} \varphi d\mu \quad a.s.;$$
 (185)

(iii) for every Borel measure μ^* on H_0^1 , one has that

$$\|P_t^*\mu^* - \mu\|_{TV} \longrightarrow 0 \quad as \ t \longrightarrow \infty,$$
 (186)

where $\|\cdot\|_{TV}$ stands for the total variation of a measure. In particularly, one has that

$$P_t^* \mu^* (B) \longrightarrow \mu (B), \quad as \ t \longrightarrow \infty,$$
 (187)

for every Borel set $B \in \mathcal{B}(H_0^1)$ (the Borel σ -algebra of H_0^1).

In order to prove Theorem 9, we only need Theorem 10 below, see [28, Theorem 4.2.1]. We define $P(t, x, \cdot), t > 0, x \in H_0^1$, to be the transition probability measure that is,

$$P(t, x, B) = P_t^* \delta_x(B) = P(u(t; x) \in B)$$
 (188)

for $B \in \mathcal{B}(H_0^1)$.

Theorem 10. Assume that the probability measures $P(t, x, \cdot), t > 0, x \in H_0^1$, are all equivalent, in the sense that they are mutually absolutely continuous. Then, Theorem 9 holds true.

In the following, we will prove the irreducibility and the strong Feller property in H_0^1 to get the equivalence of the measure $P(t, x, \cdot)$. For the two notations, we outline them below. For $y \in H_0^1, \varepsilon > 0$, let

$$B(y,\varepsilon) = \left\{ x \in H_0^1; \|x - y\|_{H^1} < \varepsilon \right\}. \tag{189}$$

(I) For any $x, y \in H_0^1$, such that for all $\varepsilon > 0$,

$$P(t, x, B(y, \varepsilon)) > 0 \tag{190}$$

for each t > 0.

(S) For all $O \in \mathcal{B}(H_0^1)$, every t > 0, and all $x_n, x \in H_0^1$ such that $x_n \to x$ in H_0^1 , it holds that

$$P(t, x_n, O) \longrightarrow P(t, x, O)$$
. (191)

Before checking the condition (I), we need Lemma 11 below. For $x \in H_0^1$ and $\phi : [0, T] \to H_0^1$, set

$$u(t, x, \phi) = v(t, x, \phi) + \phi(t), \qquad (192)$$

where $v(t, x, \phi)$ is solution of the following equation:

$$\frac{dv}{dt} + Av + B\left(v + \phi, v + \phi\right) + f\left(v + \phi\right) = 0,\tag{193}$$

for $t \in [0, T]$, with initial condition v(0) = x. As it is proved in previously this equation has a unique solution as follows:

$$v \in C([0,T]; H_0^1),$$
 (194)

when $x \in H_0^1$ and $\phi \in C([0, T]; H_0^1)$.

Lemma 11. Define $\Psi(\phi) = u(\cdot, x, \phi)$; then,

(i) the mapping

$$\Psi: C_0([0,T]; H^{3/2}) \longrightarrow C([0,T]; H_0^1)$$
 (195)

is continuous, where $C_0([0,T];B) := \{h \in C([0,T];B); h(0) = 0\}$ for Banach space B;

(ii) for every $x, y \in H^{3/2}$ and T > 0 there exists $\overline{z} \in C_0([0,T]; H^{3/2})$ such that $u(T, x, \overline{z}) = y$.

Proof. (i) is proved by (A.30) in the Appendix. To prove (ii), let $x, y, \in H^{3/2}$ and T > 0, define \overline{u} as

$$\overline{u}(t) = e^{-tA}x, \quad t \in [0, t_0],$$

$$\overline{u}(t) = e^{-(T-t)A}y, \quad t \in [t_1, T],$$

$$\overline{u}(t) = \overline{u}(t_0) + \frac{t - t_0}{t_1 - t_0} (\overline{u}(t_1) - \overline{u}(t_0)),$$

$$t \in (t_0, t_1).$$
(196)

Obviously, $\overline{u}(t) \in C([0,T]; H^{3/2})$. Define \overline{v} as the solution of the following equation:

$$\frac{d}{dt}\overline{v} + A\overline{v} + B(\overline{u}, \overline{u}) + f(\overline{u}) = 0, \tag{197}$$

with initial condition $\overline{v}(0) = x$; then $\overline{v} \in C([0,T]; H^{3/2})$. Set $\overline{z} = \overline{u} - \overline{v}$; then it satisfies all the requirements of the lemma.

Proposition 12. With conditions in Theorem 9, the irreducibility property (I) is satisfied.

Proof. Let $x \in H^{3/2}$ and \overline{z} be the same as (ii) in Lemma 11. By the above lemma, we have that for $\varepsilon > 0$, we can find $\delta > 0$, such that

$$||z - \overline{z}||_{C_{\alpha}([0,T] \cdot H^{3/2})} < \delta$$
 (198)

implies that

$$\|u\left(\cdot,x,z\right) - u\left(\cdot,x,\overline{z}\right)\|_{C([0,T]:H^{1})} < \varepsilon. \tag{199}$$

If $\theta > 1/2$ in Lemma 2, and denote z and \overline{z} the corresponding Ornstein-Uhlenbeck process satisfying conditions in the lemma, then $z, \overline{z} \in C([0,T]; H^{3/2})$. Choose $\delta_1 > 0$ such that $\delta_1 < \delta$ and

$$z \in U_{\delta_1} =: \left\{ z \in C_0 \left([0, T]; H^{3/2} \right); \|z - \overline{z}\|_{C([0, T]; H^{3/2})} < \delta_1 \right\}. \tag{200}$$

Then, for $z \in U_{\delta_1}$, we have that

$$||u(T, x, z) - y||_{H^1} < \varepsilon.$$
 (201)

Recall now that the solution u of the stochastic Burgers equation is equal to $\Psi(z)$, z being the Ornstein-Uhlenbeck process. Then, it remains to show that

$$P\left\{z\left(\cdot,w\right)\in U_{\delta_{1}}\right\}>0. \tag{202}$$

But this is obviously true. So far, we have proved that for for all t > 0, for all $x, y \in H^{3/2}$, for all $\varepsilon > 0$,

$$P(t, x, B(y, \varepsilon)) > 0. \tag{203}$$

Next, we will prove for all $x_0 \in H_0^1$, $y_0 \in H^{3/2}$, the above inequality also holds. Indeed, for 0 < h < t, by Chapman-Kolmogorov equation, we have

$$P(t, x_{0}, B(y_{0}, \varepsilon))$$

$$= \int_{H_{0}^{1}} P(t - h, x_{0}, dy) P(h, y, B(y_{0}, \varepsilon))$$

$$= \int_{H^{3/2}} P(t - h, x_{0}, dy) P(h, y, B(y_{0}, \varepsilon)) > 0.$$
(204)

Since $P(t-h,x_0,H^{3/2})=1$, we will extend (204) to the case for all $x_0\in H_0^1$, $y_0\in H_0^1$. If this is not true, there exists $t_0>0$, x_0 , $y_0\in H_0^1$, $\varepsilon>0$ such that

$$P(t_0, x_0, B(y_0, \varepsilon)) = 0.$$
 (205)

Then, we can choose $y_1 \in H^{3/2}$, $\varepsilon_1 > 0$ such that $B(y_1, \varepsilon_1) \subset B(y_0, \varepsilon)$. By (204), we have

$$P(t_0, x_0, B(y_1, \varepsilon_1)) > 0,$$
 (206)

which is contrary to (205).

In this part, it is time to check the condition (S).

We will first obtain the strong Feller property in H_0^1 for modified Burgers equation (208) below, then let $R \to \infty$ to check the condition (S).

Fix R > 0, let $K_R : [0, \infty[\to [0, \infty[\text{ satisfy } K_R \in C^1(\mathbb{R}_+) \text{ such that } |K_R| \le 1, |K_R'| \le 2 \text{ and}$

$$K_R = 1$$
, if $x < R$,
$$K_R = 0$$
, if $x \ge R + 1$. (207)

Consider the following equation:

$$du_{R}(t) + Au_{R}(t) dt + K_{R}(\|u_{R}(t)\|_{H^{1}}^{2}) B(u_{R}(t), u_{R}(t)) dt + K_{R}(\|u_{R}(t)\|_{H^{1}}^{2}) f(u_{R})(t) = dW(t).$$
(208)

Proposition 13. There exists a unique mild solution $u_R(\cdot, w) \in C([0, T]; H_0^1)$ for (208) which is Markov process with the Feller property in H_0^1 , that is for every R > 0, t > 0, there exists a constant L = L(t, R) > 0 such that

$$\left| P_t^{(R)} \phi(x) - P_t^{(R)} \phi(y) \right| \le L \|x - y\|_{H^1}$$
 (209)

holds for all $x, y \in H_0^1$, and all $\phi \in C_b(H_0^1) \leq 1$, where $P_t^{(R)}\phi(x) := \int_{H_0^1} \phi(y) P_R(t,x,dy), P_R(t,x,\cdot)$ is the transition probabilities corresponding to (204).

Proof. The proof of existence and uniqueness is similar to Section 2. Let $\phi_1 = \phi_2$ in (A.28), by the Gronwall inequality, we know that u_R is Lipschitz continuous with respect to initial value. Using the method in Proposition 4.3.3 in [24], we can prove that the solution is a Markov process. To prove the Fell property, we first consider the following Galerkin

approximations of (208). Let P_n be the orthogonal projection in H defined as $P_n x = \sum_{j=1}^n \langle x, e_j \rangle e_j, x \in H$. Clearly, $H_n := P_n H$ for every n. Consider the equation in H_n as follows:

$$du_{n}^{(R)}(t) + Au_{n}^{(R)}(t) dt + K_{R} \left(\left\| u_{n}^{(R)}(t) \right\|_{H^{1}}^{2} \right) P_{n} B\left(u_{n}^{(R)}(t), u_{n}^{(R)}(t) \right) + K_{R} \left(\left\| u_{n}^{(R)}(t) \right\|_{H^{1}}^{2} \right) f\left(u_{n}^{(R)}(t) \right) = dW(t),$$
(210)

with initial condition $u_n^{(R)}(0) = P_n u_0$. This is a finite-dimensional equation with globally Lipschitz nonlinear functions, so it has a unique progressively measurable solution with P-a.e. trajectory $u_n^{(R)}(\cdot,w) \in C([0,T];H_n)$, which is also a Markov process in H_n with associated semigroup $P_{n,t}^{(R)}$ defined as

$$P_{n,t}^{(R)}\phi(x) = E\phi\left(u_n^{(R)}(t;x)\right),$$
 (211)

for all $x \in H_n$ and $\phi \in C_b(H_n)$. For every R > 0, t > 0, we can prove that there exists a constant L = L(t, R) > 0 such that

$$\left| P_{n,t}^{(R)} \phi(x) - P_{n,t}^{(R)} \phi(y) \right| \le L \|x - y\|_{H^1}$$
 (212)

hold for all $n \in \mathbb{N}$, $x, y \in H_n$, and all $\phi \in C_b(H_n)$ with $\|\phi\|_{H^1} \le 1$. Indeed, the following remarkable formula holds true for the differential in x of $P_{n,t}^{(R)}\phi$ [29]:

$$D_{x}P_{n,t}^{(R)}\phi(x) \cdot h$$

$$= \frac{1}{t}E\left(\phi\left(u_{n}^{(R)}(t;x)\right)\int_{0}^{t}\left\langle\left(P_{n}QQ^{*}P_{n}\right)^{-1/2}D_{x}u_{n}^{(R)}(s;x)\right.\right.$$

$$\left.\cdot h,d\beta_{n}(s)\right\rangle\right),$$
(213)

for all $h \in H_n$, where β_n is a n-dimensional standard Wiener process with incremental covariance P_nQ and Q is the covariance operator of W(t). Obviously, Q is nonnegative, adjoint, Hilbert-Schmidt operator with inverse. Since the eigenvalues α_n of the Stokes operator A, in 2-space dimension, behave like n, let $\theta = 1/2 + \varepsilon$ for some $\varepsilon > 0$, in Lemma 2, we have $D(A) \subset \mathcal{R}(Q) \subset D(A^{3/4})$, where $\mathcal{R}(Q)$ is the image of Q. Therefore,

$$\left| D_{x} P_{n,t}^{(R)} \phi(x) \cdot h \right| \\
\leq \frac{1}{t} E \left(\int_{0}^{t} \left\| \left(P_{n} Q Q^{*} P_{n} \right)^{-1/2} D_{x} u_{n}^{(R)}(s; x) \cdot h \right\|_{H}^{2} ds \right)^{1/2}. \tag{214}$$

Since for $y \in H_n$

$$\|(P_{n}QQ^{*}P_{n})^{-1/2}y\|_{H}^{2}$$

$$= \langle (P_{n}QQ^{*}P_{n})^{-1}y, y \rangle$$

$$= \langle (AP_{n}QQ^{*}P_{n}A)^{-1}Ay, Ay \rangle \leq C\|y\|_{H^{2}}^{2},$$
(215)

it follows that

$$\left| D_{x} P_{n,t}^{(R)} \phi(x) \cdot h \right|$$

$$\leq \frac{1}{t} C E \left(\int_{0}^{t} \left\| D_{x} u_{n}^{(R)}(s; x) \cdot h \right\|_{H^{2}}^{2} ds \right)^{1/2}$$

$$\leq \frac{1}{t} C(R) \left\| h \right\|_{H^{1}},$$
(216)

where the last inequality follows by the Estimate 4 of the Appendix (note that C(R) is independent of $x \in H_n$ and $n \in \mathbb{N}$). Indeed, $u_n^{(R)}(t,x)$ is given by $v_n(t,x) + P_n z(t)$, where z is the Ornstein-Uhlenbeck process, and v_n is the solution of (A.2). Therefore,

$$\left| P_{n,t}^{(R)} \phi(x) - P_{n,t}^{(R)} \phi(y) \right| \\
\leq \sup_{\|h\|_{H^{1}} \le 1, k \in H_{n}} \left| D_{x} P_{n,t}^{(R)} \phi(k) \cdot h \right| \cdot \|x - y\|_{H^{1}} \\
\leq \frac{1}{t} C(R) \|x - y\|_{H^{1}}.$$
(217)

In the following step, we will let $n \to \infty$ to get the Fell property for (208). Let $x \in H_0^1$ and $\phi \in C_b(H_0^1)$ be given. From the Appendix, Remark A.1, we know that $u_n^{(R)}(t)$ converges to $u^{(R)}(t)$ strongly in $L^2(0,T;H_0^1)$, p-a.s.. By the boundedness and continuous of ϕ as well as Lebesgue dominated convergence theorem, we have

$$E\int_{0}^{T}\left|\phi\left(u_{n}^{(R)}(,;x)\right)-\phi\left(u^{(R)}(,;x)\right)\right|dt\longrightarrow0,\qquad(218)$$

which implies that for some subsequence n_k

$$E\phi\left(u_{n_{k}}^{(R)}(,;x)\right)\longrightarrow E\phi\left(u^{(R)}(,;x)\right),$$
 (219)

for a.e. $t \in [0, T]$. Take $x, y \in H_0^1$, by the previous argument, we can find a subsequence n_k such that the previous almost sure convergence in $t \in [0, T]$ holds true both x and y.

Thus, from (212), we have

$$\left| P_t^{(R)} \phi(x) - P_t^{(R)} \phi(y) \right| \le L \|x - y\|_{H^1},$$
 (220)

for a.e. $t \in [0, T]$. As $u^{(R)}(t; x)$ has continuous trajectories with values in H_0^1 , the above inequality holds for all $t \in [0, T]$.

Proposition 14. Under conditions of Theorem 9, (S) holds true.

Proof. Take t > 0, x_n , $x \in H_0^1$ satisfying $x_n \to x$ in H^1 . For every R > 0, we have that

$$\|P_{R}(t, x_{n}, \cdot) - P_{R}(t, x, \cdot)\|_{TV}$$

$$= \sup_{\|\phi\|_{C_{b}(H^{1})} \le 1} |P_{t}^{(R)}\phi(x_{n}) - P_{t}^{(R)}\phi(x)|$$

$$\le L\|x_{n} - x\|_{L^{1}} \longrightarrow 0,$$
(221)

as $n \to \infty$ by Proposition 13. Then,

$$\begin{split} & \left\| P_{R}\left(t,x_{n},\cdot\right) - P\left(t,x_{n},\cdot\right) \right\|_{TV} \\ & + \left\| P_{R}\left(t,x,\cdot\right) - P\left(t,x,\cdot\right) \right\|_{TV} \\ & = \sup_{\left\|\phi\right\|_{C_{b}(H^{1})} \leq 1} \left| P_{t}^{(R)}\phi\left(x_{n}\right) - P_{t}\phi\left(x_{n}\right) \right| \\ & + \sup_{\left\|\phi\right\|_{C_{b}(H^{1})} \leq 1} \left| P_{t}^{(R)}\phi\left(x\right) - P_{t}\phi\left(x\right) \right| \\ & = \sup_{\left\|\phi\right\|_{C_{b}(H^{1})} \leq 1} \left| E\phi\left(u_{R}\left(t;x_{n}\right)\right) - E\phi\left(u\left(t;x_{n}\right)\right) \right| \\ & + \sup_{\left\|\phi\right\|_{C_{b}(H^{1})} \leq 1} \left| E\phi\left(u_{R}\left(t;x\right)\right) - E\phi\left(u\left(t;x\right)\right) \right| \\ & \leq 2 \int_{\Omega} I_{\{\sup_{n \in \mathbb{N}} \|u(t;x_{n})\|_{H^{1}} > R\}} P\left(dw\right) \\ & + 2 \int_{\Omega} I_{\{\|u(t;x)\|_{H^{1}} > R\}} P\left(dw\right) \longrightarrow 0, \quad \text{as } R \to \infty, \end{split}$$

$$\tag{2222}$$

where the inequality follows by the consistency of u(t; x) and $u^{(R)}(t; x)$, when $||u(t; x)||_{H^1} \le R$, and the limit follows by (A.21). Therefore,

$$\|P(t, x_{n}, \cdot) - P(t, x, \cdot)\|_{TV}$$

$$\leq \|P(t, x_{n}, \cdot) - P_{R}(t, x_{n}, \cdot)\|_{TV}$$

$$+ \|P_{R}(t, x_{n}, \cdot) - P_{R}(t, x, \cdot)\|_{TV}$$

$$+ \|P_{R}(t, x, \cdot) - P(t, x, \cdot)\|_{TV} \longrightarrow 0,$$
as $n \to \infty$.

6. Example

Our theory can be applied to stochastic reaction diffusion equations or stochastic real valued Ginzburg Landau equation in high dimensions as follows:

$$\frac{\partial u}{\partial t} - \Delta u + |u|^2 u - u = dW, \quad \text{on } [0, T] \times D,$$

$$u(t, x) = 0, \quad t \in [0, T], x \in \partial D,$$

$$u(0, x) = u_0(x), \quad x \in D,$$
(224)

where $u(t,x) = (u^1(t,x), u^2(t,x))$ is the velocity field, Δ denotes the Laplace operator, W stands for the Q-Wiener process, and D is a regular bounded open domain of \mathbb{R}^2 .

Appendix

Fix R > 0 and let $K_R : [0, \infty[\to [0, \infty[$ satisfy $K_R \in C^1(\mathbb{R}_+)$ such that $|K_R| \le 1, |K_R'| \le 2$ and

$$K_R(x) = 1, \quad \text{if } x < R,$$
 $K_R(x) = 0, \quad \text{if } x \ge R + 1.$
(A.1)

Consider the following equation:

$$\frac{dv_n}{dt} + Av_n + K_R \left(\left\| v_n + P_n \phi \right\|_{H^1}^2 \right)
\times P_n B \left(v_n + P_n \phi, v_n + P_n \phi \right)
+ K_R \left(\left\| v_n + P_n \phi \right\|_{H^1}^2 \right) f \left(v_n + P_n \phi \right) = 0,$$
(A.2)

where $\phi \in C([0, T]; H^{3/2})$.

Estimate 1. We have the following estimate in H for (A.2):

$$||v_n||_{C([0,T];H)} + ||v_n||_{L^2([0,T];H^1)} \le C(||x||_H, ||\phi||_{C([0,T];H^{3/2})}, T),$$
(A.3)

where C(a, b, c) indicates a constant C depending on a, b, c. Analogously to the derivation of (147), we get

$$\frac{d}{dt} \|v_n\|_H^2 + \|v_n\|_{H^1}^2 + \|v_n\|_{L^4}^4 \le C(\|\phi\|_{H^{3/2}}^4 + 1). \tag{A.4}$$

Therefore, for all $t \in [0, T]$,

$$\|v_{n}(t)\|_{H}^{2} + \int_{0}^{t} \|v_{n}\|_{H^{1}}^{2} ds + \int_{0}^{t} \|v_{n}\|_{L^{4}}^{4} ds$$

$$\leq \|x\|_{H}^{2} + C \int_{0}^{t} (\|\phi(s)\|_{H^{3/2}}^{4} + 1),$$
(A.5)

Then, we get (A.3).

Estimate 2. We obtain the following estimate in H_0^1 for (A.2):

$$\|v_{n}(t)\|_{C([0,T];H_{0}^{1})}^{2} + \int_{0}^{T} \|v_{n}(s)\|_{H^{2}}^{2} ds$$

$$\leq C(\|x\|_{H^{1}}, \|\phi\|_{C([0,T];H^{3/2})}, T).$$
(A.6)

Since we have

$$\frac{d}{dt} \| v_n(t) \|_{H^1}^2 + \| v_n(t) \|_{H^2}^2
+ \left\langle f \left(v_n(t) + P_n \phi(t) \right), A v_n(t) \right\rangle
= \left\langle B \left(v_n(t) + P_n \phi(t), v_n(t) \right)
+ P_n \phi(t) \right\rangle, A v_n(t) \rangle,$$
(A.7)

the equation is equivalent to

$$\frac{d}{dt} \|v_{n}(t)\|_{H^{1}}^{2} + \|v_{n}(t)\|_{H^{2}}^{2}
+ \left\langle f\left(v_{n}(t) + P_{n}\phi(t)\right), A\left(v_{n}(t) + P_{n}\phi(t)\right)\right\rangle
= \left\langle B\left(v_{n}(t) + P_{n}\phi(t), v_{n}(t) + P_{n}\phi(t)\right), Av_{n}(t)\right\rangle
+ \left\langle f\left(v_{n}(t) + P_{n}\phi(t)\right), AP_{n}\phi(t)\right\rangle.$$
(A.8)

Denote by $u_n := v_n(t) + P_n\phi(t)$ and $u_n = (u_n^1, u_n^2)$; then

$$\langle |u_{n}|^{2}u_{n}, Au_{n}\rangle = 3 \int_{D} (u_{n}^{1})^{2} (\partial_{1}u_{n}^{1})^{2} dx$$

$$+ 3 \int_{D} (u_{n}^{1})^{2} (\partial_{2}u_{n}^{1})^{2} dx$$

$$+ 3 \int_{D} (u_{n}^{2})^{2} (\partial_{1}u_{n}^{2})^{2} dx$$

$$+ 3 \int_{D} (u_{n}^{2})^{2} (\partial_{2}u_{n}^{1})^{2} dx$$

$$+ \int_{D} (u_{n}^{2})^{2} (\partial_{1}u_{n}^{1})^{2} dx$$

$$+ \int_{D} (u_{n}^{2})^{2} (\partial_{2}u_{n}^{1})^{2} dx$$

$$+ \int_{D} (u_{n}^{1})^{2} (\partial_{1}u_{n}^{2})^{2} dx$$

$$+ \int_{D} (u_{n}^{1})^{2} (\partial_{2}u_{n}^{2})^{2} dx$$

$$+ 4 \int_{D} (u_{n}^{1}\partial_{1}u_{n}^{1}) (u_{n}^{2}\partial_{1}u_{n}^{2}) dx$$

$$+ 4 \int_{D} (u_{n}^{1}\partial_{2}u_{n}^{1}) (u_{n}^{2}\partial_{2}u_{n}^{2}) dx.$$

As

$$4 \int_{D} \left(u_{n}^{1} \partial_{1} u_{n}^{1} \right) \left(u_{n}^{2} \partial_{1} u_{n}^{2} \right) dx$$

$$\leq 2 \int_{D} \left(u_{n}^{1} \right)^{2} \left(\partial_{1} u_{n}^{1} \right)^{2} dx$$

$$+ 2 \int_{D} \left(u_{n}^{2} \right)^{2} \left(\partial_{1} u_{n}^{2} \right)^{2} dx,$$

$$4 \int_{D} \left(u_{n}^{1} \partial_{2} u_{n}^{1} \right) \left(u_{n}^{2} \partial_{2} u_{n}^{2} \right) dx$$

$$\leq 2 \int_{D} \left(u_{n}^{1} \right)^{2} \left(\partial_{2} u_{n}^{1} \right)^{2} dx$$

$$+ 2 \int_{D} \left(u_{n}^{2} \right)^{2} \left(\partial_{2} u_{n}^{2} \right)^{2} dx,$$

$$(A.10)$$

so, we have that

$$\langle |u_n|^2 u_n, Au_n \rangle$$

$$\geq \int_D (u_n^1)^2 (\partial_1 u_n^1)^2 dx$$

$$+ \int_D (u_n^1)^2 (\partial_2 u_n^1)^2 dx$$

$$+ \int_D (u_n^2)^2 (\partial_1 u_n^2)^2 dx$$

$$+ \int_D (u_n^2)^2 (\partial_2 u_n^2)^2 dx$$

$$+ \int_{D} (u_{n}^{2})^{2} (\partial_{1} u_{n}^{1})^{2} dx$$

$$+ \int_{D} (u_{n}^{2})^{2} (\partial_{2} u_{n}^{1})^{2} dx$$

$$+ \int_{D} (u_{n}^{1})^{2} (\partial_{1} u_{n}^{2})^{2} dx$$

$$+ \int_{D} (u_{n}^{1})^{2} (\partial_{2} u_{n}^{2})^{2} dx$$

$$= \int_{D} |u_{n}|^{2} |\nabla u_{n}|^{2} dx.$$
(A.11)

For the first term on the right hand side of (A.3), we have

$$\langle \left[\left(u_n \cdot \nabla \right) u_n \right], A v_n (t) \rangle$$

$$\leq \left\| v_n (t) \right\|_{H^2}^2 + \frac{1}{4} \int_D \left\| u_n \right\|^2 \left\| \nabla u_n \right\|^2 dx. \tag{A.12}$$

Substitute (A.11) and (A.12) into (A.8), we get

$$\frac{d}{dt} \| v_n(t) \|_{H^1}^2 + \| v_n(t) \|_{H^2}^2
\leq \left\langle f \left(v_n(t) + P_n \phi(t) \right), A \phi(t) \right\rangle
= \left\langle A^{1/4} f \left(v_n(t) + P_n \phi(t), A^{3/4} \phi(t) \right) \right\rangle .$$
(A.13)

Denote

$$u_n(t) = v_n(t) + P_n\phi(t). \tag{A.14}$$

Then,

$$\left\langle A^{1/4} f\left(v_{n}(t) + P_{n}\phi(t), A^{3/4}\phi(t)\right)\right\rangle
\leq \|\phi(t)\|_{H^{3/2}} \cdot \|A^{1/4} \left(|u_{n}(t)|^{2} u_{n}(t)\right)\|_{H}
\leq \|\phi(t)\|_{H^{3/2}}
\cdot \|\left(A^{1/4}|u_{n}(t)|^{2}\right) u_{n}(t) + |u_{n}(t)|^{2} A^{1/4} u_{n}(t) + R\|_{H}
\leq \|\phi(t)\|_{H^{3/2}}
\cdot \left[\left\|\left(A^{1/4}|u_{n}(t)|^{2}\right) u_{n}(t)\right\|_{H}
+ \|u_{n}(t)|^{2} A^{1/4} u_{n}(t)\|_{H} + \|R\|_{H} \right]
= \|\phi(t)\|_{H^{3/2}} \cdot \left[I_{1} + I_{2} + I_{3}\right], \tag{A.15}$$

where

$$R = A^{1/4} (|u_n(t)|^2 u_n(t))$$

$$- (A^{1/4} |u_n(t)|^2) u_n(t)$$

$$- |u_n(t)|^2 A^{1/4} u_n(t).$$
(A.16)

For I_1 , we have

$$I_1 \le \left\| \left(u_n(t) A^{1/4} u_n(t) + R_1 \right) u_n(t) \right\|_{H},$$
 (A.17)

where

$$R_1 = A^{1/4} |u_n(t)|^2 - 2u_n(t) A^{1/4} u_n(t).$$
 (A.18)

So,

$$I_{1} \leq C \| |u_{n}(t)|^{2} A^{1/4} u_{n}(t) + R_{1} u_{n}(t) \|_{H}$$

$$\leq C \| u_{n}(t) \|_{L^{8}}^{2} \| u_{n}(t) \|_{H^{1/2,4}}$$

$$+ \| u_{n}(t) \|_{L^{4}} \| R_{1} \|_{L^{4}}$$

$$\leq C \| u_{n}(t) \|_{L^{8}}^{2} \| u_{n}(t) \|_{H^{1/2,4}}$$

$$+ \| u_{n}(t) \|_{L^{4}} \| u_{n}(t) \|_{H^{1/4,8}}$$

$$\leq C \| u_{n}(t) \|_{H^{1}}^{3}.$$
(A.19)

Analogously, we can get the same estimate for I_2 and I_3 . Take advantage of the estimates for I_1 , I_2 , and I_3 , we have

$$\frac{d}{dt} \|v_{n}(t)\|_{H^{1}}^{2} + \|v_{n}(t)\|_{H^{2}}^{2}$$

$$\leq C \|\phi(t)\|_{H^{3/2}} \|u_{n}(t)\|_{H^{1}}^{3}$$

$$\leq C (\|v_{n}(t)\|_{H^{1}}^{3} + \|\phi(t)\|_{H^{3/2}}^{3}).$$
(A.20)

By the Gronwall inequality and (A.3), we get (A.6).

Remark A.1. It is standard to show that, for $x \in H_0^1$ and $\phi \in C([0,T];H^{3/2})$, there exists a subsequence which converges to some v, strongly in $L^2([0,T];H^1)$, weekly in $L^2([0,T];H^2)$, and weak star in $L^\infty([0,T];H^1)$. Therefore, we have

$$\|\nu(t)\|_{C([0,T];H_0^1)}^2 + \int_0^T \|\nu(s)\|_{H^2}^2 ds$$

$$\leq C(\|x\|_{H^1}, \|\phi\|_{C([0,T];H^{3/2})}, T).$$
(A.21)

Estimate 3. We compare, only in the case $R = \infty$. Let v_n^1, v_n^2 be two solutions with the same initial condition $x \in H^1$ but with different functions ϕ_1, ϕ_2 , there exists a constant $C(\|x\|_{H^1}, \|\phi_1\|_{C([0,T];H^{3/2})}, \|\phi_2\|_{C([0,T];H^{3/2})}, T)$, such that

$$\begin{aligned} & \left\| v_n^1 - v_n^2 \right\|_{C([0,T];H_0^1)} \\ & \leq C \left(\left\| x \right\|_{H^1}, \left\| \phi_1 \right\|_{C([0,T];H^{3/2})}, \left\| \phi_2 \right\|_{C([0,T];H^{3/2})}, T \right) \\ & \times \left\| \phi_1 - \phi_2 \right\|_{C([0,T];H^{3/2})}, \end{aligned} \tag{A.22}$$

for every $n, x \in H^1, \phi_1, \phi_2, T$. We have

$$\frac{dv_{n}^{i}}{dt} + Av_{n}^{i} + P_{n}B\left(v_{n}^{i} + P_{n}\phi_{i}, v_{n}^{i} + P_{n}\phi_{i}\right)
+ 9\left|v_{n}^{i} + P_{n}\phi_{i}\right|^{2}\left(v_{n}^{i} + P_{n}\phi_{i}\right) = 0,$$
(A.23)

with initial condition $v_n^i(0) = P_n x$, for i = 1, 2. Set $\eta_n = v_n^1 - v_n^2, \psi = \phi_1 - \phi_2$. Then,

$$\begin{split} \frac{d\eta_{n}}{dt} + A\eta_{n} + P_{n}B\left(v_{n}^{1} + P_{n}\phi_{1}, \eta_{n} + P_{n}\psi\right) \\ + P_{n}B\left(\eta_{n} + P_{n}\psi, v_{n}^{2} + P_{n}\phi_{2}\right) \\ + \vartheta\left|v_{n}^{1} + \phi_{1}\right|^{2}\left(v_{n}^{1} + \phi_{1}\right) \\ - \vartheta\left|v_{n}^{2} + \phi_{2}\right|^{2}\left(v_{n}^{2} + \phi_{2}\right) = 0. \end{split} \tag{A.24}$$

Take inner product in *H* with respect to $A\eta_n$, we have

$$\frac{1}{2} \frac{d}{dt} \| \eta_n \|_{H^1}^2 + \| \eta_n \|_{H^2}^2
+ \left\langle P_n B \left(\left(v_n^1 + P_n \phi_1 \right), \left(\eta_n + P_n \psi \right) \right), A \eta_n \right\rangle
+ \left\langle P_n B \left(\eta_n + P_n \psi, v_n^2 + P_n \phi_2 \right), A \eta_n \right\rangle
+ \vartheta \left\langle \left| v_n^1 + \phi_1 \right|^2 \left(v_n^1 + \phi_1 \right) \right.
- \left| v_n^2 + \phi_2 \right|^2 \left(v_n^2 + \phi_2 \right), A \eta_n \right\rangle = 0.$$
(A.25)

For the third term on the left hand side of (A.23), we have

$$\left\langle P_{n}B\left(v_{n}^{1} + P_{n}\phi_{1}, \eta_{n} + P_{n}\psi\right), A\eta_{n}\right\rangle
\leq \|\eta_{n}\|_{H^{2}} \|\eta_{n} + P_{n}\psi\|_{H^{1,4}} \|v_{n}^{1} + P_{n}\phi_{1}\|_{L^{4}}
\leq \|\eta_{n}\|_{H^{2}} \left(\|\eta_{n}\|_{H^{3/2}} + \|\psi\|_{H^{3/2}}\right) \left(\|v_{n}^{1} + \phi_{1}\|_{H^{1}}\right)
\leq \|v_{n}^{1} + \phi_{1}\|_{H^{1}} \|\eta_{n}\|_{H^{2}} \left(\|\eta_{n}\|_{H^{1}}^{1/2} \|\eta_{n}\|_{H^{2}}^{1/2} + \|\psi\|_{H^{3/2}}\right)
\leq \varepsilon \|\eta_{n}\|_{H^{2}}^{2} + C \|v_{n}^{1} + \phi_{1}\|_{H^{1}}^{4} \|\eta_{n}\|_{H^{1}}^{2}
+ C \|v_{n}^{1} + \phi_{1}\|_{H^{1}}^{2} \|\psi\|_{H^{3/2}}^{2}.$$
(A.26)

Similarly, we can get

$$\left\langle P_{n}B\left(\eta_{n} + P_{n}\psi, v_{n}^{2} + P_{n}\phi_{2}\right), A\eta_{n}\right\rangle
\leq \varepsilon \|\eta_{n}\|_{H^{2}}^{2} + C \|v_{n}^{2}\|_{H^{2}}^{2} \|\eta_{n}\|_{H^{1}}^{2}
+ C \|v_{n}^{2}\|_{H^{2}}^{2} \|\psi\|_{H^{1}}^{2}
+ C \|\phi_{2}\|_{H^{3/2}}^{2} \|\eta_{n}\|_{H^{1}}^{2}
+ C \|\phi_{2}\|_{H^{3/2}}^{2} \|\psi\|_{H^{1}}^{2},$$

$$\left\langle \left|v_{n}^{1} + \phi_{1}\right|^{2} \left(v_{n}^{1} + \phi_{1}\right) - \left|v_{n}^{2} + \phi_{2}\right|^{2} \left(v_{n}^{2} + \phi_{2}\right), A\eta_{n}\right\rangle
\leq \varepsilon \|\eta_{n}\|_{H^{2}}^{2} + C \|\eta_{n}\|_{H^{1}}^{2} \left(\left\|v_{n}^{1} + \phi_{1}\right\|_{H^{1}}^{4} + \left\|v_{n}^{2} + \phi_{2}\right\|_{H^{1}}^{4}\right)
+ C \|\psi\|_{H^{1}}^{2} \left(\left\|v_{n}^{1} + \phi_{1}\right\|_{H^{1}}^{4} + \left\|v_{n}^{2} + \phi_{2}\right\|_{H^{1}}^{4}\right).$$
(A.28)

By (A.23)–(A.27), we have
$$\frac{d}{dt} \|\eta_n\|_{H^1}^2 + \|\eta_n\|_{H^2}^2$$

$$\leq C \|\eta_n\|_{H^1}^2 \left(\|v_n^1 + \phi_1\|_{H^1}^4 + \|v_n^2 + \phi_2\|_{H^1}^4 + \|\psi_n^1 + \phi_1\|_{H^1}^2 + \|\psi_n^2\|_{H^2}^2 + \|\phi_2\|_{H^{3/2}}^2 \right) \quad (A.29)$$

$$+ C \|\psi\|_{H^{3/2}}^2 \left(\|v_n^1 + \phi_1\|_{H^1}^4 + \|v_n^2 + \phi_2\|_{H^1}^4 + \|v_n^1 + \phi_1\|_{H^1}^2 + \|\phi_2\|_{H^{3/2}}^2 \right).$$

So, by the Gronwall inequality and (A.6), we get (A.21). By (A.6), we know that v_n^i converges week star to v^i in $C([0,T];H_0^1)$, for i=1,2, we have

$$\|v^{1} - v^{2}\|_{C([0,T];H^{1})}$$

$$\leq C \left(\|x\|_{H^{1}}, \|\phi_{1}\|_{C([0,T];H^{3/2})}, \|\phi_{2}\|_{C([0,T];H^{3/2})}, T\right)$$

$$\|\phi_{1} - \phi_{2}\|_{C([0,T]:H^{3/2})}.$$
(A.30)

Estimate 4. Let us consider only the case $R \in (0, \infty)$, and denote by $v_n(t)$ the solution to (A.2). Let ξ_n be the differential mapping $x \to v_n$ in the direction h at point x, defined by, for given $x, h \in H$ as follows:

$$\xi_n(t) = D_x v_n(t; x) \cdot h. \tag{A.31}$$

Set also

$$u_n(t;x) = v_n(t,x) + P_n\phi(t),$$
 (A.32)

so that ξ_n is also the differential of the mapping $x \to u_n(t;x)$ in the direction h at the point x. Thus, ξ_n satisfies

$$\frac{d}{dt}\xi_{n} + A\xi_{n}$$

$$= 2K_{R}'(\|u_{n}\|_{H^{1}}^{2})\langle A^{1/2}u_{n}, A^{1/2}\xi_{n}\rangle B(u_{n}, u_{n})$$

$$+ K_{R}(\|u_{n}\|_{H^{1}}^{2})\{B(u_{n}, \xi_{n}) + B(\xi_{n}, u_{n})\}$$

$$+ 2K_{R}'(\|u_{n}\|_{H^{1}}^{2})\langle A^{1/2}u_{n}, A^{1/2}\xi_{n}\rangle u_{n}^{3}$$

$$+ 3K_{R}(\|u_{n}\|_{H^{1}}^{2})|u_{n}|^{2}\xi_{n}.$$
(A.33)

So, $\frac{d}{dt} \|\xi_{n}\|_{H^{1}}^{2} + \|\xi_{n}\|_{H^{2}}^{2}$ $= 2K_{R}'(\|u_{n}\|_{H}^{2}) \langle B(u_{n}, u_{n}), A\xi_{n} \rangle$ $+ K_{R}(\|u_{n}\|_{H}^{2}) \langle B(u_{n}, \xi_{n}), A\xi_{n} \rangle$ $+ K_{R}(\|u_{n}\|_{H}^{2}) \langle B(\xi_{n}, u_{n}), A\xi_{n} \rangle$ $+ 2K_{R}'(\|u_{n}\|_{H}^{2}) \langle A^{1/2}u_{n}, A^{1/2}\xi_{n} \rangle \langle |u_{n}|^{2}u_{n}, A\xi_{n} \rangle$ $+ 3K_{R}(\|u_{n}\|_{H}^{2}) \langle |u_{n}|^{2}\xi_{n}, A\xi_{n} \rangle.$ (A.34) Therefore,

$$\begin{split} &\frac{d}{dt} \left\| \xi_{n} \right\|_{H^{1}}^{2} + \left\| \xi_{n} \right\|_{H^{2}}^{2} \\ &\leq 2K_{R}' \left(\left\| u_{n} \right\|_{H}^{2} \right) \left\| u_{n} \right\|_{H^{1}} \left\| \xi_{n} \right\|_{H^{1}} \left\| \xi_{n} \right\|_{H^{2}} \left\| u_{n} \right\|_{L^{4}} \left\| u_{n} \right\|_{H^{1,4}} \\ &+ K_{R} \left(\left\| u_{n} \right\|_{H^{1}}^{2} \right) \left\| \xi_{n} \right\|_{H^{2}} \left\| \xi_{n} \right\|_{H^{1,4}} \left\| u_{n} \right\|_{L^{4}} \\ &+ K_{R} \left(\left\| u_{n} \right\|_{H^{1}}^{2} \right) \left\| \xi_{n} \right\|_{H^{2}} \left\| \xi_{n} \right\|_{L^{4}} \left\| u_{n} \right\|_{H^{1,4}} \\ &+ 2K_{R}' \left(\left\| u_{n} \right\|_{H^{1}}^{2} \right) \left\| u_{n} \right\|_{H^{1}} \left\| \xi_{n} \right\|_{H^{1}} \left\| \xi_{n} \right\|_{H^{2}} \left\| u_{n} \right\|_{L^{6}}^{3} \\ &+ 3K_{R} \left(\left\| u_{n} \right\|_{H^{1}}^{2} \right) \left\| \xi_{n} \right\|_{H^{2}} \left\| \xi_{n} \right\|_{L^{4}} \left\| u_{n} \right\|_{L^{8}}^{2} \\ &\leq C \left(R \right) \left\| \xi_{n} \right\|_{H^{1}} \left\| \xi_{n} \right\|_{H^{2}} \left(\left\| v_{n} \right\|_{H^{2}} + \left\| \phi \right\|_{H^{3/2}} \right) \\ &+ C \left(R \right) \left\| \xi_{n} \right\|_{H^{2}} \left\| \xi_{n} \right\|_{H^{1}} \\ &+ C \left(R \right) \left\| \xi_{n} \right\|_{H^{2}} \left\| \xi_{n} \right\|_{H^{1}} \\ &\leq \varepsilon \left\| \xi_{n} \right\|_{H^{2}}^{2} + C \left(R \right) \left\| \xi_{n} \right\|_{H^{1}}^{2} \\ &\times \left(1 + \left\| v_{n} \right\|_{H^{2}}^{2} + \left\| \phi \right\|_{H^{3/2}}^{2} \right). \end{split} \tag{A.35}$$

By the Gronwall inequality and (A.6), we have

$$\|\xi_n(t)\|_{H^1}^2 \le C(R) \|h\|_{H^1}^2.$$
 (A.36)

And therefore, using again the previous inequality,

$$\int_{0}^{T} \left\| \xi_{n}(t) \right\|_{H^{2}}^{2} dt \le C(R) \left\| h \right\|_{H^{1}}^{2}. \tag{A.37}$$

Acknowledgments

The authors are thankful to the referee for careful reading and insightful comments which led to many improvements of the earlier version. This work was partially supported by the Fundamental Research Funds for the Central Universities (Grant no. CQDXWL-2013-003).

References

- [1] H. Beteman, "Some recent researches of the motion of fluid," *Monthly Weather Review*, vol. 43, pp. 163–170, 1915.
- [2] A. R. Forsyth, *Theory of Differential Equations*, vol. 6, Cambridge University Press, Cambridge, UK, 1906.
- [3] D. H. Chambers, R. J. Adrian, P. Moin, D. S. Stewart, and H. J. Sung, "Karhunen Loeve expansion of Burgers' model of turbulence," *Physics of Fluids*, vol. 31, pp. 2573–2582, 1988.
- [4] H. C. Choi, R. Temam, P. Moin, and J. Kim, "Feedback control for unsteady flow and its application to the stochastic Burgers equation," *Journal of Fluid Mechanics*, vol. 253, pp. 509–543, 1993.
- [5] D. Jeng, "Forced model equation for turbulence," *The Physics of Fluids*, vol. 12, no. 10, pp. 2006–2010, 1969.
- [6] I. Hosokawa and K. Yamamoto, "Turbulence in the randomly forced, one-dimensional Burgers flow," *Journal of Statistical Physics*, vol. 13, no. 3, pp. 245–272, 1975.

- [7] M. Kardar, G. Parisi, and Y. Zhang, "Dynamic scaling of growing interfaces," *Physical Review Letters*, vol. 56, no. 9, pp. 889–892, 1986.
- [8] L. Bertini, N. Cancrini, and G. Jona-Lasinio, "The stochastic Burgers equation," *Communications in Mathematical Physics*, vol. 165, no. 2, pp. 211–232, 1994.
- [9] G. Da Prato, A. Debussche, and R. Temam, "Stochastic Burgers' equation," *Nonlinear Differential Equations and Applications*, vol. 1, no. 4, pp. 389–402, 1994.
- [10] G. Da Prato and A. Debussche, "Stochastic Cahn-Hilliard equation," *Nonlinear Analysis: Theory, Methods & Applications A*, vol. 26, no. 2, pp. 241–263, 1996.
- [11] I. Gyöngy and D. Nualart, "On the stochastic Burgers' equation in the real line," *The Annals of Probability*, vol. 27, no. 2, pp. 782–802, 1999.
- [12] M. Gourcy, "Large deviation principle of occupation measure for stochastic Burgers equation," *Annales de l'Institut Henri Poincaré*, vol. 43, no. 4, pp. 441–459, 2007.
- [13] E. Weinan, K. Khanin, A. Mazel, and Y. Sinai, "Invariant measures for Burgers equation with stochastic forcing," *Annals of Mathematics*, vol. 151, no. 3, pp. 877–960, 2000.
- [14] Z. Dong and T. G. Xu, "One-dimensional stochastic Burgers equation driven by Lévy processes," *Journal of Functional Analysis*, vol. 243, no. 2, pp. 631–678, 2007.
- [15] G. Wang, M. Zeng, and B. Guo, "Stochastic Burgers' equation driven by fractional Brownian motion," *Journal of Mathematical Analysis and Applications*, vol. 371, no. 1, pp. 210–222, 2010.
- [16] Z. Hou, J. Luo, P. Shi, and S. K. Nguang, "Stochastic stability of Ito differential equations with semi-Markovian jump parameters," *IEEE Transactions on Automatic Control*, vol. 51, no. 8, pp. 1382–1386, 2006.
- [17] F. Li, L. Wu, and P. Shi, "Stochastic stability of semi-Markovian jump systems with mode-dependent delays," *International Jour*nal of Robust and Nonlinear Control, 2013.
- [18] J. Qiu, G. Feng, and J. Yang, "A new design of delay-dependent robust H_{∞} filtering for discrete-time T-S fuzzy systems with time-varying delay," *IEEE Transactions on Fuzzy Systems*, vol. 17, no. 5, pp. 1044–1058, 2009.
- [19] J. Qiu, G. Feng, and J. Yang, "Delay-dependent non-synchronized robust H_{∞} state estimation for discrete-time piecewise linear delay systems," *International Journal of Adaptive Control and Signal Processing*, vol. 23, no. 12, pp. 1082–1096, 2009.
- [20] Y. Wei, J. Qiu, H. R. Karimi, and M. Wang, "A new design of H_{∞} filtering for continuous-time Markovian jump systems with time-varying delay and partially accessible mode information," *Signal Processing*, vol. 93, no. 9, pp. 2392–2407, 2013.
- [21] M. Hairer, J. C. Mattingly, and M. Scheutzow, "Asymptotic coupling and a general form of Harris' theorem with applications to stochastic delay equations," *Probability Theory and Related Fields*, vol. 149, no. 1-2, pp. 223–259, 2011.
- [22] J. L. Doob, "Asymptotic properties of Markoff transition prababilities," *Transactions of the American Mathematical Society*, vol. 64, pp. 393–421, 1948.
- [23] G. Da Prato and J. Zabczyk, Stochastic Equations in Infinite Dimensions, Encyclopedia of Mathematics and its Applications, Cambridge University Press, Cambridge, UK, 1992.
- [24] M. Rockner, Intruduction to Stochastic Partial Difficult Equation, Fall 2005 and Spring 2006, Version, Purdue University, 2007.

- [25] C. E. Kenig, G. Ponce, and L. Vega, "Well-posedness and scattering results for the generalized Korteweg-de Vries equation via the contraction principle," *Communications on Pure and Applied Mathematics*, vol. 46, no. 4, pp. 527–620, 1993.
- [26] F. Flandoli, "Dissipativity and invariant measures for stochastic Navier-Stokes equations," *Nonlinear Differential Equations and Applications*, vol. 1, no. 4, pp. 403–423, 1994.
- [27] A. Pazy, Semigroups of Linear Operators and Applications to Partial Differential Equations, Springer, New York, NY, USA, 1983.
- [28] G. Da Prato and J. Zabczyk, Ergodicity for Infinite-Dimensional Systems, vol. 229 of London Mathematical Society Lecture Note Series, Cambridge University Press, Cambridge, UK, 1996.
- [29] S. Pezat and J. Zabczyk, Strong Feller Property and Irreducibility for Diffusions on Hilbert Spaces, no. 510, Institute of Mathematics Polish Academy of Sciences, Warsaw, Poland, 1993.

Hindawi Publishing Corporation Abstract and Applied Analysis Volume 2013, Article ID 260578, 14 pages http://dx.doi.org/10.1155/2013/260578

Research Article

A New Real-Time Path Planning Method Based on the Belief Space

Yu-xin Zhao, Xin-an Wu, and Yan Ma

College of Automation, Harbin Engineering University, Harbin 150001, China

Correspondence should be addressed to Yu-xin Zhao; zhaoyuxin@hrbeu.edu.cn

Received 5 October 2013; Accepted 28 October 2013

Academic Editor: Xiaojie Su

Copyright © 2013 Yu-xin Zhao et al. This is an open access article distributed under the Creative Commons Attribution License, which permits unrestricted use, distribution, and reproduction in any medium, provided the original work is properly cited.

A new approach of real-time path planning based on belief space is proposed, which solves the problems of modeling the real-time detecting environment and optimizing in local path planning with the fusing factors. Initially, a double-safe-edges free space is defined for describing the sensor detecting characters, so as to transform the complex environment into some free areas, which can help the robots to reach any positions effectively and safely. Then, based on the uncertainty functions and the transferable belief model (TBM), the basic belief assignment (BBA) spaces of each factor are presented and fused in the path optimizing process. So an innovative approach for getting the optimized path has been realized with the fusing the BBA and the decision making by the probability distributing. Simulation results indicate that the new method is beneficial in terms of real-time local path planning.

1. Introduction

Recently, the development and application of autonomous robots are with growing interest in industrial and military fields. As we all know, navigation is one of the key technical problems for autonomous robots, and the most important factor of navigation is map building based on the sensor system, especially when the autonomous robots are working in an entire unknown environment. The environment is reconstructed by merging the information transferred from the sensor system during the motion. To build a practical map, one of the most difficult problems is due to the poor environment information of the sensor system which has inherent wide radiation cone and the phenomenon of multiple reflections. Thus, how to describe these uncertainties and filter out inaccurate and conflicting information and how to construct the environment view are the hot issues.

In these few years, there are about three types of approaches of constructing the environment view that appeared in exoteric literatures. The first type is the occupancy grid mapping method [1], which represents maps with fine-grained grids that model the occupied and free space of the environment. The second type is the geometrical information mapping method [2], which uses some sets of

line, angles and polygons to describe the geometry of the environment. The third way is the topological method [3, 4], which models the environment by a series of landmarks that are connected via arcs.

In order to describe the uncertainties, or filter out the conflicting information detected by sensors, the probabilistic algorithms [5] was proposed by a definitive formulation through the Bayesian technique originally. Then a family of algorithms [6] based on fuzzy theory [7] established the uncertainty information model in each cell. In a similar way, another way based on Dempster-Shafer theory described the uncertainty model by using the belief functions. In these years, the neural network technique have been introduced with using the learning ability of the neural cell [8].

There is no doubt that the optimization problem is quite important for autonomous robots path planning. So many evolutionary optimizing techniques like genetic algorithm [9–11], neural network [12], and ant colony optimization [13] are extensively used in solving the global path planning problems, on condition that the environment has been detected. But these algorithms do not work in a real-time local path planning environment, because, besides the path length, some other factors such as the underwater robot's self-characters and the influence of the special environment

(ocean current, wind speed) also influence the selection of the local target point in real-time local detecting path planning. As far as we know, few researchers consider these factors in solving real-time path planning problems.

In this paper, a novel real-time path planning approach based on the belief space is introduced. As the transferable belief model (TBM), which is popular in these years, can be used to describe a highly flexible model to manage the uncertainty information in the multisensor data fusion problems. In particular, many applications of TBM have been presented in mobile vehicles and other areas [14–17].

The rest of the paper is organized as follows. In Section 2, the uncertainty model of the sensor detection is shortly described, and the main idea of the transferable belief model is written in Section 3. In Section 4, the complex environment information is expressed by the double-safe-edges free space, which can simplify the real-time detecting environment information and prepare for the real-time path planning. In Section 5, the belief space is established according to the belief functions of the factors that affect the selection of the local target points, so the optimization local target point can be found at each step. The connection line of these optimization local target points is the optimization path of the task. Section 6 shows the experimental results of the new path planning approach and Section 7 comprises of conclusion.

2. Uncertainty Model of the Sensor Detection

Sonar is far from being an ideal sensor, mainly due to the width of the radiation cone and to the multiple reflections phenomenon. The former does not allow determining the exact angular position of the obstacle on the fixed angle θ arc of the circle corresponding to the detected distance. The latter needs a more thorough explanation. The sonar waves are reflected in two different ways depending on the surface irregularities. If their sizes are much smaller than the wavelength of the signal, we have a diffused reflection; that is, the incident energy is scattered in all directions; otherwise, the reflection is mainly specula and the beam may either reach the receiver after multiple reflections or even get lost [18].

The uncertainty model has been set up by fuzzy measure approach. A single reading r provides the information that one or more obstacles are located somewhere along the θ arc of circumference of radius r. Hence, there is evidence that points located in the proximity of this arc "occupied." On the other hand, points well inside the circular sector of radius r are likely to be "empty." To model this knowledge, we introduce the two functions [19]:

$$f_{e}(\rho, r) = \begin{cases} k_{e} & 0 \le \rho \le r - \Delta r \\ k_{e} \left(\frac{r - \rho}{\Delta r}\right)^{2} & r - \Delta r \le \rho \le r \\ 0 & \rho \ge r, \end{cases}$$
 (1)

$$f_{o}(\rho, r) = \begin{cases} 0 & 0 \le \rho \le r - \Delta r \\ k_{o} \left[1 - \left(\frac{r - \rho}{\Delta r} \right)^{2} \right] & r - \Delta r \le \rho \le r \\ 0 & \rho \ge r + \Delta r. \end{cases}$$
 (2)

That describe, respectively, how the degree of certainty of the assertions "empty" and "occupied" varies with ρ for a given range reading r. Here, ρ is the distance from the sensor k_e and k_o are two constants corresponding to the maximum values attained by the functions, and $2 \times \Delta r$ is the width of the area considered "proximal" to the arc of radius r [20].

Since the intensity of the waves decreases to zero at the borders of the radiation cone, the degree of certainty of each assertion is assumed to be higher for points close to the beam axis. This is realized by defining an angular modulation function [19]:

$$f_a(\theta) = \begin{cases} D(\theta) & 0 \le |\theta| \le \gamma \\ 0 & |\theta| > \gamma, \end{cases}$$
 (3)

$$g_d(\rho) = 1 - \frac{1 + \tanh\left(2\left(\rho - \rho_v\right)\right)}{2}.$$
 (4)

In order to weaken the confidence of each assertion as the distance from the sensor increases, the parameter ρ_{ν} plays the role of a "visibility radiuses," where a smooth transition occurs from certainty to uncertainty. The motivation for introducing this function is twofold. Firstly, as the possibility of multiple reflections increases as the beam makes a loner fly. Besides, narrow passages appear to be obstructed if seen from a large distance, due to the sensor wide radiation angle. By varying the visibility radius according to the characteristics of the environment, it is possible to obtain a more correct detection behavior [20].

3. The Transferable Belief Model (TBM)

TBM is a model for describing quantified beliefs based on belief function. Beliefs can be held at two levels: (1) a "credal" level where beliefs are entertained and quantified by belief functions; (2) a "pignistic" level where beliefs can be used to make decisions and are quantified by probability functions. The relation between the belief function and the probability function when decisions must be made is derived and justified [21].

In TBM, the actual value ω_0 of the variable whose finite domain is a given set Ω has been considered. A basic belief mass (BBM) denoted by m^{Ω} is used to represent the uncertainty about the value of ω_0 . $m^{\Omega}(A)$, which is the basic belief assignment (BBA), is given to $A \subseteq \Omega$. m^{Ω} maps 2^{Ω} , the power set of Ω on [0,1], and satisfies [22]:

$$\sum_{A \subseteq \Omega} m^{\Omega}(A) = 1. \tag{5}$$

The mass $m^{\Omega}(A)$ represents the part of belief that supports that the actual value Ω_0 belongs to A and without more specific several useful functions [23].

Belief function is defined as

$$bel^{\Omega}(A) = \sum_{B:\emptyset \neq B \subseteq A} m^{\Omega}(B).$$
 (6)

The value bel^{Ω}(A) represents the total amount of belief supporting that ω_0 is in A or without supporting that it is in \overline{A} where \overline{A} is the complement of A relative to Ω .

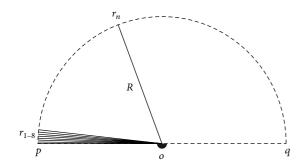


FIGURE 1: The sketch map of the sensor detection simulation.

Plausibility function is defined as

$$\operatorname{pl}^{\Omega}\left(A\right) = \sum_{B: \emptyset \cap B \neq \emptyset} m^{\Omega}\left(B\right). \tag{7}$$

The value $\operatorname{pl}^{\Omega}(A)$ represents the total amount of belief supporting that ω_0 might be in A without supporting that it might be in \overline{A} .

Combination rules: in general Bayesian theorem, the sensor detection x is the vector of plausibility $\operatorname{pl}^X[h_i](x)$ for all $h_i \in H$. The conditional belief can be written by probability function $\operatorname{pl}^X[h_i](x) = P^X[h_i](x)$. It is easier to use the likelihood of h_i given x, denoted by $l(h_i \mid x)$ [24]. So given the likelihood $l(h_i \mid x)$ for every and for every $h_i \in H$, Smets [25] has proved

$$m^{H}[x](A) = \prod_{h_{i} \in A} l(h_{i} \mid x) \prod_{h_{i} \in \overline{A}} (1 - l(h_{i} \mid x)),$$

$$pl^{H}[x](A) = 1 - \prod_{h_{i} \in A} (1 - l(h_{i} \mid x)).$$
(8)

Decision making function is defined as

Bet
$$P^{\Omega}(A) = \sum_{B \subseteq \Omega} \frac{|A \cap B|}{|B|} \frac{m^{\Omega(B)}}{1 - m^{\Omega(\theta)}} \quad \forall A \subseteq \Omega.$$
 (9)

In the TBM, when a decision has to be made, a probability functions Bet $P^{\Omega}(A)$ on Ω must be adopted. Bet P^{Ω} is a probability measure.

4. The Simulation of the Process of the Sensor Detection

4.1. The Process of Detecting of the Sensor. We will build a simulation environment about the detection process of the robot sensor for testing the new approach of the real-time path planning process. The robot sensor is an initiative sensor, the angle of the detecting is 180° , and the distance of detecting is R, so this paper will make 180 lines which starts from the particle of the robot and the length are R and the angle of each line is 1° .

In Figure 1, point o is the particle of the sensor, the sector \widehat{poq} is the detecting area of the sensor, the distance

R is the max distance of detecting, the lines $or_n = (n \in [0, 180])$ are the sound wave of the sensor, and the diameter of the sector and the y-axis of the robot is vertical. Thus, with this enactment, after each detecting of the environment, the environment information is the 181-distance, information in the sector \widehat{poq} ; they are the position information of the obstacles.

Figure 2 shows the four-detail process of the simulation of the detecting process of the sensor; in Figure 2(a) is the state of the no obstacle at time t_0 ; it gives the particle of the sensor, the 181 lines of R distance, and the sector area of the detecting; in Figure 2(b) is obstacles which the sensor needs to detect at time t_s ; in Figure 2(c) is the detection state of the sensor has detected the obstacles in Figure 2(b); it shows that some of these 181 lines have been cut in this state, so the process of detecting has been built; Figure 2(d) shows the result of the detection; the position information of the obstacles can be noted by the set Q_t $(t = 0, 1, \ldots, n)$.

4.2. The Transformation of the Detecting Space Coordinates of the Sensor. In the process of the path planning, the position information of the obstacle, and the robot, the information of the whole target point and the local target points must be described at each time, so it needs a uniform reference frame. There are two reference frames in the process of path planning of this paper: the reference frame of the robot movement and the reference frame of the sensor detection, so it needs the transition of the reference frame. In this paper, the reference frame of the robot movement is a vertical coordinate; the start point S, the whole target point G, and the position of robot O can be denoted; the reference frame of the sensor detection is a pole that coordinates the obstacle information Q and the local target point can be denoted, and the transition of these two coordinates is in Figure 3.

In Figure 3, the origin of the vertical coordinate is O_g , the position of the robot and the whole target point is o and G, the origin of pole coordinate is o, vector op is the pole axes, and the angle between the pole axes and the x-axis of the vertical coordinate is β so the coordinate of the obstacles or the local target point is (ρ_n, θ) . The vertical coordinate in the reference frame of the sensor detection is (x_p, y_p) :

$$x_p = \rho \cos \theta,$$

$$y_p = \rho \sin \theta.$$
 (10)

So the vertical coordinate in the reference frame of the robot movement is the position vector which is $[x_0, y_0, z_0]^T$:

$$x = x_{p} \cos \beta_{0} - y_{p} \sin \beta_{0} + x_{0},$$

$$y = x_{p} \cos \beta_{0} + y_{p} \sin \beta_{0} + y_{0}.$$
(11)

5. The Procedure of Confirming the Double Safe Edges Free Space

5.1. The Description of the Environment Information in Real-Time. In an uncertainty and dynamic environment, the environment information for path planning is obtained from

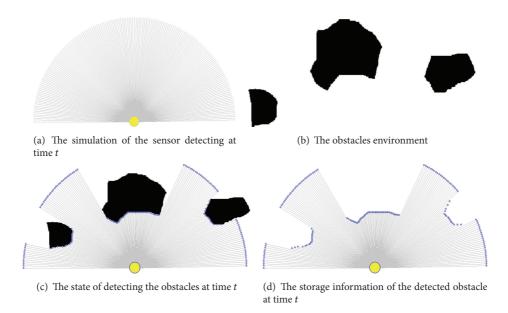


FIGURE 2: Simulation results of the sensor detection at time t.

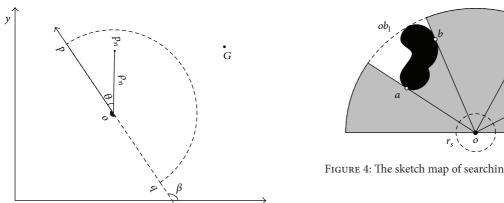


FIGURE 3: The transformation of the detecting space coordinates of the sensor.

the sensor on the robot only, so the algorithm should have well real-time ability and it is also the first step of generating the robot's motion. According to the sensor detecting model, we propose a method for searching the important information from the detecting information in this paper, which is called the double-safe-edges (DSE) information.

5.1.1. Searching for the Sensor Edges. Obviously, the sensor edges can be searched directly from the sensor detecting information, and its distance and direction can be ensured according to the position of the obstacles.

In Figure 4, point o is the particle of the robot (the sensor and robot at the same particle) and the self-safe area of the robot is a circle whose radius is the particle of the robot, and the radius is r, the range of the angle is $\pi/2$, the biggest detection radius is R_{max} , the obstacles are ob_1 and ob_2 , and the safe distance between he robot and obstacle is d_i . Because

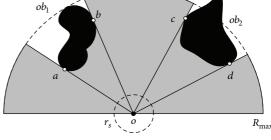


FIGURE 4: The sketch map of searching the sensor edges at time *t*.

the robot detection area is a hemicycle in front of the robot, so we use the lines to simulate the detecting process and the lines' length is R_{max} , the number is 180, and the angle of them is 1°. So it can find the sensor edges set $\{a, b, c, d\}$ quickly according to the decision parameter E_i , $E_i = R_{\text{max}} - d_i$, $i \in [0, 180]$. The rule of detecting sensor edges is as follows: if $E_i \ge 2r_s$, so the sensor edges are appearance. The rule of detecting the direction of sensor-edges is as follows: suppose the searching direction of the sensor-edges from the left of the robot, if $\min \{E_{i-1}, E_{i+1}\} = E_{i-1}$, so the direction of P_i is left, denoted by L, if min $\{E_{i-1}, E_{i+1}\} = E_{i+1}$, so the direction of P_i is right, denoted by R.

In Figure 5, it is the state curve of E at certain time, the sensor edges set is $\{a, b, c, d\}$, and the direction set is $\{R, L, R, L\}.$

5.1.2. Searching for the Double-Safe-Edges. The edges are based on the sensor as mentioned above. But the robot has its own safe area because of its special shape and kinematics, if it considers the sensor edges only, and the path planning must be failing. So it is necessary to consider the environment information and the robot's safe area together.

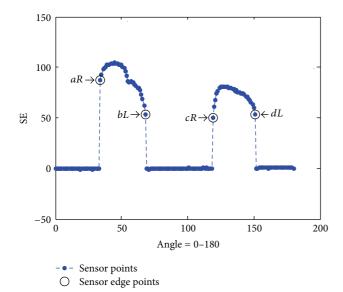


FIGURE 5: The result of the simulation of searching the sensor edges at time t.

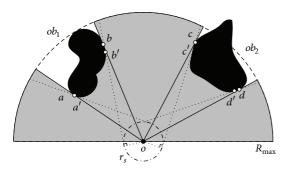


Figure 6: The sketch map of searching the double-safe-edges points at time t.

In this paper the definition of the double-safe-edges has consider the environment information and robot's safe area.

Definition 1 (double-safe-edges (DSE)). When the sensor edges been found, the algorithm will search some points which considering the environment information and robot's safe area, searching start from the sensor-edges according to its directions, the tangent lines which from these points to the robot's safe circle are tangent to the edges of the obstacles at the same time. The robot and obstacle are at the different sides of the tangent line. These points are the set of the double-safe-edges points and these lines are the set of the double-safe-edges.

In Figure 6, point o is the particle of the robot, the set of sensor-edges $\{a, b, c, d\}$, and the set direction $\{R, L, R, L\}$; the radius of the safe circle of the robot is r_s . Figure 7 shows that the state curve of E at certain time, the set of double-safe-edges $\{a', b', c', d'\}$, and the set of direction $\{R, L, R, L\}$ can be found according to the definition of the double-safe-edges. This double-safe-edges information is very important to generate the motion commands in this paper.

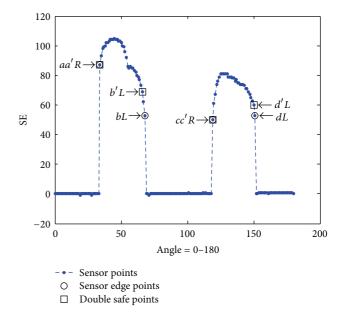


FIGURE 7: The result of the simulation of searching the double-safe-edges points at time t.

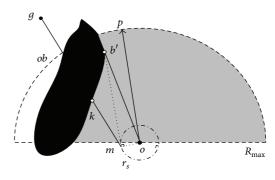


FIGURE 8: The sketch map of S-DSE at time t: DSE points set is $\{b'\}$, safe distance set is $\{mb'\}$, and safe distance set is op.

The success of finding the double-safe-edges means that the environment detected by the sensor in real-time has been analyzed and interpreted efficiently, the environment information has been simplified, the real-time has been increased, and the robot's safe area and the kinematics have been considered, so it will be efficient in generating the motion commands at the next step.

5.2. The Types of the Double-Safe-Edges. There are three types of the double-safe-edges: S-DSE, M-DSE, and Z-DSE.

(1) *S-DSE*. There is only single DSE point after analyzing and interpreting the environment information. In Figure 8, line mg connects the goal g and point m; if k is the interaction point of mg and obstacle, the robot must escape the obstacle. So the robot's safe moving direction is $\angle_s = \angle_{op}$, and the safe

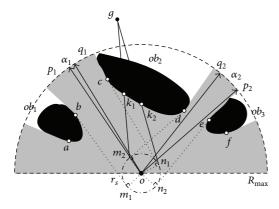


FIGURE 9: The sketch map of S-DSE at time t: DSE points set is $\{a, b, c, d, e, f\}$, safe distance set is $\{m_1b, n_1c, m_2d, n_2e\}$, and safe distance set is $\{op_1, oq_1, op_2, oq_2\}$.

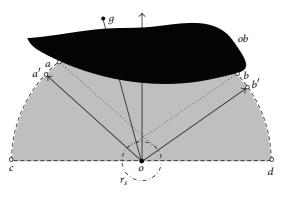


FIGURE 10: The sketch map of S-DSE at time t: DSE points set is R_{max} , and safe distance set is $\{\emptyset\}$, and safe distance set is $\{oa', ob'\}$.

moving distance is $d_{e-e} = mb'$ according to the DSE point b' and line mb', op//mb'.

(2) *M-DSE*. There is more than one DSE point after analyzing and interpreting the environment information. In Figure 9, lines m_2g and n_1g connect target point g and the interaction points m_2g and n_1g which are on the safe circle; if k_1 and k_2 are the interaction points of m_2g , n_1g , and obstacle, the robot must escape the obstacle. So the possible path set is $\{op_1, oq_1, op_2, oq_2\}$ according to the DSE points set $\{a, b, c, d\}$ and DSE lines set $\{m_1b, n_1c, m_2d, n_2e\}$ and α_1 and α_2 are the angle vector op_1 and oq_1 , op_2 and oq_2 .

(3) *Z-DSE*. There is zero DSE point after analyzing and interpreting the environment information. The first situation is that there is no obstacle around the robot, so the robot can move to the target directly; the second situation is that the part or whole of detection area that has been enveloped by the obstacle. For example, In Figure 10, there is part detection area has been enveloped by the obstacle. In this situation, there is zero DSE, so the robot enters the state of cruising in order to find the DSE. The rule of cruising is that if part of detection area cd has been enveloped, so the directions set $\{oa', ob'\}$ will be found according to the points set $\{a, b\}$ and the moving direction oc will be found according to

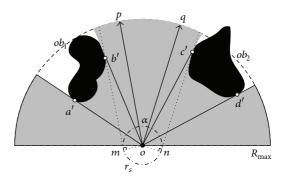


FIGURE 11: The sketch map of the safe distance and direction of the double safe edge points at time t.

the heuristic algorithm. So the robot can move according to this rule and find the DSE at the same time until the DSE appear.

5.3. The Description of the Double-Safe-Edges Free Space. After searching the double-safe-edges, the algorithm has transformed the focus from the environment information to some double-safe-edges points, and these points can be used to generate the robot's motion. We will describe the double-safe-edges free space in this part.

In Figure 11, b' and c' are the double-safe-edges points. Lines ob' and oc' are the distances from the particle to the double-safe-edges point, and points m and n are on the circle of the safe area of the robot, $om = on = r_s$. Lines mb' and nc' are the distances of the tangent lines, $mb' = \sqrt{ob'^2 - om^2}$, $nc' = \sqrt{oc'^2 - on^2}$, and op//mb', oq//nc', op, and oq are the possible planning distances of navigation. So the double-safe-edges free space can be defined by the sector area poq. This area is a free moving space and the robot can select the local target point according to some rule to finish the motion command on time.

6. The Optimization of the Real-Time Local Path Planning Based on the Belief Space

6.1. The Description of the Path Optimization in Real-Time Path Planning. Although the environment information can be detected by the sensor in real-time, the robot did not know the whole environment information; thus, optimizing the whole path in real-time path planning cannot come true. But there are still some important factors to affect the selection of the path in local environment, and we consider the six local planning factors in this paper, the avoidance collision factor R between the robot and the obstacles, the kinematics factor M, the self-safe area factor S, the path length factor L, moving obstacle factor B, and other factors (ocean current, wind speed, and so on) C, and this part will analyse the influence of the R, B, and C in real-time local detection planning.

In Figure 12, the robot's position is o_t at time t, the real-time detection space is W_t , the local target set is G_t , $G_t \subseteq W_t$, and the target is g. It is the sketch mapping of analyzing the optimization in local detection space W_t .

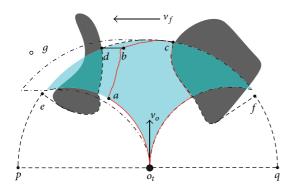


FIGURE 12: The sketch map of the analysis of the optimization in local path planning at time t.

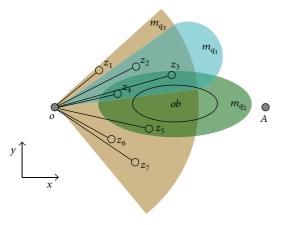


FIGURE 13: The sketch map of the base idea of the belief space at time *t*

Firstly, it can find the edge area (the broken line area) B_t , $B_t \subseteq W_t$, according to the factor R, and B_t is the selected area of G_t ; secondly, supposing that the robot's kinematics is the gyration movement, so the reachable area (the undertone area) M_t , $M_t \subseteq W_t$ according to the factor M, and finally, these two factors can makes the local goal selection area smaller. Supporting the other factor C can make the robot have the speed v_f , and this speed can make the displacement s, $s = v_f$. So it can find the reachable area (the real line area) F_t , $F_t \subset (B_t \cap M_t) \subset W_t$, at time according to the factors. This area will be smaller when the consideration factors increase, so the analysis treating and fusing these factors is a necessary method to optimize the path in real-time local detection path planning.

6.2. The Original Idea of the Belief Space in Local Target Selection. In Figure 13, it is the selection local target point situation in which the robot O must reach the target point A according to some selection rules and the local target point set is $Z = \{z_1, z_2, \ldots, z_7\}$ and the selection rules set is $Q = \{q_1, q_2, \ldots, q_j\}$, so it needs to fuse these selection rules in order to find the optimization local target point.

We note that the selection state space is $H = \{null, select, delect, unknow\}$, described by $H = \{\emptyset, S, R, U\}$, $U \neq \emptyset$. For each $z_i \in Z$, the selection state space $c_i \in H$ is known and

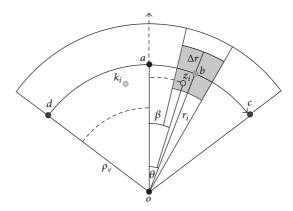


FIGURE 14: The sketch map of the belief function distribution of the sensor detection at time t.

the influence from q_j to z_i can be defined by the BBA in the selection state space H, denoted by $m_{q_1}^H(z_i)$, so the BBA set in H is $M = \{m_{q_1}^H(z_1), m_{q_1}^H(z_2), \ldots, m_{q_1}^H(z_1)\}$. Three gray areas are the area of the BBA set $\{m_{q_1}^H, m_{q_2}^H, m_{q_3}^H\}$, denoted by $\{X_{m_{q_1}}^H, X_{m_{q_2}}^H, X_{m_{q_3}}^H\}$, and these are also the descriptions of the obstacle information, kinematics, and the path length factors, so the belief space can be defined, denoted by $X_m^H = X_{m_{q_1}}^H \cup X_{m_{q_2}}^H \cup X_{m_{q_3}}^H$, the local target points' belief can be defined by the belief functions, and the belief functions can be fused according to the TBM rules. The definition of the fusing is

$$m^{H}(z_{1}) = m_{q3}^{H}(z_{1}),$$

$$m^{H}(z_{2}) = m_{q1}^{H}(z_{2}) \bigcirc m_{q3}^{H}(z_{2}),$$

$$m^{H}(z_{3}) = m_{q1}^{H}(z_{3}) \bigcirc m_{q2}^{H}(z_{3}) \bigcirc m_{q3}^{H}(z_{3}),$$

$$m^{H}(z_{4}) = m_{q1}^{H}(z_{4}) \bigcirc m_{q2}^{H}(z_{4}) \bigcirc m_{q3}^{H}(z_{4}), \qquad (12)$$

$$m^{H}(z_{5}) = m_{q2}^{H}(z_{5}) \bigcirc m_{q3}^{H}(z_{5}),$$

$$m^{H}(z_{6}) = m_{q3}^{H}(z_{6}),$$

$$m^{H}(z_{1}) = m_{q3}^{H}(z_{7}).$$

The selection of the local target point must satisfy every belief function distribution at the same time, so some local target points can be deleted and the set has been changed to $\{m^H(z_3), m^H(z_4)\}$, and the optimization local target point Z_3 can be found if the fusing belief distribution is $m^H(z_3) > m^H(z_4)$; thereby the selection of local target point at certain time in belief space has been finished and the aim of optimization came true.

6.3. The Method of Making the Belief Function

6.3.1. The Belief Function Distribution of the Sensor Detection. As the uncertainty model has been described, we further discuss the belief function distribution in Figure 14. The angle

of detection is 90°, the direction of oa is the coordinate axes, and the right is positive. The coordinate of position is (r_i, v) , and from (1)–(4), the detection distance is r_i , the angle between b and oa is θ , the uncertainty area because of the detecting of b is defined by the $\gamma_b = 12.5^\circ$ sector and the $2 \cdot \Delta r = R/4$ width approach to the detection distance, and this area is the gray area in Figure 14. The point z_i is in this area and the angle between z_i and oa is β , so the angle between z_i and b is $\alpha = |\theta - \beta|$, and the detection area uncertainty function is

$$f_{a}(\theta) = \begin{cases} D(\theta) & 0 \le |\theta| \le 45^{\circ} \\ 0 & |\theta| > 45^{\circ}, \end{cases}$$

$$g_{a}(\rho) = 1 - \frac{1 + \tanh(2|\rho - \rho_{\nu}|)}{2}, \qquad (13)$$

$$\left(0 \le \rho \le R, \ \rho_{\nu} = \frac{R}{2}\right).$$

The detection position uncertainty function is

$$f_{b}(\alpha) = \begin{cases} D(\alpha) & 0 \le |\alpha| \le 45^{\circ} \\ 0 & |\alpha| > 45^{\circ}, \end{cases}$$

$$g_{b}(\rho) = 1 - \frac{1 + \tanh(2|\rho - \rho_{\nu}|)}{2}, \qquad (14)$$

$$\left(-\Delta r \le \rho \le \Delta r, \ \rho_{\nu} = \pm \frac{\Delta r}{2}\right).$$

According to the analysis mentioned above, the detection area uncertainty distribution is from the coordinate axes to the opposition side, and the detection position uncertainty distribution is from $\pm 12.5^{\circ}$ sector to the $\pm \Delta r$ distance area. So the point k_i in the detection area plausibility function is defined as

$$\operatorname{pl}_{o}^{H}\left[x_{k}\right]\left(T\right) = f_{ak}\left(\theta\right) g_{ak}\left(\rho\right). \tag{15}$$

The point z_i in detection position plausibility function is defined as

$$\operatorname{pl}_{ob}^{H}\left[x_{z}\right]\left(T\right)=f_{as}\left(\theta\right)g_{as}\left(\rho\right)f_{bz}\left(\alpha\right)g_{bz}\left(\alpha\right).\tag{16}$$

So the position z_i "occupy" and "empty" plausibility function can be defined as

$$\begin{aligned}
&\operatorname{pl}_{ob}^{H}\left[x_{z}\right]\left(T,o\right) = f_{az}\left(\theta\right) f_{az}\left(\alpha\right) g_{bz}\left(\alpha\right) f_{o}\left(\rho,r_{i}\right), \\
&\operatorname{pl}_{ob}^{H}\left[x_{z}\right]\left(T,e\right) = f_{az}\left(\theta\right) f_{az}\left(\alpha\right) g_{bz}\left(\alpha\right) f_{e}\left(\rho,r_{i}\right), \\
&\operatorname{pl}_{ob}^{H}\left[x_{z}\right]\left(T,\left(o,e\right)\right) = 1 - \prod_{h_{i} \in \left(o,e\right)} \left(1 - l\left(h_{i} \mid x_{z}\right)\right).
\end{aligned} \tag{17}$$

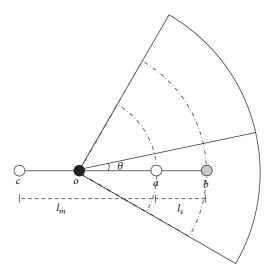


FIGURE 15: The sketch map of the belief function distribution of the safe distance at time t.

Thus, the BBA of the "occupy" and "empty" in TBM can be defined as

$$m_{ob}^{H}(o) = \prod_{h_{i} \in o} l(h_{i} \mid x_{z}) \prod_{h_{i} \in \overline{o}} l(h_{i} \mid x_{z}),$$

$$m_{ob}^{H}(e) = \prod_{h_{i} \in e} l(h_{i} \mid x_{z}) \prod_{h_{i} \in \overline{e}} l(h_{i} \mid x_{z}),$$

$$m_{ob}^{H}(o, e) = \prod_{h_{i} \in (o, e)} l(h_{i} \mid x_{z}) \prod_{h_{i} \in \overline{(0, e)}} l(h_{i} \mid x_{z}).$$
(18)

This BBA space is defined in the belief space. They are the belief functions distribution according to the base idea of the belief space, denoted by $\{X_{ob}(i)\}$.

6.3.2. The Belief Function Distribution of the Safe Distance to the Obstacle. Figure 15 shows the belief function distribution of the safe distance to the obstacle, and point o is the particle of the robot, point b is on the edge of the obstacle, the shortest safe distance is l_s , and it is the radius of the self-safe area. In a real environment, when the robot enters into a specified distance (alertness distance) l_m , it needs to calculate the dangerous degree of collision. So the safe distance function can be given as

$$f_t(\rho) = \frac{\rho - l_s}{l_m} \quad (l_s < \rho < l_m). \tag{19}$$

Then the "safe" and "dangerous" plausibility function can be defined as

$$pl_{am}^{H} [x_{t}] (T, s) = pl_{o}^{H} [x_{b}] (T) f_{t} (\rho),$$

$$pl_{am}^{H} [x_{t}] (T, d) = pl_{o}^{H} [x_{b}] (T) (1 - f_{t} (\rho)),$$

$$pl_{am}^{H} [x_{t}] (T, (s, d)) = 1 - \prod_{h_{t} \in (s, d)} (1 - l (h_{i} | x_{t})).$$
(20)

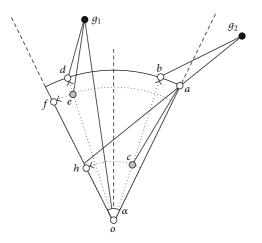


FIGURE 16: The sketch map of the belief function distribution of the optimization the path at time t.

Finally, the BBA of the "safe" and "dangerous" can be defined as

$$m_{am}^{H} [x_{t}] (s) = \prod_{h_{i} \in s} l(h_{i} | x_{t}) \prod_{h_{i} \in \overline{s}} (1 - l(h_{i} | x_{t})),$$

$$m_{am}^{H} [x_{t}] (d) = \prod_{h_{i} \in d} l(h_{i} | x_{t}) \prod_{h_{i} \in \overline{d}} (1 - l(h_{i} | x_{t})),$$

$$m_{am}^{H} [x_{t}] (s, d) = \prod_{h_{i} \in (s, d)} l(h_{i} | x_{t}) \prod_{h_{i} \in (\overline{s}, \overline{d})} (1 - l(h_{i} | x_{t})).$$
(21)

All these BBA spaces are defined in the belief space. They are the belief functions distribution according to the base idea of the belief space, denoted by $\{X_{am}(i)\}$.

So other factors can be defined and described in the belief space, it is the base step of fusing these factors to find the optimization local target point.

- 6.3.3. The Belief Function Distribution of the Optimization the Path. In Figure 16, we give the distribution of the path belief function at one movement space. Point o is the particle of the robot, the detection distance is R, and the angle of the free space is α ; thus there are two definitions of the selection of the local goal e and e for optimizing the path.
 - (1) As the global target g_1 is in a free space at this time, $l_g = og_1, l_g > R, l_g = oe + eg_1l_d = R + dg_1l_f = of + fg_1$, so the path proportion function in two ways is

$$f_{l_1}(l_e) = \frac{l_f - l_e}{l_f - l_g}.$$
 (22)

The direction of the distribution \widehat{ef} is

$$f_{l_{1}}(l_{e}) = \begin{cases} 1 & l_{e} = l_{g} \\ 0 & l_{e} = l_{f}, \end{cases}$$

$$f_{l_{2}}(l_{e}) = \frac{l_{d} - l_{e}}{l_{d} - l_{a}}.$$
(23)

The direction is *oe*:

$$f_{l_2}(l_e) = \begin{cases} 1 & l_e = l_g \\ 0 & l_e = l_d. \end{cases}$$
 (24)

So the path proportion function is

$$f_l(l_e) = f_{l_1}(l_e) f_{l_2}(l_e).$$
 (25)

(2) As the global target g_1 is out of a free space at this time,

$$l_{a} = oa + og_{2},$$

$$l_{c} = \begin{cases} oc + ca + ag_{2} & \text{in } a \\ oh + hg_{2} & \text{out } a, \end{cases}$$

$$l_{b} = ob + bg_{2},$$

$$l_{h} = \begin{cases} oh + ha + ag_{2} & \text{in } a \\ oc + cg_{2} & \text{out } a, \end{cases}$$

$$(26)$$

so the path proportion function in two ways is

$$f_{l_1}(l_c) = \frac{l_h - l_c}{l_h - l_a}.$$
 (27)

The direction of the distribution is \widehat{ch} ; then

$$f_{l_1}(l_c) = \begin{cases} 1 & l_c = l_a \\ 0 & l_c = l_h, \end{cases}$$

$$f_{l_2}(l_c) = \frac{l_b - l_c}{l_b - l_c}.$$
(28)

The direction is *ob*, so

$$f_{l_2}(l_c) = \begin{cases} 1 & l_c = l_a \\ 0 & l_c = l_b \end{cases}$$
 (29)

So the path proportion function is

$$f_l(l_c) = f_{l_1}(l_c) f_{l_2}(l_c).$$
 (30)

So the path "optimization" and "nonoptimization" plausibility function can be defined as

$$pl_{dis}^{H} [x_{e,c}] (T, \omega) = pl_{o}^{H} [x_{e,c}] (T) f_{l} (l_{e,c}),$$

$$pl_{dis}^{H} [x_{e,c}] (T, f) = pl_{o}^{H} [x_{e,c}] (T) (1 - f_{l} (l_{e,c})),$$

$$pl_{dis}^{H} [x_{e,c}] (T, (\omega, f)) = 1 - \prod_{h_{i} \in (\omega, f)} (1 - l (h_{i} | x_{e,c})).$$
(31)

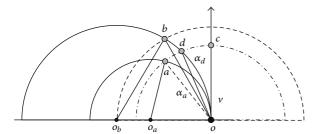


FIGURE 17: The sketch map of the belief function distribution of the dynamics of the robot at time t.

As the same way, the BBA of the "optimization" and "nonoptimization" in TBM can be defined as

$$\begin{split} m_{\text{dis}}^{H} \left[x_{e,c} \right] (\omega) &= \prod_{h_{i} \in \omega} l \left(h_{i} \mid x_{e,c} \right) \prod_{h_{i} \in \overline{\omega}} \left(1 - l \left(h_{i} \mid x_{e,c} \right) \right), \\ m_{\text{dis}}^{H} \left[x_{e,c} \right] (f) &= \prod_{h_{i} \in f} l \left(h_{i} \mid x_{e,c} \right) \prod_{h_{i} \in \overline{f}} \left(1 - l \left(h_{i} \mid x_{e,c} \right) \right), \\ m_{\text{dis}}^{H} \left[x_{e,c} \right] (\omega, f) \\ &= \prod_{h_{i} \in \left(\omega, f \right)} l \left(h_{i} \mid x_{e,c} \right) \prod_{h_{i} \in \overline{\left(\omega, f \right)}} \left(1 - l \left(h_{i} \mid x_{e,c} \right) \right). \end{split}$$

$$(32)$$

All these BBA spaces are defined in the belief space. They are the belief functions distribution according to the base idea of the belief space, denoted by $\{X_{\rm dis}(i)\}$.

6.3.4. The Belief Function Distribution of the Dynamics of the Robot. Figure 17 shows the distribution of the dynamics of the robot at one movement space, point o is the particle of the robot, and the speed of the robot is v; supposing the movement character is the nonglide movement, so the track of the movement is one part of the circle, the position of the local target point is d, the radius of the track is $r_b = o_b b$, the position b is the max distance that the robot can reach at certain time, and the min movement radius is $r_a = o_a b$, so the reached proportion function has two directions.

(1) Consider the reached proportion functions in the same track radius:

$$f_{t-dg}(l_{od}) = \frac{l_{ob} - l_{od}}{l_{ob}} \quad (0 \le l_{od} \le l_{ob}).$$
 (33)

(2) Consider the reached proportion functions in the same detection area:

$$f_{t-dg}\left(\alpha_{d}\right) = \frac{\alpha_{a} - \alpha_{d}}{\alpha_{a}} \quad \left(0 \le \alpha_{d} \le \alpha_{a}\right). \tag{34}$$

So the reached proportion function at certain detection time at local target point *d* is

$$f_{da}\left(l_{od}, \alpha_{d}\right) = f_{t-da}\left(l_{od}\right) f_{t-da}\left(\alpha_{d}\right). \tag{35}$$

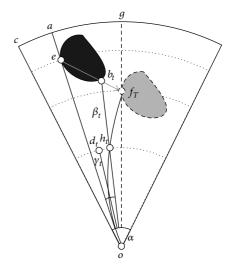


FIGURE 18: The sketch map of the belief function distribution of the escaping the movement obstacle at time t.

So the path "reach" and "unreach" plausibility function can be defined as

$$pl_{dg}^{H}[x_{d}](T,s) = pl_{o}^{H}[x_{d}](T) f_{dg}(l_{od},\alpha_{d}),$$

$$pl_{dg}^{H}[x_{d}](T,s) = pl_{o}^{H}[x_{d}](T) \left(1 - f_{dg}(l_{od},\alpha_{d})\right),$$

$$pl_{dg}^{H}[x_{d}](T,(s,h)) = 1 - \prod_{h_{i} \in (s,h)} \left(1 - l(h_{i} \mid x_{d})\right).$$
(36)

Then the BBA of the "reach" and "unreach" in TBM can be defined as

$$m_{dg}^{H} [x_{d}] (s) = \prod_{h_{i} \in s} l(h_{i} \mid x_{d}) \prod_{h_{i} \in \overline{s}} (1 - l(h_{i} \mid x_{d})),$$

$$m_{dg}^{H} [x_{d}] (h) = \prod_{h_{i} \in h} l(h_{i} \mid x_{d}) \prod_{h_{i} \in \overline{h}} (1 - l(h_{i} \mid x_{d})),$$

$$m_{dg}^{H} [x_{d}] (s, h)$$

$$= \prod_{h_{i} \in (s, h)} l(h_{i} \mid x_{d}) \prod_{h_{i} \in \overline{(s, h)}} (1 - l(h_{i} \mid x_{d})).$$
(37)

All these BBA spaces are defined in the belief space. They are the belief functions distribution according to the base idea of the belief space, denoted by $\{X_{dq}(i)\}$.

6.3.5. The Belief Function Distribution of the Escaping the Movement Obstacle. Figure 18 gives the distribution of the path belief function at one movement space, point o is the particle of the robot, the detection distance is R, the angle of the free space is α , the one side speed of the movement obstacle is v, and the belief function distribution of the movement obstacle in the free movement space can be defined.

The one side edge point of the obstacle ob is e, and this point can reach the position f_t after time T, so the double-safe-edges free space will be changed from coa to cob, and

the position of the robot can reach the position h_t after time T. If the position of the robot is h_t after time T, the angle is β_t of the eoh_t and the angle is $\gamma_t t$ of the eoh_t , so the it can describe the belief function distribution of the escaping the movement obstacle.

The collisions function of the robot which moves from the position o to the position f is

$$f_{\text{mov}}(\gamma_t) = \frac{\beta_t - \gamma_t}{\beta_t} \quad (0 < \gamma_t < \beta_t). \tag{38}$$

So the path "safe" and "collisions" plausibility function can be defined as

$$pl_{\text{mov}}^{H}[x_{t}](T, s) = pl_{o}^{H}[x_{t}](T) f_{\text{mov}}(\gamma_{t}),$$

$$pl_{\text{mov}}^{H}[x_{t}](T, h) = pl_{o}^{H}[x_{d}](T) (1 - f_{\text{mov}}(\gamma_{t})),$$

$$pl_{\text{mov}}^{H}[x_{t}](T, (s, h)) = 1 - \prod_{h_{i} \in (s, h)} (1 - l(h_{i} \mid x_{t})).$$
(39)

Then, the BBA of the "safe" and "collisions" in TBM can be defined as

$$m_{\text{mov}}^{H} [x_{t}] (s) = \prod_{h_{i} \in s} l(h_{i} \mid x_{t}) \prod_{h_{i} \in s} (1 - l(h_{i} \mid x_{t})),$$

$$m_{\text{mov}}^{H} [x_{t}] (h) = \prod_{h_{i} \in h} l(h_{i} \mid x_{t}) \prod_{h_{i} \in h} (1 - l(h_{i} \mid x_{t})),$$

$$m_{\text{mov}}^{H} [x_{t}] (s, h) = \prod_{h_{i} \in (s, h)} l(h_{i} \mid x_{t}) \prod_{h_{i} \in (s, h)} (1 - l(h_{i} \mid x_{t})).$$

$$(40)$$

All these BBA spaces are defined in the belief space. They are the belief functions distribution according to the base idea of the belief space, denoted by $\{X_{\text{mov}}(i)\}$.

6.4. The Model of Fusing the Correlation Factors in Belief Space. Suppose that, at any given time, the local target points set is $Z=\{z_1,z_2,\ldots,z_7\}$, the correlation factors set is $Q=\{q_1,q_2,\ldots,q_6\}$, and the selection state space is $H=\{\phi,S,R,U\}$, $U\neq\phi$. For each $z_i\in Z$, the BBA set in the selection state space H is $M=\{m_{q1}^H(z_i),m_{q2}^H(z_i),\ldots,m_{qj}^H(z_i)\}$, so the belief space is $X=\{X_{m_{q1}},X_{m_{q2}},X_{m_{q3}}\}$, and this part will combine the BBA in the belief space X to optimize the selection of the local target point.

6.4.1. The Structure of the Local Target Point Belief Space. Figure 19 shows three proposition spaces $(\Omega, Z)(\Omega, Q)(\Omega, H)$ and a decision-making function; supposing that Λ_1 is a multimapping from Q to Z, Λ_2 is a multimapping from H to Q; Λ_1 and Λ_2 compose the "credal" level and the decision-making function composes the "pignistic" level in TBM.

In "credal" level each local target point has its own factors, so it has to filter the fusing local target point belief space to make sure of the whole factors at the same time. Each factor has its own belief space, the whole factors BBA depend on the selection state space of the factors, and this chain structure of the local target point belief space can transform the influence

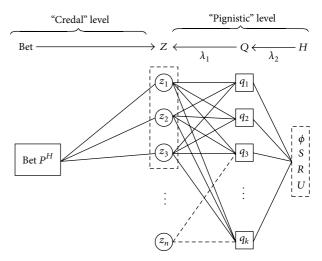


Figure 19: The structure of selecting the local target point belief space at time t.

of the factors to the BBA function in the belief space. In the "pignistic" level it denotes the influence degrees of the factors using the probability functions; it is the final form of selecting the local target point.

6.4.2. The Fusing Process of the Belief Space. It needs to fuse the belief space when the factors have been described to the BBA functions in the belief space; the details of the process at certain times are as follows.

Step 1. The local target points set is selected according to the double-safe-edges free space, denoted as Z, and the correlation influence factors are ascertained at certain time, denoted as Q.

Step 2. The BBA of the correlation influence factors set can be calculated, denoted as M, and the belief space X can be made according to the base idea of the belief space in local goal selection.

Step 3. In belief space X, the BBA set M can be combined according to the elements of the selection state space H, so the belief space X^H including M^H in the same state space can be made.

Step 4. The M^H in X^H can be transformed to the probability distribution Bet $P^H(A)$. For all $A \subseteq H$, so the optimization local target point can be selected according to the Bet $P^H(A)$.

7. The Simulation of the Local Target Point in Belief Space

In a real-time path planning process, the environment information requires to be detected at each time, so the simulation of the local target point in belief space should satisfy this character. In this paper, the maps of simulation have been made by the .bmp pictures beforehand, and the algorithm of the local target point in belief space has been written



FIGURE 20: The simulation of the path planning in special environment which has lots of edges and corners.

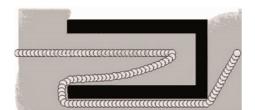


FIGURE 21: The simulation of the path planning in U-shape environment which is always called dead area.

in the software by the program, so in the process of the simulation it shows the start point and the target point, the obstacles on the map, the particle and the self-safe area, the lines of detecting, the position of the robot, and the path.

There are about two different types of simulation that will be shown in this paper to prove the feasibility of the double-safe-edges space and the idea of selecting the local target point in belief space. Simulation I is the simulation of double-safe-edges space in two conditions; it will show the special map which can show the characters of the double-safe-edges space and the death area (U shape) which can show its flexible ability. Simulation II is the simulation of efficiencies of the selecting the local target point in belief space, and it will show the changes of belief in the process of the detecting path planning.

Simulation I. The following two special maps show the simulation results of testing the double-safe-edges space. Figure 20 shows the special environment which has lots of edges and corners. In this environment, the sensor will be able to easily detect the edges points of the obstacles, so it is easy to transform these sensor edges points to the double-safe-edges points, and the double-safe-edges free space can be built each time, so the local target point will be found in real-time, and the robot will move to this position. From the simulation we can see that the method of double-safe-edges space has found the target point successfully and also keeps the path smoothness. Figure 21 shows the special environment which is called death area (U shape). Because of this special environment, when a robot enters this environment, there are zero obstacle edges that can be found, so it is hard to find the right local target point to escape from the obstacle. In the double-safe-edges space, this situation is the Z-DSE type, the robot can move along with one side of the obstacle until it finds the new edges of the obstacle. From the simulation we

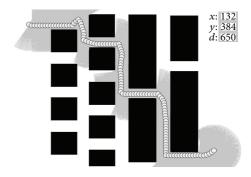


FIGURE 22: The simulation of the path in situation A for distance detecting.

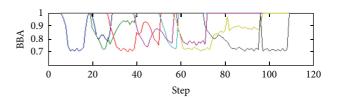


FIGURE 23: The BBA state in the process of situation A.

can see that this method can escape the death area and reach the goal successfully.

So this simulation has proved that the method of doublesafe-edges space is a feasible method to describe the real-time detecting environment.

Simulation II. This simulation results are shown in the Figures 22 and 23. Different detection areas will make the decision belief different in belief space. Figure 22 is the situation of special A. In this saturation well the maximum detection distance is shorter than the length of the right-angle line. So in this environment the delectation ability of the sensor is low, and from the simulation we can see that the robot can reach the target point after 115 steps. Figure 23 shows the belief of 7 correlation factors of each point of these 115 points at each step, and we can see that the belief is higher the line of 0.7 belief; it means the selection of each local target point in each step shows the well belief degree.

Figure 24 is the situation of special B. In this saturation the maximum detection distance is longer than the length of the right-angle line. So in this environment the delectation ability of the sensor is high, and from the simulation we can see that the robot can reach the target point after 126 steps. Figure 25 shows the belief 7 correlation factors of each point of these 126 points at each step, and we can see that the belief is higher than the line of 0.7 belief; it means that the selection of each local target point in each step shows the well belief degree. So these simulations have proved that this belief space algorithm has the well effect.

8. Conclusions

As can be seen from literature works that there are a lot of methods for robot path planning, but most of them do

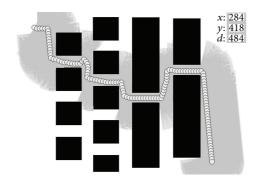


FIGURE 24: The simulation of the path in situation B for distance detecting.

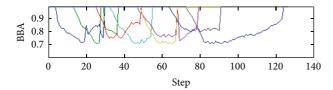


FIGURE 25: The BBA state in the process of situation B.

not work well in a complex real-time environment. In this paper, we are making some efforts for solving two problems in real-time detecting path planning: one is the expression the environment, and the second is how to optimize the path in local path planning. The double-safe-edges space has been presented to express the environment, and the simulation has proved the feasibility of this approach. Then, the belief space has fused the factors and the uncertainty of detection in real-time detecting path planning successfully, the simulation of the belief space is well running. So these achievements will help the researching of the real-time path planning effectively. Certainly, there are a lot of tough jobs such as the details of the system structure, or how to control the robot accurately. All these considerations should be further extended in our future work.

Acknowledgments

This work was supported by the National Natural Science Foundation of China (nos. 51379049 and 51109045) and the Fundamental Research Funds for the Central Universities of China (HEUCFX41302).

References

- [1] G. Ulivi, G. Oriolo, and M. Vendittelli, "Real-time map building and navigation for autonomous robots in unknown environments," *IEEE Transactions on Systems, Man, and Cybernetics B*, vol. 28, no. 3, pp. 316–333, 1998.
- [2] L. Kleeman and K. S. Chong, "Mobile-robot map building from an advanced sonar array and accurate odometry," *International Journal of Robotics Research*, vol. 18, no. 1, pp. 20–36, 1999.
- [3] A. Buecken and S. Thrun, "Integrating grid-based and topological maps for mobile robot navigation," in *Proceedings of*

- the 13th National Conference on Artificial Intelligence, pp. 944–950, AAAI, August 1996.
- [4] H. W. Jo, J. H. Park, G. T. Kim, and J. T. Lim, "On completeness of scalable path planning for multiple robots using graph with cycles," *International Journal of Innovative Computing, Information and Control*, vol. 9, no. 10, pp. 4167–4179, 2013.
- [5] H. P. Moravec and A. Elfes, "High resolution maps from wide angle sonar," in *Proceeding of IEEE International Conference on Robotics and Automation*, pp. 116–121, 1985.
- [6] E. Ramasso, M. Rombaut, and D. Pellerin, "State filtering and change detection using TBM conflict application to human action recognition in athletics videos," *IEEE Transactions on Circuits and Systems for Video Technology*, vol. 17, no. 7, pp. 944–949, 2007.
- [7] G. Ulivi, M. Poloni, and M. Vendittelli, "Fuzzy logic and autonomous vehicles: experiments in ultrasonic vision," *Fuzzy Sets and Systems*, vol. 69, no. 1, pp. 15–27, 1995.
- [8] S. X. Yang and C. M. Luo, "A bioinspired neural network for realtime concurrent map building and complete coverage robot navigation in unknown environments," *IEEE Transactions on Neural Networks*, vol. 19, no. 7, pp. 1279–1298, 2008.
- [9] F. C. J. Allaire, M. Tarbouchi, G. Labonté, and G. Fusina, "FPGA implementation of genetic algorithm for UAV real-time path planning," *Journal of Intelligent and Robotic Systems*, vol. 54, no. 1–3, pp. 495–510, 2009.
- [10] H. Lu, R. Y. Niu, J. Liu, and Z. Zhu, "A chaotic non-dominated sorting genetic algorithm for the multi-objective automatic test task scheduling problem," *Applied Soft Computing*, vol. 13, no. 5, pp. 2790–2802, 2013.
- [11] C.-C. Lin, "Hierarchical path planning for manipulators based on genetic algorithm with non-random initial population," *International Journal of Innovative Computing, Information and Control*, vol. 8, no. 3, pp. 1773–1786, 2012.
- [12] J. Yu and V. Kroumov, "3D path planning for mobile robots using annealing neural network," in *Proceedings of the IEEE International Conference on Networking, Sensing and Control (ICNSC '09)*, pp. 130–135, March 2009.
- [13] M. Dorigo, V. Maniezzo, and A. Colorni, "Ant system: optimization by a colony of cooperating agents," *IEEE Transactions on Systems, Man, and Cybernetics B*, vol. 26, no. 1, pp. 29–41, 1996.
- [14] D. Mercier, É. Lefèvre, and D. Jolly, "Object association with belief functions, an application with vehicles," *Information Sciences*, vol. 181, no. 24, pp. 5485–5500, 2011.
- [15] W. Yaonan, Y. Yimin, Y. Xiaofang et al., "Autonomous mobile robot navigation system designed in dynamic environment based on transferable belief model," *Measurement*, vol. 44, no. 8, pp. 1389–1405, 2011.
- [16] B. Marhic, L. Delahoche, C. Solau, A. M. Jolly-Desodt, and V. Ricquebourg, "An evidential approach for detection of abnormal behaviour in the presence of unreliable sensors," *Information Fusion*, vol. 13, no. 2, pp. 146–160, 2012.
- [17] G. Chalkiadakis and C. Boutilier, "Sequentially optimal repeated coalition formation under uncertainty," *Autonomous Agents and Multi-Agent Systems*, vol. 24, no. 3, pp. 441–484, 2012.
- [18] R. Kuc, "Pseudoamplitude scan sonar maps," *IEEE Transactions on Robotics and Automation*, vol. 17, no. 5, pp. 767–770, 2001.
- [19] G. Ulivi, G. Oriolo, and M. Vendittelli, "Fuzzy maps: a new tool for mobile robot perception and planning," *Journal of Robotic Systems*, vol. 14, no. 3, pp. 179–197, 1997.
- 20] M. Vendittelli, F. Gambino, and G. Ulivi, "The Transferable belief model in ultrasonic map building," in *Proceedings of*

- the 6th IEEE International Conference on Fussy Systems, vol. 3, pp. 601–608, July 1997.
- [21] A.-S. Capelle-Laizé, C. Fernandez-Maloigne, and O. Colot, "TBM for color image processing: a quantization algorithm," in *Proceedings of the 9th International Conference on Information Fusion (FUSION '06)*, pp. 1–7, July 2006.
- [22] C. Franois and J. Allaire, "Data fusion in the transferable belief model," in *Proceedings of the 3rd International Conference on Information Fusion*, vol. 1, pp. 21–33, 2000.
- [23] P. Smets, "Managing deceitful reports with the transferable belief model," in *Proceedings of the 8th International Conference on Information Fusion (FUSION '05)*, vol. 2, pp. 893–899, July 2005.
- [24] P. Smets and F. Delmotte, "Target identification based on the transferable belief model interpretation of Dempster-Shafer model," *IEEE Transactions on Systems, Man, and Cybernetics A*, vol. 34, no. 4, pp. 457–471, 2004.
- [25] P. Smets, A model mathematical-satistical stimulating the process of diagnostic medical [Ph.D. dissertation], University Libre Bruxelles, Bruxelles, Belgium, 1978.

Hindawi Publishing Corporation Abstract and Applied Analysis Volume 2013, Article ID 387890, 7 pages http://dx.doi.org/10.1155/2013/387890

Research Article

Robust Backstepping Control for Cold Rolling Main Drive System with Nonlinear Uncertainties

Xu Yang,^{1,2} Kai-xiang Peng,¹ and Chao-nan Tong¹

- ¹ Key Laboratory of Advanced Control of Iron and Steel Process (Ministry of Education), School of Automation and Electrical Engineering, University of Science and Technology Beijing, Beijing 100083, China
- ² State Key Laboratory of Mechanical System and Vibration, Shanghai Jiao Tong University, Shanghai 200240, China

Correspondence should be addressed to Kai-xiang Peng; kaixiang@ustb.edu.cn

Received 13 November 2013; Accepted 4 December 2013

Academic Editor: Ming Liu

Copyright © 2013 Xu Yang et al. This is an open access article distributed under the Creative Commons Attribution License, which permits unrestricted use, distribution, and reproduction in any medium, provided the original work is properly cited.

The nonlinear model of main drive system in cold rolling process, which considers the influence with parameter uncertainties such as clearance and variable friction coefficient, as well as external disturbance by roll eccentricity and variation of strip material quality, is built. By transformation, the lower triangular structure form of main drive system is obtained. The backstepping algorithm based on signal compensation is proposed to design a linear time-invariant (LTI) robust controller, including a nominal controller and a robust compensator. A comparison with PI controller shows that the controller has better disturbance attenuation performance and tracking behaviors. Meanwhile, according to its LTI characteristic, the robust controller can be realized easily; therefore it is also appropriated to high speed dynamic rolling process.

1. Introduction

The main drive system in cold rolling mill, as a high accuracy mechanical-electrical system, plays an important role in high speed stable rolling operation. However, the torsional vibration which usually occurs in main drive system has been recognized as a major restriction to the increase of strip yield and improvement of product quality [1, 2]. It may lead to large gauge variations [3] of strip as well as the instability of rolling speed and can even cause damage to the mechanical equipment of mill stands [4, 5]. As a matter of fact, the phenomenon of vibration exists generally in rolling process, but the time and location of where it happens cannot be easily predicted. Moreover, there are many factors that can cause the occurrence of torsional vibration, such as unstable state of friction in rolling deformation zone [6], asynchronous working between upper and lower work rolls [7], defects or failure in reduction gear box [8], influence of high order electrical harmonics excitation [9], and so on. Thus, all of these factors will cause a huge difficulty to operators on vibration-related fault detection [10-13] and suppression [14].

In order to analyze and control torsional vibration, many researchers have done a lot of work in studying the chatter mechanism. Although these mechanisms, such as negative damping effect and model matching have been identified after years of research, no clear and definite theory of their mechanics has emerged. One of the most important factors responsible for this situation is the oversimplified by neglecting nonlinearities in mechanical-electrical system, then the models can hardly be suitable for the vibration mechanism and the further control algorithms designation. Variable stiffness due to clearance in gearbox and friction coefficient should me most concerned among these nonlinearities, since the existence of nonlinear friction and stiffness terms have become the obstacle to modifying system dynamic characteristics

In addition to studying vibration mechanism in main drive system with the consideration of nonlinearity, the control strategy is also a key point in vibration suppression. With the higher demand on speed and accuracy in modern cold rolling process, the traditional control method, such as PID, has not been qualified to manage those vibration

pheromones, and some advanced control algorithms [15, 16] are not suitable to deal with the problem of model nonlinearity in rolling process. Thus, a nonlinear control algorithm is necessary to deal with this situation.

One of the recent breakthroughs in nonlinear control theory is the introduction of backstepping algorithms. The relative-degree constraints over parameterization and growth condition are removed by allowing the controlled plant to be nonlinearly dependent on structure uncertainty, such as unknown parameters or unmodeled time-varying disturbances [17-20]. Although there are many advantages in backstepping algorithm, the "explosion of complexity" problem [18, 21], caused by repeated differentiation, cannot be ignored due to its increase in calculation complexity, therefore making severe time delay on control output, which can directly influence the operation performance in cold rolling mills. In this paper, a more general case is discussed, where uncertainties are not required to satisfy matching condition or to be smooth, and then a robust control method based backstepping algorithm is introduced. The feature of this approach is that the designed controller is an LTI one, so the controller can be easily realized, and then the "explosion of complexity"

The major objective pursued in this paper is to formulate a reasonable nonlinear model with parameter uncertainty and external disturbance of cold rolling main drive system, including variable stiffness by clearance, changeable friction coefficient due to relative speed between work roll and strip, and external disturbance by load variation under dynamic working conditions. Furthermore, after proper model transformation, a robust backstepping control algorithm is stated. Finally, within actual industrial data, simulation result shows the good performance and tracking behaviors of this proposed approach, even under the influence of parameter uncertainties and external disturbances.

2. Problem Description

2.1. Mathematical Model of Main Drive System. Based on our former research, the main drive system of cold rolling mill can be defined as a "Mass-Spring System", including motor, shaft, gearbox, roll, and so on. Reasonable simplification is necessary for a better analysis of the dynamic behaviors in rolling system, which makes two parts of main drive system, mass system such as motor, as well as roll and spring system like gearbox and shaft. Therefore, the two-degreesof-freedom model within clearance, nonlinear friction coefficient, and load disturbance is established in this section. The dynamic structure of main drive system is shown in Figure 1, where J_1 , J_2 is the moment of inertia of motor and load, M_1 is the drive torque of motor, M_2 is the torque of load with load disturbance, K_{12} is defined as torsional stiffness coefficient of flexible shaft, C_1 , C_2 is the damping coefficient of motor, rolls, and shaft separately, θ_1 is the rotational angle of motor, and θ_2 is the rotational angle of work roll.

Due to wear of mechanical system, there may be a clearance [22] between gears and universal joint shaft, and its elastic recovery torque is a nonlinear function of rotational angle, as shown in Figure 2. The stiffness coefficient can be expressed in Figure 2 as

$$K_{12} = \begin{cases} K_{12} - \frac{K_{12}\Delta}{\theta_1 - \theta_2}, & \Delta \le \theta_1 - \theta_2 \le \infty \\ 0, & -\Delta \le \theta_1 - \theta_2 \le \Delta \\ K_{12} + \frac{K_{12}\Delta}{\theta_1 - \theta_2}, & -\infty \le \theta_1 - \theta_2 \le \Delta. \end{cases}$$
 (1)

Friction is necessary in rolling process, in a sense that the rolls pull the strip into roll bite by means of friction; meanwhile the lubrication state in roll gap and main drive system has a direct impact on system stability. A former model [23] utilized a constant friction factor approach between the work roll and strip. The constant friction factor model may not be adequate under excellent lubrication conditions, which are exactly happening in the case of high-speed rolling mill configuration. So a dynamic friction model is proposed considering dynamic rolling process and relative speed difference. Then the coefficient can be expressed as follows:

$$\mu = -cv + dv^3,\tag{2}$$

where c, d are variable parameters and $v = R'\dot{\theta}_2$.

Besides, when the cold rolling mill begins to vibrate, the rolling force in the roll gap is extremely high, leading to the work roll flattening effect, which cannot be neglected because that may significantly reduce the estimate of the actual contact length between the work roll and the strip, then leads to an underestimation of the rolling force. Therefore, a model of the work roll flattening effect which is more proper for practical working conditions has been shown as follows [24]:

$$R' = R \left[1 + \frac{16(1 - v_1^2) f_y}{(\Delta h + \Delta h_e) \pi E_1} \right],$$
 (3)

where R is original radius without working roll flattening effect, f_y is the roll force per width, Δh is the screw down amount of work roll, Δh_e is the elastic feedback of the strip, v_1 is Poisson's ratio, and E_1 is Young's modulus of the roll material

Based on the analyses above, the differential equation of two degrees-of-freedom model can be derived as

$$J_{1}\ddot{\theta}_{1} + C_{1}\dot{\theta}_{1} + K_{12}(\theta_{1} - \theta_{2}) = M_{1},$$

$$J_{2}\ddot{\theta}_{2} + K_{12}(\theta_{2} - \theta_{1}) + C_{2}'\dot{\theta}_{2} = -M_{2}.$$
(4)

Then it can be transformed into

$$J_{1}\ddot{\theta}_{1} + C_{1}\dot{\theta}_{1} + K_{12}(\theta_{1} - \theta_{2}) = M_{1},$$

$$J_{2}\ddot{\theta}_{2} + K_{12}(\theta_{2} - \theta_{1}) + C_{2}\dot{\theta}_{2} = -M_{2} - fR',$$
(5)

where $f = \mu P$, P is rolling force, and C_2 is the damping coefficient of vertical rolls system.

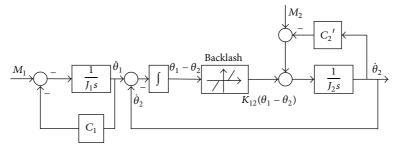


FIGURE 1: Structure of speed control model in main drive system with consideration of nonlinear influence.

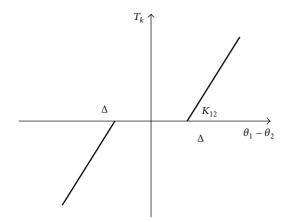


FIGURE 2: The relationship between torsional torque and rotational angle within clearance.

After substitution of (2) into (5), the new form of differential equation can be acquired:

$$J_1 \ddot{\theta}_1 + C_1 \dot{\theta}_1 + K_{12} (\theta_1 - \theta_2) = M_1,$$

$$J_2 \ddot{\theta}_2 + K_{12} (\theta_2 - \theta_1) + (C_2 - cR'^2 P) \dot{\theta}_2 = -M_2 - dR'^4 P \dot{\theta}_2^3.$$
(6)

Define $z_1 = \Delta\theta = \theta_1 - \theta_2$, $z_2 = \dot{\theta}_1$, $z_3 = \dot{\theta}_2$, then $\dot{z}_1 = \Delta\dot{\theta} = \dot{\theta}_1 - \dot{\theta}_2$.

Equation (6) can be transformed into the three following equations:

$$\dot{z}_{1} = z_{2} - z_{3},$$

$$\dot{z}_{2} = -\frac{K_{12}}{J_{1}}z_{1} - \frac{C_{1}}{J_{1}}z_{2} + \frac{1}{J_{1}}M_{1},$$

$$\dot{z}_{3} = \frac{K_{12}}{J_{1}}z_{1} - \frac{C_{2} - cR'^{2}P}{J_{2}}z_{3} - \frac{M_{2} + dR'^{4}Pz_{3}^{3}}{J_{2}}.$$
(7)

And the torsional vibration torque can be obtained as

$$M_{12} = K_{12} (\theta_1 - \theta_2) = K_{12} x_1. \tag{8}$$

2.2. Model Transformation. According to the demand of our control approach, the mathematical model of main drive system has to be transformed into a lower triangular structure.

Define $x_1 = z_3$, $x_2 = z_1$, $x_3 = z_2$, and then nonlinear torsional vibration model of main drive system can be expressed as

$$\begin{bmatrix} \dot{x}_1 \\ \dot{x}_2 \\ \dot{x}_3 \end{bmatrix} = \begin{bmatrix} -\frac{C_2 - cR'^2P}{J_2} & \frac{K_{12}}{J_1} & 0 \\ -1 & 0 & 1 \\ 0 & -\frac{K_{12}}{J_1} & -\frac{C_1}{J_1} \end{bmatrix} \begin{bmatrix} x_1 \\ x_2 \\ x_3 \end{bmatrix}$$

$$+ \begin{bmatrix} 0 \\ 0 \\ \frac{1}{J_1} \end{bmatrix} M_1 + \begin{bmatrix} -\frac{M_2 + dR'^4Px_1^3}{J_2} \\ 0 \\ 0 \end{bmatrix}.$$

$$(9)$$

2.3. Control Task. Based on (9), the drive torque of motor M_1 is the controller output. $dR^{14}Px_1^{3}$ is the nonlinear item of variable friction coefficient in dynamic cold rolling process. M_2 is the load torque within external load disturbance. Due to the variation of thickness and hardness from upstream rolling stands, as well as roll eccentricity, combined with the actual situation in rolling process, the following equation can be obtained:

$$M_2 = M_2^o + M_2^* = M_2^o + A\sin(\pi t),$$
 (10)

where M_2^o is the load of rolls side under steady state, $M_2^* = A \sin(\pi t)$ is the external disturbance, and A is defined as vibration amplitude.

As we can see from (7) and (9)

$$x_1 = z_3 = \dot{\theta}_2,\tag{11}$$

where $\dot{\theta}_2$ is the angular velocity of work roll; we aim at designing a robust controller to have $\dot{\theta}_2$ tracking the reference signals. At the same time, it is expected to show good disturbance attenuation performance for nonlinear parameters such as stiffness and friction, as well as load disturbance.

3. Control Design Procedure

Consider a nonlinear plant with lower triangular structure described by the following equations:

$$\sum x \begin{cases} \dot{x}_{1}(t) = g_{1}(x, d, t) x_{2}(t) + \phi_{1}(x, d, t) \\ \dot{x}_{2}(t) = g_{1}(x, d, t) x_{3}(t) + \phi_{2}(x, d, t) \\ \vdots \\ \dot{x}_{n}(t) = g_{n}(x, d, t) u(t) + \phi_{n}(x, d, t), \end{cases}$$
(12)

$$y_{p}\left(t\right) = x_{1}\left(t\right),\tag{13}$$

where $x_i(t)$ (i = 1, 2, ..., n) are the states, $y_p(t)$ is the output, d(t) is an external disturbance vector, $g_i(x, d, t)$ (i = 1, 2, ..., n) are unknown virtual control coefficients, and $\phi_i(x, d, t)$ (i = 1, 2, ..., n) are regarded as nonlinear timevarying uncertainties.

It is expected we will design a linear robust controller within backstepping procedure, which can produce a control input u(t) to drive the output $y_p(t)$ of the plant to track a reference output, denoted by $y_d(t)$.

The main idea of this control algorithm at each step of backstepping procedure is presented as follows [20]:

- (1) firstly, the tracking problem is transformed into a regulation problem;
- (2) then the nominal controller is designed to get desired property for the nominal disturbance-free model;
- (3) thirdly, the influence of the uncertainties and external disturbance is regarded as an equivalent disturbance;
- (4) finally, a robust compensator is designed to restrain the effect of the equivalent disturbance and to achieve robust properties.

Step 1. To start, define the variables below:

$$\tilde{y}_1(t) = y_p(t) - y_d(t) = x_1(t) - y_d(t),$$
 (14)

$$\widetilde{y}_{2}(t) = x_{2}(t) - \widehat{x}_{2}(t),$$
(15)

where $\hat{x}_2(t)$ is a virtual controller to be designed. Then according to (12) and (14), the subsystem can be established

$$\dot{\tilde{y}}_{1}(t) = q_{1}(t) x_{2}(t) + \tilde{\phi}_{1}(t),$$
 (16)

where $\tilde{\phi}_1(t) = \phi_1(t) - \dot{y}_d(t)$.

Based on (16), $\hat{x}_2(t)$ can be designed as

$$\widehat{x}_{2}(t) = -\frac{\alpha_{1}}{\underline{g}_{1}}\widetilde{y}_{1}(t) + \frac{f_{1}}{\underline{g}_{1}}w_{1}(t), \qquad (17)$$

where the first item of (17) represents nominal virtual control input to stabilize the nominal subsystem without disturbance and uncertainties and α_1 is a positive constant. The second item of (17) defines a robust compensator, and $w_1(t)$ is the compensating input; f_1 is also a positive constant to be determined. Substituting (14), (15), and (17) into (16), one can obtain

$$\dot{\tilde{y}}_{1}(t) = -\alpha_{1}\tilde{y}_{1}(t) + \hat{\phi}_{1}(t) + f_{1}w_{1}(t),$$
 (18)

where $\hat{\phi}_1(t)$ is defined as equivalent disturbance

$$\widehat{\phi}_{1}\left(t\right) = \widetilde{\phi}_{1}\left(t\right) + \underline{g}_{1}\widetilde{y}_{2}\left(t\right) + \left[g_{1}\left(t\right) - \underline{g}_{1}\right]x_{2}\left(t\right). \tag{19}$$

In order to attenuate and suppress the influence of subsystem robust property by equivalent disturbance, the robust compensating input is constructed as follows

$$w_1(t) = -F_1(s)\widehat{\phi}_1(t),$$
 (20)

where $F_1(s)$ is a robust low-pass filter in the following form:

$$F_1(s) = \frac{1}{s + f_1}. (21)$$

As shown in (21), if the filter time-constant f_1 is positive and sufficiently large, we can see that $F_1(s)$ is sufficiently small, then one can expect that $f_1w_1(t)$ would approximate $-\widehat{\phi}_1(t)$ and neutralize the effect of equivalent disturbance to gain robust property.

Since $\hat{\phi}_1(t)$ is immeasurable, it can be expressed in the form

$$\widehat{\phi}_1(t) = (s + \alpha_1) \, \widetilde{y}_1(t) - f_1 w_1(t) \,. \tag{22}$$

To get the robust compensating input $w_1(t)$, only $\tilde{y}_1(t)$ is needed in the form below:

$$w_1(t) = -\left(1 + \frac{\alpha_1}{s}\right) \tilde{y}_1(t). \tag{23}$$

According to those equations above, the subsystem can be established as

$$\dot{\tilde{y}}_{2}(t) = g_{2}(t) x_{3}(t) + \tilde{\phi}_{2}(t),$$
 (24)

where
$$\widetilde{\phi}_2(t) = \phi_2(t) - (\alpha_1^2/\underline{g}_1)\widetilde{y}_1(t) + ((f_1 + \alpha_1)/\underline{g}_1)[\widehat{\phi}_1(t) + f_1w_1(t)].$$

As the second step, the $\tilde{\phi}_2(t)$ item of subsystem (24) will be considered as disturbance and continue the similar design procedure.

Step i. Consider the ith subsystem (i = 2, ..., n-1)

$$\dot{\tilde{y}}_{i}(t) = g_{i}(t) x_{i+1}(t) + \tilde{\phi}_{i}(t),$$
 (25)

where

$$\widetilde{y}_{i}(t) = x_{i}(t) + \frac{\alpha_{i-1}}{\underline{g}_{i-1}} \widetilde{y}_{i-1}(t) - \frac{f_{i-1}}{\underline{g}_{i-1}} w_{i-1}(t),$$

$$\widetilde{\phi}_{t}(t) = \phi_{i}(t) - \frac{\alpha_{i-1}^{2}}{\underline{g}_{i-1}} \widetilde{y}_{i-1}(t)$$

$$+ \frac{f_{i-1} + \alpha_{i-1}}{\underline{g}_{i-1}} \left[\widehat{\phi}_{i-1}(t) + f_{i-1} w_{i-1}(t) \right].$$
(26)

Introduce the error variable

$$y_{i+1}(t) = x_{i+1}(t) - \widehat{x}_{i+1}(t)$$
. (27)

And regard $\hat{x}_{i+1}(t)$ as the virtual control input of the ith subsystem

$$\widehat{x}_{i+1}(t) = -\frac{\alpha_i}{\underline{g}_i} \widetilde{y}_i(t) + \frac{f_i}{\underline{g}_i} w_i(t), \qquad (28)$$

where α_i and f_i are both positive constants. Then

$$\dot{\widetilde{y}}_{i}(t) = -\alpha_{i}\widetilde{y}_{i}(t) + \widehat{\phi}_{i}(t) + f_{i}w_{i}(t), \qquad (29)$$

where $\hat{\phi}_i(t) = \tilde{\phi}_i(t) + g_i \tilde{y}_{i+1}(t) + [g_i(t) - g_i] x_{i+1}(t)$.

The robust compensating input $w_i(t)$ can be expressed as

$$w_{i}(t) = -F_{i}(s)\widehat{\phi}_{i}(t),$$

$$F_{i}(s) = \frac{1}{s+f_{i}}.$$
(30)

Note that

$$\widehat{\phi}_{i}(t) = (s + \alpha_{i}) \, \widetilde{y}_{i}(t) - f_{i} w_{i}(t) \,. \tag{31}$$

Therefore, $w_i(t)$ can also be given by

$$w_i(t) = -\left(1 + \frac{\alpha_i}{s}\right) \tilde{y}_i(t). \tag{32}$$

After differentiating $\dot{\tilde{y}}_{i+1}(t)$, one has

$$\dot{\tilde{y}}_{i+1}(t) = g_{i+1}(t) x_{i+2}(t) + \tilde{\phi}_{i+1}(t),$$
 (33)

where $\widetilde{\phi}_{i+1}(t) = \phi_{i+1}(t) - (\alpha_i^2/\underline{g}_i)\widetilde{y}_i(t) + ((f_i + \alpha_i)/\underline{g}_i)[\widehat{\phi}_i(t) + f_iw_i(t)].$

Step n. At the last step, one has

$$\dot{\tilde{y}}_{n}(t) = q_{n}(t) u(t) + \tilde{\phi}_{n}(t), \qquad (34)$$

where

$$\widetilde{y}_{n}(t) = x_{n}(t) + \frac{\alpha_{n-1}}{\underline{g}_{n-1}} \widetilde{y}_{n-1}(t) - \frac{f_{n-1}}{\underline{g}_{n-1}} w_{n-1}(t),$$

$$\widetilde{\phi}_{n}(t) = \phi_{n}(t) - \frac{\alpha_{n-1}^{2}}{\underline{g}_{n-1}} \widetilde{y}_{n-1}(t)$$

$$+ \frac{f_{n-1} + \alpha_{n-1}}{\underline{g}_{n-1}} \left[\widehat{\phi}_{n-1}(t) + f_{n-1} w_{n-1}(t) \right].$$
(35)

The real control input u(t) can be constructed including nominal control input and robust compensating input

$$u(t) = -\frac{\alpha_n}{\underline{g}_n} \widetilde{y}_n(t) + \frac{f_n}{\underline{g}_n} w_n(t), \qquad (36)$$

where $w_n(t) = -F_n(s)\widehat{\phi}_n(t)$, $F_n(s) = 1/(s+f_n)$. Note that

$$\widehat{\phi}_{n}(t) = \widetilde{\phi}_{n}(t) + \left[g_{n}(t) - \underline{g}_{n}\right]u(t). \tag{37}$$

 $w_n(t)$ can be expressed as

$$w_n(t) = -\left(1 + \frac{\alpha_n}{s}\right) \tilde{y}_n(t). \tag{38}$$

As we can see from (34) and (36), it follows that

$$\dot{\widetilde{y}}_n(t) = -\alpha_n \widetilde{y}_n(t) + \widehat{\phi}_n(t) + f_n w_n(t). \tag{39}$$

After summarizing the design results, the following system structure can be established:

$$\begin{bmatrix} \dot{\tilde{y}}_{i}(t) \\ \dot{w}_{i}(t) \end{bmatrix} = \begin{bmatrix} -\alpha_{i} & f_{i} \\ 0 & -f_{i} \end{bmatrix} \begin{bmatrix} \tilde{y}_{i}(t) \\ w_{i}(t) \end{bmatrix} + \begin{bmatrix} 1 \\ -1 \end{bmatrix} \hat{\phi}_{i}(t),$$

$$i = 1, 2, \dots, n.$$

$$(40)$$

The whole controller description is

$$u(t) = -\frac{\alpha_n}{\underline{g}_n} \widetilde{y}_n(t) + \frac{f_n}{\underline{g}_n} w_n(t),$$

$$\widetilde{y}_1(t) = x_1(t) - y_d(t),$$

$$\widetilde{y}_i(t) = x_i(t) + \frac{\alpha_{i-1}}{\underline{g}_{i-1}} \widetilde{y}_{i-1}(t) - \frac{f_{i-1}}{\underline{g}_{i-1}} w_{i-1}(t),$$

$$i = 2, 3, \dots, n,$$

$$w_i(t) = -\left(1 + \frac{\alpha_i}{s}\right) \widetilde{y}_i(t), \quad i = 1, 2, \dots, n,$$

$$(41)$$

where α_i is chosen so that $\tilde{y}_i(t)$ has desired convergent speed and f_i is needed to be determined to achieve robust stability and robust output tracking properties [20].

4. Simulation Result and Discussion

From the design procedure of the control algorithm in the last section, one can notice that the problem of "explosion of complexity" is fully avoided. Meanwhile, less information about reference output as well as the bounds of uncertainties is applied to construct the robust controller. While the price of this solution is that when there is no dynamic uncertainty or external disturbance, the tracking error cannot be guaranteed to converge to zero, it can only be made as small as desired by appropriately choosing controller parameters α_i and f_i . However, due to the actual situation in industrial fields, uncertainty and external disturbance are ubiquitous in dynamic rolling process, especially when the vibration phenomenon begins to emerge. Besides, from (9)-(11), one can notice the good applicability of our approach on the mathematical model in main drive system with the consideration of model parametric nonlinearity and external load disturbance.

In order to prove the advantage of control method, a simulation experiment with actual industrial data is built, because the torsional vibration in tandem cold rolling mill usually happens in the latter roll-stand, due to its higher rolling speed and the influence by back tension variations. Therefore, the experimental parameters come from the main

TABLE 1: Rolling parameters.

Parameters	Value and unit
$\overline{J_1}$	1552 kg⋅m²
J_2	1542 kg⋅m²
K_{12}	$5.93 \times 10^6 \text{ N} \cdot \text{M/rad}$
Δ	0.1 rad
R	0.4 m
P	932 KN
c	0.06
d	0.0024

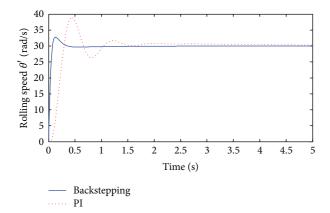


FIGURE 3: Step response of rolling speed within parameter uncertainties.

drive system data in 4th rolling stand of Baosteel. The major parameters are listed in Table 1.

At first, a comparison between robust backstepping controller and PI is made, that the PI algorithm, which is still widely used in the actual rolling field control system, is derived with application of integral square time error

$$K_{\rm PI} = 243 \left(1 + \frac{1}{0.371s} \right).$$
 (42)

Based on the results on robust property and selection of control performance index in [20], the two key parameters can be obtained separately: $\alpha_i = 3$ (i = 1, 2, 3), $f_1 = 10$, $f_2 = 1$ 100, and $f_3 = 1000$. Let us assume that the operation condition of dynamic rolling mill neglects the influence of load disturbance temporarily, while the parameter uncertainty by variable nonlinear stiffness and friction is considered. Given the system, a unit step response with rolling speed r =30 rad/s, as shown in Figure 3, although the PI controller is capable of maintaining stable rolling operation in ideal working conditions, which means the system response is not affected by variation of strip thickness or by back or front tension, it is no longer qualified in this situation as its overshoot and regulating time is unacceptable in real industrial rolling process. On the other hand, the control performance of robust backstepping algorithm is still good because of its better suppression capability on parameter uncertainties.

As demonstrated in many papers [1–8] and engineering projects, the roll eccentricity and variation of strip material

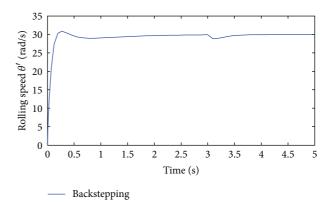


FIGURE 4: Step response of rolling speed under load disturbance.

quality (thickness, hardness, etc.) will lead to motor speed fluctuation, then generate current harmonics and therefore causing the unstable or vibration rolling process within electromechanical coupling in main drive system. Thus, those load disturbances can be derived as sinusoidal disturbance [25, 26], and based on the above parameters and process data, the value can be expressed as

$$M_2 = M_2^o + A \sin(\pi t) = [14500 + 2910 \sin(\pi t)] \text{ N·m.}$$
(43)

Figure 4 shows the system step response when the load disturbance was added at 3 s. During a short-term fluctuation, the system under robust backstepping algorithm returns to normal status quickly, mainly because of low-pass filter and robust compensating input on the attenuation to equivalent disturbance.

5. Conclusion

A nonlinear model of cold rolling main drive system has been formulated, including variable stiffness by clearance, changeable friction coefficient with consideration of relative speed between work roll and strip, and the load disturbance with roll eccentricity and variation of strip material quality.

In view of parameter uncertainty and external disturbance in dynamic cold rolling process, the mathematical model is transformed into a lower triangular structure. A robust backstepping method has been introduced to design a robust controller, which contains a nominal controller and a robust compensator, to achieve a robust tracking property for real controlled plant. The simulation results show its good performance on reference signal tracking under different operational conditions. Meanwhile, its linear and time-invariant characteristic causes the controller to be fulfilled easily.

Despite these encouraging results, the industrial application of this control algorithm should be involved. Due to the existing difficulty, such as nonlinearity, strong coupling features in rolling mill system, and requirement in fast response on control algorithm, the improvements of controller on efficiency and practically would be enormous benefits. Moreover, the possibility for expansion of this robust controller

in industrial practical plants to improve strip quality is recommended as an important issue for future investigation.

Acknowledgments

The authors gratefully acknowledge the support by National Natural Science Foundation of China (nos. 51205018 and 61074085), Research Projects of State Key Laboratory of Mechanical System and Vibration (no. MSV-2014-09), China Postdoctoral Science Foundation Funded Project (no. 2012M510321), and Fundamental Research Funds for the Central Universities (nos. FRF-TP-12-104A and FRF-SD-12-008B). Meanwhile, great thanks also goes to Baosteel Company in Shanghai, China, for data support, and the anonymous reviewers for their valuable comments and suggestions.

References

- [1] J. X. Zou and L. J. Xu, *Vibration in Rolling Mills*, pp. 88–107, Metallurgical Industry Press, Beijing, China, 1998, (Chinese).
- [2] X. Yang and C. N. Tong, "Coupling dynamic model and control of chatter in cold rolling," *Journal of Dynamic Systems, Mea*surement and Control-Transactions of the ASME, vol. 134, no. 4, Article ID 041001, 8 pages, 2012.
- [3] M. N. Skripalenko, M. M. Skripalenko, D. A. Ashikhmin et al., "Wavelet analysis of fluctuations in the thickness of cold-rolled strip," *Metallurgist*, vol. 57, no. 7-8, pp. 606–611, 2013.
- [4] P. V. Krot, "Transient torsional vibrations control in the geared drive trains of the hot rolling mills," in *Proceedings of the IEEE Conference on Control Application*, Part of 2009 IEEE Multi-Conference on System and Control, pp. 1368–1373, July 2009.
- [5] V. Panjković, R. Gloss, J. Steward, S. Dilks, R. Steward, and G. Fraser, "Causes of chatter in a hot strip mill: observations, qualitative analyses and mathematical modelling," *Journal of Materials Processing Technology*, vol. 212, no. 4, pp. 954–961, 2012.
- [6] Y. Kimura, Y. Sodani, N. Nishiura, N. Ikeuchi, and Y. Mihara, "Analysis of chatter in tandem cold rolling mills," *ISIJ International*, vol. 43, no. 1, pp. 77–84, 2003.
- [7] I. Prihod'ko, P. Krot, K. Solov'yov et al., "Vibration monitoring system and the new methods of chatter early diagnostics for tandem mill control," in *Proceedings of the International Conference* on Vibration in Rolling Mills, pp. 87–106, London, UK, 2006.
- [8] Z. J. Huang, L. X. Gao, and Y. F. Liao, *Machinery Vibration Monitoring and Fault Diagnosis*, pp. 45–80, Chemical industry Press, Beijing, China, 2010, (Chinese).
- [9] W. Liang, J. He, S. Yu, W. Long, and X. Cai, "Electromechanical coupling analysis of cold strip steel temper mill," *Journal of Central South University of Technology*, vol. 31, no. 1, pp. 78–80, 2000.
- [10] S. Yin, S. X. Ding, A. Haghani et al., "A comparison study of basic data-driven fault diagnosis and process monitoring methods on the benchmark Tennessee Eastman process," *Journal of Process Control*, vol. 22, no. 9, pp. 1567–1581, 2012.
- [11] H. Dong, Z. Wang, J. Lam, and H. Gao, "Fuzzy-model-based robust fault detection with stochastic mixed time delays and successive packet dropouts," *IEEE Transactions on Systems, Man, and Cybernetics B*, vol. 42, no. 2, pp. 365–376, 2012.
- [12] S. X. Ding, "Integrated design of feedback controllers and fault detectors," *Annual Reviews in Control*, vol. 33, no. 2, pp. 124–135, 2009.

- [13] H. Dong, Z. Wang, and H. Gao, "Fault detection for Markovian jump systems with sensor saturations and randomly varying nonlinearities," *IEEE Transactions on Circuits and Systems I*, vol. 59, no. 10, pp. 2354–2362, 2012.
- [14] S. Yin, H. Luo, and S. X. Ding, "Real-time implementation of fault-tolerant control systems with performance optimization," *IEEE Transactions on Industrial Electronics*, vol. 61, no. 5, pp. 2402–2411, 2014.
- [15] R. Zhang and C. Tong, "Torsional vibration control of the main drive system of a rolling mill based on an extended state observer and linear quadratic control," *Journal of Vibration and Control*, vol. 12, no. 3, pp. 313–327, 2006.
- [16] E. J. M. Geddes and I. Postlethwaite, "Improvements in product quality in tandem cold rolling using robust multivariable control," *IEEE Transactions on Control Systems Technology*, vol. 6, no. 2, pp. 257–269, 1998.
- [17] R. Freeman and P. Kokotovic, "Backstepping design of robust controller for a class of nonlinear systems," *Proceedings of the IFAC Nonlinear Control System Design Symposium*, pp. 307–312, June 1992.
- [18] Z. Jiang and D. J. Hill, "A robust adaptive backstepping scheme for nonlinear systems with unmodeled dynamics," *IEEE Trans*actions on Automatic Control, vol. 44, no. 9, pp. 1705–1711, 1999.
- [19] N. Yagiz and Y. Hacioglu, "Backstepping control of a vehicle with active suspensions," *Control Engineering Practice*, vol. 16, no. 12, pp. 1457–1467, 2008.
- [20] Y. Yu and Y. Zhong, "Robust backstepping output tracking control for SISO uncertain nonlinear systems with unknown virtual control coefficients," *International Journal of Control*, vol. 83, no. 6, pp. 1182–1192, 2010.
- [21] M. Krstic and M. Bernent, "Non-overshooting control of strict-feedback nonlinear systems," in *Proceedings of the American Control Conference (ACC '07)*, pp. 4494–4499, July 2007.
- [22] H. Li, G. Meng, Z. Meng, and B. Wen, "Effects of boundary conditions on a self-excited vibration system with clearance," *International Journal of Nonlinear Sciences and Numerical Simulation*, vol. 8, no. 4, pp. 571–580, 2007.
- [23] P. Hu, H. Zhao, and K. F. Ehmann, "Third-octave-mode chatter in rolling. Part 1: chatter model," *Proceedings of the Institution of Mechanical Engineers B*, vol. 22, no. 8, pp. 1267–1277, 2006.
- [24] X. Yang, C. Tong, G. Yue, and J. Meng, "Coupling dynamic model of chatter for cold rolling," *Journal of Iron and Steel Research International*, vol. 17, no. 12, pp. 30–34, 2010.
- [25] R. C. Zhang, Vibration characteristics analysis and control research of the rolling mill electromechanical coupling system [Ph.D. dissertation], University of Science and Technology, Beijing, China, 2006.
- [26] S. Mtakula, "An approach of the nonlinear control of rolling mills," in *Proceedings of the Advanced Process Control Appli*cation for Industry, Workshop of the IEEE Industry Application Society, pp. 1–8, Vancouver, Canada, 2005.

Hindawi Publishing Corporation Abstract and Applied Analysis Volume 2013, Article ID 937274, 9 pages http://dx.doi.org/10.1155/2013/937274

Research Article

Model Predictive Control of Piecewise Affine System with Constrained Input and Time Delay

Zhilin Liu, 1 Lutao Liu, 2 Jun Zhang, 3 and Xin Yuan 1

¹ College of Automation, Harbin Engineering University, Harbin, Heilongjiang 150001, China

Correspondence should be addressed to Lutao Liu; liulutao@msn.com

Received 21 September 2013; Accepted 18 October 2013

Academic Editor: Shen Yin

Copyright © 2013 Zhilin Liu et al. This is an open access article distributed under the Creative Commons Attribution License, which permits unrestricted use, distribution, and reproduction in any medium, provided the original work is properly cited.

A model predictive control (MPC) is proposed for the piecewise affine (PWA) systems with constrained input and time delay. The corresponding operating region of the considered systems in state space is described as ellipsoid which can be characterized by a set of vector inequalities. And the constrained control input of the considered systems is solved in terms of linear matrix inequalities (LMIs). An MPC controller is designed that will move the PWA system with time delay from the current operating point to the desired one. Multiple objective functions are used to relax the monotonically decreasing condition of the Lyapunov function when the control algorithm switches from a quasi-infinite horizon to an infinite horizon strategy. The simulation results verify the effectiveness of the proposed method. It is shown that, based on LMI constraints, it is easy to get the MPC for the PWA systems with time delay. Moreover, it is suitable for practical application.

1. Introduction

In engineering practice, there are many hybrid systems described by piecewise affine systems (PWA) which are composed of linear subsystems and convex polytopic regions. Hybrid systems are composed of discrete event dynamic systems and continuous time dynamic systems or discrete time dynamic systems, which interact with each other [1]. The hybrid system theory, which is proposed for the demand of the economic development, is the result of the development of computer science and control theory. Piecewise affine system is one of the most important branches of hybrid system [2]. It consists of some subsystems that integrate the logical and continuous dynamics by switching. Theoretically, any nonlinear system can be approximated as piecewise affine system [3, 4]. In [5], the PWA system is described as ellipsoid which can be characterized by a set of vector inequalities. In [6], the constraint of linear matrix inequalities (LMIs) is released. In terms of LMIs, the PWA system can be stabilized in Lyapunov theory.

Model predictive control (MPC), also known as receding horizon control, is a popular technique for the control of dynamical systems, such as those encountered in chemical process control in the petrochemical, pulp and paper industries, and in industrial hot strip mill [7]. MPC is also a popular technique for the control of dynamical system subject to input and state constraints. At any time instant, MPC requires the online solution of an optimization problem to compute-optimal control inputs over a fixed number of future time instants, known as the finite horizon or quasi-infinite horizon. Using MPC, it is possible to handle inequality constraints on the manipulated and controlled variables in a systematic manner during the design and implementation of the controller [8, 9]. MPC has become the control strategy of choice in industrial applications that typically involve linear systems subject to linear inequality constraints. However, industrial processes are in general inherently nonlinear and operated over a wide range of operating conditions [10, 11]. The use of multiple model/controllers is a common strategy in dealing with the complex of nonlinear systems and has led to the development of various multiple model/controller approaches. Considerable research has been focused on the development and utilization of multiple model/controller banks within the MPC framework [12-14] in order to cope

² College of Information and Telecommunication, Harbin Engineering University, Harbin, Heilongjiang 150001, China

³ School of Electrical and Information Engineering, Jiangsu University, Zhenjiang, Jiangsu 212013, China

with nonlinear systems. The basis of these approaches is the decomposition of the systems full range of operation into a number of operating regimes in which a simpler local model and/or controller is applied. The local models and controllers are then incorporated to give a global model and/or controller.

stability in multiple model/control Closed-loop approaches has also been studied [15] since designing local controllers that stabilize each individual model may not result in a stable global closed-loop system. In general, the use of piecewise models in a control structure necessitates a means of switching among the available models to the one that best describes the current process dynamics. The switching from one model/controller to another based on a logical argument (supervisory scheme) results in a hybrid system. A closely related work is the stability analysis of piecewise linear systems by [16] in which piecewise quadratic Lyapunov functions were constructed using convex optimization in terms of linear matrix inequalities (LMIs) as an alternative to a globally quadratic Lyapunov function.

Time delay systems are very common in industry. However, few works on control algorithms development for time delay PWA system have been reported [17, 18]. Based on this concept, we propose a MPC control algorithms for the discrete polytopic time-delay PWA systems. The MPC controller of the considered systems is solved in terms of LMIs. The sufficient conditions of stability are derived for time-delay systems. The feedback control law is obtained by convex optimization involving LMIs. The simulation results verify the effectiveness of the proposed method.

Notation. The symbol \ast will be used in some matrix expressions to induce a symmetric structure. I denotes identity matrix. For example, when H and R are symmetric matrices, then

$$\begin{bmatrix} H & * \\ T & R \end{bmatrix} = \begin{bmatrix} H & T^{\mathrm{T}} \\ T & R \end{bmatrix}. \tag{1}$$

2. Problem Formulation

Consider a discrete time-delay PWA systems with input constraints:

$$\mathbf{x}(k+1) = \mathbf{A}_{i}\mathbf{x}(k) + \mathbf{A}_{di}\mathbf{x}(k-d) + \mathbf{B}_{i}\mathbf{u}(k) + \mathbf{b}_{i},$$

$$\mathbf{x}(k) = \varphi(k),$$

$$\|\mathbf{u}\|_{2} \le u_{\text{max}},$$

$$\mathbf{x}(k) \in \mathbf{X}_{i}, \quad -d \le k \le 0, \quad k = 0, 1, \dots \infty,$$

$$(2)$$

where $\mathbf{x}(k) \in \mathbb{R}^n$ is the state of the plant, $\mathbf{u}(k) \in \mathbb{R}^m$ is the control input, and d is fixed time-delay constant. And \mathbf{b}_i is constant affine vector of the ith subsystem. i represents the switching rule, which makes value from finite set \overline{N} , and $i \in \overline{N} = \{1, 2, ..., N\}$. \mathbf{A}_i , \mathbf{A}_d , \mathbf{B}_i , and \mathbf{b}_i are sets of known

real constant matrices with appropriate dimensions of the *i*th subsystem separately. The feedback control law is

$$\mathbf{u}\left(k\right) = \mathbf{K}_{i}\mathbf{x}\left(k\right). \tag{3}$$

Substituting (3) into inequality (2), we can get

$$\mathbf{x}(k+1) = \overline{\mathbf{A}}_{i}\mathbf{x}(k) + \mathbf{A}_{di}\mathbf{x}(k-d) + \mathbf{b}_{i}, \tag{4}$$

where $\overline{\mathbf{A}}_i = \mathbf{A}_i + \mathbf{B}_i \mathbf{K}_i$. Denote X_i as the state region where subsystem i is active at moment k, and there is no switch that occurred at moment k+1 (see [5]), which is

$$\mathbf{X}_{i} = \left\{ \mathbf{x} \left(k \right) \in \mathbb{R}^{n} \mid \exists k \geq 0, \mathbf{x} \left(k \right) \in \mathbf{X}_{i}, \mathbf{x} \left(k + 1 \right) \in \mathbf{X}_{i} \right\}$$

$$i, j \in \overline{N}.$$
(5)

Commonly, X_i is ellipsoid set. The dimension of X_i is less than the dimension of state. To stabilize the PWA system (2), a state feedback control law is solved by defining a quadratic Lyapunov-Krasovskii function:

$$V\left(\mathbf{x}\left(k\right)\right) = \mathbf{x}^{\mathrm{T}}\left(k\right)\mathbf{P}_{i}\mathbf{x}\left(k\right) + \sum_{i=1}^{d}\mathbf{x}^{\mathrm{T}}\left(k-j\right)\mathbf{S}\mathbf{x}\left(k-j\right), \quad (6)$$

By solving the following two problems, the feedback control law is obtained.

Problem 1. Find a piecewise affine state feedback controller that exponentially stabilizes the PWA system when $\mathbf{x}(k) \in \mathbf{X}_i$, $\mathbf{x}(k+1) \in \mathbf{X}_i$.

Problem 2. It is the same as Problem 1 at the switching moment when $\mathbf{x}(k) \in \mathbf{X}_i$, $\mathbf{x}(k+1) \in \mathbf{X}_{i+1}$.

Lemma 3. The state region X_i can be described as same ellipsoids $X_i \subseteq \varepsilon_i$, where $\varepsilon_i = \{x \mid ||E_ix + e_i|| \le 1\}$. Denote the ellipsoid X_i as the quadratic inequalities (see [5]):

$$\begin{bmatrix} \mathbf{x}(k) \\ 1 \end{bmatrix}^T \begin{bmatrix} \mathbf{E}_i^T \mathbf{E}_i & * \\ \mathbf{e}_i^T \mathbf{E}_i & -1 + \mathbf{e}_i^T \mathbf{e}_i \end{bmatrix} \begin{bmatrix} \mathbf{x}(k) \\ 1 \end{bmatrix} \le 0.$$
 (7)

More precisely, if $d_1 < \mathbf{C}_i^T x < d_2$, then the degenerate ellipsoid is described by

$$\mathbf{E}_{i} = \frac{2\mathbf{C}_{i}^{T}}{(d_{2} - d_{1})}, \qquad \mathbf{e}_{i} = -\frac{(d_{2} + d_{1})}{(d_{2} - d_{1})}.$$
 (8)

Finally, it is assumed that the control objective is to stabilize the system to a given point x_{cl} . With the change of coordinates $z = x - x_{cl}$, the problem is transformed to the stabilization of the origin. Accordingly, the ellipsoid changes into

$$\varepsilon_i = \left\{ z \mid \left\| \mathbf{E}_i \mathbf{x} + \mathbf{e}_i^{cl} \right\| \le 1 \right\}, \tag{9}$$

where $\mathbf{e}_{i}^{cl} = \mathbf{e}_{i} + \mathbf{E}_{i} \mathbf{x}_{cl}$.

Assumption 4. In application of this formulation to multiple regions, we assume that we know the order of regions that the states will go through starting from the current region of the system to the terminal region.

Assumption 5. We also assume that we know the number of moves that the system has to take to go from one region to another adjacent operating region.

3. Main Result

Model predictive control, also known as moving horizon control or receding horizon control, has become very successful in process industries, especially in the control of processes that are constrained, multivariable and uncertain. In general, MPC solves online an open-loop optimal control problem subject to system dynamics and constraints at each time instant and implements only the first element of the control profile. At each sampling time k, plant measurements are obtained and a model of the process is used to predict future outputs of the system. Using these predictions, m control moves $\mathbf{u}(k+m\mid k)$, are computed by minimizing a nominal $J_{\infty}(k)$ over a prediction horizon as follows:

$$J_{\infty}(k) = \sum_{m=0}^{\infty} \left[\mathbf{x}^{\mathrm{T}}(k+m \mid k) \mathbf{Q}_{I} \mathbf{x} (k+m \mid k) + \mathbf{u}^{\mathrm{T}}(k+m \mid k) \mathbf{R} \mathbf{u} (k+m \mid k) \right]$$
s.t.
$$\mathbf{x} (k+m+1 \mid k)$$

$$= \mathbf{A}_{i} \mathbf{x} (k+m \mid k) + \mathbf{A}_{di} \mathbf{x} (k-d+m \mid k) + \mathbf{B}_{i} \mathbf{u} (k+m \mid k) + \mathbf{b}_{i},$$

$$\mathbf{x} (k+m \mid k) \in \mathbf{X}_{i}, \quad m = 0, 1 \dots n,$$

$$\mathbf{x} (k+n+1 \mid k) \in \mathbf{X}_{i+1},$$

$$\|\mathbf{u} (k+m \mid k)\|_{2} \leq u_{\max}, \quad m = 0, 1, \dots \infty,$$

$$(10)$$

where $\mathbf{Q}_I > 0$, $\mathbf{R} > 0$ are symmetric weighting matrices, n is control horizon, $\mathbf{x}(k+m\mid k)$ is state at time k+m predicted based on the measurements of system (2) at time k. $\mathbf{u}(k+m\mid k)$ is control move at time k+m computed by solving the optimization problem (10) at time k, $\mathbf{u}(k+m\mid k)$ is implemented to the system at time k, and then in time k+1, the maximization problem is solved by deriving an upper bound on the objective function $J_{\infty}(k)$ based on the measurements of new states of system. The control law is obtained by convex optimization based on MPC involving LMIs and ellipsoids constraints (7), which is suitable to practical application.

In this section, the problem formulation for MPC using piecewise linear models of the form (2) is discussed. The aim is to find a sequence of control input signals $\mathbf{u}(k+n\mid k)$ that will move the system from the current operating point to the desired one. The authors of [19] presented an MPC design technique (min-max MPC) in which the minimization of the nominal objective function was modified to a minimization of the worst case objective function. In this work, we extend this formulation using piecewise affine model with time delay.

Theorem 6. Consider a time-delay PWA system (2) with several operating points, where i denotes the active PWA model and \mathbf{X}_{i+1} shows the corresponding operating region which if described by $|\mathbf{E}_{i+1}\mathbf{x} + \mathbf{e}_{i+1}| \le 1$ with $\mathbf{x} \in \mathbf{X}_{i+1}$. $\mathbf{u}(k \mid k) \cdots \mathbf{u}(k+n \mid k)$ are sequences of control inputs to the PWA system. The states of PWA system (2) are steered from \mathbf{X}_i to $\mathbf{X}_{(i+1)}$ in n steps, where n is control horizon constant. If there exist

 $\mathbf{Y}_{i+1} = \mathbf{K}_{i+1} \mathbf{Q}, \mathbf{Q} \ge 0, \mathbf{W} > 0, \gamma > 0, \xi > 0,$ and a sequence of $\mathbf{u}(k \mid k) \cdots \mathbf{u}(k+n \mid k)$ satisfy the following LMI (12)–(16), the sequence of control input signals will move the system from the current operating region to the desired one, until to the origin of the system.

The modified MPC law is given by

$$\min_{\mathbf{y},\mathbf{u},\mathbf{Q},\mathbf{W},\mathbf{Y}_i} \mathbf{\gamma},\tag{12}$$

s.t.
$$\begin{bmatrix} u_{\text{max}}^2 \mathbf{I} & \mathbf{Y}_{i+1} \\ \mathbf{Y}_{i+1}^T & \mathbf{Q} \end{bmatrix} \ge 0, \tag{13}$$

$$|\mathbf{u}(k+m\mid k)| \le u_{\max}, \quad m = 0 \cdots n,$$
 (14)

$$\begin{bmatrix} \mathbf{Q} & * & * & * & * & * & * & * \\ 0 & \mathbf{W}^{-1} & \mathbf{A}_{di+1}^{\mathrm{T}} & 0 & 0 & 0 & 0 \\ \Sigma & \mathbf{A}_{di+1} & \Xi & \mathbf{b}_{i+1} \mathbf{e}_{i+1}^{\mathrm{T}} \boldsymbol{\xi} & 0 & 0 & 0 \\ \mathbf{E}_{i+1} \mathbf{Q} & 0 & \boldsymbol{\xi} \mathbf{e}_{i+1} \mathbf{b}_{i+1}^{\mathrm{T}} & t & 0 & 0 & 0 \\ \mathbf{Q}_{\mathbf{I}}^{1/2} \mathbf{Q} & 0 & 0 & 0 & \gamma \mathbf{I} & 0 & 0 \\ \mathbf{R}^{1/2} \mathbf{Y}_{i+1} & 0 & 0 & 0 & 0 & \gamma \mathbf{I} & 0 \\ \mathbf{Q} & 0 & 0 & 0 & 0 & 0 & \mathbf{W} \end{bmatrix} > 0,$$

$$(16)$$

where $\mathbf{x}(k+1\mid k)\cdots\mathbf{x}(k+n+1\mid k)$ are computed iteratively by (2) as follows:

$$\mathbf{x} (k + n + 1 \mid k)$$

$$= \mathbf{A}_{i}^{n+1} \mathbf{x} (k \mid k) + \sum_{j=0}^{n} \mathbf{A}_{i}^{n-j} \mathbf{A}_{di} \mathbf{x} (k - d + j \mid k)$$

$$+ \sum_{j=0}^{n} \mathbf{A}_{i}^{n-j} \mathbf{B}_{i} \mathbf{u} (k + j \mid k) + \sum_{j=1}^{n} \mathbf{A}_{i}^{n-j} \mathbf{b}_{i}$$
(17)

and
$$\Sigma = \mathbf{A}_{i+1}\mathbf{Q} + \mathbf{B}_{i+1}\mathbf{Y}_{i+1}$$
, $\Xi = \mathbf{Q} + \xi \mathbf{b}_{i+1}\mathbf{b}_{i+1}^{\mathrm{T}}$.

Proof

(1) *Upper Bound on the Objective Function.* The objective function can be split into two parts:

$$J_{\infty}(k) = J_0^n(k) + J_{n+1}^{\infty}(k),$$
 (18)

where

$$J_{0}^{n}(k) = \sum_{m=0}^{n} \left[\mathbf{x}^{\mathrm{T}}(k+m \mid k) \mathbf{Q}_{I} \mathbf{x}(k+m \mid k) + \mathbf{u}^{\mathrm{T}}(k+m \mid k) \mathbf{R} \mathbf{u}(k+m \mid k) \right],$$

$$J_{n+1}^{\infty}(k) = \sum_{l=n+1}^{\infty} \left[\mathbf{x}^{\mathrm{T}}(k+m \mid k) \mathbf{Q}_{I} \mathbf{x}(k+m \mid k) + \mathbf{u}^{\mathrm{T}}(k+m \mid k) \mathbf{R} \mathbf{u}(k+m \mid k) \right].$$

$$(19)$$

It is also assumed that the number of moves n required for the system to transition from one part \mathbf{X}_i to the next desired part $\mathbf{X}_{(i+1)}$ is prespecified. Using quadratic Lyapunov-Krasovskii function, the upper bound on the objective function $J_{n+1}^{\infty}(k)$ is given as

$$V\left(\mathbf{x}\left(k\right)\right) = \mathbf{x}^{\mathrm{T}}\left(k\right) \mathbf{P}\mathbf{x}\left(k\right) + \sum_{j=1}^{d} \mathbf{x}^{\mathrm{T}}\left(k-j\right) \mathbf{S}\mathbf{x}\left(k-j\right). \quad (20)$$

Suppose $V(\mathbf{x}(k))$ satisfies the following inequality:

$$V\left(\mathbf{x}\left(k+m+1\mid k\right)\right) - V\left(\mathbf{x}\left(k+m\mid k\right)\right)$$

$$\leq -\left[\mathbf{x}^{\mathrm{T}}\left(k+m\mid k\right)\mathbf{Q}_{I}\mathbf{x}\left(k+m\mid k\right)\right]$$

$$+\mathbf{u}^{\mathrm{T}}\left(k+m\mid k\right)\mathbf{R}\mathbf{u}\left(k+m\mid k\right)\right]$$
(21)

with the conditions $V(\mathbf{x}(\infty \mid k)) = 0$ and $\mathbf{x}(\infty \mid k) = 0$. Summing (21) from m = n + 1 to $m = \infty$ gives

$$J_{n+1}^{\infty}(k) \leq V\left(\mathbf{x}\left(k+n+1\mid k\right)\right)$$

$$= \mathbf{x}^{T}\left(k+n+1\mid k\right) \mathbf{P}\mathbf{x}\left(k+n+1\mid k\right)$$

$$+ \sum_{j=1}^{d} \mathbf{x}^{T}\left(k+n+1-j\mid k\right) \mathbf{S}\mathbf{x}\left(k+n+1-j\mid k\right).$$
(22)

Then, the minimization of the upper bound on the objective function $J_{\infty}(k)_{\mathbf{u},\mathbf{O},\mathbf{W},\mathbf{Y}_i,i\in\overline{N}}$ is derived as

$$\min \ J_{\infty}(k)$$

$$\mathbf{u}, \mathbf{Q}, \mathbf{W}, \mathbf{Y}_{i}, i \in \overline{N}$$

 $\leq \gamma$,

$$= \min_{\mathbf{u}, \mathbf{Q}, \mathbf{W}, \mathbf{Y}_{j}, i \in \mathbf{I}} \sum_{m=0}^{n} \left[\mathbf{x}^{T} (k + m \mid k) \mathbf{L} \mathbf{x} (k + m \mid k) + \mathbf{u}^{T} (k + m \mid k) \mathbf{R} \mathbf{u} (k + m \mid k) \right] + \mathbf{x}^{T} (k + n + 1 \mid k) \mathbf{P} \mathbf{x} (k + n + 1 \mid k) + \sum_{j=1}^{d} \mathbf{x}^{T} (k + n + 1 - j \mid k) \mathbf{S} \mathbf{x} (k + n + 1 - j \mid k)$$

$$(23)$$

where $P = \gamma Q^{-1} > 0$ and $W = \gamma S^{-1} > 0$. Using the Sprocedure [6], we get (15).

(2) The Stability of Inequality with Ellipsoids Constraints. In this section, the aim is to design an MPC controller in which the minimization of the nominal objective function was modified to a minimization of the worst case objective function. A thorough discussion of the previous problems can be found in [19]. The objective function of MPC in [19] is

$$\min J_{\infty}(k), \qquad (24)$$

where

$$J_{\infty}(k) = \sum_{m=0}^{\infty} \left[\mathbf{x}^{\mathrm{T}} (k+m \mid k) \mathbf{Q}_{I} \mathbf{x} (k+m \mid k) + \mathbf{u}^{\mathrm{T}} (k+m \mid k) \mathbf{R} \mathbf{u} (k+m \mid k) \right].$$
(25)

In this section, the objective function $\min J_{\infty}(k)$ is replaced by

min
$$(J_0^n(k) + J_{n+1}^{\infty}(k))$$

s.t. $\mathbf{x}(k+m+1 \mid k)$
 $= \mathbf{A}_i \mathbf{x}(k+m \mid k) + \mathbf{A}_d \mathbf{x}(k+m-d \mid k)$
 $+ \mathbf{B}_i \mathbf{u}(k+m \mid k) + \mathbf{b}_i \quad 0 \le m \le n,$ (26)

$$V(\mathbf{x}(k+m+1 \mid k)) - V(\mathbf{x}(k+m \mid k)) \leq -\left[\mathbf{x}^{T}(k+m \mid k)\mathbf{Q}_{I}\mathbf{x}(k+m \mid k) + \mathbf{u}^{T}(k+m \mid k)\mathbf{R}\mathbf{u}(k+m \mid k)\right] \|\mathbf{E}_{i+1}\mathbf{x}(k+m \mid k) + \mathbf{e}_{i+1}\| \leq 1$$

$$(27)$$

In this section, the MPC formulation given in [19] is extended to PWA system with form (2) that has polytopic and ellipsoid approximations for the operating region \mathbf{X}_i . The previous inequalities (27) are the stability constraints for subsystem i+1. Inequalities (27) can guarantee the PWA system to be steered from \mathbf{X}_i to \mathbf{X}_{i+1} in n steps. The control inputs $\mathbf{u}(k+mk)$, $m=0,1\dots n$ are a sequence of free variables, based on the input constraints. If \mathbf{X}_{i+1} is not the terminal operating ellipsoid region, we apply $\mathbf{u}(k+m\mid k)$, $m=0\dots n$ to PWA. Once \mathbf{X}_{i+1} is the terminal operating ellipsoid region, the feedback control law $\mathbf{u}(k)=\mathbf{K}_{i+1}\mathbf{x}(k)$ is running to reduce the calculation. The quadratic ellipsoid inequality (10) is equivalent to

$$\begin{bmatrix} \mathbf{x} (k+m \mid k) \\ \mathbf{x} (k-d+m \mid k) \\ 1 \end{bmatrix}^{\mathrm{T}} \Pi \begin{bmatrix} \mathbf{x} (k+m \mid k) \\ \mathbf{x} (k-d+m \mid k) \\ 1 \end{bmatrix} \leq 0, \quad (28)$$

where
$$\Pi = \begin{bmatrix} E_{i+1}^T E_{i+1} & 0 & E_{i+1}^T e_{i+1} \\ 0 & 0 & 0 \\ e_{i+1}^T E_{i+1} & 0 & -1 + e_{i+1}^T e_{i+1} \end{bmatrix}$$
.
Substituting (20) into (21) gives

$$\begin{bmatrix} \mathbf{x} (k+m \mid k) \\ \mathbf{x} (k-d+m \mid k) \end{bmatrix}^{\mathrm{T}} \mathbf{M} \begin{bmatrix} \mathbf{x} (k+m \mid k) \\ \mathbf{x} (k-d+m \mid k) \end{bmatrix} \le 0, \quad (29)$$

where

$$\mathbf{M} = \begin{bmatrix} \psi_{1} & \overline{\mathbf{A}}_{i+1}^{T} \mathbf{P} \mathbf{A}_{di+1} & \overline{\mathbf{A}}_{i+1}^{T} \mathbf{P} \mathbf{b}_{i+1} \\ \mathbf{A}_{di+1}^{T} \mathbf{P} \overline{\mathbf{A}}_{i+1} & \mathbf{A}_{di+1}^{T} \mathbf{P} \mathbf{A}_{di+1} - \mathbf{S} & \mathbf{A}_{di+1}^{T} \mathbf{P} \mathbf{b}_{i+1} \\ \mathbf{b}_{i+1}^{T} \mathbf{P} \overline{\mathbf{A}}_{i+1} & \mathbf{b}_{i+1}^{T} \mathbf{P} \mathbf{A}_{di+1} & \mathbf{b}_{i+1}^{T} \mathbf{P} \mathbf{b}_{i+1} \end{bmatrix}, \quad (30)$$

$$\psi_1 = \overline{\mathbf{A}}_{i+1}^{\mathrm{T}} \mathbf{P} \overline{\mathbf{A}}_{i+1} + \mathbf{S} + \mathbf{Q}_I + \mathbf{K}_{i+1}^{\mathrm{T}} \mathbf{R} \mathbf{K}_{i+1} - \mathbf{P}.$$

Using the S-procedure [6] into (28) and (29), we get $\lambda > 0$,

$$\begin{bmatrix} \mathbf{\Phi}_{1} & 0 & \lambda \mathbf{E}_{i+1}^{T} \mathbf{e}_{i+1} \\ 0 & \mathbf{S} & 0 \\ \lambda \mathbf{e}_{i+1}^{T} \mathbf{E}_{i+1} & 0 & -\lambda \left(1 - \mathbf{e}_{i+1}^{T} \mathbf{e}_{i+1} \right) \end{bmatrix}$$

$$- \begin{bmatrix} \overline{\mathbf{A}}_{i+1}^{T} \\ \mathbf{A}_{di+1}^{T} \\ \mathbf{b}_{i+1}^{T} \end{bmatrix} \mathbf{P} \begin{bmatrix} \overline{\mathbf{A}}_{i+1} & \mathbf{A}_{di+1} & \mathbf{b}_{i+1} \end{bmatrix} > 0,$$
(31)

where

$$\mathbf{\Phi}_{1} = \mathbf{P} + \lambda \mathbf{E}_{i+1}^{T} \mathbf{E}_{i+1} - \mathbf{S} - \mathbf{K}_{i+1}^{T} \mathbf{R} \mathbf{K}_{i+1} - \mathbf{Q}_{I}.$$
 (32)

By Schur complements, this is equivalent to

$$\begin{bmatrix} \mathbf{\Phi}_{1} & 0 & \lambda \mathbf{E}_{i+1}^{T} \mathbf{e}_{i+1} & \overline{\mathbf{A}}_{i+1}^{T} \\ 0 & \mathbf{S} & 0 & \mathbf{A}_{di+1}^{T} \\ \lambda \mathbf{e}_{i+1}^{T} \mathbf{E}_{i+1} & 0 & -\lambda \left(1 - \mathbf{e}_{i+1}^{T} \mathbf{e}_{i+1} \right) & \mathbf{b}_{i+1}^{T} \\ \overline{\mathbf{A}}_{i+1} & \mathbf{A}_{di+1} & \mathbf{b}_{i+1} & \mathbf{P}^{-1} \end{bmatrix} > 0. \quad (33)$$

Substituting $P = \gamma Q^{-1}$ and pre- and postmultiplying by diag{I I $\begin{bmatrix} 0 & I \\ I & 0 \end{bmatrix}$ } gives

$$\begin{bmatrix} \mathbf{\Phi}_{2} & 0 & \overline{\mathbf{A}}_{i+1}^{T} & \lambda \mathbf{E}_{i+1}^{T} \mathbf{e}_{i+1} \\ 0 & \mathbf{S} & \mathbf{A}_{di+1}^{T} & 0 \\ \overline{\mathbf{A}}_{i+1} & \mathbf{A}_{di+1} & \gamma^{-1} \mathbf{Q} & \mathbf{b}_{i+1} \\ \lambda \mathbf{e}_{i+1}^{T} \mathbf{E}_{i+1} & 0 & \mathbf{b}_{i+1}^{T} & -\lambda \left(1 - \mathbf{e}_{i+1}^{T} \mathbf{e}_{i+1} \right) \end{bmatrix} > 0, \quad (34)$$

where $\Phi_2 = \gamma \mathbf{Q}^{-1} + \lambda \mathbf{E}_{i+1}^{\mathrm{T}} \mathbf{E}_{i+1} - \mathbf{S} - \mathbf{K}_{i+1}^{\mathrm{T}} \mathbf{R} \mathbf{K}_{i+1} - \mathbf{Q}_I$. Pre- and postmultiplying by diag[**Q** I I I] gives

$$\begin{bmatrix} \mathbf{\Phi}_{3} & 0 & \mathbf{Q}\overline{\mathbf{A}}_{i+1}^{T} & \lambda \mathbf{Q}\mathbf{E}_{i+1}^{T}\mathbf{e}_{i+1} \\ 0 & \mathbf{S} & \mathbf{A}_{di+1}^{T} & 0 \\ \overline{\mathbf{A}}_{i+1}\mathbf{Q} & \mathbf{A}_{di+1} & \gamma^{-1}\mathbf{Q} & \mathbf{b}_{i+1} \\ \lambda \mathbf{e}_{i+1}^{T}\mathbf{E}_{i+1}\mathbf{Q} & 0 & \mathbf{b}_{i+1}^{T} & -\lambda \left(1 - \mathbf{e}_{i+1}^{T}\mathbf{e}_{i+1}\right) \end{bmatrix} > 0, \quad (35)$$

where

$$\Phi_3 = \gamma \mathbf{Q} + \lambda \mathbf{Q} \mathbf{E}_{i+1}^{\mathrm{T}} \mathbf{E}_{i+1} \mathbf{Q} - \mathbf{Q} \mathbf{S} \mathbf{Q}$$
$$- \mathbf{Q} \mathbf{K}_{i+1}^{\mathrm{T}} \mathbf{R} \mathbf{K}_{i+1} \mathbf{Q} - \mathbf{Q} \mathbf{Q}_I \mathbf{Q}.$$
(36)

This is equivalent to

$$\begin{bmatrix} \mathbf{\Phi}_{3} & 0 & \mathbf{Q}\overline{\mathbf{A}}_{i+1}^{\mathrm{T}} \\ 0 & \mathbf{S} & \mathbf{A}_{di+1}^{\mathrm{T}} \\ \overline{\mathbf{A}}_{i+1}\mathbf{Q} & \mathbf{A}_{di+1} & \boldsymbol{\gamma}^{-1}\mathbf{Q} \end{bmatrix} + \begin{bmatrix} \lambda \mathbf{Q}\mathbf{E}_{i+1}^{\mathrm{T}}\mathbf{e}_{i+1} \\ 0 \\ \mathbf{b}_{i+1} \end{bmatrix} \times \lambda^{-1} \left(1 - \mathbf{e}_{i+1}^{\mathrm{T}}\mathbf{e}_{i+1} \right)^{-1} \begin{bmatrix} \lambda \mathbf{Q}\mathbf{E}_{i+1}^{\mathrm{T}}\mathbf{e}_{i+1} \\ 0 \\ \mathbf{b}_{i+1} \end{bmatrix}^{\mathrm{T}} > 0.$$
(37)

Substituting **W** = γ **S**⁻¹ > 0, $\xi = \gamma \lambda^{-1}$, pre- and post-multiplying by

diag
$$\{ \gamma^{-1/2} \ \gamma^{-1/2} \ \gamma^{1/2} \ \gamma^{1/2} \}$$
, (38)

we get the inequality (16) by multiple Schur complements.

(3) *Input Constraints*. It is also possible to incorporate input constraints. We consider bounds on input at time k such as

$$|\mathbf{u}(k+m)| \le u_{\text{max}}, \quad m = 0 \dots n. \tag{39}$$

Inputs can be split into sequences:

$$\left\{\mathbf{u}\left(k\mid k\right),\mathbf{u}\left(k+1\mid k\right)\cdots\mathbf{u}\left(k+n\mid k\right),\mathbf{U}_{t}\right\},\tag{40}$$

where $\mathbf{u}(k \mid k)$, $\mathbf{u}(k+1 \mid k) \cdots \mathbf{u}(k+n \mid k)$ are free variables and \mathbf{U}_t are future control moves in the terminal region given by the state feedback law.

- (1) If PWA does not switches to the terminal operating ellipsoid region, the sequences $\mathbf{u}(k+m\mid k), m=0...n$ are free variables satisfying $|\mathbf{u}(k+m)| \le u_{\max}, m=0...n$.
- (2) If PWA switch to the terminal operating ellipsoid region,

$$\mathbf{U}_{t}: \mathbf{u}\left(k+m\mid k\right) = \mathbf{K}_{i+1}\mathbf{x}\left(k+m\mid k\right), \quad m \geq n+1,$$

$$\mathbf{K}_{i+1} = \mathbf{Y}_{i+1}\mathbf{Q}^{-1}, \qquad (41)$$

$$|\mathbf{u}\left(k\right)| \leq u_{\max},$$

where \mathbf{K}_{i+1} is state feedback matrix, which is equal to LMI (13).

Using the previous techniques, the problem of minimizing an upper bound on the worst-case objective function, subject to input and terminal operating ellipsoid constraints, is reduced to a convex optimization of $\{\mathbf{u}(k \mid k), \mathbf{u}(k+1 \mid k) \cdots \mathbf{u}(k+n \mid k), \mathbf{U}_t\}$ in terms of LMIs (12)–(16).

Remark 7. Although derived for a time-delay PWA system with ellipsoidal partitions, the optimization problem LMI (16) gives a feasible solution only when $-\lambda_i(\mathbf{I} - \mathbf{e}_i \mathbf{e}_i^T) > 0$, which means the ellipsoidal region \mathbf{X}_i does not contain origin [5]. When the ellipsoidal region contains origin, it is

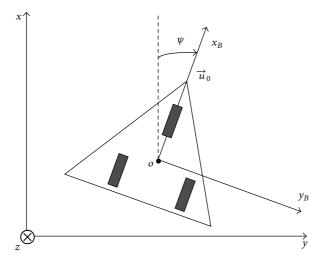


FIGURE 1: Underactuated surface vessel.

assumed that $b_i = 0$. For convenient notion, we get LMI (16) as follows:

$$\begin{bmatrix} \mathbf{Q} & * & * & * & * & * \\ 0 & \mathbf{W}^{-1} & \mathbf{A}_{di+1}^{\mathrm{T}} & 0 & 0 & 0 \\ \mathbf{A}_{i+1}\mathbf{Q} + \mathbf{B}_{i+1}\mathbf{Y}_{i+1} & \mathbf{A}_{di+1} & \mathbf{Q} & 0 & 0 & 0 \\ \mathbf{Q}_{\mathbf{I}}^{1/2}\mathbf{Q} & 0 & 0 & \gamma \mathbf{I} & 0 & 0 \\ \mathbf{R}^{1/2}\mathbf{Y}_{i+1} & 0 & 0 & 0 & \gamma \mathbf{I} & 0 \\ \mathbf{Q} & 0 & 0 & 0 & 0 & W \end{bmatrix} > 0. \quad (42)$$

Remark 8. If the ellipsoidal region X_i contains origin, it is necessary to substitute (42) into (16) to get a feasible solution.

4. Simulation Result

4.1. Example for Autonomous Land Vehicle. We use the ALV (autonomous land vehicle) model formulated by [20] in this simulation. The objective is to design a controller that forces a cart on the x-y plane to follow the straight line y=0 with a constant velocity $u_0=1$ m/s (see Figure 1). We assume that a controller has already been designed to maintain a constant forward velocity. The carts path is then controlled by the torque T about z-axis according to the following dynamics:

$$\begin{bmatrix} \dot{\psi} \\ \dot{\omega} \\ \dot{y} \end{bmatrix} = \begin{bmatrix} 0 & 1 & 0 \\ 0 & -\frac{k}{I} & 0 \\ 0 & 0 & 0 \end{bmatrix} \begin{bmatrix} \psi \\ \omega \\ y \end{bmatrix} + \begin{bmatrix} 0 \\ 0 \\ u_0 \sin(\psi) \end{bmatrix} + \begin{bmatrix} 0 \\ \frac{1}{I} \\ 0 \end{bmatrix} T, \quad (43)$$

$$|T| \le T_{\text{max}},$$

where ψ is the heading angle with time derivative ω , $I=1 \text{ kgm}^2$ is the moment of inertia of the cart with respect to the center of mass, k=0.01 Nms is the damping coefficient, and

T is the control torque. Due to the limitation of power of the drive motor, the maximum control torque T is roughly 8 Nm. Approximately the control constraint is $|T| \leq T_{\max} = 8$. The states of the system are $(x_1, x_2, x_3) = (\varphi, \omega, y)$. We assume that the trajectories can start from any possible initial angle in the range $\varphi_0 \in [-3\pi/5, 3\pi/5]$ and any initial distance from the line. The function $\sin(\psi)$ is approximated by a piecewise affine function yielding a piecewise affine system with 5 regions as follows:

$$\mathbf{X}_{1} = \left\{ \mathbf{x} \mid \mathbf{x}_{1} \in \left(-\frac{3\pi}{5}, -\frac{\pi}{5} \right) \right\},$$

$$\mathbf{X}_{2} = \left\{ \mathbf{x} \mid \mathbf{x}_{1} \in \left(-\frac{\pi}{5}, -\frac{\pi}{15} \right) \right\},$$

$$\mathbf{X}_{3} = \left\{ \mathbf{x} \mid \mathbf{x}_{1} \in \left(-\frac{\pi}{15}, \frac{\pi}{15} \right) \right\},$$

$$\mathbf{X}_{4} = \left\{ \mathbf{x} \mid \mathbf{x}_{1} \in \left(\frac{\pi}{15}, \frac{\pi}{5} \right) \right\},$$

$$\mathbf{X}_{5} = \left\{ \mathbf{x} \mid \mathbf{x}_{1} \in \left(\frac{\pi}{5}, \frac{3\pi}{5} \right) \right\}.$$

$$(44)$$

To illustrate the proposed results on the time-delay systems, we assume that the system $\mathbf{x}_2(t)$ is perturbed by time delay and the delay model is given as

$$\dot{\mathbf{x}}_{1}(t) = \alpha \mathbf{x}_{2}(t) + (1 - \alpha) \mathbf{x}_{2}(t - \tau),$$

$$\dot{\mathbf{x}}_{2}(t) = -\frac{k}{I} \alpha \mathbf{x}_{2}(t) - \frac{k}{I}(1 - \alpha) \mathbf{x}_{2}(t - \tau) + \frac{1}{I}\mathbf{u},$$

$$\dot{\mathbf{x}}_{3}(t) = \mathbf{u}_{0} \sin(\mathbf{x}_{1}(t)).$$
(45)

The constant α is the retarded coefficient [21], which satisfies the conditions: $\alpha \in [0,1]$. The limits 1 and 0 correspond to no delay term and to a completed delay term, respectively. In this example, we assume $\alpha = 0.7$. We construct the following time-delay PWA system:

$$\dot{\mathbf{x}} = \mathbf{A}_{i}\mathbf{x} + \mathbf{A}_{di}\mathbf{x}(t - \tau) + \mathbf{B}_{i}u + \mathbf{b}_{i} \quad \mathbf{x} \in \mathbf{X}_{i}$$

$$|u| \le u_{\text{max}} \quad i = 1, 2, \dots, 5,$$
(46)

where
$$\mathbf{A}_{1,5} = \begin{bmatrix} 0 & 0.7 & 0 \\ 0.309 & -0.007 & 0 \\ 0.309 & 0 \end{bmatrix}$$
, $\mathbf{A}_{3} = \begin{bmatrix} 0 & 0.7 & 0 \\ 1 & -0.007 & 0 \\ 1 & 0.007 & 0 \end{bmatrix}$, $\mathbf{A}_{2,4} = \begin{bmatrix} 0 & 0.7 & 0 \\ 0.914 & -0.007 & 0 \\ 0.914 & 0.007 & 0 \end{bmatrix}$, $\mathbf{B}_{1,2,3,4,5} = \begin{bmatrix} 0 & 1 & 0 \end{bmatrix}^{\mathrm{T}}$, $\mathbf{A}_{d1} = \mathbf{A}_{d2} = \mathbf{A}_{d3} = \mathbf{A}_{d4} = \mathbf{A}_{d5} = \begin{bmatrix} 0 & 0.30 & 0 \\ 0 & -0.003 & 0 \\ 0 & 0 & 0 & 0 \end{bmatrix}$, $\mathbf{b}_{1} = \begin{bmatrix} 0 & 0 & -0.757 \end{bmatrix}^{\mathrm{T}}$, $\mathbf{b}_{2} = \begin{bmatrix} 0 & 0 & -0.216 \end{bmatrix}^{\mathrm{T}}$, $\mathbf{b}_{3} = \begin{bmatrix} 0 & 0 & 0 \end{bmatrix}^{\mathrm{T}}$, $\mathbf{b}_{4} = \begin{bmatrix} 0 & 0 & 0.216 \end{bmatrix}^{\mathrm{T}}$, $\mathbf{b}_{5} = \begin{bmatrix} 0 & 0 & 0.757 \end{bmatrix}^{\mathrm{T}}$, $u_{\text{max}} = 8$.

 $\tau = 2$ is the time-delay constant. We construct the discrete system by sampling T = 0.02 s, and initial state $\mathbf{x}(0) = \mathbf{x}(-1) = \mathbf{x}(-2) = [\pi/2, 0, 3]^{\mathrm{T}}$. By applying Theorem 6, we get the simulation results.

Figures 2 and 3 are the simulation results. Figure 2 shows the state response of the PWA system with time delay. Obviously, all of the states are stable. Figure 3 shows control input action. Physical limitations in ALV impose hard constraints on the torque input. The simulation result in Figure 3 shows that state feedback control strategy can

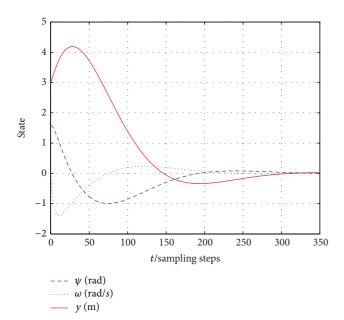


FIGURE 2: States trajectories.

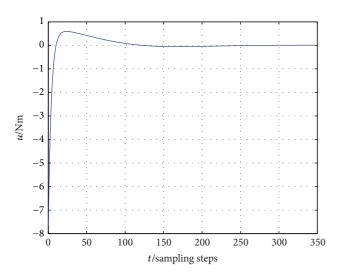


FIGURE 3: Control action.

stabilize the PWA system with time-delay subject to input constraints. In this section, the simulation shows the specified constraints on the torque input variable are satisfied.

4.2. Example for Nonlinear Circuit. This example considers a circuit with a nonlinear resistor taken from [5] and shown in Figure 4 with time in 10^{-10} seconds, the inductor current in mA, and the capacitor voltage in Volts, and the dynamics are

$$\begin{bmatrix} \dot{x}_1 \\ \dot{x}_2 \end{bmatrix} = \begin{bmatrix} -30 & -20 \\ 0.05 & 0 \end{bmatrix} \begin{bmatrix} x_1 \\ x_2 \end{bmatrix} + \begin{bmatrix} 24 \\ -50g(x_2) \end{bmatrix} + \begin{bmatrix} 20 \\ 0 \end{bmatrix} u. \quad (47)$$

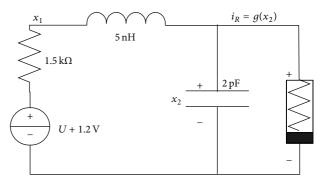


FIGURE 4: A circuit with a nonlinear resistor.

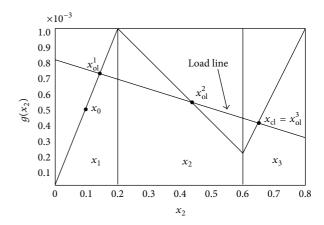


FIGURE 5: Characteristic of the nonlinear resistor.

Following [5], the characteristic of the nonlinear resistor is described as $g(x_2)$, which is defined to be the piecewise-affine function shown in Figure 5. The corresponding polytopic regions are generated as follows:

$$\mathbf{X}_{1} = \left\{ \mathbf{x} \in R^{2} \mid -L < x_{2} < 0.2 \right\},$$

$$\mathbf{X}_{2} = \left\{ \mathbf{x} \in R^{2} \mid 0.2 < x_{2} < 0.6 \right\},$$

$$\mathbf{X}_{3} = \left\{ \mathbf{x} \in R^{2} \mid 0.6 < x_{2} < L \right\},$$
(48)

where L = 100. $\mathbf{X}_{1,2,3}$ are described as ellipsoids in (10) with the following parameters: $E_1 = E_3 = [0, 0.01]$, $E_2 = [0, 5]$, $e_1 = 1.0044$, $e_2 = 1.2145$, and $e_3 = 0.9996$.

By using Lemma 3 and the characteristic of the nonlinear resistor, the dynamics (47) is transformed to the PWA system as follows:

$$\dot{\mathbf{x}} = \begin{bmatrix} -30 & -20 \\ 0.05 & -0.25 \end{bmatrix} \mathbf{x} + \begin{bmatrix} 20 \\ 0 \end{bmatrix} u + \begin{bmatrix} 0 \\ -0.1422 \end{bmatrix} \quad \mathbf{x} \in \mathbf{X}_{1},
\dot{\mathbf{x}} = \begin{bmatrix} -30 & -20 \\ 0.05 & 0.1 \end{bmatrix} \mathbf{x} + \begin{bmatrix} 20 \\ 0 \end{bmatrix} u + \begin{bmatrix} 0 \\ 0.0129 \end{bmatrix} \quad \mathbf{x} \in \mathbf{X}_{2}, \quad (49)$$

$$\dot{\mathbf{x}} = \begin{bmatrix} -30 & -20 \\ 0.05 & -0.2 \end{bmatrix} \mathbf{x} + \begin{bmatrix} 20 \\ 0 \end{bmatrix} u \quad \mathbf{x} \in \mathbf{X}_{3}.$$

Respectively, the open-loop equilibrium points of \mathbf{X}_1 , \mathbf{X}_2 , and \mathbf{X}_3 are $x_{\text{ol}}^1 = [0.71, 0.14]^T$, $x_{\text{ol}}^2 = [0.5, 0.45]^T$, and

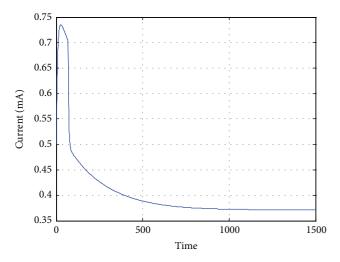


FIGURE 6: Trajectory of the current.

 $x_{\text{ol}}^3 = [0.37, 0.64]^{\text{T}}$. The objective is to design a piecewise-affine state feedback controller to steer the original state x(0) to close-loop equilibrium $x_{\text{cl}} = x_{\text{ol}}^3$; at the same time the control input constraints $|u| \le 1(V)$ must be satisfied.

Using forward differential $\dot{\mathbf{x}} = (\mathbf{x}(k+1) - \mathbf{x}(k))/T$, we get the following PWA with time delay, where T = 0.002 s, and initial state is selected as $\mathbf{x}(0) = \mathbf{x}(-1) = \mathbf{x}(-2) = [0.5; 0.1] \in \mathbf{X}_1$. To illustrate the proposed results on the time-delay system, we assume that the system $x_2(t)$ is perturbed by time delay and the delay model is given as

$$\dot{\mathbf{x}} = \mathbf{A}_{i}\mathbf{x} + \mathbf{A}_{di}\mathbf{x} (t - \tau) + \mathbf{B}_{i}u + \mathbf{b}_{i},$$

$$i = 1, 2, 3, \ \mathbf{x} \in \mathbf{X}_{i}.$$
(50)

The constant α is the retarded coefficient [21]. In this example, we assume $\alpha=0.7$. $\tau=2$ is the time-delay constant, where $\mathbf{A}_1=\begin{bmatrix} -30 & -20\alpha \\ 0.05 & -0.25\alpha \end{bmatrix}$, $\mathbf{A}_2=\begin{bmatrix} -30 & -20\alpha \\ 0.05 & 0.1\alpha \end{bmatrix}$, $\mathbf{A}_3=\begin{bmatrix} -30 & -20\alpha \\ 0.05 & -0.2\alpha \end{bmatrix}$, $\mathbf{A}_{d1}=\mathbf{A}_{d2}=\mathbf{A}_{d3}=\begin{bmatrix} 0 & 1-\alpha \\ 0 & 1-\alpha \end{bmatrix}$, $\mathbf{B}_{1,2,3}=\begin{bmatrix} 20 & 0 \end{bmatrix}^T$, $\mathbf{b}_1=\begin{bmatrix} 0 & -0.1422 \end{bmatrix}^T$, $\mathbf{b}_2=\begin{bmatrix} 0 & 0.0129 \end{bmatrix}^T$, and $\mathbf{b}_3=\begin{bmatrix} 0 & 0 \end{bmatrix}^T$. By applying Theorem 6, we get the following simulation results.

Figures 6 and 7 show the state response of the PWA system with time delay. Trajectory of the current and voltage shows that the original states are steered from \mathbf{X}_1 to closeloop equilibrium in \mathbf{X}_3 . Obviously, all of the states are stable. Figure 8 shows the control input action. The simulation result shows that state feedback control strategy can stabilize the PWA system with time delay subject to ellipsoid constraints. Moreover, the constraint on the control input is satisfied.

5. Conclusion

This work presented a stabilizing multimodel predictive control algorithm which has a contractive constraint to guarantee closed-loop stability. Moreover, the stability of the closed-loop is analyzed by employing the Lyapunov functions approach. Depending on the system state (in the terminal region or outside) the corresponding Lyapunov functions are assigned. The use of multiple objective functions has

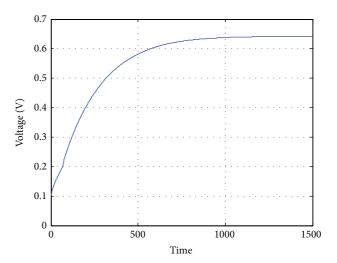


FIGURE 7: Trajectory of the voltage.

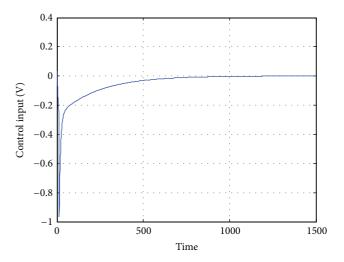


FIGURE 8: Control input.

enabled us to relax the monotonically decreasing condition of the Lyapunov function when the control algorithm switches from a quasi-infinite horizon to an infinite horizon strategy. We have developed a new controller design technique for MPC of piecewise affine systems with timedelay and input constraints. The two simulation examples proposed in Section 4 show that the driving moment (in example 1) and control voltage (in example 2) are limited in amplitude, which makes MPC approach a natural choice for the design of the controller with hard constraints. The technique in this paper leads to convex LMIs based online optimization problem when the local operating regions of the piecewise linear model family are described by ellipsoids. Perhaps the principal shortcoming of MPC proposed is their inability to explicitly incorporate plant model uncertainty. MPC involving data-driven technique is suitable to overcome the previous problem [7, 10, 11, 22, 23]. And it should also be noted that the controller proposed in this paper is developed with known order of regions. In the future work, efforts

will be made to design the data-driven MPC controller with uncertain model parameters and switching order.

Acknowledgments

The authors are grateful to the reviewers for their valuable comments. This work is partially supported by National Natural Science Foundation of China (51379044, 61304060, 61201410, and 61104037), Fundamental Research Funds for the Central Universities (HEUCF130804), and Heilongjiang Province Natural Science Foundation Projects (F200916).

References

- [1] G. Ferrari-Trecate, F. A. Cuzzola, D. Mignone, and M. Morari, "Analysis of discrete-time piecewise affine and hybrid systems," *Automatica*, vol. 38, no. 12, pp. 2139–2146, 2002.
- [2] F. A. Cuzza and M. Morari, "A generalized approach for analysis and control of discrete-time piecewise affine and hybrid system," in *Hybrid System: Computation and Control*, M. D. Di Benedetto and A. S. Vincentelli, Eds., vol. 2034 of *Lecture Notes* in *Computer Science*, pp. 189–203, Springer, Berlin, Germany, 2001.
- [3] T. A. M. Kevenaar and D. M. W. Leenaerts, "Comparison of piecewise-linear model descriptions," *IEEE Transactions on Circuits and Systems I*, vol. 39, no. 12, pp. 996–1004, 1992.
- [4] M. Johansson and A. Rantzer, "Computation of piecewise quadratic Lyapunov functions for hybrid systems," *IEEE Trans*actions on Automatic Control, vol. 43, no. 4, pp. 555–559, 1998.
- [5] L. Rodrigues and S. Boyd, "Piecewise-affine state feedback for piecewise-affine slab systems using convex optimization," *Systems & Control Letters*, vol. 54, no. 9, pp. 835–853, 2005.
- [6] S. Boyd, L. El Ghaoui, E. Feron, and V. Balakrishnan, Linear Matrix Inequalities in System and Control Theory, vol. 15 of SIAM Studies in Applied Mathematics, SIAM, Philadelphia, Pa, USA, 1994
- [7] S. Ding, S. Yin, K. Peng, H. Hao, and B. Shen, "A novel scheme for key performance indicator prediction and diagnosis with application to an industrial hot strip mill," *IEEE Transactions* on *Industrial Informatics*, vol. 9, no. 4, pp. 2239–2247, 2012.
- [8] V. Vesely, D. Rosinova, and T. N. Quang, "Networked output feedback robust predictive controller design," *International Journal of Innovative Computing, Information and Control*, vol. 9, no. 10, pp. 3941–3953, 2013.
- [9] S. Bououden, M. Chadli, F. Allouani, and S. Filali, "A new approach for fuzzy predictive adaptive controller design using particle swarm optimization algorithm," *International Journal of Innovative Computing, Information and Control*, vol. 9, no. 9, pp. 3741–3758, 2013.
- [10] S. Yin, S. Ding, and H. Luo, "Real-time implementation of fault tolerant control system with performance optimization," *IEEE Transactions on Industrial Electronics*, vol. 61, no. 5, pp. 2402–2411, 2013.
- [11] S. Yin, S. Ding, A. Haghani, H. Hao, and P. Zhang, "A comparison study of basic data-driven fault diagnosis and process monitoring methods on the benchmark Tennessee Eastman process," *Journal of Process Control*, vol. 22, no. 9, pp. 1567–1581, 2012.
- [12] C. Bruno and D. Olivie, "LMI-based multi-model predictive control of an industrial C₃/C₄ splitter," *Journal of Control*,

- Automation and Electrical Systems, vol. 24, no. 4, pp. 420-429, 2013.
- [13] D. Dougherty and D. Cooper, "A practical multiple model adaptive strategy for multivariable model predictive control," *Control Engineering Practice*, vol. 11, no. 6, pp. 649–664, 2003.
- [14] P. Falugi, S. Olaru, and D. Dumur, "Multi-model predictive control based on LMI: from the adaptation of the statespace model to the analytic description of the control law," *International Journal of Control*, vol. 83, no. 8, pp. 1548–1563, 2010.
- [15] Z. Tian and K. A. Hoo, "Transition control using a state-shared model approach," *Computers and Chemical Engineering*, vol. 27, no. 11, pp. 1641–1656, 2003.
- [16] M. Johansson and A. Rantzer, "Computation of piecewise quadratic Lyapunov functions for hybrid systems," *IEEE Transactions on Automatic Control*, vol. 43, no. 4, pp. 555–559, 1998.
- [17] G. Ferrari-Trecate, F. A. Cuzzola, D. Mignone, and M. Morari, "Analysis of discrete-time piecewise affine and hybrid systems," *Automatica*, vol. 38, no. 12, pp. 2139–2146, 2002.
- [18] G. Xinping, L. Zhiyun, and D. Guangren, "Observer-based robust control for uncertain linear systems with time-delay," *Control and Decision*, vol. 14, no. 6, pp. 716–720, 1999.
- [19] M. V. Kothare, V. Balakrishnan, and M. Morari, "Robust constrained model predictive control using linear matrix inequalities," *Automatica*, vol. 32, no. 10, pp. 1361–1379, 1996.
- [20] L. Rodrigues, Dynamic output feedback controller synthesis for piecewise-affine systems [Ph.D. thesis], Stanford University, Palo Alto, Calif, USA, 2002.
- [21] Y. Cao and P. M. Frank, "Stability analysis and synthesis of nonlinear time-delay systems via linear Takagi-Sugeno fuzzy models," Fuzzy Sets and Systems, vol. 124, no. 2, pp. 213–229, 2001
- [22] S. Yin, S. Ding, A. Haghani, and H. Hao, "Data-driven monitoring for stochastic systems and its application on batch process," *International Journal of Systems Science*, vol. 44, no. 7, pp. 1366– 1376, 2013.
- [23] S. Yin, X. Yang, and H. Karimi, "Data-driven adaptive observer for fault diagnosis," *Mathematical Problems in Engineering*, vol. 2012, Article ID 832836, 21 pages, 2012.

Hindawi Publishing Corporation Abstract and Applied Analysis Volume 2013, Article ID 726794, 15 pages http://dx.doi.org/10.1155/2013/726794

Research Article

Exponential Stabilization for Timoshenko Beam with Distributed Delay in the Boundary Control

Xiu Fang Liu and Gen Qi Xu

Department of Mathematics, Tianjin University, Tianjin 300072, China

Correspondence should be addressed to Xiu Fang Liu; liuxiu31@126.com

Received 23 October 2013; Accepted 18 November 2013

Academic Editor: Shen Yin

Copyright © 2013 X. F. Liu and G. Q. Xu. This is an open access article distributed under the Creative Commons Attribution License, which permits unrestricted use, distribution, and reproduction in any medium, provided the original work is properly cited

We consider the exponential stabilization for Timoshenko beam with distributed delay in the boundary control. Suppose that the controller outputs are of the form $\alpha_1 u_1(t) + \beta_1 u_1(t-\tau) + \int_{-\tau}^0 g_1(\eta) u_1(t+\eta) d\eta$ and $\alpha_2 u_2(t) + \beta_2 u_2(t-\tau) + \int_{-\tau}^0 g_2(\eta) u_2(t+\eta) d\eta$; where $u_1(t)$ and $u_2(t)$ are the inputs of boundary controllers. In the past, most stabilization results for wave equations and Euler-Bernoulli beam with delay are required $\alpha_i > \beta_i > 0$, i = 1, 2. In the present paper, we will give the exponential stabilization about Timoshenko beam with distributed delay and demand to satisfy the lesser conditions for $\alpha_i, \beta_i, i = 1, 2$.

1. Introduction

Since the extensive applications of Timoshenko beam in high-Tech, the stabilization problem has been a hot topic in the mathematical control theory and engineering; for instance, see [1–5] and the references therein. In many literature, the control delay problem has been neglected. Due to extensive applications of the system with delay, more and more scholars devoted to study the stabilization of the system with controller delay. It is well known that time delay caused by controller memory usually takes the form $\int_{-\infty}^0 d\alpha(s) u(t+s),$ where $\alpha(s)$ is a bounded variation function (or matrix-valued function) and u(t) is the control input. If the control is in the space $L^2_{\rm loc}(\mathbb{R})$, then the memory controller will take the form

$$\int_{-\tau}^{0} d\alpha (s) u (t + s) = \alpha u (t) + \beta u (t - \tau)$$

$$+ \int_{-\tau}^{0} g (s) u (t + s) ds.$$
(1)

Based on this reason, Xu et al. (see [6]) studied firstly stabilization of the 1-d wave systems with delay of the form $\alpha u(t) + \beta u(t - \tau)$. They proved that the system with

control delay is exponential stable if $\alpha>\beta>0$ and unstable if $\beta>\alpha$. Nicaise and Pignotti in [7] studied the stability and instability of the wave equation with delay in boundary and internal distributed delay. Nicaise and Valein in [8] extend the 1-d wave equation to the networks of 1-d wave equations. Shang et al. in [9] studied Euler-Bernoulli beam and showed that $\beta>0$ is not necessary, but the condition $\alpha>|\beta|$ is necessary. For the case of distributed delay, that is, $\beta>0$ and $\int_{-\tau}^0 |g(\eta)| d\eta \neq 0$, Nicaise and Pignotti in [10] discussed a high dimensional wave equation. Under the condition that $\alpha>\int_{-\tau}^0 |g(\eta)| d\eta \neq 0$, they proved the velocity feedback control law also stabilizes exponentially the system.

From above we see that α , β , and $g(\eta)$ are determined by the controller. We cannot determine whether or not $\alpha > \beta > 0$ including $\alpha > |\beta|$ in practice. Under the assumption of state being measurable, Shang and Xu in [11] designed a dynamic feedback controller for cantilever Euler-Bernoulli beam that stabilizes exponentially the system for any real $|\alpha| \neq |\beta|$. Recently Han and Xu in [12] extended this result to the case of output being measurable; they showed that a state observer can realize the state reconstruction from the output of the system. Xu and Wang in [13] discussed the Timoshenko beam with boundary control delay, and they also stabilized the system by a dynamic feedback controller.

Note that the difference between [11, 13], one is a system of single input and single output, the other is a system of 2 inputs and 2 outputs. Such discussion will lead us to extend the method to a general system of multiinput and multioutput. So far, however, there is no result for any α , β , and $g(\eta)$ about Timoshenko beams. In this paper, we still consider Timoshenko beam with boundary control distributed delay. We will seek for a dynamic feedback control law that exponentially stabilizes the Timoshenko beam with distributed delay under certain conditions.

The rest is organized as follows. In Section 2, we will describe the design process of controllers, including predict system and generation of signal, and then state the main results of this paper. In Section 3, we will give the representation of the transform system. In Section 4, we will prove our first result on the stabilization of the original system. In Section 5, we will prove the second result on the exponential stabilization of the induced system. In Section 6, we conclude the paper.

2. Design of Controllers and Main Results

Let w(x,t) be the displacement and $\varphi(x,t)$ the rotation angle of the beam. The motion of a cantilever beam is governed by the following partial differential equations:

$$\rho w_{tt}(x,t) - K(w_{xx} - \varphi_x)(x,t) = 0,$$

$$x \in (0,1), t > 0,$$

$$I_{\rho} \varphi_{tt}(x,t) - EI\varphi_{xx}(x,t) - K(w_x - \varphi)(x,t) = 0,$$

$$x \in (0,1), t > 0,$$

$$w(0,t) = \varphi(0,t) = 0, t > 0,$$

$$K(w_x - \varphi)(1,t) = v_1(t),$$

$$EI\varphi_x(1,t) = v_2(t),$$

$$w(x,0) = w_0(x), w_t(x,0) = w_1(x),$$

$$\varphi(x,0) = \varphi_0(x), \varphi_t(x,0) = \varphi_1(x),$$

where $v_1(t)$ and $v_2(t)$ are the control force and torque from the controllers, respectively. If the controllers have no memory, namely, $u_j(t) = v_j(t)$, j = 1, 2, where $u_j(t)$ are controller inputs, this model had been studied in [14]. If the controllers have memory, then the Timoshenko beam became

$$\begin{split} \rho w_{tt} \left(x,t \right) - K \left(w_{xx} - \varphi_x \right) \left(x,t \right) &= 0, \\ x \in \left(0,1 \right), \ t > 0, \\ I_{\rho} \varphi_{tt} \left(x,t \right) - E I \varphi_{xx} \left(x,t \right) - K \left(w_x - \varphi \right) \left(x,t \right) &= 0, \\ x \in \left(0,1 \right), \ t > 0, \\ w \left(0,t \right) &= \varphi \left(0,t \right) &= 0, \quad t > 0, \end{split}$$

$$K(w_{x} - \varphi)(1, t) = \alpha_{1}u_{1}(t) + \beta_{1}u_{1}(t - \tau)$$

$$+ \int_{-\tau}^{0} g_{1}(\eta) u_{1}(t + \eta) d\eta,$$

$$EI\varphi_{x}(1, t) = \alpha_{2}u_{2}(t) + \beta_{2}u_{2}(t - \tau)$$

$$+ \int_{-\tau}^{0} g_{2}(\eta) u_{2}(t + \eta) d\eta,$$

$$w(x, 0) = w_{0}(x), \qquad w_{t}(x, 0) = w_{1}(x),$$

$$\varphi(x, 0) = \varphi_{0}(x), \qquad \varphi_{t}(x, 0) = \varphi_{1}(x),$$

$$u_{1}(\theta) = f_{1}(\theta), \quad u_{2}(\theta) = f_{2}(\theta), \quad \theta \in (-\tau, 0),$$

$$(3)$$

where τ is the delay time, $\alpha_i, \beta_i \in \mathbb{R}$ (i = 1, 2) are the controller parameters, and $g_i(\eta) \in L^2[-\tau, 0], j = 1, 2$, and $f_i(\theta), \theta \in (-\tau, 0)$ (i = 1, 2) are bounded measurable functions that are memory values of controllers. When $g_j \equiv 0$, j = 1, 2, (3) is just the model in [13].

We suppose that the state of (3) is measurable; that is, $(w(x,t), \varphi(x,t), w_t(x,t), \varphi_t(x,t))$ is measurable. We introduce an auxiliary system as follows:

$$\widehat{w}_{s}(x,s,t) = \widehat{z}(x,s,t), \quad x \in (0,1), \ s \in (0,\tau),$$

$$\widehat{\varphi}_{s}(x,s,t) = \widehat{\psi}(x,s,t), \quad x \in (0,1), \ s \in (0,\tau),$$

$$\widehat{z}_{s}(x,s,t) = \frac{K}{\rho} \left(\widehat{w}_{xx}(x,s,t) - \widehat{\varphi}_{x}(x,s,t) \right),$$

$$\widehat{\psi}_{s}(x,s,t) = \frac{EI}{I_{\rho}} \widehat{\varphi}_{xx}(x,s,t) + \frac{K}{I_{\rho}} \left(\widehat{w}_{x}(x,s,t) - \widehat{\varphi}(x,s,t) \right),$$

$$\widehat{w}(0,s,t) = \widehat{\varphi}(0,s,t) = 0, \quad s \in (0,\tau),$$

$$K(\widehat{w}_{x} - \widehat{\varphi})(1,s,t) = \beta_{1}u_{1}(t+s-\tau) + \int_{-\tau}^{-s} g_{1}(\eta)u_{1}(t+s+\eta)d\eta,$$

$$s \in (0,\tau),$$

$$EI\widehat{\varphi}_{x}(1,s,t) = \beta_{2}u_{2}(t+s-\tau) + \int_{-\tau}^{-s} g_{2}(\eta)u_{2}(t+s+\eta)d\eta,$$

$$s \in (0,\tau), \ t > 0,$$

$$\widehat{w}(x,0,t) = w(x,t), \quad \widehat{z}(x,0,t) = w_{t}(x,t),$$

$$x \in (0,1),$$

$$\widehat{\varphi}(x,0,t) = \varphi(x,t), \quad \widehat{\psi}_{t}(x,0,t) = \varphi_{t}(x,t),$$

$$x \in (0,1), t > 0.$$

$$(4)$$

Equation (4) is a partial state predictor.

Denote the state of (4) at the moment $s = \tau$ by

$$(p_{1}(x,t), p_{2}(x,t), q_{1}(x,t), q_{2}(x,t))$$

$$= (\widehat{w}(x,\tau,t), \widehat{\varphi}(x,\tau,t), \widehat{z}(x,\tau,t), \widehat{\psi}(x,\tau,t)).$$
(5)

Using (3) we can verify that the functions group $(p_1(x,t), p_2(x,t), q_1(x,t), q_2(x,t))$ satisfy the following partial differential equations:

$$p_{1,t}(x,t) = q_1(x,t) + a_1(x)u_1(t) + a_2(x)u_2(t), x \in (0,1), t > 0,$$

$$p_{2,t}(x,t) = q_2(x,t) + a_3(x)u_1(t) + a_4(x)u_2(t), x \in (0,1), t > 0,$$

$$q_{1,t}(x,t) = \frac{K}{\rho} \left(p_{1,xx} - p_{2,x} \right)(x,t) + b_1(x)u_1(t) + b_2(x)u_2(t), q_{2,t}(x,t) = \frac{EI}{I_\rho} p_{2,xx}(x,t) + \frac{K}{I_\rho} \left(p_{1,x} - p_2 \right)(x,t) + b_3(x)u_1(t) + b_4(x)u_2(t), p_1(0,t) = p_2(0,t) = q_1(0,t) = q_2(0,t) = 0, t > 0,$$

$$K\left(p_{1,x} - p_2 \right)(1,t) = \beta_1 u_1(t), \quad t > 0, EIp_{2,x}(1,t) = \beta_2 u_2(t), \quad t > 0,$$

$$p_1(x,0) = E_1\left(w_0, \varphi_0, w_1, \varphi_1 \right)(x) - \int_{-\tau}^0 a_1(x,s) f_1(s) ds - \int_{-\tau}^0 a_2(x,s) f_2(s) ds, p_2(x,0) = E_2\left(w_0, \varphi_0, w_1, \varphi_1 \right)(x) - \int_{-\tau}^0 b_1(x,s) f_1(s) ds - \int_{-\tau}^0 b_2(x,s) f_2(s) ds, q_1(x,0) = E_3\left(w_0, \varphi_0, w_1, \varphi_1 \right)(x) + \int_{-\tau}^0 b_1(x,s) f_1(s) ds + \int_{-\tau}^0 b_2(x,s) f_2(s) ds, q_2(x,0) = E_4\left(w_0, \varphi_0, w_1, \varphi_1 \right)(x) + \int_{-\tau}^0 b_3(x,s) f_1(s) ds + \int_{-\tau}^0 b_4(x,s) f_2(s) ds,$$
 (6)

where $a_i(x, r), b_i(x, r), a_i(x), b_i(x)$ (i = 1, 2, 3, 4) are measurable function and E_i (i = 1, 2, 3, 4) are bounded linear operators on $[H^1[0, 1] \times L^2[0, 1]]^2$; they are determined later.

Equation (6) is a system without delay, but the controls appear in the system interior and boundary. First we consider the stabilization problem of (6). Let us consider the energy functional of (6)

$$E(t) = \frac{1}{2} \| (p_1, p_2) \|_{V_K^1(0,1) \times V_{EI}^1(0,1)}^2$$

$$+ \frac{1}{2} \| (q_1, q_2) \|_{L_\rho^2(0,1) \times L_{I_\rho}^2(0,1)}^2$$

$$= \frac{1}{2} \int_0^1 K |p_{1,x}(x,t) - p_2(x,t)|^2 dx$$

$$+ \frac{1}{2} \int_0^1 EI |p_{2,x}(x,t)|^2 dx$$

$$+ \frac{1}{2} \int_0^1 \rho |q_1(x,t)|^2 dx$$

$$+ \frac{1}{2} \int_0^1 I_\rho |q_2(x,t)|^2 dx .$$

$$(7)$$

A direct calculation gives

$$\frac{dE(t)}{dt}$$

$$= u_{1}(t) \left[\beta_{1}q_{1}(1,t) + \int_{0}^{1} K(p_{1,x} - p_{2}) \left[a'_{1}(x) - a_{3}(x) \right] dx + \int_{0}^{1} EIp_{2,x}(x,t) a'_{3}(x) dx + \int_{0}^{1} \rho q_{1}(x,t) b_{1}(x) dx + \int_{0}^{1} I_{\rho}q_{2}(x,t) b_{3}(x) dx \right]$$

$$+ u_{2}(t) \left[\beta_{2}q_{2}(1,t) + \int_{0}^{1} K(p_{1,x} - p_{2}) \times \left[a'_{2}(x) - a_{4}(x) \right] dx + \int_{0}^{1} EIp_{2,x}(x,t) a'_{4}(x) dx + \int_{0}^{1} \rho q_{1}(x,t) b_{2}(x) dx + \int_{0}^{1} I_{\rho}q_{2}(x,t) b_{4}(x) dx \right].$$

Set $U_{1}(p_{1}, p_{2}, q_{1}, q_{2})$ $= \beta_{1}q_{1}(1, t)$ $+ \int_{0}^{1} K(p_{1,x}(x, t) - p_{2}(x, t)) (a'_{1}(x) - a_{3}(x)) dx$

$$+ \int_{0}^{1} \rho q_{1}(x,t) b_{1}(x) dx + \int_{0}^{1} EIp_{2,x}(x,t) a'_{3}(x) dx$$

$$+ \int_{0}^{1} I_{\rho} q_{2}(x,t) b_{3}(x) dx;$$

$$U_{2}(p_{1}, p_{2}, q_{1}, q_{2})$$

$$= \beta_{2} q_{2}(1,t)$$

$$+ \int_{0}^{1} K(p_{1,x}(x,t) - p_{2}(x,t)) (a'_{2}(x) - a_{4}(x)) dx$$

$$+ \int_{0}^{1} \rho q_{1}(x,t) b_{2}(x) dx + \int_{0}^{1} EIp_{2,x}(x,t) a'_{4}(x) dx$$

$$+ \int_{0}^{1} I_{\rho} q_{2}(x,t) b_{4}(x) dx. \tag{9}$$

We take the feedback control law as

$$u_{1}(t) = -U_{1}(p_{1}, p_{2}, q_{1}, q_{2}),$$

$$u_{2}(t) = -U_{2}(p_{1}, p_{2}, q_{1}, q_{2}).$$
(10)

Then, the closed loop system associated with (6) is

$$\begin{split} p_{1,t}\left(x,t\right) &= q_{1}\left(x,t\right) - a_{1}\left(x\right)U_{1}\left(p_{1},p_{2},q_{1},q_{2}\right) \\ &- a_{2}\left(x\right)U_{2}\left(p_{1},p_{2},q_{1},q_{2}\right), \\ &x \in \left(0,1\right), \ t > 0, \\ p_{2,t}\left(x,t\right) &= q_{2}\left(x,t\right) - a_{3}\left(x\right)U_{1}\left(p_{1},p_{2},q_{1},q_{2}\right) \\ &- a_{4}\left(x\right)U_{2}\left(p_{1},p_{2},q_{1},q_{2}\right), \\ &x \in \left(0,1\right), \ t > 0, \\ q_{1,t}\left(x,t\right) &= \frac{K}{\rho}\left(p_{1,xx} - p_{2,x}\right)\left(x,t\right) - b_{1}\left(x\right)U_{1} \\ &\times \left(p_{1},p_{2},q_{1},q_{2}\right) - b_{2}\left(x\right)U_{2}\left(p_{1},p_{2},q_{1},q_{2}\right), \\ q_{2,t}\left(x,t\right) &= \frac{EI}{I_{\rho}}p_{2,xx}\left(x,t\right) + \frac{K}{I_{\rho}}\left(p_{1,x} - p_{2}\right)\left(x,t\right) \\ &- b_{3}\left(x\right)U_{1}\left(p_{1},p_{2},q_{1},q_{2}\right) \\ &- b_{4}\left(x\right)U_{2}\left(p_{1},p_{2},q_{1},q_{2}\right), \\ p_{1}\left(0,t\right) &= p_{2}\left(0,t\right) = q_{1}\left(0,t\right) = q_{2}\left(0,t\right) = 0, \quad t > 0, \\ K\left(p_{1,x} - p_{2}\right)\left(1,t\right) &= -\beta_{1}U_{1}\left(p_{1},p_{2},q_{1},q_{2}\right), \quad t > 0, \\ EIp_{2,xx}\left(1,t\right) &= -\beta_{2}U_{2}\left(p_{1},p_{2},q_{1},q_{2}\right), \quad t > 0, \\ p_{1}\left(x,0\right) &= E_{1}\left(w_{0},\varphi_{0},w_{1},\varphi_{1}\right)\left(x\right) - \int_{-\tau}^{0} a_{1}\left(x,s\right)f_{1}\left(s\right)ds \\ &- \int_{-\tau}^{0} a_{2}\left(x,s\right)f_{1}\left(s\right)ds, \end{split}$$

$$p_{2}(x,0) = E_{2}(w_{0}, \varphi_{0}, w_{1}, \varphi_{1})(x) - \int_{-\tau}^{0} a_{3}(x, s) f_{1}(s) ds$$

$$- \int_{-\tau}^{0} a_{4}(x, s) f_{1}(s) ds,$$

$$q_{1}(x,0) = E_{3}(w_{0}, \varphi_{0}, w_{1}, \varphi_{1})(x) + \int_{-\tau}^{0} b_{1}(x, s) f_{1}(s) ds$$

$$+ \int_{-\tau}^{0} b_{2}(x, s) f_{1}(s) ds,$$

$$q_{2}(x,0) = E_{4}(w_{0}, \varphi_{0}, w_{1}, \varphi_{1})(x) + \int_{-\tau}^{0} b_{3}(x, s) f_{1}(s) ds$$

$$+ \int_{-\tau}^{0} b_{4}(x, s) f_{1}(s) ds.$$
(11)

We estimate the error of the system (3) with control (10) and the system (11).

Let $(w(x,t), \varphi(x,t), w_t(x,t), \varphi_t(x,t))$ be the solution to (3) with control signals (10) and let function group $(p_1(x,t), p_2(x,t), q_1(x,t), q_2(x,t))$ be the solution to (11). Set $W(x,t) = (w(x,t), \varphi(x,t))$ and $W_t(x,t) = (w_t(x,t), \varphi_t(x,t))$, and set $P(x,t) = (p_1(x,t), p_2(x,t))$ and $Q(x,t) = (q_1(x,t), q_2(x,t))$.

To discuss the stability $(W(x,t), W_t(x,t))$, we consider the error both solutions in the energy space

$$\begin{split} \|P(\cdot,t) - W(\cdot,t+\tau)\|_{V_{K}^{1}(0,1)\times V_{EI}^{1}(0,1)}^{2} \\ + \|Q(\cdot,t) - W_{t}(\cdot,t+\tau)\|_{L_{o}^{2}(0,1)\times L_{I_{c}^{2}(0,1)}^{2}}^{2}. \end{split} \tag{12}$$

In this paper, we will prove the following results.

Theorem 1. Let $(W(x,t),W_t(x,t))$ be the solution to (3) with controls (10) and let (P(x,t),Q(x,t)) be the solution to the closed-loop system (11). If the system (11) is asymptotically (exponentially) stable, then the system (3) also is asymptotically (exponentially) stable.

Theorem 2. Suppose that $K/\rho \neq EI/I_\rho$. Let $\mu_n, n \in \mathbb{N}$ be the eigenvalues of the free system (the system (2) without controls). Set

$$\xi_{n}^{(1)} = \int_{-\tau}^{0} g_{1}(\eta) e^{-i\sqrt{\mu_{n}}(\tau+\eta)} d\eta,
\xi_{n}^{(2)} = \int_{-\tau}^{0} g_{2}(\eta) e^{-i\sqrt{\mu_{n}}(\tau+\eta)} d\eta.$$
(13)

Then the following assertions are true:

(1) *when*

$$\inf_{n} \left| \frac{\beta_{1}}{\rho} + \alpha_{1} e^{-i\tau\sqrt{\mu_{n}}} + \xi_{n}^{(1)} \right| > 0,$$

$$\inf_{n} \left| \frac{\beta_{2}}{I_{\rho}} + \alpha_{2} e^{-i\tau\sqrt{\mu_{n}}} + \xi_{n}^{(2)} \right| > 0,$$
(14)

the system (11) is exponentially stable;

(2) if for all $n \in \mathbb{N}$,

$$\left| \frac{\beta_1}{\rho} + \alpha_1 e^{-i\tau\sqrt{\mu_n}} + \xi_n^{(1)} \right| > 0,$$

$$\left| \frac{\beta_2}{I_\rho} + \alpha_2 e^{-i\tau\sqrt{\mu_n}} + \xi_n^{(2)} \right| > 0$$
(15)

but

$$\inf_{n} \left| \frac{\beta_{1}}{\rho} + \alpha_{1} e^{-i\tau \sqrt{\mu_{n}}} + \xi_{n}^{(1)} \right| = 0,$$

$$\inf_{n} \left| \frac{\beta_{2}}{I_{\rho}} + \alpha_{2} e^{-i\tau \sqrt{\mu_{n}}} + \xi_{n}^{(2)} \right| = 0,$$
(16)

then the system (11) is asymptotically stable.

In the following sections, we will prove our results. In Section 3, we will determine functions $a_i(x), b_i(x), a_i(x,s), b_i(x,s)$ (i = 1, 2, 3, 4). In Section 4, we will prove Theorem 1. In Section 5, we pay our attention to the proof of Theorem 2.

3. Representation of the System (6)

In this section, we will obtain the expressions for the functions $a_i(x)$, $b_i(x)$, $a_i(x,s)$, $b_i(x,s)$ (i = 1, 2, 3, 4) appearing in system (6) using (3) and (4).

We begin with introducing two useful lemmas.

Lemma 3 (see [13]). Define the differential operator in $L^2_{\rho}(0,1) \times L^2_{I_0}(0,1)$ as follows:

$$\mathcal{L}(w,\varphi) = \left(-\frac{K}{\rho}\left(w''(x) - \varphi'(x)\right), -\frac{EI}{I_{\rho}}\varphi''(x)\right) - \frac{K}{I_{\rho}}\left(w'(x) - \varphi(x)\right)^{T},$$
(17)

with domain

 $\mathcal{D}(\mathcal{L})$

$$= \begin{cases} (w(x), \varphi(x)) \in H^{2}(0, 1) & w(0) = \varphi(0) = 0, \\ \times H^{2}(0, 1) & K(w'(1) - \varphi(1)) = 0, \\ & EI\varphi'(1) = 0 \end{cases}.$$
(18)

Then \mathcal{L} is a positive define operator with compact resolvent in $L_o^2(0,1) \times L_L^2(0,1)$; its eigenvalues are

$$0 < \mu_1 < \mu_2 < \dots < \mu_n < \dots \tag{19}$$

and the eigenfunctions $\Phi_n(x) = (w_n(x), \varphi_n(x))^T$ corresponding to μ_n are real functions and form a normalized orthogonal basis for $L^2_{\rho}(0,1) \times L^2_{I_{\rho}}(0,1)$.

Lemma 4 (see [13]). Let $\Phi_n(x) = (w_n(x), \varphi_n(x))$ be the normalized eigenfunction corresponding to the eigenvalue μ_n of \mathcal{L} . Then it holds that

$$\int_{0}^{1} K \left| w_{n}'(x) - \varphi_{n}(x) \right|^{2} dx + \int_{0}^{1} EI \left| \varphi_{n}'(x) \right|^{2} dx = \mu_{n},$$

$$0 < \inf_{n} \left\{ \rho \left| w_{n}(1) \right|^{2} + \left| I_{\rho} \varphi_{n}(1) \right|^{2} \right\}$$

$$\leq \sup_{n} \left\{ \rho \left| w_{n}(1) \right|^{2} + \left| I_{\rho} \varphi_{n}(1) \right|^{2} \right\} < \infty.$$
(20)

Now let us return to (3). We write the equation in (3) into the vector form

$$\begin{pmatrix} w_{tt}(x,t) \\ \varphi_{tt}(x,t) \end{pmatrix} - \begin{pmatrix} \frac{K}{\rho} \partial_{xx} & -\frac{K}{\rho} \partial_{x} \\ \frac{K}{I_{\rho}} \partial_{x} & \frac{EI}{I_{\rho}} \partial_{xx} - \frac{K}{I_{\rho}} \end{pmatrix} \begin{pmatrix} w(x,t) \\ \varphi(x,t) \end{pmatrix} = 0$$
(21)

and the boundary conditions are $\binom{w(0,t)}{\varphi(0,t)} = 0$, and

$$\begin{pmatrix}
K\partial_{x} & -K \\
0 & EI\partial_{x}
\end{pmatrix}
\begin{pmatrix}
w(x,t) \\
\varphi(x,t)
\end{pmatrix}_{x=1}$$

$$= \begin{pmatrix}
\alpha_{1} & 0 \\
0 & \alpha_{2}
\end{pmatrix}
\begin{pmatrix}
u_{1}(t) \\
u_{2}(t)
\end{pmatrix} + \begin{pmatrix}
\beta_{1} & 0 \\
0 & \beta_{2}
\end{pmatrix}
\begin{pmatrix}
u_{1}(t-\tau) \\
u_{2}(t-\tau)
\end{pmatrix}$$

$$+ \int_{-\tau}^{0} \begin{pmatrix}
g_{1}(\eta) & 0 \\
0 & g_{2}(\eta)
\end{pmatrix}
\begin{pmatrix}
u_{1}(t+\eta) \\
u_{2}(t+\eta)
\end{pmatrix} d\eta.$$
(22)

The initial datum are

$$\begin{pmatrix} w(x,0) \\ \varphi(x,0) \end{pmatrix} = \begin{pmatrix} w_0(x) \\ \varphi_0(x) \end{pmatrix}, \qquad \begin{pmatrix} w_t(x,0) \\ \varphi_t(x,0) \end{pmatrix} = \begin{pmatrix} w_1(x) \\ \varphi_1(x) \end{pmatrix}. \tag{23}$$

Set $W(x,t) = (w(x,t), \varphi(x,t))^T$ and $U(t) = (u_1(t), u_2(t))^T$. Define 2×2 matrices

$$\Lambda_{1} = \begin{pmatrix} \alpha_{1} & 0 \\ 0 & \alpha_{2} \end{pmatrix}, \qquad \Lambda_{2} = \begin{pmatrix} \beta_{1} & 0 \\ 0 & \beta_{2} \end{pmatrix},
\Lambda_{3}(\eta) = \begin{pmatrix} g_{1}(\eta) & 0 \\ 0 & g_{2}(\eta) \end{pmatrix}$$
(24)

and define an operator B from \mathbb{R}^2 to $H^{-1}(0,1) \times H^{-1}(0,1)$, where $H^{-1}(0,1) = \left(V^1_{\omega}(0,1)\right)^*$ is dual space,

$$B = \begin{pmatrix} \delta(x-1) & 0\\ 0 & \delta(x-1) \end{pmatrix}, \tag{25}$$

and define an operator Γ_N from $H^2(0,1) \times H^2(0,1)$ to \mathbb{R}^2 by

$$\Gamma_N W = \begin{pmatrix} K\left(w'\left(1\right) - \varphi\left(1\right)\right) \\ EI\varphi'\left(1\right) \end{pmatrix}, \tag{26}$$

where $W(x) = (w(x), \varphi(x))^T$.

With help of these notations, we can rewrite (3) into

$$\begin{split} W_{tt}\left(x,t\right) + \mathcal{L}W\left(x,t\right) \\ &= B\left(\Lambda_{1}U\left(t\right) + \Lambda_{2}U\left(t-\tau\right) + \int_{-\tau}^{0} \Lambda_{3}\left(\eta\right)U\left(t+\eta\right)d\eta\right), \\ &\qquad \qquad t > 0, \\ W\left(0,t\right) &= 0, \qquad \Gamma_{N}W\left(1,t\right) = 0, \\ W\left(x,0\right) &= W_{0}\left(x\right) = \left(w_{0}\left(x\right), \varphi_{0}\left(x\right)\right)^{T}, \\ W_{t}\left(x,0\right) &= W_{1}\left(x\right) = \left(w_{1}\left(x\right), \varphi_{1}\left(x\right)\right)^{T}, \end{split}$$

$$(27)$$

and (4) into

$$\widehat{W}_{s}(x,s,t) = \widehat{V}(x,s,t),$$

$$\widehat{V}_{s}(x,s,t) + \mathcal{L}\widehat{W}(x,s,t) = B\Lambda_{2}U(t+s-\tau) + B\int_{-\tau}^{-s} \Lambda_{3}(\eta)U(t+s+\eta)d\eta,$$

$$\widehat{W}(0,s,t) = 0, \qquad \Gamma_{N}\widehat{W}(1,s,t) = 0,$$

$$\widehat{W}(x,0,t) = W(x,t),$$

$$\widehat{V}(x,0,t) = W_{t}(x,t),$$
(28)

where $\widehat{W}(x, s, t) = (\widehat{w}(x, s, t), \widehat{\varphi}(x, s, t))^T$, $\widehat{V}(x, s, t) = (\widehat{z}(x, s, t), \widehat{\psi}(x, s, t))^T$.

We define two families of the bounded linear operators on $L^2_{\rho}(0,1)\times L^2_{I_o}(0,1)$ by

$$\operatorname{Cos}(t\mathscr{L})F = \sum_{n=1}^{\infty} \operatorname{cos} \sqrt{\mu_n} t(F, \Phi_n)_{L_{\rho}^2 \times L_{I_{\rho}}^2} \Phi_n,$$

$$\operatorname{Sin}(t\mathscr{L})F = \sum_{n=1}^{\infty} \frac{\sin \sqrt{\mu_n} t}{\sqrt{\mu_n}} (F, \Phi_n)_{L_{\rho}^2 \times L_{I_{\rho}}^2} \Phi_n.$$
(29)

Clearly, the following equalities hold, for any $t \in \mathbb{R}$,

$$\sin(t\mathcal{L}) = \int_0^t \cos(t\mathcal{L}) dt,$$

$$\frac{d}{dt}(\cos(t\mathcal{L})) = -\mathcal{L}\sin(t\mathcal{L}).$$
(30)

It is easy to know that the vector-valued function

$$W(x,t) = \operatorname{Cos}(t\mathcal{L})W_0 + \operatorname{Sin}(t\mathcal{L})W_1$$

$$+ \int_0^t \operatorname{Sin}((t-s)\mathcal{L})B\left[\Lambda_1 U(s) + \Lambda_2 U(s-\tau)\right]ds$$

$$+ \int_0^t \operatorname{Sin}((t-s)\mathcal{L})B\int_{-\tau}^0 \Lambda_3(\eta)U(s+\eta)d\eta ds$$
(31)

is differentiable with respect to t and

$$\begin{split} W_t\left(x,t\right) &= -\mathcal{L}\sin\left(t\mathcal{L}\right)W_0 + \cos\left(t\mathcal{L}\right)W_1 \\ &+ \int_0^t \cos\left(\left(t-s\right)\mathcal{L}\right)B\left[\Lambda_1U\left(s\right) + \Lambda_2U\left(s-\tau\right)\right]ds \\ &+ \int_0^t \cos\left(\left(t-s\right)\mathcal{L}\right)B\int_{-\tau}^0 \Lambda_3\left(\eta\right)U\left(s+\eta\right)d\eta\,ds. \end{split}$$

Further, W(x, t) satisfies (27).

Similarly, we know the vector-valued function

$$\widehat{W}(x, s, t) = \operatorname{Cos}(s\mathcal{L}) W(\cdot, t) + \operatorname{Sin}(s\mathcal{L}) W_t(\cdot, t)$$

$$+ \int_0^s \operatorname{Sin}((s - r) \mathcal{L}) B \Lambda_2 U(t + r - \tau) dr$$

$$+ \int_0^s \operatorname{Sin}((s - r) \mathcal{L}) B \int_{-\tau}^{-r} \Lambda_3(\eta) U(t + r + \eta) d\eta dr,$$
(33)

$$\begin{split} \widehat{V}\left(x,s,t\right) &= -\mathcal{L}\operatorname{Sin}\left(s\mathcal{L}\right)W\left(\cdot,t\right) + \operatorname{Cos}\left(s\mathcal{L}\right)W_{t}\left(\cdot,t\right) \\ &+ \int_{0}^{s}\operatorname{Cos}\left(\left(s-r\right)\mathcal{L}\right)B\Lambda_{2}U\left(t+r-\tau\right)dr \\ &+ \int_{0}^{s}\operatorname{Cos}\left(\left(s-r\right)\mathcal{L}\right)B\int_{-\tau}^{-r}\Lambda_{3}\left(\eta\right)U\left(t+r+\eta\right)d\eta\,dr. \end{split}$$

$$(34)$$

satisfy (28).

$$P(x,t) = \widehat{W}(x,\tau,t), \qquad Q(x,t) = \widehat{V}(x,\tau,t).$$
 (35)

Then we have

$$\begin{pmatrix}
P(x,t) \\
Q(x,t)
\end{pmatrix} = \begin{pmatrix}
\cos(\tau \mathcal{L}) & \sin(\tau \mathcal{L}) \\
-\mathcal{L}\sin(\tau \mathcal{L}) & \cos(\tau \mathcal{L})
\end{pmatrix} \begin{pmatrix}
W(x,t) \\
W_t(x,t)
\end{pmatrix}
+ \int_0^{\tau} \begin{pmatrix}
\sin((\tau - r) \mathcal{L}) \\
\cos((\tau - r) \mathcal{L})
\end{pmatrix} B\Lambda_2 U(t + r - \tau) dr
+ \int_0^{\tau} \begin{pmatrix}
\sin((\tau - r) \mathcal{L}) \\
\cos((\tau - r) \mathcal{L})
\end{pmatrix}
\times B \int_{-\tau}^{-r} \Lambda_3(\eta) U(t + r + \eta) d\eta dr.$$
(36)

Thus,

$$\begin{pmatrix} P_{t}(x,t) \\ Q_{t}(x,t) \end{pmatrix} = \begin{pmatrix} \cos(\tau \mathcal{L}) & \sin(\tau \mathcal{L}) \\ -\mathcal{L}\sin(\tau \mathcal{L}) & \cos(\tau \mathcal{L}) \end{pmatrix} \begin{pmatrix} W_{t}(x,t) \\ W_{tt}(x,t) \end{pmatrix}$$

$$+ \int_{0}^{\tau} \begin{pmatrix} \cos((\tau - r) \mathcal{L}) \\ -\mathcal{L}\sin((\tau - r) \mathcal{L}) \end{pmatrix}$$

$$\times B\Lambda_{2}U(t + r - \tau) dr$$

$$+ \begin{pmatrix} 0 \\ B\Lambda_{2}U(t) \end{pmatrix} - \begin{pmatrix} \sin(\tau\mathcal{L}) \\ \cos(\tau\mathcal{L}) \end{pmatrix} B\Lambda_{2}U(t-\tau)$$
 Note that
$$- \begin{pmatrix} \sin(\tau\mathcal{L}) \\ \cos(\tau\mathcal{L}) \end{pmatrix} B \int_{-\tau}^{0} \Lambda_{3}(\eta) U(t+\eta) d\eta$$

$$+ \int_{0}^{\tau} \begin{pmatrix} \cos((\tau-r)\mathcal{L}) \\ -\mathcal{L}\sin((\tau-r)\mathcal{L}) \end{pmatrix} B$$

$$= \begin{pmatrix} 0 & I \\ -\mathcal{L} & 0 \end{pmatrix} \begin{pmatrix} W(x,t) \\ W_{t}(x,t) \end{pmatrix}$$

$$+ \int_{-\tau}^{0} \begin{pmatrix} \sin((\tau+\eta)\mathcal{L}) \\ \cos((\tau+\eta)\mathcal{L}) \end{pmatrix} B\Lambda_{3}(\eta) U(t) d\eta$$

$$+ \int_{-\tau}^{0} \begin{pmatrix} \sin((\tau+\eta)\mathcal{L}) \\ \cos((\tau+\eta)\mathcal{L}) \end{pmatrix} B\Lambda_{3}(\eta) U(t) d\eta .$$
 (38)

 $\begin{pmatrix}
P_{t}(x,t) \\
Q_{t}(x,t)
\end{pmatrix} = \begin{pmatrix}
0 & I \\
-\mathcal{L} & 0
\end{pmatrix} \begin{pmatrix}
P(x,t) \\
Q(x,t)
\end{pmatrix} \\
+ \begin{pmatrix}
\sin(\tau \mathcal{L}) B \Lambda_{1} U(t) + \int_{-\tau}^{0} \sin((\tau + \eta) \mathcal{L}) B \Lambda_{3}(\eta) U(t) d\eta \\
\cos(\tau \mathcal{L}) B \Lambda_{1} U(t) + \int_{-\tau}^{0} \cos((\tau + \eta) \mathcal{L}) B \Lambda_{3}(\eta) U(t) d\eta + B \Lambda_{2} U(t)
\end{pmatrix}.$ (39)

Therefore, we have equations

$$P_{t}(x,t) = Q(x,t) + \sin(\tau \mathcal{L}) B\Lambda_{1}U(t)$$

$$+ \int_{-\tau}^{0} \sin((\tau + \eta) \mathcal{L}) B\Lambda_{3}(\eta) U(t) d\eta,$$

$$Q_{t}(x,t) = -\mathcal{L}P(x,t) + \cos(\tau \mathcal{L}) B\Lambda_{1}U(t)$$

$$+ \int_{-\tau}^{0} \cos((\tau + \eta) \mathcal{L}) B\Lambda_{3}(\eta) U(t) d\eta,$$
(40)

$$P\left(0,t\right)=Q\left(0,t\right)=0,\qquad\Gamma_{N}P\left(\cdot,t\right)=\Lambda_{2}U\left(t\right)$$
 and initial conditions

$$\begin{split} P\left(x,0\right) &= \operatorname{Cos}\left(\tau\mathscr{L}\right)W_{0} + \operatorname{Sin}\left(\tau\mathscr{L}\right)W_{1} \\ &- \int_{-\tau}^{0} \operatorname{Sin}\left(s\mathscr{L}\right)B\Lambda_{2}f\left(s\right)ds \\ &+ \int_{-\tau}^{0} \int_{-\tau}^{s} \operatorname{Sin}\left(\left(\tau-s+\eta\right)\mathscr{L}\right) \\ &\times B\Lambda_{3}\left(\eta\right)f\left(s\right)d\eta\,ds, \end{split} \tag{41}$$

$$&+ B\Lambda_{3}\left(\eta\right)f\left(s\right)d\eta\,ds, \\ Q\left(x,0\right) &= -\mathscr{L}\operatorname{Sin}\left(\tau\mathscr{L}\right)W_{0} + \operatorname{Cos}\left(\tau\mathscr{L}\right)W_{1} \\ &+ \int_{-\tau}^{0} \operatorname{Cos}\left(s\mathscr{L}\right)B\Lambda_{2}f\left(s\right)ds \\ &+ \int_{-\tau}^{0} \int_{-\tau}^{s} \operatorname{Cos}\left(\left(\tau-s+\eta\right)\mathscr{L}\right)B\Lambda_{3}\left(\eta\right)f\left(s\right)d\eta\,ds, \end{split} \tag{42}$$

where $f(s) = (f_1(s), f_2(s))^T$.

Since all entries of B are meaningful as linear functional on $H^1(0,1)$, so for any $Z=(z_1,z_2)\in\mathbb{R}^2$ and $\Phi_n(x)\in H^1(0,1)\times H^1(0,1)$,

$$(BZ, \Phi_{n})_{L_{\rho}^{2}(0,1) \times L_{I_{\rho}}^{2}(0,1)}$$

$$= z_{1} \int_{0}^{1} \rho \delta(x-1) w_{n}(x) dx + z_{2} \int_{0}^{1} I_{\rho} \delta(x-1) \varphi_{n}(x) dx$$

$$= \rho z_{1} w_{n}(1) + I_{\rho} z_{2} \varphi_{n}(1) = [z_{1}, z_{2}] [\rho w_{n}(1), \varphi_{n}(1)]^{T}.$$
(43)

Therefore, we have the following results.

Theorem 5. Let $\{\mu_n; n \in \mathbb{N}\}$ be the list of all eigenvalues of \mathcal{L} . Then the functions that appear in (6) are

$$\begin{split} a_{1}\left(x\right) &= \rho \sum_{n=1}^{\infty} w_{n}\left(1\right) w_{n}\left(x\right) \\ &\times \left(\alpha_{1} \frac{\sin \tau \sqrt{\mu_{n}}}{\sqrt{\mu_{n}}}\right. \\ &\left. + \int_{-\tau}^{0} g_{1}\left(\eta\right) \frac{\sin \left(\tau + \eta\right) \sqrt{\mu_{n}}}{\sqrt{\mu_{n}}} d\eta\right), \\ a_{2}\left(x\right) &= I_{\rho} \sum_{n=1}^{\infty} \varphi_{n}\left(1\right) w_{n}\left(x\right) \\ &\times \left(\alpha_{2} \frac{\sin \tau \sqrt{\mu_{n}}}{\sqrt{\mu_{n}}}\right. \\ &\left. + \int_{-\tau}^{0} g_{2}\left(\eta\right) \frac{\sin \left(\tau + \eta\right) \sqrt{\mu_{n}}}{\sqrt{\mu_{n}}} d\eta\right), \end{split}$$

$$\begin{split} a_3\left(x\right) &= \rho \sum_{n=1}^{\infty} w_n\left(1\right) \varphi_n\left(x\right) \\ &\times \left(\alpha_1 \frac{\sin \tau \sqrt{\mu_n}}{\sqrt{\mu_n}} \right. \\ &+ \int_{-\tau}^0 g_1\left(\eta\right) \frac{\sin \left(\tau + \eta\right) \sqrt{\mu_n}}{\sqrt{\mu_n}} d\eta \right), \\ a_4\left(x\right) &= I_{\rho} \sum_{n=1}^{\infty} \varphi_n\left(1\right) \varphi_n\left(x\right) \\ &\quad \times \left(\alpha_2 \frac{\sin \tau \sqrt{\mu_n}}{\sqrt{\mu_n}} \right. \\ &\quad + \int_{-\tau}^0 g_2\left(\eta\right) \frac{\sin \left(\tau + \eta\right) \sqrt{\mu_n}}{\sqrt{\mu_n}} d\eta \right), \\ b_1\left(x\right) &= \rho \sum_{n=1}^{\infty} w_n\left(1\right) w_n\left(x\right) \\ &\quad \times \left(\alpha_1 \cos \tau \sqrt{\mu_n} \right. \\ &\quad + \int_{-\tau}^0 g_1\left(\eta\right) \cos \left(\tau + \eta\right) \sqrt{\mu_n} d\eta \right), \\ b_2\left(x\right) &= I_{\rho} \sum_{n=1}^{\infty} \varphi_n\left(1\right) w_n\left(x\right) \\ &\quad \times \left(\alpha_2 \cos \tau \sqrt{\mu_n} \right. \\ &\quad + \int_{-\tau}^0 g_2\left(\eta\right) \cos \left(\tau + \eta\right) \sqrt{\mu_n} d\eta \right), \\ b_3\left(x\right) &= \rho \sum_{n=1}^{\infty} w_n\left(1\right) \varphi_n\left(x\right) \\ &\quad \times \left(\alpha_1 \cos \tau \sqrt{\mu_n} \right. \\ &\quad + \int_{-\tau}^0 g_1\left(\eta\right) \cos \left(\tau + \eta\right) \sqrt{\mu_n} d\eta \right), \\ b_4\left(x\right) &= I_{\rho} \sum_{n=1}^{\infty} \varphi_n\left(1\right) \varphi_n\left(x\right) \\ &\quad \times \left(\alpha_2 \cos \tau \sqrt{\mu_n} \right. \\ &\quad + \int_{-\tau}^0 g_2\left(\eta\right) \cos \left(\tau + \eta\right) \sqrt{\mu_n} d\eta \right), \\ a_1\left(x,s\right) &= \rho \sum_{n=1}^{\infty} w_n\left(1\right) w_n\left(x\right) \\ &\quad \times \left(\beta_1 \frac{\sin s \sqrt{\mu_n}}{\sqrt{\mu_n}} \right. \\ &\quad - \int_{-\tau}^s g_1\left(\eta\right) \frac{\sin \left(\tau - s + \eta\right) \sqrt{\mu_n}}{\sqrt{\mu_n}} d\eta \right), \end{split}$$

$$a_{2}\left(x,s\right) = I_{\rho}\sum_{n=1}^{\infty}\varphi_{n}\left(1\right)w_{n}\left(x\right)$$

$$\times\left(\beta_{2}\frac{\sin s\sqrt{\mu_{n}}}{\sqrt{\mu_{n}}}\right)$$

$$-\int_{-\tau}^{s}g_{2}\left(\eta\right)\frac{\sin\left(\tau-s+\eta\right)\sqrt{\mu_{n}}}{\sqrt{\mu_{n}}}d\eta\right),$$

$$a_{3}\left(x,s\right) = \rho\sum_{n=1}^{\infty}w_{n}\left(1\right)\varphi_{n}\left(x\right)$$

$$\times\left(\beta_{1}\frac{\sin s\sqrt{\mu_{n}}}{\sqrt{\mu_{n}}}\right)$$

$$-\int_{-\tau}^{s}g_{1}\left(\eta\right)\frac{\sin\left(\tau-s+\eta\right)\sqrt{\mu_{n}}}{\sqrt{\mu_{n}}}d\eta\right),$$

$$a_{4}\left(x,s\right) = I_{\rho}\sum_{n=1}^{\infty}\varphi_{n}\left(1\right)\varphi_{n}\left(x\right)$$

$$\times\left(\beta_{2}\frac{\sin s\sqrt{\mu_{n}}}{\sqrt{\mu_{n}}}\right)$$

$$-\int_{-\tau}^{s}g_{2}\left(\eta\right)\frac{\sin\left(\tau-s+\eta\right)\sqrt{\mu_{n}}}{\sqrt{\mu_{n}}}d\eta\right),$$

$$b_{1}\left(x,s\right) = \rho\sum_{n=1}^{\infty}w_{n}\left(1\right)w_{n}\left(x\right)$$

$$\times\left(\beta_{1}\cos s\sqrt{\mu_{n}}\right)$$

$$+\int_{-\tau}^{s}g_{1}\left(\eta\right)\cos\left(\tau-s+\eta\right)\sqrt{\mu_{n}}d\eta\right),$$

$$b_{2}\left(x,s\right) = I_{\rho}\sum_{n=1}^{\infty}\varphi_{n}\left(1\right)w_{n}\left(x\right)$$

$$\times\left(\beta_{2}\cos s\sqrt{\mu_{n}}\right)$$

$$+\int_{-\tau}^{s}g_{2}\left(\eta\right)\cos\left(\tau-s+\eta\right)\sqrt{\mu_{n}}d\eta\right),$$

$$b_{4}\left(x,s\right) = I_{\rho}\sum_{n=1}^{\infty}\varphi_{n}\left(1\right)\varphi_{n}\left(x\right)$$

$$\times\left(\beta_{2}\cos s\sqrt{\mu_{n}}\right)$$

$$+\int_{-\tau}^{s}g_{1}\left(\eta\right)\cos\left(\tau-s+\eta\right)\sqrt{\mu_{n}}d\eta\right),$$

$$b_{4}\left(x,s\right) = I_{\rho}\sum_{n=1}^{\infty}\varphi_{n}\left(1\right)\varphi_{n}\left(x\right)$$

$$\times\left(\beta_{2}\cos s\sqrt{\mu_{n}}\right)$$

$$+\int_{-\tau}^{s}g_{2}\left(\eta\right)\cos\left(\tau-s+\eta\right)\sqrt{\mu_{n}}d\eta\right),$$

$$(44)$$

and the linear operators are

$$E_{1}\left(\omega_{0}, \varphi_{0}, \omega_{1}, \varphi_{1}\right)(x)$$

$$= \sum_{n=1}^{\infty} \left[\cos \tau \sqrt{\mu_{n}} \left(W_{0}, \Phi_{n}\right) + \frac{\sin \tau \sqrt{\mu_{n}}}{\sqrt{\mu_{n}}} \left(W_{1}, \Phi_{n}\right)\right] w_{n}(x),$$

$$E_{2}\left(\omega_{0}, \varphi_{0}, \omega_{1}, \varphi_{1}\right)(x)$$

$$= \sum_{n=1}^{\infty} \left[\cos \tau \sqrt{\mu_{n}} \left(W_{0}, \Phi_{n}\right) + \frac{\sin \tau \sqrt{\mu_{n}}}{\sqrt{\mu_{n}}} \left(W_{1}, \Phi_{n}\right)\right] \varphi_{n}(x),$$

$$E_{3}\left(\omega_{0}, \varphi_{0}, \omega_{1}, \varphi_{1}\right)(x)$$

$$= \sum_{n=1}^{\infty} \left[-\sqrt{\mu_{n}} \sin \tau \sqrt{\mu_{n}} \left(W_{0}, \Phi_{n}\right) + \cos \tau \sqrt{\mu_{n}} \left(W_{1}, \Phi_{n}\right)\right] w_{n}(x),$$

$$E_{4}\left(\omega_{0}, \varphi_{0}, \omega_{1}, \varphi_{1}\right)(x)$$

$$= \sum_{n=1}^{\infty} \left[-\sqrt{\mu_{n}} \sin \tau \sqrt{\mu_{n}} \left(W_{0}, \Phi_{n}\right) + \cos \tau \sqrt{\mu_{n}} \left(W_{1}, \Phi_{n}\right)\right] \varphi_{n}(x),$$

$$(45)$$

4. The Proof of Theorem 1

 $P(x,t) - W(x,t+\tau)$

In this section, we will prove Theorem 1. Here we mainly estimate the error:

$$\|P(\cdot,t) - W(\cdot,t+\tau)\|_{V_{K}^{1}(0,1)\times V_{EI}^{1}(0,1)}^{2} + \|Q(\cdot,t) - W_{t}(\cdot,t+\tau)\|_{L_{\rho}^{2}(0,1)\times L_{I_{p}}^{2}(0,1)}^{2}.$$

$$(46)$$

According to the calculation in Section 3, we have

$$= -\int_{0}^{\tau} \sin ((\tau - r) \mathcal{L}) B \Lambda_{1} U(t+r) dr$$

$$-\int_{0}^{\tau} \sin ((\tau - r) \mathcal{L}) B \int_{-\tau}^{0} \Lambda_{3} (\eta) U(t+r+\eta) d\eta dr,$$

$$(47)$$

$$Q(x,t) - W_{t}(x,t+\tau)$$

$$= -\int_{0}^{\tau} \cos ((\tau - r) \mathcal{L}) B \Lambda_{1} U(t+r) dr$$

$$-\int_{0}^{\tau} \cos ((\tau - r) \mathcal{L}) B \int_{-\tau}^{0} \Lambda_{3} (\eta) U(t+r+\eta) d\eta dr.$$

So,

$$\begin{split} &\|P(\cdot,t) - W(\cdot,t+\tau)\|_{V_{k}^{1}(0,1) \times V_{E}^{1}(0,1)}^{2} \\ &+ \|Q(\cdot,t) - W_{t}(\cdot,t+\tau)\|_{L_{\rho}^{2}(0,1) \times L_{I_{\rho}}^{1}(0,1)}^{2} \\ &\leq 4(\alpha_{1}\rho)^{2} \sum_{n=1}^{\infty} |\omega_{n}(1)|^{2} \\ &\times \left| \int_{0}^{\tau} \sin \sqrt{\mu_{n}} (\tau - r) u_{1}(r+t) dr \right|^{2} \\ &+ 4(\alpha_{2}I_{\rho})^{2} \sum_{n=1}^{\infty} |\varphi_{n}(1)|^{2} \\ &\times \left| \int_{0}^{\tau} \sin \sqrt{\mu_{n}} (\tau - r) u_{2}(r+t) dr \right|^{2} \\ &+ 4\rho^{2} \sum_{n=1}^{\infty} |\omega_{n}(1)|^{2} \\ &\times \left| \int_{0}^{\tau} \sin \sqrt{\mu_{n}} (\tau - r) \left(\int_{-\tau}^{0} g_{1}(\eta) u_{1}(r+t+\eta) d\eta \right) dr \right|^{2} \\ &+ 4I_{\rho}^{2} \sum_{n=1}^{\infty} |\varphi_{n}(1)|^{2} \\ &\times \left| \int_{0}^{\tau} \sin \sqrt{\mu_{n}} (\tau - r) \left(\int_{-\tau}^{0} g_{2}(\eta) u_{2}(r+t+\eta) d\eta \right) dr \right|^{2} \\ &+ 4(\alpha_{1}\rho)^{2} \sum_{n=1}^{\infty} |\omega_{n}(1)|^{2} \\ &\times \left| \int_{0}^{\tau} \cos \sqrt{\mu_{n}} (\tau - r) u_{1}(r+t) dr \right|^{2} \\ &+ 4(\alpha_{2}I_{\rho})^{2} \sum_{n=1}^{\infty} |\varphi_{n}(1)|^{2} \\ &\times \left| \int_{0}^{\tau} \cos \sqrt{\mu_{n}} (\tau - r) u_{2}(r+t) dr \right|^{2} \\ &+ 4\rho^{2} \sum_{n=1}^{\infty} |\omega_{n}(1)|^{2} \\ &\times \left| \int_{0}^{\tau} \cos \sqrt{\mu_{n}} (\tau - r) \left(\int_{-\tau}^{0} g_{1}(\eta) u_{1}(r+t+\eta) d\eta \right) dr \right|^{2} \\ &+ 4I_{\rho}^{2} \sum_{n=1}^{\infty} |\varphi_{n}(1)|^{2} \\ &\times \left| \int_{0}^{\tau} \cos \sqrt{\mu_{n}} (\tau - r) \left(\int_{-\tau}^{0} g_{2}(\eta) u_{2}(r+t+\eta) d\eta \right) dr \right|^{2} . \end{split}$$

Note that $\{\cos\sqrt{\mu_n}t, \sin\sqrt{\mu_n}t; n \in \mathbb{N}\}$ is a Riesz basis sequence for $L^2[0,\tau]$. Thus, there exist positive constants M_i (i=1,2,3,4) such that

$$\begin{split} \|P(\cdot,t) - W(\cdot,t+\tau)\|_{V_{K}^{1}(0,1)\times V_{EI}^{1}(0,1)}^{2} \\ + \|Q(\cdot,t) - W_{t}(\cdot,t+\tau)\|_{L_{\rho}^{2}(0,1)\times L_{I_{\rho}}^{1}(0,1)}^{2} \\ \leq M_{1}^{2} \int_{0}^{\tau} |u_{1}(r+t)|^{2} dr + M_{2}^{2} \int_{0}^{\tau} |u_{2}(r+t)|^{2} dr \\ + M_{3}^{2} \int_{0}^{\tau} \left| \int_{-\tau}^{0} g_{1}(\eta) u_{1}(t+r+\eta) d\eta \right|^{2} dr \\ + M_{4}^{2} \int_{0}^{\tau} \left| \int_{-\tau}^{0} g_{2}(\eta) u_{2}(t+r+\eta) d\eta \right|^{2} dr \\ \leq M_{1}^{2} \int_{0}^{\tau} |u_{1}(r+t)|^{2} dr + M_{2}^{2} \int_{0}^{\tau} |u_{2}(r+t)|^{2} dr \\ + M_{3}^{2} \tau^{2} \int_{-\tau}^{0} |g_{1}(\eta)|^{2} d\eta \int_{t-\tau}^{t+\tau} |u_{1}(s)|^{2} ds \\ + M_{4}^{2} \tau^{2} \int_{-\tau}^{0} |g_{2}(\eta)|^{2} d\eta \int_{t-\tau}^{t+\tau} |u_{2}(s)|^{2} ds. \end{split}$$

$$(50)$$

Let (P(x,t), Q(x,t)) be the solution to (11), and E(t) be its energy functional; then we have

$$E(t) = \frac{1}{2} \| (P(x,t), Q(x,t)) \|_{\mathcal{H}}^{2},$$

$$\frac{dE(t)}{dt} = -U_{1}^{2} (P,Q)(t) - U_{2}^{2} (P,Q)(t).$$
(51)

Therefore, we have

$$\int_{0}^{\tau} \|U(t+r)\|_{\mathbb{R}^{2}}^{2} dr$$

$$= \int_{t}^{t+\tau} \left(U_{1}^{2}(P,Q)(r) + U_{2}^{2}(P,Q)(r)\right) dr$$

$$= E(t) - E(t+\tau),$$

$$\int_{0}^{\tau} \|U(t-r)\|_{\mathbb{R}^{2}}^{2} dr = E(t-\tau) - E(t).$$
(52)

So, we can get

$$\|P(\cdot,t) - W(\cdot,t+\tau)\|_{V_{K}^{1}(0,1)\times V_{EI}^{1}(0,1)}^{2}$$

$$+ \|Q(\cdot,t) - W_{t}(\cdot,t+\tau)\|_{L_{\rho}^{2}(0,1)\times L_{I_{\rho}}^{2}(0,1)}^{2}$$

$$\leq \max_{i=1,2} \left\{ M_{i}^{2} \right\} [E(t) - E(t+\tau)]$$

$$+ \max_{j=3,4} \left\{ M_{j}^{2} \right\} \tau^{2} \int_{-\tau}^{0} \left(|g_{1}(\eta)|^{2} + |g_{2}(\eta)|^{2} \right) d\eta$$

$$\times [E(t-\tau) - E(t+\tau)].$$
(53)

If (P(x,t),Q(x,t)) is exponential stable, there exists a positive constant $\varepsilon > 0$ such that $E(t) \leq E(0)e^{-\varepsilon t}$. We can obtain the following result from above:

$$\begin{split} \|P(\cdot,t) - W(\cdot,t+\tau)\|_{V_{K}^{1}(0,1) \times V_{EI}^{1}(0,1)}^{2} \\ + \|Q(\cdot,t) - W_{t}(\cdot,t+\tau)\|_{L_{\rho}^{2}(0,1) \times L_{I_{\rho}}^{2}(0,1)}^{2} \leq Me^{-\varepsilon(t-\tau)}, \end{split}$$

$$(54)$$

where M is a positive constant. So $(W(x,t),W_t(x,t))$ also decays exponentially.

5. The Proof of Theorem 2

In this section, we will discuss the stability of system (11). At first we consider L^2 well posed of the system (6). For the sake of simplicity, we use the vector form of (6); that is,

$$P_{t}(x,t) = Q(x,t) + \sin(\tau \mathcal{L}) B\Lambda_{1}U(t)$$

$$+ \int_{-\tau}^{0} \sin((\tau + \eta)\mathcal{L}) B\Lambda_{3}(\eta) U(t) d\eta,$$

$$Q_{t}(x,t) = -\mathcal{L}P(x,t) + \cos(\tau \mathcal{L}) B\Lambda_{1}U(t)$$

$$+ \int_{-\tau}^{0} \cos((\tau + \eta)\mathcal{L}) B\Lambda_{3}(\eta) U(t) d\eta,$$

$$\Gamma_{N}P(\cdot,t) = \Lambda_{2}U(t),$$

$$P(0,t) = Q(0,t) = 0,$$

$$P(x,0) = P_{0}(x), \qquad Q(x,0) = Q_{0}(x).$$

$$(55)$$

The observation system corresponding to (55) is

$$\begin{split} W_t\left(x,t\right) &= V\left(x,t\right), \quad x \in (0,1), \ t > 0, \\ V_t\left(x,t\right) &= -\mathcal{L}W\left(x,t\right), \quad x \in (0,1), \ t > 0, \\ W\left(x,0\right) &= W_0, \\ V\left(x,0\right) &= V_0, \\ y_1\left(t\right) &= \beta_1 z\left(1,t\right) + \int_0^1 K\left(w_x\left(x,t\right) - \varphi\left(x,t\right)\right) \\ &\qquad \times \left(a_1'\left(x\right) - a_3\left(x\right)\right) dx \\ &+ \int_0^1 EI\varphi_x\left(x,t\right) a_3'\left(x\right) dx \\ &+ \int_0^1 \rho z\left(x,t\right) b_1\left(x\right) dx + \int_0^1 I_\rho \psi\left(x,t\right) b_3\left(x\right) dx; \\ y_2\left(t\right) &= \beta_2 \psi\left(1,t\right) + \int_0^1 K\left(w_x\left(x,t\right) - \varphi\left(x,t\right)\right) \\ &\qquad \times \left(a_2'\left(x\right) - a_4\left(x\right)\right) dx \\ &+ \int_0^1 EI\varphi_x\left(x,t\right) a_4'\left(x\right) dx \\ &+ \int_0^1 Pz\left(x,t\right) b_2\left(x\right) dx + \int_0^1 I_\rho \psi\left(x,t\right) b_4\left(x\right) dx, \end{split}$$

(56)

where $W(x,t) = (w(x,t), \varphi(x,t))^T$ and $V(x,t) = (z(x,t), \psi(x,t))^T$.

We can write the observation as

$$y_{1}(t) = \beta_{1}z(1,t) + \langle W(\cdot,t), (a_{1},a_{3})^{T} \rangle_{V_{k}^{1} \times V_{EI}^{1}}$$

$$+ \langle V(\cdot,t), (b_{1},b_{3})^{T} \rangle_{L_{\rho}^{2} \times L_{I_{\rho}}^{2}},$$

$$y_{2}(t) = \beta_{1}\psi(1,t) + \langle W(\cdot,t), (a_{2},a_{4})^{T} \rangle_{V_{k}^{1} \times V_{EI}^{1}}$$

$$+ \langle V(\cdot,t), (b_{2},b_{4})^{T} \rangle_{L_{\rho}^{2} \times L_{I_{\rho}}^{2}}.$$

$$(57)$$

Since

$$\begin{pmatrix} a_{1}(x) & a_{2}(x) \\ a_{3}(x) & a_{4}(x) \end{pmatrix}$$

$$= \operatorname{Sin}(\tau \mathcal{L}) B \Lambda_{1}$$

$$+ \int_{-\tau}^{0} \operatorname{Sin}((\tau + \eta) \mathcal{L}) B \Lambda_{3}(\eta) d\eta,$$

$$\begin{pmatrix} b_{1}(x) & b_{2}(x) \\ b_{3}(x) & b_{4}(x) \end{pmatrix}$$

$$= \operatorname{Cos}(\tau \mathcal{L}) B \Lambda_{1}$$

$$+ \int_{-\tau}^{0} \operatorname{Cos}((\tau + \eta) \mathcal{L}) B \Lambda_{3}(\eta) d\eta,$$

$$Y(t) = C(W, V) = \Lambda_{2} V(1, t)$$

$$+ \left[\Lambda_{1} \mathcal{L}^{1/2} \operatorname{Sin}(\tau \mathcal{L}) B\right]$$

$$+ \mathcal{L}^{1/2} \int_{-\tau}^{0} \operatorname{Sin}((\tau + \eta) \mathcal{L}) B \Lambda_{3}(\eta) d\eta \Big]^{*} \mathcal{L}^{1/2} W(t)$$

$$+ \left[\Lambda_{1} \operatorname{Cos}(\tau \mathcal{L}) B\right]$$

$$+ \int_{-\tau}^{0} \operatorname{Cos}((\tau + \eta) \mathcal{L}) B \Lambda_{3}(\eta) d\eta \Big]^{*} V(t).$$
(58)

Taking the Laplace transform for above equation leads to, for any $\Re \lambda > 0$,

$$\begin{split} \lambda P\left(x\right) &= Q\left(x\right) + \operatorname{Sin}\left(\tau\mathcal{L}\right)B\Lambda_{1}U\left(\lambda\right) \\ &+ \int_{-\tau}^{0} \operatorname{Sin}\left(\left(\tau + \eta\right)\mathcal{L}\right)B\Lambda_{3}\left(\eta\right)U\left(\lambda\right)d\eta, \\ &\quad x \in (0,1)\,, \\ \lambda Q\left(x\right) &= -\mathcal{L}P(x) + \operatorname{Cos}\left(\tau\mathcal{L}\right)B\Lambda_{1}U\left(\lambda\right) \\ &+ \int_{-\tau}^{0} \operatorname{Cos}\left(\left(\tau + \eta\right)\mathcal{L}\right)B\Lambda_{3}\left(\eta\right)U\left(\lambda\right)d\eta, \\ &\quad \Gamma_{N}P\left(\cdot,t\right) &= \Lambda_{2}U\left(\lambda\right), \\ &\quad P\left(0,t\right) &= Q\left(0,t\right) = 0, \end{split}$$

$$Y(\lambda) = \Lambda_{2}Q(1)$$

$$+ \left[\Lambda_{1}\mathcal{L}^{1/2} \sin(\tau \mathcal{L}) B\right]$$

$$+ \mathcal{L}^{1/2} \int_{-\tau}^{0} \sin((\tau + \eta)\mathcal{L}) B \Lambda_{3}(\eta) d\eta \right]^{*} \mathcal{L}^{1/2} P(\cdot)$$

$$+ \left[\Lambda_{1} \cos(\tau \mathcal{L}) B\right]$$

$$+ \int_{-\tau}^{0} \cos((\tau + \eta)\mathcal{L}) B \Lambda_{3}(\eta) d\eta \right]^{*} Q(\cdot).$$
(59)

We have the following results by solving (59):

$$(\lambda^{2} + \mathcal{L}) p(x)$$

$$= \left[\lambda \left(\sin(\tau \mathcal{L}) B\Lambda_{1} + \int_{-\tau}^{0} \sin((\tau + \eta) \mathcal{L}) B\Lambda_{3}(\eta) d\eta\right) + \cos(\tau \mathcal{L}) B\Lambda_{1} + \int_{-\tau}^{0} \cos((\tau + \eta) \mathcal{L}) B\Lambda_{3}(\eta) d\eta + B\Lambda_{2}\right] U(\lambda),$$

$$Y(\lambda) = \left[\lambda \left(\sin(\tau \mathcal{L}) B\Lambda_{1} + \int_{-\tau}^{0} \sin((\tau + \eta) \mathcal{L}) B\Lambda_{3}(\eta) d\eta\right) + \cos(\tau \mathcal{L}) B\Lambda_{1} + \int_{-\tau}^{0} \cos((\tau + \eta) \mathcal{L}) B\Lambda_{3}(\eta) d\eta + B\Lambda_{2}\right]^{*} P.$$

$$(60)$$

So we can get

$$Y(\lambda) = \left[\lambda \left(\sin(\tau \mathcal{L}) B\Lambda_{1} + \int_{-\tau}^{0} \sin((\tau + \eta) \mathcal{L}) B\Lambda_{3}(\eta) d\eta\right) + \cos(\tau \mathcal{L}) B\Lambda_{1} + \int_{-\tau}^{0} \cos((\tau + \eta) \mathcal{L}) B\Lambda_{3}(\eta) d\eta + B\Lambda_{2}\right]^{*} (\lambda^{2} + \mathcal{L})^{-1}$$

$$\times \left[\lambda \left(\operatorname{Sin} (\tau \mathcal{L}) B \Lambda_{1} \right) + \int_{-\tau}^{0} \operatorname{Sin} ((\tau + \eta) \mathcal{L}) B \Lambda_{3} (\eta) d\eta \right) + \operatorname{Cos} (\tau \mathcal{L}) B \Lambda_{1} + \int_{-\tau}^{0} \operatorname{Cos} ((\tau + \eta) \mathcal{L}) B \Lambda_{3} (\eta) d\eta + B \Lambda_{2} \right] U(\lambda),$$
(61)

and hence the transform matrix is

$$H(\lambda) = \left[\lambda\left(\sin\left(\tau\mathscr{L}\right)B\Lambda_{1}\right) + \int_{-\tau}^{0}\sin\left(\left(\tau+\eta\right)\mathscr{L}\right)B\Lambda_{3}\left(\eta\right)d\eta\right) + \cos\left(\tau\mathscr{L}\right)B\Lambda_{1} + \int_{-\tau}^{0}\cos\left(\left(\tau+\eta\right)\mathscr{L}\right)B\Lambda_{3}\left(\eta\right)d\eta + B\Lambda_{2}\right]^{*}\left(\lambda^{2}+\mathscr{L}\right)^{-1} \times \left[\lambda\left(\sin\left(\tau\mathscr{L}\right)B\Lambda_{1}\right) + \int_{-\tau}^{0}\sin\left(\left(\tau+\eta\right)\mathscr{L}\right)B\Lambda_{3}\left(\eta\right)d\eta\right) + \cos\left(\tau\mathscr{L}\right)B\Lambda_{1} + \int_{-\tau}^{0}\cos\left(\left(\tau+\eta\right)\mathscr{L}\right)B\Lambda_{3}\left(\eta\right)d\eta + B\Lambda_{2}\right]. \tag{62}$$

For any $Z = (z_1, z_2) \in \mathbb{C}^2$, we can get

$$(H(\lambda) Z, Z)_{\mathbb{C}^{2}}$$

$$= \sum_{n=1}^{\infty} \frac{1}{\lambda^{2} + \mu_{n}}$$

$$\times \left| \left(\left[\lambda \left(\operatorname{Sin} (\tau \mathcal{L}) B \Lambda_{1} \right) + \int_{-\tau}^{0} \operatorname{Sin} \left((\tau + \eta) \mathcal{L} \right) B \Lambda_{3} (\eta) d\eta \right) \right.$$

$$+ \operatorname{Cos} (\tau \mathcal{L}) B \Lambda_{1} + \int_{-\tau}^{0} \operatorname{Cos} \left((\tau + \eta) \mathcal{L} \right) d\eta \right) \right.$$

$$\times B \Lambda_{3} (\eta) d\eta + B \Lambda_{2} \left[Z, \Phi_{n} \right]_{L_{0}^{2} \times L_{1}^{2}} \right|^{2}.$$

$$(63)$$

We can easily get

$$(B\Lambda_{2}Z, \Phi_{n})_{L_{\rho}^{2} \times L_{I_{\rho}}^{2}} = \beta_{1}z_{1}\rho w_{n}(1) + \beta_{2}z_{2}I_{\rho}\varphi_{n}(1),$$

$$(Sin(\tau \mathcal{L})B\Lambda_{1}Z, \Phi_{n})_{L_{\rho}^{2} \times L_{I_{\rho}}^{2}}$$

$$= \frac{Sin(\tau \sqrt{\mu_{n}})}{\sqrt{\mu_{n}}} \left[\alpha_{1}z_{1}\rho w_{n}(1) + \alpha_{2}z_{2}I_{\rho}\varphi_{n}(1)\right],$$

$$(Cos(\tau \mathcal{L})B\Lambda_{1}Z, \Phi_{n})_{L_{\rho}^{2} \times L_{I_{\rho}}^{2}}$$

$$= Cos(\tau \sqrt{\mu_{n}}) \left[\alpha_{1}z_{1}\rho w_{n}(1) + \alpha_{2}z_{2}I_{\rho}\varphi_{n}(1)\right],$$

$$\left(\int_{-\tau}^{0} Sin(\tau + \eta)\mathcal{L}B\Lambda_{3}(\eta)d\eta Z, \Phi_{n}\right)_{L_{\rho}^{2} \times L_{I_{\rho}}^{2}}$$

$$= \int_{-\tau}^{0} \frac{Sin((\tau + \eta)\sqrt{\mu_{n}})}{\sqrt{\mu_{n}}}$$

$$\times \left[g_{1}(\eta)z_{1}\rho w_{n}(1) + g_{2}(\eta)z_{2}I_{\rho}\varphi_{n}(1)\right]d\eta,$$

$$\left(\int_{-\tau}^{0} Cos(\tau + \eta)\mathcal{L}B\Lambda_{3}(\eta)d\eta Z, \Phi_{n}\right)_{L_{\rho}^{2} \times L_{I_{\rho}}^{2}}$$

$$= \int_{-\tau}^{0} Cos((\tau + \eta)\sqrt{\mu_{n}})$$

$$\times \left[g_{1}(\eta)z_{1}\rho w_{n}(1) + g_{2}(\eta)z_{2}I_{\rho}\varphi_{n}(1)\right]d\eta.$$

$$(64)$$

Thus, we have

$$\left| \left(\left[\lambda \left(\operatorname{Sin} \left(\tau \mathcal{L} \right) B \Lambda_{1} + \int_{-\tau}^{0} \operatorname{Sin} \left(\left(\tau + \eta \right) \mathcal{L} \right) B \Lambda_{3} \left(\eta \right) d \eta \right) \right. \right.$$

$$\left. + \operatorname{Cos} \left(\tau \mathcal{L} \right) B \Lambda_{1} + \int_{-\tau}^{0} \operatorname{Cos} \left(\left(\tau + \eta \right) \mathcal{L} \right) B \Lambda_{3} \left(\eta \right) d \eta \right.$$

$$\left. + B \Lambda_{2} \right] Z, \Phi_{n} \right)_{L_{\rho}^{2} \times L_{I_{\rho}}^{2}} \right|^{2}$$

$$\leq F \left| \frac{|\lambda|^{2}}{\mu_{n}} + 2 \left| \left[\rho \left| \omega_{n} \left(1 \right) \right|^{2} + I_{\rho} \left| \varphi_{n} \left(1 \right) \right|^{2} \right] \| Z \|_{\mathbb{C}^{2}}^{2}, \quad (65)$$

where *F* is a positive constant dependent on α_i , β_i , $g_i(\eta)$, i = 1, 2. Therefore, we have the following result:

$$||H(\lambda)|| \le F \sum_{n=1}^{\infty} \frac{1}{|\lambda|^{2} + \mu_{n}} \left| \frac{|\lambda|^{2}}{\mu_{n}} + 2 \right| \times \left[\rho |\omega_{n}(1)|^{2} + I_{\rho} |\varphi_{n}(1)|^{2} \right].$$
(66)

From Lemma 4, we have

$$\sup_{\Re \lambda > \delta > 0} \|H(\lambda)\| < \infty. \tag{67}$$

Hence the system (6) is L^2_{loc} well posed (see, [15]). Next, we consider the exact observability of the system (6). **Lemma 6** (see [16]). Let \mathcal{H} be a separable Hilbert space, and let \mathcal{L} be a unbounded positive definite operator. Assume that \mathcal{L} satisfies the following conditions:

- (1) \mathscr{L} has compact resolvent and its spectrum is $\sigma(\mathscr{L}) = \{\mu_n; n \in \mathbb{N}\};$
- (2) the spectra of \mathcal{L} satisfy the separable condition

$$\inf_{n \neq m} \left| \sqrt{\mu_n} - \sqrt{\mu_m} \right| = \delta > 0; \tag{68}$$

(3) the corresponding eigenvectors $\{\Phi_n; n \in \mathbb{N}\}$ with $\|\Phi_n\|_{\mathscr{H}} = 1$ form a normalized orthogonal basis for \mathscr{H} .

Let \mathbb{Y} be a Hilbert space. Assume that $C:D(\mathcal{L})\to \mathbb{Y}$ is an admissible observation operator for \mathcal{L} . Then the following system:

$$Z_{tt} + \mathcal{L}Z(t) = 0, \qquad Z(0) = Z_0,$$

$$Z_t(0) = Z_1, \qquad Y(t) = C(Z, Z_t)$$
(69)

is exactly observable in finite time in the energy space $D(\mathcal{L}^{1/2}) \times \mathcal{H}$ if and only if

$$\inf_{n \in \mathbb{N}} \left\| C\left(\frac{\Phi_n}{i\sqrt{\mu_n}}, \Phi_n\right) \right\|_{\mathbb{V}} > 0. \tag{70}$$

Now we apply Lemma 6 to the system (55). We can easily know that the condition (68) is fulfilled when $c_1 = \sqrt{K/\rho} \neq c_2 = \sqrt{EI/I_\rho}$ (see Remark 2.1 in [8]).

For
$$\Phi_n(x) = (w_n(x), \varphi_n(x))^T$$
, we have

$$\begin{split} C\left(\frac{\Phi_n}{i\sqrt{\mu_n}},\Phi_n\right) \\ &= \Lambda_2\Phi_n(1) \\ &+ \left[\Lambda_1\mathcal{L}^{1/2}\sin\left(\tau\mathcal{L}\right)B\right. \\ &+ \left.\mathcal{L}^{1/2}\int_{-\tau}^0\sin((\tau+\eta)\mathcal{L})B\Lambda_3(\eta)d\eta\right]^*\mathcal{L}^{1/2}\frac{\Phi_n}{i\sqrt{\mu_n}} \\ &+ \left[\Lambda_1\cos\left(\tau\mathcal{L}\right)B\right. \\ &+ \left.\int_{-\tau}^0\cos\left((\tau+\eta)\mathcal{L}\right)B\Lambda_3\left(\eta\right)d\eta\right]^*\Phi_n. \end{split}$$

For any $Z = (z_1, z_2) \in \mathbb{C}^2$, we have

$$\left(\Lambda_{1}\left(\mathcal{L}^{1/2}\sin\left(\tau\mathcal{L}\right)B\right)^{*}\mathcal{L}^{1/2}\frac{\Phi_{n}}{i\sqrt{\mu_{n}}},Z\right)_{\mathbb{C}^{2}}$$

$$=\left(\mathcal{L}^{1/2}\frac{\Phi_{n}}{i\sqrt{\mu_{n}}},\mathcal{L}^{1/2}\sin\left(\tau\mathcal{L}\right)B\Lambda_{1}Z\right)_{L_{\rho}^{2}\times L_{I_{\rho}}^{2}}$$

$$=-i\sqrt{\mu_{n}}\left(\Phi_{n},\sin\left(\tau\mathcal{L}\right)B\Lambda_{1}Z\right)_{L_{\rho}^{2}\times L_{I_{\rho}}^{2}}$$

$$=-i\sin\left(\sqrt{\mu_{n}}\tau\right)\left[\alpha_{1}z_{1}\rho\omega_{n}(1)+\alpha_{2}z_{2}I_{\rho}\varphi_{n}(1)\right].$$
(72)

Similarity, we have

$$\left(\left(\mathcal{Z}^{1/2}\int_{-\tau}^{0} \sin\left(\left(\tau + \eta\right)\mathcal{Z}\right) B\Lambda_{3}\left(\eta\right) d\eta\right)^{*} \mathcal{Z}^{1/2} \frac{\Phi_{n}}{i\sqrt{\mu_{n}}}, Z\right)_{\mathbb{C}^{2}}$$

$$= -i \int_{-\tau}^{0} \sin\left(\left(\tau + \eta\right) \sqrt{\mu_{n}}\right)$$

$$\times \left[g_{1}\left(\eta\right) z_{1} \rho \omega_{n}\left(1\right) + g_{2}\left(\eta\right) z_{2} I_{\rho} \varphi_{n}\left(1\right)\right] d\eta,$$

$$\left(\Lambda_{1}(\cos\left(\tau\mathcal{Z}\right) B)^{*} \Phi_{n}, Z\right)_{\mathbb{C}^{2}}$$

$$= \cos\left(\sqrt{\mu_{n}}\tau\right) \left[\alpha_{1} z_{1} \rho \omega_{n}\left(1\right) + \alpha_{2} z_{2} I_{\rho} \varphi_{n}\left(1\right)\right],$$

$$\left(\left(\int_{-\tau}^{0} \cos\left(\left(\tau + \eta\right) \mathcal{Z}\right) B\Lambda_{3}\left(\eta\right) d\eta\right)^{*} \Phi_{n}, Z\right)_{\mathbb{C}^{2}}$$

$$= \int_{-\tau}^{0} \cos\left(\left(\tau + \eta\right) \sqrt{\mu_{n}}\right)$$

$$\times \left[g_{1}\left(\eta\right) z_{1} \rho \omega_{n}\left(1\right) + g_{2}\left(\eta\right) z_{2} I_{\rho} \varphi_{n}\left(1\right)\right] d\eta.$$
(73)

Thus it holds that

$$C\left(\frac{\Phi_{n}}{i\sqrt{\mu_{n}}},\Phi_{n}\right)$$

$$=\left(\left(\frac{\beta_{1}}{\rho}+\alpha_{1}e^{-i\tau\sqrt{\mu_{n}}}+\int_{-\tau}^{0}g_{1}\left(\eta\right)e^{-i\left((\tau+\eta)\sqrt{\mu_{n}}\right)}d\eta\right)\rho w_{n}\left(1\right)}{\left(\frac{\beta_{2}}{I_{\rho}}+\alpha_{2}e^{-i\tau\sqrt{\mu_{n}}}+\int_{-\tau}^{0}g_{2}\left(\eta\right)e^{-i\left((\tau+\eta)\sqrt{\mu_{n}}\right)}d\eta\right)I_{\rho}\varphi_{n}\left(1\right)\right)}.$$

$$(74)$$

Set

$$\xi_{n}^{(1)} = \int_{-\tau}^{0} g_{1}(\eta) e^{-i\sqrt{\mu_{n}}(\tau+\eta)} d\eta,
\xi_{n}^{(2)} = \int_{-\tau}^{0} g_{2}(\eta) e^{-i\sqrt{\mu_{n}}(\tau+\eta)} d\eta.$$
(75)

Then

$$\left\| C \left(\frac{\Phi_{n}}{i\sqrt{\mu_{n}}}, \Phi_{n} \right) \right\|_{C^{2}}^{2} = \left| \frac{\beta_{1}}{\rho} + \alpha_{1} e^{-i\tau\sqrt{\mu_{n}}} + \xi_{n}^{(1)} \right|^{2} \left| \rho w_{n}(1) \right|^{2} + \left| \frac{\beta_{2}}{I_{\rho}} + \alpha_{2} e^{-i\tau\sqrt{\mu_{n}}} + \xi_{n}^{(2)} \right|^{2} \left| I_{\rho} \varphi_{n}(1) \right|^{2}.$$
(76)

Obviously, when

$$A_{1} = \inf_{n} \left| \frac{\beta_{1}}{\rho} + \alpha_{1} e^{-i\tau\sqrt{\mu_{n}}} + \xi_{n}^{(1)} \right| > 0,$$

$$A_{2} = \inf_{n} \left| \frac{\beta_{2}}{I_{\rho}} + \alpha_{2} e^{-i\tau\sqrt{\mu_{n}}} + \xi_{n}^{(2)} \right| > 0,$$
(77)

we have

$$\left\| C \left(\frac{\Phi_{n}}{i \sqrt{\mu_{n}}}, \Phi_{n} \right) \right\|_{\mathbb{C}^{2}}^{2} \\
\geq A_{1}^{2} \left| \rho w_{n}(1) \right|^{2} + A_{2}^{2} \left| I_{\rho} \varphi_{n}(1) \right|^{2} \\
\geq \min \left\{ A_{1}, A_{2} \right\} \left(\left| \rho w_{n}(1) \right|^{2} + \left| I_{\rho} \varphi_{n}(1) \right|^{2} \right);$$
(78)

using Lemma 4,

$$\inf_{n} \left\| C\left(\frac{\Phi_n}{i\sqrt{\mu_n}}, \Phi_n\right) \right\|_{\mathbb{C}^2}^2 > 0. \tag{79}$$

According to Lemma 6, the system (56) is exactly observable in finite time, and hence the closed-loop system (11) is exponentially stable.

If for all $n \in \mathbb{N}$,

$$\left| \frac{\beta_1}{\rho} + \alpha_1 e^{-i\tau\sqrt{\mu_n}} + \xi_n^{(1)} \right| > 0,$$

$$\left| \frac{\beta_2}{I_\rho} + \alpha_2 e^{-i\tau\sqrt{\mu_n}} + \xi_n^{(2)} \right| > 0,$$
(80)

we can see that in this case, there is no eigenvalue of system (11) on the imaginary axis. Moreover, if the conditions

$$\inf_{n} \left| \frac{\beta_1}{\rho} + \alpha_1 e^{-i\tau\sqrt{\mu_n}} + \xi_n^{(1)} \right| = 0,$$

$$\inf_{n} \left| \frac{\beta_2}{I_\rho} + \alpha_2 e^{-i\tau\sqrt{\mu_n}} + \xi_n^{(2)} \right| = 0$$
(81)

hold, then the imaginary axis is an asymptote of the eigenvalues of the system (11). Therefore, the stability theorem [17] asserts then that the system (11) is asymptotically stable. Therefore, we get the result of the Theorem 2.

6. Conclusion

In this paper, we designed a new controller for a Timoshenko beam with distributed delay in the boundary that stabilizes exponentially the system. In the design process of new controllers, there are main steps: (1) to translate the delay system into a system without delay; (2) for the undelay system, we used the collocated feedback law to obtain the control signals; (3) using the obtained control signals, act on the delay system. This control strategy can be regarded as extension form of [15]. In the stability analysis, the key trick is to use the exact observability of the dual system in finite time to obtain the exponential stability of the closed-loop system.

In the proof of main result, the condition $K/\rho \neq EI/I_{\rho}$ is used to ensure the separability of the spectrum (see, the condition (2)) in Lemma 6). In the statement of our result

(Theorem 2), the conditions are stronger than the practice; in fact.

$$\begin{split} \left\| C \left(\frac{\Phi_{n}}{i\sqrt{\mu_{n}}}, \Phi_{n} \right) \right\|_{\mathbb{C}^{2}}^{2} &= \left| \frac{\beta_{1}}{\rho} + \alpha_{1} e^{-i\tau\sqrt{\mu_{n}}} + \xi_{n}^{(1)} \right|^{2} \left| \rho w_{n}(1) \right|^{2} \\ &+ \left| \frac{\beta_{2}}{I_{\rho}} + \alpha_{2} e^{-i\tau\sqrt{\mu_{n}}} + \xi_{n}^{(2)} \right|^{2} \left| I_{\rho} \varphi_{n}(1) \right|^{2}; \end{split}$$
(82)

one only needs to request

$$\inf_{n} \left\| C\left(\frac{\Phi_n}{i\sqrt{\mu_n}}, \Phi_n\right) \right\|_{\mathbb{C}^2}^2 > 0, \tag{83}$$

so, the conditions

$$\inf_{n} \left| \frac{\beta_{1}}{\rho} + \alpha_{1} e^{-i\tau\sqrt{\mu_{n}}} + \xi_{n}^{(1)} \right| > 0,$$

$$\inf_{n} \left| \frac{\beta_{2}}{I_{\rho}} + \alpha_{2} e^{-i\tau\sqrt{\mu_{n}}} + \xi_{n}^{(2)} \right| > 0,$$
(84)

are sufficient, but not necessary. Since

$$\xi_{n}^{(1)} = \int_{-\tau}^{0} g_{1}(\eta) e^{i\sqrt{\mu_{n}}(\tau-\eta)} d\eta,$$

$$\xi_{n}^{(2)} = \int_{-\tau}^{0} g_{2}(\eta) e^{i\sqrt{\mu_{n}}(\tau-\eta)} d\eta,$$
(85)

so $\lim_{n\to\infty} \xi_n^{(j)} = 0$, j = 1, 2. Therefore, when

$$\left| \frac{\beta_1}{\rho} + \alpha_1 e^{-i\tau\sqrt{\mu_n}} + \xi_n^{(1)} \right| > 0,$$

$$\left| \frac{\beta_2}{I_0} + \alpha_2 e^{-i\tau\sqrt{\mu_n}} + \xi_n^{(2)} \right| > 0$$
(86)

that means that there is no eigenvalue on the imaginary axis, and

$$\inf_{n} \left| \frac{\beta_{1}}{\rho} + \alpha_{1} e^{-i\tau\sqrt{\mu_{n}}} \right| > 0,$$

$$\inf_{n} \left| \frac{\beta_{2}}{I_{o}} + \alpha_{2} e^{-i\tau\sqrt{\mu_{n}}} \right| > 0,$$
(87)

we have

$$\inf_{n} \left\| C\left(\frac{\Phi_{n}}{i\sqrt{\mu_{n}}}, \Phi_{n}\right) \right\|_{\mathbb{C}^{2}}^{2} > 0.$$
 (88)

Clearly, when $\beta_1 \neq \rho \alpha_1$ and $\beta_2 \neq I_\rho \alpha_2$, we also have

$$\inf_{n} \left\| C\left(\frac{\Phi_{n}}{i\sqrt{\mu_{n}}}, \Phi_{n}\right) \right\|_{\mathbb{C}^{2}}^{2} > 0. \tag{89}$$

Therefore, the conditions in Theorem 2 are easily verified.

The control method proposed in this paper can be used to the system of output availed system by using the Luenberger observer. Also we have noted that the method is only fitting the continuous model; for the model of data-driven system (e.g., see, [18]), it might fail. So we need to study the corresponding control strategy for the data-driven system.

Acknowledgment

This research was supported by the National Science Natural Foundation in China (NSFC-61174080).

References

- [1] G.-Q. Xu and D.-X. Feng, "The Riesz basis property of a Timoshenko beam with boundary feedback and application," *IMA Journal of Applied Mathematics*, vol. 67, no. 4, pp. 357–370, 2002.
- [2] G.-Q. Xu and S. P. Yung, "Stabilization of Timoshenko beam by means of pointwise controls," ESAIM. Control, Optimisation and Calculus of Variations, vol. 9, pp. 579–600, 2003.
- [3] Z.-J. Han and G.-Q. Xu, "Stabilization and Riesz basis property of two serially connected Timoshenko beams system," *Journal* of *Applied Mathematics and Mechanics*, vol. 89, no. 12, pp. 962– 980, 2009.
- [4] S. A. Messaoudi, M. Pokojovy, and B. Said-Houari, "Nonlinear damped Timoshenko systems with second sound—global existence and exponential stability," *Mathematical Methods in the Applied Sciences*, vol. 32, no. 5, pp. 505–534, 2009.
- [5] A. Guesmia, S. A. Messaoudi, and A. Soufyane, "Stabilization of a linear Timoshenko system with infinite history and applications to the Timoshenko-heat systems," *Electronic Journal of Differential Equations*, vol. 2012, no. 193, pp. 1–5, 2012.
- [6] G. Q. Xu, S. P. Yung, and L. K. Li, "Stabilization of wave systems with input delay in the boundary control," *ESAIM*, vol. 12, no. 4, pp. 770–785, 2006.
- [7] S. Nicaise and C. Pignotti, "Stabilization of the wave equation with boundary or internal distributed delay," *Differential and Integral Equations*, vol. 21, no. 9-10, pp. 935–958, 2008.
- [8] S. Nicaise and J. Valein, "Stabilization of the wave equation on 1-d networks with a delay term in the nodal feedbacks," *Networks and Heterogeneous Media*, vol. 2, no. 3, pp. 425–479, 2007.
- [9] Y. F. Shang, G. Q. Xu, and Y. L. Chen, "Stability analysis of Euler-Bernoulli beam with input delay in the boundary control," *Asian Journal of Control*, vol. 14, no. 1, pp. 186–196, 2012.
- [10] S. Nicaise and C. Pignotti, "Stability and instability results of the wave equation with a delay term in the boundary or internal feedbacks," *SIAM Journal on Control and Optimization*, vol. 45, no. 5, pp. 1561–1585, 2006.
- [11] Y. F. Shang and G. Q. Xu, "Stabilization of an Euler-Bernoulli beam with input delay in the boundary control," *Systems & Control Letters*, vol. 61, no. 11, pp. 1069–1078, 2012.
- [12] Z. J. Han and G. Q. Xu, "Output-based stabilization of Euler-Bernoulli beam with time-delay in boundary input," IMA Journal of Mathematical Control and Information, p. 1, 2013.
- [13] G. Q. Xu and H. X. Wang, "Stabilization of Timoshenko beam system with delay in the boundary control," *International Journal of Control*, vol. 86, pp. 1165–1178, 2013.
- [14] J. U. Kim and Y. Renardy, "Boundary control of the Timoshenko beam," SIAM Journal on Control and Optimization, vol. 25, no. 6, pp. 1417–1429, 1987.
- [15] B.-Z. Guo and Y.-H. Luo, "Controllability and stability of a second-order hyperbolic system with collocated sensor/actuator," Systems & Control Letters, vol. 46, no. 1, pp. 45–65, 2002.
- [16] G. Q. Xu, "Exponential family, Riesz basis sequence and its applications in control theory, in preparation".

- [17] Yu. I. Lyubich and V. O. Phóng, "Asymptotic stability of linear differential equations in Banach spaces," *Studia Mathematica*, vol. 88, no. 1, pp. 37–42, 1988.
- [18] S. Yin, S. X. Ding, A. Haghani, H. Y. Hao, and P. Zhang, "A comparison study of basic data-driven fault diagnosis and process monitoring methods on the benchmark Tennessee Eastman process," *Journal of Process Control*, vol. 22, pp. 1567– 1581, 2012.

Hindawi Publishing Corporation Abstract and Applied Analysis Volume 2013, Article ID 386757, 10 pages http://dx.doi.org/10.1155/2013/386757

Research Article

Hybrid Artificial Neural Networks Modeling for Faults Identification of a Stochastic Multivariate Process

Yuehjen E. Shao and Chia-Ding Hou

Department of Statistics and Information Science, Fu Jen Catholic University, No. 510, Zhongzheng Road, Xinzhuang, New Taipei City 24205, Taiwan

Correspondence should be addressed to Chia-Ding Hou; stat0002@mail.fju.edu.tw

Received 7 October 2013; Revised 5 November 2013; Accepted 5 November 2013

Academic Editor: Shen Yin

Copyright © 2013 Y. E. Shao and C.-D. Hou. This is an open access article distributed under the Creative Commons Attribution License, which permits unrestricted use, distribution, and reproduction in any medium, provided the original work is properly cited.

Due to the recent rapid growth of advanced sensing and production technologies, the monitoring and diagnosis of multivariate process operating performance have drawn increasing interest in process industries. The multivariate statistical process control (MSPC) chart is one of the most commonly used tools for detecting process faults. However, an out-of-control MSPC signal only indicates that process faults have intruded the underlying process. Identifying which of the monitored quality variables is responsible for the MSPC signal is fairly difficult. Pinpointing the responsible variable is vital for process improvement because it effectively determines the root causes of the process faults. Accordingly, this identification has become an important research issue concerning recent multivariate process applications. In contrast with the traditional single classifier approach, the present study proposes hybrid modeling schemes to address problems that involve a large number of quality variables in a multivariate normal process. The proposed scheme includes multivariate adaptive regression splines (MARS), logistic regression (LR), and artificial neural network (ANN). By applying MARS and LR techniques, we may obtain fewer but more significant quality variables, which can serve as inputs to the ANN classifier. The performance of our proposed approaches was evaluated by conducting a series of experiments.

1. Introduction

A multivariate process monitors two or more quality variables. When a signal is triggered by the multivariate statistical process control (MSPC) chart, process personnel are typically only aware that the underlying process is in an unstable state. Identifying which of the monitored quality characteristics (or variables) is responsible for this MSPC signal is challenging. Accordingly, effective determination of the source of process faults becomes an important and challenging issue in MSPC applications, because these sources are associated with specific assignable causes that adversely affect the process.

Typically, a literature review has shown that there are different kinds of approaches to investigate on source identification of faults in a multivariate process. The first type of approach uses various graphical techniques, such as polygonal charts [1], line charts [2], multivariate profile charts [3], and boxplot charts [4] to assist in determining the quality variables at fault in a process. However, the operations of these graphical approaches are tedious and subjective.

The second type of approach uses the statistical decomposition techniques to interpret the contributors to an MSPC signal. Mason et al. [5] proposed the method to decompose the T^2 statistic into independent parts, each of which reflects the contribution of an individual quality variable. Since the decomposition of the T^2 statistic into p independent T^2 components is not unique, Mason et al. [6] provided a computing scheme that can reduce the computational effort. The same concept to decompose the T^2 statistics has been proposed by the studies [7, 8]. However, these approaches have not been analyzed in terms of the percentage of success in the classification of the variables that have actually shifted in the process [9, 10]. The study [11] investigated the method of principal components analysis (PCA) to determine the quality variables at fault in a multivariate process. The T^2 statistic is expressed in terms of normalized principal components scores of the multinormal variables. The normalized score with high values are detected when an MSPC signal is triggered. The contribution plots can then be used to determine the variables which are responsible for the signal. In addition, the contribution plots were used by the studies [12, 13]. However, the PCA approach can be argued that the dimensionality of data may not be efficiently reduced by linear transformation. Also, the problem of the PCA consists in the fact that the directions maximizing variance do not always maximize information. More recently, the study [14] developed a statistical decomposition method to estimate the sources of process variance shifts in a multivariate normal process. Although the performance of the approach was acceptable, the decomposition method requires a large sample size, which may not be feasible for some practical applications.

The third type of approach employs the machine learning (ML) mechanisms, such as artificial neural networks (ANN) and support vector machine (SVM), to identify the quality variables which are responsible for the MSPC signal. A comparative study has been conducted by the studies [9, 10]. While the study [9] made a comparison between neural network approaches with the method of Mason et al. [5], the study [10] made a comparison between ANN and SVM with the method of Runger et al. [8]. Both studies [9, 10] concluded that ML methods are in general better than those obtained using the decomposition approach. The study [15] proposed a backpropagation-net based model which can identify the group of quality variables at faults and can classify the magnitude of the process shifts. The study [16] developed a two level-based model using T^2 control chart for detecting the signals and an ANN for identifying the sources of the signals. The study [17] proposed an ANN-based model to identify and quantify the mean shifts in bivariate processes. The authors [18] developed a neural-network-based identifier to detect the mean shifts and simultaneously to identify the sources of the shifts for a multivariate autocorrelated processes. They benchmarked the run-length performance of the proposed method against the Hotelling T^2 , the MEWMA, and the Z control charts. The authors [19] investigated the sources of process variance faults with the use of ANN and SVM; however, their considerations of process variance shifts were large. The authors [20] proposed a hybrid model for online analysis of MSPC signals in multivariate manufacturing processes. Their model consisted of two modules in which the first module used a SVM to recognize the unnatural pattern, and then, the magnitude of different shifts can be determined by using the second module, the NN models. The authors [21] also proposed a hybrid model for online analysis of MSPC signals in multivariate manufacturing processes. They also used the SVM to recognize the mean and variance shifts in the first module. In the second module, they employed two neural network models to recognize the magnitude of shifts for each variable simultaneously. The study [22] proposed a hybrid scheme which is composed of independent component analysis (ICA) and SVM to decide the fault quality variables when a step change disturbance existed in a multivariate process.

The literature review has shown that most of the existing studies are concerned with the determination of which variable or group of variables has caused the signal through single step modeling. However, there is a difficulty that may not have been addressed yet. When the number of quality characteristics is large, the existing decomposition methods and/or machine learning methods may lack the capability to handle such a situation. In addition, because process faults are typically attributed to mean shifts and the multivariate normal process is one of the most widely used applications, the present study is motivated by addressing mean shift faults for a multivariate normal process with a large number of quality variables. A review of relevant literature also indicates that the application of ANN for process fault determination is promising; however, it suffers from the requirement of a large number of controlling parameters and the risk of model overfitting [23-25]. Consequently, contrary to the existing approaches, the present study proposes two-stage hybrid schemes to identify which quality variable or group of variables is responsible for process mean shift faults. The proposed schemes integrate multivariate adaptive regression splines (MARS), logistic regression (LR), and artificial neural networks, which are referred to as the MARS-ANN and LR-ANN schemes, respectively. The performance of the proposed approaches was examined by a series of computer simulations.

The rest of this paper is organized as follows. Section 2 provides brief overviews of process models and the proposed schemes. The various experimental conditions are addressed in Section 3. This study is concluded in Section 4.

2. Process Models and Methodologies

The structure of the process model is addressed. The proposed hybrid schemes are also described in this section.

2.1. Structure of the Process and the Mean Shift. This study considers the situation of process mean shifts and assumes that the multivariate process is initially in a normal state and the sample observations are derived from a k-dimensional multivariate normal distribution $N(\mu_0, \Sigma_0)$, where

$$\mu_{\sim 0} = \begin{bmatrix} 0 \\ 0 \\ \vdots \\ 0 \end{bmatrix}, \tag{1}$$

$$\Sigma_{0} = \begin{bmatrix} 1 & \rho & \cdots & \rho \\ \rho & \ddots & \ddots & \vdots \\ \vdots & \ddots & 1 & \rho \\ \rho & \cdots & \rho & 1 \end{bmatrix}. \tag{2}$$

After a certain length of time, this study assumes that the mean vector changes from $\underline{\mu}_{0}$ to $\underline{\mu}_{1}$, where

$$\mu = \mu + \begin{bmatrix} \delta_1 \\ \delta_2 \\ \vdots \\ \delta_k \end{bmatrix}. \tag{3}$$

Let

$$X_{\sim ij} = [X_{ij1}, X_{ij2}, \dots, X_{ijk}]', \quad j = 1, 2, \dots, n$$
 (4)

be a $k \times 1$ vector that represents k characteristics on the jth observation in subgroup i. The resulting sample mean vector is as follows:

$$\overline{X}_{i} = \frac{1}{n} \sum_{i=1}^{n} X_{i}.$$
 (5)

To detect a multivariate process mean shift, Hotelling [26] proposed the following chi-square statistic

$$\chi_i^2 = n \left(\overline{X}_i - \mu \right) \sum_{i=0}^{r-1} \left(\overline{X}_i - \mu \right). \tag{6}$$

This statistic is asymptotically distributed as a chi-square distribution with k degrees of freedom. The control chart that uses χ^2 as a monitoring statistic in (6) has the upper control limit

$$UCL = \chi_{\alpha}^{2}(k), \qquad (7)$$

where $\chi^2_{\alpha}(k)$ is the upper α th percentile of the chi-square distribution with k degrees of freedom. If the plotted statistic χ^2_i falls outside the UCL, the process is considered to be in an abnormal state, and our proposed method can be applied to identify the source of mean shifts. The proposed two-stage hybrid methods integrate the framework of MARS, LR, and ANN. In the initial stage, influencing variables are selected using multivariate adaptive regression splines or logistic regression. In the second stage, the significant influencing variables selected are taken as the input variables of the ANN. The following sections address these three components.

2.2. Logistic Regression. The purpose of performing logistic regression modeling in stage I was to identify important influencing variables and refine the entire set of input variables. The structure of the logistic regression model can be briefly described as follows. Let Y_1, Y_2, \ldots, Y_n represent the dependent variables ($Y_i = 1$ denotes "the abnormal state" and $Y_i = 0$ denotes "the normal state") and let

$$P_i = \Pr\left[Y_i = 1 \mid \overline{x}_{i1}, \overline{x}_{i2}, \dots, \overline{x}_{ik}\right] \tag{8}$$

be the conditional probability of event $\{Y_i = 1\}$ with a given series of independent variables $(\overline{x}_{i1}, \overline{x}_{i2}, \dots, \overline{x}_{ik})$, where \overline{x}_{im} is the sample mean of the mth characteristic. The logistic regression model is then defined as follows:

$$\ln\left(\frac{P_i}{1-P_i}\right) = \beta_0 + \sum_{i=1}^k \beta_j \overline{x}_{ij}.$$
 (9)

Before screening significant independent variables, we performed the collinearity diagnosis procedure to exclude variables that exhibited high collinearity. After this diagnosis, the remaining variables served as independent variables for logistic regression modeling and testing. The Wald forward method was applied to identify independent variables with significant influence on an abnormal state probability. These significant independent variables and the dependent variable were then substituted into the ANN to construct a two-stage model.

2.3. Multivariate Adaptive Regression Splines. The superior performance of the MARS has been reported in many applications [27–32]. MARS is typically capable of revealing important data patterns and relationships for the complex data structure that is often concealed in high-dimensional data [28, 31]. The MARS model can be represented as [33]

$$\widehat{f}(x) = b_0 + \sum_{m=1}^{M} b_m \prod_{k=1}^{K_m} \left[S_{km} \left(x_{\nu(k,m)} - t_{km} \right) \right], \quad (10)$$

where b_0 and b_m are the parameters, M is the number of basis functions (BF), K_m is the number of knots, S_{km} takes on values of either 1 or -1 and indicates the right or left sense of the associated step function, v(k,m) is the label of the independent variable, and t_{km} is the knot location. The optimal MARS model is obtained in two steps. The purpose of the first step is to construct a large number of basis functions that initially fit the data. The purpose of the second step is to delete basis functions in order of least contribution using the generalized cross-validation (GCV) criterion. The variable importance measure was obtained by observing the decrease in the calculated GCV values when a variable was removed from the model. The GCV is described as

GCV (M) =
$$\frac{1/N \sum_{i=1}^{N} [y_i - \hat{f}_M(x_i)]^2}{[1 - C(M)/N]^2},$$
 (11)

where N is the number of observations and C(M) is the cost penalty measure of a model containing M basis functions.

2.4. The Artificial Neural Network. The ANN has been widely used in many SPC applications [34, 35]. The ANN is a parallel system comprised of highly interconnected processing elements that are based on neurobiological models. The ANN processes information through the interactions of a large number of simple processing elements called neurons.

Figure 1 illustrates that neurons in networks take inputs from the previous layer and send outputs to the next layer. Typically, ANN nodes consist of three layers: the input, output, and hidden layers. The nodes in the input layers receive input signals from an external source and the nodes in the output layers generate the target output signals. The output of each neuron in the input layer is the same as the input to that neuron. For each neuron j in the hidden layer and neuron k in the output layer, the net inputs are given by

$$\operatorname{net}_{j} = \sum_{i} w_{ji} \times o_{i}, \qquad \operatorname{net}_{k} = \sum_{j} w_{kj} \times o_{j},$$
 (12)

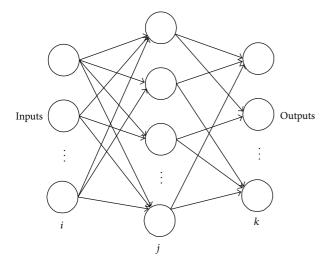


FIGURE 1: Structure of ANN model.

where i(j) is a neuron in the previous layer, $o_i(o_j)$ is the output of node i(j), and $w_{ji}(w_{kj})$ is the connection weight from neuron i(j) to neuron j(k). The neuron outputs are given by

$$o_i = \text{net}_i,$$
 (13)

$$o_{j} = \frac{1}{1 + \exp^{-(\operatorname{net}_{j} + \theta_{j})}} = f_{j} \left(\operatorname{net}_{j}, \theta_{j} \right),$$

$$o_{k} = \frac{1}{1 + \exp^{-(\operatorname{net}_{k} + \theta_{k})}} = f_{k} \left(\operatorname{net}_{k}, \theta_{k} \right),$$
(14)

where $\operatorname{net}_j(\operatorname{net}_k)$ is the input signal from the external source to the node j(k) in the input layer and $\theta_j(\theta_k)$ is a bias. The transformation function shown in (14) is called a sigmoid function and is the most commonly utilized function to date. As a result, this study used the sigmoid function.

3. Experiments and Analysis

3.1. The Parameter Settings. To evaluate the performance of the proposed approach, a series of simulations were conducted. Without loss of generality, this study assumed that each quality characteristic was initially sampled from a normal distribution with zero mean and one standard deviation. In addition, we assumed that twenty quality characteristics were monitored simultaneously (i.e., k=20), and the covariance matrix was defined as in (2).

Because we considered 20 quality characteristics for the multivariate normal process, there are $2^{20}-1$ possible types of mean shifts. They are represented by $(1,0,\ldots,0)$, $(0,1,0,\ldots,0),\ldots$, and $(1,1,\ldots,1)$, where 1 denotes a quality characteristic that is at fault and 0 denotes a quality characteristic that is not at fault. For an abnormal mean vector structure, we considered three types of mean shifts for demonstration: $(1,0,\ldots,0)$, $(1,0,1,0,\ldots,0)$ and $(1,0,1,0,1,0,\ldots,0)$. This study also considered three different values of ρ : 0.1, 0.5, and 0.9. The sample size was assumed to be 10. Two values of δ_i were considered: 0.5 and 1.0. We repeated the simulation 500 times for each data structure. The structure of the ANN

is established as follows. When applying ANN in the single stage in this study, we had 20 input nodes and one output node in the ANN structure. The hidden nodes were set to the range i - 2 to i + 2, where i is the number of input variables. Thus, in the initial phase, the hidden nodes were 18, 19, 20, 21, and 22.

According to the suggestions of the study [36], the learning rates were set to 0.01, 0.005, and 0.001. After performing ANN modeling, we obtained the $\{20-20-1\}$ topology with a learning rate of 0.01, which provides the best result with the minimum test RMSE. Here, $\{n_i - n_h - n_o\}$ denotes the number of neurons in the input layer, number of neurons in the hidden layer, and number of neurons in the output layer, respectively.

3.2. The Results. For the hybrid LR-ANN model, this study calculated the variance inflation factor (VIF) to examine the presence of collinearity, used a 0.05 significance level, and employed logistic regression analysis to select important influencing variables in the initial stage. Values of VIFs greater than 10 were considered large enough to suspect serious multicollinearity [37–39]. As shown in Table 1, all of the VIFs are less than 10. Consequently, collinearity was not too high among the independent variables. The analysis results of LR modeling are summarized in Table 2. The significant variables selected in this stage served as the input variables of the ANN.

For the hybrid MARS-ANN model, we obtained the selection results of the variables after performing the MARS procedure. Tables 3, 4, 5, 6, 7, and 8 list the selection results for the MARS models for 6 different combinations of ρ and δ_i . In this selection procedure, the important explanatory variables were chosen; their relative importance indicators are listed in the last column of Tables 3 to 8.

When the first stage of hybrid modeling was completed, the ANN topology settings were established. Table 9 displays the corresponding ANN topologies for various types of hybrid models. The network topology with the minimum test RMSE was again considered as the optimal network topology. The learning rate of 0.01 was used for all of those models.

This study used the classical single stage of an ANN model and the proposed two-stage of MARS-ANN and LR-ANN models to determine the source of mean shift faults in a multivariate process. The experimental results are displayed in Table 10.

Table 10 reveals that the two-stage MARS-ANN and LR-ANN approaches exhibit better performance than the classical single-stage ANN method in many situations. Based on the results shown in Table 10, it is noted that when the type of mean shift is $(1,0,1,0,1,0,\ldots,0)$, the LR-ANN approach exhibits the best performance in terms of accurate identification rates (AIR) for all (ρ,δ_i) combinations. The MARS-ANN approach was preferable to the single stage of the ANN in almost every case. The last two rows of Table 10 list the average and standard errors of the accurate identification rates. The proposed hybrid approaches, LR-ANN and MARS-ANN, outperformed the classical method, which is the single stage of the ANN. The proposed MARS-ANN approach had

	TABLE 1:	Collinearity	diagnosis /	for I	R models.
--	----------	--------------	-------------	-------	-----------

Variables	ρ =	= 0.1	ρ =	: 0.5	ρ =	0.9
variables	$\delta_i = 0.5$	$\delta_i = 1.0$	$\delta_i = 0.5$	$\delta_i = 1.0$	$\delta_i = 0.5$	$\delta_i = 1.0$
$\overline{\overline{x}}_1$	1.11	1.23	1.65	1.56	3.66	2.26
\overline{x}_2	1.09	1.09	1.95	1.95	9.85	9.85
\overline{x}_3	1.21	1.54	1.80	1.97	3.98	2.89
\overline{x}_4	1.07	1.07	1.91	1.91	9.54	9.54
\overline{x}_5	1.21	1.55	1.81	2.00	4.03	2.91
\overline{x}_6	1.07	1.07	1.88	1.88	9.31	9.31
\overline{x}_7	1.13	1.28	1.69	1.63	3.78	2.33
\overline{x}_8	1.11	1.11	1.98	1.98	9.82	9.82
\overline{x}_9	1.07	1.07	1.89	1.88	9.21	9.21
\overline{x}_{10}	1.05	1.05	1.81	1.80	9.21	9.19
\overline{x}_{11}	1.07	1.07	1.90	1.90	9.43	9.41
\overline{x}_{12}	1.07	1.07	1.89	1.89	9.60	9.59
\overline{x}_{13}	1.07	1.07	1.91	1.90	9.84	9.83
\overline{x}_{14}	1.06	1.06	1.83	1.82	9.13	9.11
\overline{x}_{15}	1.08	1.08	1.92	1.92	9.62	9.60
\overline{x}_{16}	1.07	1.06	1.93	1.92	9.95	9.93
\overline{x}_{17}	1.07	1.07	1.84	1.83	8.93	8.92
\overline{x}_{18}	1.09	1.09	1.96	1.96	9.78	9.78
\overline{x}_{19}	1.09	1.09	1.94	1.93	9.69	9.68
\overline{x}_{20}	1.09	1.09	1.97	1.96	9.64	9.63

TABLE 2: Significant variables selected by LR analysis.

Correlation ρ	Shift value δ_i	Significant explanatory variables
	0.5	$\overline{x}_1, \overline{x}_3, \overline{x}_5, \overline{x}_9, \overline{x}_{12}, \overline{x}_{17}, \overline{x}_{18}, \overline{x}_{20}$
0.1	1.0	$\begin{array}{l} \overline{x}_1, \overline{x}_2, \overline{x}_3, \overline{x}_5, \overline{x}_6, \overline{x}_{11}, \overline{x}_{12}, \overline{x}_{13}, \\ \overline{x}_{16}, \overline{x}_{17}, \overline{x}_{20} \end{array}$
0.5	0.5	$\overline{x}_1, \overline{x}_3, \overline{x}_4, \overline{x}_5, \overline{x}_8, \overline{x}_9, \overline{x}_{11}, \overline{x}_{12}, \overline{x}_{13}, \overline{x}_{16}$
	1.0	$\overline{x}_1, \overline{x}_3, \overline{x}_6, \overline{x}_8, \overline{x}_{12}, \overline{x}_{13}, \overline{x}_{15}, \overline{x}_{16}, \overline{x}_{20}$
0.9	0.5	$\overline{x}_1, \overline{x}_3, \overline{x}_8, \overline{x}_9, \overline{x}_{12}, \overline{x}_{13}, \overline{x}_{16}, \overline{x}_{20}$
	1.0	$\overline{x}_1, \overline{x}_{13}$

the smallest standard error, which implies the robustness of the mechanism. After comparing the performances of the LR-ANN and MARS-ANN approaches, we determined that the MARS-ANN approach is superior. The reason may be that population stratification in logistic regression analysis can lead to bias in estimates and test statistics. As a result, the results of the LR-ANN approach were somewhat unstable.

Table 11 summarizes the AIR with consideration of three different correlations, namely, the low, the moderate, and the strong correlations, respectively. The standard deviations for those AIR values are listed in parentheses. By observing Table 11, one is able to observe that the performance of the proposed hybrid models almost completely outperforms the classical single-stage ANN model. In particular, the proposed

MARS-ANN has the best and the most robust performance among those three modeling approaches.

Table 12 shows the overall improvement percentage of the proposed model in comparison with the classical single-stage model. The AIR improvements of the proposed LR-ANN model over the classical ANN model for three types of correlations are 18.73%, 10.67%, and -2.50%, respectively. Although there is a poor improvement for the case of $\rho=0.9$, the average AIR improvement is 8.97%. In addition, the AIR improvements of the proposed MARS-ANN model over the classical ANN model for three types of correlations are 14.39%, 15.85%, and 6.96%, respectively. Accordingly, the average AIR improvement reaches 12.73%.

One important result is that our proposed approach is useful in dealing with difficulties of the smaller shifts for a multivariate process. The case of the smaller shift value (i.e., $\delta_i = 0.5$) drew particular attention from industries because it is very difficult to identify the sources of small mean shifts. Considering all the cases of $\delta_i = 0.5$, Table 10 illustrates that the 21.12% and 17.00% improvement in identification can be achieved when the proposed LR-ANN and MARS-ANN schemes are used. The improvements in identification are significant.

4. Conclusions

The ANN has been criticized for its long training process; however, the combination of LR/MARS and ANN is a good alternative for performing classification tasks. Accordingly,

Function	Std. dev.	Cost of omission	Number of BF	Variable	Relative importance (%)
1	0.501	1.070	1	\overline{x}_3	100.000
2	0.500	1.065	3	\overline{x}_5	98.993
3	0.339	0.963	1	\overline{x}_1	70.614
4	0.332	0.957	1	\overline{x}_7	68.366
5	0.131	0.873	1	\overline{x}_{13}	26.827
6	0.104	0.867	1	\overline{x}_{16}	20.879
7	0.099	0.866	1	\overline{x}_{14}	19.621
8	0.093	0.865	1	\overline{x}_{17}	18.071

Table 3: Basis functions and important explanatory variables for the MARS model with $(\rho, \delta_i) = (0.1, 0.5)$.

Table 4: Basis functions and important explanatory variables for the MARS model with $(\rho, \delta_i) = (0.1, 1.0)$.

Function	Std. dev.	Cost of omission	Number of BF	Variable	Relative importance (%)
1	0.517	0.372	3	\overline{x}_5	100.000
2	0.519	0.370	2	\overline{x}_3	99.356
3	0.395	0.328	2	\overline{x}_1	85.740
4	0.369	0.310	1	\overline{x}_7	79.157
5	0.066	0.211	1	\overline{x}_{20}	15.440

TABLE 5: Basis functions and important explanatory variables for the MARS model with $(\rho, \delta_i) = (0.5, 0.5)$.

Function	Std. dev.	Cost of omission	Number of BF	Variable	Relative importance (%)
1	0.596	0.871	2	\overline{x}_3	100.000
2	0.582	0.864	2	\overline{x}_5	98.281
3	0.380	0.764	2	\overline{x}_7	68.774
4	0.369	0.763	1	\overline{x}_1	68.220
5	0.245	0.702	1	\overline{x}_{13}	40.739
6	0.234	0.700	1	\overline{x}_{16}	39.271
7	0.203	0.692	2	\overline{x}_{17}	33.836
8	0.195	0.691	1	\overline{x}_{14}	32.728
9	0.188	0.688	1	\overline{x}_{20}	30.632
10	0.186	0.688	1	\overline{x}_6	30.530

Table 6: Basis functions and important explanatory variables for the MARS model with $(\rho, \delta_i) = (0.5, 1.0)$.

Function	Std. dev.	Cost of omission	Number of BF	Variable	Relative importance (%)
1	0.540	0.352	1	\overline{x}_3	100.000
2	0.535	0.344	2	\overline{x}_5	97.416
3	0.389	0.306	1	\overline{x}_1	83.637
4	0.380	0.294	1	\overline{x}_7	78.935
5	0.174	0.217	2	\overline{x}_{13}	35.183
6	0.167	0.216	2	\overline{x}_{16}	33.487
7	0.149	0.212	1	\overline{x}_{20}	29.230
8	0.143	0.211	1	\overline{x}_{14}	29.042

the proposed combination of the LR-ANN and MARS-ANN schemes was proven to be useful for determining the mean shift faults in a multivariate process.

The rationale behind the proposed schemes was initially to obtain fewer important explanatory variables by performing LR or MARS modeling. The resulting significant variables served as inputs to the designed ANN models. The proposed

LR-ANN and MARS-ANN models not only have fewer input variables but also possess better classification capabilities.

The proposed hybrid two-stage models in this study are not the only combination techniques; other artificial intelligence techniques, such as decision tree or genetic algorithms, can be integrated with neural networks or a support vector machine to further refine the structure of the classifiers and

	atory variables for the MARS model with $(\rho, \delta_i) = (0.9, 0.5)$.	TABLE 7: Basis functions and important explanato
--	---	--

Function	Std. dev.	Cost of omission	Number of BF	Variable	Relative importance (%)
1	0.789	0.363	2	\overline{x}_5	100.000
2	0.761	0.356	2	\overline{x}_3	98.013
3	0.570	0.304	2	\overline{x}_1	79.033
4	0.531	0.289	2	\overline{x}_7	72.994
5	0.412	0.225	1	\overline{x}_{13}	35.419
6	0.402	0.225	1	\overline{x}_{16}	34.692
7	0.349	0.221	1	\overline{x}_{14}	30.760
8	0.315	0.218	1	\overline{x}_6	27.641
9	0.317	0.218	1	\overline{x}_{10}	27.426
10	0.306	0.217	1	\overline{x}_{17}	26.965

Table 8: Basis functions and important explanatory variables for the MARS model with $(\rho, \delta_i) = (0.9, 1.0)$.

Function	Std. dev.	Cost of omission	Number of BF	Variable	Relative importance (%)
1	0.579	0.179	2	\overline{x}_5	100.000
2	0.565	0.176	2	\overline{x}_3	98.746
3	0.450	0.160	2	\overline{x}_1	91.803
4	0.434	0.151	2	\overline{x}_7	87.535
5	0.295	0.072	2	\overline{x}_{13}	31.978
6	0.293	0.072	2	\overline{x}_{16}	31.287
7	0.249	0.069	1	\overline{x}_{14}	26.538
8	0.222	0.067	1	\overline{x}_6	23.337

Table 9: ANN topology settings for different hybrid LR-ANN and MARS-ANN models.

Correlation ρ	Shift value δ_i	Type of mean shifts	ANN topology for LR-ANN	ANN topology for MARS-ANN	
		(1, 0,, 0)	{8-8-1}	{8-9-1}	
	0.5	$(1, 0, 1, 0, \ldots, 0)$	{8-8-1}	{8-7-1}	
0.1		(1, 0, 1, 0, 1, 0,, 0)	{8-8-1}	{8-10-1}	
0.1		(1, 0,, 0)	{11-13-1}	{5-5-1}	
	1.0	$(1, 0, 1, 0, \ldots, 0)$	{11-12-1}	{5-6-1}	
		$(1, 0, 1, 0, 1, 0, \ldots, 0)$	{11-12-1}	{5-7-1}	
0.5		(1, 0,, 0)	{10-10-1}	{10-10-1}	
	0.5	$(1, 0, 1, 0, \ldots, 0)$	{10-10-1}	{10-10-1}	
		(1, 0, 1, 0, 1, 0,, 0)	{10-10-1}	{10-10-1}	
0.5		$(1, 0, \ldots, 0)$	{9-9-1}	{8-9-1}	
	1.0	$(1, 0, 1, 0, \ldots, 0)$	{9-7-1}	{8-8-1}	
		(1, 0, 1, 0, 1, 0,, 0)	{9-11-1}	{8-9-1}	
		(1, 0,, 0)	{8-9-1}	{10-9-1}	
	0.5	$(1, 0, 1, 0, \ldots, 0)$	{8-10-1}	{10-10-1}	
0.9		(1, 0, 1, 0, 1, 0,, 0)	{8-9-1}	{10-11-1}	
0.9		$(1, 0, \ldots, 0)$	{2-2-1}	{8-6-1}	
	1.0	(1, 0, 1, 0,, 0)	{2-2-1}	{8-8-1}	
		$(1, 0, 1, 0, 1, 0, \ldots, 0)$	{2-2-1}	{8-7-1}	

improve classification accuracy. The applications of other process faults, such as variance shift faults, for a multivariate process should be further investigated.

The data-driven methods of multivariate statistical process control have been the subject of considerable interest from both the academic community and industry as an

important implement in the process monitoring area. Since the practical systems become more and more complicated and the physical models become extremely hard to obtain, considering the related topics within data-driven framework seems more meaningful in the current and future work to achieve more industrial oriented results [40–44]. In addition,

Correlation ρ	Shift value δ_i	Type of mean shifts	ANN	LR-ANN	MARS-ANN
		(1, 0,, 0)	60.80%	61.20%	58.40%
0.1	0.5	$(1, 0, 1, 0, \ldots, 0)$	60.80%	59.20%	62.40%
		(1, 0, 1, 0, 1, 0,, 0)	56.00%	70.40%	58.80%
		(1, 0,, 0)	58.00%	80.40%	85.60%
	1.0	$(1, 0, 1, 0, \ldots, 0)$	86.40%	84.80%	81.20%
		$(1, 0, 1, 0, 1, 0, \ldots, 0)$	56.00%	92.80%	86.00%
0.5		(1, 0,, 0)	38.80%	66.00%	59.60%
	0.5	$(1, 0, 1, 0, \ldots, 0)$	46.00%	55.60%	62.00%
		$(1, 0, 1, 0, 1, 0, \ldots, 0)$	46.40%	70.80%	64.80%
		(1, 0,, 0)	90.40%	91.60%	94.00%
	1.0	$(1, 0, 1, 0, \ldots, 0)$	94.40%	63.60%	94.40%
		$(1, 0, 1, 0, 1, 0, \ldots, 0)$	85.20%	96.40%	94.00%
		(1, 0,, 0)	82.40%	93.20%	81.30%
0.9	0.5	$(1, 0, 1, 0, \ldots, 0)$	94.40%	82.80%	94.40%
		$(1, 0, 1, 0, 1, 0, \ldots, 0)$	56.00%	96.80%	92.00%
0.9		(1, 0,, 0)	98.80%	44.00%	100.00%
	1.0	$(1, 0, 1, 0, \ldots, 0)$	100.00%	100.00%	100.00%
		(1, 0, 1, 0, 1, 0,, 0)	98.40%	100.00%	99.20%
Average of accurate	e identification rates		72.73%	78.31%	81.57%
Standard error of a	ccurate identification rate	es	0.05007	0.04092	0.03767

TABLE 10: Comparison of classification accuracy among the ANN, LR-ANN, and MARS-ANN models.

TABLE 11: AIR comparison of the classical-single stage and the proposed models.

	ANN	Proposed	Proposed
	AININ	LR-ANN	MARS-ANN
$\rho = 0.1$	63.00%	74.80%	72.07%
	(0.1166)	(0.1344)	(0.1354)
$\rho = 0.5$	66.87%	74.00%	78.13%
	(0.2565)	(0.1632)	(0.1760)
$\rho = 0.9$	88.33%	86.13%	94.48%
	(0.1711)	(0.2161)	(0.0725)

Table 12: AIR improvement of the proposed models in comparison with classical ANN model.

	Proposed	Proposed
	LR-ANN	MARS-ANN
$\rho = 0.1$	18.73%	14.39%
$\rho = 0.5$	10.67%	16.85%
$\rho = 0.9$	-2.50%	6.96%
Average improvement	8.97%	12.73%

real-time implementation of fault tolerant control system with performance optimization is an important issue in modern industries [45]. Extensions of the proposed procedures to data-driven design or real-time implementation of fault tolerant control system are possible. Such works deserve further research and are our future concern.

Acknowledgment

This work is partially supported by the National Science Council of the Republic of China, Grant no. NSC 102-2221-E-030-019 and Grant no. NSC 102-2118-M-030-001.

References

- [1] L. W. Blazek, B. Novic, and M. D. Scott, "Displaying multivariate data using polyplots," *Journal of Quality Technology*, vol. 19, no. 2, pp. 69–74, 1987.
- [2] N. Subramanyan and A. A. Houshmand, "Simultaneous representation of multivariate and corresponding univariate x-bar charts using a line graph," *Quality Engineering*, vol. 7, no. 4, pp. 681–682, 1995.
- [3] C. Fuchs and Y. Benjamini, "Multivariate profile charts for statistical process control," *Technometrics*, vol. 36, no. 2, pp. 182–195, 1994.
- [4] O. O. Atienza, L. T. Ching, and B. A. Wah, "Simultaneous monitoring of univariate and multivariate SPC information using boxplots," *International Journal of Quality Science*, vol. 3, no. 2, pp. 194–204, 1998.
- [5] R. L. Mason, N. D. Tracy, and J. C. Young, "Decomposition of T² for multivariate control chart interpretation," *Journal of Quality Technology*, vol. 27, no. 2, pp. 99–108, 1995.
- [6] R. L. Mason, N. D. Tracy, and J. C. Young, "A practical approach for interpreting multivariate T² control chart signals," *Journal of Quality Technology*, vol. 29, no. 4, pp. 396–406, 1997.
- [7] N. H. Timm, "Multivariate quality control using finite intersection tests," *Journal of Quality Technology*, vol. 28, no. 2, pp. 233–243, 1996.

- [8] G. C. Runger, F. B. Alt, and D. C. Montgomery, "Contributors to a multivariate statistical process control chart signal," *Communications in Statistics*, vol. 25, no. 10, pp. 2203–2213, 1996.
- [9] F. Aparisi, G. Avendaño, and J. Sanz, "Techniques to interpret T² control chart signals," *IIE Transactions*, vol. 38, no. 8, pp. 647–657, 2006.
- [10] Y. E. Shao and B.-S. Hsu, "Determining the contributors for a multivariate SPC chart signal using artificial neural networks and support vector machine," *International Journal of Innovative Computing, Information and Control*, vol. 5, no. 12, pp. 4899– 4906, 2009.
- [11] T. Kourti and J. F. MacGregor, "Multivariate SPC methods for process and product monitoring," *Journal of Quality Technology*, vol. 28, no. 4, pp. 409–428, 1996.
- [12] J. A. Westerhuis, S. P. Gurden, and A. K. Smilde, "Generalized contribution plots in multivariate statistical process monitoring," *Chemometrics and Intelligent Laboratory Systems*, vol. 51, no. 1, pp. 95–114, 2000.
- [13] P. E. Maravelakis, S. Bersimis, J. Panaretos, and S. Psarakis, "Identifying the out of control variable in a multivariate control chart," *Communications in Statistics. Theory and Methods*, vol. 31, no. 12, pp. 2391–2408, 2002.
- [14] Y. E. Shao, C.-D. Hou, C.-H. Chao, and Y.-J. Chen, "A decomposition approach for identifying the sources of variance shifts in a multivariate process," *ICIC Express Letters*, vol. 5, no. 4A, pp. 971–975, 2011.
- [15] S. T. A. Niaki and B. Abbasi, "Fault diagnosis in multivariate control charts using artificial neural networks," *Quality and Reliability Engineering International*, vol. 21, no. 8, pp. 825–840, 2005.
- [16] R.-S. Guh, "On-line identification and quantification of mean shifts in bivariate processes using a neural network-based approach," *Quality and Reliability Engineering International*, vol. 23, no. 3, pp. 367–385, 2007.
- [17] L.-H. Chen and T.-Y. Wang, "Artificial neural networks to classify mean shifts from multivariate χ^2 chart signals," *Computers and Industrial Engineering*, vol. 47, no. 2-3, pp. 195–205, 2004.
- [18] H. B. Hwarng and Y. Wang, "Shift detection and source identification in multivariate autocorrelated processes," *International Journal of Production Research*, vol. 48, no. 3, pp. 835–859, 2010.
- [19] C.-S. Cheng and H.-P. Cheng, "Identifying the source of variance shifts in the multivariate process using neural networks and support vector machines," *Expert Systems with Applications*, vol. 35, no. 1-2, pp. 198–206, 2008.
- [20] M. Salehi, A. Bahreininejad, and I. Nakhai, "On-line analysis of out-of-control signals in multivariate manufacturing processes using a hybrid learning-based model," *Neurocomputing*, vol. 74, no. 12-13, pp. 2083–2095, 2011.
- [21] M. Salehi, R. B. Kazemzadeh, and A. Salmasnia, "On line detection of mean and variance shift using neural networks and support vector machine in multivariate processes," *Applied Soft Computing*, vol. 12, no. 9, pp. 2973–2984, 2012.
- [22] Y. E. Shao, C.-J. Lu, and Y.-C. Wang, "A hybrid ICA-SVM approach for determining the quality variables at fault in a multivariate process," *Mathematical Problems in Engineering*, vol. 2012, Article ID 284910, 12 pages, 2012.
- [23] L. Cao, "Support vector machines experts for time series forecasting," *Neurocomputing*, vol. 51, pp. 321–339, 2003.
- [24] L. J. Cao and F. E. H. Tay, "Support vector machine with adaptive parameters in financial time series forecasting," *IEEE Transactions on Neural Networks*, vol. 14, no. 6, pp. 1506–1518, 2003.

- [25] C.-J. Lu, Y. E. Shao, and P.-H. Li, "Mixture control chart patterns recognition using independent component analysis and support vector machine," *Neurocomputing*, vol. 74, no. 11, pp. 1908–1914, 2011.
- [26] H. Hotelling, Techniques of Statistical Analysis, McGraw Hill, New York, NY, USA, 1947.
- [27] Q.-S. Xu, D. L. Massart, Y.-Z. Liang, and K.-T. Fang, "Two-step multivariate adaptive regression splines for modeling a quantitative relationship between gas chromatography retention indices and molecular descriptors," *Journal of Chromatography A*, vol. 998, no. 1-2, pp. 155–167, 2003.
- [28] S.-M. Chou, T.-S. Lee, Y. E. Shao, and I.-F. Chen, "Mining the breast cancer pattern using artificial neural networks and multivariate adaptive regression splines," *Expert Systems with Applications*, vol. 27, no. 1, pp. 133–142, 2004.
- [29] Y. Zhou and H. Leung, "Predicting object-oriented software maintainability using multivariate adaptive regression splines," *Journal of Systems and Software*, vol. 80, no. 8, pp. 1349–1361, 2007
- [30] F. Vidoli, "Evaluating the water sector in Italy through a two stage method using the conditional robust nonparametric frontier and multivariate adaptive regression splines," *European Journal of Operational Research*, vol. 212, no. 3, pp. 583–595, 2011.
- [31] Y. E. Shao and C.-D. Hou, "Change point determination for a multivariate process using a two-stage hybrid scheme," *Applied Soft Computing Journal*, vol. 13, no. 3, pp. 1520–1527, 2013.
- [32] V. L. Pilla, J. M. Rosenberger, V. Chen, N. Engsuwan, and S. Siddappa, "A multivariate adaptive regression splines cutting plane approach for solving a two-stage stochastic programming fleet assignment model," *European Journal of Operational Research*, vol. 216, no. 1, pp. 162–171, 2012.
- [33] J. H. Friedman, "Multivariate adaptive regression splines," *The Annals of Statistics*, vol. 19, no. 1, pp. 1–141, 1991.
- [34] C.-C. Chiu, Y. E. Shao, T.-S. Lee, and K.-M. Lee, "Identification of process disturbance using SPC/EPC and neural networks," *Journal of Intelligent Manufacturing*, vol. 14, no. 3-4, pp. 379– 388, 2003.
- [35] Y. E. Shao and C.-D. Hou, "Fault identification in industrial processes using an integrated approach of neural network and analysis of variance," *Mathematical Problems in Engineering*, vol. 2013, Article ID 516760, 7 pages, 2013.
- [36] B. Abbasi, "A neural network applied to estimate process capability of non-normal processes," *Expert Systems with Applications*, vol. 36, no. 2, pp. 3093–3100, 2009.
- [37] F. A. Graybill and H. K. Iyer, *Regression Analysis*, International Thomson Publishing, 1994.
- [38] J. F. Hair, R. E. Anderson, R. L. Tatham, and W. C. Black, Multivariate Data Analysis, Prentice-Hall, Upper Saddle River, NJ, USA, 5th edition, 1998.
- [39] Y. E. Shao, "Prediction of currency volume issued in Taiwan using a hybrid artificial neural network and multiple regression approach," *Mathematical Problems in Engineering*, vol. 2013, Article ID 676742, 9 pages, 2013.
- [40] H. Wang, T.-Y. Chai, J.-L. Ding, and M. Brown, "Data driven fault diagnosis and fault tolerant control: some advances and possible new directions," *Acta Automatica Sinica*, vol. 35, no. 6, pp. 739–747, 2009.
- [41] S. Yin and S. X. Ding, "A comparison study of basic datadriven fault diagnosis and process monitoring methods on the benchmark Tennessee Eastman process," *Journal of Process Control*, vol. 22, no. 9, pp. 1567–1581, 2012.

- [42] S. Yin, X. Yang, and H. R. Karimi, "Data-driven adaptive observer for fault diagnosis," *Mathematical Problems in Engi*neering, vol. 2012, Article ID 832836, 21 pages, 2012.
- [43] S. J. Qin, "Survey on data-driven industrial process monitoring and diagnosis," *Annual Reviews in Control*, vol. 36, no. 2, pp. 220–234, 2012.
- [44] S. Yin, S. X. Ding, A. H. A. Sari, and H. Hao, "Data-driven monitoring for stochastic systems and its application on batch process," *International Journal of Systems Science*, vol. 44, no. 7, pp. 1366–1376, 2013.
- [45] S. Yin, H. Luo, and S. Ding, "Real-time implementation of fault-tolerant control systems with performance optimization," *IEEE Transactions on Industrial Electronics*, vol. 64, no. 5, pp. 2402–2411, 2013.

Hindawi Publishing Corporation Abstract and Applied Analysis Volume 2013, Article ID 151374, 8 pages http://dx.doi.org/10.1155/2013/151374

Research Article

State-Feedback Stabilization for a Class of Stochastic Feedforward Nonlinear Time-Delay Systems

Liang Liu, ¹ Zhandong Yu, ¹ Qi Zhou, ² and Hamid Reza Karimi³

Correspondence should be addressed to Liang Liu; smithll@163.com

Received 18 October 2013; Accepted 18 November 2013

Academic Editor: Ming Liu

Copyright © 2013 Liang Liu et al. This is an open access article distributed under the Creative Commons Attribution License, which permits unrestricted use, distribution, and reproduction in any medium, provided the original work is properly cited.

We investigate the state-feedback stabilization problem for a class of stochastic feedforward nonlinear time-delay systems. By using the homogeneous domination approach and choosing an appropriate Lyapunov-Krasovskii functional, the delay-independent state-feedback controller is explicitly constructed such that the closed-loop system is globally asymptotically stable in probability. A simulation example is provided to demonstrate the effectiveness of the proposed design method.

1. Introduction

In recent years, the study on stochastic lower-triangular nonlinear systems has received considerable attention from both theoretical and practical point of views see, for instance, [1–19] and the references therein. This paper will further consider the following stochastic feedforward nonlinear time-delay systems described by

 $dx_1 = x_2 dt + f_1(\widetilde{x}_3, \widetilde{x}_3(t - d(t))) dt$

$$+g_{1}^{T}\left(\widetilde{x}_{2},\widetilde{x}_{2}\left(t-d\left(t\right)\right)\right)d\omega,$$

$$\vdots$$

$$dx_{n-2}=x_{n-1}dt+f_{n-2}\left(\widetilde{x}_{n},\widetilde{x}_{n}\left(t-d\left(t\right)\right)\right)dt\\+g_{n-2}^{T}\left(\widetilde{x}_{n-1},\widetilde{x}_{n-1}\left(t-d\left(t\right)\right)\right)d\omega,$$

$$dx_{n-1}=x_{n}dt+g_{n-1}^{T}\left(\widetilde{x}_{n},\widetilde{x}_{n}\left(t-d\left(t\right)\right)\right)d\omega,$$

$$dx_{n}=udt,$$

$$(1)$$

where $x = (x_1, ..., x_n)^T \in \mathbb{R}^n$ and $u \in \mathbb{R}$ are the system state and input signal, respectively, $\widetilde{x}_i = (x_i, ..., x_n)^T$, $\widetilde{x}_i(t - d(t)) = (x_i(t - d(t)), ..., x_n(t - d(t)))^T$ is the time-delayed state vector,

and $d(t): R_+ \to [0,d]$ is the time-varying delay. ω is an m-dimensional standard Wiener process defined on the complete probability space $(\Omega, \mathcal{F}, \{\mathcal{F}_t\}_{t\geq 0}, P)$ with Ω being a sample space, \mathcal{F} being a σ -field, $\{\mathcal{F}_t\}_{t\geq 0}$ being a filtration, and P being a probability measure. $f_i: R^{n-i-1} \times R^{n-i-1} \to R$ and $g_j: R^{n-j} \times R^{n-j} \to R^m$ are assumed to be locally Lipschitz with $f_i(0,0) = 0$ and $g_j(0,0) = 0$, $i=1,\ldots,n-2$, $j=1,\ldots,n-1$.

Feedforward (also called upper-triangular) system is another important class of nonlinear systems. Firstly, from a theoretical point of view, since they are not feedback linearizable and maybe not stabilized by applying the conventional backstepping method, the stabilization problem of these systems is more difficult than that of lower-triangular systems. Secondly, many physical devices, such as the cart-pendulum system in [20] and the ball-beam system with a friction term in [21], can be described by equations with the feedforward structure. In the recent papers, the stabilization problems for feedforward nonlinear (or time-delay) systems have achieved remarkable development; see, for example, [22–29] and the references therein.

However, all these above-mentioned results are limited to deterministic systems. There are fewer results on stochastic feedforward nonlinear systems until now, due to the special

¹ College of Engineering, Bohai University, Liaoning 121013, China

² College of Information Science, Bohai University, Liaoning 121013, China

³ Department of Engineering, Faculty of Engineering and Science, University of Agder, 4898 Grimstad, Norway

characteristics of this system. To the best of the authors' knowledge, [30] is the only paper to consider this kind of stochastic feedforward nonlinear systems, but the assumptions on the nonlinearities are restrictive.

The purpose of this paper is to further weaken the assumptions on the drift and diffusion terms of system (1) and solve the state-feedback stabilization problem. By using the homogeneous domination approach in [26] and choosing an appropriate Lyapunov-Krasovskii functional, a delay-independent state-feedback controller is explicitly constructed such that the closed-loop system is globally asymptotically stable in probability.

The paper is organized as follows. Section 2 provides some preliminary results. The design and analysis of state-feedback controller are given in Sections 3 and 4, respectively, following a simulation example in Section 5. Section 6 concludes this paper.

2. Preliminary Results

The following notations, definitions, and lemmas are to be used throughout the paper.

 R_{+} denotes the set of all nonnegative real numbers, and \mathbb{R}^n denotes the real *n*-dimensional space. For a given vector or matrix X, X^T denotes its transpose, $Tr\{X\}$ denotes its trace when X is square, and |X| is the Euclidean norm of a vector X. $\mathscr{C}([-d,0];R^n)$ denotes the space of continuous \mathbb{R}^n -value functions on [-d,0] endowed with the norm $\|\cdot\|$ defined by $||f|| = \sup_{x \in [-d,0]} |f(x)|$ for $f \in \mathcal{C}([-d,0]; \mathbb{R}^n)$; $\mathscr{C}^b_{\mathscr{F}_0}([-d,0];R^n)$ denotes the family of all \mathscr{F}_0 -measurable bounded $\mathscr{C}([-d,0];R^n)$ -valued random variables $\xi = \{\xi(\theta) :$ $-d \le \theta \le 0$. \mathscr{C}^i denotes the set of all functions with continuous *i*th partial derivatives; $\mathscr{C}^{2,1}(R^n \times [-d,\infty); R_+)$ denotes the family of all nonnegative functions V(x,t) on $\mathbb{R}^n \times [-d, \infty)$ which are \mathscr{C}^2 in x and \mathscr{C}^1 in t; $\mathscr{C}^{2,1}$ denotes the family of all functions which are \mathscr{C}^2 in the first argument and \mathscr{C}^1 in the second argument. \mathscr{X} denotes the set of all functions $R_+ \rightarrow R_+$, which are continuous, strictly increasing, and vanishing at zero; \mathcal{K}_{∞} denotes the set of all functions which are of class $\mathcal K$ and unbounded; $\mathcal K \mathcal L$ is the set of all functions $\beta(s,t)$: $R_+ \times R_+ \rightarrow R_+$, which are of \mathcal{K} for each fixed t and decrease to zero as $t \to \infty$ for each fixed *s*.

Consider the following stochastic time-delay system:

$$dx(t) = f(x(t), x(t - d(t)), t) dt$$

$$+ g(x(t), x(t - d(t)), t) d\omega,$$
(2)

with initial data $\{x(\theta): -d \leq \theta \leq 0\} = \xi \in \mathscr{C}^b_{\mathscr{F}_0}([-d,0];R^n)$, where $d(t): R_+ \to [0,d]$ is a Borel measurable function, ω is an m-dimensional standard Wiener process defined on the complete probability space $(\Omega, \mathscr{F}, \{\mathscr{F}_t\}_{t\geq 0}, P)$, and $f: R^n \times R^n \times R_+ \to R^n$ and $g: R^n \times R^n \times R_+ \to R^{n\times m}$ are locally Lipschitz in (x(t), x(t-d(t))) uniformly in t with $f(0,0,t) \equiv 0$ and $g(0,0,t) \equiv 0$.

Definition 1 (see [6]). For any given $V(x(t),t) \in \mathcal{C}^{2,1}$ associated with system (2), the differential operator \mathcal{L} is defined as

$$\mathscr{L}V = \frac{\partial V}{\partial t} + \frac{\partial V}{\partial x}f + \frac{1}{2}\operatorname{Tr}\left\{g^{T}\frac{\partial^{2}V}{\partial x^{2}}g\right\}.$$
 (3)

Definition 2 (see [6]). The equilibrium x(t) = 0 of system (2) is said to be globally asymptotically stable (GAS) in probability if for any $\epsilon > 0$ there exists a function $\beta(\cdot, \cdot) \in \mathcal{KL}$ such that $P\{|x(t)| \leq \beta(\|\xi\|, t)\} \geq 1 - \epsilon$ for any $t \geq 0$, $\xi \in \mathscr{C}^b_{\mathcal{F}_0}([-d, 0]; \mathbb{R}^n) \setminus \{0\}$, where $\|\xi\| = \sup_{\theta \in [-d, 0]} |x(\theta)|$.

Definition 3 (see [26]). For fixed coordinates $(x_1, ..., x_n)^T \in \mathbb{R}^n$ and real numbers $r_i > 0, i = 1, ..., n$, one has the following.

- (i) The dilation $\Delta_{\varepsilon}(x)$ is defined by $\Delta_{\varepsilon}(x) = (\varepsilon^{r_1}x_1, \dots, \varepsilon^{r_n}x_n)$ for any $\varepsilon > 0$; r_1, \dots, r_n are called as the weights of the coordinates. For simplicity, we define dilation weight $\Delta = (r_1, \dots, r_n)$.
- (ii) A function $V \in \mathcal{C}(R^n, R)$ is said to be homogeneous of degree τ if there is a real number $\tau \in R$ such that $V(\Delta_{\varepsilon}(x)) = \varepsilon^{\tau} V(x_1, \dots, x_n)$ for any $x \in R^n \setminus \{0\}, \varepsilon > 0$.
- (iii) A vector field $h \in \mathcal{C}(R^n, R^n)$ is said to be homogeneous of degree τ if there is a real number $\tau \in R$ such that $h_i(\Delta_{\varepsilon}(x)) = \varepsilon^{\tau + r_i} h_i(x)$ for any $x \in R^n \setminus \{0\}, \varepsilon > 0$, i = 1, ..., n.
- (iv) A homogeneous p-norm is defined as $\|x\|_{\Delta,p} = (\sum_{i=1}^n |x_i|^{p/r_i})^{1/p}$ for any $x \in \mathbb{R}^n$, where $p \ge 1$ is a constant. For simplicity, in this paper, one chooses p = 2 and writes $\|x\|_{\Delta}$ for $\|x\|_{\Delta,2}$.

Lemma 4 (see [6]). For system (2), if there exist a function $V(x(t),t) \in \mathcal{C}^{2,1}(\mathbb{R}^n \times [-d,\infty); \mathbb{R}_+)$, two class \mathcal{K}_{∞} functions α_1, α_2 , and a class \mathcal{K} function α_3 such that

$$\alpha_{1}(|x(t)|) \leq V(x(t),t) \leq \alpha_{2} \left(\sup_{-d \leq s \leq 0} |x(t+s)| \right),$$

$$\mathscr{L}V(x(t),t) \leq -\alpha_{3}(|x(t)|),$$
(4)

then there exists a unique solution on $[-d, \infty)$ for (2), the equilibrium x(t)=0 is GAS in probability, and $P\{\lim_{t\to\infty}|x(t)|=0\}=1$.

Lemma 5 (see [26]). Given a dilation weight $\Delta = (r_1, \ldots, r_n)$, suppose that $V_1(x)$ and $V_2(x)$ are homogeneous functions of degrees τ_1 and τ_2 , respectively. Then $V_1(x)V_2(x)$ is also homogeneous with respect to the same dilation weight Δ . Moreover, the homogeneous degree of $V_1 \cdot V_2$ is $\tau_1 + \tau_2$.

Lemma 6 (see [26]). Suppose that $V: \mathbb{R}^n \to \mathbb{R}$ is a homogeneous function of degree τ with respect to the dilation weight Δ ; then (i) $\partial V/\partial x_i$ is homogeneous of degree $\tau - r_i$ with r_i being the homogeneous weight of x_i ; (ii) there is a constant c such that $V(x) \leq c \|x\|_{\Delta}^{\tau}$. Moreover, if V(x) is positive definite, then $V(x) \geq c \|x\|_{\Delta}^{\tau}$, where c is a positive constant.

Lemma 7 (see [5]). Let c and d be positive constants. For any positive number $\overline{\gamma}$, then $|x|^c |y|^d \le (c/(c+d))\overline{\gamma}|x|^{c+d} + (d/(c+d))\overline{\gamma}^{-c/d}|y|^{c+d}$.

3. Design of State-Feedback Controller

The objective of this paper is to design a state-feedback controller for system (1) such that the equilibrium of the closed-loop system is globally asymptotically stable in probability.

3.1. Assumptions. For system (1), we need the following assumptions.

Assumption 8. For i = 1, ..., n - 1, there exist positive constants a_1 and a_2 such that

$$\begin{aligned} & \left| f_{i} \left(\widetilde{x}_{i+2}, \widetilde{x}_{i+2} \left(t - d \left(t \right) \right) \right) \right| \\ & \leq a_{1} \left(\sum_{j=i+2}^{n} \left| x_{j} \right| + \sum_{j=i+2}^{n} \left| x_{j} \left(t - d \left(t \right) \right) \right| \right), \\ & \left| g_{i} \left(\widetilde{x}_{i+1}, \widetilde{x}_{i+1} \left(t - d \left(t \right) \right) \right) \right| \\ & \leq a_{2} \left(\sum_{j=i+1}^{n} \left| x_{j} \right| + \sum_{j=i+1}^{n} \left| x_{j} \left(t - d \left(t \right) \right) \right| \right), \end{aligned} \tag{5}$$

where $x_{n+1} = x_{n+1}(t - d(t)) = 0$.

Assumption 9. The time-varying delay d(t) satisfies $\dot{d}(t) \le \gamma < 1$ for a constant γ .

Remark 10. When $x_{i+1} = x_{i+1}(t - d(t)) = 0$ in diffusion term g_i (i = 1, ..., n-1), Assumption 8 reduces to the same form as in [30], from which one can see that system (1) is more general than [30]. The significance and reasonability of Assumption 8 are illustrated in that paper.

Firstly, we introduce the following coordinate transformation:

$$\eta_i = \frac{x_i}{\kappa^{i-1}}, \quad \nu = \frac{u}{\kappa^n}, \quad i = 1, \dots, n, \tag{6}$$

where $0 < \kappa < 1$ is a scalar to be designed. By (6), (1) can be expressed as

$$d\eta_{1} = \kappa \eta_{2} dt + \overline{f}_{1} \left(\widetilde{\eta}_{3}, \widetilde{\eta}_{3} \left(t - d \left(t \right) \right) \right) dt$$
$$+ \overline{g}_{1}^{T} \left(\widetilde{\eta}_{2}, \widetilde{\eta}_{2} \left(t - d \left(t \right) \right) \right) d\omega,$$
$$\vdots$$

$$\begin{split} d\eta_{n-2} &= \kappa \eta_{n-1} dt + \overline{f}_{n-2} \left(\widetilde{\eta}_n, \widetilde{\eta}_n \left(t - d \left(t \right) \right) \right) dt \\ &+ \overline{g}_{n-2}^T \left(\widetilde{\eta}_{n-1}, \widetilde{\eta}_{n-1} \left(t - d \left(t \right) \right) \right) d\omega, \\ d\eta_{n-1} &= \kappa \eta_n dt + \overline{g}_{n-1}^T \left(\widetilde{\eta}_n, \widetilde{\eta}_n \left(t - d \left(t \right) \right) \right) d\omega, \\ d\eta_n &= \kappa \nu dt, \end{split}$$

where $\overline{f}_i = f_i/\kappa^{i-1}$, $\overline{g}_i = g_i/\kappa^{i-1}$, $i = 1, \dots, n-1$, $\overline{f}_{n-1} = 0$.

3.2. State-Feedback Controller Design. We construct a state-feedback controller for system (7).

Step 1. Introducing $\xi_1 = \eta_1$ and choosing $V_1(\eta_1) = (1/4)\xi_1^4$, from (3) and (7), it follows that

$$\mathscr{L}V_1 = \kappa \xi_1^3 \eta_2 + \frac{\partial V_1}{\partial \eta_1} \overline{f}_1 + \frac{1}{2} \operatorname{Tr} \left\{ \overline{g}_1 \frac{\partial^2 V_1}{\partial \eta_1^2} \overline{g}_1^T \right\}. \tag{8}$$

The first virtual controller

$$\eta_2^* = -c_{11}\xi_1 =: -\alpha_1\xi_1, \quad c_{11} > 0,$$
(9)

leads to $\mathcal{L}V_1 \leq -\kappa c_{11}\xi_1^4 + \kappa \xi_1^3(\eta_2 - \eta_2^*) + (\partial V_1/\partial \eta_1)\overline{f}_1 + (1/2)\operatorname{Tr}\{\overline{g}_1(\partial^2 V_1/\partial \eta_1^2)\overline{g}_1^T\}.$

Step i (i = 2,...,n). In this step, we can get the following lemma.

Lemma 11. Suppose that at step i-1, there is a set of virtual controllers $\eta_1^*, \ldots, \eta_i^*$ defined by

$$\eta_1^* = 0, \qquad \xi_1 = \eta_1 - \eta_1^* = \eta_1,
\eta_k^* = -\alpha_{k-1}\xi_{k-1}, \quad \xi_k = \eta_k - \eta_k^*, \quad k = 2, \dots, i,$$
(10)

such that the (i-1)th Lyapunov function $V_{i-1}(\overline{\eta}_{i-1})=(1/4)\sum_{j=1}^{i-1}\xi_j^4$ satisfies

$$\mathcal{L}V_{i-1} \leq -\kappa \sum_{j=1}^{i-1} c_{i-1,j} \xi_{j}^{4} + \kappa \xi_{i-1}^{3} \left(\eta_{i} - \eta_{i}^{*} \right)$$

$$+ \sum_{j=1}^{i-1} \frac{\partial V_{i-1}}{\partial \eta_{j}} \overline{f}_{j} + \frac{1}{2} \sum_{p,q=1}^{i-1} \operatorname{Tr} \left\{ \overline{g}_{p} \frac{\partial^{2} V_{i-1}}{\partial \eta_{p} \partial \eta_{q}} \overline{g}_{q}^{T} \right\},$$

$$(11)$$

where α_j , $c_{i-1,j}$, $j=1,\ldots,i-1$, are positive constants. Then there exists a virtual control law $\eta_{i+1}^* = -\alpha_i \xi_i$ such that

$$\mathcal{L}V_{i} \leq -\kappa \sum_{j=1}^{i} c_{ij} \xi_{j}^{4} + \kappa \xi_{i}^{3} \left(\eta_{i+1} - \eta_{i+1}^{*} \right)$$

$$+ \sum_{j=1}^{i} \frac{\partial V_{i}}{\partial \eta_{j}} \overline{f}_{j} + \frac{1}{2} \sum_{p,q=1}^{i} \operatorname{Tr} \left\{ \overline{g}_{p} \frac{\partial^{2} V_{i}}{\partial \eta_{p} \partial \eta_{q}} \overline{g}_{q}^{T} \right\},$$

$$(12)$$

where $V_i(\overline{\eta}_i) = (1/4) \sum_{j=1}^i \xi_j^4 =: V_{i-1}(\overline{\eta}_{i-1}) + W_i(\overline{\eta}_i)$.

Proof. See the Appendix.

At step n, choosing $V_n(\overline{\eta}_n) = (1/4) \sum_{i=1}^n \xi_i^4$ and

$$v = \eta_{n+1}^* = -\alpha_n \xi_n$$

$$= -\left(\overline{\alpha}_n \eta_n + \overline{\alpha}_{n-1} \eta_{n-1} + \dots + \overline{\alpha}_1 \eta_1\right),$$
(13)

with the help of (3), (12), and (13), one obtains

$$\mathcal{L}V_{n} \leq -\kappa \sum_{i=1}^{n} c_{ni} \xi_{i}^{4} + \kappa \xi_{n}^{3} \left(v - \eta_{n+1}^{*} \right)$$

$$+ \sum_{i=1}^{n} \frac{\partial V_{n}}{\partial \eta_{i}} \overline{f}_{i} + \frac{1}{2} \sum_{p,q=1}^{n} \operatorname{Tr} \left\{ \overline{g}_{p} \frac{\partial^{2} V_{n}}{\partial \eta_{p} \partial \eta_{q}} \overline{g}_{q}^{T} \right\}$$

$$= -\kappa \sum_{i=1}^{n} c_{ni} \xi_{i}^{4} + \frac{\partial V_{n}}{\partial \eta} F + \frac{1}{2} \operatorname{Tr} \left\{ G \frac{\partial^{2} V_{n}}{\partial \eta^{2}} G^{T} \right\},$$

$$(14)$$

where $F = (\overline{f}_1, \dots, \overline{f}_{n-2}, 0, 0)^T$, $G = (\overline{g}_1, \dots, \overline{g}_{n-1}, 0)$, $\xi_n = \eta_n - \eta_n^*$, $\overline{\alpha}_i = \alpha_n \cdots \alpha_i$, c_{ni} , $i = 1, \dots, n$, are positive constants. The system (7) and (13) can be written as

$$d\eta = \kappa E(\eta) dt + F(\eta, \eta(t - d(t))) dt + G^{T}(\eta, \eta(t - d(t))) d\omega,$$
(15)

where $\eta = \overline{\eta}_n = (\eta_1, \dots, \eta_n)^T$, $E(\eta) = (\eta_2, \dots, \eta_n, \nu)^T$, and F and G are defined as in (14). Introducing the dilation weight $\Delta = (\underbrace{1, 1, \dots, 1}_{\text{for } \eta_1, \dots, \eta_n})$, by (10) and $V_n(\eta) = (1/4) \sum_{i=1}^n \xi_i^4$, one has

$$V_{n}\left(\Delta_{\varepsilon}(\eta)\right)$$

$$=\frac{1}{4}\sum_{i=1}^{n}\left(\varepsilon\eta_{i}+\alpha_{i-1}\varepsilon\eta_{i-1}+\cdots+\alpha_{i-1}\cdots\alpha_{1}\varepsilon\eta_{1}\right)^{4}$$

$$=\varepsilon^{4}V_{n}\left(\eta\right),$$
(16)

from which and Definition 3, we know that $V_n(\eta)$ is homogeneous of degree 4.

4. Stability Analysis

We state the main result in this paper.

Theorem 12. If Assumptions 8 and 9 hold for the stochastic feedforward nonlinear time-delay system (1), under the state-feedback controller $u = \kappa^n v$ and (13), then

- (i) the closed-loop system has a unique solution on $[-d, \infty)$;
- (ii) the equilibrium at the origin of the closed-loop system is GAS in probability.

Proof. We prove Theorem 12 by four steps.

Step 1. Since f_i , g_i , i = 1, ..., n, are assumed to be locally Lipschitz, so the system consisting of (13) and (15) satisfies the locally Lipschitz condition.

Step 2. We consider the following entire Lyapunov function for system (15):

$$V\left(\eta\right) = V_n\left(\eta\right) + \frac{\left(\overline{c}_{02} + \overline{c}_{03}\right)\kappa^2}{1 - \gamma} \int_{t-d(t)}^{t} \left\|\eta(\sigma)\right\|_{\Delta}^{4} d\sigma, \qquad (17)$$

where \bar{c}_{02} and \bar{c}_{03} are positive parameters to be determined. It is easy to verify that $V(\eta)$ is \mathcal{C}^2 on η . Since $V_n(\eta)$ is continuous, positive definite, and radially unbounded, by Lemma 4.3 in [31], there exist two class \mathcal{K}_{∞} functions β_1 and α_{21} such that

$$\beta_1(|\eta|) \le V_n(\eta) \le \alpha_{21}(|\eta|).$$
 (18)

By Lemma 4.3 in [31] and Lemma 6, there exist positive constants \underline{c} and \overline{c} , class \mathcal{K}_{∞} functions $\underline{\alpha}_{22}$ and $\overline{\alpha}_{22}$, and a positive definite function $U(\eta)$ whose homogeneous degree is 4 such that

$$\underline{c} \| \eta \|_{\Delta}^{4} \leq U(\eta) \leq \overline{c} \| \eta \|_{\Delta}^{4},$$

$$\underline{\alpha}_{22}(|\eta|) \leq U(\eta) \leq \overline{\alpha}_{22}(|\eta|).$$
(19)

From $d(t): R_+ \rightarrow [0, d]$ and (19), it follows that

$$\frac{\left(\overline{c}_{02} + \overline{c}_{03}\right)\kappa^{2}}{1 - \gamma} \int_{t-d(t)}^{t} \left\| \eta\left(\sigma\right) \right\|_{\Delta}^{4} d\sigma$$

$$\leq \widetilde{c} \int_{t-d(t)}^{t} \overline{\alpha}_{22} \left(\left| \eta\left(\sigma\right) \right| \right) d\sigma$$

$$\overset{\sigma=s+t}{=} \widetilde{c} \int_{-d(t)}^{0} \overline{\alpha}_{22} \left(\left| \eta\left(s+t\right) \right| \right) d\left(s+t\right)$$

$$\leq \widetilde{c} \int_{-d}^{0} \overline{\alpha}_{22} \left(\left| \eta\left(s+t\right) \right| \right) d\left(s+t\right)$$

$$\leq c \sup_{-d \leq s \leq 0} \overline{\alpha}_{22} \left(\left| \eta\left(s+t\right) \right| \right)$$

$$\leq \alpha_{22} \left(\sup_{-d \leq s \leq 0} \left| \eta\left(s+t\right) \right| \right),$$

where \tilde{c} , c are positive constants and α_{22} is a class \mathcal{K}_{∞} function. Since $|\eta| \leq \sup_{-d \leq s \leq 0} |\eta(s+t)|$, $\alpha_{21}(|\eta|) \leq \alpha_{21}(\sup_{-d \leq s \leq 0} |\eta(s+t)|)$. Defining $\beta_2 = \alpha_{21} + \alpha_{22}$, by (17), (18), and (20), one gets

$$\beta_1(|\eta|) \le V(\eta) \le \beta_2 \left(\sup_{-d \le s \le 0} |\eta(s+t)|\right).$$
 (21)

Step 3. By Lemma 6 and (14), there exists a positive constant c_{01} such that

$$\frac{\partial V_n}{\partial \eta} \kappa E\left(\eta\right) \le -c_{01} \kappa \left\|\eta\right\|_{\Delta}^4. \tag{22}$$

By Assumption 8, (6), and $0 < \kappa < 1$, one has

$$\left| \overline{f}_{i} \left(\widetilde{\eta}_{i+2}, \widetilde{\eta}_{i+2} \left(t - d \left(t \right) \right) \right) \right| \\
\leq \frac{a_{1} \left(\sum_{j=i+2}^{n} \left| \kappa^{j-1} \eta_{j} \right| + \sum_{j=i+2}^{n} \left| \kappa^{j-1} \eta_{j} \left(t - d \left(t \right) \right) \right| \right)}{\kappa^{i-1}} \\
\leq a_{1} \kappa^{2} \left(\sum_{j=i+2}^{n} \left| \eta_{j} \right| + \sum_{j=i+2}^{n} \left| \eta_{j} \left(t - d \left(t \right) \right) \right| \right) \\
\leq \delta_{1} \kappa^{2} \left(\left\| \eta \right\|_{\Lambda} + \left\| \eta \left(t - d \left(t \right) \right) \right\|_{\Lambda} \right), \tag{23}$$

where δ_1 is a positive constant. Using Lemmas 5–7 and (23), one gets

$$\frac{\partial V_{n}}{\partial \eta} F\left(\eta, \eta \left(t - d\left(t\right)\right)\right)
= \sum_{i=1}^{n-2} \frac{\partial V_{n}}{\partial \eta_{i}} \overline{f}_{i} \left(\widetilde{\eta}_{i+2}, \widetilde{\eta}_{i+2} \left(t - d\left(t\right)\right)\right)
\leq \widetilde{c}_{02} \kappa^{2} \sum_{i=1}^{n-2} \|\eta\|_{\Delta}^{3} \left(\|\eta\|_{\Delta} + \|\eta \left(t - d\left(t\right)\right)\|_{\Delta}\right)
\leq \kappa^{2} \left(c_{02} \|\eta\|_{\Delta}^{4} + \overline{c}_{02} \|\eta \left(t - d\left(t\right)\right)\|_{\Delta}^{4}\right),$$
(24)

where c_{02} , \overline{c}_{02} , and \widetilde{c}_{02} are positive constants. Similar to (23), there is a positive constant δ_2 such that

$$\left|\overline{g}_{i}\left(\widetilde{\eta}_{i+1},\widetilde{\eta}_{i+1}\left(t-d\left(t\right)\right)\right)\right| \leq \delta_{2}\kappa\left(\left\|\eta\right\|_{\Delta}+\left\|\eta\left(t-d\left(t\right)\right)\right\|_{\Delta}\right),\tag{25}$$

from which and Lemmas 5-7, one gets

$$\frac{1}{2}\operatorname{Tr}\left\{G\left(\eta,\eta\left(t-d\left(t\right)\right)\right)\frac{\partial^{2}V_{n}}{\partial\eta^{2}}G^{T}\left(\eta,\eta\left(t-d\left(t\right)\right)\right)\right\}$$

$$\leq \frac{1}{2}m\sqrt{m}\sum_{i,j=1}^{n-1}\left|\frac{\partial^{2}V_{n}}{\partial\eta_{i}\partial\eta_{j}}\right|\left|\overline{g}_{i}\left(\widetilde{\eta}_{i+1},\widetilde{\eta}_{i+1}\left(t-d\left(t\right)\right)\right)\right|$$

$$\times\left|\overline{g}_{j}\left(\widetilde{\eta}_{j+1},\widetilde{\eta}_{j+1}\left(t-d\left(t\right)\right)\right)\right|$$

$$\leq \widetilde{c}_{03}\kappa^{2}\sum_{i,j=1}^{n-1}\left\|\eta\right\|_{\Delta}^{2}\left(\left\|\eta\right\|_{\Delta}+\left\|\eta\left(t-d\left(t\right)\right)\right\|_{\Delta}\right)^{2}$$

$$\leq \kappa^{2}\left(c_{03}\left\|\eta\right\|_{\Delta}^{4}+\overline{c}_{03}\left\|\eta\left(t-d\left(t\right)\right)\right\|_{\Delta}^{4}\right),$$
(26)

where c_{03} , \bar{c}_{03} , and \tilde{c}_{03} are positive constants. With the help of (3), (15), (17), (22), (24), (26), and Assumption 9, one has

$$\mathcal{L}V \leq \frac{\partial V_{n}}{\partial \eta} \kappa E(\eta) + \frac{\partial V_{n}}{\partial \eta} F(\eta, \eta(t - d(t)))
+ \frac{1}{2} \operatorname{Tr} \left\{ G(\eta, \eta(t - d(t))) \frac{\partial^{2} V_{n}}{\partial \eta^{2}} G^{T}(\eta, \eta(t - d(t))) \right\}
+ (\bar{c}_{02} + \bar{c}_{03}) \kappa^{2} \left(\frac{1}{1 - \gamma} \| \eta \|_{\Delta}^{4} - \| \eta(t - d(t)) \|_{\Delta}^{4} \right)
\leq -c_{01} \kappa \| \eta \|_{\Delta}^{4} + \left(c_{02} + c_{03} + \frac{\bar{c}_{02} + \bar{c}_{03}}{1 - \gamma} \right) \kappa^{2} \| \eta \|_{\Delta}^{4}
= -\kappa \left(c_{01} - \left(c_{02} + c_{03} + \frac{\bar{c}_{02} + \bar{c}_{03}}{1 - \gamma} \right) \kappa \right) \| \eta \|_{\Delta}^{4}.$$
(27)

Since c_{01} is a constant independent of c_{02} , c_{03} , \overline{c}_{02} , \overline{c}_{03} , and γ , by choosing

$$0 < \kappa < \kappa^* =: \min \left\{ 1, \frac{c_{01}}{c_{02} + c_{03} + \left(\left(\overline{c}_{02} + \overline{c}_{03} \right) / \left(1 - \gamma \right) \right)} \right\}. \tag{28}$$

Equation (27) becomes $\mathscr{L}V \leq -c_0 \|\eta\|_{\Delta}^4$, where c_0 is a positive constant. By (19), one obtains

$$\mathcal{L}V \le -\frac{c_0}{\overline{c}}\underline{\alpha}_{22}(|\eta|). \tag{29}$$

By Steps 1–3 and Lemma 4, the system consisting of (13) and (15) has a unique solution on $[-d, \infty)$, $\eta = 0$ is GAS in probability, and $P\{\lim_{t\to\infty} |\eta| = 0\} = 1$.

Step 4. Since (6) is an equivalent transformation, so the closed-loop system consisting of (1), $u = \kappa^n v$, and (13) has the same properties as the system (13) and (15). Theorem 12 holds.

Remark 13. In this paper, the homogeneous domination idea is generalized to stochastic feedforward nonlinear time-delay systems (1). The underlying philosophy of this approach is that the state-feedback controller is first constructed for system (7) without considering the drift and diffusion terms, and then a low gain κ in (6) (whose the value range is (28)) is introduced to state-feedback controller to dominate the drift and diffusion terms.

Remark 14. Due to the special upper-triangular structure and the appearance of time-varying delay, there is no efficient method to solve the stabilization problem of system (1). By combining the homogeneous domination approach with stochastic nonlinear time-delay system criterion, the state-feedback stabilization of system (1) was perfectly solved in this paper.

Remark 15. One of the main obstacles in the stability analysis is how to deal with the effect of time-varying delay. In this paper, by constructing an appropriate Lyapunov-Krasovskii functional (17), this problem was effectively solved.

Remark 16. It is worth pointing out that the rigorous proof of Theorem 12 is not an easy job.

5. A Simulation Example

Consider the following stochastic nonlinear system:

$$dx_{1} = x_{2}dt + \frac{1}{10} (x_{2} + x_{2} (t - d(t)) \cos x_{2}) d\omega,$$

$$dx_{2} = udt,$$
(30)

where $d(t) = 1 + (1/2) \sin t$. It is easy to verify that Assumptions 8 and 9 are satisfied with $a_1 = 0$, $a_2 = 1/10$, and $\dot{d}(t) = (1/2) \cos t < 1$.

Design of Controller. Introducing the following coordinate transformation:

$$\eta_1 = x_1, \qquad \eta_2 = \frac{x_2}{\kappa}, \qquad \nu = \frac{u}{\kappa^2},$$
(31)

system (30) becomes

$$d\eta_1 = \kappa \eta_2 dt + \overline{g}_1 d\omega,$$

$$d\eta_2 = \kappa v dt,$$
(32)

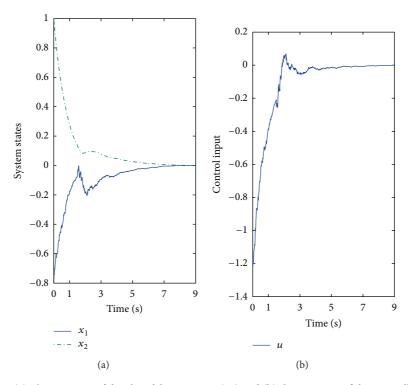


FIGURE 1: (a) The response of the closed-loop system (30) and (b) the response of the controller (37).

where $\overline{g}_1 = (1/10)(\kappa \eta_2 + \kappa \eta_2 (t - d(t)) \cos \kappa \eta_2)$. Choosing $\xi_1 = \eta_1$ and $V_1(\eta_1) = (1/4)\xi_1^4$, we obtain $\mathcal{L}V_1 \leq -2\kappa \xi_1^4 + \kappa \xi_1^3 (\eta_2 - \eta_2^*) + (1/2)(\partial^2 V_1/\partial \eta_1^2)\overline{g}_1^2$, where $\eta_2^* = -2\eta_1 =: -\alpha_1 \xi_1$. By $\xi_2 = \eta_2 - \eta_2^*$ and $V_2(\overline{\eta}_2) = V_1(\eta_1) + (1/4)\xi_2^4$, a direct calculation leads to

$$\mathcal{L}V_{2} \leq -2\kappa\xi_{1}^{4} + \kappa\xi_{1}^{3}\xi_{2} + \kappa\xi_{2}^{3}\nu + \kappa\alpha_{1}\xi_{2}^{3}\eta_{2} + \frac{1}{2}\frac{\partial^{2}V_{2}}{\partial\eta_{1}^{2}}\overline{g}_{1}^{2}.$$
 (33)

By Lemma 7, one has

$$\xi_1^3 \xi_2 \le 0.5 \xi_1^4 + 0.8438 \xi_2^4,$$

$$\alpha_1 \xi_2^3 \eta_2 \le 0.5 \xi_1^4 + 5.7797 \xi_2^4.$$
(34)

Choosing

$$v = -7.6235\xi_2 =: -\alpha_2 \xi_2 \tag{35}$$

and substituting (34) into (33), one gets

$$\mathcal{L}V_2 \le -\kappa \left(\xi_1^4 + \xi_2^4\right) + \frac{1}{2} \frac{\partial^2 V_2}{\partial \eta_1^2} \overline{g}_1^2. \tag{36}$$

By (31) and (35), one obtains the actual controller

$$u = -\alpha_2 \left(\kappa x_2 + \alpha_1 \kappa^2 x_1 \right). \tag{37}$$

The Choice of κ^* . Defining $\|\eta\|_{\Delta} = (\eta_1^2 + \eta_2^2)^{1/2}$ and choosing

$$V(\eta) = V_2(\eta) + \kappa^2 \int_{t-d(t)}^t \|\eta(\sigma)\|_{\Delta}^4 d\sigma, \tag{38}$$

by (3), (36), and $d(t) = 1 + (1/2) \sin t$, one obtains

$$\mathcal{L}V \le -\kappa \|\eta\|_{\Delta}^{4} + \kappa^{2} \left(1.5 \|\eta\|_{\Delta}^{4} + 0.5 \|\eta(t - d(t))\|_{\Delta}^{4}\right)$$

$$+ \kappa^{2} \left(\|\eta\|_{\Delta}^{4} - 0.5 \|\eta(t - d(t))\|_{\Delta}^{4}\right)$$

$$= -\kappa \left(1 - 2.5\kappa\right) \|\eta\|_{\Delta}^{4},$$
(39)

from which we get the critical value $\kappa^* = 0.4$; that is, $\kappa \in (0, 0.4)$.

In simulation, we choose the initial values $x_1(0) = -0.8$, $x_2(0) = 1$, and $\kappa = 0.3$. Figure 1 demonstrates the effectiveness of the state-feedback controller.

6. A Concluding Remark

By using the homogeneous domination approach, this paper further studied the state-feedback stabilization problem for a class of stochastic feedforward nonlinear time-delay systems (1). The delay-independent state-feedback controller is explicitly constructed such that the closed-loop system is globally asymptotically stable in probability.

There still exist some problems to be investigated. One is to consider the output-feedback control of switched stochastic system (1) by using average dwell time method in [32]. Another is to find a practical example (similar to [33–35]) for system (1). The last is to generalize the networked control systems (such as [36–41]) to stochastic feedforward networked systems.

Appendix

Proof of Lemma 11. According to (3), (7), (10), and (11), one has

$$\begin{split} \mathscr{L}V_{i} &\leq -\kappa \sum_{j=1}^{i-1} c_{i-1,j} \xi_{j}^{4} + \kappa \xi_{i-1}^{3} \xi_{i} + \sum_{j=1}^{i-1} \frac{\partial V_{i-1}}{\partial \eta_{j}} \overline{f}_{j} \\ &+ \frac{1}{2} \sum_{p,q=1}^{i-1} \operatorname{Tr} \left\{ \overline{g}_{p} \frac{\partial^{2} V_{i-1}}{\partial \eta_{p} \partial \eta_{q}} \overline{g}_{q}^{T} \right\} \\ &+ \sum_{k=1}^{i} \frac{\partial W_{i}}{\partial \eta_{k}} \left(\kappa \eta_{k+1} + \overline{f}_{k} \right) + \frac{1}{2} \operatorname{Tr} \left\{ \overline{g}_{i} \frac{\partial^{2} W_{i}}{\partial \eta_{i}^{2}} \overline{g}_{i}^{T} \right\} \\ &+ \sum_{j=1}^{i-1} \operatorname{Tr} \left\{ \overline{g}_{i} \frac{\partial^{2} W_{i}}{\partial \eta_{i} \partial \eta_{j}} \overline{g}_{j}^{T} \right\} + \frac{1}{2} \sum_{p,q=1}^{i-1} \operatorname{Tr} \left\{ \overline{g}_{p} \frac{\partial^{2} W_{i}}{\partial \eta_{p} \partial \eta_{q}} \overline{g}_{q}^{T} \right\} \\ &= -\kappa \sum_{j=1}^{i-1} c_{i-1,j} \xi_{j}^{4} + \kappa \xi_{i-1}^{3} \xi_{i} + \frac{\partial W_{i}}{\partial \eta_{k}} \kappa \eta_{i+1} \\ &+ \left(\sum_{j=1}^{i-1} \frac{\partial V_{i-1}}{\partial \eta_{j}} \overline{f}_{j} + \sum_{k=1}^{i} \frac{\partial W_{i}}{\partial \eta_{p}} \overline{f}_{k} \right) + \sum_{k=1}^{i-1} \frac{\partial W_{i}}{\partial \eta_{k}} \kappa \eta_{k+1} \\ &+ \left(\frac{1}{2} \sum_{p,q=1}^{i-1} \operatorname{Tr} \left\{ \overline{g}_{p} \frac{\partial^{2} V_{i-1}}{\partial \eta_{p} \partial \eta_{q}} \overline{g}_{q}^{T} \right\} + \frac{1}{2} \operatorname{Tr} \left\{ \overline{g}_{i} \frac{\partial^{2} V_{i}}{\partial \eta_{i}^{2}} \overline{g}_{i}^{T} \right\} \\ &+ \sum_{j=1}^{i-1} \operatorname{Tr} \left\{ \overline{g}_{i} \frac{\partial^{2} V_{i}}{\partial \eta_{p} \partial \eta_{q}} \overline{g}_{q}^{T} \right\} \right) \\ &= -\kappa \sum_{j=1}^{i-1} c_{i-1,j} \xi_{j}^{4} + \kappa \xi_{i}^{3} \eta_{i+1} + \sum_{j=1}^{i} \frac{\partial V_{i}}{\partial \eta_{p}} \overline{f}_{j} \\ &+ \frac{1}{2} \sum_{p,q=1}^{i} \operatorname{Tr} \left\{ \overline{g}_{p} \frac{\partial^{2} V_{i}}{\partial \eta_{p} \partial \eta_{q}} \overline{g}_{q}^{T} \right\} \\ &+ \kappa \xi_{i-1}^{3} \xi_{i} - \kappa \xi_{i}^{3} \sum_{k=1}^{i-1} \frac{\partial \eta_{i}^{*}}{\partial \eta_{k}} \eta_{k+1}. \end{aligned} \tag{A.1}$$

We concentrate on the last two terms on the right-hand side of (A.1).

Using (10) and Lemma 7, one obtains

$$\xi_{i-1}^{3} \xi_{i} \leq l_{i,i-1,1} \xi_{i-1}^{4} + \rho_{i1} \xi_{i}^{4},$$

$$- \xi_{i}^{3} \sum_{k=1}^{i-1} \frac{\partial \eta_{i}^{*}}{\partial \eta_{k}} \eta_{k+1}$$

$$\leq \left| \xi_{i} \right|^{3} \left| \sum_{k=1}^{i-1} \alpha_{i-1} \cdots \alpha_{k} \left(\xi_{k+1} - \alpha_{k} \xi_{k} \right) \right|$$

$$\leq \left| \xi_{i} \right|^{3} \left(\sum_{k=1}^{i-1} \left(\alpha_{i-1} \cdots \alpha_{k-1} + \alpha_{i-1} \cdots \alpha_{k+1} \alpha_{k}^{2} \right) \left| \xi_{k} \right| + \alpha_{i-1} \left| \xi_{i} \right| \right)$$

$$\leq \sum_{k=1}^{i-1} l_{ik2} \xi_{k}^{4} + \rho_{i2} \xi_{i}^{4},$$
(A.2)

where $l_{i,i-1,1}$, $l_{ik2}(k=1,\ldots,i-1)$, ρ_{i1} , and ρ_{i2} are positive constants, $\alpha_0=0$.

Choosing

$$c_{ij} = \begin{cases} c_{i-1,j} - l_{ij2} > 0, & j = 1, \dots, i - 2, \\ c_{i-1,i-1} - l_{i,i-1,1} - l_{i,i-1,2} > 0, & j = i - 1, \end{cases}$$

$$\eta_{i+1}^* = -\left(c_{ij} + \rho_{i1} + \rho_{i2}\right) \xi_i =: -\alpha_i \xi_i, \quad c_{ii} > 0,$$
(A.3)

and substituting (A.2)-(A.3) into (A.1), one gets the desired result.

Conflict of Interests

The authors declare that there is no conflict of interests.

Acknowledgments

The authors would like to express sincere gratitude to editor and reviewers for their helpful suggestions in improving the quality of this paper. This work was partially supported by the National Natural Science Foundation of China (nos. 61304002, 61304003, 61203123, and 61304054), the Fundamental Research Funds for the Central Universities of China (no. 11CX04044A), the Shandong Provincial Natural Science Foundation of China (no. ZR2012FQ019), and the Polish-Norwegian Research Programme operated by the National Center for Research and 24 Development under the Norwegian Financial Mechanism 2009–2014 in the frame of Project Contract (no. Pol-Nor/200957/47/2013).

References

- [1] N. Duan and X.-J. Xie, "Further results on output-feedback stabilization for a class of stochastic nonlinear systems," *IEEE Transactions on Automatic Control*, vol. 56, no. 5, pp. 1208–1213, 2011
- [2] M. Krstić and H. Deng, Stabilization of Uncertain Nonlinear Systems, Springer, New York, NY, USA, 1998.
- [3] S. Kuang, Y. Peng, F. Deng, and W. Gao, "Exponential stability and numerical methods of stochastic recurrent neural networks with delays," *Abstract and Applied Analysis*, vol. 2013, Article ID 761237, 11 pages, 2013.
- [4] W.-Q. Li and X.-J. Xie, "Inverse optimal stabilization for stochastic nonlinear systems whose linearizations are not stabilizable," *Automatica*, vol. 45, no. 2, pp. 498–503, 2009.
- [5] L. Liu and X.-J. Xie, "Output-feedback stabilization for stochastic high-order nonlinear systems with time-varying delay," Automatica, vol. 47, no. 12, pp. 2772–2779, 2011.

- [6] S.-J. Liu, S. S. Ge, and J.-F. Zhang, "Adaptive output-feedback control for a class of uncertain stochastic non-linear systems with time delays," *International Journal of Control*, vol. 81, no. 8, pp. 1210–1220, 2008.
- [7] S.-J. Liu, J.-F. Zhang, and Z.-P. Jiang, "Decentralized adaptive output-feedback stabilization for large-scale stochastic nonlinear systems," *Automatica*, vol. 43, no. 2, pp. 238–251, 2007.
- [8] Y.-G. Liu and J.-F. Zhang, "Practical output-feedback risk-sensitive control for stochastic nonlinear systems with stable zero-dynamics," SIAM Journal on Control and Optimization, vol. 45, no. 3, pp. 885–926, 2006.
- [9] L. Wu, P. Shi, and H. Gao, "State estimation and sliding-mode control of Markovian jump singular systems," *IEEE Transactions on Automatic Control*, vol. 55, no. 5, pp. 1213–1219, 2010.
- [10] Z.-J. Wu, X.-J. Xie, and S.-Y. Zhang, "Adaptive backstepping controller design using stochastic small-gain theorem," *Automatica*, vol. 43, no. 4, pp. 608–620, 2007.
- [11] Z.-J. Wu, X.-J. Xie, P. Shi, and Y.-Q. Xia, "Backstepping controller design for a class of stochastic nonlinear systems with Markovian switching," *Automatica*, vol. 45, no. 4, pp. 997–1004, 2009.
- [12] X.-J. Xie and N. Duan, "Output tracking of high-order stochastic nonlinear systems with application to benchmark mechanical system," *IEEE Transactions on Automatic Control*, vol. 55, no. 5, pp. 1197–1202, 2010.
- [13] X.-J. Xie and L. Liu, "Further results on output feedback stabilization for stochastic high-order nonlinear systems with time-varying delay," *Automatica*, vol. 48, no. 10, pp. 2577–2586, 2012.
- [14] X.-J. Xie and L. Liu, "A homogeneous domination approach to state feedback of stochastic high-order nonlinear systems with time-varying delay," *IEEE Transactions on Automatic Control*, vol. 58, no. 2, pp. 494–499, 2013.
- [15] X.-J. Xie and J. Tian, "Adaptive state-feedback stabilization of high-order stochastic systems with nonlinear parameterization," *Automatica*, vol. 45, no. 1, pp. 126–133, 2009.
- [16] S. Yin, S. X. Ding, A. H. A. Sari, and H. Hao, "Data-driven monitoring for stochastic systems and its application on batch process," *International Journal of Systems Science*, vol. 44, no. 7, pp. 1366–1376, 2013.
- [17] X. Yu and X.-J. Xie, "Output feedback regulation of stochastic nonlinear systems with stochastic iISS inverse dynamics," *IEEE Transactions on Automatic Control*, vol. 55, no. 2, pp. 304–320, 2010.
- [18] X. Zhao, M. Ling, and Q. Zeng, "Delay-dependent robust control for uncertain stochastic systems with Markovian switching and multiple delays," *Journal of Systems Engineering and Electronics*, vol. 21, no. 2, pp. 287–295, 2010.
- [19] X. Zhou, Y. Ren, and S. Zhong, "BIBO stabilization of discretetime stochastic control systems with mixed delays and nonlinear perturbations," *Abstract and Applied Analysis*, vol. 2013, Article ID 916357, 11 pages, 2013.
- [20] F. Mazenc and S. Bowong, "Tracking trajectories of the cartpendulum system," *Automatica*, vol. 39, no. 4, pp. 677–684, 2003
- [21] R. Sepulchre, M. Janković, and P. V. Kokotović, Constructive Nonlinear Control, Springer, London, UK, 1997.
- [22] N. Bekiaris-Liberis and M. Krstić, "Delay-adaptive feedback for linear feedforward systems," *Systems & Control Letters*, vol. 59, no. 5, pp. 277–283, 2010.

- [23] S. Ding, C. Qian, S. Li, and Q. Li, "Global stabilization of a class of upper-triangular systems with unbounded or uncontrollable linearizations," *International Journal of Robust and Nonlinear Control*, vol. 21, no. 3, pp. 271–294, 2011.
- [24] A. Isidori, Nonlinear Control Systems, Springer, London, UK, 1999
- [25] M. Krstić, "Input delay compensation for forward complete and strict-feedforward nonlinear systems," *IEEE Transactions* on Automatic Control, vol. 55, no. 2, pp. 287–302, 2010.
- [26] C. Qian and J. Li, "Global output feedback stabilization of upper-triangular nonlinear systems using a homogeneous domination approach," *International Journal of Robust and Nonlin*ear Control, vol. 16, no. 9, pp. 441–463, 2006.
- [27] X. Ye, "Adaptive stabilization of time-delay feedforward nonlinear systems," *Automatica*, vol. 47, no. 5, pp. 950–955, 2011.
- [28] X. Zhang, L. Baron, Q. Liu, and E.-K. Boukas, "Design of stabilizing controllers with a dynamic gain for feedforward nonlinear time-delay systems," *IEEE Transactions on Automatic Control*, vol. 56, no. 3, pp. 692–697, 2011.
- [29] X. Zhang, Q. Liu, L. Baron, and E.-K. Boukas, "Feedback stabilization for high order feedforward nonlinear time-delay systems," *Automatica*, vol. 47, no. 5, pp. 962–967, 2011.
- [30] L. Liu and X.-J. Xie, "State feedback stabilization for stochastic feedforward nonlinear systems with time-varying delay," *Automatica*, vol. 49, no. 4, pp. 936–942, 2013.
- [31] H. K. Khalil, Nonlinear Systems, Prentice-Hall, Upper Saddle River, NJ, USA, 3rd edition, 2002.
- [32] L. Zhang and H. Gao, "Asynchronously switched control of switched linear systems with average dwell time," *Automatica*, vol. 46, no. 5, pp. 953–958, 2010.
- [33] H. L. Dong, Z. D. Wang, and H. J. Gao, "Distributed H_{∞} filtering for a class of markovian jump nonlinear time-delay systems over lossy sensor networks," *IEEE Transactions on Industrial Electronics*, vol. 60, no. 10, pp. 4665–4672, 2013.
- [34] X. C. Xie, S. Yin, H. J. Gao, and O. Kaynak, "Asymptotic stability and stabilisation of uncertain delta operator systems with time-varying delays," *IET Control Theory and Applications*, vol. 7, no. 8, pp. 1071–1078, 2013.
- [35] S. Yin, S. X. Ding, and H. Luo, "Real-time implementation of fault tolerant control system with performance optimization," *IEEE Transactions on Industrial Electronics*, vol. 61, no. 5, pp. 2402–2411, 2014.
- [36] H. Gao and T. Chen, " H_{∞} estimation for uncertain systems with limited communication capacity," *IEEE Transactions on Automatic Control*, vol. 52, no. 11, pp. 2070–2084, 2007.
- [37] H. Gao, T. Chen, and J. Lam, "A new delay system approach to network-based control," *Automatica*, vol. 44, no. 1, pp. 39–52, 2008.
- [38] H. Gao and T. Chen, "Network-based H_{∞} output tracking control," *IEEE Transactions on Automatic Control*, vol. 53, no. 3, pp. 655–667, 2008.
- [39] H. Gao, X. Meng, and T. Chen, "Stabilization of networked control systems with a new delay characterization," *IEEE Transactions on Automatic Control*, vol. 53, no. 9, pp. 2142–2148, 2008.
- [40] H. Li, H. Gao, and P. Shi, "New passivity analysis for neural networks with discrete and distributed delays," *IEEE Transactions on Neural Networks*, vol. 21, no. 11, pp. 1842–1847, 2010.
- [41] J. Qiu, G. Feng, and H. Gao, "Fuzzy-model-based piecewise H_{∞} static-output-feedback controller design for networked nonlinear systems," *IEEE Transactions on Fuzzy Systems*, vol. 18, no. 5, pp. 919–934, 2010.

Hindawi Publishing Corporation Abstract and Applied Analysis Volume 2013, Article ID 846389, 8 pages http://dx.doi.org/10.1155/2013/846389

Research Article

Nonlinear Model Predictive Control with Terminal Invariant Manifolds for Stabilization of Underactuated Surface Vessel

Lutao Liu, ¹ Zhilin Liu, ² and Jun Zhang³

- ¹ College of Information and Telecommunication, Harbin Engineering University, Harbin 150001, China
- ² College of Automation, Harbin Engineering University, Harbin 150001, China

Correspondence should be addressed to Zhilin Liu; liuzhilin@hrbeu.edu.cn

Received 21 September 2013; Accepted 14 October 2013

Academic Editor: Xiaojie Su

Copyright © 2013 Lutao Liu et al. This is an open access article distributed under the Creative Commons Attribution License, which permits unrestricted use, distribution, and reproduction in any medium, provided the original work is properly cited.

A nonlinear model predictive control (MPC) is proposed for underactuated surface vessel (USV) with constrained invariant manifolds. Aimed at the special structure of USV, the invariant manifold under the given controller is constructed in terms of diffeomorphism and Lyapunov stability theory. Based on MPC, the states of the USV are steered into the constrained terminal invariant manifolds. After the terminal manifolds set is reached, a linear feedback control is used to stabilize the system. The simulation results verified the effectiveness of the proposed method. It is shown that, based on invariant manifolds constraints, it is easy to get the MPC for the USV and it is suitable for practical application.

1. Introduction

The waterjet propulsor is widely used to thrust existing planning surface vessels. The conventional method to control planning surface vessels is indirectly achieved through the course control which is actuated by a steerable nozzle. If the planar position and course are controlled directly, we need to regulate the angle and the thrust force of the steering nozzle to control the movements in three degrees of freedom synchronously. Obviously, the control system of planning surface vessels is typical underactuated system. In order to ensure the safety of the planning surface vessel, many constraints such as the angle of the steering nozzle and radius of gyration must be in consideration in the design process of ship motion controller; otherwise it will undermine the performance of the planning surface vessels and even lead to collapse of the hull and other serious consequences. The underactuated system with constraints is essentially nonlinear system and cannot be stabilized by any smooth time-invariant control laws. Predictive control is an effective optimization control method to deal with constrains [1-6].

In general, the use of MPC in an underactuated structure system necessitates a means of switching among the available

models to the one that best describes the current operating condition. A closely related work is the stability analysis of switched stochastic systems by [7] in which dissipativity-based sliding mode control was constructed. Since designing MPC controllers that stabilize underactuated system may not result in a stable global closed-loop system, closed-loop stability in switch model/control approaches has also been studied [8]. The study in the paper is aimed to analyse the underactuated characteristics of planning surface vessels and guarantee safe movements of the vessels. Furthermore, based on predictive control approach, the problem of the stabilization and tracking control is solved under the condition of reserved safety constraints.

Control of underactuated systems has been one of the active research topics due to its intrinsic nonlinear nature and practical applications. As a typical example of underactuated systems, control of an underactuated ship has been focused on recently. The main difficulty in the control of underactuated ships is that they are not actuated in the sway axis. This configuration is the most common among the surface ships [9]. Furthermore, unlike underactuated systems with nonintegrable constraints, the surface vessels under the consideration are a class of underactuated systems

³ School of Electrical and Information Engineering, Jiangsu University, Zhenjiang, Jiangsu 212013, China

with nonintegrable dynamics and are not transformed into a driftless system [10]. Nevertheless, several authors have studied the trajectory tracking control problem. A discontinuous control approach with two stage control laws switched on at given time is proposed based on the stability analysis of the global transformed system in [11]. In [12], the authors proposed a kinematic tracking controller that achieved global exponential practical stability of an underactuated surface vessel. In [13], a continuous time-invariant control law was proposed to obtain semiglobal exponential position and orientation tracking, provided the desired angular trajectory remains positive. Based on the cascaded approach, a global tracking result was obtained in [14, 15]. The stability analysis relied on the stability theory of linear time-varying systems. An application of the recursive technique proposed in [16] for the standard chain form systems was used in [17] to provide exponential stability of the reference trajectory. Based on Lyapunov's direct method and passivity approach, two constructive tracking solutions were proposed in [18] for an underactuated ship. The constructive control design procedure exploited the inherent cascade-interconnected structure of the ship dynamics and actually generated an explicit Lyapunov function whose availability might suit the requirements of robust and adaptive control design. With the help of the backstepping design methodology, a nonlinear time-invariant control law was proposed in [19] for an underactuated surface vessel. But the control design in [19] was not complete and lacked a further step in the backstepping procedure. In the comment letter [20], the control laws in [19] were revised and the states decayed asymptotically to zero.

Model predictive control (MPC) is a popular technique for the control of slow dynamical system subject to input and state constraints. At any time instant, MPC requires the online solution of an optimization problem to compute optimal control inputs over a fixed number of future time instants, known as the finite horizon or quasi-infinite horizon. Using MPC, it is possible to handle inequality constraints on the manipulated and controlled variables in a systematic manner during the design and implementation of the controller. Perhaps the principal shortcoming of existing MPC-base control techniques is their inability to explicitly incorporate plant model uncertainty. The fact that the rudder actuation is limited in amplitude and rate makes MPC approach a natural choice for the design of the path following controller. In [21], a standard model predictive control approach for path following with roll constraints of marine surface vessels in calm water using the rudder as the control input has been proposed. The focus is on satisfying all the input (rudder) and state (roll) constraints while achieving satisfactory path following performance. For notational convenience the ship dynamics in [21] are written into linearized matrix form based on the assumption that surge velocity is constant and the yaw moment is proportional to the rudder angle. However, the former assumption is hardly admissible in engineering. In [22], an analytic model predictive controller is presented for path following of an underactuated ship maneuvering along a predefined path. The mathematical model of ship motion is described by using

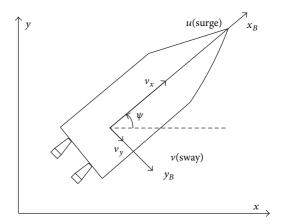


FIGURE 1: Underactuated surface vessel.

Serret-Frenet frame, and a systematic method is provided to guarantee the stability of the closed-loop system in terms of transforming the original single-input multiple-output (SIMO) into an equivalent single-input single-output (SISO) system. However, the MPC algorithm proposed in [22] is designed as an analytic model predictive controller which is affected by the accuracy of the parameters.

This paper illuminates the stabilization approach for underactuated surface vessels with only a surge force and a yaw moment. A nonlinear model predictive controller is presented for steering the states of underactuated ship into a desired terminal invariant manifolds. After the terminal manifolds set is reached, a linear feedback control is used to stabilize the system. However, in the techniques mentioned above, plant modeling is the critical step to obtain feedback controller and the control result is strongly influenced by the model; the problems inherent to plant modeling are inevitable. Moreover, even complex models cannot cover all the system dynamics [23–26]. In the future work, we will make efforts to design data-driven MPC controllers to overcome these problems.

2. Problem Formulation

In this paper, we consider the trajectory tracking control problem of a surface vessel shown in Figure 1. There is no side thruster, but two independent main thrusters are located at a distance from the center line in order to provide both surge force and yaw moment.

The dynamics and kinematics of an underactuated surface vessel are described as follows [27]:

$$M\dot{\nu} + C(\nu)\nu + D\nu = \tau, \tag{1}$$

$$\dot{\eta} = J(\eta) \, \nu. \tag{2}$$

The inertia matrix $M = \operatorname{diag}\{m_{11}, m_{22}, m_{33}\}$ and the damping matrix $D = \operatorname{diag}\{d_{11}, d_{22}, d_{33}\}$ are constant and positive definite. The vector $\tau = [\tau_1, \tau_2, \tau_3]$ denotes the control forces in surge and sway and control torque in yaw. In this paper, the surface vessel is assumed as the common thruster configuration that has no side thruster, such as $\tau_2 = 0$. So

the second component of (1) behaves as a nonholonomic constraint, which is a nonintegrable relation involving not only the generalized coordinates and velocities but also the generalized accelerations [28]. $C(\nu)$ is the matrix of Coriolis and centripetal terms also including added mass. $J(\eta)$ is the rotation matrix for the transformation between body-fixed and earth-fixed coordinates:

$$C(\nu) = \begin{bmatrix} 0 & 0 & -m_{22}\nu \\ 0 & 0 & m_{11}u \\ m_{22}\nu & -m_{11}u & 0 \end{bmatrix},$$

$$J(\eta) = \begin{bmatrix} \cos(\psi) & -\sin(\psi) & 0 \\ \sin(\psi) & \cos(\psi) & 0 \\ 0 & 0 & 1 \end{bmatrix}.$$
(3)

The vector $\eta = [x, y, \psi]^T$ denotes the North and East positions and orientation of the underactuated surface vessel in the earth-fixed coordinate system. The vector $v = [u, v, r]^T$ denotes the linear velocities in surge and sway and the angular velocity in yaw.

As a general accepted conclusion [29, 30], there is no continuous time-invariant feedback control law that makes the zero origin an asymptotically stable equilibrium of the system (1) and (2), for the system does not satisfy Brocketts condition [31]. Then time-varying and discontinuous control approaches are only taken into account in this paper.

Neglecting the motions in heave, roll, and pitch, the simplified kinematic model which describes the geometrical relationship between the earth-fixed (E-frame) and the body-fixed (B-frame) motion is given as

$$m_{11}\dot{u} - m_{22}vr + d_{11}u = \tau_1,$$

$$m_{22}\dot{v} + m_{11}ur + d_{22}v = 0,$$

$$m_{33}\dot{r} + (m_{22} - m_{11})uv + d_{33}r = \tau_3,$$

$$\dot{x} = u\cos\psi - v\sin\psi,$$

$$\dot{y} = u\sin\psi + v\cos\psi,$$

$$\dot{\psi} = r.$$
(4)

The following global coordinate transformation and feedback transformation are adopted before control design. Define

$$z_{1} = x \cos(\psi) + y \sin(\psi),$$

$$z_{2} = v,$$

$$z_{3} = -x \sin(\psi) + y \cos(\psi) + \frac{m_{22}}{d_{22}v},$$

$$z_{4} = \psi,$$

$$z_{5} = -\frac{m_{11}}{d_{22}u} - z_{1},$$

$$z_{6} = r.$$
(5)

It is proved that the state transformation (5) is a global diffeomorphism [32]. The feedback transformation is

$$w_{1} = \left(\frac{d_{11}}{d_{22}} - 1\right)u - z_{3}z_{6} - \frac{\tau_{1}}{d_{22}},$$

$$w_{2} = \frac{\left(m_{11} - m_{22}\right)uv}{m_{33}} - \frac{d_{33}r}{m_{33}} + \frac{\tau_{3}}{m_{33}}.$$
(6)

With the state and feedback transformation (5)-(6), the system (1)-(2) is eventually transformed to

$$\dot{z}_{1} = -\frac{d_{22}}{m_{11}} z_{1} - \frac{d_{22}}{m_{11}} z_{5} + z_{3} z_{6} - \frac{m_{22}}{d_{22}} z_{2} z_{6},
\dot{z}_{2} = -\frac{d_{22}}{m_{22}} z_{2} + \frac{d_{22}}{m_{22}} z_{6} (z_{1} + z_{5}),
\dot{z}_{3} = z_{5} z_{6}, \qquad \dot{z}_{4} = z_{6},
\dot{z}_{5} = w_{1}, \qquad \dot{z}_{6} = w_{2}.$$
(7)

The system (7) has the same diffeomorphism properties as the system (1) and (2) [32]; that is, if $\lim_{t\to\infty} z_i = 0$ ($1 \le i \le 6$) then (x, y, ψ, u, v, r) converges to zero as $t \to \infty$.

Lemma 1. If there exists a control law which globally uniformly asymptotically stabilizes the system

$$\dot{z}_3 = z_5 z_6, \qquad \dot{z}_4 = z_6,
\dot{z}_5 = w_1, \qquad \dot{z}_6 = w_2,$$
(8)

then the system (7) under the control law is also globally uniformly asymptotically stabilized.

Proof. An approach to prove Lemma 1 based on Lyapunov stability theorem has been given in [28]. Therefore, to stabilize the system (1) and (2), it is only needed to design a stabilizing control law for the system (8). In the following section, a discontinuous and time-varying control approach with MPC control method is proposed for the stabilization of the system (8). □

3. Control Design

Let us recall the following definitions firstly.

Definition 2. Let $\Phi: \mathbb{R}^n \to \mathbb{R}^p$ be a smooth map. A manifold $M = \{x \in \mathbb{R}^n : \Phi(x) = 0\}$ is said to be invariant for the control system $\dot{x} = f(x,u)$ if all system trajectories starting in M at $t = t_0$ remain in this manifold for all $t \ge t_0$. In other words, the Lie derivative of Φ along the vector field f is zero $(L_f\Phi(x) = 0)$ for all $x \in M$.

Definition 3. A manifold $M = \{x \in R^n : \Phi(x) = 0\}$ is said to be asymptotically attractive in an open domain Ω of R^n if, for all $t \in R_+$ such that $x(t_0) \in \Omega$, $\lim_{x \to \infty} x(t) \in M$.

3.1. Construction of the Invariant Manifold. First, in order to construct the invariant manifold of the system (8), assume that $\begin{bmatrix} w_1 & w_2 \end{bmatrix}^T$ is a linear state feedback such that

$$w_1 = -k_1 z_5 \quad (k_1 > 0),$$

$$w_2 = -k_2 z_6 - k_3 z_5 \quad (k_2 > 0, k_3 > 0, k_1 \neq k_2).$$
(9)

Substitute (9) into (8); we obtain

$$\dot{z}_3 = z_5 z_6, \qquad \dot{z}_4 = z_6,
\dot{z}_5 = -k_1 z_5, \qquad \dot{z}_6 = -k_2 z_6 - k_3 z_5.$$
(10)

The resulting closed-loop system (10) can be successively integrated to obtain

$$z_{5}(t) = z_{50}e^{-k_{1}t},$$

$$z_{6}(t) = z_{60}e^{-k_{2}t} + \frac{k_{3}z_{50}}{k_{1} - k_{2}} \left(e^{-k_{1}t} - e^{-k_{2}t}\right),$$

$$z_{4}(t) = s_{4}(z_{0}) + \left[\frac{k_{3}z_{50}}{k_{2}(k_{1} - k_{2})} - \frac{z_{60}}{k_{2}}\right]e^{-k_{2}t}$$

$$- \frac{k_{3}z_{50}}{k_{1}(k_{1} - k_{2})}e^{-k_{1}t},$$

$$z_{3}(t) = s_{3}(z_{0}) - \frac{1}{k_{1} + k_{2}}\left(z_{40}z_{60} - \frac{k_{3}z_{50}^{2}}{k_{1} - k_{2}}\right)e^{-(k_{1} + k_{2})t}$$

$$- \frac{k_{3}z_{50}^{2}}{2k_{1}(k_{1} - k_{2})}e^{-2k_{1}t},$$
(11)

where k_1 , k_2 , k_3 , $s_3(z_0)$, and $s_4(z_0)$ are the integration constants, which can be determined, at t=0, as a function of the initial conditions z_{40} , z_{50} , and z_{60} . Besides, from (11), one can easily see that $\begin{bmatrix} z_5 & z_6 & z_4 & z_3 \end{bmatrix}$ tends to $\begin{bmatrix} 0 & 0 & s_4(z_0) & s_3(z_0) \end{bmatrix}$ when t tends to infinity. So, if we take the initial conditions such that $s_4(z_0) = 0$ and $s_3(z_0) = 0$, then the whole state tends to the origin. Setting t=0 in (11), $s_4(z)$ and $s_3(z)$ can be determined. Substituting z_0 by z in the previous functions leads to

$$S_{4}(z) = z_{4} - \frac{k_{3}z_{5}}{k_{2}(k_{1} - k_{2})} + \frac{z_{6}}{k_{2}} + \frac{k_{3}z_{5}}{k_{1}(k_{1} - k_{2})},$$

$$S_{3}(z) = z_{3} + \frac{z_{5}z_{6}}{k_{1} + k_{2}} - \frac{k_{3}z_{5}^{2}}{k_{1}^{2} - k_{2}^{2}} + \frac{k_{3}z_{5}^{2}}{2k_{1}(k_{1} - k_{2})}.$$
(12)

Let

$$S = [S_4(z) \ S_3(z)]^T.$$
 (13)

From (13), it appears clearly that if the state variables belong to the 2-dimensional manifold

$$M_{S} = \{ z \in \mathbb{R}^{4} \mid S_{4}(z) = 0, S_{3}(z) = 0 \},$$
 (14)

then the whole state z tends to the origin, since z_5 and z_6 decay exponentially to zero. Furthermore, this manifold is invariant under the linear state feedback (9), as it is shown in the following result.

Proposition 4. *Consider the following functions:*

$$S_{4}(z) = z_{4} - \frac{k_{3}z_{5}}{k_{2}(k_{1} - k_{2})} + \frac{z_{6}}{k_{2}} + \frac{k_{3}z_{5}}{k_{1}(k_{1} - k_{2})},$$

$$S_{3}(z) = z_{3} + \frac{z_{5}z_{6}}{k_{1} + k_{2}} - \frac{k_{3}z_{5}^{2}}{k_{1}^{2} - k_{2}^{2}} + \frac{k_{3}z_{5}^{2}}{2k_{1}(k_{1} - k_{2})}.$$
(15)

Then $M_S = \{z \in \mathbb{R}^4 \mid S_4(z) = 0, S_3(z) = 0\}$ is an invariant manifold for the closed-loop system (8)–(10).

Proof. Denote vector fields of system (10) under the linear state feedback (9)

$$f = z_5 z_6 \frac{\partial}{\partial z_3} + z_6 \frac{\partial}{\partial z_4} - k_1 z_5 \frac{\partial}{\partial z_5} - (k_2 z_6 + k_3 z_5) \frac{\partial}{\partial z_6}.$$
(16)

Evaluating the Lie derivatives of along the vector fields (16) yields

$$L_{f}S_{4}(z) = \frac{\partial S_{4}}{\partial z} f(z)$$

$$= \begin{bmatrix} 0 & 0 & 1 \\ -\frac{k_{3}}{k_{2}(k_{1} - k_{2})} + \frac{k_{3}}{k_{1}(k_{1} - k_{2})} \end{bmatrix}^{T}$$

$$\times \begin{bmatrix} z_{5}z_{6} & 0 & 0 \\ -k_{1}z_{5} & 0 & 0 \\ -k_{1}z_{5} & 0 & 0 \\ -k_{2}z_{6} - k_{3}z_{5} \end{bmatrix}$$

$$= z_{6} + \frac{k_{1}k_{3}z_{5}}{k_{2}(k_{1} - k_{2})} - \frac{k_{3}z_{5}}{(k_{1} - k_{2})} - z_{6} - \frac{k_{3}}{k_{2}}z_{5}$$

$$= 0,$$

$$L_{f}S_{3}(z)$$

$$= \frac{\partial S_{3}}{\partial z} f(z)$$

$$= \begin{bmatrix} \frac{\partial S_{3}}{\partial z_{3}}, \frac{\partial S_{3}}{\partial z_{4}}, \frac{\partial S_{3}}{\partial z_{5}}, \frac{\partial S_{3}}{\partial z_{6}} \end{bmatrix} f(z)$$

$$= \begin{bmatrix} 1, 0, \frac{z_{6}}{k_{1} + k_{2}} - \frac{2k_{3}z_{5}}{k_{1}^{2} - k_{2}^{2}} + \frac{2k_{3}z_{5}}{2k_{1}(k_{1} - k_{2})}, \frac{z_{5}}{k_{1} + k_{2}} \end{bmatrix}$$

$$\times [z_{5}z_{6}, z_{6}, -k_{1}z_{5}, -(k_{2}z_{6} + k_{3}z_{5})]^{T}$$

$$= 0.$$
(17)

It appears clearly that the state variables M_S belong to the 2-dimensional invariant manifold.

Hence, we can construct the invariant manifold of the system (10) as M_S , which has the following characters:

- (1) $z = 0 \in M_s$;
- (2) to stabilize system (8) exponentially, it suffices to bring the state variables $\begin{bmatrix} z_5 & z_6 & z_4 & z_3 \end{bmatrix}$ into M_S by an additional state feedback, namely, w_1, w_2 .

Now it appears clearly that if the initial conditions are locating in the invariant manifold M_S , the system variables decay exponentially to zero in terms of linear feedback control. If the initial conditions locate outside of M_S , in order to stabilize the system, we should force the system variables into M_S firstly and then use the feedback control to stabilize the system.

In this paper, an MPC method is proposed for system (8) with the initial conditions out of the manifolds M_S . Consider an initial state $\begin{bmatrix} z_5 & z_6 & z_4 & z_3 \end{bmatrix}$ and a control horizon of T. At initial time, let the manifolds M_S be the terminal constraint set. The first objective of the proposed algorithm is to use a T-step control horizon to steer the terminal set-valued state prediction [z(t+T)] into the terminal constraint set M_S . The detail solution can be achieved by the minimization problem

in Section 3.2. Secondly, use the feedback control to stabilize the system to the origin. \Box

3.2. Design of MPC Controller. In this subsection we focus our objective on the determination of the first term to make the MPC controller steer the state into the terminal manifold M_S , asymptotically attractive. Once on it, the whole state $\begin{bmatrix} z_5 & z_6 & z_4 & z_3 \end{bmatrix}$ tends to zero under the residual linear state feedback (9).

MPC is an attractive strategy for systems subject to terminal constraints. Due to the USV systems with terminal constraints, we obtain the control input by minimizing a nominal cost $[J(z, w_c)]$ over a finite predictive horizon as follows:

$$J(z, w_c) = \min_{u_c} \int_{t}^{t+T} L(z, w_c) dt + W(x(t+T))$$
 (18)

s.t.

$$\dot{z}_3 = z_5 z_6, \quad \dot{z}_4 = z_6,$$

 $\dot{z}_5 = w_1, \quad \dot{z}_6 = w_2, \quad z(t+T) \in M_s,$
(19)

where T, $L(z, w_c)$, and W(x(t+T)) denote the time horizon, the running, and terminal costs. M_s denotes the terminal constraint set.

Substituting $L(z, w_c) = S^2$ by $S = \sqrt{s_3^2 + s_4^2}$, we can obtain

$$M_s^2 = S^2 = \left(z_3 + \frac{z_6}{k_2}\right)^2 + \left(z_2 + \frac{z_4 z_6}{k_1 + k_2}\right)^2.$$
 (20)

Selecting $L(z, w_c) = S^2$ and W = 0 leads to

$$J(z, w_c) = \min_{w_c} \int_t^{t+T} \left(\left(z_3 + \frac{z_6}{k_2} \right)^2 + \left(z_2 + \frac{z_4 z_6}{k_1 + k_2} \right)^2 \right) dt.$$
(21)

Proposition 5. If the optimization problem in (18) and (19) is feasible, the closed-loop underactuated system (10) with terminal invariant manifolds constraints M_s is asymptotically stable in terms of MPC controller.

Proof. Firstly, define the "MPC value function" as V; $(\overline{z}, \overline{w}_c)$ denotes the optimal solution of (18), δ denotes the sampling time, and T denotes the predictive and control horizon. There exists a scalar $\varepsilon > 0$ such that for each time $t \in [T, \infty)$ and each $z_t \in M_s$, we can choose a control function \overline{w}_c : $[t, t + \varepsilon] \to R^2$, satisfying [33]

$$\frac{\partial W\left(z_{t}\right)}{\partial z}f\left(z_{t},\overline{w}_{c}\left(t\right)\right) \leq -L\left(z_{t},\overline{w}_{c}\left(t\right)\right). \tag{22}$$

In sampling time t_i , the value function for $J(t_i, z_t, T)$ is

$$V_{t_{i}} = \int_{t_{i}}^{t_{i}+T} L\left(\overline{z}\left(t\right), \overline{w}_{c}\left(t\right)\right) dt + W\left(\overline{z}\left(t_{i}+T\right)\right). \tag{23}$$

Choose sample time $\delta < \varepsilon$ small enough such that extending the process $(\overline{z}, \overline{w}_c)$ to $[t_i, t_i + T + \delta], \overline{u}_c[t_i + T, t_i + T + \delta]$ will

satisfy (22). To this control it will correspond to the extended trajectory $\overline{z}[t_i+T,t_i+T+\delta]$. The condition (22) guarantees that the extended process $(\overline{z},\overline{w}_c)$ taken in the interval $[t_i+\delta,t_i+T+\delta]$ is admissible for problem $J(t_i+\delta,\overline{z}_{t_i+\delta},T)$. However, since this process is not necessarily optimal, we have

$$V_{t_{i}+\delta}\left(t_{i}+\delta,\overline{z}\left(t_{i}+\delta\right)\right) \leq \int_{t_{i}+\delta}^{t_{i}+T+\delta} L\left(\overline{z}\left(t\right),\overline{w}_{c}\left(t\right)\right) dt + W\left(\overline{z}\left(t_{i}+T+\delta\right)\right).$$

$$(24)$$

Hence

$$V_{t_{i}+\delta}\left(t_{i}+\delta,\overline{z}\left(t_{i}+\delta\right)\right)-V_{t_{i}}\left(t_{i},\overline{z}\left(t_{i}\right)\right)$$

$$\leq-\int_{t_{i}}^{t_{i}+\delta}L\left(\overline{z}\left(t\right),\overline{w}_{c}\left(t\right)\right)dt$$

$$+\int_{t_{i}+T}^{t_{i}+T+\delta}L\left(\overline{z}\left(t\right),\overline{w}_{c}\left(t\right)\right)dt$$

$$+W\left(\overline{z}\left(t_{i}+T+\delta\right)\right)-W\left(\overline{z}\left(t_{i}+T\right)\right).$$
(25)

Integrating (22), we have

$$W\left(\overline{z}\left(t_{i}+T+\delta\right)\right)-W\left(\overline{z}\left(t_{i}+T\right)\right) + \int_{t_{i}+T}^{t_{i}+T+\delta} L\left(\overline{z}\left(t\right),\overline{w}_{c}\left(t\right)\right) dt \leq 0.$$
(26)

Finally, we obtain

$$V_{t_{i}+\delta}\left(t_{i}+\delta,\overline{z}\left(t_{i}+\delta\right)\right)-V_{t_{i}}\left(t_{i},\overline{z}\left(t_{i}\right)\right)$$

$$\leq-\int_{t_{i}}^{t_{i}+\delta}L\left(\overline{z}\left(t\right),\overline{w}_{c}\left(t\right)\right)dt.$$
(27)

Due to $L(z, w_c) \ge 0$, we know the value function is decreasing on each interval $[t_i, t_i + \delta]$ for any i and the function V is smaller at t_{i+1} than at t_i . Hence the close-loop system (8) is asymptotically stable.

The stabilizing properties of this approach can be confirmed by the existence of an admissible solution to the openloop optimization (21) at initial time t, and so stability is guaranteed provided that M_s is reachable in time. Then the condition $L(z,w_c)=0$ is guaranteed by using the linear feedback control w_c . Because $L(z,w_c)=0$, the condition $\dot{W}=0 \leq L(z,w_c)=0$ is satisfied. It is clear that condition (22) is satisfied. (A thorough discussion of the previous problems can be found in [33].)

The approach was first described in [33]. In this case, outside the invariant manifolds centered at the origin, we have to solve the open-loop optimal control problem with (21). Before we reach M_s , we have a free time problem. After the set M_s is reached, we switch to a linear stabilizing feedback controller for the linearized system. The course of solution is described as follows:

$$w_c = w_{cMPC}, \quad z \notin M_s, \qquad w_c = w_{cM_s}, \quad z \in M_s, \quad (28)$$

where w_{cMPC} denotes the control law by using nonlinear MPC and denotes the linear feedback control law.

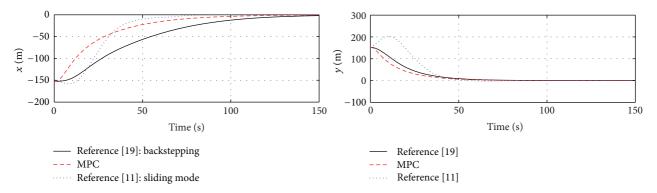


FIGURE 2: Trajectory of x and y.

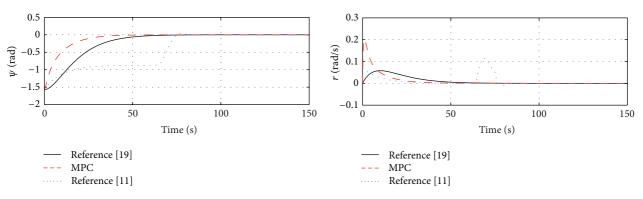


Figure 3: Trajectory of ψ and r.

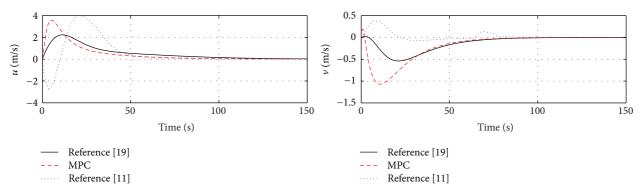


FIGURE 4: Trajectory of u and v.

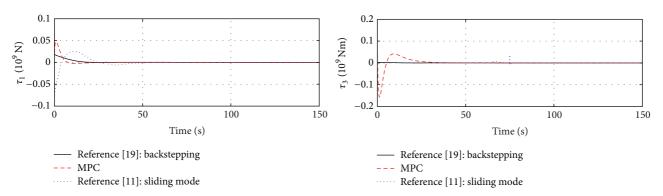


FIGURE 5: Control input.

4. Simulation Results

In [9], an underactuated actual ship named "Northern Clipper" is introduced. Consider the simulation model with parameters as "Northern Clipper" in [9]: $m_{11} = 5.312 \times 10^6$ kg, $m_{22} = 8.283 \times 10^6$ kg, $m_{33} = 3.745 \times 10^6$ kg, $d_{11} = 5.024 \times 10^4$ kg/s, $d_{22} = 2.722 \times 10^5$ kg/s, and $d_{33} = 1.189 \times 10^8$ kg/s. Length of "Northern Clipper" L = 76.2 m, and mass $m = 4.6 \times 10^6$ kg. In this section, the effectiveness of the proposed MPC control law is verified by following simulation. For the purpose of comparisons, more simulations with sliding mode control approach proposed in [11] and backstepping control proposed in [19] are done to verify the advantage of the MPC method. The control law is selected as Proposition 5, and the initial values are selected as x(0) = -152.4 m, y(0) = -152.4 m, y(0) = -m/2 rad, y(0) = 0 m/s, and y(0) = 0 m/s, and

The control parameters are selected as $k_1=1.2$, $k_2=0.8$, and $k_3=1.5$. The performance cost is selected as (21). The terminal manifolds are selected as M_s . Sampling time is selected as $\delta=0.5$ s. Predictive and control horizon are selected as T=5 s.

Simulation results are shown in the following figures, and the simulation time is set as 150 s. Figure 2 gives the time response of the position x, y. Figure 3 gives the time response of the orientation ψ and orientation velocity r. Figure 4 gives the time response of the velocities u, v. The responses of the control inputs τ_1 and τ_3 are shown in Figure 5.

Figures 2–5 show that the three control laws all asymptotically stabilize the underactuated surface vessel to the zero origin. Since the MPC control law guarantees a faster convergence rate of the simulation system, the MPC method may be superior to the other two. Furthermore, Figure 5 shows that surge control force τ_1 given by MPC is always positive. Compared with reverse thrust for an actual ship, positive thrust is easier to achieve in practice. Therefore, the MPC approach gets a more favorable control effect.

5. Conclusion

This paper proposes the stabilization approach for underactuated surface vessels with only a surge force and a yaw moment. The invariant manifolds constraints are studied, and stability theory of MPC controller is further developed, which is applied to the stabilization control of underactuated surface vessel. For the stabilization control of underactuated surface vessel, a nonlinear MPC control law with terminal invariant manifolds constraints is designed through coordinate transformation and state feedback transformation based on diffeomorphism and Lyapunov stability theory. The simulation results show that the proposed control law can effectively deal with the problem of stabilization control of underactuated surface vessel.

It should be noted that the controller proposed in this paper is developed with constant parameters. In the future work, efforts will be made to design the data-driven controller with uncertain parameters to reduce the effect of noisy data and computational complexity.

Acknowledgments

The authors are grateful to their colleagues from the College of Information and Telecommunication and the College of Automation in Harbin Engineering University for providing helpful comments. This work is partially supported by the National Natural Science Foundation of China (61201410 and 51379044), Fundamental Research Funds for the Central Universities (HEUCF130804), and Heilongjiang Province Natural Science Foundation Projects (F200916).

References

- [1] R. Hedjar, "Adaptive neural network model predictive control," *International Journal of Innovative Computing, Information and Control*, vol. 9, no. 3, pp. 1245–1257, 2013.
- [2] V. Vesely, D. Rosinova, and T. Nguyen Quang, "Networked output feedback robust predictive controller design," *International Journal of Innovative Computing, Information and Control*, vol. 9, no. 10, pp. 3941–3953, 2013.
- [3] S. Bououden, M. Chadli, F. Allouani, and S. Filali, "A new approach for fuzzy predictive adaptive controller design using particle swarm optimization algorithm," *International Journal of Innovative Computing, Information and Control*, vol. 9, no. 9, pp. 3741–3758, 2013.
- [4] V. Vesely and J. Osusky, "Robust multivariable generalized predictive control design," *International Journal of Innovative Computing, Information and Control*, vol. 9, no. 8, pp. 3377–3390, 2013.
- [5] X. Su, P. Shi, L. Wu, and Y. -D. Song, "A novel control design on discrete-time takagi-sugeno fuzzy systems with time-varying delays," *IEEE Transactions on Fuzzy Systems*, vol. 20, no. 6, pp. 655–671, 2013.
- [6] X. Su, X. Yang, P. Shi, and L. Wu, "Fuzzy control of nonlinear electromagnetic suspension systems," *Mechatronics*.
- [7] L. Wu, W. X. Zheng, and H. Gao, "Dissipativity-based sliding mode control of switched stochastic systems," *IEEE Transac*tions on Automatic Control, vol. 58, no. 3, pp. 785–793, 2013.
- [8] L. Wu, X. Su, and P. Shi, "Output feedback control of markovian jump repeated scalar nonlinear systems," *IEEE Transactions on Automatic Control*.
- [9] T. I. Fossen, Marine Control Systems, Marine Cybernetics, Trondheim, Norway, 2002.
- [10] K. D. Do and J. Pan, "Robust path-following of underactuated ships: theory and experiments on a model ship," *Ocean Engineering*, vol. 33, no. 10, pp. 1354–1372, 2006.
- [11] J. Cheng, J. Yi, and D. Zhao, "Stabilization of an underactuated surface vessel via discontinuous control," in *Proceedings of the American Control Conference*, pp. 206–211, New York, NY, USA, July 2007.
- [12] K. Y. Pettersen and H. Nijmeijer, "Global practical stabilization and tracking for an underactuated ship—a combined averaging and backstepping approach," *Modeling, Identification and Control*, vol. 20, no. 4, pp. 189–199, 1999.
- [13] K. Y. Pettersen and H. Nijmeijer, "Tracking control of an underactuated surface vessel," in *Proceedings of the 37th IEEE Conference on Decision and Control*, pp. 4561–4566, Tampa, Fla, USA, December 1998.
- [14] E. Lefeber, *Tracking control of nonlinear mechanical systems* [*Ph.D. thesis*], Department of Mechanical Engineering, Twente University, Twente, The Netherlands, 2000.

- [15] E. Lefeber, K. Y. Pettersen, and H. Nijmeijer, "Tracking control of an underactuated ship," *IEEE Transactions on Control Systems Technology*, vol. 11, no. 1, pp. 52–61, 2003.
- [16] Z. P. Jiang and H. Nijmeijer, "A recursive technique for tracking control of nonholonomic systems in chained form," *IEEE Transactions on Automatic Control*, vol. 44, no. 2, pp. 265–279, 1999.
- [17] K. Y. Pettersen and H. Nijmeijer, "Underactuated ship tracking control: theory and experiments," *International Journal of Control*, vol. 74, no. 14, pp. 1435–1446, 2001.
- [18] Z. P. Jiang, "Global tracking control of underactuated ships by Lyapunovs direct method," *Automatica*, vol. 38, no. 2, pp. 301– 309, 2002.
- [19] J. Ghommam, F. Mnif, A. Benali, and N. Derbel, "Asymptotic backstepping stabilization of an underactuated surface vessel," *IEEE Transactions on Control Systems Technology*, vol. 14, no. 6, pp. 1150–1157, 2006.
- [20] Z. Liu, R. Yu, and Q. Zhu, "Comments on asymptotic backstepping stabilization of an underactuated surface vessel," *IEEE Transactions on Control Systems Technology*, vol. 20, no. 1, pp. 286–288, 2012.
- [21] Li Zhen, Path following with roll constraints for marine surface vessels in wave fields [Ph.D. thesis], University of Michigan, Ann Arbor, Mich, USA, 2009.
- [22] X. F. Wang, T. S. Li, Z. J. Zou, and W. L. Luo, "Nonlinear model predictive controller design for path following of underactuated ships," *Journal of Ship Mechanics*, vol. 14, no. 3, pp. 217–227, 2010.
- [23] S. Yin, S. X. Ding, A. Haghani, H. Hao, and P. Zhang, "A comparison study of basic data-driven fault diagnosis and process monitoring methods on the benchmark Tennessee Eastman process," *Journal of Process Control*, vol. 22, no. 9, pp. 1567–1581, 2012.
- [24] S. Yin, S. Ding, and H. Luo, "Real-time implementation of fault tolerant control system with performance optimization," *IEEE Transactions on Industrial Electronics*, vol. 61, no. 5, pp. 2402–2411, 2013.
- [25] S. Yin, S. Ding, A. Haghani, and H. Hao, "Data-driven monitoring for stochastic systems and its application on batch process," *International Journal of Systems Science*, vol. 44, no. 7, pp. 1366– 1376, 2013.
- [26] S. Yin, X. Yang, and H. Karimi, "Data-driven adaptive observer for fault diagnosis," *Mathematical Problems in Engineering*, vol. 2012, Article ID 832836, 21 pages, 2012.
- [27] T. I. Fossen, Guidance and Control of Ocean Vehicles, Wiley, New York, NY, USA, 1994.
- [28] K. Y. Wichlund, O. J. Sordalen, and O. Egeland, "Control properties of underactuated vehicles," in *Proceedings of the IEEE International Conference on Robotics and Automation*, vol. 2, pp. 2009–2014, Nagoya, Japan, May 1995.
- [29] C. I. Byrnes and A. Isidori, "On the attitude stabilization of rigid spacecraft," *Automatica*, vol. 27, no. 1, pp. 87–95, 1991.
- [30] K. Y. Pettersen and O. Egeland, "Exponential stabilization of an nderactuated surface vessel," in *Proceedings of the 35th IEEE Conference on Decision and Control*, pp. 967–972, Kobe, Japan, 1996.
- [31] R. W. Brockett, "Asymptotic stability and feedback stabilization," in *Proceedings of Conference Progress in Mathematics*, vol. 27, pp. 181–208, Boston, Mass, USA, 1983.
- [32] F. Mazenc, K. Y. Pettersen, and H. Nijmeijer, "Global uniform asymptotic stabilization of an underactuated surface vessel," in *Proceedings of the 41st IEEE Conference on Decision and Control (CDC '02)*, pp. 510–515, Las Vegas, Nev, USA, December 2002.

[33] F. A. C. C. Fontes, "A general framework to design stabilizing nonlinear model predictive controllers," *Systems and Control Letters*, vol. 42, no. 2, pp. 127–143, 2001.